HYDRAULICS

8th National Conference on Hydraulics in Water Engineering

Editorial Notes
Keynote Speakers
Henderson Oration
Papers

HYDRAULICS THE next wave

ISBN 085825 850 1

13 - 16 July 2004

ANA Hotel Surfers Paradise Queensland Australia

CONFERENCE PROGRAMME

EXIT

ENGINEERS AUSTRALIA

8th National Conference on Hydraulics in Water Engineering Technical Program

Tuesday 13th July, 2004

4.00 - 5.30pm ***Registration - Pre-Function Area, Level 2***

5.30 - 7.00pm ***Welcome Reception - Tarcoola Pre-Function Area, Level 4***

Wednesday 14th July, 2004 Abstracts pages 13 - 39

7.30 - 8.30am Registration - Pre-Function Area, Level 2

8.45 - 10.00am ***SESSION 1: Opening Ceremony and Keynote Presentation***

Room: Tatiara Chair: Toby McGrath

8.45 - 9.00am Official Welcome - His Worship the Mayor Councillor Ron Clarke

Paul Banfield from Wallingford Software - Gold Sponsors

9.00 - 10.00am *"Estuary Hydraulics for the Year 3004" Pg 14*

Keynote Associate Professor Jon Hinwood, Monash University VIC

10.00m - 10.30am ***Morning Tea and Trade Exhibition - Tarcoola Pre-Function Area, Level 4***

10.30 - 12.10pm	***SESSION 2A: Coastal Hydraulics*** ***Room: Tallangatta Chair: Jörg Imberger***	***SESSION 2B: Hydraulic Design*** ***Room: Tatiara Chair: Bruce Melville***
10.30 - 10.55am	*"Swash Overtopping and Sediment Transport – Application to Bermed Beaches and Lagoon Entrances" Pg 15*	*"Development of a Device for Direct Measurement of Bed Shear Stress Induced by a Wave Spectrum" Pg 19*
	T E Baldock, University of Queensland - Brisbane QLD	Hamid Mirfenderesk, Griffith Centre for Coastal Management, Griffith University - Gold Coast QLD
10.55 - 11.20am	*"Numerical Modelling for Wave-Induced Pore Pressure in Marine Sediments: Case Study at Gold Coast" Pg 16*	*"Estimating the Uncertainty of Flow Measurement for the In situ Calibration of Large Water Meters" Pg 20*
	Hong Zhang, Griffith University - Gold Coast QLD	Edgar Johnson, Grampians Region Water Authority - Melbourne VIC
11.20 - 11.45am	*"The Complexity Of Numerical Modelling Of The Singapore Coastal Waters" Pg 17*	*"Direct Measurement of Roughness of Bed Covered with Gravel and Ripples" Pg 21*
	Ainslie Frazer, Water Research Laboratory University of New South Wales - Sydney NSW	Hamid Mirfenderesk, Griffith Centre for Coastal Management, Griffith University - Gold Coast QLD
11.45 - 12.10pm	*"A Methodology For Predicting Berm Crest Elevation Fronting Coastal Lagoons" Pg 18*	*"Steep Gradient Waterway Stabilisation – An Innovative Design Technique" Pg 22*
	Felicia Weir, University of Sydney - Sydney NSW	Chairs Choice - John Macintosh, Water Solutions - Brisbane QLD

12.10 - 1.10pm ***Lunch and Trade Exhibition - Tarcoola Pre-Function Area, Level 4***

1.10 - 2.50pm	***SESSION 3A: Environmental Hydraulics*** ***Room: Tallangatta Chair: Robert Schwartz***	***SESSION 3B: Hydraulic Design*** ***Room: Tatiara Chair: John Macintosh***
1.10 - 1.35pm	*"Physical Modelling and Hydraulic Modifications to a Power Station Weed Settling Pond" Pg 23*	*"Scale Effects in Moderate Slope Stepped Spillways Experimental Studies in Air Water Flows" Pg 27*
	James Walker, University of NSW - Sydney NSW	Carlos Gonzalez, University of Queensland - Brisbane QLD

1.35 - 2.00pm	*"Deterioration of Conduit Efficiency Due to Biofouling" Pg 24*	*"Assessment Of Predicted Near Field Dilution And Hydraulic Head Requirements For A Range Of Outfall And Diffuser Configurations" Pg 28*
	Andrew Barton, University of Tasmania - Tasmania	Brett Miller, University of NSW - Sydney NSW
2.00 - 2.25pm	*"Simulation of Turbidity Generation for Proposed Dreging Operations at Port Adelaide" Pg 25*	*"Diverse Drop Structure Applications in an Open Channel" Pg 29*
	Andrew McCowan, Water Technology - Melbourne VIC	Luke Toombes, Connell Wagner - Brisbane QLD
2.25 - 2.50pm	*"Assessment of Deposited Sediments in Roadside Stormwater Retention Basins" Pg 26*	*"Design of an Automated Floodgate Control System to Enhance Tidal Flushing: Case study, Broughton Creek, NSW" Pg 30*
	James Ball, Water Research Laboratory University of NSW - Sydney NSW	Brett Miller, University of NSW - Sydney NSW
2.50 - 3.20pm	***Afternoon Tea and Trade Exhibition - Tarcoola Pre-Function Area, Level 4***	
3.20 - 5.00pm	***SESSION 4A: Computational Fluid Dynamics***	***SESSION 4B: Water Supply and Stormwater***
	Room: Tallangatta Chair: Colin Apelt	***Room: Tatiara Chair: Brett Phillips***
3.20 - 3.45pm	*"Integrated High Order Water Quality and Hydrodynamic Models – An Essential Tool for Lake Management" Pg 31*	*"Hydraulic Risk Assessment of Water Distribution Systems" Pg 35*
	Robert Swan, Lawson and Treloar P/L - Melbourne VIC	Holger Maier, The University of Adelaide - Adelaide SA
3.45 - 4.10pm	*"Application of Data-Driven Models and Computational Intelligence in Hydrology and Hydraulics" Pg 32*	*"Integrating Overland Flooding and Drainage Pipe Newtorks" Pg 36*
	David McConnell, Patterson Britton & Partners Pty Ltd. - North Sydney NSW	Siebe Bosch, Lawson and Treloar P/L - Brisbane QLD
4.10 - 4.35pm	*"A Data Framework for Hydrodynamic Modelling" Pg 33*	*"Modelling a Combined Sewage and Stormwater Flood Detention Basin" Pg 37*
	Susan Shield, Umwelt Australia - Newcastle NSW & Andrew Goodwin, School of Engineering, Univeristy of Newcastle - NSW	Ann Pugh, Wallingford Software - Sydney NSW
4.35 - 5.00pm	*"Scale Similarity Models for Large Eddy Simulations" Pg 34*	*"An Efficient Geospatial Approach to Comprehensive Management and Protection of Water Distribution Systems" Pg 38*
	Francesco Gallerano, Universita La Sapienza Di Rome Italy - Rome ITALY	Brett Stewart, MWH Soft - Brisbane QLD
5.00 - 6.00pm	***Henderson Oration Drinks - Pre-Function Area, Level 2***	
6.00 - 7.00pm	***SESSION 5: Henderson Oration***	
	Room: Tatiara Chair: John Macintosh	
	"Influence of Stratification, Rotation, Wind Forcing and Basin Shape on the Hydrodynamics of Lakes" Pg 39	
	Professor Jörg Imberger, University of Western Australia - Crawley WA	

Thursday 15th July, 2004 Abstracts pages 40 - 54

8.00 - 8.30am ***Registration - Pre-Function Area, Level 2***

8.30 - 9.25am ***SESSION 6: Keynote Presentation***

	Room: Tallangatta ***Chair: Toby McGrath***	
	"Bridge Abutment Scour: Estimation and Protection" P 41	
	Professor Bruce Melville, University of Auckland - Auckland NZ	
9.30 - 10.45am	***SESSION 7A: River Hydraulics***	***SESSION 7B: Hydraulic Design***
	Room: Tallangatta ***Chair: Vladimir Nikora***	***Room: Tatiara*** ***Chair: James Ball***
9.30 - 9.55am	*"Modelling the 3-Dimensional Flow Between the Nerang River Estuary and Burleigh Lakes System, Gold Coast" Pg 42*	*"Analysis and Design of Sediment Basins" Pg 45*
	Sasha Zigic, Asia-Pacific ASA - Surfers Paradise QLD	Robert Janssen, Bechtel Services - Brisbane QLD
9.55 - 10.20am	*"Hydrodynamic Modelling of the Lower Meking River and Delta for Basin Planning" Pg 43*	*"Rock Chutes: A Review of Damage and Failure Mechanisms" Pg 46*
	Richard Harpin, Halcrow Group Pty Ltd - Melbourne VIC	Anthony Ladson, Monash University - Melbourne VIC
10.20 - 10.45am	*"Overview of Hydraulic Modelling of the Yangtze River for Flood Forecasting Purposes" Pg 44*	
	Steve Clark, Sagric International P/L - CHINA	
10.45 - 11.15am	***Morning Tea and Trade Exhibition - Tarcoola Pre-Function Area, Level 4***	
11.15 - 12.55pm	***SESSION 8A: Environmental Hydraulics***	***SESSION 8B: Flood Management***
	Room: Tallangatta ***Chair: Kuhan Kuhanesan***	***Room: Tatiara*** ***Chair: Rob Ayre***
11.15 - 11.40am	*"Modelling Saturation Excess Runoff with SWAT" Pg 47*	*"Delivering Property Specific Flood Advice" Pg 51*
	Brett Watson, Deakin University - Geelong VIC	Bruce Druery, Patterson Britton & Partners Pty Ltd - North Sydney NSW
11.40 - 12.05pm	*"Hydraulic and Ecological Modelling of the Pimpama River Estuary" Pg 48*	*"Safety of People in Flooded Streets and Floodways" Pg 52*
	Stefan Szylkarski, DHI Water and Environment - Gold Coast QLD	Ron Cox, University of New South Wales - Sydney NSW
12.05 - 12.30pm	*"Hydrodynamic, Water Quality and Ecological Study of Eprapah Creek Estuarine Zone: a Multi-Disciplinary, Cross-Institutional Approach" Pg 49*	*"Hydraulics in Floodplain Management for the Gold Coast" Pg 53*
	Hubert Chanson, University of Queensland - Brisbane QLD	Khondker Rahman, Gold Coast City Council - Gold Coast QLD
12.30 - 12.55pm	*"Evaluating the Application of Absorbent Polymers on Soil Hydraulic Properties" Pg 50*	*"A New Generation, GIS Based, Open Flood Forecasting System" Pg 54*
	Jahangir Abedi-Koupai, Isfahan University of Technology - IRAN	Terry Van Kalken, DHI Water and Environment - Gold Coast QLD
12.55 - 5.00pm	***Lunch and Technical Tours - Pre-Function Area, Level 2***	
6.30 - 7.00pm	***Pre Dinner Drinks - Margaritas on the Water, Bundall***	

7.00 - 10.30pm ***Conference Dinner***

Friday 16th July 2004 Abstracts pages 55 - 78

8.00 - 8.30am ***Registration - Pre-Function Area, Level 2***

8.30 - 9.25am ***SESSION 9: Keynote Presentation***

Room: Tatiara ***Chair: Hubert Chanson***

"Hydrodynamic Effects in Aquatic Ecosystems" Pg 56

Dr Vladimir Nikora, NIWA - Christchurch NZ

9.30 - 10.45am

	SESSION 10A: Computational Fluid Dynamics	***SESSION 10B: Hydraulic Design***
	Room: Tallangatta ***Chair: Andrew McCowan***	***Room: Tatiara*** ***Chair: Robert Schwartz***
9.30 - 9.55am	*"1-D and 2-D Hydraulic Modelling of Extreme Floods in a Steep Urban Stream" Pg 57*	*"Physical Modelling of Preliminary Design for Eidsvold Weir Spillway & Fishway" Pg 60*
	Brett Phillips, Cardno Willing (NSW) Pty Ltd - Sydney NSW	James Carley, University of NSW - Sydney NSW
9.55 - 10.20am	*"Application of CFD Modelling to Free Surface Flow Around Bluff Bodies – A Case Study Using a Bridge Superstructure" Pg 58*	*"Hydraulic Model Study of Tilapia Fish Exclusion Using Coanda Screens" Pg 61*
	Mark Jempson, WBM Oceanics - Melbourne VIC	Franz Jacobsen, SunWater Qld - Brisbane QLD
10.20 - 10.45am	*"Modelling Flood Inundation of Urban Areas in the UK Using 2D / 1D Hydraulic Models" Pg 59*	*"The Implementation of PIV-PTV Techniques for Measurement of Velocities in Large Physical Models" Pg 62*
	Bill Syme, WBM Oceanics - Brisbane QLD	Doug Anderson, University of NSW - Sydney NSW

10.45 - 11.15am ***Morning Tea and Trade Exhibition - Tarcoola Pre-Function Area, Level 4***

11.15 - 12.55pm

	SESSION 11A: Computational Fluid Dynamics	***SESSION 11B: Flood Management***
	Room: Tallangatta ***Chair: Bill Syme***	***Room: Tatiara*** ***Chair: Khondker Rahman***
11.15 - 11.40am	*"Analysis of Spillway Flow by Computational Fluid Dynamics Technique" Pg 63*	*"Emergency Action Planning for the Dee River Dams" Pg 67*
	Karen Riddette, Advanced Analysis Worley P/L - Sydney NSW	Andrew Chapman, Kellogg Brown & Root - Brisbane QLD
11.40 - 12.05pm	*"Three Dimensional Modelling of Various Stratified Reservoirs. Data Requirements, Limitations and use of Model Results to Aid Management and Engineering Decision Making" Pg 64*	*"Wivenhoe Dam Upgrade Adopted Strategy and Downstream Impacts" Pg 68*
	Rohan Hudson, University of NSW - Sydney NSW	Greg Roads, Wivenhoe Alliance, Brisbane QLD
12.05 - 12.30pm	*"A Finite Volume Solution for a Ring Tank Failure Parametric Study" Pg 65*	*"Disaster Mitigation in Central Vietnam: Application of Two-Dimensional Hydraulic Model" Pg 69*
	Alexander Nielsen, SMEC Sydney - Sydney NSW	Ian Wood, Kellogg Brown & Root - Brisbane QLD
12.30 - 12.55pm	*"Aspects of Numerically Modelling Transcritial Flows" Pg 66*	*"Evaluation of Hydrologic and Hydraulic Models for Real-time Flood Forecasting use in the Yangtze River Catchment" Pg 70*

	Anthony Wicht, Water Research Laboratory University of NSW - Sydney NSW	Sharmil Markar, Sagric International P/L - China
12.55 - 1.55pm	***Lunch and Trade Exhibition - Tarcoola Pre-Function Area, Level 4***	
1.55 - 3.35pm	***SESSION 12A: Coastal Hydraulics***	***SESSION 12B: Water Supply and Stormwater***
	Room: Tallangatta Chair: Tom Baldock	***Room: Tatiara Chair: Ann Pugh***
1.55 - 2.20pm	*"Measured and Modelled Flow Velocities in the Swash Zone of a Steep Beach: With Implications for Sediment Transport Modelling" Pg 71*	*"Asset and Pressure Management – A Combined Approach" Pg 75*
	Michael Hughes, University of Sydney - Sydney NSW	Alex McKenzie, MWH Australia - Melbourne VIC & Simon Pearce Higgins, Yarra Valley Water - VIC
2.20 - 2.45pm	*"Storm Tide Modelling of the Whitsunday Coast and Resort Islands" Pg 72*	*"Development and Calibration of Detailed Sewer Models for the Brisbane Sewerage System" Pg 76*
	Ross Fryar, GHD Pty Ltd - Brisbane QLD	Stefan Szylkarski, DHI Water and Environment - Gold Coast QLD
2.45 - 3.10pm	*"Tropical Cyclone Storm Surge Modelling of the Coast of Queensland" Pg 73*	*"Genetic Algorithm Optimisation for Water Distribution System Design at the Gold Coast" Pg 77*
	Juan Savioli, DHI Water and Environment - Gold Coast QLD	Angus Simpson, University of Adelaide - Adelaide SA & Scott Sherriff, Gold Coast Water - Gold Coast QLD
3.10 - 3.35pm	*"Queensland Climat Change and Community Vulnerability to Tropical Cyclones Project" Pg 74*	*"Finding a Solution for the Hammonds Drain Problem" Pg 78*
	Chairs Choice - Robert Schwartz, Environmental Protection Agency - Brisbane QLD	Kevan Blake, Connell Wagner - Adelaide SA
3.35 - 4.05pm	***Afternoon Tea and Trade Exhibition - Tarcoola Pre-Function Area, Level 4***	
4.05 - 5.00pm	***Closing Ceremony***	
	Room: Tatiara Chair: Toby McGrath	

Evaluating the Application of Super Absorbent Polymers on Soil Hydraulic Properties

Jahangir Abedi-Koupai BSc., MSc., PhD.
Assistant Professor, Isfahan University of Technology, Iran

Farahnaz Sohrab B.Sc., MSc.
Former Graduate Student, Isfahan University of Technology, Iran

The Implementation of PIV-PTV Techniques for Measurement of Velocities in Large Physical Models

D.J. Anderson B.E., M.Eng.Sc.
Water Research Laboratory, School of Civil and Environmental Engineering,
University of New South Wales, Australia.

A. Frazer B.E.
T. Jancar B.E.
B.M. Miller B.E., B.Sc., M.Eng.Sc., MIEAust

Swash Overtopping and Sediment Transport – Application to Bermed Beaches and Lagoon Entrances

T. E. Baldock B.Eng., PhD.
Lecturer, Division of Civil Engineering, University of Queensland, St Lucia, Brisbane, Qld 4072.

K. Day B. Eng.
GHD Pty Ltd, GPO Box 668 Brisbane, QLD, 4001

M. G. Hughes B.Ec., Ph.D
Senior Lecturer, School of Geosciences and Institute of Marine Science, University of Sydney NSW 2006

F. Weir B.Sc.
School of Geosciences and Institute of Marine Science, University of Sydney NSW 2006.

Assessment of Deposited Sediments in Roadside Stormwater Retention Basins

J. E. Ball B.E., M.E., PhD., M.I.E.Aust., CPEng.
Associate Professor, Water Research Laboratory, Civil & Environmental Engineering, University of NSW, Sydney, Australia

J. W. Walker B.E., MEngSci
Senior Project Engineer, Water Research Laboratory, Civil & Environmental Engineering, University of NSW, Sydney, Australia

S. Isles
Roads & Traffic Authority NSW, Australia

C. Blake
Roads & Traffic Authority NSW, Australia

Deterioration of Conduit Efficiency Due to Biofouling

A. F. Barton BE(Hons), MEngSc, MIAHR, MAWA, MIEAust
PhD Student, School of Engineering, University of Tasmania, Australia

M. W. Sylvester BE(Hons), MIPENZ, MIEAust
Senior Hydropower Engineer, Hydropower and Water Resources, Maunsell Ltd, New Zealand

J. E. Sargison BE(Hons), PhD, MASME, MIEAust
Research Fellow, School of Engineering, University of Tasmania, Australia

G. J. Walker BSc, BE(Hons), PhD, FASME, FIEAust, CPEng
Reader, School of Engineering, University of Tasmania, Australia

A. B. Denne DipCivEng, MIEAust, CPEng
Principal Asset Engineer (Civil), Hydro Tasmania, Australia

Finding a Solution for the Hammonds Drain Problem

K.R.K. Blake B.Sc.,MSc.,Dip.Hydraulics., M.E.Aust.
Project Engineer, Connell Wagner Pty. Ltd., Australia

Integrating Overland Flooding and Drainage Pipe Networks

Siebe Bosch
Senior Engineer, WL | Delft Hydraulics (1 year secondment to Lawson & Treloar)
Rotterdamseweg 185, 2629 HD Delft, THE NETHERLANDS

Ian Clark
Senior Engineer, Lawson and Treloar Pty. Ltd
Level 1 40-44 Blackwood Street, Mitchelton QLD 4053

Chris Catalano
Associate, Lawson and Treloar Pty. Ltd
Level 1 40-44 Blackwood Street, Mitchelton QLD 4053

An Efficient Geospatial Approach to Comprehensive Management and Protection of Water Distribution Systems

P.F. Boulos B.S., M.S., MBA, Ph.D
President and COO, MWH Soft, Inc., USA

S.F. O'Brien BEng, Grad Dip Eng
Manager Planning & Environment, MWH Australia, Australia

B. Stewart BEng
Senior Planning Engineer, MWH Australia, Australia

Physical Modelling of Preliminary Design for Eidsvold Weir Spillway and Fishway

James T. Carley B.Build., M.Eng.Sc., M.I.E.Aust.
Senior Engineer, Water Research Laboratory, School of Civil and Environmental Engineering, University of NSW, Australia

James W. Walker B.E., M.Eng.Sc.
Senior Engineer, Water Research Laboratory, School of Civil and Environmental Engineering, University of NSW, Australia.

James E. Ball B.E., M.E., Ph.D., F.I.E.Aust. C.P.Eng
Associate Professor, Water Research Laboratory, School of Civil and Environmental Engineering, University of NSW, Australia

John C. Macintosh B.E., Ph.D., R.P.E.Q., F.I.E.Aust. C.P.Eng
Director/Principal, Water Solutions Pty Ltd, Australia

Hydrodynamic, Water Quality and Ecological Study of Eprapah Creek Estuarine Zone : a Multi-Disciplinary, Cross-Institutional Approach

R. Brown B.E., B.Th., Ph.D., MIEAust
Lecturer, School of Mechanical, Manufacturing and Medical Engineering, Q.U.T., Brisbane 4000, Australia

J. Ferris
Principal Technical Officer, Water Quality Monitoring Group, E.P.A., Indooroopilly 4068, Australia

K. Warburton M.E., Ph.D
Senior Lecturer, Dept. of Zoology and Entomology, The University of Queensland, Brisbane 4072, Australia

H. Chanson M.E., ENSHMG, INSTN, Ph.D., DEng., Eur.Ing., MIEAust., MIAHR
Reader, Dept of Civil Engineering, The University of Queensland, Brisbane 4072, Australia

Emergency Action Planning for the Dee River Dams

A. Chapman B.E., Grad.I.E.Aust.
Graduate Engineer, Kellogg Brown & Root Pty Ltd, Australia

T. O'Connell B.E., GradDipMgt (TechMgt), M.I.E.Aust, CPEng
Senior Hydraulics and Hydrology Engineer, Kellogg Brown & Root Pty Ltd, Australia

Overview of Hydraulic Modelling of the Yangtze River for Flood Forecasting Purposes

S.Q. Clark BE Hons (Civil), MEng Sc, M.I.E.Aust.
Contractor to Sagric International Pty. Ltd., Australia
Director, Water Technology Pty. Ltd., Australia

M.S. Markar B.Sc (Eng)., Ph.D., M.I.E.Aust.
Contractor to Sagric International Pty. Ltd., Australia
Director, WRM Water & Environment Pty. Ltd., Australia

Min Yaowu B.E., M.Sc
Senior Engineer, Bureau of Hydrology, Changjiang Water Resources Commission, PR China

Wu Daoxi B.E., M.Sc.
Vice Director, River Management Bureau, Changjiang Water Resources Commission, PR China

Safety of People in Flooded Streets and Floodways

R.J. Cox BE, PhD, MIEAust, CPEng
Water Research Laboratory, Civil and Environmental Engineering, University of New South Wales, Sydney, Australia

M. Yee
Honours Student, Civil and Environmental Engineering, University of New South Wales, Sydney, Australia

J. E. Ball ME, PhD, MIEAust, CPEng
Water Research Laboratory, Civil and Environmental Engineering, University of New South Wales, Sydney, Australia

Delivering Property Specific Flood Advice

Bruce Druery B.E., DipSci (Geol), M.App.Sci., M.I.E.Aust
Principal, Patterson Britton & Partners

David McConnell B.E., M.I.E.Aust.
Patterson Britton & Partners Pty. Ltd., Australia

Neil Allen B.E., M.I.E.Aust
City Engineer, Bathurst City Council

The Complexity of Numerical Modelling of the Singapore Coastal Waters

A. Frazer B.E.
Project Engineer, Water Research Laboratory
School of Civil and Environmental Engineering, UNSW, Australia

W.C. Glamore B.E., Ph.D
Senior Engineer, Water Research Laboratory
School of Civil and Environmental Engineering, UNSW, Australia

J.W. Walker B.E., MEngSc
Senior Engineer, Water Research Laboratory
School of Civil and Environmental Engineering, UNSW, Australia

Storm Tide Modelling of The Whitsunday Coast and Resort Islands

R. M. Fryar B.E., MEngSt, CPEng, NPER3, CPESC
Principal Engineer, GHD Pty Ltd, Brisbane.

B. A. Harper B.E., Ph.D., FIEAust, CPEng, RPEQ
Director, Systems Engineering Australia Pty Ltd

I. B. Botev B.E., Ph.D., MEng,
Senior Engineer, GHD Pty Ltd, Brisbane,

Scale Similarity Models For Large-Eddy Simulations

F.Gallerano
Professor, Università “La Sapienza” di Roma, Italy

E.Pasero
Ph.D Student, Università di Perugia, Italy

G.Cannata
Ph.D Student, Università “La Sapienza” di Roma, Italy

Scale Effects in Moderate Slope Stepped Spillways Experimental Studies in Air-Water Flows

C.A. Gonzalez B.E., M.E.
Ph.D. student, Dept of Civil Engineering, The University of Queensland, Brisbane 4072, Australia

H. Chanson M.E., ENSHMG, INSTN, Ph.D., DEng., Eur.Ing., IEAust., IAHR
Reader, Dept of Civil Engineering, The University of Queensland, Brisbane 4072, Australia

Hydrodynamic Modelling of the Lower Mekong River and Delta for Basin Planning

Dr Richard Harpin
Director, Halcrow, UK

Dr Jon Wicks
Associate Director, Halcrow, UK

Tony Green
Principal Engineer, JBA Consulting, UK

Dr Trinh Hoa
Professor, Hanoi University, Vietnam

Nguyen Xuan Hien
Deputy Director, Sub Institute of Water Resources Planning, HCM, Vietnam

Measured and Modelled Flow Velocities in the Swash Zone of a Steep Beach: With Implications for Sediment Transport Modelling

M.G. Hughes B.Ec. (Hons.), Ph.D.
Senior Lecturer, The University of Sydney, Australia

T.E. Baldock B.E. (Hons.), Ph.D.
Lecturer, The University of Queensland, Australia

Influence of stratification, rotation, wind forcing and basin shape on the hydrodynamics of lakes

Jorg Imberger
Centre for Water Research, University of Western Australia,

Hydraulic Model Study of Tilapia Fish Exclusion Using Coanda Screens

Franz Jacobsen B,Eng, Dip Eng
Civil Engineer, SunWater, Australia

Dr Mohand Amghar B.Eng,. M.Eng.Sc., PhD
Civil Engineer, SunWater, Australia

Analysis and Design of Sediment Basins

R.H.A. Janssen Ph.D., M.I.E.Aust.
Senior Engineering Specialist, Bechtel Services Pty. Ltd., Australia

Application of CFD Modelling to Free Surface Flow Around Bluff Bodies – A Case Study Using a Bridge Superstructure

M.A. Jempson B.Eng,. M.Eng.Sc., PhD, M.I.E.Aust, CPEng
Manager, Water & Environment, Victoria, WBM Oceanics Australia

N.D. Maxwell B.E., PhD
Design Engineer, Machinery Division, WBM Pty Ltd, Australia

C.J. Apelt B.E., D.Phil(Oxon)
Professor Emeritus, Department of Civil Engineering
The University of Queensland, Australia

Estimating the Uncertainty of Flow Measurement for the Insitu Calibration of Large Water Meters

E.H.Johnson M.I.E.Aust.
Grampians Region Water Authority, Australia

Rock Chutes: A Review of Damage and Failure Mechanisms

A. R. Ladson B.E., M.Sc. Ph.D.
Institute for Sustainable Water Resources and CRC for Catchment Hydrology,
Department of Civil Engineering, Monash University Australia

R. J. Keller B.E., Ph.D.
Institute for Sustainable Water Resources and CRC for Catchment Hydrology,
Department of Civil Engineering, Monash University Australia

Steep Gradient Waterway Stabilization – An Innovative Design Technique

Dr. John C Macintosh BE(Hons), PhD, FIEAust, CPEng, RPEQ
Director / Principal Water Engineer, Water Solutions Pty Ltd

Hydraulic Risk Assessment of Water Distribution Systems

Michael Leonard B.E. (Hons)
Honours Student, University of Adelaide, Australia

Holger R. Maier B.E. (Hons), Ph.D., M.I.E. Aust.
Senior Lecturer, University of Adelaide, Australia

Angus R. Simpson B.E. (Hons), M.Sc., Ph.D., F.I.E. Aust.
Associate Professor, University of Adelaide, Australia

Aaron C. Zecchin B.Sc., B.E. (Hons)
Honours Student, University of Adelaide, Australia

Andrew J. Roberts B.E. (Hons)
Honours Student, University of Adelaide, Australia

Matthew J. Berrisford B.E. (Hons)
Honours Student, University of Adelaide, Australia

John B. Nixon B.Sc. (Hons) , Ph.D.
Senior Research Scientist, United Water International, Adelaide, Australia

Evaluation of Hydrologic and Hydraulic Models for Real-Time Flood Forecasting use in the Yangtze River Catchment

M.S. Markar B.Sc (Eng)., Ph.D., M.I.E.Aust. R.P.E.Q.
Contractor to Sagric International Pty. Ltd., Australia
Director, WRM Water & Environment Pty. Ltd., Australia

S.Q. Clark BE Hons (Civil), MEng Sc, M.I.E.Aust.
Contractor to Sagric International Pty. Ltd., Australia
Director, Water Technology Pty. Ltd., Australia

Min Yaowu B.E., M.Sc.
Senior Engineer, Bureau of Hydrology, Changjiang Water Resources Commission, PR China

Zheng Jing B.E.
Engineer, Bureau of Hydrology, Changjiang Water Resources Commission, PR China

Application of Data-Driven Models and Computational Intelligence in Hydrology and Hydraulics

Dr Zoran Vojinovic Ph.D., M.E., B.E., MIPENZ.
Patterson Britton & Partners Pty. Ltd., Australia

David McConnell B.E., M.I.E.Aust
Patterson Britton & Partners Pty. Ltd., Australia

Simulation of Turbidity Generation for Proposed Dredging Operations at Port Adelaide

A.D. McCowan B.E.(Hons), Dip.H.E.(Delft), PhD, F.I.E.Aust.
Director, Water Technology Pty. Ltd., Australia

T.J. Womersley B.E.(Hons),
Project Engineer, Water Technology Pty. Ltd., Australia

Asset and Pressure Management – A Combined Approach Mitcham-Morang Water Supply Zone

S. A. Pearce Higgins B.Eng (Hons) MIEAust.,
Yarra Valley Water Ltd, Australia

A. McKenzie B.Eng (Hons), B.Sc., G.I.E.Aust.
MWH Australia Pty Ltd, Australia

Assessment Of Predicted Near Field Dilution And Hydraulic Head Requirements For A Range Of Outfall And Diffuser Configurations

B.M. Miller B.E., B.Sc., M.Eng.Sc, M.I.E.Aust.
Manager, Water Research Laboratory, School of Civil and Environmental Engineering,
University of New South Wales, Australia

R.M. Hudson B.E.
Project Engineer, Water Research Laboratory, School of Civil and Environmental Engineering,
University of New South Wales, Australia

Design of an automated floodgate control system to enhance tidal flushing: Case Study, Broughton Creek, NSW

W. C. Glamore B.Sc., PhD
Senior Project Engineer, Water Research Laboratory, School of Civil and Environmental Engineering,
University of New South Wales, Australia

B. Indraratna BSc (Eng), MSc, PhD, CEng, CPEng, FGS, FIEAust
Professor of Civil Engineering, University of Wollongong, Australia

Development of a Device for Direct Measurement of Bed Shear Stress Induced by a Wave Spectrum

Hamid Mirfenderesk
Griffith Centre for Coastal Management, Griffith University, PMB 50 Gold coast Mail Centre, QLD 9726, Australia

Ian R. Young
Swinburne University of Technology, PO Box 218 Hawthorn, Victoria 3122, Australia

Direct Measurement of Roughness of Bed Covered with Gravel and Ripples

Hamid Mirfenderesk
Griffith Centre for Coastal Management, Griffith University, PMB 50 Gold coast Mail Centre, QLD 9726, Australia

Ian R. Young
Swinburne University of Technology, PO Box 218 Hawthorn, Victoria 3122, Australia

A Finite Volume Solution for a Ring Tank Failure Parametric Study

A.F. Nielsen B.E., M.Eng.Sci., M.I.E.Aust., C.P.Eng.
Manager, Coastal and Fluid Dynamics, SMEC Australia

C.A. Adamantidis B.E., M.Eng.Sci
Senior Engineer, Coastal and Fluid Dynamics, SMEC Australia

S.G. Roberts B.Sc.(Hons), PhD (Maths),
Senior Lecturer, Mathematical Sciences Institute, Australian National University

C. Zoppou B.E., PhD (Civil Eng),
Project Leader, Risk Modelling Project, Minerals and Geoharzards Division, Geosciences Australia

Modelling a Combined Sewage and Stormwater Flood Detention Basin

A. Pugh B.E. (Hons), Member A.W.A.
Sales and Support Manager, Wallingford Software Pty Ltd, Australia

S. Ratcliffe B.Sc(Hons), Grad Dip App Comp, ME, MIE Aust, CP Eng, CEng MICE
Launceston City Council, Australia

Hydraulics in Flood Management For the Gold Coast

Khondker Rahman
Gold Coast City Council, PO Box 5042 GCMC Queensland 9129 Australia

Hamid Mirfenderesk
Gold Coast City Council, PO Box 5042 GCMC Queensland 9129 Australia

Analysis of Spillway Flow by Computational Fluid Dynamics Technique

D.K.H. Ho, B.Sc. (Hons), Ph.D., M.I.E.Aust., C.P.Eng.
echnical Manager, Advanced Analysis, Worley Pty. Ltd., Australia

K.M. Riddette .E. (Hons), Dip.Eng.Prac
Engineer/Analyst, Advanced Analysis, Worley Pty. Ltd., Australia

S.M. Donohoo B.Sc., B.E.(Hons)
Manager, Advanced Analysis, Worley Pty. Ltd., Australia

Wivenhoe Dam Upgrade Adopted Strategy and Downstream Impacts

G. Roads E (Civil) (Hons), M.I.E.Aust, RPEQ
Hydrology/Hydraulics Manager, Wivenhoe Alliance
Director, WRM Water & Environment Pty Ltd

B Maher BE (Civil) (Hons), RPEQ
Design Manager, Wivenhoe Alliance
Project Engineer, NSW Department of Commerce

Tropical Cyclone Storm Surge Modelling of the Coast of Queensland

J. Savioli PhD
Principal Coastal and Marine Engineering
DHI Water and Environment Pty. Ltd., Australia

S. Szylkarski
QLD Manager, DHI Water and Environment Pty. Ltd., Australia

Queensland Climate Change and Community Vulnerability to Tropical Cyclones Project

R. Schwartz B.Eng., M.Eng., MBA
Senior Principal Engineer, Coastal Services Unit, Queensland Environmental Protection Agency

D. Robinson B.Eng., B.Econ, Grad. Dipl. in Hydraulic Engineering (Distinction) Delft,
Manager, Coastal Services Unit, Queensland Environmental Protection Agency

M. Allen B.Eng., MIEAust
Principal Engineer, Planning Division, Queensland Environmental Protection Agency

Jim Davidson B. Sc.
Regional Director, Bureau of Meteorology

Owen Harvey
Principal Research Officer, Disaster Mitigation Unit
Department of Emergency Services

A Data Framework for Hydrodynamic Modelling

Susan E. Shield B.E. (Hons), M.E. (Water), CPEng, M.I.E.Aust.
Senior Civil/Environmental Engineer, Umwelt (Australia) Pty. Ltd., Australia

Andrew J. Goodwin B.E. (Env)
School of Engineering, University of Newcastle, Australia

Genetic Algorithm Optimisation for Water Distribution System Design at the Gold Coast

Andrew J. Roberts B.E. (Hons)
Engineer, Optimatics Pty. Ltd.

Angus R. Simpson B.E. (Hons), M.Sc., Ph.D., F.I.E.Aust.
Technical Director, Optimatics Pty Ltd, Australia. Associate Professor,
School of Civil and Environmental Engineering, University of Adelaide, Australia

Scott Sherriff B.E., M.I.E.Aust
Supervising Engineer Network Analysis, Gold Coast Water, Australia

Peter Griffiths B.E (Hons), Grad.I.E.Aust
Network Analyst, Gold Coast Water, Australia

Integrated High Order Water Quality and Hydrodynamic Models – An Essential Tool for Lake Management

R.C. Swan B.E., M.I.E.Aust.
Project Engineer, Lawson and Treloar Pty. Ltd., Australia

N.I. Collins B.E.(Civil), M.Eng.Sc, M.I.E.Aust, CPEng, RPEQ
Director, Lawson and Treloar Pty. Ltd., Australia

Modelling Flood Inundation of Urban Areas in the UK Using 2D / 1D Hydraulic Models

W.J. Syme B.E., M.Eng.Sc.
Associate, WBM Pty. Ltd., Australia

M.G. Pinnell Bsc Msc MCIWEM
Principal Hydrologist, Symonds Group Ltd, England

J.M. Wicks BSc PhD CEng MICE
Associate Director, Halcrow, UK

Hydraulic and Ecological Modelling of the Pimpama River Estuary

S. Szylkarski B.E., MEngSc., M.I.E.Aust.
State Manager, DHI Water and Environment Pty. Ltd., Australia.

J. Dorge MSc. Biology
DHI Water and Environment, Denmark.

D. Toomey B.E.
Gold Coast City Council.

R. Burch B.E., M.I.E.Aust.
Sinclair Knight Merz.

Development and Calibration of Detailed Sewer Models for the Brisbane Sewerage System

S. Szylkarski B.E., MEngSc., M.I.E.Aust.
State Manager, DHI Water and Environment Pty. Ltd., Australia.

D. Heape B.E., MengSc., M.I.E.Aust.
Network Planner, Brisbane Water.

D Kane B.E.
Senior Engineer, DHI Water and Environment Pty. Ltd., Australia.

J. Wilson B.E.
Engineer, DHI Water and Environment Pty. Ltd., Australia.

Diverse Drop Structure Applications Iin an Open Channel

L. Toombes B.E., Ph.D., Grad.I.E.Aust.
Engineer, Connell Wagner Pty. Ltd., Australia

A New Generation, GIS Based, Open Flood Forecasting System

T. van Kalken B.E., M.Sc. (Delft), MICE
Chief Engineer, DHI Water and Environment Pty Ltd

C. Skotner M.Sc., Ph.D
Senior Engineer, DHI Water and Environment, Denmark

H. Madsen M.Sc. Ph.D
Senior Engineer, DHI Water and Environment, Denmark

Physical Modelling & Hydraulic Modifications to a Power Station Weed Settling Pond

J. W. Walker B.E., MEngSci.
Senior Project Engineer, Water Research Laboratory, Civil and Environmental Engineering
University of NSW, Australia

A Methodology for Predicting Berm Crest Elevation Fronting Coastal Lagoons

F.M. Weir B.Sc. (Hons.)
Ph.D Student, School of Geosciences and Institute of Marine Science, University of Sydney, NSW 2006.

M.G. Hughes B.Ec. (Hons.), Ph.D
Senior Lecturer, School of Geosciences and Institute of Marine Science, University of Sydney, NSW 2006.

T.E. Baldock B.Eng. (Hons.), Ph.D
Lecturer, Division of Civil Engineering, University of Queensland, St Lucia, Brisbane, Qld 4072.

Disaster Mitigation in Central Vietnam: Application of Two-dimensional Hydraulic Models

I.F. Wood B.E., MEngSc
Senior Engineer, Kellogg Brown & Root Pty. Ltd., Australia

S.E. Murphy B.E., MEngSc
Senior Engineer, Kellogg Brown & Root Pty. Ltd., Australia

N.H. Phuong M.E.
Hydraulic Engineer, Institute of Water Resources Planning, Ministry of Agriculture & Rural Development, Vietnam

Numerical Modelling for Wave-Induced Pore Pressure in Marine Sediments: Case Study at East Coast in Australia

H. Zhang B.E., Ph. D.
Lecturer, Griffith University, Australia

D.-S. Jeng B.E., M. E., Ph.D.
Senior Lecturer, The University of Sydney, Australia

Modelling The 3-Dimensional Flow Between The Nerang River Estuary And Burleigh Lakes System, Gold Coast

S.Zigic DEng., BEng
Director, Asia-Pacific ASA Pty. Ltd., Australia & PhD Candidate, Griffith University Gold Coast Campus School of Engineering

B.A.King BSc., Ph.D.,
Director, Asia-Pacific ASA Pty. Ltd., Australia

C.Lemckert Bsc., MPhilSc., Ph.D
Senior Lecturer, Griffith University Gold Coast Campus School of Engineering

Three Dimensional Modelling of Stratified Reservoirs
Limitations, Data Requirements and the use of Model Results to Aid Management and Engineering Decision Making.

R.M Hudson B.E
Project Engineer, Water Research Laboratory, The University of NSW, Australia

B.M Miller B.E, B.Sc.,MEngSc.
Manager, Water Research Laboratory, The University of NSW, Australia

1-D and 2-D Hydraulic Modelling of Extreme Floods in a Steep Urban Stream

B.C Phillips B.E (Civil), MEng Sc, Ph.D , F.I.E Aust.
Director, Cardno Willing (NSW) Pty Ltd, Sydney, Australia

B.Boon, B.E, E.W.S (Vic), H.E.C (Tas)., M.I.E Aust.
Director, Thompson and Brett Pty Ltd, Hobart, Australia

Modelling Saturation Excess Runoff with SWAT

B.M Watson B.E, B.Sc., Grad. I.E Aust
Post Graduate Student, Deakin University, Australia

S.Selvalingam, B.Sc.(Eng), Ph.D, M.I.E Aust
Senior Lecturer, Deakin University, Australia

M. Ghafouri, B.Sc., M.Sc., Ph.D.
Lecturer, Deakin University, Australia

Aspects of Numerically Modelling Transcritical Flows

A.C Wicht
School of Civil and Environmental Engineering, University of NSW

B. Cathers, B.E, Ph. D
Water Research Laboratory, School of Civil and Environmental Engineering, University of NSW

Paper Review Process

All papers including the Keynote Addresses have been peer reviewed through a formal and rigorous process, as outlined below.

In response to the Call for Abstracts sent out in 2003, the Organising Committee received 115 abstracts of proposed papers. Members of the Organising Committee used a purpose-designed 'Abstract Evaluation Sheet' to review all abstracts with regard to their suitability for the Conference.

A Panel of Reviewers, selected from experts in fields relevant to the Conference sub-themes, was established to peer review the 75 full manuscripts submitted for publication in the Conference Proceedings. All manuscripts submitted for podium presentation were peer reviewed by at least two independent reviewers according to a set of criteria established by the conference Technical Program Committee. Based on these criteria, reviewers were asked to complete a review form for each paper they reviewed. All review forms were forwarded to the Technical Program Committee who combined both reviewers comments. These combined comments were then forwarded to each author. All papers were given classifications: Accepted, minor changes required, major changes required or declined. Authors were then requested to revise their manuscripts in accordance with reviewer's comments and to resubmit for final review before inclusion in the Conference Proceedings.

Technical Review Committee

H. Chanson	University of Queensland
J. Macintosh	Water Solutions

Manuscript Review Panel

R. Ayre	SunWater
J. Ball	University of New South Wales
R. Brown	Queensland University of Technology
P. Cummings	Kellogg Brown & Root
C. Gonzalez	University of Queensland
J. Hinwood	Monash University
R. Janssen	Bechtel Services (Australia)
M. Jempson	WBM Oceanics Australia
D. Sheng-Jeng	Griffith University, Gold Coast Campus
K. Kuhanesan	Department of Natural Resources, Mines & Energy
M. Lambert	The University of Adelaide
T. McGrath	SunWater
B. Melville	University of Auckland
P. Nielsen	University of Queensland
V. Nikora	NIWA
K. Rahman	Gold Coast City Council
R. Schwartz	Environmental Protection Agency
R. Tomlinson	Griffith University, Gold Coast Campus
L. Toombes	Connell Wagner
M. Wallis	Hydro Tasmania

HENDERSON ORATION

The Henderson Oration was established in 1998 in recognition of Professor Frank Henderson's contribution to the knowledge and practice of hydraulic engineering in general but in Australian practice in particular. Professor Henderson's book "Open Channel Hydraulics" is used as a standard text in almost all engineering schools in Australia and many others throughout the world.

The Award aims to recognise the contribution of the science of hydraulics to the practice of water engineering in Australia. The address is given at each Hydraulics Conference, held approximately every 3 years. The National Committee on Water Engineering selects the Orator after receiving nominations from the conference organising committee. The Orator should have made a significant contribution to hydraulics in Australia but need not be either an engineer or an Australian.

The inaugural oration was held in Adelaide in 1998 by Dr Martin Lambert, an ex-PhD student of Professor Henderson, on Professor Henderson's behalf.

Honour Roll:

1998	Dr Martin Lambert (on behalf of Prof. Henderson)
2001	Prof. Colin Apelt
2004	Prof Jörg Imberger

Imberger Bio **Imberger Paper**

Jörg Imberger is Professor of Environmental Engineering and Chair of the Centre for Water Research at the University of Western Australia. He is currently Chair of the Western Australian Estuarine Research Foundation, former Scientific Advisor to Earthwatch and former member of the United Nations High Level Advisory Board on "Sustainable Development".

His main research interested is in the motion of stratified fluid in the context of environmental fluid dynamics. Specifically, this research includes the study of the motion and quality of water in estuaries, reservoirs and lakes. The interaction of the biological system and the water motion is also a primary focus.

Jörg has held various visiting and academic positions at the University of Padova, University of California (Berkeley), Stanford University, Caltech, University of Karlsruhe and The University of Western Australia.

Jörg is the recipient of numerous local, national and international awards.

In 1999, Jörg was awarded an Honorary Doctorate from the Democritus University of Thrace in Greece.

In 1996 he was awarded the Stockholm Water Prize for his outstanding contribution to the water industry. In 1995 Jörg was awarded the Onassis Prize for the Environment for his contribution to environmental issues.

Jörg is one of a handful of people in Australia to be elected to both the Australian Academy of Science and the Australian Academy of Technological Sciences and Engineering.

Jörg is currently the Walter Bean Scholar at the University of Waterloo in Canada, and Fellow to the Sackler Institute of Advanced Studies in Israel.

Jörg has published 21 books, 114 refereed journal papers, 74 conference papers and 107 published reports.

Centre for Water Research, UWA, 35 Stirling Hwy, Crawley 6009, W. Australia 618 9380 3911

Influence of stratification, rotation, wind forcing and basin shape on the hydrodynamics of lakes

Jorg Imberger
Centre for Water Research
University of Western Australia,
Nedlands, Western Australia, 6009

The water column in a lake responds to meteorological forcing at five energy levels. First, thermal energy is communicated through the lake surface, heating the lake in spring and cooling it in autumn. The energy changes involved in this process are enormous and the water motion is secondary to these heat fluxes. Second, wind forcing imparts momentum to the surface layers which then sets up basin scale internal waves which are characterized, if the lake is large enough, by a rotation-buoyancy balance. Such waves form a spectrum of Kelvin and Poincare waves and these waves may be viewed as first order motions, but the energy fluxes associated with these first order waves is orders of magnitude smaller than the zeroth order processes leading to temperature changes. Third, if the wind is strong enough non linear processes cascade energy to surges, high frequency waves and horizontal eddies that may be termed the second order motions. Fourth, another order down in energy level differential heating, cooling and wind mixing may lead to gravitational motions combining to form slow moving tertiary motions which have great ecological importance as they are most often responsible for net advective transport of material. Lastly, all these motions combine to trigger and then maintain intermittent turbulence in the water column. In terms of energy levels turbulence may be viewed as fourth order motions that are weak, but again of great ecological importance as they lead to net mixing of material and also a weak benthic boundary layer updraft. Recent results are used from Lake Kinneret, a topographically simple lake, the Bodensee, a lake where topographic deviations from a round basin are simple, but significant and the Gulf of Aqaba where capes and headlands trigger extensive gyre motions to illustrate the factors influencing the transfer of energy between the four levels.

Jon Hinwood

BE, MEngSc, PhD, FIEAust.

Jon Hinwood is Associate Professor of Coastal and Ocean Engineering at Monash University and a Director of AMOG Consulting. His current research and consulting includes the dynamic response of subsea pipelines and moorings for which he has developed data analysis and modelling software and a major wave flume. He has directed large multi-disciplinary environmental studies, and is currently working to simulate the evolution of estuaries over thousands of years.

View Paper

Bruce Melville

Professor Bruce Melville is Head of the Department of Civil and Environmental Engineering at the University of Auckland. His academic career spans 23 years, prior to which he spent 6 years working for civil engineering consultants in NZ and overseas. He is an active researcher with an international reputation in the field of fluvial sediment transport. His expertise encompasses most aspects of water resources engineering, including hydraulic, river, environmental and hydro-electric engineering. He is Associate-Editor of the (ASCE) Journal of Hydraulic Engineering, has served on local and international research committees, and has been a member of many tribunals for water consent hearings. He received the 2002 ASCE Hydraulic Structures Medal, in recognition of his contributions in the field.

View Paper

Vladimir Nikora

Vladimir Nikora is a Principal Scientist at the National Institute of Water and Atmospheric Research (NIWA, New Zealand), where he leads the Freshwater Hydrodynamics Group. Over a period of 25 years, Vladimir's research has covered a wide range of topics, from turbulence and sediment transport to flow-biota interactions. He published two books and more than 100 journal papers.

View Paper

The Institution of Engineers, Australia
8th National Conference on Hydraulics in Water Engineering
ANA Hotel Gold Coast, Australia 13-16 July 2004

Estuary Hydraulics for the Year 3004

J.B. Hinwood
B.E., MEngSc, PhD, F.I.E.,Aust.
Associate Professor, Department of Mechanical Engineering, Monash University

Abstract: Management of rivers and estuaries requires the choice of a strategy, which could have impacts over a very long term. The ability to predict the geomorphic evolution of an estuary would provide a useful tool for assessment of the impact of management strategies. Progress in developing a numerical modelling scheme, based on the hydraulics, to hindcast the geomorphological evolution of an estuary over the last 6,000 years and to predict the next 1000 years is described. The data needs for model operation and validation, model stability, time scales, role of extreme events, chaos and self-regulation are discussed. It is concluded that despite large uncertainties such a model can be developed, will have value and that at worst it will have an explanatory if not a predictive use. Issues raised are common to a variety of hydraulic problems where long term prediction is now required.

Keywords: Estuary, hydrodynamics, geomorphology, modelling, evolution, non-linear dynamics, attractors.

1. INTRODUCTION

At the end of the last ice age the sea level rose and flooded river valleys, creating coastal bays. Over the last 6,000 years the sea level has been nearly constant and these bays have evolved into complex estuaries, through formation of coastal barrier dunes and infilling by fluvial sedimentation. In south-eastern Australia, the evolution of the estuaries has followed one of several sequences identified and described by Roy (1984). Roy's sequences are descriptive and do not attempt to quantify the states of the estuary or to estimate the time between the different states.

Sustainable management of these estuaries requires knowledge of the present hydraulic and sedimentation regimes, and of their long term behavior, to ensure that environmentally sustainable strategies are adopted. Some of these strategies involve altering the channel geometry directly – e.g. by breakwaters, reclamation or dredging – or indirectly by preventing natural bank erosion, changing the sediment supply or the river inflows. Any of these changes may have unanticipated consequences such as increased tidal action causing bank erosion or instability of shoals. These changes may reduce or increase in time, in the latter case leading to long term loss of land or wetlands or to shifts in channel alignment or entrance location. The responses to impacts such as the greenhouse effect, clearing of land and hence change of run-off patterns and water extraction are of great interest. So too is the response to extreme events – e.g. the impact of a major storm with a return period of hundreds of years. A model would assist greatly in managing an estuary by predicting the effects of these changes, and could provide insights into the roles of the different processes.

To enable the effects of such changes to be modeled and to provide a time scale for the changes requires that the model be process-based. Coastal process models which include currents, wave action and sediment transport and have been extended to model shoreline evolution during a storm and some of these studies have been extended to decadal scales (de Vriend et al, 1993; Kaminsky et al, 2001; Steetzel, 2001; Green et al, 2003). Dennis et al (2000) and Mason and Garg (2001) have each run a two-dimensional hydrodynamic/sediment/morphology model of a large intertidal zone for about a 5 year period, with limited success when measured against changes in a DEM. There are several projects currently underway in Europe and the US to extend these models or develop improved models to predict coastal evolution on decadal time scales, including COAST3D, SEDMOC and HUMOR. Some of these joint projects are considering estuarine environments as well as open coasts.

Most models of the bed level and morphological changes within an estuary have been one of two types (Carter & Woodroffe, 1994). The first type is a process model based on two or three dimensional fluid-dynamic models with sediment transport and depth change modules added. These models are usually based on the primitive dynamic equations, are spatially explicit and run in the time domain with time steps of a few seconds to a couple of minutes. Examples are Delft3D, SMS (incorporating RMA2 and SED2D) and Sedsim Wave (Martinez and Harbaugh, 1993).

The second type is the geological or geomorphological evolution model, which is designed either to simulate changes over very long periods and may have time steps of 1000 years or more (Kirkby, 1994) or to predict only a final "equilibrium" without specifying the time scale (Willgoose et al, 1994). Such models do include some processes but are more strongly based on the statistics of actual landscapes rather than the physical processes. Neither of these two types of model meets the aims of this study; the former are not designed to run for such long times or to treat major changes in bed or channel geometry while the latter have omitted the detailed physics and cannot simulate the effects of management or environmental changes.

Thus we have been led to develop a process-based model which is designed to run for long simulation times. It is evident that this will require some novelty in the way the physics is implemented in the model. The practicability of achieving useful results, the adequacy of knowledge of processes, the adequacy of operating and validation data are addressed in the remainder of the paper.

2. CONCEPT OF THE EVOLUTION MODEL

The model which is being developed is based on the hydrodynamic equations of continuity and motion and the sediment mass conservation equation, which includes scour/deposition and hence change in bed level. Some details have been parameterized to reduce computation time and, as discussed below, the model will treat gradual changes in morphology separately from rapid transitions from one state to another. The model is restricted to the barrier type estuary typical of the south coast of NSW, following the initial formation of the barrier.

Inputs to the model comprise the initial depths and time series of river and sediment inflows and ocean tide levels. Outputs comprise statistics of the probable form of the estuary at different dates, and water level and velocity sets for various tide and river flow combinations throughout the period of evolution.

2.1 Operational Data

To enable the model to be set up and run we require initial values and boundary conditions. The initial values comprise bed elevations and an assumed set of water levels and velocities. Only for a model run starting at the present time are these values accurately known. The boundary conditions comprise the river inflow, the sediment inflow, the ocean tide and the entrance opening at all time steps of the model run.

Because the boundary conditions (with the exception of the astronomical part of the tide) cannot be known in advance, estimates based upon a selected global climate scenario must be used. The probability distributions of the required variables will be determined and then a Monte Carlo procedure will be used to select a number of sequences for modelling. In principle, one complete simulation will require each boundary variable to be specified at every time step. The intelligent Monte Carlo method (Melchers, 1984) will then be used to select sufficient sets to provide reliable statistics for the boundary variables and hence for the computed variables.

Most climate predictions are in terms of annual means for very large regions of the Earth – the standard is the IPCC (2001) global mean compilation, figure 1. At best seasonal means for 400 x 400 km regions (Pittock, 2003) have been published, and only up to 2100AD. To predict the statistics of daily rainfall in 3004 requires the use of assumptions about the statistics of the future weather. This is a major source of unreliability of the long term predictions. The necessity to use climate modelling predictions leads inevitably to a statistical approach to modelling estuary evolution and to a statistical prediction of the estuary form, comprising the most probable form and the set of possible, but less probable forms.

2.2 Time Scales And Time Stepping

The long simulation time is a key issue in the design of the model, most obviously as it could lead to impractically long computation times. In addition round off and truncation errors accumulate over many steps. These concerns lead to a consideration of the time scales of the processes which must be simulated.

The hydrodynamic modelling requires a time step of a few minutes to enable detailed two- or three-dimensional velocity fields to be correctly predicted. Over 7,000 years that would mean about 10^{10} calculations of the velocity field for each of the Monte Carlo simulations. However, other quantities do not need to be evaluated so frequently.

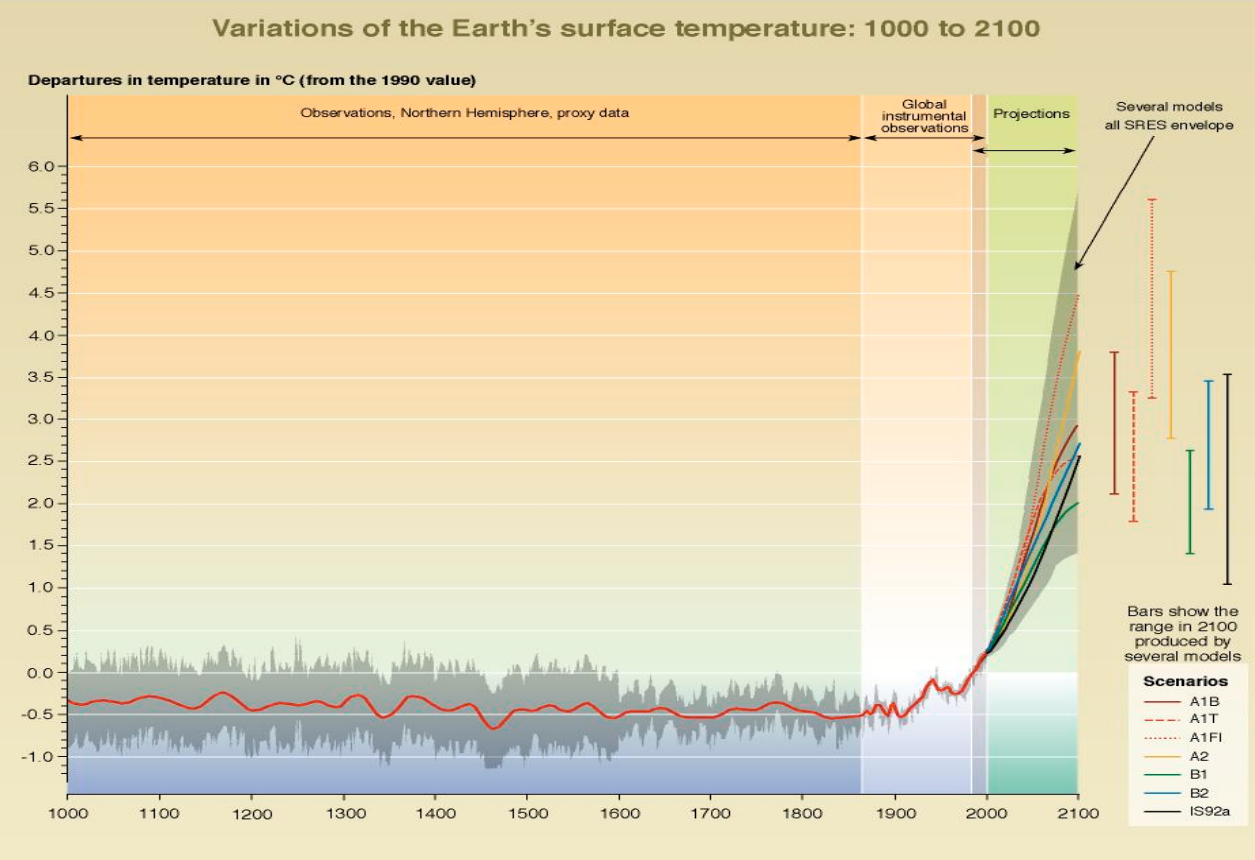

Figure 1 - Global Mean Temperature Predictions (IPCC, 2001)

As the sediment concentration is changing relatively slowly and does not affect velocity directly, many modellers only calculate the sediment transport every fifth time step or so (this must reduce sediment diffusion but no one seems to worry). Bed elevation too changes slowly so that feedback into the hydrodynamics is very weak and longer computation intervals have been used. Figure 2 shows the times for which the indicated quantities undergo a significant change. Transitions in regime or morphology, such as breaching a levee, have two ranges, about a day for the actual event and decades for the interval between events.

While variables may change throughout a tide cycle, enforcing a short time step for the hydrodynamics and sediment transport, conditions are often little changed at the end of a tide cycle and essentially the same sequence is repeated. This suggests that once the changes of morphology over a tide have been computed they may be applied unchanged for several more tides, provided that the tides and river flows remain the same.

This notion has been extended in the model to utilise two time steps as shown in figure 3 (Hinwood and McLean, 2002). A short time step is used for the hydrodynamics and sediment transport, then the changes in morphology are extrapolated for a long time step during which it is assumed that changes are small. The short time step loop of the model simulates in detail processes occurring on a tidal time scale using a network of one-dimensional hydrodynamic models. Total sediment transport (suspended + bed load) is simulated over tidal times in the same network. Six to ten sets of river inflow/sediment inflow/ocean tide data are used on the basis of their probability of occurrence. The resultant sediment transports and depth changes are computed for each data set and combined with appropriate weighting to provide an estimate of the change in bed level after many tide cycles. Each cell is then tested for its sensitivity to regime change – is it in the middle of a regime or is it close to a boundary where it may be pushed over, resulting in a sudden change in its regime. This information is used if necessary to revise the time step and to set the next long time step.

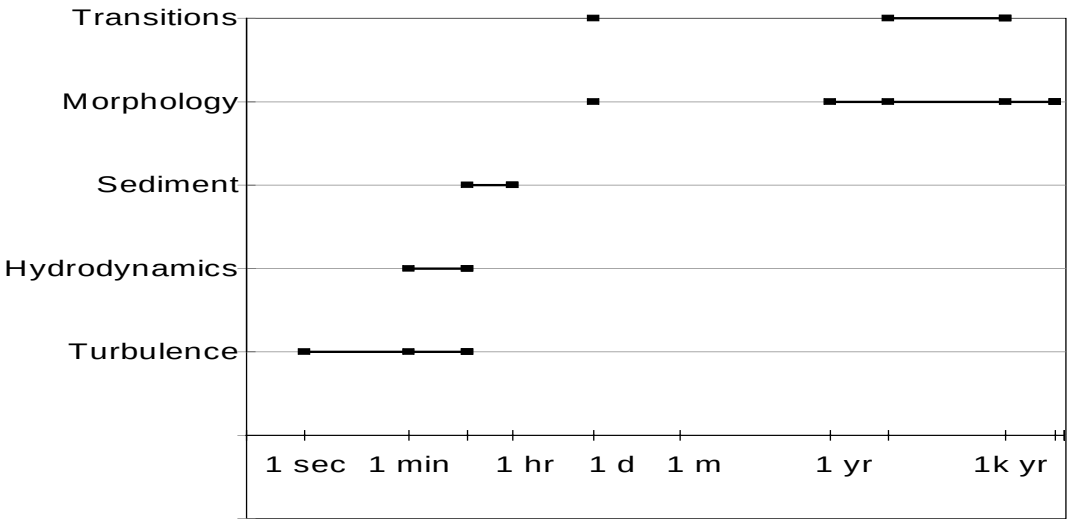

Fig. 2 - Schematic Showing Times For Significant Changes In The Variables

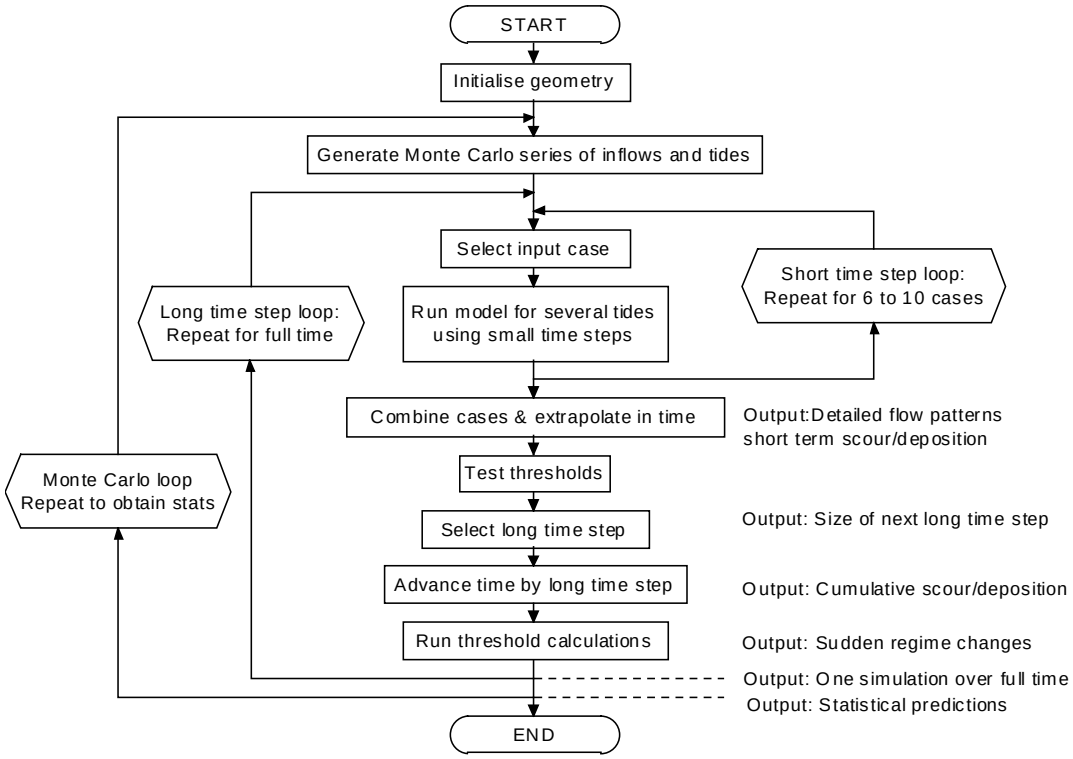

Figure 3 - Proposed Modelling Scheme

The long time step loop of the model extrapolates the gradual changes using the rates determined in the detailed simulation with the short time step. The flows and depth changes are extrapolated on the basis of the long time step. At the end of the long time step all cells are again tested for regime changes. That completes the advance of a long time step. The computation then loops back to the selection of the next set of inflows and advances a short time step and so on until the entire time selected within the Monte Carlo loop is finished. At that point the time history for that model run is generated as output. The computation then returns to the start and a new Monte Carlo sequence of river inflows/sediment inflows/ocean tides is generated and the entire computation repeated. Finally the statistical results of the simulations are output.

2.3 Model Validation

Validation is essential because of the simplifications and uncertainties which are inherent in any modelling. Validation ideally involves two steps. The first is a calibration in which poorly specified variables or parameters (often a resistance coefficient) are adjusted until the model output matches one or more data sets. Ideally these data sets test all the physical processes and assumptions and show the effect of each so that the appropriate adjustment may be made. The second step, often called verification, then confirms that the model matches one or more data sets which resemble conditions of interest. Almost invariably the parameters are tweaked again at this step.

Following this ideal as well as possible we are using well established laws for the different physical processes, e.g. sediment transport (van Rijn, 1993). In addition we plan to conduct extensive sensitivity tests of all "constants" and parameters. Poorly determined quantities which are shown to have little effect on the output need not cause concern, and the significance of all the physical factors can be shown. The sensitivity tests will also establish the likely responses of the estuary to different conditions and different parameter values over a range of evolutionary stages.

For verification we plan to use data from the last 6,000 years, that is the whole period from the date that the sea level reached (approximately) its present value. This poses the question "What was the weather in July 2004 BP [before present]"?. Paleoclimatologists can provide some indications through a range of techniques (Bradley, 1999), the principal techniques of use in the south east of Australia are outline below.

2.3.1 Dendrochronology

Tree ring studies provide a measure of the favourability of conditions during the growing season, which may be dominated by one climatic variable. Thus huon pine rings from Tasmania have been interpreted to give mean summer temperatures back to 3,600 BP (Cook et al, 1998). The summer temperature reconstruction for the last 3,600 years is shown in figure 4. The bristle cone pine of California has enabled similar data to be obtained back to 7,000 BP for mountain sites where these pines grow.

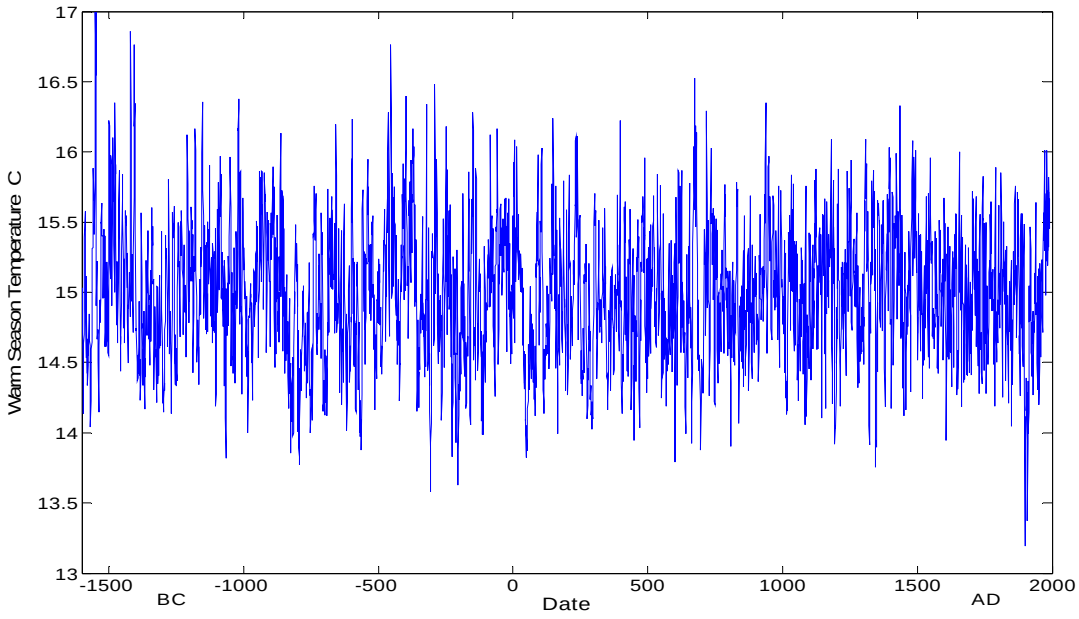

Figure 4 Mean Summer Temperatures In Tasmania From Dendrochronology (Cook et al, 1998)

2.3.2 Lake and lagoon sediments

While sediments in temperate zones lack the sharply defined stratification of glacial deposits, in some localities they may dated and counted, then correlated with stream flows. Problems include mixing of strata by bioturbation and incomplete series caused by scour or variable deposition. The resulting data are less complete than the dendrochronology as only a small number of intervals of each sediment core is dated

2.3.3 Palynology

The pollens in sedimentary deposits indicate the type and vigour of plant communities when each layer of sediment was deposited. Dating of selected levels from core samples has provided comprehensive climatologies (Kershaw, 1998), generally at intervals of several hundreds or thousands of years.

Presuming that annual or summer mean temperatures and rainfalls can be obtained for all years from 6,000 BP to the present, which is not the case at present, there remain two problems: how to transpose from the location where the climate has been determined (e.g. where the huon pine grew) to SE NSW and how to convert annual or decadal climate to daily weather. As a first pass we are using correlations based on the present climate and weather, but the possibility that the global Hadley circulation extended further south in earlier times is under study. The Monte Carlo sets of data will be extracted from the statistics of the weather calculated in this way. We look to achieving a prediction set which includes the present state and assigns it a moderate to high probability.

3. MODELLING OF COMPLEX SYSTEMS – CAN THEY BE MODELLED?

3.1 Estuary Evolution As A Problem In Non-Linear Dynamics

The recognition that river geomorphology is a highly non-linear system has lead to concerns that such systems are unstable or chaotic (e.g. Phillips, 1999) and essentially unpredictable from a process based approach (Leopold and Langbein, 1962; Pethick, 1991, de Vriend et al, 1993). Furthemore, the perturbations caused by fluctuating external conditions, like the “butterfly effect”, are considered likely to lead to radically different outcomes (Schumm, 1977, 1988; Nanson and Erskine, 1988). At time scales longer than the typical fluctuations of say 100 years Rigon and Rodruigez-Iturbe (1994) and Phillips (1999) and others assert that chaotic behavior leading to self organization is common (although Sapoznikov and Foufoula-Georgiou, 1996 reject this). Each of these authors offers a justification for their views but falls short of a convincing case. The same could be said of the following discussion although it does go a little further than the previous authors.

Numerous non-linearities are active in estuarine systems. For example the hydrodynamic resistance is non-linear which results in the response to any tidal constituent being dependent on all the other constituents present, while the resistance and hence tidal response also depends on water depth and hence varies non-linearly with the tidal elevation (Hinwood et al, 2003). The sediment transport depends approximately on the cube of the velocity. Most of the morphological processes are asymmetric introducing strong non-linearities, in particular bank erosion/deposition and channel scour/deposition which have phase lags with respect to velocity.

For a dynamical system we can define a state vector consisting of the coordinates and velocity components of all the particles in the system. Changes in the system may then be computed by an operator which is an expression of the dynamic laws applicable to the system. If the dynamic laws (operator) are non-linear there usually will be states (sets of values of the state vector) to which the state tends over time – attractors.

The operator is based on the hydrodynamic equations derived from the Navier-Stokes equations, the continuity and salt convection-diffusion equation, and the equations governing scour, deposition and transport of sediment. While this specification provides no information on the location of individual grains it does specify the whole of the estuary on an aggregated scale compatible with our ability to measure, describe and manage the system.

Applying this idea to an estuary, the state vector comprising coordinates and velocities of all particles may be replaced by a set of dimensions and parameters, for example the following:

- water plane area, cross sectional area, bed sediment diameter, tidal prism, mean tidal volume, residence time and salinity, all as functions of distance from the sea
- ocean tide, river inflows, sediment inflows, surface wind.

Following Roy (1984) many of the estuaries of south-eastern Australia fit a sequence of states from open bay to barrier lagoon to tidal river channel bounded by coastal plain (figure 5). This sequence may be thought of as an attractor. Alternatively some or all of the states on the sequence may be thought of as attractors on a short time scale with the final state as an attractor on a long time scale as depicted in figure 6. The figure shows the main sequence of change (a possible attractor) and a number of intermediate states which act as short term attractors, with one simulated “history” of an evolution. A model, such as the one we are developing, is required to determine the

location of the main attractors in the state variable space, then an estuary may be positioned on such a diagram and its probable evolutionary course and sensitivity to disturbances may be assessed from the diagram.

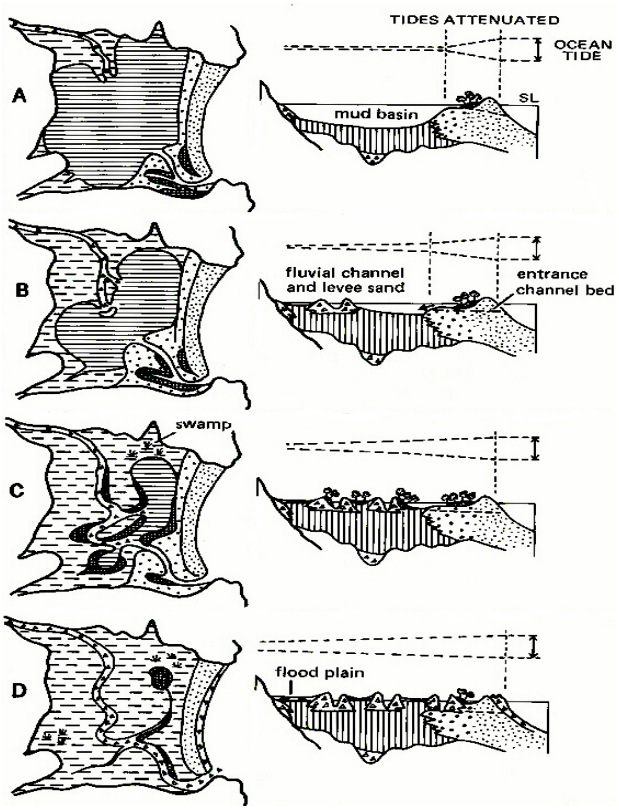

Figure 5 - Sequence Of Evolution Of A Barrier Estuary (Roy, 1984)

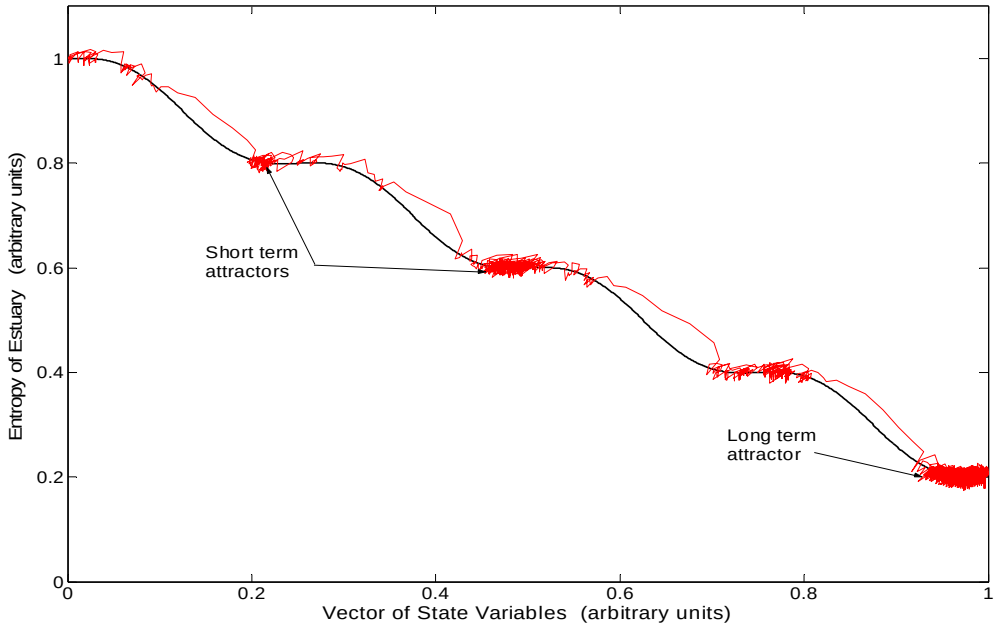

Fig. 6 - Schematic Of Estuary Evolution Via A Sequence Of Attractors (irregular line shows one “history”)

If only some of the states are attractors (on a short time scale) the estuary may evolve rapidly from one attractor state to another but only slowly, and possibly with reversals, in the vicinity of an attractor state. Change from one attractor state to another will occur if the state vector is sufficiently perturbed, for example if an extreme flood occurs. A sufficiently large change may lead to a shift from one attractor state to one which is not adjacent, or even to one which is not on the main sequence as shown on figure 6. In figure 6 the parameter which characterises the evolution of the estuary has been called "entropy" by analogy with thermodynamics. Parameters available for this role are discussed below.

The attractors proposed above may be specific to a given reach or geomorphic zone of the estuary. Accepting that there are likely to be attractors which are effective on short time scales for given geomorphic zones, a couple of the most likely attractors for the inlet channel are now outlined; similar schemes have been developed for other geomorphic zones of these estuaries.

For an estuary with a sandy inlet channel, if the throat area is too small it will scour and enlarge to the "O'Brien" area, A_{ob}, (O'Brien, 1931) which is the attractor. The O'Brien area will depend on tides and river flow and so will vary with some lag, leading to oscillation about the attractor. If area is too large deposition will occur and it will reduce to the O'Brien area.

If the inlet area is very much too small, the tidal range in the estuary will be significantly reduced and hence flow and velocity will be reduced and the entrance area will reduce. The attractor is closure with the flow percolating through the barrier or evaporating, as in figure 7. Examples of the "O'Brien attractor" are the Tomaga River, NSW, which maintains its area fairly well tidally. The Snowy river is close to the O'Brien dimension some months after a flood but tends to gradually close (It maintains open area via flood scouring). Lake Conjola, NSW has throttled tides and heads towards closure.

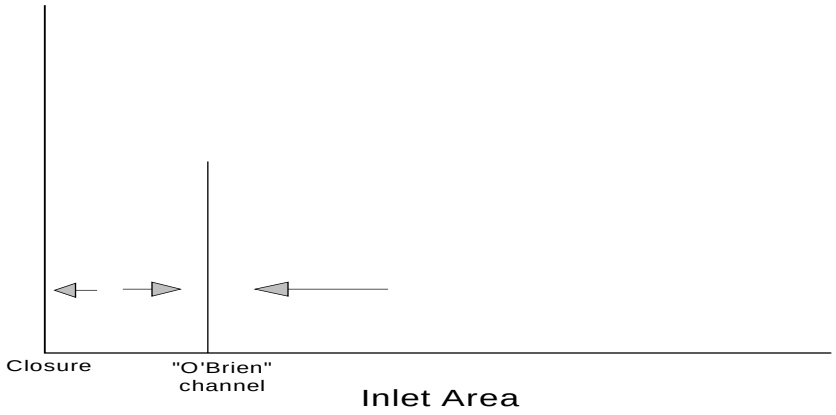

Figure 7 Attractors For An Inlet Channel

The existence of attractors is consistent with the concept of self regulation and is the converse of the butterfly effect, stating that a given final state is likely to be achieved for a range of initial states or disturbances.

3.2 Global Parameters

The concepts of energy and entropy have proved invaluable in characterizing the state and changes of state of physical, chemical and biochemical systems. In such systems energy is conserved although it may change its form, while (due to irreversibilities and hence losses) entropy increases with every change in state. Analogies to these quantities have been sought in the context of landscape evolution by Leopold and Langbein (1962). Their great insight was marred by sliding from an analogy to actually identifying energy and entropy with physical variables, incorrectly, however the analogy remains potentially very useful in attempting to quantify the state of an estuary. "Energy" and "entropy" may most usefully be defined in terms of the external variables which describe a fluid system. In his river evolution studies, Schumm (1977) used valley elevation, which is appropriate for a given upland stream, but values of this local dimensional variable are not transferable to other parts of the same stream or to other streams.

An example from another branch of fluid dynamics is the hydraulic turbine. The external variables for a turbine are the flow, Q, the head differential, H, the impeller diameter, D, the rotational speed, N, and the shaft power output, P (the torque may be formed from these quantities). The input power is

$$P_i = \rho QgH \tag{1}$$

and hence the efficiency is

$$\eta = \frac{P}{\rho QgH} \tag{2}$$

The turbine design most suitable for the conditions depends, in addition, on the diameter and speed, and thus on the kinematic parameter Q/ND^3 . A combined parameter is the specific speed, given by

$$N_S = \frac{N\sqrt{P/\rho}}{(gH)^{5/4}} \tag{3}$$

It has been found that the highest efficiency is obtained by selecting an appropriate internal design of the turbine for a given range of specific speed. For $3 < N_S < 16$ (high head, low flow) a Pelton turbine is most efficient, while for $90 < N_S$ (low head, high flow) an axial flow design is most efficient. Note that both η and N_S are dimensionless ratios, and without the scaling provided by the use of dimensionless parameters terms such as "high head" are meaningless.

Although a qualitative ranking may be made from physical principles, the numerical values of N_S which are most suitable cannot be predicted from the external variables. Prediction requires either a detailed analysis of the internal flows or experience (i.e. test data). Furthermore a poorly designed turbine of the most suitable type may well have an efficiency lower than that of a well designed one of a less suitable type, and an innovation in design may change the boundaries of the "most suitable" design.

In river hydraulics and geomorphology the external variables are Q, valley slope S_v , the river energy slope S_e (the counterpart of H/D for the turbine), the sediment fall velocity, w, the valley length, L, etc. These may be grouped to give stream power, which is the rate at which the stream dissipates potential energy, either locally or globally:

$$P_S = \tau_o V = \rho g Q S_e \tag{4}$$

Observations have shown (Hey, 1978; Chang, 1988) that many river channels adopt cross sectional dimensions and alignments which minimize the stream power. The minimum unit stream power, minimum global stream power, minimum energy dissipation rate, maximum sediment transport and maximum friction factor hypotheses have all been proposed to close the set of one-dimensional equations of water and sediment transport – without three-dimensional dynamics there are insufficient equations to solve for velocity, channel dimensions and sediment transport. All of these "laws" have been shown (Phillips, 1991; Bettess and White, 1987) to be basically equivalent for the "at-a-station hydrologic geometry ..". More exactly, these "laws" minimize the stream power subject to the constraint of available stream power. Thus the scaled, dimensionless quantity is P_S/P_a . In the form of regime theory (Blench, 1964; Chang 1988) these methods provide a guide to suitable channel dimensions and correlate with bedform (Simons and Richardson, 1966), the occurrence of meandering and the dimensions of meanders (Yang, 1971; Schumm, 1977), and the sediment load carried by the stream. (Bagnold, 1964). In the light of the turbine analogy, we use "correlate" rather than the authors' causal verbs.

Entropy may be identified with disorder or the levelling out of differences, thus Schumm (1977) used valley elevation for classifying the evolution of a river system. More generally, a trend towards uniform stream power or $P_S/P_a \to 1$could be considered as an increase in entropy. Other quantities which could serve as an index for comparison of an estuary at different stages of its evolution, or to compare the stages of evolution of two different estuaries include the ratio of the water volume of the estuary to the total volume of water in the original embayment, or the annual discharge of sediment to the ocean divided by the annual sediment inflow, or the shoreline length of the estuary divided by the valley length. Each of these captures some aspect of estuary evolution but all are too simplistic to capture adequately the changes between Roy's stages of evolution. Until such a measure is developed

the study of estuarine morphology will remain qualitative and difficult to transfer from one locality to another. Development of such a measure is one aim of the present study.

4. CONCLUSIONS

The following conclusions may be drawn from the experience of model development to date and the above discussion:

- There is a good case for attempting to model the long term evolution of an estuary to assist sustainable management and to improve the quantification of the factors affecting estuarine evolution.
- Chaos leading to self regulation is not a problem in the modelling.
- Chaos leading to the butterfly effect is unlikely to be a problem in any model run. If it arises, the statistical nature of the predictions will still enable meaningful results to be obtained.

For long term simulations of estuarine, coastal or landscape evolution:

- Data limitations mean that only statistical results may be obtained for pre-settlement hindcasts and all predictions.
- For any long term simulations, the time required for computation and the accumulation of residual errors are problems but solution can be found by use of multiple time scales while observing convergence and stability conditions.
- Validation of any long running model cannot match the ideal as inferred statistics only are available. Following calibration of the physical process equations, the direct validation must be supplemented by sensitivity analyses.

5. ACKNOWLEDGEMENTS

This research is part of the project Geo-Hydrodynamic Modelling and Estuarine Evolution, partly funded by ARC Linkage Grant LP0347365. The author's collaborators and students Errol McLean, Colin Woodroffe, Brian Jones, Owen Gould, Mark Trevethan and Marko Polic have contributed ideas and data.

6. REFERENCES

Abbott, M.B. (1979). *Computational Hydraulics*, Pitman, London, 324pp.

Bagnold, R.A. (1964). cited in Leopold, L. B., Wolman, M. G. and Miller, G.P. (1964) *Fluvial Processes in Geomorphology*, W.H. Freeman and Co., San Francisco, 552p.

Bettess, R. and White, W. R. (1987). Chapter 24: Extremal hypotheses applied to river regime. In, *Sediment Transport in Gravel-bed Rivers*, (Eds, Thorne, C. R., Bathurst, J. C., et al.), John Wiley and Sons Ltd, Chichester, New York, pp. 767-789.

Blench, T. (1964). Dynamical statements of regime formulas, *ASCE Hydraulics Division Vicksburg Meeting - Panel Discussion on "The Pros and Cons of Regime Theory"*, American Society of Civil Engineers.

Bradley, R. S. (1999). *Paleoclimatology. Reconstructing Climates of the Quaternary*, Academic Press, Amherst, Massachusetts, 613p.

Carter, R. W. G. and Woodroffe, C. D. (1994). Chapter 1. Coastal evolution: an introduction. In, *Coastal Evolution: Late Quaternary Shoreline Morphodynamics*, (Eds, Carter, R. W. G. and Woodroffe, C. D.), Cambridge University Press, Cambridge, pp. 1-31.

Chang, H. H. (1988). *Fluvial Processes in River Engineering*, John Wiley and Sons, New York, 432p.

Cook, E. R., D'Arrigo, R. D.and Buckley, D.M. (1998). Tasmania temperature reconstruction. International tree-ring data bank., *Data Contribution Series #98-040*, Vol. 2004NOAA/NGDC Paleoclimatology Program, Boulder CO, USA, IGBP PAGES/World Data Center-A for Paleoclimatology.

de Vriend, H., Capobianco, M., Chesher, T., de Swart, H.E., Latteus, B. and Stive, M.J.F. (1993). Approaches to long-term modelling of coastal morphology: A review., *Coastal Engineering*, 21**,** pp. 225-269.

Dennis, J. M., Spearman, J. R. and Dearnaley, M.P. (2000). The development of a regime model for prediction of the long-term effects of civil engineering activities on estuaries, *Physics and Chemistry of the Earth, Part B: Hydrology, Oceans and Atmosphere*, 25**,** pp. 45-50.
Green, M. O., Williamson, B., Collins, R., Senior, A., Adams, R. and Timperley, M. (2003). Prediction of decadel-scale contaminant accumulation in estuaries, *Coasts and Ports 16th Australasian Coastal and Ocean Engineering Conference*, The Institution of Engineers Australia, Auckland, New Zealand, pp. Paper No. 53.

Hey, R. D. (1978). Determinate hydraulic geometry of river channels, *ASCE Journal of the Hydraulics Division*, 104**,** pp. 869-885.

Hinwood, J. B. and McLean, E. J. (2002). Modelling the evolution of an estuary, *Proceedings Littoral 02*, European Coastal Zone Association for Science and Technology, Porto, Portugal, pp. 245-252.

Hinwood, J.B., Trevethan, M. & McLean, E.J. (2003). The effects of entrance parameters on tides in inlets, Proc. 16th Australasian Conference on Coastal and Ocean Engineering, September 2003, Auckland, NZ, paper 155, 8p.

IPCC (2001). IPCC Third Assessment Report – Climate Change 2001, Intergovernmental Panel on Climate Change, also available from www.ipcc.ch updated 4 march 2003.

Kaminsky, G. M., Buijsman, M. C. and Ruggiero, P. (2000). Predicting shoreline change and decadal scale in the Pacific North West USA, *ICCE 27th International Conference on Coastal Engineering*, 3, American Society of Civil Engineers, Sydney, Australia, pp. 2400-2413.

Kershaw, A. P. (1998). Estimates of regional climatic variation within southeastern Australia since the last glacial maximum from pollen data, *Palaeoclimates - Data and Modelling*, 3**,** pp. 107-134.

Kirkby, M. J. (1994). Thresholds and instability in stream head hollows: a model of magnitude and frequency for wash processes. In, *Process Models and Theoretical Geomorphology*, ed Kirkby, M.J., Wiley, pp. 295-314.

Leopold, L. B. and Langbein, W. B. (1962). *The Concept of Entropy in Landscape Evolution*, Geological Survey Professional Paper No. 500-A, US Dept of the Interior, Washington, pp. 20.

Mason, D.C. and Garg, P.K. (2001). Morphodynamic modelling of intertidal sediment transport in Morecambe Bay, *Estuarine, Coastal and Shelf Science*, 53, 79-92.

Martinez, P. A. and Harbaugh, J. W. (1993). Simulating nearshore environments, *Computer Methods in the Geosciences*, 12**,** pp. 265.

Melchers, R. E. (1984). *Efficient Monte Carlo Probability Integration* , Report of Dept. of Civil Engineering, Monash University, Melbourne.

Nanson, G. C. and Erskine, W.D. (1988). W. D. Episodic changes of channels and flood plains on coastal rivers in New South Wales. In, *Fluvial Geomorphology of Australia*, (Ed, Warner, R. F.), Academic Press, pp. Chapter 10, pp. 201-221.

O'Brien, M. P. (1931). Estuary tidal prisms related to entrance areas, *Civil Engineering*, 1**,** pp. 738-39.

Pethick, J. (1991). Tidal dynamics and estuarine management in the Humber Estuary, England, Coastal Zone 91, ed. Magoon, O.T., ASCE, pp1456-1468.

Phillips, J. D. (1991). Multiple modes of adjustment in unstable river channel cross-sections, *Journal of Hydrology*, 123**,** pp. 39-49.

Phillips, J. D. (1999). *Earth Surface Systems: Complexity, Order and Scale*, Blackwell, Oxford, England, 180p.

Pittock, B. ed (2003). Climate Change – An Australian Guide to the Science and Potential Impacts, Australian Greenhouse Office, Canberra, 250 pp.

Rigon, R., Rinaldo, A. and Rodriguez-Iturbe, I. (1994). On landscape self-organization, *Journal of Geophysical Research,* 99**,** pp. 11971-11993.

Roy, P. S. (1984). Chapter 5. New South Wales estuaries: Their origin and evolution. In, *Coastal Geomorphology in Australia*, (Ed, Thom, B. G.), Academic Press, Sydney, pp. 99-121.

Sapozhnikov, V. B. and Foufoula-Georgiou, E. (1996). Do the current landscape evolution models show self-organized criticality?, *Water Resources Research,* 32**,** pp. 1109-1112.

Schumm, S. A. (1977). *The Fluvial System,* Wiley-Interscience, New York; London, 338p.

Schumm, S. A. (1988). Chapter 12. Variability of the fluvial system in space and time. In, *Scales and Global Change*, (Eds, Rosswall, T., Woodmansee, R. G., et al.), Scientific Committee on Problems of the Environment, John Wiley and Sons Ltd, pp. 225-250.

Simons, D. B. and Richardson, E. V. (1966). *Resistance to Flow in Alluvial Channels*, Geological Survey Professional Paper No. 422-J, US Geological Survey, pp. 61.

Steetzel, H. J., de Vroeg, H., Ryan B.A.N., Rijan, L.C. and Stam, J.M. (2000). Long-term modelling of the Holland coasts using a multi-layer model, *ICCE 27th International Conference on Coastal Engineering*, 3, American Society of Civil Engineers, Sydney, Australia, pp. 2943-2955.

van Rijn, L. C. (1993). *Principles of Sediment Transport in Rivers, Estuaries and Coastal Seas*, Aqua Publications, Amsterdam.

Willgoose, G., Bras, R. L. Rodriguez-Iturbe, I. (1994). Hydrogeomorphology modeling with a physically based river basin evolution model. In, *Process Models and Theoretical Geomorphology*, (Ed, Kirkby, M. J.), John Wiley and Sons, Chichester; New York, pp. 271-294.

Yang, C. T. (1971). On river meanders, *Journal of Hydrology,* 13**,** pp. 231-253.

7. APPENDIX - CONSTRAINTS ON THE TIME STEP

The hydrodynamic time step must be small to meet the Courant condition. This kinematic condition is necessary for numerical stability for explicit codes and for convergence of both explicit and implicit codes (Abbott, 1979). It specifies that the computation must advance faster than the fluid (u) and the speed of disturbances traveling through the fluid, c:

$$(u+c)\Big/\frac{\delta x}{\delta t} \quad < \quad \alpha \quad < \quad 1 \tag{5}$$

where δx is the spatial step and δt is the time step. Condition (5) is required for both implicit and explicit models: for first order explicit models $\alpha \le 0.2$. The wave speed $c = \sqrt{gy}$ may be large and so this condition restricts δt. In addition there is a dynamic stability condition to ensure that disturbances die out rather than grow under the action of internal and bed shear stresses.

A Courant condition arises also from the equation of mass conservation for the sediment, leading to

$$u\Big/\frac{\delta x}{\delta t} \quad < \quad \beta \quad < \quad 1 \tag{6}$$

Even for first order models $\beta \sim 1$ is satisfactory in our experience.

Changes in u, y and c resulting from changes in morphology may cause divergence or numerical instability of the hydrodynamic equations. Morphological changes alter the form of the dynamic stability condition. Numerical trials

with a branched channel undergoing very rapid scour or deposition displayed numerical instability but with slower, more realistic rates of deposition, the stability conditions imposed above on the hydrodynamics and sediment mass balance ensured stability during quite large bed level changes. It is not yet clear whether the abrupt transitions will cause instability problems, however there are several possible fixes.

The Institution of Engineers, Australia
8th National Conference on Hydraulics in Water Engineering
ANA Hotel Gold Coast, Australia 13-16 July 2004

Bridge abutment scour: Estimation and protection

B.W. Melville
B.E., Ph.D., FIPENZ, MASCE
Professor, The University of Auckland, New Zealand

Abstract: A comprehensive method for estimating local scour depths at bridge abutments is presented. The method was developed in New Zealand on the basis of an extensive series of laboratory investigations. Application of the method ensures that the various influences on local scour depths are systematically addressed. These are the characteristics of the flow approaching the bridge crossing, the shape of the river channel in the vicinity of the bridge, the characteristics of the bed sediments in the vicinity of the bridge, the geometry of the bridge abutments, and the peak value and duration of the design flood. Application of the method is highlighted.

Preliminary results from a current investigation of the use of riprap and cable-tied blocks to protect bridge abutments are presented. The experiments apply to spill-through abutments sited on the flood-plain of wide river crossings, and wing-wall abutments sited near the bank of narrow crossings.

Keywords: Erosion, scour, bridge, abutment, estimation, protection, countermeasure, river

1. INTRODUCTION

Scour at bridge foundations during floods is the main cause of damage to bridges at river crossings. In New Zealand, an average of at least one serious bridge failure each year can be attributed to scour of the bridge foundations. The damage can result in complete failure of the bridge structure or its road approach, or it can be minor such as erosion at an adjacent river bank or bridge approach. Complete failure results in severe disruption to local traffic flows. The frequency of bridge failures due to scour has spurred many research projects of this vexing problem.

A comprehensive treatment of the present state of knowledge on bridge scour is given in Melville and Coleman (2000). The monograph makes use of New Zealand's extensive experience with scour problems. It addresses all aspects of bridge scour, including general scour, contraction scour, local scour, scour countermeasures and 31 case histories of scour failures. The methodology for local scour at bridge abutments is summarised in this paper. Examples of application of the method are included. Some preliminary results from a current investigation of the use of riprap and cable-tied blocks to protect bridge abutments against scour are also presented.

2. ESTIMATION OF LOCAL SCOUR DEPTHS

The method for estimation of local scour depths at bridge abutments by Melville and Coleman (2000) is presented. The basic data required to apply the method are:

- mean velocity V, flow depth y and Manning's coefficient n for the flow in the main channel;
- median size d_{50}, maximum size d_{max} and geometric standard deviation σ_g of the particle size distribution. In practice, d_{90} (or a similar size) can be used in place of d_{max}, which is unlikely to be known;
- length L, shape Sh and alignment θ of the abutment, and;
- for compound channels, the flow depth y^*, Manning's coefficient n^* and width L^* for the flow in the flood channel.

The following equation for the depth of local scour d_s is the basis of the design method:

$$d_s = K_{yL} K_I K_d K_s K_\theta K_G K_t \quad (1)$$

The *K*-factors in this equation are empirical expressions accounting for the various influences on scour depth. The length of the abutment relative to the depth of flow is the primary influence on scour depth and is represented by the depth-size factor K_{yL}. The remaining scour-depth influences are flow intensity, represented by K_I; sediment size, represented by K_d; abutment shape and alignment, represented by K_s and K_θ, respectively; channel geometry for compound channels, represented by K_G; and duration of scouring (time effects), represented by K_t. K_I is formulated to include sediment gradation effects as well as flow velocity effects. $K_{yL} = f(y, L)$ and d_s have the dimension of length, while the other *K*-factors are dimensionless.

Expressions for the various *K*-factors are summarised in Table 1 and illustrated in Figure 1. The expressions are derived from envelope curves fitted to laboratory data. K_I is a function of the threshold velocity V_c, the armour velocity V_a and the velocity parameter $[V-(V_a-V_c)]/V_c$. The procedure for estimating these velocities is explained below and summarised in Table 1.

Table 1 Factors influencing local scour depth at bridge abutments

Factor	K	Method of Estimation	
Flow depth-abutment size	K_{yL}	$K_{yL} = 10y$	$\frac{y}{L} \le 0.04$
		$K_{yL} = 2\sqrt{yL}$	$0.04 < \frac{y}{L} \le 1$
		$K_{yL} = 2L$	$\frac{y}{L} > 1$
Flow intensity	K_I	For uniform sediments: $d_{50a} \equiv d_{50}$ and $V_a \equiv V_c$ For nonuniform sediments: $d_{50a} = d_{max}/1.8 \approx d_{84}/1.8 = \sigma_g d_{50}/1.8$; and $V_a = 0.8V_{ca}$, where V_{ca} is V_c calculated for d_{50a}	
		$K_I = \frac{V-(V_a-V_c)}{V_c}$	for $[V-(V_a-V_c)]/V_c <$ 1
		$K_I = 1.0$	for $[V-(V_a-V_c)]/V_c \ge$ 1
Sediment size	K_d	$K_d = 1.0$	$\frac{L}{d_{50a}} > 60$
Foundation shape		Shape	K_s
	K_s	Vertical-wall	1.0
		Wing-wall	0.75
		Spill-through 0.5:1 (H:V)	0.6
		Spill-through 1:1	0.5
		Spill-through 1.5:1	0.45
	K_s^*	$K_s^* = K_s$	$\frac{L}{y} \le 10$
		$K_s^* = K_s + 0.667(1 - K_s)\left(0.1\frac{L}{y} - 1\right)$	$10 < \frac{L}{y} < 25$
		$K_s^* = 1.0$	$\frac{L}{y} \ge 25$

<table>
<tr><td rowspan="3">Foundation alignment</td><td rowspan="2">K_θ</td><td>θ (°)</td><td>30</td><td>45</td><td>60</td><td>90</td><td>120</td><td>135</td><td>150</td></tr>
<tr><td>K_θ</td><td>0.90</td><td>0.95</td><td>0.98</td><td>1.0</td><td>1.05</td><td>1.07</td><td>1.08</td></tr>
<tr><td>K_θ^*</td><td colspan="8">$K_\theta^* = 1.0 \qquad \frac{L}{y} \le 1$
$K_\theta^* = K_\theta + (1 - K_\theta)\left(1.5 - 0.5\frac{L}{y}\right) \qquad 1 < \frac{L}{y} < 3$
$K_\theta^* = 1.0 \qquad \frac{L}{y} \le 1$</td></tr>
<tr><td rowspan="4">Approach-channel geometry</td><td></td><td colspan="8">Case A (Fig. 1): [Simple rectangular river channel] $K_G \equiv 1.0$</td></tr>
<tr><td></td><td colspan="8">Case C (Fig. 1): [Abutment well back from the flood-channel edge]
Consider only the flood channel flows of y* and set $K_G = 1.0$</td></tr>
<tr><td>K_G</td><td colspan="8">Case B (Fig. 1): [Abutment in the main channel]
$K_G = \sqrt{1 - \left(\frac{L^*}{L}\right)\left[1 - \left(\frac{y^*}{y}\right)^{5/3}\left(\frac{n}{n^*}\right)\right]}$</td></tr>
<tr><td></td><td colspan="8">Case D (Fig. 1): [Abutment near the flood channel edge]
Abutment at about the flood-channel edge: Case B with L^*/L=1.0.</td></tr>
<tr><td rowspan="2">Time</td><td></td><td colspan="8">$t_e(days) = 20.83\frac{L}{V}\left(\frac{V}{V_c}\right)^3\left(\frac{y}{L}\right)^{0.8}$ for $y/L < 1$
$t_e(days) = 20.83\frac{L}{V}\left(\frac{V}{V_c}\right)^3$ for $y/L \ge 1$</td></tr>
<tr><td>K_t</td><td colspan="8">$K_t = \exp\left[-0.07\left(\frac{V}{V_c}\right)^{-1}\left|\ln\left(\frac{t}{t_e}\right)\right|^{1.5}\right]$ for $V/V_c < 1$
$K_t = 1.0$ for $V/V_c \ge 1$</td></tr>
</table>

The local scour depth is given by (1), in which K_I, K_d, K_G and K_t are always less than or equal to unity. Thus the maximum possible equilibrium local scour depth is

$$d_{se)\max} = K_{yL} K_s K_\theta \qquad (2)$$

2.1 Physical Basis Of Scour Depth Methodology

In the following sections, the various physical influences on local scour depth, as represented by the *K*-factors in (1), are discussed. These influences are determined from systematic laboratory-based tests.

2.1.1 Flow Depth - Foundation Size (Depth - Size) Factor, K_{yL}

The influence of $K_{yL} = f(y, L)$ on local scour depth is demonstrated by the data given in Figure 2. The data plotted are from Gill (1972), Wong (1982), Tey (1984), Kwan (1984, 1988), Kandasamy (1989), and Dongol (1994). These data are unaffected by flow intensity, sediment size, sediment gradation, foundation shape and alignment, channel geometry and time.

In Figure 2, the solid lines are envelopes to the data. The lines apply, from left to right respectively, to long, intermediate length and short abutments at threshold conditions. It is apparent that, for clear-water scour at reduced flow velocities, lesser scour depths are developed. The equations of the upper-limit lines define the depth-size factors for abutments. These equations are given in Table 1.

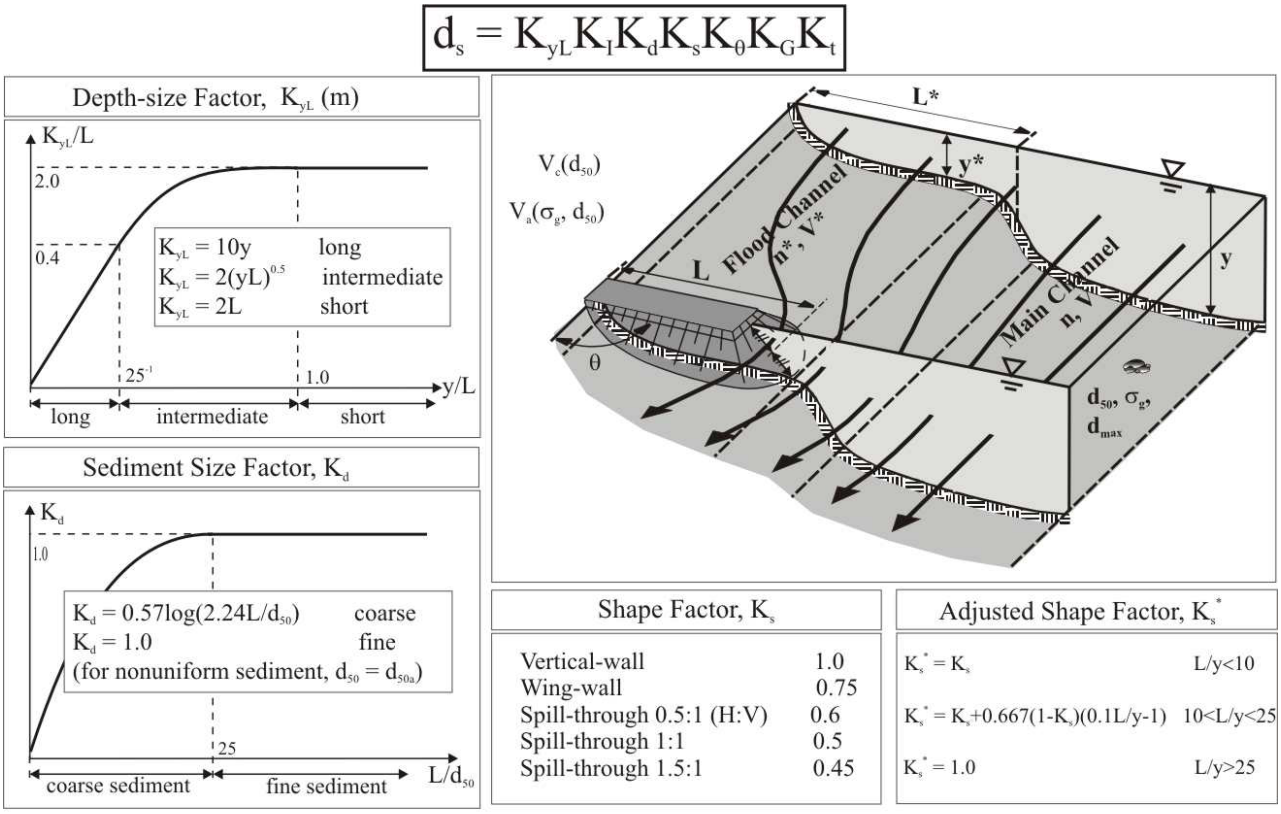

Figure 1 Method for estimation of local scour depth at abutments.

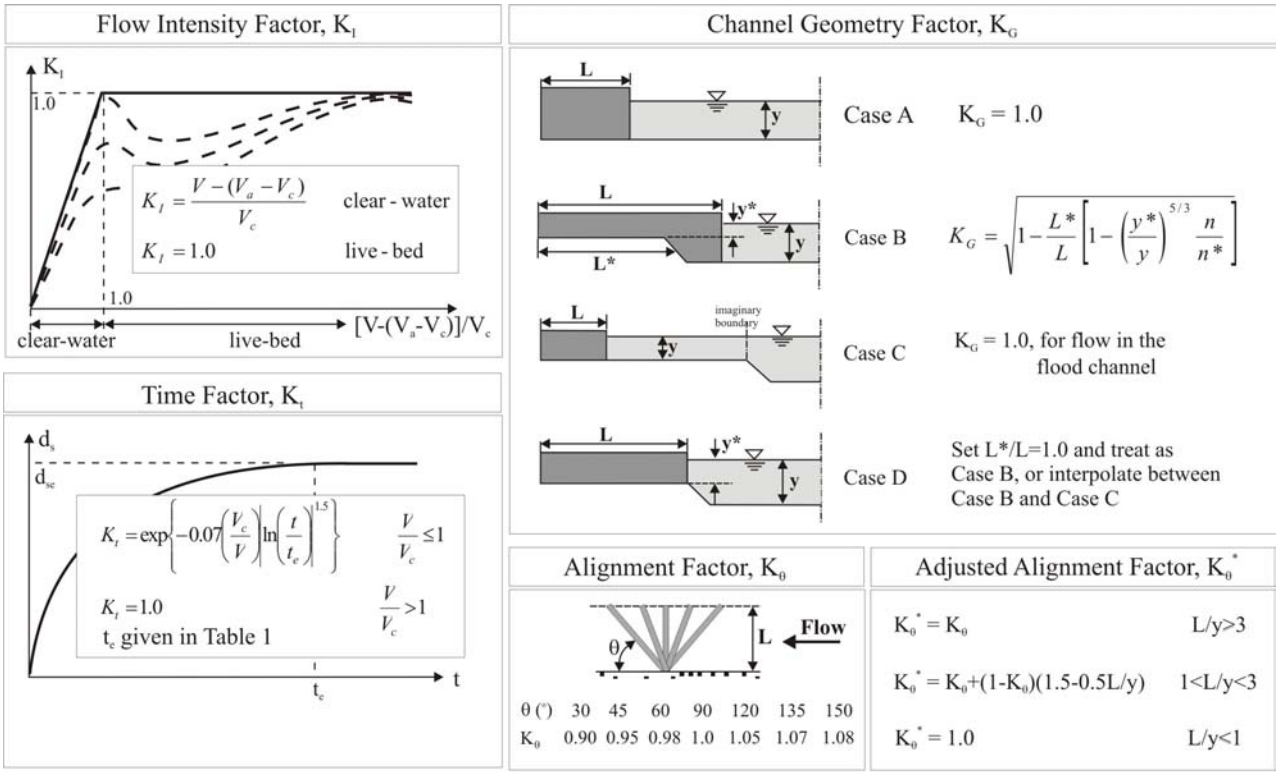

Figure 1 (cont.) Method for estimation of local scour depth at abutments.

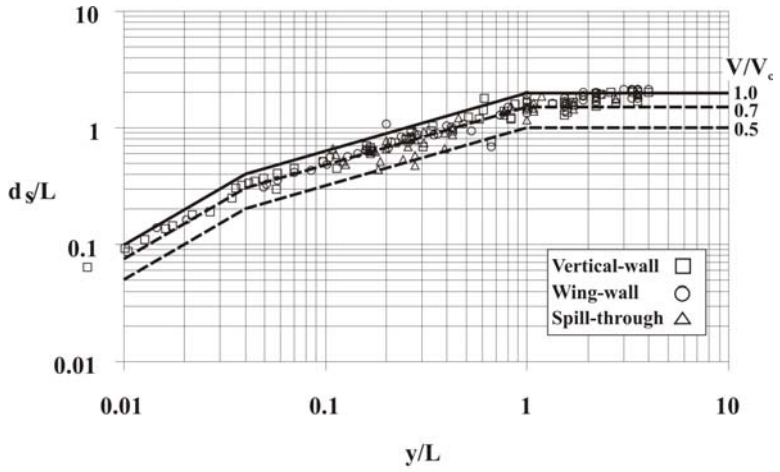

Figure 2 The influence of flow shallowness on local scour depth

2.1.2 Flow Intensity Factor, K_I

The effects of flow intensity on local scour depth are represented by K_I , which is defined, for each set of data, as the scour depth at a particular flow intensity divided by the maximum scour depth for the data set. For each data set, V is systematically varied and all other dependent parameters are held constant. The scour maxima used occur at the threshold peak for uniform sediments and the live-bed peak for nonuniform sediments.

Figures 3 and 4 are plots of laboratory data from many sources for local scour at abutments in terms of K_I. Figure 3 applies to uniform sediments, while Figure 4 applies to nonuniform sediments. The data are all enveloped by a value of K_I increasing linearly from zero to unity at the threshold condition and thereafter remaining unchanged. The nonuniform sediment data are plotted in terms of a transformed velocity parameter, as shown. The transformed velocity parameter aligns the armour peaks (that is $V=V_a$) for nonuniform sediments with varying σ_g with the threshold peak (that is $V=V_a$) for uniform sediments. It is apparent that for uniform sediments, $V_a \equiv V_c$ and $[V-(V_a-V_c)]/V_c \equiv V/V_c$. The transformed velocity parameter incorporating V_a largely accounts for the effects of sediment nonuniformity as well as those of flow velocity, although the smaller values of scour depth at $[V-(V_a-V_c)]/V_c \approx 1$, as σ_g increases, remain. Thus, the effects of sediment nonuniformity are mostly represented by the flow intensity factor.

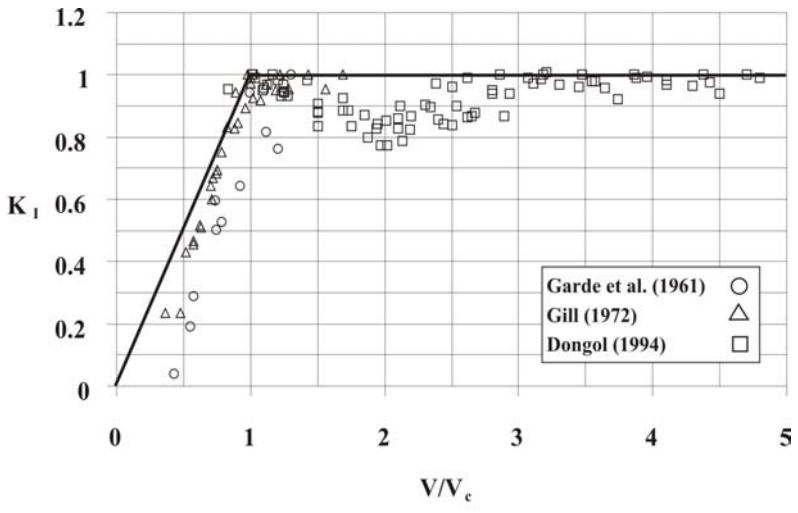

Figure 3 The influence of flow intensity on local scour depth in uniform sediment

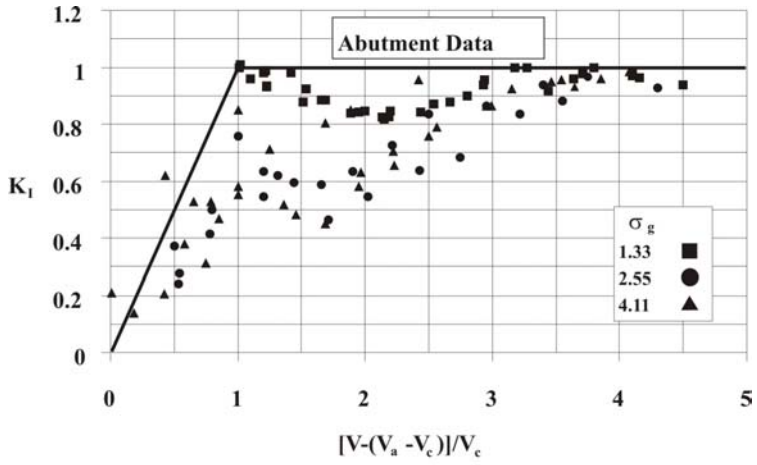

Figure 4 Influence of flow intensity on local scour depth in nonuniform sediment

The velocities V_c and V_a can be determined using the logarithmic velocity distribution equation:

$$\frac{V_c}{u_{*c}} = 5.75 \log\left(5.53 \frac{y}{d_{50}}\right) \tag{3}$$

where u_{*c} is critical shear velocity determined from the Shields' diagram. For determination of the armour peak velocity, V_a, d_{50} and u_{*c} are replaced by d_{50a} (median size of the armour layer = $d_{max}/1.8$) and u_{*ca} (critical shear velocity of the armour layer), respectively.

2.1.3 Sediment Size Factor, K_d

Dongol's (1994) data are plotted in Figure 5 in terms of the sediment size multiplying factor, K_d, which is defined generally as the ratio of the scour depth for a particular L/d_{50} to that for $L/d_{50} \geq 50$. The envelope curves in Figure 5 define the sediment size factor for design purposes.

Separate plots are given for uniform and nonuniform sediments. It is seen that the influence of relative sediment size on scour depth is the same for both piers and abutments. It is considered that the few abutment data shown in Figure 5 are adequate for definition of K_d for abutments, because the condition $L/d_{50} < 50$ is unlikely in practice.

For nonuniform sediments, channel bed armouring is important, as discussed earlier. In Figure 5, the nonuniform sediment data are plotted for different values of the velocity parameter $[V-(V_a-V_c)]/V_c$ = 1.0, 2.0, 3.0 and 4.0. The data are plotted in terms of L/d_{50a} because the median size of the armour layer is considered to be the characteristic sediment size.

2.1.4 Foundation Shape Factor, K_s

Recommended shape factors for shorter abutments are given in Table 1. The shape factor K_s is defined as the ratio of the scour depth for a particular foundation shape to that for the standard shape. Vertical-wall abutments are selected as the standard shape.

For longer abutments, shape effects are less significant, and an adjusted shape factor K_s^* is applied. K_s* is given in Table 1.

2.1.5 Foundation Alignment Factor, K_θ

Recommended alignment factors for longer abutments are given in Table 1. The alignment factor K_θ is defined as the ratio of the local scour depth at a skewed bridge foundation to that at an aligned

foundation. For shorter abutments, alignment effects are less significant. The adjusted alignment factor K_θ^* for shorter abutments is given in Table 1.

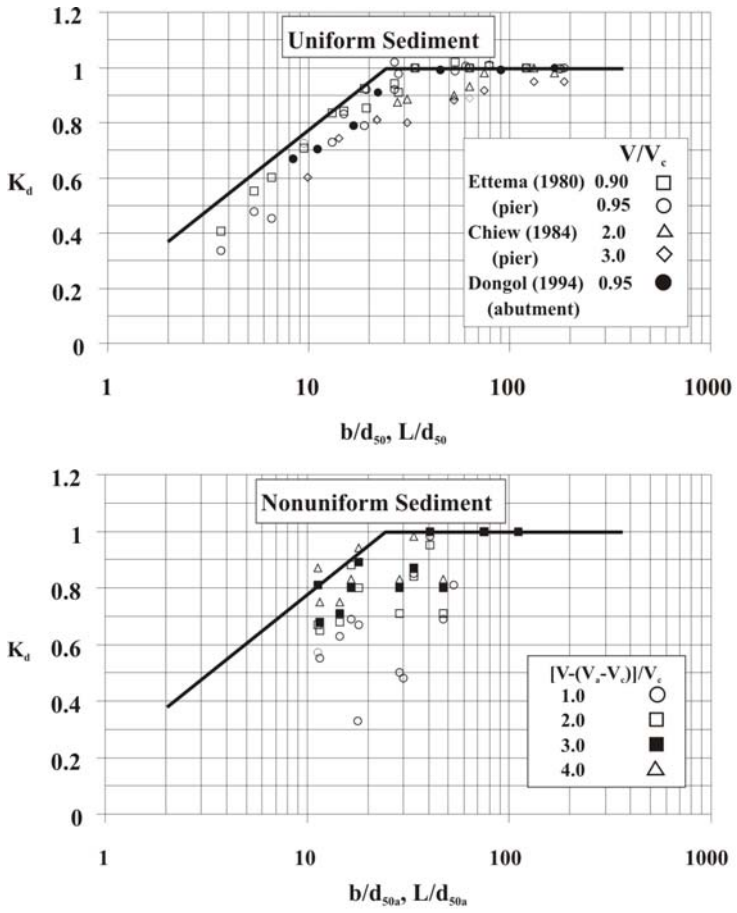

Figure 5 Influence of sediment coarseness on local scour depth

2.1.6 Approach Channel Geometry Factor, K_G

Scour depths at an abutment situated on the flood plain of a compound river channel are reduced from those in equivalent rectangular river channels. The equivalent rectangular channel is defined as having the same depth as the main channel depth in the compound river channel. The approach channel geometry factor K_G is the ratio of the local scour depth at a bridge foundation to that at the same foundation sited in the equivalent rectangular channel.

For bridge abutments in rectangular channels (Case A of Figure 1), K_G=1.0 by definition. For abutments in compound channels, K_G depends on the position of the abutment in the compound channel (Figure 1). The equation given in Table 1 is recommended for Case B abutments. It is derived from a simple theoretical analysis based on the ratio of flows deflected by the abutment, including the bridge approach, in a compound channel to such flows in the equivalent rectangular channel. In this equation, L and L^* = total projected length of the abutment (including the bridge approach) and projected length of the abutment (including the bridge approach) spanning the flood channel, respectively; y and y^* = flow depths in the main and flood channels, respectively; and n and n^* = Manning roughness coefficients for the main and flood channels, respectively. The equation is plotted in Figure 6 for ranges of values of the ratios L^*/L, y/y^* and n/n^*. Case C can be considered to be a special condition of Case A if the flow in the main channel is ignored; thus K_G=1.0. For Case D abutments where the abutment is sited at about the edge of the main channel, K_G can be estimated from the equation for Case B, with L^*/L=1.0. No specific information is available to aid estimation of K_G for

other Case D abutments; such situations could be treated by interpolating conservatively between scour depth estimates for longer (Case B) and shorter (Case C) abutments sited in the same channel.

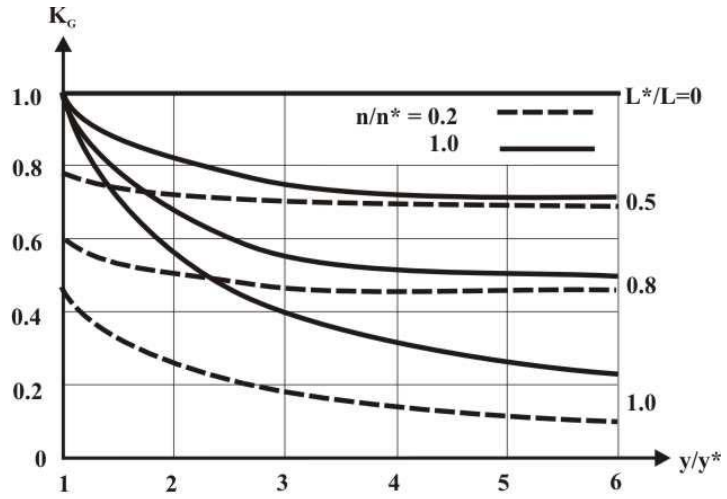

Figure 6 Influence of channel geometry on local scour depth at bridge abutments

2.1.7 Time Factor, K_t

The time factor is defined as the ratio of local scour depth d_s at a particular time t to the equilibrium scour depth d_{se}, which occurs at time t_e. The value of K_t at a site depends on whether conditions are clear-water or live-bed. Under live-bed conditions, the equilibrium depth of local scour is attained rapidly and $K_t = 1.0$ can be assumed.

A function for the time factor at abutments is given in Table 1. The function is given in Coleman et al (2003) and represents an updating of the recommendations in Melville and Coleman (2000). K_t depends on t_e, the time to equilibrium scour depth. An equation for estimation of t_e is also given in Table 1.

2.2 Example Of Application Of Methodology

A bridge is situated at a channel bend, as illustrated in Figure 7. The peak flow rate is 440 m^3/s and this lasts for 2 days. The sediment is a medium sand with $d_{50} = 0.5$ mm. The calculations are presented in Table 2. The estimated local scour depth is 4.5 m.

Because the bridge narrows the channel, contraction scour would occur. Mobile-bed conditions would exist (Table 2). Laursen's (1960) equation for contraction scour is used to estimate the contraction scour depth. The equation is

$$\frac{y_2}{y_1} = \left(\frac{Q_2}{Q_{1m}}\right)^{6/7} \left(\frac{W_1}{W_2}\right)^{k_1} \tag{4}$$

where y_1 = average depth in the approach main channel; y_2 = average depth in the main channel of the contracted section; W_1 = bottom width of the approach main channel; W_2 = bottom width of the main channel in the contracted section; Q_{1m} = discharge in the approach main channel transporting sediment; Q_2 = total discharge through the bridge; and k_1 = a coefficient depending on the mode of sediment transport. For the given example, $Q_{1m} = Q_2$.

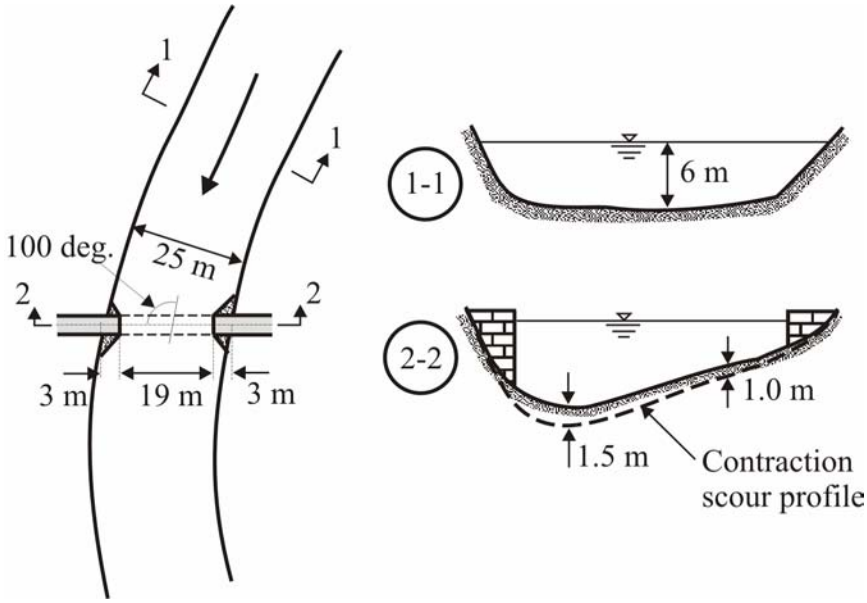

Figure 7 Abutment scour example

Table 2 Abutment Scour Example

The threshold velocity is, V_c = 1.3 m/s, for y = 6 m and d_{50} = 0.5 mm (using Neill's 1987 competent velocity chart. $V_2 = \frac{Q}{W_2 y} = \frac{440}{19 \times 6} = 3.86 \text{ m/s} >> V_c$ and conditions are live-bed
Using (4) with k_1 = 0.69 to estimate contraction scour: $\frac{d_s}{y_1} = \left(\frac{W_1}{W_2}\right)^{k_1} - 1 \quad \text{giving:} \quad d_{s)contraction} = 1.25 \text{ m}$ $d_{s)contraction} = 1.5 \text{ m, RHS}, d_{s)contraction} = 1.0 \text{ m, LHS}$ It is assumed that the contraction scour is distributed as shown in Figure 7
Flow depth after contraction scour is: $y = 6 + d_{s)contraction} = 7.25 \text{ m}$
$\frac{L}{y} = 0.42, K_{yL} = 6 \text{ m}$
$V = \frac{Q}{W_1 y} = \frac{440}{25 \times 7.25} = 2.43 \text{ m/s}$
$u_{*c} = 0.016 \text{ m/s}, V_c = 0.45 \text{ m/s}, \frac{V}{V_c} = 5.4, K_I = 1.0 \text{ and } K_t = 1.0 \text{ for live-bed conditions}$
$\frac{L}{d_{50}} > 25, K_d = 1.0$
$K_s = 0.75$, for wing-wall abutment, $K_s^* = K_s$
$\frac{L}{y} < 1, K_{\theta)LHS} = K_{\theta)RHS} = 1.0$
$K_G = 1.0$
$d_s = K_{yL} K_I K_d K_s K_\theta K_G K_t \quad$ and $d_s = 4.5 \text{ m}$
Total scoured depth: $y_{s)total} = y_1 + d_{s)contraction} + d_s, y_{s)total} = 6 + 1.5 + 4.5 = 12.0 \text{ m (RHS)}, = 11.5 \text{ m (LHS)}$

3. SCOUR COUNTERMEASURES

3.1 Background

Protection of bridge abutments from scour includes countermeasures that alter flow and scour patterns and those that armour the bed, bank, floodplain and embankment slopes, such as riprap. Armour protection frequently includes the coverage of susceptible portions of embankment slopes. Many design guidance documents recommend that an apron be constructed around the toe of the embankment slope. Armour aprons can protect vertical-wall abutments founded on spread footings. Filters have been recommended below the protection to prevent piping of soils through the armor layers. The filters also may be beneficial to prevent winnowing of soils from beneath aprons especially where the armour layer is used to protect embankments under live-bed conditions.

Riprap is a commonly used technique to protect bridge abutments and bridge approach embankments from scour. The increased weight of the riprap stones enables them to resist the increased turbulence caused by the presence of the abutment in the flow, and thereby provide an armour layer protection to the underlying sediments. Interlocking forces between adjacent stones also act to stabilise the riprap layer. Typically, the riprap is placed on the embankment slopes to protect the sediment from scour. Riprap can also be placed in a launching apron to fall onto the sides of a developing scour hole. This riprap acts to reduce the scour depth, and protect the abutment foundation from undermining.

Riprap is subject to certain failure mechanisms, dependent on where it is placed in respect to the bridge abutment. Riprap placed in the apron is subject to similar failure mechanisms as riprap placed about a bridge pier, whereas riprap placed on the embankment slopes are subject to not only dislodgement by the flow, but also slump and slide failures where the riprap moves down the embankment slope. Parola (1993), Chiew (1995) and Lauchlan (1999) identified four failure mechanisms for riprap placed in an apron, viz. shear failure, winnowing failure, edge failure, and bed-form undermining. Similarly, Blodgett and McConaughy (1985) identified the principle failure modes for riprap placed on sloping embankments. These are particle erosion failure, translational slide failure, and slump failure.

Cable-tied blocks consist of concrete blocks or slabs interconnected with metal or non-metallic cables. The cables used can be fabricated from steel, copper or synthetic materials, such as polypropylene (Przedwojski et al, 1995). A key feature of cable-tied blocks is the interconnecting of small units, which may be unstable as individual blocks, into a framework capable of withstanding much higher flow velocities. The term is used typically to describe relatively small units; articulated concrete mattresses, which rely on the same principles, are larger units commonly used for bank protection. Previous studies and experiments on the use of cable-tied blocks for scour protection of bridge foundations are limited and are focussed on bridge piers (McCorquodale et al, 1993; Bertoldi et al, 1994; Jones et al, 1995; Parker et al, 1998). Recently, Eve (1999) and Hoe (2001) completed experimental investigations.

Parker et al (1998) identified three possible failure mechanisms: ***overturning and rolling-up*** of the leading edge, which is exacerbated if the edge is not anchored; ***uplift*** of the centre of the mat, which typically occurred in cases where the edge was adequately anchored; and ***winnowing*** of sediment between the mat and the bridge pier, if the mat is not sealed tightly to the pier.

3.2 Experimental Investigation

An experimental study of scour countermeasures at bridge abutments is briefly reported. Two types of bridge abutment are considered, namely wing-wall (WW) abutments situated near the bank of relatively narrow bridge crossings where mobile-bed conditions exist, and spill-through (ST) abutments situated on the flood plain of wide river crossings where clear-water conditions pertain. Riprap and cable-tied block protection were included in the study.

The purpose of the WW abutment study was to determine the required apron size to protect an abutment from live-bed scour for different flow depths, flow velocities, and apron burial depths. Apron widths for both riprap and cable-tied block countermeasures were varied. Under mobile-bed conditions, it was observed that the troughs of the bed forms that bypass the abutment undermine the

apron, causing the outer edge of the countermeasure to settle, i.e. bed form undermining 'failure' occurs. Typical experiments using riprap and cable-tied block protection are shown in Figure 8.

The results show that as the flow depth and flow velocity are increased, the outer edge of the apron settles into the sand, to a depth proportional to the height of the bed forms developed in the flume. When the apron width is increased, the depth to which the outer edge settles remains constant. When the apron is pre-buried below the average bed level, the settlement of the outer edge is less, but the depth of the outer edge of the apron below the average bed level is the same as for the corresponding apron placed on top of the bed.

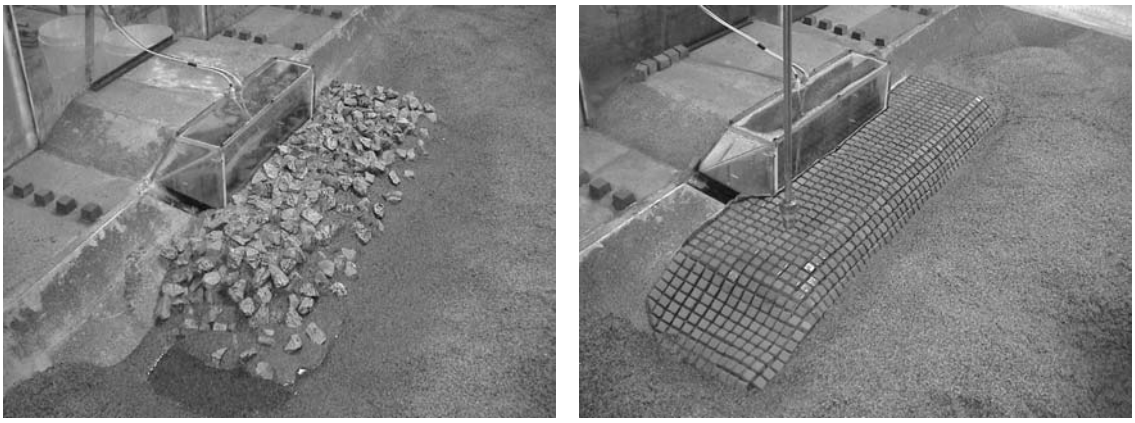

Figure 8 Riprap and cable-tied block protection at wing-wall abutments

The results also show that riprap and cable-tied block aprons respond in different ways. Stones in riprap aprons at the outer edge tend to settle and translate away from the abutment, pushing the bed form troughs further away from the abutment. Conversely, because cable-tied block aprons are constrained from moving laterally, the aprons settle allowing the troughs of the bed forms to pass closer to the abutment face. Also, under very high flow velocities, the cable-tied aprons curl over at the leading edge, allowing the flow to erode bed material from beneath the apron, resulting in excessive scour adjacent to the abutment.

From the study, it is concluded that the scour at abutments under live bed conditions is governed by the size of the bed forms that pass the abutment. Therefore, the design of riprap and cable-tied block scour protection for abutments under live bed conditions should be based upon the largest expected bed forms. This will enable the settlement of the outer edge of the apron to be determined, and the required apron width to be chosen, depending on the tolerable distance between the troughs and the abutment.

The ST abutment study was undertaken using a compound channel. The purpose of the study was to determine the variations in the scour-hole geometry under clear water conditions, by varying the compound channel and abutment geometries, and the extent of riprap and cable-tied block scour protection provided. This approach avoids one of the inherent difficulties in conducting scour countermeasure experiments, i.e. the subjectivity of determining whether the countermeasure used in the experiment is a success or failure. Riprap and cable-tied block countermeasures are incorporated. Typical results for both riprap and cable-tied block protection are shown in Figure 9.

The results show that for most cases, as the countermeasure apron width is increased, the scour hole is deflected further away from the abutment and reduces in size. However, for abutment and compound channel configurations where the scour hole forms close to the main channel bank, the scour hole increases in size as the apron width is increased. When the floodplain width is increased, the scour hole size increases for most cases, because less flow is diverted into the main channel upstream of the abutment. The results also show that cable-tied block mats allow the scour hole to form closer to the abutment compared to equivalent riprap aprons, and result in deeper scour holes. The project represents an improvement on the current, rather-simplified practice of providing aprons of fixed width equal to twice the flow depth.

The results enable determination of the local equilibrium scour formation for an abutment in question, for any level riprap and cable-tied block scour protection. If the level of protection provided predicts an undesirable scour hole formation locally at the abutment, the designer can increase the level of protection or change the type of protection, until the expected scour-hole formation at the abutment is tolerable. This method has the advantage that the countermeasure protection can be designed to be site specific for each bridge abutment. Abutments with deep foundations may not require much countermeasure protection, because larger scour-hole formations closer to the abutment may be tolerable. Conversely, abutments with shallow foundations may require more countermeasure protection, because scour-hole formations close to the abutment would be unacceptable.

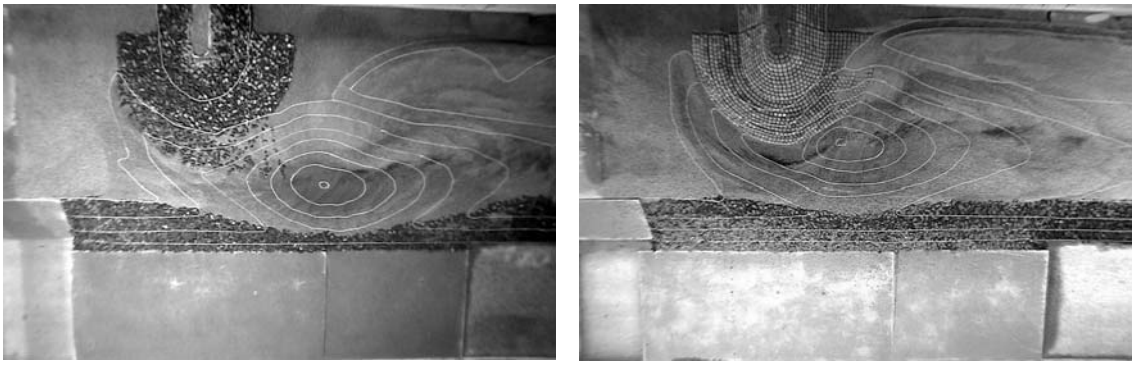

Figure 9 Riprap and cable-tied block protection at spill-through abutments

Preliminary results have been analysed using regression techniques to give the following expression for W_{min} the minimum width of apron after scour hole development (refer Figure 10):

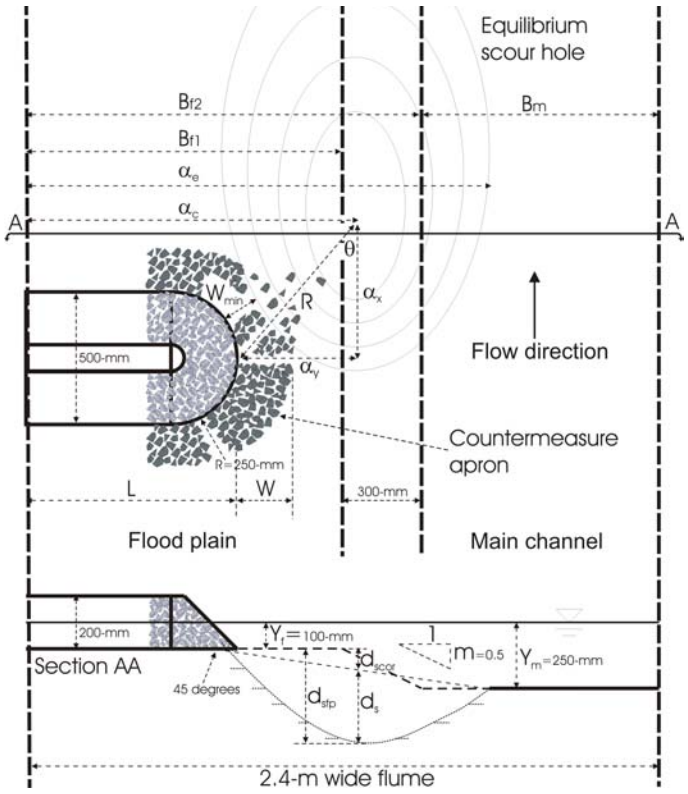

Figure 10 Set-up for spill-through abutment protection experiments

$$\frac{W_{\min}}{L} = \begin{cases} \omega \left(\frac{\sqrt{R^2 + d_{sfp}^2}}{L} \right)^{-0.012} \left(\frac{\alpha_c}{L} \right)^{-0.020} \left(\frac{L}{B_{f1}} \right)^{0.003} + \xi & W_{\min} < W \\ \frac{W}{L} & W_{\min} > W \end{cases} \quad (5)$$

In (5), $\alpha_c = R\sin\theta + L$, ξ = 49.3 and 28.3 and ω = -50.0 and –28.5 for riprap and cable-tied blocks, respectively. Expressions, obtained from the data, for R and d_{sfp} are given in Appendix A.

When the value of W_{min} is negative, insufficient protection has been provided for the given abutment geometry. The scour hole that is formed will undermine the abutment, causing the material from the abutment to slump into the scour hole. When $W_{min} > W$, the edge of the scour hole forms next to the apron, and the condition is reached for which the resultant scour hole no longer erodes the outer edge of the apron. This means that a further increase in apron width will deflect the scour hole further away from the abutment by the same distance. The scour hole will also become smaller until eventually the apron is wide enough that all scour has been eliminated locally at the abutment.

4. ACKNOWLEDGEMENT

The first part of this paper is based on an extensive programme of research conducted at The University of Auckland, much of which was funded by Transfund New Zealand. The work of the many postgraduate students involved in the research programme is acknowledged. The current study on scour countermeasures is funded by the US National Cooperative Highway Research Programme.

5. REFERENCES

Bertoldi, D.A. et al. (1994) "An experimental study of protection alternatives at bridge piers," Federal Highway Admin., Turner-Fairbank Laboratory, Virginia.

Blodgett, J.C. and McConaughy, C.E. (1985) "Evaluation of rock riprap design practices for protection of channels near highway structures - Phase I," Preliminary Report subject to revision, prepared by the U.S. Geological Survey in cooperation with Federal Highway Administration.

Chiew, Y.M. (1984) "Local scour at bridge piers," Report No. 355, School of Engineering, The University of Auckland, Auckland, New Zealand, 200pp.

Chiew, Y.M. (1995) "Mechanics of riprap failure at bridge piers," *Journal of Hydraulic Engineering,* A.S.C.E., 121(9), 635-643.

Coleman, S.E., Lauchlan, C.S. and Melville, B.W. "Clear-water scour development at bridge abutments," *Journal of Hydraulic Research*, IAHR, 41(5), 521-532.

Dongol, D. M. S. (1994). "Local scour at bridge abutments." Report No. 544, School of Engineering, The University of Auckland, Auckland, New Zealand, 409pp.

Ettema, R. (1980) "Scour at bridge piers," Report No. 216, School of Engineering, The University of Auckland, Auckland, New Zealand, 527pp.

Eve, N.J. (1999), "Riprap protection of bridge abutments", M.E. Thesis, Civil and Resource Engineering Department, The University of Auckland, Auckland, New Zealand.

Hoe, D.A. (2001) "Cable-tied block protection of bridge abutments," Project Report No. PCRE 01:18, Department of Civil and Resource Engineering, The University of Auckland, Auckland, New Zealand, 75pp.

Garde, R.J. (1961) "Local bed variation at bridge piers in alluvial channels," *Univertsity of Roorkee Research Journal*, Vol. IV, No. 1, 101-116.

Gill, M.A. (1972) "Erosion of sand beds around spur dikes," *Journal of the Hydraulics Division*, A.S.C.E., 98(9), 1587-1602.

Jones, J.S., Bertoldi, D.A. and Stein, S. (1995) "Alternative scour countermeasures," Proc., Hydraulic Engineering '95, San Antonio, Texas, U.S.A.

Kandasamy, J.K. (1989) "Abutment scour," Report No. 458, School of Engineering, The University of Auckland, Auckland, New Zealand, 278pp.

Kwan, T. F. (1984). "Study of abutment scour." Report No. 328, School of Engineering, The University of Auckland, Auckland, New Zealand, 225pp.

Kwan, T.F. (1988) "A study of abutment scour," Report No. 451, School of Engineering, The University of Auckland, Auckland, New Zealand, 461pp.

Lauchlan, C.S. (1999) "Countermeasures for pier scour," PhD thesis, The University of Auckland, Auckland, New Zealand.

Laursen, E.M. (1960) "Scour at bridge crossings," *Journal of the Hydraulics Division*, A.S.C.E., 86(2), 39-54.

McCorquodale, J.A. et al. (1993) "Guide for Design and Placement of Cable-Tied Block Erosion Protection," Proceedings Hydraulic Engineering, San Francisco, 1357-1362.

Melville, B. W., and Coleman, S. E. (2000). *Bridge scour*. Water Resources Publications, LLC, Colorado, U.S.A. 550pp.

Parker, G., Toro-Escobar, C. and Voigt, R.L., Jr. (1998) "Countermeasures to protect bridge piers from scour," Draft Final Report (Project NCHRP 24-7) prepared for National Co-operative Highway Research Program, University of Minnesota, Minneapolis, Minnesota, U.S.A., 402pp.

Parola, A.C. (1993) "Stability of riprap at bridge piers," *Journal of Hydraulic Engineering*, A.S.C.E., 119(10), 1080-1093.

Przedwojski, B., Blazejeski, R. and Pilarczyk, K.W. (1995) *River Training Techniques*, A.A. Balkema, Rotterdam, Netherlands.

Tey, C. B. (1984). "Local scour at bridge abutments." Report No. 329, School of Engineering, The University of Auckland, Auckland, New Zealand, 111pp.

Wong, W.H. (1982) "Scour at bridge abutments," Report No. 275, School of Engineering, The University of Auckland, Auckland, New Zealand, 109pp.

6. APPENDIX A

Expressions, obtained from the data, for R and d_{sfp} are given below (refer Figure 10)

$$\frac{R}{L} = 1.8\left(\frac{W}{L}\right)^{\psi}\left(\frac{L}{B_{f1}}\right)^{\zeta} + .014 \tag{6}$$

where ψ =0.48 and 1.18, and ζ = 0.23 and –0.22 for riprap and cable-tied blocks, respectively. The scour depth below the flood channel level is given by

$$d_{sfp} = d_s + d_{scor} \tag{7}$$

where

$$\frac{d_s}{L} = -18\left(\frac{\alpha_c}{L}\right)^{0.012}\left(\frac{L}{B_{f1}}\right)^{0.012} + 18 \tag{8}$$

The scour depth correction, which allows for the effect on scour hole formation when this intersects the main-channel bank, is given by the following expression

$$d_{scor} = \begin{cases} 0 & 1 > \dfrac{\alpha_e}{B_{f1}} \\ \left[\dfrac{\alpha_e - B_{f1}}{\alpha_e^* - B_{f1}}\right]\left(\dfrac{\alpha_c\left(y_m - y_f\right)}{B_{f2}}\right) & \dfrac{\alpha_e}{B_{f1}} > 1 > \dfrac{\alpha_c}{B_{f1}} \\ \dfrac{\alpha_c\left(y_m - y_f\right)}{B_{f2}} & \dfrac{\alpha_c}{B_{f1}} > 1 > \dfrac{\alpha_c}{B_{f2}} \\ y_m - y_f & \dfrac{\alpha_c}{B_{f2}} > 1 \end{cases} \qquad (9)$$

in which $\alpha^*_e = 0.65\alpha_c^{14} L^{-0.4} + L$ is the value of α_e when $\alpha_c = B_{fl}$.

The Institution of Engineers, Australia
8th National Conference on Hydraulics in Water Engineering
ANA Hotel Gold Coast, Australia 13-16 July 2004

Hydrodynamic Effects in Aquatic Ecosystems

V. Nikora
B.E., Ph.D.
Principal Scientist, National Institute of Water and Atmospheric Research, New Zealand

Abstract: The strategic goals of flow-biota interactions studies are to develop their better understanding and to build process-based, robust and practical computer models capable of predicting biota responses to various physical processes occurring in aquatic systems. To achieve these goals two key inter-connected components of the problem are being studied: (i) physical interactions between flow and organisms (e.g., due to drag forces); and (ii) ecologically relevant mass-transfer-uptake processes (e.g., due to molecular and turbulent diffusion). These issues can be addressed using double-averaged (in time and in space) hydrodynamic equations, which are briefly discussed. To illustrate application of this relatively new methodology, three examples are provided: (1) identification of specific flow layers and flow types depending on relative submergence of roughness elements, including near-bed organisms; (2) vertical distribution of the double-averaged velocity in the biologically active near-bed region; and (3) mass-transfer-uptake processes in periphyton community.

Keywords: aquatic systems, flow-biota interactions, mass-transfer-uptake processes, periphyton, turbulence.

1. INTRODUCTION

Many recent studies have shown that near-bed hydrodynamics controls most of the biophysical processes that determine benthic communities in streams, estuaries, lakes and seas (e.g., Hart and Finelli, 1999; Boudreau and Jorgensen, 2001). The importance of biophysical processes in developing better management strategies for aquatic systems has led to the emergence of several quickly growing branches of fluid mechanics and hydraulics known as ecohydraulics, environmental hydraulics, environmental fluid mechanics and biofluiddynamics. These new disciplines, although still emerging and vaguely defined, cover a wide range of aquatic environments, scales and organisms, and represent a good example of a multidisciplinary approach in modern science. A comprehensive consideration of hydrodynamic aspects of this topic is hardly possible, as it would involve too many habitat types, species, research approaches and practical issues. Instead, we will briefly review some recent results obtained at the National Institute of Water and Atmospheric Research (NIWA) in New Zealand, where this multidisciplinary research direction has been quickly developing in response to changing resource management needs. NIWA conducts extensive biophysical studies in streams, estuaries, lakes, coastal waters and deep seas. In this paper, however, we will mainly focus on biophysical processes in streams, which are closer to the writer's main research interests.

The main goals of NIWA's flow-biota interactions studies are to develop their better understanding and to build process-based, robust and practical computer models capable of predicting biota responses to various physical processes occurring in streams. To achieve these strategic goals we study two key inter-connected components of the problem: (i) physical interactions between flow and organisms (e.g., due to drag and viscous forces); and (ii) ecologically relevant mass-transfer-uptake processes (e.g., due to molecular and/or turbulent diffusion). Both components are organism-specific and may differ significantly among species. They may also strongly depend on particular physical conditions such as turbulence characteristics, bed topography, substratum, and permeability. Our approach combines the advantages of both field and laboratory experiments, and is based on the 'double-averaging' methodology originally developed for the 'air flow-terrestrial canopy' problem (e.g., Finnigan, 2000). While time (ensemble)-averaged hydrodynamic equations are standard and widely used in research and applications, double-averaged (in time and in space) equations are much less known in hydraulics and are mainly used in atmospheric physics for describing flows in terrestrial canopies. Double-averaging methodology provides a better tool for investigating rough-bed flows, including those within and above benthic communities, and therefore we adopt it in our aquatic research. This approach will be summarized first. Then, some examples of near-bed processes addressed using this methodology will be provided and discussed.

2. NEAR BED HYDRODYNAMICS IN AQUATIC SYSTEMS

Most researchers have studied natural stream flows and their effects on flow biota using the time (ensemble)-averaged Navier-Stokes equations for fluid (known as the Reynolds equations) and advection-diffusion equations for passive substances, often referred to as "scalars". These equations have been used as a key tool for both modelling and interpreting numerical and experimental results. However, in many situations these equations are not practicable due to the highly heterogeneous three-dimensional structure of the mean flow and turbulence, especially in the biologically active near-bed region. For example, 2-D approximations based on the Reynolds equations, as well as similarity considerations for time-averaged variables, are not possible for the near-bed region in rough-bed flows. Also, most applications deal with spatially-averaged roughness parameters that cannot be linked explicitly with local flow properties provided by the Reynolds equations. These conceptual contradictions have been essentially ignored in many studies. For instance, in some studies the 2-D Reynolds equations were artificially modified by introducing the form drag as an extra body force term and then used to describe the 3-D near-bed flow structure.

To resolve the problem conceptually, the time (ensemble) averaging of the Navier-Stokes and advection-diffusion equations should be supplemented by volume averaging (within a thin slab) or area averaging in the plane parallel to the bed. The double-averaged (in time and space) equations relate to the time (ensemble) averaged equations as the latter relate to the Navier-Stokes and advection-diffusion equations for instantaneous hydrodynamic variables. The double-averaging procedure gives new momentum and continuity equations for fluid, which explicitly contain important additional terms such as form-induced stresses, and form and viscous drag terms. Similarly, the double-averaged advection-diffusion equations for passive substances and suspended sediments explicitly contain form-induced fluxes as well as terms describing interface transport (e.g., nutrient uptake by aquatic vegetation or sediment erosion). These terms do not appear in the conventional time (ensemble)-averaged equations. Within this approach, similarity hypotheses and 2-D assumptions may be developed and applied even for the flow region below roughness crests, which is impossible using the conventional time-averaged variables. An additional advantage of using double-averaged hydrodynamic parameters is a better link of the surface fields of hydrodynamic variables with their sub-surface counterparts within the porous bed, where volume-averaged variables are traditionally used. Note that the term 'roughness elements' is used in this paper to describe both types of roughnesses: physical (e.g., bed cobbles) and biological (e.g., mussel field).

The double-averaging methodology stems from multi-phase and groundwater flow hydrodynamics, in which it has been developing since the sixties (an extensive mathematical treatment of the problem may be found, e.g., in Slattery, 1999). In the seventies, a similar approach was introduced in the aerodynamics of canopy flows (Wilson and Shaw, 1977; Rapauch and Shaw, 1982; Finnigan, 1985). Later, this methodology was adopted for studying rough-bed hydrodynamics and flow-biota interactions in open-channels and streams (Lopez and Garcia, 2001; Nikora et al., 2001, 2002a,b, 2003a,b, 2004; Walters, 2002; Nikora, 2004). However, implementation of the double-averaging methodology in modelling, experimental design, and data interpretation in biophysical studies of streams has only begun. A brief overview of the double-averaged equations, based on Nikora (2004), is provided below. The right-handed coordinate system is implied throughout the paper, i.e., *x*-axis is oriented along the main flow parallel to the averaged bed (*u*-velocity component), *y*-axis is oriented to the left bank (*v*-velocity component), and *z*-axis is pointing towards the water surface (*w*-velocity component), with an arbitrary origin.

The time (ensemble)-averaged momentum and continuity equations may be written for the case of open-channel flows as (e.g., Monin and Yaglom, 1971):

$$\frac{\partial \overline{u}_i}{\partial t} + \overline{u}_j \frac{\partial \overline{u}_i}{\partial x_j} = g_i - \frac{1}{\rho}\frac{\partial \overline{p}}{\partial x_i} - \frac{\partial\, \overline{u_i' u_j'}}{\partial x_j} + \frac{\partial}{\partial x_j}\left(\nu \frac{\partial \overline{u}_i}{\partial x_j}\right), \qquad \frac{\partial \overline{u}_i}{\partial x_i} = 0 \tag{1}$$

which, after volume averaging, give the following double-averaged momentum and continuity equations:

$$\frac{\partial \langle \overline{u}_i \rangle}{\partial t} + \langle \overline{u}_j \rangle \frac{\partial \langle \overline{u}_i \rangle}{\partial x_j} = g_i - \frac{1}{A\rho}\frac{\partial A\langle \overline{p} \rangle}{\partial x_i} - \frac{1}{A}\frac{\partial A\langle \overline{u_i' u_j'} \rangle}{\partial x_j} - \frac{1}{A}\frac{\partial A\langle \tilde{u}_i \tilde{u}_j \rangle}{\partial x_j} + \frac{1}{A}\frac{\partial}{\partial x_j} A\left\langle \nu \frac{\partial \overline{u}_i}{\partial x_j} \right\rangle - \frac{\langle \overline{u}_i \rangle}{A}\frac{\partial A}{\partial t} +$$

$$+ \frac{1}{V_f \rho}\iint_{S_{\text{int}}} \overline{p} n_i dS - \frac{1}{V_f}\iint_{S_{\text{int}}} \left(\nu \frac{\partial \overline{u}_i}{\partial x_j}\right) n_j dS - \frac{1}{V_f}\iint_{S_{\text{int}}} \langle \overline{u}_i \rangle \overline{u}_j n_j dS + \frac{1}{V_f}\iint_{S_{\text{int}}} \overline{u}_i (\overline{u}_j - \upsilon_j) n_j dS + \frac{1}{V_f}\iint_{S_{\text{int}}} \overline{u_i' u_j'} n_j dS ,$$

$$\left\langle \frac{\partial \overline{u}_i}{\partial x_i} \right\rangle = \frac{1}{A}\frac{\partial A\langle \overline{u}_i \rangle}{\partial x_i} - \frac{1}{V_f}\iint_{S_{\text{int}}} \overline{u}_i n_i dS = 0 \qquad \text{or} \qquad \frac{1}{A}\frac{\partial A\langle \overline{u}_i \rangle}{\partial x_i} = \frac{1}{V_f}\iint_{S_{\text{int}}} \overline{u}_i n_i dS \tag{2}$$

For 'frozen' roughness elements we have $(1/V_f)\iint_{S_{\text{int}}} \overline{u}_i n_i dS = 0$ and, thus, $(1/A)\partial A\langle \overline{u}_i \rangle / \partial x_i = 0$, i.e., $\partial A\langle \overline{u}_i \rangle / \partial x_i = 0$. For some biologically modified beds (e.g., waving vegetation) this simplification may not be valid. The time-averaged advection-diffusion equation for passive scalars (e.g., dissolved nutrients) may be written as (e.g., Monin and Yaglom, 1971):

$$\frac{\partial \overline{\varphi}}{\partial t} + \frac{\partial \overline{u}_j \overline{\varphi}}{\partial x_j} = \frac{\partial}{\partial x_j}\left(\chi_m \frac{\partial \overline{\varphi}}{\partial x_j} \right) - \frac{\partial\, \overline{u_j' \varphi'}}{\partial x_j} + F \tag{3}$$

which, after volume averaging, provides the following double-averaged advection-diffusion equation:

$$\frac{\partial \langle \overline{\varphi} \rangle}{\partial t} + \langle \overline{u}_j \rangle \frac{\partial \langle \overline{\varphi} \rangle}{\partial x_j} = \frac{1}{A}\frac{\partial}{\partial x_j} A\left\langle \chi_m \frac{\partial \overline{\varphi}}{\partial x_j} \right\rangle - \frac{1}{A}\frac{\partial A\langle \overline{u_j' \varphi'} \rangle}{\partial x_j} - \frac{1}{A}\frac{\partial A\langle \tilde{u}_j \tilde{\varphi} \rangle}{\partial x_j} - \frac{\langle \overline{\varphi} \rangle}{A}\frac{\partial A}{\partial t} - \frac{1}{V_f}\iint_{S_{\text{int}}} \left(\chi_m \frac{\partial \overline{\varphi}}{\partial x_j} \right) n_j dS -$$

$$- \frac{1}{V_f}\iint_{S_{\text{int}}} \overline{u}_j \langle \overline{\varphi} \rangle n_j dS + \frac{1}{V_f}\iint_{S_{\text{int}}} \overline{\varphi}(\overline{u}_j - \upsilon_j)\, n_j dS + \frac{1}{V_f}\iint_{S_{\text{int}}} \overline{u_j' \varphi'} n_j dS + \langle F \rangle \tag{4}$$

In the equations above, the straight overbar and angle brackets denote the time (ensemble) and spatial averaging of flow variables, respectively; the wave overbar denotes the disturbance in the flow variables, i.e., the difference between the double-averaged ($\langle \overline{\theta} \rangle$) and time-averaged ($\overline{\theta}$) values, ($\tilde{\theta} = \overline{\theta} - \langle \overline{\theta} \rangle$), similar to the Reynolds decomposition ($\theta' = \theta - \overline{\theta}$); S_{int} is the surface of bed features (e.g., boundary between water and sediment particles or plants) within the averaging domain defined by the longitudinal, transverse, and vertical length-scales of roughness elements; $A = V_f / V_o$ is 'porosity' that for the flow-bed interface may be interpreted as the roughness geometry function (Nikora et al, 2001), where V_f is the averaging volume occupied by fluid within an averaging region *R* with the total volume V_o centred at level *z*; φ is the passive substance concentration; υ_i is the velocity of bed surface features (e.g., waving plants or moving gravels); *F* is the source/sink of the substance φ; χ_m is molecular diffusion coefficient for substance φ; ν is kinematic viscosity; **n** is the inwardly directed (into the fluid) unit vector normal to the bed (organism) surface; g_i is the *i*-th component of the gravity acceleration; and ρ is fluid density. In the equations above we assume that the flow variables are 'well-behaved', i.e., $\left\langle \langle \overline{\theta} \rangle \right\rangle = \langle \overline{\theta} \rangle$ and $\left\langle \tilde{\theta} \right\rangle = 0$. An equation similar to (4) may be also obtained for suspended sediments (Nikora, 2004).

The volume averaging has several advantages over the area averaging considered in Raupach and Shaw (1982), Gimenez-Curto and Corniero Lera (1996) and Nikora et al. (2001). The key advantages include: (1) volume averaging better suits real measurements which are always made within a finite volume, not area; (2) transformations of hydrodynamic equations are simpler; (3) volume averaged equations can be equally applied for surface and subsurface flows, with variable sizes of the averaging domain *R* depending on the heterogeneity of the studied flow region. In open-channels and many natural streams, there are strong vertical gradients in flow properties, especially near the biologically active bed, and therefore the volume-averaging domain should be designed as a thin slab parallel to the bed. For reasonably homogeneous and uniform flow regions (e.g., well below the sediment-water interface) the averaging window may be thicker. The dimensions of the averaging domain in the plane parallel to the bed should be much larger than the longitudinal and transverse correlation lengths of rough bed elevations, but much smaller than the large-scale features in bed topography. For example, for gravel-bed rivers it should be much larger than gravel particles but much smaller than riffles or pools. Similar criteria apply for biologically modified beds such as streambeds covered by macrophyte or mussel patches.

Equations (2) and (4) describe relations between spatially-averaged flow properties and contain some additional terms in comparison with the conventional time-averaged equations (1) and (3). These terms include dispersive or form-induced stresses $\langle \tilde{u}_i \tilde{u}_j \rangle$ and fluxes $\langle \tilde{u}_j \tilde{\varphi} \rangle$ due to spatial disturbances in time-averaged fields, the form drag $f_{p_i} = 1/V_f \iint_{S_{\text{int}}} \overline{p} n_i dS$ and viscous drag $f_{vi}/\rho = -1/V_f \iint_{S_{\text{int}}} \left(\nu \partial \overline{u}_i / \partial x_j \right) n_j dS$ on roughness elements

(including near-bed organisms such as periphyton, mosses, macrophytes, or mussels), flux at the water – organism interfaces $R_V = -1/V_f \iint_{S_{int}} \left(\chi_m \partial\overline{\varphi}/\partial x_j\right) n_j dS$, and other surface integrals describing potential interfacial transport mechanisms. In principle, all terms in the double-averaged equations (2) and (4) may be important. Their significance for different hydrodynamic and biological conditions on the bed awaits proper assessment. Note that the quantities $\langle \tilde{u}_i \tilde{u}_j \rangle$ and $\langle \tilde{u}_j \tilde{\varphi} \rangle$ in equations (2) and (4) follow from spatial averaging, similar to $\overline{u_i' u_j'}$ and $\overline{u_j' \varphi'}$ in the time-averaged equations, which appear due to time averaging of the Navier-Stokes and advection-diffusion equations for instantaneous variables. An important feature of the double-averaged equations is the dependence on the roughness geometry accounted for by the function $A(x, y, z)$, which is $A \equiv 1$ above roughness tops and $A < 1$ below them (Nikora et al., 2001).

In many respects equations (2) and (4) represent a better basis for mathematical and numerical models of flow-biota interactions and mass-transfer-uptake processes, designing new experiments, and interpreting experimental data, compared to their time-averaged counterparts (1) and (3). Some of parameterizations based on equations (2) and (4) and their preliminary tests are discussed below. Before we proceed further, it is worth noting that as with equations (2) and (4), the double-averaged equations for turbulence energy, shear stresses, and scalar fluxes also contain important additional transport and production terms such as wake production (due to wake effects behind near-bed organisms) and waving production (due to the effects of mobile interfaces, e.g., when plants wave in response to fluctuating hydrodynamic forces or due to the bedload in gravel-bed streams).

3. SPECIFIC FLOW LAYERS AND FLOW TYPES

To simplify applications of the double-averaged equations (2) and (4) it may be useful to subdivide the flow into specific layers as well as to identify flow types possessing distinct specific properties. Based on an analysis of the double-averaged momentum and scalar transport equations, four flow types may be suggested (Nikora, 2004) depending on flow submergence H_m/Δ, where H_m is the maximum flow depth and Δ is the characteristic roughness height applied for both physical and/or biological features (Figure 1). In general, roughness elements of physical origin (e.g., cobbles) may be much smaller, comparable, or much larger than the roughness elements of biological origin (e.g., periphyton).

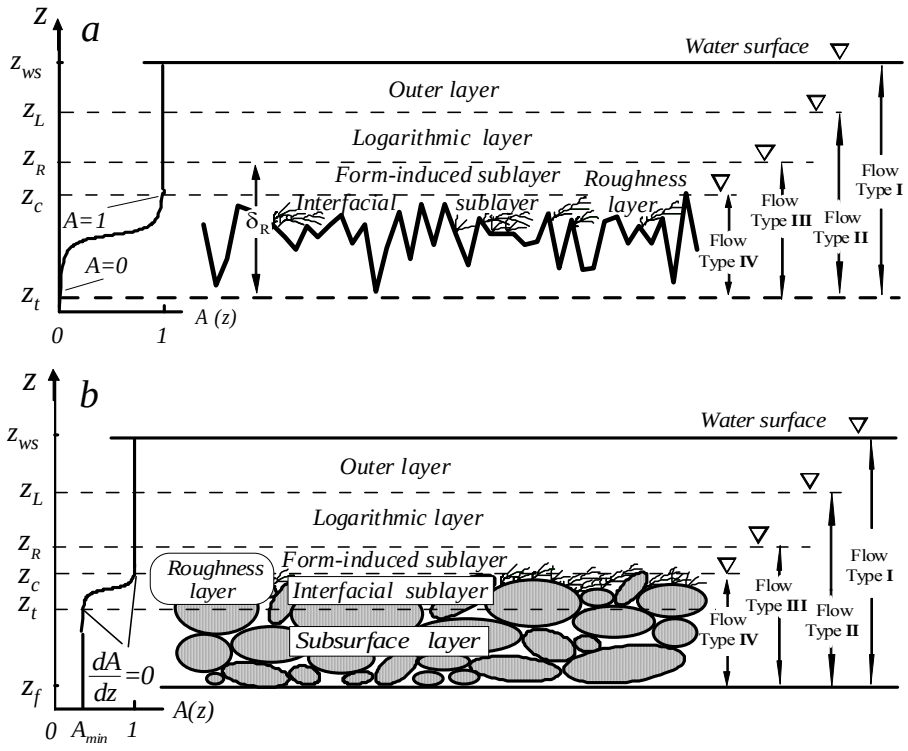

Figure 1 – The flow subdivision into specific regions: (a) impermeable bed, and (b) permeable bed.

The flow type **I** is the flow with high relative submergence, which contains several layers and sublayers: (1) the outer layer, where viscous effects and form-induced momentum and substance fluxes are negligible, and the

double-averaged equations are identical to the time-averaged equations; (2) the logarithmic layer; (3) the form-induced (or dispersive) sublayer, just above the roughness crests, where the time-averaged flow may be influenced by individual roughness elements, and thus the terms $\langle \tilde{u}_i \tilde{u}_j \rangle$ and $\langle \tilde{u}_j \tilde{\varphi} \rangle$ may become non-zero; and (4) the interfacial sublayer, which is also influenced by individual roughness elements, and which occupies the flow region between roughness crests and troughs (or between the bed surface and organism tops). The key distinct features of the interfacial sublayer are the form and viscous drag forces acting on roughness elements (including near-bed organisms) as well as interfacial transport of substances between the flow, organisms, and the bed. Together the form-induced and interfacial sublayers form *the roughness layer*. In case of permeable beds there is also an additional, subsurface layer below the roughness layer (Figure 1). The other three flow types are: (**II**) flow with intermediate relative submergence consisting of the subsurface layer (if applicable), a roughness layer, and an upper flow region which does not manifest logarithmic velocity and concentration profiles as the ratio H_m / Δ is not large enough; (**III**) flow with small relative submergence with a roughness layer extending to the free surface; and (**IV**) flow over a partially-inundated rough bed with the interfacial sublayer as the upper (or only) flow region (Figure 1). These four flow types cover the whole range of possible flow submergence H_m / Δ. For each flow type, a specific set of relationships/parameterizations describing 'double-averaged' flow properties may be developed, and some examples are considered in the sections below.

4. DRAG FORCES AND FLOW VELOCITY BELOW ROUGHNESS TOPS

The double-averaged momentum equation (2) contains two drag terms f_p and f_v that need to be parameterized. In this section we demonstrate that even a simple parameterization of these terms may lead to meaningful and testable results. In particular, we describe several relationships for the vertical distribution of the double-averaged longitudinal velocity in the biologically active region from roughness troughs to roughness tops. Following Nikora et al. (2004), consider the simplest case of two-dimensional, steady, uniform, double-averaged flow over a rigid rough bed with a flat free surface. The momentum equation (2) for such 'double-averaged' flow may be simplified as:

$$\rho g S_b + \frac{1}{A}\frac{dA\tau}{dz} + f_p + f_v = 0 \tag{5}$$

where the total fluid stress τ contains three components: viscous, turbulent, and form-induced (or dispersive) stresses, and S_b is the bed slope. Equation (5) may be further simplified by assuming that $(f_p + f_v) \approx -0.5 \rho C_D a < \overline{u} >^2$, where $a(z)$ is the local roughness density, i.e., the ratio of the frontal area of roughness elements to fluid (averaging) volume, and C_D is the drag coefficient (e.g., Finnigan, 2000). In Nikora et al. (2004) it has been shown that there are several specific expressions for velocity distribution within the interfacial sublayer (Figure 1), which may be deduced using equation (5). Simple phenomenological considerations suggest that at least three such expressions or models may exist. In practice, the double-averaged velocity profiles may be composed of some combination of these models. Within such composite profiles the combination, the existence, and the extent of the different regions (models) will depend on flow conditions, relative submergence, and the roughness geometry.

Model 1 relates to flows with vertically homogeneous roughness elements where wake turbulence dominates in the near-bed region:

$$\langle \overline{u} \rangle = \left(g S_b / 0.5 C_D a \right)^{0.5} \tag{6}$$

If C_D and a (or their product) do not depend on z then $\langle \overline{u} \rangle$ is constant within the interfacial sublayer (the constant velocity model). Examples may include partially submerged vegetation in streams or on an inundated floodplain (e.g., Rowinski and Kubrak, 2002).

Model 2 applies when the effect of the momentum flux downwards dominates over the gravity term in (5) that leads to the exponential velocity distribution:

$$\langle \overline{u} \rangle (z) = \langle \overline{u} \rangle (z_c) \exp \beta (z - z_c) \tag{7}$$

where $\langle\overline{u}\rangle(z_c)$ is the double-averaged velocity at the roughness tops z_c, and β is a parameter. A typical example is a low-slope flow over well-submerged aquatic plants such as reed.

Model 3 is represented by the linear velocity distribution:

$$\left[\langle\overline{u}\rangle(z)-\langle\overline{u}\rangle(z_c)\right]/u_* = (z-z_c)/l_c \tag{8}$$

where u_* is the shear velocity, and $l_c = \langle\overline{u}\rangle(z_c)/(d\langle\overline{u}\rangle/dz)_{z_c}$ is the shear length scale characterizing flow dynamics within the roughness layer. The parameter l_c scales with the thickness of the interfacial sublayer (Figure 1) and does not depend on the vertical coordinate z. The most realistic scenario for this case is the flow through roughness elements with $\partial A/\partial z > 0$. In principle, relationships (6)-(8) may be applicable for the interfacial sublayer for all four flow types defined above, from flows with large relative submergence to flows with partial submergence. Figure 2 shows examples of vertical distribution of the double-averaged velocities obtained in laboratory experiments covering roughness types with various densities and arrangements (Nikora et al., 2004). The data in Figure 2 support two types of velocity distribution, exponential (7) and linear (8). There are also some published data that support equation (6), e.g., Rowinski and Kubrak (2002).

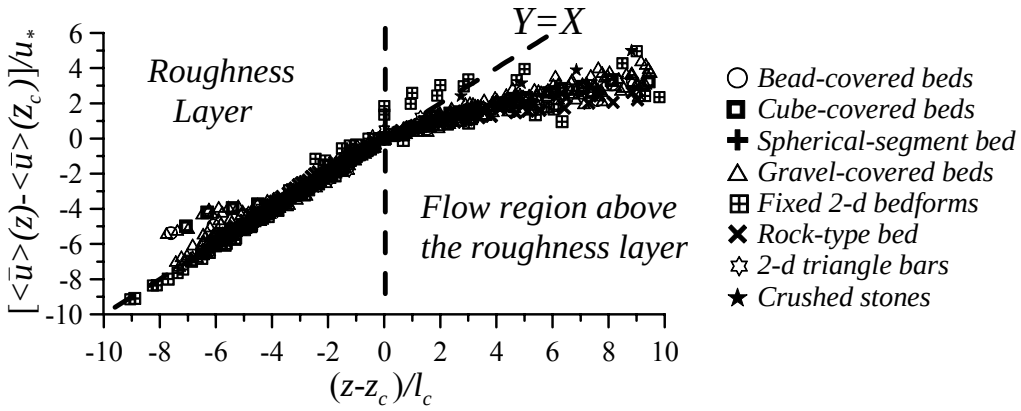

Figure 2 – Vertical distribution of the double-averaged velocities for various roughness types (Nikora et al., 2004). Deviations of the data points from Y=X are consistent with the exponential distribution (7).

5. MASS-TRANSFER-UPTAKE PROCESSES AND THEIR PARAMETERIZATION

5.1 Conceptual considerations

Mass-transfer-uptake processes in benthic communities represent interplay between turbulence, viscous effects, and the complex geometry of dynamic aquatic communities or canopies, which may be combined with hydraulically rough porous substrata such as gravel particles or sand ripples. In equation (4) the exchange between water flow and bed features (e.g., uptake by near-bed organisms) is mainly represented by the term $R_V = -1/V_f \iint_{S_{\text{int}}} \left(\chi_m \partial\overline{\varphi}/\partial x_j\right) n_j dS$ that needs to be parameterized (other 'interfacial' terms may also be important in some conditions).

Here we present an example of such parameterization for the case of a periphyton community in open-channel flow with a flat bed. Note that in the following considerations we use symbol *C* to define nutrient concentration, for consistency with other studies. Nikora at al. (2003b) and Larned et al. (2004) postulated that there are at least three distinct uptake regimes defined by the interactions between flow hydrodynamics and periphyton canopy, as illustrated in Figure 3. The uptake regime depends on the ratio of the canopy height h_c to the thickness of the diffusive sublayer $\delta_D = Sc^{-1/3}\delta_\nu$, where $Sc = \nu/\chi_m$ is the (molecular) Schmidt number, χ_m is a coefficient of molecular diffusion for a particular substance, $\delta_\nu = \alpha_\nu(\nu/u_*)$ is the thickness of the viscous sublayer, and α_ν is a constant (Levich, 1962). Note that we use the symbol δ_{Ds} to define the diffusive sublayer associated with the bed (substratum) surface, which may be different from the thickness δ_{Df} of the diffusive sublayer associated with the organism surface, i.e., an individual periphyton filament.

In regime 1, the periphyton canopy of height h_c is deeply submerged in the diffusive sublayer (i.e., $\delta_{Df} \approx \delta_{Ds} >> h_c$, Figure 3). The volume-averaged uptake rate $R_{V1}(x,y,z)$ for this regime may be parameterized as:

$$R_{V1} = \frac{n_f R \Delta A_f}{V_f} = \frac{n_f R \gamma d_f \Delta h_f}{V_f} = \gamma a \left(\frac{h_f}{h_c}\right)^2 \frac{h_c}{\delta_{Ds}} \left[\frac{\chi_m}{h_f} \Delta C_{f\infty}\right] = \gamma a \left(\frac{h_f}{h_c}\right)^2 \frac{h_c}{\delta_{Ds}} R_N \qquad (9)$$

where n_f is the number of periphyton filaments within the averaging domain with the vertical size Δz; $R = (\chi_m / \delta_{Df}) \Delta C_{f\infty}$ is the nutrient flux to a filament (per unit area) where δ_{Df} is the thickness of the diffusive sublayer associated with a filament, assumed to be equivalent to δ_{Ds} for this uptake regime (Figure 3), i.e., $\delta_{Df} \approx \delta_{Ds}$; $\Delta A_f = \gamma d_f \Delta h_f$ is the filament surface area within the averaging domain; Δh_f is the filament length within the averaging domain assumed to be equal to $\Delta z (h_f / h_c)$ where h_f is the total filament length; d_f is a filament diameter; γ is the shape coefficient representing a filament cross-section; $a = (n_f d_f \Delta z)/V_f$ is the local roughness density (recall that we used this parameter in section 4 and equation 6); $\Delta C_{f\infty}$ is the difference between the concentration in an upper fully mixed flow region and the concentration on the filament surface; and $R_N = (\chi_m / h_f) \Delta C_{f\infty}$ is the nominal uptake rate.

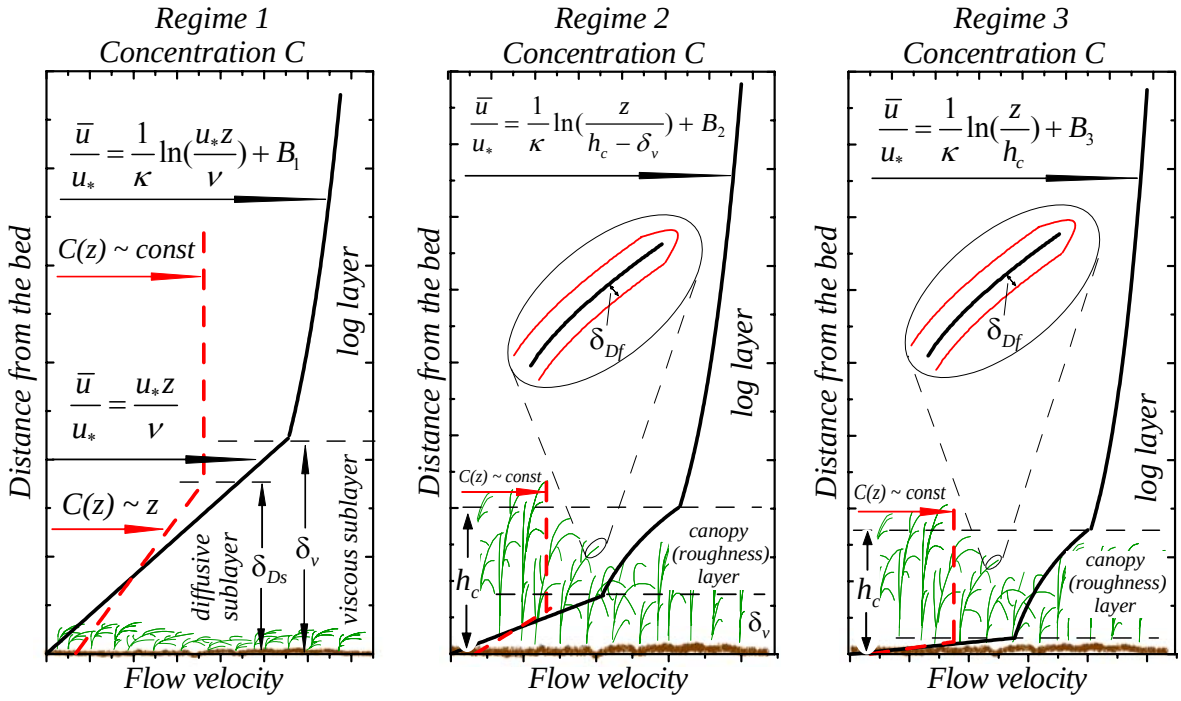

Figure 3 – Schematic diagram showing three mass-transfer-uptake regimes for stream periphyton.

Before we proceed to the intermediate uptake regime 2 we need to consider the other extreme, i.e., regime 3. In regime 3, the diffusive sublayer thickness δ_{Ds} is comparable to the filament diameter and, therefore, does not play any substantial role in the uptake processes, i.e., $\delta_{Ds} \approx d_f << h_c$ (Figure 3). Instead, uptake is controlled by the thickness δ_{Df} of the diffusive sublayers surrounding individual periphyton filaments. These filaments protrude for most of their length into the upper turbulent region (Figure 3). Thus, δ_{Df} becomes a dominant factor controlling the uptake rate R_{V3}, which may be parameterized, similar to R_{V1}, as:

$$R_{V3} = \gamma a \left(\frac{h_f}{h_c}\right)^2 \frac{h_c}{\delta_{Df}} R_N \qquad (10)$$

Regime 2 occupies an intermediate position between regimes 1 and 3 (Figure 3). For this regime, the thickness δ_{Ds} of the diffusive sublayer over the bed is less than the canopy height but larger than the filament diameter, i.e., $d_f < \delta_{Ds} < h_c$. Therefore, equation (9) applies for $z < \delta_{Ds}$ while equation (10) applies for $\delta_{Ds} < z < h_c$. For $\Delta z = h_c$ equations (9) and (10) are still valid for regimes 1 and 3 if the roughness density *a* does not depend on *z*. The uptake rate R_{V2} for regime 2 in this case will be a combination of (9) and (10), i.e.,

$$R_{V2} = R_{V1}\frac{\delta_{Ds}}{h_c} + R_{V3}\frac{h_c - \delta_{Ds}}{h_c} = \gamma a\left(\frac{h_f}{h_c}\right)^2 \frac{h_c}{\delta_{Dg}} R_N \qquad (11)$$

assuming that the roughness geometry function *A*, introduced in (4), is approximately the same for $z < \delta_{Ds}$ and for $\delta_{Ds} < z < h_c$, and where $\delta_{Dg} = \delta_{Df} h_c / (\delta_{Df} + h_c - \delta_{Ds})$ is the generalized thickness that combines effects of both regimes 1 and 3. Indeed, for regime 1 we have $\delta_{Df} \approx \delta_{Ds}$ and, therefore, $\delta_{Dg} = \delta_{Df} h_c / (\delta_{Df} + h_c - \delta_{Ds}) \approx \delta_{Ds}$. For regime 3 we have $h_c >> \delta_{Df}$, $h_c >> \delta_{Ds}$ and, therefore, $\delta_{Dg} = \delta_{Df} h_c / (\delta_{Df} + h_c - \delta_{Ds}) \approx \delta_{Df}$. Note that the ratio h_c / δ_{Dg} is proportional to the canopy Peclet number, which is a ratio of convective (turbulent) effects to molecular diffusion effects in the transport of substances. Our conceptual model shows that molecular diffusion will still control uptake even at very large Peclet numbers, as the diffusive sublayers surrounding individual filaments are the key regions limiting mass-transfer.

Equations (9) to (11) include two parameters, δ_{Dg} and h_c, which depend on interactions between periphyton and flow. The thickness of the diffusive sublayer δ_{Dg} can be obtained using the relationship $\delta_{Di} = Sc^{-1/3}\delta_v = Sc^{-1/3}\alpha_{vi}(\nu / u_*) \propto u_*^{-1}$ where the factor α_{vi} depends on the uptake regime *i* = 1, 2, or 3. Its value for regime 1 can be assumed as $a_{v1} \approx 10$ (Levich, 1962) while for other regimes it needs to be obtained from experiments. To define h_c as a function of hydrodynamic conditions, let us consider the following arguments. From the physical point of view, the periphyton mat on the bed is a special case of a rough boundary: its roughness properties are not stable and change depending on many environmental conditions. A full analytical description of the interaction between periphyton and flow is not possible at this stage since many details of this process are not yet known. However, some simplified analysis, which may be useful as a first step, is possible. Let us assume that the main forces acting upon a given periphyton filament are the drag force $F_d = \rho(C_d / 2)h_c d_f u_*^2$ and the difference between the buoyancy force and the gravity force $F_b = g(\rho - \rho_p)\chi d_f^2 h_f$, where $h_c = h_f \sin\psi$; ψ is the angle between the bed plane and a filament, which depends on the flow velocity near the bed ($\psi \approx 90^o$ in still water and tends to zero at large flow velocity); C_d is the drag coefficient that depends on a filament Reynolds number; ρ_p is periphyton mass density (which also accounts for air micro-bubbles attached if any); and χ is the coefficient which depends upon the cross section shape of a filament (Figure 4a).

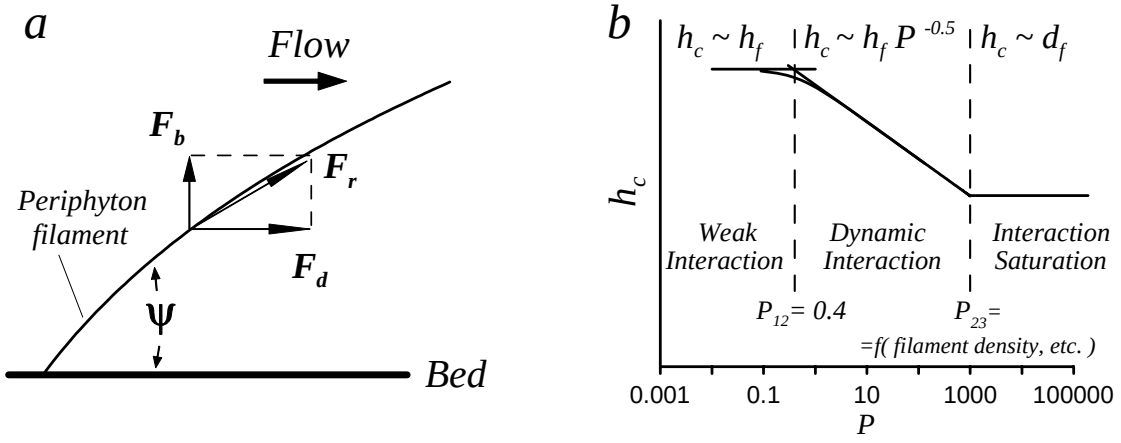

Figure 4 – The main forces acting upon a periphyton filament (a) and a schematic plot $h_c = f(P)$ (b).

Note that a periphyton mat is often positively buoyant because, in part, oxygen produced during photosynthesis is usually trapped in the mat or attached to filaments as air micro-bubbles. When the buoyancy and drag forces resolved normal to the filament are balanced, the filament will be in stable equilibrium. In this case the balance of forces is $F_d \sin\psi = F_b \cos\psi$ that gives a relationship for the angle ψ :

$$\frac{\cos\psi}{1-\cos^2\psi} = \frac{C_d}{2}\ \frac{1}{\chi}\ \frac{\rho}{\rho-\rho_p}\ \frac{u_*^2}{gd_f} \quad \text{or} \quad \psi = f(P)\ , \quad P = \frac{C_d}{2}\ \frac{1}{\chi}\ \frac{\rho}{\rho-\rho_p}\ \frac{u_*^2}{gd_f} \tag{12}$$

Here *P* is the ratio of the main scale of the drag force to the main scale of the buoyancy force. The ratio *P* can be considered as a characteristic 'periphyton' number describing the periphyton-flow interaction. Equations (12) can be reasonably approximated as $\psi \approx 57.3P^{-0.5}$.

At small *P*, we expect a weak interaction when a periphyton filament resists the flow successfully and keeps an approximately vertical position (in this case $h_c \approx h_f$). At intermediate *P*, a dynamic interaction should occur when a periphyton filament changes its position under the flow influence according to the relationship $h_c \approx h_f P^{-0.5} \propto C_d^{-0.5} u_*^{-1}$ that follows as a reasonable approximation from (12) and $\sin\psi \approx 0.0174\psi$ for $0 \le \psi \le 80^o$ (i.e., $h_c = h_f \sin\psi \approx 0.0174\psi\ h_f \approx 0.0174 * 57.3 h_f P^{-0.5} \approx h_f P^{-0.5}$). At large *P*, the filament-flow interaction saturates with a periphyton filament lying completely on the bed or on other filaments supporting it (in this case the increase of *P* value does not change periphyton mat thickness, which can be approximated as $h_c \propto d_f$). The schematic change of h_c with *P* is shown in Figure 4b. Thus, in the regime of dynamic interaction the volume-averaged uptake rate can be presented as $R_{Vi} \propto (h_c \delta_{Di})^{-1} \propto (C_d^{-0.5} u_*^{-2})^{-1} \propto C_d^{0.5} u_*^2$ (assuming that $a \approx const$ and $R_N \approx const$).

5.2 Experimental tests

Recent laboratory experiments support both discussed relationships $h_c \approx h_f P^{-0.5} \propto C_d^{-0.5} u_*^{-1}$ and $R_{Vi} \propto (h_c \delta_{Di})^{-1}$ (Nikora at al., 2003b; Larned et al., 2004). In these experiments, acrylic plates (80 cm long, 38 cm wide, 0.5 cm thick) were used as substrata on which to grow periphyton in a local stream over 13 – 26 days. Then, the measurements were made in a 150 cm long × 40 cm wide acrylic flow tank. Water in the tank was circulated from the upper working section to the lower return section. Water depth during the experiments was 8.5 cm, and tank volume was 150 L. Irradiance to maintain healthy periphyton was provided by a 1500 watt quartz halogen lamp 1.5 m above the tank. The experiments involved instantaneous release of nitrate and dissolved reactive phosphorous into flowing water, and measurement of nutrient depletion due to uptake by periphyton over five hours. Uptake rates were obtained from rates of dissolved nutrient depletion. Hydrodynamic conditions during these experiments were measured with an array of three acoustic Doppler velocimeters.

The experiments showed that for a wide range of flow velocities the canopy height h_c decreases with the increase of the bed shear stress as $h_c \propto (u_*^2 / gd_f)^{-\varphi}$ (Figure 5). Such behaviour is consistent with the relationship $h_c \propto P^{-0.5} \propto [C_d (u_*^2 / gd_f)]^{-0.5}$ for the regime of dynamic interaction between periphyton and flow (Figure 4b). Assuming that a periphyton filament is approximately cylindrical we can reasonably approximate C_d for an observed range of $\mathrm{Re}_f = \overline{u}_f d_f / \nu$ =0.08-1.2 as $C_d \propto (\overline{u}_f d_f / \nu)^{\zeta \approx -0.7}$ where $\overline{u}_f$ is the flow velocity at the midpoint of the filament. If the filaments are largely submerged within a viscous sublayer with the linear velocity distribution $\overline{u} = (u_*^2 / \nu) z$ then the flow velocity at the midpoint of the filament is $\overline{u}_f \approx (u_*^2 / \nu)(h_c / 2)$. This leads to $C_d \propto (u_*^2 h_c)^{\zeta}$ which, after substitution into $h_c \propto P^{-0.5} \propto [C_d (u_*^2 / gd_f)]^{-0.5}$, gives $h_c \propto [u_*^{2\zeta} h_c^{\zeta} (u_*^2 / gd_f)]^{-0.5} \propto u_*^{-(\zeta+1)} h_c^{-0.5\zeta}$ or, finally, $h_c \propto (u_*^2 / gd_f)^{-\varphi}$ with $\varphi = 0.5(\zeta+1)/(1+0.5\zeta) \approx 0.25$. However, if the filaments largely protrude above a viscous sublayer into the turbulent region, then $\overline{u}_f \propto u_*$ leading to $C_d \propto u_*^{\zeta}$, $h_c \propto u_*^{-0.5\zeta-1}$ and, finally, $h_c \propto (u_*^2 / gd_f)^{-\varphi}$ with $\varphi = 0.5(1+0.5\zeta) \approx 0.33$. Figure 5 shows the data for the flat bed experiments that can be approximated as a power function $h_c \propto (u_*^2 / gd_f)^{-\varphi}$ with $\varphi \approx 0.24$. The difference between the measured (0.24) and predicted (0.25 and 0.33) exponents is not significant if we account for errors involved in the measurements.

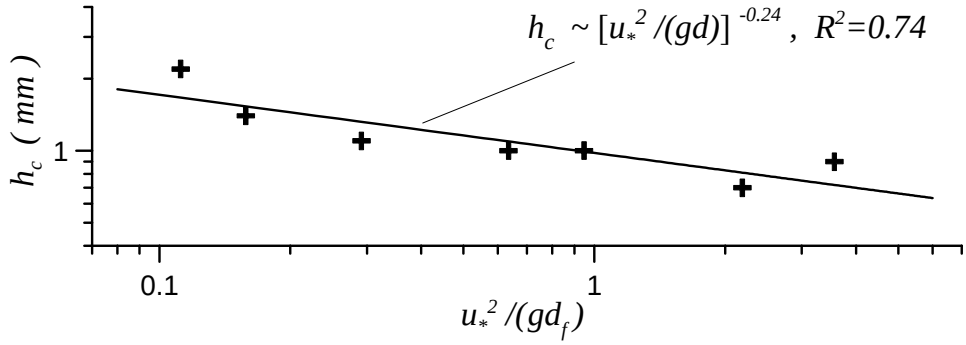

Figure 5 – Change of the periphyton canopy height with increase in u_*^2 / gd_f .

Figure 6 shows dependence of the normalised uptake rates R_V / ρ_B on the shear velocity, where ρ_B is the biomass density (biomass per unit fluid volume). Note that R_V / ρ_B represents the uptake rate per unit biomass. Bearing in mind that $\rho_B \propto h_c^{-1}$, one may deduce that $R_V / \rho_B \propto R_V h_c \propto \delta_D^{-1} \propto u_*$. This prediction is well supported by experiments (Figure 6). More details on these experiments may be found in Larned et al. (2004).

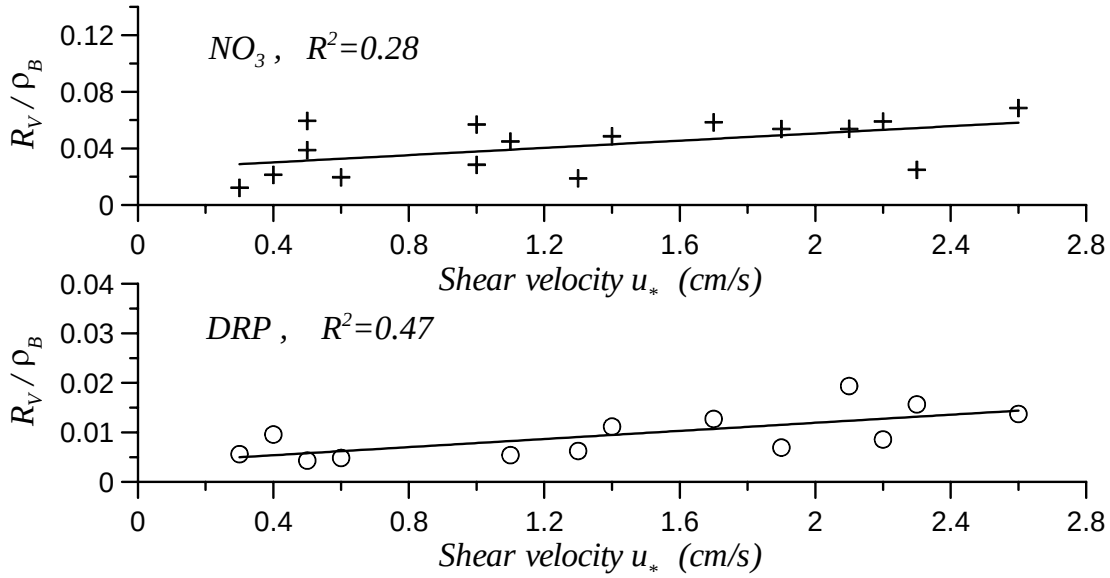

Figure 6 – Relationships between the normalised uptake rates R_V / ρ_B (mg mg chlorophyll a^{-1} min^{-1}) for nitrate (NO_3) and dissolved reactive phosphorous (DRP) and the shear velocity.

The above relationships have been developed for conditions when periphyton filaments cover an initially flat bed, i.e., $h_c >> \Delta_p$ where Δ_p is the height of roughness elements of physical origin (e.g., sediment particles). However, in real streams we also have background roughness elements, which are similar to, or larger than, filament characteristic sizes h_c, h_f, and d_f. In such situations the "biological" contribution to the total bed roughness and transport processes will depend on the filament density, the interaction regime, and the ratios h_c / Δ_p, h_f / Δ_p, and d_f / Δ_p (Nikora et al., 1998a). The periphyton-flow interactions and mass-transfer-uptake processes may also include some additional effects such as the swaying of periphyton filaments, which should be addressed in future considerations.

6. CONCLUSIONS

To develop better understanding and to build process-based computer models for predicting biota responses to various physical processes, two key issues should be addressed: (i) physical interactions between flow and organisms (e.g., due to drag forces); and (ii) ecologically relevant mass-transfer-uptake processes (e.g., due to

molecular and turbulent diffusion). We advocate that this may be better achieved using a double-averaging methodology, which explicitly includes form-induced stresses and fluxes, viscous and form drag forces acting on the near-bed communities, interfacial transport processes, and some other potentially important transport terms. Some of these factors were missed in previous considerations while others were introduced as ad hoc terms. Within the double-averaging approach, all these terms appear naturally as a result of applying conservation laws. The double-averaging methodology has become nearly a standard in atmospheric applications and the time has arrived to start its active use for solving aquatic issues. The application of this methodology at NIWA is illustrated in this paper with three examples: (1) identification of specific flow layers and flow types depending on relative submergence of roughness elements, including organisms; (2) vertical distribution of the double-averaged velocity in the biologically active near-bed layer; and (3) mass-transfer-uptake processes in periphyton community. These examples demonstrate that even simple considerations and parameterizations within the double-averaging methodology may lead to meaningful and testable results. Other examples may be found in Nikora et al. (1998b), Lopez and Garcia (2001), Nikora et al. (2002a,b; 2003a,b), and Walters (2002). Our NIWA group is currently working on implementation of this methodology into a computer code for various practical applications (Walters, 2002).

7. ACKNOWLEDGEMENTS

The research was partly funded by the New Zealand Foundation for Research, Science and Technology (C01X0307 and C01X0308) and the Marsden Fund (UOA220 and LCR203) administered by the New Zealand Royal Society. The author is grateful to B.J.F. Biggs, J. Finnigan, D. Goring, S. Larned, I. McEwan, A. Smith, and R. Walters for useful and stimulating discussions and comments.

8. REFERENCES

Boudreau, B. and Jorgensen, B.B. (2001). *The Benthic Boundary Layer*, Oxford University Press, Oxford, 404 p.

Finnigan, J.J. (1985). Turbulent transport in flexible plant canopies, *In: The forest-atmosphere interactions*, B.A. Hutchinson and B.B. Hicks, eds., D. Reidel Publishing Company, 443-480.

Finnigan, J.J. (2000). Turbulence in plant canopies, *Annu. Rev. Fluid. Mech.*, 32, 519-571.

Gimenez-Curto, L.A. and Corniero Lera, M.A. (1996). Oscillating turbulent flow over very rough surfaces, *J. Geophys. Res*., 101(C9), 20,745-20,758.

Hart, D.D. and Finelli, C.M. (1999). Physical-biological coupling in streams: the pervasive effects of flow on benthic organisms, *Annu. Rev. Ecol. Syst.*, 30, 363-395.

Larned, S., Nikora, V. and Biggs, B. (2004). Mass-transfer-controlled nitrogen and phosphorus uptake by stream periphyton: a conceptual model and experimental evidence, *Limnology and Oceanography* (accepted).

Levich, V.G. (1962). *Physicochemical Hydrodynamics*, Plentice-Hall, N.J., 705 p.

Lopez, F. and Garcia, M.H. (2001). Mean flow and turbulence structure of open-channel flow through emergent vegetation, *J. Hydraul. Eng., ASCE*, 127(5), 392-402.

Monin, A.S. and Yaglom, A.M. (1971). *Statistical Fluid Mechanics: Mechanics of Turbulence*, vol. 1, MIT Press, Boston, Mass, 769 p.

Nikora V.I., Goring D.G. and Biggs B.J.F. (1998a). A simple model of stream periphyton-flow interactions, *Oikos*, 81, 607-611.

Nikora V.I., Suren A.M., Brown S.L.R. and Biggs B.J.F. (1998b). The effects of the moss *Fissidens rigidulus* (Fissidentaceae: Musci) on near-bed flow structure in an experimental cobble bed flume, *Limnology and Oceanography*, 43(6), 1321-1331.

Nikora, V.I., Goring, D.G. McEwan, I. and Griffiths, G. (2001). Spatially-averaged open-channel flow over a rough bed, *J. Hydraul. Eng., ASCE*, 127(2), 123-133.

Nikora, V., Goring, D. and Biggs, B. (2002a). Some observations of the effects of micro-organisms growing on the bed of an open channel on the turbulence properties, *J. Fluid Mech.*, 250, 317-341.

Nikora, V., Green, M., Thrush, S., Hume, T., and Goring, D. (2002b). Structure of the internal boundary layer over a patch of horse mussels (*Atrina zelandica*) in an estuary, *Journal of Marine Research*, 60(1), 121-150.

Nikora, V., Aberle, J., Biggs, B., Jowett, I., and Sykes, J. (2003a). Effects of fish size, time-to-fatigue, and turbulence on swimming performance: a case study of *Galaxias maculatus* (inanga), *Journal of Fish Biology*, 63, 1365–1382.

Nikora, V., Larned, S. and Biggs, B.J.F. (2003b). Hydrodynamic effects in aquatic ecosystems with a focus on periphyton, *Recent Research Developments in Fluid Dynamics*, vol. 4, 41-70.

Nikora, V. (2004). Spatial averaging concept for rough-bed open-channel and overland flows. *Book of Abstracts and CD-ROM Proceedings of the Sixth International Conference on Hydro-Science and Engineering*, Brisbane, Australia.

Nikora, V., Koll, K., McEwan, I., McLean, S. and Dittrich, A. (2004). Velocity distribution in the roughness layer of rough-bed flows, *J. Hydraul. Eng., ASCE* (submitted).

Raupach, M.R. and Shaw, R.H. (1982). Averaging procedures for flow within vegetation canopies, *Boundary-Layer Meteorology*, 22, 79-90.

Rowinski, P.M. and Kubrak, J. (2002). A mixing-length model for predicting vertical velocity distribution in flows through emergemnt vegetation, *Hydrological Sciences Journal*, 47(6), 893-904.

Slattery, J.C. (1999). *Advanced Transport Phenomena*, Cambridge University Press, Cambridge, 709 p.

Walters, R.A. (2002). From river to ocean: a unified modeling approach, *Proceedings of the Seventh International Conference on Estuarine and Coastal Modeling*, Florida, 2001, 683-694.

Wilson, N.R. and Shaw, R.H. (1977). A higher order closure model for canopy flow, *J. Appl. Meteorology*, 16, 1197-1205.

The Institution of Engineers, Australia
8th National Conference on Hydraulics in Water Engineering
ANA Hotel Gold Coast, Australia 13-16 July 2004

Evaluating the Application of Super Absorbent Polymers on Soil Hydraulic Properties

Jahangir Abedi-Koupai
BSc., MSc., PhD.
Assistant Professor, Isfahan University of Technology, Iran
Farahnaz Sohrab
B.Sc., MSc.
Former Graduate Student, Isfahan University of Technology, Iran

Abstract: Nowadays, adding super absorbent polymers in soil is an appropriate method for increasing the efficiency of irrigation and soil water capacity, particularly in arid and semiarid regions. Super absorbent polymers could absorb irrigation and rain water and prevent from deep percolation. The objective of this study was to evaluate the application of super absorbent polymers on soil water capacity and soil moisture characteristic curve (WRC). Two computer models, RETC and Rosetta, were used for data analysis. Two polymers, Snf and Tarawat A100 in four levels, 2, 4, 6 and 8 g/kg were mixed with three soil textures, sandy, loamy and clay. The results of the soil moisture characteristics models showed that for each texture, super absorbent polymers caused the residual water content (θ_r), saturated water content (θ_s), and soil moisture gradient curve increase. Air entry value, $h_b=1/\alpha$, increases in sandy soil, but decreases in the other soils. The results of the statistical analysis showed that there is significant difference between samples containing polymers and control group (without polymer), level of polymer application and between types of polymers. Plant available water increases from 1.5 to 3.5 with super absorbent polymers in two levels, 6 and 8 g/kg. Also soil capillary porosity increased, particularly in the sandy soil.

Key words: Super absorbent polymer, Soil water capacity, Soil water characteristic curve models, RETC.

1 INTRODUCTION

World population growth is reaching the point where available freshwater is insufficient for the basic needs of mankind. This is becoming particularly acute in arid and semi-arid regions of the world. Hence, there is a growing need to utilize different methods to improve water use efficiency (Abedi-Koupai et al., 2001). Treatments of soils with chemical amendments, to improve or maintain soil structure may be one means of maintaining high water infiltration. The effects of polymers as soil conditioners were reviewed by Hariss et al. (1966). However, most of the initial studies with polymers dealt with applying copious amounts of polymers either dry or by spraying and then mixing to create soil aggregates. Synthetic chemical polymers improve soil physical properties (Gardeners, 1972). The effect of low concentration (10 mg/L) of 10 synthetic chemicals with varying chemical properties on flocculation of three California soils was reported by Helalia and Latey (1988). All products were found to be effective in enhancing soil flocculation. Incorporation of polymers in irrigation water may have potential benefits of maintaining or improving hydraulic conductivity of soils when irrigated with waters of poor quality (El-Morsy, 1990). Much work has been done in floriculture with hydrophilic polymers (hydrogels) to describe their effect on water holding capacity of media in pot-grown crops (Eikhof et al., 1974, Still, 1976 and Gehring et al., 1980). Hydrogels have been reported to improve aeration and drainage of the medium (Bearce and McCollum, 1977), improve market life of container grown plant (Eikhof et al., 1974, Still, 1976 and Bearce and McCollum, 1977), and reduce irrigation requirements ((Eikhof et al., 1974, Still, 1976). Gehring and Lewis (1980) reported moisture stress of plants decreased by incorporation of a hydrogel into the medium. Application of 1% polyacrylamide increased aggregate stability up to 48% in a silty loam soil, as reported by Cabaut et al. (1979). Wallace and Wallace (1986b) concluded that generally the most favorable results for seed emergence and water infiltration came from an anionic polymer and that a cationic polymer was less effective. Helalia and Letey (1989) reported that polymers added with water at very low concentration (10 to 50 mg/L) affect such soil properties as penetrometer resistance, aggregate stability, and clay flocculation, which in turn can affect seedling emergence. The relative effectiveness of the polymers depends upon chemical properties of the polymer, such as molecular size and charge, and these polymer properties tend to have differing effects on various soil properties.

The purpose of this study was to investigate the application of super absorbent polymers on soil water capacity and soil moisture characteristic curve.

2 MATERIAL AND METHODS

Three soils classified as sandy loam, loamy and clay were used in this study. The physical and chemical characteristics of the soils are shown in Table 1. The samples were collected from the upper soil layer (0-50 cm) in Ardestan located in the east of Isfahan province. The soil samples were crushed and sieved to < 2mm particle size.

Table 1. The Physical and Chemical Characteristics of the Soils.

Soil Texture	Soil particles (%)			θ_r cm^3/cm^3	θ_s cm^3/cm^3	OM (%)	CEC mol/kg	SAR	EC ds/m	pH	ρ_b g/cm^3
	Clay	Silt	Sand								
Sandy loam	13	10	77	0.041	0.31	0.055	16.64	10.54	5.81	7.8	1.78
Loamy	27	28	47	0.10	0.43	0.22	24.71	14.42	7.28	7.1	1.48
Clay	37	52	11	0.19	0.48	0.17	27.36	37.71	22.15	7.7	1.36

The amendments were two polymers. One was Snf (PR3005A) produced in France and the other was Tarawat A100 produced in Iran. The amounts of polymer application were 2, 4, 6 and 8-g/kg soil. The gravimetric water content for each treatment was determined under 6 levels of soil matric suction, 0, 0.3, 3, 5 and 15 bar using pressure plate apparatus. The soil volumetric water content was determined by soil bulk density and gravimetric water content. Two computer models, RETC (Van Genachten et al., 1990) and Rosetta (Schaap et al., 1998), were used for data analysis. The RETC program used the parametric models of Brooks-Corey (Eq. 1) and van Genuchten (Eq. 2) to represent the soil water retention curve, and the Rosetta used the Van Genuchten model based on neural networks.

$$\theta = \theta_r + (\theta_s - \theta_r)[1+(\alpha h)^n]^{-m} \quad (1)$$

$$\theta = \theta_r + (\theta_s - \theta_r (\alpha h)^{-\lambda} \quad (2)$$

θ_s = saturated water content, θ_r = residual water content, α = inverse of air entry value, n , m = coefficients. Multiple comparisons by Post Hoc Least Significant Difference (LSD) test for the various treatments were done by SAS package.

3 RESULTS AND DISSCUTION

3.1 Effect of Polymers on WRC Parameters

3.1.1 Saturated Water Content (θ_s)

In each soil texture, adding the polymers and increasing the amount of application, increased volumetric water content (Figure 1). In all soil textures maximum value of θ_s is associated with Snf. The maximum value of θ_s is related to 8, 6, 4 and 2 g/kg, respectively.

3.1.2 Residual Water Content (θr)

The variations of (θr) in each soil texture are shown in Figure 2. The value of θr is increased with polymer addition and increasing the amount of application. The maximum value of θr obtained with Snf in the application level of 8 g/kg. The increase of θr in sandy loam soil was more than the others. The residual water content in sandy loam is 5 fold of the control. This is related to less anionic nature of sandy loam soil compared with the other soil textures. As a result the inflation of polymers and water adsorption is increased.

3.1.3 Air Entry Value (h_b=1/a)

Commonly the WRC changes sharply in air entry value. Due to coarser porosity in sandy loam soils, water is released with lower matric suction. In other words the value of a is high. Adding and increasing the amount of

polymer reduced the coarser voids in soil and more pressure is required for the water release and consequently the value of *a* is reduced. In clay and loamy control soils the air entry value is increased or *a* is decreased due to frequently of small pores. The polymer addition to this sort of soils cause to increase the small pores. Hence less pressure is needed to desorb water and the value of *a* is increased.

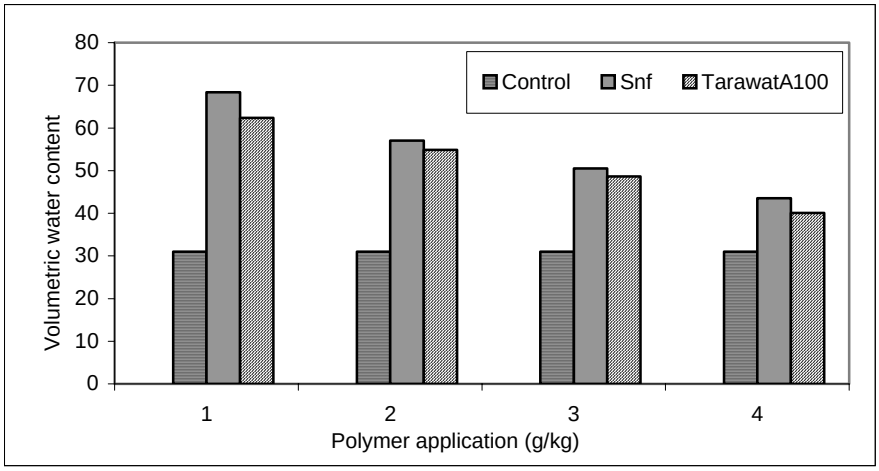

(a)

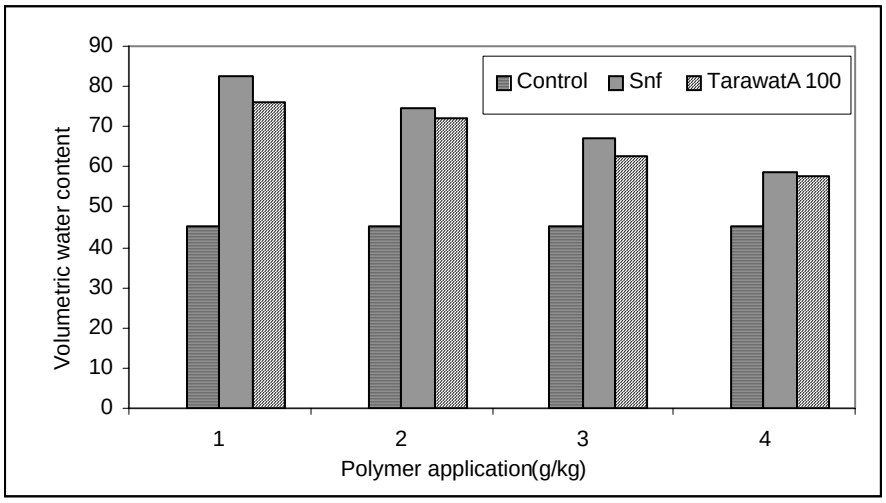

(b)

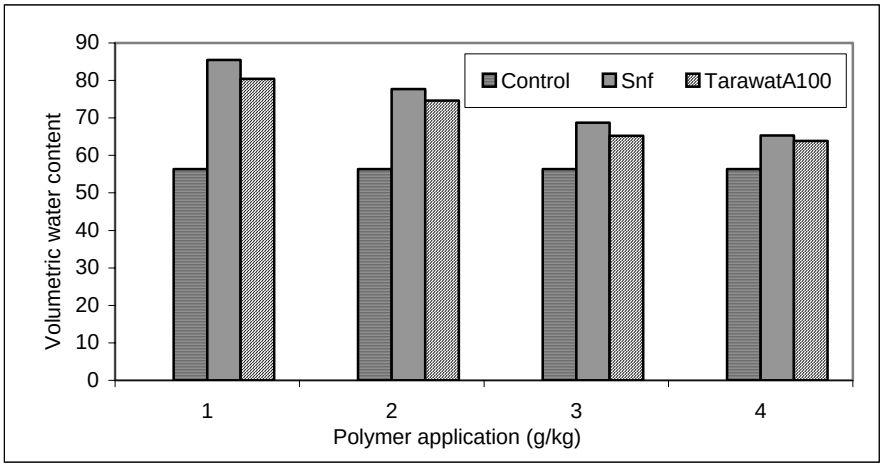

(c)

Figure 1. The variations of saturated water content due to polymer application (control without adding polymer): a) sandy loam, b) loam and c) clay.

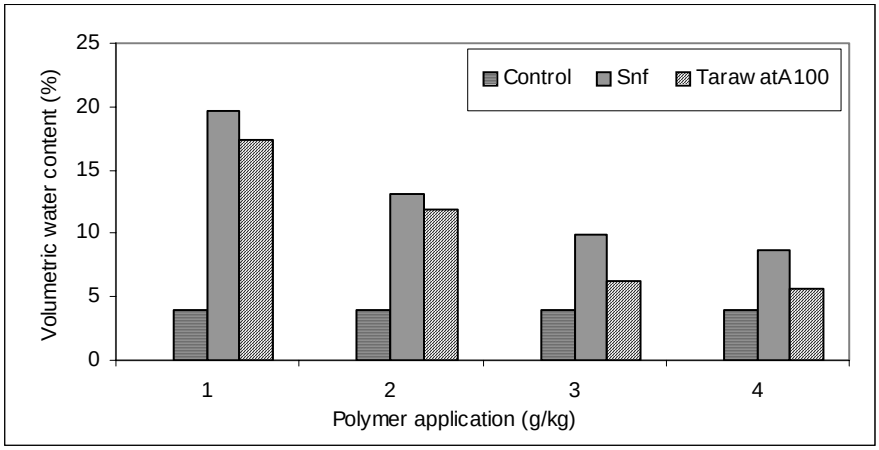

(a)

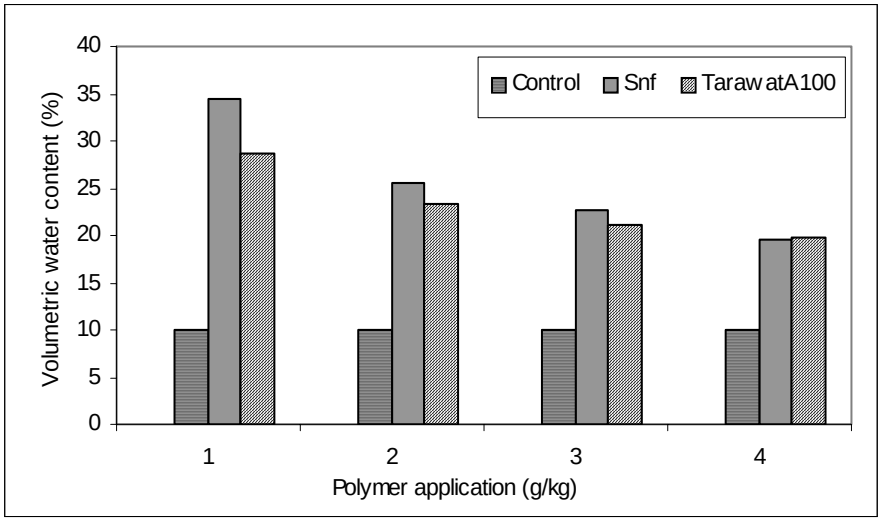

(b)

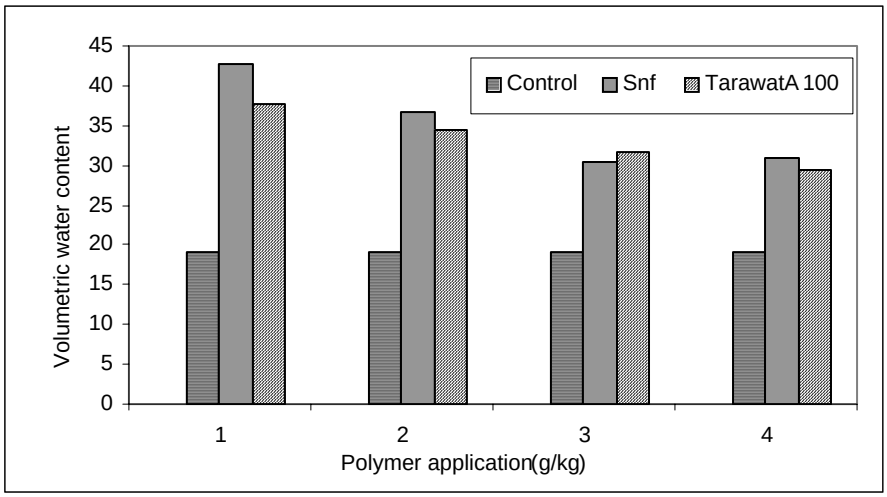

(c)

Figure 2. The variations of residual water content due to polymer application (control without adding polymer): a) sandy loam, b) loam and c) clay.

3.1.4 Water Retention Characteristic Curve (WRC)

There is significant difference (99% confidence level) between two polymers, between polymers and the control and between the amount of polymer applications in each soil texture and soil matric suction. Both polymers had

the same effect on volumetric water content (θv). The maximum increase obtained with Snf at the level of 8 g/kg. The value of volumetric water content was increased 2-4 fold of the control. In loamy soil the volumetric water content was increased between 1.5-2 fold of the control in each matric suction. Application of higher levels of polymer (6-8 g/kg) is recommended in these types of soils. In clay soil the application of polymers caused to increase the volumetric water content in each matric suction. However, the effect was less than the other soil textures. This is because of less inflation of polymers in clay soil. Application of lower levels of polymer (2-4 g/kg) is recommended in clay soils.

3.1.5 Available Water Content (AWC)

There is significant difference (99% confidence level) between two polymers, between polymers and the control and between the amounts of polymer applications on available water content in three soil textures (Tables 2, 3 and 4). In sandy loam the maximum increase of available water content obtained with Snf at the level of 8 g/kg. The amount of increase of available water content is 3 fold of control. The results of polymer addition at two levels of 4 and 6 g/kg are similar for both polymers. The value of volumetric water content in FC, PWP and AWC (FC-PWP) compared to the control are shown in Table 3 for three soils. The results indicate that the volumetric water content in FC and PWP is increased 1.5-5 fold of the control. In clay soil, AWC is doubled at maximum compared to the control (Table 4). There is significant difference (99% confidence level) between two levels of 6 and 8 g/kg compared with two levels of 2 and 4-g/kg polymer addition.

Table 2. Water Content at FC, PWP and AWC in Sandy Loam Soil Compared with the Control.

Situation of water content	Type of polymer	Control	Amount of polymer addition (g/kg)			
			2	4	6	8
FC	Snf	7.28	14.78	18.18	21.56	29.68
	TarawatA100		11.74	14.07	19.67	25.64
PWP	Snf	4.11	9.47	11.17	13.41	19.62
	TarawatA100		6.46	8.17	12.18	17.32
AWC	Snf	3.17	5.31	7.01	8.15	10.06
	TarawatA100		5.28	5.90	7.49	8.32

Table 3. Water Content at FC, PWP and AWC in Loamy Soil Compared with the Control.

Situation of water content	Type of polymer	Control	Amount of polymer addition (g/kg)			
			2	4	6	8
FC	Snf	17.43	27.4	29.51	32.76	40.75
	TarawatA100		27.09	27.97	30.71	35.68
PWP	Snf	13.16	22.01	24.47	24.65	31.2
	TarawatA100		21.56	22.26	23.57	27.12
AWC	Snf	4.27	5.39	5.04	8.11	9.55
	TarawatA100		5.53	5.90	7.49	8.32

Table 4. Water Content at FC, PWP and AWC in Clayey Soil Compared with the Control.

Situation of water content	Type of polymer	Control	Amount of polymer addition (g/kg)			
			2	4	6	8
FC	Snf	25.41	37.73	39.93	43.65	47.46
	TarawatA100		35.90	38.08	41.09	43.57
PWP	Snf	20.76	32.18	33.16	35.6	39.07
	TarawatA100		31.12	32.85	33.18	35.28
AWC	Snf	4.65	5.55	6.77	8.05	8.39
	TarawatA100		4.78	5.23	7.91	8.29

3.1.7 WRC at low Matric Suction (0-3 bar)

As presented in Figures 3 to 8, considerable water content is released through the change of matric suction from 0 to 3 bar. For instance with the amount of 8 g/kg Snf in sandy loam soil, volumetric water content is reduced from 68.4 to 25.0 due to the change of matric suction from 0 to 3 bar (Figure 3). The related values for loamy and clayey soils are from 83 to 36 (Figure 5) and 86 to 43 percent (Figure 7), respectively. Hence the release of water at low matric suction is a beneficial effect for clayey soils.

3.1.6 WRC at High Matric Suction (3-15 bar)

Comparison of volumetric water content of treated soils with the control in the range of matric suction between 3 to 15 bar indicates a considerable change in volumetric water content with the polymer addition. For instance with the amount of 8 g/kg Snf in sandy loam and loamy soils, the value of volumetric water content is between 4.5-5 fold (Figure 3) and 1.5-2.5 fold of control (Figure 5).

4 CONCLUSION

The effect of incorporating of polymers on soil hydraulic properties can be summarized as follows:

- Promotion of soil physical structures particularly in the light soil texture
- Increase of saturated and residual water content in each soil matric suction
- Release of water at low matric suction particularly for the heavy soil texture
- Increase of soil water holding capacity in the light soil texture
- Application of high levels of polymer addition in the light soil texture enhanced available water content 4 fold compared to the control.

Thus, the above mentioned concluding remarks cause to reduce the irrigation frequency which is an important issue in arid and semi-arid regions of the world.

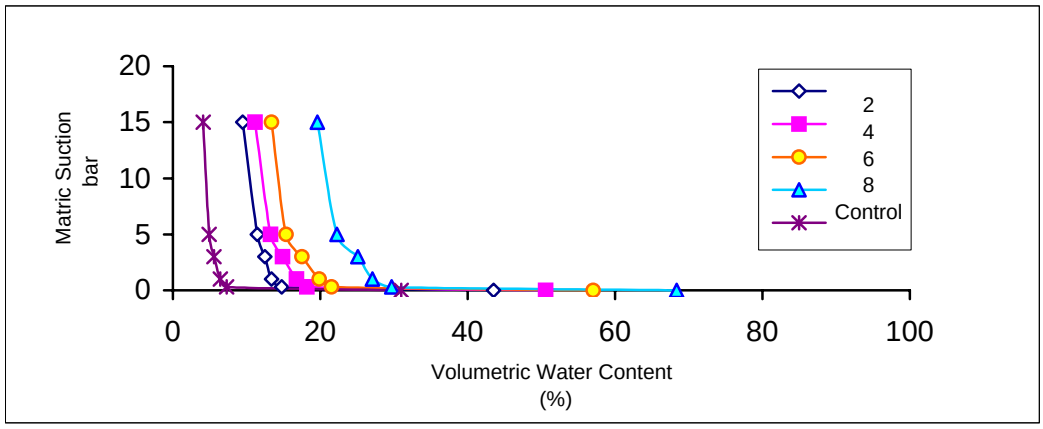

Figure 3. Water Retention Characteristic Curves in Sandy Loam Soil due to Application of Snf Polymer.

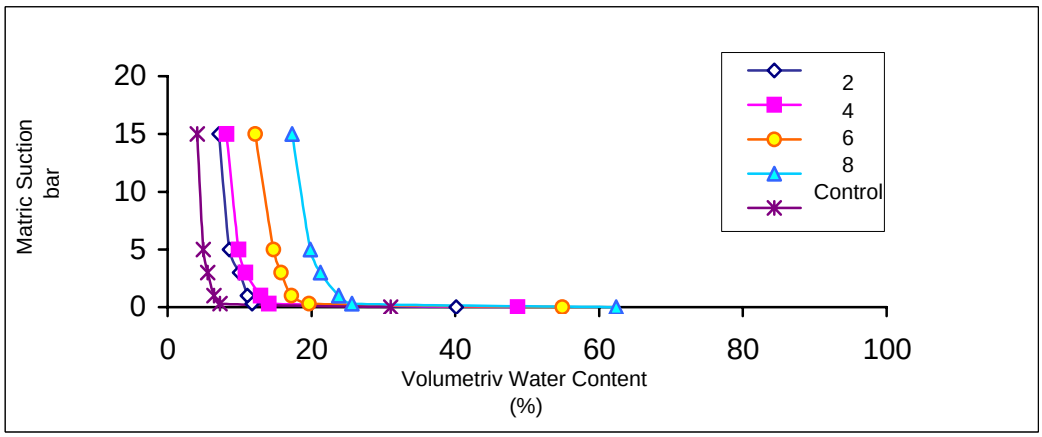

Figure 4. Water Retention Characteristic Curves in Sandy Loam due to Application of TarawatA100 Polymer.

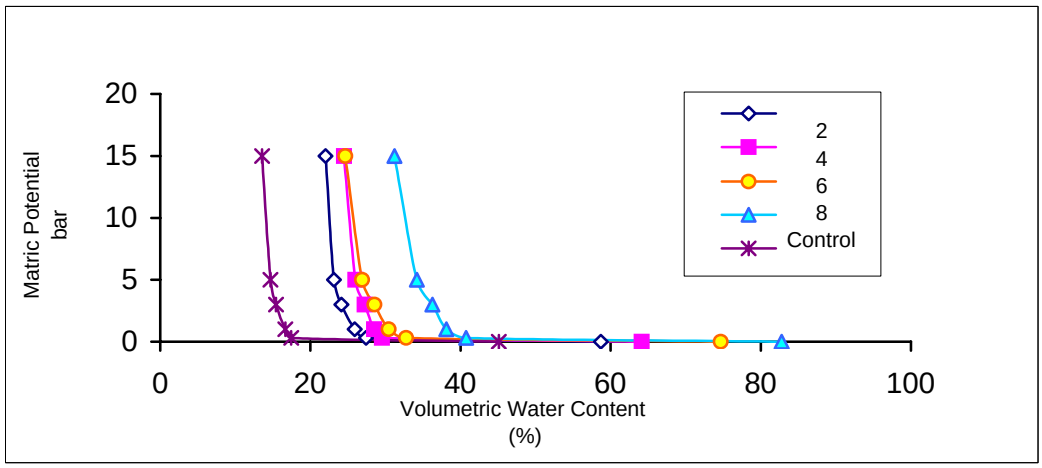

Figure5. Water Retention Characteristic Curves in Loamy Soil due to Application of Snf Polymer.

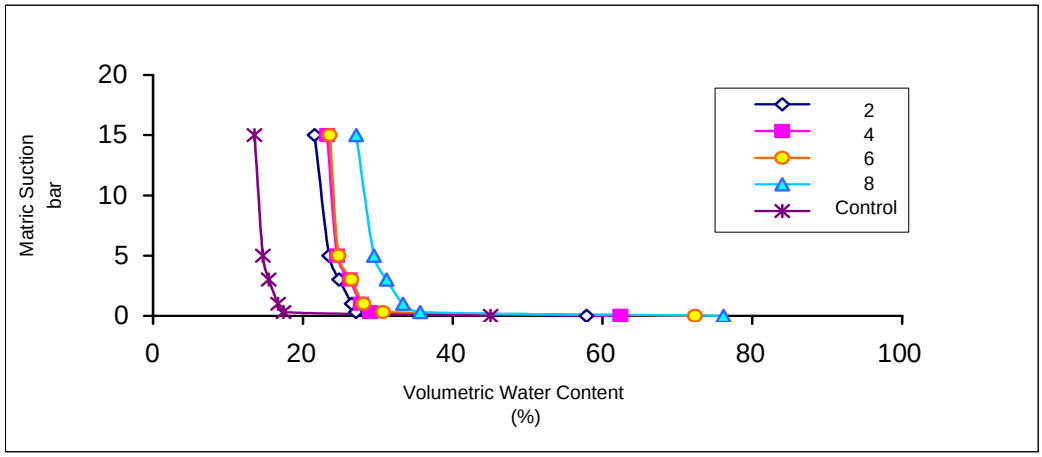

Figure 6. Water Retention Characteristic Curves in Loamy Soil due to Application of TarawatA100 Polymer.

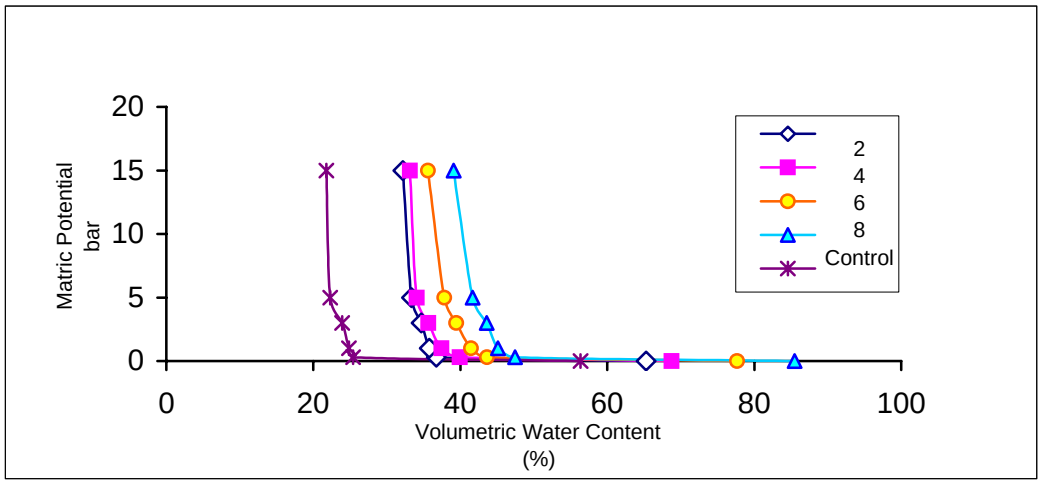

Figure 7. Water Retention Characteristic Curves in Clayey Soil due to Application of Snf Polymer.

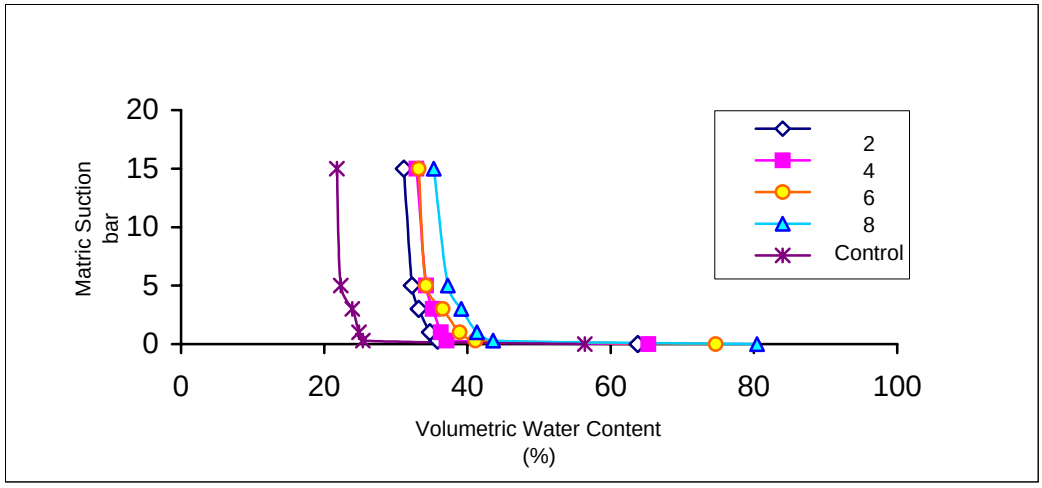

Figure 8. Water Retention Characteristic Curves in Clayey Soil due to Application of TarawatA100 Polymer.

5 REFERENCES

Abedi-Koupai, J. Afyuni, M., Mostafazadeh, B. and Bagheri, M. R. (2001). Influence of treated wastewater and irrigation systems on soil physical properties in Isfahan province. 52nd IEC Meeting & 1st Asian Regional Conference of the International Commission on Irrigation and Drainage (ICID), Proceeding of International workshop on wastewater reuse management R. Ragab, G. Pearce, J. C. Kim, S. Nairizi, and A. Hamdy (Eds.). Seoul, Korea, Sept, 2001. pp. 165- 173.

Bearce, B. C. and McCollum, R. W. (1977). A comparison of peat lite and noncomposted hardwood- bark mixes for use in pot and bedding-plant production and the effect of a hydrogel on their performance. *Flor. Rev.*, 161(4169): 21-23, 66.

Callebaut, F., Gabriels, D. and DeBoodt, M. (1979). The effect of polymer structure on soil physico-chemical properties and soil water evaporation. *J. Chem. Tech. Biotechnol.* 29: 723-729.

Eikhof, R. H., King, P. A. and Koven, G. H (1974). Control of wilting in potted plants. Ohio Flor. Assoc. Bul. 532.

El-Morsy, E. A. (1991). Polymer effect on the hydraulic conductivity of saline and sodic soil conditions. *Soil Sci*., 151(6): 430-435.

Gardner, W. H. (1972). Use of synthetics soil conditioners in the 1950s and some implications to their future development, p 1046-1061. In M. DeBoodt (ed). Proc. Symp. On the Fundamentals of Soil Conditioners, Ghent, 17-21 April. State University Ghent, Faculty of Agric Sci., Ghent, Belgium.

Harris, R. F., Chesters, G. and Allen, O. N. (1966). Dynamic of soil aggregate stability, and hardness. *Soil Sci.*, 148(3):199-203.

Helalia, A. M. and Letey, J. (1989). Effects of different polymers on emergence aggregate of tomato seedling. *Soil Sci.* 141:321-323.

Still, S. M., (1976). Growth of Sunny Mandalay chrysanthemums in hardwood-bark amended medium as affected by unsolubilized polyethylene oxides. *Hort. Science.* 11(5): 483-484.

Schaap, M. G., Leij, F. J and Van Genuchten, M. Th. (1998). Neural network analysis for hierarchical prediction of soil water retention and saturated hydraulic conductivity. *Soil Sci. Soc. Am. J.,* 62: 847-855.

Van Genuchten, M. Th., Leij, F. J. and Yates, S. R. (1990). The RETC code for quantifying the hydraulic functions of unsaturated soils. Res. Rep. 6002-91065. USEPA, Ada, OK.

Wallace, A. D. and Wallace, G. A. (1986b). Effect of polymeric soil conditioners on emergence of tomato seedling. *Soil Sci.* 141:321-323.

The Institution of Engineers, Australia
8th National Conference on Hydraulics in Water Engineering
ANA Hotel Gold Coast, Australia 13-16 July 2004

The Implementation of PIV-PTV Techniques for Measurement of Velocities in Large Physical Models

D.J. Anderson[1]
B.E., M.Eng.Sc.
[1]Water Research Laboratory, School of Civil and Environmental Engineering,
University of New South Wales, Australia.
A. Frazer[1]
B.E.
T. Jancar[1]
B.E.
B.M. Miller[1]
B.E., B.Sc., M.Eng.Sc., MIEAust

Abstract: Particle Image Velocimetry (PIV) and Particle Tracking Velocimetry (PTV) methods for visually detecting velocities in water bodies are widely recognised, as are their advantages. This has seen PIV and PTV techniques being adopted as a velocity measurement tool in many small scale laboratory studies. With improvements in image analysis algorithms and digital imaging and computer technology, it is now possible to employ these methods in large scale physical models to support detailed qualitative and quantitative velocity analysis; something traditionally constrained to the field of numerical modelling.

This paper details the application of the techniques used to successfully interpret velocities in a large physical model using commercially available computing equipment. An overview of the theory behind the methods, the implementation of the data capture and data analysis, the validation of the image analysis algorithms used and the practicalities of various implementations and techniques is provided. The study revealed that lighting, tracer seeding strategies and particle identification algorithms all require careful consideration in large scale physical models.

Keywords: PIV PTV velocity measurement physical modelling remote sensing

1. INTRODUCTION

PIV and PTV techniques are widely recognised in the literature (e.g. Willert and Gharib, 1991; Adrian, 1991). PIV and PTV analysis systems work by capturing video footage of tracer movements in a water body and, with the aid of sophisticated image analysis algorithms, decoding these images of tracer movement into velocities. In contrast to conventional 'in-situ' metering techniques, these methods allow for the rapid and easy collection of spatially and temporally detailed velocity data; all without disturbing the measured flow field. These characteristics have made PIV and PTV based systems an ideal tool for the study of detailed flow field behaviour in a range of small physical scale laboratory studies.

Historically, conventional in-situ velocity measurements in large physical models have required significant rationalisation regarding the required spatial and temporal resolution of the collected data. With improvements in image analysis algorithms and digital imaging and computer technology, it is now possible to employ PIV and PTV methods to collect spatially detailed real-time velocity data in large scale physical models with a single test (Mingzhang et. al., 2000). This has allowed large scale physical modelling to support detailed qualitative and quantitative velocity analysis; something traditionally constrained to the field of numerical modelling.

During 2003, the Water Research Laboratory (WRL), University of New South Wales (UNSW) developed PIV and PTV based techniques suited to large physical models for, and with funding from, Penrith Lakes Development Corporation (PLDC). The development included the design, application and validation of a scalable 3-camera computer system capable of measuring surface velocities in large physical models in real-time (25 frames per second). In July 2003, these techniques were applied to a 50m² (1250ha prototype) region of the Penrith Lakes Scheme Physical Model to collect velocity data that would assist in the determination of flood risk over a proposed urban development area during design floods.

This paper summarises the practicalities facing the application of PIV-PTV techniques to the measurement of surface velocities in large scale physical models and details a set of techniques and experimental methods that were devised to work within these practicalities. The discussion includes an overview of the data capture, experimental setup and data analysis techniques. A brief discussion of the application and validation of the techniques in the Penrith Lakes physical model flood study is also provided.

2. PRACTICALITIES OF LARGE SCALE PIV-PTV

In previous PIV-PTV experimental setups at WRL (Peirson, 1997) a target plane, typically in a tank or flume, is illuminated by strobe or laser sheet lighting (see Figure 1). The light highlights small neutrally buoyant tracer particles whose movement is recorded on one or more video cameras. PIV and PTV algorithms then extract velocity data from the video record of particle movement. These experimental setups were typically carried out on a small physical scale collecting only small volumes of digital data.

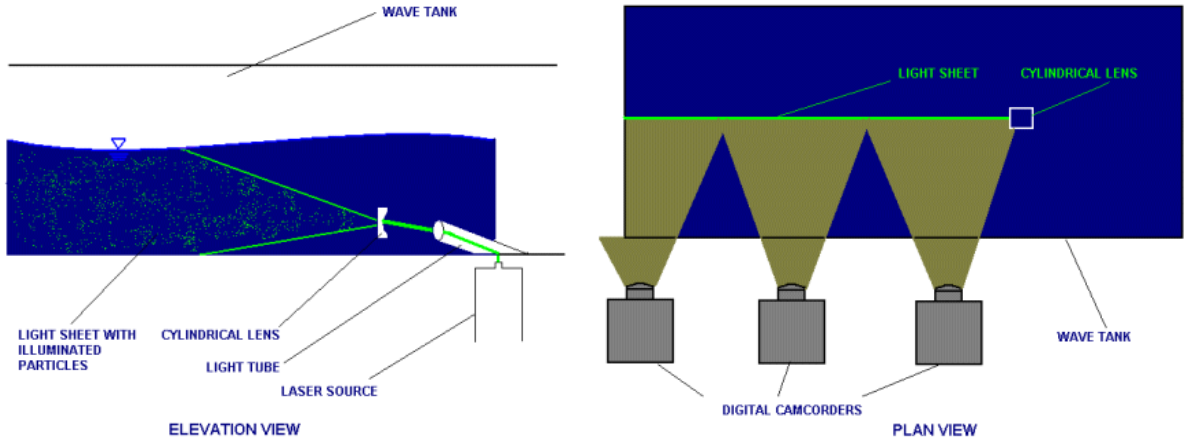

Figure 1 – Example of a Conventional PIV-PTV Experimental Setup

Application of these techniques to measure surface velocities in large scale physical models requires the resolution of a number of practicalities:

- Large models can require many overhead cameras to provide coverage. This requires the use of a collection system capable of simultaneously managing these cameras and storing the large volumes of digital data that are created.
- Access above large physical models is often restrictive. This poses practical challenges for camera installation that can control the height at which cameras are installed. This can have implications for the number of cameras required for coverage, the size of the tracer particle and hence the effective resolution of the velocity measurements.
- Tracers must be positively buoyant and have a small vertical footprint so that they travel with the surface waters. They must also be sized so that they are visible to the video cameras and PIV-PTV algorithms while still being small enough to provide the appropriate measurement resolution in the scaled prototype.
- Bright and diffuse illumination of the target areas is critical for obtaining appropriately exposed images. However, most large physical models are constructed inside buildings that suffer from either poor or non-uniform overhead lighting. Both of these situations cause problems for PIV-PTV data analysis. Poor lighting can result in under-exposed images or, when longer shutter times are used, blurred images. When the overhead lighting is not diffuse, images exhibit both under and over-exposed regions. In the over-exposed regions it is typically impossible to identify the movement of tracer particles.
- Flow patterns in large physical models are generally very complex with significant variations in the path of flow in both time and space. This decreases the likelihood of tracer particles, introduced at an upstream point in the model, arriving at target locations in densities appropriate for PIV-PTV analysis.
- At the model and prototype scales being considered, errors in the position, magnitude and direction of velocity measurements, due to camera lens distortions, can become significant.
- Velocities measured in each cameras coordinate system need to be merged into a single matrix in the prototype coordinate system for presentation and analysis.

3. A PIV-PTV TECHNIQUE FOR LARGE PHYSICAL MODELS

To scale WRL's existing PIV-PTV techniques to suit surface velocity measurement in large physical models and address the various practicalities in doing so, WRL has developed:

- a data capture and analysis system capable of sampling multiple cameras at rates of up to 25 frames per second for extended periods of time,
- experimental techniques to:
    - select a tracer particle that is positively buoyant, large enough to be visible to the cameras, and small enough to provide velocity information at the desired spatial resolution,
    - place acquisition cameras at a position in space above the model commensurate with the required coverage and resolution,
    - provides enough lighting to sufficiently illuminate the large target area,
    - seed the model with tracer particles at a density sufficient for PIV-PTV without interfering with data capture,
- a PIV-PTV analysis algorithm capable of performing in less than ideal conditions, and
- post processing tools to remove distortion in and rectify, scale, and merge the camera images and PIV-PTV velocities to the prototype coordinate system

An overview of the developed systems and techniques is provided below.

3.1 Data Collection System

The image acquisition system was developed from commercially available Digital Video (DV) cameras and computer components. DV cameras are capable of recording digital video at 25 frames per second and transferring this, in real-time via fire-wire cables (IEEE 1394a), to an acquisition PC where it is recorded directly to disk. With current commercially available computing hardware, a Linux based system can be designed to easily record a total of 250GB of footage from up to six digital video cameras. This equates to 16 camera hours of footage at 25 frames per second.

3.2 Experimental Setup and Techniques

A schematic of the experimental setup used to acquire video footage of moving particles is shown in Figure 2. A discussion of this setup and the techniques involved is detailed below.

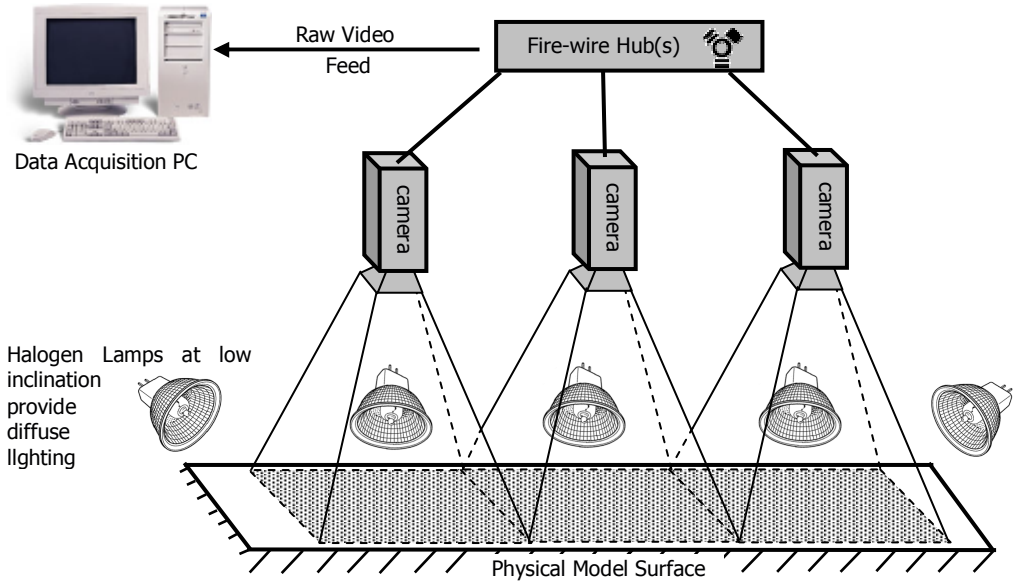

Figure 2 – Schematic Example of the Adopted PIV-PTV Experimental Setup for a Large Physical Model

3.2.1 Camera Installation

Cameras are fixed in place above the model by means of an extendible aluminium arm attached to scaffolding erected beside the model, or if access to the roof of the building is safe, directly to any appropriate ceiling structure. Once installed, the position and coverage provided by the cameras is carefully surveyed into the model and prototype coordinate systems.

A constraint balancing technique was developed to determine the elevation and position at which the cameras should be placed. This technique considers the availability of cameras and, for each possible camera elevation, whether suitable coverage and resolution would be achieved. Suitable resolution is determined by balancing the size of the tracer particle required for identification by the PIV-PTV algorithms and the required resolution of the velocity field. For example, if a tracer particle needs to be 25mm² model units to be identified by the PIV-PTV algorithm at a particular camera height and the model scale is 1:500, the movement of each tracer particle will reflect the average velocity of a 6.25m² prototype area.

3.2.2 Light Source

WRL's previous PIV-PTV experiments (Peirson, 1997) were typically side-looking and made use of a single source of strobe or laser light to illuminate the study area. In large physical models this is not practicable or feasible. Experimentation suggested that the most appropriate way to compensate for poor overhead lighting in large physical model setups was to eliminate non-uniform overhead lighting and introduce high powered halogen lights at low inclinations at several points around the model. The low inclination prevents light reflecting off the water surface back into the cameras. In cases where model topography results in the casting of shadows, means of diffusing the light are required.

3.2.3 Tracer Selection

1.5mm thick squares of balsa wood painted with reflective white paint were found to be suitably thin and buoyant enough to travel with the surface waters. Conventional PIV-PTV algorithms work with particles ranging in size from 1-4 pixels. Experimentation indicated that deliberately over sizing particles to represent at least 4 pixels in the video footage allowed PIV-PTV algorithms to identify significantly more particles in poorly lit regions of the model. As described in Section 3.2.1 a methodology was developed to select an appropriate physical size for the tracer particles.

3.2.4 Tracer Seeding Strategy

The following methodology was developed to maintain suitable tracer particle densities within the physical model:

- prior to initiation of the model run, the target areas are seeded with an initial uniform distribution of tracer particles and the results of previous runs are analysed to determine times when it is acceptable to potentially interfere with video footage by seeding the model with particles
- throughout the test, operators observe flow patterns and particle densities over the target area. When particle densities are observed to drop below a threshold level, the operators, subject to the previously determined times, seed the model with particles. Seeding is achieved by throwing more particles into the model. Where possible the model is seeded outside the field of view of the cameras.

3.3 PIV-PTV Implementation

A hybrid PIV-PTV algorithm, based on work by Cowen and Monismith (1997), was used to extract velocities from the video footage. This hybrid technique is often referred to as "super resolution analysis" (Keane et. al., 1995; Stitou and Riethmuller, 2000).

The technique starts by statistical evaluation of a tracer's displacement using traditional PIV. First, the collected digital images are pre-processed to remove the image background and isolate images of the particles. An algorithm then identifies the locations of the particles in these images by searching for objects whose size matches that of the particle and whose intensity exceeds a preset threshold level. This process is summarised in Figure 3.

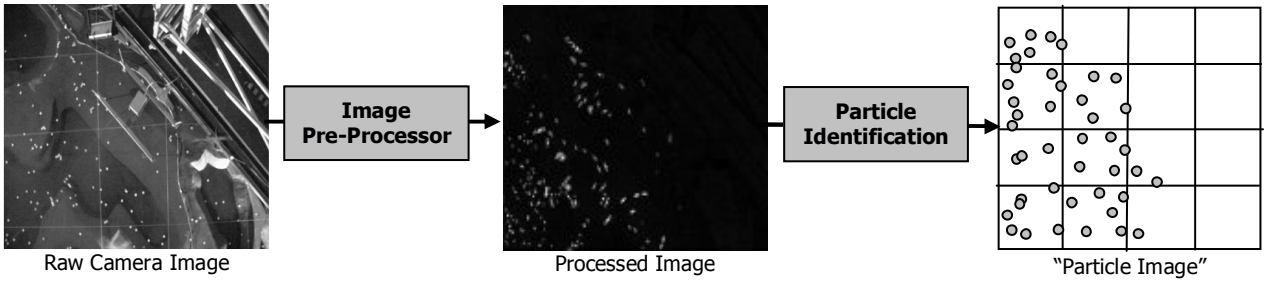

Figure 3 – PIV-PTV Digital Image Pre-Processor

Fast Fourier Transform (FFT) and auto-cross correlation techniques are used to track the movement of corresponding intensity peaks in time and determine a PIV velocity field in each image sub-window. To account for varying particle speeds and densities, the PIV algorithm was programmed to study sub-windows of 16, 32 and 64 pixels over the specified time-step. This allows the determination of a spatial analysis resolution that gives the most detailed PIV velocity field. The optimal PIV velocity field is then refined by tracking individual particles with PTV. Particles are paired between corresponding image frames using a search zone based upon the PIV velocity field, the local velocity gradient and the local particle seed density. These general principles are summarised in Figure 4.

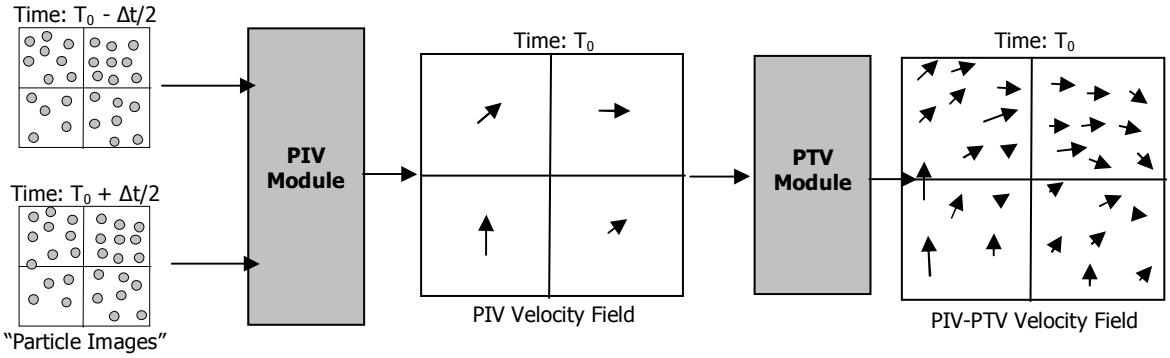

Figure 4 – PIV-PTV Analysis Principle

Synthesised images of various velocity fields were used to test the PIV-PTV algorithm. In the majority of circumstances the initial velocity field was reproduced satisfactorily. Performance of the algorithm suffered in regions of low particle density and camera-wide uniform flow.

3.4 Geo-Rectification and Scaling

The PIV-PTV analysis algorithms described above report velocity data in units of pixels per image frame step and may contain spatial distortions generated by lens defects and camera orientation. Examples of some possible distortion modes are schematised in Figure 5. To interpret results in the prototype coordinate system it is necessary to remove these distortions and then scale the results from the camera to the prototype coordinate system.

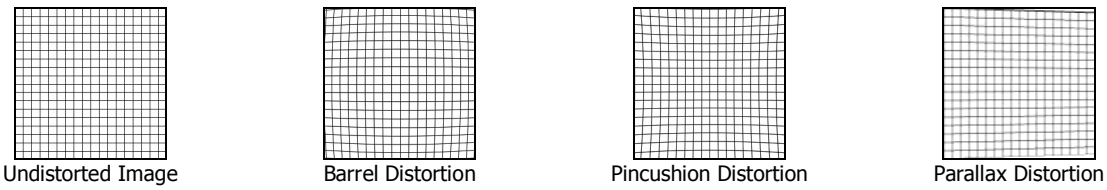

Figure 5 – Examples of Potential Distortion in PIV-PTV Images and Velocity Data

A one-step technique to remove these distortions and convert the results from the camera to the prototype coordinate system was developed. In this technique, an image registration algorithm creates a camera pixel to prototype unit mapping file from ground control points (GCPs) collected during camera installation. This mapping file is then used in the interpretation of all PIV-PTV displacements. Differences between the camera frames and the prototype time scales are corrected by dividing the frame step by the frame rate (25 frames per second) and multiplying the result by the model to prototype time scale factor.

Note that the number of GCPs required to remove distortion depends on the distortion modes that are exhibited in the camera images. Most types of distortion can be corrected using two to ten control point pairs. Collection of additional control point pairs allows a least-square methodology to be applied to the correction.

4. APPLICATION TO A PHYSICAL MODEL STUDY

Since the 1980's, WRL has been variously commissioned by PLDC to investigate aspects of flooding within the Penrith Lakes Scheme, NSW, Australia. These studies included the construction and testing of a physical model of the Penrith Lakes region in 1992 (see Figure 6: Panel A). During 2003, WRL was commissioned by PLDC to determine velocities and risk over a proposed urban development area in the Penrith Lakes Scheme. The complex interacting flow regimes over river to lake and lake to lake weirs and embankments made the physical model an ideal tool for studying this problem.

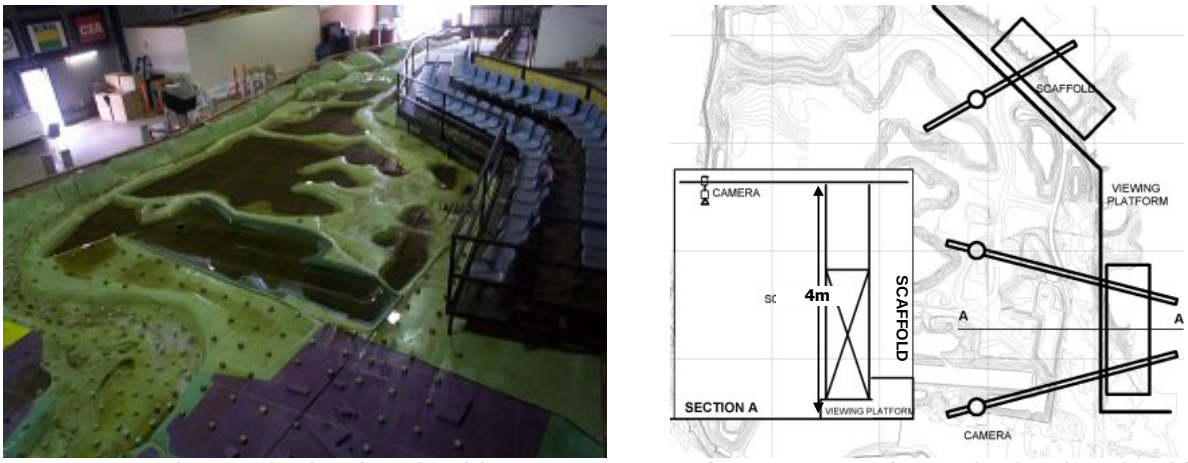

Panel A: Penrith Lakes Physical Model Panel B: Camera Setup for Penrith Lakes Physical Model

Figure 6 – Penrith Lakes Physical Model and Camera Setup

Applying the techniques discussed in this paper, PIV-PTV methods were used to gather velocity fields at several times throughout the rising limb of several design hydrographs. By combining this data with water level measurements over the urban development area ARC-GIS was used to produce contours of water level, velocity field and risk; something previously only possible in numerical studies. These maps were then used as a tool to assess flooding and flood risk over the proposed urban development area. An example of the risk contours and velocity vectors, developed from the physical model, for a given time during a large flood is shown in Figure 7.

During application of the described PIV-PTV analysis techniques, a number of practicalities were encountered. Details regarding the experimental setup and resolution of these practicalities are discussed below.

4.1.1 Experimental Setup

As indicated in Panel B of Figure 6, three cameras were fixed in place approximately 4m above the urban development area by means of an extendable aluminium arm attached to scaffolding erected on a viewing platform beside the model. These cameras provided coverage of a 50m² area of the physical model (1250ha prototype). A detailed ground control survey was performed to allow for subsequent distortion removal and geo-rectification of the camera images and velocity results.

The target areas in the model were illuminated with three 1000W halogen lamps (approximately 60W/m²) and the overhead lights directly above the model were turned off to prevent un-even exposure problems. Safety issues and a lack of suitably rated power outlets in the building prevented additional halogen lamps from being deployed. White balsa particles of dimension 25×25×1.5mm (12.5×12.5×0.1m prototype) were used as tracers and cast into the model using the previously described techniques. Tests were run for several hydrographs and the video footage of particle movement was recorded on the image acquisition system and returned to the computing laboratory for analysis on a high powered workstation.

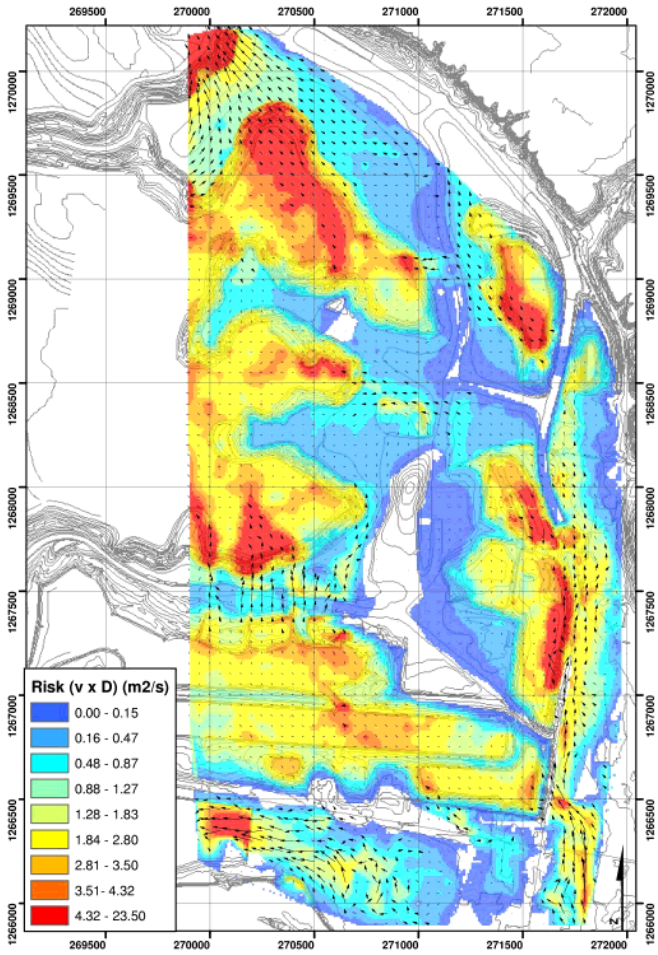

Figure 7 – Risk Contours and Velocity Vectors for a Given Time during a Large Flood

4.1.2 PIV-PTV Analysis

Velocity data was extracted from the video footage using the PIV-PTV techniques described in section 3.3. On a number of occasions it was found that particle densities within the model were too low for the PIV module to predict PIV velocity fields with statistical certainty. While this was initially attributed to non-ideal tracer seeding density, it was also observed that the many particles within the model were not identified in the particle images probably due to insufficient or inadequate lighting, shadows and a lack of robustness in the image pre-processing algorithm.

To counter these problems, it was necessary to remove the PIV module from the analysis program and predict PTV velocities without initial knowledge of the velocity field. This drastically increased the chances of the PTV program pairing incorrect particles and calculating spurious velocity vectors. To prevent this occurring, the PTV module was run many times with time-steps ranging from 0.08 to 5.00 seconds and a localised region based processing algorithm was applied to analyse the particle velocity variability over the different sized time-steps. Regions exhibiting significant variability in velocity over these 5 second periods were discarded. To validate the performance of this technique a manual verification system, described below, was devised.

4.1.3 Manual Verification of Image Analysis Algorithms

To determine the performance and accuracy of the modified PTV technique at extracting velocities under laboratory conditions a manual MATLAB based PTV analysis program was developed. Within this program several image frames are merged to create a time-exposure image as shown in Panel A of Figure 8. Particle displacements are then generated by an engineer from a series of these time-exposures to create a velocity field image as shown in Panel B of Figure 8. PIV and PIV-PTV vectors determined by the image analysis algorithms were then loaded into this program and compared with the manually calculated velocities.

Panel A: Time Exposure Image

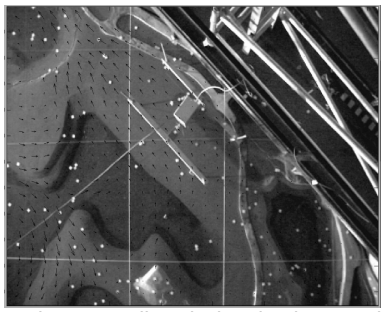

Panel B: Manually Calculated Velocity Field

Figure 8 – Time Exposure Image for Manual PTV Analysis

The two methods for velocity extraction were found to compare well given the subjectiveness of manually selecting particle centres. In most cases there was a good match between the magnitudes of the PTV and manually calculated velocities. The maximum differences in magnitude were observed to be about 20%. Matches in velocity direction, however, were typically much poorer with maximum directional differences of 45º. These large differences were typically associated with very slowly moving particles and given the subjectiveness of the manual particle digitisation process are not unexpected. It was also evident that there were conditions in which the automatic techniques picked more velocities than the manual method and vice-versa. Both techniques had difficulties extracting velocity data where clumps of particles existed.

5. CONCLUSION

PIV-PTV techniques are widely recognised as a velocity measurement tool suitable for application in many small scale studies and the ability to beneficially apply these techniques to large scale physical model studies is beginning to be realised. WRL has successfully developed, applied and tested a PIV-PTV technique for the measurement of surface velocities in large scale physical model flood studies. These techniques allow for spatially detailed quantification of flood velocities and flood risk from a physical model. Due to limitations with conventional velocity metering techniques, this type of analysis capability has been traditionally constrained to the field of numerical modelling. This represents a significant step forward for the field of physical modelling.

Various practicalities were encountered during the large-scale application of the described PIV-PTV techniques. Within poorly lit regions of the model, the image pre-processing algorithm was found to lack robustness and in some circumstances there may have been insufficient tracer particles for optimal analysis. These particular issues were resolved with the implementation of specially modified PTV algorithms and manual PTV analysis. Future work will focus on improvements to the experimental methods and particle identification algorithms.

6. ACKNOWLEDGEMENTS

The Water Research Laboratory, School of Civil and Environmental Engineering, UNSW gratefully acknowledges the support and funding provided by Penrith Lakes Development Corporation to undertake this work.

7. REFERENCES

Adrian, R.J. (1991). Particle-Imaging Techniques for Experimental Fluid Mechanics, *Annual Review of Fluid Mechanics*, 23, pp. 261-304.

Cowen, E.A. and Monismith S.G. (1997). A Hybrid Digital Particle Tracking Velocimetry Technique, *Experiments in Fluids*, 22, pp. 199-211.

Mingzhong, Y., Xingkui, W., Dianchang, W., Danxun, L. (2000). Application of PTV to Flow Field Measurement in Large-Scale Physical Models, 9th International Symposium of Flow Visualization, August 2000, Edinburgh, Scotland.

Peirson, W.L. (1997). Measurement of surface velocities and shears at a wavy air-water interface using particle image velocimetry, *Experiments in Fluids*, 23, pp. 427 – 437.

Stitou A. and Riethmuller M.L. (2000), Extension of PIV to Super Resolution using PTV, *Measurement Science Technology*, 12-9, pp. 1398-1403.

Willert, C.E. and Gharib, M. (1991). Digital particle image velocimetry, *Experiments in Fluids*, 10, pp. 181-193.

The Institution of Engineers, Australia
8th National Conference on Hydraulics in Water Engineering
ANA Hotel Gold Coast, Australia 13-16 July 2004

Swash Overtopping and Sediment Transport – Application to Bermed Beaches and Lagoon Entrances

T. E. Baldock
B.Eng., PhD.
Lecturer, Division of Civil Engineering, University of Queensland, St Lucia, Brisbane, Qld 4072.
K. Day
B. Eng.
GHD Pty Ltd, GPO Box 668 Brisbane, QLD, 4001.
M. G. Hughes
B.Ec., Ph.D.
Senior Lecturer, School of Geosciences and Institute of Marine Science, University of Sydney NSW 2006.
F. Weir
B.Sc.
School of Geosciences and Institute of Marine Science, University of Sydney NSW 2006.

Abstract: This paper presents new experimental data on swash overtopping and sediment overwash on a truncated laboratory scale beach. The experiments were designed to allow direct measurement of total uprush sediment transport rate past a fixed section of beach. The overtopping data are compared to an existing analytical solution and predictions based on a recently developed numerical model, and show good agreement with the latter. The improvement is a result of more realistic predictions of the flow depth in the swash zone by the numerical model. Subsequently, the model is extended to enable predictions of sediment overwash using well accepted sediment transport equations. Model predictions using standard coefficients are in good agreement with the data. The model performance suggests it may be applicable for modelling the accretion of berms on natural beaches, a process which requires overtopping and sediment transport above the existing berm crest.

Keywords: Estuaries, lagoons, ICOLLs, swash, sediment transport, overtopping, beach berms.

1. INTRODUCTION

Coastal lagoon and coastal creek entrances along Australia's wave dominated coastline are frequently closed or partially closed by a sand berm. The behaviour of such Intermittently Closed and Open Lakes and Lagoons (ICOLLs) is dependent on rainfall and beach behaviour, with the presence of a sand berm leading to restricted tidal flushing of the estuarine system and increasing flood risk by preventing catchment run-off (figure 1). Closure also leads to declining water quality due to the build up of pollutants, eutrophication and acid sulfate soil run-off. The behaviour of such systems is often seasonal and management often requires artificial entrance opening to mitigate these hazards. This impacts on the natural ecosystem, however, particularly in the case of coastal wetland habitats that are sensitive to changes in salinity. Entrance management of these systems is hampered by a poor scientific understanding of lagoon entrance behaviour, which stems from an incomplete understanding of swash zone hydrodynamics and berm morphodynamics.

The present study aims to address this issue and compares novel laboratory scale data with predictions from an existing analytical solution (Peregrine and Williams, 2001) and a recently developed numerical model (Hughes and Baldock, 2004). The analytical solution provides estimates of swash overtopping flow on a truncated beach and the initial hypothesis behind the experiments was that any sediment overwash would be well correlated with the overtopping flow, for which a solution was available. This is found to be the case, but the analytical solution is found to under-estimate the overtopping rate. The numerical model results show better agreement with the overtopping data, and also provides good estimates of the total sediment transport rate. Consequently, the model may be applicable for modelling the berm building process on natural beaches, where the hydrodynamic conditions are similar. Section 2 below outlines previous related work, together with the basis for the numerical model. Section 3

describes the experimental setup, with results and data comparisons presented in Section 4, followed by final conclusions in Section 5.

2. PREVIOUS WORK

The build up of a sand berm above mean sea level requires sediment transport on the upper beach face or swash zone, and is due to wave runup, or uprush, above the local tidal level. Indeed, to build the berm higher requires an overtopping flow and sediment overwash above the existing berm crest (figure 1). The runup may be due to broken waves or standing long waves, with the maximum runup height well correlated with offshore wave height (Hunt, 1959). For broken waves, however, the runup is controlled by the bore height on arrival at the shoreline. The subsequent shoreline motion can be described analytically (Shen and Meyer, 1963), hereafter SM63, with frictional effects included if required (Hughes, 1995). This approach is well verified for both laboratory and field data (Yeh et al, 1989; Hughes, 1992; Baldock and Holmes, 1999; Puleo and Holland, 2001). Peregrine and Williams (2001), hereafter PW01, extended the Shen and Meyer solution to include the internal flow kinematics in the absence of friction. Alternatively, full numerical solutions of the shallow water wave equations yield reasonable descriptions of the flow field (Hibberd and Peregrine, 1979), but appropriate input conditions are more difficult to obtain. This is a highly dynamic zone and although much research progress has been made in the last decade, the sediment dynamics in this region are still poorly understood. In particular, no reliable models exist for shoreward sediment transport and data (both laboratory and field) is very limited (see Elfrink and Baldock, 2002 for a recent review).

The shoreline motion given by SM63 is parabolic and equivalent to a simple ballistic motion under constant gravitational acceleration (figure 3). Friction modifies the parabolic nature of the shoreline path (Hughes, 1995), but does not alter the underlying ballistic principle. SM63 provide an expression for the flow depth close to the runup tip, subsequently used by PW01 to obtain the flow kinematics (again for inviscid flow). PW01 extended this solution to calculate the overtopping flow over a truncated beach, which led to the idea of using a similar approach to measure uprush sediment transport experimentally (Section 3 below). However, the SM63 solution typically over-estimates flow depths (Hughes, 1992), while the interpretation of the SM63 solution by PW01 leads to what appear to be unrealistically small flow depths. In addition, the analytical solution is not valid in the early stages of the runup. Consequently, a recent pragmatic approach adopted by Hughes and Baldock (2004), hereafter HB04, combines the SM63 approach with a similarity profile for the swash lens, scaled according to the terminal bore height, H_b (figure 4). This compares well with laboratory and field data and provides the hydrodynamic model used in the present study.

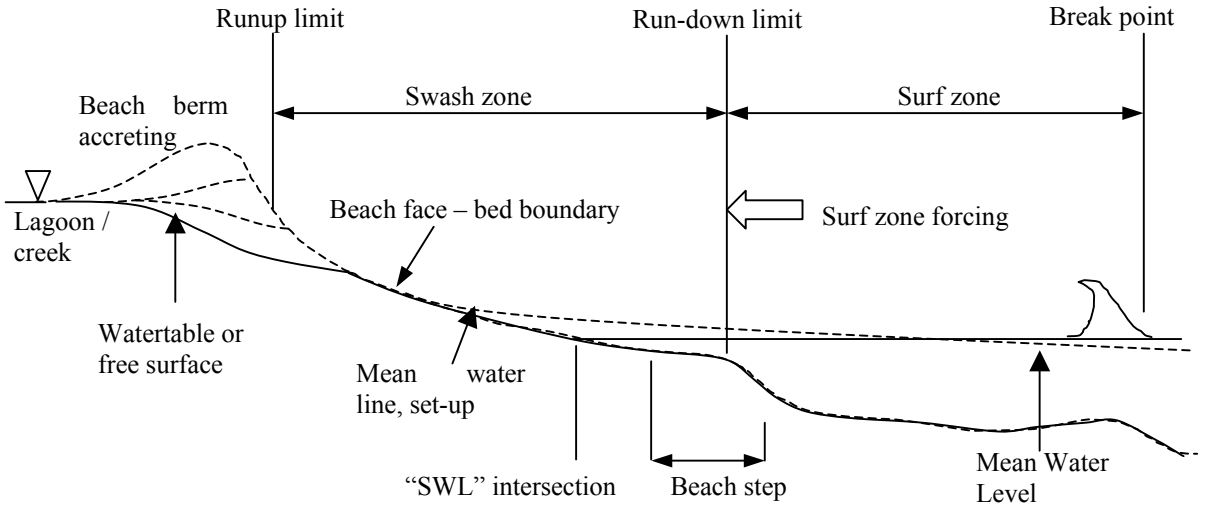

Figure 1. Definition Sketch Of Nearshore Zone And ICOLL (After Elfrink And Baldock, 2002).

3. EXPERIMENTAL SET-UP

Laboratory measurements of swash hydrodynamics and sediment transport are difficult to obtain, due to the small flow depths and thin layers of moving sediment. In the field, this is not so restrictive, but flow conditions are much more variable and less certain. Here, inspired by the overtopping solution of PW01, novel uprush sediment transport data was obtained by truncating the beach below the maximum runup elevation and allowing the flow and sediment to overtop the beach. It is then simple to measure both flow volumes and the sediment passing the truncation point. The experiments were carried out in the Coastal Engineering wave flume in the Civil Engineering Department at the University of Queensland. The flume is 20m long and 0.9m wide, and was used with water depths ranging from 0.3-0.45m (figure 2). A plane beach, gradient β=0.1, was installed 7m from the wavemaker and truncated at an elevation of 0.5m. Overtopping flow volumes were collected in a measuring tank, with overtopping sediment volumes trapped by a fine gauge mesh collecting tray above the tank. Offshore wave conditions were measured with an electronic wave gauge. Overtopping measurements were obtained for wave heights ranging between 0.04m and 0.1m, with periods varying from 1.5s to 3.0s. A non-dimensional measure of the truncation point, E, varies between 0 (corresponding to the SWL) and 2 (at the expected usual runup limit, R). For each wave condition, R was determined by running the same wave conditions on a non-truncated beach, with the data comparing well with Hunt's (1959) formula ($R=\sqrt{(H_oL_o)}\tan\beta$, where H_o and L_o are the deep water wave height and wave length respectively. Overtopping flow volumes were first collected with a fixed beach (in the absence of sand). A 50mm thick sand layer (0.3mm median grain size) was then added parallel to the underlying beach and regraded before each test. The same wave conditions were then repeated and the sediment overwash collected, dried and weighed to derive the total uprush transport per wave.

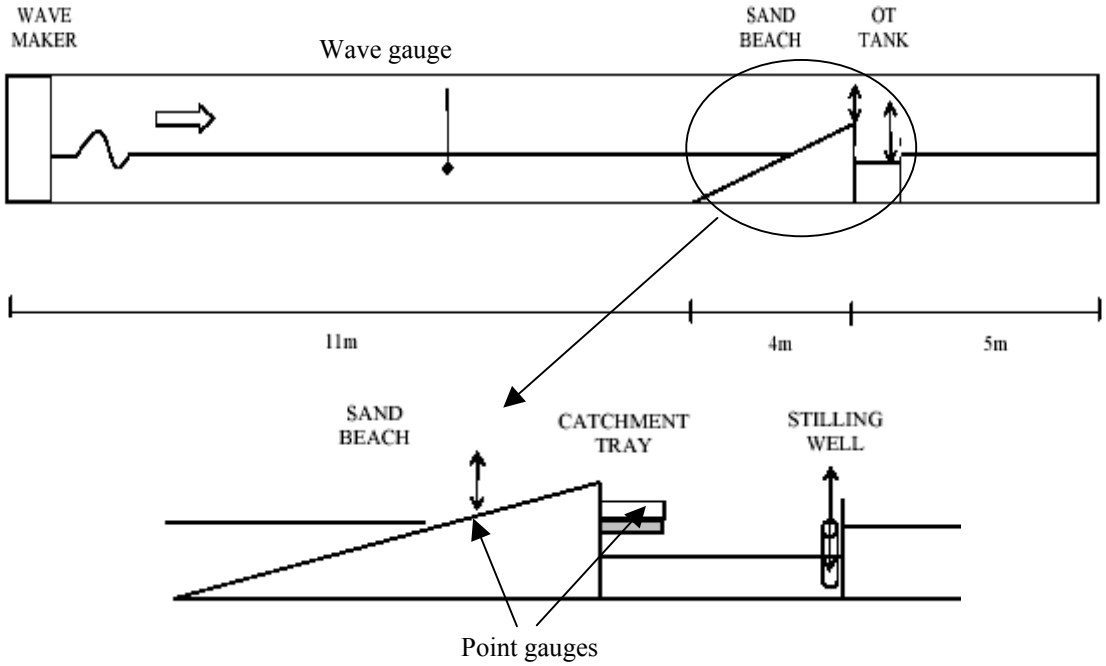

Figure 2. Experimental Set-up, Wave Flume And Overtopping Arrangement

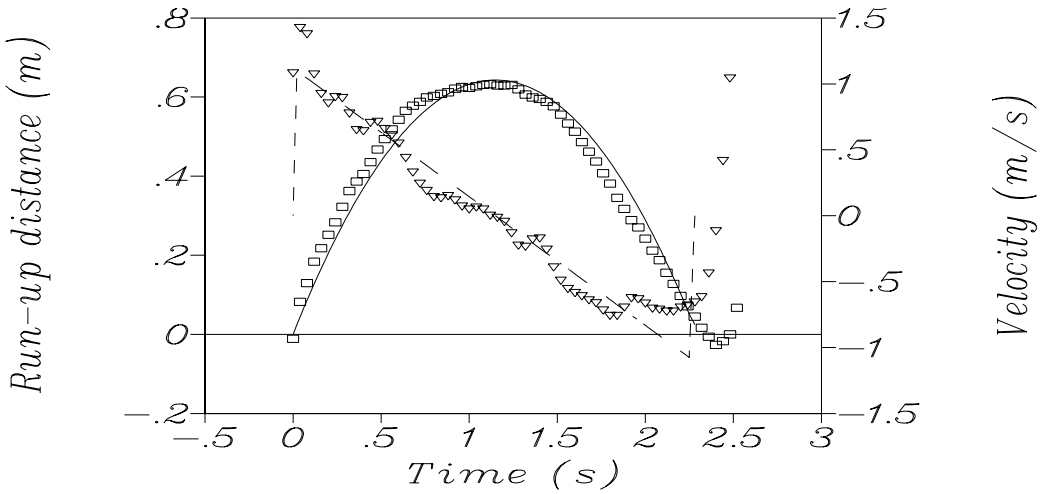

Figure 3. Measured And Predicted Shoreline Motion, X_s (t),And Velocity, H_b=0.032m.
□□□□ Runup wire, ——— X_s(t), SM63.
∇∇∇∇ Shoreline Velocity, Measured (rhs), – – – Shoreline Velocity, SM63 (rhs).

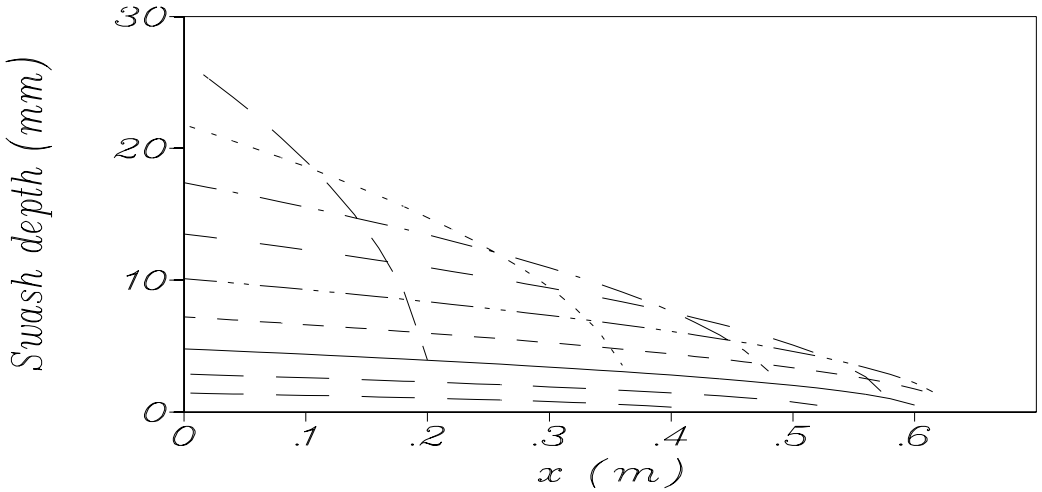

Figure 4. Similarity Profile For Swash Lens. H_b=0.032m. x=0 Is Position Of Start Of Bore Collapse

4. RESULTS

Figure 5 compares the non-dimensional flow depth and velocity at the truncation point (E=1, i.e. halfway between the SWL and maximum runup) from the PW01 solution and the numerical model results from HB04. Note that the PW01 solution includes the influence of the edge on the subcritical overtopping flow, whereas the model results do not. The maximum flow depth from the PW01 solution is approximately $1/36H_b$, which appears too small on the basis of laboratory and field data. The numerical model gives depths an order of magnitude greater, but does not tend to zero at the end of overtopping, which is unrealistic but does not unduly affect the results since the flow velocity tends to zero at this time. For a full swash (i.e. non-truncated beach), flow reversal occurs prior to the time of maximum uprush at non-dimensional time t=2 (halfway through the swash cycle). Dimensional depths can be obtained from these plots by multiplying by the terminal bore height, H_b, or half the maximum runup distance predicted by the SM63 model, A. In contrast, PW01 and HB04 give similar flow velocities at this location, since these calculations are largely governed by the shoreline velocity which comes directly from the SM63 ballistic solution (figure 3 above). Again, dimensional velocities can be obtained by multiplying by $\sqrt{(gH_b)}$ or $\sqrt{(gA)}$. The dimensional height of the truncation point above the SWL is given by EH_b or EA.

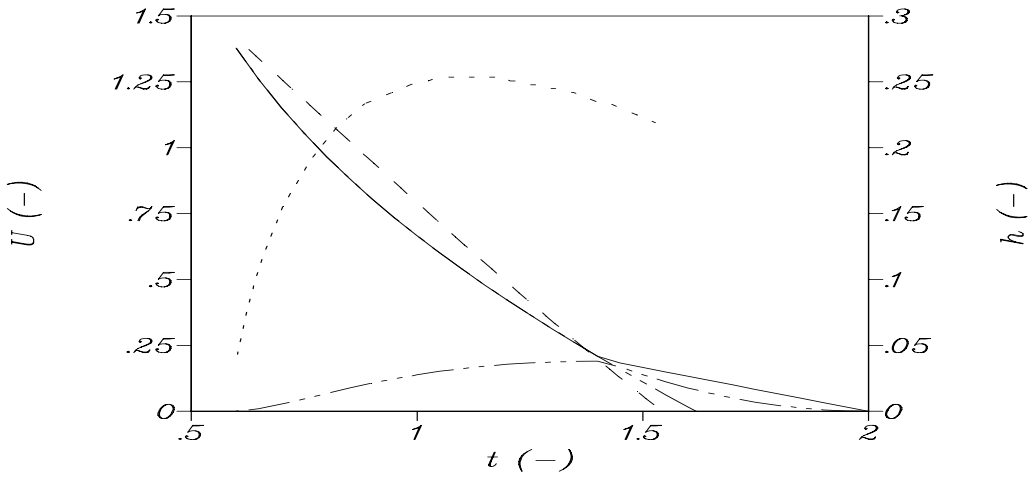

Figure 5. Non-dimensional Flow Velocity And Depth At Truncation Point, E=1.
—— Velocity (PW01); — — — Velocity (HB04); —· · — Depth (PW01); – – – – Depth (HB04)

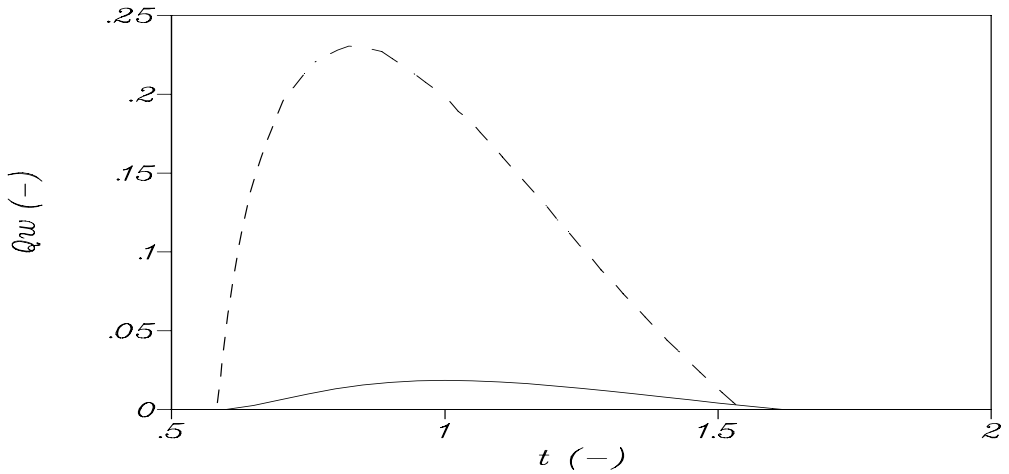

Figure 6. Non-dimensional Overtopping Volume at Truncation Point, E=1.
—— PW01; — — — HB04

Clearly, therefore, the two approaches yield quite different overtopping volumes, both in terms of the variation with time (figure 6) and the total overtopping volume (figure 7). Dimensional overtopping volumes are obtained by multiplying by $2A^2/\sin(2\beta)$ (see PW01 for details). The measured laboratory data are also shown on figure 7 and appear more consistent with the numerical model calculations than the analytical solution. The scatter in the data suggest that the overtopping volume may not solely be a function of E, a result which arises from the assumption that the swash is uniquely defined by the terminal bore conditions. Hunt's formula suggests a dependence on wave period, which also influences the degree of swash-swash interaction (Baldock and Holmes, 1999). Such interactions are ignored in PW01 and the numerical model.

The measured sediment overwash per wave is generally well correlated with the overtopping flow as hypothesised in the initial experimental design, but again considerable scatter exists for individual events (figure 8). Theoretically, sediment overwash may still be a unique function of E if only bed load transport occurs, since both the Shields parameter and wave friction factor could be defined in terms of E. This remains to be investigated further. In reality, a proportion of the uprush sediment transport will be suspended load, partly advected into the swash from the surf zone. In this instance, the transport will not uniquely depend on E. Nevertheless, the data suggest the dependence on E remains strong.

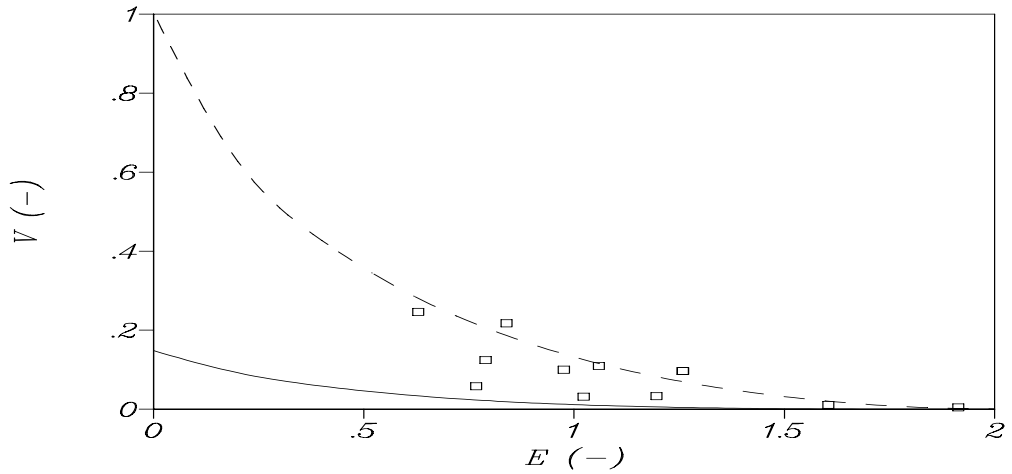

Figure 7. Measured Versus Predicted Total Non-dimensional Overtopping Volume.
□□□ Data; —— PW01; — — — HB04

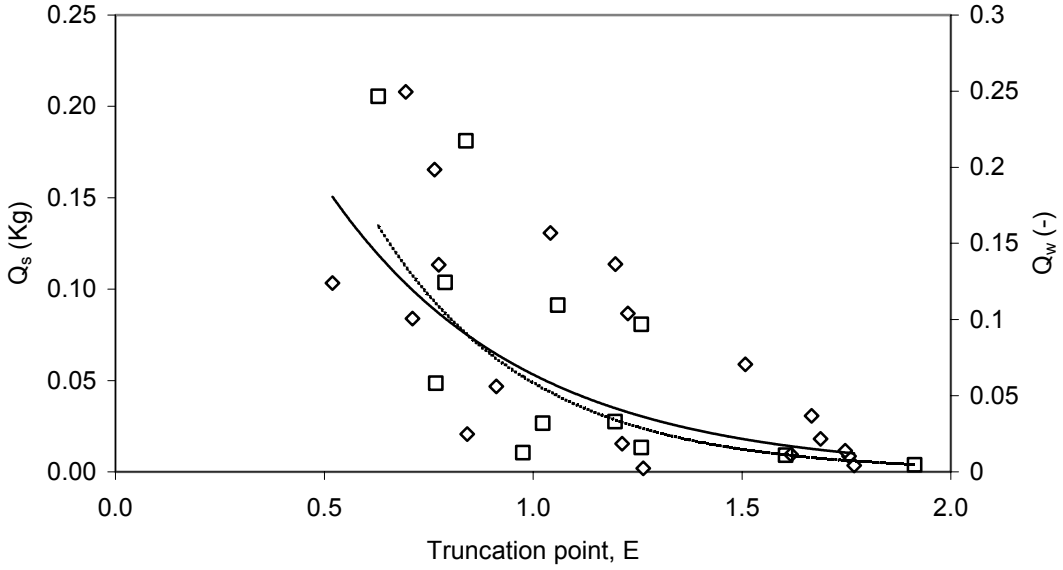

Figure 8. Sediment Overwash And Non-dimensional Water Overtopping Volume Per Wave.
—◊— Sediment Overwash, Q_b; – –□– – Overtopping volume, Q_w.

Total uprush sediment transport rates past the truncation point were calculated for each individual wave condition using the velocity field predicted by the numerical model. The sediment transport model was based on a standard bed load Shields model for wave motion (Nielsen, 1992, p112), where the total bed load transport Q_b is:

$$Q_b = \Phi d\sqrt{(s-1)gd} \tag{1}$$

with

$$\Phi = C(\theta - 0.05)\sqrt{\theta} \tag{2}$$

and

$$\theta = \frac{1/2\, f_w u|u|}{(s-1)gd} \tag{3}$$

where d is the median grain diameter, s is the specific gravity of the sediment, u is the free stream horizontal velocity, and f_w is the wave friction factor. Estimates of f_w for the swash zone range from 0.01 to 0.06 (Hughes, 1995; Raubenheimer et al., 2004), leading to large differences in the transport rates given by (1)-(3). Similarly, estimates of the multiplier C, typically 12 for steady flow data (Nielsen, 1992) range from 8-20 (Masselink and Hughes, 1998). However, in calibrating sediment transport equations of the form above with data, C and f_w are not independent and depend on the details of the model adopted. For the present data set, estimates of f_w based on standard expressions yields values of order 0.01, which combined with a multiplier C=20 slightly underpredicts the measured transport rates. A choice of f_w=0.021 and C=12 provides a better fit to the data. An example calculation for an individual swash event is shown in figure 9, which illustrates the similar dependence of Q_b and Q_w on E. However, Q_w reduces more quickly with increasing E (truncation point further shoreward) since the volume discharge is a function of flow depth, whereas Q_b is not. Finally, comparisons between measured and predicted total transport rate per wave are shown in figure 10. Given the use of the typical transport coefficients and friction factor noted above, the overall agreement is excellent.

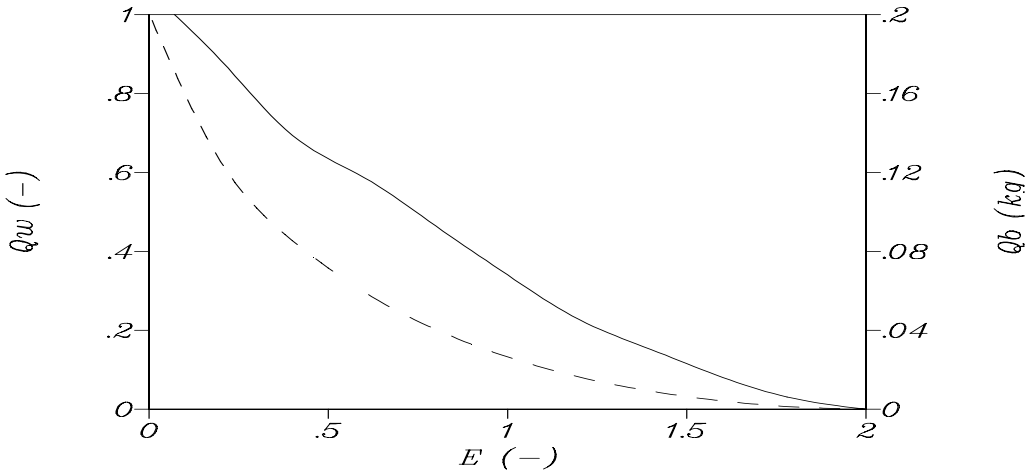

Figure 9. Predicted Sediment Overwash And Non-dimensional Water Overtopping Volume Per Wave, Numerical Model Results.
—— Sediment Overwash, Q_b; – – – – Overtopping Volume, Q_w.

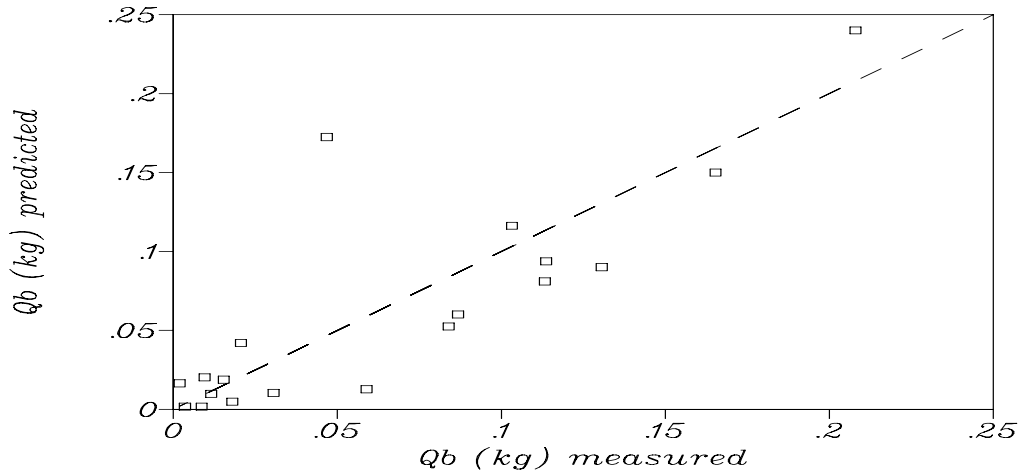

Figure 10. Measured Versus Predicted Sediment Overwash, *C*=12, *f*=0.021.

5. CONCLUSIONS

New laboratory data on swash overtopping volumes and sediment overwash on a truncated beach have been presented. The experimental design allowed direct measurement of the total uprush sediment transport rate past a fixed section of the beach, which is otherwise not easily achievable at laboratory scale. The overtopping flow is compared to an analytical solution (Peregrine and Williams, 2001) and predictions based on a recently developed numerical model (Hughes and Baldock, 2004). The analytical solution gives small flow depths compared to the model and appear unrealistic for typical nearshore bore conditions. The overtopping rates predicted by the model and the analytical solution are therefore approximately an order of magnitude different, with the model results in closer agreement with the data. The flow field predicted by the numerical scheme is then used to estimate sediment transport rates over the truncated beach. Good agreement between the model and measurements are found using conventional transport formulae and standard friction and transport coefficient. The good performance of the model suggests it may be applicable for modelling the accretion of berms on natural beaches, a process which requires overtopping and sediment transport above the existing berm crest.

6. ACKNOWLEDGEMENTS

The authors gratefully acknowledge the support from UQ staff grants and the CRC for Sustainable Tourism, grant number 70058.

7. REFERENCES

Baldock, T. E., and Holmes, P. (1999). Simulation and prediction of swash oscillations on a steep beach, *Coastal Eng*., 36, 219-242.

Elfrink, B. and Baldock, T. E. (2002). Hydrodynamics and sediment transport in the swash zone: a review and future perspectives. *Coastal Eng.,* 45, 149-167.

Hibberd, S. and Peregrine, D. H. (1979). Surf and runup on a beach: a uniform bore. *J. Fluid Mech.*, 95, 323-345.

Hughes, M.G. (1992) Application of a non-linear shallow water theory to swash following bore collapse on a sandy beach, *J. Coastal Res.,* 8, 562-578

Hughes, M.G. (1995) Friction factors for wave uprush, *J. Coastal Res.,* 11, 1089-1098.

Hughes, M. G. and Baldock, T. E., 2004. Eulerian flow velocities in the swash zone: Field data and model predictions. J. Geophys. Res, in review.

Hunt, I. A., 1959. Design of seawalls and breakwaters. *Proc. Amer. Soc. Civ. Eng*., 85, 123-152.

Masselink G. and Hughes, M.G. (1998). Field investigation of sediment transport in the swash zone. *Cont. Shelf Res.,* 18, 1179-1199.

Nielsen P., 1992. *Coastal bottom boundary layers and sediment transport*, Advanced series on ocean engineering, World Scientific, Singapore, 324p.

Peregrine, D.H. and Williams, S.M. (2001). Swash overtopping a truncated plane beach. *J. Fluid Mech.*, 440, 391-399.

Puleo, J.A. and Holland K.T. (2001). Estimating swash zone friction coefficients on a sandy beach, *Coastal Eng.,* 43, 25-40.

Raubenheimer, B., Elgar, S. and Guza, R.T. (2004). Observations of swash zone velocities: a note on friction coefficients. *J. Geophys. Res.,* 109.

Shen, M.C., and Meyer, R. E. (1963). Climb of a bore on a beach. Part 3, Runup, *J. Fluid Mech.,* 16, 113-125.

Yeh, H.H., Ghazali, A. and Marton, I. (1989). Experimental study of bore runup, *J. Fluid Mech.,* 206, 563-578.

The Institution of Engineers, Australia
8th National Conference on Hydraulics in Water Engineering
ANA Hotel Gold Coast, Australia 13-16 July 2004

Assessment of Deposited Sediments in Roadside Stormwater Retention Basins

J. E. Ball
B.E., M.E., PhD., M.I.E.Aust., CPEng.
Associate Professor, Water Research Laboratory, Civil & Environmental Engineering, University of NSW, Sydney, Australia
J. W. Walker
B.E., MEngSci
Senior Project Engineer, Water Research Laboratory, Civil & Environmental Engineering, University of NSW, Sydney, Australia
S. Isles
Roads & Traffic Authority NSW, Australia
C. Blake
Roads & Traffic Authority NSW, Australia

Abstract: Previous studies have shown stormwater runoff from road surfaces to contain numerous contaminants. Most of these contaminants are bound to silt or clay sized particles. Hence, the fine sediments trapped in roadside retention basins may potentially have high concentrations of contaminants. This study was undertaken to assist in the development of a maintenance strategy for RTA retention basins. A key outcome from the study was determination of the contaminant concentrations in the sediments and hence the "Waste Classification" in accordance with the NSW EPA Waste Guidelines.

Ten retention basins located on major highways in NSW were selected for the study. All retention basins were located in predominantly rural regions. Based on the chemical analysis of the sediments all contaminants except lead met the Inert classification criteria as outlined in the NSW EPA Waste Guidelines. Lead leachate concentrations in some samples (4 basins) were sufficiently high for the sediments to be classified as Solid Waste.

Keywords: Stormwater, retention basin, contaminant, road runoff.

1. INTRODUCTION

Stormwater runoff from road surfaces impacts on the environment in several ways. Firstly, the impervious road surface may alter the flux and volume of stormwater runoff and secondly, the quality of the runoff may be affected by contaminants originating from vehicular traffic using the roadway and the road surface itself.

In recognition of the potential impacts that stormwater runoff from road infrastructure may have on the natural environment the Roads and Traffic Authority (RTA) for a number of years has been constructing stormwater retention basins. These retention basins vary widely in design, with some basins being of natural earth construction, some lined with shotcrete, others excavated in sandstone and some formed using Gabion wire baskets. Basin dimensions also vary widely, as does catchment type, catchment size, hydrology and runoff characteristics. The majority of basins incorporate a low flow siphon pipe and an overflow spillway.

Most contaminants found in road runoff are found bound or attached to silt and clay sized particles (Ball et al., 2000). Thus, the capture of contaminants in retention basins is strongly correlated to their performance in removing fine sediments from stormwater road runoff.

A strategic study was undertaken to assess the nature and performance of road runoff interception devices (retention basins) at a number of major sites in New South Wales. A key outcome from the study was the determination of the concentrations of various contaminants contained in the sediments and hence the "Waste Classification" in accordance with the NSW EPA Waste Guidelines. The study will form a basis from which the RTA can formulate a management and maintenance plan for other road runoff interception locations.

Described in this paper are the sampling methodology and results for the selected retention basins. Interpretation of results and disposal options for contaminated sediments are discussed also.

2. GENERAL BACKGROUND INFORMATION

2.1 Relevant Literature

The majority of published literature on pollutant loads for road surface runoff has focussed on either the availability or transport of pollutant constituents. For example, Sartor and Boyd (1972), Shaheen (1975), Ellis and Revitt (1982) and Ball et al. (1996) have all investigated the availability of pollutant constituents on road surfaces. In a similar manner, Barrett et al. (1993), Batley et al. (1994), Sansalone et al. (1998), Brockbank et al. (1999) and Drapper et al. (2000) have investigated the chemical composition of stormwater runoff from road surfaces.

While some published literature is available on the sediment removal efficiency of stormwater retention basins, few studies (if any) have been undertaken on the levels of road surface contaminants contained in the sediments trapped in the basins. The concentration of contaminants in the sediments has ramifications for the maintenance of the retention basins. Of particular concern is the classification of the sediment toxicity which dictates the handling and disposal options for the waste.

2.2 NSW EPA Waste Guidelines

The classification and licensing requirements for the disposal of non-liquid wastes in New South Wales is outlined in the document "Environmental Guidelines: Assessment, Classification and Management of Liquid & Non-liquid Wastes", (NSW EPA, 1999). In summary, the management and disposal of solid wastes is based on the classification of the waste as Inert, Solid, Industrial or Hazardous.

If the waste is classified as either industrial or hazardous a license is required to generate, store, transport or dispose of the waste material. Waste classification criteria are set out in the Environmental Guidelines. Relevant waste criteria are summarised in Tables 1 and 2.

Contaminant	Inert Waste	Solid Waste	Industrial Waste
Arsenic	10	100	400
Cadmium	2	20	80
Chromium	10	100	400
Lead	10	100	400
Mercury	0.4	4	16
Nickel	4	40	160
Benzene	1	10	40
Toluene	28.8	288	1152
Ethyl benzene	60	600	2400
Xylene	100	1000	4000
C6-C9 petroleum Hydrocarbons	NA	NA	NA
C10-C36 petroleum Hydrocarbons	NA	NA	NA
PAH	NA	NA	NA

Table 1
Contaminant Threshold Values for Classification of Non-liquid Wastes without Leaching Test (mg/kg)
(NSW EPA, 1999)

Table 1 provides contaminant threshold values if leaching tests are not undertaken as part of the waste assessment. Table 2 provides contaminant threshold values where leachable concentrations (TCLP) and total concentrations (SCC) are used together to determine the classification of the waste. The total concentration (SCC) values specified in Table 2 are considerably higher than those specified in Table 1. Thus, in some waste samples it may be beneficial to measure the Leachable Concentration (TCLP) if a lower waste classification is desirable.

Contaminant	Inert Waste		Solid Waste		Industrial Waste	
	TCLP mg/L	SCC mg/kg	TCLP mg/L	SCC mg/kg	TCLP mg/L	SCC mg/kg
Arsenic	0.5	500	5	500	20	2000
Cadmium	0.1	100	1	100	4	400
Chromium	0.5	1900	5	1900	20	7600
Lead	0.5	1500	5	1500	20	6000
Mercury	0.02	50	0.2	50	0.8	200
Nickel	0.2	1050	2	1050	8	4200
Benzene	0.05	18	0.5	18	2	72
Toluene	1.44	518	14.4	518	57.6	2073
Ethyl benzene	3	1080	30	1080	120	4320
Xylene	5	1800	50	1800	200	7200
C6-C9 petroleum Hydrocarbons	NA	650	NA	650	NA	2600
C10-C36 petroleum Hydrocarbons	NA	5000	NA	10000	NA	40000
PAH	NA	200	NA	200	NA	800

Table 2
Leachable Concentration (TCLP) and Total Concentration (SCC) Values for Classification of Non-liquid Wastes (NSW EPA, 1999)

3. RETENTION BASIN SITES AND SAMPLING METHODOLOGY

Ten retention basins located on major highways in NSW were selected for the study. All retention basins were located in predominantly rural regions. Each of the basins and their catchments were surveyed. Summary details of each of the ten basin sites are presented in Table 3.

Basin ID	Road	Site Location				Retention Basin	
		Region	Side of Road	AMG Coords		Catchment Size	Age
				E	N	Ha	Yrs
1	F3 Freeway	Berowa	Northbound lane	328258	6277160	2.72	15
2		Cowan	Southbound lane	329455	6279611	2.01	15
3		Cowan	Southbound lane	329341	6279171	2.65	15
4	Great Western Highway	Valley Heights	Westbound Lane	276912	6266793	1.85	6
5		Woodford Bends	Eastbound Lane	267264	6264774	1.22	10-15
6		Woodford Bends	Eastbound Lane	267277	6264846	1.52	10-15
7	Federal Highway	Lake George	Southbound lane	717856	6126083	1.50	7
8		Lake George	Southbound lane	716564	6118513	1.10	4
9	Hume Highway	Hovells Creek	Southbound lane	694862	6146066	2.20	10
10		Hovells Creek	Southbound lane	694794	6146010	1.15	10

Table 3. Summary of Site Locations.

Six sediment samples were collected from each of the 10 basins (60 samples in total) and analysed for particle size distribution and those pollutants normally associated with road surface runoff. Samples were collected near the inlet, outlet and centre of the basin. Where sediment depths were sufficient, a sample was collected from the top 100mm of the bed and a second sample collected at a depth of between 200 and 400mm. Where sediment depths were shallow, duplicate samples were collected from the top 100mm of the bed.

4. SEDIMENT CHEMICAL COMPOSITION

4.1 Total Concentrations

Trace Elements

For many of the trace elements, metal concentrations varied widely within each basin and between basins. Lead concentrations varied between 42mg/kg and 350mg/kg on the F3, and 10mg/kg to 22mg/kg on the Hume Highway. The maximum lead concentrations were measured on the F3. The lowest lead concentrations were measured on the Great Western Highway (7.9mg/kg) and probably reflect the capture efficiency of the basin rather than pollutant loads. Based on the EPA waste guidelines (Table 1, no leaching test), sediments in five of the ten basins (Basin Nos. 1 to 5) would be classified as Industrial Waste due to lead concentrations. Sediments in all remaining basins would be classified as Solid Waste due to lead concentrations.

Arsenic concentrations varied between 1.2mg/kg and 16mg/kg. Based on the EPA waste guidelines (Table 1, no leaching test), sediments in one of the ten basins (Basin No. 1) would be classified as Solid Waste due to arsenic concentrations. All other retention basins are classified as containing Inert Waste for the contaminant arsenic.

Cadmium was only detectable in Basin Nos. 1 to 4. The maximum concentration of cadmium measured was 2.3mg/kg. Based on the EPA waste guidelines (Table 1, no leaching test), sediments in one of the ten basins (Basin No. 1) would be classified as Solid Waste due to cadmium concentrations. All other retention basins are classified as containing Inert Waste for the contaminant cadmium.

Chromium concentrations were relatively consistent in all basins. Concentrations varied from 2.3mg/kg to 41mg/kg in the sediment samples. Based on the EPA waste guidelines (Table 1, no leaching test), sediments in all ten basins would be classified as Solid Waste due to chromium concentrations.

Mercury concentrations were below detection limits.

Nickel concentrations in the sediments varied from 2.9mg/kg to 48mg/kg. Based on the EPA waste guidelines (Table 1, no leaching test), sediments in all ten basins would be classified as Solid Waste due to nickel concentrations.

Polycylic Aromatic Hydrocarbons (PAH)

For all sediment samples PAH concentrations were below analytical detection limits.

Phthalates

Phthalate plasticiser bis (2ethyl-hexyl) was detected in 7 of the 10 retention basins. The maximum plasticiser concentration measured in the sediments was 9.9mg/kg.

BTEX

For all sediment samples BTEX compounds were below analytical detection limits.

Total Petroleum Hydrocarbons (TPH)

The lighter TPH fractions (C6-C9) were below analytical detection limits in all sediment samples. The heavier TPH fractions (C10-C36) were detected in all basins. The maximum TPH concentration in each of the basins varied from 300mg/kg up to 2100mg/kg. Based on the EPA waste guidelines (Tables 1 and 2), sediments in all ten basins would be classified as Inert Waste for TPH concentrations.

Nitrogen and Phosphorus
Within each of the basins phosphorus and nitrogen concentrations varied widely depending on the sample location. For example, Total Nitrogen levels in Basin No. 1 varied from 320mg/kg near the inlet to 3,300mg/kg near the outlet. For the same basin phosphorous levels varied from 120mg/kg near the inlet to 450mg/kg near the outlet.

Maximum concentrations of Total Nitrogen in the sediments in each of the basins ranged from 790mg/kg to 3,300mg/kg. For phosphorous, maximum concentrations in the sediments in each basin ranged from 93mg/kg to 450mg/kg.

Organochlorine Pesticides (OC) and Organophosphate Pesticides (OP)
For all sediment samples OC and OP compounds were below analytical detection limits.

Herbicides
Glyphosate (Roundup) was detected in all 3 retention basins on the F3 (Basin Nos. 1-3) and on the Great Western Highway at Basin No. 4. At all other sites glyphosate was below detection limits.

4.2 Leachable Concentrations

Leachate tests were undertaken for each of the 60 sediment samples for the contaminants arsenic, cadmium, lead and nickel. These contaminants were selected for determination of leachate concentrations (TLCP) in accordance with Table 2 and the EPA Waste Guidelines.

For all sediment samples, leachate concentrations for arsenic were below detection limits. Leachate concentrations for cadmium and nickel were mostly below detection limits or were very low (maximum concentrations of 0.03mg/L and 0.09mg/L for cadmium and nickel respectively). Based on the EPA waste guidelines (Table 2, leaching test), sediments in all ten basins could be reclassified as Inert Waste for the trace metals of arsenic, cadmium and nickel following leachate analysis.

The maximum lead leachate concentration measured in the sediment samples was 2.7mg/L. Based on the EPA waste guidelines (Table 2, leaching test), sediments in four of the ten basins (Basin Nos. 1 to 4) could be reclassified as Solid Waste for the trace metal of lead. Sediments in the remaining six basins could be reclassified as Inert Waste. Eleven of the sixty sediment samples tested for lead leachate concentrations exceeded the Inert Waste classification threshold of 0.5mg/L.

The total concentration values (SCC) specified in Table 2 were compared to each of the 60 sediment samples collected and analysed. No sample, for any contaminant, exceeded the SCC value for Inert Waste, although individual samples from four of the ten basins exceeded the leachable lead concentration (TLCP) for Inert Waste.

4.3 Sediment Chemical Composition – Statistical Interpretation

In Basin No. 2 lead levels were highest near the inlet, and in Basin No.3 were highest near the mid-section of the basin. This variability within each basin and between basins poses several questions in relation to the classification of the sediment toxicity, namely:

- are the sediment concentrations within any basin representative of all other basins, and;
- where within a basin can we collect a sample representative of the contaminant concentrations?

To answer the first question, analysis of variance was undertaken using metal concentrations to identify if at least two of the basins were not similar. This statistical test indicated that contaminant levels in any single basin could not be considered representative of contaminant levels in all other retention basins.

To answer the second question, one would need to know in some detail the hydraulic and sediment depositional behaviour of each basin. Thus, in reality it is probably much simpler to take a set of samples within each basin. On the other hand, a statistical approach can be employed whereby each of the 60 sediment samples collected may be considered part of a larger population (ie the larger population being all of the basins within NSW). A distribution can than be fitted to the 60 samples for each contaminant and a mean and standard deviation determined. Thus, the probability of a contaminant exceeding specified threshold levels for any basin in NSW can than be specified.

This approach was adopted for each of the contaminants detected in the analytical tests and also listed in Tables 1 and 2. A log-normal fit was deemed the most suitable to represent the sample populations. An example of a distribution fit is presented in Figure 1. A statistical summary of the data and distributions is presented in Table 4.

Contaminant	**Mean Concentration**		**Standard Deviation (SD)**	**Mean+2SD**		**Mean +3SD**	
	Ln	mg/kg	Ln	Ln	mg/kg	Ln	mg/kg
Arsenic	1.383	4	0.591	2.565	13	3.156	23
Cadmium	-0.955	0.4	0.763	0.571	1.8	1.334	3.8
Chromium	2.712	15	0.594	3.900	49	4.494	89
Copper	3.141	23	0.754	4.649	100	5.403	220
Lead	3.773	44	1.022	5.817	340	6.839	930
Nickel	2.401	11	0.710	3.821	46	4.531	93
Zinc	4.946	140	0.951	6.848	940	7.799	2,400
C10-C36 petroleum hydrocarbons	6.094	580	0.806	7.706	2200	8.512	5000

Table 4. Log-Normal Contaminant Distributions (Total Concentrations)

Mean contaminant concentrations reported in Table 4 are significantly lower than those measured by Ball (1998, 2000) who sampled accumulated sediments on road surfaces. For example, mean copper concentrations as measured by Ball are approximately 120-130mg/kg, compared to mean concentrations measured during this study of 23mg/kg. Similar comparisons can be made for lead, zinc and chromium. The lower concentrations of contaminants measured in the sediments may reflect the efficiency of the retention basins, catchment characteristics (Ball's work was undertaken in mostly urban environments) and the sampling methodologies of the various historical studies.

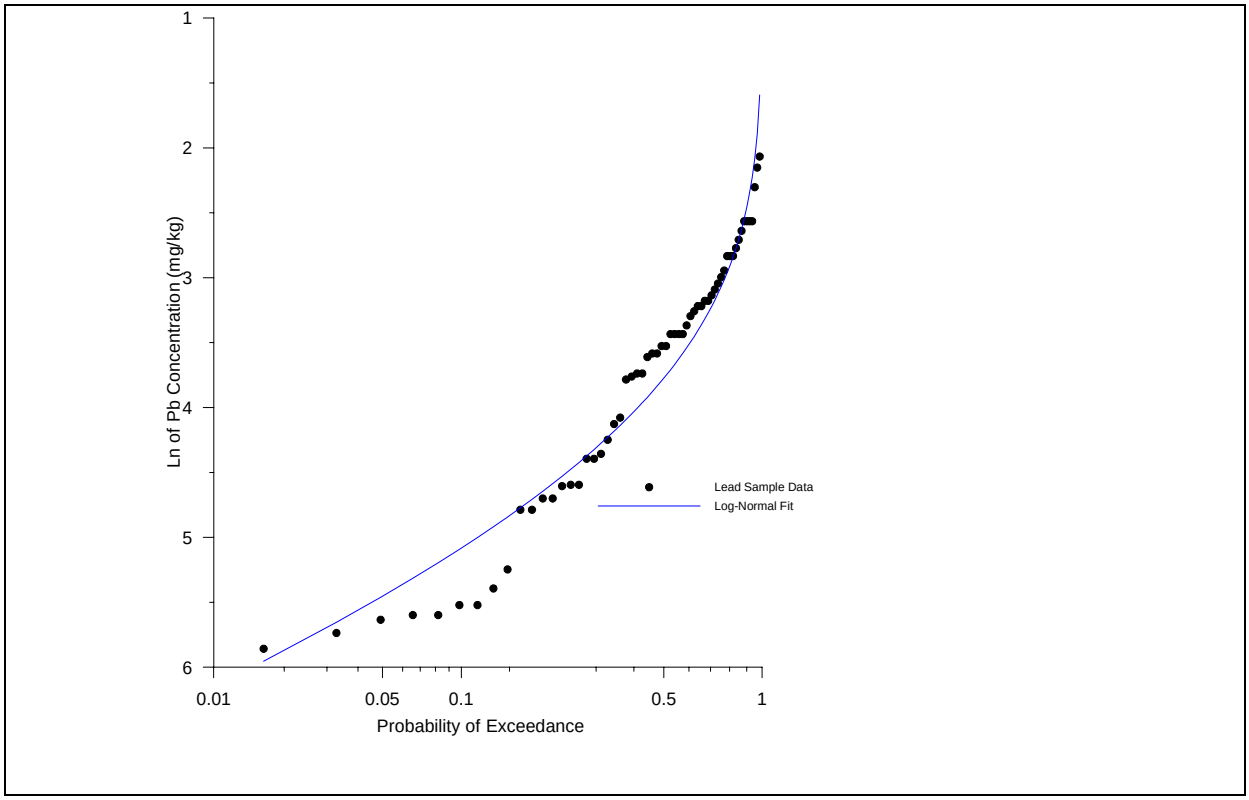

Figure 1 – Lead Concentrations

Leachate concentrations for lead were much higher than the other contaminants. As such, a statistical fit of the data for lead leachate concentrations was undertaken. A log-normal fit was deemed the most suitable to represent the sample population. A statistical summary of the data and distribution is presented in Table 5.

Contaminant	**Mean Concentration**		**Standard Deviation (SD)**	**Mean+2SD**		**Mean +3SD**	
	Ln	mg/L	Ln	Ln	mg/L	Ln	mg/L
Lead	-2.220	0.11	1.556	0.892	2.4	2.448	12

Table 5. Log-Normal Contaminant Distributions (Leachate Concentrations)

No empirical relationship was evident between total concentration and leachate concentration for lead, other than the observation that when the total concentration of lead in a sample was relatively low, the leachate concentration for that sample was generally below detection limits.

By adopting the mean plus 2SD for each contaminant (ie 98% of the population) from Tables 4 and 5 as the acceptable contaminant level that will not be exceeded by any given sediment sample in any basin, then it is possible to draw the following conclusions:

- No contaminant exceeds the total concentration (SCC, Table 2) threshold for inert waste classification;
- Only lead levels exceed the leachate concentration (TCLP, Table 2) threshold for inert waste classification;
- Lead leachate concentrations (TCLP, Table 2) do not exceed the leachate concentration threshold for solid waste classification.

Based on the above findings, deposited sediments in RTA stormwater retention basins may be classified as Solid Waste for disposal purposes. If leachate testing had not been undertaken, contaminant threshold values as specified in Table 1 would apply, in which case the deposited sediments would be classified as Industrial Waste for disposal purposes.

5. DISCUSSION

Mean contaminant concentrations in the sediments measured during the course of this study are significantly lower than those measured by Ball (1998, 2000) in NSW. As discussed earlier, this may reflect the efficiency of the retention basins, catchment characteristics (Ball's work was undertaken in mostly urban environments) and the different sampling methodologies adopted in historical studies. Of further interest, the road runoff contaminant concentrations as reported by Ball (1998, 2000) are an order of magnitude lower than similar overseas studies. Consequently, overseas studies on road runoff cannot be directly applied to Australian environments.

Sediment contaminant concentrations were shown to vary widely between and within each of the basins. A statistical assessment of contaminant concentrations for the 60 sediment samples was undertaken to determine contaminant levels which would not be exceeded by 98% of RTA retention basins. Using this statistical criteria it would then be possible to classify the waste (sediments) in each basin without sampling and chemical analysis.

In accordance with the EPA Waste Guidelines all sediment contaminant concentrations (both total and leachate) are below the Inert threshold except for lead leachate concentrations. Thus, for waste disposal purposes the sediments retained in the retention basins are classified as Solid Waste.

With reference to waste disposal/classification, the contaminant of concern is lead. Lead concentrations vary significantly between basins. For example, the basins on the Federal Highway (relatively new) show lead levels well below the Inert threshold specified in the EPA Waste Guidelines, while those on the F3 (15 year old basins) would be classified as Solid Waste. The recent introduction of lead replacement additives in motor vehicle fuel may help to explain these variations in lead concentrations. Thus, with some additional monitoring, new basins or basins that have been recently cleaned could possibly be reclassified to contain Inert rather than Solid Waste.

An alternative to classifying sediments in all basins as Solid Waste is to undertake sampling and chemical analysis within each basin to be cleaned. Based on the statistical assessment (and approval from the EPA), the only parameter required to be tested for would be lead leachate concentrations.

It should be noted that each of the 10 basins selected for this study are rural catchments with high traffic volumes. The assessment and classification undertaken in this study may not be applicable to urban and industrial regions.

6. CONCLUSIONS

Ten RTA retention basins located on major highways in rural NSW were selected for sampling of sediments and subsequent analysis for road runoff contaminants. Sediment contaminant levels were considerably lower than other published data, suggesting that the findings of many overseas studies are not directly applicable to Australian conditions.

Based on the statistical methodology used in this study, all sediments in RTA retention basins with predominantly rural catchments may be classified as Solid Waste. Only lead leachate concentrations exceeded the criteria for the sediments to be classified as Inert Waste. With the introduction of lead replacement fuel, new retention basins may be able to meet the criteria for the sediments to be classified as Inert Waste.

7. REFERENCES

Ball, J.E., Jenks, R. and Aubourg, D. (1996), Dry Weather Build-up of Constituents on Catchment Surfaces", *Proccedings Seventh International Conference on Urban Storm Drainage*, Hanover Germany, Vol.2, pp785-790.

Ball, J.E., Jenks, R. and Aubourg, D. (1998), "An Assessment of the Availability of Pollutant Constituents on Road Surfaces", *The Science of the Total Environment*, 209:243-254.

Ball, J.E., Wojcik, A. and Tilley, J. (2000), "Stormwater Quality from Road Surfaces – Monitoring of the Hume Highway at South Strathfield", *Research Report No. 204*, University of New South Wales, Water Research Laboratory, Sydney, Australia.

Barrett, M.E., Zuber, R.D., Collins, E.R., Malina, J.F., Charbeneau, R.J. and Ward, G.H. (1993), "A Review and Evaluation of the Literature Pertaining to the Quality and Control of Pollution from Highway Runoff and Construction", *Report No. CRWR 239*, Centre for Research in Water Resources, University of Texas, Austin, USA.

Batley, G.E., Brockbank, C.I., Hogan, P.M. and Ball, J.E. (1994), "The Chemical Composition of Stormwater Runoff from Roads", *Investigation Report CET/IR263*, Centre for Analytical Chemistry, Division of Coal and Energy, CSIRO.

Brockbank, C.I., Batley, G.E., Ball, J.E. and Tilley, J.H. (1999), "Metals and Hydrocarbons in Stormwater Runoff from Urban Areas", *Report No. Et/IR98R*, Centre for Advanced Analytical Chemistry, CSIRO, Lucas Heights, Australia.

Drapper, D., Tomlinson, R. and Williams, P. (2000), "Pollutant Concentrations in Road Runoff: Southeast Queensland Case Study", *Journal of Environmental Engineering*, ASCE, 126(4), 313-320.

Ellis, J.B. and Revitt, D.M. (1982), "Incidence of Heavy Metals in Street Surface Sediments: Solubility and Grainsize Studies", *Water Air Soil Pollution, 17:87-100*.

NSW EPA (1999), "Environmental Guidelines: Assessment, Classification and Management of Liquid & Non-liquid Wastes", Sydney, Australia, ISBN 0 7313 0215 X.

Sansalone, J.J., Koran, J.M., Smithson, J.A. and Buchberger, S. G. (1998), "Physical Characteristics of Urban Roadway Solids Transported During Rain", *Journal of Environmental Engineering*, ASCE, 124(5), 427-440.

Sartor, J.D. and Boyd, G.B. (1972), "Water Pollution Aspects of Street Surface Contaminants", *Report No. EPA-R2-72/081*, US Environmental Protection Agency, Washington DC, USA.

Shaheen, D.G. (1975), "Contributions of Urban Roadway Usage to Water Pollution", *Report No. EPA 600/2-75-004*, US Environmental Protection Agency, Washington DC, USA.

The Institution of Engineers, Australia
8th National Conference on Hydraulics in Water Engineering
ANA Hotel Gold Coast, Australia 13-16 July 2004

Deterioration of Conduit Efficiency Due to Biofouling

A. F. Barton
BE(Hons), MEngSc, MIAHR, MAWA, MIEAust
PhD Student, School of Engineering, University of Tasmania, Australia
M. W. Sylvester
BE(Hons), MIPENZ, MIEAust
Senior Hydropower Engineer, Hydropower and Water Resources, Maunsell Ltd, New Zealand
J. E. Sargison
BE(Hons), PhD, MASME, MIEAust
Research Fellow, School of Engineering, University of Tasmania, Australia
G. J. Walker
BSc, BE(Hons), PhD, FASME, FIEAust, CPEng
Reader, School of Engineering, University of Tasmania, Australia
A. B. Denne
DipCivEng, MIEAust, CPEng
Principal Asset Engineer (Civil), Hydro Tasmania, Australia

Abstract: Hydro Tasmania operates a network of open channels and pipelines to supply their 29 hydroelectric power stations with a total combined output capacity in excess of 2,200MW. These hydraulic conduits are susceptible to deterioration in their capacity over time due to biological growths on their internal surfaces. A research program involving Hydro Tasmania and the University of Tasmania is currently underway to alleviate the problem. This paper reports on the effects of having biological fouling material removed from a high velocity pipeline in the headworks of a hydroelectric power station. Pipeline cleaning was discovered to produce significant changes in both friction headloss and equivalent wall roughness. The broad aim of this project is to optimise pipeline maintenance procedures, minimise biological growth effects, and increase the economic return from existing infrastructure. Preliminary testing has indicated the potential for significant economic benefit.

Keywords: Biofouling, hydraulic conduit, friction loss, sand grain roughness, penstock, turbine, guide vane.

1. INTRODUCTION

Hydro Tasmania operates 29 hydroelectric schemes with an installed capacity in excess of 2,200MW. Within this system is an extensive network of open and closed hydraulic conduits. There are currently 62 pipelines and penstocks, with a combined approximate length of 42 kilometres. They vary in length from 26 metres to 8.93 kilometres, and in diameter between 1.04 metres and 7.3 metres. There are 30 tunnels and shafts, between 1.4 metres and 9.1 metres in diameter, with a total length of approximately 63 kilometres. There are 21 open channel systems with a combined approximate length of 124 kilometres, of various geometries. These conduits are susceptible to deterioration in their carrying capacity over time due to biological growths that attach to internal surfaces. This process of biofouling is attributed to a combination of bacteria, algae, fungi, and invertebrate organisms. The problem of biofouling for Hydro Tasmania relates directly to the economic returns it receives from its hydropower systems. In pipes for example, the increase in wall resistance results in increased headloss. A reduction in head at a power station equates to a reduction in power generating capacity, and reduced generation revenue. Problems associated with biofouled conduits were earlier established to be significant in the Hydro Tasmania system though studies by McFie (1973; 1976) and Brett (1980). However, there are currently no systematic maintenance programs implemented to keep friction losses due to biofouling to an acceptable level in Hydro Tasmania's hydraulic conduit systems (Hydro Consulting 2000). This is primarily due to a limited understanding of the effect biofouling has within the hydraulic conduit system. Furthermore, the current understanding has little theoretical emphasis and is based more on immediate costs and savings rather than longer-term improvements in efficiency and benefits that result.

Biofouling is thought to create additional energy dissipation mechanisms by the visco-elastic nature of some biofilms, which are able to vibrate in the flow regime (Lewandowski and Stoodley 1995). The effect is typically represented by an equivalent sand grain roughness (see Nikuradse 1933), that may differ from the physical roughness height. This concept of equivalent roughness for biofouling material is yet to be fully characterised in engineering literature. As a first step in a broader research program to control the biofouling problem, this paper presents the results for the first of a series of field tests to be undertaken on Hydro Tasmania's hydraulic

conduits. The aim is to study the effects of cleaning conduits using testing procedures to characterise the before and after friction factors and equivalent sand grain roughnesses. Tests have been carried out on a typical high velocity pipeline with results showing a significant drop in friction headloss and associated changes in the equivalent wall roughness as a result of cleaning.

2. CONDUIT DESCRIPTION AND METHOD

2.1 Conduit Description

The conduit studied brings water to a power station consisting of one 32 MW Francis turbine with nominal operating head of 252m. The water flows from an upstream storage through an intake screen and then a tunnel of various horseshoe type cross sections (Figure 1). Flow then enters a transition and penstock, which is lined with cold tar enamel on its internal surface. The water travels through the penstock to the turbine and discharges into a tailrace and receiving storage. The flow incurs minor local energy losses at each of: a hilltop valve (HTV); four vertical bends; a pipe off-take; and a machine inlet valve (MIV). The penstock is fixed at a slope of approximately 34.6 degrees from the horizontal on the hillside. Only the penstock was cleaned for the present study.

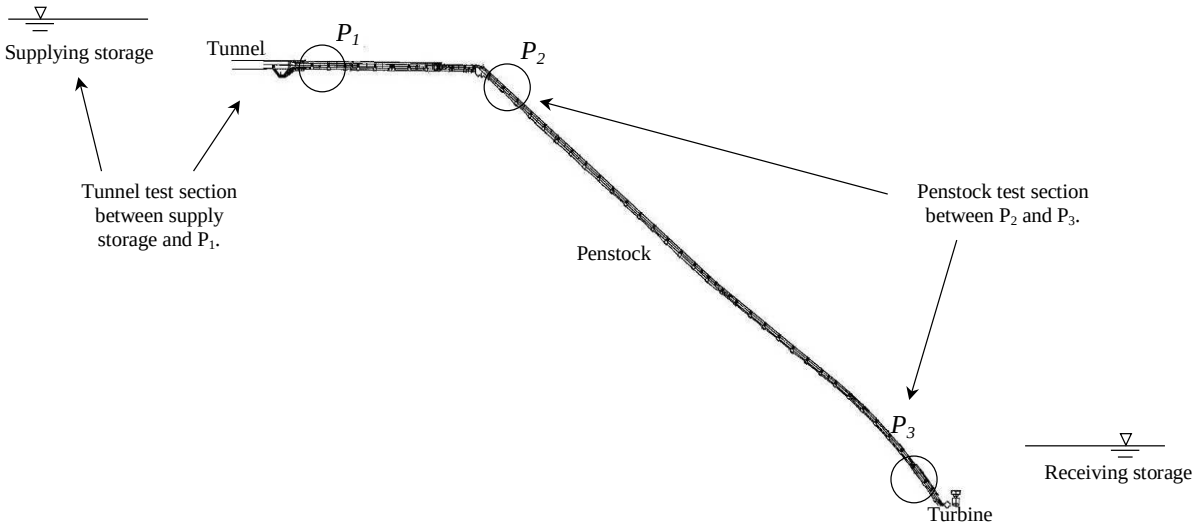

Figure 1 – Schematic Diagram of Conduit.

The turbine is located below the water surface of the receiving storage, whose level is subject to variation. This makes observation of the water surface elevation for both up- and downstream storages important for determining the effective operating head on the turbine.

2.2 Method

To measure the headloss for the upstream tunnel test section depicted in Figure 1, a pressure tapping denoted P_1 was used. The pressure difference between this point and the supplying water storage (open to atmosphere) provided the total headloss, H_L, for the tunnel conduit test section using the energy equation shown in equation 1. Since only the penstock was cleaned, the headloss characteristics in the tunnel remained constant for the tests.

$$\frac{P_{upstream}}{\rho g} + \frac{V_{upstream}^2}{2g} + y_{upstream} = \frac{P_{downstream}}{\rho g} + \frac{V_{downstream}^2}{2g} + y_{downstream} + H_L \qquad (1)$$

where P is pressure (Pa), V is velocity (m/s) calculated from the flow rate and cross sectional area, g is gravitational acceleration (m/s^2), ρ is the water density (kg/m^3), y is the height from a horizontal datum (m) taken as the supply lake level. Similarly for the penstock test section, the energy equation was used where up- and downstream pressure tappings P_2 and P_3 enabled the total headloss to be determined. The flow rate was determined by using two purpose built strap-on meters for large diameter pipes, the details of which are described subsequently in section 2.4.

Table 1 presents the general information on the tunnel, penstock and test section geometry.

Table 1 - Conduit General Information.

Conduit section description	*Length (m)*	*Area (m^2)*
Tunnel test section (storage to P_1)	4077	11.09
Start of penstock, P_1 to P_2	163	3.08
Penstock test section (P_2 to P_3)	332	3.08
P_3 to turbine	31	3.08
Total length of conduit	4598	

Both friction losses and surface roughness characteristics were specifically of interest. The total headloss, H_L, for the penstock is described in equation 2 as the combined total of friction losses, h_f, and minor losses, h_l.

$$H_L = h_f + h_l \tag{2}$$

Minor losses, h_l, due to valves, pipe branches, bends, and pipe transitions, were represented by a generic loss coefficient, K. This coefficient was applied to the velocity head at each point of interest, i, in the pipe and summed over all elements to give equation 3.

$$h_l = \sum_i K_i \frac{V_i^2}{2g} \tag{3}$$

This value was subtracted from measured H_L in the penstock to give h_f. Table 2 summarises the K values used for headloss determination in the penstock section.

Table 2 - Penstock Loss Coefficients.

Pipe section description	*K loss factor*	*Section area (m^2)*
Tunnel to pipe transition	0.02	3.08
Hilltop valve	0.11	3.08
Bend 1	0.18	2.87
Bend 2	0.01	3.07
Bend 3	0.05	3.04
Bend 4	0.31	2.37
Pipe off take	0.04	1.51
Machine inlet valve	0.11	2.11

The Darcy-Weisbach equation was used to describe the conduit friction losses as shown in equation 4.

$$h_f = f \frac{L}{D} \frac{V^2}{2g} \tag{4}$$

Here h_f is the headloss due to friction (m), f is the Darcy friction factor, V is flow velocity (m/s), L is pipe length (m), and D is pipe diameter (m). h_l is subtracted from H_L to give h_f. Once friction factors are found, the equivalent sand grain roughness, k_s (see Nikuradse 1933) can be determined using the Colebrook-White type equation shown as equation 5:

$$\frac{1}{\sqrt{f}} = -2\log\left(\frac{k_s}{3.7D} + \frac{2.51}{R_e\sqrt{f}}\right) \tag{5}$$

where R_e is the Reynolds number, $R_e = \frac{\rho VD}{\mu}$, for the given flow based on pipe diameter (see Colebrook and White 1937).

2.3 Lake Level Correction

Operational conditions prevented lake levels being the same for both pre- and post-clean tests. This meant that power output and flow rate corrections were needed to compare turbine outputs on a common basis. Constant turbine guide vane positions were used in the tests, and corrections to power and flow values were made by assuming, $P \propto H^{\frac{3}{2}}$, and $Q \propto H^{\frac{1}{2}}$ as follows:

$$P' = \left(\frac{H_{pre} - H_{L\_post}}{H_{post} - H_{L\_post}} \right)^{\frac{3}{2}} P \tag{6}$$

$$Q' = \left(\frac{H_{pre} - H_{L\_post}}{H_{post} - H_{L\_post}} \right)^{\frac{1}{2}} Q . \tag{7}$$

Here P and P' denote the power output and corrected power output respectively, and similarly for the flow rates Q and Q'. H_{pre} and H_{post} denote the gross head for the pre- and post-clean conditions respectively, and H_{L_post} is the headloss for the post clean tests.

2.4 Instrumentation and measurement of data

Static pressures were measured with *Druck PTX1400* 0-4,000KPa gauge *Industrial pressure transmitters* with a quoted error no greater than +/-1% (Druck Limited 1997). Four pressure tappings set diagonally from each other were attached to a ring bus where two transducers were located at the centreline of the pipe. The average of the two transducer readings were used at each station.

The flow rate was determined by using two *Panametrics* flowmeters giving velocity readings of +/-6% accuracy (McGuinness 2003 pers. comm.), and the known cross sectional area. Two sets of flow meters were mounted horizontally and vertically opposite from each other.

Guide vane openings for the Francis turbine were recorded as a percentage where 0% = closed, and 100% = fully open. A linear displacement transducer measured the stroke of the guide vane servomotor. This is linearly related to the rotation of the guide vanes.

All data was either logged directly to a PC or datalogger to be sent electronically back to a PC for storage.
Lake level readings were taken from level sensors linked by telemetry to a time series database within Hydro Tasmania. Readings were taken at both the upstream and downstream lake storages.

A *Center_305 data logger thermometer* was used to record penstock water temperatures periodically for both pre- and post-clean testing in order to calculate water viscosity, and test Reynolds number.

3. RESULTS

Subtraction of the downstream receiving storage levels from the upstream supply storage levels gives the gross operating head on the turbine. This is shown in Figure 2 for both the pre- and post-clean testing periods. It should be noted that allowance for daylight saving time was made when retrieving and preparing lake level data. The conduit testing was performed over a range of turbine output conditions. The direct results of the tests are presented in Tables 3 and 4. Both tests began with static flow conditions with zero power output, then increased incrementally to full flow and power output levels. Some tests were taken in the reverse order to check for consistency in measurement. All tests were given an appropriate amount of time to stabilise after the previous test to minimise pressure fluctuations in the conduit. Improvement in pipe performance is shown as an increase in net head (m) and an increase in turbine output (MW) for the same flow rate and gross head. These results are shown respectively as Figures 3 and 4.

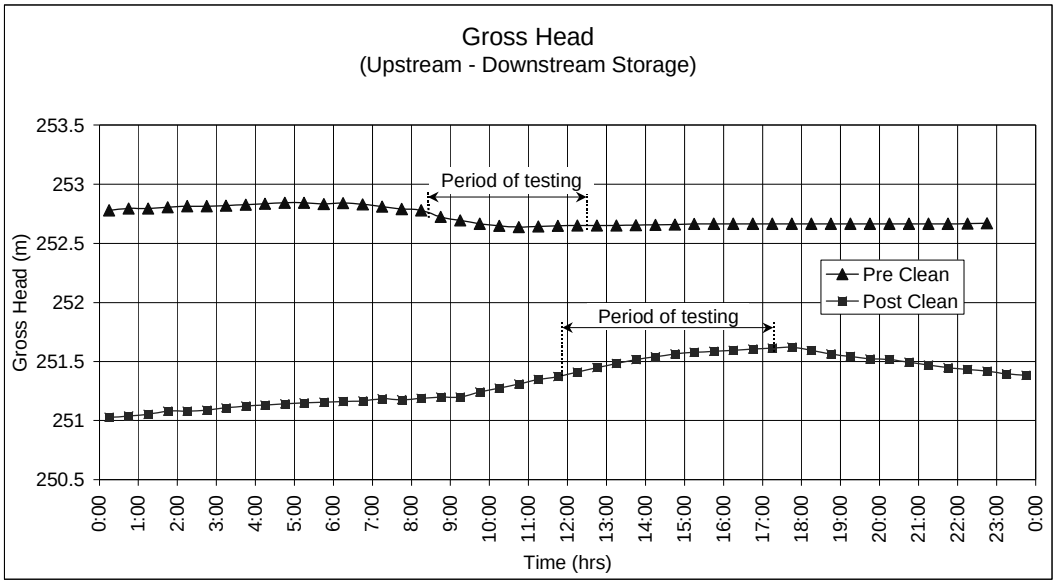

Figure 2 – Gross Head Levels During Conduit Testing

Table 3 – Pre-Clean Test Summary.

Guide Vane Position (%)	Power Output (MW)	Gross Head (m)	Flow Rate (m^3/s)
0.60	0.00	252.72	0.03
10.42	0.25	252.70	1.52
45.94	11.15	252.68	6.17
58.72	16.61	252.66	8.31
61.36	18.13	252.65	8.96
64.56	19.45	252.65	9.50
71.94	22.17	252.65	10.65
77.44	24.63	252.64	11.70
82.07	26.43	252.64	12.49
88.53	28.74	252.65	13.49
93.74	30.84	252.65	14.44
100.38	32.71	252.65	15.41

Table 4 - Post-Clean Test Summary.

Guide Vane Position (%)	Power Output (MW)	Gross Head (m)	Flow Rate (m^3/s)
0.01	0.00	251.41	0.02
9.32	0.09	251.46	1.42
47.68	11.98	251.49	6.39
61.51	18.04	251.53	8.65
76.38	23.99	251.57	11.26
79.65	25.52	251.58	11.90
79.39	25.48	251.60	11.89
83.93	27.01	251.62	12.54
87.80	28.51	251.58	13.20
93.75	30.98	251.61	14.28
100.09	32.79	251.59	15.20

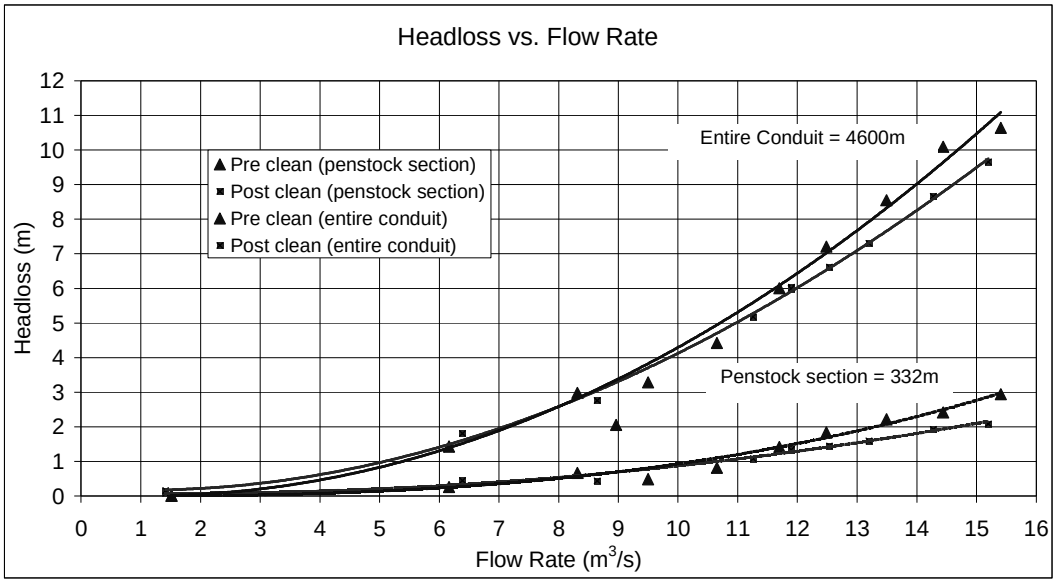

Figure 3 - Headloss for the Penstock Test Section, and for Entire Conduit.

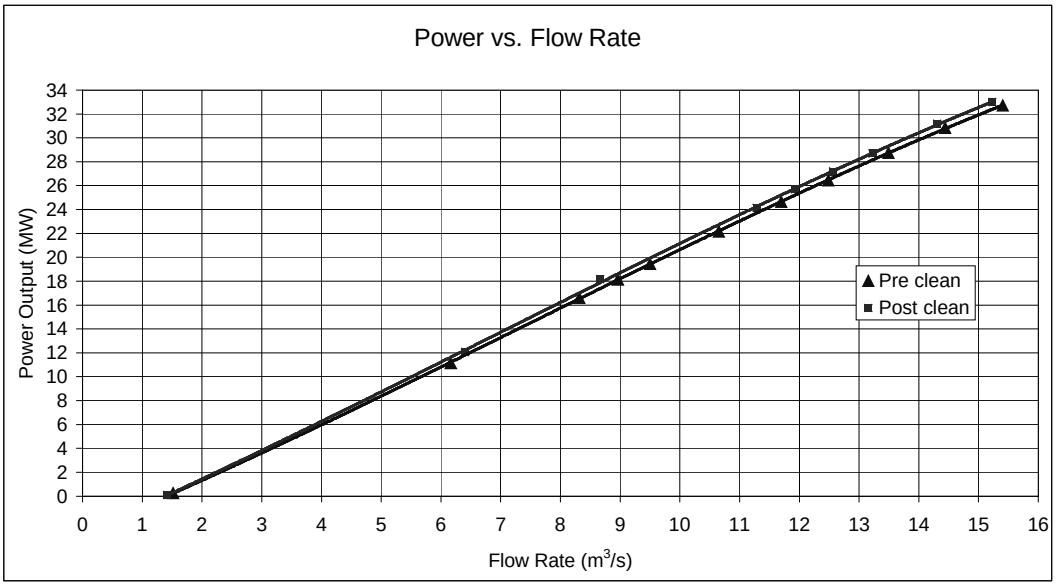

Figure 4 - Turbine Power Output for Given Flow Rate for Pre and Post-Clean Tests.

To present a realistic indication of the economic benefits of conduit cleaning at this particular station, typical summer and winter operating scenarios were modelled. These operating characteristics were derived from output duration curves using data covering the full period of record, sampled at a 1-hour period. This data can be seen in Figure 5. The definition for the winter months are 1 April to 30 September, and for the summer months 1 October to 31 March.

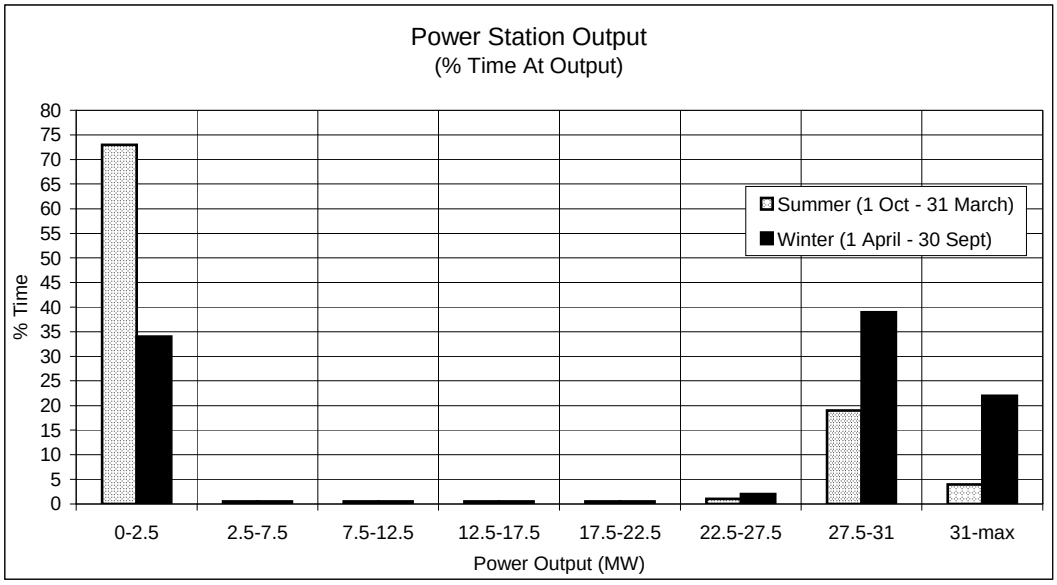

Figure 5 - Typical Summer and Winter Operating Scenarios Showing the % time of Particular MW Outputs.

The potential gains to be made in dollar terms are not presented here, but can be found by simply multiplying the power gained by the duration operated. Also of financial importance to Hydro Tasmania, is the possibility of additional revenue though Renewable Energy Certificate (REC) conditions.

The calculated friction headloss and associated equivalent sand grain roughness for the pre-cleaning and post-cleaning tests are shown in Table 5 for the penstock test section.

Table 5 – Friction Headloss and Equivalent Sand Grain Roughness for Cleaned Penstock Test Section (P_2 to P_3) with Reynolds Number Range of 8×10^5 to 6×10^6.

	Friction headloss h_f	Equivalent sand grain roughness k_s	Relative roughness k_s/D
Pre-clean	$3\text{m} \pm 0.2\text{m}$	$0.3\text{ mm} \pm 0.05\text{ mm}$	0.105
Post-clean	$2\text{m} \pm 0.2\text{m}$	$0.04\text{ mm} \pm 0.01\text{ mm}$	0.014

4. DISCUSSION

The pressure tests of the conduit have shown that the equivalent sand grain roughness, k_s, of the biological growths on the internal walls of the pipe have been reduced as a result of the cleaning process. Pre-clean test results in Table 5 show a value of approximately 0.3mm. The post-clean tests reveal a reduction of k_s to approximately 0.04mm. This reduction in wall roughness has produced a drop in headloss due to friction of approximately 1.5m over the length of the entire conduit at full machine load and a flow of approximately $15\text{m}^3/\text{s}$ (see Figure 3). This increase in available head is where the significance of cleaning conduits is realised for a hydroelectric power station, equating directly to an increased available output. Figure 4 shows this, where the post-clean power is higher than the pre-clean power for the same flow rate due to the reduction in headloss.

It must be noted that the conduit was dewatered during January and February 2002. This undoubtedly would have had an effect on the existing biological growths. It is reasonably speculated (with supporting eyewitness reports from Hydro Tasmania personnel) that a substantial portion of the biological growth was removed due to the drying and subsequent peeling of the growth because of air flowing through the dewatered penstock. This method was in fact a common past technique of reducing biological growth effects in Hydro Tasmania conduits (McFie 1956). This means that the pre-clean tests on the penstock in 2003 had effectively only 12 months of biological growths.

The biological matter in the penstock can be described as two main types. A soft black deposit adhering to the internal cold tar enamel painted surface of the penstock found to have high levels of manganese, and a hard brown deposit on some exposed steel surfaces and weld joints found to have high levels of iron.

Figure 3 shows that higher flow rates yield the greatest improvement in performance as a result of cleaning the penstock. It can be appreciated from Figure 3 that the greatest potential to generate more revenue would also be at these higher flow rates. Winter conditions usually provide periods of higher flow due to higher rainfall. Additional revenue may be available under Renewable Energy Certificate conditions.

5. CONCLUSIONS

It was found that the equivalent sand grain roughness values, k_s, for pre- and post-cleaning tests were approximately 0.3mm and 0.04mm respectively. A penstock outage occurred in January and February 2002. This outage is thought to have affected biological growths inside the penstock, effectively giving only 12 months of regrowth. The benefit of cleaning is different under winter and summer operating scenarios. At typical winter operating conditions, where the power station is operated at a higher load and for longer periods, the benefit would be additional revenue. However, during typical summer period operation, the benefit would also be a saving of storage volume for the same power output when the turbine is operated solely for efficiency. The present study marks the commencement of a broad program to investigate the effect of cleaning hydraulic conduits of biofouling material. It is clear from this study that deterioration of conduit efficiency due to biofouling is significant, and appropriate procedures to minimise biological growths are desirable in order to maintain and improve the economic return from existing infrastructure.

6. ACKNOWLEDGEMENTS

The authors gratefully acknowledge assistance from the following Hydro Tasmania personnel: Michael Wallis for hydraulic engineering assistance; Anthony McGuiness, Nick Cole and Paul Henderson for assistance with the instrumentation and field testing and coordination. Andrew Heath (School of Agricultural Science, University of Tasmania) assisted with the analysis of the biological samples within the penstock.

7. REFERENCES

Brett, T. M. (1980). "Head-Loss Measurements on Hydroelectric Conduits." ASCE Journal of the Hydraulics Division HY1: 173- 190.

Colebrook, C. F. and White, C. M. (1937). "Experiments with fluid-friction in roughened pipes." Proceedings of the Royal Society of London (A) 161: 367-381.

Druck Limited (1997). PXT 1400 Industrial Pressure Transmitter. Leicester, England, Druck Limited.

Hydro Consulting (2000). Pre Feasibility Study - Regular cleaning of the Fisher conduit system. Hobart, Hydro Tasmania.

Lewandowski, Z. and Stoodley, P. (1995). "Flow induced vibrations, drag force, and pressure drop in conduits covered with biofilm." Water Science and Technology 32(8): 19-26.

McFie, H. (1956). Report - Algae and Moss in Canals. Hobart, Tasmania, Hydro-Electric Commission.

McFie, H. H. (1973). Biological, Chemical and Related Engineering Problems in Large Storage Lakes of Tasmania. Man-made Lakes: Their Problems and Environmental Effects. W. C. Ackermann, White, G.F. and Worthington, E.B. Washingston, D.C., American Geophysical Union. 17: 56-62.

McFie, H. H. (1976). Power Storage Lakes: Biological Depositions and Energy Losses in Tasmania. 47th ANZAAS Congress, Hobart.

McGuinness, A. (2003), Personal Communication, Hydro Tasmania.

Nikuradse, J. (1933). Laws of flow in rough pipes. Washington, National Advisory Committee for Aeronautics. Technical Memorandum 1292.

The Institution of Engineers, Australia
8th National Conference on Hydraulics in Water Engineering
ANA Hotel Gold Coast, Australia 13-16 July 2004

Finding a Solution for the Hammonds Drain Problem

K.R.K. Blake
B.Sc.,MSc.,Dip.Hydraulics., M.E.Aust.
Project Engineer, Connell Wagner Pty. Ltd., Australia

Abstract: Hammonds Drain drains stormwater from a large area of the northern section of Port MacDonnell township, South Australia, to the sea through an open canal. The flat topography and low land levels behind the beach fore-dunes have proved difficult to drain effectively, leading to stagnation of water in the drain and saturation of the low-lying land during the winter months. Over the years a number of options had been considered and several reports written discussing the problem. For the most part, the solutions muted in these reports either did not meet the needs of the users or were cost prohibitive. Connell Wagner set out to provide a solution that would meet, in the first instance, the budget at hand whilst addressing the majority of the users needs. Despite the time and effort put into finding a solution for this problem over the past years, it was still possible to formulate an innovative design that met the tight criteria, including the available budget set for this site.

Keywords: Hammonds Drain, Flap gate, Outfall.

1. INTRODUCTION

Hammonds Drain is an open canal, draining stormwater from a large area of the northern section of Port MacDonnell township, South Australia, to the sea approximately 600 m west of the fishing pier. The flat topography and low land levels behind the beach fore-dunes have proved difficult to drain effectively, leading to stagnation of water in the drain and saturation of the low-lying land during the winter months. A number of studies have been undertaken over several years to address the problem. However, for various reasons (including some conflicting demands), none of these had been acceptable.

Connell Wagner was engaged by the District Council of Grant to review the previous studies and to make recommendations for a solution to the problem. This paper reviews and re-assesses the past proposals and details the solution that most adequately addressed all the relevant issues and is currently being constructed.

2. STUDY AREA

2.1 Site Description

The section of drain under investigation is west of the Mount Gambier to Port MacDonnell road. This is an open channel, unlined earth canal with grassed banks. Road crossings have been built across the drain at Pascoe Road and Sea Parade. The section of drain between Pascoe Road and Sea Parade tended to pond water as it had an uneven bed due to deposits of silt, weeds and rubbish. From the Sea Parade crossing downstream to the beach, the drain has been confined between vertical walls formed from large sandstone blocks. Finally from the beach section, two groynes have been constructed either side of the drain, extending approximately 90 m out to sea.

The groynes were constructed by Transport South Australia (TSA) as experimental methods of preventing sand and seagrass accumulation in the seaward sections of the drain. TSA advised that the western groyne was built first and was quite successful at keeping excess sand out of the drain mouth, but not the drifting dead seagrass. The eastern groyne was built later but has not solved the problem with the seagrass and may arguably exacerbate the sand problem again. A significant volume of sand and seagrass regularly accumulated in the channel.

Earlier reports stated that salinity of the low-lying areas behind the fore-dunes had been a problem due to seawater inundation. Consequentially a tidal control structure had been constructed in the section of drain just downstream of the Sea Parade road crossing, to prevent high tides and storm surges from entering the drain. The structure consisted of two vertical lift steel sluice gates. These were lifted open by a chain or rope attached to

the gate and the bucket of a front end loader or similar plant. The gates were held open using a locking pin. This method relied on plant and labour being available when required.

The gates were in poor condition, being heavily corroded with large holes in the faces. As such the gates were largely ineffective in preventing tidal flow up the drain.

Approximately 800 m west of the Hammonds Drain outlet, the Cress Creek drains out to sea. Due to perennial river flow this drain was reported not to be subject to the same problems of seagrass blockage. Besides having a constant flow, the channel downstream of the Pascoe Road crossing is slightly steeper than Hammonds Drain, allowing a self cleansing flow velocity in the creek.

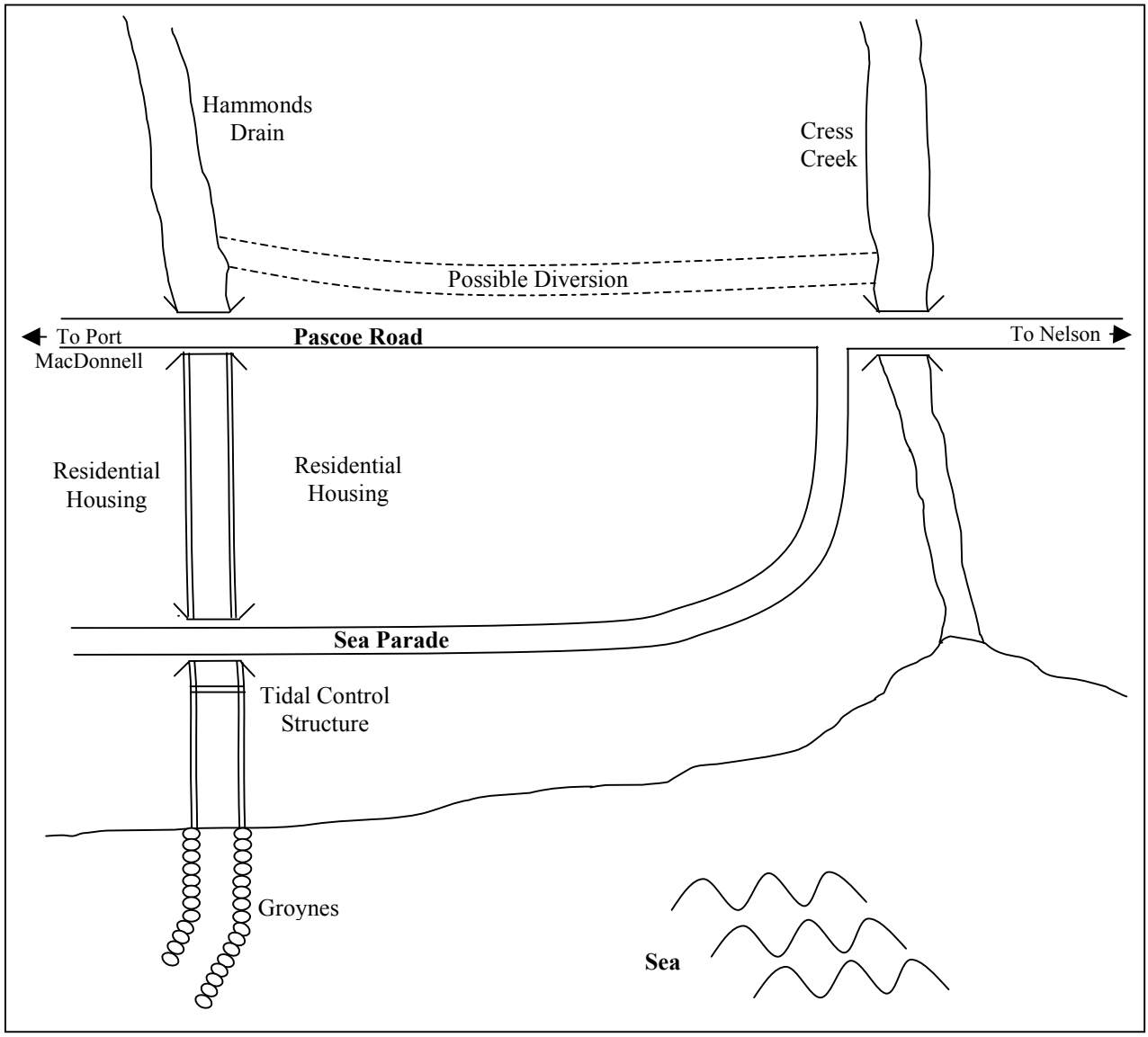

Figure 1 – Site Plan

2.2 Drainage Problems

There are a number of problems associated with the drain, some of which have been resolved, some of which were still present and others that may be a problem in the future if some remedial work was not undertaken. The major issues that needed to be taken into account when addressing possible options for the drainage problem are outlined below.

2.2.1 Tidal Flooding of the Low Lands

Salinisation of the soil was occurring after the construction of the drain due to tidal inundation of the low-lying land during high tides and coastal storm surges. To alleviate this problem the sluice gates were installed. However, in their corroded condition, these gates were no longer fully effective and the issue of salinity would become a problem again if tidal inflows were not effectively prevented. Therefore any new works had to be designed to prevent sea inflow into the drain upstream of Pascoe Road and into the low-lying areas.

2.2.2 Stormwater Flooding

Due to its size, the drain was incapable of passing large stormwater runoff flows without overtopping its banks and flooding the low-lying areas. The degree of flooding would also be influenced by when the tide gates were opened. The solution therefore needed to maximise the hydraulic efficiency of the drain and the flood control gates. The solution also had to address the consequences of flooding and the possibility of the need for retardation basins. The design discharge rate and volume of runoff needed to be evaluated in order to achieve the most economic solution.

2.2.3 Water Stagnation

Water ponding in the flat section of drain between Pascoe Road and Sea Parade was unsafe and in summer tended to stagnate, posing a potential health risk and odour problem. The new works therefore needed to ensure that this section of the drain was self-draining and capable of being easily cleaned by mechanical equipment.

2.2.4 Saturation of the Lowlands

Due to the drain's inability to effectively drain the low-lying land, particularly in winter when tides are elevated, the ground water level rose and the soil became saturated. As this land was used for stock grazing, this was a problem for the land owners. The new works therefore had to consider means of maintaining a lower ground water level during the winter months.

2.2.5 Natural "Irrigation" of the Lowlands

In contrast to the above, as the land was used for stock grazing, it was beneficial for the owner to have some water retained in the drain to provide summer irrigation of his fields. Therefore, the new works also had to consider methods to enable the land owner to maintain some form of control over the water levels in the drain.

3. OVERVIEW OF PAST STUDIES

A number of studies had been conducted over the years to look into possible solutions for the problems being experienced at Hammonds Drain. A very brief overview is given below.

- In January 1982 the Urban and Environmental Planning Group recommended a diversion of the drain to feed into the Cress Creek, although in their report they recognised that this raised some technical difficulties.

- In June 1985 a Coastal Management Branch report supported this recommendation.

- In June 1986 the Connell Group looked at the possible solutions in greater depth. Their report recommended re-grading Hammonds Drain to 0.1 % and the installation of a weir at the outlet, a sedimentation basin upstream of the weir, a sea wall with floodgates downstream of the weir, culverts between the weir and Pascoe Road and lining of the invert further upstream. However, this extensive solution had an estimated cost of construction in 1986 at over $ 500 000 and therefore was never implemented.

- In 1995 TSA-Marine Facilities constructed a rock groyne on the eastern side of the Hammonds Drain outlet in an attempt to prevent sand and seagrass build-up across the outlet. This was reported to have some success but not sufficient to prevent blockage. As a result, an additional groyne was installed on the western side of the outlet some time later. This was reported as being successful in keeping the sand out, but not the seagrass.

- From June 1999 to August 2002 Sinclair Knight Merz (SKM) carried out extensive analyses of the problems associated with the drain. They prepared a series of comprehensive reports of their investigations and looked into at least seven possible options. A study of the tidal characteristics at the site and the invert levels of the drain concluded that the only practical solutions to controlling runoff in Hammonds Drain were:

    1. Store runoff in the low lying areas for later release at low tide (as is being done at present, albeit rather inefficiently) and
    2. Install a drainage pump scheme.

  The SKM reports investigated seven major options, being variations of piped options, pumping stations and a diversion across to the Cress Creek. Estimates of cost (in 1999) for the options varied from $ 140 000 to $ 640 000. The report states the do-nothing option as having no costs but this neglects the intangible costs involved with the ongoing maintenance of the drains, loss of amenity to the residents and economic losses due the pasture conditions. The report recommended the Cress Creek diversion option as being the most cost-effective of those considered.

- On 06 July 2000 at a Council meeting a decision was taken not to implement the Cress Creek option on the basis of reservations from the South East Drainage Board who would have to take over maintenance responsibilities on completion of the project. The ongoing operating and maintenance costs appeared to be excessive and unacceptable for a rural drainage scheme. SKM were then requested to investigate further an alternative design based on a piped outfall solution.

- SKM developed a piped option that drained the low flow water through a 1200 mm diameter pipe (later reduced to a 900 mm diameter) from Pascoe Road to Sea Parade. The pipe would be installed in the base of a grassed swale designed to take the major flows. Three silt traps were included as well as a new mechanically operated sluice gate to prevent tidal inundation from the sea. To overcome the cost problem it was planned to install this solution in two stages. However, the costs of this option once again stalled the project.

4. DESIGN OPTIONS

Connell Wagner were invited to review the past studies and propose some alternative solutions. Aside from the various problems discussed above, the primary criteria was to find a solution that could be constructed within the limited budget available. The final three options presented to Council are described below.

4.1 Tides and Hydrology

The SKM study indicated that the section of Hammonds Drain between Pascoe Road and Sea Parade could handle the full major flow without overtopping the banks or reaching the soffits of the bridges. However, sections of the drain further upstream could not contain the major flow and the drain would overtop during such events. This would be expected for a major flood event. The report estimated that the maximum capacity of the drain at present is of the order of 2.0 m^3/s. This flow capacity was reliant on the sluice gates being fully open and tidal levels low enough to allow discharge to sea. It should be noted that this would not always be the case, resulting in periods during which flooding may occur in the low-lying areas during high tides.

Historic tidal data for this site was not readily available. However, for the design of the proposed solutions only limited tidal data was required and this was taken from the Ports Corp Tide Tables. These gave the average tidal range as only 0.9 m with the mean high water springs at approximately 0.29 m AHD. The drain bed levels at the downstream road crossings are 0.37 m AHD for Hammonds Drain and approximately 0.37m AHD for Cress Creek. This meant that the drains were above the normal tidal range. It was theoretically possible therefore to increase the capacity of the drains by deepening them. The bed level of the Hammonds Drain was slightly lower upstream of the Sea Parade Culvert. The bed level of the Cress Creek upstream of the Pascoe Road culvert is generally higher than at the culvert but the bed was filled with at least 300mm of soft mud and was uneven for at least one hundred metres upstream.

4.2 Option 1 : Cress Creek By-Pass

This option re-looked at the construction a new open drain from Hammond Drain (upstream from the Pascoe Road Crossing) across to Cress Creek (refer Figure1). Some form of non-return device would be required in the drain to prevent flooding of the low lying land during very high tidal events or particularly high flows in Cress Creek.

The SKM study indicated that the capacity of Cress Creek outlet was of the order of 5 m^3/s. Thus, taking the design peak for Hammonds Drain at 2 m^3/s, any flow greater than 3 m^3/s from the Cress Creek, could potentially cause backing up of the Cress Creek water and possible flooding upstream of the junction. As this would be a problem created by the Hammonds Drain diversion, a careful hydrological analysis of the probability and extent of such flooding would need to be undertaken before consideration of this option. However based on the limited data available at the time the Cress Creek option appeared to be technically sound.

By diverting Hammonds Drain across to Cress Creek, it would then fall under the responsibility of the South East Drainage Board rather than the District Council of Grant. It was noted that at a Council meeting in July 2000 the Drainage Board expressed concern at having to take over the responsibility for such a scheme. Therefore, before this option could be re-considered, it would be necessary to obtain an agreement with the Drainage Board on how the maintenance and responsibility for the scheme was to be handled.

4.3 Option 2 : Existing Drain with Piped Outlet

This option came from the basis of one of the options originally proposed in the SKM feasibility report. The existing Hammonds Drain would be retained with some reworking of the control works downstream of the Sea Parade culvert. A low level weir to form a head wall would be constructed at the position of the existing gates. A small diameter high density polyethylene pipe would run from this weir to approximately the end of the drainage channel (the extent of the groynes). A tideflex type non-return valve would be fitted at the end of the pipe to prevent seawater running back up the pipe and entering the drain at high tides. This would have to be located in a position where it was unlikely to be covered by drift sand and seagrass. This pipe would discharge low flows to open water. It could effectively drain the low-lying land down to about low tide level if the existing floor of Hammonds Drain was regraded to suit.

Major flows in the drain would flow out to sea over the top of the weir structure. A flap gate would be constructed on top of the weir to prevent tidal surge from entering the upstream end of the drain. The height of the weir would be set to ensure that major storm flows down the drain do not cause additional flooding upstream whilst still ensuring that the flap gate was well clear of the seagrass levels. Therefore the build up of seagrass in the seaward section of the drain would then not inhibit the operation of the drain and thus the gate would be less likely to leak due to debris.

4.4 Option 3 : Existing Drain with Pump

This was a variation of the above option in which a short rising main replaced the gravity pipe. A small pump installed at the weir structure would pump the water over the weir (and hence drain to the sea) through a small diameter pipe. A flap gate would still be required on top of the weir as before (refer Figure 2).

The advantage of the pump option over the pipe option was that it could operate during all tidal ranges and the pump system would be less prone to blockage. Consideration was also given to using alternative power sources to drive the pump, eg. solar or wind power.

4.5 Sediment Basins

Some of the past reports had made allowance for sediment basins along the route of the drain. Given that the majority of the flows would be very low velocity (due to the flat gradients) it was not expected that sediment would be a significant issue for the options proposed. If a sediment basin was warranted, the costs of such a structure could add significantly to the low cost options that were proposed. As a sediment basin could easily be added to any of the above options, it was considered more prudent to omit the basins at that stage and monitor the performance of the system. If maintenance of the system suggested that a sediment basin was warranted, it could easily be constructed.

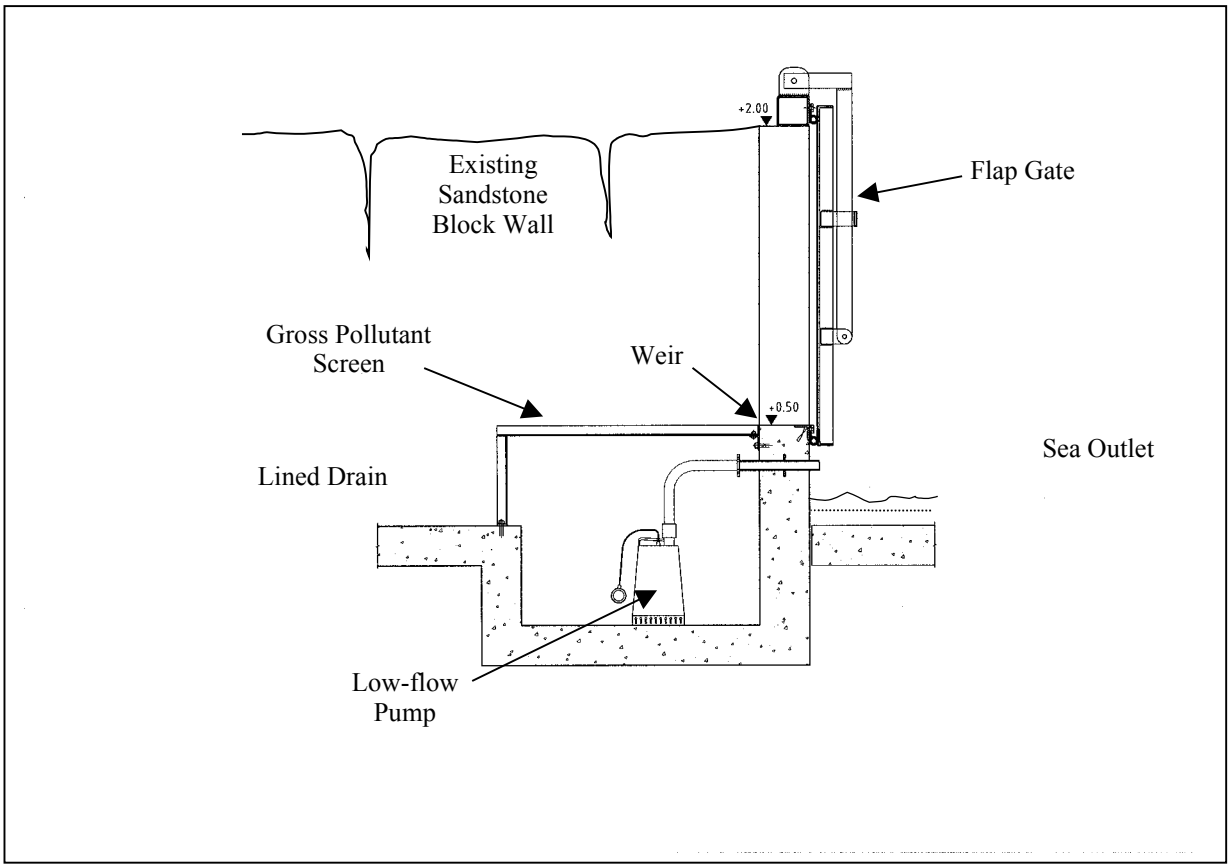

Figure 2 – Section at Weir Showing Pump

4.6 Recommended Option

The three options proposed above were recommended on the basis that they meet most of the requirements for the drain (as discussed in Section 2). Given that some of these requirements were conflicting to some extent, it is unlikely to find a solution that met all the needs of all the stakeholders all the time. The options were assessed on how well they met these requirements.

Based on this assessment, we recommended the pumped option as being the most suitable. Even though it will have on going running costs, it is not as vulnerable to the effects of littoral drift of sand and seagrass as the piped option. This relatively low cost option still retains some control of the water in the canal through the use of the pump. If the land owners wish to keep some water back to irrigate their fields (assuming this practice was acceptable to other interested parties), the pump could be switched off, or the automatic on/off switch moved to a higher level. As the weir still has automatic flap gates, the flood immunity of the system will not be compromised in the event of an unexpected rainfall event.

The Cress Creek by-pass option although technically viable is not preferred mainly due to the higher costs and the uncertainty of the Drainage Board's acceptance of the scheme.

4.7 Community Consultation

The three recommended options were put forward at a public meeting held at the District Council offices. The topic was hotly debated by members of the public and Council representatives. The presentation first had to overcome the scepticism of the local residents that had built up over the years due to the various options proposed in the past. The final outcome of the meeting was an agreement to go ahead with the pumped option but include lining the section of drain between Pascoe Road and Sea Parade. This latter requirement came out of the concern of pooled water in this section of the drain stagnating over summer and creating health and odour problems.

5. DETAILED DESIGN

Following the commitment of the local residents to the project, Connell Wagner went ahead with the detailed design of the proposed solution. This involved confirming the sizes and levels of various aspects of the proposal, structural design of a number of elements and looking at the methods to be employed in the construction of the project.

5.1 Weir and Drain Invert Levels

The design of the weir had its crest level set above the high tide level at 0.5 m AHD. The drain invert was set at 0.0 m AHD at the weir and rose at a slope of 0.2 % for the lined section which extended to Pascoe Road. Upstream of this the drain depth and size would not be altered. To check that this option would not cause flooding problems upstream, the drain was modelled using steady state HEC-RAS model.

Due to the lining and the increased capacity of this section of the drain, it was found that the water levels upstream actually dropped from those expected for the existing drain condition (refer Figure3). Therefore, there would be no issues of upstream flooding due to the construction of the new works.

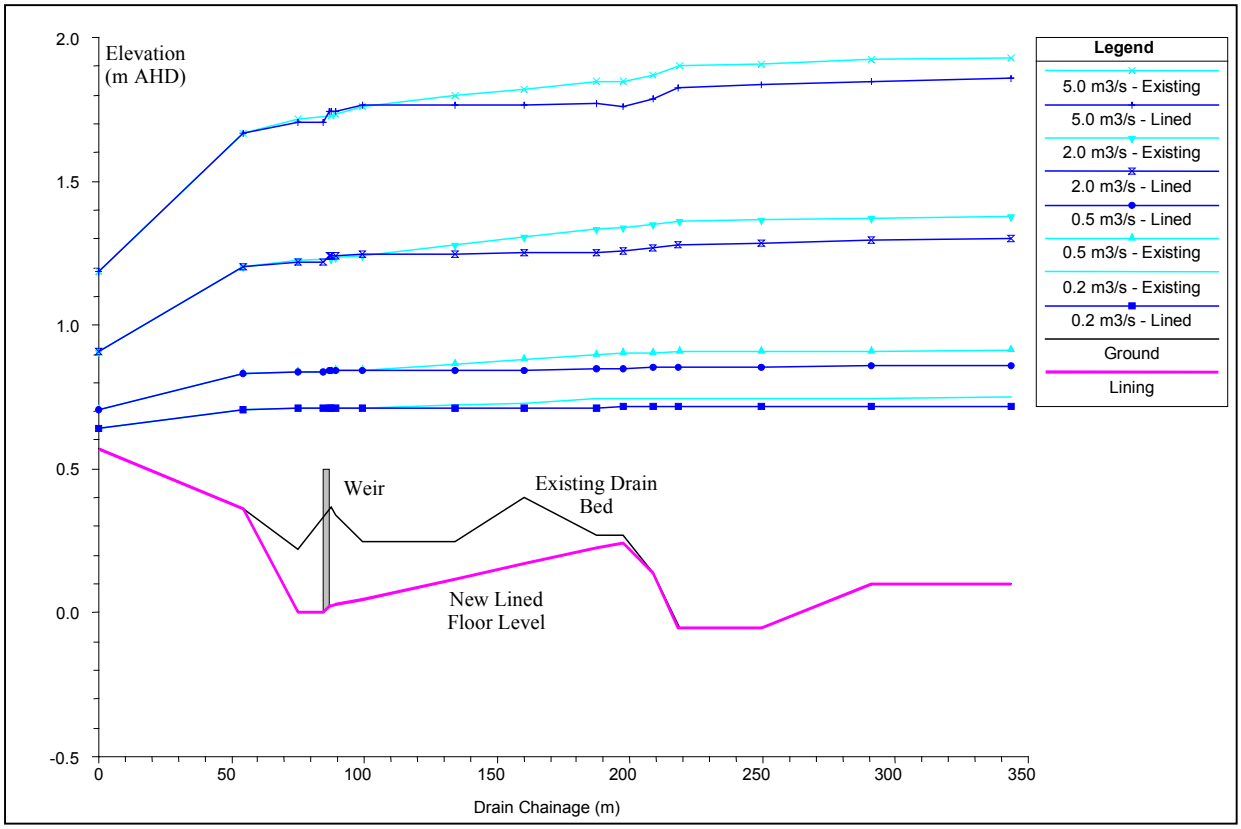

Figure 3 – Water Surface Levels for Various Flows

5.2 Flap Gate Design

Flap gates were proposed in lieu of the existing sluice gates so that no human intervention would be required in the event of flood flows. Therefore, need for monitoring and hence the risk of flooding upstream would be greatly reduced.

Initially it was proposed to use a proprietary type flap gate on top of the weir. However, during the design phase it was found that no suitable units existed. Therefore, the flap gate was designed specifically for this project. This consisted of a 2.9 m wide by 1.7 m high stainless steel gate, sealing against a stainless steel frame mounted on the weir and side walls. The rubber sealing bulb was attached to the downstream side of the frame rather than the gate to protect it from damage due to debris being carried in the flood waters at high flows. The gate was hinged with a double hinge system to ensure correct sealing all around the gate.

5.3 Pump Design

The pump was sized to drain the channel from a full level (that is weir crest level) to dry within 48 hours. This required a small submersible pump that was positioned in a sump at the weir. The sump incorporated screens to keep gross pollutants away from the pump. Pump on and off control was to be automated with float switches in keeping with the premise that no human intervention would be required in the event of a high flow in the drain.

6. PROJECT OUTCOMES

The ongoing problem at Hammonds Drain had attracted a number of investigations over the years without coming up with an economical solution. Despite the time and effort put into finding a solution for this problem, it was still possible to formulate an innovative design that met the tight criteria, including the available budget set for this site. The success of the design was the fact that we were able to satisfy the users who, due to the number of past proposals, were highly sceptical of further options. Furthermore, the final design is independent of human intervention and therefore should have a very low risk of future flooding problems. The fact that the pump only serves the low flow conditions means that a power failure will have no effect on the capacity of the system. The only time flooding upstream could occur is if the storm event was coincident with a major surge tide and the flap gates could not open due to the high tide.

The success of this project demonstrates that despite what has occurred in the past, new solutions may still be available to solve old problems. Furthermore, what may appear to be complex problems may have relatively simple solutions.

7. ACKNOWLEDGMENTS

Connell Wagner wish to thank the District Council of Grant for their help and guidance during this project and for granting permission to submit this paper. We also thank Doug Smart of Connell Wagner for his assistance both in the design phases of the project and the preparation of this paper.

8. REFERENCES

Transport South Australia (2003). Pers.comms.
Sinclair Knight Merz, (2002). Hammonds Drain Port MacDonnell. Letters to the District Council of Grant.

Sinclair Knight Merz, (1999). Rural Drainage – Hammonds Drain and Cress Creek at Port MacDonnell, Feasibility Study. Report to the District Council of Grant.

Connell Group, (1986). Report on Investigation into Problems Associated with the Outfall of Hammonds Drain, Report to the District Council of Port MacDonnell.

The Institution of Engineers, Australia
8th National Conference on Hydraulics in Water Engineering
ANA Hotel Gold Coast, Australia 13-16 July 2004

Integrating Overland Flooding and Drainage Pipe Networks

Siebe Bosch[1], Ian Clark[2] and Chris Catalano[3]

[1] Senior Engineer
WL | Delft Hydraulics (1 year secondment to Lawson & Treloar)
Rotterdamseweg 185, 2629 HD Delft, THE NETHERLANDS
siebeb@lat.com.au

[2] Senior Engineer
Lawson and Treloar Pty. Ltd
Level 1 40-44 Blackwood Street, Mitchelton QLD 4053
iqc@lat.com.au

[3] Associate
Lawson and Treloar Pty. Ltd
Level 1 40-44 Blackwood Street, Mitchelton QLD 4053
clc@lat.com.au

Abstract: Traditionally, urban drainage systems have solely been modelled using one-dimensional (1D) hydraulic models. This method has been found suitable for most situations. However, in relatively flat areas, where overland flow paths are not well defined, thus predicted flood extents can be highly inaccurate.

Two-dimensional (2D) models do not require pre-determined flow paths and can therefore more accurately determine overland flooding. This approach is limited however, as 2D models are unable to precisely compute flow within an underground pipe drainage network.

1D and 2D models are therefore more commonly being implemented in conjunction, utilising the strengths of each approach. The 1D model estimates pipe system capacity and surcharge whilst the 2D model describes the overland flow component.

This paper discusses recent, more accurate computational methods for conducting combined surface and sub-surface flood assessments, as applied for an urban subdivision in Brisbane. It also comments on challenges still to overcome regarding this type of modelling.

Keywords: Delft, SOBEK, 1D, 2D, hydraulic, hydrodynamic, modelling, subsurface, pipe flow, surcharge, overland flow, urban drainage

1 INTRODUCTION

Urban stormwater flooding can be very complex in nature, especially in relatively flat areas where the overland flow paths are not well defined. Surcharge of creeks and drainage pipe networks can result in hard-to-predict overland flow patterns affecting numerous properties. In modelling these processes both a 1D-only approach and a 2D-only approach can result in inaccurate flood estimations. A 1D-only approach would require the modeller to pre-define the overland flow paths, which can be a difficult task requiring considerable modelling experience and may not be valid for all times during a flood or for all magnitudes of flooding. Using a 2D-only approach however, one would be incapable of simulating small overland channels or subsurface pipe flow and surcharge without heavy schematisation.

A recent trend in Urban Stormwater Modelling therefore is to model 2D surface flow in conjunction with 1D subsurface flow. The advantages of such integration are clear: the modeller does not have to pre-define the overland flow paths; and processes that are 1D in nature, such as pipe or culvert flow, can still be modelled likewise with

industry accepted accuracy. Finally, using 1D elements within a 2D environment allows for coarser 2D grids, thus considerably saving computational time.

This paper discusses the design of a stormwater drainage system for an urban subdivision in Brisbane, Australia and demonstrates how an integrated 1D and 2D model can successfully be applied to complex urban stormwater flood studies. Finally, this paper will discuss the major challenges that still lay ahead regarding this type of urban stormwater modelling.

Other recent applications of combined 1D2D modelling have been given by Bishop and Catalano (2001) and by Collins and Catalano (2001).

The SOBEK-1D2D package from Delft Hydraulics in The Netherlands has been applied for the project as it provides full integration of finite difference 1D and 2D hydrodynamics. For both 1D and 2D modules the Navier-Stokes shallow water approximations of the Saint Venant equations are applied and are implicitly coupled within the program. Both modules are also designed to simulate relatively shallow flood propagation and recession across initially dry ground [Stelling et. al, 2003]. Super-critical flow and hydraulic jumps are also accurately simulated, which can occur when floods overtop embankments or encounter structures. These sorts of phenomena can be notorious as a source of problems in models that can only handle sub-critical flow [Domanti et. al., 2001].

2 DESCRIPTION OF THE SITE

The site is an undeveloped parcel of land situated amongst urban development in the Bracken Ridge suburb of Brisbane, Australia. The site is bounded by Childs Street to the north, Denham Street to the west, Telegraph Road to the south and Quinlan Street to the east as shown on Figure 1.

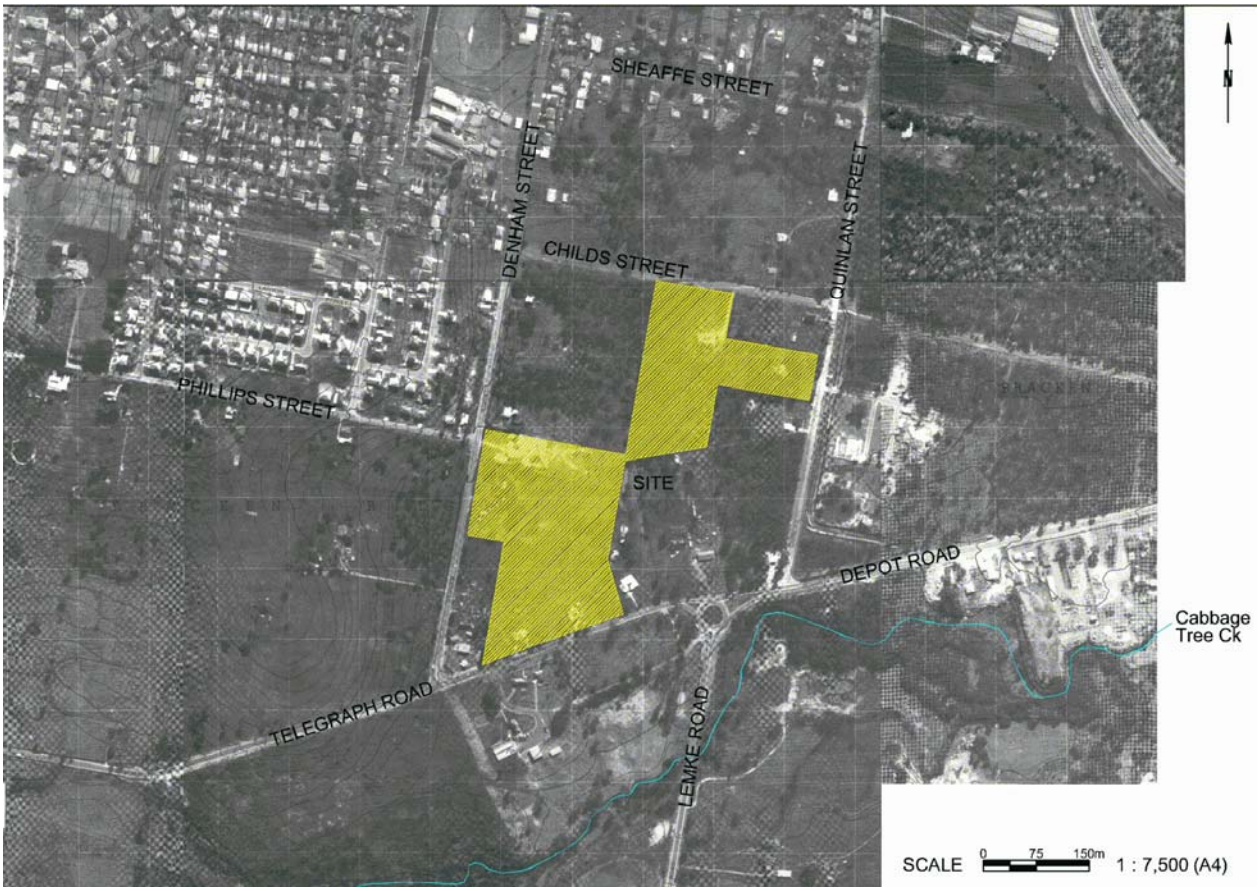

Figure 1- Proposed development site.

The area is extremely flat, except for the portion of the development site in the immediate vicinity of Denham Street, and there are no well defined channels to convey the flow to the downstream extents along the eastern and southern boundaries of the site. Stormwater from the catchment to the west of the site is discharged via a pipe culvert under Denham Street to the western boundary of the site.

Based on this, the flow paths that result from a stormwater pipe surcharge are best simulated in a dynamic 2D modelling environment. In addition, the 1D flow through the pipes is significant and therefore should not be ignored or inaccurately assessed in the simulations.

3 THE PROPOSED DEVELOPMENT

The proposal consists of residential infill development. The development has been designed with a network of grassed swales adjacent to the internal roads. These swales have dual purpose, firstly to help attenuate the increased runoff produced as a result of the additional impervious area created by the development and secondly to act as water quality improvement devices. Additional stormwater piping is also proposed which links with the swales to form the overall site stormwater drainage system.

4 MODELLING SYSTEM OVERVIEW

The integrated one- and two-dimensional vertically averaged finite difference hydrodynamic model SOBEK-1D2D was adopted for analysis. The 1D component of this program is suited to simulation of 1D channel flow and subsurface pipe flow. The 2D component is especially designed for simulation of the dynamic behaviour of overland flow over initially dry land as well as flooding and drying processes in both flat and steep terrain. SOBEK's 2D computational scheme has been frequently used to predict the influence of planned infrastructure on flooding processes, land use, vegetation characteristics and urban areas (Domanti et. al., 2001).

The basic equations used are the so-called shallow water equations, firstly described by Jean-Claude Barre de Saint Venant (1797-1886) (Saint Venant, 1871). These are:

$$\frac{\partial \zeta}{\partial t} + \frac{\partial (uh)}{\partial x} + \frac{\partial (vh)}{\partial y} = 0 \qquad (1)$$

$$\frac{\partial u}{\partial t} + u\frac{\partial u}{\partial x} + v\frac{\partial u}{\partial y} + g\frac{\partial \zeta}{\partial x} + g\frac{u \mid u \mid}{C^2 h} + au \mid u \mid = 0 \qquad (2)$$

$$\frac{\partial v}{\partial t} + u\frac{\partial v}{\partial x} + v\frac{\partial v}{\partial y} + g\frac{\partial \zeta}{\partial y} + g\frac{v \mid v \mid}{C^2 h} + av \mid v \mid = 0 \qquad (3)$$

where:

u	velocity in x-direction
v	velocity in y-direction
C	Chézy coefficient
h	water depth
a	wall friction coefficient

ζ water level above plane reference

The first equation describes conservation of mass, whereas the latter ones describe the conservation of momentum. For 1D flow, the above equations can be simplified by completely removing equation (3) and removing all terms that contain the parameters *v* and *y* from the remaining equations.

The solution scheme for SOBEK-1D2D has been developed by Stelling et al. (2003) and is based upon the following:

1. The continuity equation is approximated such that mass is conserved not only globally but also locally and the total water depth is guaranteed to be always positive, which excludes the necessity of "flooding and drying" procedures. Each time step is pre-calculated by performing Courant and positive water depth checks at every node
2. In flow expansions, a numerical approximation is applied that is consistent with the momentum principle; in flow contractions, a numerical approximation is applied that is consistent with the Bernoulli principle. Both approximations are consistent with the shallow water equations, so under sufficiently smooth conditions they converge to the same solution.
3. The momentum equation is approximated such that a proper momentum balance is fulfilled near large gradients
4. Upwind differencing of water levels in the local flow direction is used.

The combination of positive water depths and mass conservation assures a stable solution.

4.1 Coupling of 1D and 2D hydrodynamics

The SOBEK computational scheme uses a so-called *staggered* grid for its numerical approximation. The mass balance is solved at the 1D grid points and 2D grid cell centres whereas the momentum balance is solved within the segments that interconnect them. This means that the water levels (ζ) are calculated at the 1D grid points and the 2D cell-centroids and the velocities *v* and *u* are calculated on the segments interconnecting those points.

Figure 2 shows how 1D channels and 1D stormwater drainage systems are automatically connected to the 2D topographic grid. For channels this coupling is established through the 1D grid points. Every 1D grid point that is located within a 2D grid cell's geometric extent is automatically linked to the centre-point of that 2D cell. In case of 1D subsurface drainage systems, the coupling can be established through manholes or gully pits. The user can also turn off a 1D-2D coupling if, for example, a manhole is bolted down.

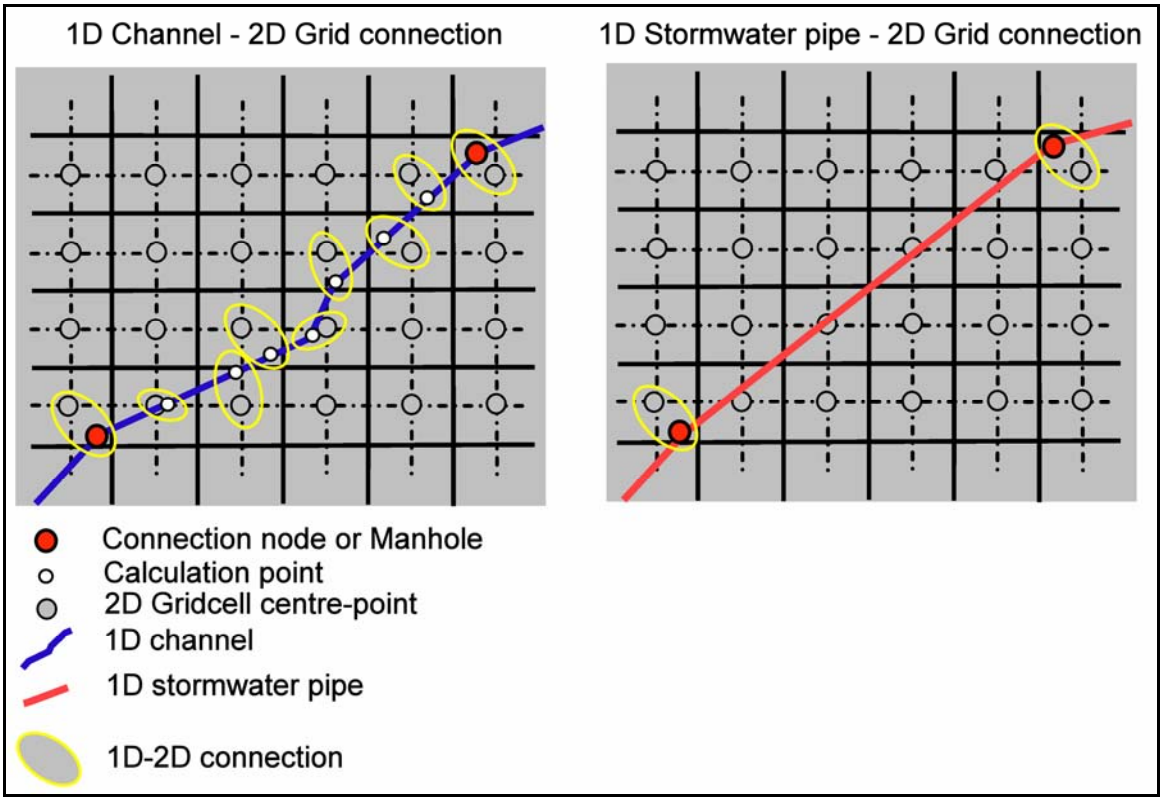

Figure 2 – Automatic establishment of a connection between 1D and 2D schematisations in SOBEK.

When a 1D grid point is located within a certain 2D cell, the water level (ζ) is solved implicitly for both points, which results in a single value of ζ every time step for both the 1D object and 2D cell whilst ensuring conservation of mass.

4.2 Analysis

As the area is very flat and overland flow passes through the site from several sources it was difficult to predict the overland flow paths. In addition, the proposal required some on-site filling which would require careful re-schematisation for the proposed case analysis. Hence a combined 1D-2D analysis was employed.

The existing case consisted of the following:

- A 2D rectilinear grid, representing the overland topographic levels, measuring 582 by 663 meters and having a cell size of 3 m.
- A 2D rectilinear grid representing manning roughness values for each of the topographic cells.
- 1D stormwater pipes interconnected by 1D manholes for all the major stormwater drainage lines in the study area.

For the proposed case, additional 1D pipe elements for the newly designed sub-surface stormwater drainage system and 1D channels for the proposed streets and adjacent swales within the development were incorporated.

Figure 3 shows the combined 1D and 2D schematisations that represent the post-development situation. The major overland flow direction is west to east and is a direct result from surcharge of the Denham Street drainage system

and inflow from western catchments. Another flow path, from the north to the east boundary, is caused by surcharge of the Childs Street drainage system.

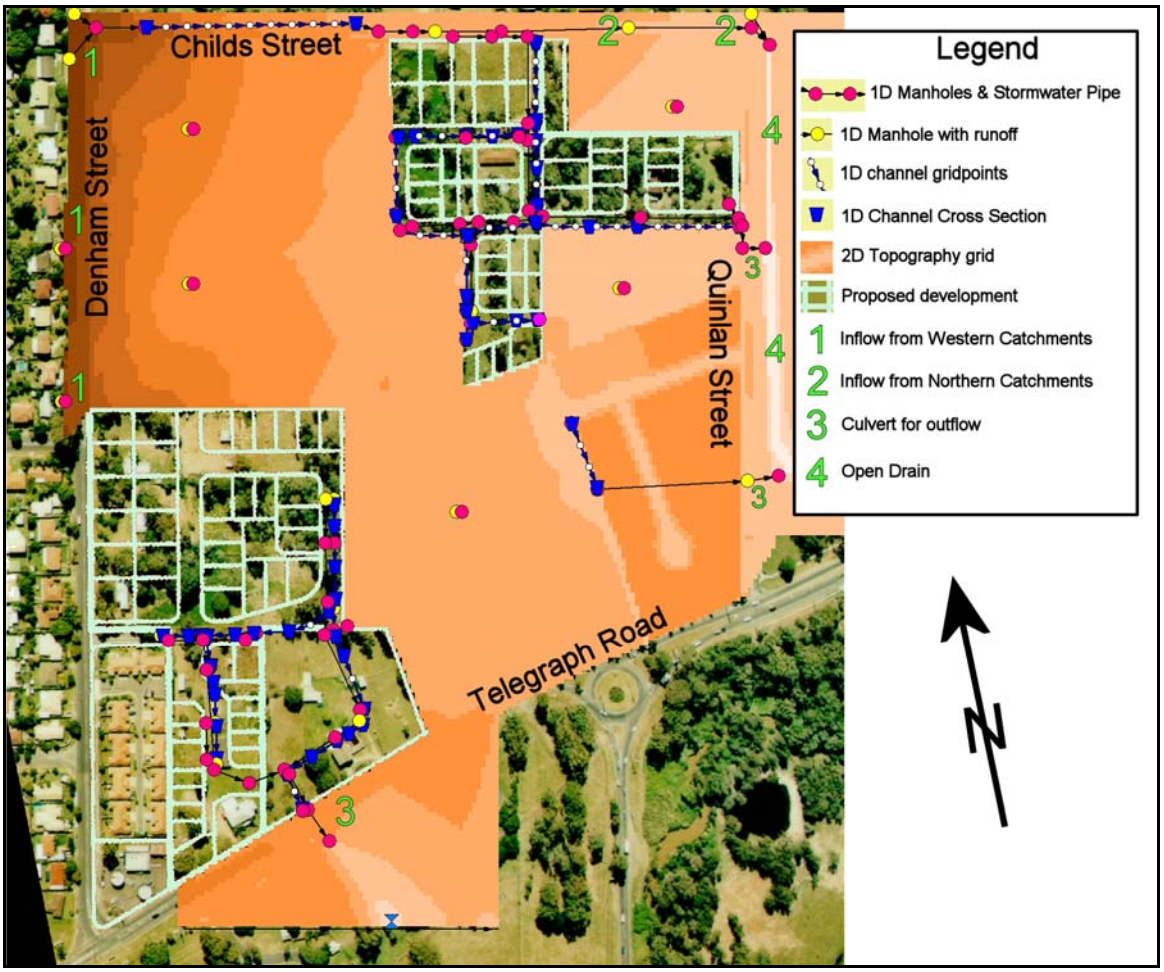

Figure 3 – Combined 1D and 2D hydraulic schematisation of the site in SOBEK.

4.3 Simulation results

Both the pre- and post-development schematisations were run with 10 and 50 year return period hydrographs. The results for the 50y post-development case are presented in Figure 4 in terms of peak overland flood depths and velocity vectors.

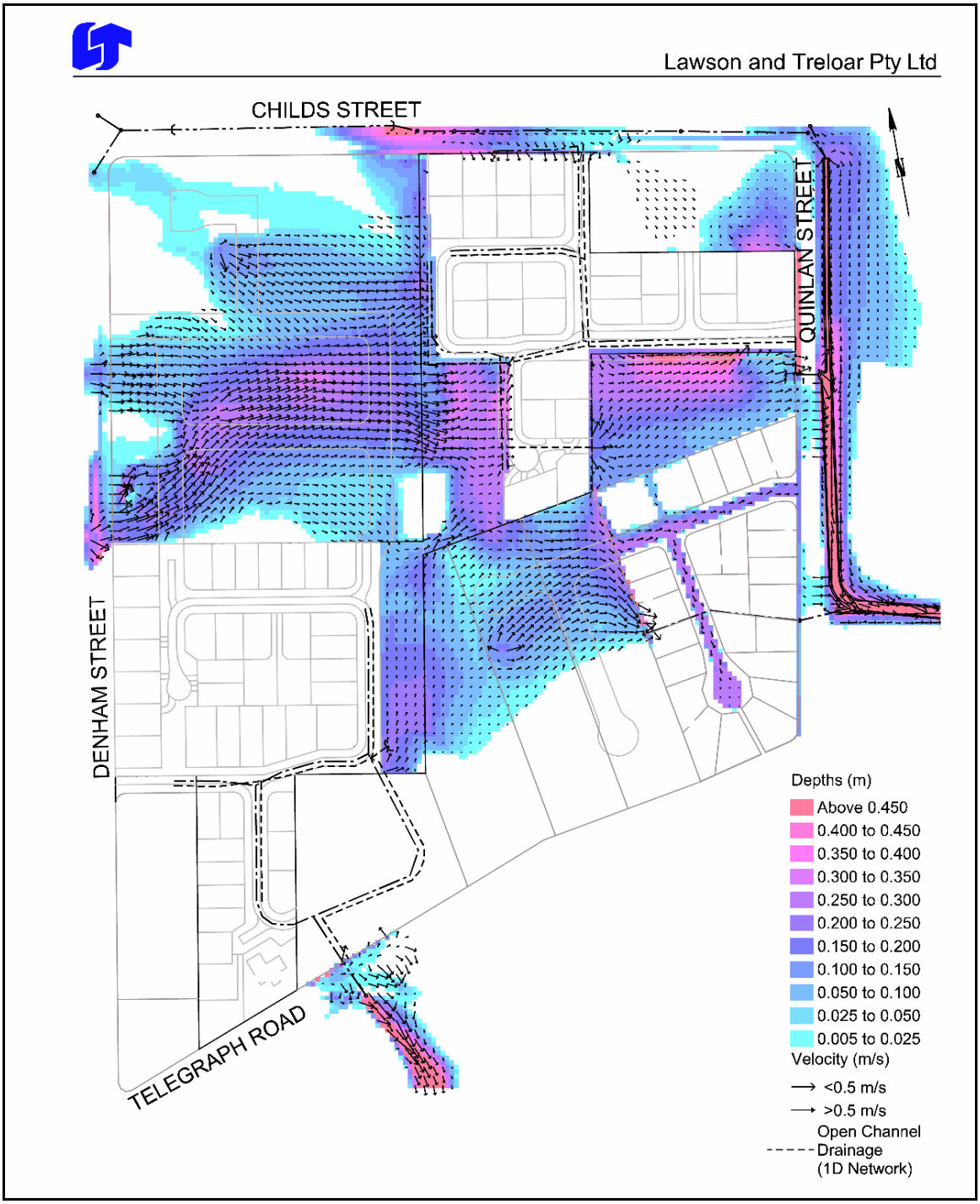

Figure 4 – Developed Situation 50 year return period flood depths and flow velocities.

From Figure 4 it can clearly be seen that the pipe drainage system along Childs Street surcharges to street level, which results in overland flooding of the area. Similarly the figure shows the overland flow from the west of the site being conveyed by the swale and pipe system along the boundary of the site and then discharged to the east of the open drain, adjacent to Telegraph Road.

A general decrease in peak flood levels was achieved on neighbouring properties for the proposed case. this being primarily a result of the additional storage and attenuation effects of the swale and pipe network system.

5 CHALLENGES IN 1D2D MODELLING

One of the first decisions to make when constructing a 2D model is the resolution of the topographic grid. Using too large grid cells can result in an inaccurate representation of the topography whereas too small grid cells can result in excessively long model development and computational times and may affect model stability.

With the ever increasing power of today's computers and the growing accuracy of laser altimetry data and aerial photogrammetry there seems to be a tendency amongst consultants to make 2D grids as fine as possible. Cell sizes of 1 to 2 metres are no longer an exception. It will not take long before small fences and brick walls that influence sheet flow paths are modelled individually as part of normal procedure. Although it is an advantage to have this capability, it can lead to a model being "over-done", thus immensely increasing the costs of modelling and data gathering.

It is questionable whether such extreme refinement in modelling gives sufficiently more accurate results. Bishop et. al. (1999) did some interesting tests on this matter. They compared flood simulation results for an urbanised floodplain modelled in a 15m spaced grid with those of a 2m spaced grid. The authors concluded that the general flow characteristics could be adequately reproduced by using a uniform high roughness value on relatively coarse grid models rather than individually modelling all small urban features in a fine grid. This was accredited to the fact that the majority of flow is conveyed by the roads, whereas urban housing lots mainly act as objects of flood storage. One should therefore base the choice for a topographic grid resolution upon the characteristics of the main flow paths rather than individual housing lots.

Further research and effort is also required at the 1D/2D interface to accurately model directional momentum transfer and accurately model inflow and outflow from stormwater inlet systems. Also, as 1D/2D systems are now capable of analysing 2D flow convergence into a 1D structure, such as a bridge located within a 2D floodplain, 1D structure losses may need to be reviewed [Collins et. al., 2001].

6 CONCLUSIONS

2D flow modelling has become more accessible thanks to the increasing computer power over the last decade and the improved availability of digital terrain data. It is a highly useful tool for overland flood flow but in some cases it is unable to accurately assess some important hydraulic structures and features that can be modelled quite sufficiently with a 1D modelling package. Hence, implicitly coupled 1D and 2D computer models for hydrodynamics are an extremely powerful tool for use in complex urban flood studies. They combine the strengths of both 1D and 2D modelling approaches and, if well applied, enhance the accuracy of the results over 1D-only and 2D-only approaches and can save considerable model development effort and computational time.

For the case analysis in this paper, the ability to couple 1D and 2D schematisations was invaluable as it enabled complex overland flow paths to dynamically interact with small 1D surface channels and 1D sub-surface pipes.

The combination of 1D and 2D hydrodynamic modules therefore creates a flood modelling package of wide applicability and is the next step forward in computational hydraulic analysis.

Care must be exercised to ensure the model has not over prescribed the study area. More research is also required on the behaviour of 1D/2D, particularly at the interface and whether 1D structures require the same level of losses when convergence and divergence from a 1D structure is modelled explicitly in the 2D model. Calibration is, as always, necessary to gain the most confidence in hydraulic modelling.

Over the last four years there have been considerable advances in coupling techniques and interfaces for 1D/2D models allowing seamless transition between the modules. Delft Hydraulics contributions in this area are acknowledged.

7 REFERENCES

Bishop, W.A., Collins, N.I., Callaghan, D.P., Clark, S.Q. (1999) *Detailed Two-Dimensional Flood Modelling of Urban Developments*, 8th International Conference Urban Storm Drainage September 1999, Sydney, Australia p1466-1473.

Bishop, W.A. and Catalano, C.L. (2001), *Benefits of Two-Dimensional Modelling of Urban Flood Projects*, 6th Conference on Hydraulics in Civil Engineering, Hobart, Australia.

Collins, N.I., Catalano C.L., *Specialised 2D Modelling in Floodplains with Steep Hydraulic Gradients*, 6th Conference on Hydraulics in Civil Engineering, Hobart, November, 2001.

Domanti, A.M. (2001) *Two Dimensional Hydraulic Modelling – Townsville Port Access Impact Assessment Study*, 6th conference on hydraulics in engineering, Hobart, Tasmania, p463.

Max Q (2004) *Stormwater Inlet Systems*, Sales Catalogue

Saint-Venant, A.J.C. de (1871). *Théorie du mouvement non-permanent des eaux, avec application aux crues des rivières et a l'introduction des marées dans leur lit*. C. R. Acad. Sc. Paris, 73:147–154.

Stelling, G.S., Duinmeijer, S.P.A. (2003) *A staggered conservative scheme for every Froude number in rapidly varied shallow water flows, International Journal for numerical methods in fluids*, #431, p329-1354.

Verwey (2001), *Latest Developments in Floodplain modelling – 1D/2D integration*, Conference on hydraulics in civil engineering, Hobart, 28-30 November 2001

WL | Delft Hydraulics (2003) *SOBEK User Manual*

The Institution of Engineers, Australia
8th National Conference on Hydraulics in Water Engineering
ANA Hotel Gold Coast, Australia 13-16 July 2004

An Efficient Geospatial Approach to Comprehensive Management and Protection of Water Distribution Systems

P.F. Boulos
B.S., M.S., MBA, Ph.D
President and COO, MWH Soft, Inc., USA
S.F. O'Brien
BEng, Grad Dip Eng
Manager Planning & Environment, MWH Australia, Australia
B. Stewart
BEng
Senior Planning Engineer, MWH Australia, Australia

Abstract: Geographic Information System offers sophisticated data management and spatial analysis capabilities that can greatly improve and facilitate network modeling applications. This paper presents a comprehensive GIS-based decision support system that integrates several advanced technologies for use in the effective management of water distribution systems. It links water quality, dynamic and transient network simulators with geospatial technology and optimization theory to address every facet of network management. The resulting system will effortlessly read GIS data, extract necessary modeling information, and automatically construct, skeletonize, load, calibrate, analyze and optimize a representative model considering hydraulic, water quality and transient design and operational requirements. It also makes it easy to simulate various scenarios, identify deficiencies, and determine cost-effective improvements for optimum performance. The innovative GIS integration approach offers a consistent geospatial environment to assist water utilities and consulting engineers in formulating and evaluating reliable water supply protection and management strategies and protecting public health.

Keywords: water distribution, optimization, surge analysis, waterhammer, geographical information systems.

1. INTRODUCTION

Computer simulation models of water distribution systems represent the most effective and viable means for providing insight into the dynamics of water distribution systems performance and evaluating their response to various management strategies. To be effective, these models require extensive spatial and infrastructure data readily available from GIS. This information system format is unique in its ability to capture and store facility data and spatial reference for asset management and network simulation model integration. It provides functions for development and preparation of pertinent spatial information for input to network models as well as functions to facilitate graphical output display for evaluating results. Added visualization tools can be applied using spatial and a spatial queries of model results to help identify correlation between input parameters and model results. Therefore, melding the strengths of network simulation models and GIS will result in more powerful modeling tools for the planning and management of water distribution systems.

Effective water distribution management requires the linking of specialized computer modeling to the GIS. The role of the GIS is to provide up-to-date and accurate data to be used in the various engineering analysis applications. For years, engineers have exported data from GIS data sets to third party software for analysis, design and optimization of water distribution systems. Applications and functionalities such as energy and fire flow analyses with the ability to analyze different demand loadings and operating scenarios were not fully recognized in GIS software. Therefore, leaving the GIS environment was necessary to use this data with other advanced modeling and planning tools. While many powerful water distribution modeling and optimization software exist, few are currently fully embedded within a GIS platform keeping engineering professionals reluctant to embrace and utilize this vital technology.

One potential problem with exporting data outside of a GIS and into a third party software application for engineering analysis is the fact that a duplication of data may be created. Once this occurs it becomes very difficult to ensure integrity between the two data sets for future applications (one data set from the GIS and the other from the hydraulic model). This occurs because engineering models take on a life of their own outside of a

GIS (Miles and Ho, 1999). Engineers spend hours tailoring the model to match existing field conditions. Pumps, pressure reducing valves, storage reservoirs, wells, closed pipes, etc. are all addressed by the engineer in the hydraulic modeling software that would otherwise be disregarded by the GIS manager. The engineer also goes to great lengths to ensure data integrity within the model for the purpose of running a hydraulic simulation. Pressure zone boundaries are delineated, demand area polygons are created and point loads are determined. All of these activities bring about the modification and adjustment of existing facilities as well as the creation of new facilities, further complicating the task of taking modeling data back to the GIS.

This paper presents an integration of water quality, dynamic and transient hydraulic models with a sophisticated planning level GIS (ArcGIS developed by ESRI, Redlands, California) and an efficient variation of computational genetic algorithms (GAs) optimization technology to address every facet of water distribution management activities. The resulting software system, called InfoWater Suite, will effortlessly read GIS data, extract necessary modeling information, and automatically construct, skeletonize, load, calibrate, analyze and optimize a representative model considering hydraulic, water quality and transient design and operational requirements. It also makes it easy to simulate various scenarios, identify deficiencies, and determine cost-effective improvements for optimum performance. It is a single software platform that addresses the requirements of both water utility engineers and GIS professionals and provides an informative structured framework for complete network model construction, analysis, and results presentation. Water utilities can use it for pipeline design and rehabilitation, system expansion, pump scheduling, developing multiple simulation scenarios, analyzing transient flows and pressures, evaluating surge protection devices, performing water quality analyses, assessing fire flow capabilities, planning sampling and unidirectional flushing programs, locating and sizing storage facilities, and monitoring SCADA operations.

2. A GEOSPATIAL DECISION SUPPORT SYSTEM – INFOWATER SUITE

The InfoWater Suite decision support system (Boulos, 2003) approaches water distribution modeling from a GIS-centric point of view and works to avoid the duplication effort involved in the creation of a hydraulic network model. Built entirely with ESRI ArcObjects technology, InfoWater Suite is a full-featured network modeling and optimization software solution. As shown in Figure 1, the core of the geospatial decision support system is the central geodatabase for storage, manipulation, and display of the collective simulation model results. No data conversion is required and the user interacts directly with the GIS. The geospatial user interface (Figure 2) initializes the GIS environment, creates all the necessary input files, builds network topology, sets hydraulic and water quality parameters and optimization constraints, runs any user-specified simulation model, and displays and tabulates results.

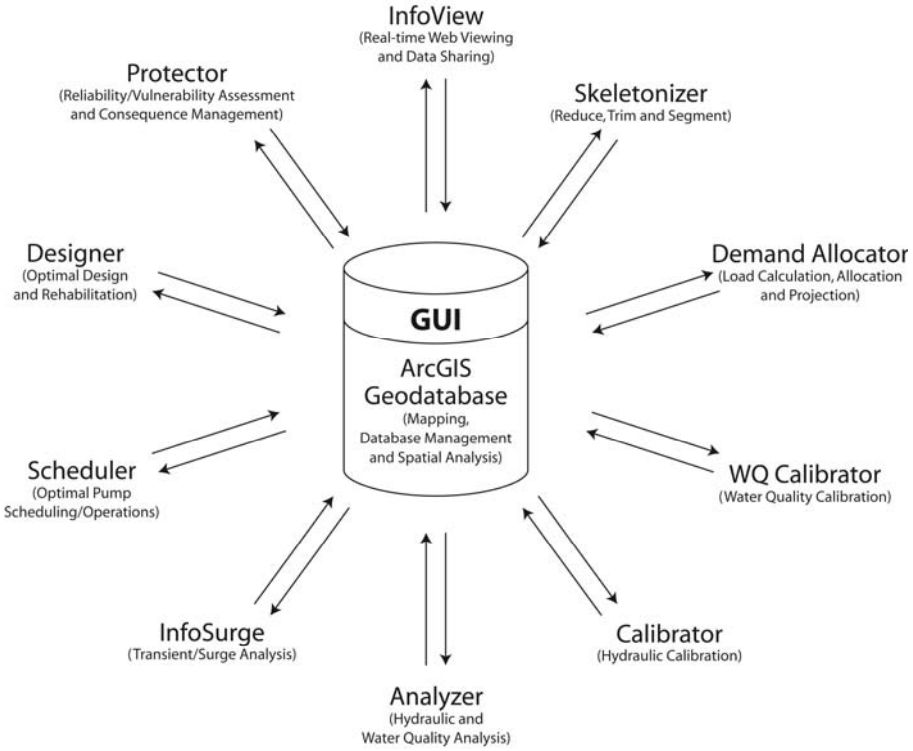

Figure 1 – The InfoWater Suite Comprehensive Geospatial Decision Making Model Architecture

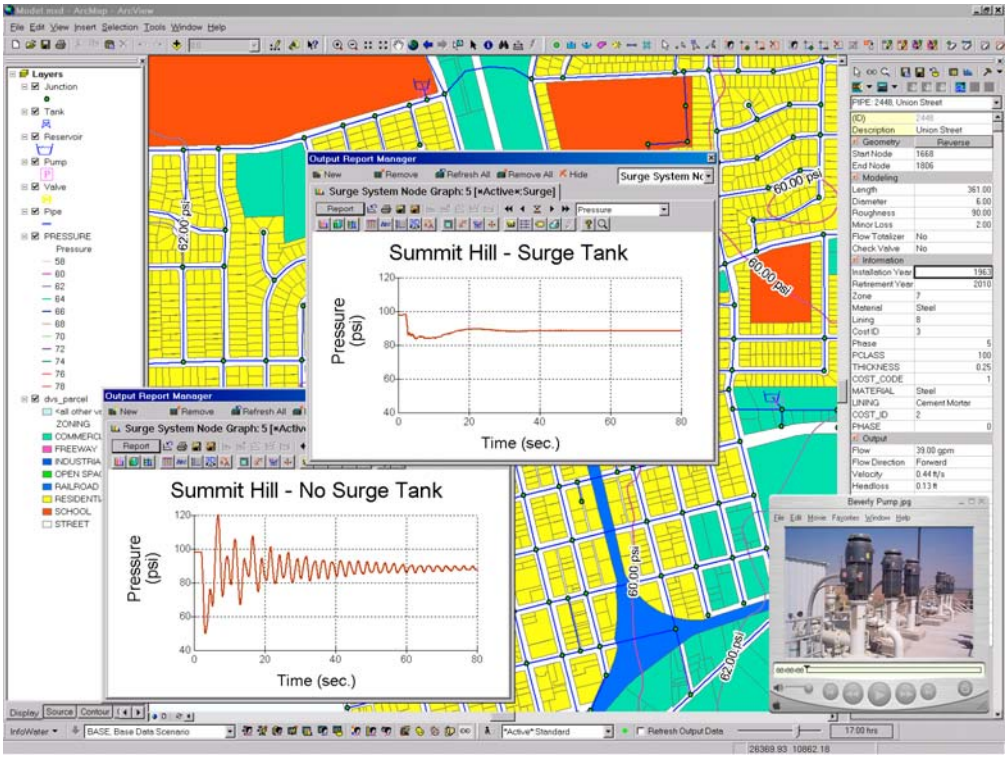

Figure 2 – The InfoWater Suite ArcGIS User Interface

The InfoWater Suite hosts in a unifying framework the variety of processes required for loading, skeletonizing, calibrating, analyzing, and optimizing water distribution network models. These are divided into eight embedded simulation modules for automated demand estimation and allocation (Allocator); network skeletonization (Skeletonizer); hydraulic and water quality analysis (Analyzer); transient simulation (InfoSurge); water security and vulnerability analysis (Protector); optimal hydraulic calibration (Calibrator); optimal water quality calibration (WQ Calibrator); least-cost design, expansion and rehabilitation (Designer); and optimal pump scheduling (Scheduler). It combines the ability to accurately build network topology, prepare requisite data, conceive and evaluate multiple scenarios, execute optimization runs, and provide both hardcopy reporting and graphical output display for evaluating and presenting results. In addition, GIS data and network modeling and simulation results can be distributed and analyzed over the internet and corporate intranets (InfoView), allowing users to interactively manage and share the information displayed with various departments.

The optimization modules are predicated on the use of the fast messy genetic algorithm (fmGA), which is one of the most competent types of GA delivering reliable solutions in sub-quadratic time (Boulos et al., 2001; Goldberg et al., 1993). They operate jointly with the hydraulic and water quality network solver (simulation module) to provide direct feedback on impacts of computed solutions on water distribution network performance. Both modules are applied in a convergent scheme as follows. The optimization model initially creates a population of candidate solutions, which are then passed to the network solver to analyze the hydraulic and water quality performance in satisfying the imposed constraints. The computed solutions are then passed to the decision support system for use in quantifying the objective function and any constraint violations. This information is then used to produce a new population with better-fit members which is then passed back to the network solver for subsequent evaluation. The iteration continues until a specified level of convergence is reached. Because the decision support software was built using an open-system architecture approach, it can be easily expanded to incorporate additional simulation and optimization modules planned in the future.

Each module of the geospatial decision support system is described below.

2.1 Network Model Reduction (Skeletonizer)

Because GIS facilities are typically created for Automated Mapping/Facilities Management (AM/FM) applications (e.g., water distribution system maintenance and management), this format is generally not suitable for construction of hydraulic network models. Common data format problems encountered by practicing

modelers who import to the network model are the inclusion of hydrants, line valves, tees or crosses from the GIS.

The Skeletonizer module is used to simplify and reduce large GIS models to a manageable size ready for hydraulic analysis. It expeditiously processes detailed GIS data, efficiently constructs reliable water system network models using three automated data segmentation applications: data reduction (Reduce), skeletonization (Skeletonize), and trimming (Trim) applications (or RST applications), and re-allocate nodal demands. Data reduction application is the ability to remove excessive pipe segmentation caused by valves, fire hydrants or other data capture processes, by dissolving interior nodes on pipe reaches and combining the associated pipe segments into single pipes. For example, merging all series pipes of common diameter, material, roughness coefficient and age, or consolidating parallel pipes and series pipes into a single hydraulically equivalent pipe. Data skeletonization application refers to the capability of removing all pipes with diameters less than a specified value (e.g., removing all 250 mm and smaller pipes). The data trimming application is the ability to remove short pipe segments leading to dead ends such as service laterals and hydrant leads. A network topology preservation algorithm (derived from graph theory) prohibits any network disconnections and ensures network model integrity and its hydraulic equivalency (using the equivalent pipe concept for series and parallel pipes) at all times.

2.2 Demand Estimation and Allocation (Demand Allocator)

Determining consumption and the spatial distribution of consumption throughout the network model is a key element of modeling. Models are loaded with existing and future demands, depending on the type of analysis performed. All sources, distribution pipelines and available storage within the system are supporting elements that provide service to meet these system demands. The variation of demand during the course of a day must also be accounted for during an extended period simulation (EPS). For static analyses, total system demand for various modeling conditions, such as average day, maximum day, peak hour, etc., is spatially distributed as a set of individual demand values allocated to selected junction nodes. For extended time period (EPS) analyses (e.g., water quality), additional temporal characteristics, typically represented by their respective diurnal variations (hydrographs), are also required. Generally, the spatial demand levels are first estimated for all junction nodes. The temporal effects are then adjusted based on individual consumption categories. The Demand Allocator module was developed to assist practicing engineers to greatly improve, simplify and fully automate the process of generating and allocating network consumption data for existing system conditions and for various planning horizons and offers six methods for processing geometric polygons to accurately compute and load network models based on demand type, location, and variation (Figure 3). These are:

1. Geocoded meter billing data (meter consumption database)
2. Polygon Processing – spatial intersection of multiple polygon layers
3. Polygon Processing – spatial summation of consumption category area polygons
4. Closest (nearest) junction method
5. Closest (nearest) pipe method
6. Large users as individual point loads

The first method makes use of GIS layers to automatically geocode consumption. The demand at each junction node is determined by identifying and summing all the customers/meters within its associated service area polygon. In the second method, demands are automatically calculated based upon a direct spatial intersection between demand categorization polygons (e.g., land use polygons, population polygons, pressure zone polygons, TAZ polygons, census tract polygons, meter route polygons, and others) and the demand node area coverage polygons (service area polygons). In the third method, nodal demands are calculated by summing the individually assigned consumption category polygons. Both the fourth and fifth methods work in conjunction with geocoded billing/meter data. The fourth method automatically assigns geocoded customer meters to the nearest junction demand node. In the fifth method, efficient geospatial search algorithms are used to locate the closest pipe to each meter. Demands are then assigned to the closest or furthest junction node on either side of the pipe or divided equally or based on a distance-weighted approach. In the last method, consumption levels for major users such as major industries, schools, parks, golf courses, hospitals, etc. are identified directly from their billing records and their demands are automatically assigned as individual point loads at their respective junction nodes.

These comprehensive capabilities give users considerable flexibility to effectively utilize their engineering knowledge and experience and leverage existing GIS data investments to strategically define/forecast their network demand distribution for various planning horizons in their master planning effort.

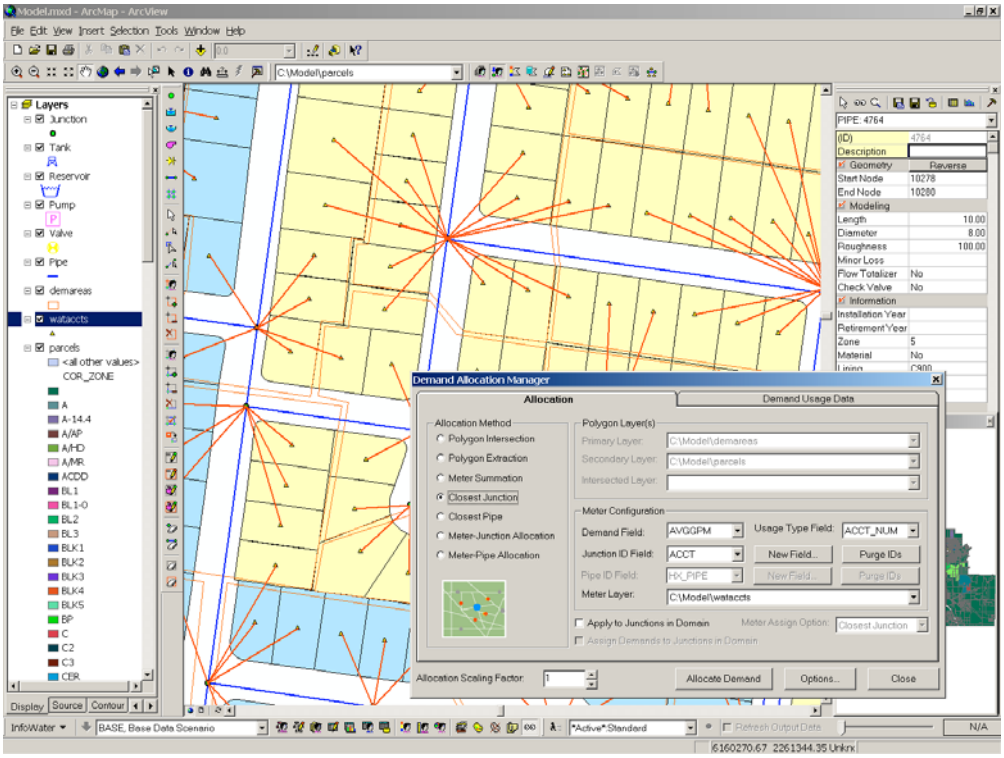

Figure 3 – The InfoWater Demand Allocator Module

2.3 Hydraulic and Water Quality Network Solver (Analyzer)

The hydraulic and water quality network solver is based on an improved version of the EPANET software. The modified Hybrid (or modified Gradient) method is used to solve the conservation of mass and energy equations and the water quality transport process is solved using the efficient Lagrangian-based Time Driven Method (Boulos et al., 2004). Both conservative and reactive species can be analyzed. A multi-level inheritance scenario manager is provided that allows the user to alternate between scenarios, merge models of any size, and compare results.

2.4 Transient (Waterhammer) Analysis (InfoSurge)

Transients in water distribution systems are a major concern for pipeline analysis, design and operation as they have the potential to wreck or damage pipeline systems and equipment, reduce system efficiency, induce adverse water quality conditions, and threaten the integrity and quality of supply as well as public safety. Pressure surges developed during startup and shutdown, and/or under accident conditions such as loss of power to the pumps or inadvertent valve closure, may exceed (steady-state) design values. Cavitation or excessive pressure surging during transient operation can lead to pipeline or component failure. Surge control devices are often required to prevent the development of such conditions. The proper selection and evaluation of these devices requires a reliable transient flow analysis.

The InfoSurge module (Boulos et al., 2003) provides advanced pressure surge simulation capabilities for analyzing mission-critical transient events, including cavitation and various commonly employed surge suppression/protection devices such as open surge tanks, closed surge tanks, discharge tanks, pressure relief valves, surge anticipation valves, air release/vacuum valves, flywheels and pump bypass lines. Vapor cavitation and liquid column separation are explicitly modeled, allowing the effect of pressure surges due to vapor cavity collapse to be properly evaluated. The program utilizes the full four quadrant pump characteristics in addition to using the moment of inertia of the moving pump parts to compute pump rundown speeds. This approach is essential for modeling situations where abnormal pump operation occurs such as turbining, flow and speed reversal, etc. These capabilities will allow the user to determine system's response to pump station power failures, valve closures, and pump speed changes, as well as assess the relative merits of various surge protection measures to reduce leaks, avoid breaks, investigate control actions and strategies, and improve water quality in the distribution system. Water utilities can then design and operate their systems with greater reliability and safety by avoiding the potential catastrophic effects of waterhammer and other undesirable system transients.

2.5 Water Security and Vulnerability Analysis (Protector)

The Protector module is designed to help water utilities reduce their infrastructure vulnerability and enhance their ability to prepare for and respond to natural disasters and emergencies. The program can be effectively used to identify viable solutions before an incident or disaster occurs, or to assist in responding should it occur. It allows the user to model the propagation and concentration of naturally disseminated, accidentally released, or intentionally introduced contaminants and chemical constituents throughout water distribution systems; assess the effects of water treatment on the contaminant; and evaluate the potential impact of unforeseen facility breakdown (e.g., significant structural damage and/or operational disruption). It enables utilities to locate areas of their systems affected by contamination; calculate population at risk and report customer notification information; and identify the appropriate valves to close to isolate a contamination event. Finally, it helps utilities track contaminants to the originating supply source(s); compute required purging water volume; develop efficient flushing strategies; determine the resulting impact on fire-fighting capabilities; and prepare data for eventual prosecution.

2.6 Network Model Calibration (Hydraulic and Water Quality Calibrator)

After a network model is properly constructed, it must be calibrated to the physical system so that model predictions can be interpreted with confidence (Boulos and Ormsbee, 1991). Calibration entails adjusting certain model parameters, usually the aggregate pipe roughness coefficients for hydraulic calibration and pipe wall decay coefficients for water quality calibration, until the model results coincide with observed field conditions. The field conditions most commonly used in network calibration correspond to pressure (fire flow tests) readings for hydraulic calibration and chlorine concentration measurements for water quality calibration. The price for neglecting network calibration is basing decisions on a model that may be seriously in error.

Typically, engineers will attempt to calibrate their network models using a tedious and inexact trial-and-error process in which the pipe roughness and wall decay coefficients are adjusted until computed and observed data are within reasonable agreement. However, since there is a vast number of possible combinations of pipe roughness and wall coefficient values that need to be considered, the trial-and-error evaluation of all options is unlikely to be practically feasible or manageable, and even knowledgeable modelers often fail to obtain good results. As a result, network model calibration has generally been neglected or done haphazardly.

In order to improve the reliability of network models as well as eliminate the need for trial-and-error calibration methods, the network model calibration problem is cast an optimization problem and solved using the fmGA. Pipes are lumped together in separate logical groups based on common physical characteristics (e.g., material, age, diameter, and location) and an average roughness and wall decay coefficient is applied to each group. The number of pipe groupings must equal or be less than the number of field measurements, the more measurements the better the accuracy of the calibration. The optimization model then proceeds by finding the set of roughness and wall decay coefficients that simultaneously minimizes the deviation between the predicted and observed data for all field measurements. Both single and multiple scenarios (e.g., maximum day + fire flow tests) and continuous dynamic (e.g., 24 hour extended period simulation) calibrations can be considered (a dynamic simulation is required for water quality calibration). Calibration results are then stored in the geodatabase and accessed by the software's object-oriented interface for graphical reporting and display.

2.7 Network Design and Rehabilitation (Designer)

Cost-effective design and rehabilitation of water supply and distribution systems is a problem of great importance in engineering practice. Water utilities have been using network models to assist them in planning their system rehabilitation and designing new systems. New system design (or expansion to existing systems) is required to cope with sustained growth while rehabilitation (or upgrading) of an existing system is required to maintain adequate levels of service.

The network design and rehabilitation problem is cast as an optimization problem and solved using the fmGA. It consists of determining the optimal rehabilitation alternatives and pipe sizes for selected pipes in the network that produce the minimum overall cost for a given set of demand loading and operating conditions while satisfying the hydraulic operational requirements of the system. The decision variables include any selected combination of rehabilitation and design options such as cleaning or cleaning and lining of existing pipes, pipe expansion, and/or installing new pipes that can either parallel or replace existing pipes. Cost data is specified for each option and for a range of pipe sizes. This data will vary with pipe material and geographical location. System operational constraints include minimum and maximum pressures at nodes, minimum and maximum velocity and hydraulic gradient requirements for pipes, and maximum flow rates (or flow volumes) for pumps.

The results of an optimization run are then stored in the geodatabase and can be displayed in both tabular and dynamic color graphic forms. The Designer module (Figure 4) can simulate any modeling condition time frame (e.g. maximum day), multiple design scenarios (e.g. maximum day plus fire), and complete extended period simulation (dynamic) designs (e.g. 24-hour operational design).

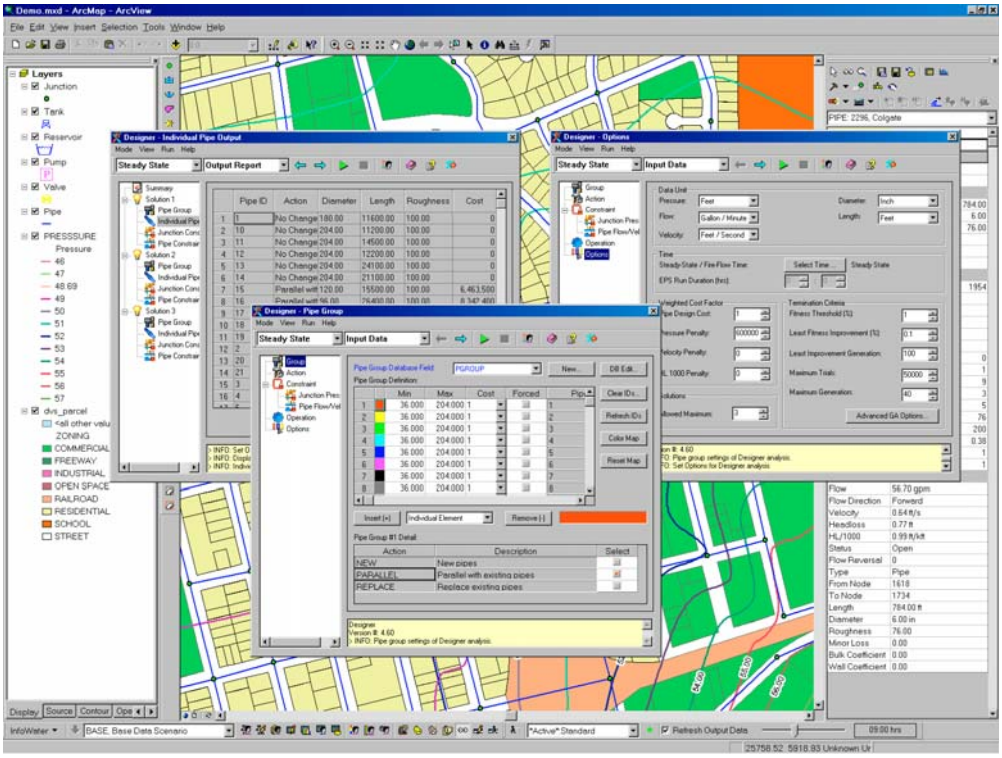

Figure 4 – The InfoWater Designer Module

2.8 Pump Scheduling (Scheduler)

Energy costs generally constitute the largest expenditure for nearly all water utilities worldwide and can consume 65 percent of a water utility's annual operating budget. One of the greatest potential areas for energy cost-savings is the scheduling of daily pump operations.

Energy-saving measures in water supply and distribution systems can be realized in many ways from field testing and proper maintenance of equipment to the use of optimal computer control. Energy usage can be reduced by decreasing the volume of water pumps (e.g., adjusting pressure zone boundaries), the head against which it is pumped (e.g., optimizing tank water level range), or the price of energy (e.g., avoid peak hour pumping and make effective use of storage tanks such as filling them during off-peak periods and draining them during peak periods), and increasing the efficiency of pumps (e.g., ensuring that pumps are operating near their best efficiency point). Water utilities can further reduce energy costs by implementing on-line telemetry and control systems (SCADA) and by managing their energy consumption more effectively using optimized scheduling of daily pump operations.

The pump scheduling problem is cast as an optimization problem and solved using the fmGA. The optimization problem consists of determining the least-cost pump operation policy that will best meet target hydraulic performance requirements. The operation policy for a pump station represents a set of temporal rules or guidelines (pump operating times) that indicate when a particular pump or group of pumps should be turned on and off over a specified period of time (typically 24 hours). The optimal operation policy is defined as that schedule of pump operations that will result in the lowest total operating cost for a given set of boundary conditions and system constraints. System constraints prescribe lower and upper limits on nodal pressures, pump and valve flow rates, pipe velocities, and storage tank levels, and final tank volumes at the end of a specified time period (normally 24 hours) to ensure hydraulic periodicity. The resulting optimal control rules for each pump in the system are then stored in the geodatabase and passed back to the decision-support system interface for graphical results presentation.

2.9 Web-Based Data Viewing and Analysis (InfoView)

The internet and the World Wide Web are rapidly evolving. Among their many benefits are greater accessibility, efficient distribution, effective administration, and cross-platform flexibility (Molenaar and Songer 2001). The Infoview module is a comprehensive ArcIMS-based (ESRI, Redlands, California) geospatial data viewer and data distribution software that enables the rapid deployment of GIS data and modeling results over the Internet and corporate intranets. GIS and modeling data are combined and made available in a common web-based map viewer allowing simultaneous users to display, analyze, query, share, and report detailed hydraulic and water quality modeling results directly from their web browser. Users can also color-code their maps according to any network characteristic, such as pipe diameter, age, velocity, flow rate, head loss, junction elevation, pressure, grade, etc.; annotate their maps with any combination of facilities and calculated results; and create contours of key modeling parameters such as pressures, water quality concentrations, and fire flows. The module greatly facilitates real-time decision making process by enabling multiple departments (including non GIS-oriented employees) within an organization to maximize their interaction with GIS data and modeling results.

3. CONCLUSIONS

Today's water utilities are discovering a wide variety of uses for GIS technology. In particular, GIS information is critical to water distribution system planning and analysis. A new geospatial software methodology has been presented as a decision support system to provide a GIS-based solution for water distribution system modeling and management. Built entirely with ESRI's ArcObjects technology, the software system seamlessly integrates sophisticated GIS features and functionalities with a hydraulic network simulator and optimization theory allowing accurate network model construction and providing a reliable and effective means for decision makers to quickly assess and address the implications of alternative design, rehabilitation and operational changes on system performance. Through the exploitation of GIS graphical data visualization capabilities, potential system deficiencies can be quickly identified where improvements are required. As the current trend towards the creation of comprehensive geodatabases continues, the proposed ArcGIS-based decision support software would be useful for planning and managing water distribution systems. It allows a wide range of network improvement and enhancement alternatives to be modeled, analyzed, contrasted, and evaluated, providing water utility managers with the ability to readily optimize their system operations and capital improvement programs. It also makes it easy for any utility to work seamlessly across platforms and to manage water systems management activities in a single environment.

4. REFERENCES

Boulos, P.F. (2003). *InfoWater Suite – Users Guide*. MWH Soft, Inc., Pasadena, CA.

Boulos, P.F. et al. (2001). Using Genetic Algorithms for Water Distribution System Optimization. In *Proceedings of the ASCE Environmental and Water Resources Institute's (EWRI's) World Water & Environmental Resource Congress*, May 20-24, Orlando, FL.

Boulos, P.F., Lansey, K.E. and Karney, B.W. (2004). *Comprehensive Water Distribution Systems Analysis Handbook for Engineers and Planners*. 1st ed., MWH Soft, Inc. Publ., Pasadena, California, 584 p.

Boulos, P.F. and Ormsbee, L.E. (1991). Explicit Network Calibration for Multiple Loading Conditions. *Journal of Civil Engineering Systems*, Vol. 8, pp. 153-159.

Boulos, P.F., Wood, D.J. and Lingireddy, S. (2003). *InfoSurge – Users Guide*. MWH Soft, Inc., Pasadena, CA.

Goldberg, D.E., Deb K., Kargupta H., and Harik G. (1993). Rapid, Accurate Optimization of Difficult Problems Using Fast Messy Genetic Algorithms. *Proceedings of the Fifth International Conference on Genetic Algorithms*, University of Illinois at Urbana Champaign, Urbana-Champaign, IL, pp. 56- 64.

Miles, S.B and Ho, C.L. (1999). Applications and Issues of GIS as a Tool for Civil Engineering Modeling. *Journal of Computing in Civil Engineering ASCE*, Vol. 13, No. 3, pp. 144-152.

Molenaar, K.R. and Songer, A.D. (2001). Web-Based Decision Support Systems: Case Study in Project Delivery. *Journal of Computing in Civil Engineering ASCE*, Vol. 15, No. 4, pp. 259-267.

The Institution of Engineers, Australia
8th National Conference on Hydraulics in Water Engineering
ANA Hotel Gold Coast, Australia 13-16 July 2004

Physical Modelling of Preliminary Design for Eidsvold Weir Spillway and Fishway

James T. Carley
B.Build., M.Eng.Sc., M.I.E.Aust.
Senior Engineer, Water Research Laboratory, School of Civil and Environmental Engineering, University of NSW, Australia
James W. Walker
B.E., M.Eng.Sc.
Senior Engineer, Water Research Laboratory, School of Civil and Environmental Engineering, University of NSW, Australia.
James E. Ball
B.E., M.E., Ph.D., F.I.E.Aust. C.P.Eng
Associate Professor, Water Research Laboratory, School of Civil and Environmental Engineering, University of NSW, Australia
John C. Macintosh
B.E., Ph.D., R.P.E.Q., F.I.E.Aust. C.P.Eng
Director/Principal, Water Solutions Pty Ltd, Australia

Abstract: This paper details two parallel physical model studies associated with the preliminary design for the proposed Eidsvold Weir project on the Burnett River in Queensland. The project incorporates a fishway to facilitate the migration of fish. A model of the entire spillway was constructed at a scale of 1:55 and a separate model of the fishway portion of the spillway was constructed at a scale of 1:12. The principal objectives of the spillway model were: to provide a faithful three dimensional visual presentation of the design; to determine a head versus discharge relationship; to identify downstream flow patterns and velocities; and to measure crest pressures over the weir. The fishway model simulated a prototype area of approximately 108 m long by 90 m wide in the vicinity of the fishway and outlet works, with its aim being to determine flow paths and velocities. Due to the complex flow patterns and interactions, it is contended that physical modelling provided the most economical, reliable and robust method of measurement of velocities downstream of the weir.

Keywords: Physical Modelling, Dam, Weir, Spillway, Fish, Fishway, Burnett, Eidsvold, Environmental Flows.

1. INTRODUCTION

Burnett Water Pty Ltd is directing the proposed construction of a weir on the Burnett River, near Eidsvold Queensland (Figure 1). A preliminary design was developed, with the final design being undertaken as part of a design and construct contract. Key design requirements for the weir are the incorporation of a fishway (to facilitate the upstream and downstream migration of fish) and outlet works (for environmental and downstream irrigation flows). The Water Research Laboratory (WRL) of the University of New South Wales was commissioned to undertake two separate physical models of the preliminary design during the tender stage of the project. A 55 scale model was constructed of the weir and a 12 scale model was constructed of the outlet works and fishway. These models were operational at the tender stage of the project for inspection by tenderers. The models were then used and modified by the successful tenderer (underway at the time of writing).

2. PRELIMINARY DESIGN

2.1 Spillway

Design flow for the weir is 2300 m^3/s and bank full flow 6600 m^3/s. A plot of flow versus average recurrence interval is shown in Figure 2. A photo of the spillway model is shown in Figure 3 and comprised the following:

- An ogee (curved) spillway, crest level 153.0 m AHD (Australian Height Datum – mean sea level), with the geometry determined for the design flow condition (2300 m^3/s). The potential crest length of the ogee is 125 m, however, 8.6 m is occupied by a low flow outlet and fishway structure, giving 116.4 m of ogee crest length. The ogee tangentially intersects a planar spillway with a slope of 1V:0.75H.
- An outlet and fishway structure, occupying 8.6 m of crest with an upper surface level of 156 m AHD.
- Stepped spillways on both sides, with the steps having dimensions of 2.0 m riser (vertical) and 6.0 m going (horizontal). The stepped portion on the left hand side (looking downstream) had a total crest length of 70 m, consisting of 36 m of horizontal and 34 m sloping down the river embankment. The

stepped portion on the right hand side (looking downstream) had a total crest length of 50 m, consisting of 22.5 m of horizontal and 27.5 m sloping down the river embankment. The horizontal portion of stepped spillway on the left hand side incorporated a 300 mm high nib/kerb giving a crest level of 153.3 m AHD, while that on the right hand side had a crest level of 153.0 m AHD.

- At the base of the ogee are two horizontal concrete aprons having levels of 140.5 m AHD on the left hand side and 140.7 m AHD on the right hand side.
- At the base of the fishway is a curved and angled trapezoidal channel which blends into the natural river topography approximately 90 m downstream of the vertical upstream face of the spillway.

2.2 Fishway

The fishway is required to operate in river flows of up to 150 m^3/s, with up to 15 m^3/s passing through the low flow outlet. A photo of the fishway model is shown in Figure 4. The conceptual design and operation of the fishway is described by Beitz (2002): "*The operating principle of a fish lock is very similar to that of a navigation lock. The migrating fish are attracted into a downstream holding chamber, and from here, enticed into the lock chamber. The bottom lock chamber gate is then closed and the chamber filled to the upstream storage level. The top gate on the lock chamber is then opened and the fish encouraged to leave the lock by creating an appropriate flow in the upstream exit channel leading to the storage*."

3. MODEL STUDY OBJECTIVES

The principal objectives for the spillway model were:

- To provide a faithful three dimensional visual presentation of the preliminary design.
- To determine a head versus discharge relationship for the weir.
- To identify flow patterns and any other concerns associated with the project.
- To measure velocities downstream of the structure for assessment of bank scour potential.
- To measure crest pressures over the weir.

The principal objective for the fishway model was to identify flow paths and velocities downstream of the weir for various low flow scenarios. Interpretation of the results was undertaken by fish migration experts.

4. DESCRIPTION OF MODELS

.

4.1 Scaling

As the models were free surface flow, scaling was in accordance with Froudian similitude. The spillway model had a length scale of 1:55 and the fishway model had a length scale of 1:12. Under Froudian similitude, the discharge scale is equal to the length scale to the power of 2.5, that is, the discharge scale in the spillway model was 1:22,434 and in the fishway model it was 1:499.

4.2 Extent of Models

The 55 scale spillway model extended approximately 300 m upstream and 700 m downstream of the weir (Figure 5), with a photo of the spillway area shown in Figure 3. Due to known flow limitations for the chosen scale, for flows over 3400 m^3/s, a central dividing wall was put in place and the model was run at half width. The 12 scale fishway model encompassed a prototype area of approximately 108 m by 90 m (Figure 4).

4.3 Control and Instrumentation

Flows were measured with electromagnetic flow meters, "rotameters" (tapered tube flow meters) and orifice plates. Water levels within the channels were measured with piezometer tappings connected to a stilling pot containing a vernier point gauge. Crest pressures were measured with a manometer board. Spillway crest tapping point locations are shown in Figure 6. Tailwater level within each model was adjusted by means of a tailgate weir at the downstream extent of the model. The design tailwater level for each flow rate was obtained from numerical modelling undertaken by Water Solutions (2002), with additional tests undertaken with lowered levels to assess sensitivity. Velocities within each model were measured with a propeller type mini current meter except where they were below the threshold (approximately 5 cm/s model), in which case, surface velocities were measured by timing surface drogues. Flow patterns were determined by injecting dye.

5. TESTING AND RESULTS FROM PHYSICAL MODELS

5.1 Spillway Model

A list of the variables tested in the spillway model is shown in Table 1. The hydraulic rating curve for the spillway model is shown in Figure 7 for three separate tailwater conditions. It can be seen that the headwater level was only sensitive to lowering the tailwater level above flows of approximately 4000 m^3/s. For the range of tailwater levels tested, the weir became submerged at flow rates above approximately 4000 m^3/s. Depth averaged velocities and flow patterns for one flow rate (3400 m^3/s) are shown in Figure 8. Crest pressures were measured for flow rates of 500, 3400 and 6200 m^3/s. As stated previously, the ogee crest shape is designed for a flow of 2300 m^3/s. No local negative pressures were measured at 500 m^3/s on the ogee, however, some minor negative pressures were measured on the stepped spillway. At 3400 m^3/s, some local negative pressures were measured on the ogee near the peak of the crest, with the results shown in Table 2. It is of note in Table 2 that several tappings (listed as n/a) became blocked in this test. No negative pressures were measured for flow rates of 6200 m^3/s due to the submergence of the weir.

Table 1 – Summary of Tests Undertaken in Spillway Model

Test	No of Tailwater Conditions	No of Full Width Flow Rates Tested	No of Half Width Flow Rates	Number of Test Permutations
Hydraulic rating	3	8	8	48
Velocities	1	2	1	3
Flow patterns	1	3	1	4
Crest pressures	1	2	1	3

Table 2 – Local Crest Pressures, Q = 3400 m^3/s, Ogee Spillway

	Local Pressure Relative to Tapping Level (m) for Transect (Figure 6)					
Tapping	**C**	**D**	**E**	**F**	**G**	**H**
1	0.1	-0.7	-0.7	-0.4	n/a	0.1
2	-0.2	-0.4	-0.5	-0.5	1.7	0.6
3	0.2	0.4	0.1	-0.1	0.8	n/a
4	1.9	0.8	0.8	0.9	0.5	1.6
5	3.3	2.4	2.5	2.3	n/a	2.7
6	4.3	4.2	4.3	4.3	n/a	3.9
7	6.9	7.0	7.1	7.1	6.5	6.1
8	9.4	9.9	9.9	9.8	9.3	8.9

5.2 Fishway Model

Flow conditions tested in the fishway model are shown in Table 3. Results from Test 2 are shown in Figure 9.

Table 3 – Summary of Tests Undertaken in Fishway Model

Test No.	Flow Rate (m^3/s)		
	Fishway (Q_F)	**Spillway (Q_S)**	**Outlet Works (Q_O)**
1	1	0	0
2	1	20	0
3	1	15	0
4	1	10	0
5	1	5	0
6	1	2	0
7	1	1	0
8	1	0	1
9	1	0	2
10	1	0	5
11	1	0	8
12	1	0	11
13	1	0	14.5

6. CONCLUSIONS

6.1 Spillway Model

A hydraulic model study at a length scale of 55 was undertaken for the preliminary design of the Eidsvold Weir spillway. Design flow for the ogee geometry was 2300 m^3/s. Testing was undertaken for flow rates ranging from 100 m^3/s to 6200 m^3/s. The structure was rated for up to 16 flow rates (eight full width and eight half width) with three separate tailwater conditions. The rating for the design tailwater curve matched the theoretical curve.

Velocities were measured at three downstream sections, located 75, 150 and 300 m downstream of the weir crest. At higher flows, higher velocity jets were observed along the banks due to the interaction of the river banks with the stepped spillway.

Crest pressures were measured for three flow rates. At the lower flow rate tested (500 m^3/s) minor negative pressures were measured on the stepped spillway but all ogee crest pressures remained positive. For a flow rate of 3400 m^3/s, minor negative pressures as low as –0.7 m were measured near the crest of the ogee, with no negative pressures measured on the stepped spillway. No negative pressures were measured for the highest flow rate (6200 m^3/s) due to the submergence effect of the higher tailwater level.

6.2 Fishway Model

A hydraulic model study at a length scale of 12 was undertaken for the preliminary design of the fishway and outlet works within the Eidsvold Weir project. Testing was undertaken with flow rates of 1 m^3/s discharging from the fishway, spillway discharges of up to 20 m^3/s and outlet works flows of up to 14.5 m^3/s. Model testing indicated that a definable flow path emanated from the fishway holding chamber under the following circumstances:

- Discharge was only from the fishway.
- Discharge from the outlet works was less than approximately 5 m^3/s.
- Discharge over the spillway was less than 2 m^3/s.

6.3 Project Overview

Flow patterns, and velocity distributions observable (both quantitatively and qualitatively) in both physical models have helped in later design optimisation and the sizing of many components in the final design (being undertaken at the time of writing). In terms of contemporary practice, it is no longer necessary to physically model large lengths of river, however, the detailed physical modelling of hydraulic structures such as the Eidsvold Weir spillway and fishway, using input from a numerical model from longer reaches of river, provides the best insight into the likely future performance of hydraulic structures. The findings in the physical model of the preliminary design have been used to optimise the final design.

7. ACKNOWLEDGEMENTS

Burnett Water Pty Itd funded the model study for the preliminary design. Model construction at WRL was undertaken by John Hart, David Clouston and Steven Pells . Doug Anderson assisted with testing.

8. REFERENCES

Beitz, E. (2002 draft), “Conceptual Design of Eidsvold Weir Fishway”, Burnett Water, November 2002.

Carley, J.T., Anderson, D.J. and Ball, J.E., (2003), “Physical Modelling of Eidsvold Weir Spillway – Preliminary Design”, *WRL Technical Report No 2003/35,* Water Research Laboratory, University of New South Wales.

Walker, J.W. and Ball, J.E., (2003), “Physical Modelling of Eidsvold Weir Fishway – Preliminary Design”, *WRL Technical Report No 2003/33,* Water Research Laboratory, University of New South Wales.

Water Solutions Pty Ltd (2002), “Preliminary Weir Headwater/Tailwater Rating Data”, Document No WS020360-Rev1 (draft).

9. FIGURES

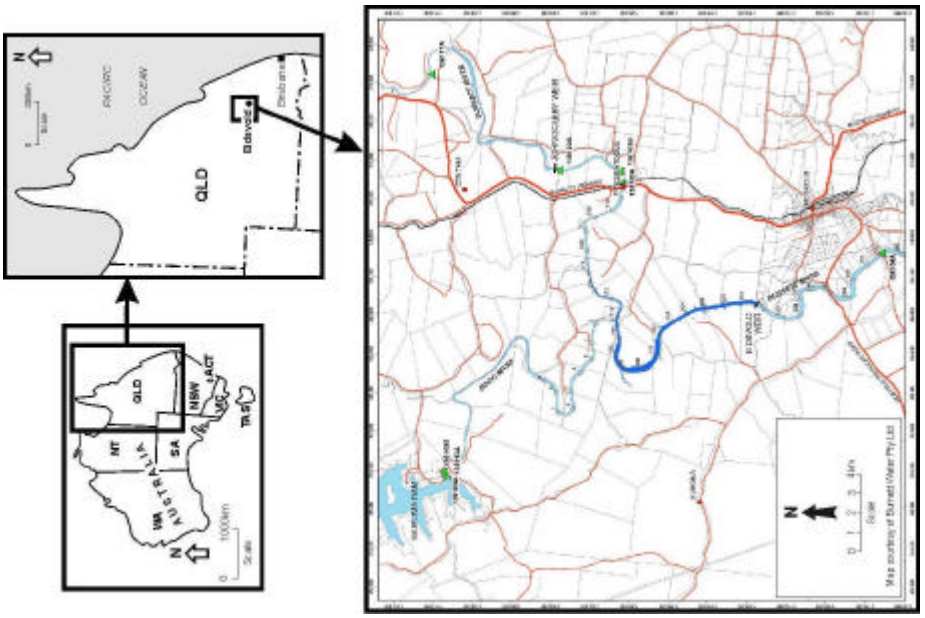

Figure 1 – Location

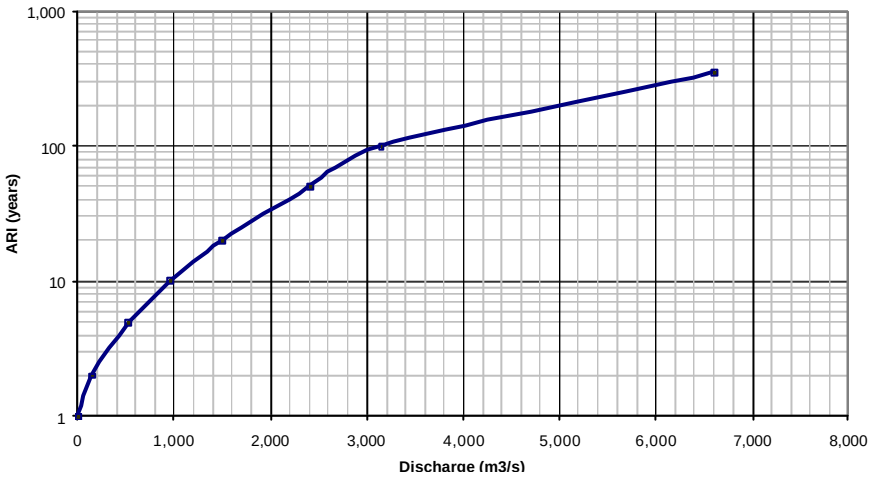

Figure 2 – Flood Frequency Curve

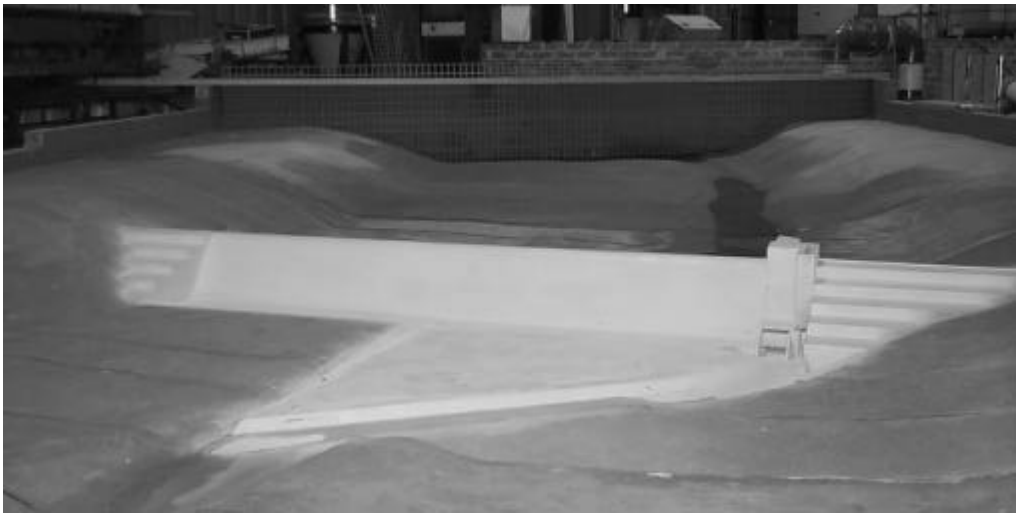

Figure 3 – Photo of Spillway Model

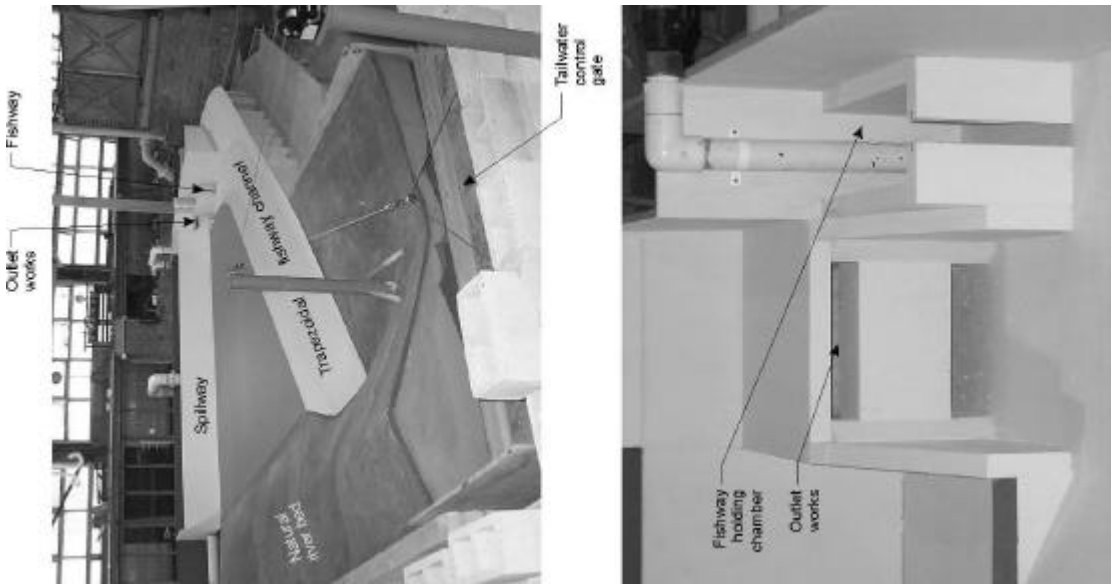

Figure 4 – Photos of Fishway Model

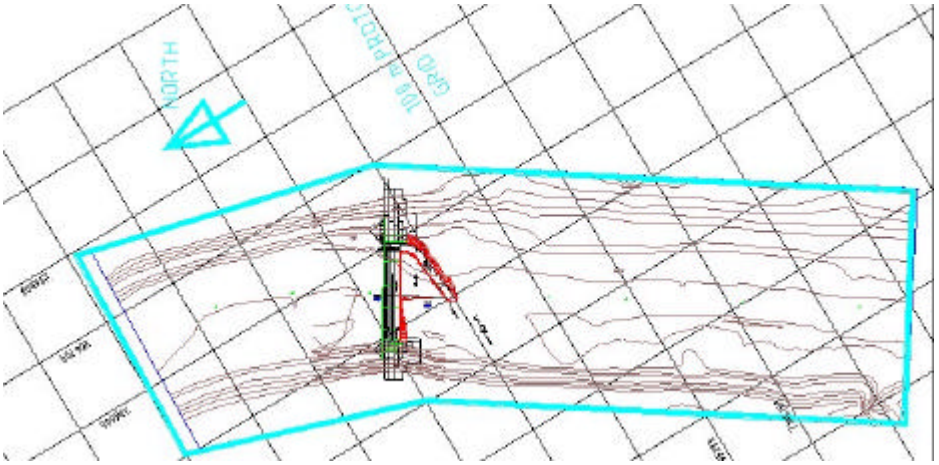

Figure 5 – Extent of Spillway Model

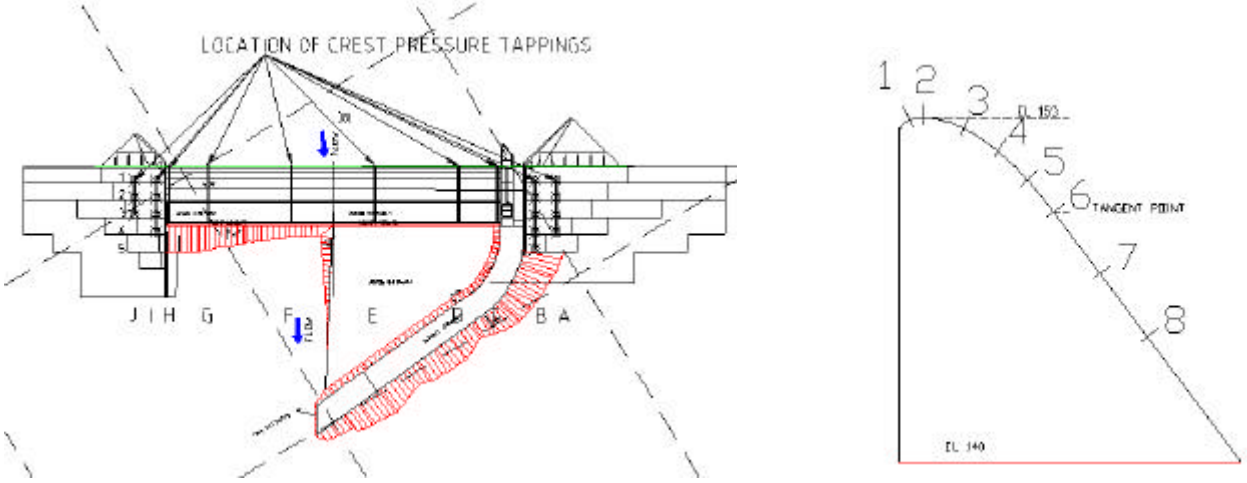

Figure 6 – Crest Pressure Tappings Location

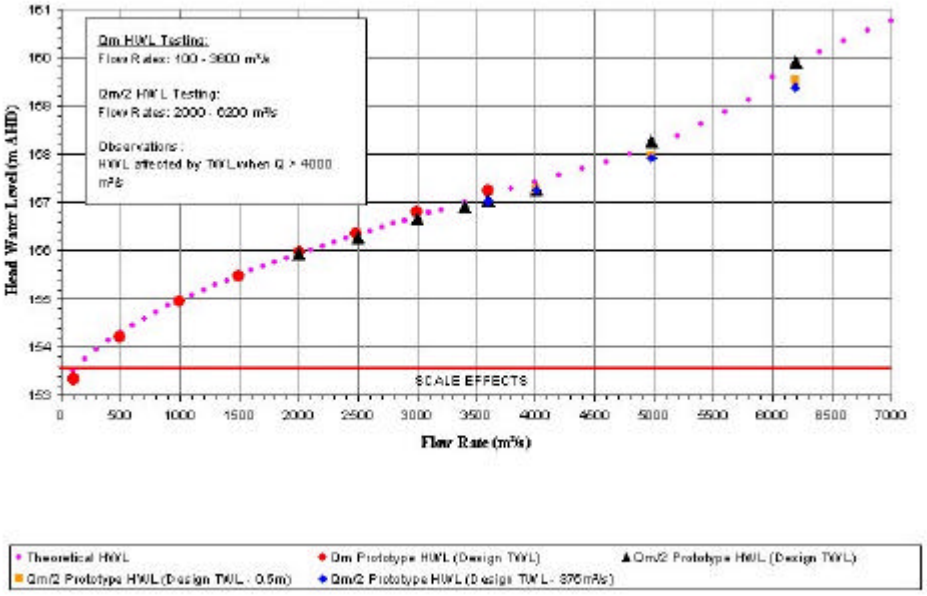

HWL = head water level (upstream of weir). TWL = tailwater level (downstream of weir).
Qm = full width flow. Qm/2 = model tests undertaken at half width (and converted back to full width).
TWL – 0.5 m refers to the tailwater level being set to 0.5 m below the design value.
TWL – 375 m^3/s refers to the tailwater level being set to the design value for a flow 375 m^3/s below the actual flow, that is, a lowered tailwater level.

Figure 7 – Hydraulic Rating Curve

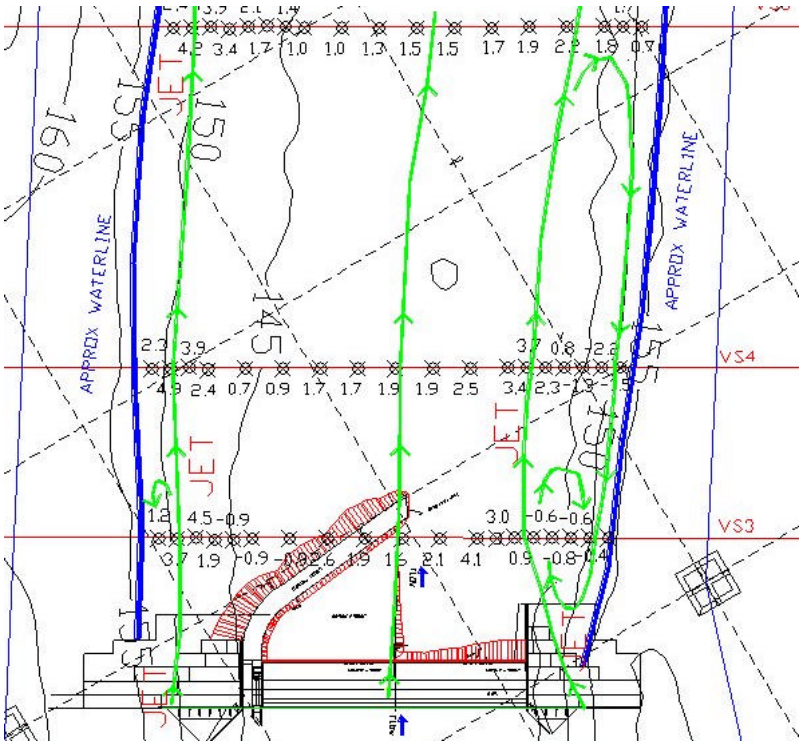

Figure 8 – Example Velocities Spillway Model

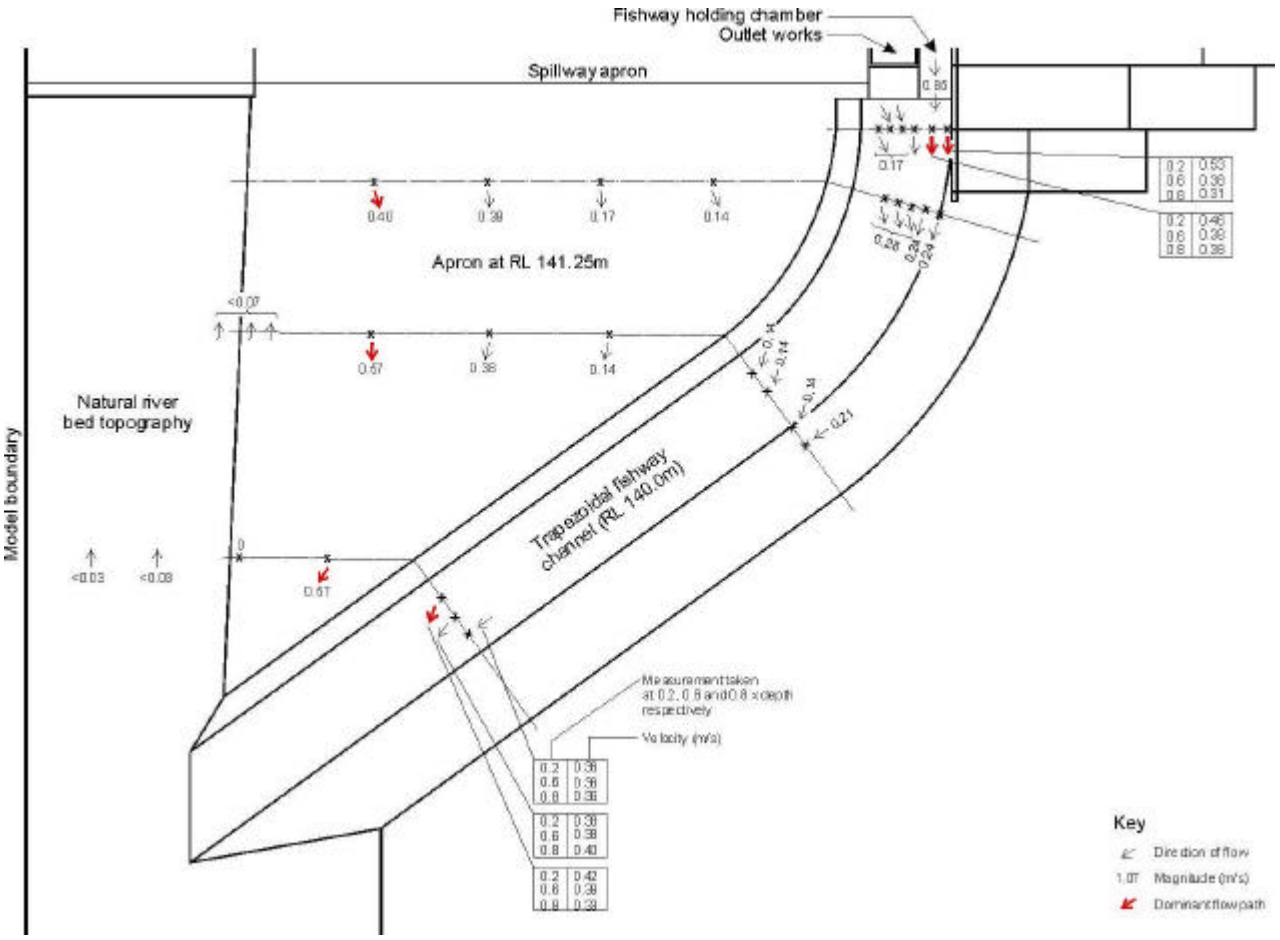

Figure 9 – Example Velocities Fishway Model

The Institution of Engineers, Australia
8th National Conference on Hydraulics in Water Engineering
ANA Hotel Gold Coast, Australia 13-16 July 2004

Hydrodynamic, Water Quality and Ecological Study of Eprapah Creek Estuarine Zone: a Multi-Disciplinary, Cross-Institutional Approach

R. Brown
B.E., B.Th., Ph.D., MIEAust
Lecturer, School of Mechanical, Manufacturing and Medical Engineering, Q.U.T., Brisbane 4000, Australia
J. Ferris
Principal Technical Officer, Water Quality Monitoring Group, E.P.A., Indooroopilly 4068, Australia
K. Warburton
M.E., Ph.D.
Senior Lecturer, Dept. of Zoology and Entomology, The University of Queensland, Brisbane 4072, Australia
H. Chanson
M.E., ENSHMG, INSTN, Ph.D., DEng., Eur.Ing., MIEAust., MIAHR
Reader, Dept of Civil Engineering, The University of Queensland, Brisbane 4072, Australia

Abstract: A series of detailed multi-disciplinary field studies was conducted in a small subtropical creek : i.e., Eprapah Creek, Victoria Point Queensland. Hydrodynamic and ecological measurements were conducted simultaneously in the river mouth to assess the complexity of the estuarine zone and the interactions between hydraulic engineering, environmental issues, biology and ecology. The results provide unique and original snapshots of a subtropical creek, and the methodology sets new standards for the comprehensive surveys of estuaries in the sub-tropical zone. A key feature of the field studies was the contrasted outcomes, and the results impact on the selection of "key indicators". Fauna observations showed strong bird and fish activities, but other results demonstrated on-going pollution.

Keywords: Field study, sub-tropical estuary, turbulence, water quality, ecology, key water quality indicator.

1. INTRODUCTION

Mixing and dispersion of matter in estuaries is of considerable importance. Applications include sediment transport and smothering of seagrass and coral, release of organic and nutrient-rich wastewater into the ecosystem (e.g. from treated sewage effluent), toxicant release and fate within the environment, and storm-water runoff during flood events. The monitoring of estuaries and marine environments is based upon key water quality parameters, including biological indicators (e.g. Ramsay et al. 2002). The effects of mixing are often ignored in assessing the overall ecosystem health of the waterways and how the water is impacted from activities such as wastewater treatment plant discharges. Although calibrated and validated water quality models are required to predict future changes in ecosystem health, their reliability depends on how well their structure and parameters best describe fundamental mechanisms such as mixing and dispersion.

In natural systems, mixing is driven by turbulence. Current knowledge is however limited since the vertical mixing coefficient is approximated by the momentum exchange coefficient, while transverse mixing and dispersion coefficients are often assumed constant. Both sets of assumptions are nearly always untrue. Predictions of contaminant dispersion in estuaries are almost always based upon empirical mixing coefficients. These coefficients are highly sensitive to the natural systems and flow conditions, and must be measured in-situ. Experimental findings are however accurate only "within a factor of 10" (at best!), and they can rarely be applied to another system (Ippen 1966, Fischer et al. 1979, Aoki 1999, Chanson 2004a). While there has been some research into pollutant dispersion in individual river catchments, very little research has been done on turbulent mixing and dispersion in complete estuarine systems, and in particular in subtropical zones. One reason for the minimal attention to this problem in the literature is the very complex behaviour of an estuary (Chanson 2004a).

In 2003, a series of detailed hydrodynamic, environmental and ecological field studies were conducted in the estuarine zone of Eprapah Creek (Victoria Point QLD). The purpose of field works was to assess the complexity of a small estuarine system, the interactions between hydraulic engineering, biology and ecology, and to gain a new understanding of basic mixing and dispersion processes in the estuarine system.

2. A CASE STUDY

Eprapah Creek is a small sub-tropical stream in Eastern Australia. Located in the Redlands shire, close to Brisbane QLD, the catchment is mostly urban in the lower reaches and semi rural/rural residential in the upper reaches (Fig. 1). The creek flows directly to the Moreton Bay at Victoria Point. It is basically 15 km long with about 3.8 km of estuarine zone. In the latter, the water depth is typically about 1 to 2 m in average in the middle of the channel, while the catchment includes several conservation areas hosting endangered species : e.g., koalas, swamp wallabies, sea eagles.

Water quality and ecology have been closely monitored at Eprapah Creek (Victoria Point QLD) for more than 30 years. The creek was heavily polluted in 1998 by illegal discharges of TBT and chemical residues leading to the first jail sentences as part of the 1994 Queensland Environmental Protection Act. Although the estuarine zone includes two environmental parks, there are some marinas and boat yards, and a sewage treatment plant impacting heavily on the natural system (Jones et al. 1999). The upstream catchment has been adversely affected by industrial poultry farms, land clearance and semi-urban development. Recent developments included the constructions of new shopping centres and residential lots.

In 2003, comprehensive hydrodynamic, environmental and ecological field studies were conducted (Table 1). The aim of investigations was to assess the complexity of the estuarine system, and to gain a new understanding of basic mixing processes in a system that was heavily impact about 4-5 years ago.

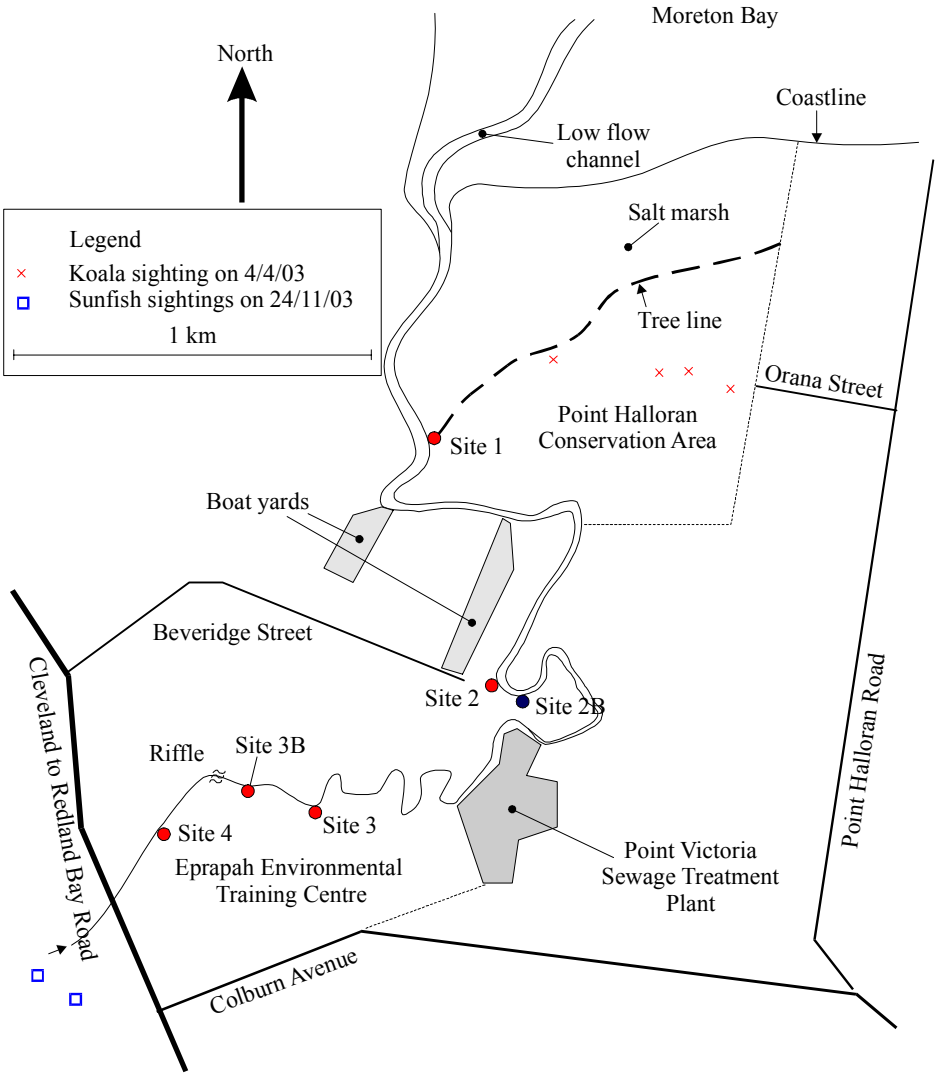

Fig. 1 - Estuary of Eprapah Creek, Redlands (Queensland)

3. EXPERIMENTAL PROCEDURES

Field works took place at several sites along the estuarine zone on three different days (Fig. 1, Table 1). They involved more than 80 people, including researchers, students, professionals and local community groups for a single-day each time (Fig. 2). Measurements were conducted for between 8 and 12 hours. The tidal and weather conditions are summarised in Table 2. On the night before the first field work, an intense but short rain storm

took place around 6:00 pm, with possibly more showers overnight. The freshwater runoff was felt on 4 April 2003 and impacted on the results (e.g. salinity).

Table 1. Experimental measurements

Field work (1)	Period (2)	Parameters (3)	Location (4)	Remarks (5)
4 April 2003				Flood and ebb tides
Series 1	06:00-18:00	Hydraulics, Water quality	Sites 1, 2, 3, 4	Measurements from banks every 15 min..
Series 2	08:00-14:00	Water quality	Sites 1, 2, 3	Measurements from boat (YSI 6920).
Series 3	10:10-14:05	Turbulence, Water quality	Site 2B	ADV and YSI 6600 probes (25 & 0.2 Hz respectively) at 14.2 m from left bank.
Series 4	06:00-18:00	Bird observations	Sites 1, 2, 3, 4	Incl. wildlife observations. Continuous observations.
Series 5	06:00-18:00	Fish sampling	Sites 1, 2, 3, 4	Incl. crustaceans and invertebrates. One trap and net every 30 min.
17 July 2003				Flood tide
Series 1	06:00-14:00	Hydraulics, Water quality	Site 2	Measurements from banks. Every 20 min.
Series 2	13:15	Water quality	Site 2	Measurements from boat (YSI 6920).
Series 3	06:10-14:05	Turbulence, Water quality	Site 2	ADV and YSI 6600 probes (25 & 0.2 Hz respectively) at 8.0 m from left bank.
Series 4	06:00-14:00	Bird observations	Site 2	Continuous observations.
Series 5	07:00-12:00	Fish sampling	Site 2 and surroundings	Several traps each hour.
24 Nov. 2003				Ebb tide.
Series 1	09:20-10:00	Hydraulics, Water quality	Sites 3B, 4	Measurements from banks.
Series 2	08:00-16:00	Water quality	Sites 1, 2, 3, 3B	Measurements from boat (YSI 6920).
Series 3	09:18-15:55	Turbulence, Water quality	Site 2B	ADV and YSI 6600 probes (25 & 0.5 Hz respectively) at 10.8 m from left bank.
Series 4	08:00-16:00	Bird observations	Site 2	Incl. wildlife observations. Continuous observations.
Series 5		Fish sampling	Site 3B, 4 and u/s of Site 4	
Series 6	07:20-16:00	Fish behaviour	Site 2	Behaviour in recirculation zones next to outer bend

On each day, several sites were simultaneously monitored (Table 1). Their location was AMTD 0.6, 2, 2.1, 3.1, 3.5 and 3.8 km for Sites 1, 2, 2B, 3, 3B and 4 respectively, where AMTD is the upstream distance from river mouth (Fig. 1). At each site, a series of hydraulic, water quality and ecological data were recorded from the bank: e.g., water elevations, surface velocity, air and water temperatures, conductivity, pH, dissolved oxygen, turbidity. Most readings were taken every 15 to 30 minutes while bird watching was continuous (Table 1). Vertical profiles of water quality parameters were conducted in the middle of the creek. These were performed at high tide and during ebb flow using a water quality probe YSI™6920 lowered from a boat drifting with the flow. Measurements of water temperature, conductivity pH, conductivity, dissolved oxygen content and turbidity were performed every 20 to 50 cm. In addition, a Sontek™ ADV velocitymeter and a water quality probe YSI™6600 were deployed and data-logged continuously at respectively 25 Hz and 0.2 Hz. The probes were located at Sites 2 and 2B (Fig. 1, Table 1). They were installed about the middle of the main channel in a moderate bend to the right when looking downstream. The two probes were positioned 300 mm apart and held by a metallic frame sliding on two poles (Fig. 2 Left). The measurement sensors were located 0.50 m beneath the free-surface and maintained at a constant depth below the free-surface for all studies. The probes were installed outside of the support system (i.e. outside of two poles) to limit the wake effects of the support.

For measurements from the bank, the data accuracy was about 1 cm for water level elevation, 0.2 to 0.5 ºC for water temperature, 1 to 2% for conductivity, 0.2 to 0.5 for pH measurement with pH paper, 5 cm on turbidity Secchi disk length, 10% on the surface velocity and 5 to 10% on the dissolved oxygen concentration. With the water quality probe YSI6920, the data accuracy was : ±2% of saturation concentration for D.O., ±0.5% for conductivity, ±0.15ºC for temperature, ±0.2 unit for pH, ±0.02 m for depth, ±1% of reading for salinity, and ± 5% for turbidity. With the water quality probe YSI6600, the accuracy of the data was : ±2% of saturation concentration for D.O., ±0.5% for conductivity, ±0.15ºC for temperature, ±0.2 unit for pH, ±0.02 m for depth, ± 1% of reading for salinity, and ±5% for turbidity. No information was available on the data accuracy on

chlorophyll levels. Further details are available in Chanson et al. (2003) and in the the website {http://www.uq.edu.au/~e2hchnas/eprapa.html}.

Fig. 2 - Photographs of field investigations
(Left) ADV and YSI6600 probes at Site 2B on 4 April 2003 in position, looking from the left bank
(Right) Interactions between students and professionals on 4 April 2003 at Site 2 (Courtesy of Student Group 2)

3.1 Discussion : practical issues

Some high level of noise was observed in the 3 velocity components recorded with the ADV velocitymeter. At rest, the measured ADV signal represents the Doppler noise itself. In the stream, the velocity fluctuations characterise the combined effects of the Doppler noise, velocity fluctuations and installation vibrations. It is acknowledged that the Doppler noise level increases with increasing velocity although it remains of the same order of magnitude as the Doppler noise at rest. Nikora and Goring (1998), Chanson et al. (2002) and more specifically Lemmin and Lhermitte (1999) discussed in details the inherent noise of an ADV system. In the present study, the ADV system was relatively old and some problems were experienced with the turbulent velocity fluctuation and vertical velocity component data. All suspicious data were discarded.
During the first two field studies, the YSI6600 water quality probe was set to record data every 5 seconds. But a few points were not recorded once every five minutes when the wiper cleaned the lens. The problem was not critical because the data acquisition timing was accurate within 1/100th of a second and it did not affect the data accuracy. The problem was resolved in the last field study when the data were recorded every 2 seconds.
The clocks of YSI6600 probe and of ADV data acquisition computers were synchronised within one second. For each study, it was expected that the cumulative errors on the time were less than 1 second for both YSI and ADV probes.

4. BASIC OBSERVATIONS

4.1 Hydraulic and water quality

Water level observations showed consistently maxima and minima slightly after the reference high and low tides (Brisbane bar). This is consistent with observed high tides at Victoria Point behind Brisbane bar records, and it is also typical of an estuarine system where the information on tide reversal must travel upstream. Surface velocity observations indicated that the flow reversal was clearly observed with greater delay than that observed with water depth data. This might be the result of possible recirculation zones next to the banks at high tide. For all 3 studies, the tidal influence was felt up to Site 3B but not at Site 4. The latter site was basically a freshwater system for each study. For the greatest tidal range (24 Nov. 2003), a very-shallow water zone was seen at low tide between Sites 2B and the sewage plant : i.e., depth less than 0.5 m. This "bar" reduced drastically mixing between the upper and lower estuarine zones at very low tides.
Water quality observations were conducted systematically from the bank (Table 1, Series 1), from a boat mid-stream (Table 1, Series 2) and with continuous recording 0.5 m beneath the free-surface at one site (Table 1, Series 3). Basic water quality results are summarised in Table 2, including the mean values, minima and

maxima. Water temperature data indicated an increase in water temperature near the middle of the day as the surface waters were heated by the sun. The flood tide also brought in some warm waters from the Moreton Bay. Measurements indicated further that the dissolved oxygen (DO) contents were maximum around high tide. The downstream waters were more oxygenated than waters at upstream sites. Basically waters rich in oxygen were brought from the Moreton Bay by the flood tide. Turbidity data showed consistently a greater water clarity at high tide and at the beginning of ebb flow. Secchi disk and YSI probe turbidity data were about constant along the creek. Water conductivity data followed the tidal cycle with an influx of saltwater during the flood flow and a reflux during the ebb at Sites 1 to 3B. The data at Site 4 indicated a freshwater pool. Conductivity data suggested clearly a decrease in conductivity with increasing distance from the river mouth. Similarly, a decrease in pH with increasing distance from the river mouth was observed on all 3 studies. On 4 April 2003, pH data ranged from 6.4 to 7 which corresponded to slightly acidic waters, associated with a marked decrease in pH with increasing distance from the river mouth (Chanson et al. 2003). It is likely that the freshwater runoff contributed to the lower pH levels.

Vertical profiles of water quality parameters showed that the distributions of water temperature, dissolved oxygen content, turbidity and pH were reasonably uniform at high tide and in the early ebb flow for all studies. Conductivity data showed however a stratification of the flow with a fresh water lens above a saltwater wedge on all 3 days. The stratification was possibly the strongest on 4 April 2003 because of substantial freshwater runoff.

Table 2. Experimental flow conditions and basic observations

Flow conditions (1)	4 Apr. 2003 (2)	17 July 2003 (3)	24 Nov. 2003 (4)	Remarks (5)
Tides	04:58 (0.53 m) 10:49 (2.02 m) 17:06 (0.43 m) 23:17 (2.20 m)	*23:42 (2:41 m)*] 06:30 (0.46 m) 12:01 (1.73 m) 17:47 (0.45 m)	03:09 (0.09 m) 09:36 (2.52 m) 16:11 (0.34 m) 21:39 (1.91 m)	Brisbane bar.
Weather conditions	Sunny	Overcast	Overcast with few short showers	
Water temperature (Celsius)	23.7 [20.4-28.4]	16.7 [15.5-18.5]	25.5 (*) [22.7-28.0]	Sites 2 & 2B.
Air temperature (Celsius)	22.2 [15.5-29]	17.2 [10.5-21.5]	-- *[19-29]*	Site 2.
Conductivity (mS/cm)	34.5 [23.9-48.3]	37.2 [29.8-48.4]	50.0 (*) [42.7-55.1]	Sites 2 & 2B.
Dissolved Oxygen content (% Sat)	0.85 [0.62-1.0]	0.82 (*) [0.66-1.06]	0.81 (*) [0.76-0.85]	Sites 2 & 2B.
pH	6.8 [6.4-7]	7.4 [6.6-7.8]	7.8 (*) [7.4-8.0]	Sites 2 & 2B.
Turbidity (m Secchi)	0.68 [0.53-1.0]	0.84 [0.5-1.2]	--	Site 2.
Average turbidity (NTU)	9.4 (*) [5.8-13.9]	11.0 (*) [7.2-*24.6*]	19.9 (*) [7.1-43]	Sites 2 & 2B.
Others :	Storm event night before. Runoff felt on 4/4/03			

Notes : Mean [Min.-Max.] : average value and range; (*) : measurement 0.5 m below free-surface.

4.2 Short-term fluctuations of velocity and water quality

Turbulent velocity records, measured with the ADV, suggested distinct periods : i.e., a slack time around high and low tides, and some strong flushing during the flood tide (17 July) and ebb tides (4 April & 24 November). Around high tide, the velocity magnitude was small : i.e., typically less than 10 cm/s, and the velocity direction was highly fluctuating. The velocity magnitude increased with time after slack, and the strongest currents were observed during mid-ebb tides on 4 April and 24 November 2003 with instantaneous velocities of about 0.2 to 0.3 m/s. The detailed records showed consistently significant fluctuations with time of both velocity magnitude and direction, with fluctuations in instantaneous velocity directions of typically about 30º. During ebb tides, the velocity data showed significant flushing of the estuarine zone. The estimated discharge at mid-tide was important (up to 5 to 10 m^3/s) and such a mass flux would contribute to significant freshwater drainage out of the estuary associated with seawater renewal at the next tide. Instantaneous water quality data results showed relatively small fluctuations of water quality parameters with time. These fluctuations were at least one order of

magnitude smaller than observed turbulent velocity fluctuations. Typical periods of fluctuations ranged from few minutes to 30 minutes. Such large periods would correspond to the effect of large vortical structures. Figure 3 presents a short series of instantaneous measurements of turbulent velocity and water quality parameters on 17 July 2003. Both graphs show results obtained around mid flood tide. The results emphasise the lesser fluctuations of water quality parameters compared to turbulent velocity fluctuations.

4.3 Fish sampling and bird observations

During each field investigation, more than 200 birds corresponding to more than 25 species were sighted at each site (Table 3, 1st and 2nd rows). Results must be considered with care since flocks of birds were seen and accounted for up to 1/3rd of the total number of sightings. Overall bird sightings showed a strong activity at all sites, particularly in the morning between 7:00 and 10:00. Yet, on 4 April 2003, there was always a minimum of five bird species seen every hour of day between 6:00 and 18:00 at each Site. This suggests a fair diversity of the bird population in the Eprapah Creek estuarine zone. Cooper (1978) indicated 120 bird species at Eprapah, while Melzer and Moriaty (1996) listed more than 70 bird species in Eprapah Creek between Cleveland-to-Redland Bay road and the river mouth. Present findings (Table 3) suggest that the bird population was diverse and active. However the surveys were limited and it is difficult to make any definite conclusion.
Fish sampling was possibly more intensive on 4 April 2003. Altogether more than 400 fish were caught corresponding to 21 species then. The largest numbers of fish were caught between 10:00 and 17:00. It is very likely that the combination of flood flow with higher dissolved oxygen contents and sun light induced significant fish activities during the period 10:00 to 16:00. At Site 4 (freshwater pool), 98.6% of the catches were Mosquito fish, an exotic species tolerant to environmental extremes. This might suggest that native species had difficulties in reduced dissolved oxygen conditions, although native fish activity were present. For example, Empire gudgeon, Firetail gudgeon and Flat headed gudgeon were caught on 4 April 2003 at Sites 3 and 4, while sun fish were observed in Eprapah Creek upstream of Site 4 on 24 November 2003.
A large amount of macro invertebrates and crustaceans were also observed during each investigation: i.e., shrimps, prawns, Fiddler crabs, mud crabs.

Table 3. Experimental observations (2) Fish and bird activities

Observations (1)	4 Apr. 2003 (2)	17 July 2003 (3)	24 Nov. 2003 (4)	Remarks (5)
Nb of bird sightings	189 (496)	200 to 300	293	Site 2 (Sites 1, 2, 3 & 4)
Nb of bird specie sighting	27 (72)	28	38	Site 2. (Sites 1, 2, 3 & 4)
Nb of fish catch	111 (437)	185	--	Site 2. (Sites 1, 2, 3 & 4)
Nb of fish specie catch	8 (21)	5	--	Site 2. (Sites 1, 2, 3 & 4)
Nb of fish sighting in recirculation zones	--	--	> 500	Site 2, outer bend.
Nb of fish specie sighting in recirculation zones	--	> 2	> 7	Site 2, outer bend.

4.4 Discussion

Depth-averaged water quality parameters were calculated from vertical water quality profiles. Despite some salinity stratification, similar trends were observed between depth-averaged data and surface water data. These observations were valid on three specific days but should not be extrapolated without further comparative tests. Although such results confirm that surface water quality parameters were reasonable indicators of Eprapah Creek health, it is essential to understand that surface water sampling does not provide any information on the flow stratification nor on turbulence characteristics.
Along an estuarine zone, the depth-averaged density increases with increasing seaward distance. Basic momentum considerations show that a slope of the mean water surface must counterbalance the mean density gradient while the solution of the motion equation gives vertical residual velocity distributions (Chanson 2004a). The results yield residual surface velocities of up to 1 cm/s. The residual circulation is relatively significant, corresponding to a renewal of the estuarine waters in about one week.
During all 3 field works, recirculation zones were observed in the outer bend of the river (Site 2). On 17 July and 24 November 2003, some toad fish were seen utilising these recirculation regions for feeding, and detailed observations on 24 November 2003 are summarised in Table 3. The findings confirm the existence of an outer bank secondary current cell at Eprapah Creek (Site 2), discussed more broadly by Blanckaert and Graf (2001).

The observations showed that recirculation zones varied in space and in time with the tide, but they were always observed. The occurrence of recirculation regions is important since outer bend cells contribute to a reduction in bend scouring. They are "dead zones" which are thought to explain long tails of tracer observed in natural rivers. Their existence implies that the turbulence is not homogeneous across the river, and that the time taken for contaminant particles to penetrate the entire flow may be significantly enhanced (e.g. Valentine and Wood 1979a,b, Chanson 2004a).

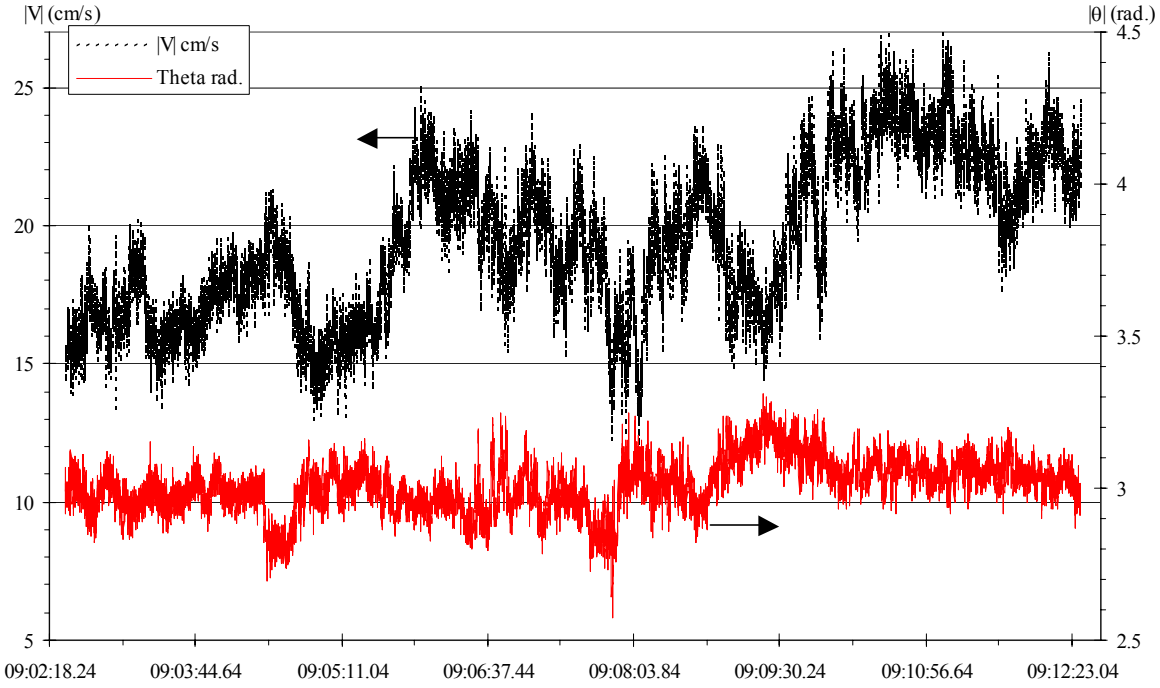

(A) Instantaneous horizontal velocity magnitude |V| and velocity direction θ (ADV data)

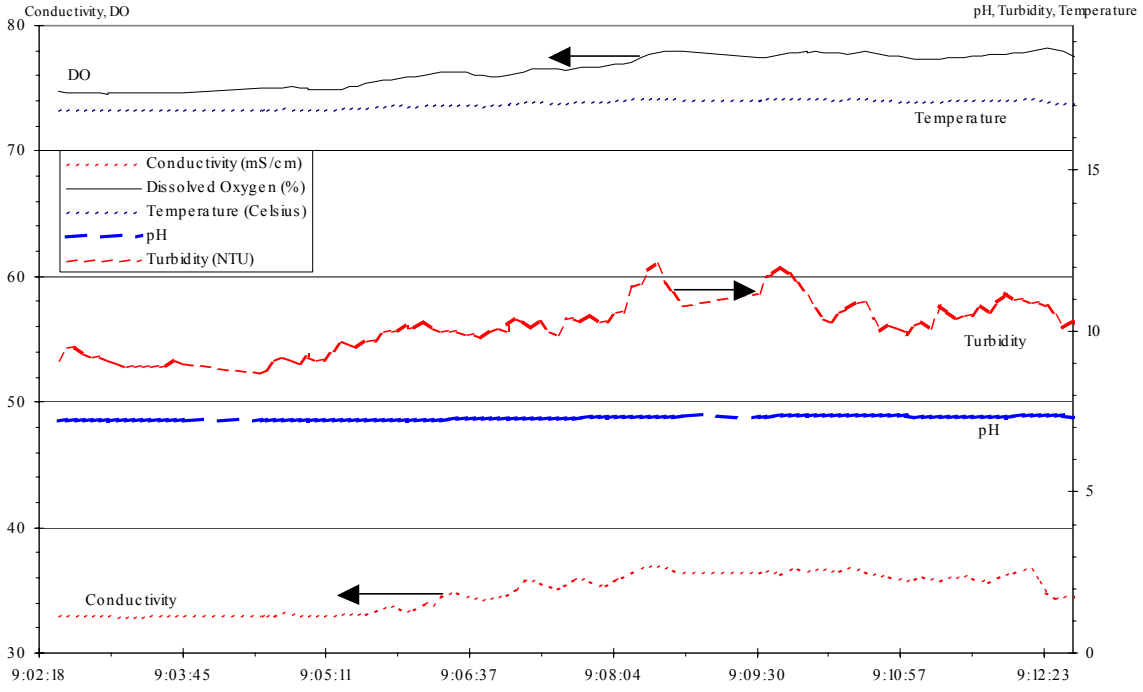

(B) Instantaneous water quality parameters (YSI6600 data)

Fig. 3 - Short-term fluctuations of turbulent velocity and water quality on 17 July 2003 during mid flood tide

5. SUMMARY AND CONCLUSION

The results and outcomes of three field studies in a subtropical estuary are three-fold. First, these investigations provided unique snapshots of a small estuarine system. The single-day studies complemented long-term monitoring, and results should not be extrapolated without care and caution. The works provided a broad range of simultaneous data encompassing hydrodynamics, water quality and ecology, and they constitute the first comprehensive hydrodynamic survey of a subtropical system. It is the opinion of the writers that the methodology sets new standards for multidisciplinary, cross-institutional, comprehensive field studies.

Second, the measurements provided contrasted outcomes. Fish sampling and bird observations suggested a dynamic eco-system, while velocity measurements indicated high turbulence levels and a strong flushing process in the estuary. But other results highlighted poor water quality parameters in the upstream sections of the estuary. Serious concerns included low dissolved oxygen and pH levels (Sites 3 and 4), surface slicks (Sites 2 and 3), a large number of exotic fish (e.g. Site 4) competing with native fish species, and surface runoff (e.g. construction sites, shopping centres). All these demonstrated on-going pollution. Clearly a major issue is the definition of so-called "key indicators" which cannot describe the complexity and diversity of sub-tropical estuaries.

Third, the field works provided unique personal experiences to all parties involved. They fostered interactions between academics, professionals, and local community groups, while they contributed to the students' personal development. Field studies complement traditional lectures and laboratory work and anonymous student feedback demonstrated a strong student interest for the field works (Chanson 2004b). Group work contributes to new friendships and openings: e.g., between civil and environmental students, between Australian and international students, between students and professionals involved in the study. Such personal experiences are at least as important as the academic experience.

6. ACKNOWLEDGMENTS

The writers acknowledge the help from all participants, including the Epraph Creek and Landcare Association (ECCLA), Mrs Lyn Roberts, Dr Bernard Stone and Mrs Jan Ellis. Richard Brown, Kevin Warburton, and Hubert Chanson thank all their students for their field work contributions.

7. REFERENCES

Aoki, S. (1999). "New Coastal Engineering in Global Environment." *Fuji Technosystems*, T. Sawaragi Ed..

Blanckaert, K., and Graf, W.H. (2001b). "Mean flow and turbulence in open-channel bend." *Jl of Hyd. Engrg.*, ASCE, Vol. 127, No. 10, pp. 835-847.

Chanson, H. (2004a). "Environmental Hydraulics of Open Channel Flows." *Butterworth-Heinemann*, Oxford.

Chanson, H. (2004b). "Enhancing Students' Motivation in the Undergraduate Teaching of Hydraulic Engineering: the Role of Field Works" *Jl of Prof. Issues in Eng Educ. and Practice*, ASCE, Vol. 130, No. 2.

Chanson, H., Aoki, S., and Maruyama, M. (2002). "Unsteady Two-Dimensional Orifice Flow: a Large-Size Experimental Investigation." *Jl of Hyd. Res.*, IAHR, Vol. 40, No. 1, pp. 63-71

Chanson, H., Brown, R., Ferris, J., and Warburton, K. (2003). "A Hydraulic, Environmental and Ecological Assessment of a Sub-tropical Stream in Eastern Australia: Eprapah Creek, Victoria Point QLD on 4 April 2003." *Report No. CH52/03*, Dept. of Civil Engineering, University of Queensland, Brisbane, Australia, June.

Cooper, V. (1978). "Bird of Eprapah." *Scout Association of Australia*, Kelvin Grove Qld, Australia, 46 pages.

Fischer, H.B., List, E.J., Koh, R.C.Y., Imberger, J., and Brooks, N.H. (1979). "Mixing in Inland and Coastal Waters." *Academic Press*, New York, USA.

Ippen, A.T. (1966). "Estuary and Coastal Hydrodynamics." *McGraw-Hill*, New York, USA.

Jones, A.B., Prange, J., and Dennison, W.C. (1999). "An Assessment of the Ecological Health of Eprapah Creek." *Report*, Marine Botany, Univ. of Queensland, Brisbane, Australia, 23 pages.

Lemmin, U., and Lhermitte, R. (1999). "ADV Measurements of Turbulence: can we Improve their Interpretation ? Discussion" *Jl of Hyd. Engrg.*, ASCE, Vol. 125, No. 6, pp. 987-988.

Melzer, R., and Moriarty, C. (1996) "Flora and Fauna of Eprapah Creek" *Eprapah Creek Catchment Landare Association*, Victoria Point Qld, Australia, 56 pages.

Nikora, V.I., and Goring, D.G. (1998). "ADV Measurements of Turbulence: can we Improve their Interpretation ?" *Jl of Hyd. Engrg.*, ASCE, Vol. 124, No. 6, pp. 630-634.

Ramsay, I., Counihan, R, Webb, G. and Conrick, D. (2002) "Southern South-East Queensland Waterway Monitoring Technical Report 2000." *Queensland Environmental Protection Agency*, Brisbane.

Valentine, E.M., and Wood, I.R. (1979). "Experiments in Longitudinal Dispersion with Dead Zones." *Jl of Hyd. Div.*, ASCE, Vol. 105, No. HY9, pp. 999-1016.

Valentine, E.M., and Wood, I.R. (1979). "Dispersion in Rough Rectangular Channels." *Jl of Hyd. Div.*, ASCE, Vol. 105, No. HY12, pp. 1537-1553.

The Institution of Engineers, Australia
8th National Conference on Hydraulics in Water Engineering
ANA Hotel Gold Coast, Australia 13-16 July 2004

Emergency Action Planning for the Dee River Dams

A. Chapman
B.E., Grad.I.E.Aust.
Graduate Engineer, Kellogg Brown & Root Pty Ltd, Australia
T. O'Connell
B.E., GradDipMgt (TechMgt), M.I.E.Aust, CPEng
Senior Hydraulics and Hydrology Engineer, Kellogg Brown & Root Pty Ltd, Australia

Abstract: The Queensland Department of Natural Resources, Mines and Energy owns three dams on the Dee River within the town of Mount Morgan, near Rockhampton. The dams were found to be referrable under the *Water Act 2000* during a Failure Impact Assessment (FIA). An Emergency Action Plan (EAP) was created to give residents warning of an impending flood and any potential dam failure. The EAP incorporated real time rainfall inputs that could give up to three hours warning of an oncoming flood. This paper aims to demonstrate the methods used in obtaining an accurate representation of the dam failure flood wave and highlight some problems had in working with FLDWAV (the hydraulic model). Flood warnings need to be accurate and local council and emergency services properly informed of the population at risk. FIA of dams will become more frequent under the new *Water Act* and this paper provides a platform for comparison.

Keywords: FLDWAV, Dam-break, Failure Impact Assessment, Emergency Action Plan, Dee River, Mount Morgan

1. INTRODUCTION

The new referable dam provisions in the *Water Act 2000* took effect on 19 April 2002. Under the new legislation a dam will no longer be considered referable in Queensland simply by its height and volume. To be referable, population will need to be at risk in the event of the failure of the dam. The act requires owners of particular dams to assess the impacts of dam failure on the safety of people living downstream of the dam, by way of a 'dam failure impact assessment', to determine whether the dam is a referable dam.

The Queensland Department of Natural Resources, Mines and Energy (NRM&E) is responsible for three dams located adjacent to the now closed Mount Morgan Mine site. The dams were built in the 1880s and 90s as a water source when the Mine was in operation and since then parts of them have been significantly undermined and are subject to increased risk of failure. The three dams are named Dam No 6, Dam No 4, and Dam No 5 from upstream to downstream. A failure impact assessment (FIA) of Dam No 6 in accordance with the *Water Act 2000* and *Guidelines for Failure Impact Assessment of Water Dams* (NRM&E, 2002) was undertaken. The objective was also to determine the need for a FIA for Dam No 5 and to consider the risk of cascade (domino effect) failure of the three structures.

The three dams are all located on the Dee River within the town of Mt Morgan (Figure 1) near Rockhampton in central Queensland. The downstream end of the reach of concern is located at the gauging station of Kenbula (Ref: 130355A) operated by NRM&E, some 3.9 km downstream of Dam No 6. The catchment area of this station is 65 km^2. The only tributary of any significance in the region of concern is Dairy Creek, which enters the Dee River in the ponded area just upstream of Dam No 6. Most of the catchment area is undeveloped with grazing and forest the main land use. The town and mining area of Mt Morgan is located in the lower reaches of the catchment, but this covers a small portion of the total area. The land is hilly with the highest point of the catchment having an altitude of the order of 500 m. There is another dam located almost 4 km upstream of Dam No 6 called Dam No 7, and is used for water supply to the town of Mt Morgan. While this dam would have limited impact on major flood discharges in the downstream reach, it has been included in this analysis to enable an upstream warning system for emergency action.

Figure 1 – Locality Plan (Dam No 7 and Kenbula Gauging Station Not Shown).

The Dee River channel in this reach has well defined beds and banks with a steep rock formation slope on one side and limited floodplain on the other. As a consequence of the operation of the mine, the reservoirs upstream of each dam are filled with substantial quantities of tailings.

Whilst solutions will be planned to some degree within a year from the completion of the FIA, an interim Emergency Action Plan (EAP) was considered necessary especially prior to the oncoming wet season.

The analysis for the EAP required the assessment of trigger flows in the upper reach of the Dee River upstream of Dam No 6. These trigger flows allowed for the preparation of warning systems with extended warning time prior to onset of potential dam failure. The warning time however, is extremely limited because of the small catchment area.

2. DAM-BREAK MODEL

NRM&E's FIA guidelines allow the use of both one dimensional and two dimensional flow analyses for the determination of population at risk. A two-dimensional flow analysis assessment is used if the population at risk is situated close to a possible dam breach location and there is a risk that the population will be inundated by water from the dam before it concentrates in downstream channels. This is not the situation here, as identified earlier, and hence a two dimensional analysis is not warranted.

The FIA was originally undertaken using Danish Hydraulic Institute's MIKE 11 Dam-break Module, but the switch was made to FLDWAV prior to the EAP to take advantage of its public availability. Proprietary equivalent graphical input and output processors are available for FLDWAV but they were not used in this study.

The flood wave routing model FLDWAV (Fread and Lewis 1988), the flow model developed at the US National Weather Service Hydraulics Laboratory, provides real-time forecasts of discharges, water-surface elevations, and velocities at specified locations along a river. The model is based on an implicit (four-point, nonlinear) finite-difference solution of the complete one dimensional Saint-Venant unsteady flow equations coupled with an

assortment of internal boundary conditions representing flows controlled by a wide spectrum of hydraulic structures. This dynamic wave method accounts for the acceleration effects associated with the dam-break wave.

Additional capabilities of FLDWAV include: 1) the ability to dynamically model dam failures, as well as flows which are affected by bridge constrictions: 2) the ability to simulate flows which overtop and crevasse levees located along either or both sides of a main stream and/or its principal tributaries; 3) the ability to handle flows in the subcritical and/or supercritical flow regime; and 4) the ability to handle non-Newtonian (mud/debris, mine tailings) flow.

The essential component of the FLDWAV model is the computational hydraulic routing algorithm that determines the extent and time of occurrence of flooding when subjected to an unsteady flow hydrograph. The hydrograph is attenuated, lagged and distorted as it is routed through the channel due to the effects of floodplain storage, frictional resistance to flow, flood wave acceleration components, flow losses and gains, and downstream channel constrictions and/or flow control structures.

The equations of Saint-Venant, expressed in conservation form, with additional terms for the effect of expansion/contractions, channel sinuosity and non-Newtonian flow (Fread and Lewis, 1998) consist of a conservation of mass equation, i.e.,

$$\frac{\partial Q}{\partial x} + \frac{\partial s_{co}\left(A + A_0\right)}{\partial t} - q = 0 \tag{1}$$

And a conservation of momentum equation, i.e.,

$$\frac{\partial\left(s_m Q\right)}{\partial t} + \frac{\partial\left(\beta Q^2 / A\right)}{\partial x} + gA\left(\frac{\partial h}{\partial x} + S_f + S_e + S_i\right) + L + W_f B = 0 \tag{2}$$

where Q is the discharge or flow, h is the water-surface elevation, A is the active cross-sectional area of flow, A_0 is the inactive (off-channel storage) cross-sectional area, s_{co} and s_m are sinuosity factors which vary with h, x is the longitudinal distance along the river, t is the time, q is the lateral inflow or outflow per lineal distance along the channel, β is the momentum coefficient for velocity distribution, g is the acceleration due to gravity, S_f is the channel boundary friction slope, S_e is the expansion-contraction slope, S_i is the additional friction slope associated with internal viscous dissipation of non-Newtonian fluids, L is the momentum effect of lateral flow, B is the active river top width at water-surface elevation h, and W_f is the effect of wind resistance on the surface of the flow.

Implicit finite difference techniques have no restrictions on the size of the time step due to mathematical stability; however, convergence considerations may require its size to be limited. The weighted four-point scheme appears beneficial since it can readily be used with unequal distance and time steps and its stability-convergence properties can be conveniently controlled.

Modifications to the flood wave manifest as attenuation of the flood-peak magnitude, spreading-out or dispersion of the time-varying flood-wave volume, and changes in the celerity (propagation speed) or travel time of the flood wave.

Even when the channel approaches that of a uniform rectangular shape, as is the case for this reach, the dam-break flood wave can experience appreciable attenuation of the flood peak and reduction in the wave celerity as the wave progresses through the channel/floodplain.

For significant dam structures, the magnitude of the peak discharge of a dam-break wave is usually much greater than the runoff flood of record having occurred in the same river. The above-record discharges make it necessary to extrapolate certain coefficients used in various flood routing techniques and make it impossible to fully calibrate the routing technique. Because of the small storage volumes associated with the three dams this shouldn't be the case here.

Another distinguishing characteristic of typical dam-break floods is the very short duration time, and particularly the extremely short time from beginning of rise until the occurrence of the peak. This time to peak is similar to the period of breach formation time and therefore is in the range of a few minutes to about an hour. This

relatively rapid time causes it to have acceleration components of a far greater significance than those associated with a runoff-generated flood wave.
FLDWAV is a PC-DOS based system with parameter data user-specified through a batch mode and output files written in text format. The output files can be very large, especially when small time steps combined with maximum debug information are used, and must be interrogated for confirmation that the run was successful. Generally FLDWAV will execute runs even when insufficient inputs are included, thus making it important to thoroughly check output files for errors.

3. MODEL SETUP AND CALIBRATION

Information about the dam spillways and non-overflow crest (Table 1) were included in the model.

Table 1. Dam Properties at Full Supply Level (FSL)

Dam	Type	Height above bed (m)	Capacity (ML)	Surface area (ha)	Overall length (m)	Spillway length (m)
6	Mass concrete monolithic wall with buttresses & earth levee	9.7	63.6	4.6	240	86.5
4	Vertical concrete wall	3.0	29.5	2.6	70	63.5
5	Mass concrete monolithic wall	4.8	42.0	1.3	110	62.5

In addition to the physical data on the dams, there were two groups of data relevant to this project, namely the hydrology data and the survey data.

The hydrology data was used to define the relevant design floods and to assess the risk of occurrence of these floods using the routing runoff program RORB (Laurenson and Mein 1995), based on the gauging station at Kenbula, which has about ten years of stream flow records. This station has been used to assist in the assessment of design floods and to calibrate the hydraulic model.

Whilst the gauging station period of record was short, the occurrence of several larger floods and more than 30 gaugings plus communication with NRM&E's hydrologists led the designers to adopt the recordings for calibration. The relevant data extracted from the records at the gauging station included daily maximum flood peak discharges, for use in flood frequency estimation; the published rating curve, for use as the downstream boundary of the hydraulic model; measured flow velocities, for use in calibration of the hydraulic model; and a recorded flood hydrograph for the February 2003 event with a peak of 355 m^3/s, for calibration of both the hydrology and hydraulic model.

Elevation-storage-outflow data for Dam No 7, with a catchment area of 37.5 km^2, was included in the hydrology model.

A series of flood hydrographs were calculated for the catchment using RORB. With 100 year ARI design rainfall intensities, appropriate rainfall losses given by *Australian Rainfall and Runoff* (Institution of Engineers, Australia, 1998), temporal patterns scaled from the recorded flood, and catchment storage-discharge parameters from the calibration run, a peak discharge of 455 m^3/s for a critical storm duration of 6 hours was calculated for the 100 year ARI event.

The February 2003 recorded flood hydrograph is straddled by the two design floods and hence is considered appropriate for the calibration. The peak at Kenbula is only 1 to 1.5 hours after the peak at Dam No 7 for the range of floods considered, meaning flood warning systems based on peak discharges alone are not likely to give sufficient mobilisation times.

Active cross section areas and inactive areas are user-specified in FLDWAV as a table of wetted top widths which vary with elevation. Survey data was needed for the river to allow accurate calculation of water levels and flow velocities, and also for location and level of the houses and other facilities near to the Dee River, to assess the risk and potential damage to the downstream community. The rail bridge between Dam Nos 4 and 5 was included in the survey but assumed to have little or no effect on the hydraulics of a dam failure case. The survey provided cross-sections of the river from upstream of Dam No 6 to the Kenbula gauging station (a total distance of about 5.3 km). These sections are spaced about 100 m apart giving a total of 47 sections and are at right angles to the flow. They extend up to high ground above the level of the expected highest flood level, estimated as about 10 m above the bed of the river and extend below standing water level behind the dams to the existing

river bed. Small cross-section spacing is necessary to propagate the peaked flood wave accurately. Interpolated cross-sections at generally 5 m centres achieved this.

The hydraulic roughness coefficients for the river, which may vary with elevation or discharge and with location along the waterway, were set to a Manning's 'n' of 0.05 globally based on limited data and to achieve calibration.

Once the model was calibrated it was run for a 100 year ARI event without dam break. The model was then used to calculate the flood hydrographs throughout the catchment for the Property Damaging Flood (PDF), which is defined as the greatest flood without a dam-break that would not inundate habitable structures downstream. The peak discharge of 330 m^3/s was calculated for the PDF.

All properties were assigned a river chainage based on visual inspection of the survey data. This allowed comparison with the flood profiles from the FLDWAV output files. Results are presented and compared with failure cases in Section 4. Dam No 4, the smallest of the structures, is drowned in these sized floods.

One point of particular significance in the recorded data was the large flow velocities measured at the gauging station, with velocities of over 3 m/s for the higher discharges on record. This high flow velocity appears to be well supported by observations of the conditions of the stream channel (NRM&E hydrologist Pers. Comm., photo collection), especially in the downstream part of the river reach where the river bed appears to have been scoured by the high velocity flows. In addition to the calibration to the February 2003 recorded level hydrograph at the gauge, these velocities were used to verify the calibration (Table 2).

Table 2. Model Verification Using Average Flow Velocities

Flood Event	Velocity in last 2km reach (m/s)
PDF	2.3
ARI 100 year	2.6

4. DAM-BREAK RESULTS

In the event of a dam wall failure, the expected flooding effects need to be known for emergency procedures. As it produces worst case flooding downstream, the cascade failure (i.e. first dam flood wave causes breaching of second dam and so on) of all three dams in the same rainfall event was considered.

The flow at the dam-break structure is quite similar to a broad-crested weir, but there are differences in that the shape of the dam changes with time, i.e. the breach increases and the dam crest is shortened. As a consequence the critical flow characteristics *(Q-h)* relationship of the crest and of the breach cannot be calculated beforehand. Additionally, the *Q-h* relationship for the dam crest and the breach are different. Therefore the flow over the crest and the flow through the breach are calculated separately. For each of these two flows the equations used are the same as for a broad-crested weir.

The breach dimensions and timing were determined from a literature review of similar breaches on similar dams. This led to the adoption of instantaneous dam failure for all dams. The theoretical breach begins in the centre of the dams and develops in a trapezoidal shape until it reaches the river bed at the downstream face of the dams. This produces conservative results.

Surveyed cross-sections represented the current level of tailings/silt in the dams and not the original construction bed or natural ground level within the ponded areas upstream of the dams. It was assumed that the tailings material would be eroded away prior to the onset of the dam-break flood peak. Tailings depths were interpolated from 12 borelogs along the reach of concern and assumed to extend bank-to-bank at each cross-section. The exact composition and extent of the material is not known with certainty, but it is likely that, in the real situation, part of the material would erode away leading to a situation intermediate between the two assumptions. Assuming that all the material erodes leads to a greater impact of the dam failure, given the potential for larger water storage at failure.

Dam failure by overtopping was timed to occur when the peak of the flood wave, produced from the runoff or a combination of runoff and breach waves, arrived at each dam wall. Since the dams were to fail instantaneously, this produced a sharply spiked flood profile. This was achieved by using very small time steps, and specifying the dams to break at water levels accurate to three decimal places.

Figure 2 plots the water surface elevation difference due to dam failure for the PDF and ARI 100 year events. It can be seen that the failure impact is fairly similar for both cases, however, the increase in flood level is more pronounced for the smaller PDF event. This is due to the dam failure flood wave being larger in proportion to the PDF event than the ARI 100 year event. The failure impact is 1.3m maximum immediately downstream of Dam No 6. Downstream of Dam No 5, the maximum increases to 1.7m due to the combined failure peaks.

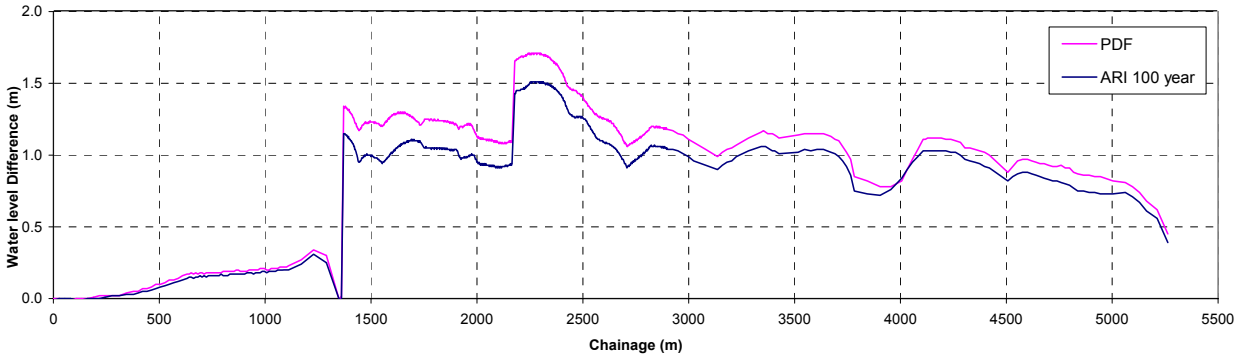

Figure 2 – Difference Between Flood Profiles for Failure and No Failure Cases

The failure impact zone is defined in the guidelines as the region where the incremental effect of the dam failure is 300 mm or greater. Based on this criterion, the whole reach from Dam No 6 down to the Kenbula gauging station is located in the failure impact zone for these flood events, since the incremental effect of the dam failure in both PDF and ARI 100 year events caused an increase in flood water levels of greater than 300 mm.

Figure 3 presents the inundation profiles of the PDF and ARI 100 year events with cascade dam failure. The figure also shows a number of property ground levels and the mine causeway entrance as being affected by the dam-break flood waves, giving a referable dam with a Category 1 failure impact rating (between 2 and 100 people at risk).

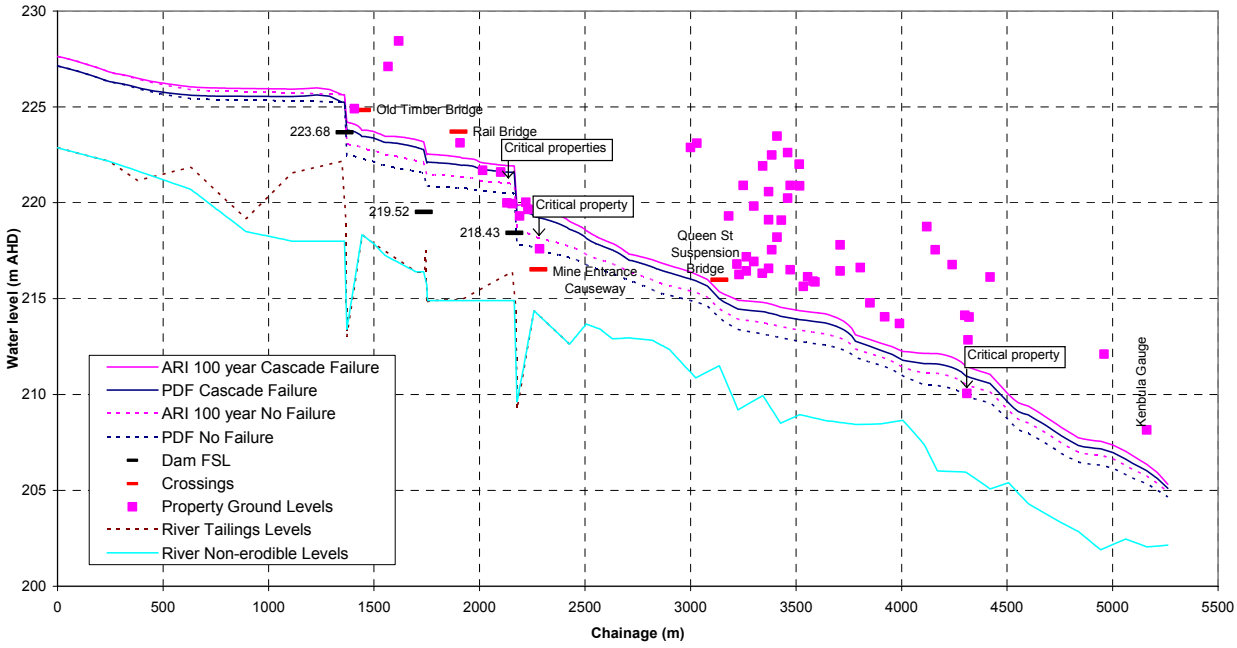

Figure 3 – Flood Profiles For Failure and No Failure Cases

5. RAINFALL TRIGGERS

Consultation with Bureau of Meteorology staff ruled out the use of proprietary flow warning systems due to the extremely short lead-time to the onset of the wet season. Hence a simplistic flow and rainfall trigger system needed to be implemented and remain in place until solutions are found, presumably one wet season.

The analysis for the EAP required the assessment of trigger floods in the upper reaches of the Dee River. Gauges exist on Dam No 7 and in Dairy Creek and these were automated and upgraded for the purposes of real-time warning. The calculation of trigger flows at those upstream gauges combined with trigger rainfall at Dam No 6 allowed for the preparation of warning systems that would give a minimum of 1.5 hours notice to evacuation personnel before the onset of property inundation. The warning time however is extremely limited because of the small catchment area.

Historical point rainfall data for Kenbula station was provided by NRM&E. This data extends from December 1992 through to early June 2003, representing over ten years of complete instantaneous rainfall depths. The data was processed to provide hourly totals and analysed to find incidences of intense rainfall. The EAP defines this intense rainfall as anything over 25 mm in one hour.

For each rainfall event in the data period, for which in one or more hours 25 mm of rain was recorded, a RORB model and corresponding FLDWAV model was set-up. Peak discharges were recorded at Kenbula station for most of the dataset, allowing calibration using rainfall losses. Assumptions included all dams being at FSL prior to the start of the rainfall event, all tailings removed prior to the onset of the flood for conservative results and rainfall at Kenbula being indicative of uniform rainfall over the entire catchment.

There were fourteen occurrences of this intense rainfall, with up to 310mm total in the February 2003 event with an average of 78mm. Peak discharges were not recorded in 6 of these events with a maximum of 463mm in January 1996 and an average of 117m^3/s.

Only twice in the fourteen occurrences (January 1996 and February 2003) was the rainfall of sufficient intensity and duration to produce floods large enough to inundate downstream property. This is equivalent to twelve false alarms to the authorities that crossings downstream of the dam may be inundated. For both these occurrences, the combined rainfall and discharge triggers of the EAP would have resulted in a call to the relevant authorities to evacuate. In 1996 there would have been over 6 hours warning from recorded intense rainfall at Dam No 6. In 2003, there would have been 9 hours warning from recorded trigger flow at Dam No 7. Given dam failure, especially cascade failure of all three dams, the timing from triggers to inundation of crossings and properties would be much reduced.

Whilst the incidence of potential false alarms is high, the triggers are warranted to provide the necessary warning times, and given the temporary nature of the EAP the high incidence was considered acceptable.

6. CONCLUSIONS

The public domain software FLDWAV contained all the necessary components to accurately define the flood inundation due to both the runoff flood and the breach generated flood wave. Whilst the lack of a graphical pre- and post-processor increased model set-up and reporting times, results were still achieved. The model, as it is set up, allows for future solution planning.

Closely spaced and accurate survey to sufficient elevations above the channel proper is vital.

Modelling of reach hydrology and hydraulics for all historical rainfall produced interim trigger flows and rainfalls that could be used by NRM&E staff to give emergency services adequate warning of impending property damage.

7. ACKNOWLEDGEMENTS

The authors would like to thank NRM&E's Rockhampton based project officer for initial and continued support of this regulatory exercise. Technical expertise has been drawn from NRM&E's and the Environmental Protection Agency's dam sections in Brisbane, which has been invaluable. Project overview by Kellogg Brown & Root's chief engineer and technical sector leader (Water Resources) is appreciated.

8. REFERENCES

Department of Natural Resources and Mines, Queensland Government. 2002. Guidelines for Failure Impact Assessment of Water Dams. http://www.nrm.qld.gov.au/compliance/wic/referable_dams.html

Fread, D.L. and Lewis, J.M. 1998. NWS FLDWAV Model Theoretical Description, User Documentation. Hydrologic Research Laboratory, Office of Hydrology, National Weather Service, NOAA, Maryland USA.

Institution of Engineers, Australia. 1998. Australian Rainfall and Runoff – A Guide to Flood Estimation. Editor-in chief D.H. Pilgrim, Volume 1.

Kellogg Brown & Root Pty Ltd. 2003. Mount Morgan – Dee River Dams –Final Failure Impact Assessment (BEW316-W-DO-003 Rev A).

Kellogg Brown & Root Pty Ltd. 2003. Mount Morgan – Dee River Dams –Emergency Action Plan – Final Modelling Inputs (BEW316-W-DO-004 Rev 0).

Laurenson, E.M. and Mein, R.G. 1995. RORB Runoff Routing Program User Manual, Version 4. Monash University, Department of Civil Engineering, Victoria, Australia.

Water Act 2000 (Qld).

The Institution of Engineers, Australia
8th National Conference on Hydraulics in Water Engineering
ANA Hotel Gold Coast, Australia 13-16 July 2004

Overview of Hydraulic Modelling of the Yangtze River for Flood Forecasting Purposes

S.Q. Clark
BE Hons (Civil), MEng Sc, M.I.E.Aust.
Contractor to Sagric International Pty. Ltd., Australia
Director, Water Technology Pty. Ltd., Australia
M.S. Markar
B.Sc (Eng)., Ph.D., M.I.E.Aust.
Contractor to Sagric International Pty. Ltd., Australia
Director, WRM Water & Environment Pty. Ltd., Australia
Min Yaowu
B.E., M.Sc.
Senior Engineer, Bureau of Hydrology, Changjiang Water Resources Commission, PR China
Wu Daoxi
B.E., M.Sc.
Vice Director, River Management Bureau, Changjiang Water Resources Commission, PR China

Abstract: A significant component of the Yangtze River Flood Control and Management Project (YRFCMP) is the development of a integrated real-time Flood Forecasting System (FFS) for the upper and middle reaches of the Yangtze River. A series of hydrologic and hydraulic models are utilised within the FFS to provide this functionality.

Of key importance to the success of the project is a full understanding of the markedly different hydraulic behaviour of the upper and middle reaches. The upper reach is a predominantly confined, stable channel with relatively minor local inflows. In contrast, the middle reach is characterised by relatively flat hydraulic gradients, complex flow paths, significant local inflows and several extensive lake systems.

This paper provides firstly a description of the hydraulics of these reaches of the Yangtze River, followed by an overview of the hydraulic models that have been developed for flood warning purposes under the YRFCMP.

Keywords: Yangtze River, Upper Reach, Middle Reach, Hydraulic Modelling, Flood Forecasting

1. INTRODUCTION

The five-year Yangtze River Flood Control and Management Project (YRFCMP) commenced in 2001 under the program of technical cooperation for development between the governments of Australia and Peoples Republic of China. A significant component of this project is the development of an integrated real-time Flood Forecasting System (FFS) for the upper and middle reaches of the Yangtze River between Chongqing and Wuhan. Hydrologic and hydraulic models are utilised within the FFS to provide this forecasting ability. The selection of the most appropriate hydrologic and hydraulic models is the subject of an accompanying paper (Markar et al, 2004).

Based on observed rainfall and discharges, the various hydrologic models provide discharge forecasts at all the key inflow locations of the Yangtze hydraulic models. To enable the FFS to provide accurate forecasts of the hydraulics of the system (flow distributions and river levels), an extensive hydraulic model development, calibration and implementation program is currently in progress.

Based on the work completed as part of this model development program, this paper provides an overview of the hydraulics of the Yangtze River system (from a flood warning perspective) and a brief description of the implications for flood warning activities.

2. THE UPPER AND MIDDLE REACHES OF THE YANGTZE RIVER

2.1 General

The Yangtze River catchment is some 1.8 million km^2 in extent. The upper catchment, which runs from source of the river in the Qinghai-Tibetan plateau to the city of Yichang has a catchment area of 1.0 million km^2. The middle catchment, lying between Yichang and the city of Wuhan has a catchment area of 0.68 million km^2 (Government of Australia, Government of the People's Republic of China, 2000).

For convenience, a slightly different reach delineation is used when considering the river reaches for flood forecasting purposes. As illustrated in Figure 1 below, the area referred to as the upper reach extends from ChongQing to Yichang. The area referred to as the middle reach extends from Yichang to Jiujiang and includes the extensive lake system known as the Dongting Lakes.

Figure 1 provides an indication of the upper and middle reaches of the Yangtze River as adopted for the YRFCMP and for this paper.

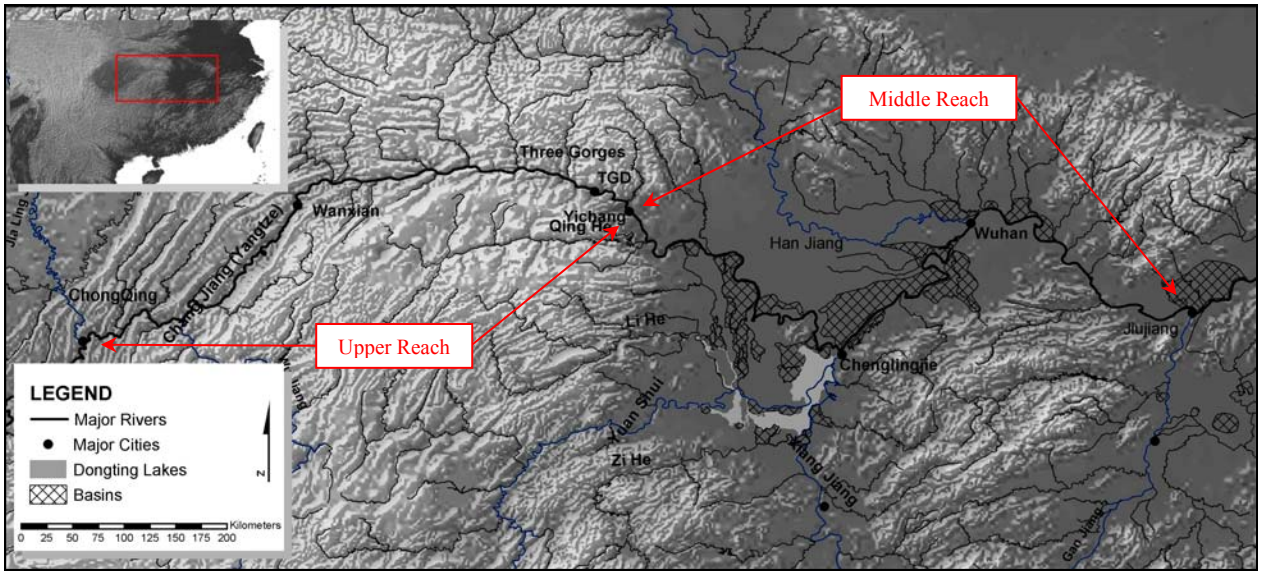

Figure 1 – The Upper and Middle Reaches of the Yangtze River

As will be discussed in the following sections, these reaches have strikingly different hydraulic characteristics. Similarly the problems for the relevant authorities from a flood warning and a flood management perspective vary significantly between the reaches.

Figure 2 presents the observed flood behaviour for two years at two stations, namely Wanxian and Wuhan. As illustrated in Figure 1, Wanxian is in the top half of the upper reach, upstream of the "Three Gorges". While not as confined as the three gorges sections, the Yangtze River at this point is still predominantly a single channel. Extensive floodplain inundation does not occur as river stage increases.

Wuhan is the major population centre within the middle reach of the Yangtze and is protected by extensive levees and detention basin works. Hydraulic gradients through this reach are significantly lower than those within the upper reach. In the absence of the flood protection works (ie levees), extensive floodplain inundation would occur through the middle reach under flood flows.

The 1981 and 1998 flood events illustrate well the wide variety of flood behaviour that may be experienced by the upper and middle reaches of the Yangtze.

The 1981 event was predominantly an upper catchment event, with a flood peak of approximately 80,000 m^3/s travelling through the Three Gorges to the middle reach of the Yangtze. To the study team's knowledge, this is the single largest flood peak experienced through the upper reach this century. Note in Figure 2 the 35m increase in river stage at Wanxian corresponding to the 1981 flood peak.

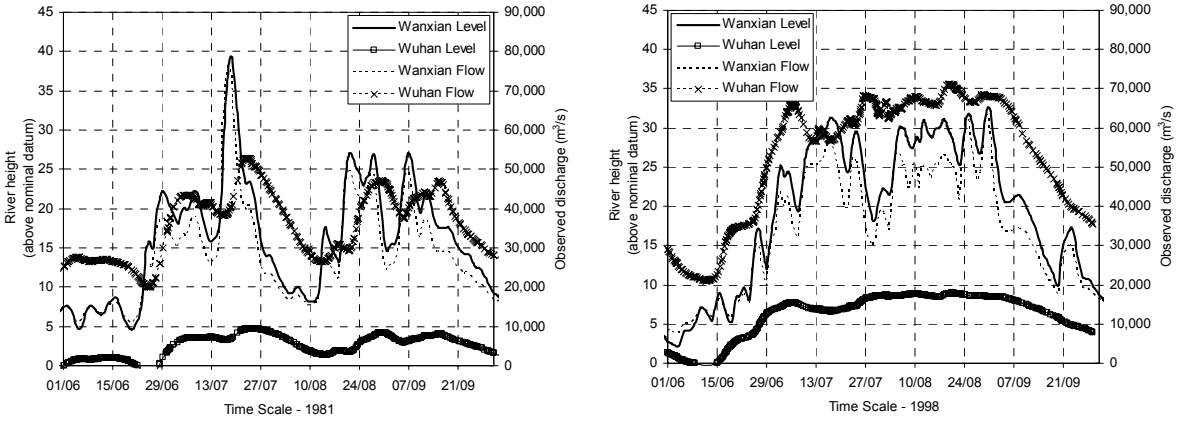

Figure 2 – Comparison of hydraulic behaviour of the Yangtze River at Wanxian (upper reach) and Wuhan (middle reach)

However, as the event was relatively brief (less than one week), and there was little contributing inflow to the middle reach (apart from the Yangtze River flow itself), the 1981 event was not a significant event at Wuhan. The storage available within the system reduced the flood peak of 80,000m^3/s at Wanxian to (approximately) 50,000m^3/s at Wuhan.

In contrast, the 1998 event was the product of sustained rainfall. This produced increased discharge both from the Yangtze upper catchment, and the (significant) catchments contributing directly to the middle reach. As can be seen from Figure 2, significantly elevated flows were experienced for a period of approximately two months, effectively utilising all available storage within the lake systems and leading to dangerously elevated river levels throughout the entire middle reach.

The hydraulic characteristics of the upper and middle reaches are discussed in more detail in the following sections.

2.2 The Upper Reach

The upper reach of the Yangtze River is some 600km in length and includes the famous "Three Gorges" section of the river. Flows during the flood season (June to September) are substantial with discharges in excess of 70,000m^3/s experienced on at least 4 occasions within the last 20 years. Outside of the flood season, flows drop to less than 10,000m^3/s. Within the upper reach of the Yangtze, these high flows do not lead to extensive lateral inundation as the flow is largely confined through the gorge sections of the upper reach of the river. However, these high flows do lead to large changes in flow depth associated with relatively small changes in flow width.

For the purposes of flood forecasting, this reach is essentially a single (albeit extremely large) channel. Thus, the hydraulic model for the upper reach consists of a single branch extending 600km from ChongQing to Yichang (the site of the Three Gorges Dam) with a tributary representing the lower reaches of the Wu River.

Figure 3 presents a long section of the upper reach. Note the dramatic variations in depth through the reach with 90m deep sections present under low flow conditions (less than 10,000m^3/s) at some locations. With an average hydraulic gradient of 0.02%, the upper reach of the Yangtze is still steep when compared to the middle reach.

Under low flow conditions, average stream velocities are generally between 1 and 2 m/s with associated Froude numbers typically in the range of 0.2 to 0.3. In some constricted sections, much higher Froude numbers (up to 0.6) are present under low flows.

Figure 3 provides an indication of the conditions experienced under flood flow conditions (specifically the 1981 event as simulated by the hydraulic model). Increases in depth of up to 50m are common. Average stream velocities are predicted to be typically between 2 and 4m/s, although higher velocities are present. Note that for these higher flows, Froude numbers generally decrease to between 0.1 and 0.2. This decrease is associated with a significant increase in flow depth (often by a factor of 2 or 3) under flood flows, but the corresponding increase in velocity is relatively small.

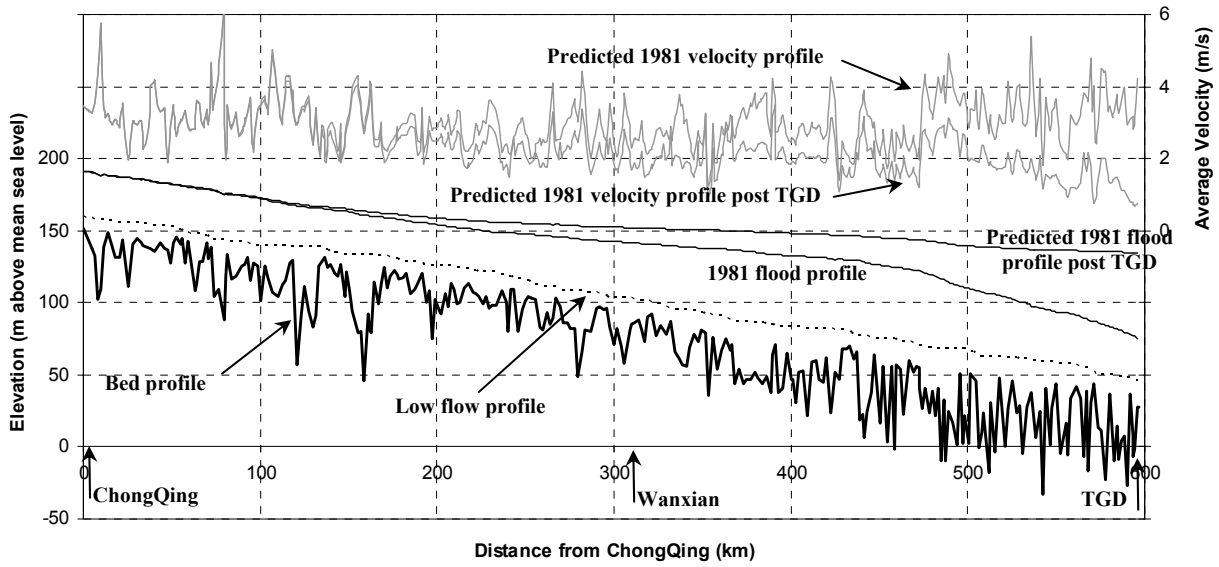

Figure 3 – Long section of predicted water surface profiles associated with low flow conditions and the 1981 flood event through the upper reach of the Yangtze River under pre and post Three Gorges Dam conditions

2.3 The Three Gorges Dam

In June, 2003, the completion of the first stage of the Three Gorges Dam (TGD) was marked by the closure of the dam wall and the raising of the reservoir level to the interim "flood control level" of RL 135m. The "Introduction to Technical Studies on the Three Gorges Dam" (ChangJiang Water Resources Commission (CWRC), 2000) provides an overview of the design considerations behind the TGD. One of the fundamental goals of the design is to raise the present 10 year "flood control standard" for the reach immediately downstream of the Three Gorges to a 100 year "flood control standard".

The following is a brief summary of the operating regime (CWRC, 2000). Note that this summary is only an overview of a quite complex series of operating rules.

1. During the May/June period, the reservoir level will be dropped from the "normal pool level" (NPL – 175m) to the "flood control level" (FCL – 145m). Note that until scheduled completion in 2009, the interim pool level is set at 135m. Also note that the "check flood level" or 10,000 year frequency flood + 10% is set at 180.4m.
2. During the flood season, the flood control level will be maintained until flood runoff surpasses safe discharge for the lower reaches.
3. The reservoir will then be allowed to impound water until the flood passes, raising the pool level.
4. Once the flood passes, the reservoir will once again be drawn down to the flood control level.
5. During October, the water level will be allowed to rise to the normal pool level.
6. Over the period November to April, the reservoir will be operated according to the demands of the power network, but maintained above the limiting water level for the dry season (155m).

Figure 3 also provides an indication of the predicted impact on hydraulic conditions associated with the 1981 event through the upper reach of the Yangtze following construction of the TGD. As could be expected, velocities decrease through the lower reaches associated with the construction of the reservoir, although they are still significant (generally in excess of 2m/s). As the reservoir extent is confined by the natural gorge sections at all stages, under flood conditions a significant hydraulic gradient along the full length of the reservoir is maintained.

Note that these results correspond to the interim operating procedures of the pool level at the dam wall being maintained at 135m. One of the implications of this mode of operation is that until final completion of the TGD, the progression of flood waves through the upper reaches of the Yangtze will be faster than under pre-TGD conditions.

The theoretical speed of flood wave progression or wave celerity can be expressed as $(g.depth)^{0.5}$. Note that in this situation, the actual wave celerity is significantly less than the theoretical value due to friction through the

confined gorge sections. Prior to completion of the TGD the full active storage capacity of the dam can not be utilised and the speed of flood wave progression down the upper reach of the river increases associated with the significantly increased flow depth. As a result of the confined "gorge" sections, there is little increased active storage available to provide any attenuation of the flood wave. Prior to completion of the structure, floods will thus progress faster through this reach of the river, making accuracy of the flood forecasts all the more critical.

Again considering the 1981 event, under pre-TGD conditions, peak discharge at Yichang was experienced approximately 60 hours after it was experienced at ChongQing, some 600km upstream. Preliminary simulations indicate that for a repeat of the 1981 event with the current TGD operating regime, the time to peak discharge at Yichang would be reduced to approximately 48 hours.

2.4 The Middle Reach

As illustrated in Figure 1, downstream of the "Three Gorges", the Yangtze enters what is termed the middle reach. Some 80 million people live in the middle and lower reaches of the Yangtze along with vast areas of cropland and major industrial development. In order to protect people and assets in these floodplains, for over 3000 years a complex system of levees has been constructed and continually raised. While providing a measure of protection (1 in 15 year flood protection for less populated areas and 1 in 200 year flood protection for major cities such as Wuhan), there are increased risks associated with catastrophic failure should the levees be overtopped (Government of Australia, Government of the People's Republic of China, 2000).

This occurred in a disastrous flood event in 1954 when some 40,000 people perished in the middle and lower reaches of the Yangtze Basin. Following this flood event, a series of substantial detention basins were constructed (indicative locations shown on Figure 1). When flood levels in either the Yangtze River or the lake systems approach critical levels, the detention basins are deliberately flooded to reduce flood levels on the river and avert overtopping of the main levee systems.

The major lake system within the middle reach is known as the Dongting Lakes. As flows and stage increase in the Yangtze through the flood season, four major effluents take flow from the Yangtze River and deliver it to the Dongting Lake system. Inflows to the local catchment of the Dongting Lakes may contribute substantial volumes as well. There are constructed storages present on most of these tributary inflows meaning there is some flood mitigation potential through the use of upstream storages.

Entering the Yangtze just upstream of Wuhan, the Han River may also contribute significant flows to the middle reach. As for the Dongting Lakes, there are numerous on and offline storages constructed within the Han River catchment leading to a significant capacity for flood mitigation through the use of these storages.

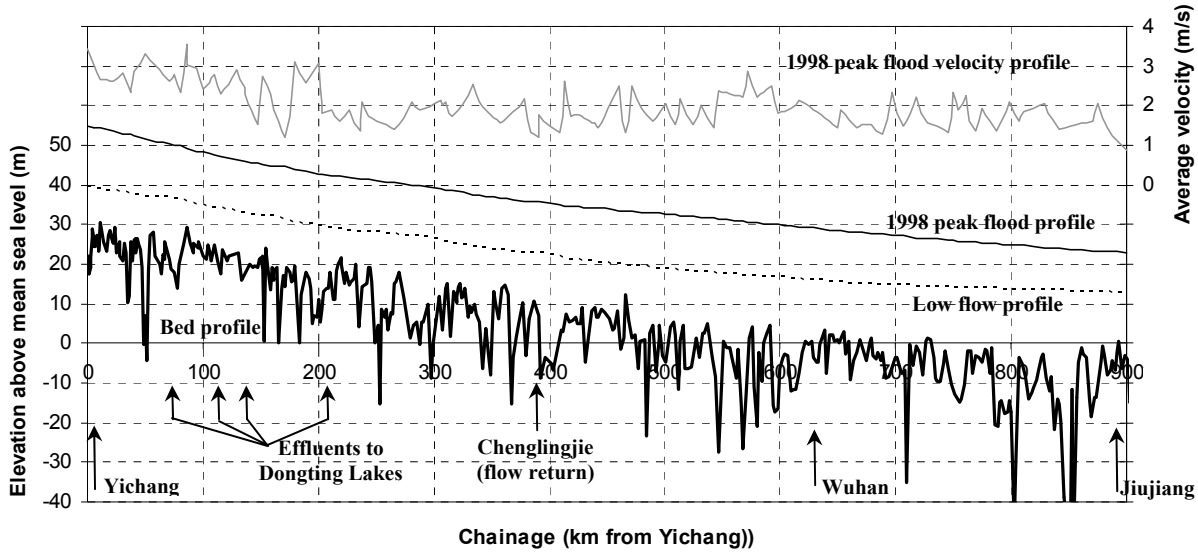

Figure 4 – Long section of predicted water surface profiles associated with low flow conditions and the 1998 flood event through the middle reach of the Yangtze River.

Figure 4 presents a long section of the middle reach of the Yangtze River. Ranging from 0.002% to 0.005%, the hydraulic gradients through the middle reach are an order of magnitude smaller than those through the upper reach. Average low flow velocities are typically less than 1m/s and rise to between 1 and 2 m/s during flood events. Correspondingly, Froude numbers are typically 0.1 for low flows and increase to (approximately) 0.15 during flood events.

There are four major effluent flow paths allowing outflow from the Yangtze River to the Dongting Lakes. The locations of these outflows are indicated on both Figures 1 and 4. Significant outflows from the Yangtze River via these effluents start when the Yangtze River flow reaches approximately 8,000m^3/s. Gauging records for recent years indicate that for flow rates above 8,000m^3/s, typically between 25% and 30% of the total Yangtze River flow is delivered to the Dongting Lakes i.e. for a Yangtze River flow of 60,000m^3/s downstream of Yichang, approximately 17,000m^3/s exits the main channel and flows to the Dongting Lakes. This flow is in addition to the 5 significant river systems draining directly to the lakes from the west and south. These river systems have a combined catchment area of approximately 0.26 million km^2. Outflow from the Dongting lakes re-enters the Yangtze river at Chenglingjie (indicated in Figure 4). Note that the outflow capacity is controlled by backwater effects from the Yangtze River.

3. IMPLEMENTATION OF HYDRAULIC MODELS

As discussed previously, a core component of the YRFCMP is the development or enhancement of CWRC's flood forecasting capacities. The development of hydraulic models as part of this process has then been aimed at providing systems that:

a) accurately represent the hydraulics of the Yangtze River system through the reaches of interest,
b) have the capacity to represent both the operation of the TGD in the upper reach, and the numerous detention basins in the middle reach,
c) have facilities to operate in a real time flood forecasting mode with (potentially) gauge data of varying quality, and
d) are practical to use in real time operation.

The flood forecasting models have been developed using DHI's MIKE 11 one dimensional (quasi two dimensional) hydrodynamic modelling system. The Structures Operation Module has been utilised to represent both the TGD operating regime and detention basin operations. Real time operation and error correction facilities have been developed using the Flood Forecast module.

At the time of this paper's preparation, the MIKE Flood system was being utilised to investigate two dimensional effects in the major lake systems. It is also being utilised to investigate the complex hydraulics associated with detention basin operations. While the possibility of using MIKE Flood in real time operations is being investigated, due to the lengthy simulation times associated with the use of two dimensional models, it is not anticipated that this will be practical. Instead, the results of the two dimensional simulations are currently being utilised to improve the schematisation and accuracy of the one dimensional flood forecasting models.

The upper and middle reaches of the Yangtze have been the subject of previous investigations (DHI, 1998), so previously established models were available to the study team. In many places, these models have been enhanced through work undertaken as part of the YRFCMP and additional data has been incorporated. A significant amount of effort has been put into the detailed calibration of these hydrodynamic models prior to incorporation into the flood forecasting system.

The following is a very brief discussion of some of the issues encountered to date within the hydraulic modelling component of the project.

3.1 The Upper Reach

Not surprisingly, the combination of extremely high flow rates and the confined nature of the flow through the gorge sections mean that the accuracy of hydraulic model predictions through these areas were found to be extremely sensitive to hydraulic roughness. In order to accurately reproduce hydraulic behaviour at both low and high stages it was necessary to introduce vertical variation in hydraulic roughness on a reach by reach basis. These variations were not large. Within the "Three Gorges", Manning's n values ranging (vertically) from 0.055 to 0.070 were adopted. Upstream of the "Three Gorges" Manning's n values ranging (vertically) from 0.030 to 0.045 were adopted. Note that through the upper reach of the Yangtze River, due to the combination of extremely high discharges and gorge sections, an increment in Manning's n of 0.001 can produce variations in predicted flood levels of up to 10m depending on the length of reach being considered.

During initial system trials in the 2003 flood season, it became evident that once the interim pool level for the reservoir had been reached, additional storage was mobilised. It is thought that this storage is principally associated with backwater into lateral gorges associated with some of the larger tributaries. Although a substantial number of cross sections are available for the upper reach, these are predominantly Yangtze River sections. At present, the topographic information necessary to accurately define this additional storage is not available. The distribution of floodplain storage at high river stages was also then a key factor in calibration of the hydraulic model.

Varying methods of representing the TGD operating regime have been trialled. During system testing in the 2003 flood season, variability in the day to day operating regime of the TGD has meant that utilising preset operating rules has not produced satisfactory results. To date, the most robust procedure has been to represent the structure simply as the downstream boundary condition of the model with the anticipated dam operation for the forecast period based on discussions with the TGD operators. Note that the key outcome of the upper reach model in a flood forecasting context is the accurate prediction of discharge (via the TGD) delivered to the middle reach.

3.2 The Middle Reach

Accurate modelling of the middle reach of the Yangtze River represents a significant challenge due to the combination of a number of factors that include:

a) Approximately 900km of the main channel of the Yangtze, in addition to the adjacent lake systems must be considered due to the relatively flat hydraulic gradients.
b) Although extensive gauging data exists, local (ungauged) runoff to the Donting Lakes is significant and must be considered.
c) In some reaches, there appears to be the potential for significant bed movement over the course of a flood season.
d) The effects of dyke breaches associated with detention basin operations during flood events, and those associated with dyke failures are present in the gauge records for larger events, but in most cases, it is difficult to determine the exact timing and extent of these breaches/failures with sufficient accuracy for hydraulic model calibration purposes.
e) Conversely, any model intended for real time application must have the ability to accurately represent the impact of dyke breaching.
f) The ongoing alterations to the system associated with levee construction/alteration activities.
g) As noted in point c) above, there are substantial ongoing geomorphological processes occurring within the system whose effects are visible, even in the short term. Of particular importance is the potential for bed movement along the main stem of the Yangtze. There is also rapid sedimentation occurring in some sections of the Dongting Lakes. Following closure in 2003, the TGD has the potential to alter the both of these, and other geomorphological processes occurring in the downstream reaches.

Despite these difficulties, promising results have been obtained utilising the existing middle reach model with some degree of recalibration and enhancement.

At the time of writing, a significant data gathering effort has resulted (as far as is possible) in a comprehensive and current data set being compiled. This data has been utilised to reconstruct the hydraulic model of the middle reach for the Yangtze, utilising a much higher degree of detail than has been previously available. Previously, Yangtze River cross sections have been available with an average spacing of approximately 9km. New cross sections are now being incorporated at approximately 2km centres. Detailed bathymetric survey of the lake systems is currently being processed and significantly increased detail will be available to more accurately represent these features.

A detailed calibration process will follow this model reconstruction process with the intention of incorporating the model into the flood forecasting system for the 2004 flood season.

Investigation into the impacts of detention basin operations, utilising the structures operation module of the MIKE 11 modelling system, has also yielded promising results. Work is progressing on the incorporation of the major middle reach detention basins within the hydraulic model. This is critical for the assessment of the impact of potential basin operation scenarios. It is also critical for the accuracy of the flood forecasts to incorporate the effect of detention basins that have been previously opened.

4. SUMMARY OF FINDINGS/CONCLUSIONS

As part of the YRFCMP's Flood Forecasting System, the development of hydraulic models for the upper and middle reaches of the Yangtze River has progressed well. The integration of these models within the Flood Forecasting System is also progressing well. More specifically, the work associated with data gathering, processing, model trials and calibration has lead to a (quantitatively) better understanding of the Yangtze River system.

Of key importance to the success of the project is a full understanding of the different characteristics of the upper and middle reaches of the Yangtze River. Due to the markedly different hydraulic behaviour of these two reaches, significantly different approaches to hydraulic analysis and flood forecasting are required for each reach.

Following first stage completion in 2003, and prior to full completion (2009), the interim operating rules of the TGD will result in faster flood progression through the upper reach of the river, making accuracy of flood forecasts all the more critical.

Trial flood forecasting activities undertaken utilising the upper reach hydraulic model during the 2003 flood season have produced promising results and the model was actively used by CWRC during the 2003 flood season. Note that during this period, the first stage of the TGD became operational.

The evaluation of the existing middle reach model indicated that quantitative improvements in the accuracy of predictions were possible through additional schematisation and recalibration effort. On this basis, an extensive data gathering and model enhancement process for the middle reach is currently in progress, with the intention to integrate the middle reach model (in addition to the already present upper reach model) into the FFS for testing during the 2004 flood season.

5. ACKNOWLEDGEMENTS

This project has been funded by the governments of Australia and Peoples Republic of China under the development cooperation program with China, managed by the Australian Agency for International Development (AusAID).

6. DISCLAIMER

The views expressed in this publication are those of the authors and not necessarily those of the Commonwealth of Australia. The Commonwealth of Australia accepts no responsibility for any loss, damage or injury resulting from reliance on any of the information or views contained in this publication

7. REFERENCES

ChangJiang Water Resources Commission (2000). *Introduction to Technical Studies of the Three Gorges Dam*. Hubei Science and Technology Press,

Danish Hydraulics Institute in association with Danish Meteorological Institute and the University of Copenhagen, (1998) *Heavy Rains and Flood Forecasting in the Middle Yangtze River Valley – Final Report, Phase 2*. Report prepared for Changjiang Water Resources Commission

DHI. (2002). *MIKE-11 User Guide,* Danish Hydraulic Institute, Denmark.

Government of Australia, Government of the People's Republic of China (2000) *Yangtze River Flood Control and Management Project, Project Design Document*.

Markar, S.M., Clark, S.Q., Min, Y., Jheng, Z. (2004). *Evaluation of Hydrologic and Hydraulic Models for Real Time Flood Forecasting use in the Yangtze River Catchment*, 8th National Conference on Hydraulics in Water Engineering, Gold Coast, Australia.

The Institution of Engineers, Australia
8th National Conference on Hydraulics in Water Engineering
ANA Hotel Gold Coast, Australia 13-16 July 2004

Safety of People in Flooded Streets and Floodways

R.J. Cox
BE, PhD, MIEAust, CPEng
Water Research Laboratory, Civil and Environmental Engineering, University of New South Wales, Sydney, Australia
M. Yee
Honours Student, Civil and Environmental Engineering, University of New South Wales, Sydney, Australia
J. E. Ball
ME, PhD, MIEAust, CPEng
Water Research Laboratory, Civil and Environmental Engineering, University of New South Wales, Sydney, Australia

Abstract: The safety of people on floodways or flooded streets is of major concern in urban stormwater design and floodplain management. Current design guidelines for safety on floodways (in Australia and overseas) are simplistic, generally given in terms of a critical value of Depth * Velocity (D*V) which has been based on limited laboratory testing. Cox and Ball (2001) updated the primal 1973 data for 6 children from Australia with tests of 3 adults from Japan. This paper incorporates further analysis of laboratory test data for adults from USA and Finland. The worldwide laboratory test data was found to be deficient in not testing very small/young children nor very frail/older persons. The authors have thus completed additional testing on 4 young children. A predictive model has been developed and proven against the test data for stability failure of human subjects. The commonly adopted guideline for designing floodways by specifying a critical Depth*Velocity (D*V) value of 0.4 m^2s^{-1} does not ensure the safety of all children - young children with low muscular coordination (typified by Height*Mass values less than 20 mKg) are not safe at this criteria. It is most likely that many frail/older persons also may not be safe under this criteria.

Keywords: Urban, Stormwater, Flooding, Floodplain management, Floodway, Safety

1. INTRODUCTION

The safety of people on floodways or flooded streets is of major concern in urban stormwater design and floodplain management. Human activity in floodways is inevitable with much development already in flood prone areas. The safety of people can be compromised when exposed to flows ranging from low depth-high velocity to high depth-low velocity cases.

Current design guidelines for safety of people on floodways in Australia are simplistic, generally given in terms of a critical value of Depth*Velocity (D*V) which has been based on the limited testing by Foster and Cox (1973) for 6 male children, ages 9 to 13 years. Currently the Australian Rainfall and Runoff (ARR) guidelines (O'Loughlin and Robinson, 1998) stipulate that floodways should have a product of depth and velocity (D*V) of less than 0.4 m^2/s to ensure pedestrian safety. In contrast, the velocity depth relationships presented in Figure 1 (extract from NSW Floodplain Development Manual, Department of Public Works, 1986) as defining unsafe wading and vehicle instability do not indicate constant D*V relationships which would plot on this diagram as a hyperbolic curve (similar to that indicated for damage to light buildings). Besides the safety of the general community, floodway safety is important to rescue workers who are frequently required to operate in hazardous conditions. Emergency Management Australia (EMA) is the national government agency responsible for managing disaster situations. EMA has published a series of manuals to assist other agencies and local governments to assist in the planning of emergency situations regarding flooding. In regard to "Flood Hazard", EMA advice is that wading by able-bodied adults becomes difficult and dangerous when the depth of still water exceeds 1.2 m or when the velocity of shallow water exceeds 0.8 m/s and for various combinations of depth and velocity between these limits. EMA acknowledge other local site factors other than depth and velocity need to be taken into account.

Due to the varied circumstances that may occur, there are many qualifications to the safety criteria for people on floodways. In the application of these criteria, many assumptions are employed since the basic laboratory testing on which the criteria were developed was not holistic but rather considered

particular conditions. It is worthwhile collating and reviewing all relevant major studies to highlight the explicit and implicit assumptions incorporated in results and subsequent safety criteria.

2. LABORATORY TEST RESULTS

Cox and Ball (2001) reported in detail on the laboratory test data and analyses by Foster and Cox (1973) and Takahashi et al (1992). In reviewing the relevancy of a single (D*V) criteria for floodway safety, further laboratory test data from USA (Abt et al, 1989) and Finland (RESCDAM, 2001) were acquired and interpreted. The worldwide laboratory test data was found to be deficient in not testing very small/young children nor very frail/older persons. Yee (2003) subsequently completed additional testing on young children.

2.1 Foster and Cox (1973)

Foster and Cox (1973) identified four conditions that could affect the safety of a child:-

- The child's physical attributes – this includes age, height, weight and muscular development.
- Psychological factors – an aggressive child may be more capable of movement in certain conditions whilst a passive child may struggle in such conditions.
- Hydraulic Conditions – the flow regime is important to a person's safety, in particularly depth and velocity.
- Other Factors – such as friction between the ground and child's feet, the type of clothing worn, the movement of the child in the flow, uneven ground and possible impact of floating debris.

Experiments were undertaken in a flume 6m long, 0.6m wide and 0.75m deep. The base of the flume consisted of painted timber. The velocity and depths were controlled by sluice gates at each end of the flume.

The following situations were used to define limits for safe flow conditions:-

- Child standing - when the child standing in the flume felt unsafe and reached for the sides of the flume;
- Child standing - when the child in the flume could walk upstream or downstream and turn around without assistance from his hands, then the situation was considered safe.
- Child sitting - the flow depth and velocity that resulted in the child starting to slide on the flume base.

Safety criteria were based on the perception of the child as to safe and unsafe conditions. Consequently, inherent in the criteria developed for safe and unsafe flow conditions is the psychological tendency of the child; an aggressive child may feel safe in a flow situation where an identical twin who is passive may feel unsafe. This point is noted in the report by Foster and Cox (1973) but is rarely noted in most safety criteria.

The subjects consisted of 6 male children aged from 9 to 13 years, 1.27 to 1.45 m tall, 25 to 37 Kg mass and Height*Mass (H*M) from 32 to 53 mKg (Table 1). All subjects wore shorts. Clothing drag was negligible in all tests as water levels never reached the height of the shorts. Shoes were not worn during experimentation. All safety criteria/failure were due to loss of friction between the child's feet and the flume floor in supercritical flow conditions ("sliding" failure as shown in Figure 2).

The safety criteria/failure results from this testing are shown in Figures 7 and 8.

2.2 Takahashi et al. (1992)

Takahashi et al. (1992) included detailed measurements of drag, friction and force moments when testing 3 adult males 1.64 to 1.83 m tall, 63 to 73 Kg mass and Height*Mass from 107 to 134 mKg (Table 1). The research (published in Japanese) focus was the safety of dock workers in conditions of wave overtopping of harbour structures. The experiments were undertaken in a basin of 50m length and 20m width. As opposed to other experiments which used a flume, this facility operated by funneling large amounts of water to generate higher velocities and depths. The subjects stood on a load cell platform that was capable of measuring force, friction and sliding. The subjects were exposed to increasingly more dangerous combinations of water flow depth and velocity until they were physically washed off their feet in either "sliding" or "tumbling" mode as sketched in Figure 2.

Testing was undertaken for three different types of clothing (long boots, dry waterproof suit, and normal cotton trousers) and for a range of leather and rubber soled shoes on a range of surfaces including smooth and rough concrete as well as concrete covered with algae and seaweed. Coefficients of friction were measured and found to be typically around 0.6 and 1.0 respectively for smooth and rough concrete under wet conditions. The lowest values reported for concrete covered with relatively slippery seaweed are around 0.4. These values are all significantly higher than the apparently conservative value of 0.3 adopted by Keller and Mitsch (1993). No data exists for asphalt road surfaces and/or grassed floodway surfaces. It is recommended that such basic coefficient of friction data be undertaken for a range of shoe sole types.
With the benefit of continuous monitoring of depth, velocity and resultant forces (on the persons/subjects) during each test, Takahashi et al. (1992) were able to specifically calculate drag force coefficients C_D and examine the stability of persons for water exposure from different directions. For front on water exposure and feet together the drag coefficient C_d was found to vary between 0.6 and 1.1 depending upon the subject and the clothing being worn. Keller and Mitsch (1993) appear to have adopted a conservative value in choosing $C_d = 1.2$.

Takahashi et al (1992) developed a computational model for stability incorporating the resolution of forces and moments including weight, flow drag and friction. Based on human ergonomic data, they adopted a human shape standardised in respect of height. For any given person's height and weight, computational resolution of weight, drag and frictional forces enables an estimate of critical velocity for either “sliding” or “tumbling rotation” modes of stability in a given water depth. In comparisons with the experimental measurements for the exposed human subjects, the calculated critical conditions using the computational procedure proved quite reliable for front and side exposure with either feet together or braced feet wide apart.

For water depths less than "in seam" (less than 0.48 person height), only two feet and legs are exposed to drag forces. Under such conditions for a relatively slippery surface such as concrete covered with seaweed or algae ($C_d = 0.37$), critical values of D*V were found in the experiments to be 0.4 to 0.6 m^2/s for front or rear exposure and 0.7 to 0.8 m^2/s for side on exposure. If exposed in a sitting position, increased body drag reduces the critical D*V value to 0.3 to 0.5 m^2/s.
The safety criteria/failure results from this testing are shown in Figures 7 and 8.
Being adults it is not surprising that the data indicate significantly higher stability than the data for children from Foster and Cox (1973).

2.3 Abt, Wittler, Taylor and Love (1989)

In conducting a test program to allow prediction of the approximate depth and velocity of flow in which a person will topple in flood flow, Abt et al (1989) completed testing of 20 adults (male and female, 1.52 to 1.83 m tall, 41 to 91 Kg mass and Height*Mass from 62 to 172 mKg: Table 1).

Experiments were undertaken in a flume 61m long, 2.44m wide and 1.22m deep. The slope of the flume could be changed between 0 and 3 percent grade, experiments were undertaken using 0.5 and 1.5 percent grades. The facility was able to produce up to $2.83 m^3/s$ of flow. Velocity was measured using a magnetic flow meter and depth was measured using pressure transducers and periodically checked using a staff.
A change in surface (from steel to concrete to gravel to turf) did not significantly affect the stability - most tests were conducted in relatively high depths (>1m) and hence friction underfoot is less important, thereby biasing towards tumbling failure as opposed to clear sliding (friction) failure. If tests were undertaken at lower depths with high velocities, it would be expected that there would be a measurable difference in safety on different surfaces.
The safety criteria/failure results from this testing are shown in Figures 7 and 8.

This set of data indicates substantially higher stability than all other data for adults. This cannot fully be explained.
It is partially explained in that the purpose of the experiments was to determine the absolute limit of stability of the subjects to failure (personal communication with Abt, SR, 10 October 2003), that is the subjects were made to fail as opposed to determining if safety was compromised. Clothing had lower drag than that applicable to testing by Takahashi et al (1992) and RESCDAM (2001). The safety equipment used is likely to have provided additional stability to the limit of failure. The failure mode for each subject is not known - this information would be of value in interpreting the results.

Computational model prediction (see section 3) indicates most of the data is in the transitional failure mode between sliding and tumbling.

2.4 RESCDAM (2001)

The Helsinki University of Technology (RESCDAM, 2001) completed a study primarily focussed on defining the limits of human stability for a safe rescue action in a dam break situation. The study recognises that the limit of safety is affected by other factors such as lighting and turbidity.

Seven adult subjects were used in these experiments, consisting of 5 males and 2 females, 1.6 to 1.95 m tall, 48 to 100 kg in mass and Height*Mass from 77 to 195 mKg (Table 1). Two of the subjects were professional rescue personnel. As the focus of this study was on rescue worker mobility, all subjects wore Gore Tex rescue suits (equivalent to a dry suit) and one subject also wore waders. It is unknown how the dry suits were adjusted. It is possible to increase the buoyancy of some suits by increasing the air volume within the suits. It is also possible to decrease the volume but this may increase drag as the suit does not perfectly conform to the body and will increase the roughness of a subject's body dramatically. Subjects also wore fall arrest harnesses for safety. It is assumed that all subjects wore boots. Experiments were undertaken in a basin 130m long, 11m wide and 5.5m deep. The water temperature was approximately 16 degrees. The water within the basin was stagnant. A moving platform was used to replicate flow. The platform consisted of two steel grates resulting in a 1.13m wide and 1.17m long platform. To induce failure the velocity of the platform was increased with fixed depth which was altered between test runs.
The safety criteria/failure results from this testing are shown in Figures 7 and 8.
The critical failure values of D*V from this study are considerably less the values from Abt et al.(1989) and more comparable to Takahashi et al (1992). This is to be expected due to the similar clothing worn by subjects in the experiments of Takahashi et al. The aim of these experiments was '*to define the limits for a safe rescue action'*, which would be expected to be considerably lower than the higher "*limit of stability failure*" which was sought by Abt et al. The method of this study is unique in that a platform was moved through stagnant water as opposed to exposing subjects to flowing turbulent water in a flume or the like.

	Foster and Cox	**Abt et al.**	**Takahashi et al.**	**RESCDAM**
Setup	Flume	Flume	Funnelled basin	Moving platform through basin
Surface	Painted timber	Concrete, turf, gravel and steel.	Metal load cell	Steel grating
Subject Characteristics	Children-Young Teenagers	Civilian Adults with safety equipment	Adults	Rescue workers with safety equipment
Subject Action	Standing, turning and sitting	Walking around in flow	Standing	Walking around in flow
Number of subjects	6	20	3	7
Range of D, m	0.09-0.17	0.43-1.2	0.44-0.93	0.4-1.1
Range of V, m/s	0.76-3.12	0.82-3.05	0.58-2.0	0.6-2.6
Range of DV, m^2/s	0.16-0.52	0.71-2.13	0.64-1.26	0.6-1.3
Range of HM, mKg	32-53.2	62.3-172.8	106.6-133.6	77-195

Table 1: Comparison of experimental methodologies and test subjects.

2.5 Yee (2003)

The various worldwide laboratory test data presented above have been analysed in detail to better understand the mechanisms by which stability failure of people on floodways occurs. The data was found to be deficient in not testing very small/young children nor very frail/older persons. Yee (2003)

thus completed additional testing on 4 young children (2 male and 2 female, ages 6 to 8 years, 1.09 to 1.25 m tall, 19 to 25 Kg mass and Height*Mass from 20.7 to 32.5 mKg: Table 2).

Subject	Sex	Age	Height (m)	Mass (Kg)	HM (mKg)
1	Female	7	1.25	22	27.5
2	Female	6	1.24	24	29.76
3	Male	8	1.3	25	32.5
4	Male	6	1.09	19	20.71

Table 2: Experiment subject characteristics Yee (2003).

The testing procedures were similar in most aspects to those previously reported by Foster and Cox (1973). Testing of the subjects in a sitting position was not however carried out. The flume used in the experiments was 6m long, 0.6m wide and 0.75m deep. The maximum flow was approximately 400 L/s. The base of the flume consisted of painted timber. The velocity and depths were controlled by sluice gates at each end of the flume – measurements being made with propeller velocimeter and water depth gauges. All subjects wore swimming attire and were barefooted. Subjects 3 and 4 are shown in Figure 5. Due to the nature of the experiments, safety equipment was required. Safety measures as depicted in the general photograph of testing in Figure 6 included helmet, harness, safety procedures, padded railing, covered drain and subject assistant(s).
Failure was determined through observation and consultation with the subject. This is quite subjective and was open to much interpretation. Video recording of all subject tests allowed failure scenarios to be clearly identified as either:

- a loss in stability resulting in the subject slipping or falling with assistance required; or
- a situation where the subject did not feel confident in undertaking set movements in the generated flow (depth and velocity) and stabilised themselves by grabbing the flume sides or an assistant.

The two failure definitions are not the same. The first defines failure of stability whilst the second defines the limit of safety. In presenting the experimental results in Figures 7 and 8, either of the 2 failure scenarios is considered as failure in general. The results are seen to be consistent with whilst extending the stability criteria originally determined for older and larger children by Foster and Cox (1973).

The results showed that subjects 1, 2 and 3 (with similar H*M values between 27.5 and 32.5 mKg) have very similar failure behaviour with critical D*V values from 0.51-0.55 m^2/s. Subject 4 with a H*M of 20.7 mKg has a significantly lower critical failure value of D*V from 0.33-0.38 m^2/s. The lower stability of subject 4 cannot be explained merely in terms of his smaller height and mass. Based on detailed observations of behaviour of all subjects during testing, it is postulated that the difference in behaviour of subject 4 is due to his lower level of muscular development and coordination.

3. COMPUTATIONAL MODEL

The various data have been analysed in detail to better understand the mechanisms by which stability failure of people occurs. These mechanisms have been incorporated by Yee (2003) in an improved predictive computational model which has been directly compared with the various test data. The model is based on the work of both Takahashi et al (1992) and Keller and Mitsch (1993) with the incorporation of additional parameters. The model examines the stability of a standing subject facing the flow and incorporates velocity, depth (up to 1.5m), mass, height and body shape, drag, friction and buoyancy. Failure occurs by either sliding (friction) or tumbling (moment) failure as shown in Figure 2. Sliding failure is due to loss of friction between the subject's foot and the floodway surface – this generally occurs with low depths and high velocities. Tumbling failure, or overtopping, occurs when the subject is rotated about their foot (either heel or toe depending on their orientation within the flow) by imbalance of the horizontal drag force and the vertical weight of the subject - this generally occurs with higher depths as buoyancy effects reduce the vertical weight normal force. The standardised human body shape proposed originally by Takahashi et al (1992) was adopted after it had been validated against 16 adults of height 1.64 to 1.98 m.

Adopting coefficients of 1.1 and 0.4 for drag and friction respectively, the model was found to reliably predict stability criteria comparable with the test results of Takahashi et al (1992), Foster and Cox (1973) and all but the smallest subject in Yee (2003). In these applications the lever arm between heel and weight force was single valued at 0.1m. In contrast, the majority of subjects in the Abt et al (1989) and RESCDAM (2001) research were relatively tall and heavy adults (many wearing boots) being tested in relative deep water - in applying the predictive model to these data sets a larger lever arm between heel and weight force equal to 0.15*height was indicated. For the Abt et al data in which the subjects were wearing normal clothes it was not surprising to find that a lower drag coefficient was indicated than that for either the Takahashi et al or RESCDAM testing in which the subjects were clothed in high drag waders or dry suits. Figures 3 and 4 present predictive model comparisons with specific subject test results from RESCDAM (2001) and Yee (2003).

4. DISCUSSION

The results of all testing by various researchers are presented in Figure 7 as depth versus velocity. For discussion purposes curves with constant Depth*Velocity (D*V) values of 1.5, 1.0 and 0.4m^2/s are plotted. Figure 8 shows all the data presented in terms of critical Depth*Velocity (D*V) versus Height*Mass (H*M) of the subject.
Analysis of Figures 7 and 8 leads to the following conclusions:-

- The Abt et al (1989) data indicates substantially higher and unexplained stability than all other data for adults. The data must be considered an upper limit inconsistent with other research until clarified.
- Safety of able healthy adults is almost guaranteed at D*V values below 0.6m^2/s. The current guideline stipulated by O'Loughlin and Robinson (1997) of D*V=0.4m^2/s is conservative for healthy adults, many of whom could safely negotiate conditions up to D*V=1.0m^2/s.
- Children, depicted on the figures as having H*M value less than 50, may not be able to negotiate flow conditions with a D*V even as low as 0.4m^2/s. This is dependent upon many factors beyond the Height*Mass (H*M) product – additional factors include the age of the child and their level of physical and muscular development. Note the failures below the D*V = 0.4m^2/s criteria in both Figures 7 and 8.

5. CONCLUSIONS

Human stability has been found to be dependent on many factors. The two most important factors affecting human stability in floodways are firstly depth and secondly velocity. Depth was found to dictate what type of failure is to occur, either sliding (friction) or tumbling (moment) failure. High depths increase buoyancy and reduce friction underfoot. Low depth-high velocity flows may cause sliding instability but the chances of drowning are less than in the more dangerous deepwater situations where a person is more prone to being swept away once they lose their footing.

From the analysis of all the available data and through modeling and experimentation a better understanding of human stability was gained. It has been shown that the commonly adopted guideline for designing floodways (to ensure that the safety of children is preserved) by specifying a critical Depth*Velocity (D*V) value of 0.4 m^2s^{-1} does not ensure the safety of all children. Very young children with low muscular coordination typified by H*M less than 20 mKg are not safe at this criteria. It is most likely that many frail/older persons may also not be safe under this criteria.

The laboratory test data on personal human safety in floodway conditions remains limited with many deficiencies. Additional testing which would be of significant benefit is recommended to include:

- Testing with varied clothing, varied footwear and varied ground surfaces on a large scale – to date the only study that has concurrently examined to some degree changes in clothing, footwear and ground surface is Takahashi et al. (1989). To define limits of rescue worker safety a comparison between civilian clothing and rescue suits should be undertaken. By quantifying flows at which rescuers are able to operate will reduce the risks involved in such emergency situations.
- Repeat tests on larger range of subjects changing multiple flow and environmental variables including lighting, visibility, water clarity, debris and surface discontinuities.
- Testing on elderly persons – due to the large variance in physical capabilities of elderly persons, testing would need to be carefully managed with adequate statistical power requiring large sample sizes.

6. REFERENCES

Abt, S.R, Wittler, R.J, Taylor, A and Love, DJ. (1989). Human Stability in a High Flood Hazard Zone, *Water Resources Bulletin*, American Water Resources Association, Vol. 25, No. 4, pp881-890.
Cox, R.J & Ball, J.E. (2001). Stability and Safety in Flooded Streets, *Conference on Hydraulics in Civil Engineering*, Hobart, The Institution of Engineers, Australia.
Department of Public Works, (1986), *Floodplain Development Manual*, New South Wales Government, Sydney, Australia
Foster, D.N and Cox, R.J (1973). Stability of Children on Roads Used as Floodways, *Technical Report No. 73/13*, Water Research Laboratory, The University of New South Wales, Manly Vale, NSW, Australia.
Keller, R.J and Mitsch, B. (1993). Safety Aspects of the Design of Roadways as Floodways, *Research Report No. 69*, Urban Water Research Association of Australia.
New South Wales State Flood Plan,(2001), Sub-Plan of the New South Wales State Disaster Plan (DISPLAN), State Emergency Management Committee, Sydney.
O'Loughlin, G.G and Robinson, D.K. (1997). *Urban Stormwater Management - Book 8, Australian Rainfall and Runoff - A guide to Flood Estimation*, Edited by DH Pilgrim, The Institution of Engineers, Australia.
RESCDAM. (2001). The Use Of Physical Models In Dam-Break Flood Analysis, Development of Rescue Actions Based on Dam-Break Flood Analysis, *Final report of Helsinki University of Technology*, Finnish Environment Institute.
Takahashi, S, Endoh, K and Muro, Z-I, (1992), Experimental Study on People's Safety against Overtopping Waves on Breakwaters, *Report on the Port and Harbour Institute*, Vol 34, No 4, pp 4-31 (in Japanese)
Yee, M (2003). Human Stability in Floodways, *Undergraduate Honours Thesis*, School of Civil and Environmental Engineering , University of New South Wales, Sydney, Australia.

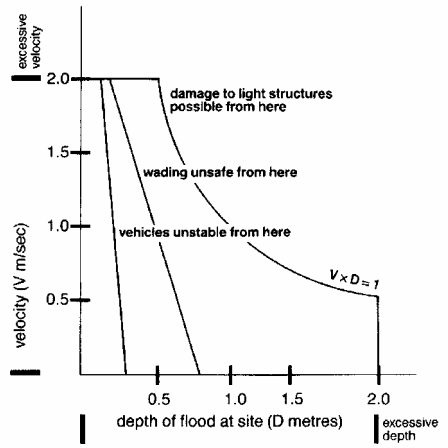

Figure 1 - Depth Velocity Relationships For Floodway Design (After Department Public Works, NSW, 1986)

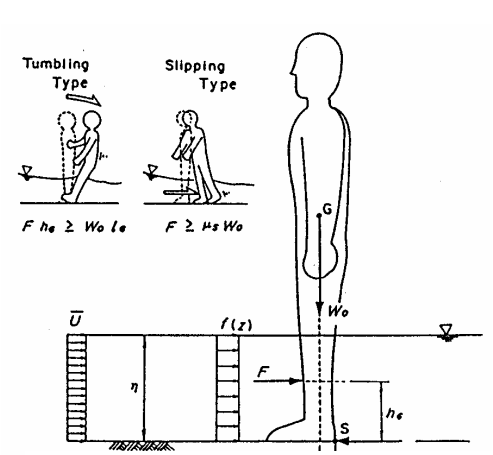

Figure 2 - Human Stability Failure Modes (After Takahashi et al, 1992)

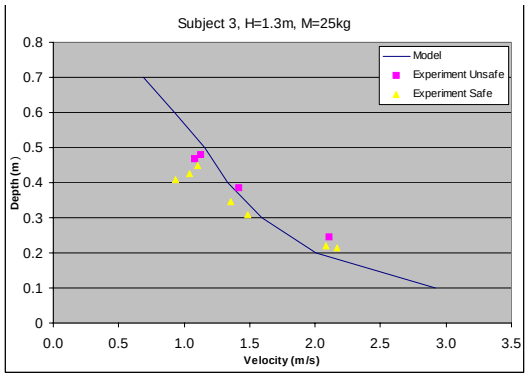

Figure 3 - Predictive Model For Stability Vs Test Data RESCDAM (2001) Subject 2, 1.95m, 100Kg

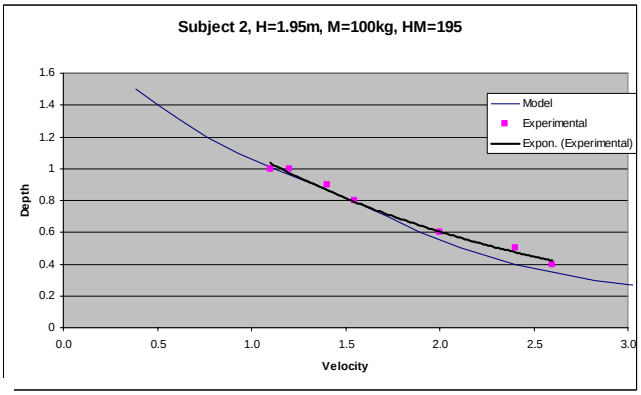

Figure 4 - Predictive Model For Stability Vs Test Data Yee (2003) Subject 2, 1.3m, 25Kg

Figure 5 - Photograph Yee (2003) Subjects 3 and 4

Figure 6 - Photograph Yee (2003) Test Example

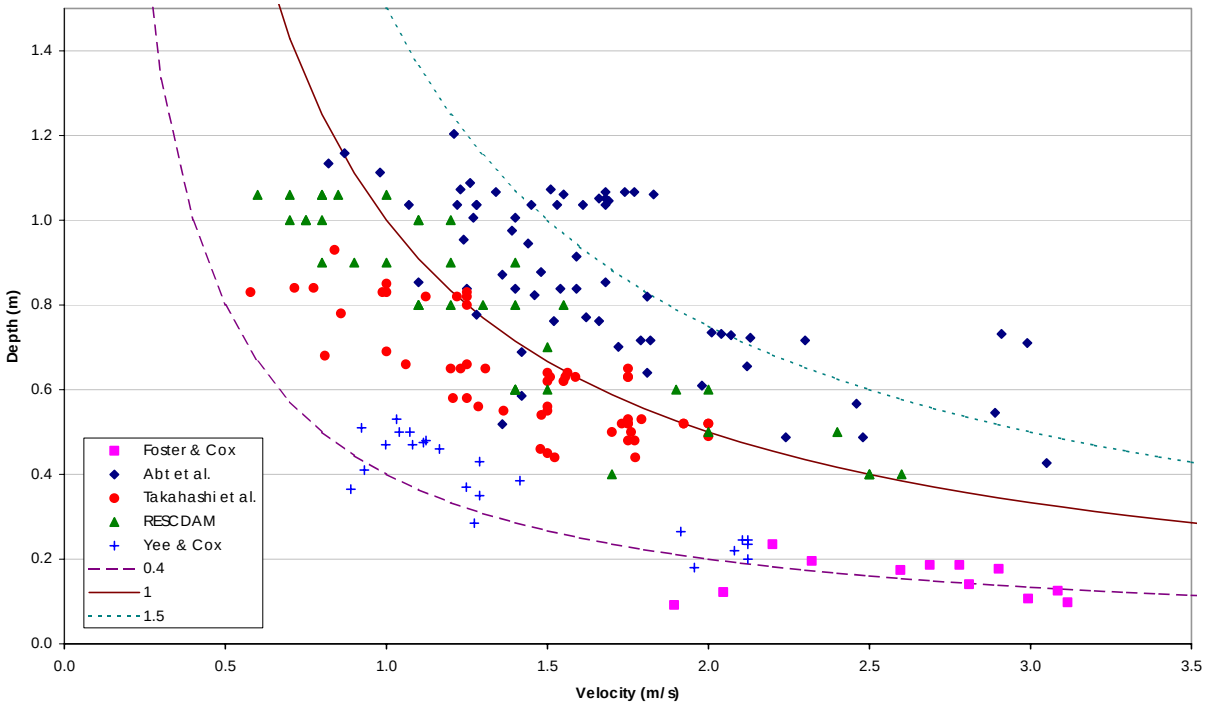

Figure 7 - Test results: Depth Vs Velocity

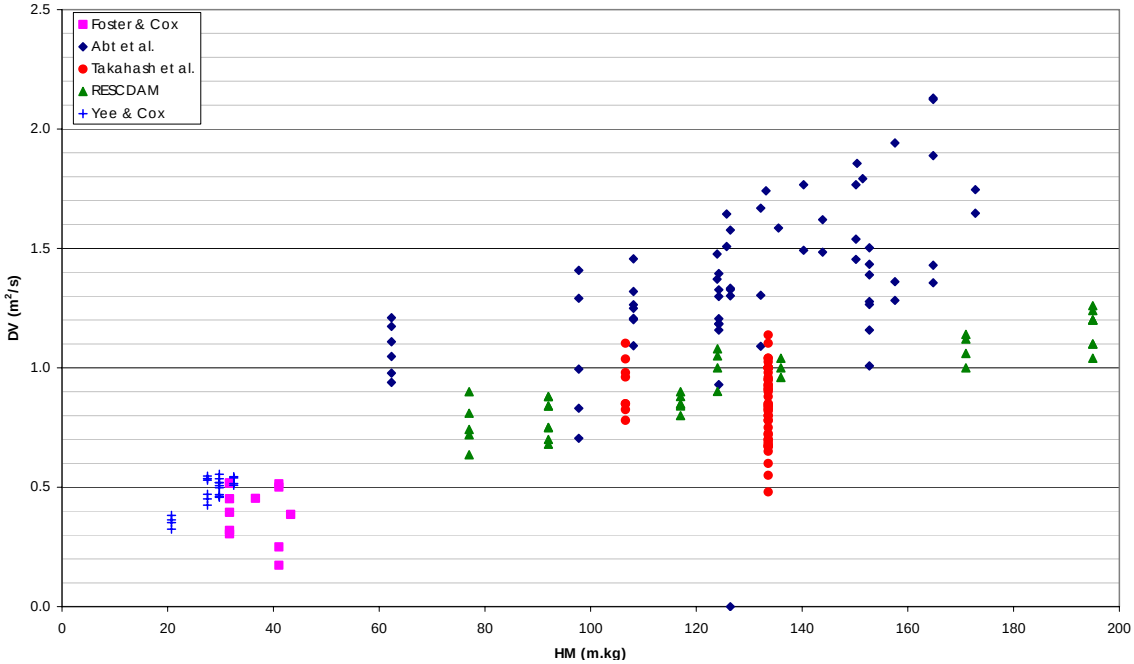

Figure 8 - Test Results: Depth*Velocity (D*V) Vs Height*Mass (H*M)

The Institution of Engineers, Australia
8th National Conference on Hydraulics in Water Engineering
ANA Hotel Gold Coast, Australia 13-16 July 2004

Delivering Property Specific Flood Advice

Bruce Druery
B.E., DipSci (Geol), M.App.Sci., M.I.E.Aust
Principal, Patterson Britton & Partners
David McConnell
B.E., M.I.E.Aust.
Patterson Britton & Partners Pty. Ltd., Australia
Neil Allen
B.E., M.I.E.Aust
City Engineer, Bathurst City Council

Abstract: The translation of discrete time varying results of 1D and 2D hydraulic models into a geospatial continuum using spatial framework technology is described. This technology allows model results to be established as interactive geospatial layers in GIS which integrate hydraulic results at the resolution of an individual property and other data stored in property databases. Spatial technology involves the manipulation of DTMs, creation of TINs and spatial enhancement of hydraulic data. There is an increasing repository of fine mesh topographic data emanating from laser surveys. These laser generated fine meshes can be used to create fine mesh TINs for the display of hydraulic model results.

Keywords: Hydraulic models, geospatial frameworks, GIS, DTM, TIN, cadastre, data mining, flood animation.

1. INTRODUCTION

1.1 What Does Flood Data Entail?

Understanding flood behaviour and flood risks requires knowledge of the data shown in Table 1.1.

(i)	Floodplain Topography	-	the variability in height of flood prone land.
(ii)	Floodplain Cadastre	-	the shape and distribution of properties across the floodplain.
(iii)	Floodplain Property Database	-	floor level and details of buildings located on the floodplain.
(iv)	Historical Flood Levels	-	usually at a small number of historical reference points.
(v)	Hydraulic Model Results	-	hydraulic model simulations of a range of design floods of different return intervals. Information is generated about flood depths, flow velocities and relative timing of flood peaks at discrete points on the floodplain.
(vi)	Flood Hazard	-	involves interpretation of hydraulic model results [ie. depth (D) and velocity (V)] in relation to the likely risk to life and property damage.
(vii)	Impacts of Development Options	-	quantified by hydraulic model simulations.
(viii)	Emergency Response	-	Strategic evacuation plans based on the above information.

Table 1.1 - Flood Data Components

1.2 The Emerging Role of ICT

Over the last decade, local flood authorities have embraced information and communication technology *(ICT)* to varying degrees to expand their capabilities and improve the effectiveness of corporate databases and community services. Councils are using geographic information system (GIS's), MapInfo, ArcView

and Genamap to establish property databases within spatial frameworks eg. cadastre and property information.

However, ICT has traditionally evolved out of the "IT Industry" and it has not involved mainstream hydraulic engineering. As a consequence, most Council databases embrace only (i) – (iv) above and often only partially.

The emergence of ICT has created demand for quicker and more easily understood flood advice. The demand is focused on the needs of the individual. Broad brush flood reports which provide flood information at selected points on the floodplain are no longer acceptable. Local flood authorities are faced with providing more personalised flood data "on demand" or they face criticism for not meeting public expectations of service delivery.

Many Councils are restricted to varying degrees by their existing flood models which may be either too discrete (ie. present flood levels only and at selected locations only) or non geospatial ie. the flood model output is not directly linked to Council's cadastre, property database and/or aerial photographs. Hence there is a need to fully integrate the results of hydraulic modeling of floods within the spatial framework of Council GIS.

2. THE LIMITATIONS OF NON GEOSPATIAL FLOOD DATA

Access to flood data should be considered in the context of the Council floodplain manager who, in most instances, does not have the expertise or time to interrogate sophisticated flood models developed by specialist flood hydraulics engineers.

Traditionally, this crucial information has been supplied only in hard copy as flood study reports, floodplain management studies and associated maps. The subsequent application of this information to development applications, flood policy initiatives and strategic floodplain planning has always required interpretation of the hard copy by the Council floodplain manager. This can be time consuming and can be subject to inaccuracies and inconsistencies when changing or inexperienced staff are involved.

Allen, Druery et al (2003) describe the limitations of hydraulic data provided by a traditional 1D network model of the Bathurst floodplain based on the EXTRAN system. The hydraulic behaviour was represented as a series of flow channels/conduits connected to nodes. The channels/conduits were arranged to represent the geometry and hydraulic features of the floodplain and the main channel – see Figure 1. The model output results provide water levels at each node of the model in tabular form and as graphical output – see Figure 2.

3. THE NEED FOR A GEOSPATIAL PARADIGM

The traditional hydraulic modelling paradigm described in Section 2 is a technical format which suits engineers. However, it is not convenient for non engineers involved in planning and community services. These officers need to relate flood hazard to Council's cadastre, property data bases and statutory certification responsibilities. This requires flood hazards to be available at any point on the floodplain, not just the nodes of the model.

To facilitate community understanding of flood behaviour, presentation of hydraulic model results needs to be readily recognisable by the lay person ie. the presentation needs to be realistic so that understanding becomes intuitive. Technical formats are not effective in conveying flood behaviour to the general community for the purposes of improving flood awareness. Spatial information technology can be used to embed the time varying results of hydraulic models in a "live" GIS.

Figure 3 shows schematically how the time varying results of a 1D or 2D hydraulic models can be integrated within a GIS system. The objective is to create a live link between the spatial results of a hydraulic model and a GIS system incorporating multiple layers of information.

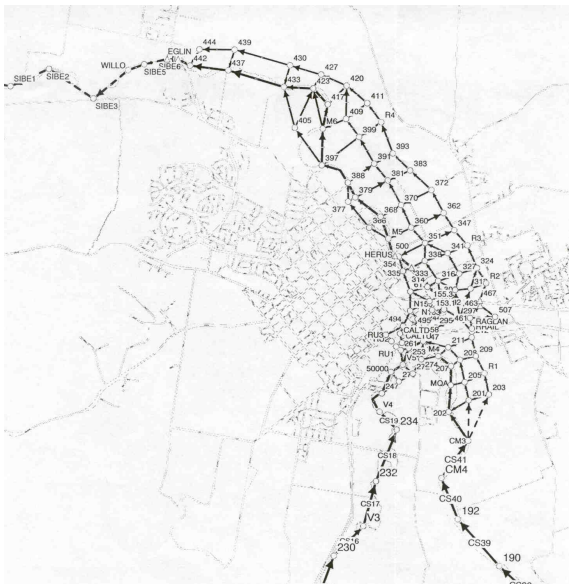

Figure 1 – 1D Model Network Of Bathurst Floodplain

Macquarie River at Bathurst, Aug 98 flood

Label	Chainage	Model '98	Observed	1% AEP	0.05% AEP	PMF
SIBE3	0.000	644.41		644.74	645.81	647.85
WILLO	0.720	645.16		645.52	646.70	648.94
SIBE5	1.000	645.46		645.85	647.13	649.69
SIBE6	1.390	645.86		646.33	647.95	651.14
EGLIN	1.550	645.95		646.45	648.15	651.54
442	1.800	646.00		646.68	648.19	651.81
437	2.410	646.50		647.06	648.28	651.98
433	3.350	647.14		647.58	648.76	652.14
423	3.840	647.57		647.84	648.95	652.22
417	4.200	647.73		647.97	649.10	652.28
M6	4.600	648.47		648.61	649.33	652.31
397	5.180	649.04		649.15	649.75	652.40
388	5.720	650.39		650.60	651.25	652.95
379	5.990	650.85		651.07	651.79	653.29
368	6.500	651.15		651.37	652.09	653.54
M5	6.880	651.86		652.04	652.65	653.92
HERUS	7.200	652.20		652.41	653.13	654.39
333	7.550	652.48		652.72	653.53	654.79
314	7.940	653.09		653.34	654.16	655.36
300	8.210	653.48		653.76	654.56	655.67
292	8.430	653.55		653.94	655.00	656.45
244	8.840	653.58		653.97	655.03	656.48
458	8.960	653.95		654.39	655.51	656.82
198	9.130	654.99		655.57	657.33	659.93
M4	9.490	655.27		656.50	657.63	660.00
207	9.750	656.34		656.56	657.71	660.03
MQA	10.070	656.43		656.66	657.81	660.13
202	10.510	656.78		657.04	658.46	660.58
CM3	11.090	657.18		657.38	658.69	660.76
CM4	11.840	658.89		659.07	659.77	661.24
192	12.570	659.50		659.54	660.13	661.51
190	13.600	659.65		659.76	660.53	661.89
M3	14.520	662.01		662.26	663.51	664.53
186	15.250	662.29		662.58	663.69	665.34
M2	15.720	663.38		663.62	664.90	666.43
182	16.390	663.86		664.08	665.32	666.85
180	17.250	664.13		664.37	665.63	667.18
178	18.060	665.10		665.32	666.50	668.04
M1	18.820	666.07		666.35	667.79	670.00

Figure 2 – Typical Model Output in Tabular Form

Figure 3 shows how the fundamental model results (ie. water level and velocity) and any type of derived data (eg. depth, V x D, flood damages) can be linked geospatially as separate layers to fixed GIS data sets eg. digital terrain model (DTM), cadastre, property data base and air photography.

In an integrated GIS dataset, all data, including the hydraulic model results, can be polled or mined at any chosen point irrespective of whether the original hydraulic model (1D or 2D) predicted the fundamental variables at that arbitrarily chosen point. The key to incorporating hydraulic model results as a geospatially linked 2D continuum is the conversion of the hydraulic model results to a spatial framework.

4. THE CONVERSION OF HYDRAULIC MODEL RESULTS TO A SPATIAL FRAMEWORK

4.1 Overview

Hydraulic models produce fundamental hydraulic data as water levels and velocity (refer **Figure 3**).

The basic requirement of a hydraulic model results layer(s) in a GIS system is that it be a spatial framework. 1D model data is discrete ie. the data is restricted to a limited number of cross-sections; 2D model data is continuous but isolated to itself data wise. The results are geared for 2D presentation on a computer screen and as such they are not readily transferable or interactive with other data. Hence 2D results are often produced in hard copy in a discrete manner eg. contours of water surface in hard copy.

4.2 Creating A Spatial Framework For 2D Models

Creating a spatial framework for 2D models is relatively easy. It involves the translation of the intrinsic finite difference grid or finite element network of the model into a spatial framework suitable to be read as a GIS layer ie. the creation of a triangular irregular network (ie. TIN).

A triangle defines a planar surface and a set of connected triangles *(ie. a TIN)* defines a continuous surface upon which the hydraulic model results can be imposed. The nodes in this spatial framework are where the results of the hydraulic model are stored.

Hence in a 2D model, the TIN merely involves the triangulation of the nodes of the model network or grid and translating the time varying results into a suitable format that can be read as a GIS layer for each time step of the model results.

The 2D model results can be conceptualized as a "cube of data" where the 1st slice is a spatial framework of the model results at the first time step. Following slices represent the spatial frameworks of subsequent timesteps.

4.3 Creating A Spatial Framework For 1D Models

1D models don't have a spatial framework as they are constructed from a series of cross sections linked by branches, usually located to a co-ordinate system. Each cross-section constitutes a series of offset points *(ie. distance from an origin and a level)*. Provided the order or "adjacency" of the cross sections is known then the offset points from each cross-sections can be connected to create a series of triangles which define the space between any two adjacent cross-sections. This process can be continued for all cross-sections in the model to provide a derived continuous topographic surface represented by the model.

The time varying results of both water level and velocity, related to each cross-section are indexed to the relevant nodes in the spatial framework to create separate results TINS similar to that produced in 2D models. The outcome of this process is a derived spatial layer, as a TIN, for both water level and velocity that can be used in the GIS process.

Whilst the velocity TIN has the appearance of a 2D velocity field, it is important to appreciate that the velocity at any point is a planar interpolation of the discrete model velocities determined by the 1D model at each cross-section. Conservation of mass is preserved on the scale of control volumes defined by the model cross-sections but not at the much finer scales of the velocity TIN and DTM. However, provided the original 1D model constitutes a reasonable schematisation of the 1D waterway hydraulics and average floodplain geometry, the velocity TIN should provide a good interpretation of local velocities.

Similarly, the velocity TIN assumes that the cross-sectional velocities can be interpolated purely spatially without reference to the DTM. Provided the 1D model schematisation is a good representation of average floodplain geometry, the interpolation produces reasonable results.

The main difficulty with mapping the velocity TIN onto a fine scale DTM is where the 1D model sections do not closely define a meandering thalweg. This leads to velocity vectors which tend to truncate the thalweg when displayed on air photo or cadastre. In this case it is necessary to increase the resolution of the 1D model by adding intermediate, dummy sections whose properties are interpolated between the original cross-sections but whose offsets define the channel thalweg accurately.

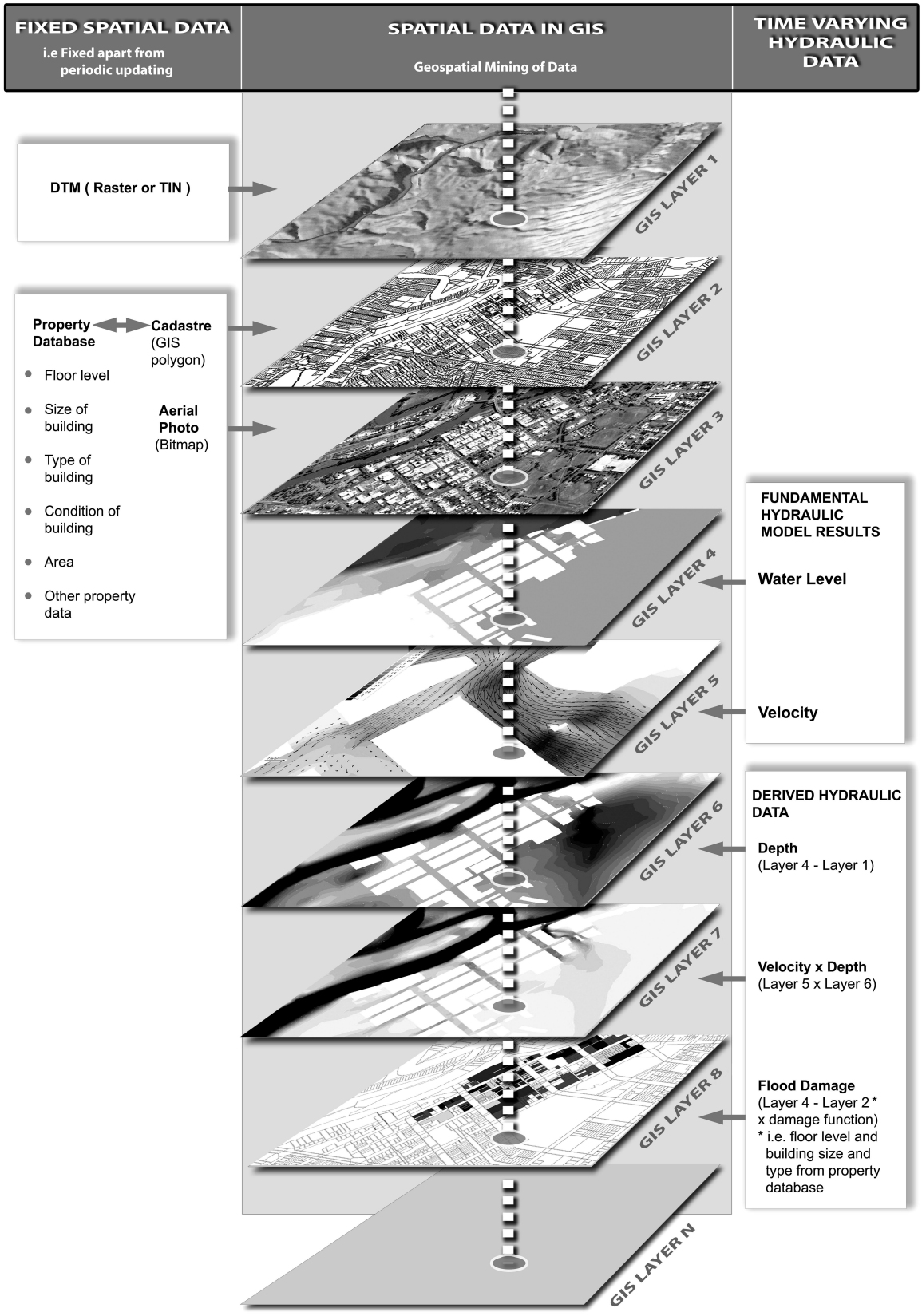

Figure 3 – Schematic showing Integration of Hydraulic Model Results in GIS

Another finesse in developing the velocity and water level TINS is to ensure that the 1D model cross-sections extend beyond the limit of inundation so that an intersection of the water surface and the DTM is created. Otherwise the water inundation surface will not be defined properly.

4.4 Mapping/Translating The Model Results TIN To a DTM

The model results TIN derived through the above process, especially for 1D models, but often for 2D models, is coarse in relation to the variation of the terrain. Because water level and velocity, to a lesser extent, usually represent gradually varying results surfaces, estimates of the variation of these fundamental model results can be interpolated within this coarse framework.

This is not the case with depth or other derived parameters based on depth. Hence a further spatial refinement is necessary to translate the fundamental model results TIN onto the much finer spatial framework of the DTM.

Improvements in field survey data techniques such as laser and high precision photogrammetry are making fine mesh DTM's more readily available. Many local government authorities are acquiring laser survey data and the translation of model results to the finer mesh of the DTM is an opportunity to make more effective use of this expensive data.

The first step in the translation process is to transfer the water level and velocity results TIN across to the fine meshed, spatial framework of the DTM. This is done by taking every node of the fine meshed framework of the DTM and determining the model results of water level and velocity within the triangles of the model results TIN by planar interpolation. This translation is repeated for every time set of model results.

4.5 Derived Hydraulic Data

Hydraulic models generate only water level and velocity as the fundamental variables. As described above they are incorporated into the GIS as a spatial layer (ie. layers 4 and 5 of Figure 3). Other parameters such as depth *(D)*, V x D, hazard *(combination of D, V x D and V)*, local Froude Number, bed shear etc. can be derived from the fundamental ones and the ground surface defined by the fine mesh DTM. These derived parameters do not have to be stored as they are readily calculated "on the fly".

A derived data set which is of particular value to floodplain managers and planners is the peak data set ie. the peak value of every parameter *(fundamental or derived)* at each individual node, regardless of time.

5. EXAMPLE OF APPLYING A GEOSPATIAL INTERFACE TO BATHURST

Figures 4 to 6 show the non spatial results of the 1D network model of Bathurst translated to the geospatial paradigm using a geospatial interface developed by PBP (ie. waterRIDE™).

5.1 Flood Animation

Figure 4 shows a snapshot of the time varying inundation of the Bathurst floodplain as a thematic surface or as a translucent "blue wash" spreading over an airphoto bitmap. Standard GIS functions of zooming and panning allow flood behaviour to be focussed on an individual region or group of buildings. Cadastre can be superimposed on the animation to facilitate interrogation of the flood surface for water level (m AHD at any time or peak value) at any property location. As shown the time history of water level variation at any selected point can be called up as a water level versus time plot.

Water level surfaces translate very easily onto the DTM because most flood situations involve gradually varying flow and the water surface slopes are gradual and well suited to planar interpolation. Topographic controls such as embankments and gullies which are not defined in the 1D network show up well in animations because of the realistic fine scale interaction of the gradually varying water surface with the fine scale DTM.

5.2 Floodplain Velocities

The flood flow along the conduits/channels of the model network were converted to section average velocities using model cross-section areas. These velocities were vectorised and used to produce a continuous, time varying velocity solution surface (ie. TIN) across the entire Bathurst floodplain within waterRIDE^{TM}. Figure 5 shows a thematic plot of velocities of portion of the floodplain.

5.3 Floodplain Hazard Map

The ground surface from the DTM is subtracted from the water surface to determine water depth at any point. Depth is multiplied by velocity to determine flood hazard (V x D; refer to layers 6 and 7 of Figure 3).

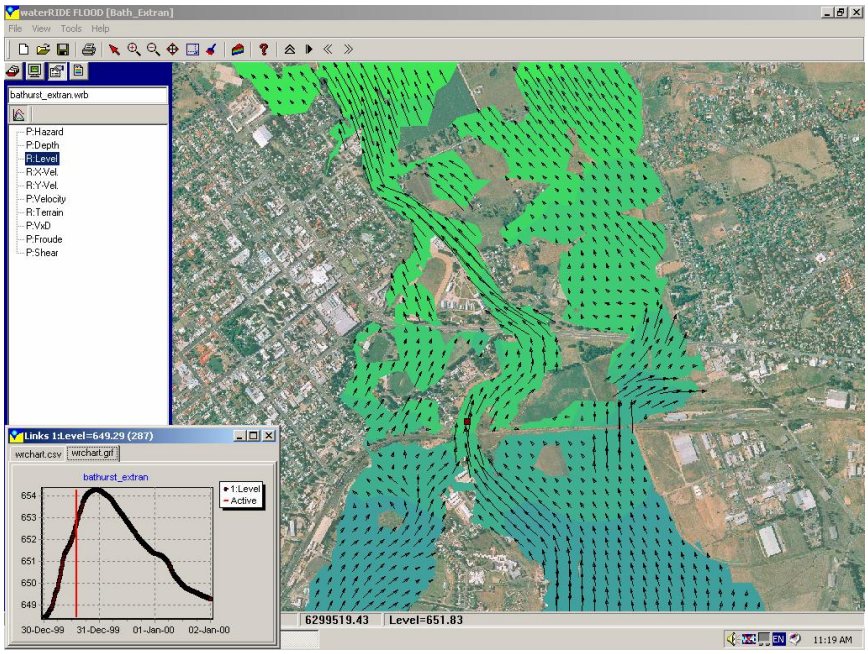

Figure 4 – Screen Shot of Water Surface Animation Showing Water Level TIN and Velocity TIN Results (as vectors) and Time Plot at a Location Downstream of Railway Bridge.

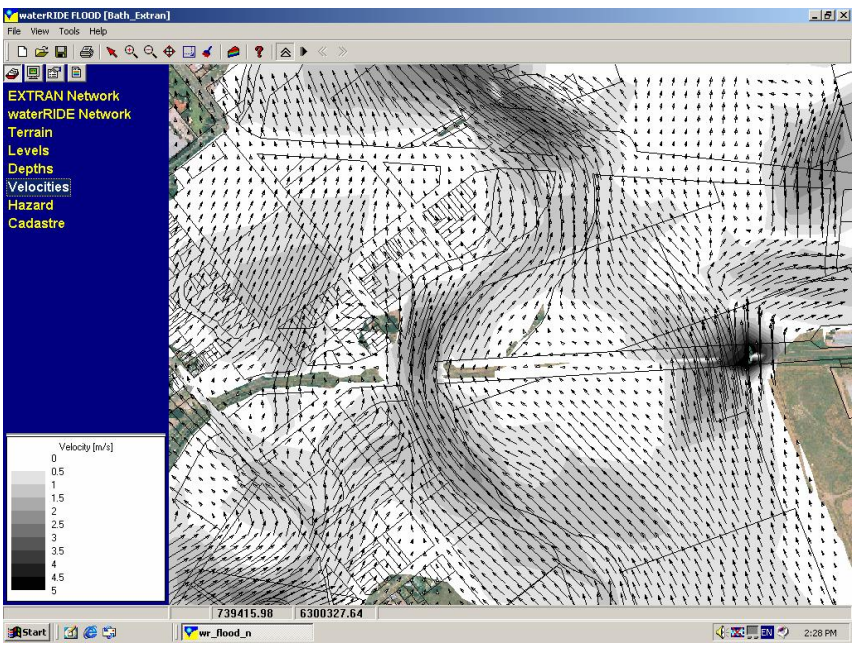

Figure 5 – Thematic Plot of Peak Velocities with Superimposed Cadastre and Velocity Vectors

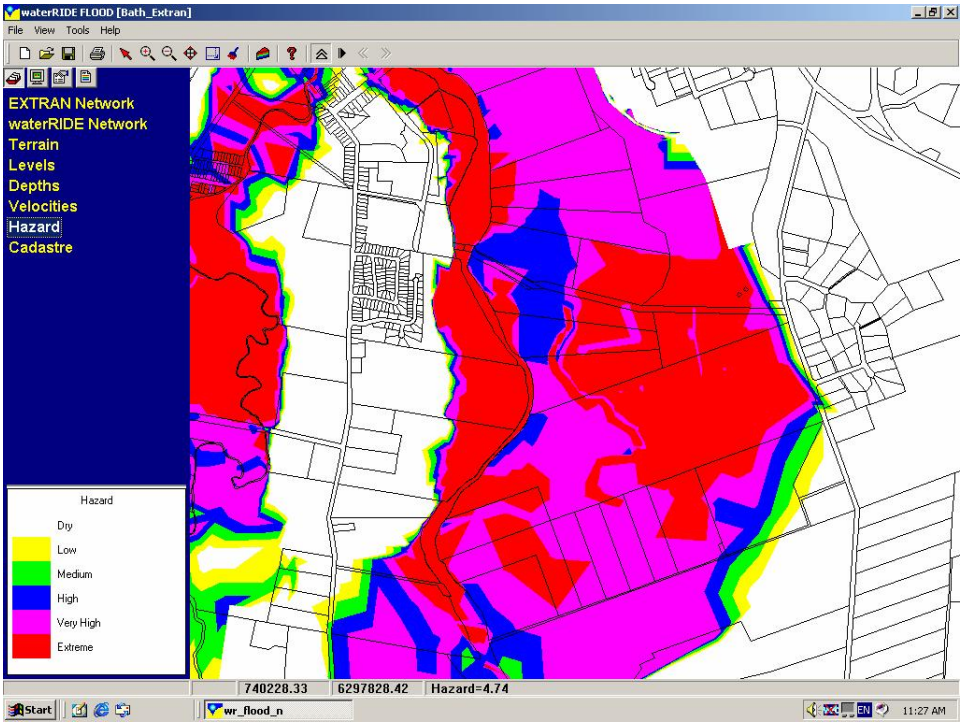

Figure 6 – Flood Hazard Map

5.4 Integration of Model results and Council Property Map

The results of the Bathurst flood model (ie. peak values of water level, velocity, depth, velocity x depth, ground level) were linked in the geospatial interface to Council's cadastre and property database. In its native form, this allows an airphoto image, with superimposed cadastre, to be panned and the cursor clicked on any property to show flood level and property details related to that to the air photo image. Any geosptatially tagged information can be called up this way.

6. CONCLUSIONS

There is a tendency to think that 1D models are outdated and most flood modeling should be 2D. 1D modeling still has its place and the need to make 1D model results more compatible with the need to give individual property advice, can be met by the use of geospatial integration.

Geospatial integration can be done retrospectively utilizing new land survey technologies such as laser surveys to make old 1D and 2D flood models more relevant to giving flood advice about individual properties.

Hydraulic modeling technology of itself can not be improved much further. However, there are great advances occurring in remote sensing of ground terrain *(laser survey)* and geospatial integration *(GIS)* and engineers and floodplain managers need to integrate established hydraulic modeling methods with these new technologies to make flood data more accessible and understandable to the general community.

7. REFERENCES

Neil, A., Druery, B. and Fisher, J. (2003) Getting Better Value from your Flood Model, *Proc FMA NSW Annual Conference*, Forbes, NSW

Druery, B., McConnell, D., Ross, C. and Moorhouse B. (2002) Making Flood Data Accessible, *Proc FMA NSW Annual Conference*, Kempsey, NSW

The Institution of Engineers, Australia
8th National Conference on Hydraulics in Water Engineering
ANA Hotel Gold Coast, Australia 13-16 July 2004

The Complexity of Numerical Modelling of the Singapore Coastal Waters

A. Frazer
B.E.
Project Engineer, Water Research Laboratory
School of Civil and Environmental Engineering, UNSW, Australia
W.C. Glamore
B.E., Ph.D
Senior Engineer, Water Research Laboratory
School of Civil and Environmental Engineering, UNSW, Australia
J.W. Walker
B.E., MEngSc
Senior Engineer, Water Research Laboratory
School of Civil and Environmental Engineering, UNSW, Australia

Abstract: Large scale land reclamation has taken place in Singapore since the 1960's. The relatively rapid changes to the Singapore coastline and increasing environmental awareness, require that the hydrodynamic environment of the coastal waters is better understood. Numerical modelling, using two-dimensional finite element hydrodynamic modelling software, has been undertaken to examine hydrodynamic behaviour at three sites around Singapore. The model was driven by predicted time series data at open ocean boundaries and calibrated with measured water level and tidal current data. Results show that the model can successfully reproduce both the elevation and phasing of the tides across the model domain for a neap-spring-neap tidal cycle. Hydrodynamic modelling results have been incorporated into suspended sediment models and used to determine impacts of other developments such as a proposed ocean outfall into Singapore Strait. This paper discusses the issues encountered when developing calibrated hydrodynamic models of the Singapore coastal waters.

Keywords: numerical modelling, hydrodynamics, Singapore, land reclamation.

1. INTRODUCTION

Since becoming independent in 1965, Singapore has become one of the worlds most prosperous countries. Given Singapore's relatively small size (673 km^2), a policy of land reclamation has been adopted since the 1960's to meet land use demands. Increasing environmental awareness and concerns over the impacts of land reclamation and other coastal developments has necessitated a comprehensive understanding of the hydrodynamics of Singapore's coastal waters. Singapore is located at the confluence of the South China Sea and the Indian Ocean (Figure 1) where a highly complex hydrodynamic environment exists due to the interacting tidal regimes of these water bodies, combined with variable bathymetry and monsoonal weather patterns.

To represent the natural environment with a numerical model requires simplifications and assumptions which lead to inherent inaccuracies in the model predictions. This is particularly the case with Singapore's coastal waters as they are notoriously complex, due to the interaction of the tidal regimes. With the technology and software currently available, it is possible to incorporate a significant amount of complexity into the hydrodynamic model. With high quality data for driving and calibrating the model, a reasonable representation of natural processes can be attained.

Three studies have been undertaken that have required the development of a two-dimensional hydrodynamic model to predict changes that may occur to the tidal regime. The results of the hydrodynamic model have in turn been used to predict changes to water quality due to these projects.

The RMA suite of software has been used to develop the hydrodynamic model of Singapore's coastal waters and are driven by predicted time-series tide level data applied at open ocean boundaries. The highly complex hydrodynamics in the area, coupled with the limited availability of measured data, creates a challenge for any numerical modeller to

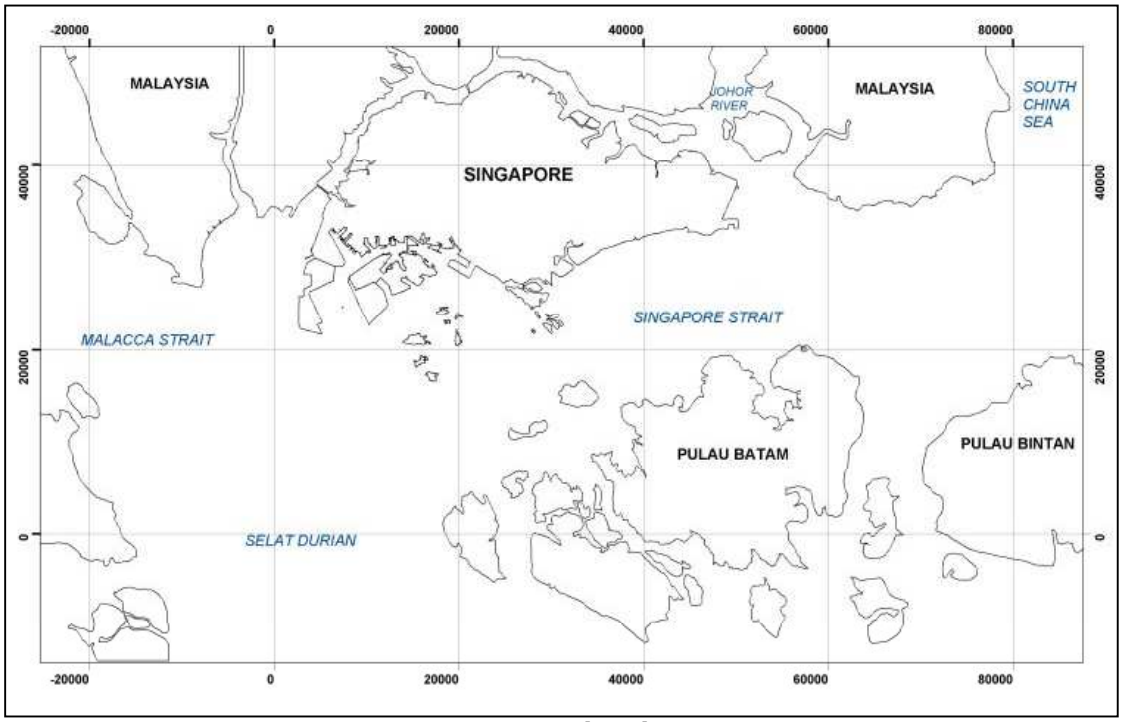

Figure 1 – Locality Plan

accurately replicate the tidal processes. In these studies, numerous model runs have been undertaken to improve the predictions made by the model and subsequent results indicate that accurate predictions of the ocean hydrodynamics are achievable.

This paper describes the environmental processes taken into consideration in the hydrodynamic modelling, details the methodology used to develop and calibrate the model and discusses the results achieved by the model.

2. BACKGROUND

An understanding of the processes that impact Singapore's coastal environment is important in order to appreciate the complexity of the hydrodynamics. These factors had to be taken into consideration when developing and validating the numerical model.

2.1 Meteorology

The hydrodynamics of Singapore waters are influenced by three distinct weather systems during the year (after Turner and Tate (2001)):

- *North East Monsoon:* Generally occurring between December and March, the NE monsoon season is characterised by the highest portion of annual rainfall, with winds typically between 20-40 km/hr.
- *South West Monsoon:* Generally drier than the NE monsoon, the SW monsoon occurs during June to September and is characterised by thunder and gusty surface winds.
- *Inter-monsoon Periods:* The periods between the NE and SW monsoons generally exhibit light, variable breezes with thundery showers occurring late in the day.

2.2 Oceanography

The bathymetry of Singapore's coastal waters is highly variable, with deep water channels in the Singapore Straits varying in depth from 40-100 m. Furthermore, the bathymetry in localised areas around Singapore has been constantly changing due to reclamation activities taking place. There are also many small islands that exist in the coastal waters of Indonesia and Singapore.

Shankar *et al.* (1991) noted that the hydrodynamics of the Singapore region are dominated by tides and associated currents, with tides in the Singapore Strait being predominantly diurnal and having typical tidal ranges of 2.5-3.0 m (springs) and 0.7-1.2 m (neaps). Greig (1992) also reported that winds have a limited impact

on the current patterns in the region and tides dominate the hydrodynamics. The broader tidal dynamics are extremely complex, being driven by distinctly different tidal forces from the Indian Ocean (via the Malacca Straits) and the South China Sea. Typical velocities of the tidal stream vary from 1.5-2.0 m/s in the open waters of Singapore Strait.

3. AVAILABLE DATA

The ability of a model to produce accurate and meaningful results is highly dependent on a number of factors including the data that is used to configure and validate the model. Ideally, high quality data for the temporal and spatial scales is required to initialise and run the model, although in reality this is rarely the case. For the hydrodynamic modelling of Singapore, data requirements included bathymetric, tide level and current data. Data that has been collected in the Singapore region includes long term background data and specific project oriented data, usually of limited applicability. This section describes the data limitations identified in the development of the models and how they have been taken into account.

3.1 Water Level and Current Data

Due to the strong influence that tides have on the current patterns within the Singapore region (Grieg, 1993, Hadi, 1992), accurate water level data is imperative to drive the hydrodynamic model. The Maritime and Port Authority of Singapore operate tidal stations at various locations and supply predicted data for Singapore Waters (Figure 2). For the modelling carried out to date, predicted tide level data, supplied by tide prediction software such as WXTide32 and the British Admiralty's Totaltide package, has been used to describe the boundary conditions of the model. Measured, study specific water level data has been used in the calibration and verification stages of the model development.

The models are driven with tide water level data, however tide current data is necessary to ensure that the model is making accurate predictions. Measured current data has been collected or made available at strategic locations within the study area for the three studies. Extensive data was collected in the Johor River area where no data had previously been collected and was essential for the calibration of the model. Predicted tidal stream data can also be extracted from the aforementioned tide prediction software, which provides current information at a number of locations around Singapore (Figure 2). Due to the complex nature of tidal currents across the study region, these predictions were used to discern indicative flow/tidal patterns but were not employed during model calibration or verification.

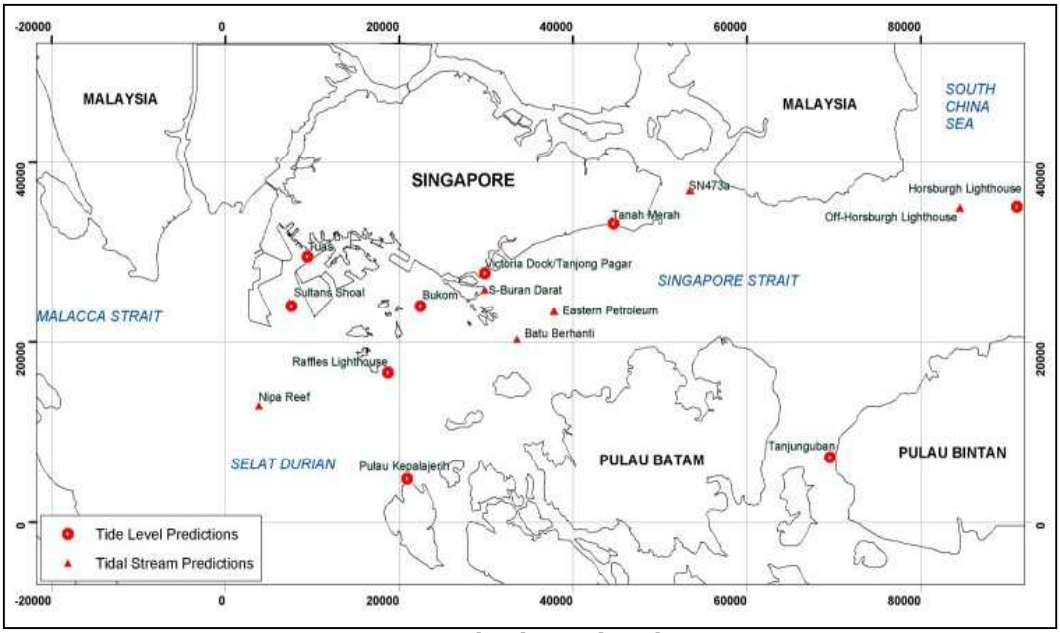

Figure 2 – Current Stream and Tide Level Prediction Locations

3.2 Bathymetry Data

Bathymetry of the broader Singapore waters region has been sourced from British Admiralty (BA) Nautical Charts covering the study domain. The bathymetry from several BA Charts was digitised into electronic format for use in defining the bathymetry of the study domain. Detailed data sets that define the bathymetry in the vicinity of proposed developments were made available to refine the model in the areas of interest.

The vertical reference used for all bathymetric data was Singapore Chart Datum (CD). The horizontal reference used was SVY95 datum. Data in WGS84 geographical positions was projected into SVY95 using datum definitions provided by the Land Survey Department, Singapore Land Authority.

4. MODEL DEVELOPMENT AND CALIBRATION

4.1 Overview of Methodology

A numerical model covering the broader coastal waters of Singapore was established using the RMA-2 modelling software. The two-dimensional model was used to define the hydrodynamics as opposed to a three-dimensional model due to study requirements, data limitations and the computational time that would be required. The boundary conditions were defined at each of the open water boundaries with tide level predictions based on British Admiralty Tide Tables and WXTide32 software.

To calibrate the model, an extensive series of runs were undertaken, the results of which were compared to recorded current and water level data. From these comparisons, model parameters and input conditions were modified so as to best reproduce the hydrodynamics at the site of interest.

4.2 Hydrodynamic Modelling

4.2.1 RMA-2 Finite Element Flow Modelling Software

RMA-2 is a two-dimensional finite element hydrodynamic model for depth-averaged flow (King, 1998). The Navier-Stokes equations are solved in two-dimensions combined with the continuity equation to obtain velocities and water surface elevations at each node on the finite element mesh. One or two dimensional elements may be integrated within the same mesh to enable varied mesh detail according to the dominant processes and importance of different areas in the model. The model can be operated in either steady state or dynamic modes.

4.2.2 RMA-2 Model Configuration and Boundary Conditions

For each of the Singapore scenarios that were modelled, the broader study domain was discretised into a finite element mesh consisting of both triangular and quadrilateral elements (Figure 3). Fine spatial resolution was adopted in areas of interest and in other areas where there were sharp gradients in topography or flow velocities. The bathymetry of the mesh was defined using the data discussed previously in Section 3.2.

The model boundaries were positioned so as to limit both boundary effects and uncertainty within the model. In the absence of recorded current or water level data at the model boundaries, time-varying predicted water levels were used. The time series of water levels at each open boundary was based upon the predicted tide levels at selected stations in proximity to the model boundaries. In some cases, the time-series tide level predictions were adjusted to account for phasing and/or mean sea level differences between the location of the tide station and the actual location of the RMA model boundaries.

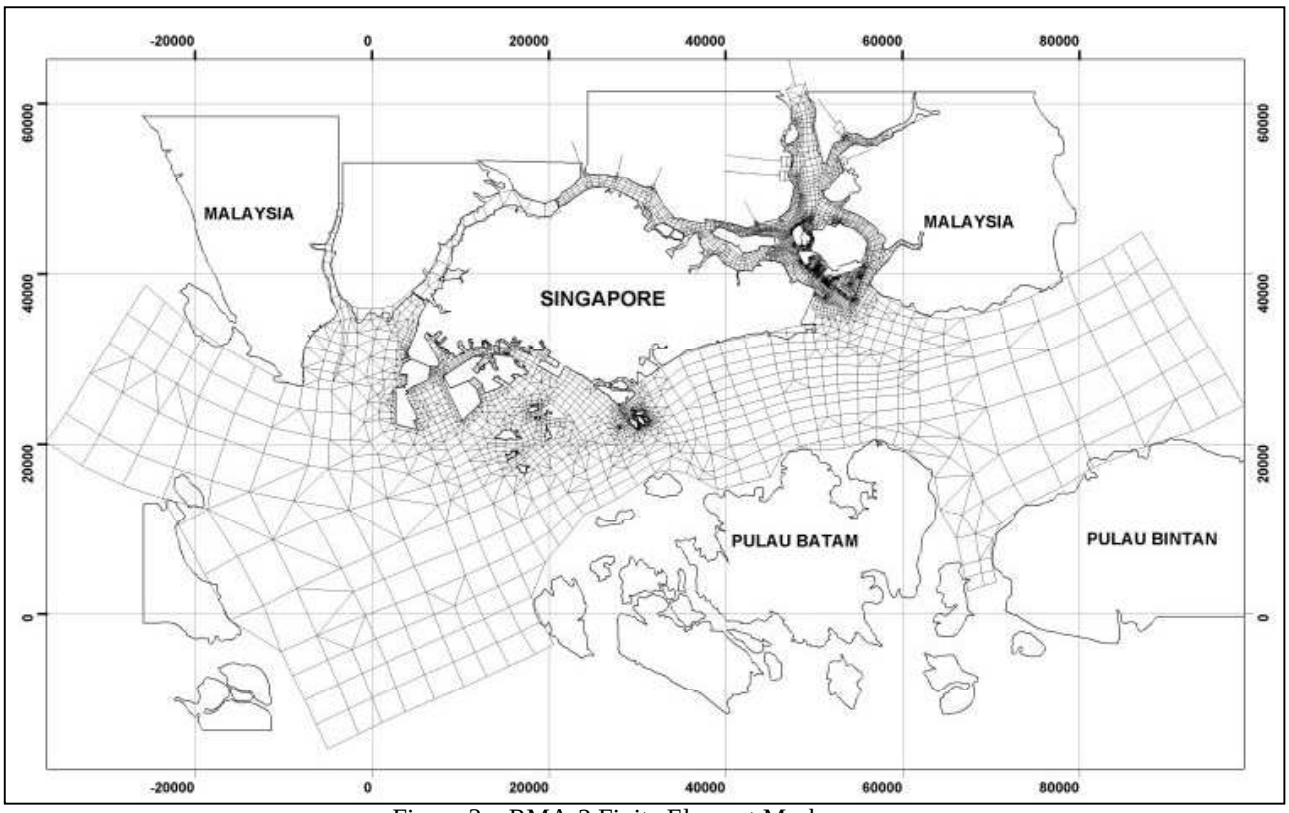

Figure 3 – RMA-2 Finite Element Mesh

4.3 RMA-2 Model Calibration

Using the finite element mesh and the model boundary conditions, the RMA-2 model was employed to simulate the hydrodynamics of the study domain for a neap-spring-neap periods for which measured data was available. The model was run with a 15 minute time-step for the duration of the simulations. To find the best configuration of the model, an extensive calibration process was carried out for each of the studies. Various calibration and input parameters were adjusted to obtain the best fit of the simulated data to the measured data.

The key model calibration parameters were the Manning's bed roughness and eddy viscosity, which were initially set to values based on previous investigations. These values were then examined with a range of sensitivity tests. It was found that altering the Manning's roughness to take into account the main shipping channels better replicated current patterns measured along ADCP transects. Thus, the value of Mannings roughness was set at 0.013 in the major shipping channels and 0.023 throughout the remainder of the model. A nominal eddy viscosity was specified across the whole model domain with the exception of elements at the open water boundaries where a higher value was employed to maintain stability. The nominal eddy viscosity was specified in terms of a scaled velocity and element size described by Equation 1.

$$\varepsilon_{x,y} = \alpha(x, y, t) \cdot V(x, y, t) \cdot \Delta_{elt}(x, y) \tag{1}$$

where ε is the horizontal eddy viscosity (m^2/s)
V is a velocity (m/s)
α is a non-dimensional scaling factor; and
Δ_{elt} is a length representative of the element size (m)

The values of $\alpha \cdot V$ were varied to investigate the impact of phenomena such as eddy currents within the model. Figure 4 illustrates the impacts of altering the eddy viscosity scaling factor on the current patterns. Values of $\alpha \cdot V$ were specified at 1 m/s as it was felt that this value was reasonable as the model current patterns appeared to agree with field observations. No measured data existed to confirm or deny the existence or magnitude of such patterns.

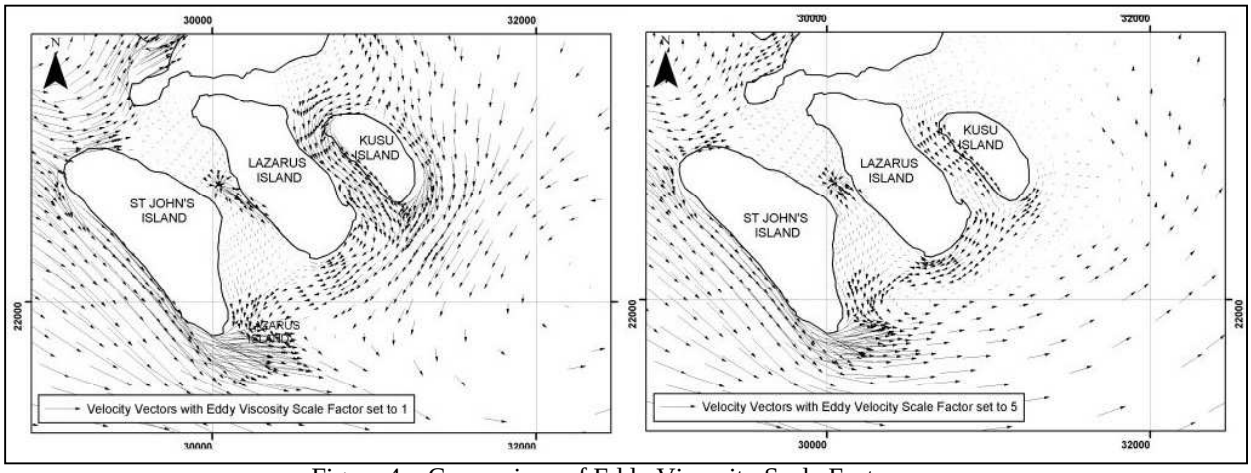

Figure 4 – Comparison of Eddy Viscosity Scale Factors

To improve the model predictions, the impact of having an open or closed south-west boundary was also investigated as the predominant current direction through the Malacca Strait and Singapore Strait was east-west.

Preliminary model runs also identified that the tidal hydrodynamics across the study domain were sensitive to variations in mean sea level at the model boundaries. After rigorous testing, a single set of boundary mean sea level and phase lag adjustments were made to the boundary conditions so that the model results best fit the recorded current meter data.

Other issues encountered during the calibration phase of the modelling included taking into consideration the amount of storage in major rivers such as the Johor River which may be associated with features such as marshes and tidal tributaries. Estimates of the upstream storage were derived from ADCP current data.

Another consideration, was the ability of the model to simulate hydrodynamics for the distinct weather patterns that are observed in Singapore. In the cases where measured data was available, the model was verified using data from a contrasting time period.

A comparison of simulated water levels against predicted tide levels and current predictions during the calibration phase and with the final model configuration at one location in the model domain are shown in Figure 5. The main differences in the model configuration between the calibration plots include the phase lag and MSL shift of the western boundaries of the model and the representation of the islands in Singapore Strait

4.3.1 Discussion of Model Calibration

The results of the hydrodynamic modelling carried out to date have shown that by understanding and incorporating the complexity of the natural environment, the accuracy of model predictions can be improved. The final model results reveal that there is still inaccuracy in the models but that they can adequately reproduce both the elevation and phasing of the tides across the model domain for a neap-spring-neap tidal cycle.

As indicated by the current directions shown in Figure 5, the flood and ebb tide currents through the Singapore Strait were able to be simulated by the model throughout the spring-neap phases of the tidal cycle. With respect to current speeds, the complexity of the hydrodynamics were apparent in the results as it was observed that the models under-estimated the current speeds in some locations and over-estimated current speeds at other locations with no discernible pattern. However, it should be noted that the error in the simulated currents was generally within the acceptable accuracy of the predicted current speeds (± 30%). Importantly, the models were able to match the phasing and the direction of the currents at the chosen locations with acceptable accuracy and in the areas of interest the model was able to reproduce the hydrodynamics accurately. The current patterns were able to be reproduced with greater accuracy in the estuaries around Singapore as these areas were generally not

effected by the interaction of the tidal regimes. Model results were particularly accurate in the Johor River region where additional data was collected for calibration.

There are a number of factors that may contribute to the under- or over-estimation of the current speed results, including mesh complexity, poor bathymetry data or other data limitations. For instance, at some locations within Singapore Strait current speeds are over-estimated and it is possible that model simplifications, such as the exclusion of complex areas around the Indonesian islands south of Singapore or the accuracy of the representation of islands within Singapore Strait, may influence the accuracy of the current predictions. In contrast, at other location within Singapore Strait, it is evident that the model slightly underestimates the current velocity.

The coverage and accuracy of the data used to define the bathymetry of the model may also be a contributing factor between the measured and simulated currents. Simplifications of the bathymetry in the study site may have had implications on the accuracy of the current velocities. Furthermore, in some cases it is possible that inaccuracies may be present in the supplied current data, as the tide levels are accurately replicated throughout the various time-periods.

The development of a calibrated hydrodynamic model of Singapore's coastal waters has been further put to use in a number of ways. An RMA-11 sediment transport model using the hydrodynamics from the RMA-2 model has been successfully developed to predict the movement of dredge material in the area. The model has also been used with other software such as CORJET to predict the transport of pollutant plumes in Singapore Strait.

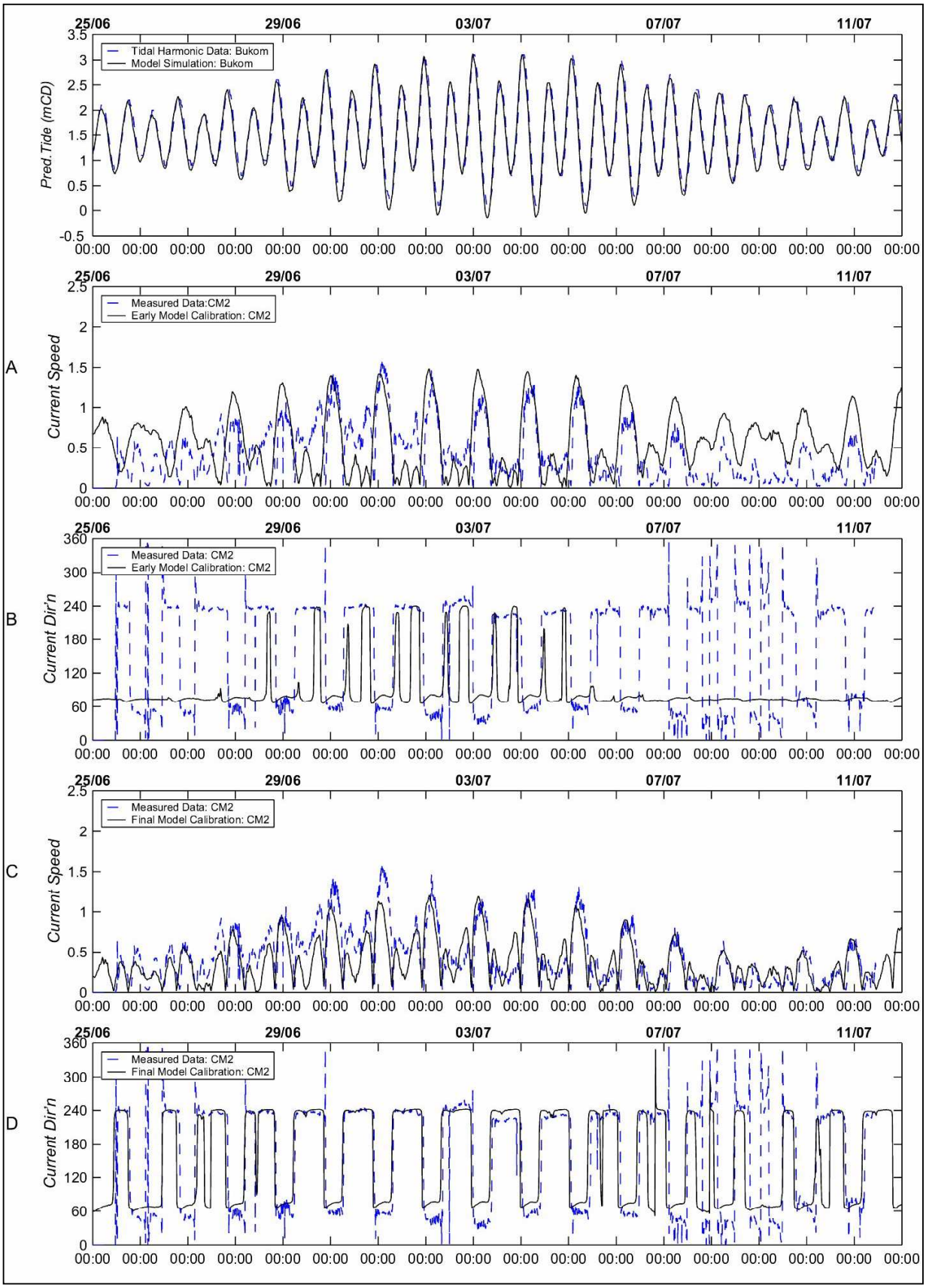

Figure 5 – Model Calibration Results with Initial Model Calibration (A&B) and Final Model Calibration (C&D)

5. CONCLUSIONS

A calibrated model of Singapore's coastal waters has been developed, the results of which have been used in subsequent water quality studies. Although there is still some uncertainty evident in the model results, a large degree of complexity has been incorporated into the model configuration by carrying out rigorous testing of combinations of boundary conditions and calibration parameters such as the Mannings roughness and eddy viscosity to determine the model configuration that would best fit measured data. These values and the configuration of the model has been based on an understanding of the complexity of the coastal environment and the dominant processes impacting on the hydrodynamics. The model performs particularly well in estuarine areas, which are not impacted greatly by the interacting tidal regimes.

It considered that although reasonable estimates have been made by the model across the broader Singapore region, in areas where there is still uncertainty additional tidal level, current, and bathymetric information at key locations within the model domain would enhance future modelling.

6. REFERENCES

Greig, M.J. (1993). *Ocean Currents and Bathymetry*, Report on Field Measurements, New Zealand Oceanographic Institute, Report Prepared for WORKS Consultancy Services Ltd

Hadi, D. (1992). Hydrodynamics model of the Malacca Strait, *Proceedings of the Third Asean Science and Technology Week*, Vol 5, pp. 121-129

King, I.P. (1998*). RMA2 – A Two Dimensional Finite Element Model for Flow in Estuaries and Streams Version 6.5*, Department of Civil Engineering, University of California, Davis Ca

Shankar, N.J., Cheong, H. and Chan C.T. (1991). A Hydrid Model for Singapore Coastal Waters, *Journal of the Institution of Engineers, Singapore*, Vol. 31 No. 4

Storm Tide Modelling of The Whitsunday Coast and Resort Islands

R. M. Fryar
B.E., MEngSt, CPEng, NPER3, CPESC
Principal Engineer, GHD Pty Ltd, Brisbane,
B. A. Harper
B.E., Ph.D., FIEAust, CPEng, RPEQ
Director, Systems Engineering Australia Pty Ltd
I. B. Botev
B.E., Ph.D., MEng,
Senior Engineer, GHD Pty Ltd, Brisbane,

Abstract: A comprehensive modelling assessment has been made of the storm tide risk in the Whitsunday Shire Council region due to the possible effects of tropical cyclones. The assessment was aimed at the delivery of a fundamental risk management tool with respect to the development of a sound vulnerability-reduction (risk allocation) strategy for the shire and was based on return periods. These provide a conceptual basis for quantifying the uncertainties associated with wind, wave, and storm tide due to tropical cyclones. In total, 236 possible cyclones were modelled in detail laying the ground for statistical estimates of storm tide levels based on an artificially generated time series of 91,304 cyclones over a 50,000-year period.

The study provided high level guidance, to the local Council, on the interpretation of storm tide return periods and how such information might be used for decision-making in urban and emergency response planning.

Keywords: Storm tide, tropical cyclones, hydrodynamics, hazard mapping, emergency response planning.

1 INTRODUCTION

Tropical cyclones generating storm tides and flooding in Australia rank on top of the list of extreme events (geohazards) according to the most recent natural risk assessment completed by the Natural Hazards Research Centre (Newton et al., (2001)). Despite this, the theory and application of storm tide predictions are generally poorly understood, especially by those most likely to have a need to apply the results. With this fact in mind, the need for studies to be undertaken is therefore of paramount importance.

The paper details (1) a comprehensive assessment of the storm tide risk in the Whitsunday Shire region (Figure 1) due to the possible effects of tropical cyclones and (2) the adopted methodology. The assessment was aimed at the delivery of a fundamental risk management tool with respect to the development of a sound vulnerability-reduction (risk allocation) strategy for the shire, which should always be based on statistical return periods. These provide a conceptual basis for quantifying the uncertainties associated with wind, wave, and storm tide due to tropical cyclones.

It is important to understand that a return period (or average recurrence interval or ARI) is simply the expected average elapsed time in years between equalling or exceeding a specified event level. This concept does not guarantee that the nominated event's return period number of years will have elapsed before such an event occurs again. In fact, the probability of experiencing the "n" year return period event within any consecutive period of "n" years is approximately 64%, i.e. more likely than not. For example, the 100 year and 1000 year event could both occur in the same year or one might occur twice in the same year, etc.

In total, 236 discrete synthetic cyclones have been modelled in detail laying the ground for statistical estimates of storm tide levels based on an artificially generated time series of 91,304 cyclones over a 50,000-year period.

State-of-the-art wind, spectral wave (ADFA1) and storm surge (Delft3D) models have been applied with the complex results from the latter two summarized into a parametric model before being rendered for inundation mapping purposes by a discrete Monte-Carlo statistical model (SATSIM).

The adopted methodology for the project was based on the "Queensland Climate Change and Community Vulnerability to Tropical Cyclones: Ocean Hazards Assessment" - the "de facto" best practice guidelines approved by Bureau of Meteorology (BOM) for storm tide studies in Queensland. The principal author (and editor) for these guidelines is also one of the authors of this paper. The outcomes from the project were reviewed by a five-member Advisory Committee including the Environment Protection Agency (EPA) and the Department of Emergency Services.

Figure 1 - Study Area With Regions Requiring Hazard Mapping Highlighted.

2 METHODOLOGY OVERVIEW

2.1 Philosophy

Extreme storm tide levels caused by tropical cyclones cannot be estimated solely on the basis of historically measured water levels. This is because the available record of tropical cyclones affecting any single location on the coast is quite small, the resulting storm surge response is often complex and very site specific, and the final storm tide is dependent on the relative phasing with the astronomical tide. Hence, measured storm tide data alone is typically inadequate for extrapolation to very low probabilities of occurrence.

To overcome this problem, it is necessary to formulate a statistical model of the coastal region that will attempt to re-create the observed region-wide tropical cyclone climatology and numerically generate long sequences of potential storm tide scenarios. The statistical model must be supported by a series of deterministic hydrodynamic models that will describe the effect that an individual cyclone has on the coastal region, i.e. the relationship between the wind speed and atmospheric pressure patterns and the resulting storm surge and wave setup for a given cyclone scenario. This is then combined with a tidal description of the region that recreates the known tidal characteristics. When the effect of a single cyclone can be adequately described, the statistical model is used to generate many thousands of possible situations and the resulting statistics are used to determine the probability of storm tide levels throughout the study area.

The accuracy of the model predictions is checked against historical data on a case by case basis where possible, or compared with long term measurements of wind speed in the region, which are less subject to localised effects.

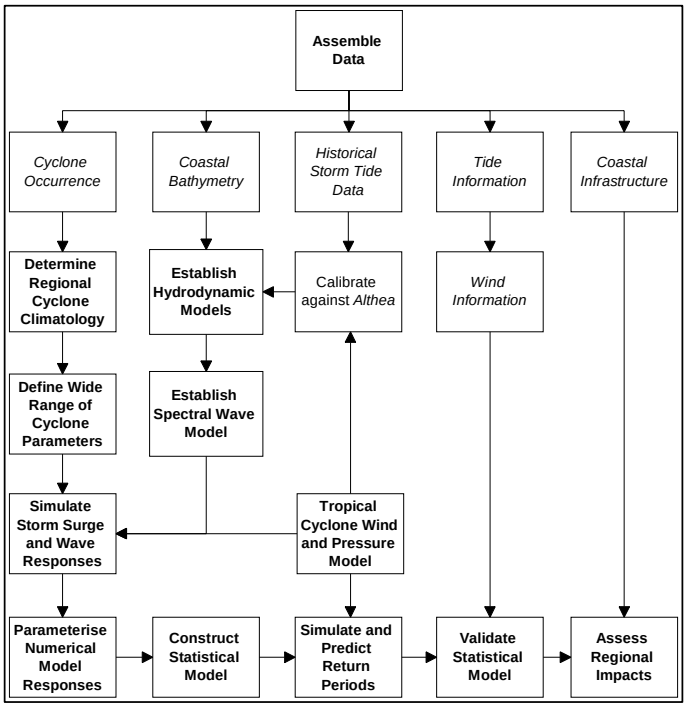

Figure 2 – Overview Of Study Methodology

2.2 Methodology

The adopted methodology utilises a number of sophisticated numerical models, some addressing the deterministic (cause and effect) elements of the problem and others addressing the probabilistic (chance) aspects. Each has been applied to a comparable level of detail and together demonstrate a good degree of accuracy against historical datasets.

Figure 2 provides an overall conceptual view of the study methodology. The first aspect of this relates to the availability of data to describe the tropical cyclone threat to the region, data to describe the coastal geography, and

historical storm tide data for calibration and for defining the regional tide characteristics. Data on regional winds must also be used for model validation, and finally, the coastal infrastructure assets must be identified.

A climatological risk assessment of the threat from tropical cyclones in the Whitsunday region was undertaken to obtain statistical descriptions that can be extrapolated to return periods of interest. This includes statistics describing the expected variation in cyclone frequency, intensity, path and size.

In parallel with the development of the cyclone climatology, numerical models that can estimate the impacts of tropical cyclones on the underlying ocean were established. A numerical hydrodynamic model is used to estimate the strength of the wind driven currents and resulting storm surge, while a spectral wave model is used to estimate wave heights and periods, which contribute the breaking wave setup water level component. The models are constructed based on regional bathymetry data, comprising several nested numerical grids to resolve the numerous near-shore islands and narrow inlets and passages.

The numerical storm surge and wave models are driven by a tropical cyclone wind and pressure field model that generates the complex winds produced by a moving tropical cyclone, according to a set of parameters supplied to it. For example, the set of parameters that approximate tropical cyclone Althea, which impacted Townsville in 1971, was used, in part to verify the storm surge model. A much wider set of parameters was then used to simulate the effects of many hundreds of possible cyclones in the Whitsunday region. These parameters were chosen based on the identified range of values from the long-term climatology of the region.

Once the results of simulating the wide range of possible cyclones are known, the resulting storm surge and wave heights are parameterised (simplified) into a form that is amenable to statistical modelling. This enables the otherwise very computationally intensive numerical surge and wave model results to be re-generated and interpolated very efficiently to enable a simulation of many thousands of years of possible cyclone events. The accuracy of this parameterisation is checked to ensure it is consistent with the other analysis assumptions.

After the parametric surge and wave models are established and tested, the statistical model is built by combining them with the climatology description. At this point, the local astronomical tide is included and also the wave height and period is converted to wave set up so that the overall height of the combined storm tide (surge + set up + tide) can be determined at any location in the study area during the passage of a synthetic cyclone. The probability of water level exceedence can then be obtained by simulating an extended period of possible tropical cyclones affecting the region (50,000 years has been used) and accumulating the resulting time history of the surge, the tide and the wave set up at each coastal location. In this context, the model is not used to predict the future, but rather to suggest what the past experience up until this date might have been if 50,000 years of measurements had been available. A very long period is simulated simply to enable very low probabilities to be reliably estimated.

The statistical model is then verified by comparing its probability predictions against other data wherever possible. Clearly this is not possible in the case of the storm tide itself, but the astronomical tide statistics can be checked against their known probability of exceedence and also the predicted wind speeds (which are separately accumulated by the model) are compared with the available long-term regional wind records. Other checks are also done to ensure that the linear superposition of tide, surge and set up is a reasonable approximation to the real situation where there may be some interaction between these events.

Finally, the predicted exceedence of coastal water levels generated from the statistical modelling process for each point of interest is subjected to extreme value analysis. The results are then mapped to define the 50, 100 and 1,000 year storm tide elevations. Additionally, the Probable Maximum Flood or PMF is defined here by the nominal 10,000 year return period estimate (PMF being a term used in inland-based flood studies).

The possible effects of greenhouse-induced climate change are considered in a subsequent step, whereby a possible future climate scenario is simulated and those results compared with the estimates for “present climate”.

3 DEVELOPMENT AND TESTING OF THE MODELLING SYSTEM

The first module of the system – the tropical cyclone wind and pressure model, has been used extensively throughout Australia and internationally to represent the broad-scale wind and pressure fields of a mature tropical cyclone. It relies on a series of parameters to describe a tropical cyclone when it is over an open ocean environment, namely: (1) the central Mean Sea Level (MSL) pressure p_0; (2) the surrounding, or ambient, pressure p_n; (3) the radius to maximum winds R; (4) the windfield peakedness factor B; (5) the storm track (speed V_{fm} and direction θ_{fm}). The method used in this study (as developed by SEA) also accounts for the effect of storm attenuation when the eye crosses the coast.

The model generates estimates of the 10-minute average wind speed and direction at a height of 10m above the ocean surface for supply to the hydrodynamic models for storm surge and waves. It also estimates the 3-second wind gust for comparison with long-term wind records at Mackay. The estimated MSL pressure field is also supplied to the hydrodynamic model as it has an influence on the generation of the storm surge.

The hydrodynamic (storm surge) modelling has been carried out using the FLOW module of the Delft3D suite of models developed by Delft Hydraulics (The Netherlands). The model has been forced by space and time varying wind and atmospheric pressure fields applied at the free surface of the ocean and operated in two-dimensional, depth-integrated mode. A single, three-dimensional application of the hydrodynamic model was used to conduct

sensitivity tests involving tropical cyclone Althea. Two levels of nesting (using BOM-approved class A, B and C grids, kindly provided by the James Cook University Marine Modelling Unit) were used, achieving a maximum coverage of some 0.9×10^{-6} square kilometres along the coast of Queensland.

As the Delft3D model had not previously been coupled with the Harper and Holland (1999) tropical cyclone wind and pressure model, it was deemed necessary to ensure that the combined model, with the above assumptions, would operate reliably in estimating storm surge levels for this study. Ideally, the model would be tested against an historically measured event in the Whitsunday Region but since no suitable data is available, the nearby well-documented 1971 event of Althea at Townsville has been used. Results of the calibration check showed a very favourable comparison between the measured surge component at the Townsville Harbour tide gauge and the Delft3D model combined with the Harper and Holland wind and pressure model. The predicted storm surge levels (2.8 m range) were within a 3.5% margin of error with respect to the magnitude of the peak storm surge (2.89 m) recorded at the Townsville tide gauge. The accuracy of the prediction is comparable to the accuracy achieved in reconstructing the wind and pressure fields (3.5% for peak wind speeds and bias within 5% for the majority of anemometers available).

Estimates of the breaking wave set up component of the total storm tide (3rd row in Figure 2) were provided by a numerical spectral wave model of the Whitsunday Region established using the ADFA1 model – a 2nd generation spectral wave model (Young 1987) which has been widely applied throughout Australia, especially on the North West Shelf, with great success in reproducing the measured waves from tropical cyclones (e.g. Harper et al. 1993).

There is no site-specific wave data for the region that would be suitable for verifying the operation of the wave model. Reliance was therefore made on the well-established performance of this model in many similar studies. However, a number of sensitivity tests were done to determine the effect of different model computational time steps. Due to the complex island features and the presence of extensive shoals and banks to the south of the study area (Figure 1), a 600 s time step was retained to maintain highest accuracy.

Parametric models (bottom row in Figure 2) were developed to summarise the complex results from the full-scale hydrodynamic and spectral wave models and to express their output in a form that can be readily assimilated by the statistical model. These resulted in 3 sets of tracks, chosen to represent the best coverage of the likely storm surge response: 140° - parallel to the coast; 180° - oblique crossing; 230° - perpendicular crossing.

The tracks were combined with intensity, speed, size and location and were simulated by the hydrodynamic model and the spectral wave model. This required a total of 2 x 2 x 3 x 2 x 9 = 216 simulations, each of which considered an elapsed real time of 30 h, with the start of the cyclone being 18 h before “landfall” and continuing until 12 h afterwards. In the case of the parallel storms, “landfall” is the time of closest approach to Airlie Beach. Each model cyclone also underwent an additional initial 12 h build up period, with the storm held stationary, to reduce numerical transient effects.

In addition to the base set of storms, a series of 18 special tests were also undertaken to explore the surge and wave response at the upper and lower limits of some of the parameter ranges and to check linearity and scaling assumptions.

Finally, since all the preceding simulations were conducted at Mean Sea Level (MSL), a special set of sensitivity tests was undertaken at +1.5m and -1.5m, representative of approximately the Mean High Water Springs and Mean Low Water Springs tidal condition in the region (point of reference Shute Harbour).

Therefore, a total of 236 detailed numerical hydrodynamic and spectral wave model runs have been undertaken, each utilising the three nested grid systems and providing time history output of water elevation, wave height, period and direction each 10 minutes at 336 coastal locations in the region.

Each of the above full scale numerical model simulations were processed according to a method developed by SEA (2002), which combines the output in such a way as to extract the underlying regional and local storm surge and wave responses. The parametric model is optimised for highest accuracy at the time of the predicted peak condition (surge or wave height) and typically reproduces the numerical model results to within about 5% for surge and within 0.5 m for wave height.

The statistical module of the system – SATSIM, generates an artificial history of tropical cyclones based on the climatology. The model calculates the occurrence of cyclonic events based on random number sequences and then allocates the necessary parameters, randomly sampled from the climatology distributions. Each cyclone’s predicted wind, surge and wave response at each of the sites of interest is then generated by the parametric models. The wave height and period estimate is converted into a breaking wave set up height before being added to the surge and both are superimposed on the background astronomical tide for that date in time. This is repeated for 50,000 years of synthetic cyclones and the exceedence statistics of the combined total water level at each site then forms the basis of the probabilistic storm tide level predictions. There is no absolute way that the statistical model can be verified, other than ensuring that the various component parts of the model are performing correctly. Performed checks relate to the model’s re-creation of the astronomical tide statistics and a comparison of its wind speed predictions with long term regional values.

4 RESULTS

Key results of the study were presented in the form of hazard maps for planning and emergency services related applications with the maps indicating zones of potential inundation as a function of return periods for the coastal areas at risk. The locations most exposed to storm tide in the Shire were identified and categorized relative to the risk incurred in strict compliance with the Australian regulatory practices. The estimated return periods (50-year, 100-year, 1000-year and 10000-year) of total storm tide levels for key locations allowed for a detailed assessment of impacts of storm tide on critical infrastructure in inundated areas and a consequent review of Council's evacuation plans. In addition to the principal predictions of extreme storm tide levels undertaken within the concept of "present" climate, the possible influence of "enhanced greenhouse" climate by the year 2100 has been also estimated.

The study gave guidance to Council authorities on the interpretation of storm tide return periods and how such information might be used for decision-making in urban and emergency response planning. A computerized database of predicted inundation levels with possibility of extracting data for any point of the affected areas was delivered using high-resolution hazard mapping at 1 m contour intervals for the most populated areas. The ability to query the outcomes of the parametric model for future planning and emergency services applications without re-running the expensive and time consuming full scale hydrodynamic model will likely be of great benefit to the local authorities.

Results from the hydrodynamic (surge-only) modelling of all 236 cyclones were transferred to the parametric model in the form of time series of storm surge elevation at 10-minute intervals and at 336 coastal locations in the region. In addition, for each cyclone, a series of maps illustrating the current fields (in response to the cyclone) in the nearshore zone overlain on water elevation are generated at 15-minute intervals and stored for presentation purposes.

Results from the statistical model are presented in two different formats: (1) Absolute levels relative to Australian Height Datum (AHD), and (2) Inundation depths relative to the local Highest Astronomical Tide (HAT).

Each of these is then provided as: (1) Tabulated values for the identified townships and resorts; (2) Regionally ranked summary graphs; (3) Selected site-specific return period graphs; (4) Selected detailed regional mapping.

It should be noted that the actual depth of inundation will vary as the local ground level, storm tide level, and difference between the two will all vary in their own right. The depth of inundation (where referenced to HAT) will provide the highest expected depth at the "shoreline", over and above where the highest astronomical tide would normally reach. Hence, any depth relative to HAT indicates the maximum depth that seawater is expected to reach in excess of the normal human experience of the highest tide level.

4.1 Storm Tide Levels

Figure 3 summarizes the estimated total storm tide levels for selected sites, grouped by geographic proximity. As a general rule, the further offshore an island site, the lower the expected storm tide, assuming it is also sheltered from extreme waves. Likewise, coastal sites that are located in large shallow bays are likely to experience increased storm tide levels but open coast sites may also be exposed to high breaking wave set up levels.

Figure 4 shows the relative storm tide rankings. The highest indicated storm tide levels of the selected locations occur at Wilson and Conway Beaches, near the mouth of the Proserpine River, followed by the area to the south of Cape Gloucester and then Airlie Beach. The lowest indicated levels are offshore, at Hook Island Observatory and Hayman Island. The majority of locations have an estimated 10000-year level between 4.0 and 5.0 m AHD.

Figure 5 provides a sample of a series of colour-shaded inundation maps (relative to AHD) designed to enhance the presentation of storm tide data and to facilitate its use by Council's planning department and engineering units. All maps are delivered in digital format and are accessible on ESRI's Arcview Version 8.x and MapInfo Professional Version 6.0 (and later) GIS platforms.

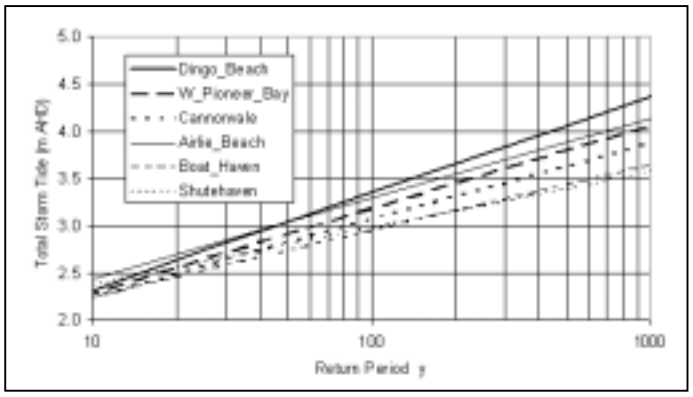

Figure 3 - Estimated Total Storm Tide Levels For Selected Sites

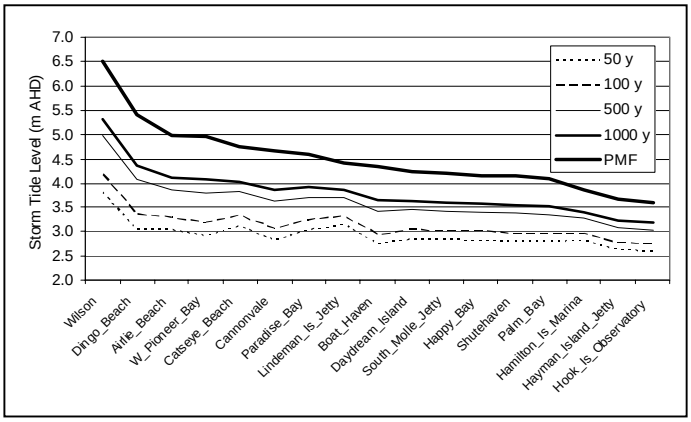

Figure 4 - Relative Ranking Of Estimated Storm Tide Levels

This series of maps is designed for town planning purposes and contains Council's cadastral plan, major roads and localities overlaid on the topography of the area. Storm tide impacts on land use can be assessed by overlaying Council's Planning Scheme on the map and by conducting spatial analysis. Spatial analysis relies on the categories included in the Whitsunday Shire Council Planning Scheme to produce a detailed statement of consequential loss per land category. Table 1 provides an example of the land area of one township (represented by four zones) and the area that will be inundated by the 50-year, 100-year, 1000-year and the 10000-year return period storm tide.

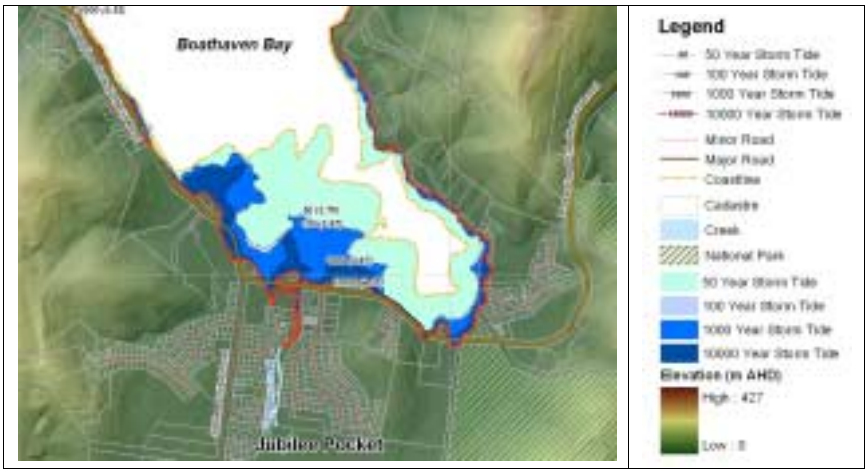

Figure 5 - Example Of Impact Map For Town Planning Applications

4.2 Inundation Depths

A summary of inundation depths is shown in Figure 6. Inundation depths are expressed relative to the highest astronomical tide (HAT) and therefore represent the additional depth of sea water over and above that associated with HAT.

The relative ranking of storm tide inundation depths for the selection of townships is similar to that for the absolute elevations. Dingo Beach is the highest, followed by Wilson/Conway Beaches and then Airlie Beach. The lowest indicated levels are again at Hook Island Observatory and Hayman Island. The majority of locations have an estimated 10000-year return period storm tide inundation depth between 1.5 and 2.0 m above HAT.

As discussed in earlier sections, the increasing tidal range from north to south acts to raise the HAT tidal plane. This is combined with the regional sensitivity to storm surge. For example, Wilson Beach is located in a region where the storm surge will always be amplified due to the shallow waters, but is somewhat protected against extreme waves and set up. Dingo Beach however, is a more open coast site with modest exposure to storm surge and a high exposure to extreme waves and set up. The intervening sites, by comparison, are somewhat protected by the complex island geography.

Table 1 - Land Use Areas Affected by the 1 in 50-y, 1 in 100-y, 1 in 1000-y and 1 in 10000-y return period storm tide

	Areas in hectares				
Land Use Zone	**50-y**	**100-y**	**1000-y**	**10000-y**	**Zone**
Urban Residential	0.00	2.27	6.26	10.15	455.00
Part Development	7.73	8.14	9.66	11.88	102.00
Rural Protection	18.58	23.76	40.70	51.25	939.90
Commercial	0.84	0.97	1.36	2.02	16.53
Open Space	12.81	15.82	22.97	28.74	86.04
Public Purpose	10.97	11.57	12.48	13.10	2739.20

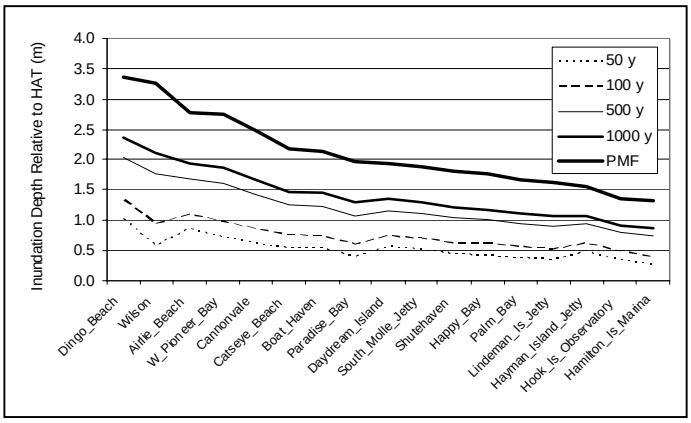

Figure 6 - Relative Ranking Of Estimated Storm Tide Inundation Depths

4.3 Interpretation Of The Results

Figure 7 presents the variation in probability of at least one event occurring (the encounter probability) versus the period of time considered (the design life). The intersection of any of these chosen variables leads to a particular return period and a selection of common return periods is indicated. For example, this shows that the 200-year return period has a 40% chance of being equalled or exceeded in any 100-year period.

The level of risk acceptable in any situation is necessarily a corporate or business decision. Figure 7 is provided to assist in this decision making process. Combinations of design life and a comfortable risk of occurrence over that design life can be used to yield the appropriate return period to consider. For example, accepting a 5% chance of occurrence in a design life of 50 years means that the 1000-year return period event should be considered. A similar level of risk is represented by a 1% chance in 10 years. By comparison, the 100-year return period is equivalent to about a 10% chance in 10 years. AS1170.2 (Standards Australia 1989), for example, dictates a 5% chance in 1000-year criteria or the 1000-year return period as the minimum risk level for wind speed loadings on engineered structures.

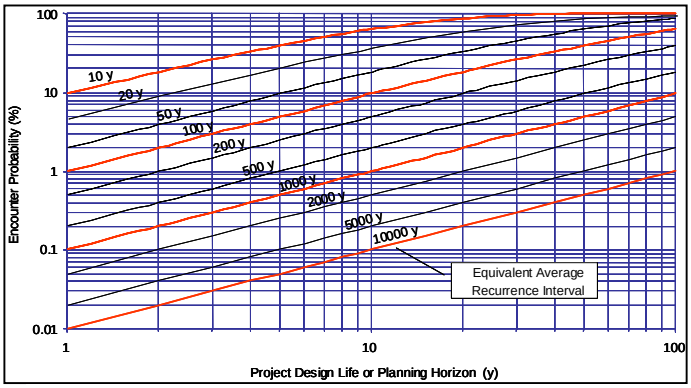

Figure 7 – Relationship Between Return Period and Encounter Probability

5 CONCLUSIONS

A comprehensive assessment has been made of the storm tide risk in the Whitsunday Shire region due to the possible effects of tropical cyclones. The analyses have used a combination of historical data analysis, detailed numerical hydrodynamic modelling and state-of-the-art statistical modelling. The regional impacts have been assessed based on Council-supplied infrastructure information.

The study has considered: (1) the long-term historical record of cyclones in the region, including preferred tracks, speeds, directions and intensities; (2) the spatial and temporal characteristics of storm surges generated by cyclones interacting with the complex coastal features; (3) associated extreme waves and breaking wave set up levels at the coastline; (4) the astronomical tide, which varies significantly across the region.

The accuracy of the various models has been confirmed by comparison with available historical wind and storm surge data and also the published tide tables. The adopted method of modelling has not only provided an accurate assessment of storm tide, but also the means (i.e. a database of levels) to re-estimate the extent of inundation in the future without the need to rerun the models.

While the principal predictions of extreme storm tide levels has been undertaken within the concept of "present" climate, additional guidance on the possible influence of an "enhanced greenhouse" climate by the year 2100 has also been included.

Guidance has also been provided on the interpretation of storm tide return periods and how such information might be used for decision making. It is important to note that this guidance must always be provided responsibly, and that local authorities should be wary of accepting models as tools for self-prediction, as this may have legal implications.

6 REFERENCES

Harper, B. A., Mason, L. B. and Bode, L., (1993). Tropical Cyclone Orson - A Severe Test for Modelling, Proc 11th Australasian Conference on Coastal and Ocean Engineering, IEAust, Townsville, August, pp 59-64.

Harper, B. A. and Holland, G. J., (1999). An Updated Parametric Model of the Tropical Cyclone. Proc. 23rd Conf. Hurricanes and Tropical Meteorology, American Meteorological Society, Dallas, Texas, 10-15 January.

Harper, B. A. (Ed), (2001). Queensland Climate Change and Community Vulnerability to Tropical Cyclones: Stage 1 - Ocean Hazards, Queensland Government, March.

SEA (2002). Parametric Tropical Cyclone Wave Model for Hervey Bay and South East Queensland. Queensland Climate Change and Community Vulnerability to Tropical Cyclones: Ocean Hazards Assessment - Stage 2. Prepared by Systems Engineering Australia Pty Ltd for JCU Marine Modelling Unit and the Bureau of Meteorology, March.

Young, I. R. (1987). A General Purpose Spectral Wave Prediction Model. Research Report No 16, University College, Australian Defence Force Academy, Canberra, January.

Newton, P. W. et al., (2001). Australia State of the Environment Report 2001. CSIRO Publishing on behalf of the Department of the Environment and Heritage, http://www.deh.gov.au/soe/2001/settlements/settlements04-5.html, March 15, 2004.

The Institution of Engineers, Australia
8th National Conference on Hydraulics in Water Engineering
ANA Hotel Gold Coast, Australia 13-16 July 2004

Scale Similarity Models For Large-Eddy Simulations

F.Gallerano
Professor, Università "La Sapienza" di Roma, Italy
E.Pasero
Ph.D Student, Università di Perugia, Italy
G.Cannata
Ph.D Student, Università "La Sapienza" di Roma, Italy

Abstract: Over the last two decades, many authors have proposed LES models based on the scale similarity assumption. The scale similarity models (SSM) assume that the SGS stress tensor is equal to the product of a scalar and a resolved stress tensor obtained by multiple filtering operations. Because of the strong dependence of this coefficient on the type of flow and its wide spatial variability, it is not possible to assume a constant value for such scalar coefficient, thus requiring a dynamic adjustment. In this work it is proved that SSMs computing such a scalar dynamically by means of the Germano Identity (e.g. Liu et al., 1994) are not dissipative enough, since they do not take into account the smallest unresolved scales where most dissipation of turbulent SGS kinetic energy takes place. It is shown that the coefficient of proportionality between the SGS stress tensor and the modified Leonard tensor is uniquely related to the generalised SGS kinetic energy and to the modified Leonard tensor. This relation makes it possible to obtain SSMs that are adequately dissipative.

Keywords: Large Eddy Simulation, Scale Similarity, SGS turbulent kinetic energy.

1. INTRODUCTION

The first step in the LES–approach consists of filtering a flow variable, e.g., the velocity component u_i as follows:

$$\bar{u}_i(x,t) = \int \overline{G}(x-z)u_i(z,t)dz \tag{1}$$

Where $\overline{G}$ is a filter function. If this operation is applied to the Navier Stokes equation, subgrid-terms appear which are expressed in the turbulent stress tensor:

$$\tau_{ik} = \tau(u_i, u_k) = \overline{u_i u_k} - \bar{u}_i \bar{u}_k \tag{2}$$

that is an objective tensor (Gallerano and Napoli, 2000; Gallerano et al., 2002) and can be split into three tensors (Germano, 1986; 1992):

$$\tau(u_i, u_k) = L_{ik}^m + C_{ik}^m + R_{ik}^m \tag{3}$$

where:

$$L_{ik}^m = \overline{\bar{u}_i \bar{u}_k} - \bar{\bar{u}}_i \bar{\bar{u}}_k \tag{4}$$

$$C_{ik}^m = \overline{\bar{u}'_i \bar{u}_k} - \bar{u}'_i \bar{\bar{u}}_k + \overline{\bar{u}_i u'_k} - \bar{\bar{u}}_i \bar{u}'_k \tag{5}$$

$$R_{ik}^m = \overline{u'_i u'_k} - \bar{u}'_i \bar{u}'_k \tag{6}$$

respectively called the modified Leonard tensor, the modified cross tensor and the modified Reynolds tensor, are objective tensors (Gallerano et al., 2002). The last two tensors have to be modelled in terms of resolved quantities in order to close the filtered equations of motion.

A group of SGS models is made up of those models based on the assumption of scale similarity, according to which there is a strict analogy between the hydrodynamic characteristics of the scales of motion which are contiguous in wavenumber space. This assumption is evidently justified by the characteristics of the energy cascade process that transfers the turbulent kinetic energy from the mean velocity field towards the largest turbulent scales and then towards the smallest by vortex stretching. The scale similarity models of Bardina et al. (1983) and of Liu et al. (1994) unlike the Smagorinsky-type models, assume neither local isotropy of the

turbulence scales, nor alignment of the generalised SGS turbulent stress tensor with the resolved strain-rate tensor, nor local balance between production and dissipation of generalised SGS turbulent kinetic energy. In particular, Bardina et al. (1983) use the scale similarity and assume that the smallest resolved scales (similar to the contiguous largest unresolved scales which are the most active in the energy transfer from large to small scales) are represented by the difference between the filtered and the twice filtered velocity field, $\bar{u}_i - \bar{\bar{u}}_i$. Consequently, Bardina et al. relate the cross and Reynolds terms (which are not objective tensors) to the above-mentioned difference velocity field, and therefore expresses the generalized SGS turbulent stress tensor by the equation:

$$\tau_{ij} = L_{ij} + C_b \cdot (\overline{\overline{u_i u_j}} - \bar{\bar{u}}_i \bar{\bar{u}}_j) \tag{7}$$

in which L_{ij} is the Leonard term and C_b is a dimensionless coefficient. This constitutive equation respects the form invariance under Euclidean transformations of the frame and the frame indifference (and not merely the Galilean invariance requested by Speziale (1985) and Spalart and Speziale (1999) if and only if the coefficient C_b is set to one. The previous equation (when C_b =1) therefore reads:

$$\tau_{ij} = L_{ij}^m \tag{8}$$

In which L_{ij}^m is the modified Leonard tensor . In this equation it is evident that in the modelling of τ_{ij} only the modified Leonard tensor appears, and the modified cross tensor and the modified Reynolds tensor are, therefore, completely neglected. The neglecting of these tensors (which are associated with the unresolved scales, at the level of which the most of turbulent kinetic energy dissipation occurs) therefore implies an underestimation of the energy drain process from the resolved to the unresolved scales. Consequently, the scale similarity model of Bardina et al. and those derived from it, even though they eliminate the main inconsistencies of the Smagorinsky dynamic models (i.e. the assumption of local isotropy of the turbulence scales and of local balance between production and dissipation of generalized SGS turbulent kinetic energy), have the drawback of being insufficiently dissipative, i.e. they are not able to guarantee an adequate energy drain from the grid scales to the subgrid scales.

Liu et al. (1994) propose a scale similarity model in which the SGS stress tensor τ_{ij} is related to the resolved tensor L_{ij}^L according to the following relation:

$$\tau_{ij} = C_L L_{ij}^L \tag{9}$$

where

$$L_{ij}^L = T_{ij} - \langle \tau_{ij} \rangle = \langle \overline{u_i}\,\overline{u_j} \rangle - \langle \overline{u_i} \rangle \langle \overline{u_j} \rangle \tag{10}$$

and where the overbar represents the convolution operator with a grid filter and the angular brackets represent the convolution operator with a filter having the characteristic dimension which is double that of the grid filter. Liu et al. proposed for the calculation of the coefficient C_L the use of the dynamic procedure based on the following Germano identity:

$$T_{ij}^T - \langle \tau_{ij} \rangle = L_{ij}^L = C_L \left(\widehat{\langle \overline{u_i} \rangle \langle \overline{u_j} \rangle} - \langle \widehat{\overline{u_i}} \rangle \langle \widehat{\overline{u_j}} \rangle \right) - \langle C_L L_{ij}^L \rangle \tag{11}$$

where the filtering operation at the test scale of dimensions 4Δ is indicated by the symbol $\widehat{\ }$.
The model of Liu et al., like Bardina's, does not guarantee the adequate drain of kinetic energy from the mean motion. Liu et al. (1994) found that the cause of such behavior lies in the very nature of the scale similarity models, stating that these models are generally not dissipative. The authors of this paper do not agree with this statement. The model of Liu et al, using the alignment assumption between the SGS stress tensor and the L_{ij}^L tensor and not formulating any hypothesis on the energy cascade process, makes the mistake of not sufficiently representing the non-resolved scales of the turbulence in correspondence with which the kinetic energy dissipation takes place. The tensor L_{ij}^L represents the turbulence scales included among the scales corresponding to the grid filter and those corresponding to the filter having the characteristic dimension which is double that of the grid filter.

The right-hand term of equation (11) represents the turbulence scales included among the scales corresponding to the grid filter and those corresponding to the filter having the characteristic dimension which is equal to four times that of the grid filter. It follows that the right-hand term Q_{ij} of equation (11) and the tensor L_{ij}^L represents scales belonging to the same range of the turbulence spectrum, which generally lies between the range of scales in which most subgrid kinetic energy is produced and the range in which it is dissipated. The model of Liu et al.

does not therefore sufficiently represent either the production of subgrid kinetic energy, which takes place at the large scales, or its dissipation that takes place at the smallest scales of the energy spectrum. Furthermore, in the near-wall and buffer layers the dynamic procedure for the calculation of the coefficient C_L gives suspect results. This may be due to the fact that the Liu et al. scale similarity model requires three levels of filtering. In high Reynolds number flows simulations the largest filter width is significantly larger than the most of the eddies that govern the momentum and energy transfer in the buffer layer (Sarghini et al. 1999). Moreover, coefficient C_L is calculated, according to the procedure proposed by Lilly (1992), with a least squares minimization method. This method identifies a single value of the scalar coefficient C_L from a system of five independent scalar equations relating the components of the generalized SGS turbulent stress tensor to the components of the resolved tensor Q_{ij}. This procedure may not give absolutely reliable results.

In this paper a scale similarity model is presented in which the closure coefficient C that appears in the constitutive equation is uniquely determined without adopting Germano's dynamic procedure (Germano et al., 1991). Such coefficient is related exclusively to the modified Leonard tensor and the generalized SGS turbulent kinetic energy, which is calculated by its balance equation. The constitutive equation at the basis of the proposed model: a) complies with the principle of material frame indifference (Truesdell, 1977); b) takes into account both the anisotropy of the turbulence velocity scales and of the turbulence length scales; c) removes any assumption of balance between the production and dissipation of turbulent kinetic energy; d) allows the use of a filter whose width is not necessarily associated with the wavenumbers lying within the inertial subrange; e) guarantees an adequate energy drain from the grid scales to the subgrid scales and guarantees backscatter; f) overcomes the inconsistencies linked to the dynamic calculation of the closure coefficient used in the modelling of the generalized SGS turbulent stress tensor.

2. THE PROPOSED MODEL

The generalized SGS turbulent stress tensor is expressed in the following form:

$$\tau_{ij} = C L_{ij}^{m} \tag{12},$$

The generalized SGS turbulent stress tensor is expressed in equation (12) by means of a tensor whose principle axes are aligned with those of the modified Leonard tensor L_{ij}^{m}. The constitutive relation expressed by equation (12) is obtained without any assumption of local balance between production and dissipation of generalized SGS turbulent kinetic energy and thus may be considered applicable in LES with the filter width falling into the range of wave numbers greater than the wave number corresponding to the maximum turbulent kinetic energy. On the other hand, in the range of wavenumbers which are lower than the latter the scale similarity assumption may not be reasonably formulated. In this range, in fact, the part of the turbulent kinetic energy produced by the largest unresolved eddies is high and consequently the above-mentioned turbulent structures may not entirely represent the energy dissipation process (a basic assumption of scale similarity models).

In order to close the equations governing turbulent flows, it is necessary to determine the coefficient C which appears in equation (12). Some authors, including Bardina, have proposed models in which the scalar coefficient of proportionality between the generalized SGS turbulent stress tensor and the scale similarity term is assumed to be constant and is calculated by means of calibration. It has however been found that the above-mentioned coefficient is extremely variable within the calculation domain and it may vary with the type of flow, the Reynolds number and the discretisation scheme. Consequently, the scale similarity models in which this coefficient is assumed to be constant do not correctly estimate the value of the SGS turbulent stress tensor.

In order to calculate the value of the coefficient C which appears in Eq. (12) it is not necessary to make an empirical calibration or use the dynamic procedure based on Germano's identity which is not able to fully represent the dynamic processes of the unresolved scales at which important dissipative processes affecting the entire domain occur. The coefficient C which appears in (12) is uniquely determined by using the existing relation between the generalized SGS turbulent kinetic energy and the generalized SGS turbulent stress tensor.
By definition, the generalized SGS turbulent kinetic energy is equal to half the trace of the generalized SGS turbulent stress tensor:

$$E = \tau_{kk}/2. \tag{13}$$

Introducing equation (12) in (13) gives:

$$\tau_{kk} = 2E = C L_{kk}^{m} \tag{14}$$

from which is obtained:

$$C = 2E / L_{kk}^{m} \tag{15}$$

Equation (15) gives coefficient C as a function only of the resolved quantity L_{kk}^{m} and the generalized SGS turbulent kinetic energy E. Introducing equation (15) in constitutive equation (12), the generalized SGS turbulent stress tensor becomes:

$$\tau_{ij} = (2E / L_{kk}^{m})\ L_{ij}^{m} \tag{16}$$

It may be easily demonstrated that equation (16) complies with the principle of Material Frame Indifference, since it relates the generalized SGS turbulent stress tensor exclusively to objective tensors.

The generalized SGS turbulent kinetic energy, E, is calculated by solving its balance equation, defined by the following equation:

$$\frac{DE}{Dt} = -\frac{1}{2}\frac{\partial \tau(u_k, u_k, u_m)}{\partial x_m} - \tau_{mk}\frac{\partial \bar{u}_k}{\partial x_m} - \frac{\partial \tau(p, u_m)}{\partial x_m} + \nu\frac{\partial^2 E}{\partial x_m \partial x_m} + \tau(F_{Ok}, u_k) - \nu\tau\left(\frac{\partial u_k}{\partial x_m}, \frac{\partial u_k}{\partial x_m}\right) \tag{17}$$

Equation (17) is form-invariant under Euclidean transformations of the frame and frame-indifferent (Gallerano et al. 2002).

The 1st and 3rd terms of the right-hand side of equation (17) express the turbulent diffusion of generalized SGS turbulent kinetic energy:

$$\frac{1}{2}\frac{\partial \tau(u_i, u_i, u_k)}{\partial x_k} + \frac{1}{\rho}\frac{\partial \tau(p, u_k)}{\partial x_k} = \frac{\partial T_{Ek}}{\partial x_k} \tag{18};$$

The following equation is used for the calculation of T_{Ek} (Ghosal et al. 1995; Gallerano and Napoli, 2000):

$$T_{Ek} = D\sqrt{E}\ \bar{\Delta}\frac{\partial E}{\partial x_k} \tag{19}.$$

Scalar coefficient D is dynamically calculated by means of the following identity:

$$T_{Ek}^{T} - \widetilde{T_{Ek}} = -\frac{1}{2}\left(\widetilde{\bar{u}_i \bar{u}_i \bar{u}_k} - \tilde{\bar{u}}_i \tilde{\bar{u}}_i \tilde{\bar{u}}_i\right) + \widetilde{\bar{u}_k \tau(u_i, u_i)} - \tilde{\bar{u}}_k \tau^{T}(u_i, u_i) - \widetilde{\bar{u}_i \tau(u_i, u_i)} + \tilde{\bar{u}}_i \tau^{T}(u_i, u_k) - \frac{1}{\rho}\left(\widetilde{\bar{u}_k \bar{p}} - \tilde{\bar{u}}_k \tilde{\bar{p}}\right) \tag{20};$$

where symbol $\sim$ indicates the filter operation at the Test scale. Using equation (19), the left-hand side term of equation (20) takes the following form:

$$T_{Ek}^{T} - \widetilde{T_{Ek}} = D\sqrt{E^{T}}\ \tilde{\bar{\Delta}}\frac{\partial E^{T}}{\partial x_k} - D\sqrt{E}\ \bar{\Delta}\frac{\partial E}{\partial x_k} \tag{21}$$

from which the coefficient D is calculated.

The 5th term on the right-hand side of equation (17) expresses the generalized central moment related to the force density and the velocity components.

The 6th term expresses the viscous dissipation of the generalized SGS turbulent kinetic energy.

$$\varepsilon = \nu\,\tau\left(\frac{\partial u_i \partial u_i}{\partial x_j \partial x_j}\right) \tag{22}.$$

The following equation is used to model ε:

$$\varepsilon = C * E^{3/2} / L \tag{23};$$

where L is a characteristic length scale assumed to be equal to the distance from the wall. The scalar coefficient $C*$ is calculated by means of a dynamic procedure based on the following scalar equation:

$$C* E^{T\,3/2}/L - C* \widetilde{E^{3/2}/L} = \nu\left(\widetilde{\frac{\partial \bar{u}_i}{\partial x_j}\frac{\partial \bar{u}_i}{\partial x_j}} - \frac{\partial \tilde{\bar{u}}_i}{\partial x_j}\frac{\partial \tilde{\bar{u}}_i}{\partial x_j} \right) \quad (24);$$

3. RESULTS AND DISCUSSION

Turbulent channel flows (flows between two flat parallel plates placed at a distance of 2δ) have been simulated with the proposed Large Eddy Simulation model at friction-velocity-based Reynolds numbers, Re*= 1655 and 2340 (corresponding to centerline-velocity-based Reynolds numbers respectively equal to 39700 and 63200). The filtered Navier-Stokes equations, the generalized SGS turbulent kinetic and the energy balance equation are integrated on a non staggered grid with a finite volume method using a fractional step method.

Fig. 1 shows the profile of the average streamwise velocity component for a channel flow at Re* = 2340 obtained with the proposed model compared with the profile of the analogous velocity component measured experimentally. The agreement between the two velocity profiles is very good.

Fig. 2 compares the profile of the component <u¦u ¾> of the Reynolds stress tensor calculated with the proposed model with the profile of the similar component of the Reynolds tensor obtained from experimental measurements, for channel flow at Re* = 2340. Fig. 2 shows that at Re* = 2340 the proposed model provides a profile of the component <u¦u¾> in agreement with that of the corresponding component of the Reynolds stress tensor obtained from the experimental measurements.

Fig. 3 shows the time-averaged profile of the scalar $C = (2E)/L_{kk}^{m}$, for channel flow simulations at Re* = 1655 and Re* = 2340 carried out with the same calculation grid. The profile of C is similar in both cases: C has values near to two in the viscous sublayer, maximum values at the top of the buffer layer (y+ = 30) and a minimum value at the centre of the channel. Fig. 3 shows that the values of C decrease with an increase in the Reynolds number. The dimensions of the filters used are such that with an increase in the Reynolds number the kinetic energy associated with the smallest resolved scales increases at a greater rate than the kinetic energy associated with the unresolved scales. Consequently, scalar C, which is equal to the ratio between the kinetic energy associated with the unresolved scales and the kinetic energy associated with the smallest resolved scales, decreases with an increase in the Reynolds number.

Figures 4 and 5 show the profiles of the various terms of the balance equation of the generalized SGS turbulent kinetic energy E (production term: P_E ; turbulent tranport term: T_E ; convection term: C_E ; viscous diffusion term: D_E; and viscous dissipation: ε) calculated with this model and averaged over time and over homogeneous planes, for channel flows respectively at Re* =1655 and 2340. Figures 4 and 5 demonstrate that the balance between production and dissipation of generalized SGS turbulent kinetic energy is confirmed only in a limited region between the buffer layer and the log layer ($20<y^{+}<40$) whilst it is not confirmed in other regions of the domain.
The production of E is balanced in the viscous sublayer ($y^{+}<5$) by the viscous diffusion term and by the viscous dissipation of E. Moving away from the wall, in the first part of the buffer layer, the production term of E increases until it reaches its maximum value ($y^{+} \sim 10$) and the terms of turbulent transport and viscous diffusion of E are comparable with the production term of E. In the region between the buffer layer and the log layer ($20< y^{+} <40$) the convective and turbulent transport terms and the viscous diffusion terms are negligible compared with the production and dissipation terms. Only in this limited region is there a balance between the production and dissipation of E. Towards the center of the channel ($y^{+} >30$) the viscous dissipation tends towards a minimum but not negligible value. In this region the production term of E is balanced, not only by the dissipation, but also by the turbulent transport of E.

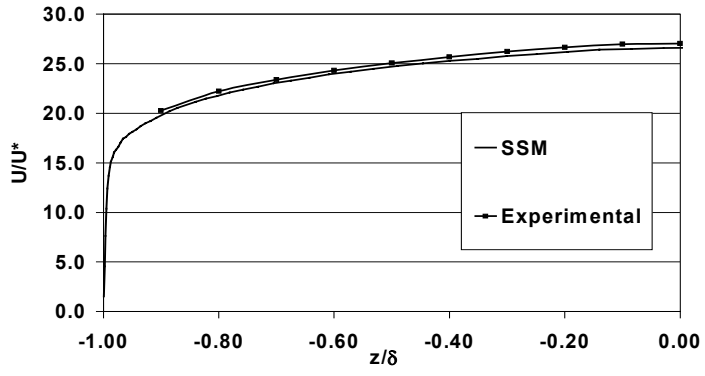

Fig. 1. Time-averaged streamwise velocities. Comparison between experimental measurements and LES results obtained with the proposed model (SSM). Channel flow, Re*=2340.

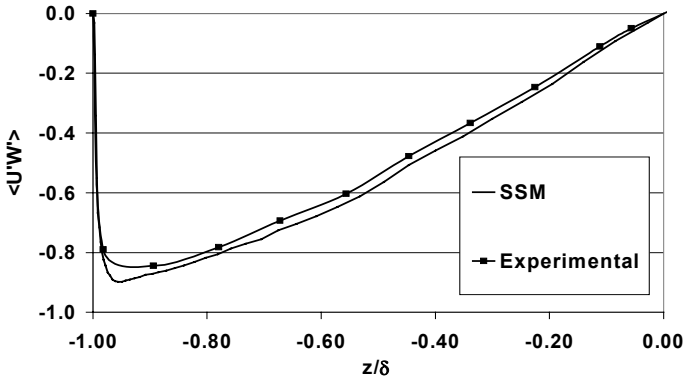

Fig. 2. Reynolds stress <U'W'>. Comparison between experimental measurements and LES results obtained with the proposed model (SSM). Channel flow, Re*=2340.

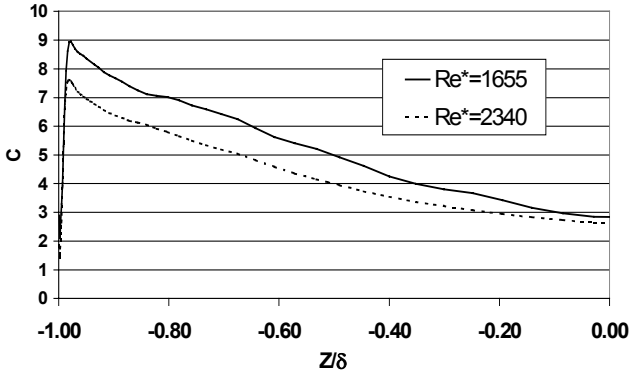

Fig. 3. Values of the coefficient C averaged over time and over homogeneous planes. Channel flow Re*=1655, 2340.

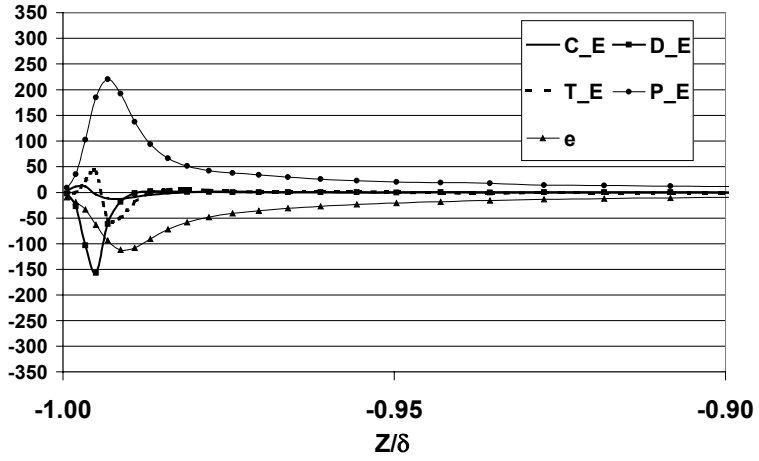

Fig. 4. Generalized SGS turbulent kinetic energy balance terms averaged over time and over homogeneous planes. Production: P_E ; Turbulent transport: T_E ; Convection: C_E ; Viscous diffusion: D_E ; Viscous dissipation: ε. Channel flow, Re*=1655.

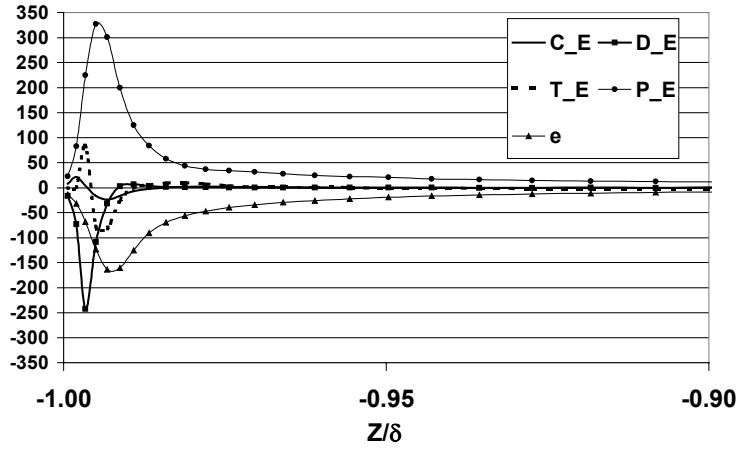

Fig. 5. Generalized SGS turbulent kinetic energy balance terms averaged over time and over homogeneous planes. Production: P_E ; Turbulent transport: T_E ; Convection: C_E ; Viscous diffusion: D_E; Viscous dissipation: ε. Channel flow, Re*=2340.

4. CONCLUSIONS

In this work it is proved that the SSMs of Bardina *et al*. and of Liu *et al*. are not dissipative enough because in the calculation of the proportionality coefficient between the SGS stress tensor and the resolved tensor, obtained by multiple filtering operations, they do not take into account the smallest unresolved scales, where most dissipation of turbulent SGS energy takes place.

In this paper a scale similarity model is presented in which the closure coefficient *C* that appears in the constitutive equation is uniquely determined without adopting Germano's dynamic procedure. Such coefficient is related exclusively to the modified Leonard tensor and the generalized SGS turbulent kinetic energy that is calculated by its balance equation. The constitutive equation at the basis of the proposed model: a) complies with the principle of material frame indifference (Truesdell, 1977); b) takes into account both the anisotropy of the turbulence velocity scales and of the turbulence length scales; c) removes any assumption of balance between the production and dissipation of turbulent kinetic energy; d) allows the use a filter whose width is not necessarily associated with the wavenumbers lying within the inertial subrange; e) guarantees an adequate energy drain from

the grid scales to the subgrid scales and guarantees backscatter; f) overcomes the inconsistencies linked to the dynamic calculation of the closure coefficient used in the modeling of the generalized SGS turbulent stress tensor.

Turbulent flows have been simulated with the proposed model between two flat and parallel plates (turbulent channel flow) at friction-velocity-based Reynolds numbers Re*= 1655 and 2340, thus obtaining results that agree with the experimental data.

5. REFERENCES

Bardina J, Ferziger JH, Reynolds WC (1983) Improved turbulence models based on large eddy simulation of homogeneous, incompressible, turbulent, flows. Ph.D. dissertation. Department of Mechanical Engeenireng, Stanford University.

Gallerano F, Napoli E (2000) Balance equation of the generalized sub-grid scale (SGS) turbulent kinetic energy in a new tensorial dynamic mixed model. Continuum Mech. Thermodyn. 19, 1-16.

Truesdell C. (1977) A first course in rational continuum mechanics. New York, San Francisco, London, Academic Press.

Gallerano F, Cannata G, Pasero E, (2002) L'equazione di trasporto degli sforzi di sottogriglia generalizzati e il terzo assioma di Noll nella large eddy simulation. 28° Convegno di idraulica e Costruzioni idrauliche.

Germano M (1986) A proposal for a redefinition of the turbulent stresses in the filtered Navier-Stokes equations. Phys. Fluids 29, 2323-2324.

Germano M, Piomelli U, Moin P, Cabot WH (1991) A dynamic subgrid scale eddy viscosity model. Phys. Fluids A3, 1760-1765.

Germano M (1992) Turbulence: the filtering approach. J. Fluid Mech. 238, 323-336.

Ghosal S, Lund TS, Moin P, Aksevoll K (1995) dynamic localization model for large-eddy simulation of turbulent flows. J. Fluid Mech. 286, 229-255.

Lilly DK (1992) A proposed modification of the Germano subgrid scale closure method. Phys. Fluids A4, 633-635.

Liu S, Meneveau C, Katz J (1994) On the properties of similarity subgrid-scale models as deduced from measurements in a turbulent jet. J Fluid Mech. 275, 83-119.

Sarghini F, Piomelli U, Balaras E (1999) Scale-similar models for large-eddy simulations. Phys. Fluids 11, 1596-1607.

Spalart PR, Speziale CG (1999) A note on constraints in turbulence modelling. J. Fluid Mech. 391, 373-376.8.

Speziale CG (1985) Galilean invariance of subgrid-scale stress models in the large-eddy simulation of turbulence. J. Fluid Mech. 156, 55-62.

The Institution of Engineers, Australia
8th National Conference on Hydraulics in Water Engineering
ANA Hotel Gold Coast, Australia 13-16 July 2004

Scale Effects in Moderate Slope Stepped Spillways Experimental Studies in Air-Water Flows

C.A. Gonzalez
B.E., M.E.
Ph.D. student, Dept of Civil Engineering, The University of Queensland, Brisbane 4072, Australia
H. Chanson
M.E., ENSHMG, INSTN, Ph.D., DEng., Eur.Ing., IEAust., IAHR
Reader, Dept of Civil Engineering, The University of Queensland, Brisbane 4072, Australia

Abstract: Air-water flow measurements were conducted in two large-size stepped chute facilities (θ = 3.4 & 16º) to study experimental distortion caused by scale effects and result extrapolation to prototypes. The stepped geometries corresponded to moderate slopes typical of embankment dams and storm waterways. Experimental data included distributions of air concentration, air-water flow velocity, bubble frequency, bubble chord length and turbulence intensity. For a Froude similitude, scale effects were observed in both facilities, although the geometric scaling ratio was only $L_r = 2$ in each case. The criterion selection for scale effects is a critical issue. In the 16º chute, major differences (i.e. scale effects) were observed in terms of bubble chord sizes and turbulence levels although little scale effects were seen in terms of void fraction and velocity distributions. The findings emphasise that physical modelling of stepped chutes based upon a Froude similitude is more sensitive to scale effects than classical smooth-invert chute studies. This is consistent with basic dimensional analysis.

Keywords: physical modelling, scale effects, stepped spillways, air entrainment, embankment dams.

1. INTRODUCTION

During the last three decades, research in the hydraulics of stepped spillways has been very active (Chanson 2001, Ohtsu and Yasuda 1998). For a given stepped chute, water flows as a succession of free-falling nappes (nappe flow regime) at small discharges. For an intermediate range of flow rates, a transition flow regime is observed. Most prototype spillways operate at large discharges per unit width (i.e. skimming flow regime) for which the waters skim as a coherent stream over the pseudo-bottom formed by step edges (Fig. 1 & 2). Skimming flows are characterised by very-significant form losses and momentum transfer from the main stream to the recirculation zones. There is an obvious analogy with skimming flows past large elements and boundary layer flows past d-type roughness: e.g., Knight and Macdonald (1979), Djenidi et al. (1999).Stepped chute hydraulics is not simple, because of different flow regimes, but most importantly because of strong flow aeration, very-strong turbulence, and interactions between entrained air and turbulence (Chanson and Toombes 2002). To date, little research was conducted at the microscopic scale on the complex nature of the flow and its physical modelling.

It is the purpose of this study to discuss similitude and scale effects affecting stepped chute flows. The analysis is supported by a series of systematic measurements conducted in two large-size facilities (θ = 3.4 and 16º) with two step sizes each. The geometric scaling ratio was $L_r = 2$ in each case. The results provide a new understanding of scale effects affecting stepped chute flows.

2. DIMENSIONAL ANALYSIS AND SIMILITUDE

2.1 Basic analysis

A dominant characteristic of stepped chute flows is the strong flow aeration ('white waters') clearly seen in prototype and laboratory (Fig. 1). Hence the relevant parameters needed for any dimensional analysis include the fluid properties and physical constants, the channel geometry and inflow conditions, the air-water flow properties including the entrained air bubble characteristics, and the geometry of the steps. Considering a skimming flow down a stepped chute with flat horizontal steps at uniform equilibrium and for a prismatic rectangular channel, a complete dimensional analysis yields a relationship between the local air-water flow properties, the fluid properties and physical constants, flow conditions, and step geometry :

$$C, \frac{V}{\sqrt{g*d}}, \frac{u'}{V}, \frac{d_{ab}}{d}, \ldots = F_1\left(\frac{x}{d}; \frac{y}{d}; \frac{q_w}{\sqrt{g*d^3}}; \rho_w * \frac{q_w}{\mu_w}; \frac{g*\mu_w^4}{\rho_w * \sigma^3}; \frac{d}{h}; \frac{W}{h}; \theta; \frac{k_s'}{h}\right) \quad (1)$$

where C is the local void fraction, V is the local velocity, g is the gravity acceleration, d is the equivalent water depth at uniform equilibrium, u' is a characteristic turbulent velocity, d_{ab} is a characteristic size of entrained bubble, x is the coordinate in the flow direction measured from a step edge, y is the distance normal from the pseudo-bottom formed by the step edges, q_w is the water discharge per unit width, ρ_w and μ_w are the water density and dynamic viscosity respectively, σ is the surface tension between air and water, W is the chute width, h is the step height, θ is the angle between the pseudo-bottom and the horizontal, and k_s' the skin roughness height (Fig. 2). For air-water flows, the equivalent clear water depth is defined as :

Fig. 1 - Skimming flow down Santa Cruz dam spillway at low overflow (Courtesy of US Bureau of Reclamation) - The 23-m wide stepped spillway is designed to accommodate the 25-year flood (57 m^3/s peak), wit larger floods passing over the dam crest - Note the splitter piers to aerate the undernappe (dam height: 46 m)

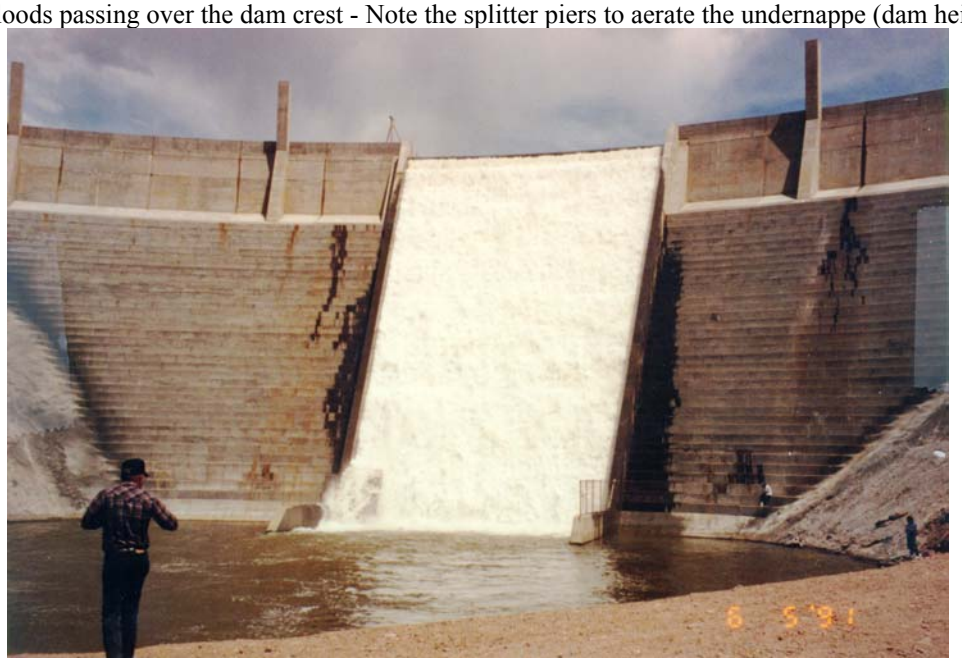

Fig. 2 - Skimming flow over a stepped chute : definition sketch

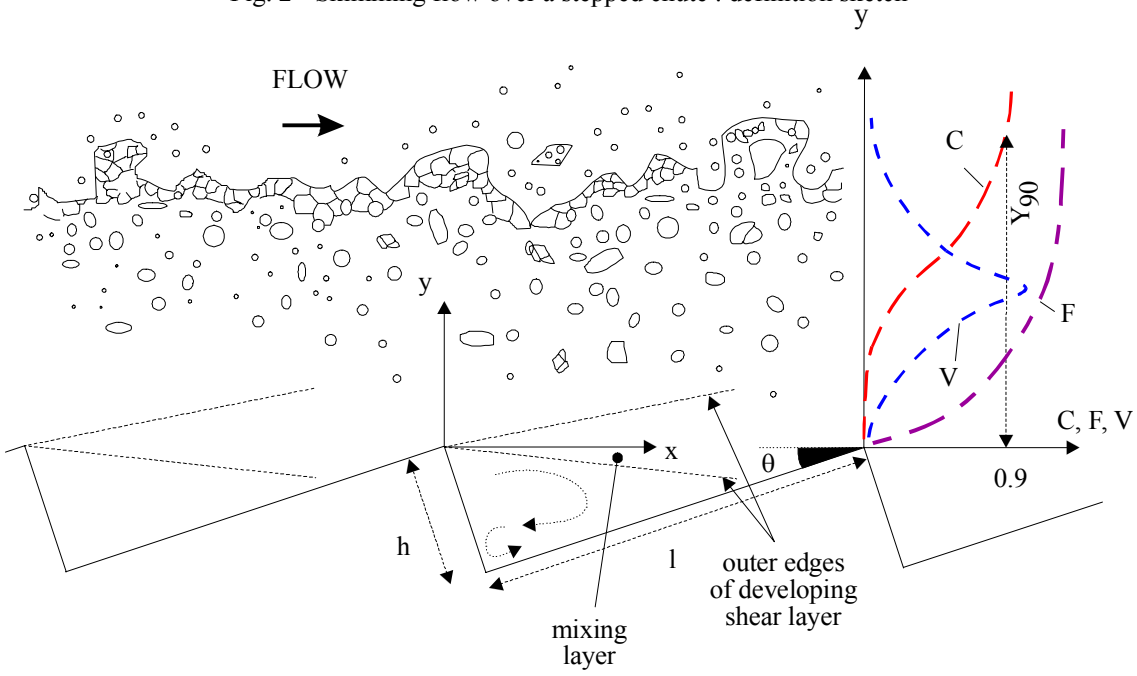

$$d = \int_{y=0}^{y=Y_{90}} (1 - C) * dy \quad (2)$$

where Y_{90} is the depth where C = 0.9. In Equation (1) right handside, the 3rd, 4th and 5th dimensionless terms are Froude, Reynolds and Morton numbers respectively, and the last four terms characterise the step cavity shape and the skin friction effects on the cavity wall. Note that any combination of dimensionless numbers is also dimensionless. One parameter among the Froude, Reynolds and Weber numbers can be replaced by the Morton number $Mo = (g*\mu_w^4)/(\rho_w*\sigma^3)$ as seen in Equation (1) where the Weber number was replaced. Further simplifications may be derived by considering the depth-averaged air-water flow properties. For a skimming flow at uniform equilibrium, Equations (1) yields :

$$F_2\left(\frac{U_w}{\sqrt{g * d}}; \rho_w \frac{U_w * d}{\mu_w}; \frac{g * \mu_w^4}{\rho_w * \sigma^3}; C_{mean}; \frac{d}{h}; \frac{W}{h}; \theta; \frac{k_s'}{h}\right) = 0 \quad (3)$$

where U_W is the mean flow velocity ($U_W = q_W/d$) and C_{mean} is the depth-averaged void fraction:

$$C_{mean} = \frac{1}{Y_{90}} * \int_{y=0}^{y=Y_{90}} C * dy \quad (4)$$

Despite very simplistic assumptions, Equation (1), and even Equation (3), demonstrate that dynamic similarity of stepped chute flows is impossible with geometrically similar models, unless working at full-scale, because of the large number of relevant parameters. In free-surface flows, most laboratory studies are based upon a Froude similitude (e.g. Henderson 1966, Chanson 2004). But cavity recirculation and momentum exchanges between cavity and stream flow are dominated by viscous effects suggesting the need for a Reynolds similitude. If L_r is the geometric scaling ratio defined as the ratio of prototype to model dimensions, it is impossible to satisfy simultaneously Froude and Reynolds similarities unless $L_r = 1$, and significant scale effects are expected on small size models ($L_r >> 1$). Usually the same fluids (air and water) are used in model and prototype, and the Morton number becomes an invariant.

Table 1. Summary of systematic studies on stepped chutes based upon a Froude similitude

Study (1)	Definition of scale effects (2)	Limiting conditions to avoid scale effects (3)	Experimental flow conditions (4)
BaCaRa (1991)	Flow resistance & energy dissipation	$L_r < 25$	Model studies: θ = 53.1º, h = 0.06, 0.028, 0.024, 0.014 m L_r = 10, 21.3, 25, 42.7
Boes (2000)	Void fraction & velocity distributions	Re > 1E+5	Model studies: θ = 30 & 50º, W = 0.5 m, h = 0.023 to 0.093 m L_r = 6.6, 13, 26 (30º) / 6.5, 20 (50º)
Chanson et al. (2002)	Flow resistance	Re > 1E+5 h > 0.02 m	Prototype & model studies θ = 5 to 50º, W = 0.2 to 15 m, h = 0.005 to 0.3 m, 3E+4 < Re < 2E+8, 32 < We < 6.5 E+6
Present study	Void fraction & bubble count rate distributions	$L_r < 2$	θ = 3.4º, W = 0.5 m, h = 0.143, 0.0715 m, 2.4 E+5 < Re < 6 E+5 L_r = 1, 2
	Void fraction, bubble count rate, velocity & turbulence level distributions, Bubble sizes & clustering	$L_r < 2$	θ = 16º, W = 1 m, h = 0.10, 0.05 m, 1.2E+5 < Re < 1.2 E+6 L_r = 1, 2

Notes : D_H : hydraulic diameter; L_r : geometric scaling ratio; $Re = V*D_H/\nu_W$; $We = \rho_W*V^2*d/\sigma$.

2.2 Discussion

Few studies tested systematically the validity of a Froude similitude with geometric similarity using same fluids in model and prototype (Table 1). BaCaRa (1991) described a systematic laboratory investigation of the M'Bali

dam spillway with model scales of L_r = 10, 21.3, 25 and 42.7. For the smallest models (L_r = 25 & 42.7), the flow resistance was improperly reproduced. Chanson et al. (2002) re-analysed more than 38 model studies and 4 prototype investigations with channel slopes ranging from 5.7º up to 55º, with Reynolds numbers between 3 E+4 and 2 E+8. They concluded that physical modelling of flow resistance may be conducted based upon a Froude similitude if laboratory flow conditions satisfy h > 0.020 m and Re > 1E+5. They added that true similarity of air entrainment was achieved only for model scales L_r < 10. However detailed studies of local air-water flow properties yielded more stringent conditions suggesting the impossibility to achieve dynamic similarity, even in large-size models (Table 1). In the present study, a Froude similitude was used as for most open channel flow studies and past studies.

3. EXPERIMENTAL SETUP

Experiments were performed in two facilities with flat horizontal steps (Table 2). The first channel was 24 m long 0.5 m wide with a 3.4º slope. Two step sizes were used : h = 0.143 and 0.0715 m. In both cases, the first drop was located 2.4 m downstream of a smooth nozzle (d_n = 0.03 m), and the channel invert, upstream of the vertical drop, was flat and horizontal for all experiments. Water was supplied by a pump, with a variable-speed electronic controller (Taian™ T-verter K1-420-M3 adjustable frequency AC motor drive), enabling an accurate discharge adjustment in a closed-circuit system. The flow rates were measured with a Dall™ tube flowmeter, calibrated on site. The accuracy of the discharge measurement was approximately 2%. The second channel was 1 m wide with a 15.9º slope. It consisted of a broad-crest followed by nine identical steps (h = 0.1 and 0.05 m). The flow rate was delivered by a pump controlled with an adjustable frequency AC motor drive, enabling an accurate discharge adjustment in a closed-circuit system. The discharge was measured from the upstream head above crest with an accuracy of about 2%, after complete calibration on the crest profile site.

Air-water flow properties were measured using a single-tip resistivity probe (∅ = 0.35 mm) in Channel 1 and a double-tip probe (∅ = 0.025 mm) in Channel 2. Both probes were developed at the University of Queensland and excited by an air bubble detector (AS25240). The probe signal was scanned at 5 kHz for 60 to 180 s in Channel 1, and at 20 kHz per sensor for 20 s in Channel 2. The probe signal outputs were post-processed using the method outlined by Chanson (2002) and Chanson and Toombes (2002). The translation of the probes in the direction normal to the channel invert was controlled by a fine adjustment travelling mechanism connected to a MitutoyoTM digimatic scale unit (Ref. No. 572-503). The error on the vertical position of the probe was less than 0.025 mm. Flow visualisations were conducted with a digital video-camera and high-speed still photographs.

Table 2. Summary of experimental flow conditions

Reference	θ deg.	q_W m^2/s	h m	d_c/h	Flow regime	Instrumentation	Remarks
(1)	(2)	(3)	(4)	(5)	(6)	(7)	(8)
Channel 1	3.4	0.150	0.143	0.92	Transition flow	Single-tip conductivity probe (∅ = 0.35 mm).	L = 24 m. W = 0.5 m. Inflow: pressurised intake. Experiment CR98.
		0.06	0.0715	1.0			Experiment EV200.
		0.08		1.2			
Channel 2	15.9	0.075 to 0.220	0.10	0.85 to 1.7	Transition & Skimming flows	Double-tip conductivity probe (∅ = 0.025 mm).	L = 4.2 m. W = 1 m. Inflow: uncontrolled broad-crest.
		0.020 to 0.08	0.05				

Notes : L : chute length; W : chute width.

4. EXPERIMENTAL RESULTS

4.1 Basic results

Detailed measurements of void fraction and air-water flow properties were conducted for a number of dimensionless flow rates d_c/h. Identical experiments were repeated with two step sizes in each Channel based upon a Froude similitude (Table 2). Systematic comparisons were performed. Overall the results showed that the distributions of air concentration were properly scaled with a Froude similitude, for the investigated flow conditions (Table 2). This is illustrated in Figures 3 and 4A for Channel 1 and 2 respectively, showing

dimensionless distributions of void fraction C. In addition, the void fraction distributions are compared with an analytical solution of the advection diffusion equation for air bubbles (Chanson and Toombes 2002).

Good agreement was observed also in terms of dimensionless distributions of velocity, as well as in terms of mean air content C_{mean}, dimensionless flow velocity U_w/V_c and air-water flow velocity V_{90}/V_c, where V_{90} is the air-water flow velocity at $y = Y_{90}$ and Y_{90} is the characteristic depth where C = 0.90 (Fig. 3 and 4A). However significant differences, hence scale effects, were observed in terms of dimensionless distributions of bubble count rates F^*d_c/V_c and of turbulence intensity Tu as functions of y/d_c where F is the bubble count rate defined as the number of bubbles impacting the probe per second, and d_c and V_c are the critical flow depth and velocity respectively. In both Channels 1 and 2, lesser dimensionless bubble count rates by about 30 to 50% were observed with the smallest step heights : i.e., h = 0.0715 and 0.05 m for θ = 3.4 and 15.9º respectively. This is illustrated in Figures 3 and 4B, and the finding implies significant scale effects in terms of number of entrained bubbles and bubble sizes. In Channel 2, differences in turbulence intensity distributions were consistently observed, with lesser maximum turbulence levels for the smallest step height (h = 0.05 m). This is well illustrated in Figure 4B. Further, in Channel 2, a comparative analysis of bubble chord size distributions, for similar flow rate, identical location and local void fraction, showed consistently differences between the two step heights : entrained bubbles were comparatively larger for the smallest model (Fig. 5A). Figure 5 compares dimensionless bubble and droplet chord sizes ch/d_c recorded at the same dimensionless distance from the inception point and for the same dimensionless flow rate with two step heights (h = 0.1 and 0.05 m). Figure 5A shows dimensionless bubble chord distributions for C = 0.1. Figure 5B presents dimensionless droplet chord distributions for C = 0.96, at the same locations as in Figure 5A for the two step heights. Basically entrained bubble sizes were not scaled at 2:1 (Fig. 5A). A similar observations was made in terms of water droplet size distributions in the spray region (Fig. 5B). In dimensional terms, the size distributions of the smallest bubbles and droplets were about the same for both step heights, but a broader range of large particles were seen with the largest step height (h = 0.1 m).

Overall the results demonstrated significant scale effects in terms of bubble and droplet size distributions that were not approximated properly by a Froude similitude.

Fig. 3 - Comparison of dimensionless distributions of void fraction C and bubble count rate F^*d_c/V_c in Channel 1 (θ = 3.4º, $d_c/h \sim 1$) for h = 0.143 and 0.0715 m - Step 9, x/l = 1 (step brink)

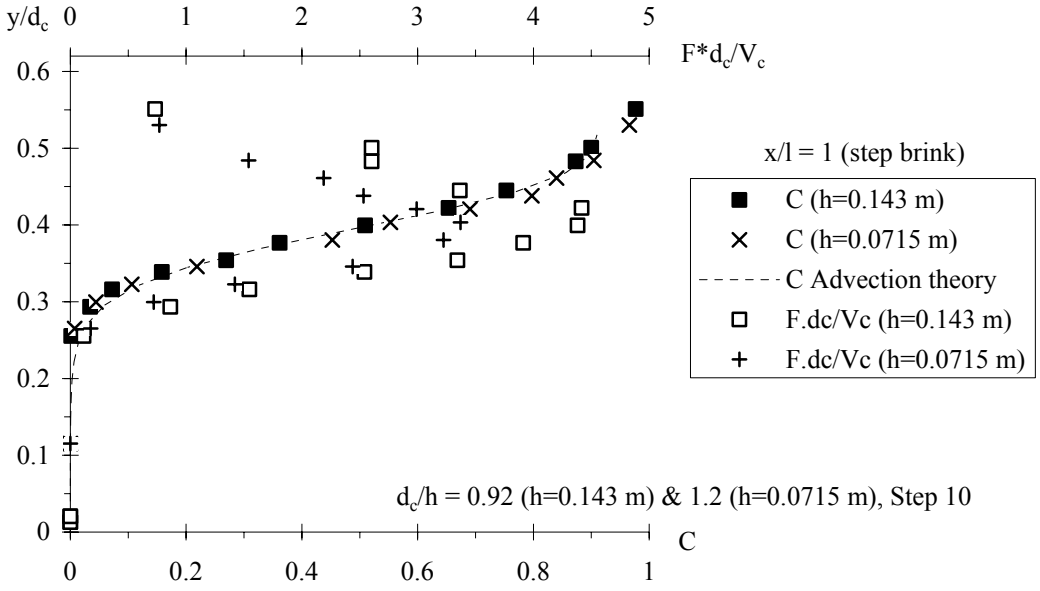

4.2 Discussion

A basic result is the lesser number of entrained bubbles and comparatively greater bubble sizes observed in the smallest flumes, as well as lower turbulence levels. The findings have direct implications on the flow structure and the interactions between turbulence and entrained bubbles. Chanson and Toombes (2002) demonstrated that the air-water flow turbulence level was a function of bubble count rate : $Tu \propto F^{1.5}$. Lesser turbulence levels in small laboratory flumes must imply lesser rate of energy dissipation, particularly on long chutes. That is, small-

size models are likely to underestimate the rate of energy dissipation of prototype stepped spillways for similar flow conditions. Similarly, the lesser number of entrained bubble sizes in laboratory flumes must affect the rate of air-water mass transfer on the chute. Present results imply that the air-water interface area, hence the rate of air-water mass transfer, are underestimated in small-size physical-models, and extrapolation are not reliable.

Fig. 4 - Comparison of dimensionless distributions of void fraction C, bubble count rate F^*d_c/V_c, velocity V/V_c and turbulence intensity Tu in Channel 2 (θ = 15.9°, d_c/h = 1.5) for h = 0.10 and 0.05 m at 3 step edges downstream of the inception of free-surface aeration

(A) Dimensionless distributions of void fraction C and velocity V/V_c

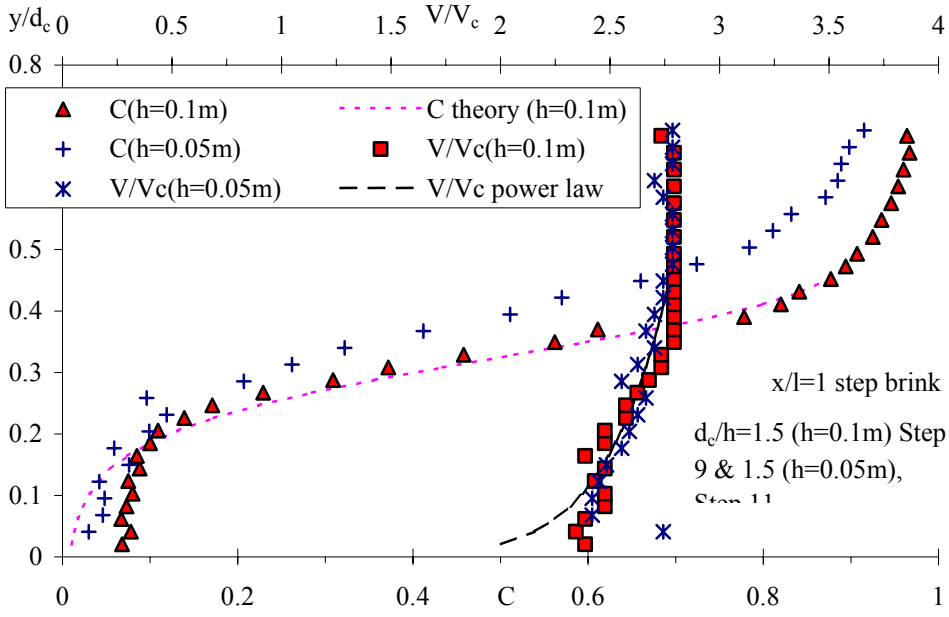

(B) Dimensionless distributions of bubble count rate F^*d_c/V_c and turbulence intensity Tu

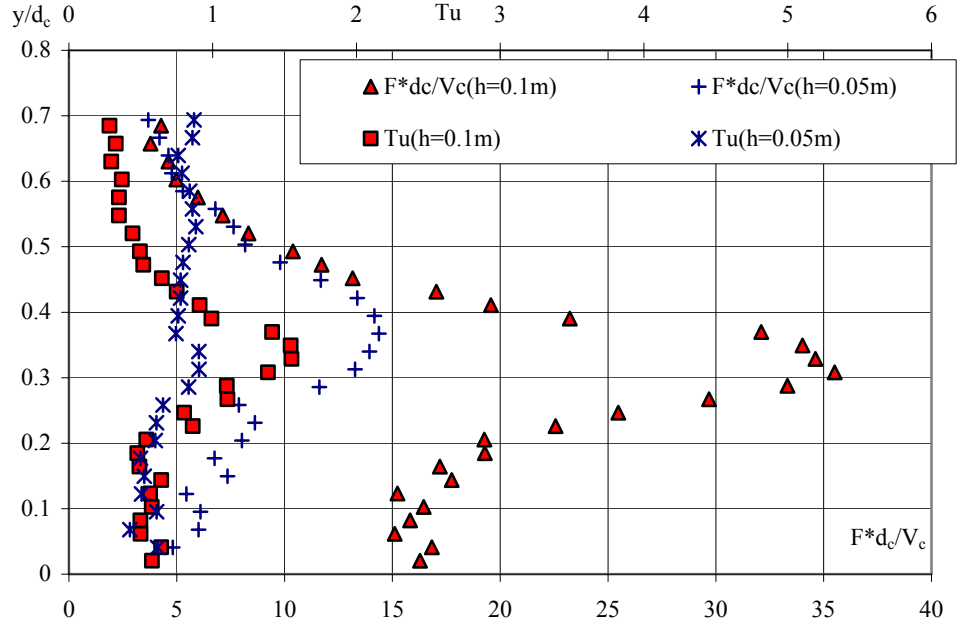

Fig. 5 - Comparison of dimensionless bubble and droplet chord size ch/d_c distributions in Channel 2 (θ = 15.9º, d_c/h = 1.5) for h = 0.10 and 0.05 m at step edges 9 and 14 respectively
(A) Bubble chord size distributions for C = 0.1

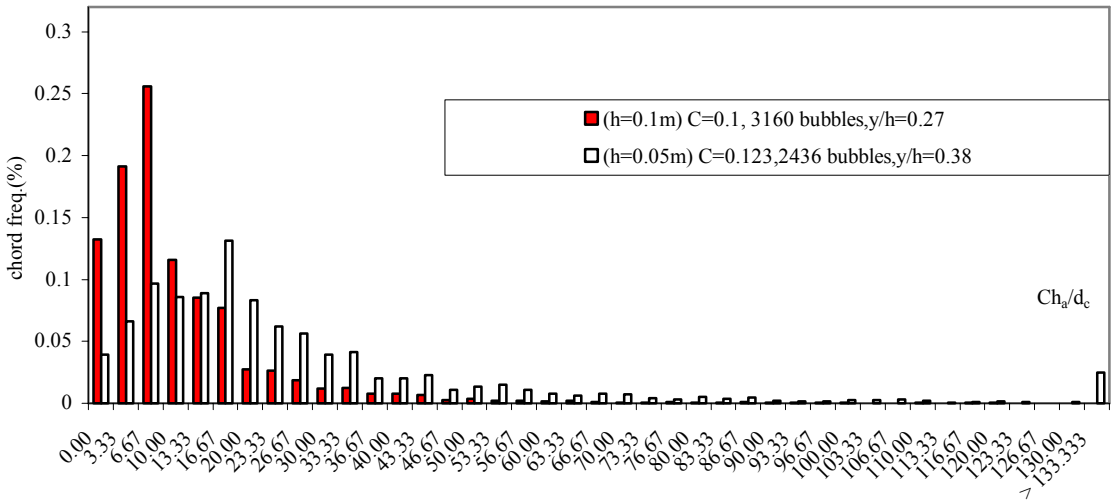

(B) Droplet chord size distributions for C = 0.96

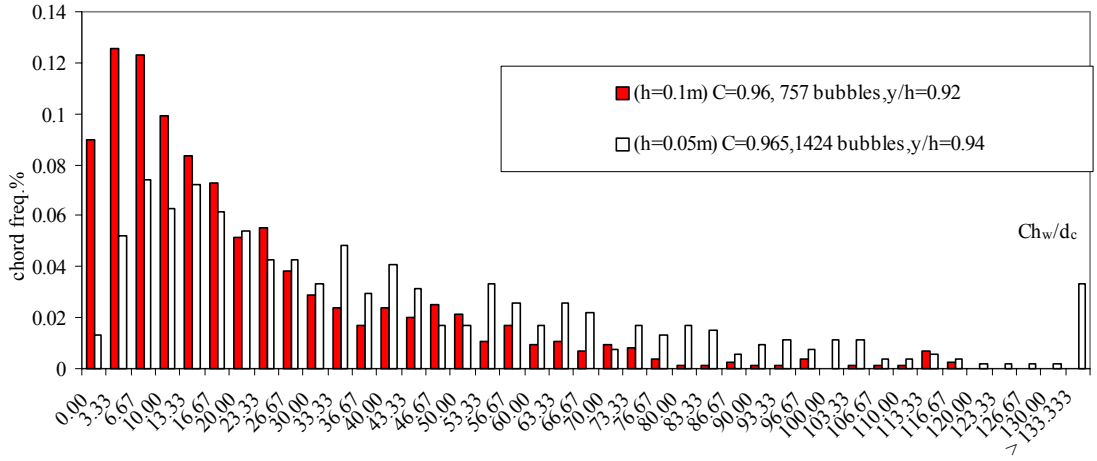

5. SUMMARY AND CONCLUSION

The study of stepped chute hydraulics is still based primarily upon physical modelling. It is understood that stepped chute hydraulics is complex because of different flow regimes, strong flow aeration, and interactions between entrained air and turbulence. A complete dimensional analysis yields two basic equations (1) and (3) corresponding respectively to two-dimensional and one-dimensional air-water flows. The analysis emphasises the complexity of stepped chute hydrodynamics, and the limitations of the Froude similitude. Systematic studies of scale effects affecting stepped chute flows are few and the results are sometimes contradictory.

New experimental works were conducted with two slopes (θ = 3.4 & 16º) and two large step sizes for each large-size facility. Identical experiments were performed based upon a Froude similitude with geometrically similar channel configurations. A geometric scaling ratio L_r = 2 was selected for both invert slopes (θ = 3.4 & 16º). Significant scale effects were observed in terms of distributions of bubble count rates, turbulence intensity and bubble/droplet chord sizes. Basically the number of entrained bubble sizes and turbulence levels were drastically underestimated with the smallest step sizes. Further it is demonstrated that the selection of the basic criterion to define scale effects is critical : e.g., flow resistance, air concentration distributions, or turbulence levels.

It is believed that the new results are the first systematic study of scale effects in air-water flows at microscopic scales. The results emphasise that physical modelling of stepped chutes is more sensitive to scale effects than classical smooth-invert chute studies, and this is consistent with basic dimensional analysis. While the findings

were obtained for two moderate slopes (θ = 3.4 & 16º), it is thought that the outcomes are valid for a wider range of chute geometry and flow conditions.

6. ACKNOWLEDGMENTS

The writers acknowledge the assistance of Mr Graham Illidge and Dr L. Toombes. The first writer acknowledges the financial support of the National Council for Science and Technology of Mexico (CONACYT). The second author acknowledges the assistance of his students L. Rowlands, M. Condon, M. Eastman and N. Van Schagen.

7. REFERENCES

BaCaRa (1991). "Etude de la Dissipation d'Energie sur les Evacuateurs à Marches." ('Study of the Energy Dissipation on Stepped Spillways.') *Rapport d'Essais*, Projet National BaCaRa, CEMAGREF-SCP, Aix-en-Provence, France, Oct., 111 pages (in French).

Boes, R.M. (2000). "Zweiphasenstroömung und Energieumsetzung an Grosskaskaden." ('Two-Phase Flow and Energy Dissipation on Cascades.') *Ph.D. thesis*, VAW-ETH, Zürich, Switzerland (in German). (also *Mitteilungen der Versuchsanstalt fur Wasserbau, Hydrologie und Glaziologie*, ETH-Zurich, Switzerland, No. 166).

Chanson, H. (2001). "The Hydraulics of Stepped Chutes and Spillways." *Balkema*, Lisse, The Netherlands, 418 pages. {http://www.uq.edu.au/~e2hchans/reprints/book4.htm}

Chanson, H. (2002). "Air-Water Flow Measurements with Intrusive Phase-Detection Probes. Can we Improve their Interpretation ?." *Jl of Hyd. Engrg.*, ASCE, Vol. 128, No. 3, pp. 252-255.

Chanson, H. (2004). "The Hydraulics of Open Channel Flows : An Introduction." *Butterworth-Heinemann*, Oxford, UK, 2nd edition. {http://www.uq.edu.au/~e2hchans/reprints/book3_2.htm}

Chanson, H., and Toombes, L. (2002). "Air-Water Flows down Stepped chutes : Turbulence and Flow Structure Observations." *Intl Jl of Multiphase Flow*, Vol. 27, No. 11, pp. 1737-1761.

Chanson, H., Yasuda, Y., and Ohtsu, I. (2002). "Flow Resistance in Skimming Flows and its Modelling." *Can Jl of Civ. Eng.*, Vol. 29, No. 6, pp. 809-819.

Djenidi, L., Elavarasan, R., and Antonia, R.A. (1999). "The Turbulent Boundary Layer over Transverse Square Cavities." *Jl Fluid Mech.*, Vol. 395, pp. 271-294.

Henderson, F.M. (1966). "Open Channel Flow." *MacMillan Company*, New York, USA.

Knight, D.W., and Macdonald, J.A. (1979). "Hydraulic Resistance of Artificial Strip Roughness." *Jl of Hyd. Div.*, ASCE, Vol. 105, No. HY6, June, pp. 675-690.

Ohtsu, I., and Yasuda, Y. (1998). "Hydraulic Characteristics of Stepped Channel Flows." *Workshop on Flow Characteristics around Hydraulic Structures and River Environment*, University Research Center, Nihon University, Tokyo, Japan, November, Edited by I. Ohtsu and Y. Yasuda, 55 pages.

The Institution of Engineers, Australia
8th National Conference on Hydraulics in Water Engineering
ANA Hotel Gold Coast, Australia 13-16 July 2004

Hydrodynamic Modelling of the Lower Mekong River and Delta for Basin Planning

Dr Richard Harpin
Director, Halcrow, UK
Dr Jon Wicks
Associate Director, Halcrow, UK
Tony Green
Principal Engineer, JBA Consulting, UK
Dr Trinh Hoa
Professor, Hanoi University, Vietnam
Nguyen Xuan Hien
Deputy Director, Sub Institute of Water Resources Planning, HCM, Vietnam

Abstract: Halcrow has been involved for the last three years in developing a hydrodynamic model of the Lower Mekong river including the Great Lake in Cambodia and the delta in Vietnam. The model has been built as part of a decision support system intended for use by the four members countries of the Lower Mekong Basin: Thailand, Vietnam, Cambodia and Laos PDR. The system is designed to be used as a mechanism for the four countries agreeing on the basin development plan and in setting rules for water utilisation, with the Mekong River Commission acting as a "clearing house". The paper explains the background and context of the model and how it fits into a Decision Support Framework. It then outlines the issues in developing a hydrodynamic model of a highly complex system to be used for planning purposes with some model runs to span 15 years so that statistical analysis can be undertaken to feed into a variety of socio-economic and environmental impacts. The paper presents details of the model and its calibration together with some of the results and examples of impact assessments.

Keywords: Mekong, Hydrodynamic Model, Basin Modelling, Flood Simulation, Salinity, Impact Assessment,

1. BACKGROUND AND CONTEXT OF THE MODEL

1.1 The Water Utilisation Programme Start-Up Project

The development and wide availability of ever more powerful personal computers and modern user friendly interfaces for hydrodynamic models has enabled comprehensive developments in the integration of models and GIS based results processing for a wide user base that would not have been possible or even contemplated previously. For the Mekong River Commission (MRC) a system has been developed that encompasses the data storage and handling for three complementary models covering the hydrological and hydraulic processes of the whole Lower Mekong Basin, which in turn are integrated within a user orientated environment for testing and assessing impacts of developments and interventions in terms of flooding, water shortage and environmental impacts.

The models used within the system are SWAT (from USDA) for runoff processes, IQQM (from DLWC) for system simulation upstream of the delta and ISIS (from Halcrow and Wallingford Software) for hydrodynamic and water quality modelling (especially salinity) for the Mekong floodplain and delta in Cambodia and Vietnam. The system has been developed as part of the Water Utilisation Programme (WUP), which is intended to help the Mekong River Commission member states to implement key elements of the 1995 Mekong Agreement. It will provide the technical and institutional capacities required for longer-term co-operation for sustainable management of the basin's water and ecological resources. There are three components to the WUP Start-up Project:

A Basin Modelling and Knowledge Base
B "Rules" for Water Utilisation
C Institutional Strengthening and Capacity Building

1.2 The Basin Modelling and Knowledge Base Development Sub-Project

The Basin Modelling and Knowledge Base Development Sub-Project (WUP-A) is being undertaken by Halcrow Group Ltd for the MRC under Component A of the WUP. An important outcome of this project is a Decision

Support Framework (DSF), which contains a Knowledge Base, a Basin Modelling Package and Impact Analysis Tools. The DSF was written specifically for the MRC by Halcrow as part of the project.

Now completed, the WUP DSF is to be used to assist in developing rules for water sharing amongst the four riparian countries in the Mekong River Commission (MRC) and to support decision making for basin planning and management through assessment of the environmental and socio-economic impacts of development options.

1.3 Requirements Of The 1995 Mekong Agreement

The process for Basin Development Planning draws its mandate from and must be guided by the 1995 Agreement signed by each of the four Governments[1]. The Agreement prescribes a number of conditions that need to be followed in planning and managing the water and related resources of the Mekong River Basin. Key aspects of the Agreement relevant to the planning process and to the DSF are highlighted below.

Objectives: The key phrases in the Agreement refer to cooperation in a manner that optimises multiple-use and mutual benefits of all riparians and develops the full potential of the basin. Emphasis and preference are to be placed on joint and/or basin-wide development, whilst protecting the environment from harmful effects due to the use of water and related resources. The basin development plan should prioritise projects and programmes to implement at basin level.

Definitions: These make clear that the Basin Development Plan is viewed as a general planning tool and process to prioritise projects and programmes and that a proposed use relates to any definite use proposed by a Riparian, excluding domestic and minor uses of water not having a significant impact on mainstream flows.

Principles: Each Riparian should utilise the Mekong River system in a reasonable and equitable manner in their respective territories, subject to rules and provisions.

Rules: The Rules for Water Utilisation and Inter-Basin Diversions will prescribe inter alia the definitions of wet and dry seasons (which, as shown below, affect how the terms of the Agreement are implemented), the minimum flow level requirements and the means by which these are measured, and the criteria by which water is judged to be surplus to requirements during the dry season on the mainstream. The Agreement also obliges the countries to cooperate in maintaining in the mainstream to enable acceptable natural reverse flow to Tonle Sap during the wet season and to prevent average daily flows greater than those naturally occurring on average.

Provisions: The provisions for water utilisation are different for the tributaries and the mainstream. On the tributaries, intra-basin and inter-basin diversions are subject to notification, whereas on the mainstream in the wet season only intra-basin use is subject to notification and inter-basin diversion is subject to prior consultation. In the dry season on the mainstream, more stringent provisions are made such that intra-basin use is to be subject to prior consultation and inter-basin diversion is subject to specific agreements, or if there is an agreed and confirmed surplus of flow, with prior consultation.

Environment and Other Provisions: Riparians are obliged to make every effort to avoid, minimise and mitigate harmful environmental effects, and must cease immediately an activity that is alleged to be causing substantial damage to another, until such time as the matter is resolved. Also, navigation in the mainstream is to be protected.

Institutional Requirements: The Agreement vests authority for all decisions relating to implementation of the Agreement in the four-member Council, with day-to-day executive powers delegated to a Joint Committee.

[1] Agreement on the Co-operation for the Sustainable Development of the Mekong River Basin, signed in Chiang Rai, Thailand on 5th April 1995 between the Governments of the Kingdom of Cambodia, the Lao People's Democratic Republic, the Kingdom of Thailand and the Socialist Republic of Viet Nam.

2. DEVELOPMENT OF THE HYDRODYNAMIC MODEL COMPONENT

2.1 Distinguishing Features of Mekong Delta

The Mekong delta has a number of unique distinguishing features that create a challenging task for the development of a comprehensive hydrodynamic model:

- A large proportion of the delta is liable to inundation for long periods of time affecting a significant proportion of the populated land area of Cambodia and South Vietnam.
- High out of bank flows occur such that peak flood flows in the mainstream are reduced downstream (Figure 1).
- Significant flows in the Mekong and the total inflow from the Tonle Sap Basin in Cambodia is stored within the Great Lake at the height of the monsoon period resulting in a reversal of flow of the Tonle Sap River at Phnom Penh twice yearly.
- Tides of around 2.5m amplitude at the mouths of the Mekong that interact during floods and low flow with the very low lying land within Vietnam.
- Numerous major and minor canals distribute water to the one of the productive agricultural and fisheries areas of the world.
- Saline intrusion and gates to control salinity intrusion.
- Low embankments and major roads affecting distribution of flood flows.
- Floodwater runs through and is stored on the higher ground of the Cambodian floodplain but at a critical stage in a large flood it rapidly floods across the border into Vietnam through a number of paths causing widespread overtopping of local banks protecting land from flooding (Figure 2).

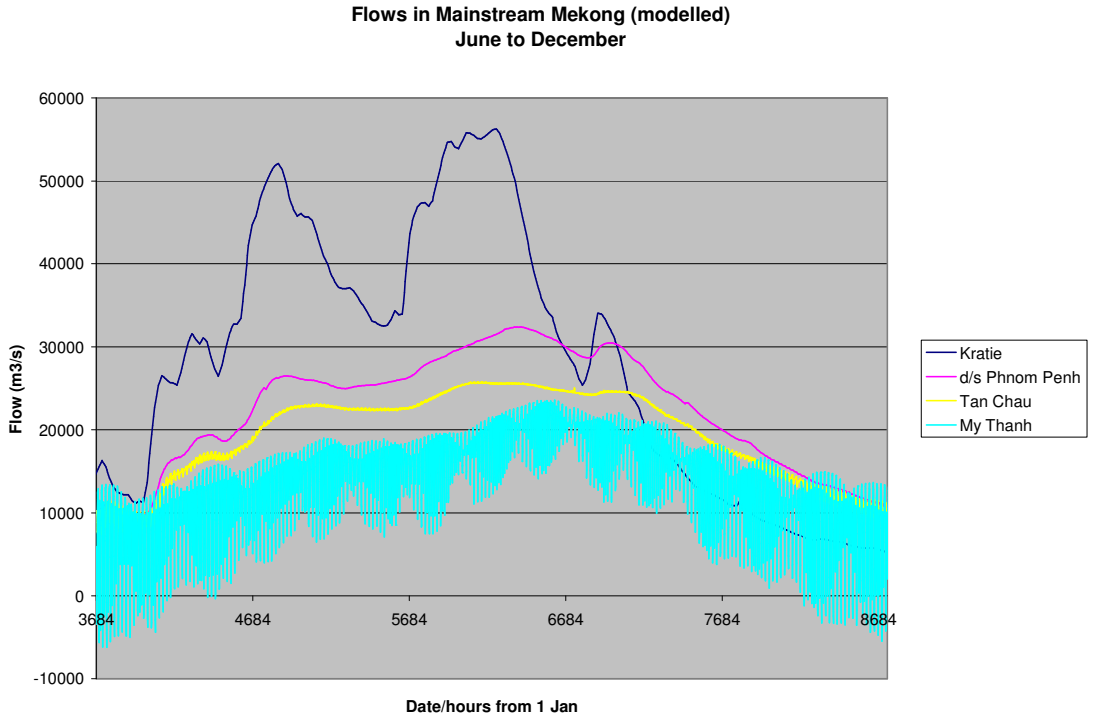

Figure 1 - Attenuation and Alternative Flood Routes Change the Flow Significantly in the Mekong Mainstream (448km, 346km, 235km and 127km from sea)

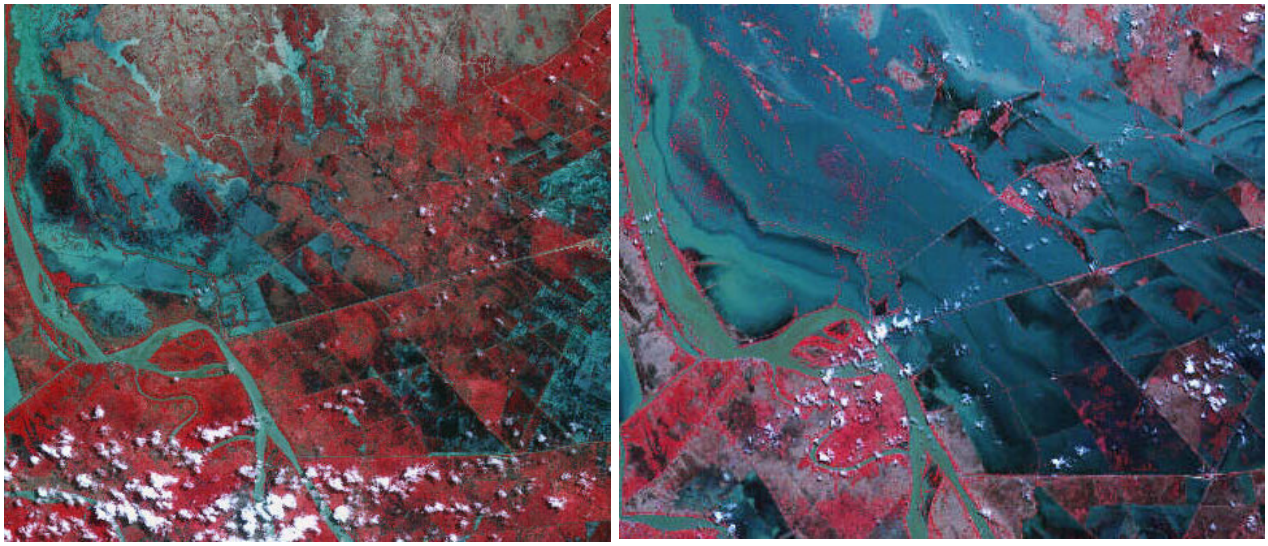

Figure 2 - Satellite Imagery Showing Onset of Flooding 20 July 2000 and Progress of Flood 10 Days Later

2.2 Model Selection

Selection of the three components of the overall modelling package for use by MRCS and each member State was based on a number of criteria. Thesefall into three main categories: Technical, User Friendliness and Synergy, and Sustainability:

Eight hydrodynamic modelling programs were reviewed, as listed on the right. Four were excluded on technical criteria, generally related to absence of sediment transport and/or water quality modules. SAL is technically of a high standard, but the interfaces are based on text files and the programme would not be easy to use.

Hydrodynamic Models Conmsidered	Technical	User Friendliness	Sustainabilty
HEC-RAS/UNET	❖	❑	❖
HYDROGIS	❖	❑	❑
ISIS	■	■	■
KOD	❖	❑	❑
Mike 11	■	❑	❑
SAL	❑	❖	❑
Sobek-River	■	❑	❑
VRSAP	❖	❑	❑

Legend: ■ *Fully complies*
❑ *Some reservations*
❖ *Major shortcomings*

The main candidates were iSIS, Mike-11 and possibly Sobek. Both Sobek and Mike 11 comply with the specifications and are widely used. However, neither had a comparative advantage over iSIS, which the Consultants proposed to use in their contract bid. The specific advantage to MRCS and the member States of adopting iSIS over these other programmes was that, with the ready access to and familiarity with the source code, the Consultants, being joint owners of iSIS were in the best position to tailor the model to the needs of all parties and to integrate the hydrodynamic model seamlessly with the other models and the Knowledge Base. Specific features of iSIS include:

- It is user-friendly with a well developed Windows based interface
- It models backwater influences
- It includes flood plain processes including convergence and divergence of flow at various points along the river system.
- It represents a wide variety of water quality components and their interactions
- It models of tidal influences.
- It includes saline intrusion
- It includes erosion, deposition and sediment transport
- It has modules to enable output of inundation depth-duration-frequency relations.
- It can provide primary data for development of Impact Analysis Indicators

2.3 Requirements for the Model

The hydrodynamic model is not required solely for use by experts for a flood study as might be a typical use of a hydrodynamic model - it is a tool developed and maintained at the MRC but in use at a number of sites in the four riparian countries by users of different experience for:

- Simulation of flood regimes - for example, assessing changes due to dam construction upstream for which typical years or long term simulations may be carried out and compared with the base case
- Simulation of changes in saline intrusion
- Providing outputs for impact assessment tools including making use of GIS for spatial analyses

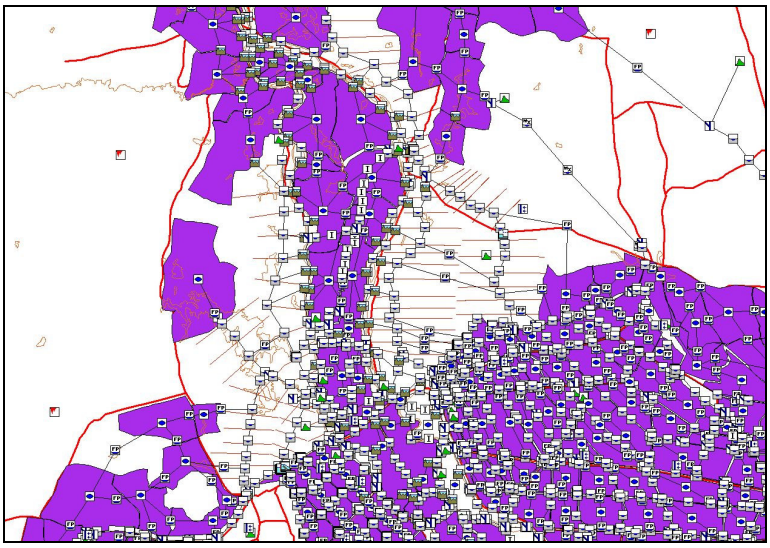

Figure 3 – Example Schematisation

For practical use there is a limit on the times taken for simulations, which places a limit on the spatial complexity of the model that can be used, balanced against the need to represent the system adequately for planning purposes. Extensive discussions and tests on levels of schematisation detail were carried out and agreement with the parties was obtained on a relatively complex model with around 5000 nodes comprising major rivers, canals and flood storage and conveyance. The node location diagram for the part of the network downstream of Phnom Penh is shown in Figure 3, which illustrates the complexity of the model.

2.4 Data Inputs and Model Calibration

In a hydrodynamic model the bulk of the data used relates to physical data such as river sections, banks or fields. The ISIS model was built up using GIS processing to extract data from digital models of the terrain and bathymetry derived from existing data sets within the MRC. Some data were also extracted from the existing VRSAP model used in Vietnam. The geographical location of the model nodes were integrated within the model, thus facilitating future updating of the model and enabling the model outputs to directly link into spatial tools for analysis of results. For example the soundings of river depth from the hydrographic atlas of the major rivers in Vietnam and Cambodia were combined with land surveys of banks and ground levels to create a digital terrain model within the ESRI ArcView environment. River sections, embankments and flood storage units could then be abstracted directly into the model input data. Where river sections were not available in such a form, for example for smaller canals, the centre of each section was registered to the same coordinate system enabling direct comparison with satellite data on flood extent for example.

The model calibration stage covered both flooding and low flows for 2000 as a calibration year and 2001 and 1998 as verification events. The model was calibrated for 31 permanent water level stations on the mainstream and floodplain, and 5 permanent flow gauging stations. The calibration was assessed using threshold parameters indicating the goodness of fit to the field data for wet and dry seasons and year round statistics for flood peaks, mean absolute differences and tidal ranges. The approach taken is more rigorous than originally envisaged but provides an easier way to assess results than can be seen from comparison plots and quickly highlights areas for potential improvement (Table 1). For the tide-affected stations the comparison of observed and model outputs was calculated using hourly intervals for the whole year. Sample time series comparison plots are shown in Figures 4 and 5. Note that for more detailed modelling for specific interventions the updated VRSAP model from the Sub Institute of Water Resources Planning, HCM, Vietnam may provide increased accuracy.

Table 1. Summary of Year 2000 Calibration Results

				DRY SEASON				WET SEASON				YEAR ROUND	
Location		Country	Label	Mean Daily Peak Flow (%)	Tidal Range Observed (m)	Tidal Range Simulated (m)	Difference in Tidal Range (m)	Mean Daily Deviation (tide filtered) (m)	Mean Daily Peak Flow (%)	Flood Peak (m)	Mean Daily Deviation of Water Levels (m)	Mean Daily deviation of tidal range (m)	Mean Daily Deviation (m)
Tan Chau	Mainstream	VietNam	MK235001	-11	0.77	0.83	-0.06	0.10	-1	0.05	0.13	0.03	0.11
Chau Doc	Mainstream	VietNam	BA221000	-5	0.83	0.88	-0.05	0.18	0	0.24	0.11	0.01	0.15
Vam Nao	Mainstream	VietNam	VAM18600	-1	1.01	1.11	-0.10	0.14	3	-0.06	0.12	0.08	0.13
Long Xuyen	Mainstream	VietNam	BA162000		1.20	1.49	-0.29	0.19		0.23	0.23	0.25	0.20
CanTho	Mainstream	VietNam	BA106000	4	1.75	1.66	0.09	0.05	-3	-0.28	0.14	-0.11	0.09
My Thuan	Mainstream	VietNam	MK127000	20	1.51	1.79	-0.28	0.09	10	-0.01	0.05	0.32	0.08
Tra Vinh	Mainstream	VietNam	COC32000		2.32	2.12	0.20	0.03		-0.06	0.06	-0.12	0.04
Tan An	Flood Plain	VietNam	VCT06000		1.39	1.75	-0.36	0.14		0.26	0.09	0.02	0.12
Tuyen Nhon	Flood Plain	VietNam	VCT14000		0.83	1.24	-0.41	0.24		-0.05	0.16	0.33	0.21
Moc Hoa	Flood Plain	VietNam	VCT210U2		2.22	2.23	-0.01	0.28		-0.17	0.26	-0.09	0.27
Hung Thanh	Flood Plain	VietNam	DON45000		0.22	0.34		0.24		-0.20	0.34		0.28
Kienbinh	Flood Plain	VietNam	DON73000		0.20	0.57		0.24		-0.25	0.24		0.24
My Tho	Mainstream	VietNam	MK069000		2.15	2.15	0.00	0.06		-0.02	0.04	-0.01	0.05
DaiNgai	Mainstream	VietNam	TRANDE14		2.48	2.35	0.13	0.04		-0.04	0.05	0.00	0.04
XuanTo	Flood Plain	VietNam	VTE25000		0.25	0.36		0.13		-0.03	0.24		0.17
Tan Hiep	Flood Plain	VietNam	CAI28001		0.21	0.31		0.13		0.08	0.15		0.14
Vi Thanh	Flood Plain	VietNam	XAN34001		0.23	0.07		0.09		0.05	0.07	-0.07	0.08
Phung Hiep	Flood Plain	VietNam	XCH00000		1.33	1.26	0.07	0.11		0.03	0.05	0.00	0.08
Phuoc Long	Flood Plain	VietNam	QLP35000		0.07	0.02		0.10		0.07	0.13		0.11
Ca Mau	Flood Plain	VietNam	TTH09000		0.71	0.71	0.00	0.06		0.14	0.22	0.03	0.12
My Hoa	Flood Plain	VietNam	BTR03700		2.22	2.23	-0.01	0.05		-0.03	0.05	-0.09	0.05
Kratie	Mainstream	Cambodia	M558000					0.18		0.19	0.21		0.19
Kompong Cham	Mainstream	Cambodia	M448000U					0.26		0.20	0.24		0.25
Mekong Phom Penh	Mainstream	Cambodia	M348000U					0.13		-0.14	0.15		0.13
Neak Luong	Mainstream	Cambodia	M292000					0.25		0.26	0.16		0.21
K Luong	Mainstream	Cambodia	G40000					Obs not continuous		-0.15	0.10		Obs not continuc
Tonle Sap	Mainstream	Cambodia	T0					0.14		-0.11	0.08		0.12
Prek Dam	Mainstream	Cambodia	T32000					0.11		-0.08	0.16		0.13
K Chhanang	Mainstream	Cambodia	T100000					0.18		-0.02	0.31		0.24
Bassac Phom Penh	Mainstream	Cambodia	B344000					0.13		-0.09	0.11		0.12
Kho Khel	Mainstream	Cambodia	B296000					0.23		-0.11	0.26		0.24

Initially the model was calibrated separately for wet season and dry season periods, however, as the planning model had to run continuously for 16 years, it was necessary to calibrate the model for both dry season and wet season conditions in a single model. Depth variable roughness was introduced into the ISIS software and much effort was taken to produce a robust model that would run stably for long-term simulations with ranges of boundary conditions.

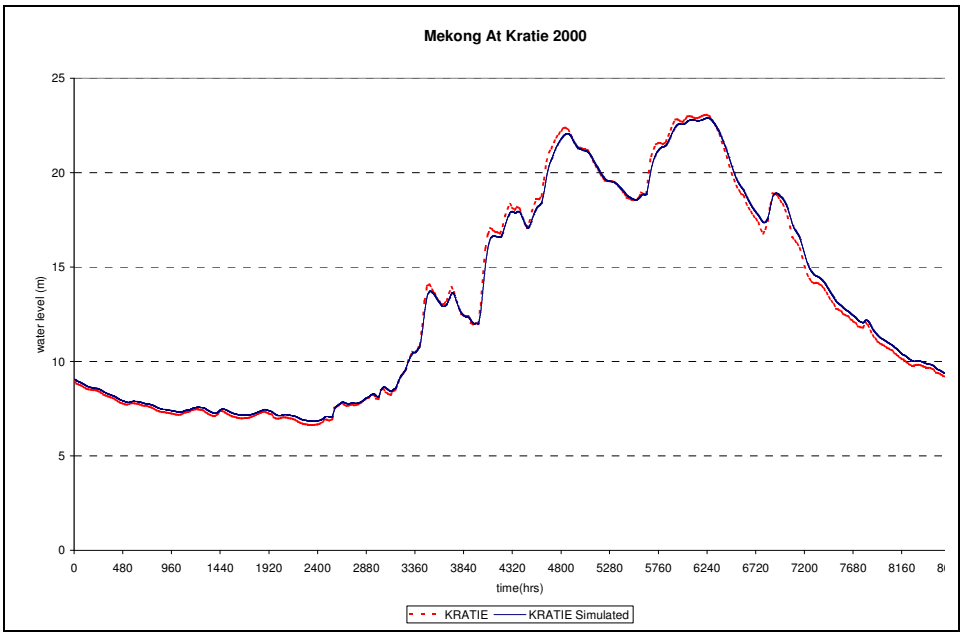

Figure 4 – Simulated and Observed 2000 Water Levels at Kratie

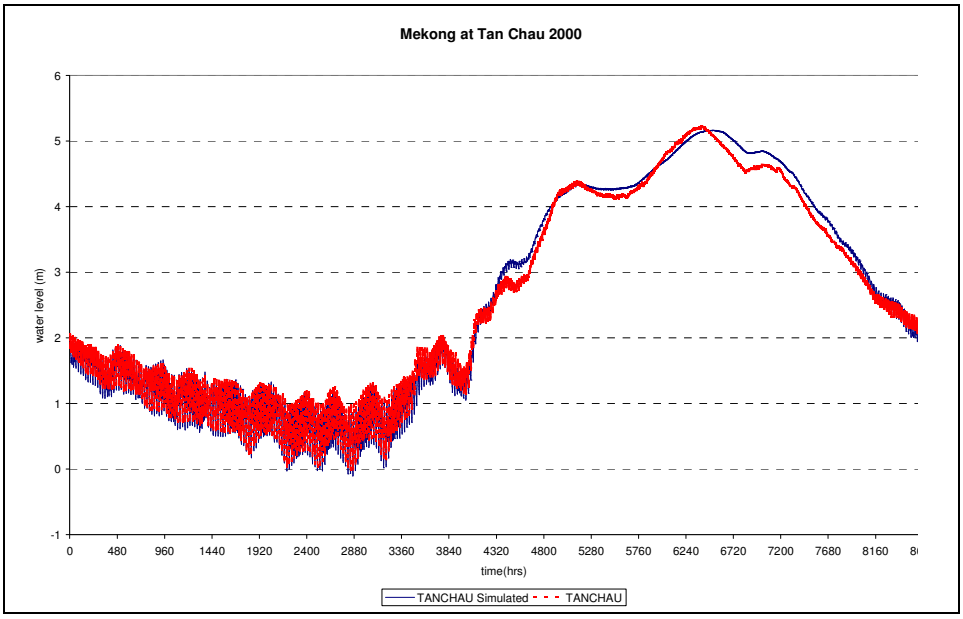

Figure 5 – Simulated and Observed 2000 Water Levels at Tan Chau

2.5 Salinity Modelling

The ISIS hydrodynamic modelling package is also able to take the hydrodynamic results obtained with the full model and use these to drive a water quality simulation. For the Mekong, the most important water quality parameter is salinity, as saline intrusion into the river and canal system in the delta affects the use of water for irrigation. The preparation and calibration of the salinity model is relatively straightforward comprising primarily the definition of salinity boundaries and dispersion coefficients to be used. The SMART algorithm used in the ISIS Quality computation enables fast and accurate simulation of the advection-dispersion process. The main difficulties for development of a calibrated salinity model lay in the sparseness of data for definition of the boundaries and points for comparison. Within the DSF the results can be spatially processed, again in a GIS environment to produce, for example, contours of maximum salinity in a particular month as shown in Figure 6.

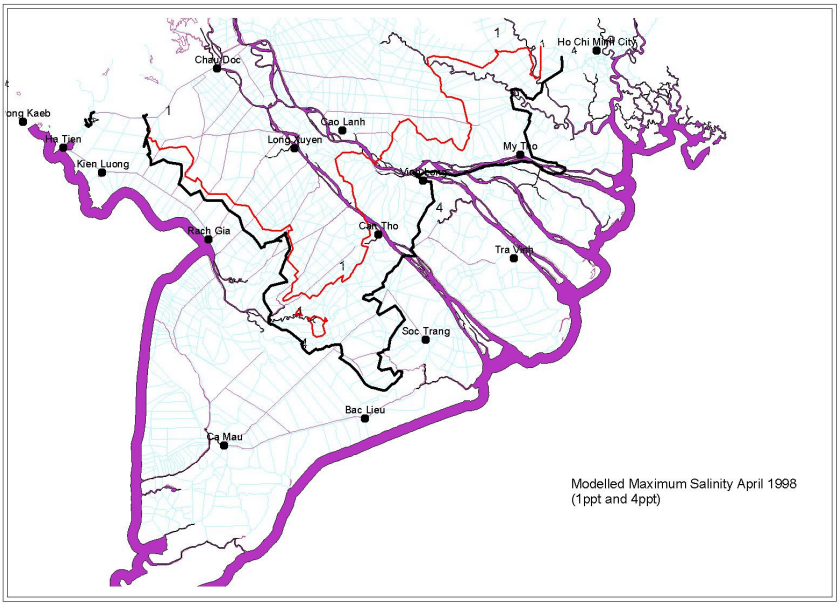

Figure 6 – Modelled Salinity Contours

3. TOOLS FOR PROCESSING OF RESULTS AND IMPACT ANALYSIS

Impact Analysis Tools
Main categories

Time-Series River Flow and Water Quality Impact Analysis Tools
- Generic Hydrologic Analysis Tools
- Flood Analysis Tools
- Low Flow Analysis
- Tonle Sap Flow – Reversal Analysis

Spatial Impact Analysis Tools
- Planning Sub-Area Classification
- Habitat Classification
- Multi-Theme Habitat Analysis
- Analysis of Spatial Changes Over Time
- Network Analysis
- Combined Spatial – Time Series Analysis

Functional Relationship Impact Analysis Tools
- Environmental Risk Analysis
- Decision Trees
- Statistical Analysis

There is a range of environmental and socio-economic impact analysis tools that can be used within the context of the DSF. These are summarized in the adjacent text box. The foundation of the needs for Impact Analysis Tools lies with the transboundary issues of concern identified by the riparian countries under another component of the Water Utilisation Programme. Through discussions with the WUP team, the MRC's Environment Program and the BDP team, as well as with other MRC programs including fisheries, flood mitigation and management, navigation and hydropower, the main categories of transboundary issues have been sub-divided into 36 sub-issues, in order to characterise the relevant concerns and potential transboundary impacts of different development scenarios. The main categories of transboundary issues are:

- Water Quality Deterioration and Sedimentation
- Fisheries Productivity and Ecosystem Functioning
- River Bank Erosion
- Obstruction to Navigation
- Inadequate Dry Season Flows
- Flooding

The analytical tools for environmental impact assessment required for the DSF need to be issue-specific and predictive in a manner that is replicable, objective, quantitative and sensitive to impacts. Quantitative tools are not confined to those that produce numerical results, but include those that rank, or categorise results based on analysis of numeric data. Expert knowledge, including traditional knowledge, is an integral part of many of these tools. Based on the identified issues and sub-issues, a range of generic tools has been identified for analysis of time-series data, spatial data and simple functional relationships of environmental responses. The principal limitation on the application of such first order impact tools is the level of current quantifiable knowledge of environmental responses to various land use, geomorphic, fisheries management, river flow and water quality changes.
It is recognised that many of the likely socio-economic impacts are driven by environmental change and other impacts, which are also important for macro-planning, are not directly related to changes in water regime. Thus application of the socio-economic tools often will follow assessment of environmental impacts, and planners will need to consider socio-economic issues outside the scope of the DSF impact analysis tools.

The impact analysis tools provided with the DSF rely on the results of the hydrologic and hydraulic simulation models. For example, Figure 7 shows the impact of a hypothetical embankment on the Mekong left bank on flood durations (calculated by the ISIS model) – these data can be intersected with ecological or socio-economic data to assess positive and negative impacts.

4. CONCLUSIONS

The Decision Support Framework and hydrodynamic model have been successfully set up in the Mekong River Commission Secretariat offices in Phnom Penh and in local offices in the four riparian countries. The ISIS hydrodynamic model successfully runs for the target 16-year simulations despite its complexity, and produces a representation of the system that is adequate and acceptable to the client. This has been a complex undertaking with the model development taking place within a consultative framework with representatives of the four countries each of which have their own views and requirements. Extensive on the job training has been given and at the time of writing the client organisation is finalising the acceptance testing for the whole system, before putting the system into practice. A follow up period to assist the client and riparian users through the initial period of implementation has been proposed.

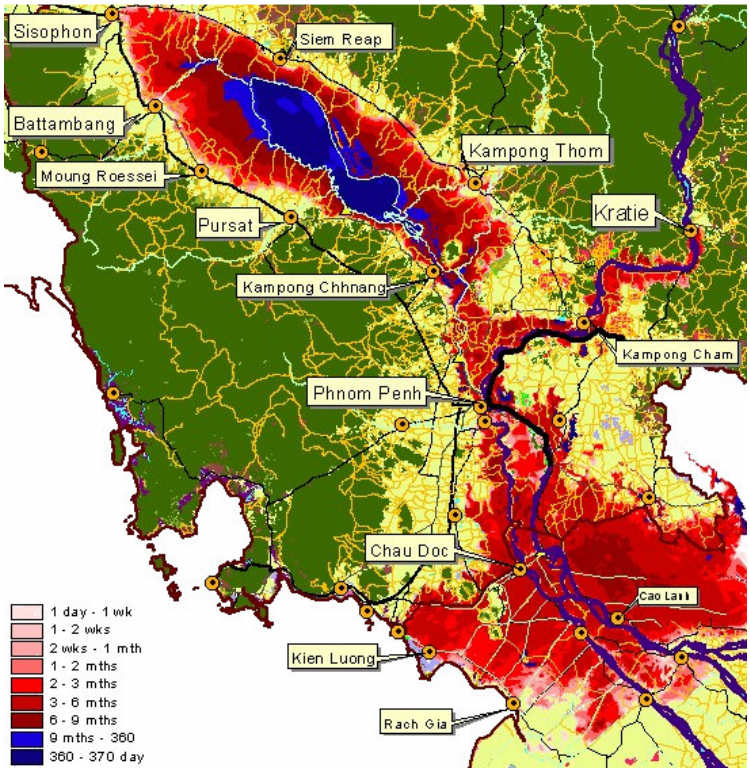

Figure 7 – Impact of Hypothetical Embankment on Flood Durations

REFERENCES

1. Mekong River Commission, 2000, Hydrologic and Environmental Modelling in the Mekong Basin

2. Halcrow, March 2004, Decision Support Faremework Final Report, Mekong River Commission, Phnom Penh, Cambodia

2. Harpin R, Wicks JM, Wallace, M, Dac NT, Sukhsri C, Mekong River Basin Decision Support Framework, International Water Association, 9th International Specialised Conference on Watershed and River Basin Management

3. Hien, Nguyen Xuan. 1999. Hydraulic modelling and flood control planning in the Mekong Delta. In: Flood Management and Mitigation in the Mekong river basin. Food and Agriculture Organization of the United Nations, RAP Publication 199/14, Bangkok, 131-143.

4. Nguyen Tat Dac. 1987. Mathematical model of the tidal flow and salinity intrusion in the Mekong main branches by fractioned step method. Report No. 9. Ho Chi Min City: Institute for Water Resources Planning and Management.

5. ISIS User Manual, 1999, Halcrow and HR Wallingford

6. SOGREAH/UNESCO. 1966. Mathematical model of the Mekong Delta: Comprehensive report of the different determinations of the Grand Lac capacity, Cambodia.

The Institution of Engineers, Australia
8th National Conference on Hydraulics in Water Engineering
ANA Hotel Gold Coast, Australia 13-16 July 2004

Three Dimensional Modelling of Stratified Reservoirs. Limitations, Data Requirements and the use of Model Results to Aid Management and Engineering Decision Making.

R.M. Hudson
B.E.
Project Engineer, Water Research Laboratory, The University of NSW, Australia
B.M. Miller
B.E., B.Sc., MEngSc.
Manager, Water Research Laboratory, The University of NSW, Australia

Abstract: Thermal stratification of a reservoir or water impoundment influences the hydrodynamics of the water body, changing the transport and diffusion of constituents within the water column. RMA-10 a three-dimensional (3-D) hydrodynamic model for stratified flow has been successfully used to model a range of different sized water impoundment's including large dams, a 400 ML distribution reservoir and naturally occurring riverine weir pools.

The model studies have been undertaken to aid the formulation of management strategies that are aimed at alleviating water quality issues. The paper focuses on two different studies and discusses data requirements, modelling capabilities, limitations and the application of model results. The first study involved predicting the reservoir water age and hence loss of chlorine residual due to a range of proposed changes to reservoir configuration. The second study involved determining the most efficient environmental release required to destratify naturally occurring weir pools on a degraded river system. Numerical modelling revealed that high magnitude, short duration releases were the most efficient, greatly reducing the required release volume needed for destratification.

The model studies have highlighted the need for accurate data to fully define water body heat budgets. Interpretation of model results including the development of a viewer (WRLPOND-3D) capable of displaying results on a 3-D mesh are also discussed.

Keywords: three dimension hydrodynamic modelling, stratification, destratification, water age, water quality, data.

1. INTRODUCTION

Numerical hydrodynamic and constituent models have been increasingly applied to a variety of problems in the field of water engineering. In situations where a water body is not vertically homogeneous (ie. stratification is present) or wind driven currents are important, a model with multiple vertical layers is required so that processes through the water column can be adequately represented. Each additional vertical layer greatly increases the number of computational points within the numerical model, resulting in much longer run times and much larger result files. With recent advances in computer technology, three-dimensional (3-D) hydrodynamic model studies can now be undertaken using PC's in a reasonable time frame.

This paper discusses important issues relating to three-dimensional numerical modelling and focuses on two recent studies undertaken by the Water Research Laboratory (WRL) where computational models were used successfully to aid management and engineering decision making. The first model investigation was of a 400 ML distribution reservoir in the Sydney Region while the second study investigated the destratification of natural weir pools on the Nepean River due to environmental releases. These projects will be discussed after a brief background to numerical modelling and a description of the RMA-10 modelling suite.

2. OVERVIEW OF NUMERICAL MODELLING METHODOLOGY

Numerical models can be an invaluable tool for investigations into physical and ecological processes. However, it is important to understand the modelling process, assumptions, capabilities and limitations. Numerical models require accurate parameterisation of the physical processes they are attempting to simulate. Once a phenomenon such as river flow or temperature flux is adequately parameterised, complex models can be developed that allow for the prediction of an outcome for a given set of boundary conditions. This allows numerical models once properly calibrated to rapidly determine the outcomes of a variety of management options (such as proposed alterations to a reservoir) and ensure that the best option is selected.

A three dimensional hydrodynamic model with appropriate internal density, mixing and turbulence parameterisation can theoretically predict the effect on a stratified body of water if it is flushed by an environmental release. It is important to realise that the results from a numerical model will only be as good as the schematisation of the model area (element mesh), the parameterisation of the processes, the ability of the numerical solution technique to solve the given parameterisation and of course the applied boundary conditions (BC's). Most numerical models have a range of internal parameters (such as eddy viscosity and diffusivity) that allow the parameterisation of the natural phenomena to be appropriately tuned so that the natural processes can be adequately simulated.

To ensure that the model can be used in a predictive sense it is necessary to calibrate the model. If sufficient data is available model verification will further increase confidence in model results. Calibration is the most important model procedure where internal model parameters are tuned until the model is able to replicate a recorded event. To enable calibration we require suitable and accurate model boundary conditions (including initial conditions) and a recorded data set to compare to the model results.

2.1 Description of RMA-10 Numerical Model

RMA-10 (King, 1999) is a three-dimensional finite element hydrodynamic model that solves the shallow water wave equations. The model is suitable for simulating density stratified flows and includes the parameterisation of a number of vertical turbulence closure options that can be used to model vertical mixing processes such as the breakdown of stratification. The model can be run either without stratification or density coupled to up to three density effecting constituents (temperature, salt and suspended sediment).

As RMA-10 uses the shallow water wave form solution of the Navier-Stokes equation, it does not include vertical momentum. Horizontal flows are solved on both momentum and conservation of mass equations, whereas the vertical flows are solved only for conservation of mass.

RMA-10 includes the provision of a full surface heat budget that can be used to predict the build up of stratification given appropriate meteorological data. Thermal stratification can also be imposed on the model by specifying the temperature at each vertical node in the model. The model also includes wind induced mixing by the application of surface shear based on the model wind field.

3. MODELLING OF IMPROVEMENTS TO A RESERVOIR

WRL was commissioned to help evaluate a range of proposed changes to a large 400 ML (~190x210x10 m) covered storage reservoir that would minimise water age and hence chlorine loss within the reservoir. The reservoir in its current configuration (where due to valve failure the intake/offtake structures are used to both fill and drain the reservoir) experiences long residence times resulting in a decay of chlorine below acceptable levels. In addition to the existing reservoir configuration, six different proposed changes to the reservoir were modelled. The model of the existing reservoir was calibrated against thermistor data collected during two, ~2-month data collection exercises over a summer and winter period. The six proposed reservoir configurations (Table 1) were then initially tested and evaluated based on their ability to flush a tracer over a 5-day summer operation period. Three favoured options (a, c & d) and the existing reservoir setup were then subjected to a further two tests using 14 days of operational simulations for both a typical summer and winter period. The first test was on the ability of a tracer mass in the system to be flushed from the system. The second test evaluated the age of the water within the reservoir and the age of water extracted during draw down. Determination of water age within the reservoir allows for a consideration of chlorine loss within the reservoir. While chlorine decay is primarily a function of water age, its loss is difficult to

directly model because it also depends on a number of different factors that were beyond the scope of the modelling exercise.

Table 1. Summary of Scenarios

Scenario	Title	Description	Model Implementation
	Existing	Existing conditions	Base Scenario
a.	Inlet/Outlet	Restoration of separate inlet/outlet functionality by replacing broken valves	Change inflow / outflow BC's
b.	Surface Inlet	Change the inlet location in the reservoir	Apply inflow to surface layer
c.	Mixers	Incorporating mixers into the reservoir	Locally increase vertical eddy diffusivity
d.	Baffles	Adding baffles to redirect flow	Change mesh to incorporate baffles
e.	Subdivide	Subdividing the reservoir into sections	Split mesh in two
f.	Insulate	Insulation of the roof.	Change the surface heat budget

3.1 Modelling Approach & Field Data Requirements

The purpose of the model study was to evaluate a number of proposed reservoir configurations in regards to improvements in water age and hence ensure acceptable levels of chlorine loss. By changing the design or operation of the reservoir, preferable reservoir mixing and circulation patterns should lead to a reduction in the occurrence of "pockets" of old water which have been associated with lower chlorine concentration. A model calibration process was undertaken to increase confidence in model predictions. In order to run and calibrate the model, suitable data was required. Data sets for the project include information on reservoir water level, intake/offtake pipe flows, inflow and outflow water temperature, thermistor data, and heat budget data. Five thermistor strings each consisting of four thermistors (surface, 2m below the surface, 4m above the bed, 2m above the bed) were used to measure temperature data throughout the reservoir and gain an understanding of mixing processes.

3.2 Model Configuration

The model mesh of the existing reservoir is shown in Figure 1. Horizontal mesh resolution is typically 20 m, though much finer mesh resolution was required in several places to represent the intake / offtake structures and the resultant hydraulic-jet features. Seven vertical layers were used with layer boundaries defined at 9 m, 7 m, 4 m, 2.3 m, 1.4 m and 0.7 m for an initial water surface elevation of 10 m and reservoir bed at 0 m. Adequate representation of hydraulic properties of the intake & offtake structure was an issue due to their complexity and a lack of data on flow fields within the reservoir. JETLAG (Lee & Cheung, 1990) near-field model simulations were undertaken to determine the approximate jet characteristics of the inflows. While RMA-10 is not formulated to resolve all the physics of a near field jet, a suitable mesh resolution and set of eddy viscosity parameters was selected that was able to closely reproduce expected momentum and velocity features.

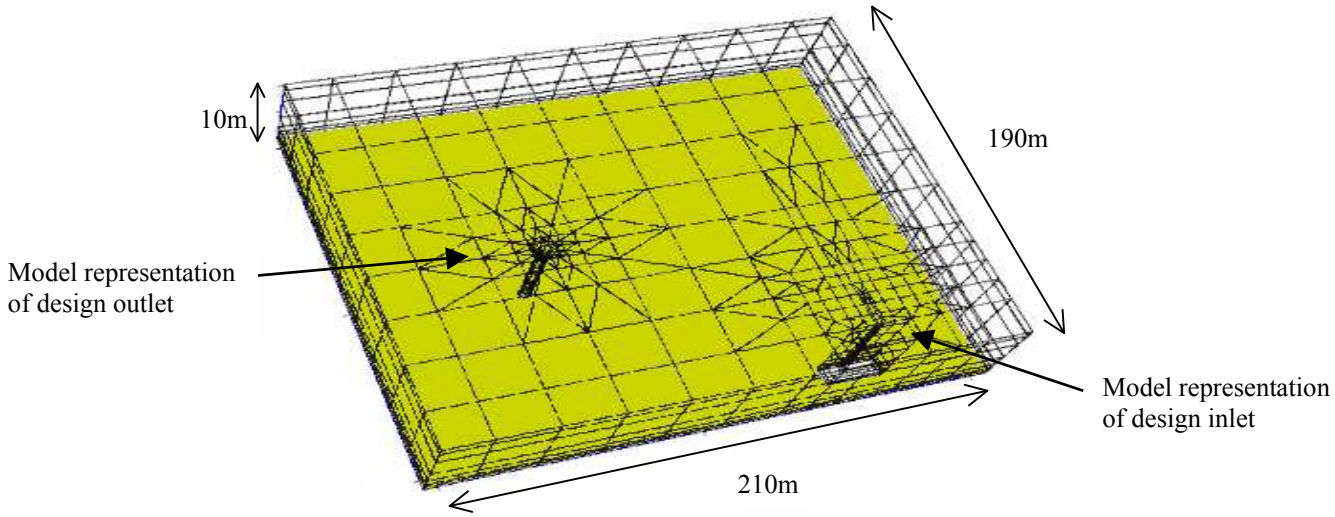

Figure 1 – WRLPOND-3D Image of Finite Element Mesh of Existing Reservoir

Model boundary conditions included inflow and outflow volumes and temperatures and the surface heat budget. At low pipe flows, slow pipe velocities resulted in small inaccuracies in flow measurements. The flow errors resulted in differences between recorded water volumes based on water level measurements and an integration of inflows and outflows. To ensure that the correct volume of water circulated through the reservoir, model water inflow and outflows were based on observed water level change and pipe inflow and outflow correlations. Flow data shows strong correlations ($R^2 > 0.996$) between the amount of water entering and leaving the two inflow / outflow structures. During filling of the reservoir 67% of the flow was through the design inlet (near the wall) structure while the remaining 33% arrived through the design outlet (centre left of reservoir) structure. When draining the reservoir 58% of the outflow is through the design inflow structure and 42% leaves through the design outlet structure. The derived flows were in very close agreement to the measured flows.

A modified surface heat budget was applied to the model to ensure that the correct level of stratification was present in model hydrodynamics. As the reservoir is covered by a corrugated steel roof no short wave radiation contributes to the surface heat-budget. The surface heat-budget was driven by a measurement of air temperature under the roof. The temperature of the roof was also collected so that long-wave radiation effects could be added into the heat budget if required. Humidity below the roof was assumed to be 100%. Inflow and outflow temperatures were applied to the model using data measured by a thermistor placed in the inflow pipe.

3.3 Model Calibration

Model calibration was based on: ensuring the correct volume of water entered and left the reservoir, checking that the flow field behaved as expected and ensuring that the correct level of stratification was present so that mixing behaviour was appropriately simulated. As inflows and outflows were based on a differentiation of measured water levels flow volume calibration was more a check than a true calibration and model volumes replicated measured volume change as expected. As no velocity measurement in the reservoir were taken due to OH&S and health reasons, the model was only able to be calibrated against near field (JETLAG) model results and experienced gained during previous reservoir modelling exercises. Horizontal and vertical eddy viscosity parameters as well as element size and shape were all optimised until a representative model flow pattern was achieved.

For the model to be able to simulate the correct level of stratification within the water column, it was necessary to calibrate internal mixing parameters (vertical and horizontal eddy diffusivity) and to specify an appropriate surface heat budget. Thermal heat budget calculations found that the surface heat budget made a minimal contribution to the overall heat budget of the reservoir which was dominated by the amount of heat transported into and out of the reservoir during the filling and draining cycles.

The calibration procedure resulted in the model being able to predict approximately the right amount of stratification that was observed in the reservoir. The model surface heat budget slightly over predicted the observed diurnal changes in the surface layer, but as the problem was restricted to the surface layer and the general trend of stratification was reproduced, this would have only minimal impact on model results. The main cause in the discrepancy between model and observed temperature data is attributed to spurious inflow water temperature measurements. Analysis of air and inflow water temperature data shows a strong correlation, indicating that the thermistor located in the inflow pipe was being strongly influenced by the temperature of the metal pipe. The impact of this inaccuracy in an important boundary condition resulted in the model not being able to match the observed temperature data for a number of events. However, as the same data was used to drive all scenario models and all of the mixing processes were adequately represented within the model, this problem would have little impact on the ability to compare the performance of different reservoir configurations.

3.4 Model Results

The performance of the existing reservoir and that of the three proposed modified reservoirs was evaluated against a range of results from the two tracer runs for each scenario for a typical 14-day summer and winter period. The first tracer test involved flushing a conservative tracer of initial concentration 100 from the reservoir. New inflows were defined to have zero tracer concentration and the mass of tracer leaving the reservoir was calculated so that the percentage of tracer flushed from the reservoir could be assessed. The second tracer run used a decaying tracer to calculate water age. Initial reservoir tracer concentration and new water entering the reservoir was defined to have a tracer concentration of 100 units/volume. Each time step all the tracer in the reservoir was exponentially decayed. This meant that “newer” water had a higher tracer concentration than “older” water. As the decay rate is known and

so is the initial tracer concentration, water age can be determined at all location within the reservoir and at the reservoir offtakes. The results of the flushing and water age reservoir simulations are shown in Table 2.

Table 2. Summary of Results for Detailed Reservoir Simulations of Tracer Flushing and Water Age

	Existing		Mixers		Inlet – Outlet		Baffles	
	Summer	Winter	Summer	Winter	Summer	Winter	Summer	Winter
% Tracer Mass Remaining (day-14)	32	25	29	25	21	6	10	1
Tracer Conc. at Outlet (day-14)	26	18	25	18	20	8	10	2
Poor Vertical Mixing	Y	N	N	N	Y	N	Y	N
Depth av. Tracer Conc. (centre reservoir, day-14)	33	20	25	22	19	5	14	0
Max Res. Tracer (day-14)	49	28	28	29	39	12	32	0
Water Age (hr) at design offtake (Range of Maximums & Expected Value)	96-132 Ex=108	96-111 Ex=90	108-132 Ex=115	92-114 Ex=90	N/A	N/A	N/A	N/A
Water Age (hr) at design intake (Range of Maximums & Expected Value)	72-100 Ex=90	75-84 Ex=75	87-126 Ex=105	69-84 Ex=70	N/A	N/A	N/A	N/A
Water Age (hr) at offtake (Range & Expected Value)	N/A	N/A	N/A	N/A	65-141 Ex=125	93-120 Ex=114	105-195 Ex=160	130-150 Ex=144
Max Res. Water Age (hr) (day-14)	243	171	160	164	242	160	270	160

The results show that there are large differences in reservoir performance depending on whether the reservoir is operated with separate inlet, outlet functionality (inlet-outlet & baffles) or with the design inlet and design outlet being used to both fill and empty the reservoir (existing & mixer). The results also show that by breaking down summer stratification maximum water age within the reservoir can be greatly reduced.

In terms of being able to flush the reservoir, the reinstatement of separate inlet – outlet functionality, improves reservoir flushing. Further significant gains in reservoir flushing are made with the installation of baffles. Stratification, which results in inhibited vertical mixing, appears to reduce the effectiveness of the baffles (compare inlet-outlet to baffles results for summer and winter). While in winter better flushing may be a result of the reservoir being operated at a lower volume, model results show it is also attributed to an absence of stratification, which during summer results in vertical short-circuiting of the reservoir. The use of mixers, only slightly increases reservoir flushing above the existing case, however, in the absence of stratification, maximum reservoir tracer concentration is reduced. In the existing and mixer simulation, reservoir flushing is greatly inhibited because diffusion and not advection of the tracer is the primary factor influencing tracer removal.

A comparison of the various reservoir configurations shows that existing case provides the “youngest water” during draw-down. However, to assess the risk of drawing off water with very low chlorine concentrations, it is important to consider maximum reservoir water age along with the age of water that is removed from the reservoir during typical daily fill/drain cycles. The existing scenario allows for withdrawal of the youngest water out of the four options, because it is able to withdraw water that was only put into the reservoir during the previous cycle. Water from the mixer scenario, is slightly older than that from the existing scenario, because the water column is fully mixed. For both options where separate inlet-outlet functionality has been restored, water age is typically older – though it is much more consistent. Water age is greater for the baffles case than for the inlet-outlet scenario, because the flow path is longer and the influence of diffusion is reduced by the additional reservoir divisions.

The selected operation (filling and draining) of the reservoir is also likely to significantly influence offtake water age results for the inlet-outlet and baffles scenario. During summer where fill/drain cycles vary considerably, offtake water age also fluctuates significantly, depending on the relative magnitude of inflows and outflows and the water level.

It is important to consider the volume of old water in the reservoir and not just the magnitude of oldest water at a single point within the reservoir. 3-D plots helped to provide further information on water age volumes. During the winter simulation, maximum water age for the baffles case is 160 hours, while for the winter case it is 164 hours. However, the volume of old water (> 150 hours) is far greater in the mixer case than for the baffles scenario. The volume of old water in the reservoir will influence the quality of water that is withdrawn, when the reservoir is significantly drawn-down (to a low water level). A 3D image created using WRLPOND-3D shows that during summer, stratification causes pockets of old water to exist above the thermocline in all but the mixer scenario. The maximum water age in a stratified reservoir appears to be much older than that in a non-stratified reservoir (compare summer and winter results – though some consideration of the different reservoir operation between these times is required).

3.5 Study Outcomes and Discussion

The results indicate that the operation of the reservoir in a plug flow mode, in an unstratified environment (i.e. baffles with mixers) will produce the best performance reservoir. Slightly spurious temperature inflow data resulted in the model not being able to completely replicate observed thermistor data, though the calibrated model was able to reproduce similar levels of stratification to that observed, ensuring important mixing processes could be adequately simulated. The use of software capable of displaying 3D results greatly assisted the interpretation of model results. This model study highlights how a 3D numerical modelling study can aid engineering and management decisions by helping to evaluate a number of proposed changes to a reservoir.

4. MODELLING WEIR POOL DESTRATIFICATION DUE TO ENVIRONMENTAL FLOWS

Stratification within a deeper section of a river results in reduced vertical mixing processes. In a stratified weir pool, warm water flowing into the pool will tend to move above cooler hypolimnic waters (below the thermocline) without mixing vertically through the water column. This results in long residence times for water in deeper pools, which, coupled with inhibited vertical oxygen transfer, can result in anoxic conditions below the thermocline. These anoxic conditions found at the bottom of deeper holes, if persistent, have been associated with negative ecological impacts such as eutrophication and fish kill.

Thermal density stratification occurs when there is a net surface heat flux (solar) into the water and insufficient mixing (wind or flow) to prevent stable density profiles developing. Destratification due to a mixing event will only occur when the destabilising force of the fluid shear is greater than the density difference caused by stratification.

WRL was commissioned by the Hawkesbury Nepean River Management Forum to study using a numerical model, environmental release strategies able to destratify naturally occurring weir pools. The study identifies primary processes that must be included in the modelling of destratification. The study also identifies additional processes that may be of importance to pool stratification and flushing but which could not be incorporated into the current model due to lack of data.

RMA-10 was used to numerically model the breakdown of stratification in deep pools. The model was calibrated using data collected by MHL (1999) at Bents Basin on the Nepean River during an environmental flow release in February 1999. Appropriate mixing parameters including horizontal and vertical eddy diffusivity and viscosity were obtained from the Bents Basin model calibration. The model and calibrated mixing parameters were then applied to two representative shallower pools to determine the characteristics of the environmental flows required to cause adequate destratification of pools within the Nepean River system.

4.1 Description of Bents Basin & Destratification Data Set

Bents Basin is a large deep pool located in a steep reach of the Nepean River between Camden and Wallacia. The basin is oval shaped with approximate dimensions of 220 m long and 150 m wide. The maximum depth within the pool is 23 m with approximately half the pool being deeper than 10 m.

The February 1999 environmental flow release consisted of increasing discharge from base-flow (~0.5 m^3/s), up to ~25 m^3/s over 24 hours. The flow was then held above 20 m^3/s for a further 48 hours and then decreased to 3 m^3/s over the following three days. A thermistor string (with thermistors at 0.5 m intervals) was located in the deepest

point of the basin providing temperature data through the water column. Recorded thermistor and flow data is shown on Figure 2.

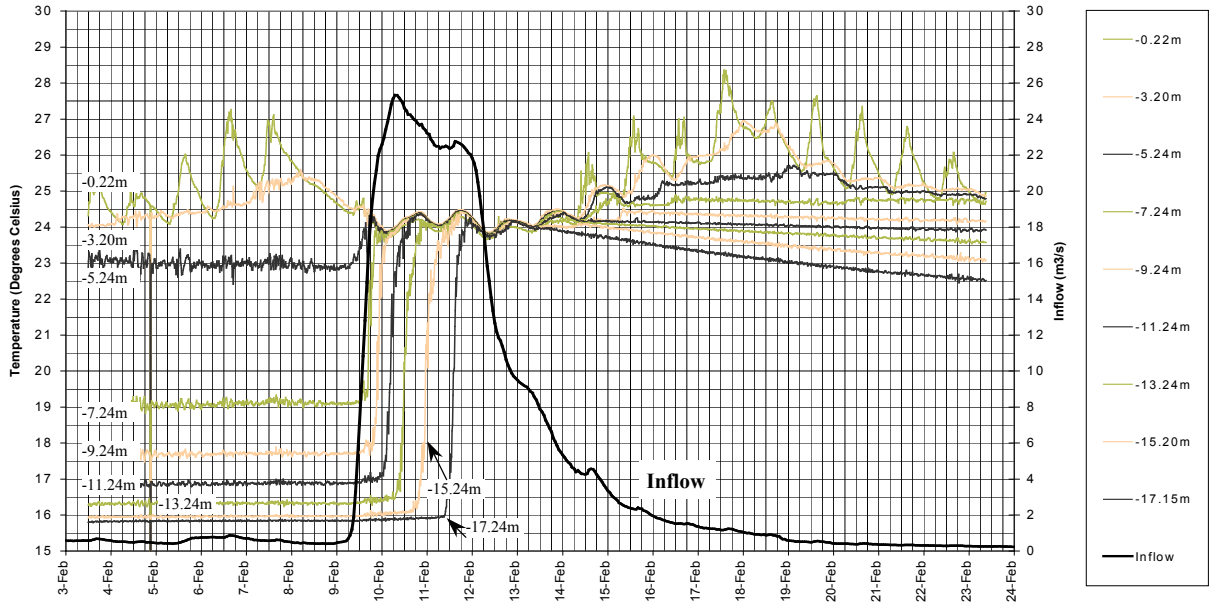

Figure 2 – Bents Basin, 1999 Environmental Flow Release - Thermistor and Flow Data

The temperature data shows that up until the arrival of the release, stratification is fairly constant with only the top 4m of the water column being influenced by the surface heat flux. From –4m to below -15m there is 8°C thermal stratification. The data shows that once the release waters arrive, destratification is rapid, with the mixed surface layer reaching –17 m within 60 hours of the inflow arrival at the basin. It should be noted that the deepest points within the basin are never fully flushed.

The restratification of the Basin that occurs on the falling limb of the hydrograph is an interesting phenomenon apparent in the data. Once the inflow is considerably reduced, a large mixed layer can no longer be maintained and the surface waters are able to be heated independently of those below them. Also the reduction in temperatures of the deeper layers indicates that there is cooler water below them, which is mixing with the warmer water through diffusive processes. This cooling from below may be an important restratification process (which may be difficult to manage through environmental releases) and is likely to result from the thermal inertia of the benethic mass (i.e. rocks and boulders) that lies at the bottom of the basin. As soon as there is no more warm inflow into the basin, the cooler large thermal mass at the bottom of the basin will begin to restratify the water from below.

4.2 Use of Numerical Model to Predict Destratifying Environmental Flows

The Bents Basin data set was used to calibrate the RMA model so that it could be used in a predictive manner to determine the required environmental flow releases required to destratify other natural weir pools. The study showed that it is possible to calibrate RMA-10 for the purpose of destratification modelling. However, it is important to realise that there are many complicated factors to consider when modelling destratification. Comprehensive sensitivity testing of all parameters that effected model destratification was undertaken. Over 180 model runs on a simplified 2-D vertical mesh of Bents Basin were used to gain an understanding of vertical mixing processes. Over 70 tests were carried out on a full 3D mesh of the Basin for model calibration. Run times for the full 3D model were typically between 0.5 - 1 times real time. Approximately 60 model runs were used to evaluate destratification of the shallower representative 3m and 4m basins before the final model parameters were selected.

The numerical model was applied to two typical (shallower) river pools: a 4 m deep x 150 m long x 20 m wide pool and a 3 m deep x 250 m long x 30 m wide pool. Various flushing scenarios were applied to each of the pools to determine the most efficient type of environmental flow to cause destratification. Six different environmental flow regimes were modelled, including magnitudes of: 2.5 m^3/s, 5.0 m^3/s and 7.5 m^3/s for durations of 1 and 2 days. It was found that high flows released for a short duration are the most efficient at destratification.

This study revealed that higher flows are more efficient at destratifying pools because of the speed at which they cause destratification. Lower flows are less efficient because of the longer duration required to cause adequate mixing. Based upon the current state of model calibration, tests indicated that a 4 m x 100 m x 20 m pool, would not be flushed by 2.5 m^3/s flows or 5 m^3/s for one day. The 4m pool would be flushed by 5 m^3/s in two days or 7.5 m^3/s for one day. The model also indicated that a 3 m x 250 m x 30 m pool, would not be flushed by 2.5 m^3/s flows in one day but would be flushed by 2.5 m^3/s flows in two days or 5 m^3/s for one day.

Model results indicate careful consideration of release efficiency could save a considerable amount of water. In the 3m deep pool the medium flow release (5 m^3/s) requires ~230 ML to destratify the pool whereas at the higher flow (7.5 m^3/s) only ~190 ML or approximately 20 % less water is required. In the 4m deep pool the model predicts that higher flows are much more efficient at destratification than lower flows. At the higher flow of 7.5 m^3/s, ~550 ML is needed to destratify the pool, whereas at the medium release approximately 50% more water (~820 ML) is required. It is important to note that the above results are only indicative and that the model requires further calibration and verification to be used accurately in a predictive manner.

4.3 Study Outcomes and Discussion

The study has shown that numerical models can be used to help determine the most efficient environmental release required to destratify deep pools. However, additional data is required to further increase confidence in model results so that the model can be used in a predictive manner. The application of calibration parameters derived from modelling a 20 m deep pool, to modelling a 4 m deep pool is not ideal, as some of the physical processes are likely to differ. Pool geometry was also found to influence the rate of destratification. It is recommended that the effect of pool geometry be more closely investigated. The study has shown that numerical modelling of weir pool destratification is extremely complicated and many complex interactions and problems were revealed. Data collected in more typical pools would allow for better model calibration and verification resulting in more accurate model predictions of destratification.

5. DISCUSSION AND CONCLUSIONS

The reservoir and pool destratification modelling studies revealed many important issues related to 3D numerical modelling. They highlight that if the modelling procedure is properly understood and limitations accepted and overcome where possible, extremely useful model results can be produced. The model results after some interpretation are of invaluable assistance to engineers and managers trying to evaluate the outcome of a number of given options.

Model exercises of any sort require appropriate data to use as both boundary conditions and calibration objectives. Inaccuracies or absences in model boundary conditions result in a model that has no chance of accurately predicting outcomes. While data collection is often an expensive and time consuming exercise having adequate data is fundamental to the modelling process.

The modelling exercises discussed in this paper revealed many unforeseen complexities. Model stability was always an important issue, that required a trade off between model resolution (both vertical and horizontal), time step and eddy viscosity and diffusivity settings. Model run times and result file sizes also had an impact on the modelling procedure. The interpretation of model results also needs to be considered and the development of a viewer (WRLPOND-3D) capable of displaying results on a 3D grid greatly assisted the studies.

6. REFERENCES

King, I.P. (1999). *A Finite Element Model For Stratified Flow – RMA-10 Users Guide Version 6.7a,* Resource Management Associates, Suisun, CA.

Lee, J.H.W. and Cheung, V. (1990). Generalised Lagrangian Model for Buoyant Jets in a Current, *J Env Eng, ASCE,* Vol No. 116, No. 6.

Manly Hydraulics Laboratory (MHL). (1999). *Hawkesbury / Nepean Environmental Flows – Stratification in Weir Pools",* DRAFT, NSW Department of Works and Services, Manly Hydraulics Laboratory, Report No. MHL983.

The Institution of Engineers, Australia
8th National Conference on Hydraulics in Water Engineering
ANA Hotel Gold Coast, Australia 13-16 July 2004

Measured and Modelled Flow Velocities in the Swash Zone of a Steep Beach: With Implications for Sediment Transport Modelling

M.G. Hughes
B.Ec. (Hons.), Ph.D.
Senior Lecturer, The University of Sydney, Australia
T.E. Baldock
B.E. (Hons.), Ph.D.
Lecturer, The University of Queensland, Australia

Abstract: Measurements of Eulerian flow velocity from the swash zone of a steep beach (gradient 1:23) are compared with a ballistic swash model. The model only requires a friction factor, beach slope angle and terminal bore velocity as input. The following model predictions matched well with observations: (1) the maximum Eulerian flow velocity during the run-up and backwash is the shoreline velocity when it arrives at the fixed point of interest; (2) at any location the time of flow reversal occurs prior to the shoreline reaching its maximum landward excursion; and (3) the duration of the uprush flow is shorter than the duration of the backwash flow. An important result of the model-data comparisons presented here is that, across most of the swash zone, there are no positive Eulerian flow accelerations during wave run-up. Sediment transport models that rely on flow acceleration as a surrogate for complicated fluid-sediment interactions are clearly inappropriate in this context.

Keywords: swash; flow velocity, wave runup; beach processes; sediment transport

1. INTRODUCTION

The research reported in this paper is motivated by the need to accurately model sediment transport and morphological change on beaches, particularly in the region above the still water level (i.e. the swash zone). The swash zone is particularly relevant to several coastal management issues. For example, the swash-deposited berm that is ubiquitous along most medium to coarse sand beaches can block the entrance to coastal creeks and lagoons for extended periods of time. In developed areas this leads to a variety of problems relating to water quality as well as flooding of lagoon foreshore properties. Due to a limited understanding of swash hydrodynamics and sediment transport there is currently no engineering model that adequately predicts the formation and maximum elevation of this berm. The model presented below provides a significant first step in redressing this shortcoming in that it successfully predicts flow velocities in the swash zone. Further development in the area of sediment transport and morphological modelling is ongoing.

2. FLOW VELOCITIES IN THE SWASH ZONE: MODEL DEVELOPMENT

The numerical model presented here is based on Shen and Meyer's (1963) analytical solution to the one-dimensional, depth-averaged, non-linear shallow water equations (NLSWE). In an inviscid flow, Shen and Meyer (1963) showed that for fully developed turbulent bores the shoreline motion is dependent only on the bore velocity upon arrival at the initial shoreline position, which subsequent laboratory experiments have shown is accurate (Yeh et al., 1989). The motion of the front of the swash lens (moving shoreline) and some details of the flow within the swash lens can be determined from a set of assumptions and corollaries of the NLSWE (Shen and Meyer, 1963). Ho et al. (1963) described a useful way to visualize the mathematical arguments by imagining that the swash lens consists of several small fluid elements, each containing the same mass of water at all times. The motion of each fluid element depends only on the pressure exerted by the adjacent elements and gravity. Freeman and LeMehaute (1964) argued that the swash lens is analogous to a rarefaction wave, thus the leading element is always moving faster than the elements behind and the horizontal pressure force acting on it will be negligible.

The problem of the shoreline climbing the beach therefore simplifies to a consideration of the balance of forces acting on the leading element alone. Including friction due to a bed shear stress, the depth-averaged equation of motion for the shoreline (which is analogous to ballistic motion) is therefore:

$$m\frac{d^2X}{dt^2} + mg\sin\beta + \tau\delta = 0 \tag{1}$$

where m is the mass of the fluid element, X is its position relative to the initial shoreline position, x=0, t is time relative to the time of bore collapse at t=0, g is the gravitational acceleration, β is beach slope, τ is the bed shear stress and δ is the nominal length (and also depth) of the fluid element. The bed shear stress is usually approximated using a quadratic friction law

$$\tau = \tfrac{1}{2}\rho f\frac{dX}{dt}\left|\frac{dX}{dt}\right| \tag{2}$$

where ρ is the fluid density, f is the friction factor and dX/dt is the shoreline velocity. Substituting (2) into (1) and dividing throughout by $m=\rho\delta^2$ yields

$$\frac{d^2X}{dt^2} + g\sin\beta + \frac{f}{2\delta}\frac{dX}{dt}\left|\frac{dX}{dt}\right| = 0 \tag{3}$$

(3) can be solved analytically for the shoreline position X through time if g, β, f and δ are assumed to be constants (Hughes and Baldock, 2004). Alternatively, when modelling evolving morphology (i.e. variable beach slope) the shoreline motion can be obtained by solving (3) using a 4th grade Runge-Kutta numerical scheme.

Once the shoreline position with time is known an estimate of the depth averaged Eulerian flow velocity $u(t)$ at any fixed location of interest $x=x_i$ on the beach face can be obtained using the mass balance principle, where the discharge of water Q (per unit width of beach) that passes x_i is

$$Q = \frac{V}{t} = hu \tag{4}$$

(Hughes, 1989; Turner and Masselink, 1998; Peregrine and Williams, 2001) and V is the time-varying volume of water up beach between x_i and the moving shoreline. In order obtain a practical expression for u we need an expression for the water depth h. While the water depth very close to the shoreline (leading edge of the swash lens) can be reasonably assumed to be constant, (1), its value elsewhere in the swash lens varies with time and distance up the beach. Baldock and Holmes (1997) proposed a semi-empirical formulation for h that closely approximates experimental observations

$$h(x,t) = H_b\left(\frac{X-x}{X}\right)^C\left(\frac{T_s-t}{T_s}\right)^D \tag{5}$$

where H_b is the terminal bore height, T_s is the swash period and C and D are empirical coefficients. (5) is based on the following constraints: i) when $(X\text{-}x)\leq 0$ then h=0; ii) when x=0 and t=0 then $h=H_b$; and iii) when x=0 and $t=T_s$ then h=0 (i.e., the water depth is equal to the height of the incident bore at the start of the uprush, x=0, reducing to zero at the end of the backwash and at the run-up tip). This formulation assumes that individual non-interacting swash events have a similar water surface profile, dependent on fixed choices of C and D for particular wave conditions and beach slope. Note that (5) describes the flow depth from the start of bore collapse, i.e., with an initially vertical front face. The volume of water shoreward of the fixed location of interest $x=x_i$ and the moving shoreline X is

$$V = \int_{x_i}^{X} h.dx \tag{6}$$

Re-arranging (4) and expressing it in finite-difference form yields the following equation for the Eulerian flow velocity u at $x=x_i$

$$u = \frac{V(t+\Delta t) - V(t-\Delta t)}{2h(t)\Delta t} \tag{7}$$

where $h(t)$ is obtained from (5) and $V(t\pm\Delta t)$ is obtained from (6).

Predictions of the viscous ballistic swash model for the shoreline position, X, shoreline velocity, U, Eulerian flow velocity, u, and local temporal acceleration, $a=\partial u/\partial t$, at two locations in the swash are shown in Figure 1. The following input conditions were used in the model: initial swash velocity u_o=3 m s^{-1}, beach gradient 1/23, friction factor for the uprush f_u=0.007 and friction factor for the backwash f_b=0.04. These values for the friction factors are in the middle of the range of those proposed by Puleo and Holland (2001). The maximum swash depth at the mid swash position is used here to represent δ_u during the uprush (Hughes, 1995), which is obtained by evaluating (5) iteratively. The backwash value δ_b was set to $0.6\delta_u$ (Puleo and Holland, 2001). In the top panel of Figure 1 the path of the shoreline through time is shown to be slightly asymmetric, with the duration of shoreward motion being less than the duration of seaward motion. The maximum shoreline velocity is equal to the collapsing bore velocity, u_o, and throughout the uprush the shoreline velocity decreases from this value until it crosses zero at the time the maximum shoreline displacement is reached (middle panel of Figure 1). Note that the maximum shoreline velocity at the end of the backwash is less than that at the start of the uprush. The first and last Eulerian flow velocity observed at any fixed location on the beach is the shoreline velocity at that location; prior to and after the swash event the velocity is undefined, not zero. The model also predicts that the flow velocity at any point seaward of the run-up limit reverses prior to the time of maximum run-up. This diverging flow has been widely observed (e.g., Raubenheimer and Guza, 1996), and is an important feature of the swash kinematics, leading to the rapid thinning of the swash lens around the time of maximum uprush. Notice that at any fixed location on the beach the local temporal flow acceleration, $\partial u/\partial t$, throughout the swash is predicted to be negative (bottom panel Figure 1).

3. FIELD DATA AND MODEL COMPARISON

3.1 Field Site and Instrumentation

North Stradbroke Island is a barrier sand island located off the Queensland coast, Australia. The seaward side of the island is exposed to a moderate energy, swell wave climate. The modal surf zone morphology varies between the 'longshore bar trough' and 'transverse bar and rip' beach states defined by Wright and Short (1984). Swash oscillations at gravity wave frequencies are driven by breaking waves, which make the site suitable for investigating swash forced by collapsing turbulent bores. The surf zone gradient was 1:55 and the mean beach face gradient 1:23, which was assumed planar for numerical modelling purposes. Sediment size on the beach face was in the medium sand range with a median diameter of 0.28 mm.

A Nortek sideways-looking acoustic Doppler velocimeter (ADV) was used to measure the shore normal flow velocity tangential to the bed, with the sampling volume maintained 1.5-2.5cm above the bed by an observer. The position of this measurement point within the fluid boundary layer is unknown, and probably varies depending on distance from the measurement point to the point of bore collapse. It is assumed, based on previous measurements of boundary layer thickness in the swash zone (Raubenheimer et al., 2004), that the ADV data represent the depth-averaged flow velocity. A Druck PTX1830 pressure sensor was used to measure swash depth at the ADV location. The shoreline location was measured with a run-up wire, again maintained 1-2 cm above the bed. A second pressure sensor measured incident wave conditions in the inner surf zone. Instruments were logged at 10 Hz for 3.5 hours at the top of the tide. The location of bore collapse varied due to both infragravity and tidal fluctuations in the water level, providing data from a wide variety of positions within the swash zone. Swash cycles were selected for analysis if there was no interaction, or if interaction was limited to the last 10 % of the swash cycle and occurred well seaward of the ADV station. A total of 214 such events had reliable data from all 3 instruments and were selected for

the analysis below. These events represent about 20% of the total individual swash events expected during this logging period. In the remainder, either significant swash interaction occurred or the ADV signal was too noisy for an accurate assessment of the data.

3.2 Data-Model Comparison

Figure 2 shows direct model versus data comparisons for ten randomly selected individual swash events. In all cases the free parameters were set to the values stated in the previous paragraph. The remaining model inputs were the beach face gradient, β=1/23, and the initial shoreline velocity, u_o, obtained from the runup wire. The bore height H_b at the initial shoreline, required in (5), was hindcast using the usual relationship $u_o = 2\sqrt{gH_b}$. The distance from the initial shoreline position to the ADV, x_i, is indicated for each event. The earliest velocity measurement shown in each swash event is the shoreline velocity when it arrived at the ADV. In most cases both the timing and magnitude of the shoreline velocity at the ADV location matches closely with model predictions. Similarly, in most examples the general shape and magnitude of the velocity time series throughout the swash event matches very well with predictions. In many cases the model predictions at the end of the swash event extend beyond the data. This is because the water level in the backwash has dropped below the ADV or the signal quality threshold was not satisfied. In all cases the measurements show no deceleration of the local backwash velocity prior to the end of the swash event, consistent with the model predictions.

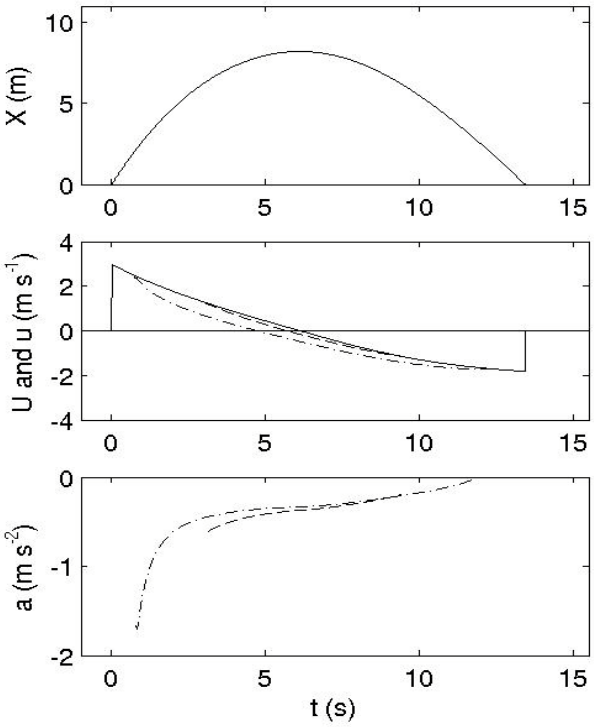

Figure 1 - An Example Of Swash Behaviour Predicted By The Ballistic Swash Model Including Friction. The Top Panels Show The Shoreline Position X As A Function Of Time. The Middle Panels Show The Shoreline Velocity U (solid line) And The Local Flow Velocity u At Two Locations on the Beach: x=2 m (dash-dotted line) and x=6 m (dashed line). The Bottom Panels Show The Corresponding Eulerian Flow Accelerations $a=\partial u/\partial t$. Initial Conditions Used In The Example Are Described In The Text.

The RMS-error between data and model predictions for swash velocity for all 214 swash events were calculated, and the frequency distribution is shown in Figure 3. The modal RMS-error for the prediction of velocity is 0.2 m s^{-1} and for most of the data set the RMS-error in the velocity is restricted to ≤0.4 m s^{-1}. Note that the model-data comparisons are relative to the start of the swash cycle, i.e. from the time of bore collapse when the shoreline starts moving shoreward (see Figure 1). This is a severe test of the model capabilities; effectively a comparison of the phase match between predicted and measured data, not just the magnitude or temporal variation. In general, the model tends to overestimate the flow velocity in the backwash (Figure 2), which is partly due to phase errors, but may be also a result of comparing depth averaged velocity predictions with measurements made close to the bed. If a roughly logarithmic boundary layer exists, then data from Raubenheimer et al. (2004) suggest that the ratio of near bed flow velocity to depth averaged flow velocity will be approximately 0.8-0.9.

A key feature of the internal swash kinematics is asymmetry in uprush/backwash flow durations and velocities, with many previous laboratory and field studies showing that $T_u<T_b$ (e.g. Raubenheimer et al, 1995*;* Baldock and Holmes, 1997*;* Masselink and Hughes, 1998*;* Raubenheimer, 2002). The swash kinematics model predicts this general behaviour (Figure 1) in agreement with the data obtained here (Figure 4). The correlation between the uprush and backwash data is positive but weak (r=0.39), since T_u and T_b differ most at positions on the lower beach near the bore collapse point (i.e., where T_u is largest) and converge on the upper beach near the limit of shoreline excursion (i.e., where T_u is smallest). The low correlation is therefore also an indicator of the asymmetry in the swash kinematics.

Model predictions for T_u versus T_b for a typical swash cycle (period 11s) are plotted on Figure 4 and show good agreement with the data set.

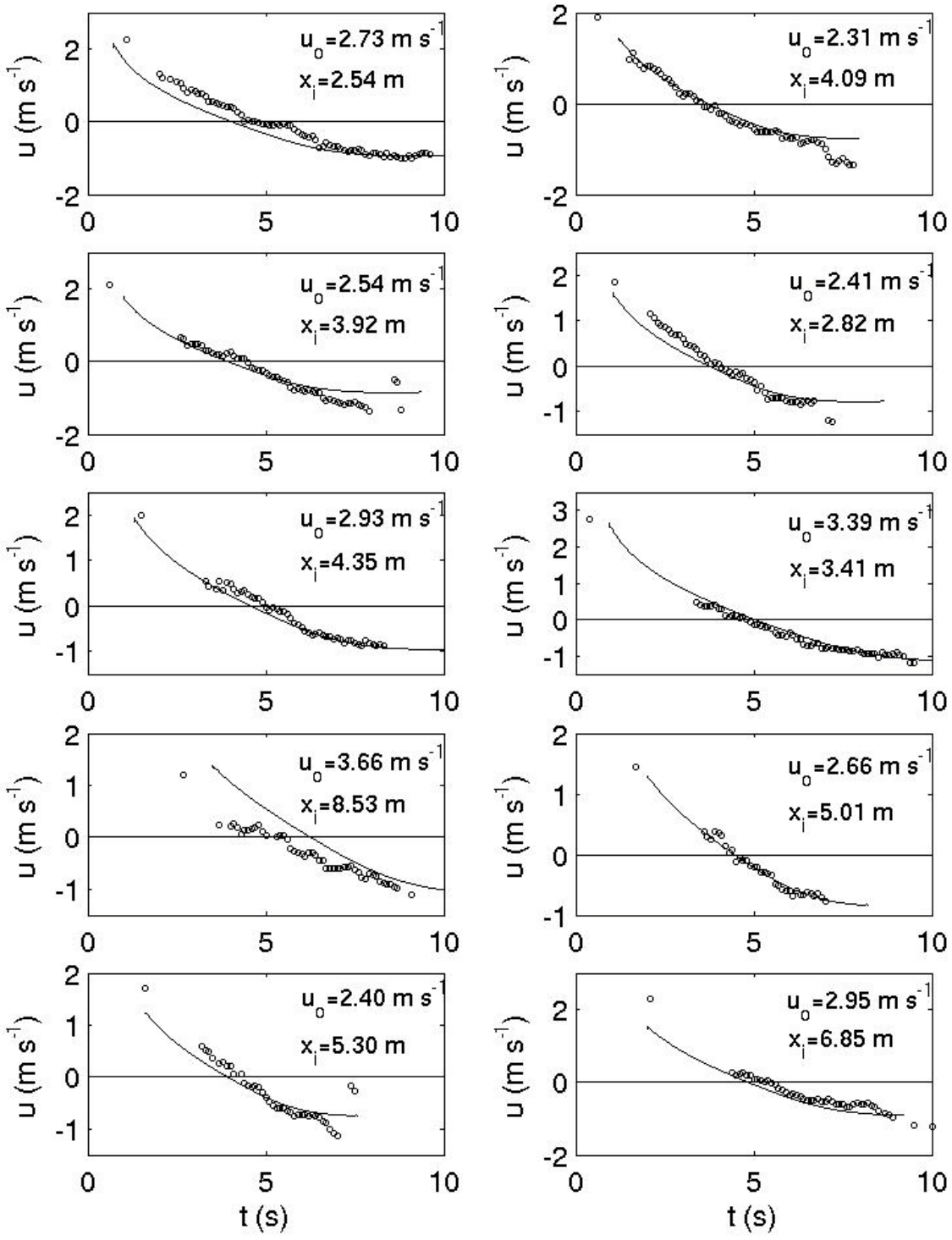

Figure 2 - Measured Eulerian Flow Velocity (open circles) Compared With Model Predictions (solid line) For 10 Individual Swash Events. The Values For Shoreline Velocity At The Beginning Of The Swash Cycle u_o (i.e. the terminal bore velocity) And Distance Of The ADV From The Shoreline Position At The Beginning Of The Swash Cycle x_i, Used To Initialise The Model In Each Case, Are Also Shown.

The peak or maximum flow velocity is an important parameter in some formulations for sediment transport rate (e.g. Masselink and Hughes, 1998). For the swash events described here, this is equivalent to the shoreline velocity when it arrives at the ADV (i.e., the start of the swash event). Data and model predictions of the magnitude, u_{max}, and timing, t_i, of the maximum flow velocity are compared in Figure 5. Again, model-data comparisons are relative to the time of bore collapse when the shoreline starts moving shoreward, i.e. they include phase errors. There is a tendency for the model to under predict the magnitude of the maximum velocity, but this is in part due to errors in estimating the exact distance from the point of bore collapse to the measurement location. The accuracy of the model is indicated by the RMS-error between model predictions and data, which in this case is 0.62 m s^{-1} and 1.14 s for the maximum velocity and timing, respectively.

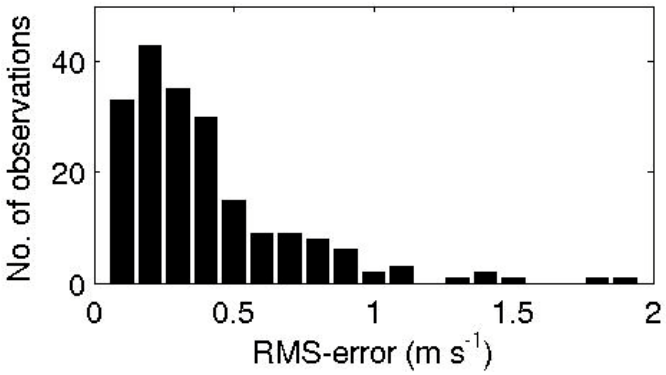

Figure 3 - Frequency Distributions Of The RMS-Error Between Measurements And Model Predictions Of Flow Velocity For Each Of The 214 Swash Events In The Data set.

4. IMPLICATIONS FOR SEDIMENT TRANSPORT AND MORPHODYNAMIC MODELING

In our presentation of Eulerian flow velocities we chose not to force the data to zero between swash events. In our view, prior to arrival of the shoreline at a point of interest the beach is 'dry' (devoid of swash) so that there can be no fluid velocity, zero or otherwise. This raises an interesting question regarding flow accelerations at a fixed point on the beach, i.e. Eulerian flow accelerations $\partial u/\partial t$. The ballistic swash model predicts that such accelerations are negative throughout the swash event (Figure 1). Previous work has tended to force velocity data to zero between swash events, implying that a strong, positive Eulerian acceleration occurs at the beginning of local uprush and at the end of the backwash. In all of our data the shoreline velocity when it arrives at the ADV location is the largest recorded flow velocity, hence there is no evidence of strong, positive Eulerian accelerations. Nevertheless, recent swash zone sediment transport modelling has focused on Eulerian flow acceleration as a potentially important factor (Puleo et al., 2003). One motivation for incorporating acceleration into the models is to produce a phase shift of the predicted bed shear stress to match the observation that most sediment is transported at the start of local uprush (Puleo and Holland, 2003). This is not necessary, however, if current meter data is used in a way that is consistent with the event like nature of swash. If the velocity data used to initialise sediment transport models is not forced to zero between events, then the first flow velocity the sediment experiences is the shoreline velocity as the front of the swash lens arrives. The data from this study and that of Petti and Longo (2001) shows that this is actually the largest flow velocity occurring in the local uprush (at least outside the bore collapse zone and in the absence of swash interactions). Consequently, the largest predicted instantaneous bed shear stress will also occur at the start of the local uprush (when most sediment transport is occurring), thus removing the need to introduce a Eulerian acceleration to produce a phase shift. It has been argued that the inclusion of Eulerian flow acceleration in swash zone sediment transport models acts a surrogate for other unaccounted for processes such as positive pressure gradients experienced by the grains (Nielsen, 2002). While a pragmatic approach to modelling swash zone sediment transport is necessary at this stage, the appropriateness of positive Eulerian flow accelerations as a proxy for these processes is not at all clear at the present time and warrants further investigation. It is true that a sediment grain on the beach face is subject to a drag force when the swash arrives, giving rise to a positive Eulerian acceleration of the grain, but this neither implies nor requires the fluid to be experiencing a positive Eulerian acceleration.

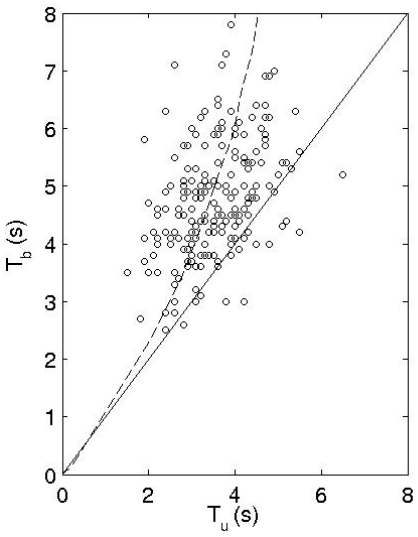

Figure 4 - Durations Of Local Uprush T_u Plotted Against Backwash T_b. The Solid Line Shows The 1:1 Relationship, And The Dashed Line Shows The Model Predictions For T_u Versus T_b For A Swash Cycle Typical Of The Data Set (T_s=11s).

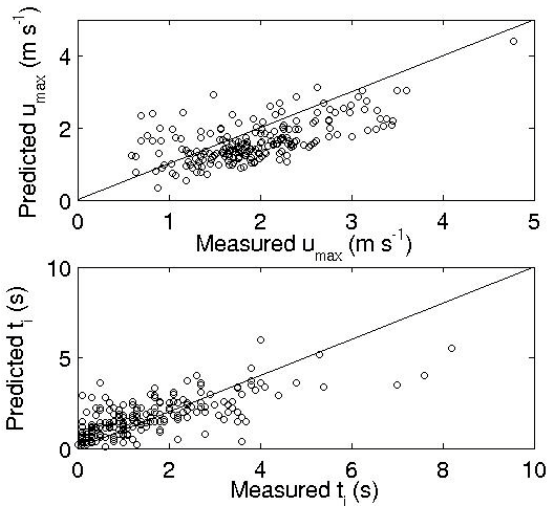

Figure 5 - A Comparison Of Measured And Model Predictions For The Magnitude (top panel) And Timing (bottom panel) Of The Maximum Flow Velocity In Each Swash Event. The Solid Lines Indicate The 1:1 Relationship.

The greatest challenge facing efforts now to model sediment transport in the swash zone relate to a poor understanding of the boundary layer structure beneath the swash. It is well known that the flow in the region immediately behind the moving shoreline carries the largest sediment loads (e.g. Butt and Russell, 1999). The relationship between the fluid velocity and the bed shear stress in this region of the flow is likely to be complicated and to evolve with distance up the beach. On the lower beach face the flow immediately behind the shoreline is likely to be associated with large stresses due to both a large mean velocity and steep velocity gradient. On the upper beach, however, the flow immediately behind the shoreline will have a smaller mean velocity, and also a more mature boundary layer (more gentle velocity gradient), leading to considerably smaller bed stresses (Masselink et al., 2004). Indeed, the relationship between the flow velocity and bed shear stress will probably vary markedly across the swash zone in an, as yet, undetermined fashion.

5. CONCLUSIONS

Model predictions for Eulerian flow velocities, flow depths and flow durations in the swash zone compare well with the field measurements, which cover different relative positions within the swash zone. In particular, the timing and magnitude of the maximum predicted flow velocity at a fixed location on the beach face matches well with the measured shoreline velocity upon its arrival at that location. Flow depths are well predicted, together with the cross-shore variation in uprush and backwash durations. Detailed comparisons of Eulerian velocity time-series from individual swash events compare very well with the data, both in terms of velocity magnitude and the time of flow reversal. The timing of the zero velocity crossing in a local swash event is correctly predicted to occur prior to the time the shoreline reaches its maximum landward displacement, thus the flow duration of the local uprush is noticeably less than the flow duration of the local backwash in both model predictions and observations. Finally, the data show no positive (shoreward directed) local accelerations, $\partial u/\partial t$, in the flow velocity at a fixed point during either uprush or backwash. This is consistent with the ballistic swash model and relevant to sediment transport modelling in the swash zone.

6. REFERENCES

Baldock, T. and Holmes, P. (1997). Swash hydrodynamics on a steep beach, in E.B. Thornton (Editor), *Coastal Dynamics '97*, A.S.C.E., Virginia, 784-793.

Butt, T. and Russell, P. (1999). Suspended sediment transport mechanisms in high-energy swash, *Marine Geology*, 161, 361-375.

Freeman, J.C. and LeMehaute, B. (1964). Wave breakers on a beach and surges on a dry bed, *Journal Hydraulics Division, Proc. A.S.C.E.*, 90, 187-216.

Ho, D.V., Meyer, R.E. and Shen, M.C. (1963). Long surf, *Journal of Marine Research*, 21, 219-230.

Hughes, M.G. (1989). *A field study of wave-sediment interaction in the swash zone*, Ph.D. thesis, University of Sydney, 249 p.

Hughes, M.G. (1995). Friction factors for wave uprush, *Journal of Coastal Research*, 11, 1089-1098.

Masselink G. and Hughes, M.G., (1998). Field investigation of sediment transport in the swash zone, *Continental Shelf Research*, 18, 1179-1199.

Masselink, G., Evans, D., Hughes, M.G. and Russsell, P. (2004). Suspended sediment transport in the swash zone of a dissipative beach, *Marine Geology*, in review.

Nielsen, P. (2002). Shear stress and sediment transport calculations for swash zone modelling, *Coastal Engineering*, 45, 53-60.

Peregrine, D.H. and Williams, S.M. (2001). Swash overtopping a truncated plane beach. *Journal of Fluid Mechanics*, 440, 391-399.

Petti, M. and Longo, S. (2001). Turbulence experiments in the swash zone, *Coastal Engineering*, 43, 1-24.

Puleo, J.A. and Holland, K.T. (2001). Estimating swash zone friction coefficients on a sandy beach, *Coastal Engineering*, 43, 25-40.

Puleo, J.A., Holland, K.T., Plant, N.G., Slinn, D.N. and Hanes, D.M. (2003). Fluid acceleration effects on suspended sediment transport in the swash zone, *Journal of Geophysical Research*, 108, 3350, doi:10.1029/2003JC001943.

Raubenheimer, B. (2002). Observations and predictions of fluid velocities in the surf and swash zones, *Journal of Geophysical Research*, 107, 3190, doi:10.1029/2001JC001264.

Raubenheimer, B. and Guza, R.T. (1996). Observations and predictions of runup, *Journal of Geophysical Research*, 101, 25575-25588.

Raubenheimer, B., Elgar, S. and Guza, R.T. (2004). Observations of swash zone velocities: a note on friction coefficients. *Journal of Geophysical Research*, 109, C01027, doi:10.1029/2003JC001877.

Shen, M.C. and Meyer, R.E. (1963). Climb of a bore on a beach. Part 3, Run-up, *Journal of Fluid Mechanics*, 16, 113-125.

Turner, I.L. and Masselink, G. (1998). Swash infiltration-exfiltration and sediment transport, *Journal of Geophysical Research*, 103, 30813-30824.

Wright, L.D. and Short, A.D. (1984). Morphodynamic variability of surf zones and beaches; a synthesis, *Marine Geology*, 56, 93-118.

Yeh, H.H., Ghazali, A. and Marton, L. (1989). Experimental study of bore run-up, *Journal of Fluid Mechanics*, 206, 563-578.

The Institution of Engineers, Australia
8th National Conference on Hydraulics in Water Engineering
ANA Hotel Gold Coast, Australia 13-16 July 2004

Hydraulic Model Study of Tilapia Fish Exclusion Using Coanda Screens

Franz Jacobsen
B,Eng, Dip Eng
Civil Engineer, SunWater, Australia
Dr Mohand Amghar
B.Eng,. M.Eng.Sc., PhD
Civil Engineer, SunWater, Australia

Abstract: Tinaroo Falls Dam is situated on the Barron River approximately 130 km upstream from Cairns (Australia). The noxious Tilapia fish was accidentally introduced into the Barron River just upstream from the dam about ten years ago. There is a possibility that the Tilapia fish could migrate from the east coast Barron River catchment to the Mitchell River catchment, which forms part of the Gulf river system, via the existing irrigation channel system.

SunWater has investigated the Coanda effect screens which consists of an inclined screen structure utilising a tilted-wire screen panel installed in the sloping downstream face of an overflow weir. The use of this tilted wire arrangement allows a significantly larger portion of flow to be forced through the screen than with conventional screens (e.g. vertical flat-plate screens). This type of screen has not been utilised very much in Australia although it has been commercially available in the U.S. for about 10 years. However, the type of the flow capacity through the Coanda screens planned by SunWater is believed to be much larger than used anywhere in the world. This paper discusses the overall design and the findings of this investigation of the Coanda effect screens using hydraulic model in two- and three-dimensional

1. INTRODUCTION

Tinaroo Falls Dam is situated on the Barron River approximately 130 km upstream from Cairns on the Atherton Tablelands and 2000 km north of Brisbane (Figure 1). The West Barron diversion channel is for irrigation of the Barron River Scheme. Fish screening is required to prevent the translocation of Tilapia fish from the east-coast Barron River into the Mitchell River catchments, which forms part of the larger Gulf of Carpenteria river system.

The Coanda screen design uses a concave arc or flat plate panel consisting of wedge wire (Strong and Ott 1988, Bestgen et al. 2001, Wahl 2001). It has been applied for nearly 15 years for exclusion of unwanted fish and other organisms from wetlands (Strong, 1989) and for debris removal upstream of hydropower projects (Strong and Ott, 1988) and has hardly been applied in Australia. Limited biological evaluations have been conducted on the Coanda screen (Buell 2000), and it is not yet considered acceptable for anadramous fisheries in California (USA). The current design was derived from other model arrangements reported in the literature (Wahl and Einhellig, 2000). For instance, Aquadyne has marketed one specific Coanda effect screen configuration under the trade name Aqua Shear. Design information available to hydraulic engineers has previously been limited. Tony Wahl (USBR, 2001) conducted extensive laboratory tests. These tests included prototype Coanda-effect screen structures.

The aim of the study is firstly to develop a solution to contain Tilapia fish to the Barron system with total exclusion from the Mitchell system, ensure that services to irrigators of the channel system are not adversely affected by the installation and operation of the screen and secondly to successfully address the issue of cleaning of the fine screens.

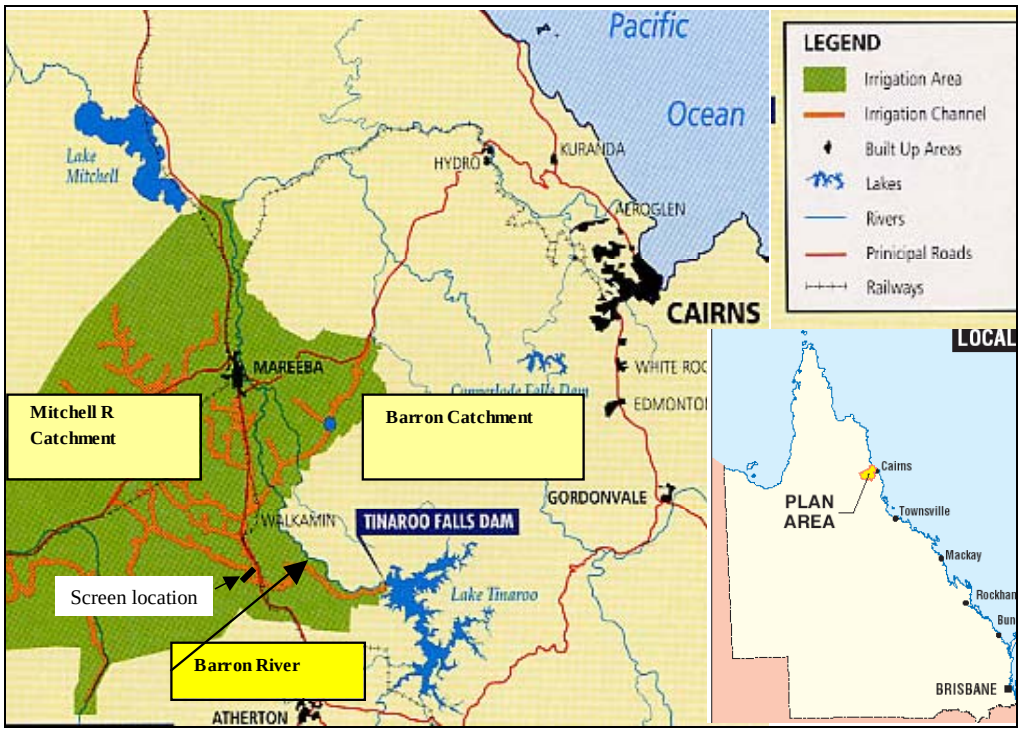

Figure 1. Location of the screen site

2. MODEL EXPERIMENT

2.1 Coanda Screen Description

The Coanda screen or profile screen is a sloped fixed screen consisting of a wedge-wire type mesh which allows water to be sheared off and through the mesh as it passes over its downstream ogee face (Figure 2). Flow passes over the crest of the weir, across a solid acceleration plate, and across and through the screen panel. Flow passing through the screen is collected in a conveyance channel below the screen, while the overflow containing fish and debris passes off the downstream end of the screen. Flow velocities across the face of the screen are highly variable, and are a function of the drop height from the upstream pool to the start of the screen (Wahl 2001). Sufficient flow depths must be maintained over the end of the screen to prevent excessive fish contact with the screen surface.

Flow depths across the screen are shallow, which increases fish exposure to the screen surface. These screens typically require a head drop of several meters. Coanda screens have high flow-handling capacities for their size, are essentially self-cleaning, and have the ability to exclude very fine debris and small aquatic organisms. The Coanda effect hydro-shear wedge wire screens were manufactured out of stainless steel, as shown in figure 3. Its name is taken from the phenomenon of fluids flowing over a solid surface.

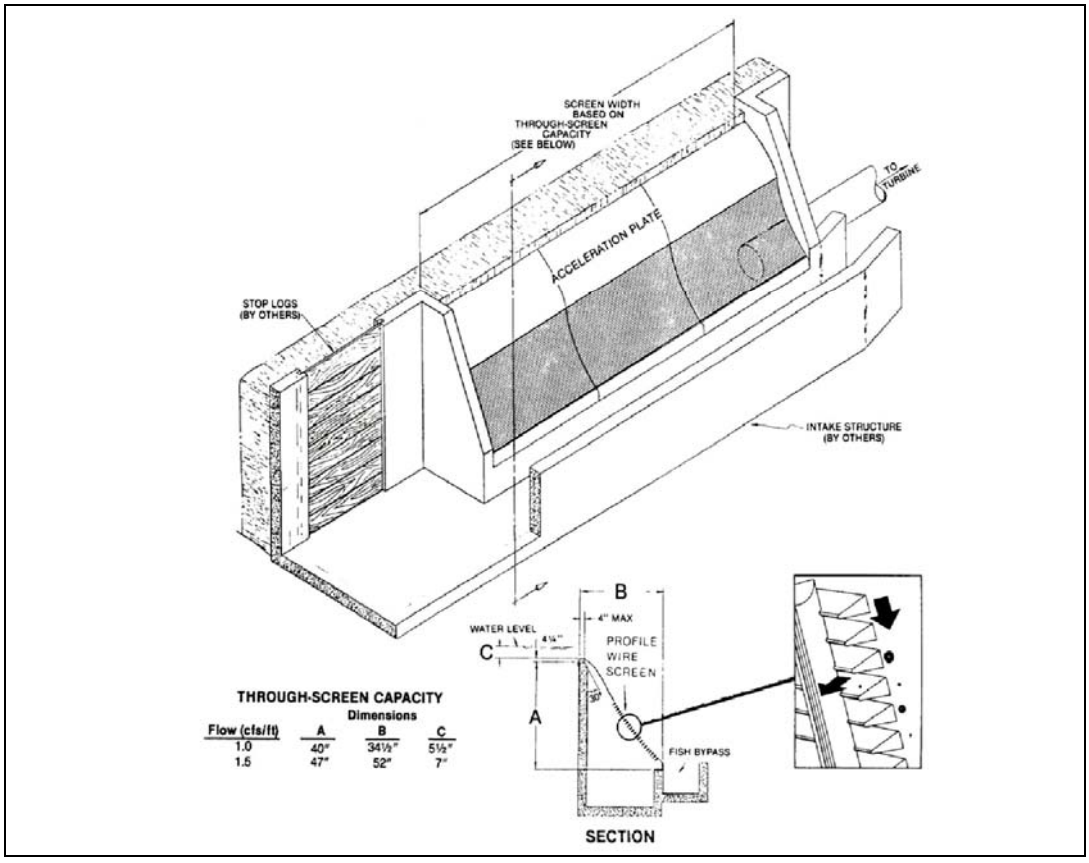

Figure 2. Example Coanda Screen (Source: Aquadyne, Inc., Healdsburg, CA

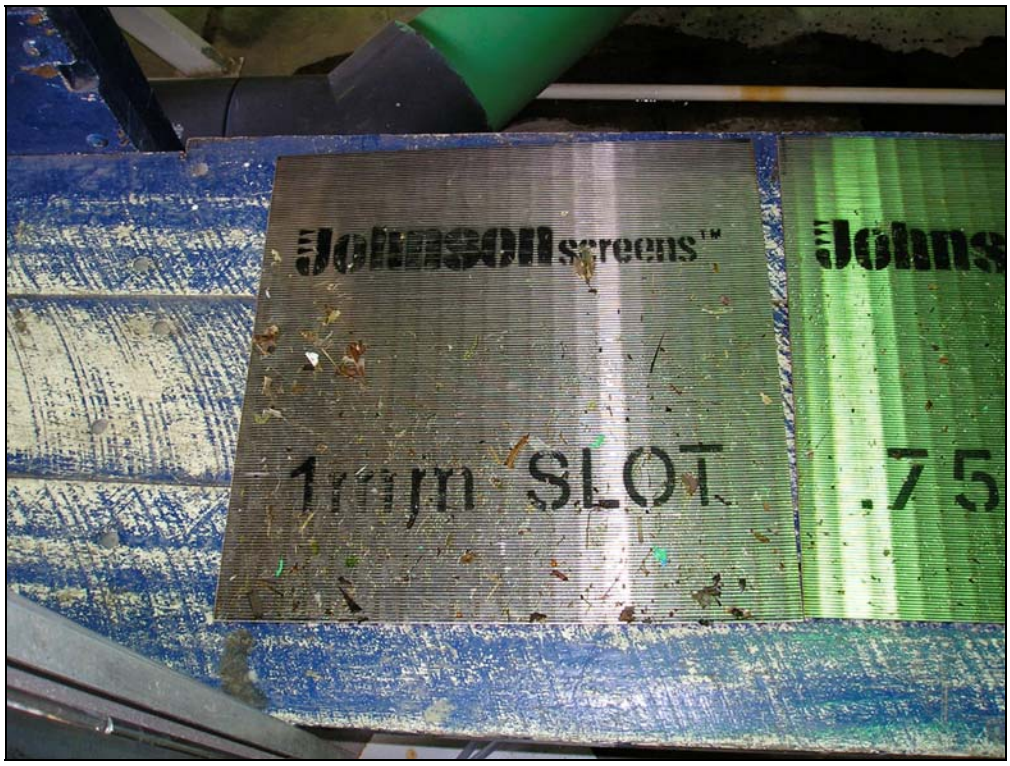

Figure 3. Coanda screen sample

2.2 Two-Dimensional Sectional Model

A flume test facility was designed to perform preliminary tests exposing fish to water velocities of up to 2.5 m/s under two types of screens (vertical flat plate and Coanda screen). The flume system, Figure 4, is 0.45 m wide, 0.90 m deep and 4.5 m length, included 1 pump, two 150 mm diameter PVC piping, and a reservoir tank. The floor of the flume was inclined at 5 degrees. The inclined floor was designed to produce the desired water velocity of 0.3 to 2.5 m/s. A flow meter was built into the supply line to monitor pump performance. The flume system was installed in SunWater Hydraulic Laboratory at Rocklea in Brisbane. The flow meter readings were used for reference and comparison only, since only velocities were measured in later tests.

The Coanda screen was mounted 0.30 m off the flume floor, inclined downstream (flow perpendicular to the screen axis). An acrylic plastic viewing window on the flume wall adjacent to the screen allowed viewing and video taping of screen operation during tests. Flow through the screen was viewed and measured using streamflow velocimeter and pointer gauge to measure water depth.

To define the functional design criteria, Sunwater designed and built a prototype facility to expose fish to water velocities of up to 2.5 m/s under the two types of screens, the maximum water velocities a fish might encounter when passing through a typical screen. The biological tests were intended to test screen-opening sizes (from 0.30 mm to 1.0 mm) where fish (eggs, fry, and larvae) were exposed to high- and lower-velocity jets.

The two-dimensional model analyses the performance of the screen sample at various position of inclination from the horizontal and the description of the flow behaviour on the screen.

Figure 4. General view of the flume showing the Coanda screen (left) and the vertical plate screen (right).

2.3 Three-Dimensional Model

It was obvious from the two-dimensional model investigation that a full three-dimensional representation/ scale model of the Tinaroo Coanda effect screen was necessary for this specific irrigation channel configuration. A Froude-model was built and an undistorted scale of 1: 8 used due to the limitation of the available supply capacity and working space of the Hydraulics Laboratory.

The 1:8 scale model reproduced approximately 24 m of the width of the screen and 30 m of the upstream approach channel including the proposed training wall and 40 m of the exit channel (figure 5). A small screen section (350 mm x 350 mm wide) with wires that are 1.6 mm wide, wires are spaced to produce 0.5 mm openings between the wires, and a 5 degrees wire tilt, was tested in the SunWater hydraulic laboratory at Rocklea, installed in 3.0 m wide test flume on 45 degree slope.

Adhering to similitude criteria results in a reduction of discharge by 1: 181 and of flow by 1:2.83.

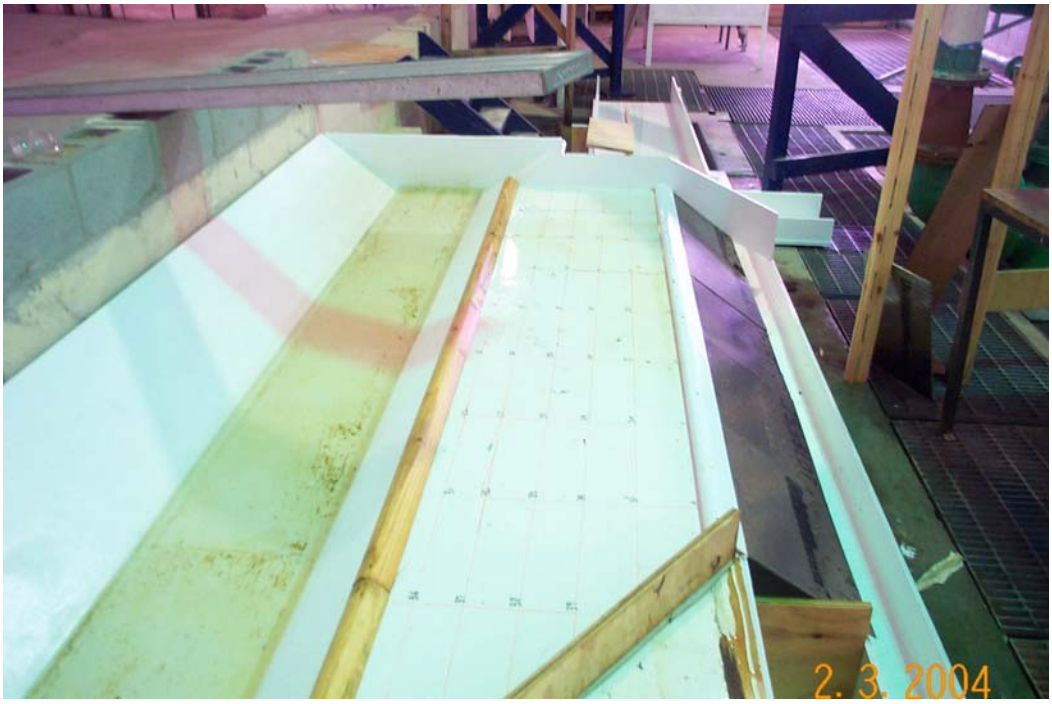

Figure 5. Three-dimensional model set-up of Coanda screen

3. RESULTS

3.1 Fish Tests

Tests were conducted to test screen performance and view fish behaviour in the vicinity of the screen. Ten each of fry, larvae and eggs (Tilapia), ranging 0.5 mm to 1.2 mm in length, were used for the screen configuration perpendicular to the flow. Three stainless steel mesh sizes with the following aperture opening of 0.75mm, 0.5mm and 1.0.mm were tested for various life history stages of the Tilapia fish. The screens were inserted into a tilted flume at right angles to the flow at SunWater's Rocklea facility. The initial flow conditions were set to represent field conditions. In these experiments, eggs were excluded by 1mm mesh and free swimming larvae by 0.5mm mesh. However a small proportion of late stage yolk sac larvae passed through the 0.5mm mesh.

As the screens tested all failed to contain the Tilapia fish, measurements of the hydraulic performance of the screens was not undertaken. However, large head losses (difference in water levels upstream and downstream of a screen) where observed. With an initial depth of flow of 400mm, approximately 300mm of head loss was encountered.

The second phase of testing was carried out utilising the Coanda-effect screen. Once again, three stainless steel mesh sizes with the following aperture opening of 0.75mm, 0.5mm and 0.4.mm were tested for various life history stages of the Tilapia fish. Figure 6 shows the layout of the test. Line 1 represents the flow of water over the ogee weir crest; line 2 shows the flow of screened water to plankton net. Line 3 indicates water that does not pass through the screen, which is directed to a second net. Line 4 denotes the perspex layer separating screened from unscreened water. With this arrangement the 0.5mm screen was successful in excluding late stage yolk sac larvae and free- swimming larvae.

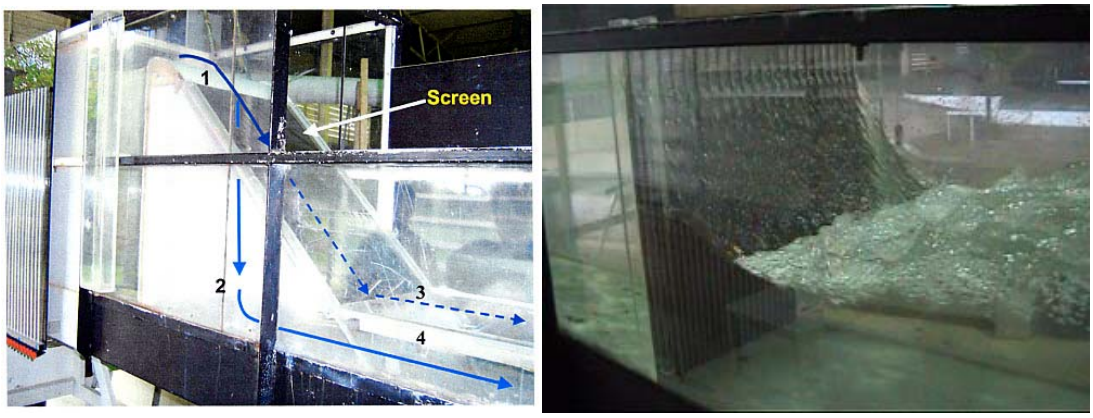

Figure 6. Coanda screen installation and vertical with large head loss.

3.2 Velocity Measurements and Dye Tests

Screen performance was evaluated by measuring approach velocities across the width of the intake channel and crest weir 2m upstream from the screen as shown in figure 5. Velocities were measured with a streamflow velocimeter at 0.2 and 0.8 of the water depth at the right, left, and centrelines along the length of intake channel to determine the overall flow distribution. Velocities were also measured at the crest 1.0 m from the screen surface with the screen oriented parallel to the flow to give an indication of the near screen velocity field (Figure 7 to 9). For all test cases, positive approach velocities indicate flow is going into the screen. Flow visualisation tests (dye tracings) were also conducted to evaluate the uniformity of the flow distribution over the screen surface and the flow though the screen and also to visually verify the results from these tests.

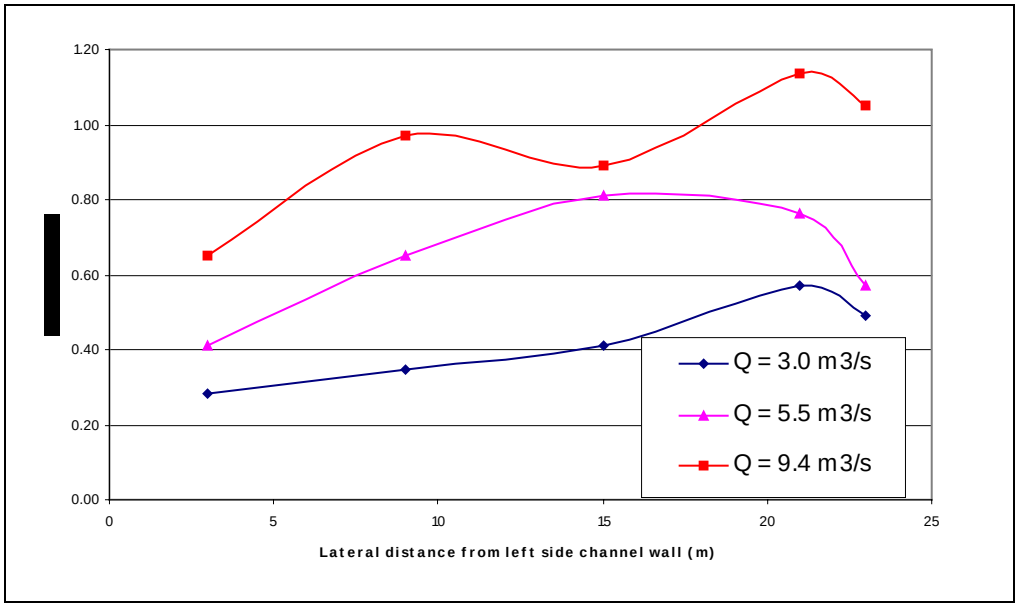

Figure 7. Approach velocities measured at 0.50 m from the crest.

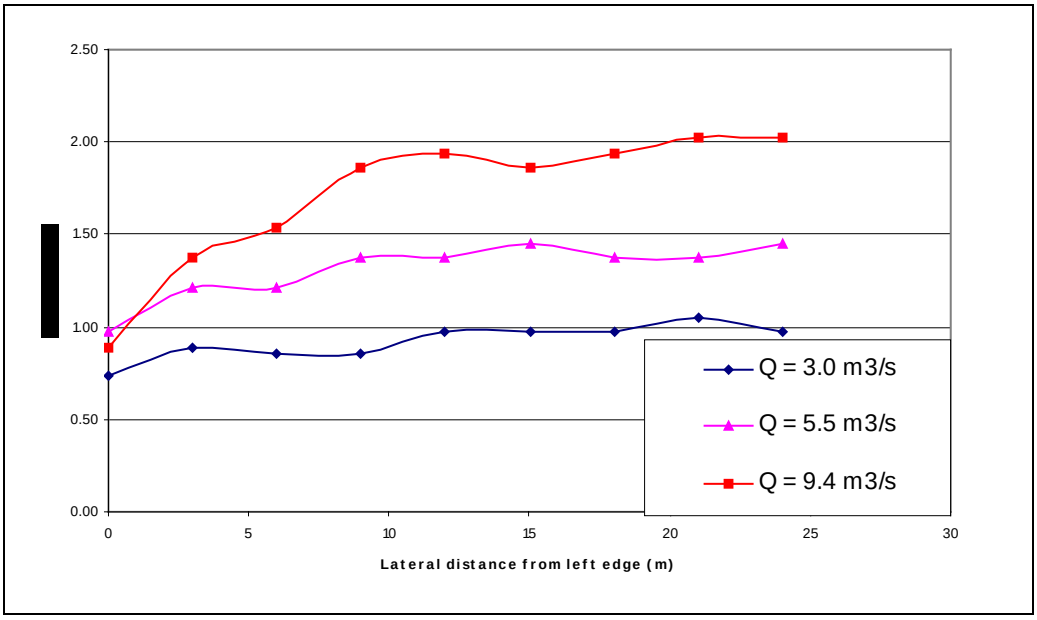

Figure 8. Approach velocities along the crest 0.8 m from the Coanda screen.

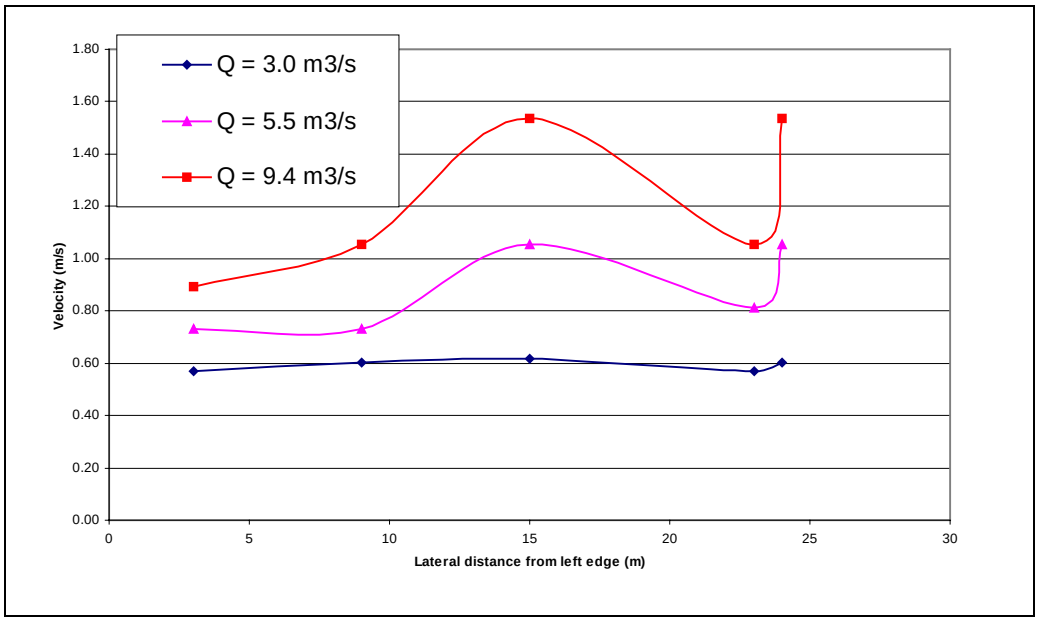

Figure 9. Approach velocities measured 1.5 m from the crest. Coanda screen is oriented 45 degree to flow.

4. CONCLUSIONS

This study focused its attention on the performance of the screen and the flow distribution along the length of the screen for each case tested. The following conclusions were drawn from the study:

Tests conducted with the screen-oriented perpendicular to the flow show that the upstream approach velocities and head losses measured along the length of the screen for the flume (two-dimensional model) conditions are about twice the magnitude of those for the Coanda screen condition. This occurs because accumulation of debris and dead fish diminish the flow diverted through the screen and in turn increases the head loss as the open area is decreased.

The approach velocities measured along the upstream of the Coanda screen (high velocity screen) show that the control structure performed well to maintain an even flow distribution into the screen, despite an uneven flow distribution across the width of the intake at the upstream side channel. Fluctuations in the velocities measured along the upstream side channel are all within 20% of the average upstream centreline velocity for each flow tested.

Dye tracings tests verified that the screen performed well in shredding large debris. Although some debris remained attached to the screen on the upstream side of the screen. Dye tests also showed that an area of recirculation on the downstream side of the left hand side of the irrigation channel.

Tests with fish showed that although many fish remained attached to the screen, none of the fish tested were passed through the mesh.

5. REFERENCES

Bestgen, K. R., J. M. Bundy, K. A. Zelasko, and T. L. Wahl. 2001. *Exclusion and survival rates of early life stages of fathead minnows released over inclined wedge-wire screens*, final report submitted to Metro Wastewater Reclamation District, Denver, Colorado, August 15, 2001.

Buell, J. 2000. Biological performance tests of East Fork Irrigation District's Sand Trap and Fish Screen Facility: Phase I. Buell & Associates, Inc.

Strong, J. J. and R. F. Ott. 1988. *Intake screens for small hydro plants*. Hydro Review VII (V): 66-69.

Wahl, T. L. 2001. *Hydraulic performance of coanda-effect screens*. ASCE Journal of Hydraulic Engineering 127(6).

Wahl, T. L. and R. F. Einhellig. 2000. *Laboratory testing and numerical modeling of Coanda effect screens*: 2000 Joint Conference on Water Resources Engineering and Water Resources Planning & Management July 30 – August 2, 2000, Minnesota, USA.

The Institution of Engineers, Australia
8th National Conference on Hydraulics in Water Engineering
ANA Hotel Gold Coast, Australia 13-16 July 2004

Analysis and Design of Sediment Basins

R.H.A. Janssen
Ph.D., M.I.E.Aust.
Senior Engineering Specialist, Bechtel Services Pty. Ltd., Australia

Abstract: Sediment basins are typically designed based on ideal settling theory, with a factor to account for turbulence. The advantage of this approach is that it is simple to use, and will often yield a reasonable approximation to actual sediment removal efficiency. However, ideal settling theory does not quantify turbulence, and various empirical and analytical methods have previously been proposed to estimate basin performance. A numerical model for computing efficiency of sediment basins is presented and is compared to these methods. The model is solved using a spreadsheet and yields similar results to Camp's (1946) detailed analytical approach. The comparison indicates that when basins are sized using ideal settling theory with typical turbulence factors, up to 15% of the target sediment particles may not be removed.

Keywords: Sediment basins, settling efficiency, turbulence, numerical simulation.

1. INTRODUCTION

Water engineering comprises facilities to collect, divert, convey, store, or discharge water in a controlled manner. The presence of sediment can hinder the performance of the water management facilities (Janssen, 2003), and can have a detrimental impact on downstream receiving water bodies. Sediment management should therefore always be considered in water engineering, and may include preventing the intake of sediment; removing sediment from water; transporting sediment through water conveyances; and discharging sediment in a controlled manner. Sediment basins are one of the most commonly used structures for sediment management, reducing the through-flow velocity to allow settling. For removal of a target sediment particle size with a fall velocity of w_t, the required surface area of a sediment basin, A, is typically given by the following relationship:

$$A = \frac{KQ}{w_t} \tag{1}$$

where Q is the design flow rate and K is a coefficient to account for turbulence. **(1)** is based on ideal settling theory described in the Appendix, and K is typically set to 1.2 (Goldman et al, 1986, as adopted by IEAus, 1996). This equation is simple to use, but care should be taken since it does not explicitly quantify the impact of turbulence on sediment settling. Increased turbulence in a sediment basin can be expected to reduce sediment removal efficiency.

The assessment of sediment removal efficiency over a range of sediment sizes is important not only to ensure that the design criteria are being met, but also to be able to plan maintenance and cleaning activities. Ideal settling theory is also applied to estimate basin removal efficiency for sediment other than the target size. Although the factor K can be adjusted to account for turbulence, it is not based on any physical hydraulic parameters. BHRA (1989), Camp (1946), Haan et al (1994) and others present analytical and empirical approaches to quantifying turbulence in sediment basins. The objective of this paper is to compare these approaches and their impact on predicted sediment removal efficiency over a range of sediment sizes. A numerical model for sediment settling in basins has been developed to provide a reference for this comparison.

Janssen (2003) presents other factors that impact sediment settling, including:

- Short-circuiting, where the active flow area does not cover the available basin surface area
- Hindered settling due to high sediment concentrations, requiring adjustment to the fall velocity
- Scour and re-suspension of deposited sediment due to excessive through flow velocity
- Variability in flow rate over time

Quantifying the impact of these factors on settling is beyond the scope of this paper, but these are addressed by others such as BHRA (1989) and Haan et al (1994).

2. PERFORMANCE OF SEDIMENT BASINS

(1) is used to size sediment basins for removal of a target sediment size. Performance of a sediment basin is the removal efficiency over a range of sediment sizes. Removal efficiency can be estimated based on ideal settling theory, or on empirical and analytical relationships.

2.1 Ideal settling efficiency

For the linear ideal settling behaviour (see Appendix), the efficiency of removal, η, for a sediment size with a fall velocity, w, is given by the following relationship:

$$\begin{aligned} \eta &= \frac{w}{KVo} & w < KVo \\ \eta &= 1 & w \geq KVo \end{aligned} \qquad \textbf{(2)}$$

Vo is the overflow rate based on the basin surface area and design flow rate, as defined in the Appendix. **(2)** yields the result that 100% of the target sediment particles ($w=w_t$) will be removed for $w>=KV_0$. Assessment of this result is provided later.

2.2 Empirical and analytical approaches for basin efficiency

Turbulent velocity fluctuations, especially those in the vertical, will result in mixing and a reduced effective average settling rate. Turbulence will tend to keep sediment suspended, and hence reduce the basin efficiency. Several approaches to providing a more realistic estimate of sediment basin efficiency have been proposed. BHRA (1989) presents the Hazen equation:

$$\eta = 1 - \left[1 + m\left(\frac{w}{Vo}\right)\right]^{\frac{-1}{m}} \qquad \textbf{(3)}$$

The parameter, m is used to quantify performance of the settling basin, where m=0 represents best performance, and m=1 represents very poor performance. m is therefore used to represent all of the non-linear effects, but in itself is not based on any physical characteristics.

The Vetter equation, as presented by Haan et al (1994), is based on high turbulence in the basin, and is given by:

$$\eta = 1 - \exp\left(-\frac{w}{Vo}\right) \qquad \textbf{(4)}$$

Neither of these methods quantifies the degree of turbulence based on hydrodynamic criteria.

Camp (1946) discusses in detail the effects of turbulence on settling, and proposes a solution to the turbulence closure equations. Camp uses this to develop an analytical relationship for sediment removal efficiency that incorporates a turbulence term. Since there is no analytical solution to Camp's relationship, this has been solved by trial and error and plotted as settling efficiency curves (Camp, 1946, also shown in BHRA, 1989, and Haan et al, 1994). These curves have been redrawn by BHRA (1989), in which efficiency is dependent on two parameters:

$$\eta = f\left(\frac{w}{Vo}, \frac{w}{U*}\right) \qquad \textbf{(5)}$$

The shear velocity $U*$ is a measure of turbulence intensity, and is given by:

$$U* = \sqrt{gRS_f} \qquad \textbf{(6)}$$

where g is acceleration due to gravity, R is the basin cross section hydraulic radius, and S_f is the friction slope, which can be computed from relationships such as Manning's equation.

3. NUMERICAL MODEL OF SEDIMENT SETTLING

Valioulis and List (1984), Haan et al (1994), Olsen and Kjellesvig (1999), and others have applied detailed hydrodynamic models to sediment settling. The model presented here is a simplified numerical approach that quantifies turbulence based on Prandtl's mixing length theory applied to flow in open channels. Within this model, suspended sediment transport is solved in a two dimensional vertical plan along the length of the basin.

3.1 Velocity profiles

Two-dimensional, uniform, steady state flow conditions are simulated, so that the velocity profile through the sediment basin is constant. The following standard logarithmic profiles (e.g. Simons and Sentürk, 1976) are used to compute the velocity, *u*, at a depth, *y*, above the bed:

Turbulent Smooth Velocity Profile:

$$\frac{u}{U*} = 5.75 \log\left(\frac{U* y}{\upsilon}\right) + 5.5 \quad \textbf{(7)}$$

Turbulent Rough Velocity Profile:

$$\frac{u}{U*} = 5.75 \log\left(\frac{y}{k_s}\right) + 8.5 \quad \textbf{(8)}$$

Two cases of sediment settling have been analysed, one with low turbulence (smooth velocity profile) and one with high turbulence (rough velocity profile). The impact of the viscous sublayer on overall settling within the basin is considered to be negligible, and has not been included. In the cases analysed, velocity profile and settling velocity were considered to be independent of sediment concentration, though this is worth further investigation.

3.2 Suspended sediment transport equations

Simulation of suspended sediment transport through the basin includes terms for horizontal transport by advection, settling due to gravity, and vertical turbulent mixing. Note that lateral mixing, bed load transport, and flocculation were not included in this sediment transport simulation. The transport velocities given below are mass transport rates per unit cross-section area ([kg/s/m^2]), at a distance *y* above the bed, where the concentration is *C* ([% by weight]).

$$\text{Horizontal transport velocity} = \rho u C \quad \textbf{(9)}$$

$$\text{Vertical transport velocity due to settling} = -\rho w C \quad \textbf{(10)}$$

$$\text{Vertical transport velocity due to mixing} = -\rho \varepsilon_s \frac{dC}{dy} \quad \textbf{(11)}$$

ε_s is the mass transfer coefficient, assumed to be equal to the momentum transfer coefficient, ε, given by Camp (1946) to be:

$$\varepsilon_s = \varepsilon = 0.075 D U* \quad \textbf{(12)}$$

For steady state conditions being considered, there is a balance between the three transport terms, which yields the following advection-diffusion equation for sediment continuity in differential form:

$$u\frac{\partial C}{\partial x} - w\frac{\partial C}{\partial y} - \varepsilon_s \frac{\partial^2 C}{\partial y^2} = 0 \quad \textbf{(13)}$$

3.3 Computational solution

The sediment continuity equation **(13)** was discretised into an implicit finite difference form, and solved by iteration on a spreadsheet. For the cases presented here, a uniform rectangular grid size of 1m horizontal by 0.1m vertical was used. The sediment deposited in the basin was computed by summing all the sediment falling vertically from the lower computational layer, using **(10)**. Once the equations had been set up, this proved to be a simple approach to implement, with no programming required.

In developing the above relationships for suspended sediment behaviour, the following assumptions were made:

- Flow velocity is constant across the width of the sediment basin
- Horizontal turbulent diffusion is negligible compared to the horizontal advection, and hence can be ignored
- Sediment is completely mixed at the inlet to the sediment basin, and the sediment concentration at the inlet is constant with depth.

4. COMPARISON OF ANALYSIS METHODS

4.1 Description of cases analysed

The numerical analysis was conducted for two cases, one with low turbulence (smooth velocity profile) and one with high turbulence (rough velocity profile). The key parameters for each case analysed are summarised in Table 1. Mannings n values for sediment basins will generally be between 0.02 and 0.03, and hence the two cases analysed are considered to be the low and high turbulence extremes of typical sediment basins.

	Low Turbulence Case	**High Turbulence Case**
Flow Rate, Q [m^3/s]	1	2
Target sediment size [μm]	50	75
Overflow velocity, *Vo* [m/s]	0.002	0.004
Manning n	0.02	0.03
Shear velocity, U^* [m/s]	0.0014	0.0052

Table 1: Summary of parameters for low and high turbulence cases analysed

The numerical model was used to compute settling efficiency for a range of sediment sizes. In addition, the two parameters in **(5)** were evaluated and the basin efficiency was read off curves shown in Camp (1946). The sediment basin efficiencies are plotted against the *w/Vo* in Figures 1 and 2, for low and high turbulence, respectively. Also plotted is the commonly used case with a turbulence factor of 1.2, and the two extreme cases of quiescent settling (K=1.0) and high turbulence Vetter equation.

Figure 1: Plot comparing the sediment removal efficiency for a range of sediment particle sizes, for low turbulence

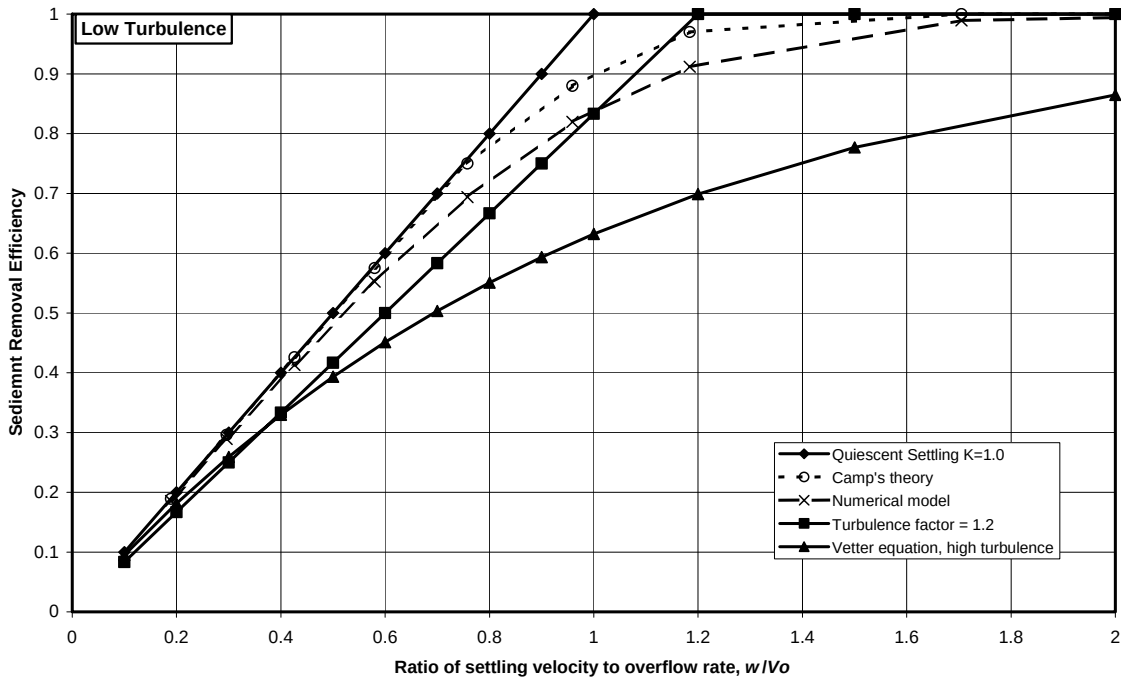

Figure 2: Plot comparing the sediment removal efficiency for a range of sediment particle sizes, for high turbulence

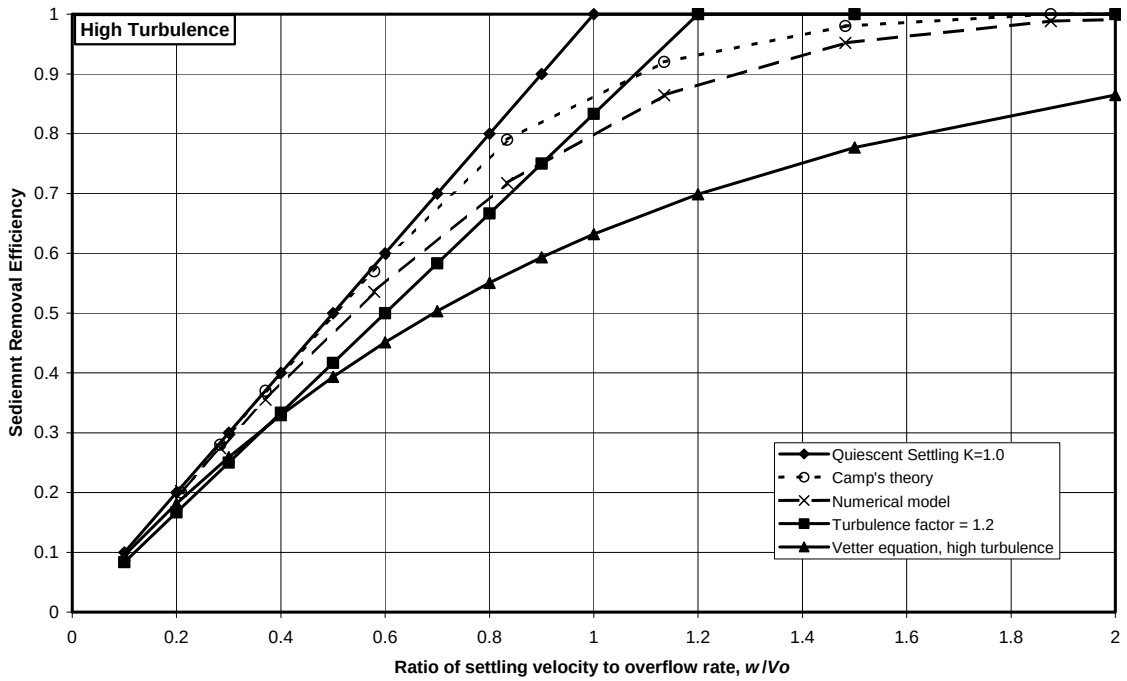

4.2 Discussion of results

Plots of the removal efficiencies for the numerical model and Camp's plots have similar shapes, and lie between the quiescent and high turbulence extremes. Settling efficiency predicted by Vetter's equation appears to be for high turbulence not normally expected in sediment basins. The linear plot for a turbulence factor of 1.2 is a reasonable linear approximation to the non-linear plots. In general, use of a turbulence factor of 1.2 tends to under-predict basin efficiency for low values of *w/Vo* (smaller than the target sediment size), but over-predicts efficiency for higher values of *w/Vo* (approximately the same as the target sediment size and larger). Although under-prediction of basin efficiency may appear to be conservative, this may not be the case when trying to assess sediment storage volumes and maintenance requirements. The example in Section 5 illustrates this impact.

The results in Figures 1 and 2 show that Camp's method predicts higher sediment basin efficiency compared to the numerical model. Since the same mass transfer coefficient given in **(12)** was used for each method, the difference is likely due to different assumptions regarding velocity distribution and numerical discretisation. However, it is encouraging that the two curves are similar enough to provide a degree of validation.

It is interesting to note that for a basin sized using a turbulence factor of 1.2, a portion of the target sediment size (*w/Vo*=1.2) will not be retained within the basin. Should 100% removal of the target sediment be required, then the factor *K* should be increased to between 1.5 and 2 (depending on the level of turbulence), which obviously results in much larger sediment basins. Designers should always consult the performance specifications of the sediment management system that they are designing, to check whether some discharge of the target sediment size is allowable.

5. EXAMPLE APPLICATION

The importance of correctly analysing the efficiency of a sediment basin for the full range of expected sediment ranges is illustrated here for the seawater supply to a processing plant in the Gulf of Mexico. Following tropical storm events, the seawater used for cooling was found to contain extremely high suspended sediment concentrations. This high sediment concentration led to abrasion and corrosion of the cooling water pipework and pump impellers, reduction in hydraulic capacity of intake pipelines, blockage of strainers, and deposition of

sediment in the pump sumps. After monitoring the performance of the existing cooling water system, Bechtel engineers presented the owner with a series of capital and operational improvements to the cooling water intake to limit future impacts and extend the life of the existing infrastructure.

Figure 3: Example Application - Suspended sediment concentration in seawater intake

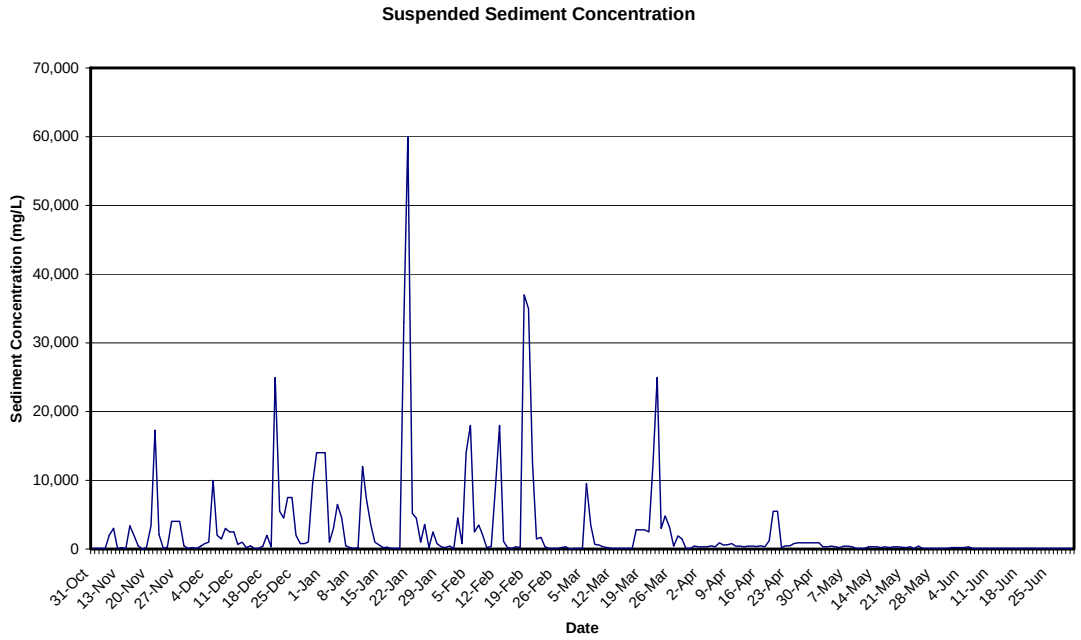

Figure 4: Example Application - Plot of results of simulation of sediment deposition depths in a settling basin

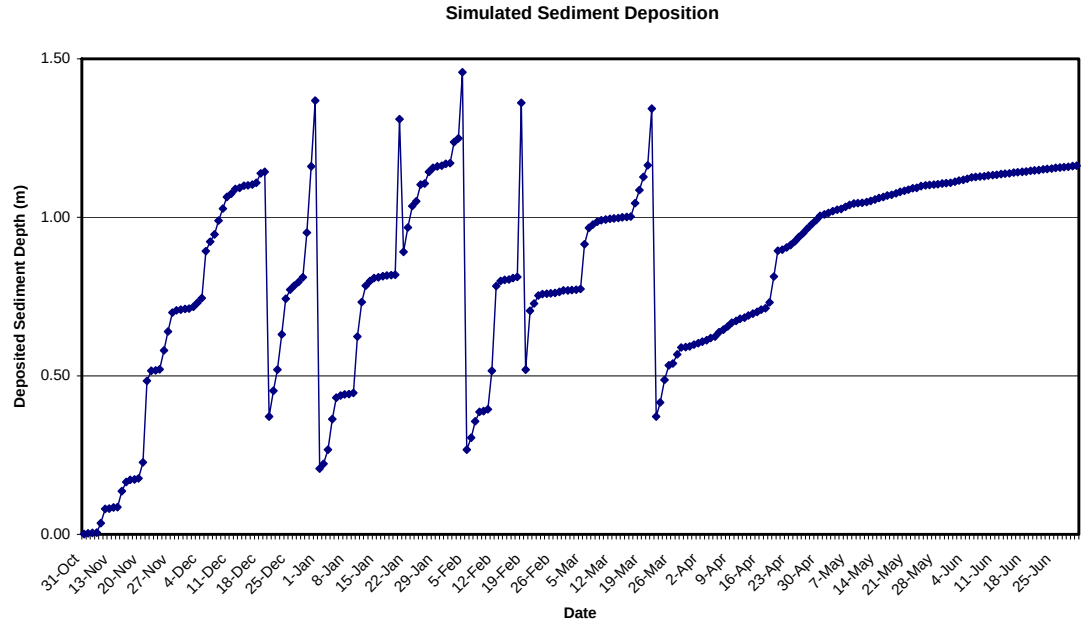

The design flow rate for the water intake was 1.2 m^3/s, and sediment concentrations reached 60,000 mg/L for several days during storm events. Sediment basins were designed for removal of sediment particles 50μm and larger. A fall velocity of 1.96mm/s was calculated for 50μm particles, taking into account the effects of hindered

settling given the 60,000 mg/L suspended sediment concentration. Using **(1)** with a turbulence factor, *K*, of 1.2, the required settling surface area was determined to be 735 m^2. Allowing approximately 5% for inactive settling areas, two parallel basins, 77m long by 10 m wide each, were designed. Two basins were used to ensure that water supply would be uninterrupted while one of the basins was being cleaned.

An 8-month record of measured daily sediment concentrations in the water is shown in Figure 3. A sediment basin model based on Camp's (1946) relationship was used to simulate daily sediment deposition over this period of record. A plot of sediment depths in the basin is shown in Figure 4. In generating this plot, it was assumed that the basin would be cleaned when the deposited sediment depth reached 1.5m, and operation would switch to the adjacent basin. The results showed that very rapid filling of the basin during storms, which led to the recommendation that both basins should be cleaned in advance of expected storms.

6. CONCLUSIONS

A numerical model for computing efficiency of sediment basins is presented. This model is solved using a spreadsheet and is simple to implement. The numerical model yields similar results to Camp's (1946) detailed analytical approach, which provides a degree of validation. The results of the numerical model and Camp's approach show that Vetter's equation significantly under-predicts efficiency. Further work is required to address the differences between the two sets of results, and sensitivity of the results to the assumptions made. In particular, re-suspension of sediment from the bed is expected to influence efficiency for small sediment sizes (relative to the target size), and hindered settling due to increasing sediment concentration with depth is expected to reduce settling velocity. Both of these impacts can be incorporated into the numerical model in the future.

Sediment basins are typically designed based on ideal settling using **(1)** with a turbulence factor of 1.2. The advantage of this approach is that it is simple to use, and will often yield a reasonable approximation of actual sediment removal efficiency. However, it is important for designers to be aware of the following:

- Up to 15% of the target sediment particles will not be removed by sediment basin. This fact is often overlooked, and 100% removal of the target sediment size is assumed. 100% removal would require use of a turbulence factor of 1.5 to 2.0.
- Sediment removal of smaller sediment sizes tends to be under-estimated, and larger sediment sizes tends to be over-estimated. This could have a significant impact on overall basin efficiency, depending on the particle size distribution.

7. REFERENCES

BHRA (1989). *Sediment control at intakes: A design guide*, edited by P. Avery, BHRA The Fluid Engineering Centre, UK.

Camp, T.R. (1946). "Sedimentation and the design of settling tanks", in *Transactions ASCE*, vol. 111, paper no. 2285, pp895-936, American Society of Civil Engineers.

Goldman, S.J., Jackson, K., and Bursztynsky, T.A., (1986). *Erosion and Sediment Control Handbook*, McGraw-Hill, Inc.

Haan, C.T., Barfield, B.J., and Hayes, J.C. (1994). *Design Hydrology and Sedimentology for Small Catchments*, pp 588, Academic Press, Inc, San Diego.

IEAus, (1996). *Soil Erosion and Sediment Control. Engineering Guidelines for Queensland Construction Sites*, prepared by G. Witheridge and R. Walker, The Institution of Engineers, Australia.

Janssen, R.H.A. (2003). "Ignore sediment at your peril - Sediment issues in water management", presented at *Water in Mining Conference*, Brisbane, 13 - 15 October 2003, pp 113 - 121, Australasian Institute of Mining and Metallurgy.

Olsen, N.R.B., and Kjellesvig, H.M. (1999). "Three-dimensional numerical modelling of bed changes in a sand trap", in *Journal of Hydraulic Research*, Vol. 37, No. 2, pp 189-198, IAHR.

Simons, D.B. and Sentürk, F. (1976). *Sediment transport technology*, pp 808, Water Resources Publications, Fort Collins, Colorado.

Valioulis, I.A., and List, E.J. (1984). "Numerical Simulation of a Sedimentation Basin. 1. Model Development", in *Environmental Science and Technology*, Vol. 18, No. 4, pp 242-247, American Chemical Society.

8. APPENDIX - IDEAL SETTLING THEORY

The theory of ideal settling in quiescent conditions is based on the following assumptions:

- There is no scouring or re-suspension of deposited material
- The through-flow velocity is steady and uniform
- Sediment particles settle at a constant fall velocity throughout the basin

For illustrative purposes, the theory of ideal settling will be applied to a rectangular basin, as shown in Figure 5, with a basin width B, length L, and depth of the settling region, D. The cross section average flow velocity (left to right in Figure 5) is assumed to be constant and uniform within the settling region, and is given by:

$$V = \frac{Q}{BD} \tag{14}$$

Figure 5: Schematic section of an ideal settling basin, illustrating linear settling paths of various different sized particles under ideal conditions

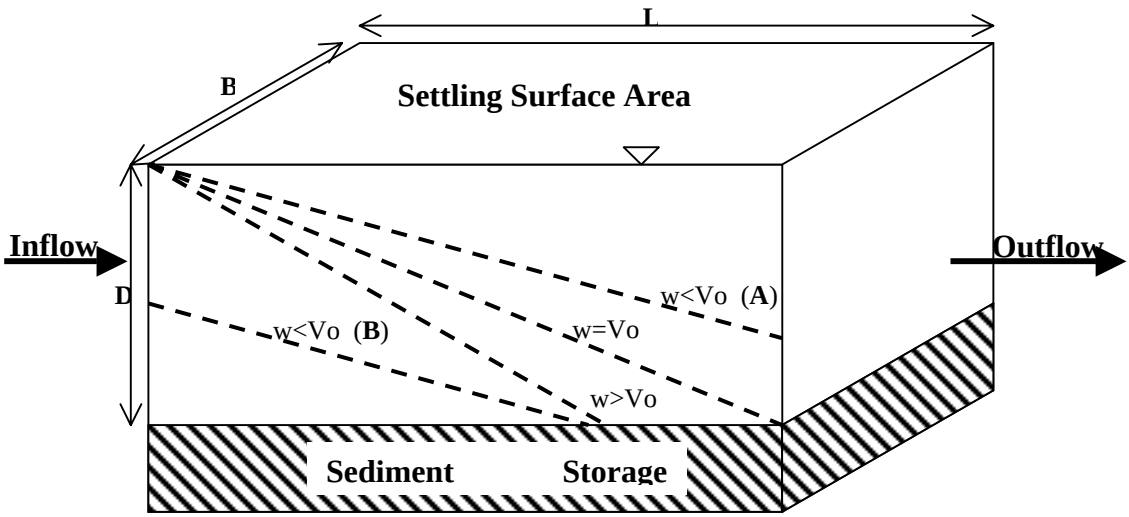

The target sediment, with a fall velocity w_t, is the size for which all particles will just settle in the basin. Equating the time taken for a sediment particle to fall to the bed to the time to be conveyed along the length of the basin, yields:

$$\frac{D}{w_t} = \frac{L}{V} \tag{15}$$

Combining **(14)** and **(15)**, we obtain:

$$w_t = \frac{Q}{BL} = \frac{Q}{A} = Vo \tag{16}$$

Note that $A=BL$ is the surface area required for settling under ideal conditions. **(1)** is obtained by including the factor K (>1) to adjust the fall velocity for non-quiescent conditions. Vo is referred to here as the *overflow rate* (not to be confused with the through flow velocity, V), also know as the "surface loading" or "surface overflow rate". Settling of various particles under ideal conditions, with fall velocities equal to, greater than, and less than Vo, is shown schematically in Figure 5. Where the fall velocity is equal to the overflow rate ($w=Vo$), a particle at the water surface at the entrance to the basin will have settled down to the deposition zone by the time it reaches the basin outlet, and hence this particle will be deposited in the basin. Hence, all particles will be removed whose fall velocity is equal to or greater than the overflow rate. Although some particles with fall velocities less than the overflow rate will not be deposited and will exit the basin ($w<Vo$ (path A)), there are some particles of the same size that will reach the deposition zone ($w<Vo$ (path B)), and hence a certain portion will be removed.

The Institution of Engineers, Australia
8th National Conference on Hydraulics in Water Engineering
ANA Hotel Gold Coast, Australia 13-16 July 2004

Application of CFD Modelling to Free Surface Flow Around Bluff Bodies – A Case Study Using a Bridge Superstructure

M.A. Jempson
B.Eng,. M.Eng.Sc., PhD, M.I.E.Aust, CPEng
Manager, Water & Environment, Victoria, WBM Oceanics Australia
majempson@wbmpl.com.au
N.D. Maxwell
B.E., PhD
Design Engineer, Machinery Division, WBM Pty Ltd, Australia
C.J. Apelt
B.E., D.Phil(Oxon)
Professor Emeritus, Department of Civil Engineering
The University of Queensland, Australia

Abstract: Laboratory data from a research program investigating flood loads on bridge superstructures was used to assess the suitability of computational fluid dynamics (CFD) in representing free surface flow around a complicated bluff body. A two-phase, two-dimensional Fluent™ model was developed and flow patterns, pressure distributions and force coefficients were compared to the laboratory data.

General agreement was achieved in the flow patterns, with the only significant discrepancy being in the separated boundary layer above the model. Uncertainty over the treatment of the fluid density in a two-phase problem in Fluent™ limited the discussion on the pressure distributions. Notwithstanding this, there was general agreement in the pressure distribution patterns. Under some flow conditions good agreement was obtained between the force coefficients, and in others the agreement was poor. Difference in the separated boundary layers was identified as a possible explanation for the discrepancies.

Further research is required to investigate the anomaly in the fluid density, the mesh resolution, turbulence intensity and other flow and geometry conditions.

Keywords: CFD, computational fluid dynamics, bluff bodies, bridge, flooding, free surface flow, flood loads, drag coefficient, lift coefficient, moment coefficient, pressure coefficient

1. INTRODUCTION

In the mid 1990's the first and third authors undertook a comprehensive laboratory program to gain an understanding of hydrodynamic and debris loadings on bridge superstructures and piers and the associated fluid mechanics phenomena. Loads on scale model bridges were measured using a custom designed dynamometer and by integrating pressure distributions measured around the centreline of the superstructure model. Test data is available for a range of flow conditions and geometric arrangements. Flow visualisation and pressure distributions were used to investigate the bluff body fluid mechanics phenomena associated with flow around bridges. Boundary layer separation and reattachment, free surface effects, and wake blockage effects were studied in detail, and related to the trends in the measured loads.

Advances in computational fluid dynamics (CFD) modelling software, particularly in the representation of turbulence, prompted the authors to utilise the laboratory data to assess the suitability of CFD in representing free surface flow around a complicated bluff body such as a bridge superstructure. The software Fluent™ was used for this assessment.

The laboratory program indicated that degree of submergence, the behaviour of the separated boundary layer, the Froude Number and the proximity of the model to the bed were key factors affecting the loads on the models. Tests selected for modelling in CFD provided a range of submergences.

This paper presents the results of this research. A comparison between the laboratory and CFD analysis is made for the load coefficients, the pressure distribution and the flow patterns.

2. LABORATORY PROGRAM

The aim of the laboratory test program was to determine C_D (drag coefficient), C_L (lift coefficient), and C_M (moment coefficient) for use in the design of submersible bridge superstructures for a range of geometric and flow conditions likely to be encountered by the designer, and to gain an understanding of the associated fluid mechanics phenomena. The test condition was defined by the relative submergence (S_R), the proximity ratio (P_r), the Froude number (**Fr**), and the superelevation. With reference to Figure 1, S_R, P_r, and **Fr** are defined by equation 1. By definition, a superstructure with the upstream water level to the top of the parapet has a S_R of 1.0. S_R ranged from 0.5 to 3.0, P_r from 1.4 to 9.1 and **Fr** from 0.09 to 0.6.

$$S_R = \frac{d_{wgs}}{d_s}, \qquad P_r = \frac{y_{gs}}{d_s}, \qquad \mathbf{Fr} = \frac{V_0}{\sqrt{g.y_0}} \tag{1}$$

where d_{wgs} is the depth from the upstream water surface to the girder soffit (m), d_s is the depth of solid superstructure (m), y_{gs} is the distance from the floor to the girder soffit (m), V_0 is the average free stream approach velocity (m/s) at the level of the superstructure, g is the gravitational acceleration (9.81 m/s/s), and y_0 is the depth of the free stream approach flow (m).

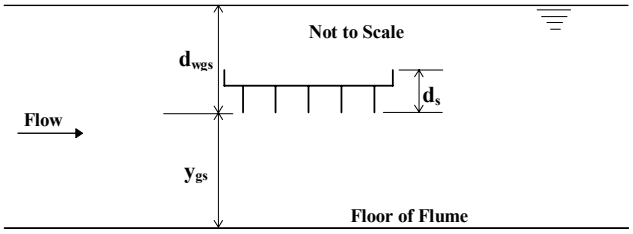

Figure 1 Dimensions for Calculating S_R and P_r

Scale models of six superstructure types were tested. Only data from the model of a typical prestressed concrete girder bridge with concrete deck and New Jersey parapet is used in this paper. The model was constructed to a scale $L_r = 25$, where L_r is the length ratio. Model dimensions are given in Figure 2. The dimension of the superstructure in the spanwise direction was 998 mm.

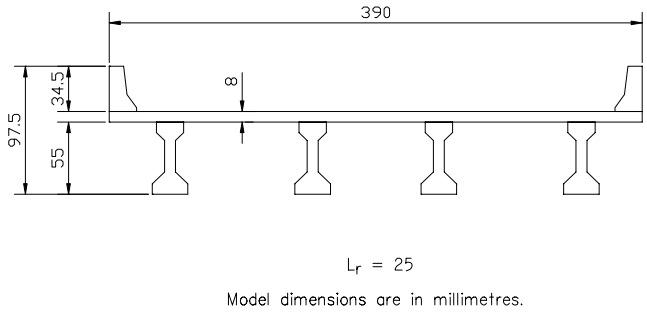

Figure 2 Dimensions of Scale Model

The experiments were done in the test flume at the Department of Civil Engineering at The University of Queensland. It is a low head, high flow circuit with a maximum flow capacity of 500 Ls^{-1}. The working section of the flume is rectangular in section, 3 m long, 1.25 m deep and nominally 1 m wide with clear perspex walls and a concrete floor. The pump is axial flow and direct coupled to a variable speed electric motor.

The hydrodynamic forces on the scale model were obtained by measuring the pressure distribution around the cross-section of the superstructure (pressure distribution method (PDM)), and by measuring the forces directly (direct force method (DFM)). The two methods were carried out independently. Although results from the DFM are not used directly in this investigation, this aspect of the laboratory program is mentioned because good correlation between the DFM and PDM was obtained for the drag and lift coefficients (Jempson, 2001). This supports the reliability of the pressure distributions measured in the laboratory.

To calculate the loads on the bridge superstructure using the PDM, the pressure distribution around the bridge was measured and then the components of the pressure forces in the direction of flow (drag force), normal to the flow direction (lift force), and the moment about the girder soffit were obtained by integration. When using the PDM the model was fixed in position. In any one PDM test, the pressure was measured at up to 40 of the

available 46 tappings shown in Figure 3. The reference pressure was the piezometric pressure at the flume cross-section 1.225 m upstream of the bridge centreline where the pressure distribution was hydrostatic. Pressures at the surface of the model greater than the reference hydrostatic pressure were recorded as positive and vice versa.

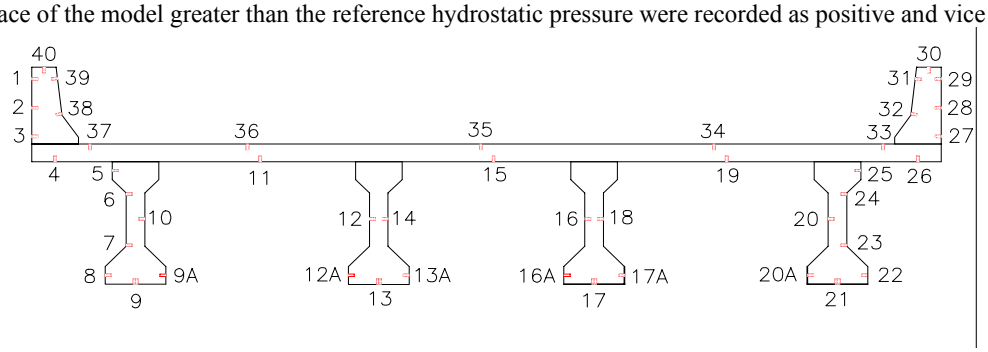

Figure 3 Location of Pressure Tappings

3. CFD ANALYSIS

Computational modelling of the two-phase system was performed using the commercial CFD package Fluent™ with the channel surrounding the bridge represented by a two-dimensional mesh of 37,364 quadrilateral elements. This mesh varied in element size and was most refined in the region surrounding the bridge and about the line of interaction between the water and air. For each test case, the inlet conditions used 5% turbulence and the particular inlet velocities and water depths specified for each case. For the outlets, outflow boundary conditions were used. Phase interactions were modelled using an implicit volume of fluid approach.

The turbulence model used was the Reynolds Stress model. This is the most complex model available in Fluent™ as it solves the Reynolds Stress transport equations in each dimension separately. It hence has a greater potential for accuracy for complex flows than the simpler Spalart-Allmaras or k-epsilon models also available in Fluent™. For three-dimensional modelling problems Fluent™ is also capable of doing Large-Eddy Simulation of flow around bluff bodies, however this approach is inapplicable to two-dimensional problems such as the current study.

Three tests were analysed in Fluent™ to give a range of submergences at a constant **Fr** and P_r to the bed. The laboratory flow and geometry conditions are summarised in Table 1 for the tests simulated using Fluent™.

Table 1 Test Conditions Modelled in Fluent

Test Number	**Fr**	**S_R**	**P_r**
Varying S_R with constant Fr and P_r			
SWOD71R	0.21	1.58	3.44
SWOD66R	0.21	2.03	3.44
SWOD72R	0.21	2.58	3.44

4. DISCUSSION

Flow patterns and pressure and force coefficients obtained in the laboratory program are compared to the CFD analysis. It is shown that, in general, good agreement was achieved.

4.1 Flow Patterns

Free surface profiles, the behaviour of the separated boundary layer, and circulation patterns within the wake region were observed in the laboratory. Dye injection was used to observe the separated boundary layer and the wake patterns. The observation of the separated boundary layers was normally limited to the location of separation and reattachment as shown diagrammatically in Figure 4. It is not intended that the lines shown as separated boundary layers represent the angle of separation, the curvature of the separation, or the wake width. The following discussion on the laboratory tests related only to the tests considered as part of this investigation. Differing patterns were observed in other tests.

In all laboratory tests, the boundary layer separated from the top of the upstream parapet, the upstream lower edge of the deck and from the leading edge of the soffit of the upstream girder. The separated boundary layer on the underside of the bridge did not reattach, but under some flow conditions reattachment occurred on the deck.

If reattachment on the deck occurred, there would be separation from the top of the downstream parapet. These flow patterns are shown in Figure 4 for a series of tests with S_R varying, but P_r and **Fr** held constant. As S_R increases, the location of reattachment moves further downstream. Jempson (2001) noted that the location of reattachment approximately coincided with the location of the low point in the free surface. It was concluded that there is most likely an interaction between the free surface and the separated boundary lower without one necessarily controlling the other. Other patterns of interest are the circulations upstream of the upstream girder, and between the girders.

Generally it was found that Fluent™ replicated these patterns reliably, with the only significant difference being the reattachment to the deck. A comparison between Figure 5, the Fluent™ velocity vectors for test SWOD72R, and the same test in Figure 4 shows that the circulation patterns under the deck are reliably reproduced by Fluent™.

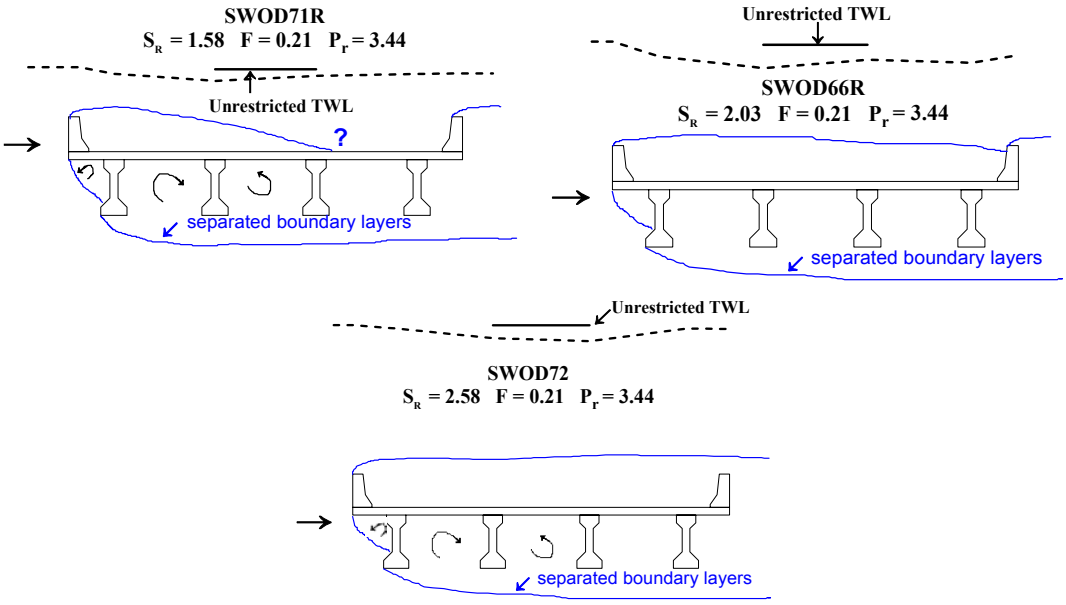

Figure 4 Laboratory Flow Patterns with Varying S_R

Figure 6 shows traces from Fluent™ that indicate the approximate positioning of the separated boundary layer. A comparison with the separated boundary layers shown in Figure 4 reveals some differences above the model. In both the laboratory and Fluent™ the reattachment point moves further downstream as the submergence increases, but the effect is greater in the laboratory with no reattachment occurring in test SWOD72. On the underside of the model there is a minor difference with the Fluent™ separated boundary layer having a greater curvature than indicated in the laboratory, although reattachment does not occur in either the laboratory or in Fluent.

The turbulence intensity of the incident flow can influence the separated boundary layer through enhanced transfer of mass, momentum and energy associated with increased levels of turbulence. Jempson (2001) noted that, in experiments where the turbulence intensity was increased to approximately 11%, the separation bubble shortened when compared to tests with equivalent flow and geometry, but normal levels of turbulence (5%). In Fluent™ the inlet boundary conditions were established with a turbulence intensity of 5%, but the turbulence intensity increased to about 8% closer to the model. This may explain some of the difference in the separated boundary layers.

Another factor that may be affecting the representation of the separated boundary layer is the mesh resolution. At the top of the upstream face of the upstream parapet, the velocity vectors are not parallel to the face of the parapet as would be expected near the separation point.

Further research is being undertaken to investigate these differences. Aspects that are being considered include the resolution of the mesh and the turbulence intensity. Additional laboratory data that is presented in Section 4.2 indicates the significance of the turbulence intensity.

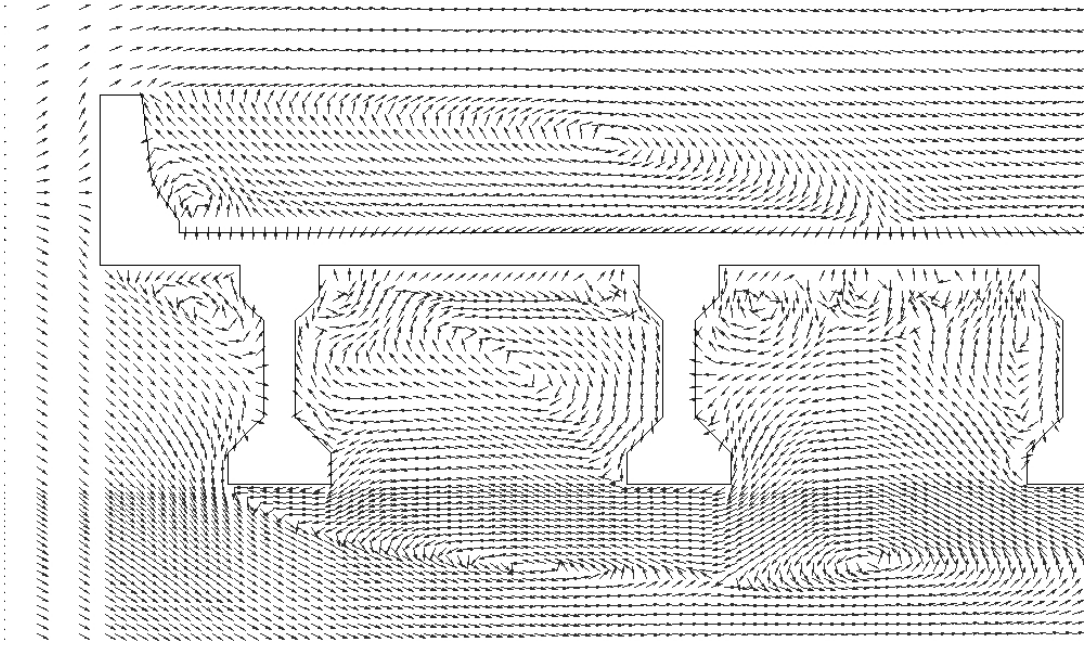

Figure 5 Velocity Vectors - SWOD72R

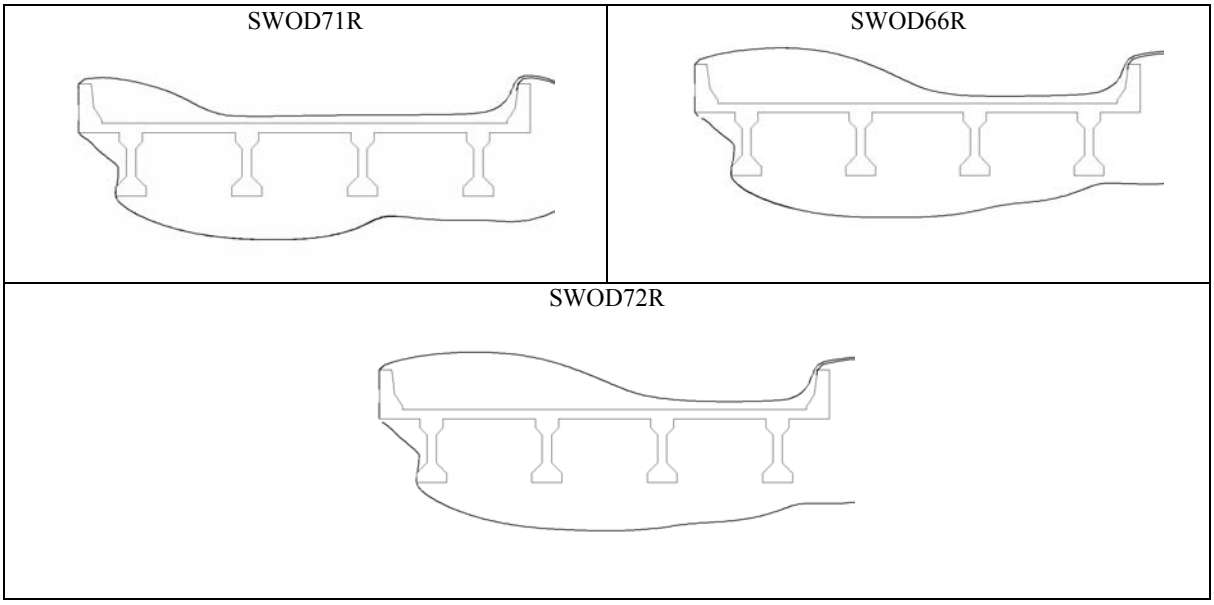

Figure 6 Flowlines from Fluent

4.2 Pressure Distributions

The pressure coefficients (C_P) derived from the laboratory data and from Fluent™ are presented in Figure 7. C_P was calculated using Equation 2 where p is the pressure on the body, p_0 is the free stream reference pressure, V_0 is the free stream velocity and ρ is the fluid density. C_p is positive when the pressure at the surface of the model is greater than the reference pressure. In these distributions, a positive pressure can be considered to be acting into the surface of the model and a negative pressure away from the surface.

The pressure coefficients and pressures output by Fluent™ appear to be calculated using a fluid density equivalent to approximately half that specified for water. This may be an outcome of an averaging process utilised by Fluent™ in two-phase problems. An adjustment to the Fluent™ C_P was made to account for this discrepancy. With this adjustment, there are still differences in the Fluent™ C_P between adjacent tappings that, according to the laboratory data, should have a similar C_P. This is typically on the underside of the model (tappings 9 to 21). Therefore further adjustment to the C_P may be required. This matter is being investigated further. Not withstanding this, it is considered that the adjusted pressure coefficients are sufficiently reliable for comparison of general patterns.

$$C_P = \frac{p - p_0}{\frac{1}{2}\rho V_0^2} \tag{2}$$

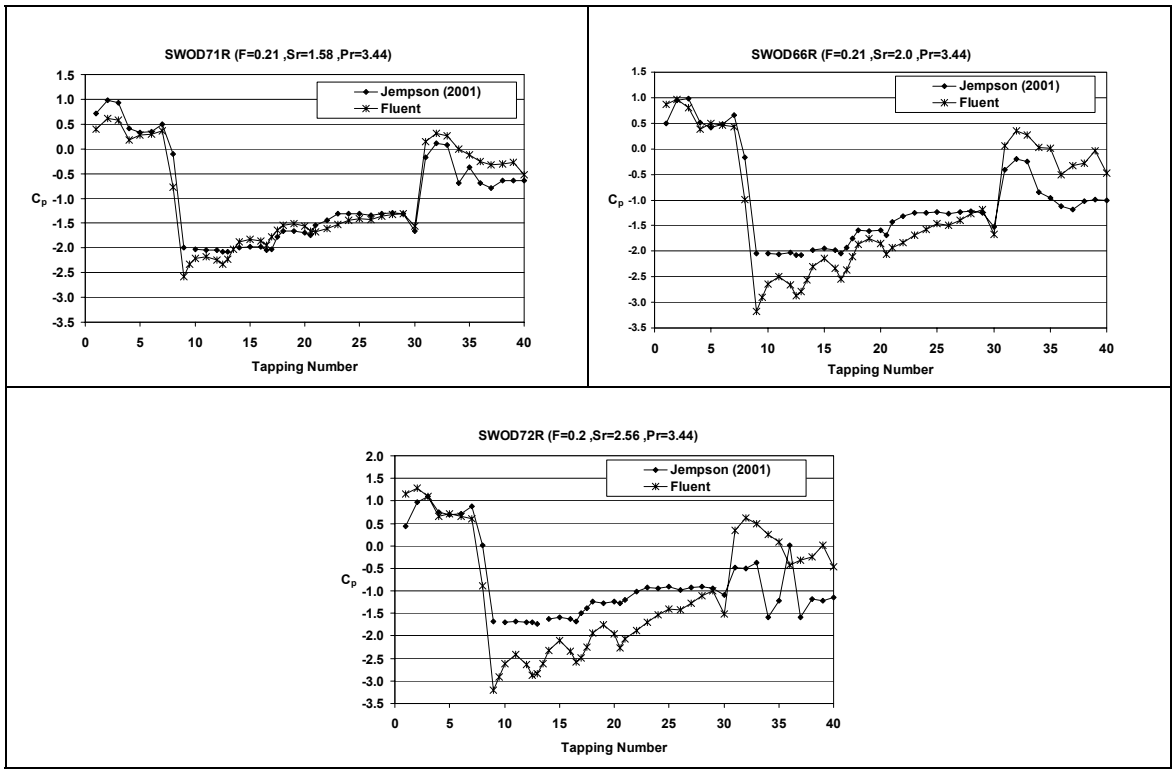

Figure 7 Pressure Distributions

There is general agreement in the pressure distribution patterns, although in some tests there are differences in the magnitude of C_P at some locations. These differences may be related to the uncertainty in the Fluent™ C_P, but differences in the behaviour of the separated boundary layers noted previously may also explain some of the discrepancies. For example, in SWOD72R the separated boundary layer above the model did not reattach in the laboratory test (Figure 4), but in Fluent™ there was reattachment (Figure 6). This difference in the behaviour of the separated boundary layer is consistent with the more positive coefficients in the deck region (tappings 30 to 40) indicated in the Fluent™ data. The difference in magnitude on the underside may be in part attributable to the adjustment of the coefficients to account for the fluid density as noted previously.

The turbulence intensity may also be a contributing factor to the differences on the underside of the model. As noted previously, the turbulence intensity of the incident flow in Fluent™ was higher than that in the laboratory. Jempson (2001) found that increasing the turbulence intensity from 5% to 11% made C_P more negative on the underside of the model. For example, in test SWOD72R, C_P was about –1.7 from tapping 9 to 13, but with the turbulence intensity increased to 11%, C_P was about –3.0. On the deck, increasing the turbulence intensity changed the C_P from about -0.5 at tapping 32 to about +0.8. The C_P obtained in the laboratory for the higher turbulence at these locations case is not dissimilar to those from Fluent.

Further research into the fluid density and turbulence intensity is being undertaken.

4.3 Force Coefficients

The drag coefficient (C_D) and the lift coefficient (C_L) are defined by Equation 3. C_D is positive in the direction of flow, C_L is positive vertically upwards.

$$C_D = \frac{F_D}{\frac{1}{2}\rho V_0^2 A}, \qquad C_L = \frac{F_L}{\frac{1}{2}\rho V_0^2 A} \tag{3}$$

where F_D is the drag force in the direction of flow (N), F_L is the lift force (N), ρ is the fluid density (kg/m^3), V_0 is the approach velocity (m/s), A is the reference area (m^2). The reference area is the wetted area of the superstructure projected on a vertical plane normal to the flow. The buoyant force was <u>not</u> included in the calculation of C_L.

The force coefficients derived from the laboratory data and from Fluent™ are presented in Figure 8. Good agreement in C_D is achieved at an S_R in the range 1.5 to 2, but at an S_R of 2.5, Fluent™ is overstating C_D. In Fluent™ at an S_R of 2.5 (SWOD72R), the separated boundary layer above the deck reattaches and then separates at the downstream parapet. In the laboratory, reattachment did not occur. When reattachment occurs on the deck there is a positive force (in the direction of flow) on the upstream face of the downstream parapet. The force on this face of the parapet is negative when reattachment does not occur, and hence a lower C_D would be expected, all else being equal. There is good agreement in C_L at an S_R of 2.0, but poor agreement at the other submergences. The discrepancies can also be attributed, in part at least, to the differences in the behaviour of the separated boundary layer. Using SWOD72R (S_R = 2.5) as an example again, the C_P along the deck is more positive (acting into the deck and hence a negative lift) in Fluent™ than was recorded in the laboratory.

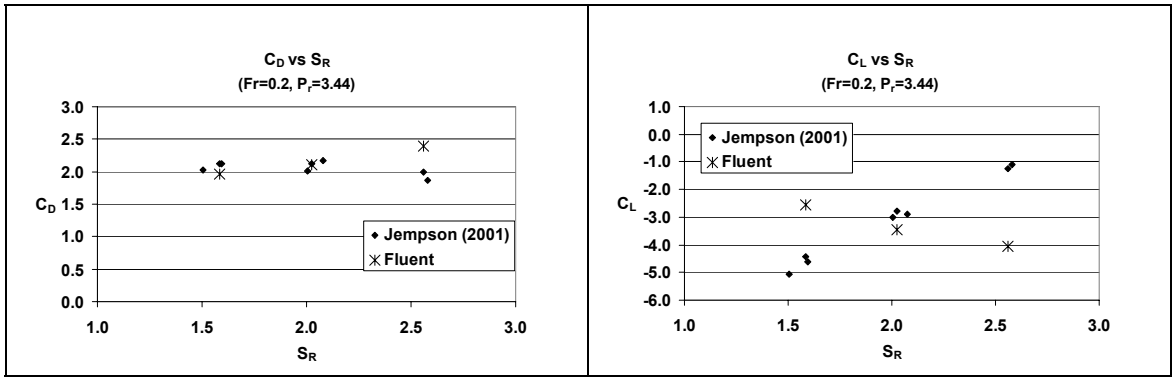

Figure 8 Force Coefficients Varying with S_R

5. CONCLUSIONS

Laboratory data was used to assess the suitability of CFD package Fluent™ in representing free surface flow around a complicated bluff body such as a bridge superstructure. A range of flow conditions was modelled to assess the ability of CFD to reliably reproduce flow patterns, pressure distributions and force coefficients. General agreement was noted in the flow patterns, with the only significant discrepancy being the separated boundary layer above the model. Differences in the turbulence intensity were identified as a possible source of this discrepancy. Uncertainty over the treatment of the fluid density in a two-phase problem in Fluent™ meant that definitive comments could not be made on the pressure distributions. Notwithstanding this, there was general agreement in the patterns. Under some flow conditions good agreement was obtained between the force coefficients obtained in the laboratory and those from Fluent, and in others the agreement was poor. Difference in the separated boundary layers was identified as a possible explanation for the discrepancies.

Further work is ongoing to investigate:

- the apparent anomaly with the fluid density;
- the turbulence intensity in the Fluent™ models and the impact this is having on the separated boundary layers;
- the resolution of the mesh in the vicinity of the model;
- other flow and geometry conditions;
- other turbulence models within Fluent.

6. REFERENCES

Jempson, M.A. (2001). *Flood and debris loads on bridges*, PhD thesis, Univ. of Queensland, Australia.

7. GLOSSARY OF TERMS

A	reference area (m^2)
C_D	drag coefficient
C_L	lift coefficient
C_M	moment coefficient
C_P	pressure coefficient
CFD	computational fluid dynamics
DFM	direct force method
d_s	depth of solid superstructure (m)
d_{wgs}	depth from the upstream water surface to the girder soffit (m)
F_D	drag force (N)
F_L	lift force (N)
Fr	Froude number
g	gravitational acceleration (9.81 m/s/s)
L_r	length ration
p	pressure on the body
p_0	free stream reference pressure
P_r	proximity ratio
PDM	pressure distribution method
ρ	fluid density (kg/m^3)
S_R	relative submergence
V_0	average free stream approach velocity at the level of the superstructure (m/s)
y_{gs}	distance from girder soffit to bed of flume (m)
y_0	depth of the free stream approach flow (m)

The Institution of Engineers, Australia
8th National Conference on Hydraulics in Water Engineering
ANA Hotel Gold Coast, Australia 13-16 July 2004

Estimating the Uncertainty of Flow Measurement for the *In situ* Calibration of Large Water Meters

E.H.Johnson
M.I.E.Aust.
Grampians Region Water Authority, Australia

Abstract: A methodology for the establishment of an *in situ* calibration approach has been determined from previous relevant theoretical and applied research, a pilot study as well as through the application of a Quality System. The Quality System ensures a holistic, ongoing and sustainable *in situ* calibration approach that facilitates confidence by stakeholders in the uncertainty of flow measurement statements for existing large in-line water meters. The Quality System is outlined in a Quality Manual that is the core document used for the purposes of obtaining accreditation from a country's National Accreditation Body. Some important components of uncertainty of measurement have been identified as well as guidance as to how they can be minimised when applying the *in situ* calibration methodology. The benefits of adopting an *in situ* calibration approach include minimising non-physical (apparent) water losses, minimising errors in measurement of the volume of potable water sold and optimal decision-making.

Keywords: Accreditation, calibration, error, insertion, *in situ*, meter, measurement, quality, uncertainty, water.

1. INTRODUCTION

The measurement of flow within pressurised piping systems is an important source of water engineering data. The errors associated with the measurement of this data are directly related to the quality of water engineering decision-making. Any programs, therefore that can determine and minimise the errors associated with these measurements on a sustainable basis will ultimately facilitate optimal decision-making.

Errors in flow measurement contribute to non-physical (apparent) water losses that is usually evident when conducting a water balance or when continuously measuring the volume of potable water to be sold to a customer.

As errors form part of any measurement they require a quantitative statement to have credibility. Uncertainty of measurement is the parameter that quantifies the boundaries of the error of a measurement. A statement of the uncertainty associated with the result of a measurement is preferred because it is more specific than the general term accuracy, which is often open to misinterpretation.

Water meters require recalibration, as on installation and over its operational life, the water meter's performance will differ from that of its original off-site laboratory calibration. There is, therefore, a need to determine the uncertainty of flow measurements within large pipelines by means of a portable meter so those in-line meters which cannot be easily removed for testing can be evaluated or previously calibrated water meters can be calibrated *in situ* to take into account particular site conditions.

The calibration of large in-line water meters in the field is required not only because of differing site conditions, which affects a water meter's performance, but also because of the expense of testing on off-site facilities and the practical problems associated with the removal and testing of some types of water meters.

A flow reference standard is generally used as the benchmark to be compared against when establishing errors in flow measurement. This standard could either be another water meter of a higher metrological quality or a technique utilising weighing methods or volumetric methods. This standard should also be traceable to the national or international flow standard such that the result of flow measurement can be related to this standard through an unbroken chain of comparisons.

To be sustainable, any *in situ* calibration approach developed should be based on best practices in the field of flow metrology. These best practices should also have a foundation in applied research, sound experience and Quality Systems. A verification procedure is an essential component of a calibration approach as it provides confidence in the results obtained. This verification procedure includes the basic components of uncertainty for a flow

reference standard. The development of a Quality System, based on ISO 17025 (1999), enhances the sustainability of *in situ* calibration programs for water authorities.

This paper provides:

- A brief review of previous studies on the subject of velocity profiling techniques utilising insertion meters.
- A description of a related empirical *in situ* calibration research project that overcame the disadvantages of a pure theoretical approach.
- An overview of a multi-phase calibration program for the *in situ* calibration of 200 large (300 - 2 000 mm diameter) water meters.
- An outline of a methodology, in the context of a Quality System that facilitates an estimation of the uncertainty of flow measurement for the *in situ* calibration of large water meters.
- A suggestion of a potential Australian application for the approach such as part of the proposed Wimmera Mallee Pipeline Project.

2. *IN SITU* CALIBRATION REFERENCE STANDARD

2.1 Previous Research

The original research conducted into the various velocity-area methods of flow determination assumed that the insertion meters were error-free and emphasised the relative accuracy of these methods. A subsequent applied research project in South Africa combined the various components of uncertainty of measurement through a direct comparison of the velocity profiles measured with an insertion meter and the flow measured by an accredited off-site laboratory. These previous studies are reviewed below.

2.1.1 Velocity-Area Methods

The determination of velocities at various points across one plane in a pipe flowing full and under pressure usually finds the maximum velocity positioned at the centre of the pipe with the velocity reducing as measurements are taken closer to the pipe wall.

Velocity-area methods require that the flow sensor be inserted at predetermined points across the plane for the measurement of the local velocity. The mean of these local velocities is the average velocity of the water flow in the pipe. Generally, the greater the number of measuring points per traverse the less the error in flow determination for a particular method.

Evaluation studies (Winternitz and Fischl, 1957; Salami, 1971) have indicated the merits of the various velocity-area methods of flow determination in pipes. The tangential method seems to be the one that was most commonly adopted in the past, while the log-linear method appears to be the most accurate. The log-linear is also more efficient in its application as it requires fewer measuring points to achieve smaller errors than other velocity-area methods with a greater number of measuring points.

The emphasis of these earlier evaluation studies was on the determination of the relative accuracy of the various velocity-area methods and not the overall accuracy of the flow measurement relevant to a reference standard. A recent related study by the National Engineering Laboratory (NEL, 2002) indicated that the quantifying of errors from mathematically derived velocity profiles for various effects are not absolute and only provide an indication of the severity of the effects.

A graphic comparison of the errors associated with different velocity-area methods for six velocity-measuring points per diameter as derived from Salami's (1971) results is given in Figure 1.

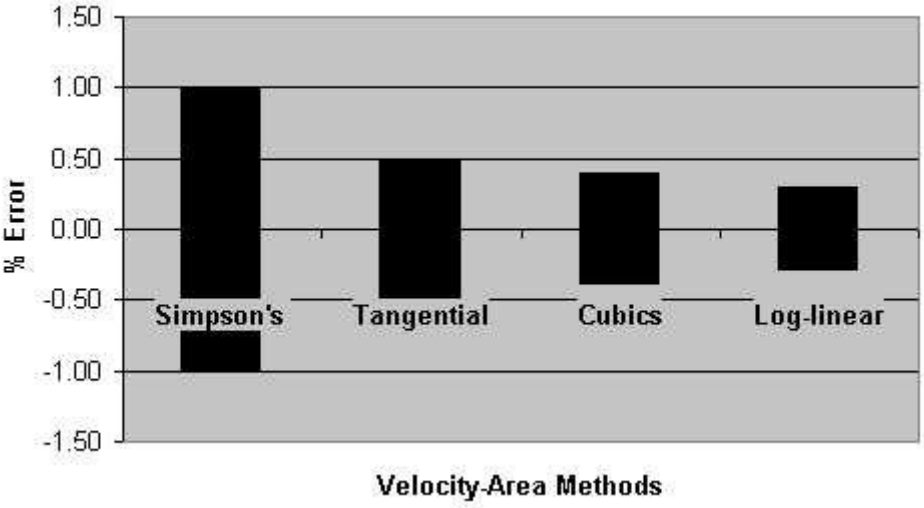

.

Figure 1 – Velocity-Area Method-Error Comparison (Salami, 1971).

2.1.2 South African Water Research Commission Project

A comprehensive review of previous studies on the subject of velocity-area methods for flow determination, and some practical guidelines as to the application of insertion meters in establishing a suitable *in situ* flow reference standard was provided by Johnson (1995). Subsequent related applied research by Johnson (1999) established a flow reference standard for the cost-effective *in situ* calibration of large in-line water meters consisting of the combined accuracy of point velocity measurements within pipes, a velocity-area method and a velocity-profile function. This previous research indicated that the *in situ* calibration of large water meters can achieve tolerances that comply with relevant standards and that these results are traceable to national and international flow reference standards.

The research undertaken to establish this flow reference standard included the measurement of velocity profiles within pipe sections of 250, 300, 400, 500, 600 and 800 mm diameter and compared to the flow measured by a large permanent flow laboratory. This flow laboratory has a best measurement capability of 0.1% uncertainty for the 95% confidence level as accredited by the South African National Accreditation System (SANAS).

Results of this empirical research are given in Figure 2 and the envelope illustrated is used to define the tolerances within which a meter's error curve is expected to be situated as well as its specified flow range. The research also identified the disadvantage of attempting to adopt a pure theoretical approach when modelling velocity profiles.

The South African Specifications SABS 1529-1 (1994), as well as the International Standards ISO 4064 (1993) was used to provide a generic definition of the error envelope for this research. The flow range for mechanical meters is defined from a minimum flow rate (Q_{min}) up to a maximum or overload flow rate (Q_s). Q_p is the normal flow rate at which the meter should operate situated between minimum and maximum flow rates. Between Q_{min} and Q_p, a transitional flow rate (Q_t) is specified dividing the flow range into two separate permissible error zones. Q_p is also referred to as Q_n and Q_s as Q_{max} in the International Standards ISO 4064 (1993) while a recent Australian Standard AS 3565.1 (2004) defines these four points over a meter's flow range as Q_1 through to Q_4.

The baseline reference defining the error envelope for existing meters in use is given by SABS 1529-1 (1994) as ±8% for flow rates less than or equal to Q_t and ±3.5% for flow rates greater than Q_t. The rationale for adoption of the error envelope for mechanical meters in use was that a portable insertion turbine meter was used in the research project and there is a paucity of references indicating the error limits of other types of meters in use. Although other types of meters could have lower error specifications than those of mechanical meters, the SABS 1529-1 (1994) error values was adopted as an upper limit.

The results of this research project therefore also indicate that the combined errors of all the factors influencing the measurement of flow by means of this *in situ* calibration method generally fall within the error limits adopted for meters in use.

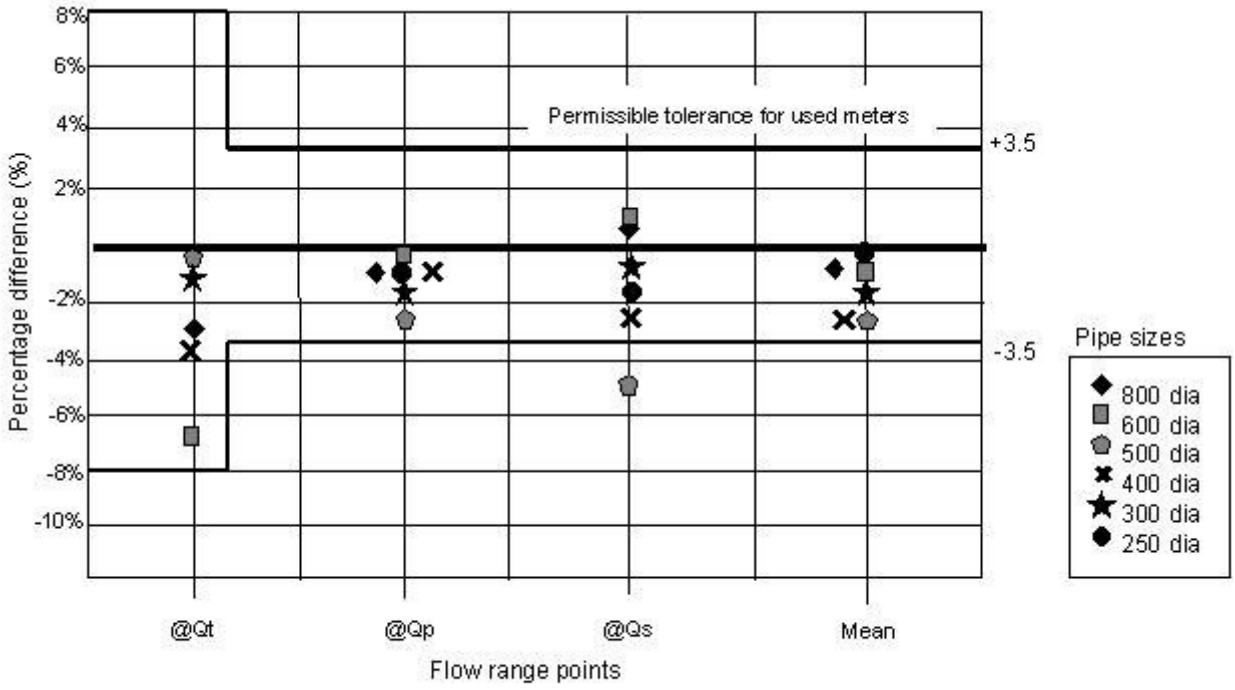

Figure 2 – *In situ* Calibration Research Results (Johnson, 1999)

2.2 Pilot Study

A holistic, ongoing and sustainable *in situ* calibration program was initiated for Rand Water, a large water authority in South Africa, based on the previously mentioned research (Johnson & Mashile, 2002). The aim of the program was to establish the confidence of stakeholders in the potable water volumes measured by large water meters. It is proposed that this multi-phase calibration program will eventually involve the regular *in situ* calibration of the authority's 200 large (300 - 2 000 mm diameter) water meters.

The program commenced with a reconnaissance survey and data collection exercise to correctly assess future access points for flow measurements as well as the ability of the hydraulic system to achieve specified flow rates required for testing meters.

Some first order measurement uncertainties were initially established at a sample of metering sites, which also gave an indication of the limitations of an approach that excludes the application of a Quality System. Accessible to the pipe at each of the proposed *in situ* measuring site was also investigated during the initial stages of the program.

The pilot study included the planning, design, specification and construction of access pipework and chambers to accommodate portable *in situ* testing equipment at a sample of sites. Subsequent Closed-Circuit Television (CCTV) inspections indicated the unsuitability of using existing pipes as test measurement sections because of the excessive roughness of the original internal protective coatings. The program was subsequently modified to include the installation of new sections of in-line piping at the portable meter's insertion point. The purchase of a portable insertion flow meter was undertaken as a result of a thorough evaluation and specification preparation process.

The electronic logging of a sample of water meters' and determination of their weighted errors of measurement was an important aspect of the program as it established each of the existing in-line meter's overall error of measurement for current operating conditions as well as whether they were correctly sized.

An accreditation process based on ISO 17025 (1999) for site calibration and testing is the core of the program. It is proposed to ultimately obtain accreditation for the *In situ* Calibration Laboratory through SANAS. The accreditation process will ultimately ensure traceability of flow measurements and included the preparation of a Quality Manual. If a Quality System was not to be implemented it would lead to an unsustainable program and inconclusive results.

During implementation of the program it was found that the water authority's institutional capacity and respective skills base required strengthening before it can proceed with an on-going *in situ* calibration program for all of its large water meters. Although training and mentorship of the authority's project team was a key component of the original project, it became apparent that establishment of the *In situ* Calibration Laboratory required a far greater involvement of the management of the authority in the application of the Quality System than was originally envisaged.

2.3 Quality System

A Quality System for an *in situ* calibration laboratory includes applicable procedures, methods, competent personnel, portable water meters and water engineering infrastructure. The code of practice ISO 17025 (1999) provides the general guidance for the establishment of Quality System for a calibration laboratory. A Quality System is outlined in a Quality Manual that sets out the quality policy and objectives as well as identifies management functions and responsibilities. Technical requirements that include the procedure to estimate uncertainty of flow measurements and validation of the calibration method are also detailed in a Quality Manual.

The aim of a Quality System is to have routine activities standardised for the benefit of all concerned and then to ensure that every individual and activity involved becomes part of the process. The established and maintenance of a calibration laboratory in accordance with a Quality System ensures a holistic, ongoing and sustainable *in situ* calibration approach. This Quality System facilitates confidence by stakeholders in the uncertainty of flow measurement statements of a water authority's large water meters.

The Quality Manual is the core document used for the purposes of obtaining accreditation of a calibration laboratory in terms of ISO 17025 (1999). A laboratory obtains its accreditation from the National Accreditation Body of a country and in Australia this organisation is the National Association of Testing Authorities (NATA). National Accreditation Bodies for various countries are linked via international Mutual Recognition Agreements to ensure consistency amongst accreditation bodies. Therefore, the previously mentioned SANAS and NATA have a Mutual Recognition Arrangement through the International Laboratory Accreditation Co-operation (ILAC).

2.4 Estimate Uncertainty of Flow Measurement

It is not possible to measure anything without error and the further the measurement is removed from a reference standard the greater the doubt in the particular measurement. A reference standard must also be related to a national and international standard through an unbroken chain of comparisons. This 'doubt' is known as measurement uncertainty.

Cook (2002) defines uncertainty as the parameter, associated with the result of a measurement that characterises the dispersion of the values that could reasonably be attributed to the measureand. The measureand is the particular quantity subject to measurement. An uncertainty statement has an associated confidence level, which is generally the 95 % confidence level. This means that there is a 95% probability that the true value lies within the stated range.

2.4.1 Components of Uncertainty for *In situ* Calibration Flow Reference Standard

A reasonable estimation of the components of uncertainty of an *In situ* Calibration Flow Reference Standard can be based on the knowledge gained from the previously mentioned applied research. The aim is to adopt a calibration approach that is based on acceptable best practices in the field of flow metrology which in turn has a foundation in applied research, sound experience and Quality Systems that provide confidence in the results through a verification process.

To facilitate the identification of some of the relevant components of uncertainty, the mathematical method known as Dimensional Analysis can be used to reduce complex hydraulic problems to the primary quantities of Length (L), Mass (M) and Time (T) as detailed in Table 1.

Table 1. Dimensional Analysis of Components of Uncertainty

Description	S.I. or other units	Components	Derived dimensions M-L-T
(i) Flow rate in a pipe	m³/s	- diameter of pipe - mean velocity of water	L³/T
(ii) Pipe diameter & ovality	m	- diameter	L
(iii) Mean velocity related to a particular velocity-area method	m/s	- velocity	L/T
(iv) Cross-sectional area of pipe	m²	- area	L²
(v) Frequency of insertion meter's turbine blade	H_z (pulses/s)	- pulses per second	1/T
(vi) Insertion meter factor (turbine)	pulses/m	- frequency - water velocity	1/L
(vii) Actual point velocity measurement of turbine insertion meter	measured frequency/meter factor	- frequency - meter factor	L/T
(viii) Insertion Blockage Factor	m²	-area /area	Dimensionless i.e. L²/ L²
(ix) Positioning of insertion meter at log-linear measuring point within the pipe	m	- length	L
(x) Measured single-traverse velocity profile with respect to the modified Pao equation.	m & m/s	- measuring position - pipe radius - velocities	Dimensionless i.e. $\frac{L}{T}$ x $\frac{T}{L}$
(xi) Steady state flow rate	m³/s	- % difference of flow rate	Δ (L³/T)
(xii) Relative roughness of pipe	m	- length/length	Dimensionless i.e. L/L

The proviso of stating that the velocity profile is dimensionless in Table 1(x) is that two extra velocity measurements are taken together with the velocity measurements taken at the positions determined by the log-linear method (i.e. at centre-line and the approximate position that mean-axle velocity occurs). The modified Pao equation describing the velocity profile within the pipe and at turbulent flows is independent of temperature changes (Johnson, 1995).

The British Standard BS1042 (1984), Part 2 provides a useful guide to identify all the uncertainty components, which are of importance when applying velocity area methods and current-meters. These components include uncertainties arising from asymmetry, swirl and turbulence.

Although each calibration site should be selected to allow for sufficient straight lengths of pipe that would facilitate the development of an axisymmetric velocity profile at the measurement point, there is a possibility that there would be some uncertainty arising from a possible asymmetric profile. The index of asymmetry relates to the anticipated maximum error and is the standard deviation (s) of the mean velocities (v) determined at each log-linear measuring point divided by the mean calculated pipe velocity (V_p), i.e.

$$E_y = \frac{s(v)}{V_p} \qquad (1)$$

Applying this index to the research results of Johnson (1999) the maximum percentage uncertainty for 6 measuring points across a single traverse (diameter) was approximately 0.13%.

The siting of the calibration sites with sufficient straight lengths upstream of the measuring point should reduce the problem of swirl. The British Standard BS1042 (1984) indicates that for swirl angles below 20° the percentage uncertainty (Es) is taken at ±5% of the maximum value (expressed in degrees) of swirl angle observed in the measuring section. There is an approximate relationship between the shape of the velocity profile and the swirl, therefore it can be assumed that if index of asymmetry is within previously stated limits, the swirl angle will be minimal (i.e. < 5°) and Es will be 0.25%. If the relative roughness of the internal walls at the measuring section of the pipe is 1.0 x 10^{-4} or better, then this uncertainty source can be minimised (Johnson, 1995).

Turbulence mentioned here must not be confused with the turbulent flow region within which most potable water pipelines operate (i.e. as defined by the Reynolds Number and relative roughness of the internal pipe surface). Although turbulence can arise from rough pipes (Rough Pipe Law) it can also be caused by similar disturbances to flow that result in profile distortion and swirl.

Some of the previously mentioned as well as other sources of measurement uncertainty can be reduced or rendered statistically insignificant through installation of precision manufactured pipe measurement sections, optimal positioning of the measurement sections within the various pipelines and restricting the time taken to measure the velocity profile with the insertion meter. Johnson (1995) provides details of other possible measures to minimise measurement uncertainties.

The code of practice ISO 17025 (1999) indicates that once a calibration method has been adopted it is to be subject to validation as part of its routine application. An appropriate validation process is the simultaneous measurement of flow rates with clamp-on ultrasonic and insertion meters within the same section of pipe. Only after the results of this validation process indicate that the flow measurements for the two portable meters agree within predefined uncertainty limits, can the calibration of that particular permanent in-line meter commence. Australian Standards AS 2360.7.1 (2001) and AS 2360.7.2 (1993) can provide initial guidance in determining appropriate uncertainty limits.

The sources of uncertainty that are associated with the application clamp-on ultrasonic meters require identification if this type of meter is to be included in an initial validation process. The National Engineering Laboratory (NEL, 2002) indicated that these sources generally relate to the geometry of the pipe section, angle of the transducer, transducer temperature, time measurements and distortion of the velocity profile. These sources of uncertainty will also be reduced through the installation of specially manufactured pipe measurement sections that can accommodate both types of portable meters.

2.4.2 Uncertainty Budget

An estimation of the uncertainty of flow measurements is established through an uncertainty budget. This uncertainty budget is used to determine the best measurement capability of an *in situ* calibration laboratory. The sources of uncertainty of the flow reference standard and the in-line meter being calibrated are evaluated as to whether they are statistically significant or insignificant for inclusion in final calculations. Engineering experience and judgement is also required to determine what sources of uncertainty should be included as well as providing an estimate of their potential influence and statistical characteristics.

The uncertainty budget procedure is detailed in the calibration laboratory's Quality Manual to ensure consistency in the approach adopted. An uncertainty budget facilitates the aiming for and maintaining of realistic tolerances for an *in situ* calibration laboratory as the objective is not attain the best measurement capabilities of an off-site flow laboratory. The achievement of tolerances of at least similar to the results of the previously mentioned applied research project should be expected for an *in situ* calibration laboratory operating within the requirements of a Quality System.

3. WIMMERA MALLEE PIPELINE PROJECT (WMPP)

A potential application for the on-going *in situ* calibration of large water meters in Australia is the proposed Wimmera Mallee Pipeline Project (WMPP). The WMPP proposes to replace a 17 500 kilometre channel system with a pipeline distribution system to reduce the approximate 112 000 megalitres lost annually to evaporation and seepage.

Making provision for an *in situ* calibration system within the proposed WMPP infrastructure and institutional arrangements will facilitate optimal use of funding. Measurement errors of the large water meters will be minimised and maintained to within acceptable tolerances reducing non-physical (apparent) water losses as well as establish the confidence of stakeholders in the water volumes measured by these water meters.

4. CONCLUSIONS

The establishment and maintenance of a comprehensive Quality System facilitates the determination of the uncertainty of flow measurement for the *in situ* calibration of large water meters. To be sustainable, the *in situ* calibration approach developed should be based on best practices in flow metrology that in turn have a

foundation in applied research, sound experience as well as Quality Systems. The determination of the uncertainty of flow measurements assists water engineering decision-making through the comprehensive identification and quantification of errors.

A pragmatic approach is required to identify the components of uncertainty. Engineering experience and judgement will ultimately facilitate estimating which components of uncertainty will be included in the determination of the overall uncertainty of *in situ* flow measurements.

The implementation of an accredited *in situ* calibration laboratory in terms of a Quality System provides confidence by stakeholders in uncertainty of flow measurement statements of a water authority's large water meters. Implications of adopting such an approach however, will be the requirement for institutional strengthening, improvement of the authority's skills base, as well as greater involvement of the management of the authority. The benefits of such an approach include minimising non-physical (apparent) water losses, minimising errors in the measurement of the volume of potable water sold to customers as well as optimal decision-making.

5. REFERENCES

Australian Standard AS 3565.1 (2004). Meters for water supply. Part 1: Cold water meters. Standards Australia. 60p.

Australian Standard AS 2360.7 (2001& 1993). Measurement of fluid flow in closed conduits Parts 7. 1 & 7.2, 60p.

British Standards Institution BS1042 (1984). *Measurement of Fluid Flow in Closed Conduits. Part* 2 Velocity Area Methods. Section 2.3, 27p.

Cook,R.R (2002). *Assessment of Uncertainties of Measurement for Calibration and Testing Laboratories,* National Association of Testing Authorities, Australia, 60p.

International Organisation for Standardisation ISO 4064 (1993). *Measurement of Water Flow in Closed Conduit Meters for Cold Potable Water, Part 1 Specifications.*

International Organisation for Standardisation ISO 17025 (1999). *The Code of Practice for General Requirements for the Competence of Testing and Calibration Laboratories.* Published by the SABS as SABS ISO/IEC 17025, 36p.

Johnson, E.H. (1995). Field Evaluation of Large In-line Flow Meters, *Water SA,* Vol 21 No 2, pp 131-137.

Johnson, E.H. (1999). *In situ* Calibration of Large Water Meters, *Water SA,* Vol 25 No 2., pp 123-135.

Johnson, E.H. and Mashile, P. (2002). A Comprehensive Programme for the *In situ* Calibration of Large Water Meters, IWA *3rd World Water Congress (Melbourne),* Paper e21441a.

National Engineering Laboratory NEL.(2002). Flowmetering Current Practice & Uncertainty Case Studies-Appendix D & F, *ProjectFDWM04,* http://www.windfall.co.uk 20 February 2002.

Salami, L.A. (1971). Errors in the Velocity-area Method of Measuring Asymmetric Flows in Circular Pipes, In Clayton G.C. *Modern Developments in Flow Measurement*. Peter Peregrinus Ltd, pp 381-400.

South African Standard Specifications SABS 1529-1 (1991). *Water Meters for Cold Potable Water, Part 1* Metrological Characteristics of Mechanical Water Meters of Nominal Bore not exceeding 100mm.

Winternitz, F.A.L and Fischl, C.F. (1957). A simplified Integration Technique for Pipe-flow Measurement, *Water Power,* (June), pp 225-234.

The Institution of Engineers, Australia
8th National Conference on Hydraulics in Water Engineering
ANA Hotel Gold Coast, Australia 13-16 July 2004

Rock Chutes: A Review of Damage and Failure Mechanisms

A. R. Ladson
B.E., M.Sc. Ph.D.
Institute for Sustainable Water Resources and CRC for Catchment Hydrology, Department of Civil Engineering, Monash University, Australia

R. H. Hardie
B.E., M.Sc.
Earth Tech Engineering Pty Ltd, Australia

R. J. Keller
B.E., Ph.D.
Institute for Sustainable Water Resources and CRC for Catchment Hydrology, Department of Civil Engineering, Monash University, Australia

Abstract: Rock chutes are an important technique for controlling erosion, and have been widely used in Victorian streams. Occasionally, for a number of reasons, they are damaged or fail. Based on a survey of 170 rock chutes, eight damage or failure modes have been identified and include loss of rock from the face and crest, downstream erosion, undermining of the chute apron, stream bed instability, abutment damage, total loss of the chute and willow infestation. The greatest risk to rock chutes arises from three mechanisms, loss of rock from the face of the chute, willow infestation and abutment damage. It is important to consider the complete range of possible failure mechanisms when designing rock chutes. Improved design procedures, especially aimed at the greatest risk to chutes, loss rock from the chute face, are discussed.

Keywords: rock chutes, erosion control, river management

1. INTRODUCTION

The stability of rivers and channels is often linked to the stability of the channel bed. Channels may be de-stabilised by (for example) the draining of a downstream wetland, which can initiate an erosion head which, unchecked, will migrate upstream with substantial subsequent bank collapse.

A rock chute is a relatively short and steep section of the bed of a channel which has been armoured with rock. It is normally intended to either stabilize an erosion head, preventing it from moving upstream in the channel, or to reduce the overall grade of a channel by providing a weir within the channel bed. A design procedure has been developed for the hydraulic design of rock chutes - Keller and Winston (2003). This procedure is embodied in the computer package CHUTE.

Despite careful hydraulic design, however, rock chutes may be damaged or fail. The purpose of this paper is to highlight potential failure modes, established from an intensive study of rock chutes in North East Victoria and Gippsland, and to highlight lessons learned from these failures to improve future performance.

2. DAMAGE MODES

Rock chutes may be damaged, or fail, in a number of ways. We have identified eight damage modes from reviewing more than 170 rock chutes in North East Victoria and Gippsland.

1. Rock lost from the face of the chute
2. Rock lost from the crest of the chute
3. Bank erosion downstream of the chute
4. Undermining of the chute apron
5. Ongoing instability in the stream bed
6. Damage to the chute abutments, or outflanking of the chute
7. Total loss of the chute crest, face and abutments

8. Willow infestation

The occurrence and frequency of the failure modes listed here should be considered to be specific to the streams where this study was undertaken (Gippsland and North East Victoria). Some of these failure modes have been identified by others (e.g. Frissell and Nawa 1992; Roper et al. 1998) but they have also identified other failure modes and different failure frequencies. The comparison of our work with these North American examples suggest that some failures are uniquely related to stream characteristics, for example, high sediment loads and presence of invasive exotic riparian vegetation. Other failure modes can probably be considered to be generic in that they could happen anywhere. There are also probably other potential failure mechanisms than those that have been documented and new ones waiting to happen. Continuing vigilance is warranted. The aim of this paper is to identify risks to chutes so that their design can be improved.

2.1 Damage Frequency and Costs

Damage frequency, and repair costs, provide information on those problems that are most likely to occur, most costly to fix, or have the greatest risk (Figure 1). For each of the identified damage modes, Figure 1 shows the percentage of chutes affected and the average repair cost.

From our review of over 170 rock chutes, the most common damage mode was willow infestation with over 36% of chutes affected; 25% had minor infestation and 11% major. Minor willow infestations were one of the least expensive problems to fix at an average cost of $6,400 per chute.

The highest cost problems were those associated with outflanking or failure of abutments or total loss of the chute. These problems occurred least often but repair costs can be equal to, or greater than the original construction cost. The average repair costs for chutes damaged by abutment failure was about $37,000 in our sample.

Looking at risk is a way of combining information on damage frequency and cost. The usual definition of risk (see A/NZS 4360:1999) is:

Risk = Consequence x likelihood

Considering consequence as equal to damage cost, and likelihood as damage frequency, the risk of the damage modes can be calculated. Three damage modes stand out, in order:

1. Rock lost from the face of the chute;
2. Willow infestation; and
3. Damage to the chute abutments, or outflanking of the chute.

To manage these risks, we can reduce the cost of repair (consequence) and/or the occurrence (likelihood) of failure. This requires a combination of good design, construction and maintenance.

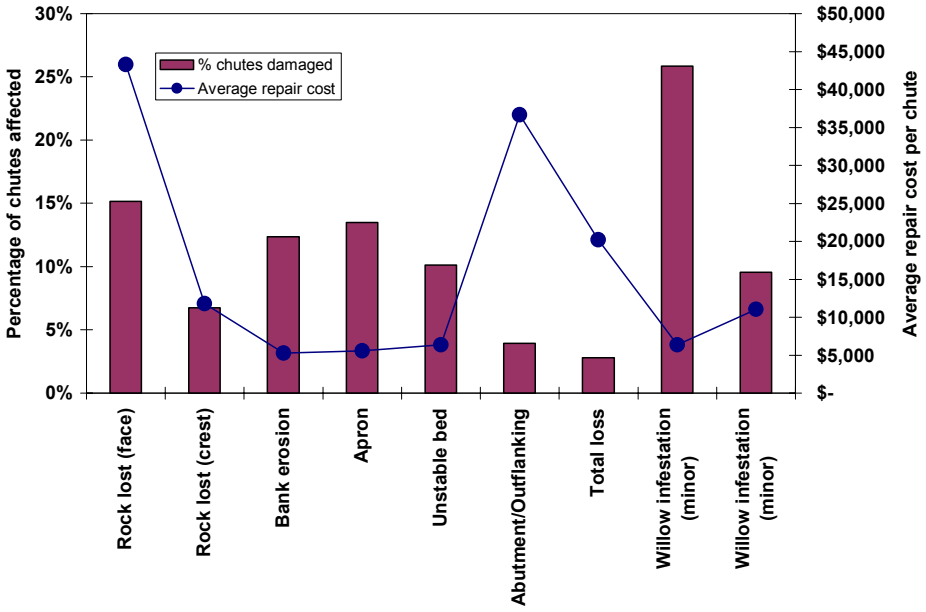

Figure 1 – Damage modes for rock chutes

2.2 Loss of rock from the face of a chute

Our analysis showed that the greatest risk to chutes is damage associated with the loss of rock from the chute face (Figures 1 and 2). Sometimes damage of this type can be associated with large floods events when it may not be unexpected. However, there are also many situations where rock is lost in relatively small events where the extent of damage is often surprising large.

Laboratory analysis on scale models of rock chutes suggests the likely failure mechanism (Topham 1994). In these model chutes, failure was initiated when forces caused by a hydraulic jump, were sufficient to pluck rocks from the chute face. Once a few rocks where removed there was progressive upstream failure and the chute unravelled. Similar removal of isolated rocks occurred in a full scale test, although there was not sufficient flow to destroy the chute (I D & A Pty Ltd 1996). Others have reported similar results e.g. (Olivier 1967).

Better design procedures can make this type of damage less likely. In the past, chutes have often been designed for a flow event of a particular recurrence interval, usually a 10-year to 50-year event. This design flow was converted into a discharge per unit width and the rock sized accordingly. This design approach should not be used as it can give a misleading indication of the required rock size.

Rock chutes need to be designed for a *critical* flow, not a flow based on a particular recurrence interval. Often the critical situation occurs for relatively small flows with the chute being drowned out as flows increase (Figure 3). The selection of rock for a chute should be based on the maximum required rock size up to the design flow event, not the size based on the design discharge. Note that some design procedures are unnecessarily conservative in that do not take into account the fact that a chute can be drowned out at high flows. Instead the required rock size is just determined from the discharge per unit width (Robinson et al. 1997). Best practice design procedures will be based on an estimate of the actual forces on the chute.

The CHUTE program (discussed below) allows rapid calculation of the critical flow and the design rock size.

Figure 2 - Rock lost off the face of a rock chute on Iguana Creek, Mitchell River Catchment

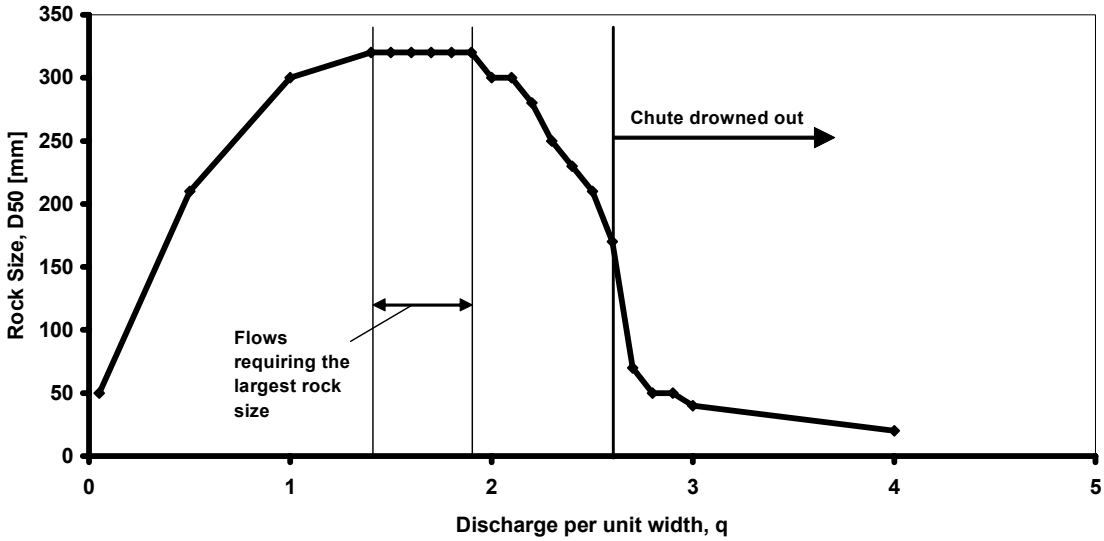

Figure 3 - The maximum required rock size does not necessarily occur at the highest discharge per unit width where the chute may be drowned out. (Figure based on example calculations carried out using the CHUTE program)

Another key cause of this type of failure is the use of rock in construction that is smaller than specified in the design. Often it can be difficult to control the size of rock that is delivered from a quarry to a construction size. If chutes are constructed from rock that is smaller than design they may be vulnerable to damage in reasonably small events.

2.3 Rock lost from the crest of a chute

Where the purpose of rock chutes is to prevent or control bed erosion upstream, the crest level is a key aspect of the design. If rock is eroded from the crest of the chute, the stream bed may no longer be protected. Losing rock from the crest is more of an issue if the crest is made from loose rock compared to situations where there is a fixed crest (commonly sheet pile, concrete or timber). However, laboratory testing suggested that the most stable chutes were those without a fixed crest but where the top of the chute was keyed into the upstream river bed (Topham 1994). Fixed crests can also be a major problem for fish passage and are generally no longer recommended.

2.4 Localised bank erosion downstream of the chute

It is important to design a rock chute so that energy is dissipated on the chute rather than downstream. If the hydraulic jump occurs downstream, a plunge pool will be created that can cause bank erosion which, in turn, can threaten the chute abutments.

2.5 Apron undermining

Apron undermining is usually a symptom of continuing bed erosion in the stream reach downstream of the chute. If a pool forms at the bottom of the apron, rock can be progressively lost as it falls into the hole, and in the worst case, the chute can progressively unravel. Apron undermining can also be a symptom of chute outflanking (Figure 4) where the sides of the apron are no longer protected as the stream widens.

Figure 4 – The apron is being undermined on this chute but there is also downstream bank erosion and the danger of outflanking.

2.6 Ongoing instability in the stream bed

As the purpose of a chutes is to control stream bed erosion, continued bed instability means the goal of building the chute has not been met, even if the chute is physically intact. The most likely cause of this problem is that the design grade, associated with a series of chutes, has been made too steep. Selection of design grades is a complex issue and requires a tradeoff between the cost of construction and selection of an appropriately low grade. Increasing the design grade can reduce the number and or height of chutes creating a major cost saving. However the risk of failure of individual chutes is increased (Hardie 1996).

2.7 Damage to the chute abutments, or outflanking of the chute

Damage to chute abutments or outflanking of the chute was found to be a costly problem as the chute will usually have to be rebuilt much larger than the original design (Figure 5). Any protection of the upstream reach against bed instability will be lost until the chute is repaired. A particular issue is where a chute is threatened by lateral migration of a stream. Chutes are designed to control vertical instability but issues of lateral erosion must also be considered.

Figure 5 – A large rock chute outflanked when river banks eroded

2.8 Total failure (crest, face and abutments)

Sometimes, most, or all, the rock on a chute is lost, or a stream can widen to such as extent that the original site of the chute is obliterated. These types of failures can be caused by extreme events that are difficult, or inappropriate, to design against. An example is the effect of flooding on Black Range Creek, north east Victoria, in 1993. This extreme event caused sections of the creek to widen from about 5 m to over 90 m. The original alignment of the stream disappeared along with any stream management works.

Another cause of this type of failure is when a chute is constructed in a section of channel where flood flows are constricted which can result in very high shear stresses. It is safer to build chutes in wider reaches, but the initial costs may be higher.

These types of extreme failures were rare, representing less than 3% of our sample (and the sample only consisted of damaged chutes). Roper et al. (1998) in their study of instream structures following floods in the Pacific Northwest also found that structural 'durability' was high which they defined as the degree to which structures remained at the site of their original placement. This contrasts with the findings of other studies such as (Frissell and Nawa 1992; Schmetterling and Pierce 1999).

2.9 Willow infestation

Willows growing on a chute can cause a number of problems:

- Flow can be concentrated between the willow trunks which may result in rock being removed from the face or crest of the chute;
- Increased flow resistance may mean that less water will flow down the chute which could increase the likelihood of outflanking.
- When willows topple, over a large part of the chute may be disturbed leading to damage in later floods

In problem areas, regular maintenance will be required to remove willows from chutes. Willows are only likely to be a problem for chutes where willows are an exotic invasive species.

3. IMPROVED DESIGN PROCEDURES

As discussed above, our results suggest that the highest risk failure mode corresponds to movement of rock from the face of a chute. We also suggest that inappropriate selection of the *critical* flow for a chute may exacerbate the risk of failure (Figure 3). Rock chute design procedures need to enable the straightforward calculation of these critical conditions.

The authors have been involved with the development of a computer program that can assist with the design of rock chutes. This has been developed as part of the Toolkit project of the Cooperative Research Centre for

Catchment Hydrology and is available for free download from www.toolkit.net.au. This program allows the computation of a water surface profile on a proposed rock chute for a given design condition. An innovative feature of the CHUTE-based design procedure is that ability to analyse the hydraulic conditions over a range of flow rates (and associated range of tail-water levels) from the lowest to the highest expected flow. The critical flow rate with respect to rock size can be identified (Keller and Winston 2003). Rock chute design guidelines based on the CHUTE program have also been prepared (Keller 2003).

It is important to note that these new guidelines, and existing design guidelines (Standing Committee on Rivers and Catchments 1993; Robinson et al. 1998) are mainly directed at designing rock chutes so they do not fail because of rock movement on the crest and face of the chute (damage mode 1 and 2 above). There has been less discussion of the best procedures to design against the other failure modes, the range of design issues has been highlighted (Biedenharn and Smith 1997; Robinson et al. 1998). Designers need to use their own skills, experience, and alternative information sources to assist with design of these aspects.

4. CONCLUSION

Rock chutes are an important technique for controlling erosion, and have been widely used to control bed instability in incising streams. Occasionally, for a number of reasons, they are damaged or fail. On the basis of an intensive study of failed chutes, we have found that the highest risk failure mode is rock lost from the face of the chute. A new computer program, CHUTE, has been specifically developed to analyse the risk of this type of failure. The program allows accurate and rapid sizing of rock, which, using existing tools, is difficult and time consuming.

The other two risks that stand out are, damage to chutes because of willow infestation, and damage to abutments or outflanking of the chute. Willow infestation was the most frequent problem. Abutment damage was the least frequent but most expensive problem to repair. Chute designers need to be aware of, and take into account, the full range of failure modes.

5. RECOMMENDATIONS

Recommendations for improved design procedures are:

- Recognise that there are a number of failure modes for rock chutes and that these need to be considered during design;
- Loss of rock from the face of a chute is likely to be the highest risk. To design against this type of failure a range of flows and tailwaters need to be considered to identify the critical conditions;
- Rock needs to be sized based on these critical conditions;
- Existing design guidelines focus on a relatively small number of failure modes. Designers need to use their own skills and experience to deal with the full range of potential problems.

6. REFERENCES

A/NZS 4360 (Australian/New Zealand Standard 4360) *Risk Management*. Standards Australia.

Biedenharn, D. S. and J. B. Smith (1997). Design considerations for grade control siting. In: *Management of Landscapes Disturbed by Channel Incision*, S.S.Y Wang, E.J. Langendoen, and F.D. Shields Jr., eds., University of Mississippi Oxford, MS, pp 229-239.

Frissell, C. A. and R. Nawa (1992). Incidence and causes of physical failure of artificial habitat structures in streams of western Oregon and Washington. *North American Journal of Fisheries Management* 12: 182-197.

Hardie, R. E. (1996). Streambed longitudinal gradient and unit stream power analysis of tributary streams of North East Victoria, Australia. Proceedings of the First National Conference on Stream Management in Australia, Merrijig, Cooperative Research Centre for Catchment Hydrology. pp 57-62.

I D & A Pty Ltd (1996). Improvements to the design and construction of rock chutes. Melbourne, Department of Natural Resources and Environment: p34.

Keller, R. J. (2003). Guidelines for the design of rock chutes using CHUTE. Melbourne, Cooperative Research Centre for Catchment Hydrology: p33.

Keller, R. J. and F. Winston (2003). Stabilisation of channel beds using rock chutes. 28th International Hydrology and Water Resources Symposium, Wollongong, NSW, Australia, Institution of Engineers, Australia pp107-113.

Olivier, H. (1967). Through and overflow rockfill dams - new design techniques." *Proceedings of the Institution of Civil Engineers* 36: 433-471.

Robinson, K. M., C. E. Rice and K. C. Kadavy (1997). Rock chutes for grade control. In: *Management of Landscapes Disturbed by Channel Incision*, S.S.Y Wang, E.J. Langendoen, and F.D. Shields Jr., eds., University of Mississippi Oxford MS.

Robinson, K. M., C. E. Rice and K. C. Kadavy (1998). Design of rock chutes. *Transactions of the American Society of Agricultural Engineers* 41(3): 621-626.

Roper, B. B., D. Konnoff, D. Heller and K. Wieman (1998). Durability of Pacific Northwest instream structures following floods. *North American Journal of Fisheries Management* 18: 686-693.

Schmetterling, D. A. and R. W. Pierce (1999). Success of instream habitat structures after a 50-year flood in Gold Creek, Montana *Restoration Ecology* 7(4): 369-375.

Standing Committee on Rivers and Catchments (1993). *Guidelines for stabilising waterways*. Melbourne, Working Group on Waterway Management.

Topham, C. (1994). Failure of rock chutes. Melbourne, University of Melbourne, Department of Civil Engineering.

The Institution of Engineers, Australia
8th National Conference on Hydraulics in Water Engineering
ANA Hotel Gold Coast, Australia 13-16 July 2004

Steep Gradient Waterway Stabilization – An Innovative Design Technique

Dr. John C Macintosh
BE(Hons), PhD, FIEAust, CPEng, RPEQ
Director / Principal Water Engineer, Water Solutions Pty Ltd

Abstract: Design of stable waterways over steep gradients can be a challenging task, particularly so if the following design criteria must also be satisfied:

- be permanent - that is, last for hundreds of years
- convey extreme flow events
- handle steep gradients, e.g. 10%
- sit in an erosive substrate
- accommodate significant settlement
- be affordable

An innovative and cost effective design technique has been developed to provide engineers with the means of tackling projects of this nature. The technique utilizes specially designed interlocking pre-cast concrete blocks to stabilize a cascade formed from relatively small rock. A novel aspect of the design is the use of baffles laid across the toe of each cascade drop which serve to stabilize the rock in this high turbulence area by creating a zone of stagnation above the bed.

Dr. John Macintosh, Director and Principal Water Engineer of Water Solutions Pty Ltd, will present the concept of this new technique including the outcomes from physical model testing. An overview of a prototype application to a permanent waterway diversion through mining spoil will also be presented.

The Institution of Engineers, Australia
8th National Conference on Hydraulics in Water Engineering
ANA Hotel Gold Coast, Australia 13-16 July 2004

Hydraulic Risk Assessment of Water Distribution Systems

Michael Leonard
B.E. (Hons)
Honours Student, University of Adelaide, Australia
Holger R. Maier
B.E. (Hons), Ph.D., M.I.E. Aust.
Senior Lecturer, University of Adelaide, Australia
Angus R. Simpson
B.E. (Hons), M.Sc., Ph.D., F.I.E. Aust.
Associate Professor, University of Adelaide, Australia
Aaron C. Zecchin
B.Sc., B.E. (Hons)
Honours Student, University of Adelaide, Australia
Andrew J. Roberts
B.E. (Hons)
Honours Student, University of Adelaide, Australia
Matthew J. Berrisford
B.E. (Hons)
Honours Student, University of Adelaide, Australia
John B. Nixon
B.Sc. (Hons), Ph.D.
Senior Research Scientist, United Water International, Adelaide, Australia

Abstract: The existence of uncertainties in water distribution systems (WDSs) has been recognised for several decades within the literature (typical examples of uncertainty include demand variability, component failures and increased roughness of pipes). The existence of these uncertainties implies that the risk of inadequate hydraulic performance needs to be identified and assessed throughout the system. In this paper, the risk of hydraulic failure of an existing WDS is assessed, both in terms of reliability (probability of non-failure) and vulnerability (probable magnitude of failure given that a failure has occurred). The WDS considered within this paper is the McLaren Vale/McLaren Flat system, which is located approximately 30 km to the south of Adelaide, South Australia. The spatial variability of both reliability and vulnerability is modelled and the results are presented using spatial contour maps. The results indicate that such maps are extremely useful for identifying and interpreting critical regions and regions of poorer performance in terms of pressure head. Furthermore, by using both reliability and vulnerability indices, a more complete description of risk, using the multiple criteria, is obtained.

Keywords: Risk; Reliability; Vulnerability; Water Distribution Systems; Network; Spatial Variation

1. INTRODUCTION

Risk assessment is a broad field within the management of water distribution systems (WDSs). It is applicable to analysing and comparing the performance of existing WDSs, for assessing the impact of various operational strategies on network performance (such as changes in valve settings or tank trigger levels), and also in the design of cost-effective and reliable network configurations or network rehabilitation schemes. Risk is defined as the measure of potential loss when the system fails to perform (Howard 2002), and is primarily due to attributes of the system that are difficult to quantify and hence considered uncertain.

A broad range of uncertain variables exists within a WDS. Examples include component failure (pipes, pumps, valves), variability in demands and demand patterns, projections of future demand, deterioration of hydraulic performance of components (i.e. unknown changes in pipe roughness, pump capacity, etc.), uncertainty in chlorine residual levels and uncertain levels in tanks and reservoirs (Bao and Mays 1990; Goulter 1995; Mays 1996). The presence of such uncertainties implies that hydraulic simulation of WDSs must be cast in a probabilistic framework, such that parameters may be characterised using probability distributions as opposed to single valued constants. Rather than provide a single set of pressure levels across the system for a single case of demands, a hydraulic model that includes uncertainties is able to provide a probability distribution of pressure values at each node. This feature enables the risk-based performance of the system to be quantitatively assessed. One of the problems associated with the incorporation of uncertainties into hydraulic simulation models is the

choice of appropriate risk-based performance measures (Goulter 1995). Within the literature, there are a large number of risk-based performance indices for WDSs due to, amongst other reasons, the many different sources of uncertainty across the various components of the system, changes in the system over time and the spatial variability of the system (Bouchart and Goulter 1991; Gupta and Bhave 1994; Tanyimboh *et al.* 1999; Xu and Goulter 1999; Gargano and Pianese 2000; Prasad and Park 2004).

The performance of WDSs has traditionally been measured by the probability that they will be in a state of failure at any given time (Goulter 1995). Initially, the probability of inadequate supply was linked to the performance of the system under abnormal conditions (i.e. in the event of component failures) (Duan and Mays 1990; Bouchart and Goulter 1991; Jowitt and Xu 1993). More recently, attention has focused on hydraulic uncertainties, such as demand variability, which can cause a system to perform inadequately (Bao and Mays 1990; Xu and Goulter 1998; Xu and Goulter 1999). Following Hashimoto *et al.* (1982), the probability of providing adequate supply to a customer (i.e. the non-failure state) is referred to as *reliability*.

While reliability provides an indication of how likely system failure is, it does not indicate how severe the consequences of failure are (e.g. whether the minimum desirable pressure has not been met by 1 mm or 5 m). In contrast to reliability assessments, the magnitude of a potential failure has not been extensively considered. Whereas several indices of a more complex nature include, amongst other indicators of risk, aspects of failure magnitude (Ostfeld and Shamir 1996; Gargano and Pianese 2000), this paper considers failure magnitude as an independent measure of risk. Following Hashimoto *et al.* (1982), the magnitude of failure, given that failure has occurred, is termed *vulnerability*.

Another aspect of risk to consider is the expected duration of a failure event, which is the inverse of the system *resiliency*, as defined by Hashimoto *et al.* (1982). Resilience can only be evaluated for situations where extended period simulations of a WDS are conducted. Therefore, resilience is more commonly associated with water quality assessments of chlorine decay rather than steady state assessments of water quantity (Ostfeld and Shamir 1996; Portielje *et al.* 2000). As the focus of this paper is not on an assessment of water quality, resilience indices have not been considered.

The primary objective of this paper is to demonstrate the application and utility of a new visualisation method for assessing and interpreting the spatial variation of risk performance across a WDS. Because of the complexity and spatial variability of WDSs, this objective overcomes inadequacies of current techniques that attempt to combine the performance across many nodes into a single overall measure for the entire system. The spatial variability of risk is assessed in terms of two different performance indices: reliability and vulnerability. By applying two different indices, a secondary objective is to demonstrate the need for using more than one aspect of risk to assess the performance of a WDS. This objective is in contrast to current techniques that do not consider or delineate between various aspects of risk. In order to meet the above objectives, a realistic case study of significant complexity is used: the McLaren Vale/McLaren Flat WDS, South Australia, which consists of 222 pipes.

2. METHODOLOGY

2.1 Characterising Uncertainty

Demand driven hydraulic solvers of WDSs are generally used in a deterministic fashion. This modelling simplification enables specific values of pressure head to be determined at individual nodes based upon specific input information for each component of the system (demands, pipe roughnesses, reservoir levels, etc.). Therefore, the hydraulic analysis of the performance of a WDS is mostly restricted to worst-case scenarios. This is achieved by making conservative assumptions about the system, such as minimum reservoir levels, or by considering the loading of the system under extreme cases, such as peak-day or fire demand scenarios. By way of contrast, risk assessment requires a distribution of possible values to be specified for certain attributes of the system. More specifically, a probability distribution is used to ascribe relative probabilities of occurrence to each value within the range of possible values of a particular quantity. As shown in Figure 1, distributions may be ascribed to characterise the degree of uncertainty about an exact (but unknown) quantity, such as the roughness of a pipe, or they may be used to characterise the inherent variability of variables over their known range, such as demand flow and reservoir level.

There are numerous instances in which data are available to characterise WDS uncertainties, for example flow meters that gauge variations in demand, historical records that indicate reservoir levels and water-authority records that contain component failure rates. In these circumstances it is possible to determine an appropriate

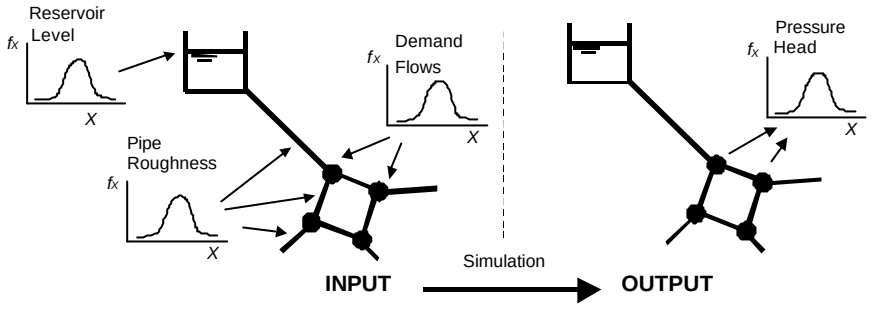

Figure 1 – Figurative example of inputs and outputs of a probabilistic framework WDS model. The inputs of reservoir level, pipe roughness and nodal demand, and the output of nodal head are described by probability distributions as opposed to single values.

type of distribution and acceptable parameter values for that distribution. Some aspects of a system or designcriteria may require subjective assumptions to be made based upon engineering judgement that reflect the modeller's degree of certainty. For example, the hydraulic capacity of a pipe may be assumed to deteriorate by 10% over 15 years, and this estimate might vary by 20% across different pipes in the network. Another example might be that a demand forecast may have an error of ± 20% due to unpredictable circumstances.

2.2 Use of Monte Carlo Simulation to Model Uncertainty

Due to the probabilistic framework of the risk model and the non-linear hydraulic relationships of flow in closed looped conduits, it is necessary to use simulation techniques rather than analytical techniques for risk assessment (Goulter, 1995). As shown in Figure 1, a simulation procedure, such as Monte Carlo Simulation (MCS), is used to evaluate the distribution of pressure heads at any given node in the WDS. MCS proceeds by generating many realisations of the state of the WDS based upon random samples from the probability distributions ascribed to the various input values. For each realisation, the hydraulic solver determines the resultant pressure head at each node, and as the simulation progresses, a distribution of pressures is developed, with some ranges of pressure occurring more frequently than others. The simulation continues until an adequate description of the pressure distributions has been achieved for all nodes. Performance indices such as reliability and vulnerability may then be expressed as functions of this pressure head distribution.

Relative to other simulation techniques (Xu *et al.* 2003; Tolson *et al.* 2004), MCS is considered to be more robust as it is able to simultaneously evaluate the pressure head distribution for every node in the system, is relatively computationally efficient for large WDSs and does not introduce model errors into the result based upon simplifying assumptions. However, the main disadvantage of MCS is that it is a computationally demanding procedure requiring many realisations to achieve adequate convergence.

2.3 Reliability and Vulnerability Indices

Using the notation of Tolson *et al.* (2004), the performance of any engineering system can be expressed in terms of its load and resistance. If $\mathbf{X}=(X_1,X_2,\ldots,X_n)$ is the vector of random variables that influence a system's load (L) and/or resistance (R), the performance function $G(\mathbf{X})$ is commonly written as $G(\mathbf{X}) = R - L$. Due to the idealisation of demand-driven hydraulic solvers, the demand at a node is assumed to be satisfied, therefore the only variable requirement (or load) upon the system is that a customer receives adequate pressure. For this research, it is assumed that the minimum pressure requirement at a node is a fixed quantity and is independent of the system's uncertainties. Since the minimum pressure requirement at each node defines the load upon the system, the ability of the system to provide pressure to meet this requirement is defined as the resistance. Therefore the system's resistance is comprised of the set of components and component attributes, both of which may be subject to random variability. Although the spatial and temporal variability of flow is conceptually a load upon a system, the idealisation of demand-driven models implies that it is mathematically modelled as a resistance. This is because the flow demand at each node influences the ability of the system to provide pressure to individual nodes. The performance function used to evaluate the reliability of the i^{th} node of a WDS for each realisation of MCS is given by

$$G_i(\mathbf{X}) = H_i(\mathbf{X}) - H_i^* \qquad \textbf{(1)}$$

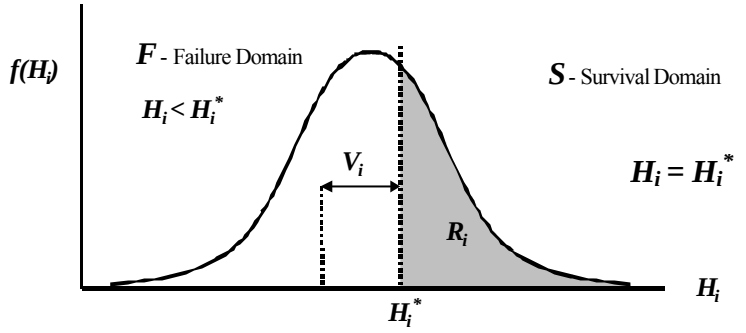

Figure 2 – Probability Distribution of Pressure Heads at a Given Node

where $H_i(\mathbf{X})$ is the head predicted at node i as a function of the random vector of system inputs and H_i^* is the minimum specified head at node i. The failure surface $G_j(\mathbf{X}) = 0$ is the boundary that separates all values of $\mathbf{X}$ that lie in the failure domain (F) from those that lie in the survival domain (S), as shown in Figure 2.

The nodal reliability R_i is defined as the probability that the random vector $\mathbf{X}$ will lie in the survival domain, which is simply the area of the survival domain, given as

$$R_i = P\{\mathbf{X} \in S\} = P\{G_i(\mathbf{X}) \geq 0\} = \int_{H>H^*} f(H_i)dH_i \quad \textbf{(2)}$$

Consequently, the nodal reliability is the probability that the pressure at a particular node is adequate given the uncertainties in the inputs used to calculate the nodal pressures. The nodal vulnerability V_i is defined as the expected magnitude of failure in the event of a failure occurring, that is,

$$V_i = E\left[G_i(\mathbf{X}) \middle| G_i(\mathbf{X}) < 0\right]. \quad \textbf{(3)}$$

In the event of failure to provide adequate pressure, the vulnerability is therefore the likely amount that a node will violate this pressure requirement, as shown in Figure 2. In the event that the node is always able to provide adequate pressure, the vulnerability assumes a value of zero. Since reliability is a probability of occurrence, its values lie between zero and one. Vulnerability on the other hand is measured in units of pressure head (metres) and can lie, realistically, anywhere between zero and H_i^* (i.e. the realistic maximum pressure violation[1]).

2.4 Spatial Contour Maps

Once nodal reliabilities and vulnerabilities have been calculated (Equations 2 and 3), they can be visualised using spatial contour maps. The EPANET2 hydraulic solver provides a graphical package that interpolates between nodes to generate contour plots[2]. Although the interpolation method is not specified, the advantage of EPANET's contouring facility is that it is able to superimpose the network configuration on top of the spatial reliability and vulnerability contour plots. It is important to note that contour maps for systems with few nodes or for values near the boundary may lack meaning due to insufficient information for accurate contouring.

3. CASE STUDY: THE McLAREN VALE / McLAREN FLAT SYSTEM

The McLaren Vale/McLaren Flat WDS, as shown in Figure 3, supplies both suburban and agricultural users and is located approximately 30 km south of Adelaide, South Australia. This WDS contains 202 nodes, 222 pipes, two water sources, two pumping stations, one tank and five main valves. Supply to the McLaren Vale/McLaren Flat system is through two valve connections to the Myponga Trunk Main, which is situated to the west of the

[1] Demand-driven models can give negative pressures at a node thus giving non-realistic vulnerabilities greater than H_i^*
[2] Custom features for graphing reliability and vulnerability are not provided by EPANET, therefore mock input files were generated by replacing variables that were able to be graphed (such as nodal elevation) with the relevant performance indexes.

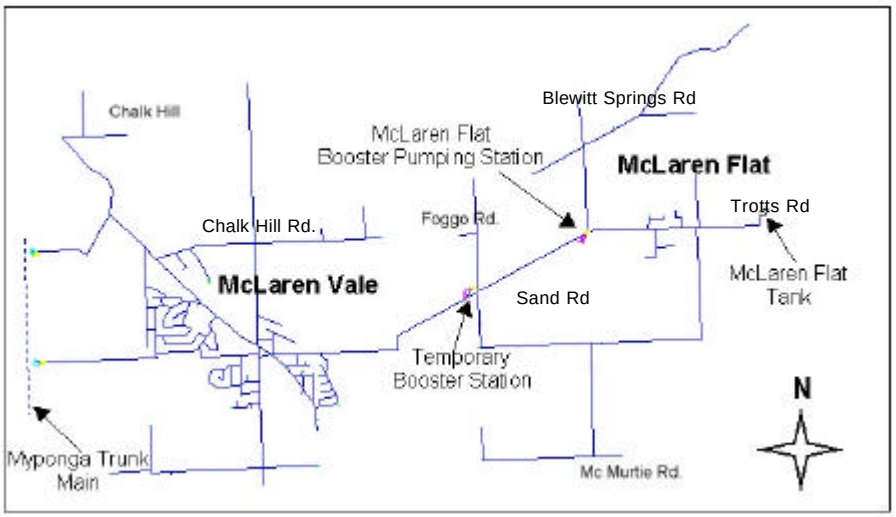

Figure 3 – McLaren Vale / McLaren Flat Water Distribution System Configuration

network, as shown in Figure 3. These connections feed a 300 mm supply main running east-west which extends into McLaren Vale/McLaren Flat where it reduces to a 250 mm diameter pipeline and runs through McLaren Flat to the McLaren Flat tank. The tank has a capacity of 1.2 ML and was established, along with the mains, in 1962.

In 1994, a booster pumping station was constructed at McLaren Flat with variable speed pumps that operate in response to the pressure downstream of the pump. Water from the McLaren Flat system does not recirculate back to McLaren Vale. Therefore the McLaren Flat system operates at pressures controlled by the pump station and the tank, rather than from the valve connection at the trunk main. In 1999, a second booster pump station was built to boost pressures supplied to customers situated in Foggo Road north.

Ground levels throughout the system range from 120 m, east of McLaren Flat, down to 50 m, west of McLaren Vale. Generally land north of the two towns is higher than the township levels. The peak-day, peak-hour demand upon the system occurs during the evening peak of a summer's night and is approximately 170 L/s. It is important to note that viticulture demands have significant variation throughout the system occurring anywhere between dusk and dawn (Woods 2000).

A review of the McLaren system prior to more recent system upgrades highlighted some of the performance issues that can be experienced in WDSs, especially those related to increasing demands. Models of the existing McLaren Vale/McLaren Flat system showed that, in the past, the system had areas that were unable to receive adequate pressure during peak-day, peak-hour demands (Woods 2000). It was demonstrated that, for the existing system, even though for the majority of the peak-day, most customers would receive in excess of 30 m pressure head, pressures were observed to drop to zero in the Foggo Road and Chalk Hill areas. Additionally, in the past, flow and pressure complaints have been received from various parts of the network including Chalk Hill Road, Foggo Road and, in the case of pipe bursts, Blewitt Springs Road and Trotts Road. Indications of possible pipe restrictions in the network were also identified in the vicinity of McMurtie Road and Sand Road.

Analyses of the McLaren system adopted a recommended minimum pressure requirement of 20 m pressure head for the desired level of supply (Woods 2000). In this research, the McLaren Vale/McLaren Flat WDS was modelled under normal operating conditions, that is, component failure was not included within the analyses. The modelled uncertainties in the system included a distribution of demand flow at every node and a distribution in the hydraulic capacity of pipes due to ageing. Using a normal distribution, a coefficient of variation of 5% was assumed for all nodal demands whilst a coefficient of variation of 20% was assumed for all pipe roughnesses. The demands were modelled for the peak-hour of the peak-day[3], with the probability distribution about this mean representing the uncertainty in the estimates of the peak flows. For the purposes of this study, the assumptions about the degree of uncertainty in demands and pipe roughnesses were intended to be representative of possible values, which are based on engineering judgement and similar values used by other

[3] As stated earlier, a risk assessment is not necessarily restricted to the analysis of a WDS under a worst-case scenario. This research adopted a peak-day peak-hour analysis nonetheless, primarily due to the availability of data. An alternate approach would be to model the WDS under 'normal' operating conditions, with the joint uncertainty distributions of demand across each node encapsulating the peak-hour peak-day event (with a corresponding low probability). This approach is however complicated by the need to account for the correlation in demands between each pair of nodes.

authors (Bao and Mays 1990; Xu and Goulter 1998; Tolson *et al.* 2004). Because the model is not of the current McLaren system and because the probability distributions were not verified using data, the case study is intended to be *realistic* rather than *real*. The emphasis of this case study is therefore placed upon the procedure and interpretation of results, rather than the results themselves.

The McLaren WDS was modelled using the EPANET2 hydraulic solver, which was linked to a Monte Carlo Simulation (MCS) program written in FORTRAN 95. Each simulation was performed using 100,000 realisations to ensure convergence of the performance indices, which resulted in run times on the order of several minutes using a 1 GHz computer. Reliability, vulnerability, elevation and flow graphs were obtained for the peak-hour peak-day demand case for the McLaren Vale/McLaren Flat WDS.

4. RESULTS AND DISCUSSION

Figure 4 shows several properties of the McLaren Vale/McLaren Flat WDS, including nodal elevations, demand flows, reliability and vulnerability. Figure 4(c) shows that the majority of the system is very reliable, with R_i = 0.999, which is an expected observation for a WDS in a developed country. This figure also shows that the areas that exhibited lower reliability values were primarily viticultural regions located on the outskirts of the system. Specifically these regions were, Chalk Hill, Foggo Road north and the eastern region of the McLaren Flat system. Without considering uncertainties within the system, the model showed adequate pressure (above 20 m) at every node, therefore, the observation of several less reliable areas is attributed to the inclusion of uncertainties within the model. From Figure 4(c), it was deduced that the node located before the McLaren Flat booster pumping station has a slightly reduced reliability (0.97), despite the fact that the surrounding region of the system has a high reliability. The assumed reason for this is that the booster pump station is situated at the extremity of the McLaren Vale/McLaren Flat system. Since the only connection between the McLaren Vale/McLaren Flat WDS is through the booster pump, the McLaren Flat region experiences increased pressures (and hence increased reliability) due to the additional pressure head provided by this pump.

A more complete description of the system performance is achieved by considering the vulnerability of the system in conjunction with reliability (Figure 4(d)). As can be seen, on the whole, the McLaren Vale/McLaren Flat WDS is not very vulnerable; however there are several regions that experience local failures of a high magnitude. For the peak-hour of the peak-day, Figure 4(c) shows that there is at least a failure probability of 5% for Chalk Hill and up to a 1% probability of failure for the northern part of Foggo Road. This result is consistent with the observation of poorer performance in the real system in these areas, as discussed in Section 3. Figure 4(d) shows that in the event of a failure, both Chalk Hill and Foggo Road will, probabilistically, experience failure magnitudes between 4 m and 8 m, which is significant.

Although Figure 4(c) shows that there is up to a 3% probability of failure in the region of the McLaren Flat booster pumps, Figure 4(d) shows that this region is not highly vulnerable with an expected failure magnitude for this region of less than 4 m. A similar conclusion can be drawn for the eastern region of the McLaren Flat system. By way of contrast, Figure 4(c) indicates that the region near the Foggo Road booster pumps has a very low failure probability (0.1%), however, there is a high vulnerability in the event of a failure occurring, with a likely magnitude of greater than 8 m. Therefore, considering two different performance indicators demonstrates that some regions may perform well in terms of one aspect (high reliability or low vulnerability), but poorly in terms of another aspect (low reliability or high vulnerability).

Apart from being able to identify areas of poor performance and account for spatial variability, one of the main aspects of topographical maps is that they can be used to correlate the performance of the WDS with factors that may influence it. For example, Figures 4(a) and 4(b) show the elevation and flow demand throughout the McLaren Vale/McLaren Flat WDS, respectively. Figure 4(a) shows that there is a significant difference in elevation throughout the system, from approximately 50 m at the Martins Road main trunk connection up to in excess of 110 m at the McLaren tank. This provides a 60 m change in pressure head throughout the system, which is significant. The McLaren Flat system is considerably higher than the McLaren Vale/McLaren Flat system and the northern and eastern outskirts of the system also have higher elevations than the majority of the system. Therefore, one explanation for the poor performance in the regions of the vineyards is that they are situated at high elevations.

Figure 4(b) provides a graphical description of the mean demands at each of the nodes for the peak-hour of the peak-day. It can be seen that, for this time period (peak-hour peak-day), the majority of the WDS has a demand of less than 0.5 L/s, however, several nodes experience flows in excess of 3 L/s. The variability of demand is attributed to the broad variety of customers including agricultural users, domestic users, commercial users,

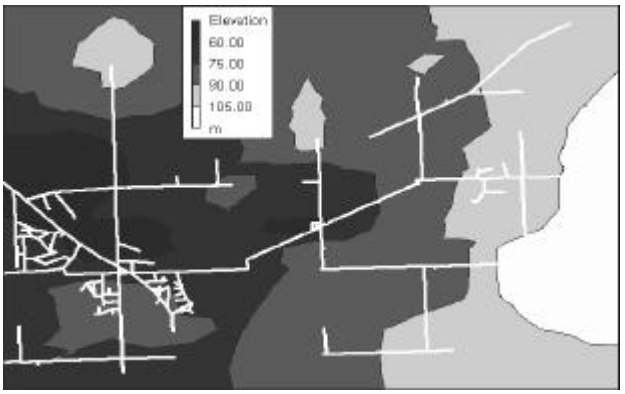

(a) Nodal Elevation

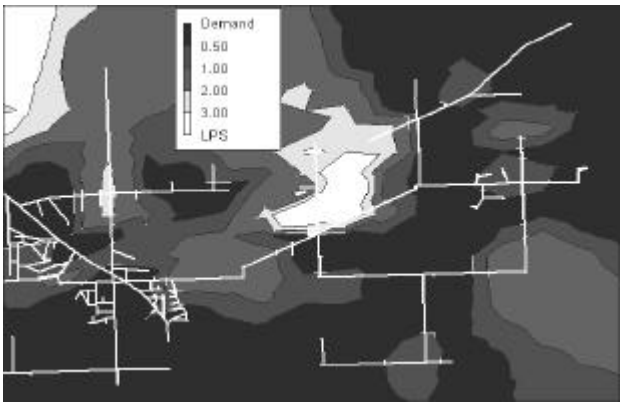

(b) Flow Demand

(c) Nodal Reliability

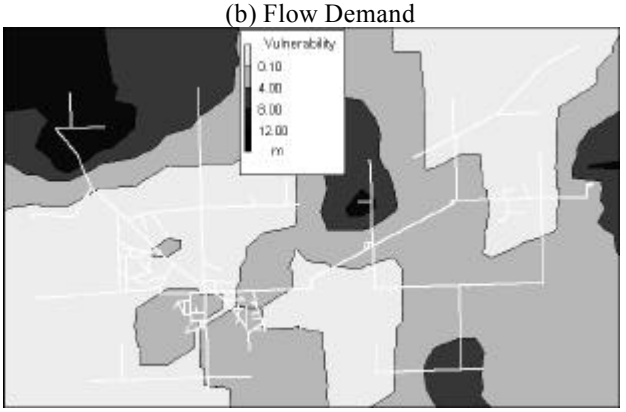

(d) Nodal Vulnerability

Figure 4 – Spatial Variation of Attributes of the McLaren Vale / McLaren Flat System, (a) Nodal Elevation, (b) Flow Demand, (c) Nodal Reliability, (d) Nodal Vulnerability

council users and government operated users. Due to agricultural users, the higher than average demands in the Chalk Hill and Foggo Road areas are another contributing factor to the poorer performance in these regions. The McLaren Flat region does not have any abnormally high flow demands; therefore the reduced performance in this region of the system can mostly be attributed to the higher elevations. In general it can be observed that the regions of poorer performance are located at the extremities of the network and can either be attributed to an increase in demands, or elevations, or both.

5. CONCLUSIONS

This paper demonstrates the application of risk assessment to WDSs using a realistic case study, the McLaren Vale/McLaren Flat WDS, South Australia. The performance of the system was assessed in terms of two different aspects, reliability and vulnerability. The spatial variability of system performance was assessed by developing contour maps of reliability and vulnerability from the performance at each node in the system. The contour maps were used to identify regions of poorer performance and it was observed that some regions performed well in terms of one aspect but not another. This indicates the need for using more than one performance index to describe risk. The performance of the system was interpreted using spatial maps of system attributes such as elevation and demand. The principles discussed in this paper could be extended easily to consider other aspects of system performance such as water quality, temporal variability of demand, uncertainty in predictions of future demand or random component failures.

6. ACKNOWLEDGMENTS

Acknowledgment is extended to United Water International for allowing the use of the McLaren Vale/McLaren Flat water distribution system as a case study and for providing computing resources, and the Cooperative Research Centre for Water Quality and Treatment for providing financial support for this project.

7. REFERENCES

Bao, Y. X. and L. W. Mays (1990). Model for Water Distribution-System Reliability. *Journal of Hydraulic Engineering*-ASCE **116**(9): 1119-1137.

Bouchart, F. and I. Goulter (1991). Reliability Improvements in Design of Water Distribution Networks Recognizing Valve Location. *Water Resources Research* **27**(12): 3029-3040.

Duan, N. and L. W. Mays (1990). Reliability-Analysis of Pumping Systems. *Journal of Hydraulic Engineering*-ASCE **116**(2): 230-248.

Gargano, R. and D. Pianese (2000). Reliability as a Tool for Hydraulic Network Planning. *Journal of Hydraulic Engineering*-ASCE **126**(5): 354-364.

Goulter, I. C. (1995). *Analytical and Simulation Models for Reliability Analysis in Water Distribution Systems*. London, Kluwer Academic.

Gupta, R. and P. R. Bhave (1994). Reliability-Analysis of Water-Distribution Systems. *Journal of Environmental Engineering*-ASCE **120**(2): 447-460.

Hashimoto, T., J. R. Stedinger and D. P. Loucks (1982). Reliability, Resiliency, and Vulnerability Criteria for Water-Resource System Performance Evaluation. *Water Resources Research* **18**(1): 14-20.

Howard, C. D. D. (2002). Sustainable Development - Risk and Uncertainty. *Journal of Water Resources Planning and Management*-ASCE **128**(5): 309-311.

Jowitt, P. W. and C. C. Xu (1993). Predicting Pipe Failure Effects in Water Distribution Networks. *Journal of Water Resources Planning and Management*-ASCE **119**(1): 18-31.

Mays, L. W. (1996). Review of Reliability Analysis of Water Distribution Systems. *Stochastic Hydraulics*, Balkema, Rotterdam, The Netherlands.

Ostfeld, A. and U. Shamir (1996). Design of Optimal Reliable Multiquality Water-Supply Systems. *Journal of Water Resources Planning and Management*-ASCE **122**(5): 322-333.

Portielje, R., T. Hvitved-Jacobsen and K. Schaarup-Jensen (2000). Risk Analysis Using Stochastic Reliability Methods Applied to Two Cases of Deterministic Water Quality Models. *Water Research* **34**(1): 153-170.

Prasad, T. D. and N S. Park (2004). Multiobjective Genetic Algorithms for Design of Water Distribution Networks. *Journal of Water Resources Planning and Management*-ASCE **130**(1): 73-82.

Tanyimboh, T. T., R. Burd, R. Burrows and M. Tabesh (1999). Modelling and Reliability Analysis of Water Distribution Systems. *Water Science and Technology* **39**(4): 249-255.

Tolson, B. A., H. R. Maier, A. R. Simpson and B. J. Lence (2004). Genetic Algorithms for Reliability-Based Optimization of Water Distribution Systems. *Journal of Water Resources Planning and Management*-ASCE **130**(1): 63-72.

Woods, M. (2000). *McLaren Vale / McLaren Flat Water Supply System.* Adelaide, Gutteridge Haskins & Davey Pty Ltd**:** 1-19.

Xu, C. C. and I. C. Goulter (1998). Probabilistic Model for Water Distribution Reliability. *Journal of Water Resources Planning and Management*-ASCE **124**(4): 218-228.

Xu, C. C. and I. C. Goulter (1999). Reliability-Based Optimal Design of Water Distribution Networks. *Journal of Water Resources Planning and Management*-ASCE **125**(6): 352-362.

Xu, C. G., I. C. Goulter and K. S. Tickle (2003). Assessing the Capacity Reliability of Ageing Water Distribution Systems. *Civil Engineering and Environmental Systems* **20**(2): 119-133.

The Institution of Engineers, Australia
8th National Conference on Hydraulics in Water Engineering
ANA Hotel Gold Coast, Australia 13-16 July 2004

Evaluation of Hydrologic and Hydraulic Models for Real-Time Flood Forecasting use in the Yangtze River Catchment

M.S. Markar
B.Sc (Eng)., Ph.D., M.I.E.Aust. R.P.E.Q.
Contractor to Sagric International Pty. Ltd., Australia
Director, WRM Water & Environment Pty. Ltd., Australia
S.Q. Clark
BE Hons (Civil), MEng Sc, M.I.E.Aust.
Contractor to Sagric International Pty. Ltd., Australia
Director, Water Technology Pty. Ltd., Australia
Min Yaowu
B.E., M.Sc.
Senior Engineer, Bureau of Hydrology, Changjiang Water Resources Commission, PR China
Zheng Jing
B.E.
Engineer, Bureau of Hydrology, Changjiang Water Resources Commission, PR China

Abstract: A key component of the Yangtze River Flood Control and Management Project is the development of an integrated real-time flood forecasting system to improve the reliability, accuracy and lead times of forecast flood discharges and flood levels along the upper and middle reaches of the Yangtze River. Central to the flood forecasting system is the use of appropriate hydrologic and hydraulic models. As part of the hydrologic and hydraulic model evaluation and selection process, a comprehensive comparative study was carried out for five well established hydrologic models and three well established hydraulic models to assess their performance and suitability for use in real-time forecasting in the Yangtze River catchment. The model evaluations were undertaken using common data sets and technical performance criteria specified in the Chinese National Standards for Flood Forecasting Models. This paper describes how the different hydrologic and hydraulic model performances were evaluated and presents the findings on their suitability for use in the Yangtze River flood forecasting system.

Keywords: Yangtze River, Hydrologic Modelling, Hydraulic Modelling, Flood Forecasting.

1. INTRODUCTION

The five-year Yangtze River Flood Control and Management Project, which commenced in 2001, aims to improve the reliability, accuracy and lead times of forecast flood discharges and flood levels along the upper and middle reaches of the Yangtze River between Chongqing and Wuhan. A key component of this project is the development of an integrated real-time flood forecasting system (FFS) for the Yangtze River, and central to the flood forecasting system is the use of appropriate hydrologic and hydraulic models. To assist in the selection of suitable hydrologic and hydraulic models, the performance of five well-established hydrologic models and three well established hydraulic models were assessed and compared. The five hydrologic models evaluated were Xinanjiang (Chinese), API (Chinese), URBS (Australian), RAFTS (Australian) and HEC-HMS (United States). The three hydraulic models evaluated were MIKE-11 (Danish), InfoWorks (United Kingdom) and HEC-RAS (United States).

The performance of the hydrological models was assessed through the application of the selected models on two tributary catchments of the Yangtze River, namely Da Ning He and Tang He. These two catchments have contrasting characteristics and were considered to be fairly representative of the range of characteristics encountered in the Yangtze catchment. The performance of the hydraulic models was assessed by applying the selected models to the upper reach of the Yangtze River between Chongqing and the Three Gorges Dam. The locations of the Da Ning He and Tang He catchments and the upper reach of the Yangtze are shown in Figure 1.

The model evaluations were undertaken using common data sets and technical performance criteria specified in the Chinese National Standards for Flood Forecasting Models (Chinese Standards, 2000). A brief description of each of

the test catchments used for hydrologic modelling, the river reach used for hydraulic modelling and the hydrologic and hydraulic models, and the findings of the evaluations are presented in the following sections.

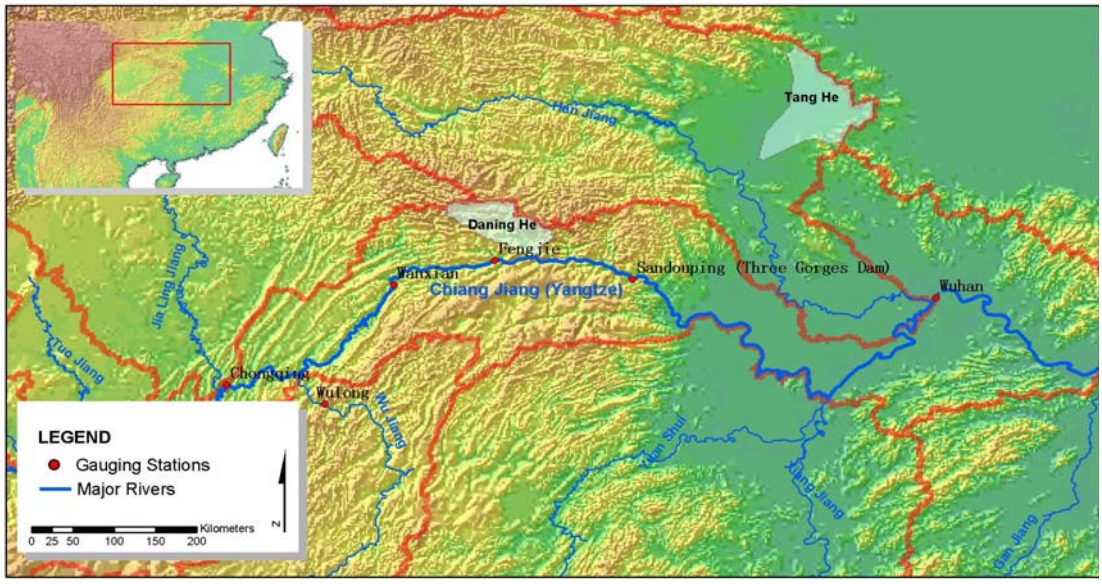

Figure 1 – Locality Map, Upper and Middle Reaches of the Yangtze River Catchment

2. TEST CATCHMENT CHARACTERISTICS

2.1 Da Ning He (River) Catchment

The Da Ning He is a minor tributary of the Yangtze River located in the Three Gorges reach. It has a total catchment area of about 4180 km^2 and a stream length of about 162 km. The catchment rises from elevations of less than 100 m at its confluence with the Yangtze to elevations of over 2000 m. The catchment is quite steep, has a thin topsoil layer and is covered with extensive marlite and karst limestone rock outcrops. Numerous groundwater flow conduits exist within these limestone formations and thus producing a steady base flow in the river. Data were available for 10 rainfall and 4 stream gauging stations spread across the catchment. Modelling was undertaken for the upper half of the catchment (2001 km^2) down to Wuxi, where the most downstream stream gauging station is located.

2.2 Tang He (River) Catchment

The Tang He is a tributary of the Tangbai He, which in turn is a major tributary of the Han River. The Han River is one of the largest tributaries of the Yangtze River. The Tang He catchment has a total area of about 8685 km^2 and a stream length of about 230 km. Upstream of the Guotan stream gauging station (the downstream limit of this study) the catchment has an area of 6877 km^2 and a stream length of 148 km. The catchment is quite flat and has extensive floodplains. Most of the catchment is within the 100 m to 200 m elevation range. The bed slopes of major streams generally vary between 0.0003 m/m to 0.0007 m/m. Base flows in the Tang He drainage system are not significant compared to flood flows.

There are 6 large storages (200 to 1300 million m^3) and numerous other smaller storages in this catchment. Only limited data are available for these storages. Levees have been constructed along both banks of the lower reaches of Tang He to protect vast areas of agricultural land and population centres. Based on available information, some of these levees have been in place for over 50 years and have been progressively upgraded. There are extensive intra and inter basin irrigation networks in the Tang He catchment. No data on this irrigation network were available for this study. Data were available for 9 rainfall and 5 stream gauging stations spread across the modelled catchment.

3. YANGTZE UPPER REACH CHARACTERISTICS

The upper reach of the Yangtze River between Chongqing and the Three Gorges Dam is about 600 km long and has a bed slope of about 0.0002 m/m. Floods in this reach occur in the wet season (May to September) and discharges in

excess of 70,000 m^3/s (at Chongqing) have been experienced on at least 4 out of the last 20 years. Although the flood flows can be very large, the river is predominantly confined or 'one-dimensional' along this reach. Downstream of Fengjie (see Figure 1), the Yangtze passes through the Three Gorges reach. As the name suggests, the river is confined through this reach and there is (relatively) little change in the flow width across a large range of flood levels (60m+) over a river distance of about 200 km. Upstream of Fengjie, whilst still passing through 'gorge' type controlling sections, the river does widen considerably. A detailed description of the hydraulic characteristics of this reach is given in an accompanying paper (Clark et. al., 2004).

The hydraulic models for the upper reach are represented by 305 cross-sections at approximately 2 km intervals. Flood storage along the main channel of the Yangtze appears to be well represented by the available cross-sectional information. However, it appears that during the flood season additional storage becomes available within this reach when the Yangtze 'backs up' into the numerous tributary rivers feeding into the main river. The model configuration was adjusted at major tributary junctions to take account of this additional storage.

The hydraulic models developed for this reach have 3 'external' boundary conditions (Chongqing on the Yangtze River and Wulong on the Wu River at the upstream end and the Three Gorges Dam at the downstream end) and 26 'internal' boundary conditions feeding lateral inflows from various tributary catchments along this reach (via hydrologic model outputs). There are 7 'intermediate' gauging stations along the Yangtze providing water level data to calibrate the models and ascertain model performance. Four of these stations also provide gauged discharge data.

4. DESCRIPTION OF MODELS

4.1 Hydrologic Models

Based on an overview of the flood forecasting models currently used in the Yangtze catchment, three well-established hydrologic models not previously tested in the Yangtze catchment (URBS, RAFTS and HEC-HMS) were selected for testing. Two of these models (URBS and RAFTS) are non-linear rainfall runoff-routing models of Australian origin. It is understood that these types of models have not been previously evaluated for use in the Yangtze catchment. The third model (HEC-HMS) is of United States origin. Two Chinese models currently in use in the Yangtze catchment (Xinanjiang and API) were also selected for comparative purposes.

URBS and RAFTS are networked runoff-routing models, which estimate flood hydrographs by routing rainfall excess through a module representing the catchment storage. HEC-HMS is also a networked rainfall-runoff-routing model. However, unlike URBS and RAFTS, HEC-HMS uses unit hydrograph theory to convert excess rainfall to direct runoff. The Xinanjiang (XAJ) model is a well-known Chinese model which was built mainly for catchments in humid and semi-humid regions, but has been extensively used throughout China for flood forecasting since 1980 (Zhao, 1992). XAJ is essentially based on unit hydrograph theory, but has an option to adopt the linear reservoir routing technique to produce runoff hydrographs. The API model has also been extensively used in China for flood forecasting for many years. The API model used by the Yangtze River Water Resources Commission is based on the principles of the American Weather Service method developed in 1969 but modified to suit the local catchment conditions.

4.2 Hydraulic Models

The worlds leading hydraulic modelling software providers were invited to provide a demonstration of their software capabilities and then provide licences to evaluate their software for suitability for use in the Yangtze FFS. Based on the response from these software providers, three well-established international hydraulic models (InfoWorks – UK; MIKE-11 – Denmark; and HEC-RAS – US) were short-listed for evaluation.

HEC-RAS is the successor of the well-known HEC-2 steady flow hydraulic Model. The unsteady flow modelling component, which is a recent addition to HEC-RAS, is capable of simulating one-dimensional unsteady flow through a full network of open channels. InfoWorks combines Wallingford's original ISIS hydraulic model engine with GIS functionality and database storage within a single environment bringing together source data and hydraulic modelling into a single product (Wallingford, 2002). MIKE-11 is described as a fully dynamic modelling tool for the detailed analysis, design, management and operation of both simple and complex river and channel systems (DHI, 2002). The hydrodynamic model is the nucleus of the MIKE-11 modelling system and forms the basis for its flood forecasting module.

5. MODEL EVALUATION

5.1 Chinese National Standards

The technical performance of the five hydrologic and the three hydraulic models was assessed in accordance with the performance criteria specified in Chinese Standards (2000). The two key performance indicators specified in the Chinese Standards are the 'Coefficient of Determination' (CD), which is a measure of the goodness-of-fit between the recorded and predicted discharge time series data, and the 'Qualifying Rates' (QR) of predicted individual flood event peak discharges and volumes. Under this terminology, a forecast peak discharge or flood volume is termed 'qualified' when the difference between the predicted and recorded values is within 20%. When flood levels are forecast the accuracy of forecast flood levels are assessed by examining the absolute error of the forecast levels.

The forecast accuracy determined on the basis of the CD and QR indicators is classified into Grades A, B or C according to criteria shown in Table 1. According to Chinese Standards (2000), the models that produce Grade A or B results are suitable for making official forecasts. Grade C models are only suitable for making 'reference' forecasts. Models that cannot make at least Grade C are not recommended for use in flood forecasting.

Table 1 - Accuracy Grading of Flood Forecast Elements

Accuracy Grade	A	B	C
Coefficient of Determination	CD>=0.90	0.90>CD>=0.70	0.70>CD>=0.50
Qualifying Rate (%)	QR>85.0	85.0>QR>=70.0	70.0>QR>=60.0

5.2 Evaluation Criteria

5.2.1 Hydrologic Models

The primary objective of the hydrologic model evaluation was to select the models that are most suited for use within the Yangtze FFS, provided they satisfied the technical performance criteria specified in the Chinese Standards. If the technical performances of different models were similar, the ease of adapting a particular model for real-time flood forecasting purposes in the Yangtze was also taken into account. Additional factors that were considered included model simplicity and flexibility, ease of use, suitability for different types of catchments (i.e. model limitations), cost and level of technical support, source code availability, and ease of integration with the selected hydraulic model and with components of the proposed FFS. The final selection involved some trade-off between model complexity (and possibly accuracy) and ease of use for flood forecasting.

5.2.2 Hydraulic Models

The primary objective of the hydraulic model evaluation was to select one model for further development and integration into the Yangtze River FFS. In order of importance, each model was evaluated for its 1) technical capability; 2) conformance to Chinese National Standards; 3) ability to interface with the FFS; 4) ease of use; and 5) Cost. The models had to satisfy the first 2 criteria (i.e. they must reproduce the flow behaviour of the Yangtze River to an acceptable level of accuracy as defined by the Chinese National Standards) to qualify for further consideration.

The technical features assessed included the accuracy of solution schemes, the flexibility to handle hydraulics roughness, the ability to handle the operation of the Three Gorges Dam, and the ability to undertake real-time error correction. The conformance to the Chinese National Standards was determined as per criteria defined in Table 1. A model's ability to interface with the FFS was determined on the basis of considerations such as ease of importing hydrologic model results from the FFS database and exporting results from the hydraulic model back to the FFS database. Model run times, and numerical stability during real-time use were also important considerations. Ease of use considerations included ease of model set up, ease of running the model in real-time and level of available technical support and documentation. The cost considerations included licensing, maintenance and training costs.

After a preliminary evaluation, only InfoWorks and MIKE-11 were selected for detailed evaluation. Although found capable of satisfying the technical criteria specified in the Chinese National Standards, HEC-RAS was not considered further for two reasons, these being: 1) there are no error correction facilities available for use in a real-

time application and 2) technical support required to integrate the model with the FFS is not available from the software provider. Thus, HEC-RAS is not discussed further in this paper.

6. COMPARISON OF MODEL RESULTS

6.1 Hydrologic Models

All models were run in a continuous mode for 6 years of historical flood season data for each catchment. Four years (1980,1981,1982&1983 for Da Ning He and 1975, 1977, 1980 & 1982 for Tang He) were used for model calibration and the remaining two years (1979 & 2000 for Da Ning He and 1984 & 1998 for Tang He) were used for model verification. For Da Ning He, the predicted hydrographs were compared to those recorded at the Wuxi gauging station. For Tang He, the predicted hydrographs were compared with those recorded at the Guotan gauging station.

6.1.1 Coefficient of Determination (CD)

The combined results of the model calibration and verification runs for Da Ning He at Wuxi and Tang He at Guotan respectively are shown in Tables 2 and 3. The results show that the average CD values obtained from the different models do not vary significantly. Interestingly, the average CD values obtained for the more complex Tang He catchment were generally better than those obtained for the simpler Da Ning catchment. This could be a reflection of the quality of available rainfall, streamflow and other catchment data.

Table 2 - CD Values for Discharge Predictions at Wuxi, Da Ning Catchment

Year	URBS	RAFTS	HEC-HMS	XAJ	API
1979	0.81	0.81	0.83	0.95	0.80
1980	0.93	0.93	0.90	0.85	0.90
1981	0.77	0.59	0.85	0.64	0.66
1982	0.91	0.90	0.90	0.64	0.91
1983	0.80	0.72	0.82	0.82	0.73
2000	0.90	0.87	0.92	0.85	0.88
Average	0.85	0.80	0.87	0.79	0.81

Table 3 - CD Values for Discharge Predictions at Guotan, Tang He Catchment

Year	URBS	RAFTS	HEC-HMS	XAJ	API
1975	0.93	0.93	0.93	0.95	0.93
1977	0.89	0.88	0.88	0.82	0.79
1980	0.94	0.88	0.86	0.88	0.89
1982	0.79	0.68	0.84	0.68	0.66
1984	0.88	0.88	0.89	0.90	0.81
1998	0.90	0.92	0.84	0.87	0.91
Average	0.89	0.86	0.87	0.85	0.83

The average CD values for all five models for both catchments are within Grade B limits. However, the gradings for different years of analysis for the different models varied for different years and catchments. For URBS and HEC-HMS, CD values for all years are within Grade A or B limits for both catchments; for RAFTS and API, CD values for all years, except one, are within Grade A or B limits for both catchments; and for XAJ, 4 out of the 6 years for Da Ning He catchment and 5 out of the 6 years for Tang He catchment are within Grade A or B limits.

6.1.2 Qualifying Rates (QR*)*

The predictions for individual flood events were extracted from continuous modelling results. Only flood events with peak discharges greater than 500 m^3/s at Wuxi for Da Ning He (35 events) and 1000 m^3/s at Guotan for Tang He (20 events) were extracted for the calculation of QR values.

Qualifying rates obtained for the different models for Da Ning He and Tang He catchments are shown in Tables 4 and 5. For the Da Ning He catchment, URBS and XAJ model results were within Grade A or B limits for both peak discharges and flood volumes; HEC-HMS model results were within Grade C limits for peak discharges and Grade A limits for flood volumes; RAFTS model results were within Grade C limits for both Peak discharges and flood volumes; and API model results were below Grade C limits for both peak discharges and flood volumes. For the Tang He catchment, URBS, XAJ and HEC-HMS model results for both peak discharges and flood volumes were within Grade A or B limits; RAFTS model results were within Grade B limits for peak discharges and Grade C limits for flood volumes; and API model results were below Grade C limits for both peak discharges and flood volumes.

Table 4 - Qualifying Rates for Event Peak Discharges and Flood Volumes, Da Ning Catchment

Model	Peak Discharges	Flood Volumes
URBS	71%	77%
RAFTS	66%	66%
HEC-HMS	60%	91%
XAJ	80%	86%
API	52%	52%

Table 5 - Qualifying Rates for Event Peak Discharges and Flood Volumes, Tang He Catchment

Model	Peak Discharges	Flood Volumes
URBS	75%	70%
RAFTS	70%	65%
HEC-HMS	90%	70%
XAJ	70%	85%
API	45%	45%

6.2 Hydraulic Models

Trial calibrations of InfoWorks and MIKE-11 models were carried out for 7 years of recorded flood season discharge and water level data (1981,1982,1983,1984,1985,1986&1998) for the upper reach of the Yangtze. The predicted water levels and discharges at the 7 intermediate gauging stations were compared with equivalent recorded water levels and discharges (where available). Due to space limitations, results are shown and discussed only for 2 of these 7 stations, namely Wanxian and Fengjie, which are located some 308 km and 433 km respectively downstream from the upstream end (see Figure 1). The findings for these 2 stations are generally similar to the other 5 stations.

6.2.1 Coefficient of Determination (CD)

The CD values obtained from the trial calibrations for the Yangtze at Wanxian and Fengjie are shown in Table 6. With MIKE-11 it was possible to achieve a GRADE A accuracy level for all years modelled. In contrast, only a mixture of GRADE A and GRADE B accuracy level could be achieved with InfoWorks. The average CD value obtained for all years at both locations with MIKE-11 was within GRADE A limits, where as the equivalent value obtained with InfoWorks was within GARDE B limits. According to these results, both InfoWorks and MIKE-11 are in conformance with the Chinese Standards (2000) with respect to the CD value. However, the calibration achieved with MIKE-11 was superior to InfoWorks. Achieving a good calibration with InfoWorks was inhibited by its limited ability to vary hydraulic roughness vertically within cross-sections. As a result, InfoWorks does not provide a mechanism to achieve a good calibration across the full range of water levels experienced during a flood event.

6.2.2 Qualifying Rate (QR)

Table 7 shows the difference between the predicted and recorded peak discharges at Wanxian and Fengjie for each year of calibration. All of the peak discharges for the years used in the trial calibrations fall within the definition of ‘qualified’ events and are within Grade A limits, with the notable exception of InfoWorks for 1981. This is

associated with the increasing discrepancy between the modelled and observed discharge for 1981 – the single largest observed discharge in these years.

Table 6 – CD Values for Discharge Predictions at Wanxian and Fengjie

Year	Wanxian		Fengjie	
	InfoWorks	MIKE-11	InfoWorks	MIKE-11
1981	0.74	0.96	0.81	0.98
1982	0.86	0.93	0.92	0.96
1983	0.69	0.90	0.83	0.96
1984	0.87	0.93	0.93	0.96
1985	0.89	0.96	0.93	0.99
1986	0.83	0.91	0.82	0.90
1998	0.91	0.98	0.94	0.98
Average	0.83	0.94	0.88	0.96

Table 7 – Relative Difference between Predicted and Recorded Peak Discharges at Wanxian and Fengjie

Year	Wanxian		Fengjie	
	InfoWorks	MIKE-11	InfoWorks	MIKE-11
1981	-25%	-2%	-20%	0%
1982	-11%	-11%	-11%	-12%
1983	-7%	-11%	-2%	-4%
1984	-9%	-14%	-1%	-6%
1985	-10%	-9%	-3%	-2%
1986	-12%	-11%	-5%	-5%
1998	-8%	-11%	0%	0%

6.2.3 Absolute Error

Table 8 shows the difference between the predicted and recorded peak flood levels at Wanxian and Fengjie for each of the calibration years. When assessing the magnitudes of absolute error values shown in Table 8 please note that the depth of flow at these two locations when the flood levels peak are usually greater than 40-50 m.

Table 8 – Absolute Error (m) in Predicted Peak Flood Levels at Wanxian and Fengjie

Year	Wanxian		Fengjie	
	InfoWorks	MIKE-11	InfoWorks	MIKE-11
1981	-4.8	0.1	-9.4	0.1
1982	-0.5	-2.2	-4.6	-2.8
1983	1.7	-0.5	-2.3	-1.0
1984	0.9	-1.0	-2.7	-1.5
1985	2.3	0.6	-0.7	0.9
1986	1.9	-0.1	-0.8	0.4
1998	2.0	0.0	-0.6	1.6

7. SUMMARY AND CONCLUSIONS

Suitability of five hydrological models (URBS, RAFTS, HEC-HMS, XAJ and API) and three hydraulic models (InfoWorks, MIKE-11 and HEC-RAS) was evaluated for inclusion in the real-time FFS for the Yangtze catchment. Common data sets from two hydrologically dissimilar tributary catchments and the upper reach main stem

respectively of the Yangtze River, and performance indicators specified in Chinese Standards (2000) were used. The models satisfying the technical criteria were then further assessed for their suitability for integration into the FFS.

7.1 Hydrologic Models

All models satisfied the CD criteria specified in the Chinese National Standards, and all models, except the API model, satisfied the QR criteria. The URBS and HEC-HMS models appeared to perform better than the other models with respect to the CD criteria. The XAJ model appeared to perform better than the other models with respect to the QR criteria.

The data available (for this investigation) on topography, reservoir storage and operation, and other catchment features that may influence runoff behaviour of the two test catchments were limited. It is believed that the model performances can be improved with better quality data.

It was interesting to note that the performance of the simpler models based on the unit hydrograph theory (XAJ and HEC-HMS) was similar to that based on non-linear catchment storage response models (URBS and RAFTS).

Based on the results of this study, four of the five models evaluated (URBS, RAFTS, HEC-HMS and XAJ) satisfy all the requirements of Chinese Standards (2000). Therefore, it is concluded that the modelling requirements of the Yangtze tributary catchments are within the capabilities of four out of the five models evaluated in this study. However, on the basis of the other criteria discussed in Section 5.2, it is further concluded that the URBS and XAJ models are more suited than the other models for use within the Yangtze FFS.

7.2 Hydraulic Models

Based on the trial calibration and other investigations conducted during the evaluation period, the following conclusions were reached with regard to the two hydraulic models evaluated in detail.

With respect to technical performance, both InfoWorks and MIKE-11 were generally in conformance with the Chinese Standards (2000). It is noted that with additional effort both sets of calibrations could be improved further. However, for the objectives of this model evaluation, such an additional effort was not considered necessary. Apart from technical performance, both models have adequate features to incorporate them into the Yangtze FFS. However, after the consideration of all evaluation criteria, MIKE-11 was found to be more suited for use within the Yangtze FFS. InfoWorks' inability to vary hydraulic roughness values vertically in cross-sections is a major weakness for Yangtze River hydraulic modelling. In addition, the model run times for MIKE-11 were much smaller and the stability of MIKE-11 runs was less sensitive to specified initial conditions.

8. ACKNOWLEDGEMENTS AND DISCLAIMER

This project has been funded by the governments of Australia and Peoples Republic of China under the 'development cooperation program' with China, managed by the Australian Agency for International Development (AusAID). The support given by the various organisations involved in the project and the technical assistance provided by the developers of URBS, RAFTS, InfoWorks and MIKE-11 models is gratefully acknowledged. The views expressed in this publication are those of the authors and not necessarily those of the Commonwealth of Australia. The Commonwealth of Australia accepts no responsibility for any loss, damage or injury resulting from reliance on any of the information or views contained in this publication.

9. REFERENCES

Chinese Standards. (2000). *Standard for hydrological information and hydrological forecasting*, Chinese Ministry of Water Resources – SL 250-2000.
Clark, S.Q., Markar, M.S., Wu, D., Min, Y. (2004). Overview of Hydraulic Modelling of the Yangtze River for Flood Forecasting Purposes, *8th National Conference on Hydraulics in Water Engineering,* Gold Coast, Australia.
DHI. (2002). *MIKE-11 User Guide,* Danish Hydraulic Institute, Denmark.
Wallingford. (2002). *InfoWorks RS 'Help' Documentation*, Version 4.5, Wallingford Software, United Kingdom.
Zhao, R.J. (1992). The Xinanjiang model applied in China, *Journal of Hydrology*, Vol. 135, pp371-381.

The Institution of Engineers, Australia
8th National Conference on Hydraulics in Water Engineering
ANA Hotel Gold Coast, Australia 13-16 July 2004

Application of Data-Driven Models and Computational Intelligence in Hydrology and Hydraulics

Dr Zoran Vojinovic
Ph.D., M.E., B.E., MIPENZ.
Patterson Britton & Partners Pty. Ltd., Australia
David McConnell
B.E., M.I.E.Aust.
Patterson Britton & Partners Pty. Ltd., Australia

Abstract: Due to the advances in information technology, data collection, storage and its retrieval many changes have taken place within the fields of hydrology and hydraulics. Many of these changes are seen through developments and use of hydroinformatics technologies for water resources planning and management. With the use of computational power and the exchange of knowledge with other disciplines we are quickly bringing together and understanding the new trends in the water related applications as we increase the knowledge of these applications. For example, we are witnessing intelligent systems entering the field such as Artificial Neural Networks, Support Vector Machines, Genetic Programming, etc., which can learn from data to produce solutions or equations as input output relationships with relatively little knowledge about the underlying processes. These new technologies, which are commonly referred to as data-driven modelling technologies, have proved in many cases to successfully complement the traditional (partial differential) knowledge-based modelling approach. There are many other areas where these advanced hydroinformatics technologies have found their successful application and the challenge is to use this power to the best advantage, and where possible sharing and building on the advances made by our colleagues in other disciplines. This paper describes key hydroinformatics technologies within the context of water resources planning and management and refers to some examples from real life applications.

Keywords: Hydroinformatics, Numerical Models, Genetic Algorithms, Genetic Programming, Fuzzy Logic Artificial Neural Networks, Support Vector Machines, Chaos Theory.

1. INTRODUCTION

The capabilities of computational modelling techniques aimed to support sustainable water resources management are nowadays making considerable progress. Also, advances in information technology, data collection, storage and its retrieval have been enormous in recent years. The hydraulic engineering community has responded to this challenge in various ways. The major response is seen in the developments occurring within the field of hydroinformatics and application of emerging data-driven technologies that are based on model induction and evolution from large data sets. In this respect, hydroinformatics can be viewed as the application of modern information technologies for solving problems associated with the aquatic environment. Hydroinformatics relates to the area of latest Information Communication Technology (ICT) developments, and at the same time it also relates to the area of developing the knowledge associated with the flow of water. The following sections of this paper summarise these novel hydroinformatics technologies and provide some examples of their successful application within the context of integrated data analysis and modelling framework.

2. HYDRAULIC MODELLING TECHNOLOGIES

Studying a physical system and its interaction with the environment is a prerequisite for effective planning and management of water resources. In this respect, as opposed to models built of material components, computer models provide effective means for well-structured and timely problem analysis. Therefore, a computer model can be viewed as a simplified, but still very powerful, representation of reality. The objective of applying a model is to gain the knowledge about the process under consideration and to perform what-if scenarios in order to arrive with better management and control strategies of water resources. The modelling process includes studying a system, posting the problem, collecting and analysing the data, building the model, testing it, optimising its parameters, running the scenarios and interpreting the results.

Traditionally, computer hydraulic models have been based on a deterministic description of the physical processes. Such an approach is based on governing laws from physics (e.g., Navier-Stokes equations) which describe the behaviour of water in particular circumstances. Another approach is based on developing the models on data alone (or rules) without the prerequisite of having the detailed knowledge about the phenomena. Both approaches are briefly described in following sections with subsequent presentation of benefits gained by applying the data-driven approach as a complementary error-correction tool for deterministic (or physically-based) models.

2.1 Physically-based modelling

A physically-based (or knowledge-driven, deterministic, behavioural, process, simulation, partial differential equation) model is based on the description of processes by physics or first-order principles of natural phenomena. The theoretical foundations for this kind of models were laid down in the 19th century with the work of de St Venant and Boussinesq, who formulated the unsteady flow equations, and with the work of Massau who in 1889 published early attempts to solve those equations. These physically-based models are widely researched, applied and taught. Despite the powerful capabilities of physically-based models, it is still deemed unfeasible to develop a fully deterministic model able to account for the high spatial and temporal variability of the processes involved (Vojinovic *et al*., 2003, Babovic, *et al*., 2001). Furthermore, the classic approach is to build a model form first principles and use it to forecast on the basis of initial conditions. Unfortunately this is not always possible. In fluid dynamics a perfect model in the form of physical equations exists, but initial conditions are difficult to obtain and therefore alternative approaches should be examined. In this contribution, the novel hydroinformatics methods based on data-driven and computational intelligence concepts are presented here and their applications pointed out.

2.2 Data-driven modelling and computational intelligence

Emerging technologies within the field of hydroinformatics are based on model induction and evolution from large amounts of data without the prerequisite of having detailed physically-based knowledge of processes under consideration. In this context, a model can be viewed on the basis of connections between the input, state and output variables. An example of such models is a linear regression or autoregressive moving average model. In the past, due to the limited capabilities in modelling nonlinear dependencies, these techniques have had a somewhat restricted success. However, during the last decade, following the tremendous developments within the field of information technology, computational intelligence, data collection and nonlinear process modelling, such concepts are again receiving a great deal of attention within the scientific community and practitioners. The data-driven modelling concept borrows methods from various areas that are related to *computational intelligence, machine learning, data mining, knowledge discovery, soft computing, artificial intelligence, etc*. The techniques that will be briefly described are evolutionary algorithms (more precisely here, genetic algorithms (GA) and genetic programming (GP)), fuzzy inference models, artificial neural networks (ANN), support vector machines (SVM) and chaos theory.

The techniques such as GA and GP have been inspired by the biological concepts of natural evolution where the solutions of the problem are evolved rather than the problems being solved directly. Although different and intended for different purposes, all evolutionary algorithms share a common conceptual base. In principle, an initial population of individuals is created within a model and allowed to evolve using the principle of inheritance (so that the offspring resembles the parents), variability (the process of offspring creation is not perfect – some mutation occurs) and selection (more fit individuals are allowed to reproduce more often and less fit less often so that their 'genealogical' trees disappear in time). Some application of GAs can be found in Babovic *et al.*, (1994). Also, very interesting approaches based on GP technique are presented in Khu et al. (2001).

Another technique is the so-called fuzzy logic approach which is based on fuzzy set theory introduced by Lofti Zadeh in 1965. This technique has found a very wide range of applications in the industrial systems control which are very complex, uncertain and cannot be modelled precisely, even under different assumptions and approximations. As such, it is also very applicable for the operation and control of water related systems and some applications in this respect can be found in Lobbrecht and Solomatine (1999).

Recent developments in non-linear dynamics have demonstrated that irregular or random behaviour in natural phenomena may arise from purely deterministic dynamics with unstable trajectories. Even though some observations may appear random, underneath their random behaviour may lie an order or pattern. Such types of non-linear dynamical systems are known as chaotic systems. Chaotic behaviour of many systems was observed by many researchers for a number of decades, but it was first described as such by

Lorenz in 1963. Chaotic systems comprise a class of signals that lie between predictable periodic or quasiperiodic signals and totally irregular stochastic signals which are completely unpredictable. Chaos theory is becoming very popular in various areas of engineering and even social sciences. Some examples of its application in water related field can be found in Solomatine *et al.,* (2000) and Babovic *et al.,* (1999).

Recently, neural networks (NNs) and support vector machines (SVM) have been applied successfully in various fields as a modelling technique for nonlinear systems. A major characteristic of these two techniques is that they are capable of approximating nonlinear functions to any arbitrary degree of accuracy (Hornik *et al,* 1989; Cybenko, 1989). As in many other processes, the nonlinearity, complexity, and lack of understanding of water related processes favour the potential use of neural networks. Mason *et al.* (1996) have shown how radial basis function neural networks can be very effective in modelling runoff for a large rainfall database. A review of NN applications in processes such as rainfall-runoff, streamflows, water quality, ground water, precipitation, hydrology is presented in detail in the ASCE Task Committee (2000). There are also other dozens of successful applications such as prediction of rainfall-runoff processes, replication of behaviour of hydrodynamic/hydrological processes aimed for model-based optimal reservoir control, replication of a channel network, surge water level prediction in the problem of ship guidance, reconstruction of stage-discharge relationship and various flood management problems.

Despite the powerful capabilities of these relatively new concepts, a typical data-driven model (which can be either linear or a nonlinear function) suffers from a drawback in that it is synthesised only on the available data, without detailed knowledge of the underlying processes (black box approach). It may be inadequate and inaccurate for prediction and extrapolation when the data are sparse or noisy. Consequently, the alternative of using a hybrid model that integrates both a deterministic (numerical) model and a data driven model for modelling water related processes appears promising, especially when more accurate model outputs (predictions) are required. The major advantage of such an approach (over using the data-driven model alone) is that the already available deterministic model quality is exploited and improved instead of starting from scratch and throwing away all knowledge. This approach also known as a data assimilation (or error correction) approach will be explained in the following section of this paper as part of the integrated data analysis and modelling framework.

3. INTEGRATED DATA ANALYSIS AND MODELLING

In order to relate direct application and values of these new technologies, which are rapidly taking place within the water related disciplines worldwide, it is beneficial to look for a moment at the practices that have been applied traditionally. A traditional perspective of the development of a catchment management plan is illustrated in Figure 1. From Figure 1 we can see that the classic approach starts with information gathering and database development (e.g., topographical data, land use data, drainage network data, hydrological data and monitoring data). Following the data gathering phase, the modelling process starts and results in a series of outputs which are used to prepare the final plan to the end user. This historically conditioned segmentation is usually present at all levels without any appropriate interaction. It is reflected through the administrative set up of the responsible organisations, as well as through the predominating engineering doctrines applied in each of the segments. Throughout the past decade, significant scientific and engineering efforts, supported by the intensified use of data processing technologies have been invested in development and application of analysis tools and engineering methodologies for water resources management. Numerical models, GIS systems, real-time data acquisition and control systems have become standard tools when dealing with water related systems. The value of the new tools and methods has been proven through applications, ranging from the long-term planning to the real-time control of these complex systems. The development and implementation of the new technologies has been driven by an increased pressure coming from ever stricter emission and environmental performance legislation, as well as by the need to increase the economical efficiency in the sector. However, this process has in general followed the traditional approach linked with the historical segmentation. Experiences in management and engineering analyses of water related systems in conditions of legislation focussed on environmental impact rather that on its emissions, have shown that proper understanding of water related systems cannot be established by focusing on each of the main segments separately without having an appropriate degree of interaction. This is because the segments are interconnected and changes in one part affect the performance of the other parts. Furthermore, the application of traditional numerical modelling technologies will not always generate fruitful results. Therefore, on a more advanced side, the emerging approach for water resources planning and management based on the hydroinformatics framework which includes the integration of information obtained from diverse sources, from field data and data from numerical models to data from non-engineering fields like ecology, economy and social science has been developed, Figure 2.

Hydroinformatics can be viewed as a socio-technical discipline which applies the latest computing technology and it makes social arrangements to support this technology. As such, hydroinformatics encourages practitioners to rethink traditional approaches from looking at the parts of a problem separately to looking at the problem as a whole. This is a very important aspect evolved from the fact that without appropriate social transformations the technologies themselves can never succeed and without appropriate technologies the social deadlocks cannot be unlocked. This certainly implies that hydroinformatics should play an important role in this process.

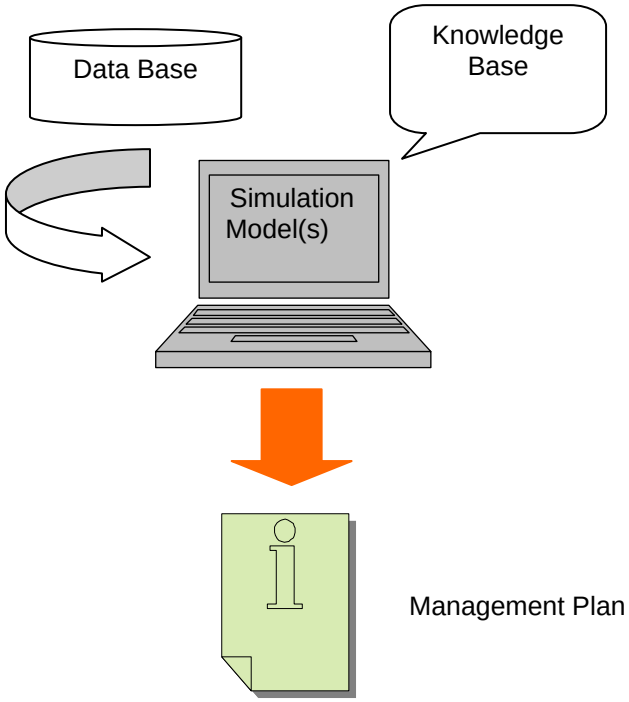

Figure 1 - Traditional approach to the development of a catchment management plan.

Figure 2 illustrates a more advanced approach within the hydroinformatics framework with additional elements such as, knowledge discovery and data assimilation, geospatial interface, application of intelligent systems and interactive user/stakeholder interface. After data gathering, the process starts with the knowledge discovery phase which refers to an effort of developing a data-driven technologies directly from databases. This is based on the fact that the database itself is a source of knowledge which sometimes cannot be explained in terms of known physical or biological laws. This phase is concerned with extracting useful information from data stores. Data mining is the step (be it automated or human-assisted) in this larger process called the knowledge discovery process. The broad knowledge discovery process includes: retrieving the data from a large data warehouse (or some other source); selecting the appropriate subset with which to work; deciding on the appropriate sampling strategy; selection of target data; dimensionality reduction; cleaning; data mining, appropriate model selection (or combination), evaluation and interpretation, and finally the consolidation and the putting to practical use of the extracted "knowledge". The data-mining step then fits models to, or extracts patterns from, the pre-processed data. The role of the human expert is to provide domain knowledge, interpret computer model results and devise further experiments that will provide even better data coverage.

Clearly, there is an enormous amount of knowledge and understanding of physical processes that should not be just thrown away. Consequently, the most appropriate way forward is to combine the best of the two approaches: theory-driven, understanding-rich with data-driven/mining discovery process (also referred to as data assimilation process). The following section refers to some practical applications in achieving just this — interaction of domain specialists with scientific discovery computer systems in order to create a knowledge discovery environment.

Probably one of the most important tasks in the development of a catchment management plan within the framework of hydroinformatics is the engagement of the end users or stakeholders. In Figure 2, this engagement is indicated by the user/stakeholder interface. The hydroinformatics tools and techniques which have been developed are capable of enabling them to effectively relate and communicate their interests and concerns.

However, there is always room for further development, and, as indicated by Abbott *et al.*, (2001), one of the major challenges for the future is to develop effective means to enable participation of stakeholders, in particular in environmentally sensitive decision-making processes.

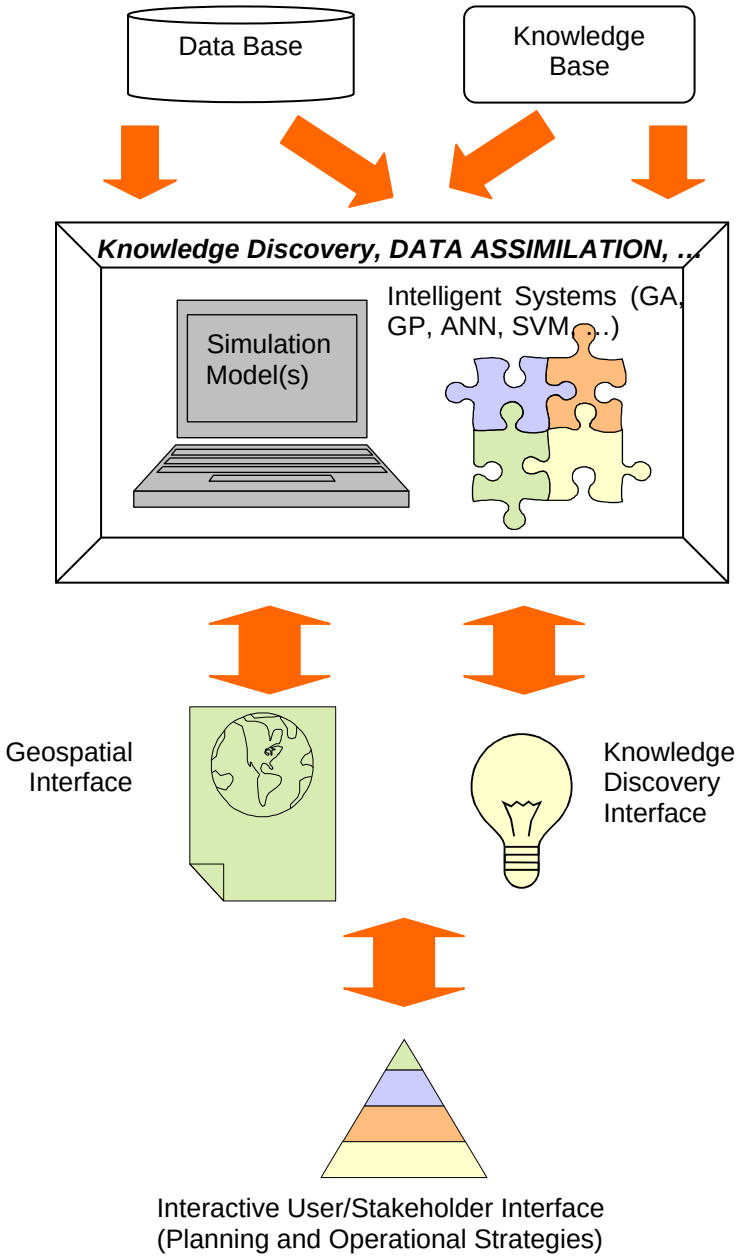

Figure 2 - Advanced approach to the development of a catchment management plan.

One of the other elements within the framework of hydroinformatics is the GIS, a system which deals with data acquisition, storage and mapping. GIS system plays an important role in the development of a catchment management plan as it provides the ability to visualise and interrogate model results so the decisions can be made easier within a rich graphical environment. Furthermore, the use of GIS thematic maps displaying model results have enabled many non-technical people to interpret and understand problems and take a part in the decision making process.

These fundamental changes in the approach to the development of a catchment management plan from providing software to assist an expert in making an analysis to providing a tool that decision makers can use, has been at the heart of much of the software development over the last few years and is well illustrated by the abundant high quality input and output systems associated with much of the “commercial” software available today.

3.1 Data Assimilation

In modelling physical processes where the underlying functions are known, the deterministic equations can be solved to generate the model output to a certain degree of accuracy. In hydraulic modelling, the governing laws are Navier-Stokes equations which provide a very accurate description of the process, if the initial conditions and forcing terms are precisely defined. In real-life applications, it is a very difficult task to create precisely boundary conditions for our models. However, even under precisely defined boundary conditions (almost ideal conditions), the model results are not fully accurate because the model deploys a number of simplifying assumptions. Therefore, the key reasons why the deterministic models often do not fully describe the modelled process are model physics, numerical solution, grid discretization, model parameters, input data, initial conditions, forcing terms and unknown subprocesses (Vojinovic *et al*, 2003).

It is a common belief within the hydraulic modelling community that the errors associated with calibrated model outputs do not accurately reflect the prototype despite our perfect knowledge of governing laws. Data assimilation is a methodology that combines a numerical model of a system with observations in order to gain a better knowledge of the state of the system. There are four different data assimilation procedures that can be applied to improve the accuracy of model outputs, Figure 3. These are designed either to improve the description of initial conditions (boundary conditions) or to provide correction of model predictions. The data assimilation procedures can be classified according to the variables modified during the updating process:

1. Updating of input parameters - This is the classical method justified by the fact that input uncertainties may be the dominant error in operational forecasting.

2. Updating of state variables - Adjustment of state variables can be done in different ways. The theoretically most comprehensive methodology is based on Kalman filtering (Gelb, 1974). Kalman filtering is the optimal updating procedure for linear systems, but can with some modifications it also provides an approximate solution for non-linear systems.

3. Updating of model parameters - continuous adaptation of model parameters is a matter of continuous debate. The prevailing view seems to be that for hydrodynamic models of non-trivial complexity recalibration of model parameters at every time step has no real advantages, as the operation of any hydrodynamic system cannot significantly change over a short interval of time.

4. Updating of output variables (error prediction) - The deviations between the observed variables and the simulation forecast are model errors. The possibility of forecasting these errors and superimposing them on the simulation model forecasts usually gives more accurate performance. This method is most often referred to as error prediction.

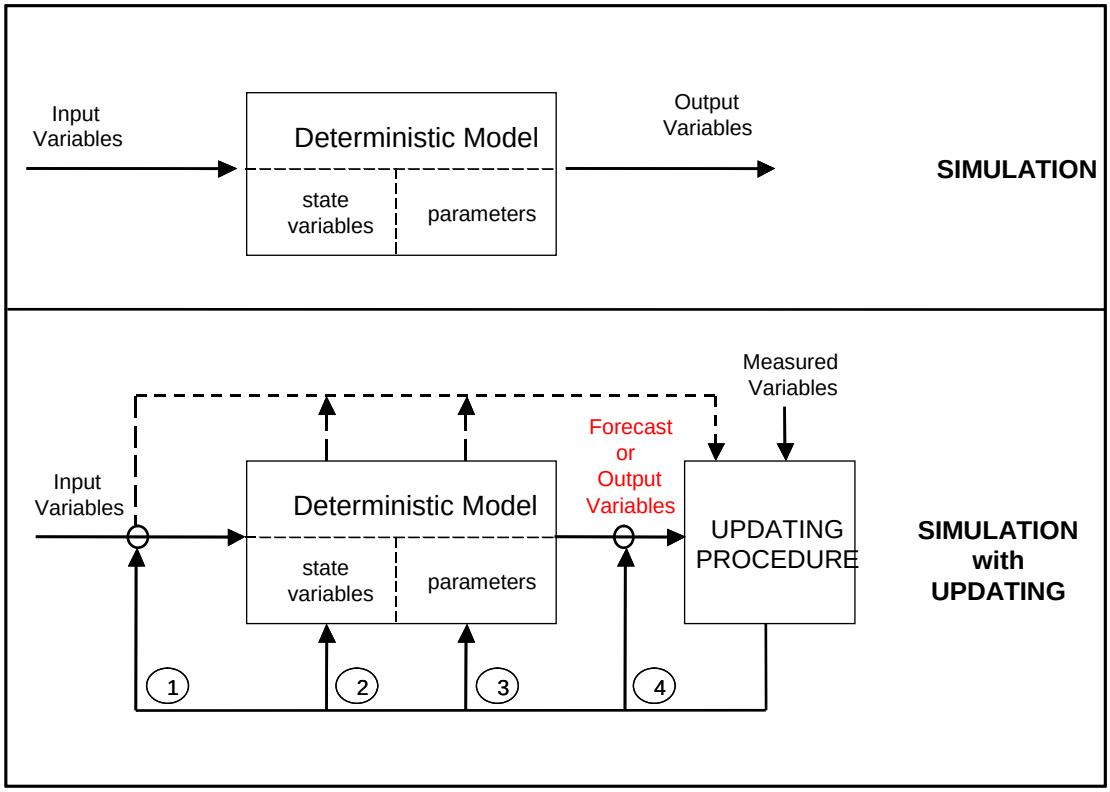

Figure 3 – Schematic diagram of simulation with emphasis on the four different updating methodologies.

There are several successful real life projects where the application of data assimilation technologies has proven to be very beneficial for the correction of deterministic models and hence for the development of operational strategies as well as for the analysis of remedial works requirements (e.g., Vojinovic *et al.,* 2003; Vojinovic and Kecman, 2003; Babovic, *et al.,* 2002).

4. CONCLUSIONS

In a nutshell, this paper illustrates novel hydroinformatics technologies and refers to some examples of their successful application within the area of water resources planning and management. Although the explanation here is fairly brief, the aforementioned discussion suggests that hydraulic engineering is advancing on several fronts. The new developments in mathematics, computer science, information communication technologies, etc., make it possible for hydraulic engineers to not only refine current practices but also to venture into the new dimensions of integrated data analysis and modelling with socio-technical interaction.

5. REFERENCES

Abbott M.B., Babovic, V.M. and Cunge, J.A. (2001), Towards the hydraulics of the hydroinformatics era, *Journal of Hydraulic Research*, 39(4), 339-349.

ASCE Task Committee, (2000). Artificial neural networks in hydrology II: Hydrologic applications. *Journal of Hydrologic Engineering*, ASCE, 5(2), 124-137.

Babovic, V., Larsen, L.C., and Wu, Z. (1994). Calibrating hydrodynamic models by means of simulated evolution, In Adri Verwey, Anthony W. Minns, Vladan Babovic, and Cedo Maksimovic, editors, *Proceedings of the First International Conference on Hydroinformatics,* pages 193-200. Balkema, Rotterdam.

Babovic, V., Keijzer, M., and Mahbub, R., (1999), Analysis and prediction of chaotic time series, D2K Technical Report 0399-2, DHI Water & Environment.

Babovic, V, Canizares, R, Jensen, H, Klinting, A, (2001), Neural networks as a routine for error updating of numerical models, *Journal of Hydraulic Engineering*, ASCE, 127(3), 181-193.

Cybenko, G., (1989). Approximation by superpositions of a sigmoidal function. *Mathematics of Control, Signals and Systems* 2, 304-314.

Gelb, A., (1974), Applied Optimal Estimation, MIT Press, Cambridge.

Hornik, M., Stinchcombe, M., and White, H., (1989). Multilayer feedforward networks are universal approximators. *Neural Networks,* 2, 359-366.

Khu, S.T., Liong, S.Y., Babovic, V., Madsen, H. and Muttil, N., (2001), GP and its application in real-time runoff forecasting, *Journal of American Water Resources Association*, Vol. 37, No 2: 439-451.

Lobbrecht A.H., Solomatine D.P. (1999), Control of water levels in polder areas using neural networks and fuzzy adaptive systems. In: Water Industry Systems: Modelling and Optimisation Applications, D. Savic, G. Walters (eds.). Research Studies Press Ltd., pp. 509-518.

Mason, J. C., Price, R. K. and Tem'me, A., (1996). A neural network model of rainfall runoff using radial basis function, *Journal of Hydraulic Research*, ASCE, Vol. 34(4), pp. 537-548.

Solomatine, D.P., Velickov, S., Rojas, C., and Wust, H., (2000), Predictive data mining in predicting surge water levels, Proc. Hydroinformatics 2000 Conference, Iowa, USA, July, Balkema.

Vojinovic, Z., and Kecman, V., (2003), Data Assimilation Using Recurrent Radial Basis Function Neural Network Model, IEEE International Symposium on Computational Intelligence for Measurement Systems and Applications, 29-31 July, Lugano, Switzerland.

Vojinovic, Z., Kecman, V., and Babovic, V., (2003), A Hybrid Approach for Modelling Wet Weather Response in Wastewater Systems, ASCE *Journal of Water Resources Planning and Management*, ASCE, Vol. 129, Issue 6, pp. 511-521.

The Institution of Engineers, Australia
8th National Conference on Hydraulics in Water Engineering
ANA Hotel Gold Coast, Australia 13-16 July 2004

Simulation of Turbidity Generation for Proposed Dredging Operations at Port Adelaide

A.D. McCowan
B.E.(Hons), Dip.H.E.(Delft), PhD, F.I.E.Aust.
Director, Water Technology Pty. Ltd., Australia
T.J. Womersley
B.E.(Hons),
Project Engineer, Water Technology Pty. Ltd., Australia

Abstract: Flinders Ports proposed to undertake capital works at Port Adelaide to allow access for larger Panamax size vessels. The works included dredging of approximately 2,000,000 m^3 of bed material with spoil disposal at sea. This paper describes the development of numerical hydrodynamic and suspended sediment transport models that have been used to investigate the likely fates of turbid plumes of suspended sediment generated during dredging and spoil disposal operations. The investigations have included a review of meteorological and oceanographic data for the area, and laboratory settling analysis of the sediments to be dredged. Modelling included the development of an overall model of Gulf St Vincent that simulated tidal and wind-driven currents and circulations, coupled to successively finer grid models of the spoil ground. A separate stand-alone fine-grid model was developed to simulate the effects of dredging within Port Adelaide.

Keywords: Dredging, Spoil disposal, Turbidity generation, Suspended sediments, Port Adelaide, Modelling

1. INTRODUCTION

Port Adelaide services the City of Adelaide and regional South Australia. It is situated at the mouth of the Port Adelaide River on the eastern coast of Gulf St Vincent, as shown in Figure 1. Flinders Ports Pty Ltd proposed to undertake capital works dredging at Port Adelaide to allow access for larger Panamax size vessels. The works included dredging approximately 2,000,000 m^3 of material at Port Adelaide to provide shipping access to a proposed new swinging basin and grain terminal. It was proposed that the dredge spoil would be disposed of at sea, approximately 40 kilometres west of Port Adelaide in water with a depth of 30 to 40 m. Figure 1 shows the location of key sites used in the investigations, including Port Adelaide and the proposed spoil disposal site.

This paper describes modelling investigations that have been used to assess turbidity generation and subsequent transport and deposition of suspended sediments associated with the proposed dredging works and spoil disposal operations.

2. DATA COLLATION

Existing meteorological and oceanographic data was reviewed to provide boundary conditions and calibration data for the models.

2.1 Tidal Data

Tide is the main parameter forcing the hydrodynamics of Gulf St Vincent. The tide propagates into the Gulf from the Southern Ocean via Investigator Strait, between York Peninsula and Kangaroo Island, and to a lesser extent through Backstairs Passage, between Cape Jervis and Kangaroo Island

Tidal information at key locations used in the study was derived from tidal constituents published in the Australian National Tide Tables (Department of Defence, 1995) and by Grzechnik & Noye (1996). The tide is predominately semi-diurnal (i.e., there are generally two tides per day), but there is a significant diurnal inequality (i.e., one tide each day has a significantly greater amplitude than the other). The amplitudes of the main solar and lunar semi-diurnal constituents are almost identical. During spring tides, the two solar and lunar semi-diurnal constituents combine to increase the tidal range. During neap tides, they tend to cancel each other

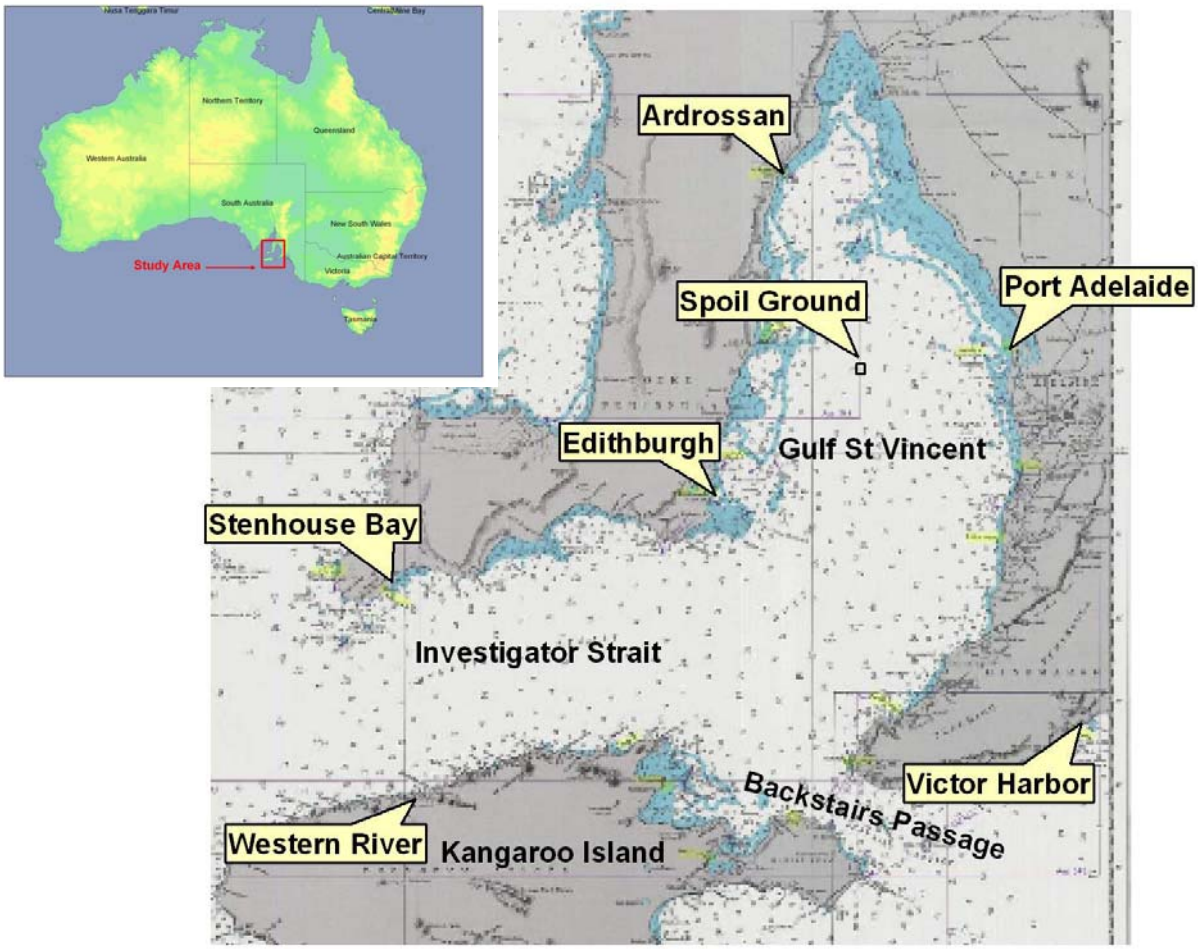

Figure 1 - Locality Plan

out and there is virtually no semi-diurnal tide (the so-called "dodge tide'). Additionally, the amplitude of the tide increases significantly with distance towards the head of the Gulf.

2.2 Wind Data

Wind data was obtained from the Bureau of Meteorology for a number of representative stations around the Gulf, including Adelaide Airport, Edithburgh and Kingscote (on Kangaroo Island). It was found that the winds in the Gulf come predominantly from the south during summer and from the north during winter. At Adelaide Airport (representative of the Port Adelaide area), the winds come from the south and southwest in summer, while the winter winds come predominantly from the north and northeast.

2.3 Survey Data

Survey data for the areas to be modelled was obtained from Royal Australian Navy charts of the area, and from detailed hydrographic surveys of the Port Adelaide River provided by Flinders Ports.

2.4 Current Data

Limited current measurements taken from Outer Harbor have shown that the currents in the Port Adelaide River tend to be aligned with the main channel. They have also shown that the current speeds can be very variable depending upon the location within the channel. On the flood tide, peak current speeds of up to 0.9 knot (0.46 m/s) were measured across most of the width of the channel. On the ebb tide, however, higher current speeds of up to 1.2 knots (0.62 m/s) were measured in the central part of the channel, with much weaker currents, typically less than 0.5 knots (0.26 m/s) measured closer to the channel edges.

2.5 Sediment Data

The results of detailed geotechnical investigations have shown that most of the material to be dredged from the existing channel is stiff to hard silty clays of the Hindmarsh Clay Formation. Shallower areas to be dredged at the edges of the proposed swinging basin include some soft clay and sit, overlying a 1.0 to 1.5 m layer of calcrete gravel and gravely sand associated with the Glanville Formation.

Settling tube analysis of clay samples representative of the material to be dredged from the channel showed that most of the sediment settled very rapidly. However, as the concentration of suspended sediment reduced, the settling rate also reduced, leaving a concentration in the order of 10 mg/L still present after 48 hours.

3. MODEL DEVELOPMENT

The hydrodynamic models were set-up using the nested hydrodynamic (HD) module of DHI Software's MIKE 21 modelling system. An overall 900 m grid model of Gulf St Vincent, including Investigator Strait and Backstairs Passage, was developed first. This overall Gulf model was then dynamically coupled to successively finer 300 m and 100 m grid models of the spoil ground area. A separate stand-alone 20 m grid of Port Adelaide and its immediate surrounds was established for simulating the effects of dredging within Port Adelaide. The bathymetry and extent of the models used in the investigations is displayed in Figure 2.

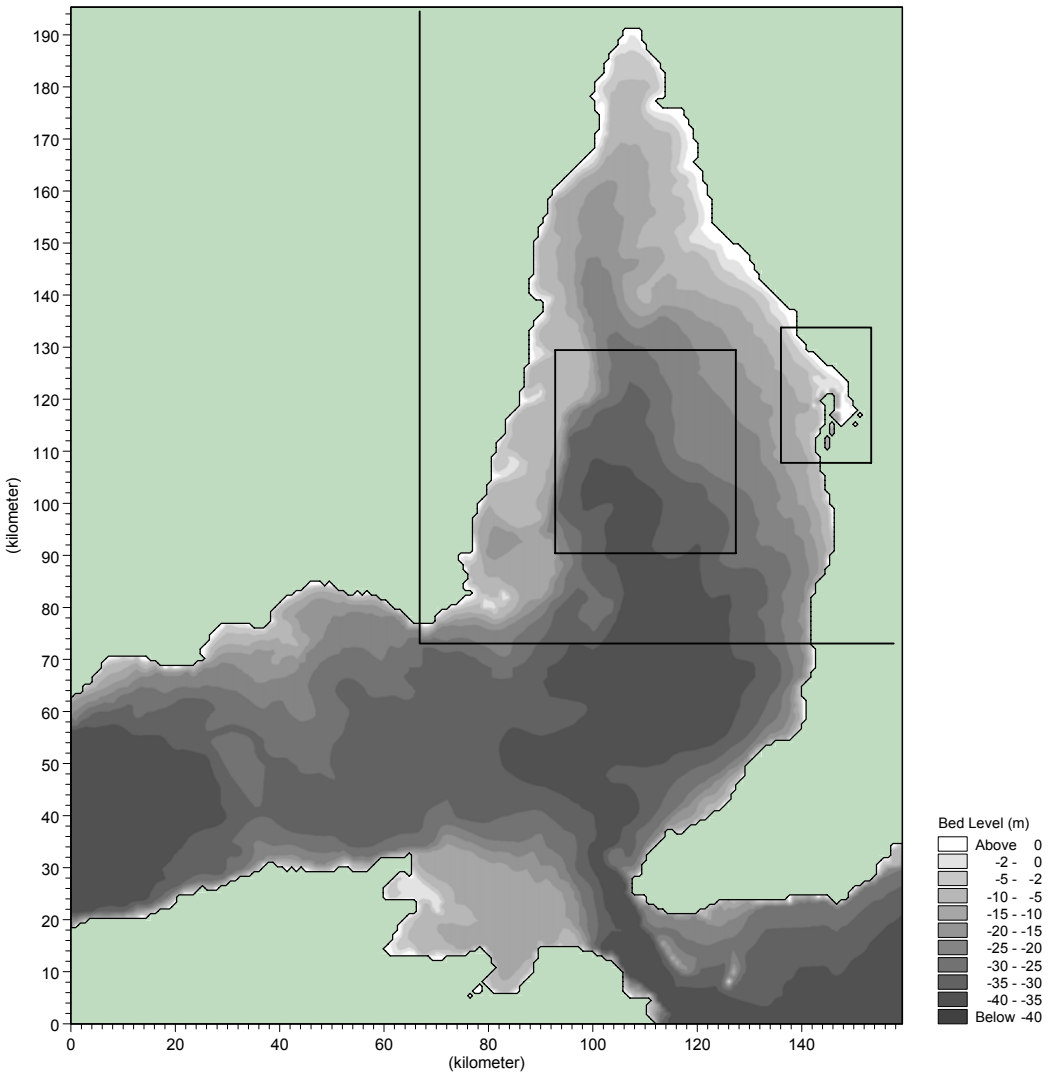

Figure 2 – Extent of the Models Used in the Investigation

3.1 The Gulf St Vincent Model

The overall Gulf St Vincent model contains two open boundaries, one at Backstairs Passage and the other through Investigator Strait. Boundary conditions at Backstairs Passage were generated from predicted tide levels at Victor Harbour. Boundary conditions at the Investigator Strait boundary were generated by averaging the phase and amplitude of the tidal constituents at Stenhouse Bay and Western River. The peak tidal range at both of these boundaries is typically of order 1.0 m.

The model was calibrated by running it for a period of one month, analysing the tidal elevations at different locations around the Gulf (e.g., Adelaide Outer Harbor, Edithburgh and Ardrossan), and comparing the tidal constituents with those provided in the Australian National Tide Tables (Department of Defence, 1995). Calibration was achieved by adjusting the bed resistance and by minor adjustment of the Investigator Strait boundary to obtain a close correlation between the tidal constituents obtained from the model results and those provide in the Tide Tables. The final bed resistance applied was equivalent to a Manning's "n" value of 0.025 throughout the model.

Figure 3 shows a plot comparing the computed tides at Ardrossan with predicted tides obtained from the tidal constituents provided in the Tide Tables. This shows that the peak tidal range at Ardossan is approximately 3.0 m (compared with about 1.0 m at the model boundaries), and that the model is capable of reproducing the strong spring/neap tide cycle, including the "dodge' tide, as well as the amplification of the tide towards the head of the Gulf.

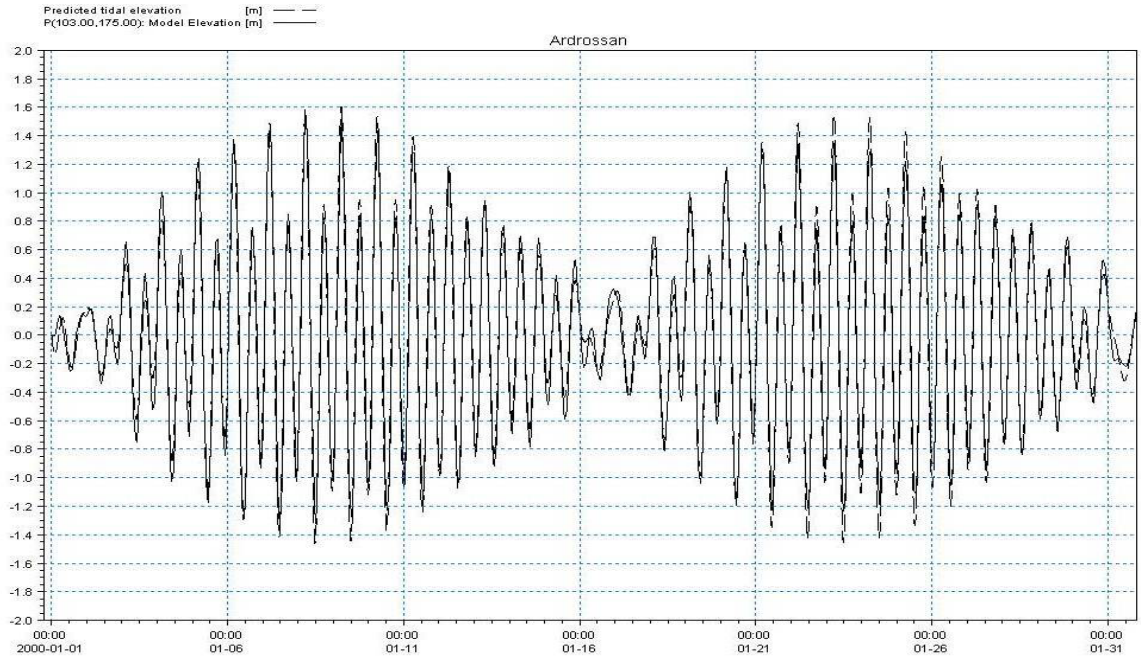

Figure 3 - Comparison of Predicted and Modelled Tidal Levels at Ardrossan

3.2 The Port Adelaide Model

The bathymetry of the Port Adelaide model is presented in Figure 4. This model was driven directly by the predicted tide at Port Adelaide Outer Harbor. Comparisons of modelled and predicted tides showed that the model was capable of reproducing the small increase in amplitude (of order 2 to 3 cm) and phase (typically 2 to 3 degrees) of the tide between the positions of the Inner and Outer Harbor tide gauges. Further, computed peak spring tide flows in the Outer Harbor were found to be consistent with the limited amount of measurements from the area.

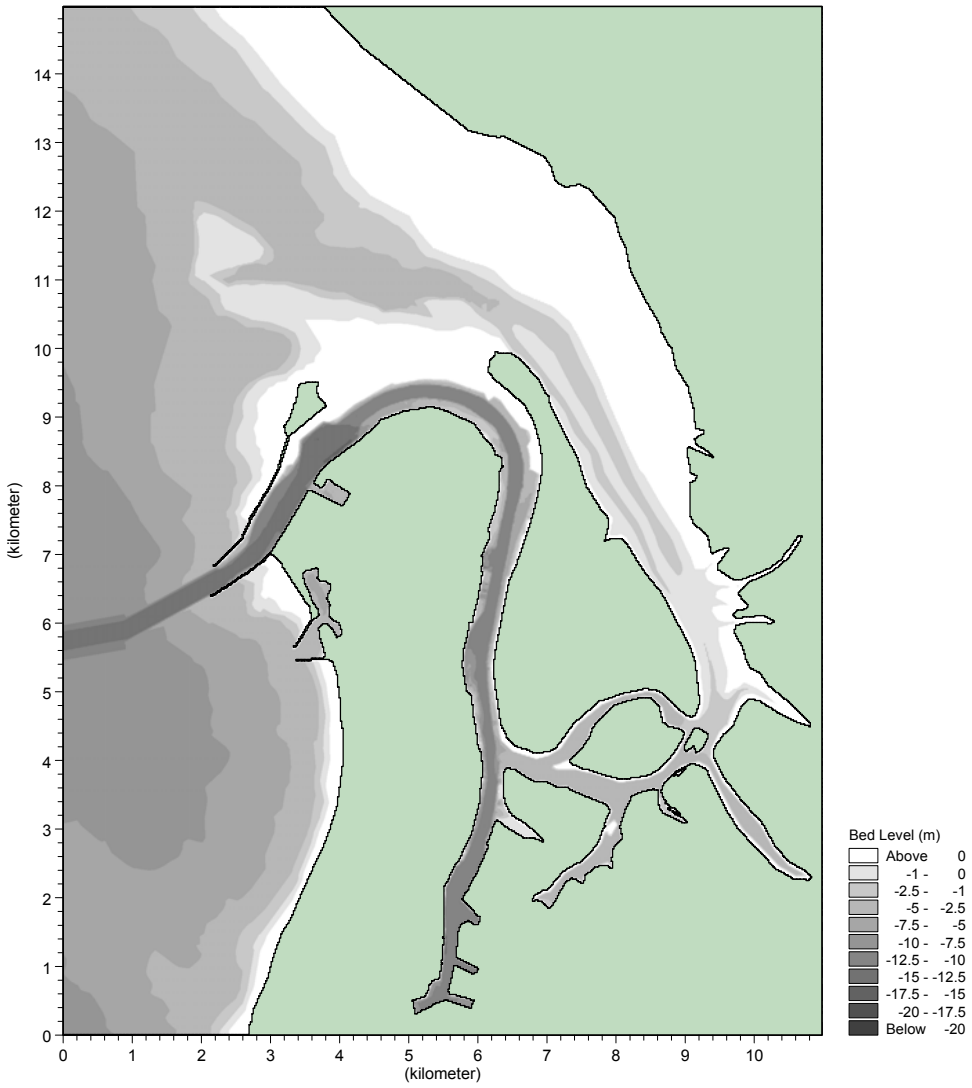

Figure 4 – The Port Adelaide Model Bathymetry

4. DREDGE SCENARIOS

It was proposed that a cutter suction dredge would be combined with a trailing suction hopper dredge to dredge the stiff to hard clays that comprise the vast majority of the material to be dredged. With this approach, the cutter suction dredge would be used to "pre-treat' the stiff to hard clays that are too hard to be dredged directly by the trailing suction hopper dredge. The cutter suction dredge would break up the clay bed and deposit the broken up material back on the channel bed for subsequent collection by the trailing suction hopper dredge. The dredged material would then be transported to, and disposed of in a new spoil ground in the central part of Gulf St Vincent.

The main physical effects of dredging will be related to the generation of turbidity during dredging and spoil disposal operations. Both the cutter suction dredge and the trailing hopper dredge would be expected to contribute to the turbidity generated during dredging, while only the trailing suction hopper dredge will contribute to the turbidity generated during spoil disposal operations. Following the work of Nakai (1984), turbidity generation has been quantified in terms of kilograms of suspended matter generated for each cubic meter of material dredged (kg/m^3). The turbidity generation rates used in this study were derived from the work of Nakai (1984), industry sources as reported by the Department of Defence (1995), and the results of a trial dredging operation in Corio Bay (Lawson and Treloar, 1996).

It was assumed that a large cutter suction dredge with a suction pipe diameter of about 850 mm would be used. Such a dredge could be expected to operate 24 hours per day for 6.5 days per week, with an effective dredging time of about 110 hours per week. For breaking up stiff to hard clays, the production rate of such a dredge could be expected to be in the order of 140,000 m^3 of bed material per week. Allowing for the effects of turbidity generation at the cutter head and at the discharge pipe, the turbidity generation rate for the operation of the cutter suction dredge was estimated to be 135 kg/m^3.

It was assumed that a medium to large trailing suction hopper would be used. Such a dredge could be expected to have a hoper capacity of 8,000 m^3, a draft of 8 to 9 m (laden), and a sailing speed of 12 to 15 knots. The biggest limitation to the productivity of this dredge will be the sailing distance of approximately 35 km to the spoil ground. Allowing for almost 2 hours of dredging and approximately 5,000 m^3 of bed material being removed each cycle, 24 hour a day and 6.5 day per week operation, could be expected to result in a production rate of approximately 160,000 m^3 of bed material per week. Allowing for the effects of the draghead, propeller wash and hopper overflows, the turbidity generation during dredging was estimated to be 300 kg/m^3. This is a relatively high value, and allowed for the fact that the material to be dredged would have already passed through the pump of the cutter suction dredge.

The amount of turbidity generated during spoil disposal operations will be very dependent upon the type of dredge being used, and the way in which it is operated. Typical turbidity generation rates could be expected to be in the range of 25 to 125 kg/m^3. For the present study, a turbidity generation rate of 75 kg/m^3 was assumed.

5. DREDGE SIMULATIONS

The physical effects of the proposed dredging operations were simulated by describing the turbidity generated during dredging and spoil disposal as sources of suspended sediment and simulating their subsequent transport and deposition in a numerical sediment transport model. As described above, two main scenarios were considered:

- Dredging in the Port Adelaide River using the combination of a cutter suction dredge and a trailing suction hopper dredge.
- Spoil disposal operations in Gulf St Vincent using a trailing suction hopper dredge.

5.1 The Sediment Transport Model

The suspended sediment transport model was set up using the nested mud transport (NMT) module of DHI Software's MIKE 21 modelling system. The model is based on critical shear stress theory where deposition occurs when the mean velocity falls below a critical deposition velocity, and erosion occurs when the mean velocity exceeds a critical erosion velocity. For the present study, erosion associated with re-suspension of recently deposited material only was considered.

5.2 Sediment Properties

The results of the settling tube analysis of the clay sediments were used to provide an indication of the likely settling rates of sediments suspended during dredging and spoil disposal operations. These results showed that the settling rate increases as a function of sediment concentration, from of order 0.01 mm/sec at a concentration of 10 mg/L, to of order 1.0 mm/s at a concentration of 1000 mg/L. The results also showed the sediments to have comparable settling characteristics to sediments from Port Giles (on the other side of the Gulf), and from Corio Bay (Department of Defence 1995). Further, in a full scale trailing suction hopper dredge trial in Corio Bay, Lawson and Treloar (1996) were able to calibrate turbidity generation rates and settling velocities used in similar dredge modelling simulations.

Applying a similar approach to the present study, the suspended sediments were divided into 5 main fractions each having settling rates varying from 3.3 mm/s down to 0.011 mm/s.

5.3 Port Adelaide Dredging

To simulate the likely extent of turbid plumes generated during dredging in the Port Adelaide channel, the suspended sediment model of Port Adelaide was run for a period of 15 days of representative winter conditions. The main inputs into the model included a full neap-spring tidal cycle as predicted for the Outer Harbour and

actual wind speeds and directions for July 1996 at Adelaide Airport (which was found to be representative of average winter conditions).

For modelling purposes the cutter suction dredge was assumed to operate continuously as a source of suspended sediment over a range of grid points within the area to be dredged. The source points operated sequentially, and were assumed to have a suspended sediment discharge rate of 31 kg/s. This corresponded to a total turbidity generation rate of 135 kg/m^3, at a weekly production rate of 140,000 m^3 of bed material. The trailing suction hopper dredge was assumed to operate on a 5 hour cycle, consisting of two hours of dredging and 3 hours of sailing to and from the spoil ground. Over the two hour dredging cycle the trailing suction hopper dredge was also assumed to operate over a range of source points within the area to be dredged. These source points were assumed to have a suspended sediment discharge rate of 208 kg/s, corresponding to a turbidity generation rate of 300 kg/m^3, at a production rate of 5,000 m^3 of bed material in each 5 hour dredge cycle.

Figure 5 shows typical suspended sediment concentrations (above background) resulting from the combined operation of the cutter suction and trailing suction hopper dredges during spring tide ebb flow.

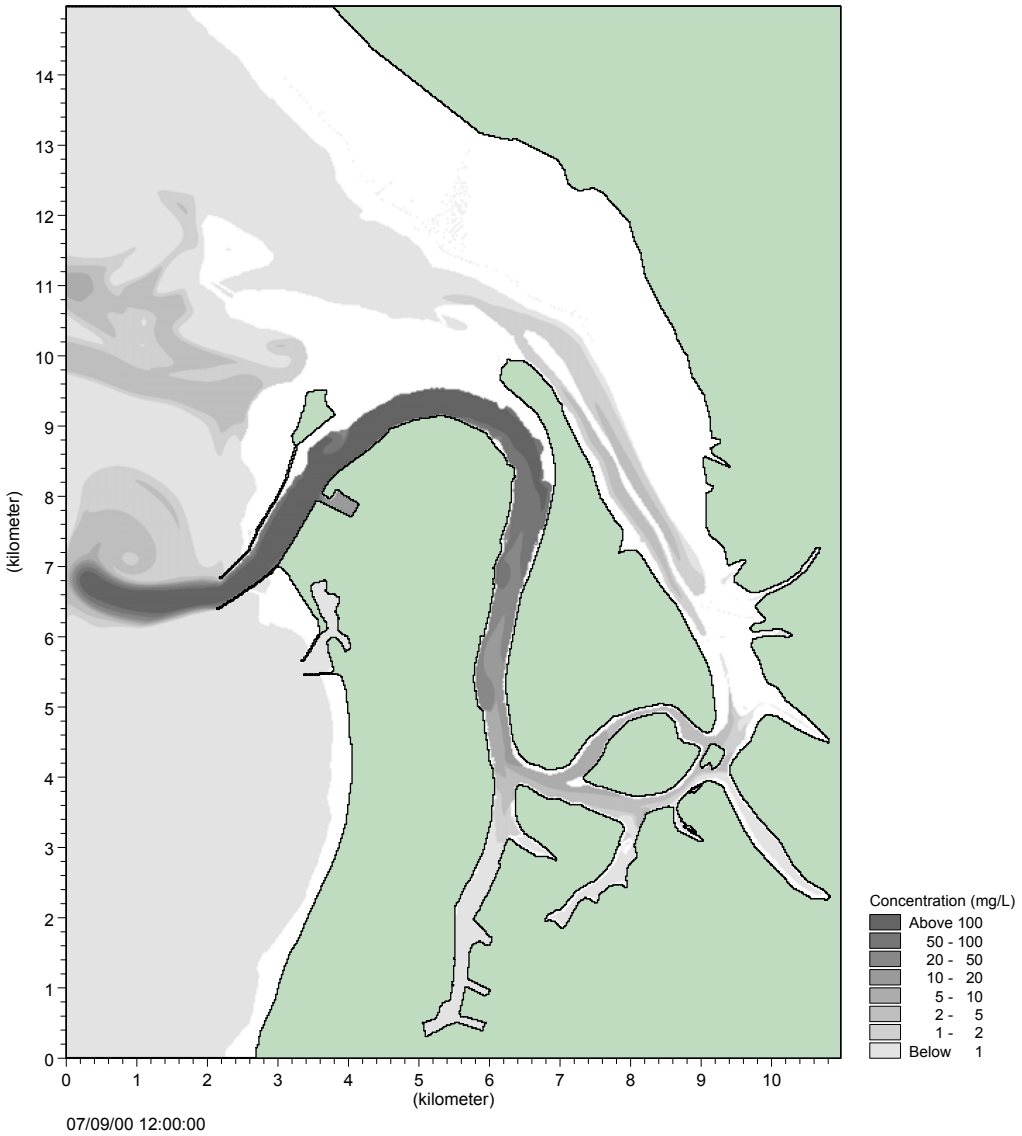

Figure 5 - Typical Suspended Sediment Concentrations During Spring Tide Ebb Currents

The model results showed that the combined operation of a cutter suction and trailing suction hopper dredge could be expected to generate turbid plumes with a relatively high suspended sediment concentrations of typically 100 to 200 mg/L above background levels over most of the area to be dredged. The model results also showed that following peak spring tide flows, turbid plumes could be expected to penetrate into the Inner Harbour and southern part of Barker Inlet (to the east) with peak sediment concentrations at the southern end of Barker Inlet up to 20mg/L above background. Similarly, turbid plumes during peak spring tide flows could be expected to be pass out into the Gulf. The turbid plumes that escape out into the Gulf are expected to be rapidly dispersed as they are advected away by tidal and wind driven currents.

Net sedimentation within the area to be dredged could be expected to be in the order of 100 mm. The model also indicates that with current speeds in excess of 0.3 m/s in the Port River during spring tides, some re-suspension of recently deposited sediments and hindering of normal settling would be expected. This would contribute to the relatively high suspended sediment concentrations computed by the model within the main channel.

5.4 Spoil Disposal Operations

To simulate the likely extent of turbid plumes generated during spoil disposal operations, the suspended sediment model of the spoil ground area was run for a period of one month of representative winter conditions. The main inputs to the model included two full neap-spring-neap tidal cycles at the Investigator Strait and Backstairs Passage model boundaries, and a month of representative average winter wind conditions. For modelling purposes, the position of spoil disposal was varied over 4 source points near the centre of the spoil ground. The source points were assumed to have a total load of 375 tonnes of suspended sediment during each disposal operation. This corresponded to 75 kg/m^3 of suspended sediment from each 5,000 m^3 load of spoil.

The model results showed that, apart from immediately following each disposal operation, the suspended sediment concentrations associated with spoil disposal would be expected to be relatively low (typically less than 20 mg/L above background levels). During neap tides, the turbid plumes would be expected to remain almost entirely within the area of the spoil ground. During spring tides, however, the greater tidal excursion together with periods of strong winds could be expected to advect the plume 1 to 2 km beyond the northern and southern boundaries of the spoil ground. The model indicated that with current speeds in excess of 0.3 m/s over the spoil ground during spring tides, some re-suspension of recently deposited spoil and hindering of normal settling could be expected. However, these effects did not appear to have a significant impact on suspended sediment concentrations in the area modelled.

6. CONCLUSIONS

The combined use of numerical hydrodynamic and suspended sediment transport models has provided a valuable tool for investigating the likely fate of sediments suspended during dredging and spoil disposal operations at Port Adelaide. With the models, realistic suspended sediment and sedimentation values could be determined for various dredging and disposal scenarios. This information then made it possible for an assessment to be made of the likely impact of the proposed dredging program on the marine environment, and to develop appropriate mitigation options and monitoring programs.

7. REFERENCES

Danish Hydraulic Institute, (1990), *Offshore Dredging Spoil Disposal*, Internal Report.

Department of Defence (1995), East Coast Armaments Complex, Submissions to the Commonwealth Commission of Inquiry.

Department of Defence (1999), *Australian National Tide Tables*, Australian Government Publishing Services, Canberra

Grzechnik, M. & Noye, J. (1996), *A Tidal Model of Gulf St Vincent, South Australia with fine grid submodels of the Outer Harbour and Port Stanvac regions*, University of Adelaide, Dept of Mathematics, Report TM1.

Lawson and Treloar Pty Ltd (1996), *Monitoring of Trial Dredge Operations in the Proposed ECAC Channel*, Report J5064/R1677.

Nakai, O. (1984), *Turbidity Generated by Dredging Projects*, Proc 3rd US-Japan Experts Meeting on Management of Bottom Sediments Containing Toxic Substances.

The Institution of Engineers, Australia
8th National Conference on Hydraulics in Water Engineering
ANA Hotel Gold Coast, Australia 13-16 July 2004

Asset and Pressure Management – A Combined Approach Mitcham-Morang Water Supply Zone

S. A. Pearce Higgins
B.Eng (Hons) MIEAust.,
Yarra Valley Water Ltd, Australia

A. McKenzie
B.Eng (Hons), B.Sc., G.I.E.Aust.
MWH Australia Pty Ltd, Australia

Abstract:

Yarra Valley Water's (YVW) water supply network has an average static pressure of supply of 73m head. Although the network was designed and constructed to accommodate these pressures, ageing pipes and natural deterioration has resulted in an increased burst rate. YVW has adopted a proactive planning approach to Asset Management, with system-wide measures, to determine the least community cost for the replacement of water supply assets.

This approach has recently been extended to include Pressure Management Areas (PMAs) and the construction of Pressure Reducing Stations (PRS) within selected water supply zones. The assessment is rigorous and includes the generation of a number of possible options with extensive testing of the final selection. There are definite advantages in combining the Asset and Pressure Assessment since the fundamental differences in supply philosophy can otherwise result in disjointed solutions.

At each PRS monitoring equipment will continuously measure the performance of the water supply zone so that areas with a high Minimum Night Flow (MNF) can be targeted for reduction in background leakage. These savings will play a key role in meeting the State Government's target of a 15% per capita reduction in water usage by 2010. The first new zones are expected to be operational in May/June 2004.

Keywords:

Asset, Pressure, Management

1 INTRODUCTION

1.1 Background

Yarra Valley Water (YVW) is one of three retail water companies in Melbourne and annually purchases approximately 190GL of water from a wholesaler, Melbourne Water. YVW supply retail water and sewerage services to 616,000 customers, comprising of 569,000 domestic customers and 47,000 industrial and commercial users. Of the 190GL's of water purchased, about 164GL are metered supplies to customers, with the remaining 24GL or 12.4% as 'Non Revenue Water'.

The Victorian Government has set a target reduction in water consumption per capita of 15% by 2010 and to achieve this YVW has set a goal of a 25% reduction in Non Revenue Water (NRW) by 2008. YVW is pursuing a number of initiatives to achieve this including the proactive preparation of Asset and Pressure Management Strategy's for each Water Supply Zone. The Mitcham-Morang Water Supply Zone is the first zone to be assessed as a combined Asset and Pressure Management Strategy. This combined Strategy approach expands the work conducted by other international water companies, primarily in the UK.

1.2 YVW Pressure Assessment

YVW experiences the second highest burst rate in Australia for large water supply systems, refer to Table 1 below *WSAA Facts 2003 Extract: Burst Rates for Retail Water Companies.* This high burst rate is attributed to the variability of soils types, particularly expansive clays, the fact that the pipes were not sand bedded prior to 1970, the high pressure of supply and the type and age of pipe materials.

Table 1 WSAA Burst Rate Comparison /100km pa

Company	98/99	99/00	00/01	01/02	02/03	Average
City West Water	77	70	58	56	103	72.8
Yarra Valley Water	42	42	56	41	57	47.6
Sydney Water	43	41	38	38	51	42.2
Brisbane Water	32	36	37	38	39	36.4
Barwon Water	53	19	28	24	32	31.2
South Australia Water	31	25	25	22	24	25.4
South East Water	24	26	26	21	29	25.2
WA Water Corp	11	12	13	13	13	12.4

The varying topography across YVW's area from the hills in the east to the lower elevated inner suburbs means the water supply pressure range from 20m to a maximum of 140m. The average water supply pressure for all customers is 73m, which is very high by comparison with other water supply systems. The average water pressure in each supply zone is show in Figure 1 below.

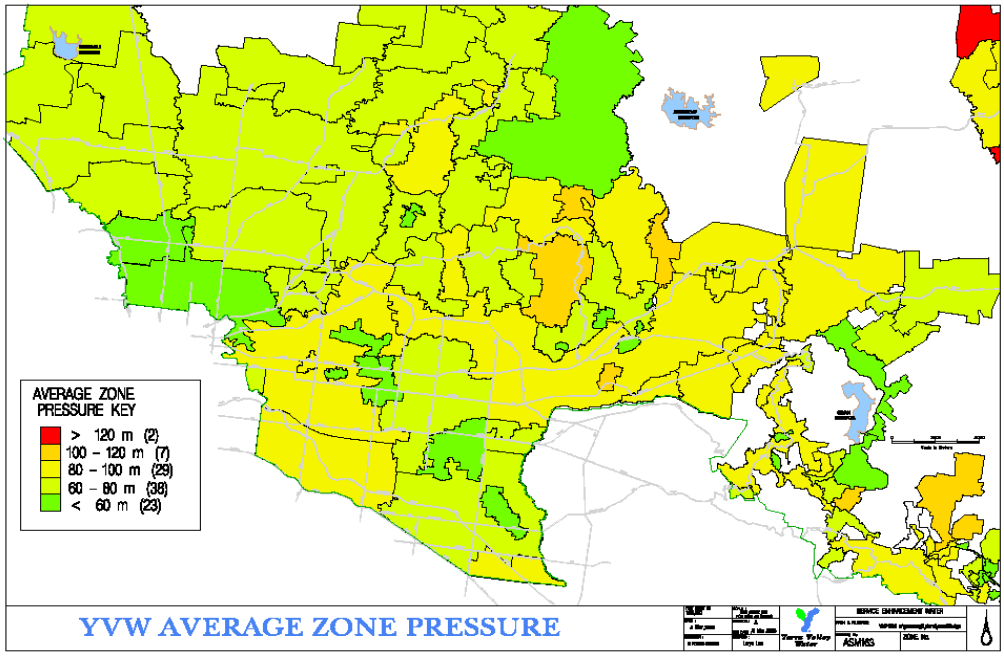

Figure 1: Average Pressures in YV W Water Supply Zones

In December 2000 YVW instigated the Kew pressure management trial in the Surrey Hills Water Supply Zone. A control area remained on the normal operating pressures and an adjacent area was pressure reduced with installation of two Pressure Reducing Station's (PRS). The average pressure inside the later was reduced from 105m to 75m. An analysis of the burst data for a period of 22 months before and after pressure reduction in the Kew trial area produced a 58% reduction in pressure related bursts for the Kew PRV Zone whilst over the same period there was a 38% increase in the control zone.

1.3 YVW Asset Assessment

YVW's water supply system comprises of a total of 8,643 km of water mains of which 820km are distribution mains with a diameter of 300mm and larger. The age/material profile of YVW water infrastructure is shown in Figure 2.

Although the pipe networks were originally designed and constructed to accommodate the high pressures, as the pipe assets age they have a declining residual strength. Remedial works in the 1960's and 1970's included in-situ cement lining which prolonged the asset life however the cost of burst rates and the associated remedial repairs and replacement costs are now starting to increase.

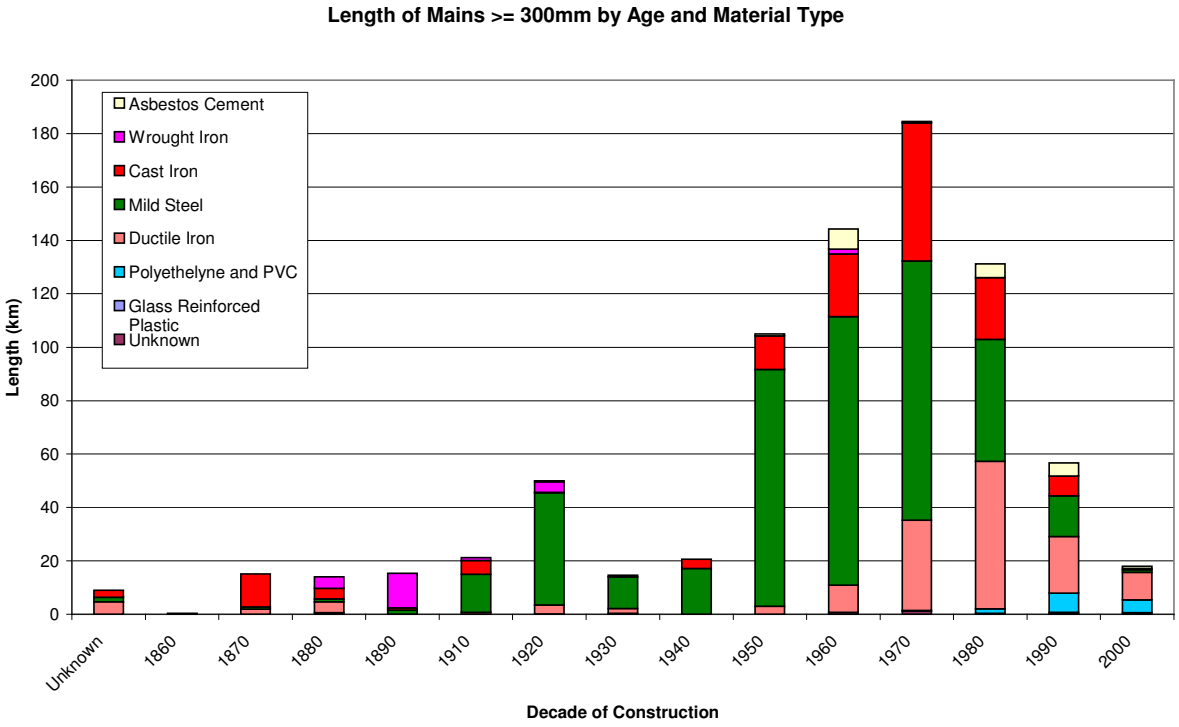

Figure 2: Age / Material Profile of Water Pipe

2 ASSET AND PRESSURE MANAGEMENT STRATEGY

2.1 Design Requirements of Asset and Pressure Management Strategies

2.1.1 Selection Criteria for Defining an Asset Management Study

An Asset Management Strategy is an examination of all mains with a diameter of 300mm or above and any other mains that are hydraulically important to zone operation. It considers the best option for the future replacement of each main when taken in context of overall zone performance relative to YVW service levels. Replacement options include abandonment, downsizing (either replacement or slip lining) and upsizing. New main alignments are also considered where such an option would allow the abandonment or downsizing of other assets.

Ongoing refinement of the strategy methodology has led to additional criteria being adopted. These criteria have been incorporated to bias the replacement of mains that are older than 50 years or have a material type that increases the likelihood of failure (AC, CICL or WI). The optimal solution is then derived by minimising the total replacement cost of all selected mains while ensuring that the level of service criteria is met.

2.1.2 Selection Criteria for Defining a Pressure Management Area

A Pressure Management Strategy is an examination of a water supply network to determine whether areas can be shifted to a lower operating pressure by the use of Pressure Reducing Valves (PRVs). This generally occurs in larger zones with high topographical variation and where a local high point has defined the operating grade. Ideally the largest possible area is moved into a Pressure Management Area (PMA) so that the unit cost is minimised, however this is not always possible due to operational or topographical reasons. High topographical variation means that there is a compromise between the size of the PMA and the final pressure reduction possible.

This assessment defined the PMA sizes as ranging between 1,000 and 10,000 customers and having at least two sources of supply. The emphasis was to be on residential areas and therefore large clusters of fire services or non-residential customers were excluded from Pressure Management. Any PMA design proposed may require improvements to the pipe network capacity to a level that ensures that supply can be maintained from one source only on a 95%ile DSD day.

If a PRV never operates fully open, then for design purposes, the water network internal and external to a PMA can be assessed independently. There are also operational advantages to maintaining the inlet grade of the PRS above the operating grade of the PMA.

2.1.3 Design Criteria

The solutions being proposed had to meet the standard YVW customer charter (minimum pressure of 20m with pipes having a headloss of less than 10m/km and a velocity less than 2m/s) and some PMA specific additional guidelines. The assessments were conducted under Dry Summer Day (DSD) demand conditions (99.9%ile from the previous 10 years). Under 95%ile DSD demand conditions the average pressure at each connection had to be above 30m.

2.2 Asset and Pressure Management Strategy for Mitcham-Morang

The Mitcham-Morang Water Supply zone covers an area of 110km², supplying approximately 95,000 customers in the northern eastern suburbs of Melbourne. It is divided into four sub zones that operate at grades between 134m and 164m. Water is supplied to the zone from one reservoir and five different pipelines regulated by Pressure Reducing Valves. There are also two booster-pumping stations to maintain system pressure during peak demand periods.

2.2.1 Preparation of a Hydraulic Model of the Zone

YVW has been building and calibrating hydraulic models for its 106 water supply zones since 1996. The provision of well calibrated hydraulic models is essential to be able to properly investigate and scope out the relevant infrastructure requirements to meet the applicable design criteria.

2.2.2 Model Calibration and Development

The Mitcham-Morang Water Supply model was calibrated using information from February 2002 and a summary of the results are shown in Figure 3. In total 106 temporary recorders (flow and pressure) and 41 permanent recorders linked to a SCADA system were used. A second day was used to validate the network model.

Using historical information from the SCADA system the model demand was increased to represent a Dry Summer Day. A future scenario, to be used for the combined asset and pressure management strategy, and representing a 2027 peak day was developed by the inclusion of new development across the zone.

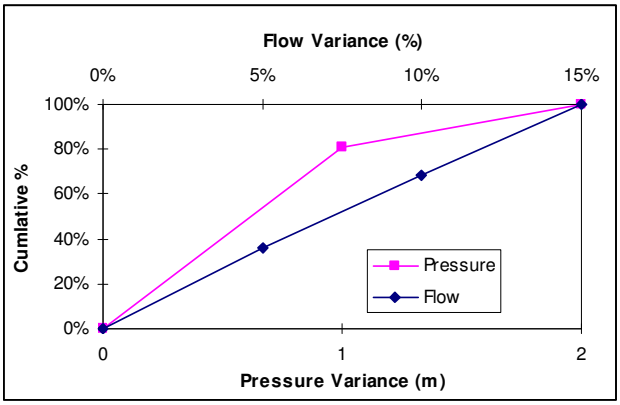

Figure 3 – Calibration Accuracy

2.2.3 Options Development

The initial PMA boundaries and operating grades were based on the zone topography. From this starting point the divergent phase of the assessment involved the generation of as many feasible options for each PMA as possible. The benefits of conducting a combined asset and pressure management strategy becomes clear at this point since the approx. 40km of mains being considered for replacement/abandonment had already been identified (based on the previously discussed criteria). This meant that when the PMA options were being developed they could be biased towards or away from these assets.

While clusters of fire services were avoided this process did not consider exact alignments for new mains or the precise positions of each PRS. Coarse statistics were prepared for each PMA option including the number of properties, length of main, operating pressure, average pressure reduction and the number of PRSs required. In the Mitcham-Morang zone a total of 8 PMAs were prepared (some including areas of network currently serviced by adjoining water supply zones).

At this point in the design process a Value Management session was held with the key stakeholders, including representatives from the planning and operations departments. An indicative cost for each option had been prepared and this information combined with the comparative statistics, detailed earlier, was discussed. The merits were debated with consideration given to issues such as alternate sources of supply or different seasonal/operational strategies. The session concluded with the three most promising options for each PMA being selected for more detailed investigation.

2.2.4 Option Refinement

This project phase moved the assessment from the desktop into the field with visits to each potential PRS location. The objective of these inspections was to ascertain whether there was site that could accommodate a PRS (including a pit and an above ground cabinet), and that the location would meet the hydraulic design requirements. At each site the dimensions were recorded and a number of photos taken. The majority of the sites selected were located in parks however in some instances they ended up in road reserves or nature strips.

A search was conducted for other underground assets including water, sewer, drainage, gas and telecommunications in the vicinity of the PRS. This information was included on a site layout drawing that showed the position of the pit, cabinet and connecting pipework. In a few instances the number of existing underground services precluded the site from being used and an alternative location had to be found. The site photos were overlaid with a mock up of the site works for aesthetic purposes, and these were later used in submissions to the local planning authorities.

With the PRS locations determined the network configuration and operation could now be adjusted to maximise the size of the PMA. In most situations the use of flow modulating PRVs was deemed to be beneficial. YVW operations specified that these could have a maximum pressure variance of only 5m to prevent cyclic loading of the mains. While this work was progressing the mains inside the PMA that were identified for asset management were also being assessed. If more capacity was required they were the first to be upsized. Conversely the PRS locations were biased towards newer mains that were not included in the asset management strategy.

The PMAs are isolated from the surrounding system by closing existing valves or installing new ones. A hydrant was required on each side of the valve to allow the main to be flushed. A plan showing the location of each valve to be closed/installed was prepared including the size of the main, the address and whether new hydrants were required.

The key statistics concerning customer numbers/length of main vs. average pressure reduction were updated and a detailed cost estimate was provided for each option including any new mains required for the PMA. YVW used this information to generate the life cycle cost of each option and the resulting benefits from the reduced operating pressure. A second Value Management workshop was convened to rank the PMA options with issues such as practicality of construction and operation being considered.

In one instance a PMA option with the best cost-benefit ratio was rejected because it would have required construction to take place in a shopping strip along major road. While hydraulically sound and financial advantageous the disruption to the local community was considered to be too high and a competing option was selected instead. At the conclusion of the VM workshop YVW selected a final option for each PMA to which more rigorous risk and customer impact assessments would be applied.

2.2.5 Final Option selected

The selection of the final PMA option meant that the previously identified asset management mains could now be examined with more confidence. In the earlier stages of the assessment a preliminary action (resize, replace or abandon) had been assigned to each main. This was initially based on the wider requirements of the network and then included the servicing requirements of the PMA options. The requirements for the mains within the PMA had already been determined and provided that the inlet grade remained above the PMA operating grade they would continue to operate as designed.

With the location of each PRS now identified a determination could be made for the remaining mains outside the PMAs. The majority of new development in the Mitcham-Morang will be multi-tenant or subdivision of existing blocks, increasing the density but not having a large impact on peak hour flows (due to a reduction in the amount of garden watering). The zone can therefore be classified as mature with limited allowance made for additional demand. When examining the asset management mains it was therefore possible to abandon or downsize those with excess capacity in situations where the network security would not be compromised. The remaining asset sizing was focussed on providing adequate supply to each PRS and to ensuring that the minimum service levels were maintained across the zone, at the least community cost.

2.2.6 Demand Sensitivity and Risk Assessment

The combined strategy had been based on a number of demand assumptions and to test its sensitivity a number of demand scenarios were considered including Low (–10% demand change from the adopted strategy figure), High (+10%) and Higher (+20%). These were analysed to determine the impact that the increase or decrease in demand would have on system performance. In the event that customer service levels in large areas of the zone would not be met under the higher demand conditions additional works could be included at YVWs discretion.

The robustness of the strategy was also examined by considering the failure of each PRS and critical main under 95%ile DSD demand conditions. Critical mains tended to be those with a diameter of 225mm and above or mains to isolated parts of the network. In the event of widespread pressure deficiencies within the system an additional PRV could be specified at that location or a new distribution main constructed to reduce the risk. The before and after results were tabulated along with the cost of the additional works. This allowed YVW to make an informed decision in whether the works should be adopted for the Final Strategy.

2.2.7 Customer Impact Assessment

One of the design parameters was that large clusters of fire services or non-residential customers were to be excluded from the PMA where possible. Critical accounts that remained inside the PMA were to be checked to ensure that their level of service would not be compromised by the implementation of pressure management. Once the strategy had been finalised, including any amendments identified by the sensitivity/risk analysis, a customer impact assessment was conducted. This assessment examined the consequences of a reduction in pressure to the available flow rate that could be supplied. Hydrant curves (flow vs. pressure) were produced for the pre and post PMA networks for 95%ile DSD and DSD peak hour scenarios.

YVW also provided the location of all fee paying fire services contained within the PMA or near the proposed boundary. A representative sample of these customers were selected and hydrant curves (flow vs. pressure) were produced for the pre and post PMA networks for 95%ile DSD and DSD peak hour scenarios. If any problems were identified then a recommendation was made on the remedial works required to overcome the deficiency.

2.2.8 Summary of Strategy Results

The Pressure Management Strategy for the Mitcham-Morang Water Supply Zone identified a total of 8 PMAs and the statistics have been tabulated in Table 2.

The key elements of the economic evaluation are the initial capital cost of building Pressure Reducing Stations, installing new boundary valves, expected replacement of old main to meter service pipes and remedial works to fire services. An allowance must also be made for ongoing maintenance of PRVs and loss of revenue, but offsetting all this are the expected savings from reduced burst rates, leakage and asset renewals. The NPV assessment for the Pressure Management Strategy is detailed in Table 3.

The Asset Management Strategy for the Mitcham-Morang Water Supply Zone identified 38.4km of main for consideration. The equivalent size cost assumes that no assessment was made of future system requirements and that a replacement main of the same size was constructed. While the final cost will depend on when individual mains are replaced it is clear from the potential savings that system wide assessments are valuable. These have been detailed in Table 4.

Table 2: Mitcham-Morang PMA Summary

PMA	Length of Mains (km)	Number of Customers	ΔP Avg. (m)	ΔP Max. (m)
Bundoora	110	10,200	15	14
Greensborough	68	5900	33	36
Ivanhoe	82	6200	7	30
Preston	182	17,000	15	12
Reservoir	144	12,600	11	10
Rosanna	45	3400	38	41
Viewbank	25	2500	39	61
West Heidelberg	46	4200	23	21
	702	62,000		

Table 3 NPV Summary

Description	Worst Case	Likely Case	Best Case
Burst Reduction	8.0%	10.0%	12.0%
Leakage Savings	85.3 ML	106.6 ML	127.9 ML
Deferred CAPEX	$200k	$250k	$300k
Revenue Loss	2.0%	1.0%	1.0%
NPV	Negative	Neutral	Positive

Table 4: Mitcham-Morang Asset Management Summary

Asset Management Strategy Cost ($ '000s)	Equivalent Size Cost ($ '000s)	Cost Difference ($ '000s)
$20,345	$34,000	$13,655

2.2.9 Strategy Implementation

The consultation phase was split into three phases with the first dealing with the initial concept. YVW engaged directly with the known critical stakeholders such as fire services and the appropriate government departments. The second phase involved the notification of business customers and the general public through the placement of advertisements in local and metro papers. The impact of the strategy was also discussed with key YVW customers.

A functional design statement was prepared by YVW using the information generated during the assessment process including the site layout plans/photos. A standard YVW PRS design for a variety of PRV sizes was developed by MWH in consultation with YVW. Construction of the Ivanhoe and West Heidelberg PMAs in the Mitcham-Morang Zone has already commenced with an expected activation date of June 2004. The third communication phase will deal with the customer reaction to the change in pressure.

2.2.10 Future Operation

Flow meters are being installed at each PRS so that the PMA zone demand and minimum night flows can be recorded. Continuous monitoring of the minimum night flow (MNF) for each PMA will be used to trigger leakage detection activities based on an economic level of return. Data will also be analysed to determine the cost effectiveness of the PMAs and the potential for further pressure management.

3 CONCLUSION

3.1 Benefits of Asset/Pressure Management Strategy's

International studies have quantitatively demonstrated that higher network pressures inherently result in elevated burst and leakage rates. Pressure Management as an approach for reducing burst and leakage rates and extending pipe asset life, is not a new concept. It has been widely implemented throughout the UK over the past decade and YVW has undertaken a number of promising trials including the one in Kew. The key drivers for YVW are improving customer service levels by reducing unplanned interruptions; environmental water conservation benefits through reduced leakage, and savings via reduced maintenance costs and renewal deferments.

Water network construction and maintenance is capital-intensive and YVW prepares Asset Management Strategies to determine the optimal hydraulic and financial solution. It is advantageous to defer the works until such time that customer supply expectations will not be met and/or the risk to the business become unacceptable. Long term planning enables these parameters to be defined and the work to be scheduled at the appropriate time.

3.2 Assessment process

The rigorous assessment process using finely calibrated models allows a detailed comparison of competing options, which in turn produces a high level of confidence in the results. The consultative process meant that all stakeholders had an opportunity to provide input.

The Mitcham-Morang Pressure Management Strategy resulted in an average reduction of pressure of 22.5m by rezoning 62,000 people and 702km of main inside PMAs. The NPV assessment resulted in cost neutral benefit over the next 25 years. The Mitcham-Morang Asset Management Strategy resulted in saving of $13.6m (in 2002 terms) on an equivalent replacement size basis.

3.3 Future Implementation

The Mitcham-Morang Asset and Pressure Management Strategy covers only one Water Supply Zone. YVW has determined that there are water conservation and service reliability benefits from reducing pressures of supply to customers. YVW has developed a Pressure Management Strategy that it will implement over a 5-year period to reduce its overall average pressure of supply from 73m to 63m. This strategy provides for establishing 64 PMAs covering 46% of customers and 36% of reticulation water mains.

The economics of the strategy depend on the assumptions relating to the amount of benefits to be achieved, particularly relating to the reduction in pipe burst rates and the associated deferral of water main renewals. The actual benefits of the strategy will be established over the implementation period of the strategy. The installation of monitoring equipment at each PRS will enable more accurate leakage detection.

4 ACKNOWLEDGMENTS

The authors would like to acknowledge the assistance provided by Tim Moulton, Ian Filby, Darryl Knox, Kein Gan, Rod McCoy, Ian Smith, Chris Povey and Kerry Brooksmith in the preparation of this strategy.

REFERENCES

- FARLEY, M. *Leakage Management and Control - A Best Practice Training Manual*, World Health Organisation, 2001
- FARLEY, M. & TROW, S. *Losses in Water Distribution Networks – A Practitioner's Guide to Assessment, Monitoring and Control*, 2003
- *The Blue Pages – Losses from Water Supply Systems: Standard Terminology and Recommended Performance Measures*, International Water Association, 2000
- *Applying Worldwide Best Management Practices in Water Loss Control (Draft Report),* American Water Works Association Water Loss Control Committee, 2002
- *A Manual of DMA Practice*, UK Water Industry Research Limited, 1999

The Institution of Engineers, Australia
8th National Conference on Hydraulics in Water Engineering
ANA Hotel Gold Coast, Australia 13-16 July 2004

Design of an automated floodgate control system to enhance tidal flushing: Case Study, Broughton Creek, NSW

W. C. Glamore
B.Sc., PhD
Senior Project Engineer, Water Research Laboratory, School of Civil and Environmental Engineering, University of New South Wales, Australia
B. Indraratna
BSc (Eng), MSc, PhD, CEng, CPEng, FGS, FIEAust
Professor of Civil Engineering, University of Wollongong, Australia

Abstract: Results from an extensive two-stage spatial analyst/water quality model indicated that restoring flows to an acid sulphate soil affected flood mitigation drain would significantly improve water quality. Using traditional floodgate designs the improvements in water quality would be offset by surface flooding of the surrounding paddocks during large tides. Furthermore, commercially available tidal control gates do not offer the functionality required to remotely control tidal flows. To overcome these limitations, an environmentally controlled SmartGate system was designed, tested and installed in a low-lying flood mitigation drain near Berry, Southeastern NSW.

The SmartGate system was designed to permit tidal flushing based on real-time water sensors installed upstream of a floodgate. The system operates within existing infrastructure and is designed to permit tidal waters to discharge through a mini-sluice gate installed within the larger steel plate. Multiple triggers within the main control network determine whether the gate should remain open or closed. The gate movements can also be remotely controlled through telemetry. Dial-in systems allow access to the remotely located gates in order to manipulate a range of controls including modifying the trigger values, downloading data and manually controlling the gate position. The SmartGate can also dial-out one of several text messages to alert a user of any potential operational concerns (i.e. low battery) or preset trigger values. The system is self-contained, does not impact drainage during floods, is solar powered and can be modified to suite a range of applications. Following installation, the SmartGates have been effective in controlling upstream tidal flushing and have successfully operated for more than 2 years. Hydraulic field tests indicate that the SmartGate effectively controls tidal flushing and drain water levels.

Keywords: SmartGate, tidal control, tidal restoration, floodgate, acid sulfate soil, telemetry

1. INTRODUCTION

Throughout coastal Australia one-way tidal restricting floodgates are currently being modified or manipulated to restore tidal flushing. Indeed, within the state of New South Wales Williams and Watford (1997) reported 5300 tidal restricting structures of which 1035 were considered easily modifiable. Floodgates modifications are usually undertaken on a case-by-case basis to address a specific water quality issue and are not presently based on any standard engineering design criteria.

Though radial and sluice gates can be found in selected flood mitigation drains, the majority of floodgates in use today are top-hinged flap gates. The working objective of flap gates is to permit drainage upstream of the floodgate and prevent flood and tidal flows from downstream waterways into the drained area. Top-hinged floodgates operate under 3 design criteria. First, when upstream water levels are higher than downstream levels hydrostatic pressure opens the gate and water is discharged from the drain. Assuming these conditions remain, water will continue to discharge until the drain invert or the sill level is reached. Second, when the downstream water elevation is higher then upstream levels hydrostatic pressure closes the gate and no reverse flow can occur. Finally, when the water level is equal on both sides the gate remains closed and acts like a non-return valve. Slanting the headwall enhances gate closure and a compression seal between the flap face and the headwall structure decreases leakage.

The above drainage conditions imply that flap gates typically operate ‘automatically’ except when manual debris removal from between the seal and headwall is required. However, drainage will not occur unless there is a significant difference between upstream and downstream water levels and therefore, the rate of fall upstream of

the gate cannot be greater than the rate of fall downstream. Nonetheless, drainage times are site specific and related to a number of factors including (Patterson and Smith, 2000):

(1) The relationship between water height and volume stored in a particular area;

(2) The size of the floodgate structure;

(3) The design of the floodgate;

(4) The size of the drain; and

(5) The hydraulic efficiency of the drain.

Limited information is available on the hydraulic considerations and stage discharge relationship of top-hinged flap gates. The majority of available information (Lewin, 1995; Pethick and Harrison, 1981) concerns the discharge of water through multiple gates and its impact on flow interference. Specifically, when a series of flap gates are close to each other discharge under and around the gate causes flow interferences and results in hydraulic loss. To maximise discharge and reduce bed-scour from flow interferences, training walls and aprons are often installed. With this in mind, any major structural modifications to the floodgate infrastructure must consider the interactions between adjoining floodgates and compensate for reduced discharge.

At present, modified floodgate designs differ throughout NSW and range from simple lifting mechanisms to complex buoyant gates. While these manually operated gates can permit tidal flushing and operate as a simple open-close valve these floodgates do not allow for full automated control of tidal levels based on real-time in-situ water parameters such as pH, salinity, dissolved oxygen and/or water pressure (i.e. elevation). Therefore, to improve functionality and to provide floodgate access via telemetry, an environmentally controlled SmartGate system was developed and implemented at several monitored field site along Broughton Creek in southeastern NSW.

This paper details the components and capabilities of the SmartGate system. First the functionality of the SmartGates are described including how the tidal fluctuations are controlled using real-time water variables. A field investigation is then detailed and tests to control the drain water level are then given. The SmartGate systems are presented as a novel means of automatically controlling tidal flushing and in addressing many of the limitations commonly encountered with manual tidal gates.

2. LIMITATIONS OF CONVENTIONAL MODIFIED FLOODGATES

While traditional modified floodgates can successfully restore tidal flushing to flood mitigation drains, they do not provide incremental control over the quantity of water within the drain. The volume of tidal water within the drain determines drain water quality and/or the extent of floodgate manipulations (i.e. overtopping concerns). In these instances, conventional modified floodgates are not suitable for drainage systems where only a small volume of tidal water is required to improve drain conditions or where full tidal flushing will cause drain overtopping. This situation is common in extremely low-lying drainage systems, in tertiary drains upstream from tidal barrage structures and in various backswamp drains with small levee banks around coastal Australia.

Access to conventional modified floodgates is also a concern during extreme events because tidal restricting flap gates are usually located along the levee bank junction where the drainage system flows into a creek or estuary (Glamore, 2004). In these conditions, the floodgates can become isolated and access to the gates may become hazardous. Therefore, floodgates that incorporate a remote access feature are advantageous because they can be operated from a central control network.

Similarly, under prolonged dry conditions salinity levels within creeks/estuaries can rise to near seawater and only a small volume of tidal flushing is required to reduce drain water acidity (i.e. low groundwater seepage) and increase creek water alkalinity. In areas with high lateral soil hydraulic conductivity (> 5 m day^{-1}), tidal flushing may need to be restricted based on salinity concentrations. Based on these and the aforementioned operational requirements, the ‘Environmentally Controlled Smart Gate System’ was developed and installed at a monitored field site along Broughton Creek, in southeastern NSW.

3. ENVIRONMENTALLY CONTROLLED SMARTGATE SYSTEM

A drawing of an 'Environmentally Controlled Smart Gate System' (or 'Smart Gate') is shown in Figure 1. The 'Smart Gate' was designed to allow a specific volume of tidal water into the study drain based on real-time water quality variables. Within the system, submersible multi-parameter data loggers located upstream and downstream of the flap gate input pH, electrical conductivity, water temperature, and water elevation into a central data-logging unit at 15-minute intervals. The control unit then compares these readings to previously set trigger points and determines whether a slotted aperture within the floodgate should be opened or closed. If a trigger point is reached, the control unit closes the appropriate electrical circuit to drive a DC motor in the open (up) or closed (down) direction.

An example of a typical gate operation is explained below:

1. Gate is open to allow tidal flushing.
2. Data logger measurements uploaded to the control unit every 10 minutes.
3. With the incoming tide, data logger readings exceed manually set trigger levels and the control system activates the close gate protocols.
4. The motor closes the gate and the system awaits further readings.
5. When acceptable levels return, the gate reopens.

The primary objectives of SmartGates are to control the volume of water upstream of the floodgate and optimise tidal buffering. To accomplish these objectives, a range of user defined triggers based on real-time data logger readings have been layered into the system program. A schematic of the SmartGate operations over a full tidal cycle are shown in Figure 2.

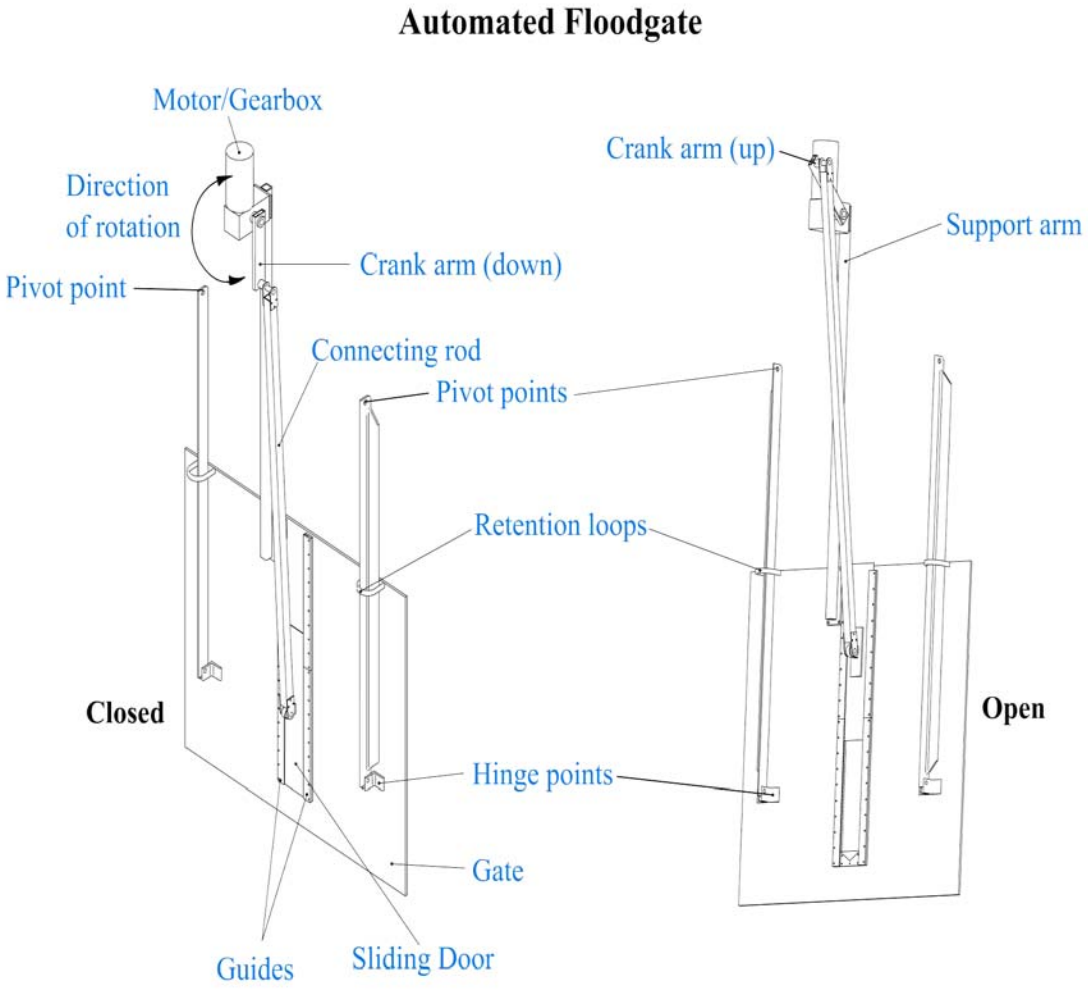

Figure 1 – Schematic of SmartGate Flap

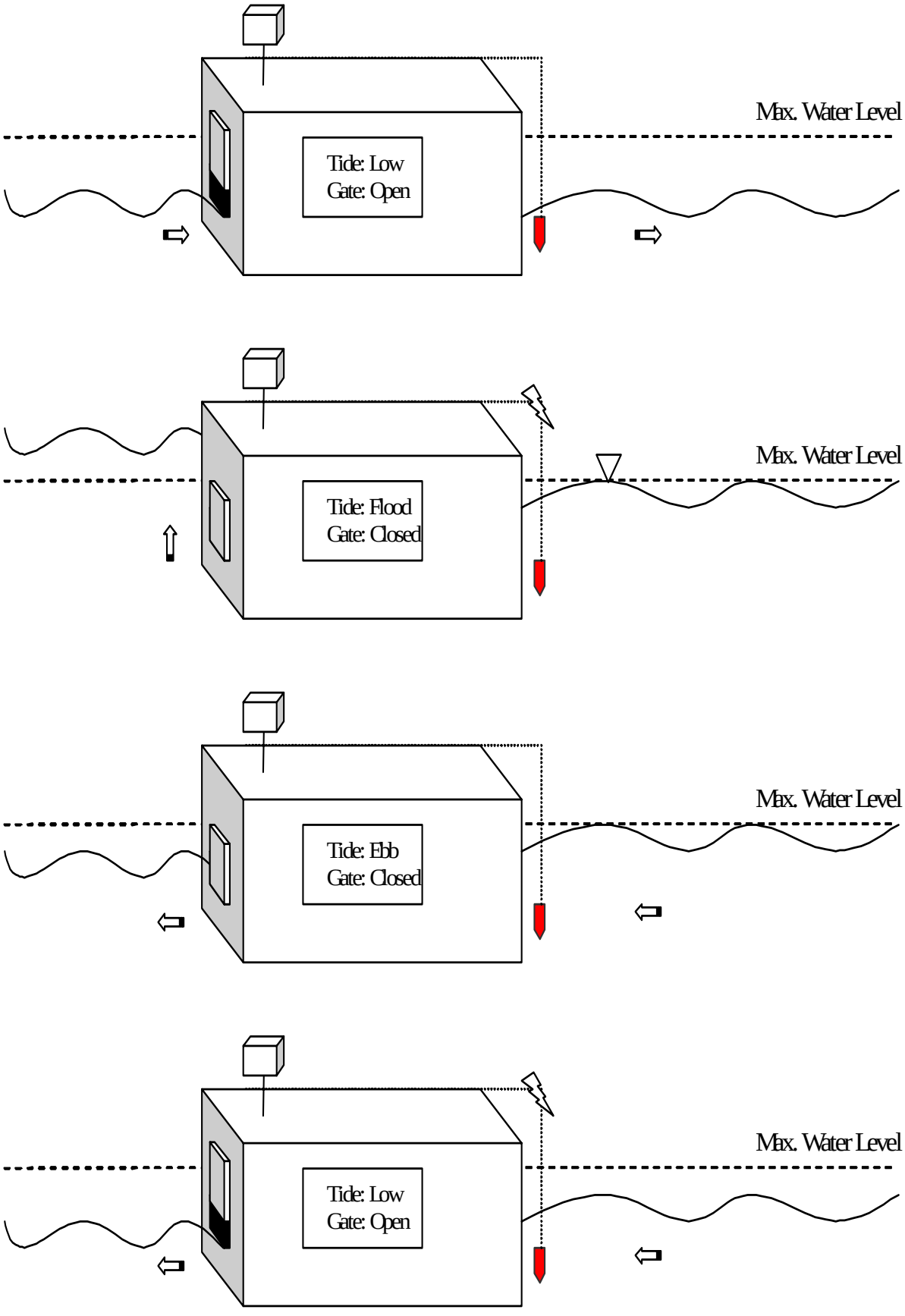

Figure 2 – SmartGate Operations over a Tidal Cycle

To increase robustness and enable remote control of the system, various 'intelligent' designs were built-in to the program. First, using a standard 56K modem and appropriate data logger support software (Campbell Scientific PC208W) the user can remotely 'dial-in' to the system. Once connected, the user can view current conditions, download previous data, change trigger levels, and override automatic functions. This ability is particularly important during flooding periods when access to the site may be restricted. Second, the control unit is also equipped with 'dial-out' technologies which were used to increase on-site safety. These safety protocols are designed to alert the user to specific problems concerning 'Smart Gate' operations (i.e., low battery, jammed gate, energy surge, etc.) or preset water quality variables (i.e., low pH, high salinity, high flow) via a SMS text message to their mobile phone. The message will read 'Gate Error Number 1-15' and, based on the gate error number, the user can determine an appropriate plan of action. This function can also be used to alert a floodplain manager to activate an automatic sampler based on real-time drain water parameters. As a fail safe, the control unit is equipped with a manual override switch which can be operated in the field to control the gate position.

The electrical components within the SmartGate were designed to provide optimal flexibility within a wide range of compatible components. The central processing unit within the control panel is the Campbell Scientific CR10X measurement and control data logger. This unit is programmed to output to the appropriate relay according to external data loggers, which then input through individual converter boxes. The converter boxes allow multiple sensors (up to 10, with 10 parameters per sensor) to be connected via this port without absorbing existing analogue and digital ports on the control unit. Based on this information, the relevant relay circuit is closed and the motor rotates in the correct direction. When the motor reaches its full position, the reed switches send a return pulse to the control unit to stop the motor. Active readings within the control unit determine when/if the GSM modem should be activated and what message to send. The entire unit, including the external data loggers and the motor, is powered by two 12V gel cell batteries connected in series. An BP 20-watt solar panel trickle charges the batteries through a solar regulator. For safety and convenience, all external cables are concealed within flexible conduit buried underground, and the external data loggers are dyna-bolted to the headwalls and encased in slotted PVC sheath.

The original SmartGate prototype was installed at the study site on December 20th 2001 and has continued to operate successfully (>2 years). Installation involved removing one of the standard top-hinged floodgates from the headwall using a hydraulic crane provided by Council. The 'Smart Gate' infrastructure was constructed and tested in the laboratory (including tests for sealant efficiency) and transported to the site as one unit. The electrical components were re-assembled at the site and total installation time was less than 4 hours.

In comparison with other buoyancy driven 'automatic' gates driven solely by hydrostatic pressure, the 'Smart Gate's' critical advantage is that it can operate using multiple parameters including pH, electrical conductivity, water temperature, dissolved oxygen, and bi-directional flows to vary water elevation levels upstream or downstream of the floodgate. This is significant because improved water quality, and not water elevation, is the key factor in restoring tidal flushing in ASS terrains.

4. HYDRAULIC FIELD TESTS

Once installed the SmartGate system effectively controlled upstream water levels, but leakage through the vertical lifting gate limited its efficiency. Figure 3 depicts a trial period to determine the effectiveness of the 'Smart Gate'. During this trial, the SmartGate system was programmed to restrict water levels upstream of the floodgate to 0.4 m AHD. In response, the SmartGate controlled upstream water levels and limited drain water elevation to 0.471 m AHD over three tidal cycles. The discrepancy between the trigger limits and the recorded values was from leakage through one of the flaps on the traditional top-hinged floodgate located adjacent to the SmartGate and via upstream inflows. Nonetheless, in future applications where leakage is minimised, the ability to remotely control the SmartGates trigger heights will maintain water retention properties of the drain during flooding events.

5. CONCLUSIONS

Throughout coastal Australia one-way tidal restricting floodgates are being modified to permit tidal flushing. While several designs have been successfully installed to manually control tidal flushing levels, no floodgates existed which automatically controlled floodgates based on real-time water quality variables. Furthermore, no existing floodgates existed which could be remotely controlled via telemetry. To overcome these limitations the Environmentally Controlled SmartGate System (or SmartGates) was developed and installed at a fully monitored field site along Broughton Creek in southeastern NSW.

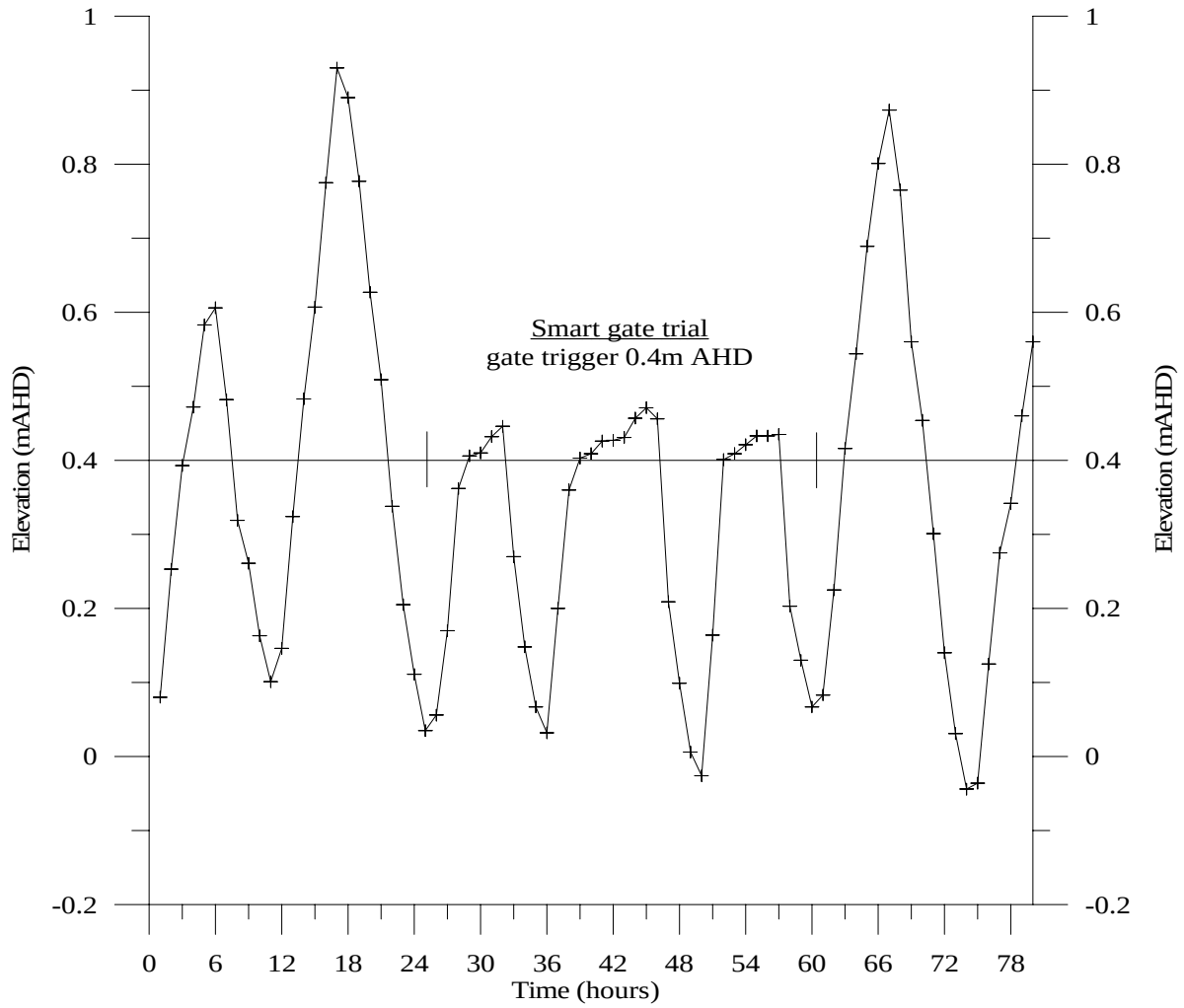

Figure 3- Drain Water Elevations during SmartGate Trials

The SmartGate systems were developed to open or close an aperture within a traditional top-hinged floodgate based on a series of water quality triggers. Data obtained from in-situ loggers is used to determine if the trigger values have been reached and if so, whether the floodgate should be open or closed. The unit can be remotely accessed and controlled via telemetry and has been equipped with dial-out warnings in case of a systems malfunction.

The prototype unit has been successfully operating in the field since December 2001. Hydraulic investigations have shown that the SmartGate is effective at controlling tidal flushing and drain water levels. Additional SmartGate installations are currently underway in the Shoalhaven region and a centralised network has been developed to control a series of SmartGates.

6. ACKNOWLEDGEMENTS

The authors wish to acknowledge the support of the Shoalhaven City Council throughout the length of the study. Additional support was given by local landholders, the NSW Department of Agricultural, and the federal government through its Natural Heritage Trust.

7. REFERENCES

Glamore, W.C (2004). *Evaluation and Analysis of Acid Sulphate Soil Remediation via Tidal Restoration.* PhD Thesis, University of Wollongong, Australia.

Lewin, J. (1995). *Hydraulic gates and valves in free surface flow and submerged outlets.* Thomas Telford Publications, London, 238p.

Patterson, C., and Smith, R. (2000). *Acid sulfate soils program: Design improvements – rural drainage schemes.* Final report prepared by Patterson Consultants Pty Limited. 41p.

Pethick, R. J. and Harrison, A. J. W. (1981). *The theorectical treatment of the hydraulics of rectangular flap gates.* 19th I.A.H.R. Congress, Karlsruhe, subject B (c), paper #12.

Williams, R. J. and Watford, F. A. (1997). Identification of structures restricting tidal flow in New South Wales, Australia. *Wetlands Ecology*, **5**, 87-97.

The Institution of Engineers, Australia
8th National Conference on Hydraulics in Water Engineering
ANA Hotel Gold Coast, Australia 13-16 July 2004

Assessment Of Predicted Near Field Dilution And Hydraulic Head Requirements For A Range Of Outfall And Diffuser Configurations

B.M. Miller
B.E., B.Sc., M.Eng.Sc, M.I.E.Aust.
Manager, Water Research Laboratory, School of Civil and Environmental Engineering,
University of New South Wales, Australia
R.M. Hudson
B.E.
Project Engineer, Water Research Laboratory, School of Civil and Environmental Engineering,
University of New South Wales, Australia

Abstract: Many ocean outfalls could achieve greater near field dilutions through optimisation of the diffuser types and configuration. However, the design of diffuser types and configurations can greatly influence the required hydraulic head to drive the necessary discharges through the outfall.

A number of diffuser configurations have been assessed using the near field model CORMIX to determine near field dilutions under varying discharge and environmental conditions. A methodology for calculating the hydraulics was programmed in FORTRAN to determine distribution of flows, head losses and limiting flows.

This paper presents the findings of "optimum" outfall configurations for a practical application. Considerations were also made of purging, sea-water intrusion and pumping costs vs gravity flow. A conclusion is that the optimum type of diffuser is very dependant on the environmental conditions, the available hydraulic head and the range of effluent discharge rates that the STP supplies.

Keywords: Near-field Dilution Hydraulic Head Diffusers.

1. INTRODUCTION

As effluent is discharged from a diffuser port, its momentum relative to the receiving water results in seawater being entrained into the plume, diluting the effluent and causing the plume to spread. The density difference between the 'fresh' effluent and the saltwater causes the plume to rise. As the plume rises, further seawater is entrained and the effluent is further diluted. Eventually the plume rises to its trap depth (for stratified receiving waters), or the density of the plume is such that the diluted effluent plume will surface. Momentum and density driven mixing are referred to as near-field mixing and account for the majority of achievable dilution. Far-field mixing occurs as the plume is advected and mixed after the initial momentum or density driven mixing processes have ceased. Significantly less dilution occurs in far-field mixing.

Near-field mixing is strongly dependent on diffuser design. The amount of initial dilution is typically maximised in order to minimise potential health or ecological problems. Typically a minimum required dilution is specified, such that the outfall does not breach required health or environmental guidelines. The minimum required initial dilution depends on the concentration of a particular constituent within the effluent and the applicable limit/guideline for that constituent in the environment.

The initial dilution for a given diffuser design will depend upon the discharge rate, port exit velocity, the ambient current, depth of the diffuser and the presence of stratification. Due to the high level of variability in these parameters, initial dilution varies widely depending on discharge rates and the receiving environment. The spatial area of the zone of initial dilution also varies depending on outfall discharge and oceanographic conditions.

While near field dilutions are optimised to minimise potential health or ecological problems, the design and location of the outfall diffusers have important hydraulic and economic factors. The factors considered in the selection of concept designs for an outfall diffuser include: outfall length/location; outfall pipe diameter;

diffuser array design; discharge vs required hydraulic head; saline intrusion; outfall purging and the use specialised nozzle valves.

The near field dilution and the hydraulic requirements of an outfall diffuser design must both be considered to find an optimised solution for operation, construction cost and operational costs. Much of the discussion in this paper is generic to all outfalls, however the emphasis is on smaller ocean outfalls with ADWF (average dry weather flow) about 20 ML/day and shallow depths to about 15m.

2. FACTORS INFLUENCING OUTFALL CONCEPT DESIGNS

2.1 Pipe Length / Location

The pipeline length and diffuser position will strongly influence required hydraulic head and initial dilution. A longer pipeline typically results in effluent being discharged at a greater depth, which increases initial dilution. A longer outfall also means that the subsequent far-field transport is further from the shoreline. Further from the shore currents are likely to be stronger which again increases initial dilution.

A longer pipeline will increase construction costs and total hydraulic head. If a longer outfall is required pipe diameter can be increased to help reduce friction losses and hence the required hydraulic pumping head.

2.2 Outfall Pipe Diameter

The outfall pipe diameter has no influence on outfall performance in terms of initial dilution, though it has a large influence on the hydraulic performance of the outfall. Required hydraulic head is strongly influenced by pipe diameter with smaller pipes incurring much higher head losses due to the resultant higher pipe velocities. Pipe diameter also influences sedimentation and slime growth, as velocities in larger pipes are lower and there is less wall shear and hence less scouring.

2.3 Diffuser Array Design

The specification of the diffuser array has a strong influence on expected initial dilution and the required hydraulic head. Port/nozzle diameter, the number of ports used, use of either tee or rosette diffusers and the use of check valves must all be considered in designing an optimal diffuser array.

The selection of port diameter has a strong influence on outfall performance. Smaller port diameters result in higher exit velocities, which increases available initial dilution but also increase exit head losses. Port diameter also influences the likelihood of seawater intrusion at low flows with larger ports being more susceptible to intrusion.

The number of ports in the diffuser array also strongly influences outfall performance, both in terms of initial dilution and hydraulic performance. Additional ports reduce the amount of flow through each port, which increases available dilution (due to a decreased mass flux through each port). Increasing the number of ports also reduces the required hydraulic pumping head because of the reduced velocity through each port. However, it is important that at low flows there are not too many ports, such that the velocity through each port is able to prevent saline intrusion. While the maximum number of ports in a diffuser array is constrained by preventing saline intrusion criteria, in terms of optimal design it is best to maximise the number of discharge ports. However, construction costs are also a consideration.

Ports should be optimally spaced so that the individual plumes do not merge, reducing further dilution. The selection of port spacing has a slight influence on diffuser hydraulics, with a longer diffuser array being associated with slightly higher pumping costs.
Two main types of diffuser arrays have been considered; tee-ports and rosettes. Rosettes are likely to be easier to protect from marine operations and are slightly easier to purge. However, due to the close positioning of ports in a rosette, plume interactions are more likely under low flow conditions.

2.4 Flow vs Required Plant Head

Outfall design will have a strong influence on the required hydraulic head needed to transport a given flow through the outfall. Hydraulic losses are a function of the effluent velocity squared so are of particularly important at high flows.

The system must be designed so that there is available hydraulic head for the maximum planned discharge. In smaller outfalls this is often the PWWF (peak wet weather flow) however consideration must be made of whether it is acceptable to bypass the outfall in high wet weather flows.

At low flows it is advantageous to design the outfall such that pumps are not required but this is dependant on the available gravitational head throughout the system. It is desirable to keep the maximum required effluent head below 15 m, which is the typical limit for centrifugal pumping.

2.5 Near Field Mixing

Initial dilution will be increased in areas of higher ambient current and increased water depth. A reduction in port diameter increases exit velocity resulting in increased initial dilution. By increasing the number of ports the flow rate through each port can be reduced. In terms of initial dilution, a diffuser array with many small ports will give the best results. However, the use of small ports increases exit head losses and therefore requires a higher head to drive the effluent out through the outfall. Also it is important that diffusers are adequately spaced so that plumes do not merge reducing available dilution.

Near field mixing can be assessed by using a near field model such as CORMIX as described in Section 3.1.

2.6 Saline Intrusion

Saline intrusion may occur if the velocity through a port is not sufficient to prevent the denser seawater from entering the port. If saline intrusion occurs and the outfall cannot be easily flushed/purged, a circulation may exist where seawater is drawn into several risers and discharged from others. This circulation results in the outfall not being able to perform as designed. Saline intrusion may also result in marine growth occurring which may result in blockages.

Wilkinson (1988) has shown that seawater intrusion will not occur as long as the densimetric port Froude number Fr' is kept well above unity. The densimetric Froude number is defined as:

$$Fr' = \frac{u_j}{\sqrt{g' d_j}} \quad where \quad g' = \frac{\rho_o - \rho}{\rho} g \tag{1}$$

where u_j and d_j are the effective velocity and diameter of the jet discharging from the port, g' is the effective acceleration due to gravity and ρ_o and ρ are the density of seawater and effluent respectively.

It can be seen that the design factor of saline intrusion can be used to estimate the maximum number of ports for an outfall diffuser if standard ports are to be used. Check valves are designed to close when there is no discharge through the port to avoid saline intrusion. However, design considerations must be made for the implications of faulty or damaged check valves.

2.7 Outfall Purging / Flushing

The ability of an outfall to be purged after construction can impact on the performance of the outfall. After outfall construction (or after maintenance work) the pipeline will be filled with seawater which must be purged (with less dense effluent) during outfall commissioning. If the outfall is commissioned at a low flow rate the pipe may become stratified with lower-density effluent flowing above the denser seawater.

If the outfall is not properly purged it will not operate as designed and seawater may actually be drawn into some risers and a circulation may exist reducing the performance of the outfall. Problems in outfall purging typically only occur in tunnelled outfalls, where the slope of the tunnel is negative (ie. it slopes down towards the landward end), and long risers are required. However, an outfall with a positive tunnel slope may still suffer from purging problems. If the diameter of the diffuser zone outfall pipe is large and there are a number of risers,

then the velocities in the final section(s) of the outfall pipe (before the last riser) may not be large enough to provide enough energy to fully purge the denser salt water from outfall pipe.

2.8 Use Of Check Valves

Check valves are designed to close when there is no discharge through the port to avoid saline intrusion. Check valves can also increase initial dilution at low flows because the port opening area is smaller and thereby the exit velocities are higher. A drawback associated with the use of check valves is that exit head-losses are often higher and they can be susceptible to ageing and damage.

Check valves are being used to advantage on many ocean outfalls of all sizes. However, consideration needs to be made of the advantages over regular ports when saline intrusion and purging can be shown to not be a problem.

3. A METHODOLOGY FOR OUTFALL CONCEPT DESIGNS

The following sub-sections provide details of the methodology used on recent projects by the Water Research Laboratory (WRL) for assessing outfall design concepts.

3.1 Near Field Modelling

Predictions of initial dilution for each of the outfall concepts were made using CORMIX-GI Version 4.1GT (Jirka, Doneker and Hinton, 1996). Initial dilutions were based entirely on the CORJET near field module. By using CORJET from within CORMIX, discharge interactions with environmental boundaries such as the sea-bottom (Coanda effect) can also be assessed. Assessment of initial dilutions were based entirely on predictions from a single discharge port which assumes that each plume acts independently and does not merge with others. While port spacing was calculated such that there would be minimal plume interaction, under low discharges the plumes may have minimal horizontal momentum and hence may merge when they form a buoyant plume. However, as plume merging is only likely to occur at very low flows, when initial dilutions are maximised it is not considered to be a problem.

CORJET is a buoyant jet, integral near-field model developed at Cornell University (Jirka, Doneker and Hinton, 1996). It solves the three-dimensional jet integral equations for submerged buoyant jets that are discharged either as a single round jet or as interacting multiple jets that comprise a multiport diffuser. The model is applicable to a wide range of environmental conditions. The ambient waters, into which the buoyant jet discharges, may be stratified or unstratified and flowing or stagnant. The buoyant jet is permitted to be positively or negatively buoyant. Detailed verification studies of the CORJET model have been undertaken, the results of which can be found in Jirka, Akar and Nash (1996).

The absolute accuracy of the concentrations (or dilutions) predicted by CORJET model is within about ± 30% when compared to the results of laboratory experiments (Jirka, Akar and Nash, 1996). However, the variance may be considerably greater when comparing with field data, due to the inherent accuracy of the field data themselves as well as the models. Comparisons of several different near-field models show variations of about a factor of two among the models. This absolute accuracy should be acknowledged when interpreting the model results.

Initial dilutions from CORMIX were taken at the end of the near-field mixing zone, which depends on both the discharge properties and the properties of the receiving environment. In the example case CORMIX was configured to discharge "fresh" effluent at 20^{o} C into an unstratified receiving water body with varying density due to temperature. Each diffuser option considered was modelled a number of times with CORMIX with each of the Average Dry Weather Flow (ADWF), Peak Dry Weather Flows (PDWF) and future Peak Wet Weather Flow (PWWF). Each simulation used a derived long time series of environmental conditions (currents and temperature) to provide probabilities of exceedance for initial dilutions.

Parameters used to define the diffuser option in the CORMIX model were the depth of water above the port, the number and size of risers and ports, the type of port, the height of the port above the bed and the angle of the port in both the vertical and horizontal planes.

3.2 Outfall Hydraulics

An in-house FORTRAN program (outfall_hydraulics.f) was used to evaluate the required effluent head to drive flows through the outfall. The methodology is described below but is a simple method of calculating the friction losses in all outfall pipes, the losses associated with flow entry into the riser and nozzle and the exit losses from the nozzle into the receiving water. The program calculates the flow for a given plant head where head losses are based on the extra head required to discharge fresh water into salt water, friction losses through the system and entrance exit losses between the pipe, riser and nozzle. Loss coefficients and friction factors were based upon published values, however, it must be noted that these coefficients allow only an estimation of outfall hydraulics. The only way to determine actual riser and port losses is through physical modelling. A slightly modified version of the program (outfall_hydraulics-duck.f) was used to evaluate the system hydraulics if check valves were used on diffuser nozzles. Parameterisation of head loss characteristics of the duckbills was after Lee, Karandikar and Horton (1998).

The outfall configuration from the head works to the diffuser outlets for the each of the design concepts were schematised in order to be modelled hydraulically. Figure 1 shows the notation used.

Specifications were given for:

$d_{N.n}$ = diameter of nozzle at n
$d_{R.n}$ = diameter of riser at n
$L_{R.n}$ = length of riser at n
$K_{1.n}$ = head loss coefficient for flow from pipeline into riser n
$K_{2.n}$ = head loss coefficient for flow from riser n into nozzle

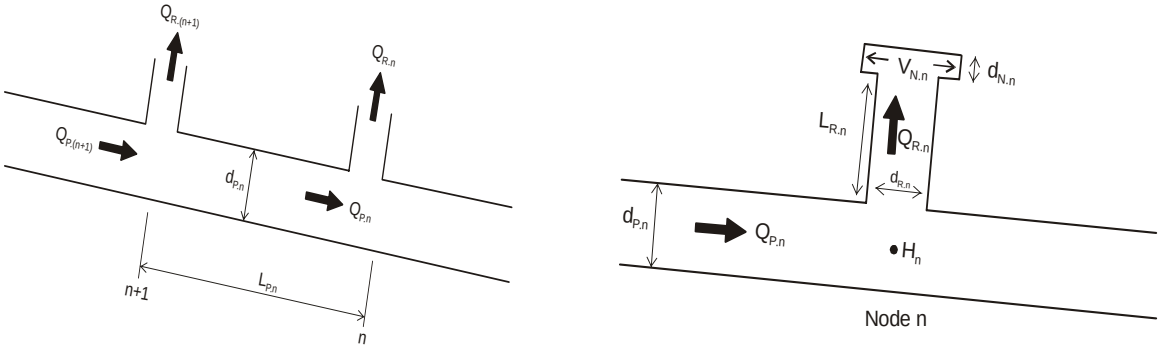

$K_{3.n}$ = head loss coefficient for flow exiting nozzle and entering ambient receiving waters
$d_{P.n}$ = diameter of pipeline (i.e. penstock) at n
$L_{P.n}$ = length of pipeline from n to next upstream node.
where "n" ranges from zero (i.e. the most seaward port) to N (at the head works), as shown in Figure 1.

Figure 1: Schemetisation Of Outfall

The total head/flow relationship across the diffuser was solved by assuming an initial value for total head at the end of the diffuser and working backwards up the pipe in a landwards direction to solve the head/flow relationship at each subsequent port. This procedure was undertaken many times with varying assumed initial total head at the end of the diffuser to give total discharge versus head at the plant curves.

More specifically, after assuming an initial value for total head in the centre of the pipeline at the end of the diffuser (H_o), the head loss to just outside the nozzle was calculated using the Bernoulli equation.

$$HL = H_n - (wselev) \times \frac{\rho_{sea}}{\rho_{effluent}} \qquad (2)$$

where:

HL is the Head Loss from the pipe centreline just before the riser to just outside the nozzle,
H_n is the total head at the centreline of the pipe,
Z is the elevation above the reference datum Indian Springs Low Water (ISLW) of the point just outside the nozzle,
wselev is the water surface elevation (m above datum),
ρ_{sea} is the density of sea water,

$\rho_{effluent}$ is the density of effluent,

The head loss (HL) was calculated by summing the entrance loss for the flow leaving the pipe and entering the riser, friction loss in the riser, nozzle constriction loss and the nozzle exit loss.

$$HL = \frac{K_1 V_R^2}{2g} + f_R \frac{L_R V_R^2}{d_r 2g} + \frac{K_2 V_R^2}{2g} + \frac{K_3 V_N^2}{2g} \quad (3)$$

where:

V_R is the velocity in the riser,
V_N is the velocity in the nozzle,
g is acceleration due to gravity,
L_R is the length of the riser,
d_R is the diameter of the riser,
f_R is the Darcy friction factor for the riser.

Darcy friction factors can be calculated from the Colebrook-White equation:

$$\frac{1}{\sqrt{f}} = -1.98 \log\left(\frac{e}{3.7d} + \frac{2.51}{\mathrm{Re}\sqrt{f}}\right) \quad (4)$$

where:

e is the wall roughness value of the pipe or riser,
d is the diameter of the pipe or riser,
Re is the Reynolds number of the flow.

For the most seaward port, the flow through the port ($Q_{P(n)}$) equals the flow through the riser ($Q_{R(n)}$). For other ports, the flow through the port equals the sum of the flow through the riser ($Q_{R(n)}$) and the flow through the preceding port ($Q_{P(n-1)}$). These equations were solved iteratively to give the head, discharge through the riser and total discharge in the pipe at each node (n).

The head (H_{n+1}) at the subsequent node was then calculated by adding the friction losses (eq. 4) along the length of pipeline (L_P) to the head at the preceding node (H_n) using:

$$H_{n+1} = H_n + f_P \frac{L_P V_P^2}{d_p 2g} \quad (5)$$

where:

f_P is the friction factor for the pipe,
L_p is the length of the pipeline between nodes (n) and (n+1),
V_P is the velocity in the pipeline,
d_p is the diameter of the pipeline,
g is the acceleration due to gravity.

This procedure was repeated for each subsequent node in order to solve equations 2 to 5 for the head, discharge through the riser and total discharge at each node.

4. OUTFALL DESIGN CONCEPTS FOR A SMALL OUTFALL

This outfall concept is based upon discharges of 6 ML/d current ADWF through to 22 ML/d future ADWF and 57 ML/d future PWWF. All discharges including PWWF were to be delivered through the outfall. While several different outfall length were considered, the preferred option was a 0.642 m diameter, 1.5 km outfall pipe. At this location water depth was approximately 14 m and unstratified. The velocity of current field at the outfall ranged from 2 cm/s (95%ile) to 23 cm/s (10%ile). Near field objectives were for a minimum initial dilution of 50 and an average initial dilution of 75.

Using the seawater intrusion criteria as a first pass to determine the maximum number of ports, the following diffuser concepts were considered: 2 rosettes x 8 ports x 75 mm bell mouthed ports, 3 rosettes x 8 ports x 75 mm bell mouthed ports, 4 rosettes x 8 ports x 75 mm bell mouthed ports and 2 rosettes x 8 ports x 100 mm bell mouthed ports

Table 1 presents the near field dilutions and pumping head requirements for the future PWWF and ADWF. It can be seen that the option of 2 rosettes x 8 ports x 100 mm bell mouthed ports provides the required near field dilution and one of the lowest pumping head requirements under PWWF.

Port Diameter, Number of Ports	**Dilution PWWF (Future) Q=0.66 m^3/s**			**Dilution ADWF (Future) Q=0.256 m^3/s**			**Pumping Head (m) (Future Flows)**	
U_a (cm/s) =	**0**	**2**	**10**	**0**	**2**	**10**	**PWWF**	**ADWF**
75 mm, 32	75	85	171	101	114	384	13.2	2.4
24	72	82	144	90	101	291	14.0	2.4
16	72	82	122	79	90	207	16.4	2.4
100 mm, 16	54	60	93	68	75	180	13.6	2.4

Table 1: Near Field Dilutions And Pumping Head Requirements

Currents of 10 cm/s were determined to be about the median current. As such, imposing an absolute minimum dilution criteria results in the median dilutions that are far above the median criteria.

The same configurations were tested hydraulically for a 0.2 m diameter check valves. Figure 2 presents the discharge versus head requirements for three different 16 port diffuser arrays and a 32 port array, for a 1500 m long, 0.642 m diameter outfall in 14 m of water.

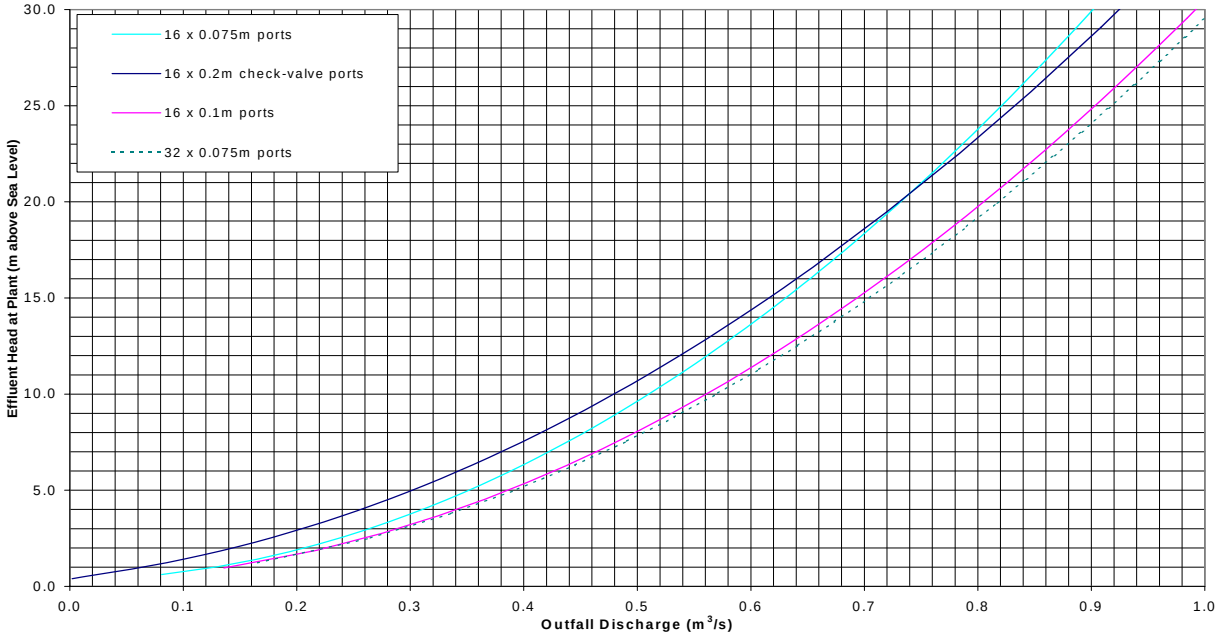

Figure 2: Hydraulic Characteristics Of 4 Diffusers

A comparison of the 0.075 m and 0.1 m, 16 port diffusers shows that by using a larger port aperture, hydraulic head requirements are decreased especially at higher discharges. However, the figure shows that by increasing the number of ports used in a diffuser array, lower hydraulic heads are required. The figure also highlights difference in the hydraulic behaviour of check valves compared to fixed aperture ports. It shows that while at lower flows a slightly higher hydraulic head is required, at higher flows the valve begins to fully open resulting in a lower required hydraulic head.

Figure 2 only shows hydraulic head requirements for a range of different diffusers on a fixed length and diameter outfall. The length and more importantly diameter of the outfall have a strong influence on the hydraulic behaviour of the outfall particularly at high discharges. Because friction losses are related to the square of velocity and pipe velocity is a square function of pipe diameter, small increases in pipe diameter can significantly reduce the required pumping head.

Figure 2 highlights the exponential increase in hydraulic head requirements with discharge which raises issues of whether all PWWF's should be required to discharge through an outfall. If the hydraulic constraints of forcing all PWWF's through a series of risers and nozzles were not required, then the number of risers and nozzles may be able to be better optimised for near field dilutions.

5. CONCLUSIONS

Both the factors influencing outfall concept designs and a methodology for assessing outfall concept designs have been presented. While near field dilutions are optimised to minimise potential health or ecological problems, the design and location of the outfall diffusers have important hydraulic and economic factors. The factors considered in the selection of concept designs for an outfall diffuser include: outfall length/location; outfall pipe diameter; diffuser array design; discharge vs required hydraulic head; saline intrusion; outfall purging and the use specialised nozzle valves.

By careful consideration and understanding of the imposed criteria of the ocean outfall in terms of initial dilutions and flow requirements, optimal outfall solutions can be found.

6. REFERENCES

Jirka G.H., Doneker R.L. and Hinton S.W. (1996) "User's manual for CORMIX: A hydrodynamic mixing zone model and decision support system for pollutant discharges into surface waters", DeFrees Hydraulic Laboratory, School of Civil and Environmental Engineering, Cornell University, Ithica New York, 14853-3501.

Jirka G.H., Akar P.J. and Nash J.D. (1996) "Enhancements to the CORMIX mixing zone expert system: Technical background", Technical Report, DeFrees Hydraulic Laboratory, School of Civil and Environmental Engineering, Cornell University, Ithica New York, 14853-3501.

Lee H.W.J., Karandikar J., and Horton P.R., (1998) " Hydraulics of "Duckbill" Elastomer Check Valves", Journal of Hydraulic Engineering, April 1998, pp. 394-405.

Wilkinson D.L. (1988) "Avoidance of sea water intrusion into ports of ocean outfalls", *J. Hyd. Eng. ASCE*, 114(2), 218-228.

Wood I.R., Bell R.G. and Wilkinson D.L. (1993) " Advanced Series on Ocean Engineering – Volume 8, Ocean Disposal of Wastewater", World Scientific, Singapore.

The institution of Engineers, Australia
8th National Conference on Hydraulics in Water Engineering
ANA Hotel Gold Coast, Australia 13-16- July 2004

Direct Measurement of Roughness of Bed Covered with Gravel and Ripples

Hamid Mirfenderesk
Griffith Centre for Coastal Management, Griffith University, PMB 50 Gold Coast Mail Centre, QLD 9726, Australia Email: hmirfenderesk@goldcoast.qld.gov.auT
Ian R. Young
Swinburne University of Technology, PO Box 218 Hawthorn, Victoria 3122, Australia
Email: iyoung@swin.edu.au

Abstract: In this study a series of experiments were conducted on different beds and under different flow conditions. The tests included a series of uni-directional near wall measurements of mean velocity. These tests were conducted in a channel covered with two types of roughness elements: i) bed covered with spherical aggregates with a diameter between 4 and 9.5mm ii) bed covered with triangular elements (an idealization of rippled beds) with a height of 13.6mm. The result shows that equivalent sand roughness associated with aggregate is of the order of the magnitude of the grain size. For rippled-like beds, the result of this study shows that this type of roughness can be adequately described with only one length scale (such as Nikuradse equivalent sand roughness) and that Dirling's empirical relation can best predict this length scale.

Keywords: roughness, Nikuradse, sand, measurement

1. INTRODUCTION

The importance of this study came from the fact that many littoral and riverine processes, such as sediment transport or dissipation of mean flow energy are strongly affected by the interaction between water particles and bed. This interaction is basically under the influence of the flow condition and the bed roughness. This study is mainly focused on bed roughness.

Roughness is a term, which describes the size, shape and spatial distribution of the protrusions on the boundary. Nikuradse conducted a series of experiments on pipe flows to obtain measurable indices for the roughness factor. He artificially roughened the inside wall of the pipes with uniform sand grains and from the experimental data descried the roughness by only a single length, k_s, which was the diameter of the uniform sands used in his experiments. In practice, roughness elements are very different from uniform grain sands. In general they can be characterized by a typical or average roughness height, ε. However, it is usually possible to establish a relationship between ε and k_s. Many authors have tried to establish such a relationship for various types of rough beds. Table (1) shows attempts made by different authors to characterize aggregate bed forms with a roughness length, k_s (Nikuradse's equivalent sand roughness). Table (1) shows that for a flat immobile bed k_s is of the order of the grain size and can be represented by Equation (1):

$$k_s \approx n.D_x \qquad (1)$$

Where x denotes that x% by weight of particles smaller than D_x .

Nikuradse's equivalent sand roughness	
Author's name	k_s
Ackers-White (1973)*	$1.25\,D_{35}$
Einstein (1953)*	D_{65}
Englund-Hansen (1967)*	$2\,D_{65}$
Hey (1979)*	$3.5\,D_{84}$
Kamphuis (1974)	$2\,D_{90}$
Mahmood (1971)*	$5.1\,D_{84}$
Nilsen (1991)	$2.5\,D_{50}$
Limerinos (1970)	$2.8\,D_{84}$
Gladki (1979)	$2.5\,D_{84}$
Leopol et al (1964)	$2.8\,D_{84}$
Bray (1979)	$2.4\,D_{84}$

Table 1 – Nikuradse's Equivalent Sand Roughness Obtained By Different Authors (* sighted at Seabed Mechanics, Sleath (1984))

2. EQUIVALENT NIKURADSE SAND ROUGHNESS

Milikan (1938), using dimensional analysis, showed a logarithmic velocity profile exists in the overlap region of the bottom boundary layer under unidirectional flow. Using Prandtl mixing length theory and Nikuradse's experimental results on roughened pipes with uniform sand grains it can be shown that the following equations hold within this overlap layer:

For smooth bed:
$$\frac{u}{u_f} = 5.75\log\frac{zu_f}{\nu} + 5.5 \qquad (2)$$

For rough bed:
$$\frac{u}{u_f} = 5.75\log\frac{z}{\varepsilon} + 8.5 \qquad (3)$$

Where $u_f = \sqrt{\tau_0/\rho}$ is friction velocity (τ_0 is bed shear stress), ν is viscosity and u is velocity at level z above bed.

To apply these results to rough walls having the same roughness height but different geometry, the concept of equivalent sand roughness can be used. The idea behind equivalent sand roughness is that, in a fully turbulent rough flow, the general form of the velocity distribution of the flow remains unchanged; only the absolute values change.

By definition, the equivalent sand roughness, k_s, of a wall with roughness element ε, is the sand grain size which induces the same resistance to flow as the roughness element ε. In using the concept of sand grain roughness it is implicitly assumed that a single dimension of roughness elements can describe roughness effects. In other words, there should be a single dimension of roughness elements that changes the velocity distribution to a logarithmic form like equation (3). Obviously it is possible to find irregular surfaces, which are not of the sand grain type, and friction cannot be determined by a single equivalent roughness. However, for most surfaces, an equivalent sand grain roughness can be determined using velocity data on the rough surface and under the flow condition of interest. The direct result of the definition of equivalent sand roughness is that the flow velocity will be the same in both cases for given z.

Figure (1) schematically shows mean velocity profile for both rough and hydraulically smooth flow. In a hydraulically smooth flow, viscous shear alone determines the flow resistance and the shear stress in the overlap layer is transmitted to wall by the action of these viscous shear stresses. In this case, the height of the irregularities is much smaller than the thickness of the viscous sub-layer and hence they are buried in the viscous sub-layer. In rough turbulent flow the turbulent wakes generated by the roughness elements are too strong to be

smoothed out by viscosity. Hence the whole inner layer becomes turbulent and the viscous sub-layer totally disappears. In a rough flow the form drag of the irregularities plus skin friction determine the flow resistance. In a rough turbulent flow the velocity profile is logarithmic throughout the boundary layer, whilst in a hydraulically smooth flow the logarithmic profile holds only in the overlap layer, as shown in figure (1).

Extrapolating the straight line of the logarithmic velocity profile to $u = 0$, figure (1a), gives an intercept on the log axis at a finite elevation z_0 above the bed.

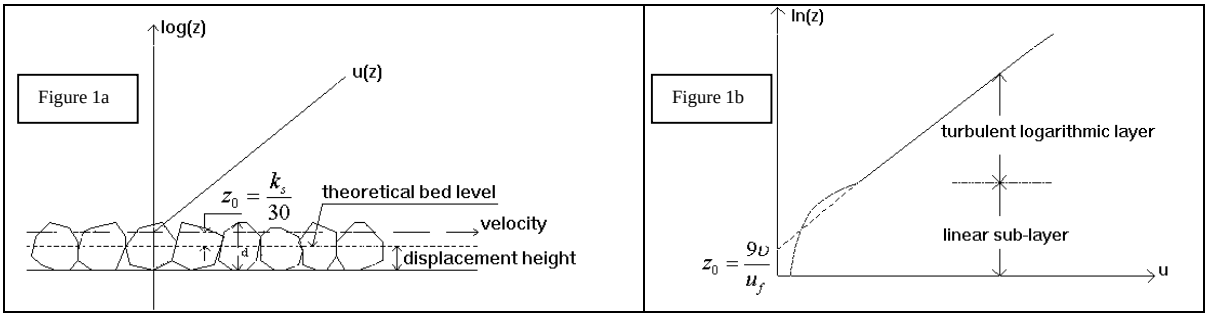

Figure 1 - Logarithmic Profile of Mean Velocity in a Rough Flow and Hydraulically Smooth Flows

Since at $z = z_0$, $u = 0$, equation (3) can be written as:

$$0 = 5.75 \log \frac{z_0}{d} + 8.5 \qquad (4)$$

Where d is the sand grain diameter used in Nikuradse's experiments, and hence

$$8.5 = -5.75 \log \frac{z_0}{d} \rightarrow \frac{z_0}{d} = \frac{1}{30} \qquad (5)$$

Irrespective of the value of d, the ratio $\frac{z_0}{d}$ is a constant. Based on equation (5) the equivalent Nikuradse sand roughness can be defined as $k_s = 30 z_0$. The value z_0 can be determined by fitting a logarithmic curve to experimental data of the velocity distribution within the boundary layer.

In the case of a turbulent smooth flow, Figure (1b), z_0 can be obtained by using equation (6):

$$\frac{u}{u_f} = 5.75 \log \frac{z.u_f}{\nu} + 5.5 \qquad (6)$$

at $z = z_0$, $u = 0$, hence

$$0 = 5.75 \log \frac{z.u_f}{\nu} + 5.5 \rightarrow z_0 = \frac{\nu}{9u_f} \qquad (7)$$

3. METHODOLOGY

As explained above, equivalent Nikuradse sand roughness can be obtained by determination of the velocity profile within the boundary layer. In this light, a series of near wall mean velocity measurements have been conducted to obtain the velocity profile within the boundary layer of the surface of interest. After each test the value of $\frac{u_f.z}{\nu}$ was calculated to make sure it was larger than 70, to ensure the existence of a turbulent rough flow around the aggregates. The value of z_0 has then been determined by extrapolating the straight line of the logarithmic velocity profile to $u = 0$. Equivalent Nikuradse sand roughness has been calculated using equation (5).

4. EXPERIMENTAL SETUP AND EQUIPMENT

Measurements were performed in the water channel shown schematically in figure (2).

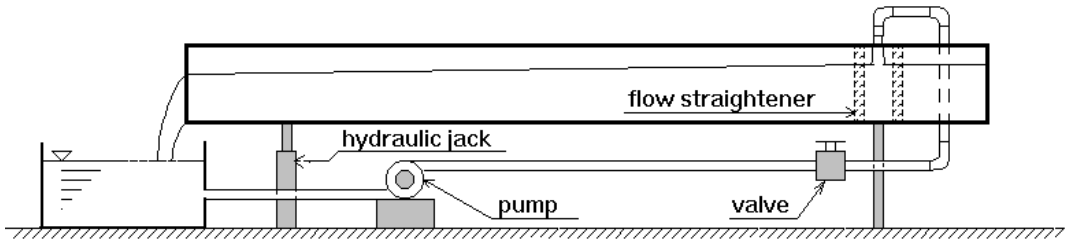

Figure 2 -Layout of the Channel Used for Sand Roughness Determination.

The measurements were performed at a point nearly 20 water depths down stream from the inlet and the width of channel was more than five times the water depth. A 10 MHz Sontek Acoustic Doppler Velocimeter (ADV), with a 5 cm focal length, was used for velocity measurements. The ADV is a non-contact acoustic-sensing instrument for measurement of water particle velocities. Determination of the velocity is based on the Doppler shift caused by the movement of small particles in the water. To obtain the Doppler shift, a transmit transducer mounted on the probe sends acoustic signals. Small particles, which are assumed to faithfully follow the water flow, backscatter the signals. Three receive transducers, related to the three components of the velocity, mounted on the probe and around the transmit transducer, sense the back scattered signal. The output of the system is a DC signal between -5 and 5 volts, which is directed to the signal processor supplied with the system. Data acquisition is conducted by software, developed by Sontek Company and installed on a IBM 486 microcomputer. A digital signal processor supplied with the system primarily processes the data. The data rate in this case is 25 Hz. The package provides a real time display of the data and also records to disc.

5. BED CONDITIONS

In this study three different bed conditions were used: i) sand paper, ii) spherical aggregates with diameters between 4 and 9.5 mm glued to the surface and iii) strip roughness elements with triangular cross-sectional shape, fastened to the bed. This element had 13.6 mm height and placed 6.6 cm apart in the flow direction.

5.1 Sand Paper

The sand paper provided a bed covered with uniform silicon carbide aggregates with a diameter of 197 micron. The aggregate was glued on backing made from woven cloth. The velocity profile within the boundary layer of a unidirectional flow over the sand paper was measured. For this purpose the Acoustic Current Meter was traversed in a vertical direction with measurements being made at .1 mm increments above the bed. Figures (3-a) and (3-b) give the mean velocity profile in both normal and wall coordinates.

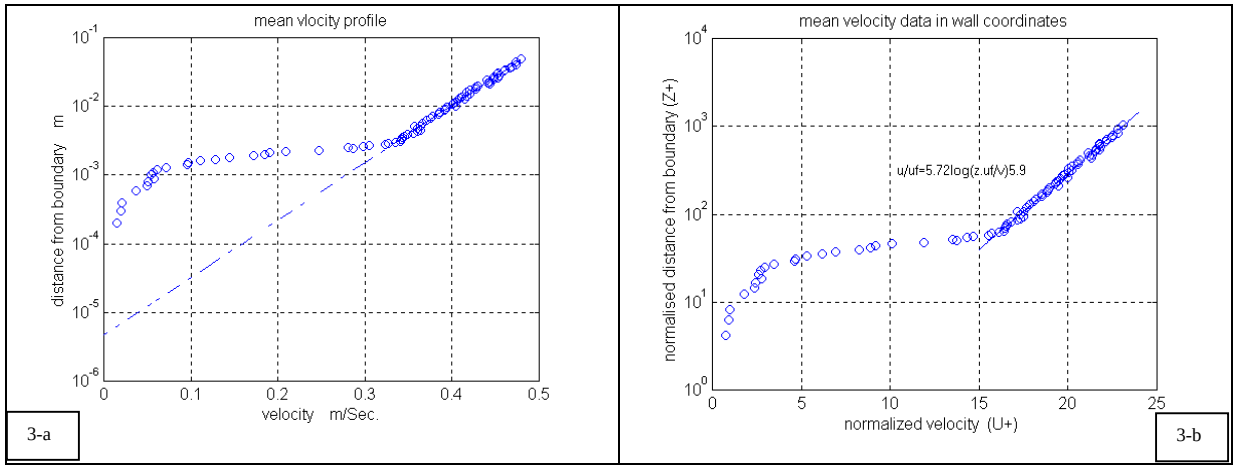

Figure 3 - Mean Velocity Profile in Wall and Physical Coordinates

The slope of the logarithmic profile of the mean velocity in the over overlap layer yields the value of u_f equal to 0.0208 m/s. The values of $U^+ = u/u_f$ and $Z^+ = zu_f/\nu$ were then calculated. The straight line fitted through the normalized parameters U^+ and Z^+ gives the logarithmic velocity profile, equation (8):

$$U^+ = 5.72 \log Z^+ + 5.9 \qquad (8)$$

Equation (8) is very close to the universal profile of mean velocity within the overlap layer of a hydraulically smooth flow, equation (3). The value of z_0 can be obtained from extrapolating the logarithmic profile of the velocity to intercept the vertical axis. Figure (3-a) shows the value of z_0 to be approximately .005 mm. The value of z_0 can also be obtained from equation (7):

$$z_0 = \frac{9\nu}{u_f} = \frac{10^{-6}}{9 \times .0208} = 0.005 \quad \text{mm}$$

It can be shown that the thickness of the viscous sub layer can be calculated as follows

$$\delta_v = \frac{11.6\nu}{u_f} = \frac{11.6 \times 10^{-6}}{0.0208} = 0.56 \quad \text{mm}$$

It shows that the thickness of the viscous sub layer is sufficient to bury all protrusions. This confirms the above finding that this case is a hydraulically smooth flow.

5.2 Aggregates

A series of tests was conducted on spherical aggregates with a diameter between 4 and 9.5 mm. The same tests as performed on the sand paper, were repeated on a bed covered with aggregates. Figure (4-a & b) shows the mean velocity profile in both physical and wall coordinates in a typical test.

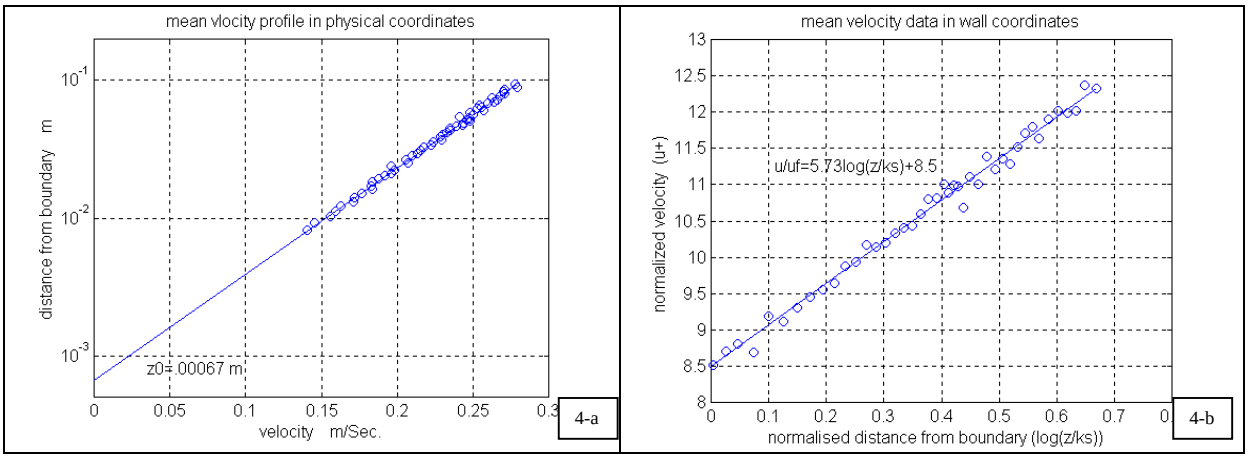

Figure 4 - Mean Velocity Profile in Wall and in Physical Coordinates, Aggregate Roughness Element

The slope of the logarithmic profile of the mean velocity in the over overlap layer yields the value of u_f equal to 0.0226 m/s. The value of U^+ was then calculated. The straight line fitted through the normalized parameters U^+ and $\frac{z}{k_s}$ gives the logarithmic velocity profile, equation (9):

$$U^+ = 5.73 \log\left(\frac{z}{k_s}\right) + 8.5 \qquad (9)$$

Equation (9) is very close to the universal profile of mean velocity within the overlap layer of a turbulent rough flow, equation (4). The value of z_0 can be obtained from extrapolating the logarithmic profile of velocity to intercept the vertical axis. Figure (4-a) shows the value of z_0 to be approximated 0.67 mm. Consequently the equivalent Nikuradse sand grain roughness is: $30 \times z_0 = 30 \times 0.67 = 20$ mm, which is approximately $2.5D_{84}$. This compares well with the empirical relations offered by other authors, table (1).

5.3 Strip Roughness Elements

To obtain friction factor results in a fully turbulent rough flow another series of tests were carried out on a surface with transverse triangular ribs. To relate the rib roughness geometry to an equivalent sand grain size, the same tests conducted on previous roughness elements were repeated on the new surface. The geometry of the roughness elements of the new surface raises some new complexities. In the following, the structure of the boundary layer above the rib surface is discussed in more detail. Reynolds (1974) stated that on such a surface, under a zero pressure gradient flow, a region near the wall develops, called the roughness layer, figure (5-a & b).

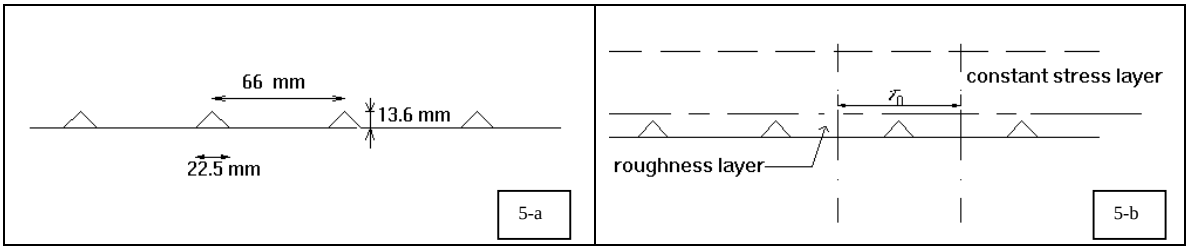

Figure 5 - Distribution of Roughness and Constant Stress Layer within the Boundary Layer

He stated that in this layer the mean flow velocity is three-dimensional and the time-mean shear stress varies from point to point. The effective average shear stress is assumed to act beyond the roughness layer at the interface between the roughness layer and the constant stress layer. The latter layer, as its name suggests, is a region where the shear stress is constant and therefore the velocity profile can be described by a logarithmic relationship, provided a proper roughness length scale is chosen.

In the following, the equivalent Nikuradse sand roughness of the surface (for $\varepsilon = 13.6mm$) is calculated using the empirical relationship suggested by Dirling (1973), equations (10) and (11). Dirling (1973) suggested the following empirical relationship for k_s.

$$\frac{k_s}{\varepsilon} = 0.0164\lambda^{3.78} \qquad (for \quad \lambda \le 4.93) \tag{10}$$

$$\frac{k_s}{\varepsilon} = 139\lambda^{-1.90} \qquad (for \quad \lambda > 4.93) \tag{11}$$

Where ε is the roughness height and λ is a roughness element geometry parameter:

$$\lambda = \frac{l_r}{k_r}\left(\frac{A_s}{A_p}\right)^{\frac{4}{3}} \tag{12}$$

Where $l_r = 6.6cm$ is the center to center roughness element spacing, $k_r = 1.36cm$ is the roughness element height, actual, $A_S = 1.36cm^2$ is the roughness element windward surface area, $A_p = 1.53cm^2$ is the roughness element cross-sectional area. Using these values and equation (11) k_S can be calculated: $k_S = 4.83cm$.
There are many other empirical relationships for the evaluation of k_S based on the geometry of the rib roughness elements, obtained by various authors. They yield values between 1.4 and 8 cm for k_S in this case.
To estimate the Nikuradse sand roughness of the triangular riblet surface experimentally, the equation of the logarithmic velocity profile within the boundary layer has again been used. Unlike the sandpaper case, the displacement height cannot be ignored for a riblet surface. The displacement height accounts for the position of the theoretical bed or the origin of the Z-axis in the velocity profile diagram. The theoretical bed is usually somewhere between the base plate and the top of the roughness elements. To the knowledge of the authors, there is no exact analytical method for determining the position of the theoretical bed. To obtain the equivalent Nikuradse roughness there is only one equation, (13) with three unknowns, u_f , d_t and k_S.

$$\frac{u}{u_f} = 5.75\log\frac{z-d_t}{k_s} + 8.5 \tag{13}$$

where d_t is the displacement height. In regard to the estimation of d_t, the suggestion of Reynolds (1974) can be used. The profile of the velocity is plotted versus the logarithm of the distance from the wall. The distance of the measurement point from the theoretical wall can be considered as the distance of the measurement point from the base plate z_t minus the displacement height, d_t, $(z = z_t - d_t)$.

The value of the displacement height is changed and every time a logarithmic line is fitted to the measured velocity. The value of d_t corresponding to the best fit is regarded as the position of the theoretical wall. Having the two unknowns, u_f and d_t, k_s can be estimated from equation (13). Figure (6) shows the variation of the distance between the roughness height and the theoretical bed versus the mean square deviation of the measured points from the fitted line. It can be seen that a theoretical bed 2.5 mm below the top of the roughness elements, gives the best fit. Considering that the roughness height is 13.6 mm, the theoretical bed level in this case can be regarded as 11.1 mm above the baseplate. In this case it is observed that, the displacement height is nearly 0.8 times the roughness height. Jackson (1981) gives the values of displacement height obtained by different authors over a wide range of roughness elements. His collection shows that 0.8 is a good approximation for the displacement height.

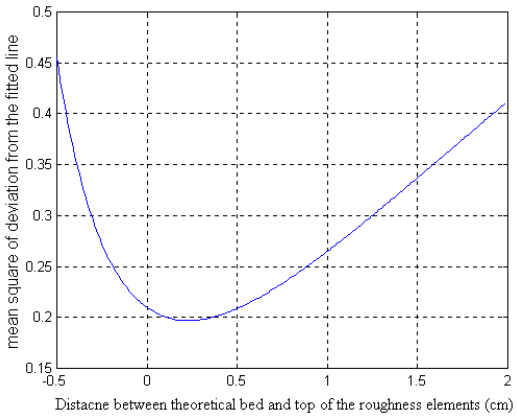

Figure 6 - Variation of the Distance between the Theoretical Bed and the Top of the Roughness Elements Versus Mean Square Deviation of Measured Points from the Fitted Line

Having the position of the theoretical bed, the logarithmic line, which is fitted to the velocity data, is extended to intercept the z axis, Figure (7-a & b).

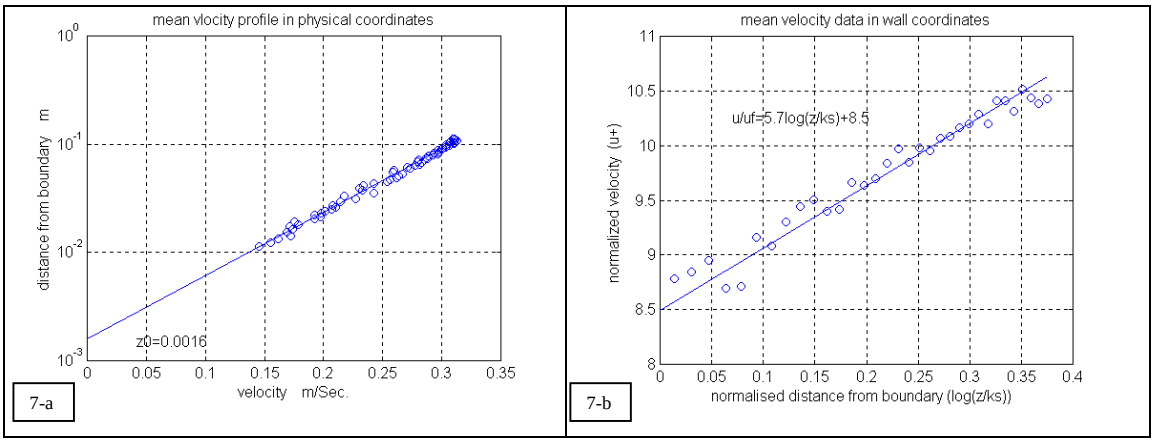

Figure 7 - Mean Velocity Profile in Wall and in Physical Coordinates, Rib Roughness Elements

Figure (7-a) shows that $z_0 = 1.6mm$. Hence the Nikuradse roughness becomes: $30z_0 = 48mm$. Figure (7-b) shows the profile of normalized velocity versus normalized distance from the boundary.
The equation of the fitted line yields:

$$\frac{u}{u_f} = 5.7 \log \frac{z}{k_s} + 8.5 \qquad (14)$$

This test was repeated many times. The equivalent sand roughness obtained in these tests scattered around 50mm which compares well with 48 mm obtained from the Dirling (1973) relationship.

6. CONCLUSION

A series of uni-directional near wall measurements of mean velocity in a channel covered with various roughness elements under fully developed turbulent flow condition was conducted. The results show that for aggregate roughness elements, equivalent Nikuradse sand roughness has a magnitude of the order of the grain diameter and can be approximated by the value of $2.5D_{84}$.

The roughness associated with a bed covered with rippled-like strip roughness elements can be adequately described with only one length scale (such as Nikuradse equivalent sand roughness). Out of many different empirical relations, Dirling's empirical formula provides a good estimation of the equivalent Nikuradse sand roughness for these beds.

This study also shows that displacement height associated with rippled-like strip roughness elements is nearly 0.8 times the roughness height.

7. ACKNOWLEDMENT

The authors thank the technical staff of the School of Civil Engineering, University College, University of New South Wales, for their support throughout this study.

8. REFERENCES

Nielsen, P. (1991). *Coastal Bottom Boundary Layers and Sediment Transport*. Advance Series on Ocean Engineering- Volume 4, World Scientific. Reynolds, A.J. (1974). *Turbulent Flows in Engineering*, John Wiley &Sons.

Sleath, John F.A. (1984). *Seabed Mechanics*, John Wiley & Sons.

Jackson, P.S. (1981). On the Displacement Height in the Logarithmic Velocity Profile, *Journal of Fluid Mechanics 111*, pp. 15-25.

Bray, D.I. (1979). Estimating Average Velocity in Gravel-Bed Rivers, *Journal of Hydraulics, ASCE* 105, pp 1103-1122.

Gladki, H. (1979). Resistance to Flow in Alluvial Channels with Coarse Bed Materials, *Journal of Hyrologic Research* 17(2), pp 121-128.

Hey, R.D. (1979). Flow Resistance in Gravel Bed Rivers. Journal of Hydraulics, *ASCE 105 No Hy4*, pp 365-379.

Kamphuis, J.W. (1974). Determination of Sand Roughness for Fixed Beds, *Journal of Hydraulic Research* 12, pp 193-203.

Dirling, R.B. (1973). A Method for Computing Rough Wall Heat Transfer Rates on Re-Entry Nosetips. *AIAA paper* No. 73-763 pp. 16-18.

Limerinos, J.T. (1970). Determination of the Manning Coefficient for Measured Bed Roughness in Natural Channels, *US Geological Survey, Water Supply Paper*, 1891-B.

Leopold, L.B. et al (1964). *Fluvial process in Geomorphology*, W.H. Greenman and Co. San Francisco.

The Institution of Engineers Australia
8th National Conference on Hydraulics in Water Engineering
ANA Hotel Gold Coast, Australia 13-16 July 2004

Development of a Device for Direct Measurement of Bed Shear Stress Induced by a Wave Spectrum

Hamid Mirfenderesk
Griffith Centre for Coastal Management, Griffith University, PMB 50 Gold coast Mail Centre, QLD 9726, Australia
Email:hmirfenderesk@goldcoast.qld.gov.au
Ian R. Young
Swinburne University of Technology, PO Box 218 Hawthorn, Victoria 3122, Australia
Email: iyoung@swin.edu.au

Abstract: This paper describes a device (shear plate), which was developed for the direct measurement of shear stress applied to the bed by the action of gravity waves in a 50-meter long wave basin. This device is capable of resolving shear stress up to .05 N/m^2 and measuring waves with a frequency of up to 5 Hz. This instrument in conjunction with a Laser Doppler Anemometer was later successfully used for the measurement of bed shear stress resulting from both monochromatic and spectrum of gravity waves. In this paper a full description of the device, some of the challenges encountered during its development, and some of the lessons learnt in the process of this exercise have been explained.

Keywords: Bed, Shear Stress, Measurement, Wave spectrum, Shear plate

1. INTRODUCTION

Accurate determination of the bed friction factor in an oscillatory boundary layer is essential to the proper estimation of wave energy dissipation and sediment transport in coastal waters. Determination of the bed friction factor under oscillatory boundary condition is one of the problems in hydraulics. Many authors have tried to express friction factor f_w in terms of measurable or calculable elements of a progressive wave field. Determination of bed shear stress under an oscillatory boundary layer is vital for the estimation of the friction factor. A potentially reliable method for determination of bed shear stress appears to be the direct measurement of the shear force exerted on a segment of the bed.

Kamphuis (1975) and Simon et al (1992) have previously used this method. The significance of direct measurement of shear stress using a shear plate comes from the fact that alternative methods are not capable of providing shear stress under the action of a wave spectrum. An alternative method widely used by other authors, e.g. Jonsson (1966) and Sleath (1988), is the measurement of the velocity field within the boundary layer and the determination of the bed shear stress by solving the momentum equation (1), numerically.

$$\frac{\tau}{\rho} = \int_{\frac{k}{30}}^{\delta} \frac{\partial}{\partial t}(u - u_b)dz \tag{1}$$

where δ is the level at which shear stress vanishes, ρ is the density of water, z the vertical coordinate measured upwards from the bed, u_b is the instantaneous bottom velocity and τ is the bottom shear stress ($\tau = \tau_0 \ \ at \ \ z = z_0$). This method, however, can only be used under monochromatic conditions.
Two other methods, which can potentially be used in unidirectional condition, i.e. measuring Reynolds stress and the similarity technique cannot be used in oscillatory boundary layer situation. Measuring the Reynolds stresses within an oscillatory boundary layer, unlike in steady flow, underestimates the bed shear stress. As stated by Sleath (1988), this can be partly due to the substantial correlation between the stream wise and the transverse components of the velocity within the oscillatory boundary layer.

Similarity techniques are based on the existence of a region adjacent to the bed where a universal law of the wall is assumed to exist. However, such a universal law of the wall in an oscillatory boundary layer is nonexistent.

2. SHEAR PLATE

In this project the shear stress is measured directly by a shear plate. The principle of this measurement technique is to detach a piece of the bed and allow it to move freely under the shear stress exerted by water flow over the bed.

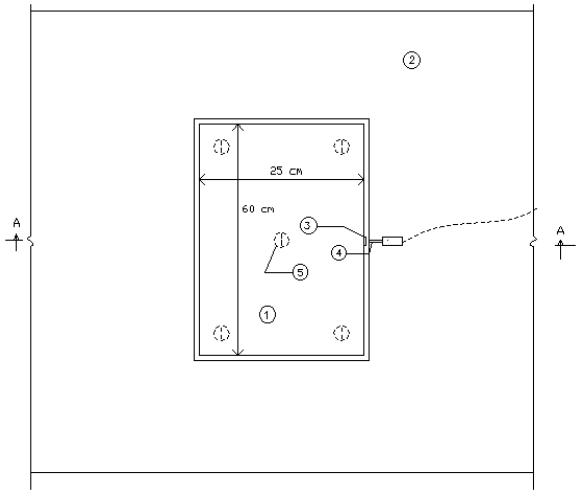

Figure 1 - Layout of the Shear Plate (plan)

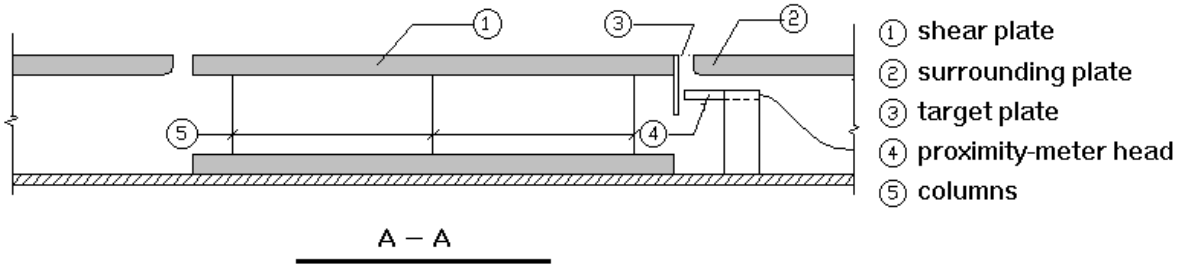

Figure 2 – Cross-Section of the Shear Plate

Figures 1 and 2 schematically show the form of the shear plate. The system consists of two major parts. The first part, the body, consists of two parallel steel plates. The plate at the top is covered with roughness elements. It is supported at its corners and at the middle by 5 legs. This plate functions as a single degree of freedom structure. The legs are rigidly joined to the plates. The structural stiffness is small enough to allow the shear plate to deflect under very small shear forces exerted to the top plate but still large enough to justify a static calibration of the plate. The second component is an eddy current proximity sensor, which measures the distance between the sensor head and a conductor, or target plate. Figure (3) shows the principle behind the structure of a proximity sensor.

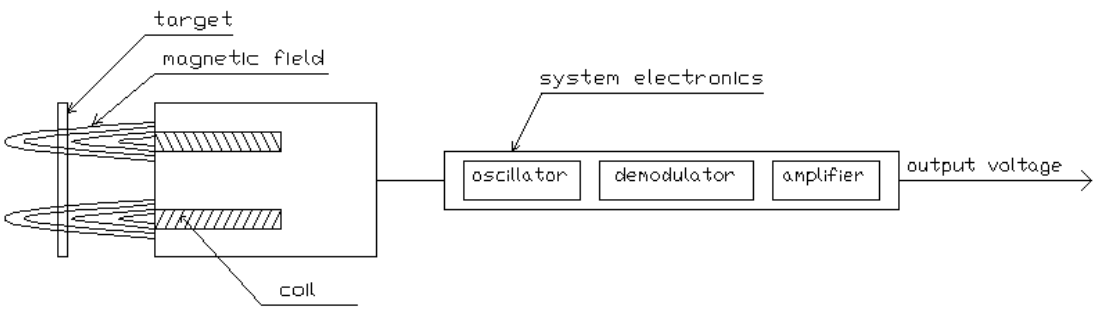

Figure 3 - Layout of the Proximity Sensor

The sensor consists of a coil, which is part of a high frequency LC resonance circuit. The circuit oscillates at its resonance frequency and generates a magnetic field around the coil. If the magnetic flux lines intersect a conducting surface (target), an eddy current will be induced in the conducting material. This eddy current causes the oscillation in the circuit to be damped and reduces the output voltage. As the distance between the sensor head and the target varies, the magnitude of the eddy current in the conducting material changes and these changes are evaluated by a demodulator. Therefore, the output voltage can be shown to be a function of the distance between the target and the sensor head. In this manner, the output voltage time history yields the time history of the position of the target from the sensor head. Having the relationship between applied force and the position of the target from the sensor head, through a calibration curve, the shear stress time history can be determined.

2.1 Data Acquisition

The signal from the shear plate is a DC voltage between -5 and 5 volt. A computer program installed on a IBM486 microcomputer acquires data at a rate of 25 Hz from the shear plate. The computer is interfaced with the instrument by an Analog Device RTI-815F card.

2.2 Calibration

The shear plate should be calibrated before every experiment. The calibration system consists of a string, weights and four low friction pulleys as shown in figure (4).

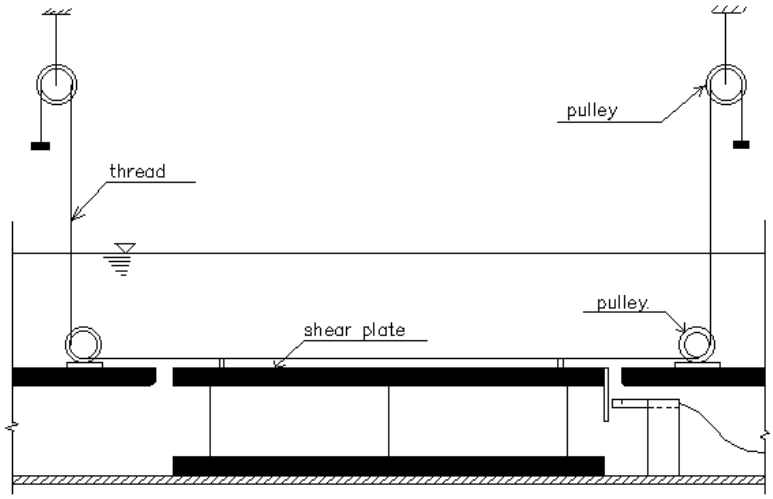

Figure 4 - Layout of the Calibration System of the Shear Plate

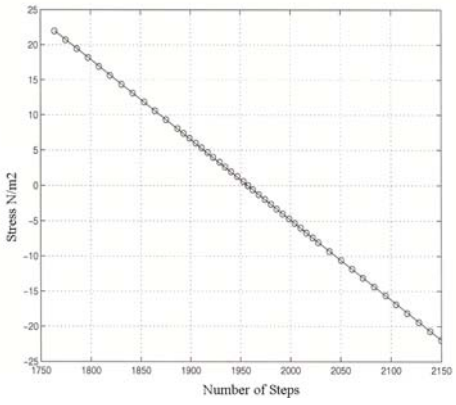

Figure 5 - A typical Shear Plate Calibration Curve. The Number of Steps Indicates the Quantisation Level of the Output Voltage by the A/D Card

The shear plate was calibrated statically in its submerged state in increments of about .05 Newton. Intermediate values were interpolated by a straight line, a typical example being shown in figure (5).

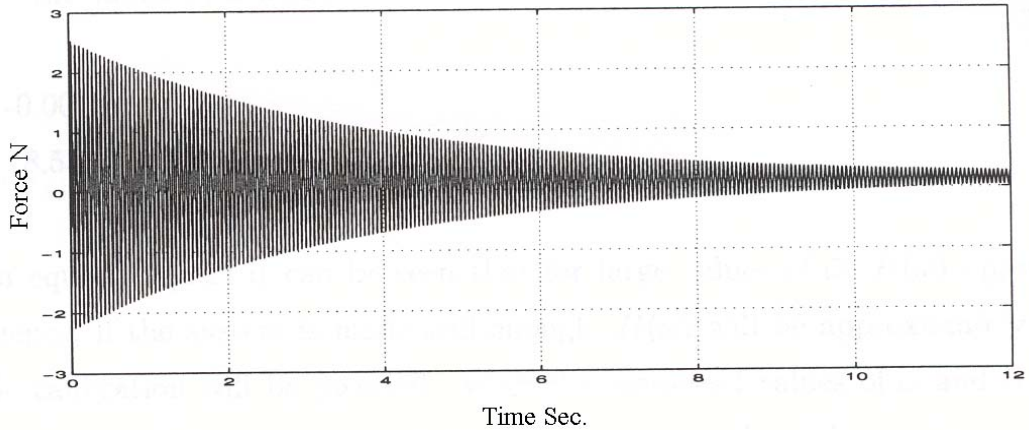

Figure 6 - Force Time History of Force Exerted on the Shear Plate

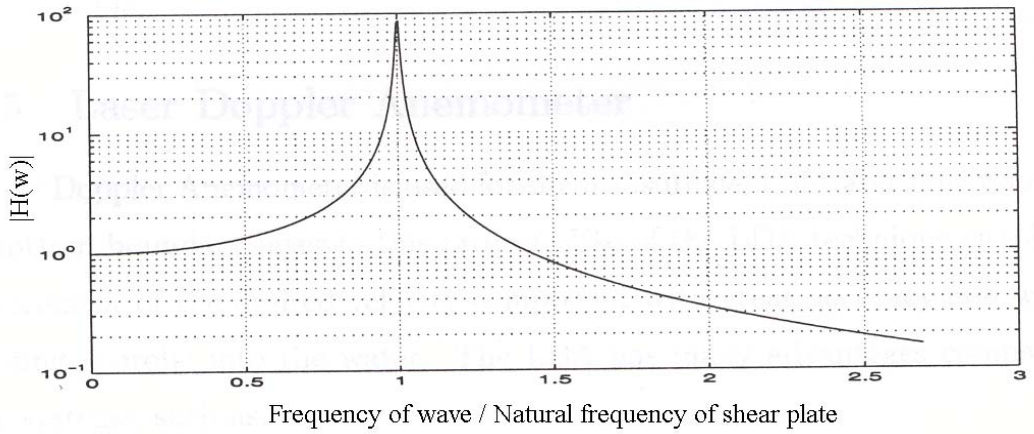

Figure 7 – Frequency Response of the System

The static calibration of the shear plate could be a source of error since an elastic system subject to a dynamic load may experience a displacement, which is different from the displacement for the equal static load used for the calibration.

The ratio of dynamic displacement to static displacement is called the dynamic magnification factor or frequency response of the system, H_ω . It can be shown that for a single degree of freedom system (SDF), (R.C. Coates et al (1972)):

$$H(\omega) = \frac{1}{\left\{\left|1-\left(\frac{\omega}{\overline{\omega}}\right)^2\right|^2 + 4\beta^2.\left(\frac{\omega}{\overline{\omega}}\right)^2\right\}^{\frac{1}{2}}} \qquad (2)$$

where β is the coefficient of critical dumping $\overline{\omega}$ is the circular natural frequency of the system and ω is the frequency of the excitation. It can be shown that for a damped free vibration response of a SDF system, the envelope of the force time history of the system, figure (6), can be expressed as, $e^{-\beta\overline{\omega}t}$. Based on the results of the measurements made, while the system vibrated freely, the values of $\overline{\omega}$ and β were determined as:
β = -0.0052
$\overline{\omega}$ = 18.5547 rad/Sec

From equation (2) it can be seen that for large values of $\overline{\omega}$, $H(\omega)$ approaches 1. Hence, if the system is made stiff enough, $H(\omega)$ will be approximately 1 and static calibration will be justified. With the measured values of $\overline{\omega}$ and β, $H(\omega)$ was determined from (2) for different values of ω. The results are shown in figure (7). It can be seen that for frequencies up to 5 Hz, $H(\omega)$ is nearly 1 and therefore, the results of the static calibration are acceptable.

3. UNCERTAINTY

There are three sources of errors for shear plate measurements, i) resolution capability of the analog to digital converter, ii) circuit noise and iii) calibration error.

3.1 Resolution Capability of the A/D Converter

The precision of the card can be estimated as 20/4096=0.0049 volt, where the numerator shows the input range of the card and 4096 is the number of steps into which an analog signal can be digitized by the card. Preliminary tests showed that every 1 N/m^2 of shear stress exerted on the shear plate induces 1.05 volt output. Therefore, the precision due to the resolution capability of the A/D converter is approximately

$$\frac{0.0049}{1.05} \approx 0.0047 \quad N/m^2$$

3.2 Uncertainty Due to Noise

Figure (8) shows that the recorded voltage for a constant distance between the target plate and the proximeter probe head scatters around an average value. The standard deviation of this scattered data is 0.003 volt. Therefore the 95% confidence interval due to this noise is

$$1.96\frac{\hat{\sigma}}{\sqrt{N}} = 1.96\frac{.003}{1000} = 0.00019 \text{ Volt}$$

Which is equivalent to 0.00019/1.05=0.00018 N/m^2. This is a very small uncertainty compared with the precision resulting from the finite resolution of the A/D conversion.

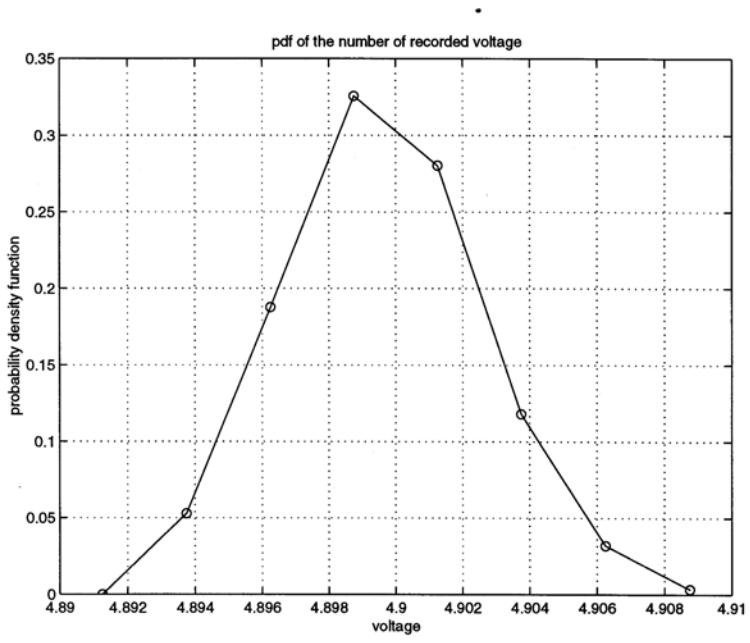

Figure 8 - Output of the Shear Plate under a Constant Force

3.3 Calibration Error

As shown in figure (5) due to the uncertainty in both the measured parameters and the small nonlinearly of the relationship between the shear stress and the deflection of the shear plate, the measured points scattered around the fitted straight line:

$$\text{Stress} = -0.1139 * \text{number of steps} + 222.9 \tag{3}$$

The mean error estimate for the points calculated by MATLAB is about $\pm 0.05\ N/m^2$ for this calibration curve. For a typical shear stress of about 2 N/m^2, it gives an error of approximately 2.5%. As can be seen, the error due to the noise and the resolution of the shear plate is insignificant compared with the error due to the calibration. Therefore, the total error of the shear plate can be attributed to the calibration error, approximately 2.5%.

It is important to note that the calculated uncertainty is associated with the reading of the shear plate. Extraction of the true value of the shear stress requires filtering out some contaminating forces from the results of the shear plate as explained in the next section.

4. CORRECTION FOR CONTAMINATING FORCES

The shear plate has the obvious advantage that it provides a direct measure of the shear stress exerted on the bed. Due to the finite height of the wave train, however, a longitudinal pressure gradient will be present. This pressure gradient will exert a contaminating force on the edge of the shear plate, and its magnitude must be carefully assessed to obtain reliable results. The pressure gradient at the bed can be estimated from equation (4).

$$\rho \frac{\partial u_b}{\partial p} = -\frac{\partial p}{\partial x} \tag{4}$$

Where u_b is the orbital velocity just outside the oscillatory boundary layer and p is the pressure. The bed velocity, $u_b(t)$, was measured directly using the LDA (Laser Doppler Anemometer) system. It was assumed that the pressure varied linearly over the length of the plate. As the shear plate was 26cm long and the wavelength was typically 4m, this seemed a reasonable assumption. Calculations using linear wave theory confirmed the accuracy of the assumption (error is less than 0.5%). The pressure difference across the plate (Δp) was assumed to act on the cross sectional area of the edge of the plate. This included both the thickness of the plate itself, plus the roughness elements attached to the plate.

The shear plate was tested using three different roughness elements: i) hydraulically smooth surface, ii) bed covered with spherical aggregates with diameters between 4 to 9.5mm, glued to the surface, iii) rippled-like roughness using triangular ribs with 13.6 mm height and placed 6.6 cm apart in the flow direction. All these roughness elements were placed on both the top plate of the shear plate device (part 1 in figure 1 and 2) and the surrounding plate (part 2 in figure 1 and 2).

The effect of the pressure gradient in the case of a smooth bed is quite significant and can, in fact, exceed the magnitude of the shear force exerted on the plate. In the case of the rippled-like elements, the effect of the pressure gradient was relatively small, less than 10% of the total shear stress, although in the case of the spherical aggregates its effect was as large as 40% of the total shear stress.

5. COMPARISON WITH SIMILAR MEASUREMENTS

To verify the reliability of the measurements, the shear stress measured by the shear plate (corrected for pressure gradient) were converted to friction factor via equation (5)

$$\tau_{0\max} = \frac{1}{2} \rho f_w U_b^{\,2} \tag{5}$$

Where f_w is a friction factor, U_b is the maximum near bed velocity measured by Laser Doppler Anemometer and $\tau_{0\max}$ is the maximum shear stress measured by the shear plate. These friction factors were compared with a set of data obtained by Kamphuis (1975). Kamphuis' results were based on direct shear stress measurement.

To make a comparison between the friction factors obtained in this study with Kamphuis' data, the experimental results are drawn on a friction factor-Reynolds Number diagram Figure (9). The numbers in this graph denote the A_b / k_s related to each data point resulted from this study. The lines belong to the Kamphuis experimental data (1975). It can be seen that the agreement between the results of this study and those of Kamphuis in the range of experimental data is good.

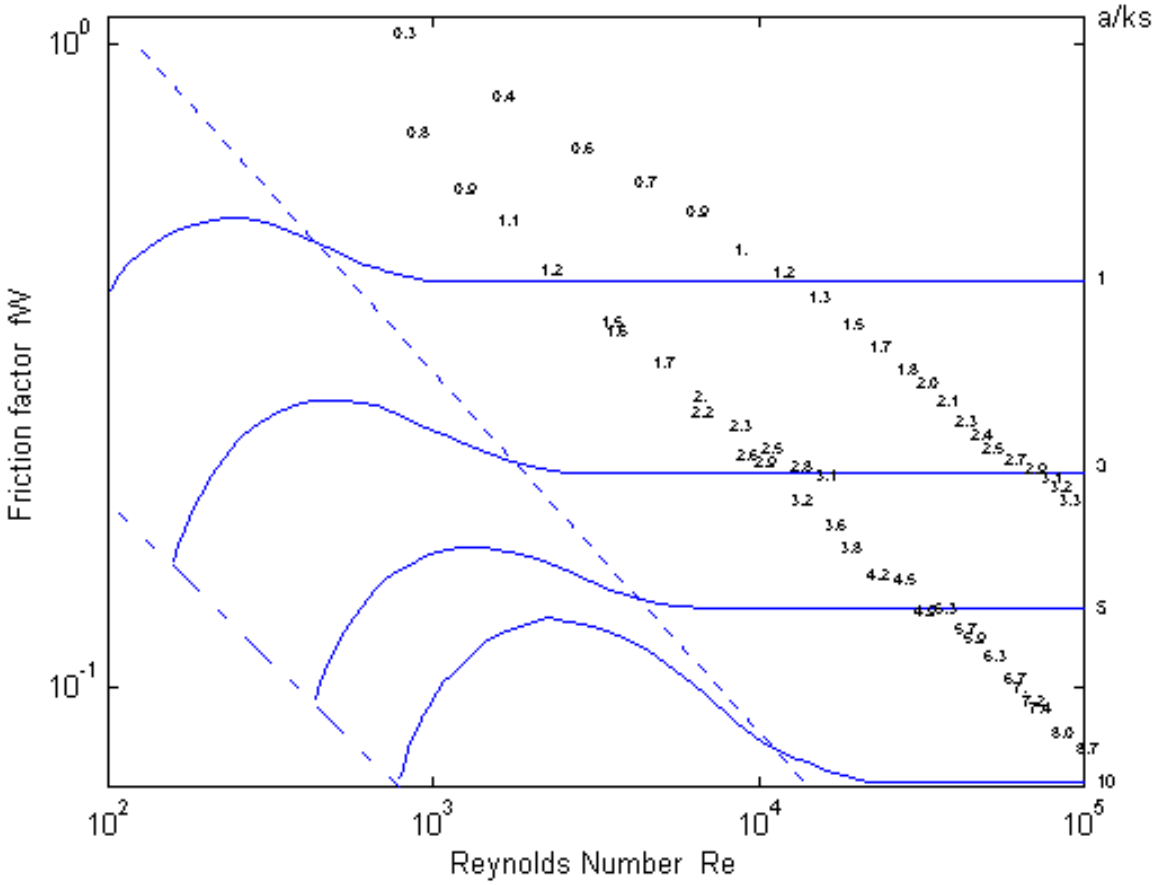

Figure 9 - Friction Factor Diagram, Comparison between Kamphuis Diagram and the Data in the Present Study. The Numbers Show the Values of A_b / k_s for the Experimental Data

6. CONCLUSION

In this study an instrument for direct measurement of shear stress under the action of monochromatic waves and wave spectrum on fixed beds was developed. It was observed that the results of the measurement were contaminated due to the action of the pressure gradient at the edge of the plate and roughness elements. However, it was demonstrated that by measuring the velocity field within the boundary layer this superfluous force could be calculated and filtered out.

Comparisons with previous laboratory experiments indicate that this approach is practical and the shear stress on fixed beds under pressure gradient can be directly measured. An improvement to this device can be achieved by installing pressure sensors to directly measure the pressure gradients on the both sides of the plate.

7. ACKNOWLEDGEMENT

The authors thank the technical staff of the School of Civil Engineering, University College, University of New South whales, for their support throughout this study.

8. REFERENCES

Simons, R.R. (1994). Bottom Shear Stresses in the Boundary Layers under Waves and Currents Crossing at Right Angles, *Proceedings of the 23rd International Conference on Coastal Engineering*, 1, pp 604-617.

Sleath, J.F.A (1988). Transition in Oscillatory Flow Over Rough Beds, *Journal of Waterway, Port, Coastal and Ocean Engineering*, 114 No. 1, pp 18-33.

Kamphuis J.W. (1975). Friction Factors under Oscillatory Waves. *Journal of Waterways, Harbors and Coastal Engineering, Proceedings of the American Society of Civil Engineers*, 101 No. ww2, pp 135-144.

Coates, R.C. et al (1972). *Structural Analysis*. First edition, Thomas Nelson and Sons Ltd London.

Jonsson, I.G. (1966). Wave Boundary Layer and Friction Factors, *Coastal Engineering Conference*, pp 125-148

The Institution of Engineers, Australia
8th National Conference on Hydraulics in Water Engineering
ANA Hotel Gold Coast, Australia 13-16 July 2004

A Finite Volume Solution for a Ring Tank Failure Parametric Study

A.F. Nielsen
B.E., M.Eng.Sci., M.I.E.Aust., C.P.Eng.
Manager, Coastal and Fluid Dynamics, SMEC Australia
C.A. Adamantidis
B.E., M.Eng.Sci.
Senior Engineer, Coastal and Fluid Dynamics, SMEC Australia
S.G. Roberts
B.Sc.(Hons), PhD (Maths),
Senior Lecturer, Mathematical Sciences Institute, Australian National University
C. Zoppou
B.E., PhD (Civil Eng),
Project Leader, Risk Modelling Project, Minerals and Geoharzards Division, Geosciences Australia

Abstract: A dam break analysis of ring tanks was carried out using an advanced 2-dimensional (*pseudo* 3D depth-averaged) finite volume numerical modelling algorithm. The objective was to determine the maximum extent of the *Failure Impact Zone* (where water flow depth exceeded 300 mm) for a range of embankment heights, storage volumes, flood plain bed slopes and Mannings *n* roughness coefficient. Combining the ranges of these parameters resulted in some 72 cases having been examined. The resulting data were analysed using a statistical package and a predictive equation was developed that allowed for the interpolation of the numerical experimental data.

Keywords: dam break; finite volume method; numerical modelling; ring tank.

1. INTRODUCTION

Within the Darling Downs area there is a proliferation of off-stream storages (known locally as ring tanks), which are used mainly for irrigation of broad-acre crops. Many ring tanks are sited close to dwellings, public roads and other infrastructure. The question arises as to the potential safety hazard in the event of dam failure.

The aim of this study was to examine the two dimensional effects of a ring-tank dam break on a floodplain. The objectives comprised carrying out a parametric study to obtain data to enable a standard solution for determining the extent of the *Failure Impact Zone* of ring tanks in Queensland.

The study was conducted in accordance with the Queensland Government Guidelines for Failure Impact Assessment of Water Dams (Queensland Government Natural Resources and Mines, 2002). These Guidelines define the *Failure Impact Zone* of a dam break as the area where the incremental effect of a dam break flood is 300 mm or higher. To this end, this study aimed to produce a methodology whereby the extent of the *Failure Impact Zone* could be determined readily for various dam and floodplain parameters, namely:

- the slope of the surrounding terrain;
- the Mannings *n* roughness of the surrounding terrain;
- the capacity of the dam; and
- the height of the dam embankment.

2. NUMERICAL ANALYSIS

2.1 Modelling Programs

Numerical modelling programs for the analysis of the two-dimensional dam-break problem attempt to solve the shallow water Saint-Venant wave equations. It is the hyperbolic character of the shallow water wave equations

that makes finding solutions to these equations difficult. Hyperbolic equations admit discontinuous and smooth solutions. Even for the case in which the initial conditions are smooth, the non-linear character combined with the hyperbolic type of the equations can lead to discontinuous solutions in finite time. The non-linear character of these equations also means that analytical solutions to these equations are limited to only very special cases. Therefore, numerical methods generally are used to obtain solutions to practical problems.

Numerical methods that can be used to solve the shallow water wave equations include the *method of characteristics*, *finite differences*, *finite-elements* and *Godunov-type* schemes. Each of these methods have limitations as described in the following:

- The characteristics associated with the governing equations converge at a shock. The method of characteristics cannot be used to follow the propagation of the shock, so a shock fitting approach is required. This makes the use of the method of characteristics very complicated for practical problems, especially for two-dimensional problems.

- Irregular geometry associated with the dam break problem in two space dimensions are poorly described using finite difference grids.

- Finite elements seem to have difficulty if subcritical and supercritical flows are present either simultaneously in different parts of the channel, or if they occur in sequence at different times.

- The local initial value problem which solves the shallow water wave equations, involving discontinuous neighbouring states is known as the *Riemann* problem. Numerical schemes based on the solution of local Riemann problems are generally known as Godunov-type schemes. Their main advantages are that they are robust and capture accurately the location of discontinuities such as shocks and contact surfaces. Two-dimensional Riemann solvers do not appear to have matured enough to be used in the construction of multi-dimensional schemes. Even if such solvers were available, the resulting schemes are likely to be too complicated for common use. Recently, a number of efficient one-dimensional approximate Riemann solvers have been proposed. These can be used to solve the two-dimensional dam break problem on a Cartesian grid using *fractional step* or *splitting techniques.*

The modelling programs that are available commercially and, hence, most likely to be used by consulting engineers for the assessment of the *far-field* effects of a dam break of a referable dam would include TUFLOW, MIKE-21 or SOBEK 1D/2D (DELFT-FLS). These programs use a finite difference solution scheme on a regular rectangular grid. Another program that may be used also is RMA-2, which uses a finite element solution scheme that provides a variable mesh that may have some advantages in modelling an expanding flow path.

All of these programs require, as input, the *near-field* schematisation of the actual dam-break mechanism and the resulting dam-break hydrograph. The most reliable *near-field* schematisation of the wall failure and resulting input hydrograph that is available commercially is the US NWS FLDWAV (formerly NWS DAMBRK) program. This is a one-dimensional (1D) modelling program based on an implicit finite difference solution to the 1D Saint-Venant equations. Therefore, the commercial analysis of the dam-break problem requires the synthesis of 1D and 2D modelling programs.

The *Finite Volume Method* (McDonald, 1971) can be used to solve the two-dimensional problem. Like finite elements, the major advantage of the finite volume method is that it can be applied to any unstructured grid. Generally, the finite volume method requires less computational effort than finite elements because it involves the solution of a local one-dimensional Riemann problem, which can be solved efficiently.

The *approximate Riemann solver* developed by Toro (1989) was found to be robust and efficient for solving the dam break problem. Unlike many other schemes, such as finite differences and other approximate Riemann solvers, it avoids the problems associated with sonic points, where a non-physical expansive shock is produced.

The finite volume method and the first-order approximate Riemann solver developed by Toro (1989) have been chosen to solve the shallow water wave equations in two-dimensions. Such a finite volume modelling program is presented in Zoppou and Roberts (2003), which was chosen for this study and was used for both the near-field and far-field two-dimensional analysis. This modelling program is based upon a robust and stable finite volume method, structured around a triangular grid. The modelling program was chosen over other available programs because the robust algorithm is able to solve the shallow water equations over two dimensional space with an initially dry bed, providing a complete 2D solution (*pseudo*-3D - depth-averaged) over the modelling domain.

2.2 Model Parameters

2.2.1 Parametric Ranges

This study used numerical modelling to produce data that covered the range of parameters associated with ring tanks in Queensland. The range of data examined for this problem included:

- embankment heights (h) of 5.0 m, 8.0 m and 10.0 m;
- storage volumes (V_w) of 250 ML, 500 ML, 1000 ML and 2000 ML;
- bed slopes (S) of the surrounding terrain of 0%, 0.05% and 0.10%; and
- Mannings n roughness coefficients (n) of 0.02 and 0.05.

Combining these parameters resulted in some 72 cases having been examined for this study. As these values covered the typical range of parameters associated with ring tanks in Queensland, it becomes possible to use interpolation for cases with parameter values intermediate to those specified above.

2.2.2 Model Schematisation

The model was set up on a regular two-dimensional triangular grid, with a node spacing of 10 metres. This grid spacing allowed for the accurate calculation of the breach flow paths as well as the accurate schematisation of the breaches and dam volumes. It has also allowed reasonable computation times for the model. For some cases, the grid spacing was set to 5 metres to represent the dam breaches more accurately.

The dam walls were schematised as *reflective* boundaries, whereas the edges of the model domain were *transmissive* boundaries. Reflective boundaries do not allow the passage of water and reflect the flow back into the model domain. Transmissive boundaries allow flow to pass through them so that flow, which reaches the edges of the two-dimensional model domain, flows out of the domain and is not reflected back into the model domain.

2.2.3 Breach Size

The procedure used to calculate the breach size was adopted from "The Guidelines for Failure Impact Assessment of Water Dams" (Natural Resources and Mines, 2002). This procedure was followed, assuming instantaneous breach formation (piping failure). A *Breach Formation Factor* (*BFF*) for each dam was calculated based on the following:

$$BFF = V_W \times h \tag{1}$$

where:

V_W = total volume of water to flow through the breach (ML); and
h = height of the dam embankment.

The Guidelines provide an empirical relationship between the *BFF* and the volume of material removed from the breach. This empirical relationship is based on a considerable scattering of data (as is evidenced in the Guidelines). Nevertheless, the empirical relationship is given by:

$$V_m = 10^{\left[\frac{\log(BFF)-3.2553}{1.0787}+3\right]} \tag{2}$$

where:

V_m = volume of material removed from the breach;
BFF = Breach Formation Factor

For the dam embankment heights and volumes considered for this problem, the volume of material removed from the breach is shown in Table 1. Moore and Power (2002) give typical section dimensions for dam embankments for ring tanks in the Darling Downs in Queensland. These comprise side slopes of 2.5:1 (outer) and 3:1 (inner). We have assumed an embankment crest width of 1m. These dimensions have been adopted for calculation of the breach widths for the ring tanks in this study, based on the volume of material removed and on the assumption that the breach shape is rectangular with the same top and bottom widths. The dimensions are given in Table 1.

Table 1. Volume of Material Removed for Dam Breach

V_w (ML)	h (m)	Dam Dimensions (m)	BFF	V_m (m^3)	Breach Width[(1)] (m)
250	5	223.6	1250	713	9.67
250	8	176.8	2000	1,103	5.99
250	10	158.1	2500	1,356	4.76
500	5	316.2	2500	1,356	18.39
500	8	250.0	4000	2,096	11.39
500	10	223.6	5000	2,578	9.05
1,000	5	447.2	5000	2,578	34.96
1,000	8	353.6	8000	3,986	21.66
1,000	10	316.2	10000	4,902	17.20
2,000	5	632.5	10000	4,902	66.47
2,000	8	500.0	16000	7,579	41.19
2,000	10	447.2	20000	9,320	32.70

Notes: (1) Assumes that side slopes are 3:1 and 2.5:1 with 1m wide crest.

For the dimensions of the embankment adopted, the breach width becomes a function of the dam capacity and embankment height through the Breach Formation Factor. As storage capacity (V_w) and embankment height (h) are two of the four independent variables used in the study, the interpretation of these results can investigate the introduction a fifth variable, being breach width, as V_w/h. The Guidelines provide ranges for the following parameters:

$0.84 < B/d < 10.93$ – ratio of breach width to breach depth; and

$1.06 < B/b < 1.74$ – ratio of the length of the top of the breach to the bottom of the breach.

The range of data that has been selected has B/d ratios varying from 0.48 to 13.29, thus encompassing the entire specified range for B/d. However, B/b is always equal to unity for the model runs used in this study.

2.3 Modelling Assumptions

The following assumptions were adopted for this analysis:

1) the breach forms instantaneously due to piping failure;

2) the ring tanks are square in shape and the side walls are infinitely thin for the purposes of calculating the dam storage capacity;

3) the surrounding terrain, initially, is dry;

4) the slope of the dam floor is the same as the slope of the surrounding terrain;

5) the breach is rectangular in shape, with the same top and bottom widths;

6) the breach size conforms to the parameters outlined in “The Guidelines for Failure Impact Assessment of Water Dams”.

These assumptions do not affect the accuracy of the computation. Instantaneous breach formation would be expected for a piping failure mechanism for the dams, and gradual overtopping failures have not been considered for this analysis.

3. RESULTS

A typical model output schema is presented in Figure 1. The dependent variable, *Distance*, is the farthest distance that the flow reaches before its depth falls to 300 mm, which, generally, is directly in front of the breach (Figure 1).

The impact of cross-slope drainage on the ring tank failure results is illustrated in Figure 2. This shows the failure of a 5 m high embankment for a 2,000 ML storage failing across a flood plain of slope 0.1% with Mannings *n* of 0.02. For this case, the maximum flow distance to the 300 mm depth was computed to be 1,880 m downslope, which compared with 2,120 m for the direct downslope failure. Across the slope, the flow to a depth of 300 mm extended 800 m.

Figure 3 presents the relationship between the maximum distance to the *Failure Impact Zone* and dam Volume for various Flood Plain Slopes and Mannings *n* for a 5 m high ring tank. The graphs illustrated the high sensitivity of the extent of the *Failure Impact Zone* to the dam capacity, as well as to flood plain slope. Variation in Mannings *n* had a relatively low impact on the result.

The results indicated also that there was not a consistent relationship between distance and embankment height and that the distance was not strongly related to embankment height (not presented). For the smaller dams, generally, the distance increased with increasing embankment height, with an increasing rate of increase for the higher structures. However, for the larger structures, this tendency was reversed.

For small ring tanks, flood plain slope was not significant in defining the extent of the *Failure Impact Zone*. However, flood plain slope was very significant for the larger capacity structures.

For the range of values tested, the maximum distance to the *Failure Impact Zone* was not very sensitive to Mannings *n*.

4. PREDICTION OF FAILURE IMPACT ZONE

A multiple regression analysis of the data points was undertaken following the method in Devore (1995). A third order interaction model was considered as well as the additional predictor, V_w/h. This predictor represented breach width and was considered to be a realistic parameter in defining *D*. The following predictor equation was developed:

$$D = 3.181\ V_w - 222.5\ h - 379.1\times10^3\ S - 1.308\times10^3\ n - 1.391\times10^{-4}\ V_w^2 + 16.46\ h^2 + 3.464\ n\ V_w - 0.1782\ h\ V_w + 724.1\ s\ V_w + 6.806\times10^6\ S\ n - 8.373\ V_w/h + 841 \quad (3)$$

where:

D = maximum extent of *Failure Impact Zone* (m);

V_w = ring tank storage volume (ML);

S = bed slope;

h = embankment height (m); and

n = Mannings *n* roughness coefficient.

This equation allowed for the interpolation of the numerical experimental data to an accuracy of ±150 m for all the results and better than ±30 m for 50% of the results.

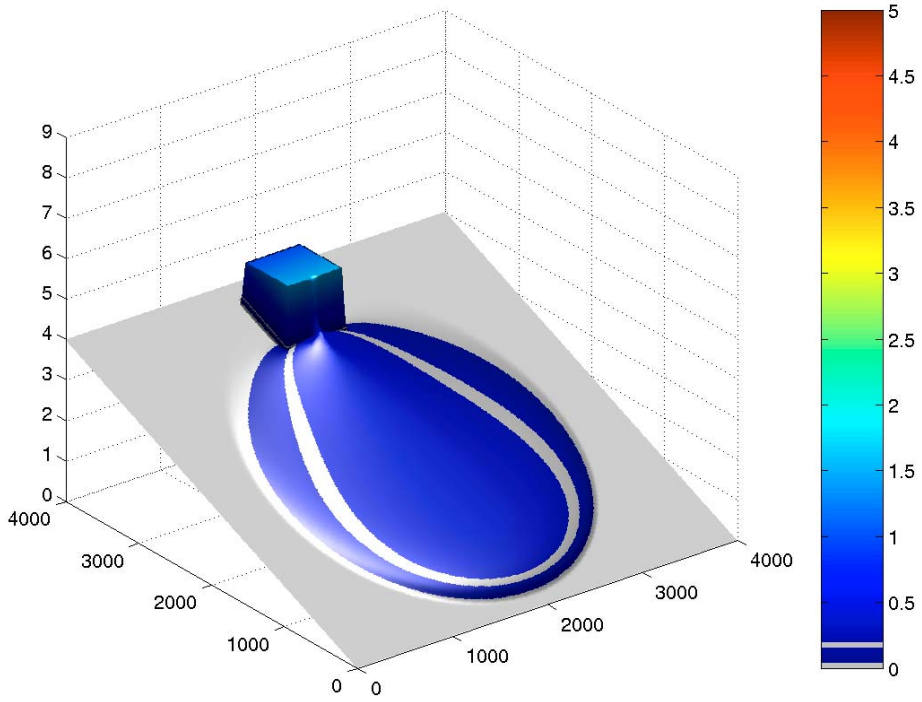

Figure 1. Model schema of a 5 m high, 2000 ML dam break on a 0.1% slope. The 300 mm depth contour is shown as white band. The maximum distance is directly in front of the breach.

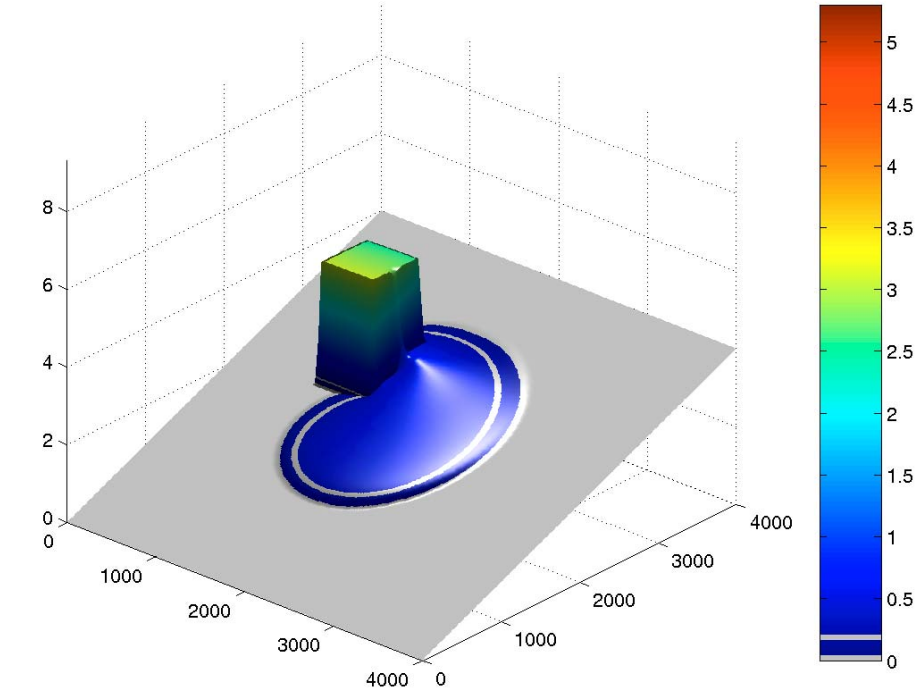

Figure 2. Model schema of a 5 m high, 2000 ML dam break on a 0.1% side slope. The 300 mm depth contour is shown as white band. The maximum distance is directed down slope rather than directly in front of the breach, as compared with Figure 1.

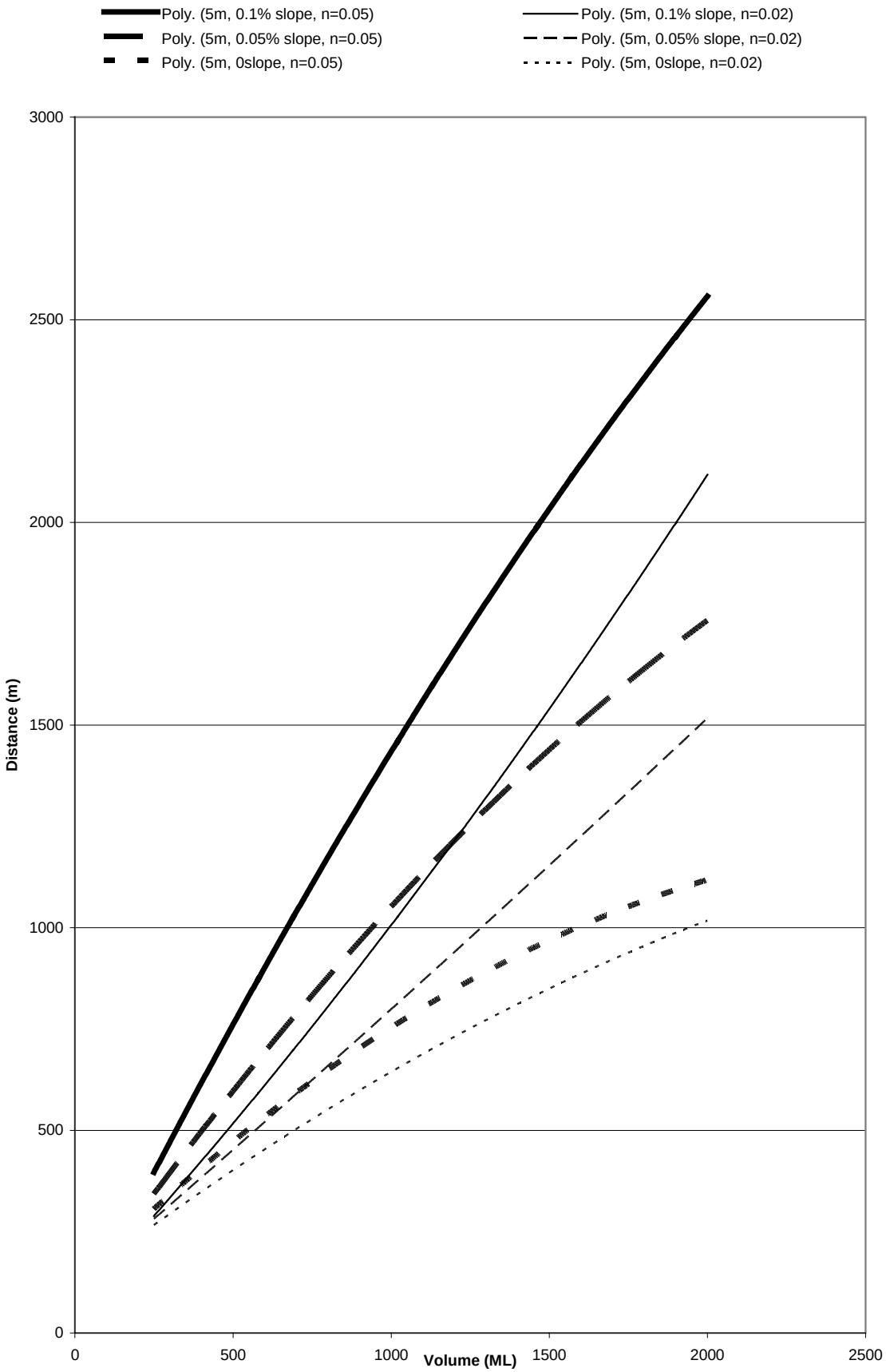

Figure 3. Relationship between the Maximum Distance to the *Failure Impact Zone* and dam Volume, Flood Plain Slope and Mannings *n* for a 5 m high ring tank

5. CONCLUSIONS

A dam break analysis of ring tanks has been carried out using an advanced 2-dimensional (*pseudo* 3D depth-averaged) finite volume numerical modelling algorithm. The objective was to determine the maximum extent of the *Failure Impact Zone* (where water flow depth exceeded 300 mm) for a range of data including:

- embankment heights (h) of 5.0 m, 8.0 m and 10.0 m;
- storage volumes (V_w) of 250 ML, 500 ML, 1000 ML and 2000 ML;
- flood plain bed slopes (S) of the surrounding terrain of 0%, 0.05% and 0.10%; and
- Mannings n roughness coefficients (n) of 0.02 and 0.05.

Combining these parameters resulted in some 72 cases having been examined. The resulting data were analysed using a statistical package and a predictive equation was developed. It was found that the ring tank storage volume and the flood plain bed slope were the most important variables determining the maximum extent of the *Failure Impact Zone*.

The *Finite Volume Method* for solving the shallow water equations (Zoppou & Roberts, 2003) that was used for the analysis proved to be a robust algorithm, allowing for the numerical simulation of flow over an initially dry bed and allowing for mixed supercritical and subcritical flow over the modelling domain.

6. REFERENCES

Devore, J.L. (1995). *Probability and Statistics for Engineering and the Sciences*, Duxbury Press, Belmont.

McDonald, P.W. (1971). The computation of transonic flow through two-dimensional gas turbine cascades, *American Society of Mechanical Engineers*, Paper 71-GT-89, 1971.

Moore, K.A. & R.K. Power (2002). Safe buffer distances for offstream earth dams, *Aust. J. of Water Resources*, IEAust, 2002; 6(1):1-16.

Natural Resources and Mines (2002). Guidelines for failure impact assessment of water dams, *Queensland Government Department of Natural Resources and Mines* Publication QNRM02014, April, 2002.

Roberts, S.G. & C. Zoppou (2000). Robust and efficient solution of the 2D shallow water equation with domains containing dry beds, *ANZIAM J*. 42 (E) pp C1260-C1282, Nov., 2000.

Toro, E.F. (1989). A weighted average flux method for hyperbolic conservation laws, *Proceedings of the Royal Society*, Series A, 423, 401-418, 1989.

Zoppou, C. & S.G. Roberts. (2003). Explicit schemes for dam-break simulations. *Journal of Hydraulic Engineering, American Society of Civil Engineers*, 129(1), 11-34.

The Institution of Engineers, Australia
8th National Conference on Hydraulics in Water Engineering
ANA Hotel Gold Coast, Australia 13-16 July 2004

1-D and 2-D Hydraulic Modelling of Extreme Floods in a Steep Urban Stream

B.C. Phillips
B.E. (Civil), M.Eng.Sc, Ph.D., F.I.E.Aust.
Director, Cardno Willing (NSW) Pty. Ltd, Sydney, Australia
B.Boon
B.E., E.W.S (Vic), H.E.C (Tas)., M.I.E.Aust.
Director, Thompson & Brett Pty. Ltd, Hobart, Australia

Abstract: Humphreys Rivulet drains a steep forested catchment of 17 km^2 in area in the City of Glenorchy in Hobart Tasmania. It flows northeast through residential and light industrial areas and the CBD of Glenorchy to Elwick Bay on the estuary of the Derwent River. There are three water supply storages within the catchment: Knights Creek, Limekiln Gully and Tolosa Park Reservoirs

Building on a series of flood and floodplain management studies undertaken in 1997 and 1999, Hobart Water and Glenorchy City Council embarked on an additional study to define inundation resulting from hypothetical dam break of Knights Creek Reservoir (for dam risk assessment) and inundation resulting from infrequent floods (for early evacuation planning). The hydrological and hydraulic investigations of the Humphreys Rivulet and Barossa Creek floodplains are outlined. A number of 2-D hydraulic models that were trialled and failed to model the Humphreys Rivulet floodplain are also briefly discussed.

It is concluded that as a result of the hydrological and hydraulic modelling investigations that Council and Hobart Water are now better informed about the inundation that could result from the failure of Knights Creek Reservoir and the inundation resulting from infrequent floods and the ramifications for early evacuation planning.

Keywords: Hydrology, Dambreak, 1-D Hydraulic modelling, 2-D Hydraulics modelling , Flood mapping.

1. INTRODUCTION

The Humphreys Rivulet catchment and Barossa Creek catchments both catchments rise on Mount Wellington and flow down into Elwick Bay on the Derwent River. The boundaries of these two catchments are shown in **Figure 1**. The Glenorchy CBD lies also within these two catchments. Humphreys Rivulet drains a steep forested catchment of 17 km^2 in area in Glenorchy. It flows north-east through a built-up area of Glenorchy to Elwick Bay on the estuary of the Derwent River. Most of the catchment remains uncleared being protected as a water supply and wildlife sanctuary.

There are three water supply storages within the catchment: Knights Creek, Limekiln Gully and Tolosa Park Reservoirs. The catchment boundary reaches an altitude of 1,250 metres above Australian Height Datum (AHD) in the south on the lower pinnacles of Mount Wellington and 800 m AHD in the west on Mount Hull.

The slope of the Rivulet is steep which can give rise to high velocity flows that are capable of scouring the stream bed and transporting gravel and small boulders down into the lower reaches. Despite being comparatively flatter in its lower reaches, the Rivulet remains steep by Australian standards. The average bed slope of the Rivulet from Wariga Road downstream to the Brooker Highway is around 2%.

The Barossa Creek catchment has an area of around 5 km^2. In the upper catchment there are steep rocky slopes with lightly timbered scrubby areas and wet sclerophyll gullies. In the mid and lower catchment there is a range of urban landuses from predominantly residential and commercial to some industrial areas. The catchment is not gauged for rainfall or flow nor are there any storages in the catchment. Barossa Creek itself comprises a series of reaches of landscaped and/or overgrown "natural" channel alternating with channelised or piped reaches.

Residential development has occurred on the floodplains of both Humphreys Rivulet and Barossa Creek. A number of residential properties located on both floodplains can be inundated by floodwaters depending on the severity of floods. This was most recently demonstrated when Humphreys Rivulet experienced major floods on 19th December 1995; 9th February 1996 and 17th April 1996 (Thompson & Brett - Willing & Partners, 1997; Phillips et al, 2001)

Subsequent to hydrological, hydraulic and sediment transport modelling investigations that were undertaken as part of a program to develop and implement a comprehensive flood mitigation strategy for the streams and watercourses of the City of Glenorchy (Phillips et al, 2001) a further study was commissioned by Hobart Water and Glenorchy City Council to define inundation resulting from hypothetical dam break (for dam risk assessment) and inundation resulting from infrequent floods (for early evacuation planning).

2. HYDROLOGY

A detailed XP-RAFTS rainfall/runoff model of the Humphreys Rivulet catchments was assembled and used to estimate flood hydrographs. The model was a modified version of the XP-RAFTS rainfall/runoff model created in 1997. The model is described in detail in Thompson & Brett – Cardno Willing, 2002).

2.1 Water Storages

Only Knights Creek Reservoir and Lime Kiln Gully Reservoir were included in the catchment model on the basis that it is very likely that Tolosa Park Reservoir will be de-commissioned and removed in the near future. Hydraulic data for each reservoir was derived from available information.

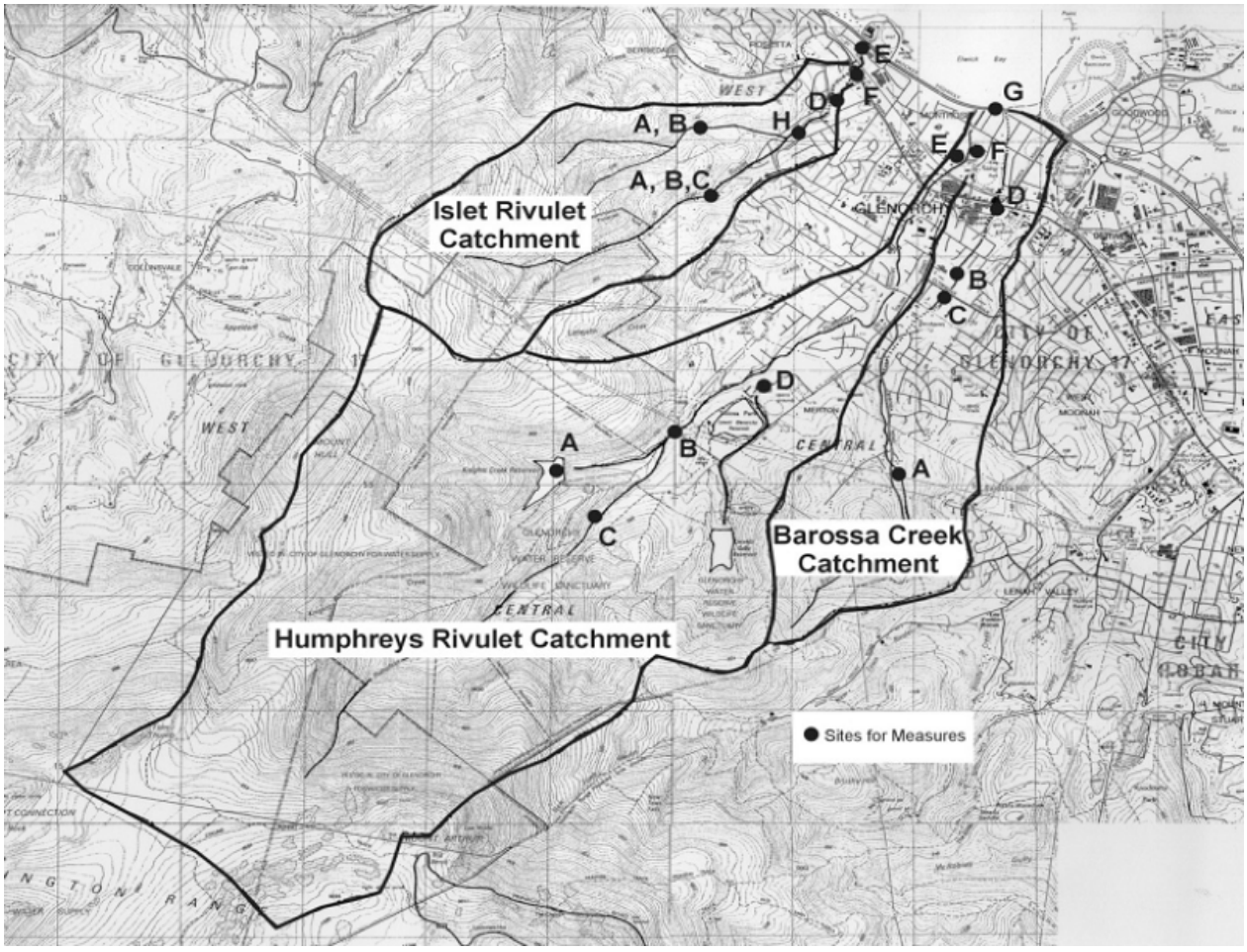

Figure 1 Humphreys Rivulet and Barossa Creek Catchment Locations

2.2 Rainfall

In a previous 1997 study, the Humphreys Rivulet catchment was divided into two rainfall zones (Phillips et al, 2001). The same rainfall zones were adopted for this study for storms up to the 2,000 yr ARI event (see **Figure 2**).

FORGE rainfall estimates for storms from 50 yr ARI to 2,000 yr ARI of durations from 0.25 to 72 hours were obtained from the HEC (Hydro Electric Commission (Tasmania)). Probable Maximum Precipitation (PMP) estimates for the Humphreys Rivulet catchment up to 6 hours duration were prepared using the GSDM procedures given in the Bureau of Meteorology's (BoM) Bulletin 53. Estimates of the rainfall intensities for storms between the 2,000 yr ARI and PMP events were prepared in accordance with the practice recommended in Book 6, AR&R, 1999.

Initial rainfall loss rates for pervious areas ranging from 20 mm (storms ≤ 100 yr ARI) to 0.0 mm (10,000,000 yr ARI) were adopted while the continuing rainfall loss rates for pervious areas varied from 2.5 mm/h (storms ≤ 100 yr ARI) to 0.0 mm/h (10,000,000 yr ARI). The adopted rainfall losses for impervious areas were 1.5 mm and 0.0 mm/h for all storms.

3. FLOOD FREQUENCY

3.1 Inflow Frequency Curves

The XP-RAFTS model was run for the 50 yr ARI, 100 yr ARI, 1,000 yr ARI, 2,000 yr ARI, 10,000 yr ARI, 100,000 yr ARI, 1,000,000 yr ARI and 10,000,000 yr ARI events for multiple storm durations to determine the peak inflows for both reservoirs and also at Node HR-14 near Wariga Avenue (the reference location adopted in the 1997 study). All these runs were for the case where both reservoirs are at 100% supply levels.

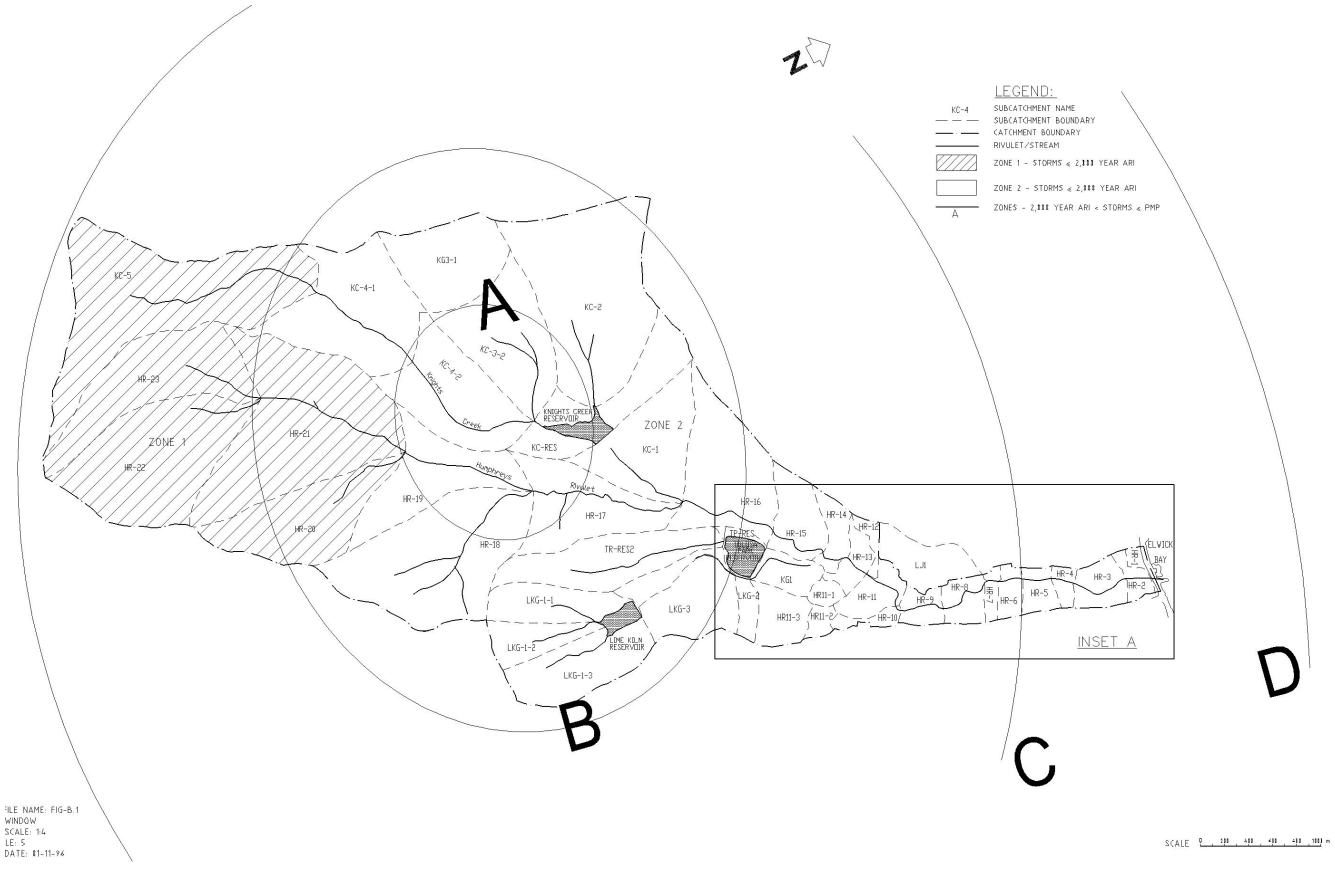

Figure 2 Humphreys Rivulet Catchment Rainfall Zones

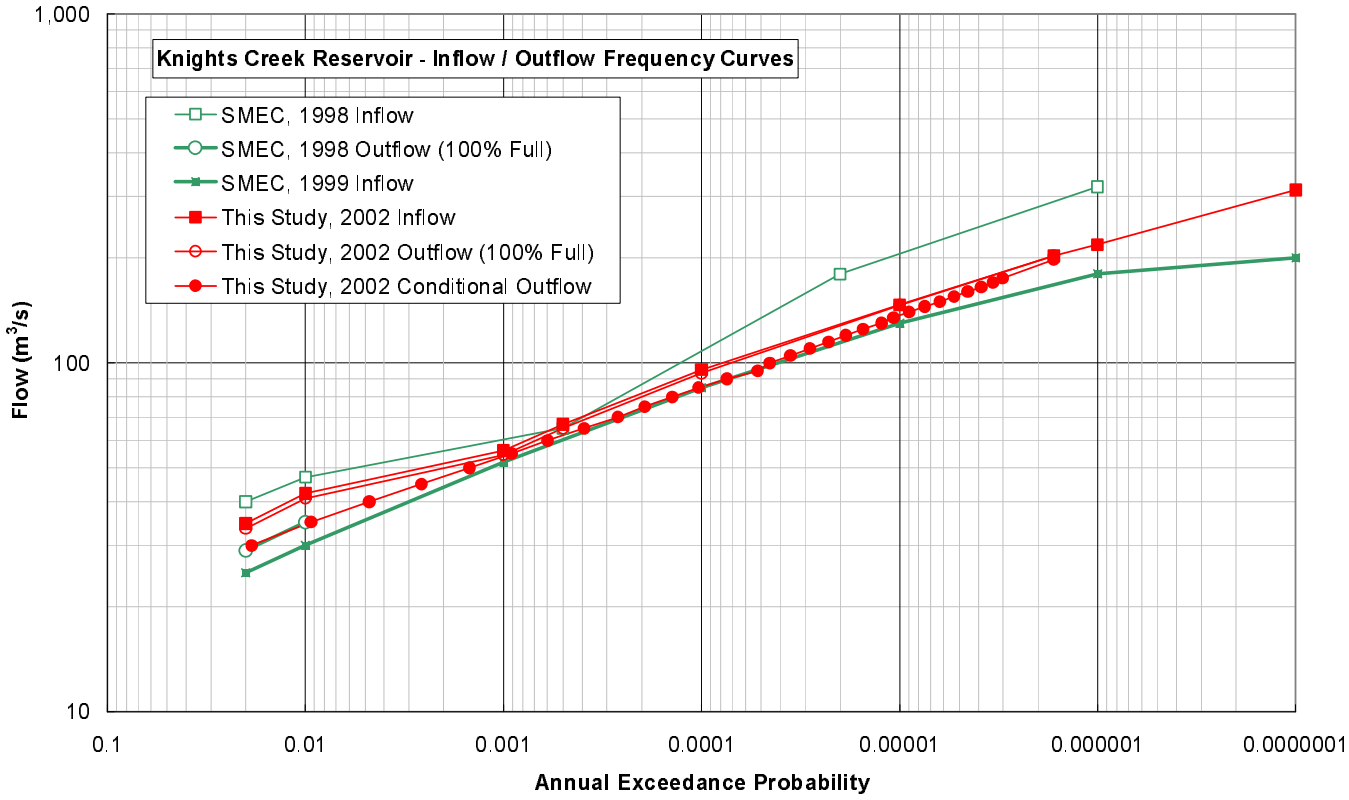

Figure 3 Knights Creek Reservoir Inflow and Outflow Frequency Curves

3.2 Outflow Frequency Curves

Outflow frequency curves were also plotted for the 100% full supply case for comparison with SMEC, 1998 and 1999 curves (refer **Figure 3**).

A conditional outflow probability analysis of both Knights Creek and Limekiln Gully Reservoirs was also undertaken in accordance with the procedure given in Section 8.4 in Book 6, AR&R, 1999. Based on the inflow frequency curve, historical variations in reservoir levels and the calculated outflow frequency curves for the 100% full, 80% full, 60% full and 40% full initial reservoir conditions, the conditional outflow frequency curves were calculated for both Knights Creek (refer Figure 3) and Limekiln Gully Reservoirs.

A comparison of 50 yr ARI and 100 yr ARI peak flows at Node HR-14 is given in **Table 1**.

Table 1
Comparison of 50 yr ARI and 100 yr ARI peak flows at Node HR-14

ARI (years)	1997 Study	2002 Study (100% Full)	2002 Study (Conditional Outflow)
50	72.1	89.2 (+24%)	Approx 69.8(-3%)
100	87.8	108.5(+24%)	Approx 92.4(+5%)

4. DAM BREAK AND SUNNY DAY FAILURE HYDROGRAPHS

For the dam beak scenarios, hydrographs immediately downstream of Knights Creek Reservoir and /or Limekiln Gully were determined using DAMBRK for the following scenarios:

(i) Dam Crest Flood (DCF) for Knights Creek Reservoir and Limekiln Gully Reservoir;
(ii) DCF + Dam Break of Knights Creek Reservoir only; and
(iii) Sunny Day Failure of Knights Creek Reservoir only

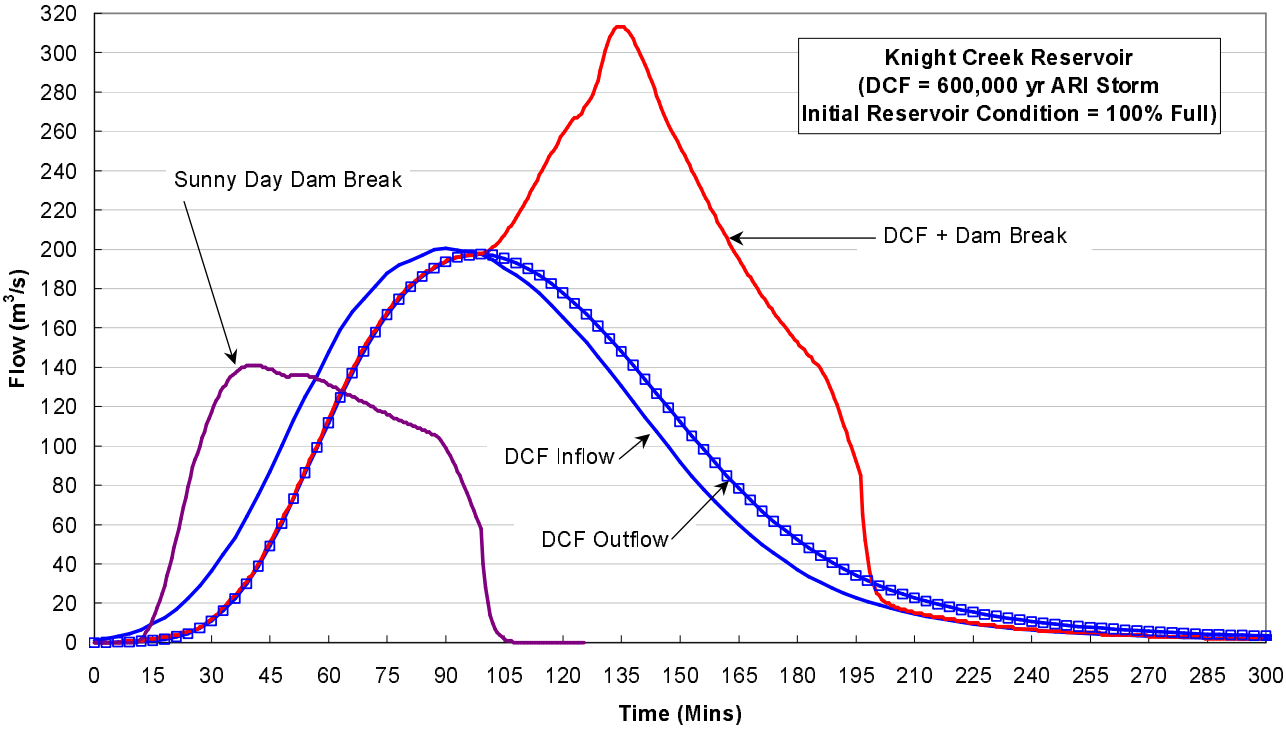

Figure 4 Dam Break and Sunny Day Failure Hydrographs – Knights Creek Reservoir

The adopted initial condition for Knights Creek Reservoir at the start of the DCF storm was the reservoir 100% full while the assumed operational condition of Limekiln Gully Reservoir at the start of the DCF storm was a reservoir level 1.3 m below the primary spillway level (ie. equivalent to around 84% full).

The breach formation parameters adopted by SMEC, 1999 for Knights Creek Reservoir were initially adopted for this study. These parameters were adjusted to reflect the dam upgrading works as appropriate.

The calculated DCF + Dam Break and Sunny Day Failure hydrographs for Knights Creek Reservoir are plotted in **Figure 4**. The breaching of Knights Creek Reservoir during the DCF increases the peak flow immediately downstream of Knights Creek Reservoir from around 200 m^3/s up to around 312 m^3/s. This is equivalent to the peak outflow in around an 8,000,000 yr ARI storm. The peak outflow under a Sunny Day Failure is around 140 m^3/s. Ignoring any attenuation due to routing of flows from Knights Creek Reservoir down to Node HR-14, the peak flow in the Sunny Day Failure equates to around the peak flow in Humphreys Rivulet in a 1,000 yr ARI storm.

5. 1-DIMENSIONAL HYDRAULICS

Two 1-D flood routing model of Humphreys Rivulet were created during previous studies. An XP-SWMM hydrodynamic model was created in 1997 to estimate design flood levels in Humphreys Rivulet. DAMBRK models of Humphreys Rivulet that extend from the Brooker Highway upstream to the Knights Creek Reservoir and Lime Kiln Gully were created in 1999 to estimate flood levels extreme flood and dambreak scenarios.

A modified XP-SWMM model was run to estimate revised 50 yr ARI and 100 yr ARI flood levels in Humphreys Rivulet. The DAMBRK model was used to assess flooding under the dambreak scenarios:

Inflow hydrographs were directly input into the hydraulic model in the form of an interface file of hydrographs generated by XP-RAFTS for both Humphreys Rivulet and Barossa Creek catchments.

Based on the outcome of the conditional outflow analysis, Knights Creek Reservoir was assumed to be 82% full and 78% full at the start of the 50 yr ARI and the 100 yr ARI storms respectively.

It was found that the revised 100 yr ARI flood levels in Humphreys Rivulet are higher in most locations than the estimates reported in 1997. These increases are attributed to:

(i) An increase in the peak outflows from Knights Creek Reservoir due to the spillway augmentation works notwithstanding the adoption of lowered starting reservoir levels; and the
(ii) Hydraulic routing of outflows from Knights Creek Reservoir and Limekiln Gully Reservoir in comparison with the hydrological routing that was undertaken in the 1997 study.

Based on a review of the results of the preliminary modelling by Hobart Water, the final model runs were based on the following conditions:

(i) The 100,000 yr ARI flood to be combined with breaching of Knights Creek Reservoir. The flood to include 100,000 yr ARI outflows from Limekiln Gully Reservoir and 100,000 yr ARI inflows from Barossa Creek and Littlejohn Creek; and
(ii) Sunny Day Failure of Knights Creek Reservoir only.

6. 2-DIMENSIONAL HYDRAULICS

Based on the cross section data that was collected for the previous Humphreys Rivulet study and the SMEC, 1999 study, a 2-D floodplain model was assembled for the Humphreys Rivulet, Barossa Creek and Littlejohn Creek floodplains from around Wariga Road downstream to the Brooker Highway.

An initial 2-D model was assembled using the BOSS SMS modelling package. A feature of the model was that despite being comparatively flatter in its lower reaches Humphreys Rivulet is a steep urban stream by Australian standards. The average bed slope of Humphreys Rivulet from Wariga Road downstream to the Brooker Highway (the 2-D model domain) is around 2% ie. a fall of 90 m over a distance of around 4.5 km. A feature of the SMS modelling system is that the 2-D model needs to start drowned with the water surface drawn down until it reaches the desired initial condition prior to the commencement of the period to be simulated. It was found that the SMS RMA-2 "engine" was unable to complete this drawn down process ie. the model crashed prior to even starting a run. This problem was attributed to the large elevation difference between the upstream and downstream boundary conditions ie. 90 m. In an attempt to overcome this problem two other numerical "engines" were trialled. Both the FESWM and HIVEL engines also proved to be incapable Humphreys Rivulet and its floodplain.

Consequently a fourth 2-D modelling package was trialled and this proved to be capable of modelling a range of floods for Humphreys Rivulet and its floodplain. This package was TUFLOW.

TUFLOW is a computer program for simulating depth-averaged, two and one-dimensional free surface flows such as occurs from floods and tides. TUFLOW was originally developed for just Two-dimensional Unsteady FLOWs. It also incorporates, the full functionality of the ESTRY 1-D network or quasi-2D modelling system based on the full one-dimensional (1-D) free-surface flow equations. The 2-D solution algorithm is based on Stelling, 1984 and was presented in Syme, 1991. It solves the full two-dimensional, depth averaged, momentum and continuity equations for free-surface flow.

Using the available survey information, a digital elevation model (DEM) of this study area was created. This formed the basis of all subsequent 2-D modelling. A digital grid was generated that accommodates all the floods to be modeled. The model used a grid of 4m square cells. Elevation values were assigned to the TUFLOW grid at 2m intervals. Elevations are assigned to each cell's center, mid-sides and corners. Along the Brooker Hwy and for the levee from just south of Young St to Grove Rd, elevations were adjusted to represent these hydraulic controls.

At bridge structures, "lids" were placed on the cells to represent the bridge deck. Flow over the top of the bridges was modeled using embedded 1-D weir structures. Culverts under the Brooker Hwy were modeled as 1-D embedded culverts and pipes.

The hydraulic roughness of the floodplain and waterways was classified into 3 categories. The categories of land use and waterway, and their adopted roughness values were as follows:

Humphreys Rivulet	0.05	Roads	0.02
Properties	0.20	(buildings, fences, gardens, etc)	

The TUFLOW model was run for the 100,000 yr ARI + dam break flood and the results were compared with the results from other modeling to establish the need or otherwise to adjust model parameters in the 2-D model. Upon completion of model adjustments, the 2-D hydraulic model was run for the following flood events:

(i) The 100,000 yr ARI flood combined with breaching of Knights Creek Reservoir;
(ii) Sunny Day Failure of Knights Creek Reservoir only;
(iii) The 100 yr ARI flood; and
(iv) The 50 yr ARI flood.

The results of the TUFLOW model runs were in turn used to prepare inundation / floodplain maps and hazard maps.

Notwithstanding a modest increase in the calculated peak 100 yr ARI flood flow, the predicted extent of flooding in the 100 yr ARI event was greater than expected. It was noted that the calculated depth of floodwaters on the floodplain outside of areas that have been historically subject to inundation eg. Fleming Street area is shallow being typically less than 0.1 m deep (refer **Figure 5**).

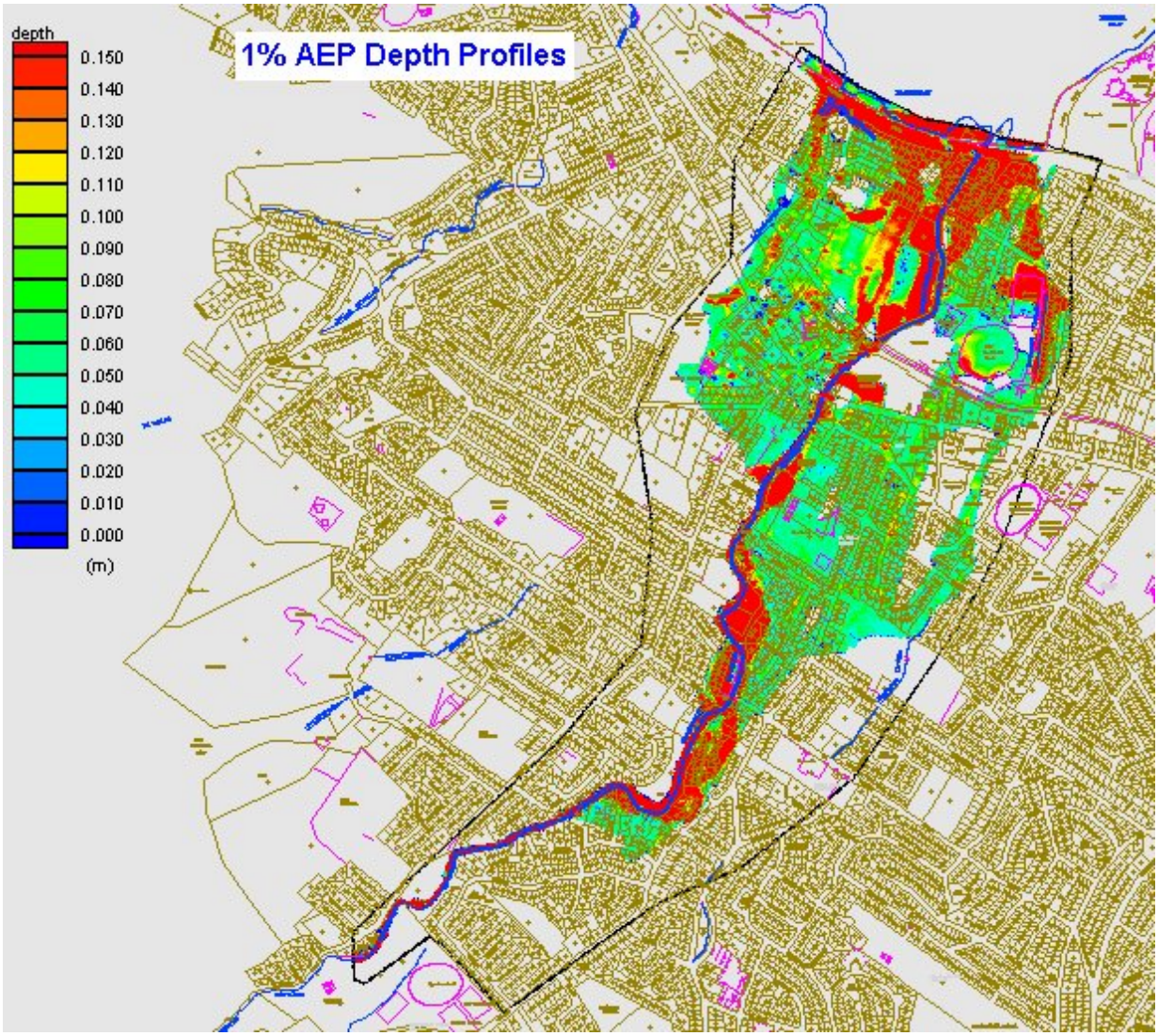

Figure 5 2-D Distribution of the Depth of 100 yr ARI Floodwaters

The extent of flooding on the floodplain in the 100 yr ARI event in particular is due to the predicted shallow overtopping of the banks of Humphreys Rivulet. It was found that a comparison of the survey levels at a number of surveyed cross sections and the digitized 2 m floodplain contours gave differences of up to +0.5 m. It is therefore possible that the top of bank levels for Humphreys Rivulet interpolated onto the 4 m grid are lower than the actual top of bank levels in a number of sections.

A further contributing factor is that the floodplain contours downstream of say Brent Street are roughly perpendicular to the alignment of Humphreys Rivulet. Once overtopping of Humphreys Rivulet occurs floodwaters have an opportunity to spread out across the floodplain.

7. FLOOD MAPPING

The floodplain maps were prepared based on the 1-D and 2-D modelling results from immediately downstream of Knights Creek and Limekiln Gully Reservoirs down to the Brooker Highway. Hazard Maps were also prepared for the floodplain area covered by the 2-D model only. Hazard maps were prepared for the 100,000 yr ARI flood combined with breaching of Knights Creek Reservoir; Sunny Day Failure of Knights Creek Reservoir only; and the 100 yr ARI flood.

8. CONCLUSIONS

It is concluded that as a result of the hydrological and hydraulic modelling investigations that Council and Hobart Water are now better informed about the inundation that could result from the failure of Knights Creek Reservoir and the inundation resulting from infrequent floods and the ramifications for early evacuation planning. It was also concluded the study highlighted the challenges that can arise when attempting to assemble and run a 2-D flood routing model of a hydraulically steep urban floodplain.

9. ACKNOWLEDGEMENTS

The permission of Hobart Water to outline the Humphreys Rivulet flood inundation investigations and hazard mapping is gratefully acknowledged. The views expressed in the paper are those of the authors and are not necessarily the views of Hobart Water.

10. REFERENCES

Institution of Engineers, Australia (1999). "*Australian Rainfall & Runoff, A Guide to Flood Estimation*", Book VI – Estimation of Large and Extreme Floods, 81 pp.

Phillips, B.C., Boon, B. and Reeve, D. (2001) "Mitigating the Impacts of Flooding in the City of Glenorchy (Tasmania)", *Proceedings*, 6th Conference on Hydraulics in Civil Engineering, 28-30 November, Hobart, pp 97-106.

Snowy Mountains Engineering Corporation (1998). "Review of Hydrology and Flood Capability for HWRA Dams – Knights Creek, Limekiln Gully, Ridgeway & Upper Reservoirs", *Report*, May, 72 pp.

Snowy Mountains Engineering Corporation (1999). "Hydrologic and Hydraulic Investigation for Reservoirs above Humphreys Rivulet", *Report*, prepared for Hobart Regional Water Authority, May, 72 pp.

Stelling, G.S. (1984). "On the Construction of Computational Methods for Shallow Water Flow Problems". Rijkswaterstaat Communications No. 35/1984, The Hague, The Netherlands.

Syme, W.J. (1991). "Dynamically Linked Two-Dimensional / One-Dimensional Hydrodynamic Modelling Program for Rivers, Estuaries & Coastal Waters". *M.Eng.Sc Thesis,* Dept of Civil Engineering, The University of Queensland, May.

Thompson & Brett – Cardno Willing (2002). "Humphreys Rivulet Flood Inundation and Hazard Mapping", Final Report, prepared for Hobart Water and Glenorchy City Council, December, 37 pp + A3 Final Drawings.

Thompson & Brett – Willing & Partners (1997). "Analysis of the Humphreys Rivulet Catchment and Concept Design of Flood Protection Measures", Final Report, prepared for Glenorchy City Council, January, 56 pp + Apps.

The Institution of Engineers, Australia
8th National Conference on Hydraulics in Water Engineering
ANA Hotel Gold Coast, Australia 13-16 July 2004

Modelling a Combined Sewage and Stormwater Flood Detention Basin

A. Pugh
B.E. (Hons), Member A.W.A.
Sales and Support Manager, Wallingford Software Pty Ltd, Australia
S. Ratcliffe
B.Sc(Hons), Grad Dip App Comp, ME, MIE Aust, CP Eng, CEng MICE
Launceston City Council, Australia

Abstract: The Margaret Street detention basin for combined sewage and stormwater flows is a unique solution to provide storm flooding protection within urban Launceston. Using a part covered and part open basin of 7ML and 23ML respectively, the basin configuration and operation provides first flush capture, containment and discharge to Council WWTP. The structure designed by GHD, is scheduled for completion by March 2004.

The purpose of this paper is to discuss the creation of the InfoWorks CS model; how the catchment model was built, calibration issues, how complex control structures were considered within the model. The model was developed to allow testing and refinement of the operation under proposed and alternative system control scenarios for the Council. The results of this testing will also be discussed.

Keywords: Hydraulic modelling, Combined, Sewer, Stormwater, Detention Basin, InfoWorks CS, WWTP.

1. INTRODUCTION

Dating from the 1840's Launceston City Council's drainage system is one of the oldest in Australia. The system was designed using the English system of collecting both stormwater and sewage discharges in the one same pipes. As Launceston expanded demands on the system increased and as a result the system became grossly overloaded with the result being regular flooding of the CBD and low lying residential areas.

Figure 1 – Historical Flooding Event.

In the 1980's Council spent approximately $20M on upgrade works in the system. These works were part of a strategy proposed by Gutteridge, Haskins & Davey (GHD) which had been developed by undertaking flow monitoring and modelling of the catchment. The strategy has so far been successful, although a major element of this strategy had yet to be constructed. The complete strategy included a 1.1 km long pressure gravity pipeline of 2.7m diameter to collect water from South Launceston and discharge directly into the river. It is estimated that this would cost $12M to complete and is considered to be beyond Council's current resources.

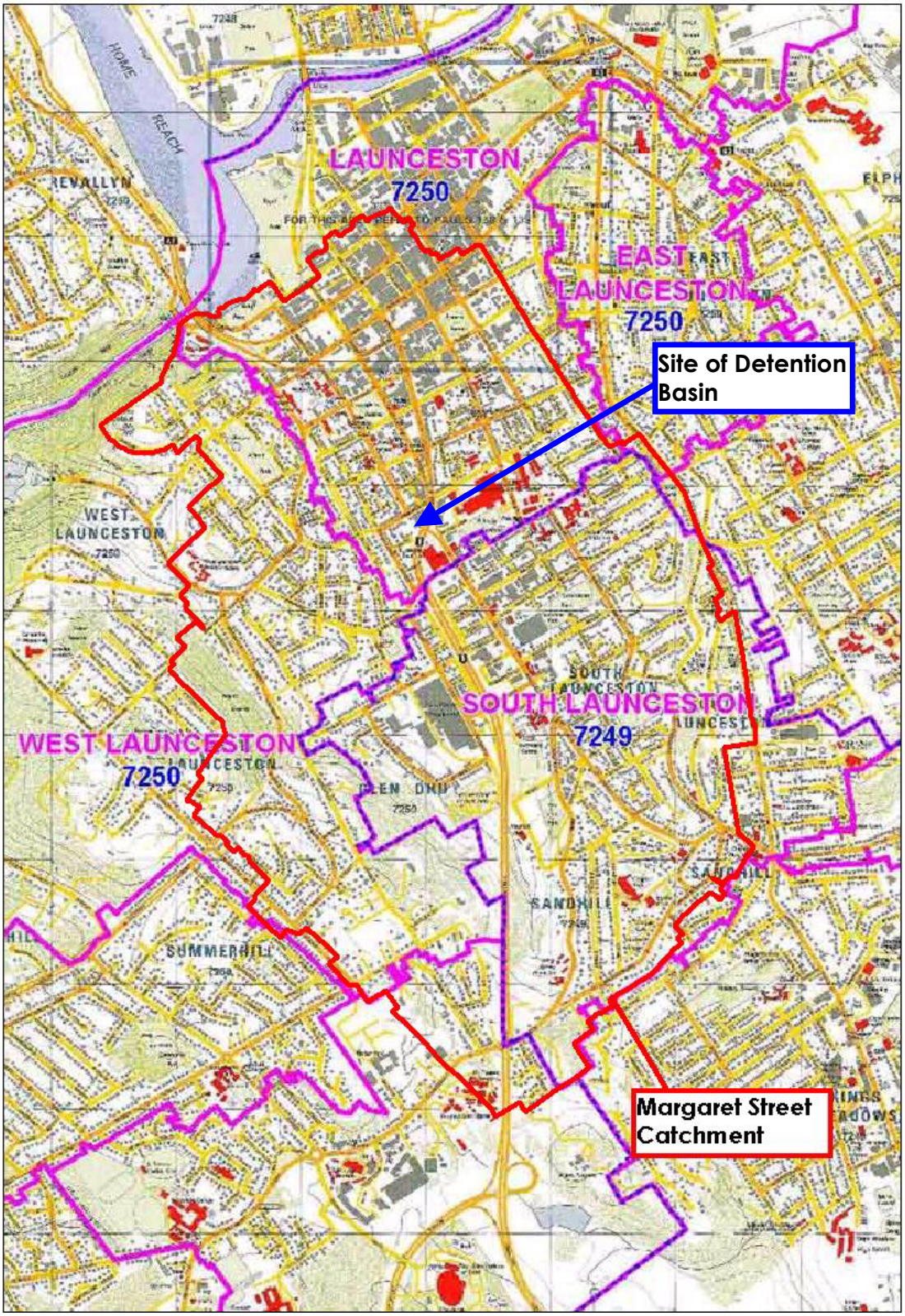

Figure 2 – Map showing the extents of the Margaret Street Catchment

As a result alternative solutions were developed for managing the flows from the catchment. The Margaret Street Detention Basin was determined to be the best alternative and is an innovative solution which, when constructed, will:

- achieve the flood protection objectives of Council's strategy;
- maximise the use of existing stormwater infrastructure,
- be significantly less expensive and within Council's capacity to fund,
- deliver a significant improvement in amenity, and
- provide environmental benefits of the project including capture and discharge to the Council wastewater treatment plant of the first flush of stormwater, grit and floatables.

In 2002 a more comprehensive hydraulic modelling study of the Margaret Street catchment was undertaken by Earth Tech Engineering with the following aims:

- To calibrate the proposed detention basin site in dry and wet weather flow conditions,
- To model the Margaret Street Detention basin and assess its performance for selected design rainfall events.

2. BUILDING THE MODEL

The raw data was provided in GIS format (ESRI SHP[1]) files and these were imported directly into InfoWorks CS[2]. Validation of the data was undertaken using the inbuilt routines within InfoWorks and where necessary data was input and/or inferred. Data flags were used during the model build to trace the data source and confidence, as this was seen to be an important Quality Assurance step. The model was simplified to approximately 1900 manholes and the ancillary structures and control regimes were created.

2.1 Sub-catchment Delineation

InfoWorks CS uses subcatchments as the mechanism for generating both dry weather sewer flows and wet weather runoff and infiltration for routing in the model. As this model contained three different systems, sewerage, stormwater and combined, it was necessary to ensure that there was no double counting of either population generated flows (sewage) or area based flow calculations (runoff and infiltration).

It was decided to use only two types of catchments – a storm catchment and a sewer catchment. This made the modelling simpler as you could view each type of catchment separately to ensure there was no overlap. For the combined network two separate sub-catchments were created. One, the foul catchment, represents the dry weather sewerage flows, and the slower inflow and infiltration effects. The storm subcatchment represents the faster wet weather rainfall runoff – which will account for the majority of the wet weather inflow into the manhole.

When delineating sub-catchments, the following aspects were considered:

- The location, grade, and system type of pipes not modelled. These pipes were considered to determine the modelled manhole into which any given discharges flows.
- The locations of properties relative to the pipework, via the cadastral base.
- Sub-catchments were delineated in such a way that their area did not exceed 10 hectares.

3. CALIBRATING THE MODEL

The model was calibrated using data collected at the proposed site of the Margaret Street Detention Basin. There was fifteen months of data available, with flow gauges being located in both of the major pipelines.

[1] Developed by the Environmental Systems Research Institute (ESRI) a shapefile (SHP) stores nontopological geometry and attribute information for the spatial features in a data set.

[2] InfoWorks CS is a dynamic hydraulic modelling tool supplied by Wallingford Software. It uses a four-point implicit finite difference scheme (the Preissmann scheme) with a non-linear Newton-Raphson iteration and an adaptive time-stepping algorithm to solve the St Venant equations.

3.1 Dry Weather Calibration

Dry weather flow data was available for the Low Level Gravity Pipeline (LLGP) and from this a representative hydrograph was developed for weekdays and weekends. This data also allowed a per capita flow rate to be established for the lower half of the catchment – this flow rate and hydrograph profile was assumed to apply to the northern section also.

In addition to calculating the generation rate, tidal levels at the outfall were obtained to improve the accuracy of the calibration. The levels were applied at the outfall to simulate boundary conditions at the outlet of the catchment.

3.2 Wet Weather Calibration

Rainfall entering the sewerage system is modelled in InfoWorks by using runoff surfaces. These surfaces have different parameters relating to both speed of response and quantity of response. Typically runoff surfaces are developed to represent flow from impervious areas as having a "fast response" whilst flows from pervious areas were classified as "slow response".

For the Margaret St catchment the four main areas were classified. The key runoff characteristics of these surfaces are:

- "Roof" and "Road" are both impervious surfaces,
- "Open Ground" assumed to be predominantly a pervious surface, and
- "Long term response" is generated from pervious surface with very slow inflow characteristics.

Ideally fast response inflow should be all directed into the stormwater or combined network, however experience indicates that a lesser percentage will also enter into the sewerage system via leakage from sealed areas such as roofs, driveways and roads, damaged manhole lids and illegal stormwater connections. Slow responses from open ground area enter the stormwater system, again with anecdotal evidence suggesting that some flow will enter the sewerage system.

As there was no way of separating the wet weather inflow into the sewerage system and the inflow into the storm water system a base level of inflow into the sewerage system was assumed. This arbitrary amount was set at approximately 4 % of the rainfall.

The total quantity of flow and shape of the predicted outflow was calibrated by adjusting the percentages of flow from the storm catchments. The inflow from the storm catchments was found to be approximately 47% of the rainfall in the urban areas, and 31% in the undeveloped catchments.

The calibration of the model was determined to be successful with the predicted wet weather flow volume for the verification event being 93% of that observed at the monitoring points. Peak flows predicted by the model were slightly lower than those observed by the field monitors. Figure 3 shows a sample calibration plot.

It was noted that the flows predicted by InfoWorks were substantially less than those predicted by other modelling exercises. While it was assumed that these earlier predictions were probably over estimations we wanted to check the realism of the model. As it was considered that some of this may be due to extra flow reaching the detention basin from surface routing, overland flow paths were added into the model. It was interesting to note that this had very little impact on the total flows received at the detention basin.

4. MODELLING THE DETENTION BASIN

The construction of the detention tank in the model was initially substantially simplified. It was noted however that this was not accurately modelling the flow situation in the tank and a more detailed model of the detention tank was developed.

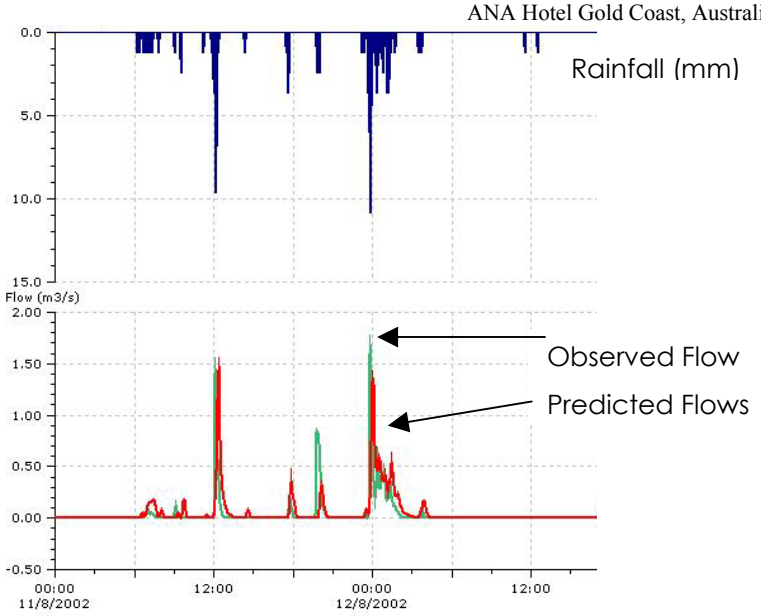

Figure 3 - Sample Calibration Plot.

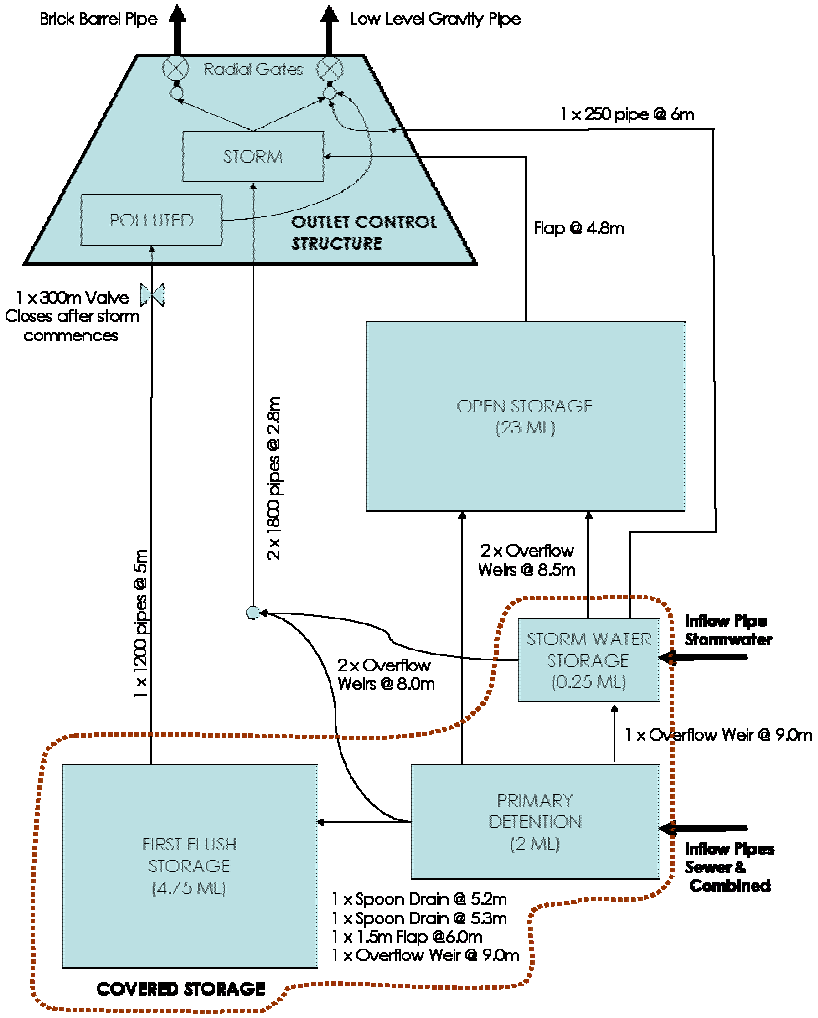

Figure 4 – Schematic showing Hydraulic Flow Paths in the Detention Basin

The flow regime (refer Figure 4) is such that in dry situations the flows pass through the primary detention, first flush storage, into the polluted chamber of the Outlet Control Structure and into the LLGP. The tank is designed to store both sewerage and stormwater flows in a covered flow control facility with the "cleaner" water from extreme rainfall events being detained in an above ground storage basin. The flows out of the tanks and the above ground basin are controlled by two large radial gates which protect the downstream system from excessive surcharge and flooding. There is also a valve that shuts the flow from the covered storage – thus storing the first flush for subsequent discharge and treatment. There are flap valves located throughout the structure to prevent back flow of polluted water into cleaner areas.

The modelling of the hydraulic elements was relatively straightforward with most elements being modelled as they would physically exist. It was necessary to create a Real Time Control (RTC) routine in the model to simulate the operation of the outlet valves, pumps and radial gates as the operation of these would be governed by conditions in the downstream pipe network. It was important that this detail was included as a key part of the project was going to be validating the set points of the telemetry for the basin.

Figure 5 shows how the model displays the different elements in the model.

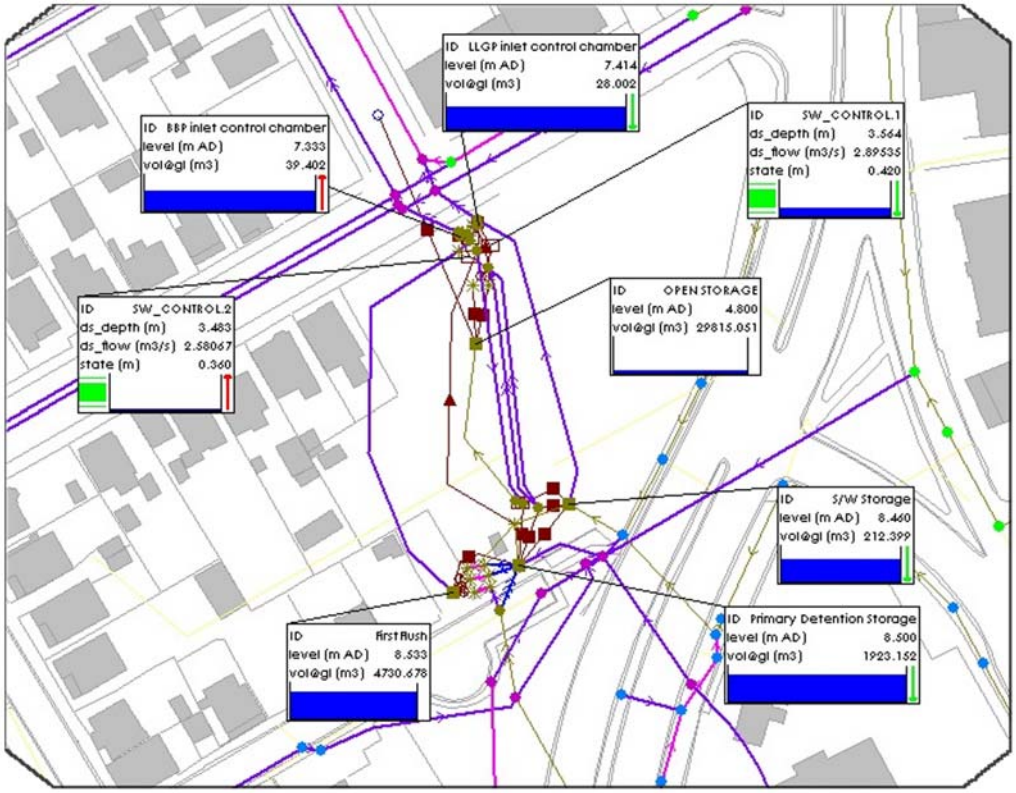

Figure 5 – InfoWorks CS Model

Figure 6 shows the difference in the flow through the radial gates by adding a new rule that controlled the flow passing through the radial gates. Originally the control on these gates was based on water level in the gate manhole. A rule was added to throttle the flows allowed out of the detention tank to reduce any downstream flooding. The rule stated that if the flow was greater than $3m^3/s$ the radial gate should start to be closed – if the flow was below $3m^3/s$ the gate should be opened. This allowed the gates to operate as the hydraulic simulation was proceeding – optimising the flows downstream.

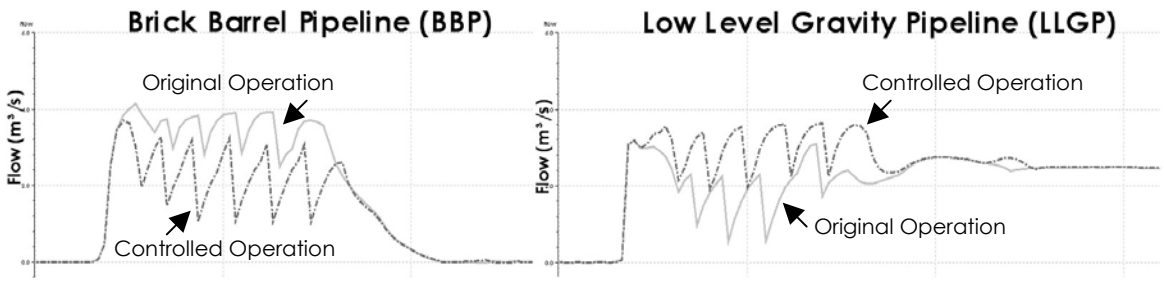

Figure 6 – Comparison of Flows Exiting the Tank with the Control Rule

The results in the model showed that downstream flooding was reduced by 75% by adding this rule to the model.

5. OUTCOMES

Launceston is one of the few cities in Australia with a combined sewerage and drainage system. By using a dynamic hydrologic and hydraulic model that was able to consider all three different system types, sewerage, drainage and combined; it has been possible to develop a model that has been calibrated to the catchment and can be used for testing the theory of the detention tank. While the model build and calibration has been completed and a preliminary investigation of the detention tank operation has occurred it is already envisaged that the model will be used to verify the following

- Fine tuning the set levels of the radial gates to reduce flooding in the downstream catchment,
- The effect of tidal position on the storage basin,
- Volume of stormwater detained in open storage for different storm durations and frequencies, and
- Water Quality analysis.

As discussed in this paper the model has already demonstrated that improvements in operation may be able to optimise the detention tank operations and reduce downstream flooding while minimising detention times.

6. ACKNOWLEDGEMENTS

The authors would like to thank both the organisations of GHD and Earth Tech Engineering for their work on this project, and their assistance in preparing this paper.

7. REFERENCES

Earth Tech Engineering (2003), *Margaret Street Catchment Model Build and Calibration Report,* Earth Tech Engineering, Melbourne.

Tabart, K and Brayford (2001), G, Unique City Detention Basin Solution for Combined Sewage and Stormwater Flood Control, *6th Conference on Hydraulics in Civil Engineering*, pp329-335

GHD (2002), Margaret Street Detention Basin Schedule of Drawings, CD 026.2002.

InfoWorks CS Online Help.

The Institution of Engineers, Australia
8th National Conference on Hydraulics in Water Engineering
ANA Hotel Gold Coast, Australia 13-16- July 2004

Hydraulics in Flood Management For the Gold Coast

Khondker Rahman
Gold Coast City Council, PO Box 5042 GCMC Queensland 9129 Australia
krahman@goldcoast.qld.gov.au
Hamid Mirfenderesk
Gold Coast City Council, PO Box 5042 GCMC Queensland 9129 Australia
hmirfenderesk@goldcoast.qld.gov.au

Abstract- Flood management in the Gold Coast has become a complex issue. The reason is that the Gold Coast has been growing rapidly in the past few decades. This growth has resulted in the urbanization of new spaces, generally located within the floodplain of the major river systems of the city. This rapid urbanization of the floodplain has created two types of issues. On one hand, each overflow can potentially result in damage to property or loss of life, on the other hand it has strengthened the feedback from drainage systems, i.e. even during average rainfall events, devastating floods can occur.

To respond to this flooding problem, the Gold Coast City Council has created an integrated flood management system based mainly on modern one and the two-dimensional hydrodynamic models. The aim of this system is mainly to address three types of problems associated with floods:

I) Future
II) Existing
III) Residual

This paper describes the Gold Coast flood management system and explains how hydraulic modelling techniques have been integrated into this system to develop strategies to address above-mentioned flooding problems in the Gold Coast.

Keyword: Hydraulic, Flood, Management, modelling

1. Introduction

Floods are natural events, which continue to be one of the most severe annual disasters in Australia and throughout the world. A single flood event in Australia on average causes $25M damage, Abbs (2000). The annual cost of flood damage in Australia is estimated to be $350M, SCARM (2000), (This amount is based on data from the Department of Primary Industry and Energy 1992, which has been adjusted for Consumer Price Index increases to 1998 $ terms). Floods are estimated to contribute 25% of the total average annual cost of natural disasters in Australia, Joy (1992). The southeast of Queensland is regarded as one of the most vulnerable regions in Australia. The damage resulting from a 100 year ARI flood within the Nerang River catchment is estimated to be $147M, resulting from the inundation of more than 4000 properties. Although flooding seems to be the most damaging natural disaster, it is the only natural disaster that can be effectively controlled and managed. Flood management is a program of corrective and preventative measures which aims at implementing the effective control of floods. This paper will provide a concise description of the role of hydraulic engineering in flood management in the context of the Gold Coast flood management development and implementation.

The structure of the paper is as follows; first a brief description of flooding in the Gold Coast region followed by the structure of flood management in the Gold Coast, then a brief description of development of flood models and at the end a demonstration of how a flood model can address flooding problems.

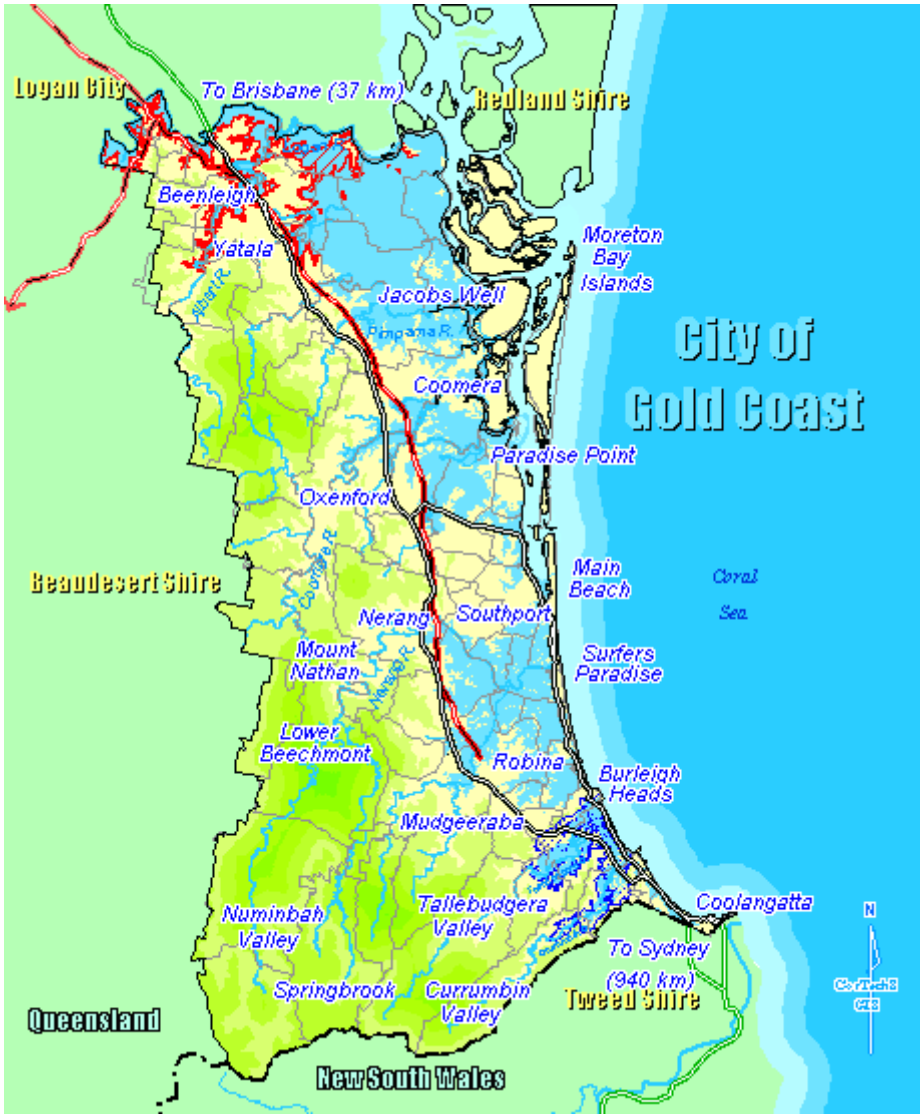

Figure 1- General Layout of the Gold Coast and its Major River System

2. Flooding in the Gold Coast

The Gold Coast as part of southeast Queensland has been vulnerable to flooding due to its meteorological and topographic features.

- The typical topographic feature of this coastal strip is parallel valleys through which rivers with high mainstream slopes flow in a generally west-east direction into the ocean. These rivers have created floodplains, which are currently inhabited by human beings. These settlements have changed the flooding behaviour of these rivers and creeks (generally it has worsened). As a result we have witnessed an increase in the level of hazards to many communities living on this coastal strip. Another topographic feature of this area is a rather abrupt change in terrain, which results in high rainfall gradients.

- The meteorological feature of the region is the existence of two types of climate. 1) Weather patterns controlled by tropical cyclones, which statistically are the source of floods with more than 30 years ARI, 2) weather patterns controlled by the southeasterly low-pressure system, which is statistically responsible for floods with less than 30 years ARI.

In the past 50 years, the Gold Coast has experienced four major floods in 1947, 1954, 1967 and 1974, implying that in the last 30 years, the floodplain has not experienced any major flood. This situation can be attributed to three things, 1) the fact that we have been in a dry cycle of long-term weather pattern variations, 2) the fact that

the region has been free from the close approach of tropical cyclones, 3) the construction of Hinze Dam, which has had a mitigation impact on flooding during the last 20 years. Facts and figures indicate that this fortunate state would not continue forever and that we should prepare ourselves for a major flood. In response to this need the Flood Strategies Section of the Gold Coast City Council was formed in year 2000, and since then has been focused on the development and implementation of an integrated flood management program.

3. Flood Management Structure in the Gold Coast

Following the recommendation of SCARM Report 73, this program was evolved around addressing three types of flood problems, namely 1) existing, 2) future and 3) residual flood problems. Figure-2 provides a snapshot of the way these problems have been addressed as part of the Gold Coast flood management program. This structure shows that flood management in the Gold Coast is not solely relying on large-scale structural and engineering measures for flood control. There is substantial emphasis on measures such as land-use control and participation of the community in flood control and management.

3.1 Existing problems

Existing problems are related to the existing properties, which are currently at risk from flooding. The management strategy to deal with this type of problems is mainly aimed at mitigating the flood impact. This is achieved in two different ways: namely 1) physical mitigation, 2) non-physical mitigation.

Physical flood mitigation has been focused on two strategies:

1) Storing floodwater at the upper reaches of the catchment. To this end comprehensive hydraulic and economic studies for raising the Hinze Dam wall in the Nerang catchment were conducted. Some of the previous mitigation work in this regard includes the construction of retardation basins in Loders Creek and Biggera Waters Creek.
2) Improving the conveyance of the lower reaches of the catchment to allow floodwater to be drained from the system as quick as possible. In this line dredging of the lower reaches of the Nerang River was studied as an alternative to raising the Hinze Dam wall. Some of the previous mitigation work in this line includes Benowa Channel in the Nerang River catchment, which as a bypass floodway provides a shortcut allowing 385 Q^3/Sec of floodwater to be conveyed from upper reaches of Nerang River to its lower reaches through an additional waterway system.

Non-physical mitigation has been focused on improving flood awareness of the community, to ensure that it would not expose itself to flood hazards and to prepare it to react as quickly as possible in the event of a flood.

3.2 Future problems

Future problems refer to buildings that will be built on flood-prone land that will be exposed to future flood risk. The strategy for dealing with this type of problem has been focused on:

1) **Land-use control;** this measure has been adopted in response to population pressure to ensure that existing hydraulic conditions of the floodplain would not be compromised because of unsustainable uses of flood prone areas.

2) **Response to future change;** such as impact of climate change on the flooding behaviour of the catchments or impact of the future developments on the hydrologic and hydraulic behaviour of the catchments. The Gold Coast City Council has undertaken extensive studies through CSIRO, McInnes (2000), Walsh (1998), in regard to the sea level rise due to climate change and has adopted 27cm sea level rise, Betts (1999), for planning purposes (to be added to the downstream boundary condition of the Council's hydraulic models). More recently, Council has commissioned CSIRO to conduct a comprehensive study on the impact of climate change on the temporal pattern of severe rainfalls in the Gold Coast Region.

Figure 2- Three Types of Problems Addressed in the Gold Coast Flood Management Program.

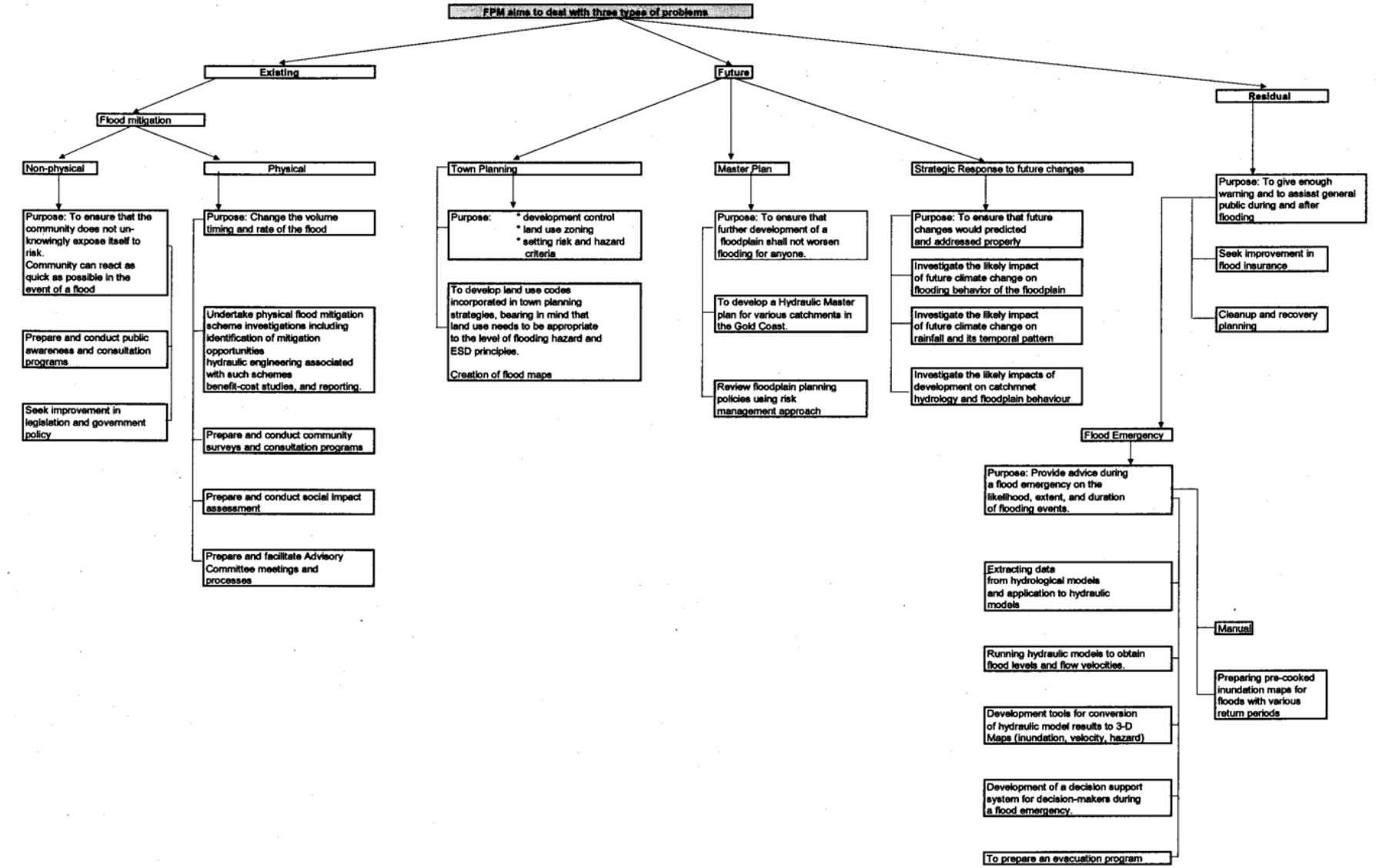

3.3 Residual problems

Residual problems refer to the residual risk associated with floods that overwhelm management measures already in place. The strategy for dealing with this type of problem has been focused on

1) Creating a forecasting and warning system.
2) Assisting the individual and the community in the preparatory, disaster and post disaster recovery phases.

4. Flood Modeling

A flood model is a predictive tool, essential for the development and implementation of a flood management program. A flood model is in fact a suite of models, comprising of a digital elevation model, hydrological model, hydraulic model and flood damage model.

4.1 Digital elevation model (DEM)

DEM converts the survey data to a raster grid representing land surface. A digital elevation model is necessary for the development of any type of two dimensional model, as in a two dimensional model ground surface is represented by a series of closely spaced grid points with a height associated with them. These grid points are one of the outputs of a digital elevation model. In this exercise the smooth land surface is generally replaced by a step like construction of usually rectangular grid cells with typical dimensions between 5 to 20 meters. Currently a widely accepted methodology in 2D flood modelling is to use commercially available GIS and CAD software for the creation of a DEM. A major shortcoming of this approach is that methodologies used for ground level representation in these software have not been specifically developed for hydraulic engineering applications. The Gold Coast City Council initiated a study on the applicability of these software in hydraulic engineering, Mirfenderesk (2003) showed that the use of this type of DEM in 2D modelling could be a source of uncertainty in results.

4.2 Hydrological Model

Hydrological models convert rainfall to runoff. It determines what fraction of rainfall becomes runoff and how fast the runoff is discharged through a stream system. The output of a hydrological model is a hydrograph, which is often used as an upstream boundary condition in a hydraulic model. Some of the main information required for the development of a hydrological model is as follows: catchment area, catchment boundaries, historical rainfall data, land use data, rainfall Intensity-Frequency-Duration (IFD) curves and rainfall temporal patterns. There are two types of hydrological models, flood emergency and land use planning.

4.2.1 Flood Emergency Model

The purpose of the development of a flood emergency model is to equip the Council with a tool for perdition of real-time flooding behaviour (extent, flood heights, flood risks etc) throughout the city in a very short period of time (to allow counter disaster measures be implemented on time). The model is based on the existing development and catchment features. The water level in natural or dam storages should reflect the existing situation. Current rainfall loss criteria should be applied for the calibration of the model.

4.2.2 Land Use Planning Model

The purpose of the development of a land use planning model is to equip the Council with a comprehensive tool for strategic planning and development assessment. These models use comprehensive land use data using city's strategic plans for growth and development sequence. All the storages and dam reservoirs are assumed to be full.

4.3 Hydraulic Model

A hydraulic model converts runoff to water level, within the floodplain. The main information required for the development of a hydraulic model is as follows: survey data, roughness coefficients, downstream boundary conditions, inflow hydrographs, hydraulic structures, roads and other structural elements within the floodplain and calibrations data. Hydraulic models are generally in two forms, one-dimensional (1D) and two-dimensional (2D).

4.3.1 One-dimensional model

In a 1-D model, the flow direction is chosen by the modeller and flow is averaged both in vertical and horizontal directions. 1-D models are generally very fast and appropriate for predicting real-time flood behaviour in a flood emergency situation. The obvious disadvantage of 1-D models is that they cannot fully represent flow characteristics on the floodplains in areas where flow is two dimensional in nature.

4.3.2 Two-dimensional model

In a 2D model, flow can occur across two dimensions. Unlike 1D models, the model determines the direction that water flows. In this case flow is depth averaged. In general a 2D model is a good representation of natural flood flow (as the flow in third dimension is generally insignificant and can be ignored). However, this type of model has several drawbacks. One of the major drawbacks is due to the poor representation of conveyance of waterways and flow paths. Obviously, by choosing an adequately small grid size, this problem can be alleviated. However, computer power, running time and applicability of turbulence models in small grid width to depth ratio are limiting factors, which prevent modellers reducing the size of grids to a desirable level.

In some of the newer software this problem has been tackled by incorporation of a nested modelling feature (both nested 1D and 2D). In some of the widely used commercial software this improvement comes at the expense of making some substantial changes to the physics and geometry of the model. In simple cases this feature can provide some comfort, but in general for complicated situations the net benefit of using this feature may not be good enough due to the above-mentioned changes to the physics and geometry of the problem. Another difficulty associated with 2D models is related to the wet and drying feature. Much better routines have been developed for modelling cells, which can be dry and wet during the modelling period in recent years, but the problem does not seem to be completely resolved yet for some of the software, which are widely used for development assessments. Another area, which needs improvement at least for some of the software used in the industry, is the way that structures are modelled. Despite these shortcomings, 2D modelling is gaining more support in the industry and is regarded as the preferred option for assessing planning and development proposals in flood affected areas.

4.4 Flood Damage Model

A flood damage model provides an estimation of damage associated with flooding. It is an important tool for planning, development assessment and economical studies associated with flood mitigation options. The Gold Coast City Council has developed a number of flood damage models for various catchments. An obvious improvement in regard to flood damage modelling is the collection of more data to make stage-damage curves used by this type of model more accurate.

4.5 How Flood Models Are Used for Flood Management

In accordance with the three types of flood problems mentioned earlier, a flood model can be used to address these three types of flood problems as follows.

4.5.1 Addressing Existing Flood Problems

Flood mitigation measures are the most important tool to address existing flood problems. There are various alternatives for mitigation, depending on their cost and the benefit that they can produce. Flood models can provide vital information in relation to the effectiveness and economical viability of these alternatives. In this line Council flood models have been used during the last few years to investigate various mitigation options for the Nerang River floodplain. This included raising the Hinze Dam, dredging lower reaches of the Nerang River, improvement in Benowa flood channel and modification of some of the bridges over the Nerang River.

To this end, initially, using the hydrological model, various types of hydrology (based on temporal pattern) were examined. After a rigorous review process the most realistic hydrology for flood mitigation study was adopted. Then using a two-dimensional hydraulic model the impact of each of these alternatives (in terms of water level and depth of inundation) was examined. In the next step, using the flood damage model, the damage associated with each alternative was determined. Comparing the damage cost with the cost of mitigation option, benefit cost ratio of each alternative was determined. This piece of information, along with some other sources of information such as social impact assessment, community consultation input, etc. enabled decision makers to opt for the best option to mitigate existing flood problem in the Nerang River catchment.

4.5.2 Addressing Future Flood Problems

Council's flood models have provided vital information in relation to the outcome of alternative development strategies. In this line, using the hydrological model, a conservative but realistic hydrology for each catchment was adopted. Then, using the hydraulic model, flood-planning level for each and every catchment throughout the city was determined. By running the hydraulic model for various development strategies, the best and the most viable strategies for development were chosen (as an example, Hope Island Canal in the Coomera floodplain). In addition, flood models are vital for development assessment. These models have made it possible to assess the flooding impact of each development proposal. It is possible to find out if a development or cumulative impact of similar developments would result in real damage to other sections of the floodplain. Council's flood models have been extensively used for development assessment. In some cases this tool has allowed planners and designers to develop plans, which not only meet the developers needs but also contribute to an overall city flood mitigation program (Clear Island Water).

4.5.3 Addressing Residual Flood Problem

Flood models can provide vital information for emergency planning. The first generation of flood emergency process, Khan (2001), included interrogation of ALERT system to obtain real time measured rainfall data, running a hydrological model to convert the measured and predicted rainfall to inflow hydrographs for one-dimensional hydraulic models, running hydraulic models to provide water levels throughout the floodplain and finally mapping the output of the hydraulic models to create flood inundation maps. This process is currently under review. The purpose of the review is to complement this system with a decision support system to enable decision makers to take quick and effective counter disaster measures.

5. Conclusion

Recent advances in computer powers and numerical analysis techniques have enabled engineers to foresee flooding related problems and to offer solution to this type of problems more effectively. This in turn has potentially enabled local authorities to minimize flood related damages to the community through the development and implementation of comprehensive flood management programs. This paper has presented an outline of the development and implementation of such a flood management program for the Gold Coat. It shows the main steps, which is needed to be taken to develop a flood model, shows how these flood models can be used for planning purpose and also for effective real time flood management. It demonstrate that how central is the role of hydraulic in the development and implementation of a successful flood management program.

In this paper we have identified several areas for further development in the hydraulic component of flood management. This includes improvement in 2D hydrodynamic software in regard to waterway conveyance, wetting and drying routines and better representation of structures.

6. Acknowledgement

The Floodplain Management Program in the Gold Coast has been achieved through strong teamwork. Its success is owed to the completion of numerous tasks and projects undertaken by both previous and current members of the Flood Strategies Section of the Gold Coast City Council. This includes, Haydn Betts, Don Carrol, Saydure Khan, Anne D'arcy, Chandra Gunarratne, Luke Adair, Tussita Eleperuma, Michael Tonks, Tim Vass and Margaret Parker.

7. References

Mirfenderesk, H. (2003), A Review of the Application of GIS to Two-Dimensional Flood Modelling, *Floodplain Management Authorities Of New South Wales 43rd Annual Conference*, February 2003.

Khan, S. Betts H. (2001). Real-Time Flood Level Forecasting For the Nerang River System, Using Integrated Hydrology, Hydraulic and GIS Models, *Floodplain Management Authorities Of New South Wales 41st Annual Conference*, May 2001.

K.L. McInnes et al (2000). *Impact of Sea-Level Rise and Storm Surges on Coastal Resort.* .CSIRO Division of Atmospheric Research.

SCARM Report 73 (2000). *Floodplain Management in Australia, Best Practice Principles and Guidelines*. CSIRO Publishing Australia.

Abbs, D. J. et al (2000). Climate Change, Urban Flooding and Infrastructure, *Hydro 2000: 3rd International Hydrology and Water Resources Symposium of the Institution of Engineers, Australia*: Perth, Australia. p. 686-691.

Betts, H. (1999): The Implication of Future Climate Change on Floodplain Planning at Gold Coast City, *NSW Floodplain Managers' Conference, Tamworth*.

K.J.E. Walsh et al (1998). *Global Warming and Sea Level Rise on the Gold Coast*, April (1998).CSIRODivisionof Atmospheric Research – CSIRO Division of Marine Research. Report prepared for he Gold Coast City Council.

Joy, C.S. (1992). Towards Better Floodplain Management in Australia, *Severe Weather and Flooding Seminar, Seaworld, Gold Coas*t, 14-15 October, 12p.

The Institution of Engineers, Australia
8th National Conference on Hydraulics in Water Engineering
ANA Hotel Gold Coast, Australia 13-16 July 2004

Analysis of Spillway Flow by Computational Fluid Dynamics Technique

D.K.H. Ho
B.Sc. (Hons), Ph.D., M.I.E.Aust., C.P.Eng.
Technical Manager, Advanced Analysis, Worley Pty. Ltd., Australia
K.M. Riddette
B.E. (Hons), Dip.Eng.Prac.
Engineer/Analyst, Advanced Analysis, Worley Pty. Ltd., Australia
S.M. Donohoo
B.Sc., B.E.(Hons)
Manager, Advanced Analysis, Worley Pty. Ltd., Australia

Abstract: Many spillway structures in Australia were designed and built based on limited hydrological information at the time of design. As a result they are under-sized for today's revised probable maximum floods. Potential problems such as the generation of excessive negative pressure over spillway crest under increased flood condition could be encountered. The raised flow profile may also have adverse impact on crest bridge and gate structures. Historically, physical models have been constructed in hydraulic laboratories to study these behaviours, but they are expensive, time-consuming and there are many difficulties associated with scaling effects. Today, with the use of high-performance computers and more efficient computational fluid dynamics (CFD) codes, the behaviour of hydraulic structure can be investigated numerically in reasonable time and expense. Several spillway structures in Australia have been investigated successfully by this technique recently. This paper describes the CFD analysis of the existing spillway for the Wivenhoe Dam upgrade project. The results have been validated against physical model test data. It was found that the predicted raised flood level could interfere with the control gates. The analysis revealed how the discharge would change from a spillway free flow to an orifice flow through a transition flow region. Some interesting behaviour in this transition zone and in the downstream plunge pool will be described in the paper.

Keywords: Spillway, Flow Analysis, Computational Fluid Dynamics, Orifice Flow, Wivenhoe Dam.

1. INTRODUCTION

The reservoirs provided by the Wivenhoe, Somerset and North Pine dams are a major source of water supply to the south-east Queensland region. The Wivenhoe Dam upgrade project is the result of a significant increase in the estimation of the probable maximum flood (PMF) since the original design of the dam and spillway structure. The dam owner, SEQWater, has formed an alliance (Wivenhoe Alliance) with Leighton Contractors, Coffey Geosciences, Montgomery Watson Harza and Department of Commerce (NSW) to upgrade the dam. Details of this project conducted by the Wivenhoe Alliance have been reported by Chandler et al (2003).

One aspect of the upgrade was to assess the spillway discharge capacity and the impact on the raised gates and bridge structures due to the estimated revised PMF. Traditionally this would have been analysed using a physical scaled model of the spillway. However, the Wivenhoe Alliance decided to carry out this investigation numerically using a three-dimensional computational fluid dynamics (CFD) model because of the time and cost constraints. This method of analysis has been successfully applied to spillways overseas, and more recently in Australia (Ho et al, 2003).

The objectives of the investigation were to determine: (1) the flow behaviour through the spillway gate bays under various flood levels, (2) the pressure distribution along the spillway crest, (3) whether the free surface would impinge on the radial gate trunnion pier structure, (4) whether the free surface would impinge on bridge structure and, (5) if orifice flow behaviour could occur when high water levels impinged on the raised radial gate. In order to have confidence in the analysis technique and to validate the model, the computed results were validated against physical model test data. As the upstream head water levels increased, the analysis was able to capture both the spillway free discharge and the orifice discharge behaviours. A rather complex transitional discharge was also encountered in the analysis.

2. SPILLWAY MODEL

A mixture of 2D and 3D CFD models were generated for the study. The models incorporated a portion of the upstream and downstream topography, channel features, spillway and gate structures, the downstream flip bucket and plunge pool. A combination of coarse and fine grids was utilised to minimise the computational time required and to capture the flow in the regions of interest.

The non-flow regions were treated as obstacles that were created by importing the topographic data and by defining the geometry directly from drawings. Both the flow and non-flow regions were modelled within a grid system. The fractional area/volume obstacle representation (FAVOR) technique was used to model the complex interface between the flow region and the obstacles. The model consisted of the following features:

- Local topography
- Upstream and downstream spillway channel, including the plunge pool
- Upstream groynes
- Training walls
- Spillway surface, including flip bucket and downstream apron
- Piers
- Underside of road and service bridges
- Upstream side of raised radial gate (skin plate only)

An elevation along the centreline of the spillway showing the important components is shown in Figure 1. Figure 2 shows a view of the 3D model of the obstacle without the bridges and gates. The spillway was designed to the US Army Corps of Engineers (USACE) pre-1970 standard crest shape, consisting of two upstream radii of $0.5H_d$ and $0.2H_d$, and a downstream curve shape of:

$$2H_d^{0.85}y = x^{1.85} \quad (1)$$

where x is distance downstream of crest centreline, y is distance below crest level and H_d is the design head.

The piers are mitre-shaped, similar to the USACE Type 3/3A pier. The downstream ends of the piers are tapered. The spillway gate slots and radial gate trunnion corbel were not modelled due to the fineness of these details.

The upstream and downstream boundary conditions were set to zero-velocity, hydrostatic pressure boundaries at the specified water level. A combination of head and tail water levels as shown in Table 1 was analysed.

The fluid properties used in the analysis were for water at 20°C. The water was assumed to be incompressible with a constant density, ρ, of 1000 kg/m^3 and a dynamic viscosity, μ, of 0.001 kg/m/s. Previous experience showed that variations in water temperature of up to 10°C did not have a significant influence on the fluid flow (Worley, 2003).

The two-equation k-ε turbulence model was used for the analysis. Although a number of turbulence models are available, this is the recommended model for flow with relatively high Reynolds number. The air entrainment and cavitation effects were not activated in the analysis. However, the computed negative pressure was checked for any

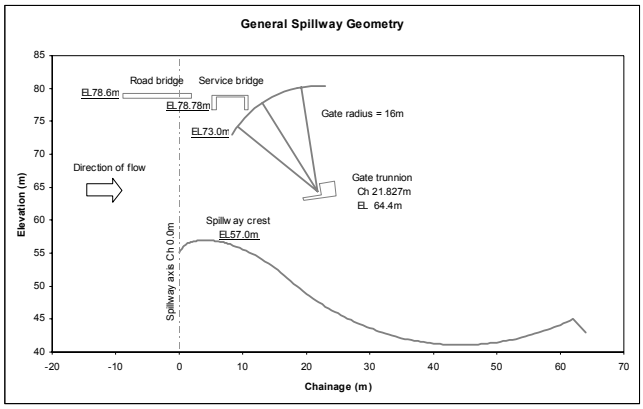

Figure 1 - Spillway, Gate and Bridge Geometry

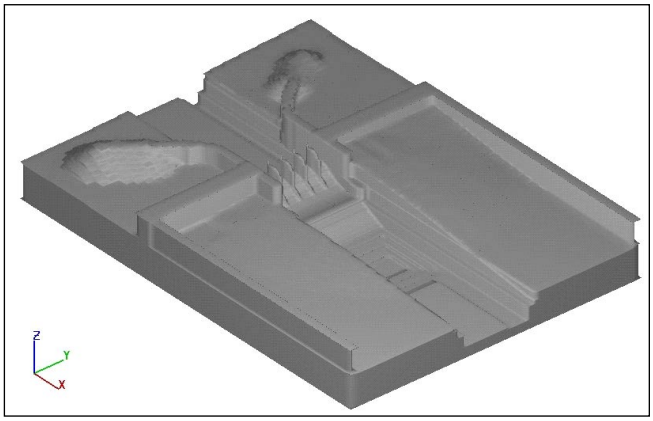

Figure 2 - 3D Model of Spillway Geometry (Bridges and Radial Gates Excluded for Clarity)

potential cavitation. Acceleration due to gravity of 9.81 m/s^2 was applied to the model to activate the inertia or body load of the water in the transient analysis.

Traditionally, open channel flow calculations used the empirical Manning equation to include the effects of surface roughness. Values for the Manning's 'n' roughness coefficient have been widely investigated for many different surface conditions. Based on advice from the Wivenhoe Alliance and published data from Chow (1959), the roughness values shown in Table 2 were assumed in the analysis.

Table 1 – Analysis Cases.

Case	Head water (EL)	Tail water (EL)	H/H_d
1	RL77.0m	RL52.0m	1.33 (for validation purposes)
2	RL79.0m	RL63.5m	1.47
3	RL79.7m	RL63.2m	1.51
4	RL80.0m	RL62.8m	1.53
5	RL80.5m	RL62.8m	1.57

Table 2 – Roughness Coefficients.

Location	Manning's 'n'
Upstream groynes	0.100
Excavated rock channel	0.040
Concrete spillway, piers and training walls	0.011

3. CFD ANALYSIS

The Navier-Stoke equation governing the water flow behaviour was solved numerically by an explicit finite difference method. The velocities and pressures in the domain were solved for each time step in a transient analysis. The Reynolds-averaged Navier-Stokes equation was used to model turbulence. The two-equation (k-ε) turbulent kinetic energy dissipation equations were used for calculating the Reynolds stresses.

One important aspect in the modelling was the accurate tracking of the free surface. Multiple free surfaces occurred in the model where the jet of water entered the plunge pool after leaving the flip bucket. A well-known computational technique was developed by Hirt (1994), and was implemented in the CFD code, FLOW-3D, which was used for the spillway analysis described in this paper. It utilizes a true volume of fluid (true VOF) method for computing free surface motion (Hirt and Nichols, 1981) and the FAVOR technique to model complex geometric regions (Hirt and Sicilian, 1985). The true VOF method tracks the sharp interface accurately and does not compute the dynamics in the void or air regions. The portion of volume occupied by the obstacle in each cell (grid) is defined at the beginning of the analysis. The fluid fraction in each cell is also calculated. The continuity, momentum or transport equation of fluid fraction is formulated using the FAVOR function.

The basic algorithm for advancing a solution in one time increment consists of the following three steps (Flow Science, 2000):

1. Compute the velocities in each cell using the initial conditions or previous time-step values for all advective, pressure, and other accelerations based on the explicit approximations of the momentum (Navier-Stokes) equations.
2. Adjust the pressure in each cell to satisfy the continuity equation.
3. Update the fluid free surface or interface to give the new fluid configuration based on the volume of fluid value in each cell.

The transient analysis began by assigning a volume of water just upstream of the spillway crest and defining the upstream (inflow) and downstream (outflow) boundary conditions. The water would flow into the domain during each time step until a steady-state flow was established. The histories of flow rate through the upstream boundary, volume of water in the domain and kinetic energy of the system were monitored to determine when the flow reached a steady-state.

4. MODEL SENSITIVITY STUDY

The analysis run time depended predominantly on the size and aspect ratio of the grid. In order to minimise the run time without losing too much accuracy, different grid sizes were investigated. Also, the results were compared with the physical model results to determine the degree of accuracy and validity of the model.

4.1 2D Model

The extent of downstream boundary was investigated in two 2D models: with the downstream boundary 300m and 500m away from the spillway crest. In general a 2D model will be much faster to compute than a 3D model. This was carried out to optimise the extent of the 3D model in terms of computational run time. A comparison of the flow rates (Figure 3) shows that the inflow rate for both models stabilised quickly. The average inflow rate for both models was almost identical, indicating that the downstream outflow location did not affect the spillway discharge. The presence of the hydraulic jump created a fluctuation in the downstream outflow rate due to the unsteady nature of this type of flow.

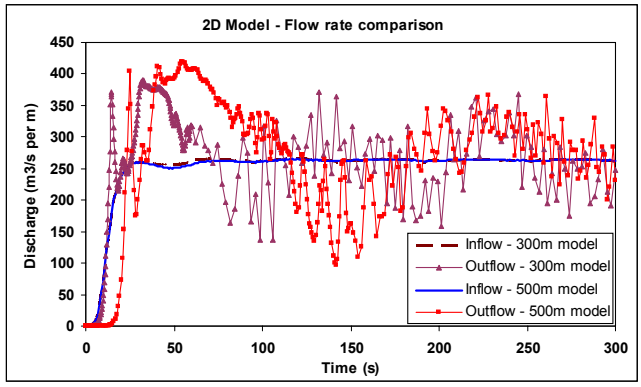

Figure 3 – History of Inflow and Outflow for the 2D Models.

The results from these 2D models indicated the presence of a hydraulic jump in the vicinity of the downstream edge of the plunge pool (Figure 4). They demonstrated that the models (3D and 2D) needed to be extended at least 300m downstream of the spillway crest to capture the effects of the hydraulic jump and high tail water levels.

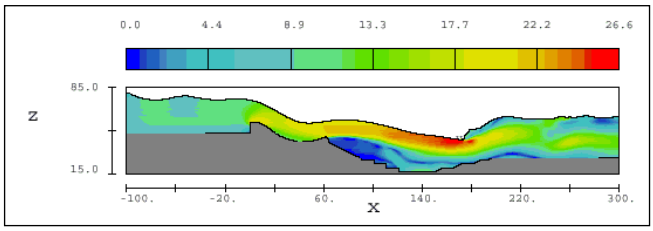

Figure 4 – 2D Model: Hydraulic Jump at the Downstream End of the Plunge Pool.

4.2 Half-3D Model

In order to reduce the computational run time the full 3D model was cut down to a half model with a symmetry boundary through the central bay. A validation test of the two models (the full 3D and the half-3D) was carried out with the head water elevation set to EL77.0m and the downstream tail water set to EL52.0m. An examination of the flow across the crest in the full model indicated that although there was some slight asymmetry in the flow, the half model would be sufficiently accurate for the purposes of the calibration comparison.

A comparison of the average flow rate for each model gives 12,300 m^3/s for the full model, compared with 12,400m^3/s for the half model. This indicates that the spillway flow may be slightly biased to one side (west side) of the spillway in the full model.

A plot showing the volume of fluid with velocity contours of the half-3D model is shown in Figure 5. It can be observed that for the given head and tail water levels the flip bucket was not drowned, and the hydraulic jump occurred in the middle of the plunge pool.

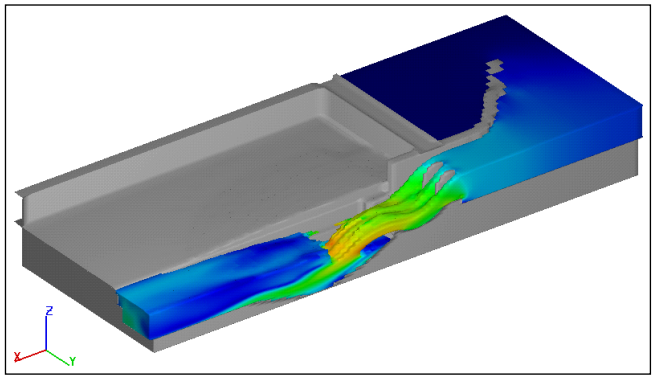

Figure 5 – Half-3D Model: Velocity Distribution.

4.3 Validation Using Physical Model Test Data

The results of the CFD study were validated through comparison with existing experimental data obtained from physical model (1:80 scale) studies undertaken by the Queensland Water Resources Commission (Wilke, 1979). The maximum probable inflow case (flow rate of 11,700 m^3/s) was chosen for the validation. This flow rate represented a flow for a head level of $1.33H_d$, corresponding to an upstream head level of RL77.0m. It should be noted that the CFD and physical models have differing upstream boundary conditions. In the physical model, the upstream flow rate was set at 11,700 m^3/s, and the corresponding upstream head level was determined through measurement on the model. It was reported that the measured head water ranged from RL77.0m to RL77.52m indicating some fluctuation in the measurement. In comparison, the CFD model used a fixed or predefined upstream head level to determine the corresponding discharge rate.

The change in flow rate over the analysis time period is shown in Figure 6. The average inflow rate at the final time steps was about 12,400 m^3/s, which was 6% higher than the value obtained by the physical testing. Previous spillway analyses undertaken by Worley (2003) have found that discharges computed by CFD modelling were generally slightly higher than the theoretical and physical model results. It should be noted that with CFD analyses there will be some 'error bars' (as there are with all numerical analyses) associated with mesh discretisation, and with the physical model there will be errors associated with measurement and inherent scale effects.

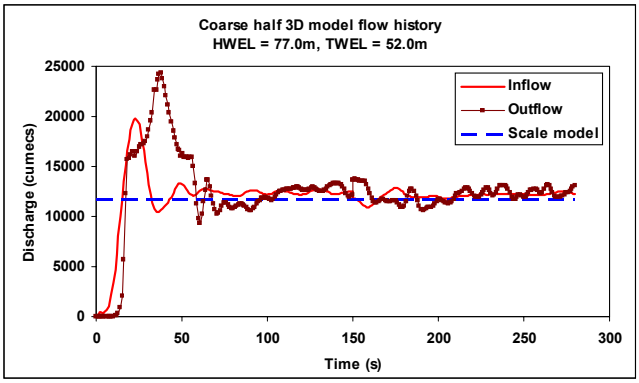

Figure 6 - Comparison of Discharge.

A comparison of the crest pressures at the central bay is shown in Figure 7. Results from both the coarse and fine grid models are shown. Close to the crest, the CFD pressure results have a good correlation to those from the physical model. The coarse model results slightly underestimated the scale model values, while the fine model results have a slight overestimation. Further downstream in the flip bucket the pressure computed by the coarse model was higher (up to 8%) than those obtained from the scale model, however the fine model values were close to those of the physical model.

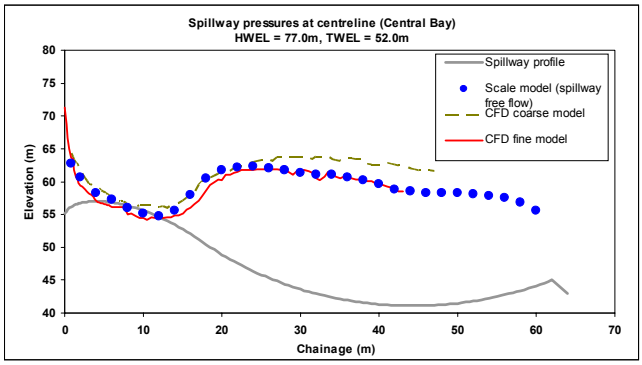

Figure 7 - Comparison of Pressure Distribution.

The flow surface profiles at the central bay for the CFD analysis and physical model are shown in Figure 8. They indicated a generally good correlation, although the CFD analysis appeared to have a slightly higher upstream water level than the physical model. The CFD results also indicated a slightly greater water depth at the downstream spillway trough. The flow surface profiles for both the fine and coarse mesh were virtually identical.

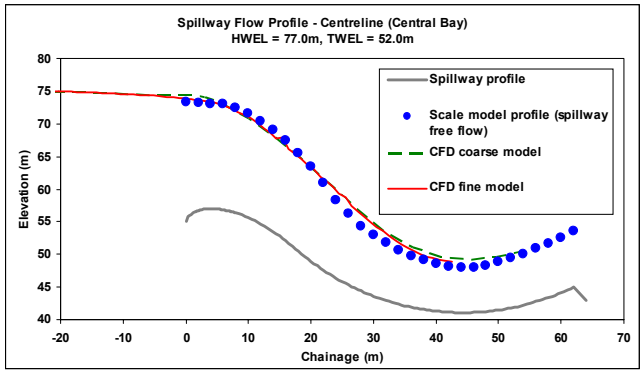

Figure 8 – Comparison of Flow Surface Profile.

Generally, the coarse model results were within reasonable range of the physical test values. The higher upstream level noted in the flow profile comparison may indicate that the boundary conditions of the CFD and physical models did not correspond exactly. This may also account for the slight overestimation of the flow rate and crest pressure. On balance the coarse model has sufficient accuracy to be used to analyse the subsequent cases as shown in Table 1.

5. ANALYSIS RESULTS

The numerical investigation yielded the following results that were useful for the Wivenhoe Alliance to carry out the upgrade design:

- head-discharge curve
- discharge interference with the raised gates
- discharge interference with the crest bridge
- forces acting on the bridge structure and gates
- pressure and velocity distributions at the crest, around the piers, over the apron and plunge pool

Due to space constraint, only the head-discharge curve and the flow behaviour in the plunge pool will be described in this paper. Details of the other results can be found in the report by Worley (2004).

5.1 Head-Discharge Curve

Three types of flow were captured in the analysis and they were:

- Spillway free flow at low head water levels
- Transitional flow (partial orifice flow) at some intermediate head water levels
- Pure orifice flow at high enough head water levels

The discharge rate was determined when a steady-state inflow condition was achieved. The outflow rate was not used because of the high levels of variability in the flow beyond the hydraulic jump. The head-discharge relationship for the half-3D cases is shown in Figure 9. When the upper nappe did not interfere with the underside of the bridge or the gates' skin plates, the discharge was of spillway free flow. Under orifice flow condition, as shown in Figure 10, it was found that for increasing head water level in the range analysed, the average discharge actually decreased. This was due to the presence of a transition zone between free flow and orifice flow, at which point the flow fluctuates between the two discharge rates (see Figure 11). A similar transition zone was reported by the physical model study, occurring over a head water range of up to 3m.

This transitional flow was further complicated because the water level varies between each bay. As a result, the change from spillway free flow to orifice flow occurred at different head water levels in the different bays as shown in Figure 12. With the higher head levels, the range of discharge fluctuation became progressively smaller. It would be expected that if head levels beyond the transitional zone were analysed, the flow would become purely an orifice discharge, and the flow rate would then begin to increase again. Furthermore, at some point the bridge and gate will be overtopped, again modifying the flow pattern and discharge curve.

The orifice discharge rates were also dependent upon the edge conditions of the radial gate. The CFD model used a sharp edged obstacle to represent the skin plate of the gate; however the actual edge geometry and seal type may affect the discharge coefficient.

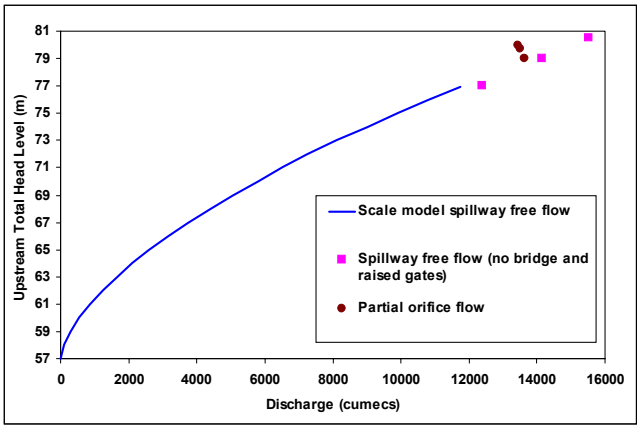

Figure 9 – Head-Discharge Curve 3D Model.

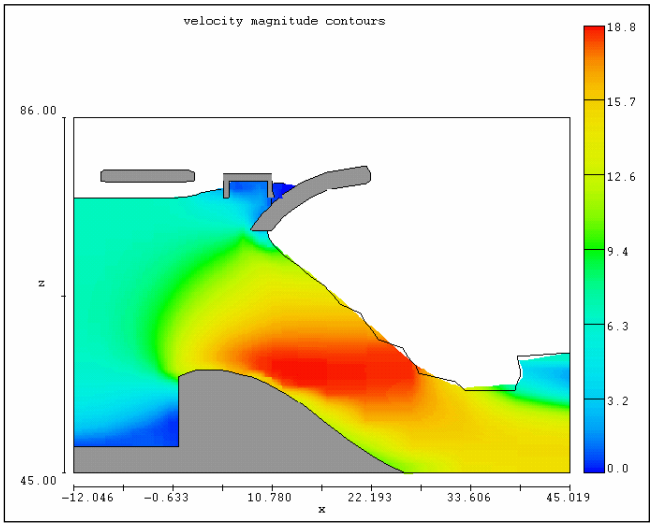

Figure 10 – A Sectional View of an Orifice Flow.

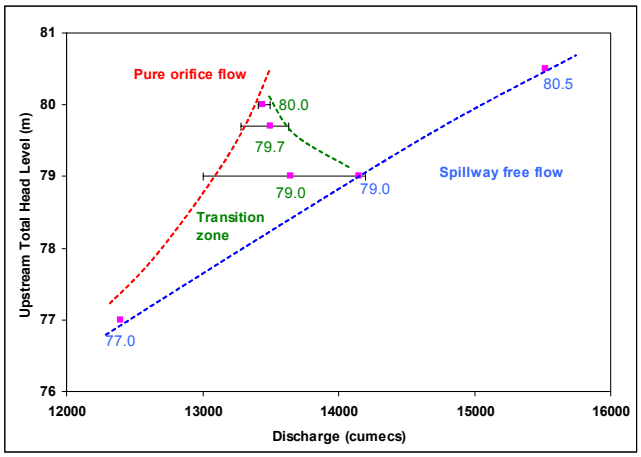

Figure 11 – Discharge in the Transition Zone.

5.2 Plunge Pool

The flow patterns in the plunge pool were examined using the 2D model, which simplified the flow patterns by excluding 3D effects. Due to the time-varying nature of the flow in the plunge pool, the flow patterns varied considerably with each time step. Two extreme conditions were identified; the first with very little recirculation in the plunge pool, and the second with high level of recirculation. A high level recirculation was defined as the condition where the large volume of water has velocity heading back upstream.

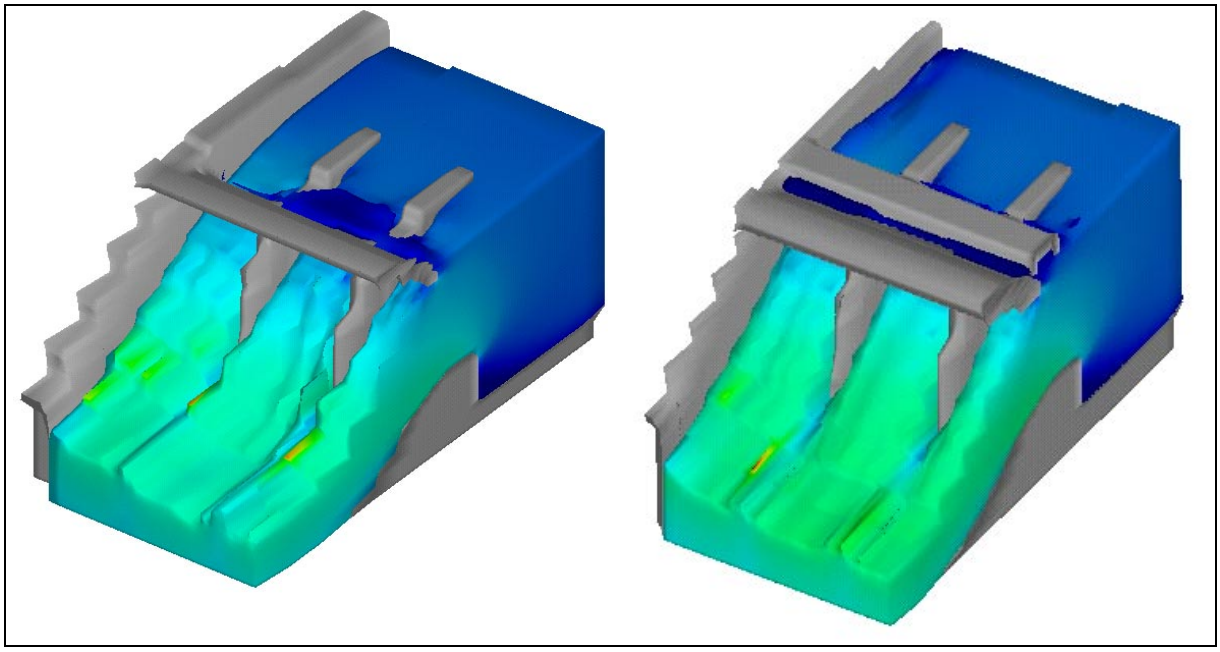

Figure 12 - Partial Orifice Flow (left). Pure Orifice Flow Through all Bays at Higher Head Water (right)

Under low recirculation, the maximum velocity in the pool was 29.4m/s, occurring at the water surface (Figure 13). Backwards flows of up to 19m/s occurred at the bottom of the apron, and flows of approximately 10m/s impinged on the upstream steps of the plunge pool. It can be observed that the velocities close to the bottom and downstream steps of the pool were quite low (< 2m/s).

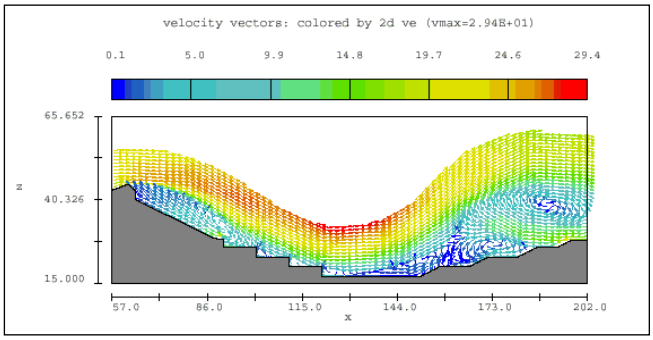

Figure 13 – Velocity Vectors with Low Recirculation.

Under high recirculation, the maximum velocity in the pool was 27.5m/s, again occurring at the water surface (Figure 14). Backwards flows occurred throughout the plunge pool, reaching velocities of up to 15m/s in the lowest section. The velocities at the apron and upstream steps of the pool were quite low (< 2m/s).

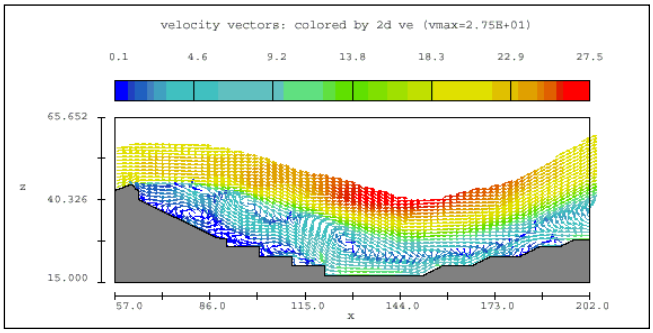

Figure 14 – Velocity Vectors with High Recirculation.

Despite the time varying flow in the plunge pool, the pressures on the apron and pool floor were relatively steady, with no negative pressures occurring at any location. Figure 15 shows the pressure distribution in the pool. This result was taken into consideration for the assessment of the anchoring requirement for the apron slabs stability.

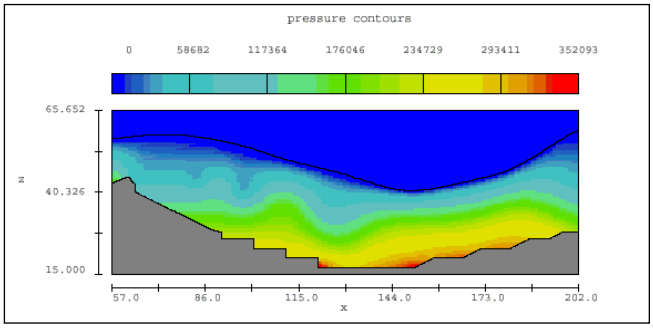

Figure 15 – Typical Plunge Pool Pressure Plot. No Negative Pressures at the Apron or Plunge Pool.

6. CONCLUSIONS

The following conclusions can be made from the investigation:

- When validated against the physical test results, the CFD model provided good correlation for crest pressures and flow profiles. The computed discharge rate was approximately 6% higher than that reported by the physical model.
- For head water elevations greater that EL79.0m, the spillway discharge was likely to impinge upon the raised radial gate skin plate and the gate trunnion, resulting in full and/or partial orifice flow.
- As the head water level increased, the flow passed through an unsteady transition zone, where the discharge rate and gate forces oscillate between spillway free flow and orifice flow conditions.
- The flow patterns occurring in the plunge pool were highly unsteady due to the presence of the hydraulic jump, with the level of recirculation varying significantly. No negative pressures were found to occur in the plunge pool or apron area.
- The CFD analysis was able to provide useful results for the Wivenhoe Alliance to carry out the upgrade design at a reasonable cost and within a tight time frame.

7. ACKNOWLEDGEMENTS

The authors wish to thank the Wivenhoe Alliance and SEQWater for their permission to publish some of the analysis results in this paper.

8. REFERENCES

Chandler, K., Gill, D., Maher, B, Macnish, S. and Roads, G. (2003) Coping with Probable Maximum Flood – An Alliance Project Delivery for Wivenhoe Dam. *Proceedings 43rd ANCOLD conference*, Hobart, Tasmania, pp.24-29 October.

Chow, V.T. (1959) *Open-Channel Hydraulics*, Mc-Graw Hill Book Company, New York.

Flow Science, Inc. (2000) *FLOW-3D User's Manual*.

Hirt, C.W. (1994) Weir Discharge and Counter Currents, *Proceedings 1st International Conference on Hydroinformatics*, Delft, 19-23 September.

Hirt, C.W. and Nichols, B.D. (1981) Volume of Fluid (VOF) Method for the Dynamics of Free Boundaries, *J. Comp. Phys.* 39, No.201.

Hirt, C.W. and Sicilian, J.M. (1985) A Porosity Technique for the Definition of Obstacles in Rectangular Cell Meshes, *Proc. 4th Int. Conf. Ship Hydro*., National Academy of Science, Washington, DC, September.

Ho, D.K.H, Boyes, K.M., Donohoo, S.M. and Cooper, B. (2003) Numerical Flow Analysis for Spillways. *Proceedings 43rd ANCOLD conference*, Hobart, Tasmania, 24-29 October.

Wilke, M. (1979) Wivenhoe Dam Spillway Hydraulic Model Studies, *Queensland Water Resources Commission Hydraulics Laboratory Report*.

Worley (2003) *Hume Dam Spillway – Computational Fluid Dynamics Analysis*, Report No. 251-00436-RP001-5, March. (Not published).

Worley (2004) *Wivenhoe Dam Spillway CFD Study*, Report No. 251-05448-RP002, March. (Not published).

The Institution of Engineers, Australia
8th National Conference on Hydraulics in Water Engineering
ANA Hotel Gold Coast, Australia 13-16 July 2004

Wivenhoe Dam Upgrade
Adopted Strategy and Downstream Impacts

G. Roads
BE (Civil) (Hons), M.I.E.Aust, RPEQ
Hydrology/Hydraulics Manager, Wivenhoe Alliance
Director, WRM Water & Environment Pty Ltd
(Formerly Senior Engineer, Water Studies)
B Maher
BE (Civil) (Hons), RPEQ
Design Manager, Wivenhoe Alliance
Project Engineer, NSW Department of Commerce

Abstract: SEQWater is proposing to upgrade the flood discharge capacity of Wivenhoe Dam, the main water supply source for the cities of Brisbane and Ipswich, to safely pass all floods up to the probable maximum flood (PMF). To achieve PMF capacity, two auxiliary spillways will be constructed consisting of a secondary, three bay fuse plug and a tertiary, one bay fuse plug. Works will also be undertaken on the main embankment to raise the maximum lake level from 77 m AHD to 80 m AHD. Hydrological and hydraulic investigations were undertaken to determine the impact of the proposed works on downstream flood levels and flood flows. The works do not change design flows for events more frequent than the 1 in 5,000 annual exceedance probability (AEP) design flood. For more extreme floods, peak flood depths rise by 0.7m to 1.4 m (or less than 4%) up to 20 river km downstream of the dam and 0.0 to 0.6 m (or less than 3%) through Brisbane. Overall, the proposed works improve the safety of Wivenhoe Dam whilst maintaining the existing flood mitigation benefits.

Keywords: Wivenhoe Dam, Fuse Plug Spillway, Brisbane, PMF, Hydraulic Model, Downstream Impacts.

1. INTRODUCTION

Wivenhoe Dam is located on the Brisbane River about 80 kilometres by road from the centre of Brisbane. Its primary function is to provide a safe water supply to the people of Brisbane and adjacent local authorities. At full supply level the dam holds 1.16 million megalitres (ML), or about 2000 times the daily water consumption of Brisbane. It holds a further 1.45 million ML of flood storage at the maximum lake level of 77 m AHD.

Changes to extreme rainfall estimates have resulted in significant increases in the Probable Maximum Flood (PMF) estimate at the dam since the original design. SEQWater, the owner of Wivenhoe Dam, is proposing to upgrade the flood discharge capacity of the dam to safely pass all floods up to the PMF. To do this, SEQWater has formed an alliance with Leighton Contractors, Coffey Geosciences, MWH Global and the NSW Department of Commerce to design and construct the upgrade works.

This paper details the configuration of the proposed auxiliary spillways and the outcomes used to design the spillways, including the concepts on how a fuse plug spillway operates. The methodology and results of hydraulic investigations used to determine the adequacy and downstream impacts of the proposed auxiliary spillways are also presented.

2. PROPOSED AUXILIARY SPILLWAYS

2.1 Design Outcomes

The upgrade of Wivenhoe Dam is driven by the need to improve the safety of the dam and to reduce flood risk to the downstream community. To achieve this, the following design outcomes were adopted:

- To allow Wivenhoe Dam to safely pass the latest estimate of the PMF;
- To preserve the flood mitigation benefits of Wivenhoe Dam for more frequent flood events;
- To ensure that outflows are less than inflows for all flood events;
- To limit the frequency of operation of the auxiliary spillway to reduce downstream damage; and
- To minimise the cost of the upgrade option.

2.2 Proposed Auxiliary Spillway Configuration

The option selected to upgrade the dam consists of a secondary, three bay fuse plug on the right abutment, and a tertiary, one bay fuse plug at Saddle Dam 2, some 2.8 km southeast of the existing spillway. Works will also be undertaken on the main embankment to raise the maximum lake level to 80 m AHD. In setting the maximum lake level, zero freeboard is proposed. The works will be undertaken in two stages. Stage 1 works involve the construction of the right abutment spillway and works on the main embankment to raise the maximum lake level. Stage 2 involves the construction of the Saddle Dam 2 spillway, which will be completed within the next 20 years. The location and alignment of the spillways is shown in Figure 1.

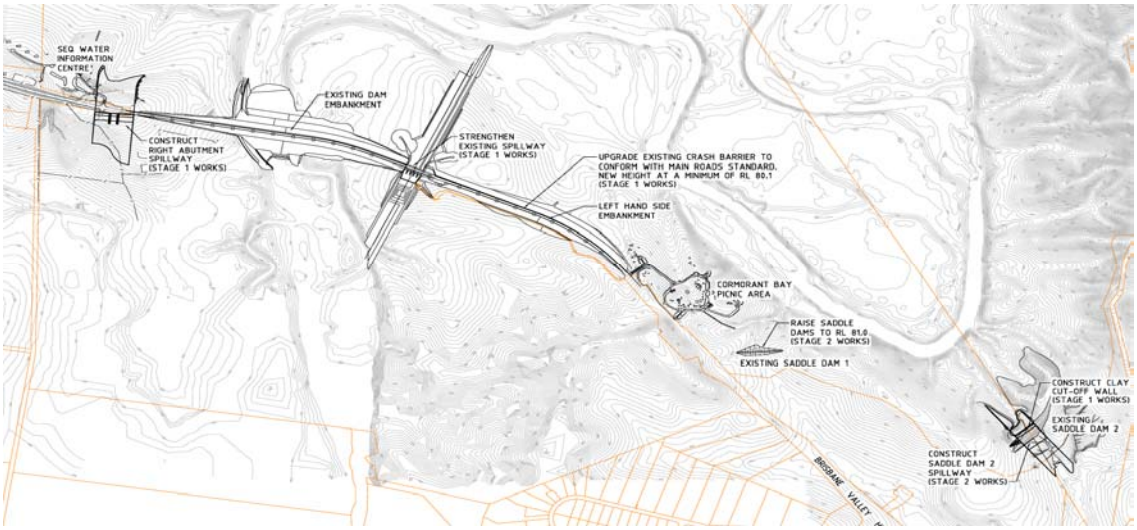

Figure 1 – Location and General Arrangement of the Wivenhoe Dam Auxiliary Spillways

Table 1 provides details of the auxiliary spillways and peak lake levels when the fuse plugs initiate. An ogee crest was selected for the spillways to reduce the width and cost of the structure. Stage 1 works allow the dam to safely pass the 1 in 100,000 annual exceedance probability (AEP). Stage 2 works safely pass the latest PMF.

Table 1 - Peak Lake Water Levels at Fuse Plug Initiation, Wivenhoe Dam

Auxiliary Spillway Location	Spillway Crest Control Type	Spillway Crest Width (m)	Spillway Crest Level (m AHD)	Peak Lake Level at Fuse Plug Initiation (m AHD)
Right Bank				
Fuse plug 1	Ogee	34	67	75.7
Fuse plug 2	Ogee	64.5	67	76.25
Fuse plug 3	Ogee	65.5	67	77.2
Saddle Dam 2				
Fuse plug 4	Ogee	100	67	78.3

2.3 Concept of Controlled Fuse Plug Spillway

Figure 2 shows a cross section of a typical fuse plug embankment. It is effectively a zoned earth and rock fill embankment that is constructed on a non-erosive sill or weir. The embankment is designed to erode in a controlled manner when the lake water level reaches a pre-determined level. Below this level, the embankment impounds water in the same manner as a typical zoned earth and rock fill embankment. The upstream face of the embankment consists of a riprap layer to protect against wave action. Consecutive layers consist of coarse rock followed by a coarse filter and then the impermeable clay core laid on a similar slope to the riprap. Downstream of the sloping clay core are more layers of filters that lie on a wedge of compacted rock fill.

A low point, or pilot channel, is located in the embankment crest, which initiates the controlled erosion. A narrow vertical slot of coarse filter is located immediately downstream of the pilot channel that extends to the downstream slope of the dam and replaces the compacted rock fill. As the lake water level rises above the pilot channel crest to a depth of about 0.15 m, fast flowing water starts to erode the coarse filter in the vertical slot, which removes the material supporting the sloping clay core eventually causing it to collapse. The material adjacent to the slot is then exposed to the fast flowing water initiating lateral erosion.

2.4 Fuse Plug Performance

Fuse plug performance is largely based on two research projects undertaken by Tinney & Hsu (1961) and Pugh (1985). The Tinney & Hsu study was conducted as part of the design of the Oxbow fuse plug at Snake River in the United States. In the study, scale model tests were conducted in the laboratory and the field to investigate the behaviour of the fuse plug spillways. Pugh's study used laboratory models to simulate full sized fuse plugs from 3 m to 9 m high. Both studies found that the fuse plugs washed out in an orderly and predictable manner. They found that the rate of erosion is proportional to the type of material used and height of the embankment.

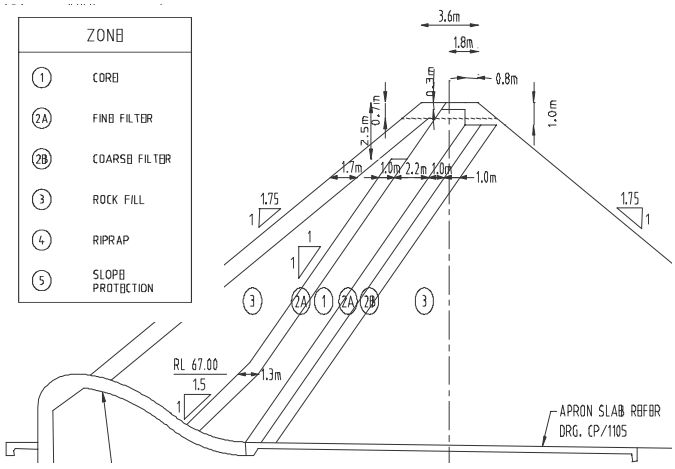

Figure 2- Typical Fuse Plug Embankment Cross Section

The NSW Public Works and Services, now the NSW Department of Commerce, extrapolated the results of these studies to design the 15 m high fuse plug embankments at Warragamba Dam in Sydney (DPWS, 1998). The analysis undertaken for Warragamba Dam has been used to select the material and estimate the lateral erosion rates for the proposed fuse plugs at Wivenhoe Dam. Based on the fuse plug material selected for Wivenhoe, lateral erosion rates of 100 m per hour are expected.

3. DESIGN FLOW ESTIMATES

3.1 Previous Flood Studies

The current spillway capacity of Wivenhoe Dam is based on a PMF inflow of 15,090 m^3/s (Hausler and Porter, 1977). This estimate was based on a 48-hour duration probable maximum precipitation (PMP) estimate of 480 mm and synthetic unit graphs. The design flood estimate was revised in 1983 to 48,000 m^3/s. The increase was mainly attributed to the changes in the PMP, which increased to 1,000 mm for the 48-hour duration storm. The Department of Natural Resources (DNR) (formally WRC) revised the design flows again as part of a comprehensive safety review of the dam undertaken between 1990 and 1994 (DNR, 1994). DNR estimated the PMF inflow to be 39,900 m^3/s. The different PMF estimate was mainly attributed (again) to changes in the PMP, which was revised down to 870 mm for the 48-hour duration storm. Flood operating procedures were also incorporated into the models to estimate design outflows.

The BOM recently updated the PMP estimates for Wivenhoe using the revised Generalised Tropical Storm Method (GTSMR) (BOM, 2003). BOM also provided the latest temporal patterns and spatial rainfall weightings to be used with the new PMP data. The 2003 PMP estimates are some 20% higher than the previous PMP estimates. As a result, the new PMF estimate for the catchment is significantly higher than the 1994 estimate and much larger than the current spillway capacity of Wivenhoe Dam.

3.2 Design Flows

Figure 3 shows the inflow and outflow flood frequency curves for the existing dam and upgraded dam. Peak inflows represent the sum of inflows from the Upper Brisbane River catchment and outflows from Somerset Dam. Details of the methodology used to derive the design flows are presented in Wivenhoe Alliance (2004).

- The rapid increase in flood frequency curve flows represent the releases from the various fuse plugs;
- The AEP of the dam crest flood (DCF) for the existing dam is about 1 in 22,000 rising to 1 in 100,000 AEP for Stage 1 and PMF for Stage 2;
- Both Wivenhoe and Somerset Dams have a significant impact on design flood outflow peaks. Somerset Dam alone reduces the PMF inflow peak to Wivenhoe Dam by over 6,000 m^3/s. Combined Stage 1 and Stage 2 works reduce the PMF peak outflow by a further 11,000 m^3/s;
- The existing dam is designed for a maximum flood level of 77 m AHD, which is the top of the existing clay core and filters. The flood AEP at this level is about 1 in 10,000;
- The proposed works do not change outflows for flood events up to the 1 in 2,000 AEP event.

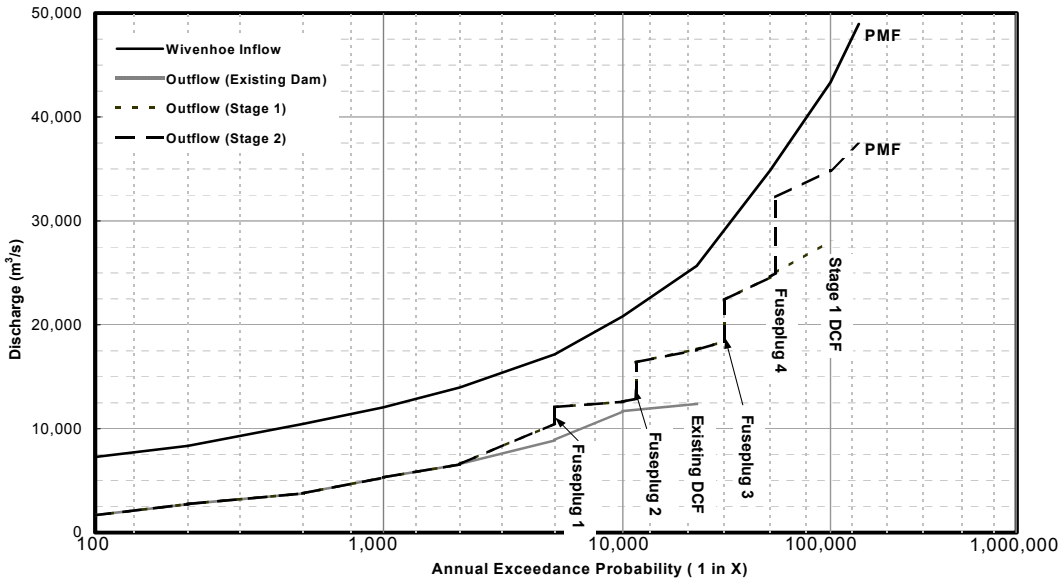

Figure 3 - Inflow and Outflow Flood Frequency Curves for the Existing, Stage 1 and Stage 2 Upgrades.

3.3 Fuse Plug Discharges

Table 2 shows peak outflows from each spillway and maximum lake water levels for floods that just initiate a fuse plug breach. The results show that:

- The capacity of each fuse plug bay increases incrementally as the flood AEP decreases.
- The first fuse plug breach increases downstream flows by about 1,600 m^3/s within about 20 to 30 minutes. The second fuse plug breach increases flows by 3,300 m^3/s within about 30 to 40 minutes and the third by 4,000 m^3/s in about the same time. The final fuse plug at Saddle Dam 2 increases downstream flows by 7,400 m^3/s in about an hour. (Refer to Figure 3)

Table 2 - Peak Outflows and Maximum Lake Levels at Fuse Plug Initiation, Wivenhoe Dam

Fuse Plug No. Initiated	Approx. AEP (1 in X Years)	Peak Outflow (m^3/s)			Lake Water Level at Initiation (m AHD)
		Gated Spillway	Right Abutment Spillway	Saddle Dam 2 Spillway	
1	5,000	10,500	1,600	0	75.7
2	11,000	11,000	5,300	0	76.25
3	30,000	12,200	10,200	0	77.2
4 (SD2)	53,000	13,000	11,850	7,400	78.3

4. DOWNSTREAM IMPACTS OF A FUSE PLUG DISCHARGE

The downstream impacts of the auxiliary spillways were determined using a MIKE 11 one-dimensional hydraulic model (DHI, 2003) of the Brisbane River. The model extends from Wivenhoe Dam to Moreton Bay, a river distance of 150 km, and includes the Bremer River and its tributaries. The model was used to determine the difference in peak discharges and peak water levels along the Brisbane River between events just prior to and just after a fuse plug initiates; and to determine the depth of flood water and the rate of water level rise at various locations when a fuse plug initiates.

4.1 Hydraulic Model Development

The Ipswich Rivers Improvement Trust (IRIT) made available the MIKE 11 hydraulic model of the Brisbane and Ipswich Rivers, developed by SKM (2000). The model was based on the Brisbane River MIKE 11 model, also developed by SKM, for Brisbane City Council. Details of the model development and calibration are given in the Ipswich Rivers Flood Study Report (SKM, 2000). The IRIT model was updated and recalibrated for this study. The modified model configuration is shown in Figure 4. The changes made to the model are as follows:

- Brisbane River cross sections in the IRIT MIKE 11 model were extended to encompass the GTSMR PMF maximum water levels;

- The model was extended from the Ipswich and Esk Shire boundary to Wivenhoe Dam and up to Lyons Bridge on Lockyer Creek using cross sections provided by DNR&M.
- Thirty eight additional branches were used to represent the overland flow paths that occur at high flows;
- Additional floodplain storage on the Bremer River and its tributaries, not represented by the existing cross sections was modelled using stage-surface area curves;
- The stage – storage relationship representing floodplain storage within Oxley Creek was extended up to the new PMF level; and
- A number of bridge structures were modified to remove model instabilities. According to discussions with DHI, the developers of MIKE 11, the algorithms used to estimate afflux at bridges has been changed between the 1999 and 2003 versions of MIKE 11. The two model versions will often produce different affluxes using the same parameters and can produce instabilities.

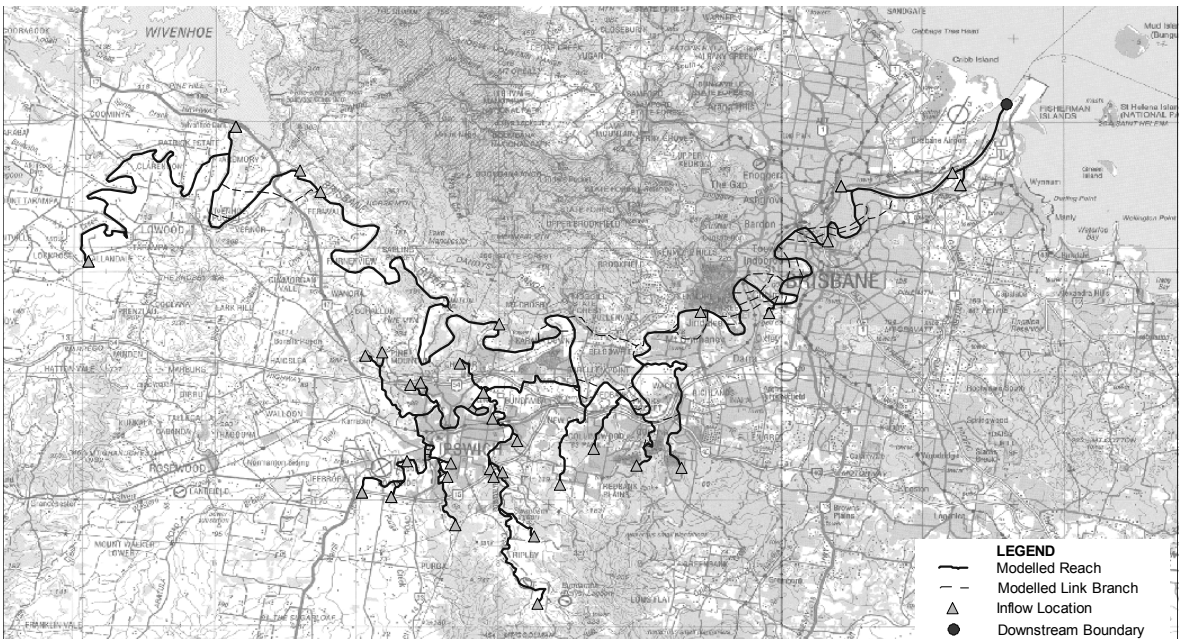

Figure 4 – Modified MIKE 11 Hydraulic Model Configuration, Brisbane River and Tributaries

4.2 Model Calibration

The MIKE 11 model was re-calibrated against historical water level data and water levels and flows predicted using the IRIT model. The 1974 historical flood was used for this purpose, as it is the largest historical flood with recorded water level and flow data. The 1974 flood calibration parameters were also adopted by SKM in their study to estimate design flows. The 1974 flood had an AEP of about 1 in 100 at Wivenhoe Dam.

Manning's 'n' values used in the IRIT model varied from 0.03 to 0.13 for the Brisbane River main channel, and from 0.04 to 0.22 on the floodplain. The adopted Manning's 'n' values account for channel roughness and bend losses (which are not explicitly modelled in MIKE 11). Re-calibration of the model was achieved by increasing Brisbane River channel and floodplain Manning's 'n' values by 5% downstream of the Bremer River.

It is noted that the IRIT model used very high overbank Manning's roughness values (up to 0.22). The adopted values are likely to be adequate for events up to the 1974 flood as buildings will slow overbank velocities. As the flood level rises, overbank velocities are likely to increase and Manning's 'n' values will correspondingly decrease. The IRIT model values have been adopted for this study in the absence of better data. Thus, flood levels for events much larger than the 1974 flood are likely to be marginally over-predicted.

There is generally good agreement between predicted and recorded flood level data with predicted data generally within +/- 0.2 m of recorded values. The predicted afflux at the bridges generally compares well with recorded data. The difference between Brisbane River maximum water levels predicted in this study and in the IRIT study for the 1974 event is generally within +/- 0.2 m. The maximum flows predicted in this study are generally 200 to 300 m^3/s lower than those predicted using the IRIT. This represents a difference of less than 4 % of the peak flow. Overall the model calibration is considered satisfactory for the purposes of this investigation.

4.3 Concurrent Downstream Flows

Table 3 - Adopted Concurrent Downstream Flows, Brisbane River

Fuse Plug	Wivenhoe Dam Inflow AEP (1 in X)	Concurrent Lower Brisbane River Flow AEP (1 in X)
1	5,000	120
2	8,500	300
3	25,000	1,000
4	52,000	5,000

Table 3 shows the AEP of the design flows in the downstream catchments used concurrently with the various design floods at Wivenhoe Dam. Approximately half of the Brisbane River catchment is located downstream of Wivenhoe Dam. The concurrent downstream flow was determined using the approximate procedures recommended in Australian Rainfall and Runoff (IEAUST, 1999). This assumes that design flows in the Wivenhoe Dam catchment occur concurrently with flows in the Lower Brisbane River catchment generated using 0.6 times the Wivenhoe Dam catchment design rainfall .

4.4 Impact of Fuse Plug Flows on Downstream Discharges

Table 4 - Increase in Peak Flow due to Fuse Plug Initiations

Fuse Plug No.	Peak Flow Increase (m^3/s)		
	Wivenhoe Dam	Savages Crossing	Moggill Gauge
1	1,600	800	300
2	3,300	1,700	700
3	4,000	1,800	600
4	7,400	3,500	2,000

Table 4 shows the difference in peak flows at various locations along the Brisbane River between floods that just do not and just do initiate a fuse plug. Savage Crossing is located about 20 river km downstream of the dam. Moggill gauge is located about 75 river km downstream just below the Bremer River confluence. The results show that the biggest reduction in flood peak occurs between the dam and Savages Crossing. A review of the available elevation data shows that there is about 840,000 ML of flood storage available between the dam and Savages Crossing below the approximate flood level when fuse plug 4 initiates. This is more than half the available flood storage in Wivenhoe Dam. Savages Crossing appears to act as a "choke" on downstream flows.

4.5 Impact of Fuse Plug Flows on Downstream Water Levels

Figure 5 shows the differences in water levels along the Brisbane River between Moreton Bay and Wivenhoe Dam between floods immediately prior to and just after the various fuse plugs initiate. The greatest impact occurs between Savages Crossing and Mt Crosby Weir where water levels rise by around 0.7 m for fuse plug 1 and by 1.4 m for fuse plug 4. Downstream of the Bremer River confluence, water levels increase by less than 0.4 m for fuse plugs 1 and 3 and less than 0.7 m for fuse plug 4.

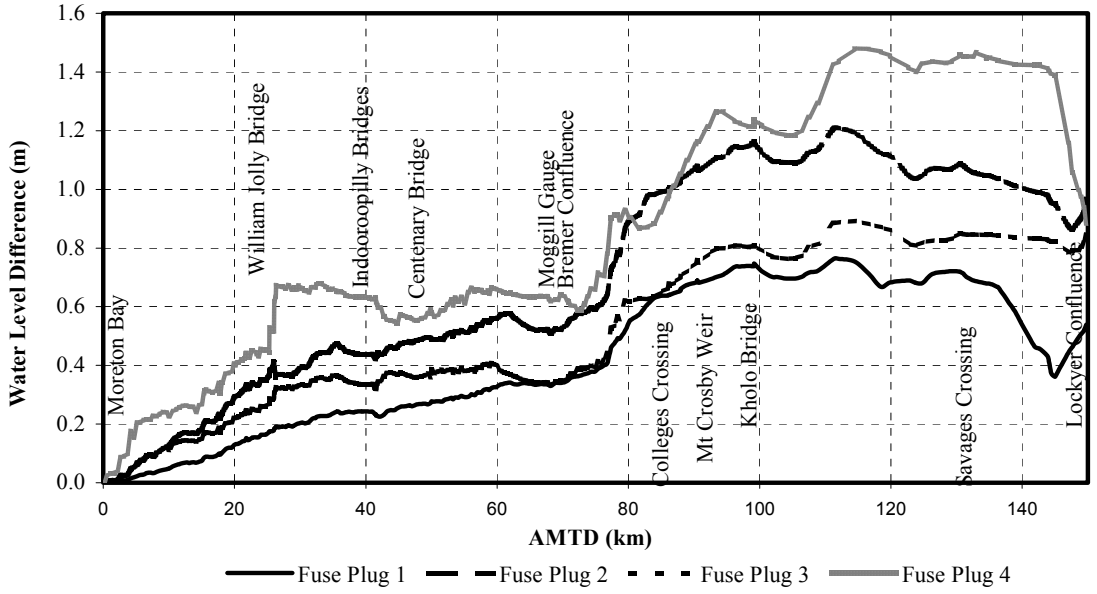

Figure 5 - Peak Water Level difference along Lower Brisbane River for Pre and Post Fuse Plug Initiating Events

4.6 Impact of Fuse Plug Flows at Savages Crossing and Moggill Gauge

Figure 6 and Figure 7 show the water level hydrographs at Savages Crossing and at Moggill Gauge respectively for floods immediately prior to and just after the various fuse plugs initiate. The 1974 peak water level and the upper limit of non damaging flows through Brisbane and Ipswich are also shown. The following is of note:

- The percentage increase in flood depth due to a fuse plug initiating at Savages Crossing varies from 2.5% for fuse plug 1 and 4% for fuse plug 4. The depth of water at Savages Crossing prior to the fuse plugs initiating is well above the level of non damaging flows.
- The percentage increase in flood depth due to a fuse plug initiating at Moggill gauge varies from 1.8% for fuse plug 1 to 3% for fuse plug 2. The depth of water at Moggill prior to the fuse plugs initiating is well above the level of non damaging flows.
- Water levels are higher during the recession of the flood when the fuse plugs initiate. Modifications to the main spillway gate closing procedures are likely to reduce releases and hence receding water levels;
- The rate of water level rise caused by the fuse plugs initiating does not significantly change from the pre fuse break rate of rise at both Savages Crossing and Moggill. The large floodplain storage available between the dam and Savages Crossing appears to mitigate the rapid increase in discharges resulting from the fuse breaks.

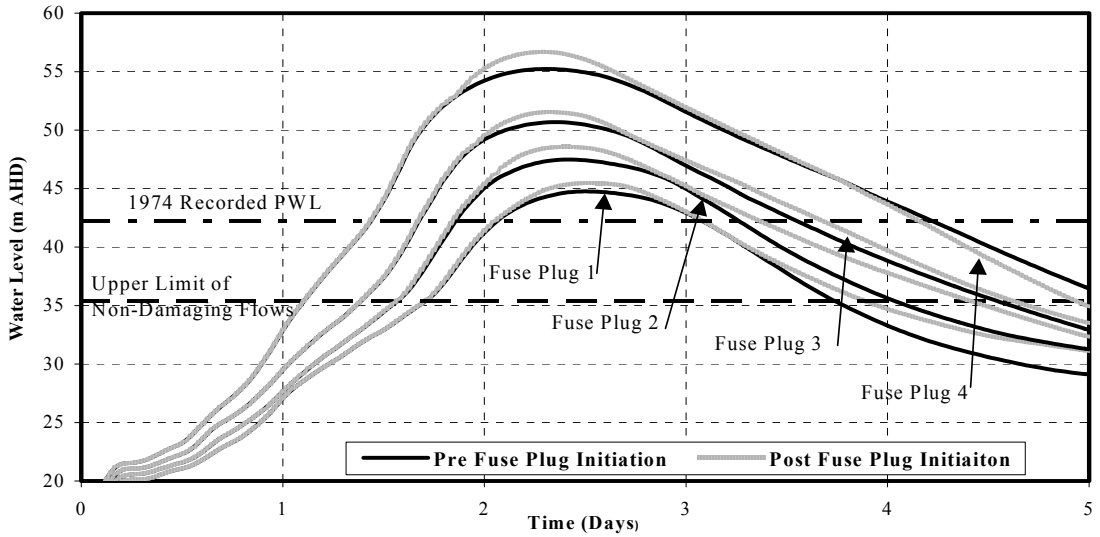

Figure 6 - Water Level Hydrographs at Savages Crossing (Fernvale) for Pre and Post Fuse Plug Initiating floods

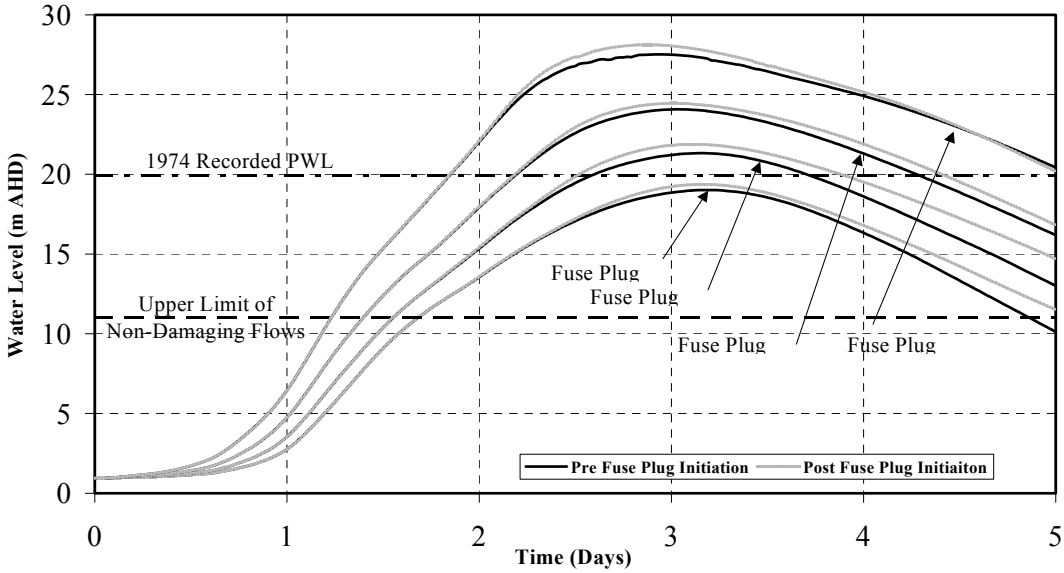

Figure 7 - Water Level Hydrographs at Moggill Gauge for Pre and Post Fuse Plug Initiating floods

- The 1974 flood peak water level at Moggill is higher than the peak level generated from 1 in 5,000 AEP flood at Wivenhoe and the 1 in 120 AEP flood in the downstream catchments, even though the 1974 flood was much smaller. It appears that the dam holds back the flood peak from the Upper Brisbane River until the peak from the downstream tributaries has passed the Moggill gauge. Had the dam been constructed prior to the 1974 flood, downstream flood levels would have been substantially lower.

5. CONCLUSIONS

Overall, the proposed works will improve the safety, or flood discharge capacity, of Wivenhoe Dam whilst maintaining the existing flood mitigation benefits. All design objectives outlined in Section 2.1 are met by the proposed option. The key conclusions of the study can be summarised as follows:

- The AEP of the dam crest flood is 1 in 22,000 for the existing dam, decreasing to 1 in 100,000 AEP after Stage 1works and PMF after Stage 2 works;
- The four fuse plugs initiate at AEP's of 1 in 5,000, 1 in 11,000, 1 in 30,000 and 1 in 53,000 AEP. The capacity of each fuse plug increases as the probability of the flood decreases.
- The proposed upgrade works do not change outflows for flood events up to the 1 in 5,000 AEP event. This is substantially higher than the 1974 flood, which had an AEP of about 1 in 100 at the dam;
- Initiation of the three fuse plugs on the Right Abutment spillway increase peak water levels by 0.7 m to 1.1 m at Savages Crossing, and by 0.3 m to 0.5 m at Moggill Gauge. The initiation of fuse plug 4 (Saddle Dam 2 spillway) increases peak water levels by almost 1.5 m at Savages Crossing and by 0.6m at Moggill Gauge. This equates to a maximum water level increase of 4% at Savages and 3% and Moggill from the fuse plug flows.
- The rate of water level rise downstream of Savages Crossing is not significantly affected by the fuse plug breaches. It appears that the rapid increase in flows from all fuse plug breaches is mitigated by the large floodplain storage upstream of Savages Crossing.

6. REFERENCES

BOM (2003) *Generalised Probable Maximum Precipitation Estimates for the Wivenhoe Dam Catchment*. Report prepared for SEQWater by the Hydrometeorological Advisory Service of the Commonwealth Bureau of Meteorology (HAS report No. GTSMR/03R).

DHI (2003) *MIKE 11 A Modelling System for Rivers and Channels Reference Manual*, DHI Software June 2003

DNR (1994) *Brisbane River Flood Study Suite of Reports*. Reports prepared by the Department of Natural Resources (1994).

DPWS (1998) *Warragamba Dam Auxiliary Spillway – Concept Design Report* NSW Department of Public Works and Services, Dams and Civil Section, Report No. DC98058

IEAUST (1999) *Australian Rainfall and Runoff. A Guide to Flood Estimation*. Institution of Engineers Australia (1999)

Hausler and Porter (1977) *Report on the Hydrology of Wivenhoe Dam*, Water Resources Commission, QDPI Hydrology Report 143005.PR Brisbane

Pugh C.A. (1985), *Hydraulic Model Studies of Fuse Plug Embankments*, Hydraulics Branch, Division of Research and Laboratory Services, Engineering and Research Center, Denver Colorado, United States Department of the Interior, Bureau of Reclamation.

SKM (2000) *Ipswich Rivers Flood Studies*, Report prepared for Ipswich Rivers Improvement Trust SKM (2000)

Tinney E.R and Hsu H.Y (1961), Mechanics of Washout of an Erodible Fuse Plug, *Journal of the Hydraulic Division*, Proceedings, American Society of Civil Engineers, vol 87, No. HY3 May 1961

WIVENHOE ALLIANCE (2004) *Design Discharges and Downstream Impacts of the Wivenhoe Dam Upgrade*, Report prepared by the Wivenhoe Alliance for SEQWater, Item ID:003684308.

The Institution of Engineers, Australia
8th National Conference on Hydraulics in Water Engineering
ANA Hotel Gold Coast, Australia 13-16 July 2004

Tropical Cyclone Storm Surge Modelling of the Coast of Queensland

J. Savioli
PhD, Principal Coastal and Marine Engineering.
DHI Water and Environment Pty. Ltd., Australia
S. Szylkarski
QLD Manager
DHI Water & Environment, Pty Ltd, Australia

Abstract: Tropical cyclones are large scale and severe low-pressure weather systems. These systems typically affect the north-eastern coast of Australia between November and April and combine strong winds, intense rainfall and induced ocean effects including extreme waves, currents and storm surge. To facilitate the assessment of storm surge flooding, DHI has applied a methodology based on the application of the two dimensional coastal modelling system MIKE21. This system allows the simulation of hydraulics, waves and related phenomena in coastal areas and seas and also the generation of wind and pressure fields of cyclones using a parameterised description of the cyclone shape with predefined historical records tracks and design tracks and also the effects of waves. The model was calibrated against tidal measurements and storm surge events along the Queensland coast to verify it correct behaviour. The model results provided accurate surge inundation maps that provide information on hazard zones, areas where the inundation depths combined with various other factors constitutes an unacceptable hazard.

Keywords: storm surge, tropical cyclones, wave modelling.

1. INTRODUCTION

Tropical cyclones are large scale and severe low-pressure weather systems that affect the north-eastern coast of Australia typically between November and April. These cyclones combine strong winds, intense rainfall and induced ocean effects including extreme waves, currents and storm surge and pose a real threat to many coastal communities along the northern coast of Queensland every year. As an example, in 1989 tropical cyclone Aivu passed through the Burdekin Shire inundating large areas of the Shire resulting in significant material and rural losses.

In the event of future cyclones the Burdekin Shire Council decided to facilitate a disaster risk management plan to develop a disaster risk management strategy. This strategy was based on the development of a storm surge forecast model to be operated by Council, which would provide storm surge prediction during cyclone events. The storm surge model was used to develop disaster risk management plans, including evacuation plans and storm surge mitigation measures for the Burdekin Shire. The primary aim of the study was to minimize the risk of death and injury due to storm surge events with a secondary aim of reducing flooding isolation and infrastructure damage.

2. MODEL DESCRIPTION

A methodology was developed based on the modelling of the cyclones with the two dimensional coastal modelling system MIKE21 that is applicable to the simulation of hydraulics, waves and related phenomena in coastal areas and seas. The complexity of the area and the tropical cyclones required the use of nesting facilities in MIKE 21 to define a modelling area large enough to avoid perturbations along the boundary conditions and small enough to allow accurate description of the complex reef and channel systems. Five model areas, nested in 4 levels were defined; the layout of the model set-up is illustrated in Fig. 1.

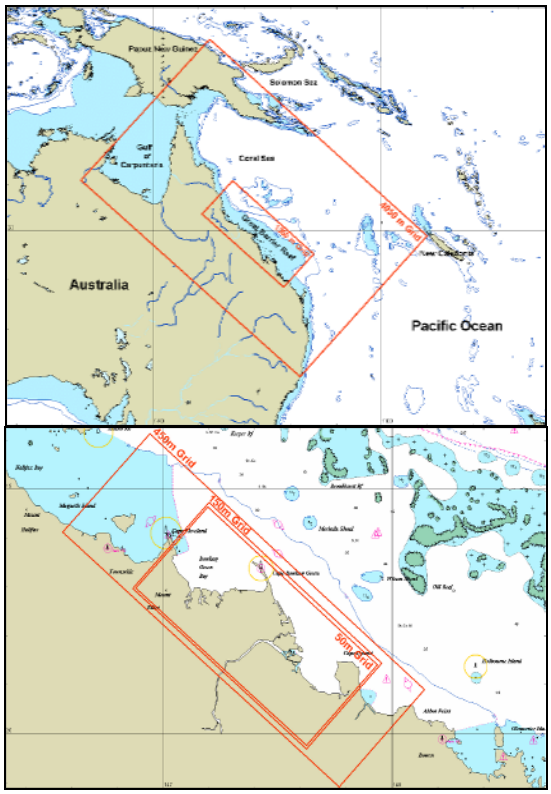

Figure 1 - Overview Of The Model Set-up

The study area is complex due to the presence of the offshore coral reefs and low-lying hinterland areas. Therefore, data from different sources was collected and this information was supplemented with a detailed airborne laser scanning of the coastal areas and the hinterland. Fig. 2 illustrates the detailed bathymetry of the study area after being processed with MIKE 21.

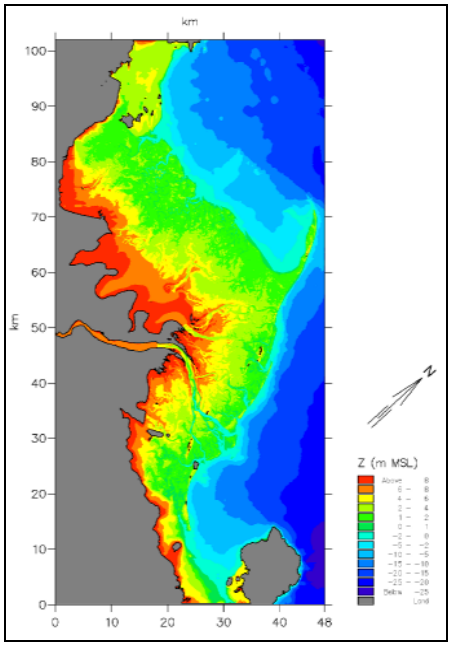

Figure 2 - Detailed Bathymetry

The MIKE 21 model allows for automatic generation of wind and pressure fields of cyclones using a parameterised description of the cyclone shape with a predefined track. Wind and pressure fields have been generated from the parameterised data sets and in conjunction with the results prepared for the hydrodynamic and wave modelling scenarios.

The impact of wave set-up on the storm surge was also investigated to obtain the contribution of the waves on the total surge. For this purpose the spectral wind-wave MIKE21 SW based on unstructured meshes was established for the area. The model simulates the growth, decay and transformation of wind-generated waves and swells in offshore and coastal areas and is particularly applicable for simultaneous wave prediction and analysis on (global), regional and local scale. The computed wave field was applied in the hydrodynamic model simulations.

2.1 Calibration Of The Model

The numerical model was calibrated for two different conditions:

- Normal tidal conditions.
- Storm surge events.

2.1.1 Tidal Calibration

The model was calibrated against predicted tidal levels of the area to ensure its correct behaviour under normal tidal conditions. Comparisons at 14 locations along the Queensland coast were carried out. Fig. 3 presents the model water level predictions (red) compared to water levels based on tidal constituents (black). The results show good agreement.

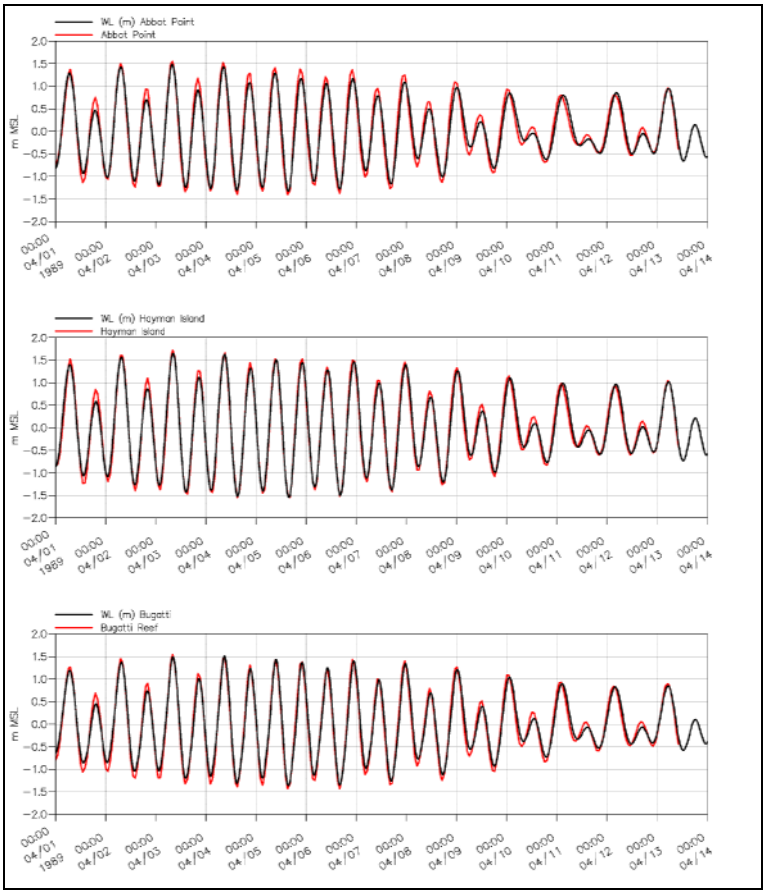

Figure 3 - Comparison Of Predicted And Computed Water Levels At Four Stations Along the East Coast of Australia

This calibration exercise provided a good insight of the influence of the barrier reef on the tidal conditions of the area. It was observed that the reef with its narrow deep channels regulates the inflow and outflow of water and consequently plays a key role on the hydrodynamic conditions of the study area. This was particularly so in the Mackay region, where large tidal ranges are experienced due to the influence of the reef convergence of tidal currents.

2.1.2 Storm Surge Calibration

The model calibration was extended to include the full storm surge model including wave setup for two cyclone events, Althea (1971), which hit Townsville to the north of the study area and Aivu (1989). A comparison of the water level predictions for tropical cyclone Althea is presented in Fig. 4 for the recorder locations of Townsville and Bowen. The model results show good agreement, especially during the peak surge conditions.

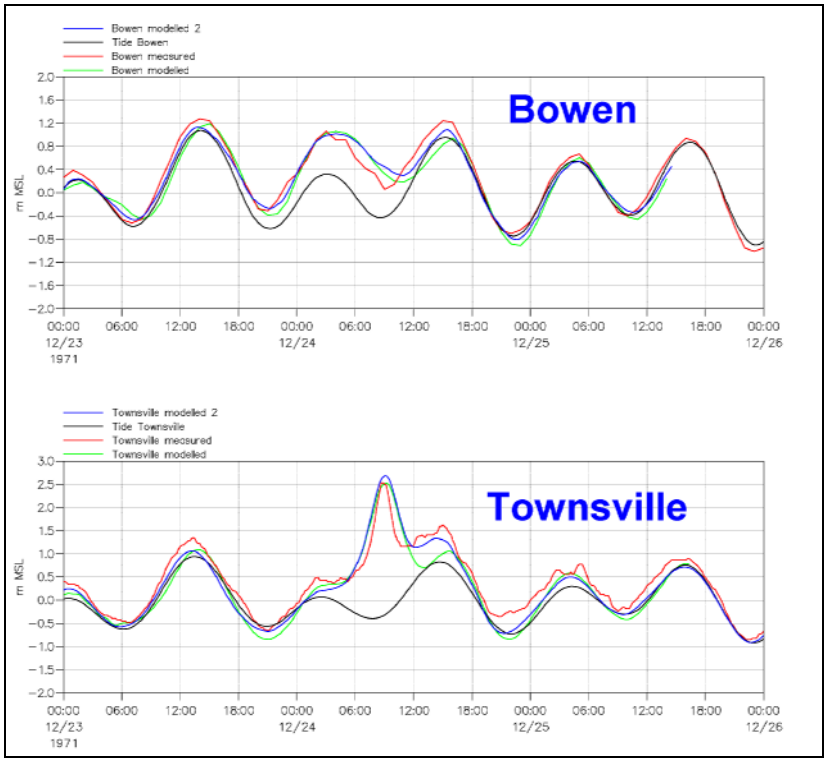

Figure 4 - Comparison of water level measurements and prediction for cyclone Althea.

Fig. 5 presents the model results for Cyclone Aivu in 1989. The left picture shows the wave height and direction predictions, the centre the predicted water levels and to the right the wind and pressure field at a particular time step. Unfortunately, no measurements were available to compare this event to model results, however anecdotic information of the flooding timing and pattern agree with the model results.

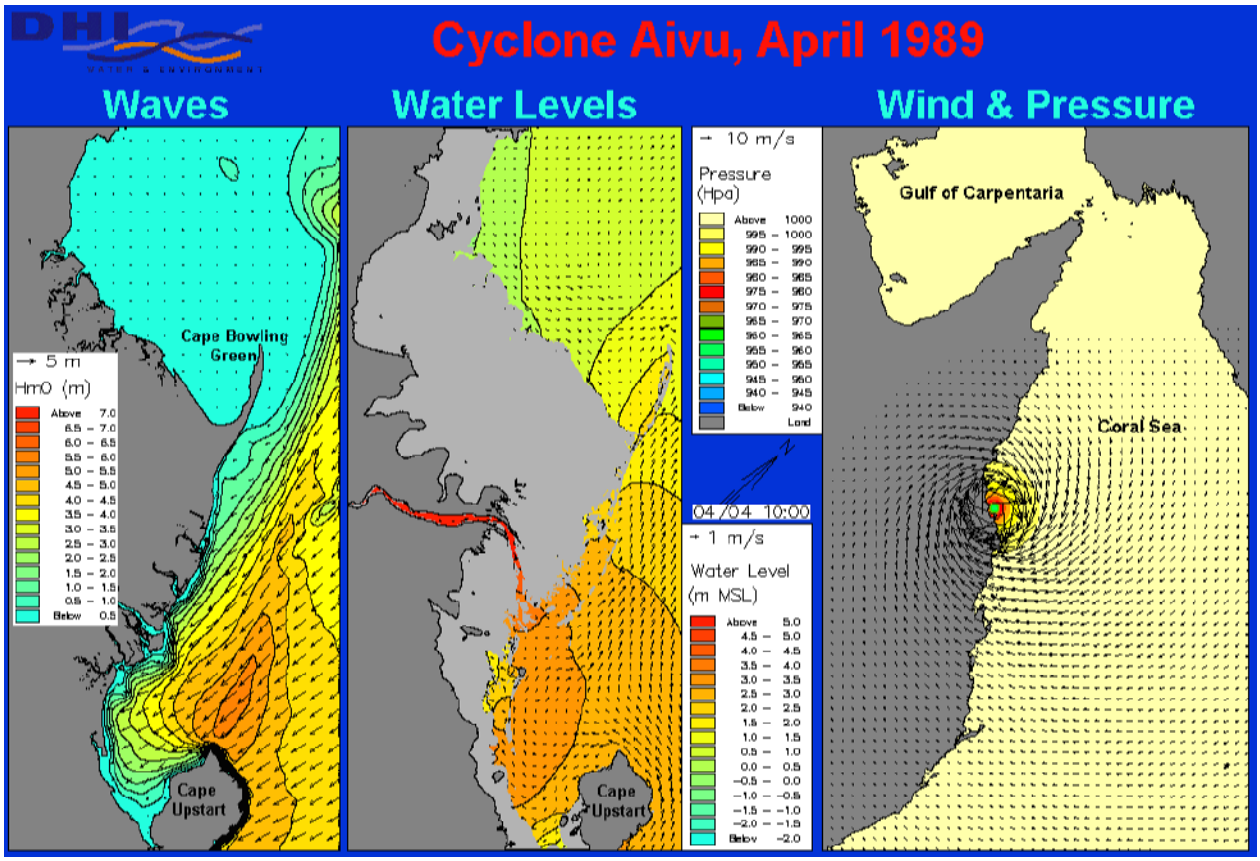

Figure 5 - Wave, Water Levels And Wind And Pressure Predictions During The Model Calibration.

3. CYCLONE STORM SURGE ANALYSIS

The assessment of water levels and the inundation areas during design storm conditions was carried out for a number of conditions. These conditions were defined based on a sensitivity analysis of different possible storm conditions and the scope and the schedule of the project, and four variables were found to be the most relevant as follows: .

- Cyclone strength
- Cyclone bearing
- Cyclone landfall area and
- Tidal water level conditions.

Therefore a matrix of 36 simulations was defined to describe those four variables. Each of the modelled conditions are presented in Table 1. The results of these simulations provided the basis to determine the maximum storm surge water levels as well as the inundation areas for each of the design events.

Table 1. Description of the design storm matrix

Tide\Cyclone Category	1	3	5
High Water Level	6 landfalls and directions	6 landfalls and directions	6 landfalls and directions
Mean Water Level	3 landfalls and directions	3 landfalls and directions	3 landfalls and directions
Low Water Level	3 landfalls and directions	3 landfalls and directions	3 landfalls and directions

These results were applied to define a disaster risk management plan. A typical example of the inundation results from a Category 2 cyclone crossing the Burdekin River delta is presented in Figure 7. The depth of inundation is described by the blue intensity with darker areas indicating deeper flow. The figure illustrates a small area of the Burdekin Delta showing the coastal village of Wunjunga in the south and the Burdekin River in the north.

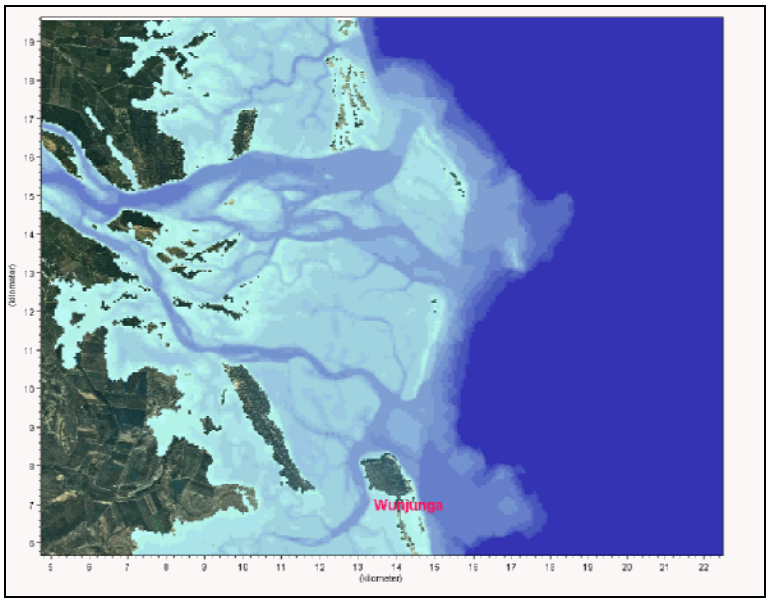

Figure 7 - Typical Example Of The Inundation Mapping From Model Results For The Burdekin River

Another requirement of the Council in this project was the delivery of a forecast model to be operated by the Council to provide storm surge prediction during cyclone events, which DHI implemented and delivered. Due to the complexity of the operation of this type of model, training was also provided to the personnel of the Council.

4. CONCLUSIONS

A numerical cyclone storm surge model has been successfully implement to determine maximum water levels and inundated areas of the Burdekin Shire that will be the input to a disaster risk management process and development of storm surge counter disaster plans for the Shire. The numerical model includes the combined effect of tides, wind/pressure fields and waves and was calibrated against tidal predictions and water level measurements during two cyclone events. The comparisons show good agreement against the measured data.

The approach proved to be optimal for the prediction and analysis of water levels and the associated inundation areas for a range of design storm conditions based on: cyclone strength and bearing, cyclone landfall area and tidal water level conditions. The application of this type of approach certainly provides a powerful tool in the analysis and forecasting of cyclone events.

A forecast model was also implemented and delivered to the Council to forecast future storm events.

5. RECOMMENDATIONS

This study recognizes also the need to keep on monitoring water levels and waves to further improve the understanding the behaviour of tropical cyclones and the numerical description of these effects. This will certainly enhance the prediction capability of numerical models.

6. ACKNOWLEDGEMENTS

The authors wish to acknowledge the following groups and individuals who have made important contributions to the study:

- Representatives of the Burdekin community and the Council, for providing important anecdotal records of storm surge and other data.
- AAM GeoScan and Burdekin Shire Council for the supply of Aerial laser Scanning data of the Shire.
- Department of Natural Resources and Mines (DNR&M), Bureau of Meteorology (BOM), Environmental Protection Agency (EPA) and Queensland Transport, who made available data for the study.
- Maunsell Pty Ltd Townsville who carried out the risk assessment study.

7. REFERENCES

Department of Natural Resources and Mines, The State of Queensland (2001*). Queensland Climate Change and Community Vulnerability to Tropical Cyclones, Ocean Hazards Assessment, Stage 1 Report*.

DHI Water and Environment (2002). MIKE21 Hydraulics, User Manual.

Holland, G.J. (1980) An analytic model of the wind and pressure Profiles of Hurricane, *American Meteorological Society, Monthly Weather Review, Vol 108*.

Young, I.R. and Sobey,R.J. (1981). The Numerical Prediction of Tropical Cyclone Wind-Waves, *James Cook University of North Queensland, (Dept of Civil & Systems Eng., Research Bulletin No. CS20).*

The Institution of Engineers, Australia
8th National Conference on Hydraulics in Water Engineering
ANA Hotel Gold Coast, Australia 13-16 July 2004

Queensland Climate Change and Community Vulnerability to Tropical Cyclones Project

R. Schwartz
B.Eng., M.Eng., MBA
Senior Principal Engineer, Coastal Services Unit, Queensland Environmental Protection Agency
D. Robinson
B.Eng., B.Econ, Grad. Dipl. in Hydraulic Engineering (Distinction) Delft,
Manager, Coastal Services Unit, Queensland Environmental Protection Agency
M. Allen
B.Eng., MIEAust
Principal Engineer, Planning Division, Queensland Environmental Protection Agency
Jim Davidson
B. Sc.
Regional Director, Bureau of Meteorology
Owen Harvey
Principal Research Officer, Disaster Mitigation Unit
Department of Emergency Services

Abstract: The *Queensland Climate Change and Community Vulnerability to Tropical Cyclones Project* encompasses three separate studies designed to update and extend the present understanding of storm tide inundation threats in Queensland, including the effects of cyclonic wave conditions in selected areas and estimates of potential Greenhouse impacts.The results from these studies will assist coastal management planners and engineers, local government, disaster management agencies, and the Bureau of Meteorology in land use management planning and design of coastal protection structures; developing appropriate disaster response strategies; and improving the accuracy of warnings for storm tides and cyclonic wave conditions. Comparisons with the results from previous studies will also be presented and discussed.

Keywords: Tropical Cyclone, Storm Tide, Greenhouse

The Institution of Engineers, Australia
8th National Conference on Hydraulics in Water Engineering
ANA Hotel Gold Coast, Australia 13-16 July 2004

A Data Framework for Hydrodynamic Modelling

Susan E. Shield
B.E. (Hons), M.E. (Water), CPEng, M.I.E.Aust.
Senior Civil/Environmental Engineer, Umwelt (Australia) Pty. Ltd., Australia
Andrew J. Goodwin
B.E. (Env)
School of Engineering, University of Newcastle, Australia

Abstract: The data management demands of hydrodynamic modelling are huge. Establishing and checking the developed digital terrain model and analysis of model results present substantial challenges which represent a significant proportion of the modelling process. These issues present the need to streamline data manipulation, analysis and reporting.

The example presented in this paper focuses on the data management issues associated with a hydrologic study of the Mandalong Valley. The Mandalong Valley has limited channel capacity and a broad low gradient floodplain. Sections of the valley are to be subsided by longwall mining. In setting up, running and analysing results of the flood model, three major issues are encountered:

- Handling large volumes of survey data (over 12 million data points) and using this information to create a digital terrain model.
- Representing the hydraulic features of the landform with a simplified terrain model / finite element mesh suitable for use in hydrodynamic modelling.
- Being able to model the subsided landforms for each of the longwall panels planned to be mined so that the model can be used as a mine planning tool.

This paper discusses the development and application of methods to facilitate the above process. The tools and methods developed are flexible and can be easily extended to link to different flood models, import/export data to and from numerous file formats, utilise custom analysis methods and link to CAD/GIS software packages.

Keywords: Database; Digital Terrain Modelling; Aerial Laser Scanning; Polygonal Surfaces; RMA-2; Finite Element; Hydrodynamic Modelling; Multiresolution modelling

1. INTRODUCTION

Hydrodynamic modelling presents many challenges. One of these challenges is the volume of data required to be handled for setup and analysis of two dimensional (2-D) finite element hydrodynamic models. Substantial effort is involved in creating an appropriate model network that accurately represents the hydraulic characteristics of a landform from detailed survey data. This is generally the first step taken by model developers after checking the quality of the survey data. Similarly, extracting and comparing data from hydrodynamic models, for example calculating flood depths, velocities and flood hazards, can present many difficulties.

These challenges require the development of new approaches to modelling including processes and techniques to streamline model development and analysis. A data management framework has been developed to overcome some of these issues. The framework provides considerable flexibility in digital terrain modelling and manipulation, and facilitates the linking of spatially orientated data sets.

The primary example used in this paper is the application of the developed data management framework to a hydrologic study of the Mandalong Valley where an underground longwall mining operation is planned. The Mandalong Valley is generally broad and flat with the lower valley forming a floodplain. The characteristics of the valley require that a two dimensional flood model be developed in order to determine flood depths and velocities.

This paper details the processes and steps within the data management framework that has been developed, see Figure 1. The solid arrows represent the pathway taken to achieve a given outcome. Third party utilities/programs, where used, are listed on the process arrow. The dashed arrows represent optional pathways of data flow into and out of the relational database.

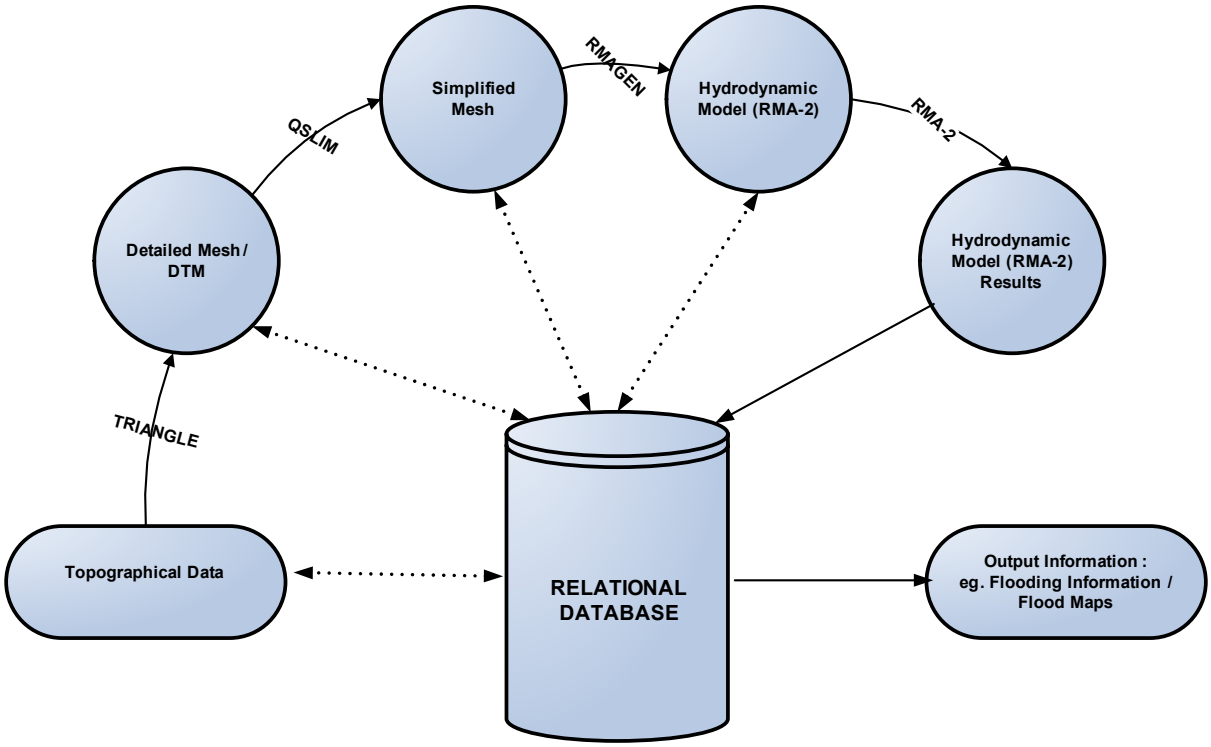

Figure 1 - Data Framework Schematic

2. TOPOGRAPHICAL DATA

Topographical data can be obtained by a number of methods including traditional surveys, aerial photogrammetry and Global Positioning Systems (GPS). The recent introduction of Aerial Laser Scanning (ALS) as a method of topographic data collection has resulted in a substantial increase in the density of height samples that may be obtained for a given site. While ALS greatly increases the resolution with which the surface can be described, a number of difficulties arise due to the sheer volume of the data obtained using such methods.

Survey measurements from the field are often samples of height at a given location, but may also contain information about how these samples are joined, i.e. breaklines. Such information may be utilised in a terrain model by ensuring that the breakline forms one of the edges in the resulting triangulated surface.

In order to facilitate the storage and retrieval of potentially very large terrain models, a database structure has been devised that is capable of storing various geometric objects. Databases are able to store models several orders of magnitude larger than those which can be typically stored and operated upon using computer memory alone. In practice entire ALS runs may be stored in the database and subsets of interest may be selected using Structured Query Language (SQL) for subsequent analysis and manipulation.

3. DIGITAL TERRAIN MODELLING USING POLYGONAL SURFACES

A digital terrain model provides a method of estimating the height of the ground surface at a given point. The examples discussed in this paper use polygonal meshes to represent surfaces. Polygonal surfaces consist of a series of three or more sided polygons arranged in such a way that the original data samples comprise the vertices of the polygons. An estimate of the height at any given point within the boundaries of the terrain model can be obtained by linear interpolation across the triangle in which that point lies.

Although grid based models are also commonly used to represent terrain surfaces, polygonal surfaces have been found to be more suitable for the examples used in this paper. They offer several major advantages:

- Polygonal surfaces are able to describe features of different size within the same model, allowing for greater detail where the surface elevation is changing rapidly (i.e. by utilising smaller triangles).
- Polygonal surfaces are able to utilise the original height samples directly while grid based methods require the original samples to be pre-processed in order to obtain a regular grid.
- The hydrodynamic model used for the floodplain model in the examples used in this paper was RMA-2 (Resource Modelling Associates Pty Ltd, 2004). RMA-2 utilises a finite element network that requires data structures that are similar in nature to those used to describe a polygonal surface, allowing for easy and transparent translation between the two model types.

4. MESH GENERATION / SIMPLIFICATION

A 2-D mesh generator was used for the creation of the surface from the original sample points. The mesh generator used, Triangle (Shewchuk, 1995), can robustly generate 2-D Delaunay Trianglulations from a list of x,y co-ordinates. Furthermore, Triangle can generate Constrained Delaunay Triangulations (Sloan, 1993) from a list of points and breaklines. Each of the co-ordinates used also has an associated z value which can represent the value of any parameter at that location. For terrain modelling the third co-ordinate represents the height of the ground surface at that location. Figure 2 shows an example of a Constrained Delaunay Triangulation produced from aerial photogrammetry spot heights and breaklines obtained from a ground survey. The resulting triangles are shown in the figure with the surveyed breaklines shown in red.

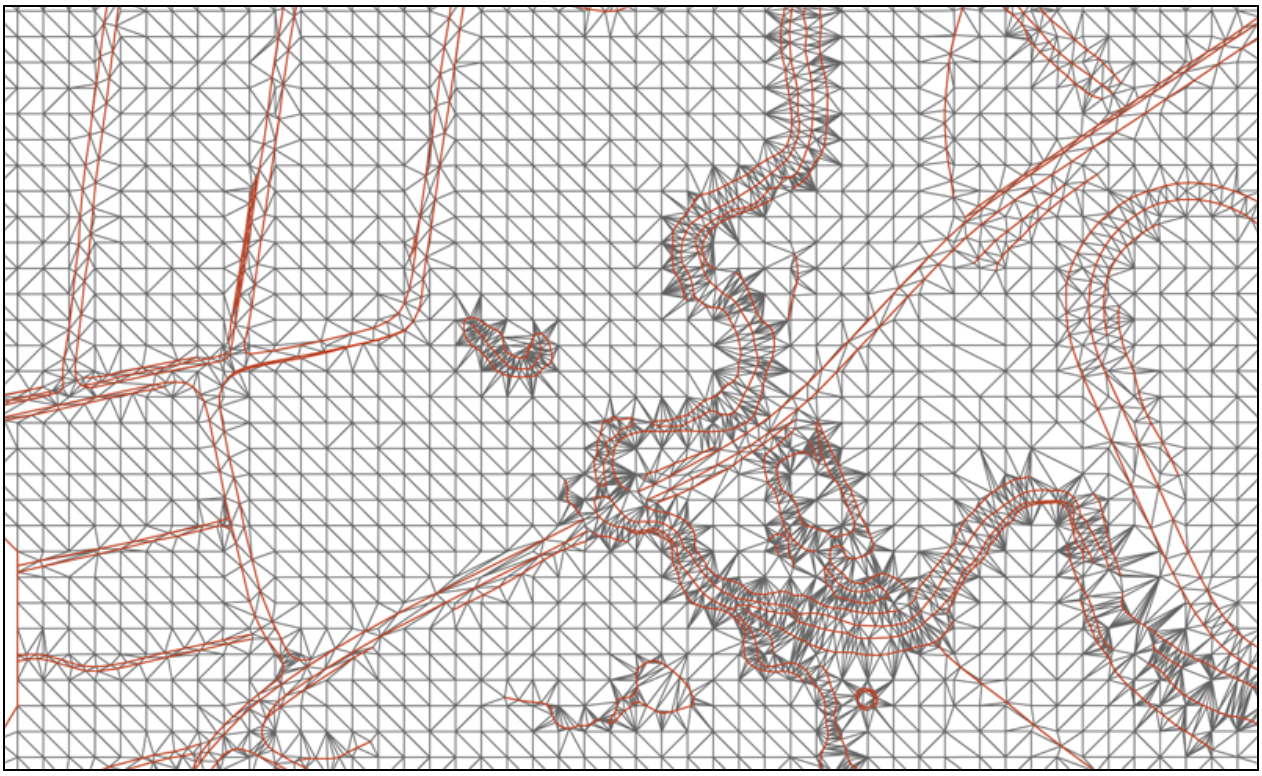

Figure 2 – Polygonal Surface Incorporating Surveyed Breaklines

Delaunay Triangulations of ALS samples produce extremely dense meshes that are often unsuitable for direct use in a finite element model due to the required computer processing time. An example of a Delaunay Triangulation using every point in the ALS data for the Mandalong Valley is shown in Figure 3. The resulting triangles, see Figure 3(A), have a side length of the order of 2 metres. Such small elements are computationally inefficient for use in large scale finite element hydrodynamic models. The sample density is too high for direct modelling and a method for reducing the level of detail is required. If samples are decimated randomly then features such as drainage lines and other hydrological features may not be retained. Any process used to simplify meshes must be able to retain hydraulically significant features. Furthermore, any errors that are introduced during the simplification process need to be quantified to provide a check on the quality of the resulting mesh.

Qslim (Garland & Heckbert, 1995) is an application that can reduce the level of detail in a polygonal surface whilst maintaining landform characteristics. The reduction in level of detail is achieved by an algorithm designed to minimise both the error and the number of triangles.

Figure 3 shows the mesh characteristics before and after mesh simplification has occurred. Three different levels of mesh detail are shown for the given 36.6 ha area of terrain. Figure 3(A) shows the detailed mesh produced directly from ALS and contains approximately 110,000 vertices. The next two panels, Figures 3(B) and 3(C), show two different levels of simplification of the detailed mesh. Figure 3(B) has approximately 11,000 vertices, with Figure 3(C) being further simplified with approximately 1,100 vertices. The definition that remains in the digital terrain model of the creek system and surrounding landform can be seen in the contour plots shown for each of the three polygonal models. The production of contour plots can provide a quick qualitative check of the integrity on the mesh characteristics.

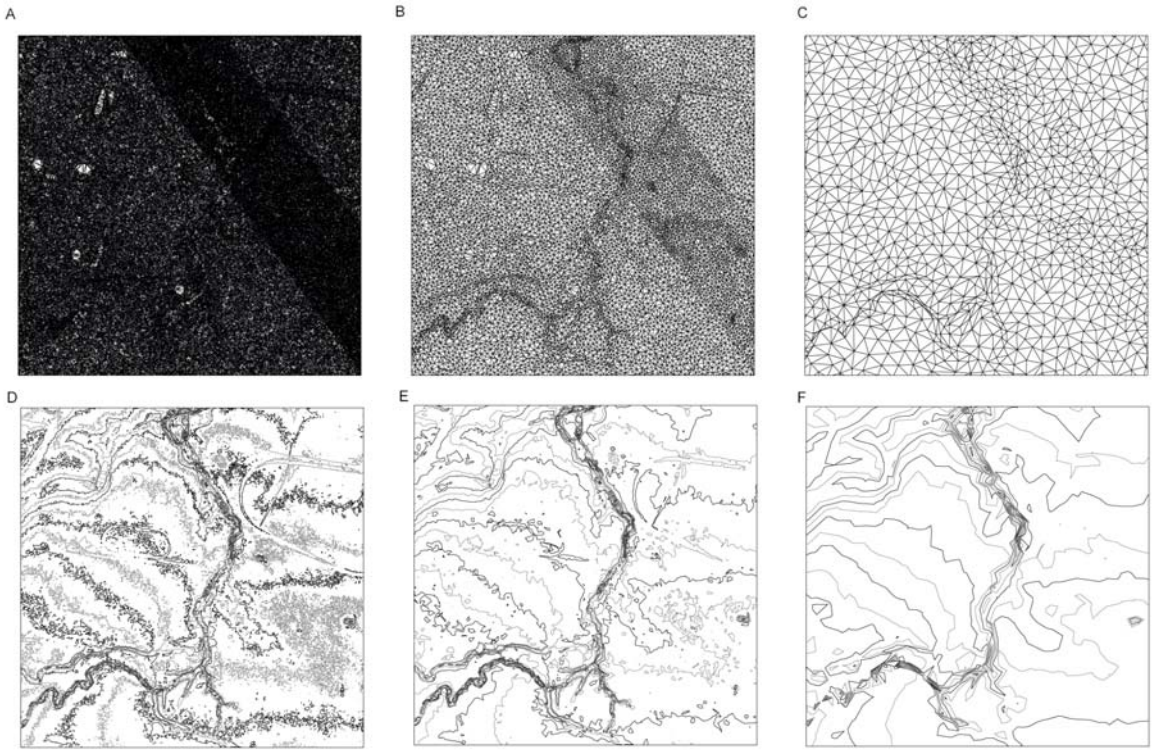

Figure 3 – Levels of Detail in a Polygonal Mesh

Whenever mesh simplification is performed, a parallel process of mesh validation must be undertaken. The changes to the modelled landform that are inferred from the mesh simplification process need to be quantified and either accepted or modified. The validation process can be undertaken by comparing the detailed mesh with the selected simplified mesh. The change in surface representation that has occurred can then be considered.

After a suitable mesh is created, the mesh can be stored in the database and then exported as a network file for use in hydrodynamic models, in this instance RMA-2.

5. VISUALISATION OF DIGITAL TERRAIN MODELS

Figure 4 shows a visualisation derived from the polygonal model shown in Figure 3(A). The visualisation was created by draping a spatially rectified aerial photograph over a 1m grid. Many visualisation software packages require the input data to be supplied as a regular grid. A grid can be readily derived from a polygonal model by interpolating values. However, the process cannot be undertaken in reverse, i.e. deriving a polygonal model from a grid risks loss of required detail in the represented surface. Feature size in any polygonal model derived from a grid is limited to the level of definition in the original grid.

Figure 4 - Visualisation

Visualisation facilitates rapid checking of the digital terrain model and easy presentation to peer review groups to demonstrate data integrity.

6. ANALYSIS OF MODELLING RESULTS

A suite of tools was developed to allow import of RMA-2 model results at each node for each timestep into the database. The imported modelling results are stored in the database with a primary key of node and timestep. For each node and timestep the velocity in the *x* direction, velocity in the *y* direction, water surface elevation and RMA-2 calculated depth of water are stored.

The modelling results are able to be linked to the corresponding mesh stored in the database using the node number, allowing the allocation of x and y coordinates to the modelling results. This relationship between the modelling results and spatial node details allows spatial analysis of data and gives the ability to import modelling results in CAD and GIS packages.

Using SQL, the model results are then manipulated to populate tables with the actual water depth and absolute water velocity at each node for each timestep of the model run. The maximum predicted water depth, water elevation and velocity can then be extracted for each node.

Flood hazard categories can also be determined for each node at each timestep of the model results. Flood hazard categories are defined in the Floodplain Management Manual (NSW Government, 2001) by the relationship between absolute velocity and depth of water. Equations were defined, in terms of velocity and depth, to differentiate between the four different flood hazard categories used in the Floodplain Management Manual. These equations were used in database queries to populate a table with flood hazard at each node for each timestep of the model.

Queries of the database tables with the absolute velocity, water surface elevation, water depth and flood hazard at each node for each timestep of the model allow the maximum, minimum and range of values at each node to be determined, or the time series at each node for each variable to be analysed.

Model run results for a range of scenarios with different characteristics, such as recurrence interval or elevation data, can be stored in the database for the same RMA-2 network. The results from the different runs can be compared. Using query statements the changes in velocities, water surface elevations, water depth, flood hazards and other salient variables can be compared between the model runs.

7. CREATION OF FLOOD INFORMATION MAPS

Flood maps can be created for any variable at each or any timestep or combination of timesteps at any node within the database. CAD data files can be produced using the results contained in the database to display a visual representation of the hydrodynamic modelling results. The x and y coordinates correspond to the coordinate of the node in the plane, with an arbitrary variable plotted as the z coordinate. The data can then be loaded on to a drawing file as spot values, or processed to form a polygonal surface that uses the same data structures as the original terrain model. These surfaces can then be plotted with other spatial information, such as topographical contours, roads and buildings etc. overlaid.

Figure 5 shows the maximum predicted flood depths for a 1:100 year ARI storm event for the Mandalong Valley. The proposed longwall layout and cadastre information have been superimposed.

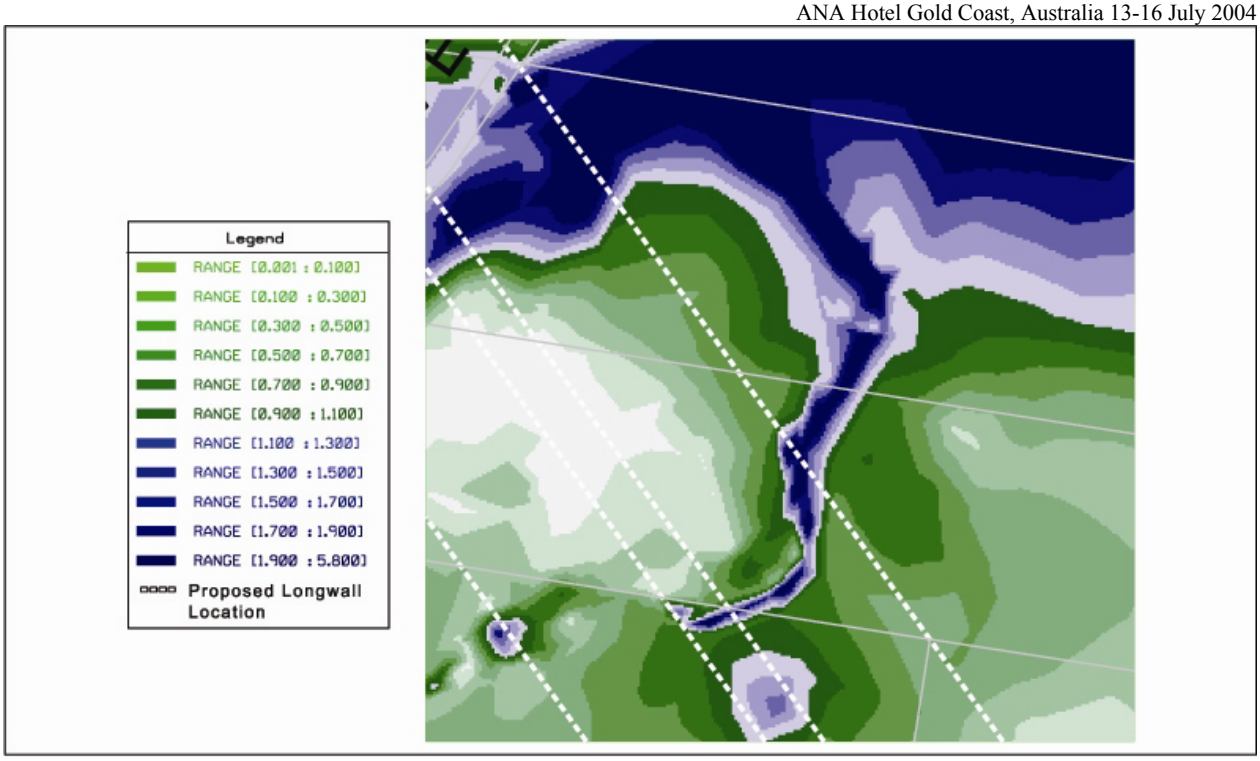

Figure 5 – Maximum Flood Depths

The maximum predicted flood hazards are shown in Figure 6 for the same area for which flood depth is defined in Figure 5. The displayed flood hazard has been derived using the polygonal surface generated from the maximum predicted flood hazard at each node for any timestep of the model run.

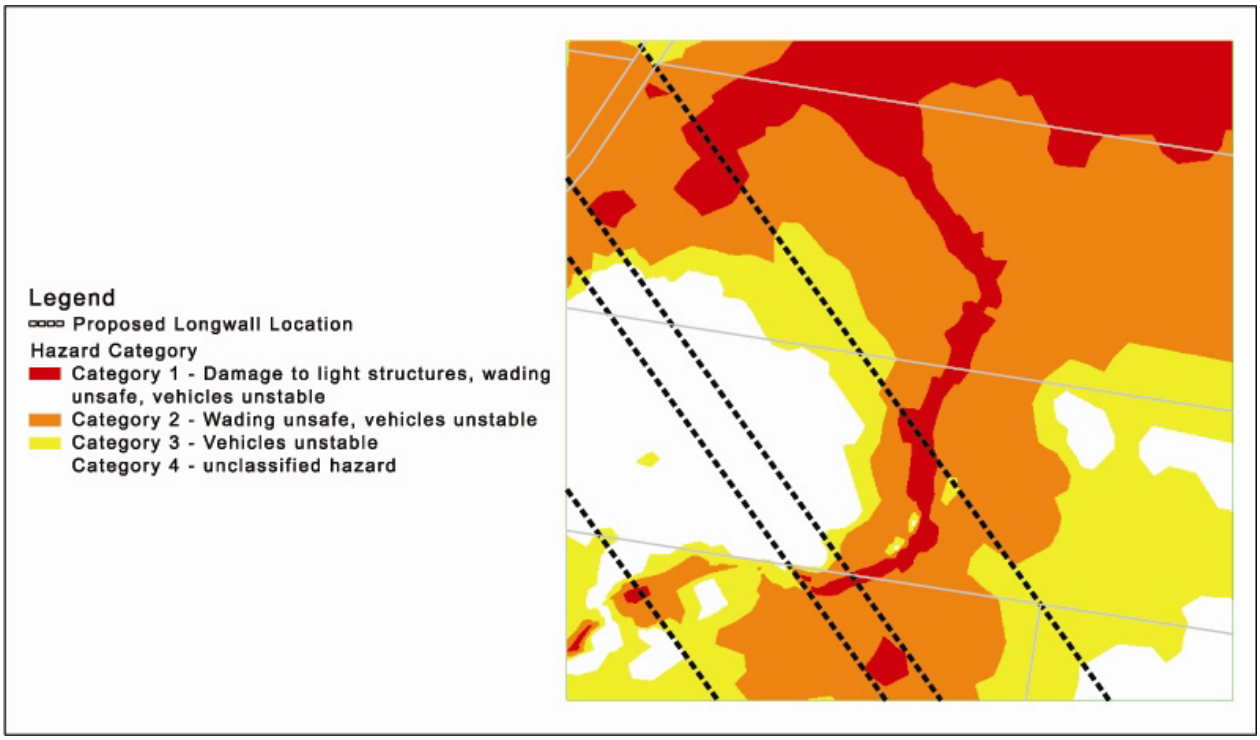

Figure 6 – Maximum Flood Hazards

8. CONCLUSIONS

This paper has discussed the development and application of methods aimed at facilitating the interaction between the hydrodynamic model, in this case RMA-2, and other software packages for management of input and output data. The tools and methods facilitate the operation of various stages of the modelling process and allows the integrity of the finite element mesh used to be checked through direct comparison with the digital terrain information. The data management framework developed also enables the hydrodynamic model of the Mandalong Valley to be iteratively used as part of mine planning to facilitate assessment of hydrodynamic inputs of mining a single or group of longwalls. The tools and methods are also flexible and able to be easily extended to link to different flood models, import data from various sources, apply different analysis methods and link to CAD/GIS software packages.

9. ACKNOWLEDGEMENTS

The authors wish to thank Peter Jamieson of Umwelt (Australia) Pty Ltd for his input into writing this paper and for his support during the development of the data management framework.

We thank Ian King of Resource Modelling Associates Pty Ltd for his review and on going support of this process to enable a more streamlined approach to RMA-2 modelling.

10. REFERENCES

Garland, M. and Heckbert, P. S. (1995). Fast Polygonal Approximation of Terrains and Heightfields, http://graphics.cs.uiuc.edu/~garland/papers/scape.pdf, 19 September 1995.

King. I. P. (1990), RMA2 – A Two Dimensional Finite Element Model For Flows In Estuaries and Streams, Resource Management Associates

NSW Government (2001). *Floodplain Management Manual: The Management of Flood Liable Land*, NSW Government, G-3p.

Shewchuk, R. S. (1995). Triangle: Engineering a 2D Quality Mesh Generator and Delaunay Triangulator, WACG: *1st Workshop on Applied Computational Geometry: Towards Geometric Engineering, WACG*,

Sloan. S. W. (1993). A Fast Algorithm for Generating Constrained Delaunay Triangulations, *Computers and Structures,* Vol 47., pp. 441-450.

The Institution of Engineers, Australia
8th National Conference on Hydraulics in Water Engineering
ANA Hotel Gold Coast, Australia 13-16 July 2004

Genetic Algorithm Optimisation for Water Distribution System Design at the Gold Coast

Andrew J. Roberts
B.E. (Hons)
Engineer, Optimatics Pty. Ltd.
Angus R. Simpson
B.E. (Hons), M.Sc., Ph.D., F.I.E.Aust.
Technical Director, Optimatics Pty Ltd, Australia. Associate Professor,
School of Civil and Environmental Engineering, University of Adelaide, Australia
Scott Sherriff
B.E., M.I.E.Aust
Supervising Engineer Network Analysis, Gold Coast Water, Australia
Peter Griffiths
B.E (Hons), Grad.I.E.Aust
Network Analyst, Gold Coast Water, Australia

Abstract: A two part optimisation study using the computer search technique of Genetic Algorithm optimisation has been carried out for the Gold Coast area. The study covered ten water supply zones from Nerang South to Coolangatta. Part one of the study focussed on three water supply zones. The Optimatics Genetic Algorithm (OGA) was used to optimise pipe sizes, zone boundary locations and storage sizes that satisfied Gold Coast Water's (GCW) hydraulic constraints whilst dramatically reducing the cost of the augmentations to the system. Part two focussed on the transmission mains for all ten water supply zones in the area. The OGA was able to optimise pipe sizes, pump sizes and valve settings to satisfy the GCW tank refill, node pressures and pipe velocity criteria, whilst again reducing the overall cost of the required augmentations to the system.

Keywords: Water Distribution System Design, Genetic Algorithms, Optimisation, Gold Coast, Optimatics.

1. INTRODUCTION

The Southern Trunk Water Distribution Network within Gold Coast Water's supply area includes ten water supply zones reaching from Nerang South to Coolangatta. The Gold Coast area has recently experienced significant growth and will require system augmentations to satisfy the projected future water demands. An optimisation study has been completed for the improvements to this system using an evolutionary computer search technique called a Genetic Algorithm (GA). The aim of the GA study was to identify augmentations that satisfy the projected year 2056 demands, called the ultimate demand case, whilst minimising the sum of capital and operating costs. The GA study was undertaken in two parts with two sets of genetic algorithm runs in each part.

The aim of Part 1 of the study was to identify the optimal locations for two water supply zone boundaries whilst minimising the cost of new pipes and tanks required to satisfy the ultimate demand case. One of the two water supply zone boundaries was a new boundary used to separate the two existing water supply zones into three. The locations of these water supply zone boundaries influenced the size of the storages for each of the water supply zones. The storage required for any given water supply zone was related to the total demand inside each water supply zone. Part 2 of the study focussed on the trunk main system with the aim to minimise the costs of additional pipes, pumps, valves and tanks required to satisfy the projected ultimate demands. Both operating costs and capital costs were considered for the skeletonised trunk distribution network.

2. GENETIC ALGORITHMS AND THE OGA PROCESS

A genetic algorithm is an advanced search tool that uses a "survival of the fittest" technique to iteratively improve a group of "solutions" called a population. Each "solution" contains a set of selected values, whether that is a pipe size selection, pump schedule, valve setting etc, for every decision variable in the GA. This means

that each "solution" is a potential augmentation scheme for the system. Optimisation of water distribution systems using genetic algorithms was pioneered by Murphy and Simpson (1992). Other papers include Simpson et al. 1994, Dandy et al. 1996, Savic and Walters 1997, Lippai et al. 1999, Wu and Simpson 2001 and Wu and Simpson 2002. More recently another evolutionary type algorithm – Ant Colony Optimisation has been investigated for optimisation of water distribution systems (Maier et al. 2003).

After a population of solutions is generated in a genetic algorithm run, every solution in that population is hydraulically tested to determine its performance against a series of hydraulic design criteria. To perform this hydraulic analysis, the OGA uses a link to the EPANET hydraulic engine. The hydraulic results from EPANET are used to calculate a penalty cost for each solution in the population if the hydraulic design criteria are not met.

The OGA also evaluates the cost of each of the members of the population representing the selected augmentations and, if applicable, the operating costs of the system over the design life. These calculated costs along with the penalty cost indicate the hydraulic performance of the solutions, and are used to determine an overall solution "fitness" for each solution. The fitness values of the solutions are then used in the application of the GA operator of tournament selection to form a mating pool for the next generation. Other operators of crossover and mutation are used to produce a new population for the next iteration or "generation".

As part of the OGA process, cycles of optimisation runs and client reviews are invaluable. Not only do these review points allow possible errors in the GA setup or inadequacies of the hydraulic model or constraints to be identified, but they also provide an opportunity for the client to express any preferences between solutions produced. With thorough discussion, to ensure that these preferences are properly understood, and careful consideration, into how to include the preferences into the OGA setup, further sets of OGA runs can be undertaken that are more directed and produce low cost solutions that suit the client's needs.

One of the most important requirements for a successful GA study is the involvement of the client. The client usually has an intimate familiarity with the hydraulic model and the system the model represents. This local knowledge of the system is of vital importance when identifying options for the OGA to select from, as well as evaluating the solutions produced.

3. DETAILS OF THE SYSTEM AND HYDRAULIC MODELS

The Southern Trunk Main Distribution Network has two water purification plants (WPPs) that supply water through a trunk main system to the ten water supply zones. These zones and the model are shown in Figure 1 with the zone boundaries in grey and the pipes in black. In the north, the Molendinar WPP sources water from the Hinze Dam Lower Intake (HLI). The Mudgeeraba WPP in the west of the system sources water from the Hinze Dam Upper Intake (HUI) and the Little Nerang Dam (LND).

The water is transferred through a transmission main system into tanks for each of the ten water supply zones. These tanks have been sized depending on the amount of demand in the water supply zone serviced. The individual zones are supplied from these tanks using a gravity supply system. The tanks act as a buffer for the WPPs so that the quantity of flow required from the WPPs is steady over the day and can provide emergency storage for expected or infrequent demands such as fire flow. These tanks allow the transmission main system upstream of the tanks to be modelled almost independently from the water supply zones downstream of the tanks.

The original GCW hydraulic model of this system was in H2ONet format. The level of detail in that model was too great for the purpose of this study. For Part 1 GCW skeletonised the model by replacing each water supply zone with a dummy demand node except the two water supply zones that were to be optimised. These two water supply zones, Reedy Creek and Worongary, were further simplified by removing all pipes below 100 mm and reallocating demands along the pipes to the most appropriate remaining node. This model was then exported to an EPANET format, so it could be integrated into the OGA software. The demand case analysed for these water supply zones was the peak hour of the maximum day steady state demands.

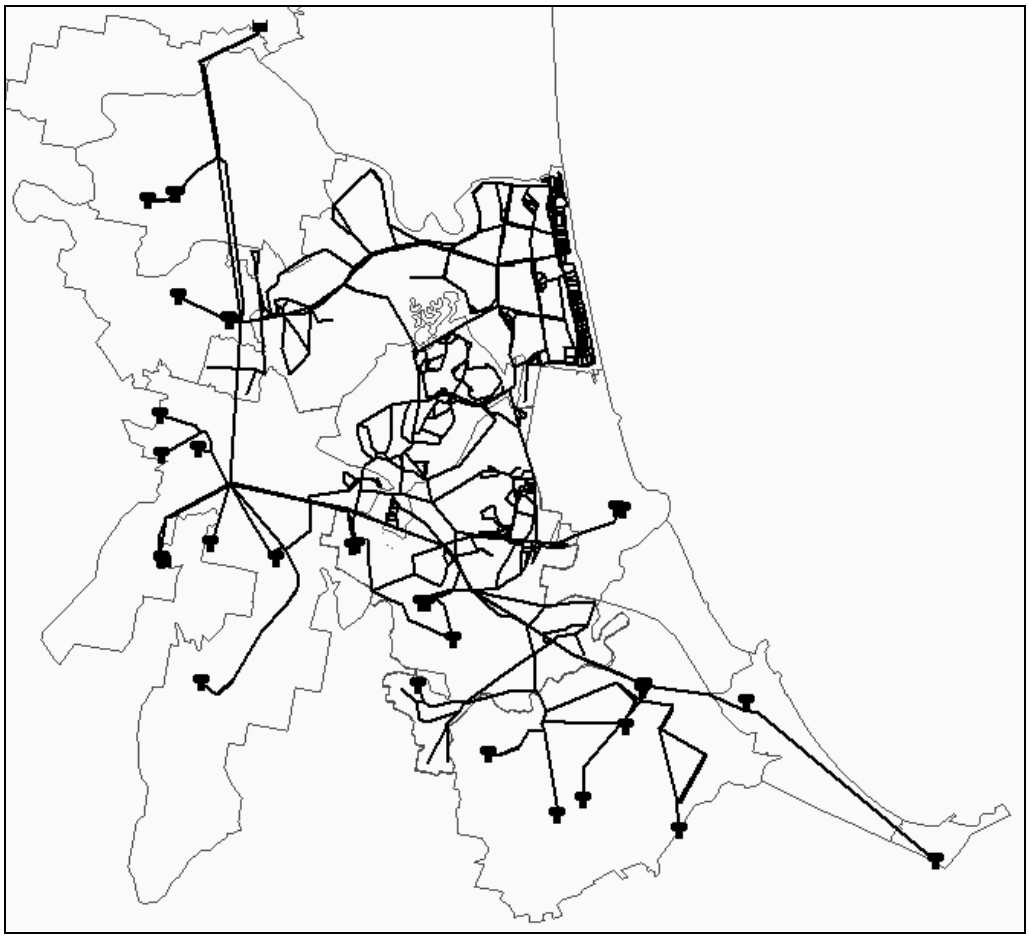

Figure 1. Whole System Showing Original Zone Boundaries

The Part 2 model was very similar to the Part 1 model, however, the Worongary, Reedy Creek, and new Reedy Creek North water supply zones were also represented by dummy demand nodes. The demand at each of these dummy demand nodes was calculated based upon the locations of the zone boundaries selected as part of the GA optimisation study in Part 1.

The demand case used for designing the transmission mains (Part 2) was an extended period simulation (EPS) of the mean day of the maximum month (MDMM) using 5 minute time steps. Similar to Part 1, this model was provided by GCW in EPANET format after being exported from H2ONet.

4. THE GA OPTIMISATION STUDY

4.1 Part 1 Study

Prior to Part 1 of the study commencing, a coordination meeting was held at which GCW requested that the cost of the GCW original hydraulic augmentation solution be evaluated as a baseline solution for comparison purposes. This baseline solution was very important because not only did it give GCW a method for measuring how effective the optimisation study had been, but it also provided the opportunity for GCW to review the method Optimatics would use to calculate the capital and operating costs during the OGA runs. In addition, potential zone boundary locations were discussed with GCW for a new water zone to be incorporated into the network. During this discussion GCW helped Optimatics identify four potential new locations for the northern water supply zone boundaries and four new potential locations for the southern water supply zone boundary. GCW also requested that Optimatics investigate the original planned locations for the water supply zones.

After hydraulic modelling was carried out it was determined that the northern boundary location in GCW planning was no longer suitable and as such this was not considered as an option for the remainder of the study. With this option removed there were four northern water supply zone boundary options as shown in Figure 2. The southern boundary location in GCW planning was investigated as a fifth option for the southern zone boundary. The five southern zone boundary location options are given in Figure 3.

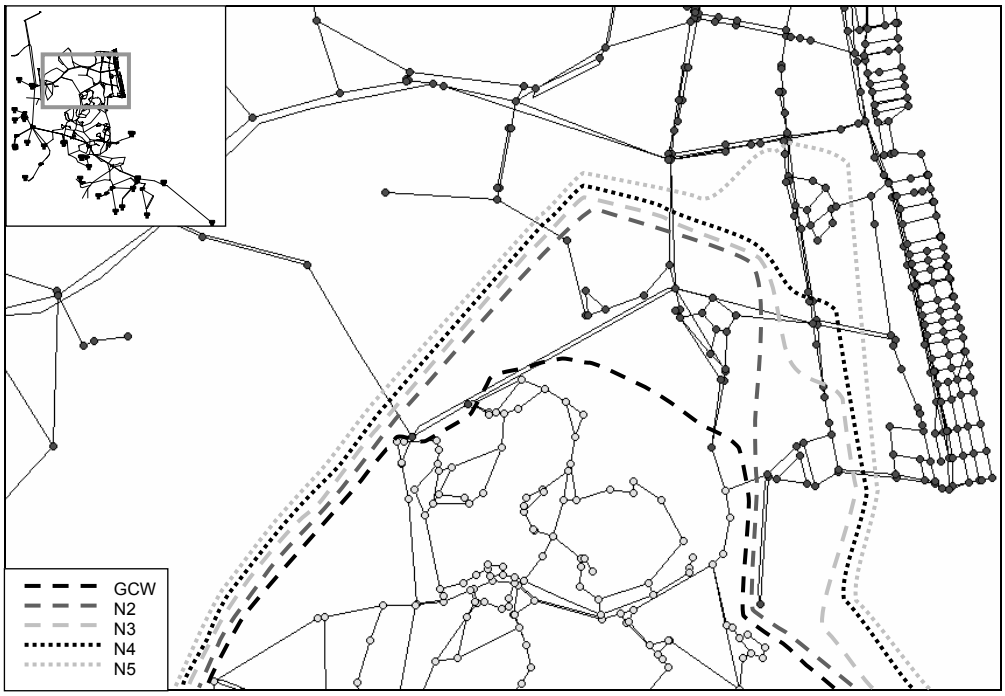

Figure 2. Northern Water Supply Zone Boundary Locations (Locater Box Shows Part 1 Study Area)

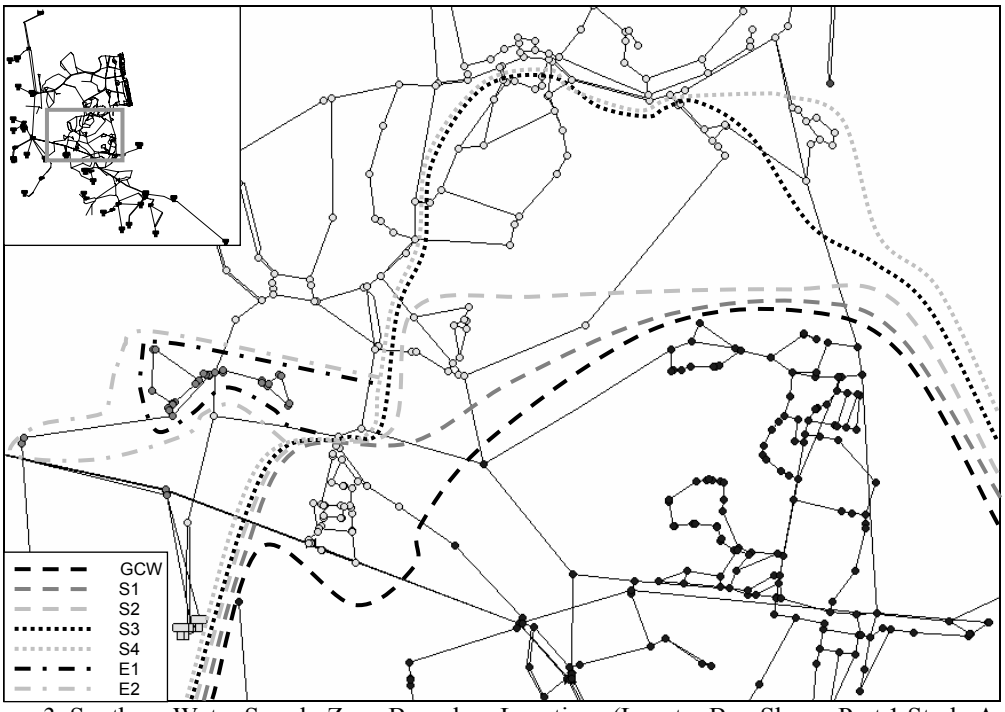

Figure 3. Southern Water Supply Zone Boundary Locations (Locater Box Shows Part 1 Study Area)

The water supply zone boundaries were modelled as closed pipes to simulate shut-off valves. All demands inside a zone boundary were supplied only from the storage designated for that supply zone. Whilst the OGA could have been set up to select the zone boundary locations during the OGA runs using a zone boundary location decision, it was judged to be more productive to run each of the zone boundary location combinations separately. If all the zone boundary locations were considered at once, during the OGA runs, all of the solutions may use the same boundary locations. By running all twenty combinations separately the cost of each of the zone boundary combinations could be determined and thus the cost difference between each twenty combinations of zone boundaries determined. The piping and storages capital costs of the best ten solutions using different zone boundary combinations are shown in Table 1.

The effects of incorporating two other expansion zones into the Reedy Creek North zone were also investigated. These zones were called expansion zone 1 (E1) and expansion zone 2 (E2). The four least cost solution designs with different zone boundaries were presented to GCW in a memo summarising the outcomes of Part 1 of the GA optimisation study for review at the end of the first set of optimisation runs.

After the first set of optimisation runs a workshop was held at the Gold Coast to discuss the benefits of each of the zone boundary combinations. From the four solutions presented, GCW selected a preferred zone boundary location combination (N3_GCWS) for Optimatics to consider in the second set of OGA runs. GCW also expressed a concern that the skeletonized system used for the OGA runs may not adequately represent the full system. GCW resolved that the minimum pressure constraint should be raised to 27 m from 22 m to take into account the detail missing due to the model skeletonization. GCW requested that additional pipes be included into a group previously specified by GCW to be security of supply pipes. These security of supply pipes have diameters of at least 600 mm in the solutions.

Table 1. Pipe Capital Costs of Solutions for the Best Ten Water Supply Zone Boundary Combinations

North Boundary	South Boundary	Capital Cost of Pipes and Storages ($m)
N3	GCWS	$14.562
N4	S1	$14.604
N2	GCWS	$14.677
N3	S1	$14.748
N4	GCWS	$15.876
N2	S1	$16.023
N5	GCWS	$16.529
N5	S2	$17.098
N4	S2	$17.358
N3	S2	$17.439

The second set of OGA runs for Part 1 incorporated all comments and feedback from GCW about the memo and the workshop. These OGA runs were focussed on redesigning the system for the selected zone boundary combination including the revised constraints and data identified through the previous OGA runs. In traditional methods of design, a change in design criteria like this would require a large time commitment to amend the previous design and perhaps even beginning again wasting all the work to date. However using the OGA to aid design meant that only minor changes needed to be made in the OGA setup to account for these changed constraints and the majority of the setup from the first set of runs could be reused. A final solution was produced from this second and final set of OGA runs for Part 1, called “Final Solution N3_GCWS”. The capital cost breakdown for Final Solution N3_GCWS is given in Table 2. The pipe cost for Final Solution N3_GCWS is greater than the costs shown in Table 1 because it includes the cost of the security of supply pipes ($2.960 million) and the cost of the additional piping required to satisfy the revised minimum allowable pressure criteria of 27 m ($0.246 million). The final solution costs shown in Table 2 also include some additional pipes that were already in early stages of construction. These pipes were not considered by the GA but the costs ($3.140 million) have been included to ensure a fair comparison with the GCW baseline solution.

Table 2. Comparison of Solution Capital Costs

	Final Solution N3_GCWS	GCW Baseline Solution	Percentage Savings
Pipes Inside Three Zones of Concern for Part 1	$ 13,994,025	$ 21,838,021	35.9%
Storages	$ 6,913,799	$ 7,692,922	10.1%
Total	*$ 20,907,824*	*$ 29,530,943*	*29.2%*

4.2 Part 2 Study

A Part 2 coordination meeting was held following the Part 1 workshop. At this meeting GCW discussed their goals and expected outcomes for Part 2 of the project. GCW explained that some parts of the system were becoming increasingly difficult to operate and alternative operating methods for these locations should be investigated.

GCW identified nine major decisions to be considered. In addition, the OGA was used to select; diameters for 64 potential future pipes, settings for 9 existing valves, settings and sizing for 8 potential future valves, set operating schedules for 8 existing pumps, sizes and setting the operating schedules for 7 potential future pumps and sizes for 11 potential future tanks. The locations of the nine major decisions are given in Figure 4.

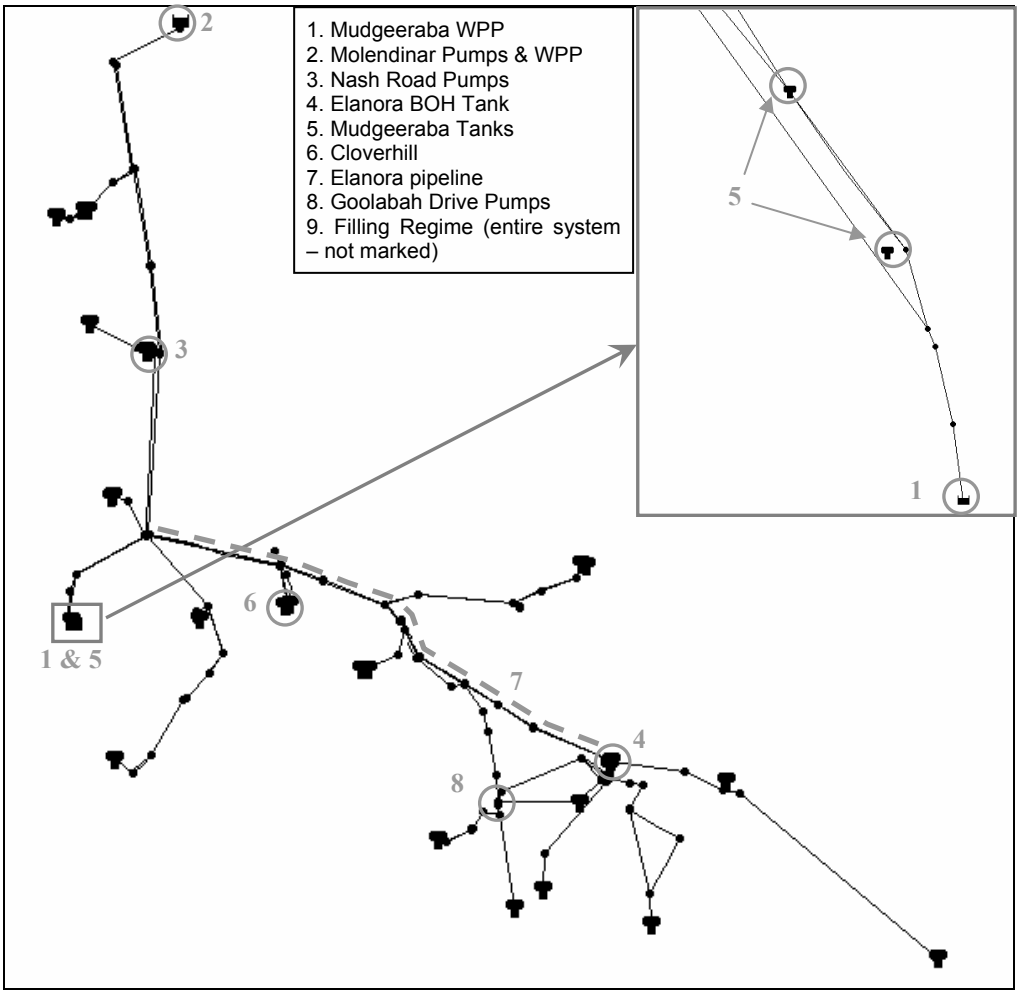

Figure 4. System Map Showing Major Decision Locations

The nine major decisions included WPP upgrades, tank decommissioning, storage operation, pump operation and pipeline operations. It was identified that of these nine major decisions, only decision 2 was suited to being selected by the OGA during the OGA runs. Decisions 1 and 3 were to be investigated using scenarios and as such four different scenarios were identified. The remaining six major decisions, which were not investigated as GA decisions or scenarios, were investigated to determine if the options were feasible. In some cases only one of the proposed options was feasible and was therefore implemented. In some other cases it was found that the effects were isolated and could be investigated easily using modelling rather than included in the optimisation. The best option for each decision was incorporated into the model and used for all scenarios during the OGA runs for Part 2.

Four solutions were produced from the first set of OGA runs for Part 2. Each of these four solutions utilised a different combination of options for decisions 1 and 3. Gold Coast Water, when reviewing the solutions, expressed some concerns about some aspects of the study. These concerns prompted GCW to undertake a review of both the project and their "Standards of Service". During this review GCW were able to use many of the conclusions made during the first set of OGA runs for Part 2. The review investigated different upgrade schemes for the water purification plants and which zones were to be supplied from which WPPs. The results of this review were presented in a report produced by GCW (2003). In this report, GCW produced three designs. The designs were called Option 1, Option 2 and Option 3 and featured elements of the OGA designs produced during the first set of runs for Part 2. GCW requested that the second set of runs for Part 2 focus on using the OGA to identify any savings that could be made for the designs of Option 2 and Option 3. The detailed cost evaluation in the GCW report included a complete staging analysis and thus was beyond the scope of this project. Option 2 was recosted using the data available in the GCW review report and sent to GCW for review. GCW gave feedback on how the costing was to be performed, as well as clarifying other questions and indicating the preferred method for net present valve (NPV) calculation. The requested NPV cost calculation included assuming specific proportions of the total capital cost were constructed at key years into the future. Then these proportions of the total capital cost were factored back to NPV costs using a discount rate of 6.5% and a design life of 50 years.

The number of pipes to be sized by the OGA for the second set of OGA runs was reduced from the number considered by the OGA in the first set of runs. These revised pipe decisions are numbered and shown in Figure 5. For many of the pipe alignments diameters had been decided upon by GCW. Optimatics was instructed to formulate the OGA to only optimise the sizes of 33 pipes, 2 pumps and 3 valves in Option 2 and 28 pipes, 2 pumps and 3 valves in Option 3. Optimatics was also informed that to preserve the separation of the water from the two water purification plants the open/closed status of all pipes was to remain the same as in the EPANET models provided by GCW.

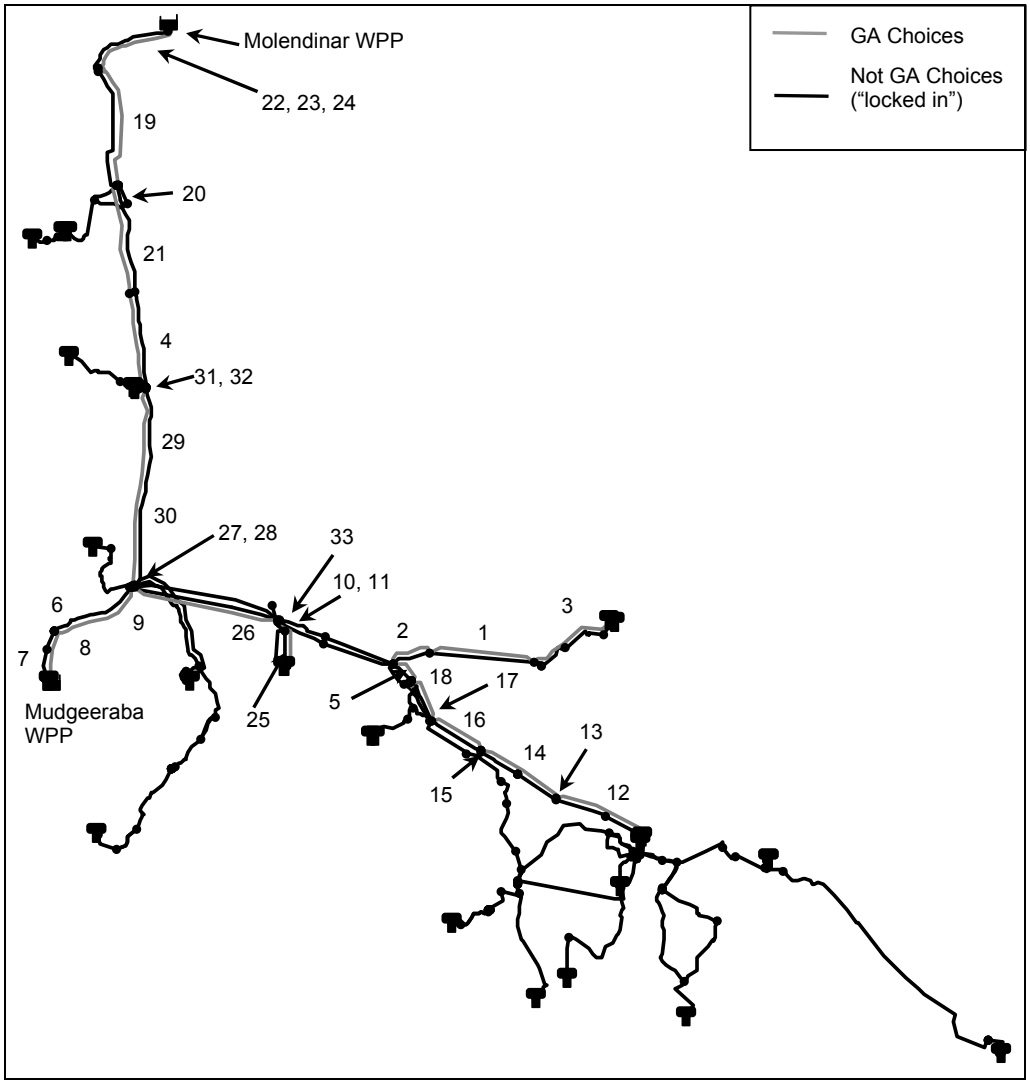

Figure 5. Pipe Decisions for Part 2

The appropriate changes were made to the OGA setup and a final set of OGA runs undertaken. Two solutions were produced in the final set of OGA runs called "Option 2 Final Solution" and "Option 3 Final Solution". The costs for the final Part 2 solutions are given in Table 3. It can be seen that for the "GA Optimised Option 2 Solution" minor savings were made for the capital costs while larger savings were made for the operating costs. For the "GA Optimised Option 3 Solution" greater savings were made for capital costs while similar cost savings were made for operating costs.

Table 3. Comparison of NPV Costs

	GCW Original Solution	GA Optimised Option 2 Solution	GA Optimised Option 3 Solution
Capital Cost	$ 21,828,256	$ 19,735,479	$ 13,509,629
Operating Cost	$ 19,093,966	$ 13,381,995	$ 13,231,203
Total	**$ 40,922,222**	**$ 33,117,474**	**$ 26,740,832**
Savings	**-**	**$ 7,804,748**	**$ 14,181,390**
percentage	**-**	**19.1 %**	**34.7 %**

5. CONCLUSIONS

The Gold Coast study is a clear example of the importance for a client to be closely involved in both the original setup of the GA optimisation runs including the identification of options for the GA and the constraints by which solutions are evaluated. The input from GCW during the setup together with careful reviewing of solutions at points during the study helped result in GCW receiving final designs which achieved their clearly defined goals for the study as well as making significant cost savings. Engineering experience and judgement is also clearly a necessary component of any optimisation study.

The OGA process used in this study, proved successful at including GCW in all major decisions and allowing GCW to drive the study whilst not having to worry about the technical issues involved in achieving the desired outcome using the OGA. The iterative approach where the OGA setup was adapted to include the feedback from GCW on the designs produced in the early runs ensured that GCW's in depth knowledge of the system was incorporated in the decisions and solutions. GCW's detailed knowledge of the hydraulic models, and the system they represent, was another factor in the success of this study. This gave GCW a strong grounding to give thorough, constructive and proactive feedback on the system designs presented.

This study clearly showed that using the OGA is an excellent method for investigating "what if" scenarios such as the water supply zone boundaries in Part 1 or the different WPP upgrade schedules in Part 2. Since the OGA can quickly optimise and evaluate criteria for the many options, the different options are independent and can be compared fairly. It is difficult to produce independent solutions for a fair comparison of all of the options using traditional trial and error methods of design. Time restrictions would limit investigating all twenty options thoroughly.

Part 2 of the study illustrated that whilst the OGA was a powerful tool for analysing many inter-related and complicated decisions, the OGA did not and should not replace engineering judgement and careful consideration to ensure that solutions are both realistic and satisfy all the desired standards of service of the client. It requires experience in using GA optimisation to be able to effectively determine where the GA can be applied without compromising the role of engineering judgement. This judgement was demonstrated by using a combination of scenarios, modelling and OGA runs to investigate the options in Part 2.

6. REFERENCES

Dandy, G.C., Simpson, A.R. and Murphy, L.J. (1996). "An Improved Genetic Algorithm for Pipe Network Optimisation." *Water Resources Research*, Vol. 32, No. 2, Feb., 449-458.

Lippai, I., Heany, J. P., and Laguna, M. (1999). ''Robust Water System Design with Commercial Intelligent Search Optimizers.'' *J. Comput. Civ. Eng.,* ASCE, Vol. 13, No. 3, 135–143.

Maier, H.M., Simpson, A.R., Zecchin, A., Foong, W.K., Phang, K.Y., Seah, H.Y., and Tan, C.L. (2003). "Ant Colony Optimization for Design of Water Distribution Systems." *Journal of Water Resources Management and Planning*, American Society of Civil Engineers, Vol. 129, No. 3, May/June, 200-209.

Murphy, L.J. and Simpson, A.R. (1992). "Pipe Optimisation Using Genetic Algorithms," *Research Report No. R93*, Department of Civil Engineering, The University of Adelaide, June, 53pp.

Savic, D.A. and Walters, G.A (1997). "Genetic Algorithms for Least-Cost Design of Water Distribution Networks." *Journal of Water Resources Planning and Management*, ASCE, Vol. 123, No. 2, 67-77.

Simpson, A.R., Dandy, G.C. and Murphy, L.J. (1994). "Genetic Algorithms Compared to Other Techniques for Pipe Optimisation," *Journal of Water Resources Planning and Management,* American Society of Civil Engineers, 120 (4), July/August, 423-443.

Wu, Z.Y. and Simpson, A.R. (2001). "Competent Genetic-Evolutionary Optimization of Water Distribution Systems." *Journal of Computing in Civil Engineering*, American Society of Civil Engineers, Vol.15, No.2, April, 89-101.

Wu, Z.Y. and Simpson, A.R. (2002). "A Self-Adaptive Boundary Search Genetic Algorithm and its Application to Water Distribution Systems." *Journal of Hydraulic Research*, International Association of Hydraulic Research, Vol. 40, No. 2, 191-203.

The Institution of Engineers, Australia
8th National Conference on Hydraulics in Water Engineering
ANA Hotel Gold Coast, Australia 13-16 July 2004

Integrated High Order Water Quality and Hydrodynamic Models – An Essential Tool for Lake Management

R.C. Swan
B.E., M.I.E.Aust.
Project Engineer, Lawson and Treloar Pty. Ltd., Australia
N.I. Collins
B.E.(Civil), M.Eng.Sc, M.I.E.Aust, CPEng, RPEQ
Director, Lawson and Treloar Pty. Ltd., Australia

Abstract: The provision of man-made lakes for recreation and visual amenity has led to a greater emphasis on the design and operational management of these systems, to ensure appropriate water quality outcomes. The use of integrated water quality and hydrodynamic models allows lake designers and managers to understand what the critical physical processes are in a lake system and which management strategies will be required to obtain acceptable water quality outcomes. This paper provides a framework for the development of these models and examines the use of the integrated models SOBEK, Delft3D and Mike21 in residential lakes systems at Emerald Lakes in Queensland and Sanctuary Lakes in Victoria

Keywords: Water Quality, Hydraulics, Hydrology, Modelling, Lakes.

1. INTRODUCTION

This paper has been prepared to demonstrate a range of techniques, from simple inception planning tools, to complex high order water quality analysis used in detailed investigations, for assessment of the water quality performance of lakes. An integral component of lake performance is the management of nutrient loads, aquatic vegetation, fish and other fauna. The authors draw on recent experiences from several large artificial lake projects in Queensland and Victoria. The demand for water views in urban development will see an increase in demand for lake developments.

2. ANALYSIS LEVEL VERSUS APPLICATION AND RISK

The level of analysis required to properly assess lake water quality varies with:

- Lake depth (at greater than 6 metres stratification may become more dominant)
- Lake salinity; salt, brackish or fresh (fresh water lakes can have more issues with aquatic vegetation)
- Lake shape and batters (shape effects circulation and turnovers, batters effect fringing vegetation)
- External sediment and nutrient loads
- Temperature and seasonal variability

Simple turnover and residence time analysis may be appropriate for a shallow (<5m deep) off line lake with direct connection to a healthy estuary. However, generally, the larger the lake and external load potential, the more complex the analysis required.

A common investigation requirement is to quantify the potential frequency of algal blooms or aquatic vegetation harvesting required. i.e. the risk of a major water quality issue. The potential risk should be a determinant in the selection of the analysis level required.

3. PROJECT PLANNING

At the project planning stage, decisions as to whether lakes are on or off line, depths, shapes and turnover, aeration and mixing requirements are made. This lends itself to simple tools to allow rapid elimination of non-feasible solutions, and to broadly examine lake management risk. Nutrient budgeting, using long-term catchment pollutant yield as an input, is a commonly used approach. A typical flow chart for the project planning stage is as follows:

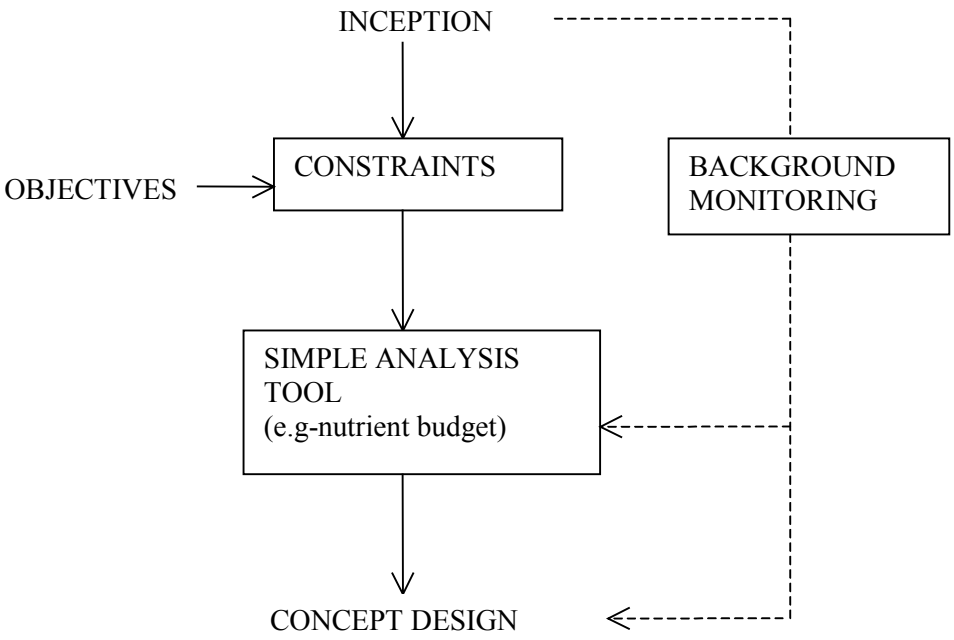

4. PROJECT PRELIMINARY DESIGN

Key analysis stages required for preliminary design are:

- Catchment and downstream (e.g. tidal) impacts (flow, sediment, salinity, nutrients).
- Lakes and turnover hydrodynamics
- Advection / dispersion, turnover rates and residence times

Long term simulations based on up to 50 years of rainfall and/or streamflow data is desirable. Catchment modelling can be undertaken with MUSIC or AQUALM and turnover modelling with a hydrodynamic model (usually 1D at this stage) e.g. SOBEK (WL|Delft Hydraulics, 2003) or MIKE11 (Danish Hydraulic Institute, 2003a) with advection dispersion parameters based on monitoring results. For complex plan shaped lakes, full two dimensional hydrodynamics may be required at this stage (e.g. SOBEK, 1D / 2D or MIKE21) and for deep lakes, 2D vertical analysis may be warranted (e.g. Delft3D or Dyresm). As part of the preliminary design, the need for supplementary turnover, mixing and aeration devices should also be considered. Figure 1 shows a typical one dimensional model arrangement for initial turnover and residence time assessments.

Background water quality monitoring should continue, particularly on an event basis, through the preliminary design stage.

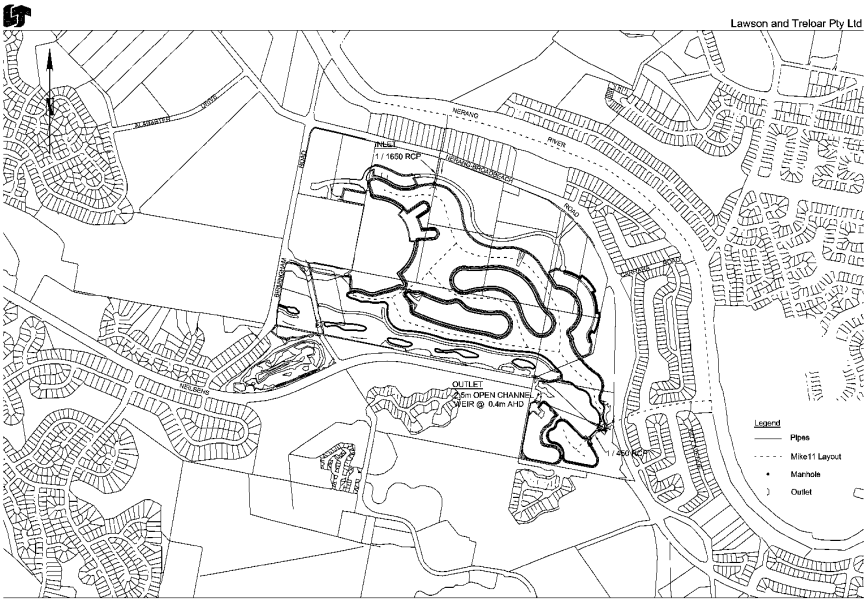

Figure 1 – Emerald Lakes One-Dimensional Hydraulic Model Schematisation (MIKE11)

5. DETAILED DESIGN

Once the feasibility of the project is established and an acceptable level of risk and practical and affordable management strategies are considered achievable, detailed design can proceed. Typical design requirements include:

- Wind effect on circulation and turnover modelling artificial mixing and aeration devices.
- Higher order water quality analysis, with eutrophication and/or aquatic plant growth modelling.
- Faecal coliform die-off (particularly where primary and secondary recreational contact is envisaged).

The design of any higher order coupled water quality and hydraulic model must be undertaken with consideration given to those items identified in sections 2 and 4.

To accurately model wind effects, full 2D (shallow lake) or 3D (deep lakes) modelling may be required. Figure 2 shows the results of wind mixing / turnover simulations for the Emerald Lakes Project. This work was completed with Delft3D (WL|Delft Hydraulics, 2002). Figure 3 shows die-off results for faecal coliforms following a catchment runoff event, as modelled with MIKE21 (Danish Hydraulic Institute, 2003d).

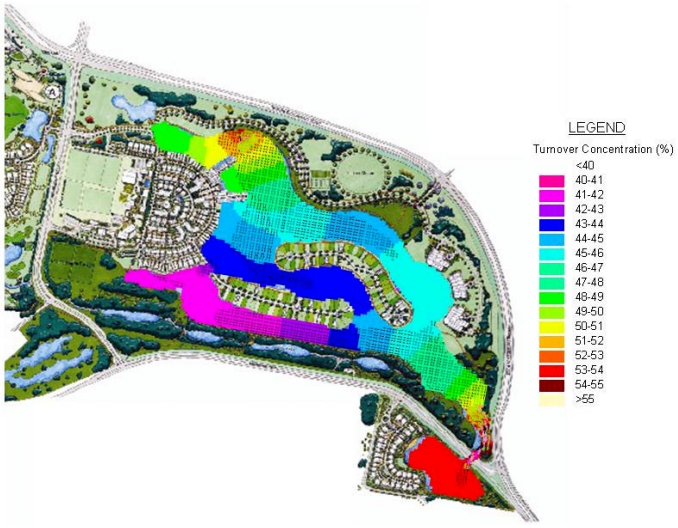

Figure 2: Wind Mixing and Lake Turnover at Emerald Lakes

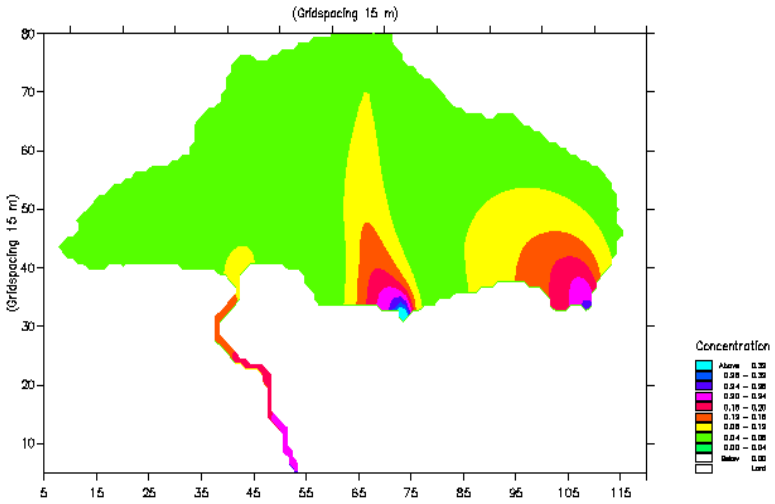

Figure 3: In-Lake Faecal Coliform Concentration Following Runoff Event

6. OPERATIONAL MANAGEMENT AND MAINTENANCE

Results from the model study must be integrated into the construction and operational phases of a lake system. The outcomes from the modelling and from other studies should be incorporated into both a lake management plan and operational guidelines. The lake management plan should include the following items:

- The design intent of the lake (eg. recreation, visual amenity etc.);
- Maintenance responsibility for the lake and it's surrounding features;
- An on-going water quality and flow monitoring plan, and;
- Emergency response procedures.

Lake operational guidelines should be written in plain english, be specific in their instructions and allow a layperson to implement them. They should include, where applicable:

- Operational parameters of any pumping or turnover system;
- Procedures for water quality sampling;
- Emergency notification and response procedures and;
- Maintenance and inspection schedules.

7. MODEL CASE STUDY - SANCTUARY LAKES

The Sanctuary Lakes Project used high order integrated water quality and hydraulic modelling to examine the potential for algal blooms in a residential lake system near Melbourne, Victoria. The approach used for the integrated model is discussed below. Figure 4 shows the schematisation of the integrated model.

7.1 Input requirements

An integrated lake system model can be described in terms of hydraulics (water levels and water movement) and water quality (changes in concentrations of various parameters

Lake hydraulics and water quality are controlled by the following factors:

- Lake Bathymetry (cross-sections or digital elevation models are used to describe the lake bottom topography)
- Catchment Inflows (Various inputs determined by an appropriate method)
- Direct Rainfall and Evaporation (flow input and outputs from the above ground sources occurring within the lakes)
- Groundwater Inflows (natural flow input from underground occurring within the lakes)
- Tidal Exchange (natural flow input due to tidal actions)
- Pumped Inflows (unnatural flow input from underground sources occurring within the lakes)

The construction of a higher order model requires large data sets that can be difficult to obtain. Ideally, there should be flow data available for catchments that discharge to the water body of interest, that are coupled with the required water quality parameters. For many catchments, this data does not exist or, if a catchment area is developing, the available data set may not be appropriate to the future land use. If water quality and flow data is not available, artificial generation of the raw data set, through the use of appropriate catchment models, can be appropriate. For example, the MUSIC model generates a time series of flows and pollutant concentrations based on recorded rainfall data, which can be used as an input data set.

The Sanctuary Lakes project had extensive water quality data for the existing constructed lake, however no flow or concentrations had been recorded for any of the catchment inflow points. A SOBEK one-dimensional flow and water quality model was set-up to simulate the lake system. MUSIC (CRCCH, 2002) was used to generate a time series of flows and corresponding pollutant concentrations for a time series of recorded rainfall corresponding to the in-situ water quality data set. The results of the MUSIC model were transformed to separate pollutants into their component forms, as required by SOBEK.

The final design runs occurred over a modelled period of 12-years, which is considered to be more representative of physical process than the oft used dry, wet and average year analysis.

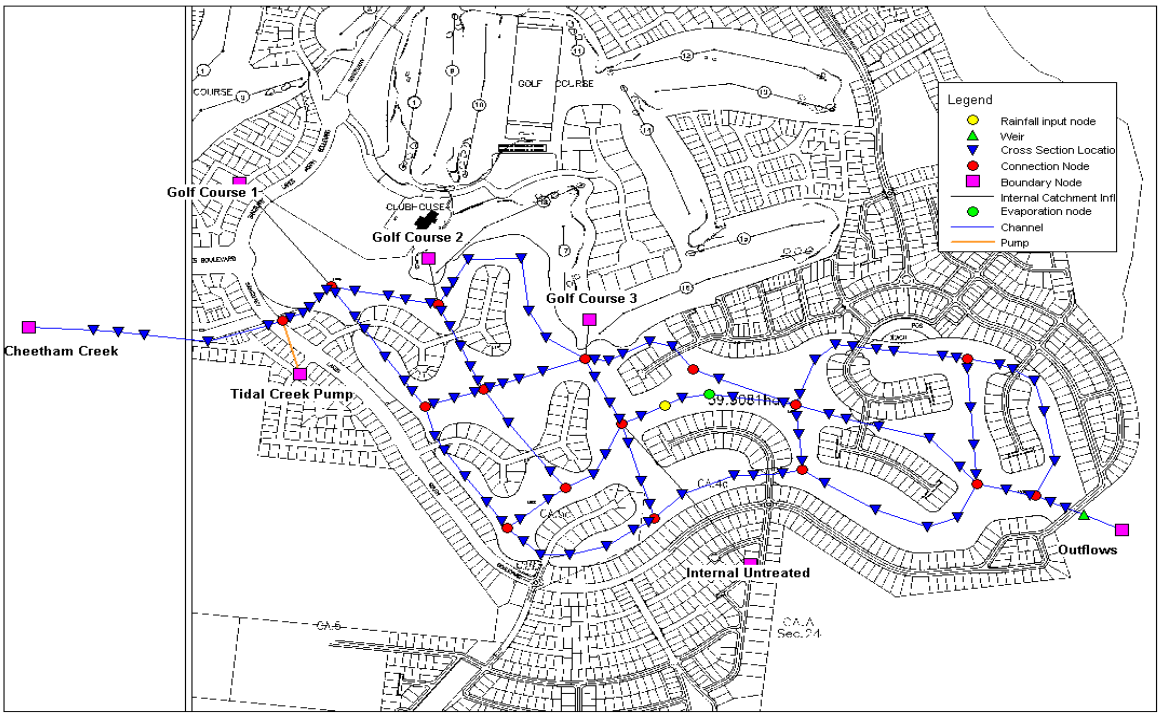

Figure 4: SOBEK Model Schematisation, Sanctuary Lakes

7.2 Water Quality Processes

The selection of appropriate water quality process to model has a major impact on the design and data requirements of the integrated model. These processes must be selected based on the required outcomes of the modelling project. The Sanctuary Lakes model was required to include modelling of algal concentrations by the Responsible Authority. To achieve this objective the so-called “simple eutrophication model” in SOBEK was used.

The simple eutrophication model is a pre-defined set of selected state variables, active processes, process parameters and output parameters (WL|Delft Hydraulics, 2003). State variables are the inputs to the model and active processes are the water quality interactions that can be physical or chemical in nature. The process parameters allow changes to coefficients evaluation schemes and constants that are involved in the process calculations. For the simple eutrophication model used at Sanctuary Lakes, there are approximately 50 process parameters that can be edited by the user.

The simple eutrophication model distinguishes 11 state variables that are input to the model as a time series of concentrations in mg/L. Each state variable has a number of processes that are applied to it for the modelling of both physical and chemical interactions. The state variables and the modelled processes applied to each are shown in Table 1

Table 1: Sobek Water Quality Process Simple Eutrophication Model

State Variable	**Interacting Processes**
Nitrate	Denitrification in water column Nitrification of ammonium Uptake of nutrients by growth of algae
Ammonium	Nitrification of ammonium Mineralisation of detritus nitrogen Uptake of nutrients by growth of algae Release (nutrients/detritus) by mortality algae Diffusive waste ammonium
Detritus Nitrogen	Mineralisation of detritus Release (nutrients/detritus) by mortality algae Sedimentation
Phosphate	Ad(De)Sorption ortho phosphorus to inorganic matter Mineralisation of detritus phosphorus Uptake of nutrients by growth of algae Release (nutrients/detritus) by mortality algae Diffusive waste Phosphate
Absorbed Phosphates	Ad(De)Sorption ortho phosphorus to inorganic matter Sedimentation Adsorbed Phosphates
Detritus Phosphorous	Mineralisation of detritus Release (nutrients/detritus) by mortality algae Sedimentation
Detritus Carbon	Mineralisation of detritus Release (nutrients/detritus) by mortality algae Sedimentation
Inorganic Matter	Sedimentation Resuspension Diffusive waste Inorganic Matter
Green Algae	Net primary production and mortality green algae
Dissolved Oxygen	Denitrification in water column Nitrification of ammonium Reaeration of oxygen Mineralisation of detritus carbon Sediment oxygen demand (additional) Net primary production and mortality green algae
Chloride	Concentration Only

7.3 Model Outputs

The higher order integrated models allow examination of the key operational parameters of the lake system, both for hydraulic and water quality processes, which are defined during the project planning stages. Sufficiently long simulation times will provide information on seasonal effects on the lake system, data for statistical analysis of lake behaviour at varying timescales and enable examination of the effect of various management strategies.
For the Sanctuary Lakes project, the Responsible Authority required that certain target concentrations of specific water quality parameters were achieved at the 90th-percentile level and that saline level were maintained in a brackish range (10-25ppt NaCl) to prevent lake damage by European carp. Additionally, the developer of the estate wished to examine the average lake water level and the effect of pumping from a nearby creek on water level, circulation and water quality. The effect of constructed water quality treatment measures in the upstream catchment was also examined. Figure 5 shows the predicted salinity concentrations in the lake for two options, one with pump and one without.

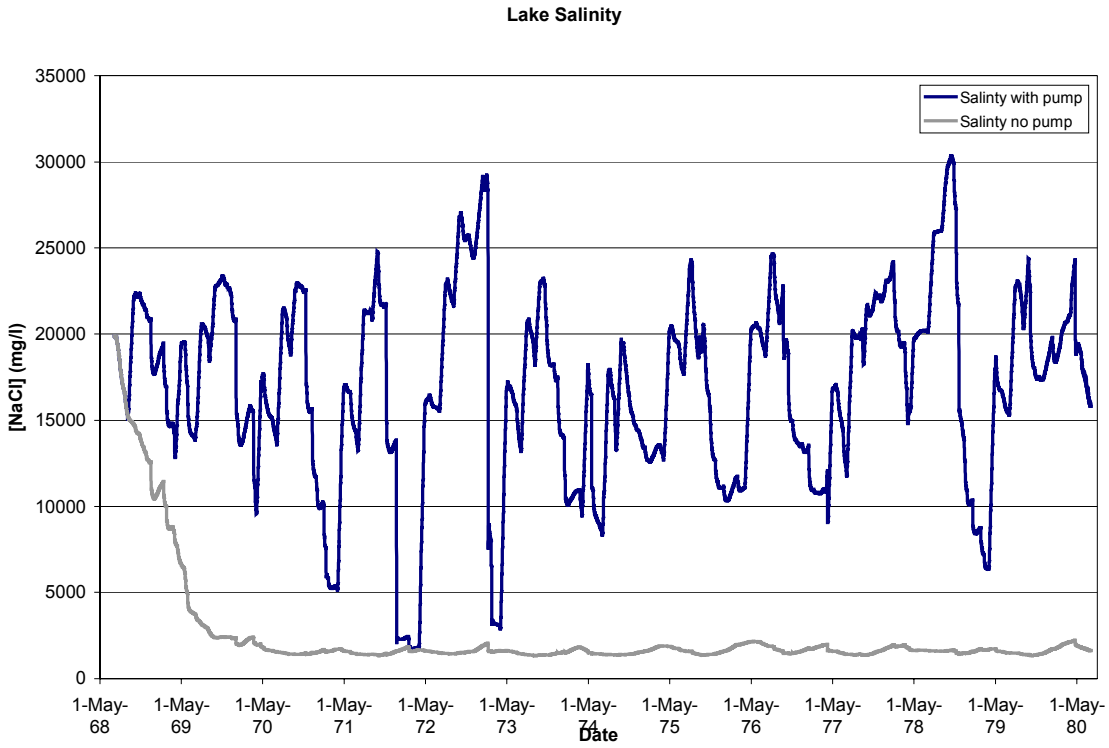

Figure 5 – Predicted Salinity Concentrations

Long term statistical analysis can also be generated as shown in Tables 2 and 3

Table 2: Integrated Modelling Results, No Pumping

Parameter	[Chlorophyll-a] (μg/L)	[TN] (mg/L)	[TP] (mg/L)	[DO] (mg/L)	[NaCl] (mg/L)	Water Level (m)
Mean	2.87	1.130	0.017	9.6	2466	1.79
Median	0.73	1.121	0.010	9.8	1608	1.80
Maximum	26.81	2.530	0.361	11.7	19871	1.95
Minimum	0.00	0.926	<0.001	<2	1332	1.55
10th percentile	0.02	0.990	0.003	8.5	1396	1.74
90th percentile	8.69	1.263	0.035	11.3	2491	1.81

Table 3: Integrated Modelling Results, Pumping

Parameter	[Chlorophyll-a] (μg/L)	[TN] (mg/L)	[TP] (mg/L)	[DO] (mg/L)	[NaCl] (mg/L)	Water Level (m)
Mean	4.31	0.596	0.022	8.7	16873	1.79
Median	1.88	0.577	0.016	9.0	17354	1.81
Maximum	27.89	2.515	0.361	10.5	30354	1.95
Minimum	0.00	0.092	0.002	<2	1751	1.55
10th percentile	0.11	0.323	0.007	7.7	10145	1.75
90th percentile	12.79	0.872	0.038	10.0	22990	1.82

These results allow the formulation of management plans and strategies to address issues identified through the modelling process. The results of management decisions may also be incorporated into the model to examine their potential effect.

8. CONCLUSIONS

The use of integrated water quality and hydraulic models is becoming essential for the planning and design of large residential lake systems as demand for waterfront residential land increases. Stringent environmental controls determined by Responsible Authorities require long term analysis be undertaken to enable statistical analysis and prediction of lake behaviour. A structured approach that is tailored to the specific project is essential, as the level of detail of a model is dependent on the required outcomes. The key requirements of the approach are:

- Defining the level of analysis required based on lake use and design intent;
- The use of simple water quality analysis tools in the concept design phase;
- Preliminary design should include consideration of lake hydrodynamics and catchment water and nutrient yields and impacts;
- Detailed modelling through a process based integrated model of higher order water quality functions, such as eutrophication, wind circulation and faecal coliform death. These modelled parameters should be defined in the early stages of the project, and;
- Incorporate the model results in lake management plans and operational procedures.

It is recommended that the structured approach to integrated modelling detailed in this paper be adopted when considering the design and construction of large residential lakes.

9. REFERENCES

Cooperative Research Centre for Catchment Hydrology (CRCCH) (2002). *MUSIC Version 1.0 User Manual,* Cooperative Research Centre for Catchment Hydrology, Melbourne

Danish Hydraulic Institute (2003a). *MIKE 11 Version 2003b,* http://www.dhisoftware.com/mike11, 1 February 2004.

Danish Hydraulic Institute (2003b). *MIKE 21 Version 2003,* http://www.dhisoftware.com/mike21, 1 February 2004.

WL|Delft Hydraulics (2002). *Delft3D User Manual,* WL|Delft Hydraulics, Delft.

WL|Delft Hydraulics (2003). *SOBEK User Manual,* WL|Delft Hydraulics, Delft.

The Institution of Engineers, Australia
8th National Conference on Hydraulics in Water Engineering
ANA Hotel Gold Coast, Australia 13-16 July 2004

Modelling Flood Inundation of Urban Areas in the UK Using 2D / 1D Hydraulic Models

W.J. Syme
B.E., M.Eng.Sc.
Associate, WBM Pty. Ltd., Australia

M.G. Pinnell
Bsc Msc MCIWEM
Principal Hydrologist, Symonds Group Ltd, England

J.M. Wicks
BSc PhD CEng MICE
Associate Director, Halcrow, UK

Abstract: Urbanised floodplains present significantly more complex hydraulic modelling challenges than those for rural floodplains. Urban areas require consideration of fences, highly varying land-use, buildings, narrow flow paths and underground stormwater drainage. The application of a 2D/1D hydraulic modelling approach to an urban flood study in Bristol, and a comparison of approaches benchmarked for the Thames Embayments Inundation study are presented. The Bristol study demonstrates the successful use of a 2D/1D system to model overland urban flows in 2D, whilst the river (open channel and long sprung arch culverts), stormwater sewer and narrow gaps are modelled as 1D elements. The Thames study is investigating the inundation risk from a breach or overtopping of the flood defence walls of 23 embayments along the River Thames, London. The findings from Stage 2a of the study provide an interesting comparison of four approaches, ISIS, LISFLOOD, TUFLOW and TELEMAC, when benchmarked to the Greenwich embayment.

Keywords: flood; hydraulic modelling; 1D; 2D; raster routing; finite difference; finite element

1. INTRODUCTION

In the UK, national planning guidance policies on Development and Flood Risk (PPG25) states "Policies in redevelopment plans should outline the consideration which will be given to flood issues, recognising the uncertainties that are inherent in the prediction of flooding, and that flood risk is expected to increase as a result of climate change" (DTLR, 2001). It goes on to state that "Planning authorities should apply the precautionary principle to the issue of flood risk, using a risk-based search sequence to avoid such risk where possible and managing it elsewhere".

The Environment Agency (EA) of England and Wales is charged with advising planning authorities on the application of PPG25, which in part it discharges through the creation and publication of maps that indicate areas considered to be at risk from flooding. This national dataset is, and by necessity remains, indicative, the intention being that refinement of the understanding of flood risk be considered more closely at a local level through the planning process. The methods used to derive these indicative maps are based on well-understood and standard techniques, and are applied through a national specification. However, in considering flood risk at a local level, and in particular in circumstances where the assumptions inherent in these techniques are exceeded, there is a need to reduce the uncertainties associated with estimation of flood water levels and flood extents. This is particularly the case in urban environments where the predominance of culverted watercourses, extensive development on the natural floodplain, and the interaction of urban drainage systems warrant close scrutiny of the techniques used to determine flood risk (Pinnell, 2003).

This paper describes innovative approaches that have been adopted to understand and reduce the uncertainty associated with defining the flood risk. The paper draws upon two investigations recently carried out for:

- fluvial (catchment flood) study for the centre of the City of Bristol, England; and
- benchmarking of different hydraulic modelling approaches for predicting storm tide inundation of urban areas along the River Thames in the City of London, England.

2. BRISTOL CASE STUDY

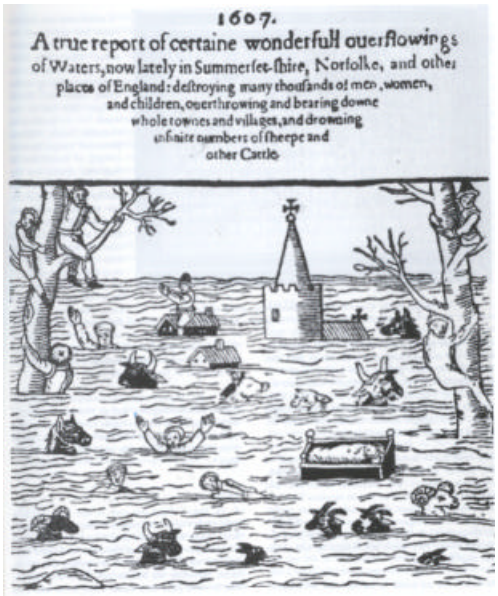

The city of Bristol has long suffered from flooding. There are records of significant flood events of the River Frome in the city of Bristol dating back to the 1600's. Many significant floods have occurred in the 20th century with documented events occurring in 1926, 1935, 1936, 1937, 1960, 1974, 1980, 1982, 1999 and 2000.

Upstream of Bristol the Frome catchment is dendritic and drains a number of rural and semi-rural sub-catchments. The catchment and study area include significant areas of urbanisation, notably Bristol, and in recent years there has been extensive development in the lower catchment. Within the city, the Frome culvert system is intended to carry floodwaters entirely underground through to the floating harbour. Despite the construction of these large culverts, and also major flood attenuation and diversion schemes further upstream, flood risk in the city remains a concern.

In 2002 the EA completed a study to prepare indicative flood mapping (IFM) as part of the Agency's commitments to defining the flood risk. In addition to mapping a river length of approximately 47km, a baseline unsteady ISIS 1D hydraulic model was developed. A number of assumptions in the ISIS modelling were made that were considered acceptable for the production of indicative flood risk maps.

The indicative flood maps were constructed using engineering judgement applied to the results of the ISIS model. This involved the extension of predicted flood levels outwards to either high ground or to parallel flow paths in the model. However, in urban areas ground levels typically vary greatly over small distances, and the built environment, channel walls, buildings, road and hard surfaces etc, heavily influence the topography and flood flow patterns creating significant uncertainties and difficulties in producing flood maps.

For the lower, fully culverted section of the River Frome that passes through the City of Bristol, the uncertainties were deemed too great and flood risk mapping for this section was not produced. It was accepted that the overland flooding in this area would require more detailed analysis that considers the interaction of the culverted watercourse, stormwater sewers and manholes, and overland flooding routes along roads, pathways and other open areas.

In August 2002, the EA was consulted on a planning application relating to the redevelopment of low-lying areas of the centre of Bristol for mixed retail, office, residential and public open space. In part, because of the results of the IFM study, the EA advised that the redevelopment area was affected by extreme fluvial flows in the River Frome and tidal events from the River Avon.

Symonds Group was commissioned by the Bristol Alliance (the development proposers) to undertake a Flood Risk Assessment (FRA) for the urban redevelopment proposal. The scope of works included detailed computational modelling to more clearly define the flood risk resulting from overland flows, surface and sub-surface flow interactions, and the operation of the culverted sections of the River Frome.

In these areas, the characteristics of the built environment dominate and control the flood risk. The more detailed hydraulic modelling needs to be able to represent the following characteristics:

- Complex flow routes and variation in flood levels through the built environment.
- The presence of discrete lengths of flood defences along open channels.

- Interaction between overland flows and sub-surface pipe systems.

For these reasons, it was decided to research two-dimensional (2D) modelling systems and select one for carrying out the more detailed hydraulic modelling.

In addition, the benefits of fully 2D hydraulic modelling are noticeably realised in the urban environment where the flood hazard needs to be mapped in addition to flood extent. It is not only the frequency and extent of flooding that needs to be quantified, but also the depth, duration and velocity. 2D models provide detailed information on these parameters and deliver the required strategic planning information. The benefits accrued through the use of 2D fully hydrodynamic models in the urban environment can be summarised as:

- Improved analysis of floodplain (out of bank) flows via better definition of physical situations and hence improved accuracy and confidence in results.
- Prediction of flood hazards through parameters such as the velocity depth product and flood duration.

For the detailed flood risk assessment, a 2D/1D hydrodynamic model was constructed to overcome these limitations. The modelling package chosen was TUFLOW. WBM Pty Ltd were contracted to provide training and help develop and validate the model.

TUFLOW solves the full 2D depth averaged momentum and continuity equations for shallow water free surface flow, and incorporates the full functionality of the ESTRY one-dimensional (1D) hydrodynamic network software (Syme 2001). A powerful feature of TUFLOW is its ability to dynamically link 1D and 2D domains. Its strengths include rapid wetting and drying, powerful 1D and 2D linking options, multiple 2D domains, 1D and 2D representation of hydraulic structures, automatic flow regime switching over embankments, 1D and 2D supercritical flow, effective data handling and quality control outputs.

The TUFLOW Bristol model is constructed from several connected 1D domains and a single, regular grid, 2D domain using a cell size of 4m. The 1D and 2D domains represent a variety of flowpaths as follows:

- 1D open channel flow upstream of the culverted section.
- Culverted section of the River Frome as branches of 1D culvert elements.

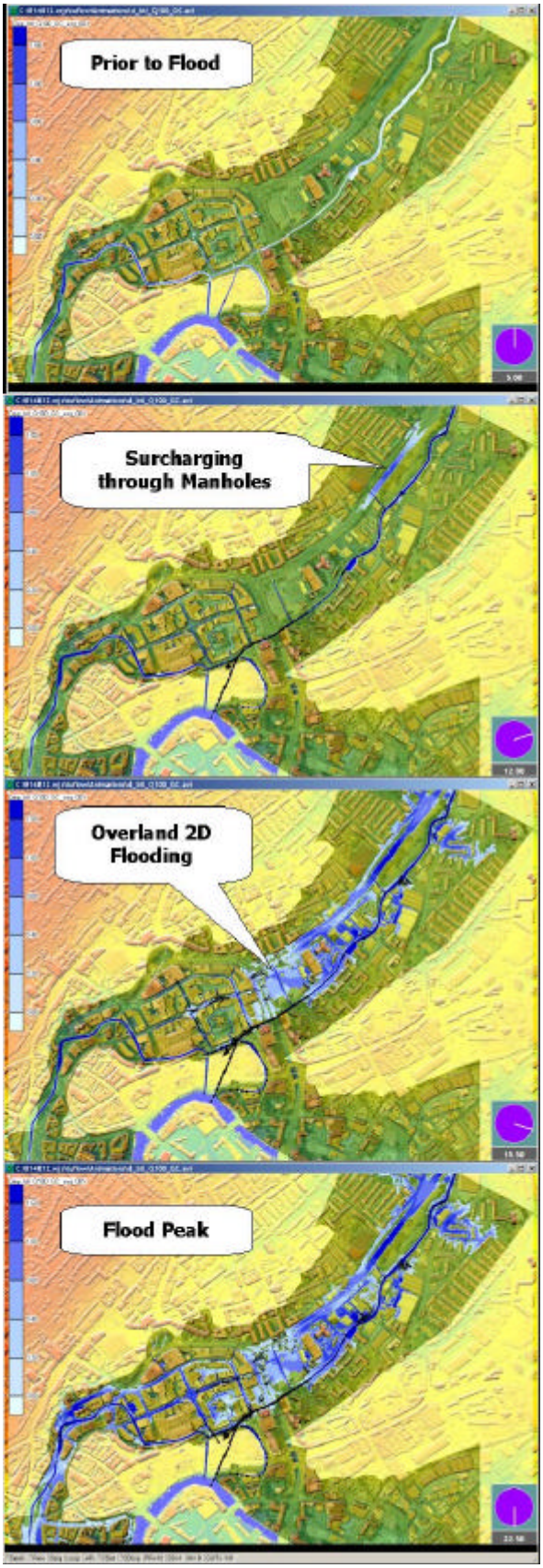

Figure 1 Predicted Flood Depths, Bristol TUFLOW Model

- Stormwater sewer pipes as a 1D system of culverts with connections between stormwater pipes and the overland 2D domain at manhole locations.
- Low-lying overland areas of the centre of Bristol as a 2D domain linked to the 1D domains.
- Replacement of 2D solution in three narrow and critical flowpaths between buildings that could not be adequately represented by the resolution of the 2D 4m cells.

The 1D open channel and culverted sections were based on those in the existing ISIS model. The stormwater sewer data was provided via a GIS layer. The 2D domain was based on sampling elevations from LIDAR (air-borne laser) DEMs provided by the UK, Environment Agency. DEMs were available with buildings and vegetation unfiltered or filtered from the data. For the TUFLOW model, the DEM with vegetation filtered out and buildings remaining was used. The DEM was problematic in that some re-working of elevations was required to remove features such as pedestrian bridges and overpasses that were incorrectly blocking overland flows. Also, key hydraulic controls, such as a stone wall alongside the open channel, are poorly defined in the DEM, and need to be incorporated into the TUFLOW model as 3D survey lines. Bed roughness (Manning's n) values were assigned to the 2D domain using existing GIS layers of land-use. Each land-use category was assigned a Manning's n value using a lookup table. For the 1D domains, similar Manning's n values as in the ISIS model were adopted.

The upstream inflow boundary condition was extracted from the existing ISIS model. Comparisons were made between the ISIS and TUFLOW results up until the point where flow was confined to the 1D domains (this is close to the 100 year event). A good correlation between the models resulted providing a validation of the TUFLOW model's 1D domains.

No major problems were encountered whilst setting the model up and carrying out simulations. As much of the data was available in digital formats, the setting up of the model was relatively straightforward. A site inspection carried out after preliminary modelling helped cross-check the predicted inundation and flow patterns, and to identify any need for additional detail in the model. Several locations were identified as needing more detail, such as the insertion of 1D elements for three key flowpaths between buildings as mentioned above.

Outputs of water level, depth, velocities and velocity depth product were generated from the 2D/1D model for a number of scenarios. Figure 1 shows predicted flood depths at different times of the simulation for one of the scenarios modelled.

As part of the flood risk assessment ongoing studies are investigating mitigation methods through the incorporation of additional storage, culverted and surface flow routes and building thresholds and floor levels for development proposals planned for the city centre. The ability of the TUFLOW 2D/1D model to represent a wide range of hydraulic processes within the urban environment was of considerable benefit in establishing accurately the flood risk, and for identifying measures to manage the risk.

3. TIDAL THAMES EMBAYMENTS INUNDATION STUDY

Over the course of history, development in and around London has encroached significantly into the River Thames floodplain. As a result, approximately 116 km2 between Teddington Weir and Dartford Creek, covering 23 hydraulically discrete embayments, is at risk of storm tide flooding during an extreme event. The risk is predicted to increase in the future due to a combination of sea level rise and geological settlement of southeast England. There are also the risks associated with failure of flood defence walls and/or the Thames Barrier.

The EA requires a tool to improve its ability to plan for and manage a tidal flood event that breaches or overtops the defences. This tool would generate predictions to give emergency response teams and the public reliable information regarding the extent, timing and nature of the propagation of floodwaters. On this basis, Halcrow, in conjunction with HR Wallingford, and WBM as a sub-consultant, were commissioned to carry out the Tidal Thames Embayments Inundation Study.

The first stage in the development of the tool involved the benchmarking of different modelling approaches on a single representative embayment, and make recommendations on the most suited modelling solution. The Greenwich embayment, located adjacent to the Thames Barrier, was selected as the trial area. Ideally an embayment for which observed flood extents are available would have been selected, however, in the absence of such data, an embayment was selected that was of 'average' size, contains many of the relevant features of the other embayments and is well known by the Agency team.

For modelling of floodplains, the main approaches used in the UK industry are:

- Quasi-2D (1D network) models
- 2D raster routing models
- Full 2D regular grid (typically finite difference) hydrodynamic models
- Full 2D irregular grid (typically finite element) hydrodynamic models
- Combinations of 1D hydrodynamic models with one of the above

The quasi-2D approach delimits a series of cells that correspond to distinct flood compartments, often separated by topographic features. This approach is incorporated in many standard 1D modelling packages as a means of representing off channel storage as a series of networked flood cells. The flow between the cells is modelled using simple analytical formulae such as the Manning or weir equations, or using the 1D St. Venant equations as used in the main river channels. Level/volume or level/flooded surface area relationships are used to define the storage of the floodplain.

More recently, the availability of topographic data in a grid format (eg. from air-borne laser) has led to the development and use of the storage cell concept applied to a raster DTM grid. These models use the raster DTM to discretise the floodplain as a regular grid with each pixel in the grid treated as an individual storage cell. Inter-cell fluxes use the uniform flow formulae or the weir equation (see for example Bates and De Roo, 2000). Each cell is assigned an elevation derived from the raster DTM. The computational burden compared with the quasi-2D approach is increased, but set up costs are greatly minimised. Raster routing methods are known to suffer from scale dependency (different results are generated with different grid sizes / time steps), and these are being investigated as part of the Greenwich Embayment application.

Fully 2D hydrodynamic models solve the complete 2D free-surface shallow water flow equations. They differ with the raster routing approach in that they model inertia, turbulence and other physical processes. The numerical solution of the full 2D equations requires increased computational effort.

For regular numerical grids (as predominantly used in finite difference models), model set up is relatively easy and similar to that for raster routing models as described above. The difficulty with regular numerical grids, of any type, is that the narrow and important flow routes (such as streams and drains) may force the cell or pixel size to be very small, and may create large, unworkable grids (on present day computers).

Irregular numerical grid models (as used in finite element solutions) are more difficult to construct and tend to be subject to a degree of user subjectivity. Irregular grid models, however, better represent linear features on the floodplain in a computationally efficient mesh (ie. higher density of elements through narrow flow paths). Set up costs in terms of time and necessary operator skill can be significant, and run times can be substantial.

One of the most important recent advances in floodplain modelling is the adaptation and use of full 2D hydrodynamic models dynamically linked with 1D models (Syme 2001). These combined models provide an efficient modelling environment in which small or narrow flowpaths (such as weirs, pipes and narrow streams) are modelled using 1D equations, while 2D flow (eg. overland flow) is solved using the full 2D solution. The 1D solution takes as input cross-sections, pipe dimensions, etc, providing a better representation of the geometry of these small or narrow flowpaths.

In order to provide recommendations on the most appropriate techniques to adopt, the following software were selected and applied to the Greenwich embayment to assess their accuracy and fitness for purpose.

- ISIS Flow (Quasi-2D)
- LISFLOOD-FP (Raster Routing)
- TUFLOW (Fully 2D, Regular Grid with 1D/2D dynamic linking)
- TELEMAC 2D (Fully 2D, Irregular Grid)

Experts in each of the modelling systems applied a consistent approach to development of the Greenwich models. Unfiltered (ie. includes buildings) air-borne laser data was used to generate a 1m raster DEM from which each model sampled its elevation data. The same distribution of five different bed roughness values was applied to all models using 30,000 polygons extracted from land-use mapping of London. Three scenarios were defined (an upstream breach, a downstream breach and an extreme overtopping event). The results of the

upstream breach are presented in this paper. The following discussion, and Figures 2a, 2b and 3, on the comparison of modelling approaches are taken from Wicks, et al (2004).

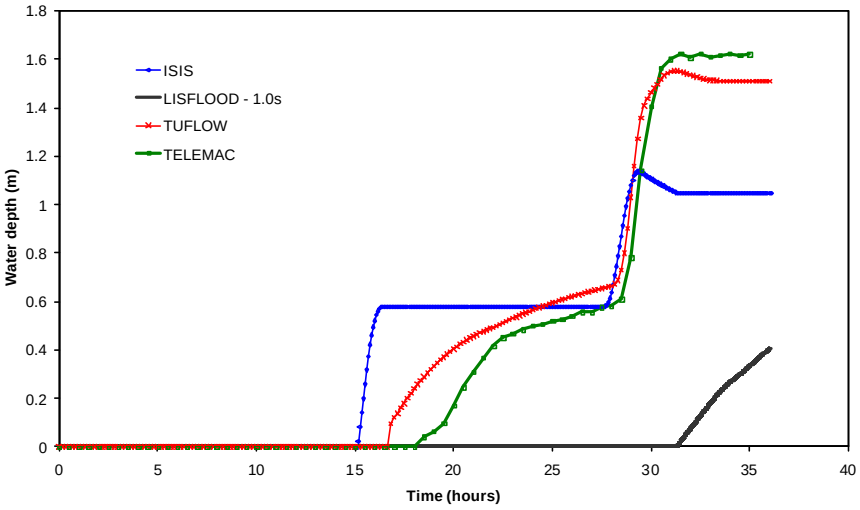

Figure 2a Comparison of Flood Depths at Location A (Wicks et al, 2004)

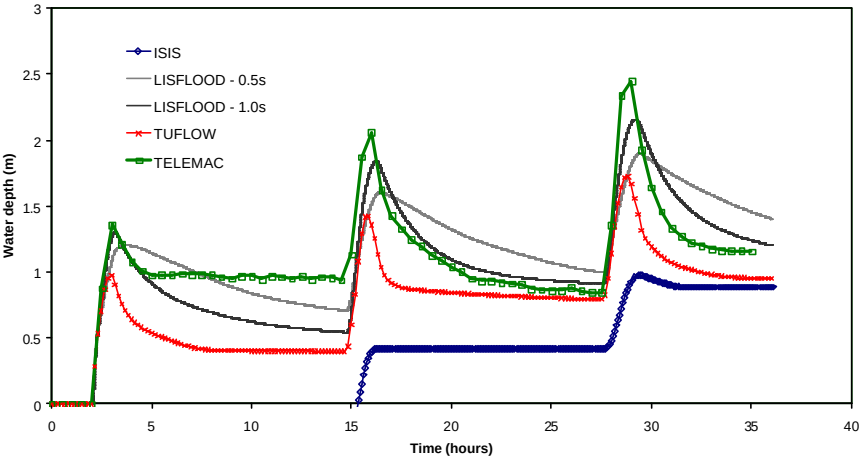

Figure 2b Comparison of Flood Depths at Location B (Wicks et al, 2004)

Based on the limited results presented in this paper a number of interesting conclusions can be made. Firstly, the time series of water depths in the floodplain demonstrate different aspects of the behaviour of the models. Depth time-series charts are presented in Figures 2a and 2b for locations A and B (refer to Figure 3). Location A is located further from the breach at an elevation of 1.3m above sea level, whilst location B is close to the breach at an elevation of 1.8m. At location A the TUFLOW and TELEMAC time series are very similar and the ISIS results are quite similar (but give a 0.5m lower final water depth). The LISFLOOD result at location A is very different - the predicted flooding does not reach this location until about 15 hours after that predicted by the other three models. It also appears that the final LISFLOOD water level has not been reached at this location during the 36-hour simulation. At location B larger water depths are predicted and the TUFLOW, LISFLOOD and TELEMAC results show similar behaviour. LISFLOOD results were also shown to be dependent on the computational timestepThe effect of changing time step in raster routing approaches is clearly seen from the 0.5s and 1s LISFLOOD simulation results. ISIS predicts onset of flooding at location B to occur about 13 hours after the other models but the final ISIS predicted flooding depth is close to that predicted by TUFLOW.

Secondly, the ISIS and TUFLOW maximum flood depth/extent maps (Figure 3) are both similar and seem reasonable. The LISFLOOD maximum extent is similar to the ISIS and TUFLOW extents in the southern part of the embayment but the LISFLOOD flooding does not extend northerly towards the Millennium Dome (as does the ISIS and TUFLOW extents). The TELEMAC extent is similar in the southern part and does extend further north than the LISFLOOD results (but not as far as the ISIS or TUFLOW results). In the TELEMAC results there are a number of large buildings that are shown flooded which are not shown flooded in the results of the other three models. Table 1 contains a summary of flooded areas for the models – the LISFLOOD flooded area is clearly the smallest.

As no 'observed' or theoretical data are available, it is not possible to definitely state that one particular model is more accurate than another. However, a subjective assessment of the results suggests that the TUFLOW model appears to give reasonable results that in all comparisons are similar to at least one other approach. For the other three models their results seem less reasonable in at least one of the comparisons.

For the selection of the most appropriate approach for the next stage of the Thames Embayment project, the criteria include run time, robustness, total cost, likely sustainability and ease of linkage to the ISIS 1D Tidal Thames model and other systems, as well as expected accuracy. The EA will be assessing the results presented

here (and further results presented in the formal project report) to inform their decision on which modelling approach to adopt.

Table 1: Comparison Summary – Upstream Breach Scenario, 36h Simulation

Model	Cell Size (m)	Timestep (s)	Approx Simulation Run Time	Flooded Area (km^2)
ISIS	n/a	Adaptive	< 1min	0.417
LISFLOOD	10	0.5	8 hrs	n/a
LISFLOOD	10	1	2 hrs	0.244
TUFLOW	20	10	4 min	0.466
TUFLOW	10	5	23 min	0.448
TUFLOW	5	3	2.5 hrs	0.437
TELEMAC	10 - 25	2	> 24 hrs	0.580

4. CONCLUSIONS

A number of drivers are changing the needs for floodplain mapping and flood risk assessment in the UK. The publication of PPG25 in July 2001 led to a major change in the way local planning authorities consider flood risk as part of the Town and Country Planning process. Additionally other organisations (financial planning services and insurance bodies) are increasingly using flood risk information. There is therefore a fundamental need to recognise the limitations and uncertainties of the (mapped) data available to such organisations, and where required there must be amendment and improvement of the techniques which underpin these studies.

In the urban environment in particular, it is essential that the model and techniques adopted for the study be fit for purpose. The model selected must accurately reflect the flow/flood mechanisms; be calibrated and verified wherever possible and must demonstrate that it is not sensitive to the selection of influential parameters.

Incumbent upon specialists in the field of flood risk and flood mapping is the need to identify concerns and uncertainties in the hydrological and hydraulic models used. Whenever required these uncertainties must be reduced through the application of the most appropriate techniques available, together with the collection of good quality hydrometric and supporting information.

In urban areas, fully 2D modelling offers a major step forward in the prediction of flood extents through superior representation of the complex hydraulic processes. Additional benefits include velocity and flood hazard mapping at a much finer resolution and greater accuracy than quasi-2D or 2D raster routing methods can offer. For hydraulic features that are poorly represented by the 2D domain (eg. pipe networks, narrow waterways, etc), 2D/1D dynamically linked modelling offers a near complete solution. In the case of the Thames Embayments Inundation study, the ability to dynamically link 2D domains along the length of the established and calibrated 1D ISIS model of the River Thames would be a very powerful tool.

Through the use of this next generation of flood modelling tools, considerable assistance is given to those required to make decisions where flood risk is an issue.

5. REFERENCES

Bates P.D. and De Roo A.P.J. (2000). *A simple raster-based model for flood inundation modelling,* Journal of Hydrology, 236, pp54-77.

DTLR (2001). *Office of the Deputy Prime Minister*, *Planning Policy Guidance Note 25 – Development and Flood Risk*, July 2001, HMSO, London.

Pinnell M. (2003). *Urban Hydrology: Stormwater Management*, Irish National Hydrology Symposium, November 2003.

Syme W.J. (2001). *TUFLOW – Two & one-dimensional Unsteady FLOW Software for Rivers, Estuaries and Coastal Waters*, IEAust Water Panel Workshop on 2D Models, Sydney, NSW, 2001.

Wicks J.M., Syme W.J., Hassan M.A.A.M., Lin B, Tarrant O. (2004). *2D Modelling Of Floodplains – Is It Worth The Effort*, Submitted in March 2004 for 2004 DEFRA Conference, UK.

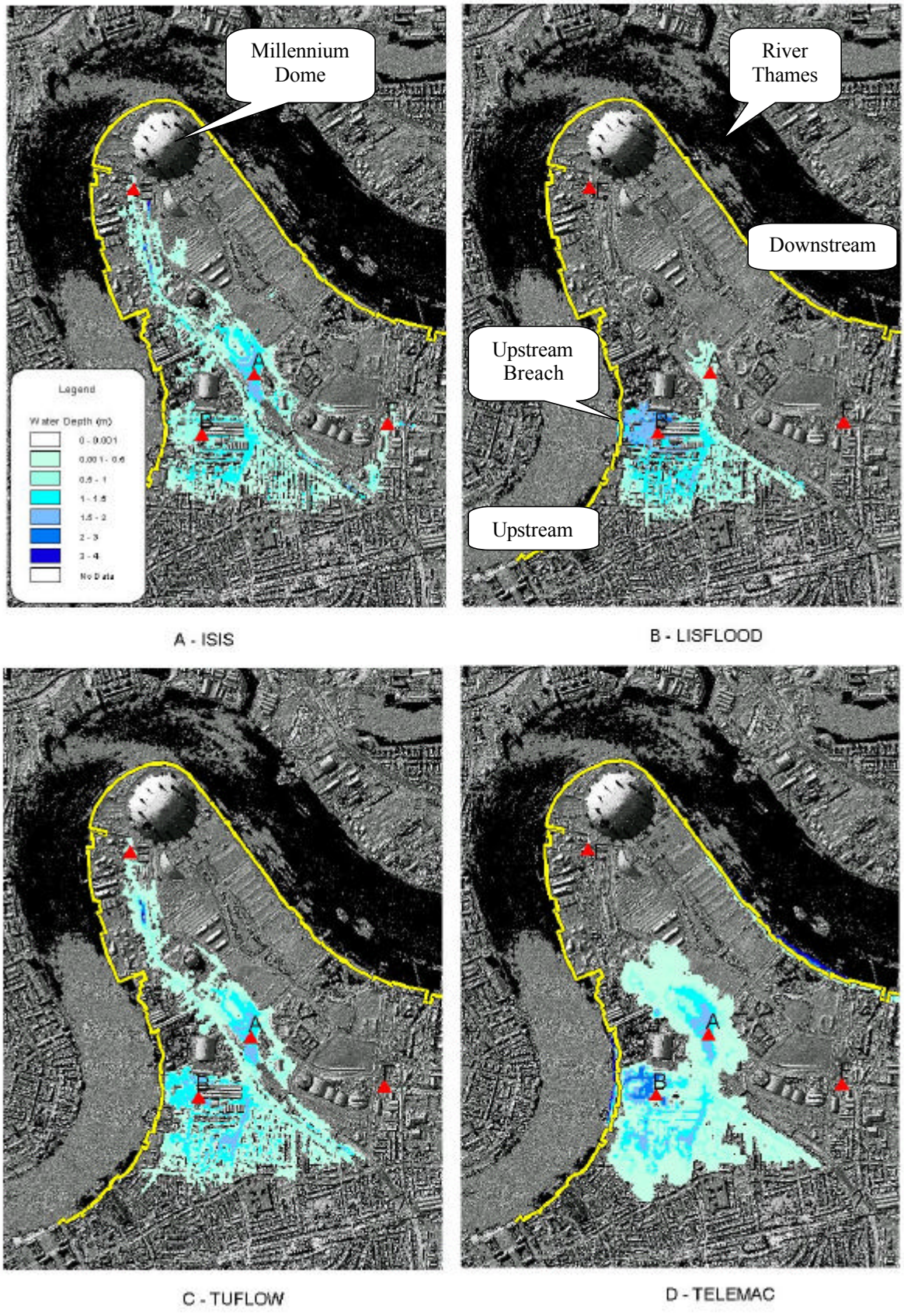

Figure 3 Comparison of Simulated Maximum Flood Depths (Wicks et al, 2004)

The Institution of Engineers, Australia
8th National Conference on Hydraulics in Water Engineering
ANA Hotel Gold Coast, Australia 13-16 July 2004

Development and Calibration of Detailed Sewer Models for the Brisbane Sewerage System

S. Szylkarski
B.E., MEngSc., M.I.E.Aust.
State Manager, DHI Water and Environment Pty. Ltd., Australia.
D. Heape
B.E., MengSc., M.I.E.Aust.
Network Planner, Brisbane Water.
D Kane
B.E.
Senior Engineer, DHI Water and Environment Pty. Ltd., Australia.
J. Wilson
B.E.
Engineer, DHI Water and Environment Pty. Ltd., Australia.

Abstract: The Brisbane City Council has a commitment to the South East Queensland Regional Water Quality Management Strategy to improve the health of Brisbane waterways. To facilitate the implementation of this commitment, Brisbane Water is developing strategic plans for the abatement of the impacts of wet weather sewer overflows throughout the City of Brisbane.

The basis of the overflow abatement plans is the development of detailed planning level hydraulic models of the waste water collection system.

In this paper we present the process for the development and calibration of hydraulic models for Brisbane City using the MOUSE modelling system. The models were developed for all pipes of 225mm in diameter and greater and include all known overflow structures connected to these pipes. The resulting models contained approximately 22,000 manholes and a similar number of pipes, over 150 pumps and over 490 overflow structures. The models were calibrated to over 380 flow monitoring gauges and/or pump stations, which represent a significant calibration process.

Keywords: Brisbane City, MOUSE, Sewer Modelling.

1. INTRODUCTION

To facilitate investigation of strategic plans for the abatement of the impacts of wet weather sewer overflows, Brisbane Water is developing detailed planning level hydraulic models of the sewerage system. The models will eventually be used to assess current performance and to optimise engineering options for a range of wet weather performance criteria.

The development of an overflow abatement model requires a thorough understanding of the sewerage system behaviour and an extensive set of dry and wet weather flow records. Hydraulic models are essential tools for assessing a sewer system performance under wet weather conditions and developing wet weather flow gauging campaigns. A robust hydraulic model is developed by first carrying out a thorough calibration of the sewer network under Dry Weather Flow (DWF) conditions. The model can then be used under various design loading scenarios to test wet weather flow behaviours and as a base for wet weather flow calibration. A DWF hydraulic model can also give a wide range of operational benefits such as transit time for Biological Oxygen Demand (BOD), load balancing at treatment plants, pumping station optimisation, power saving through flow smoothing, time to overflow for emergency and programmed shut downs, required bypass pumping parameters, as well as assistance in odour management and main criticality and condition.

The fundamental stages in model building and calibration for dry weather flow conditions are detailed below.

1. **Model Network Definition** – Definition of the contributing areas that are to be included in the model and the extent of the sewerage network to be modelled.
2. **Data Scrubbing** - Implementation of a series of checks and processes to ensure that validated data is used

for all facilities in the MOUSE model.

3. **Network Structures Definition.** Processing of available data for structures such as weirs, pumps, rising mains, one way valves, storage facilities and siphons to a format suitable for MOUSE. This may include Real Time Control (RTC) logic for pumps and other moveable structures.
4. **Network Parameter Definition.** Processing of hydraulic parameters for the model network such as head loss coefficients, storage allowances roughness, manhole sealing and rising main definitions.
5. **Catchment Definition and Population Modelling.** Processing land use, population and water consumption data to develop loading catchments for input to the network model.
6. **Preparation of Flow Survey Data**. Analysis of flow, depth and rainfall survey data to develop a common time series format for use in the model data bases. Analysis and preparation of normalised dry weather flow curves for use in MOUSE DWF calibration.
7. **Model Build.** Connecting of MapInfo and MOUSE data bases for data transfer and model build. Input of structures and network parameters.
8. **Dry Weather Flow Calibration.** Application of the DWF curves to the MOUSE model and analysis of the model results against flow gauging using Brisbane Water calibration sheets.
9. **Model Verification**. Application of the calibrated MOUSE model to an alternative DWF period to confirm the calibration.
10. **Mapping and Reporting**. Preparation of thematic mapping, calibration sheets and documentation.

The hydraulic models have been developed using DHI Water and Environment's MOUSE modelling system. MOUSE is a professional engineering software package for the simulation of surface runoff, dry weather flows, water quality and sediment transport in urban catchments and sewer systems. The MOUSE model carries out computation of unsteady flows in pipe networks using an implicit finite difference numerical solution of the one dimensional free surface flow equations. The MOUSE model includes specialised facilities for the modelling of looped pressure networks, pump facilities and ODBC connectivity for integrating with databases and GIS system.

The hydraulic models include all sewer pipes greater than 225mm in diameter, pump stations, overflows and rising mains needed for model linkage in the sewer network of Brisbane. A number of small sewers and mains (such as 150mm sewers) which were important for system analysis or connectivity have also been included.

This paper details the model development and calibration process that was carried out. The sewer models developed are some of the largest and most comprehensively calibrated models that have been developed in the MOUSE system and provide a case study on the application of models to large scale sewer systems.

2. DATA SCRUBBING

In order to develop reliable models the base data sets from the Council's MapInfo Geographical Information System (GIS) were passed through an extensive "data scrubbing" process to ensure the integrity of the data sets. Erroneous, duplicate and missing data were identified using Standard Query Language (SQL) – a feature of GIS MapInfo. Integrity tests were specific to each asset type (manhole, pipes/segments and pump station) and were developed for each data set. A typical example of integrity tests for manholes information includes:

- Duplication of data,
- Missing data,
- Ground level of the manhole was less than the sum of invert level and pipe diameter,
- Null values,
- Manhole diameter is less than pipe diameter,
- Excessively large, erroneous data entries,
- Upstream and downstream invert levels larger or smaller respectively.

Missing data and "gaps" in the data sets were resolved by interpolation of information and through model based assessments. Model based assessments involve the running of a non-calibrated model and using the results as a tool to determine the characteristics of the elements in question. In some cases a field inspection was required to resolve conflicting information.

3. MODEL DEVELOPMENT

The Brisbane sewer system is comprised of 7 catchments referred to as S1 S2, S3, S4, S5, S6 and S7 as shown in Figure 1. Each sewer catchment predominantly drains to a Waste Water Treatment Plant (WWTP) which is characterised as an outlet in the MOUSE models. The S1 system is by far the largest of the systems and incorporates the Brisbane CBD and the surrounding inner suburbs. The S1 system drains to the Eagle Farm Pump Station which then pumps to the Luggage Point Waste Water Treatment Plant at the mouth of the Brisbane River.

Sewer models for each of these catchments with the exception of the S4 catchment were developed by importing the "scrubbed" MapInfo data sets into MOUSE using an ODBC database import facility. A summary of the MOUSE modelled sewer system characteristics is presented in Table 1.

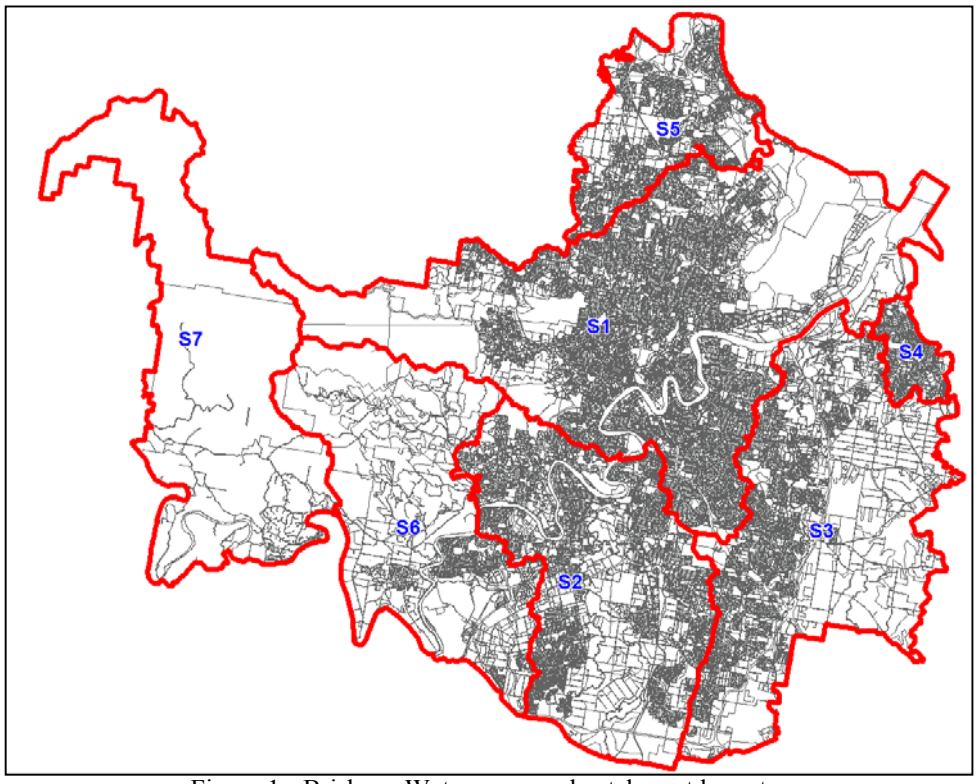

Figure 1 - Brisbane Water sewer subcatchment layout.

Table 1 - Brisbane sewer system model characteristics.

CATCHMENT	EP	FLOW MONITORS	PUMP STATIONS	MANHOLES ON PIPES >=225mm	OVERFLOW STRUCTURES	TOTAL KM GRAVITY PIPES >=225mm	TOTAL KM PRESSURE MAINS
S1	575,342	173	22	7,922	255	459	20
S2	241,095	59	60	5,334	207	293	50
S3	183,377	Nil	31	4,151	46	210	27
S4	30,933	35	9	698	20	36	2
S5	84,244	Nil	27	2,112	39	113	14
S6	23,000	Nil	11	675	11	26	12
S7	2,546	Nil	8	78	8	2.5	1
TOTAL	1,140,537	267	168	20,970	586	1,139	126

A specific feature of the MOUSE model developed for the Brisbane system is the modelling of pressure mains. In circumstances were the pressure main is not under outlet control but contains areas of gravity driven flow

within the pressure main line a specific schematisation has been developed to provide an approximation to the flow characteristics. This circumstance will often arise where the pipeline contains internal control points such as 'high elevation points' along the pressure main. These internal control points can determine the static head on the pump and often influence the dynamic performance of the pump. In such cases it is necessary to model the pressure main as a combination of rising main and gravity driven flow.

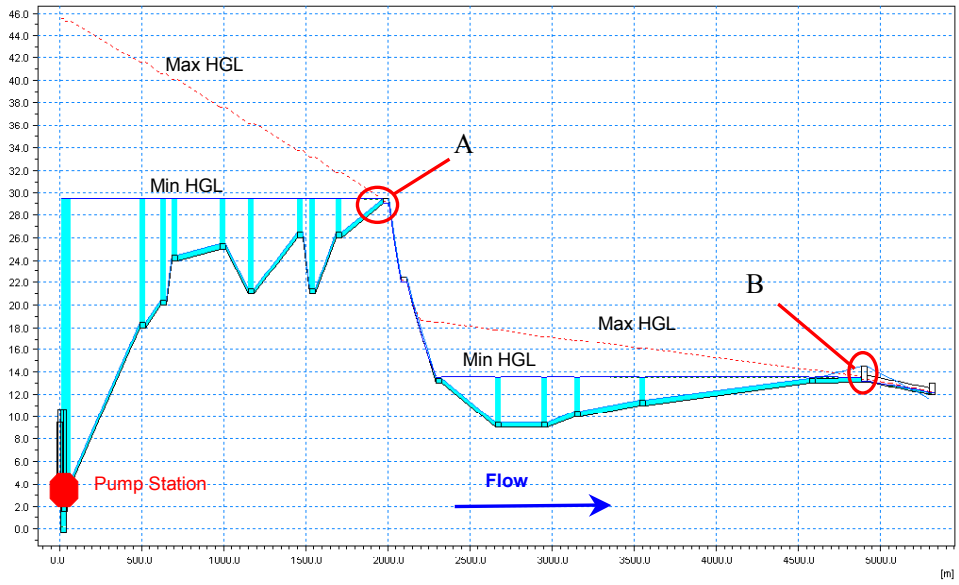

Figure 2 - Example of Internal Controls on Pressure Mains in MOUSE

The overflow structures were incorporated into the MOUSE model as a combination of 3 elements: the overflow pipe, the flap valve manhole and an overflow weir. The crest level of the overflow pipe is the overflow control level, while the overflow manhole and weir structure are included for the purposes of completeness and reporting.

4. DRY WEATHER FLOW PROFILE DEVELOPMENT

To successfully calibrate the hydraulic sewer models, accurate dry weather flow (DWF) 'patterns' were necessary. Dry weather flow 'patterns' define the distribution of the average sub-catchment flow at all times and are based on the principle of summation of repetitive diurnal flow 'profiles' for each day. In this study, the diurnal 'profiles' represent daily flow variations while 'patterns' define weekly flow variations.

The dry weather flow contributions within a catchment can vary significantly within a 24-hour period but substantial differences also occur from day-to-day during a typical week. In this study, the daily variation between a typical Weekday and typical Weekend day were determined to be significant and separate profiles were developed for each of these categories. In some instances, where the significant variation occurred from a Saturday to a Sunday, a separate profile was developed for each Weekend day. The combination of daily Weekday and Weekend (or Saturday and Sunday) profiles defines the flow distribution in the catchment over a typical week, which is referred to as the dry weather flow pattern.

A critical issue when developing dry weather flow profiles from gauging data is selecting appropriate time periods to represent 'typical' flow. The analysis period should not occur during school holiday periods when many households are vacant; should not include any periods that may be adversely influenced by inflow and infiltration due to wet weather and should avoid public holidays and major events when people's typical behaviour patterns are altered.

Review of the gauge records indicated that the effects of infiltration and inflow on the flow and level records were usually negligible after about four days of dry weather conditions. Based on that observation, rainfall records throughout Brisbane were analysed to determine the 5-day antecedent rainfall conditions at each gauge.

The results were then superimposed over a record of school and public holiday periods both in Queensland and Interstate. Finally, these results were superimposed over the periods of the gauging campaigns. A selection of suitable dry weather flow gauge periods was then made by observation.

In the selected DWF analysis periods a 'primary' week and a 'secondary' week were identified. The primary week was the primary source of data for analysis of dry weather flow profiles with the secondary week used to supplement data in the primary record when data dropouts occurred in the primary set. An example of the primary and secondary week dry weather flow from a gauge site is presented in Figure 3. The combined primary and secondary week flow records were then manipulated in order to identify averaged daily dry weather flow profile ordinates for weekdays and weekends. The normalised DWF profiles for all flow monitors is presented in Figure 3. In total, 70 gauge records were analysed using the dry weather analysis technique described above. The normalised ordinates (ADWF flow factors) varied from a maximum of 2.5 (peaking factor) to a minimum of 0.15. The minimum ordinate indicates that base flow in the system is typically between 15 to 30 percent of the average dry weather flow.

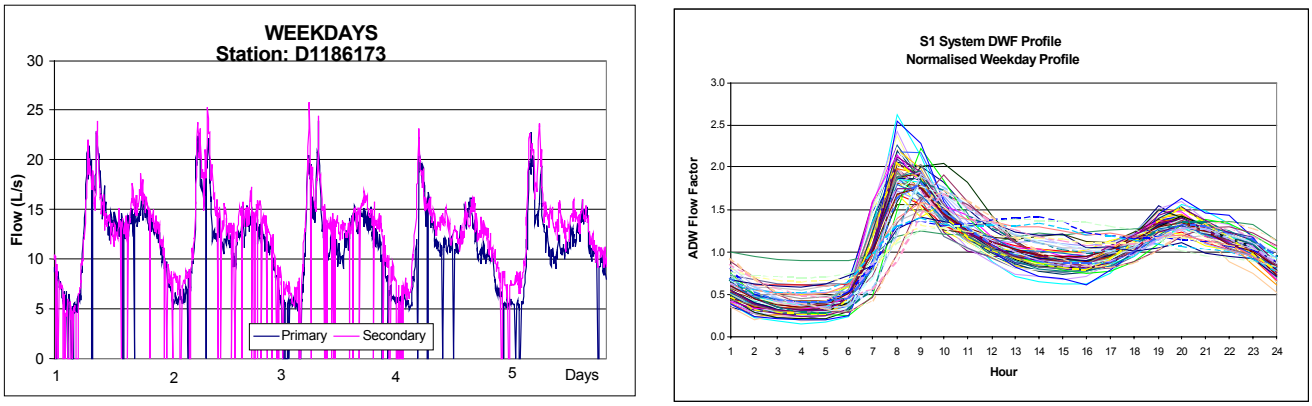

Figure 3 - Typical Flow Gauge Data for Weekday (left) and Normalised DWF Profiles(right - 70 flow monitors).

The 70 normalised DWF profiles were analysed in detail and a series of land use specific profile were derived from the total set. The unique land use profiles were developed for residential(slow response), residential (fast response), commercial, industrial, shopping centre, educational, Brisbane central business district and hospital. An example of the residential and commercial profiles is presented in Figure 4.

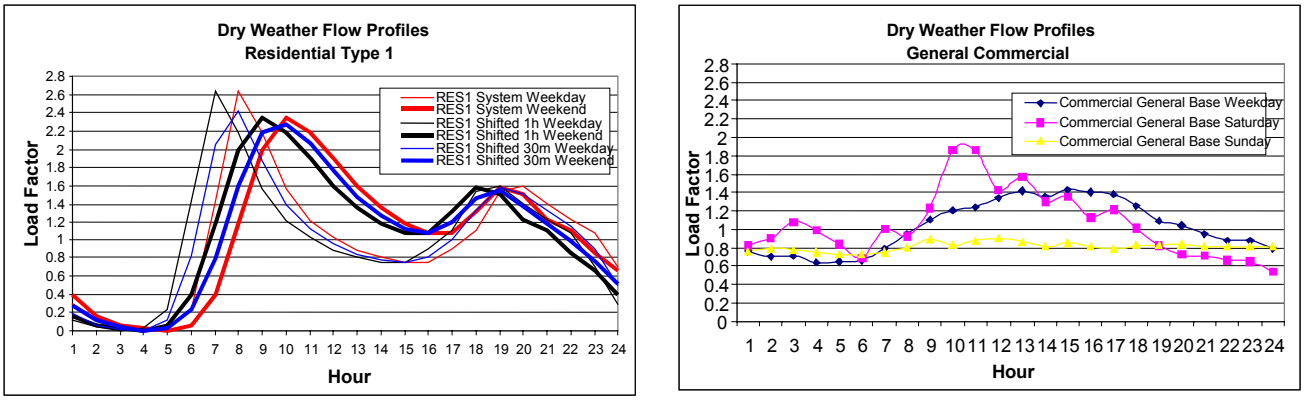

Figure 4 - Typical Residential and Commercial DWF Profiles for Brisbane City.

5. MODEL CALIBRATION

The calibration of the MOUSE models for dry weather flows is a deterministic process and is generally carried out as both a calibration and a verification process. A separate verification process is not necessary because of the repetitive characteristics exhibited by dry weather loads. The calibration is carried out to ensure that the repetitive flow and depth characteristics are consistent over time and as such the verification will produce the same results as the calibration.

The model calibration is primarily focused on reproducing the observed flow behaviour in terms of the flow depth and discharge over time at each flow gauge location. The calibration also focused on reproducing the pumping characteristics of the pump stations within the system. The pump station calibration is focused on reproducing the observed number of pump starts and stops and the overall volume of pumping.

Calibration of models is not an exact procedure and requires the modeller to make engineering judgements on the suitability of model parameters and results. However, a sequence of general tasks can be specified which will result in a calibration outcome. Divergence from these general tasks may be required in some instances where the calibration outcome is unusual and does not fit within the expected outcome. The intuition and experience of the modellers is paramount in determining the reliability of the calibration results.

The calibration results for each flow and water level gauge has been documented on a "calibration sheet", which covers a 48 hour period from Friday morning at 12:00 (midnight) to Sunday morning at 12:00 (midnight). The Friday and Saturday period are selected specifically to ensure that the change in diurnal behaviour between the weekday and the weekend is reproduced by the model. The pump stations were calibrated using a specific calibration sheet developed for pump stations which only covers a 24 hour period from Friday morning at 12:00 (midnight) to Saturday morning at 12:00 (midnight).

The calibration sheets are used to produce the correlation analysis between the model and the flow gauging data. The calibration sheets form the basis of the quality control for the model calibration and include details of the model simulation files and parameters, local catchment loadings, visual profile plot of system geometry at gauge location and general calibration observations and comments. A typical calibration sheet is presented in Figure 5.

A set of calibration targets and standards were set for each calibration station. Calibration stations were specified on the basis of available flow monitoring data and pump station operational data resulting in a total of 267 calibration stations for flow and depth and 168 calibration stations at pump stations. The calibration criteria at each station are dependant on the size of the catchments as detailed in Table 2. The model met or exceeded the calibration standards in over 90% of cases while divergence in the accuracy in the other 10% of cases was attributed to errors in the observed data.

Table2 Calibration Criteria and Targets

CALIBRATION CRITERIA	**EP > 10,000**	**EP 5,000 - 10,000**	**EP 5,000**
Variation in Total Discharge Volume (m^3)	±5%	±10%	±15%
Discharge (L/s) Scattergraph	Coefficient of Determination (R^2) > 0.85		
Depth (L/s) Scattergraph	Coefficient of Determination (R^2) > 0.85		
Maximum Variation in Depth	±10%		
Variation in Pump Station Starts per Hour	±15%		

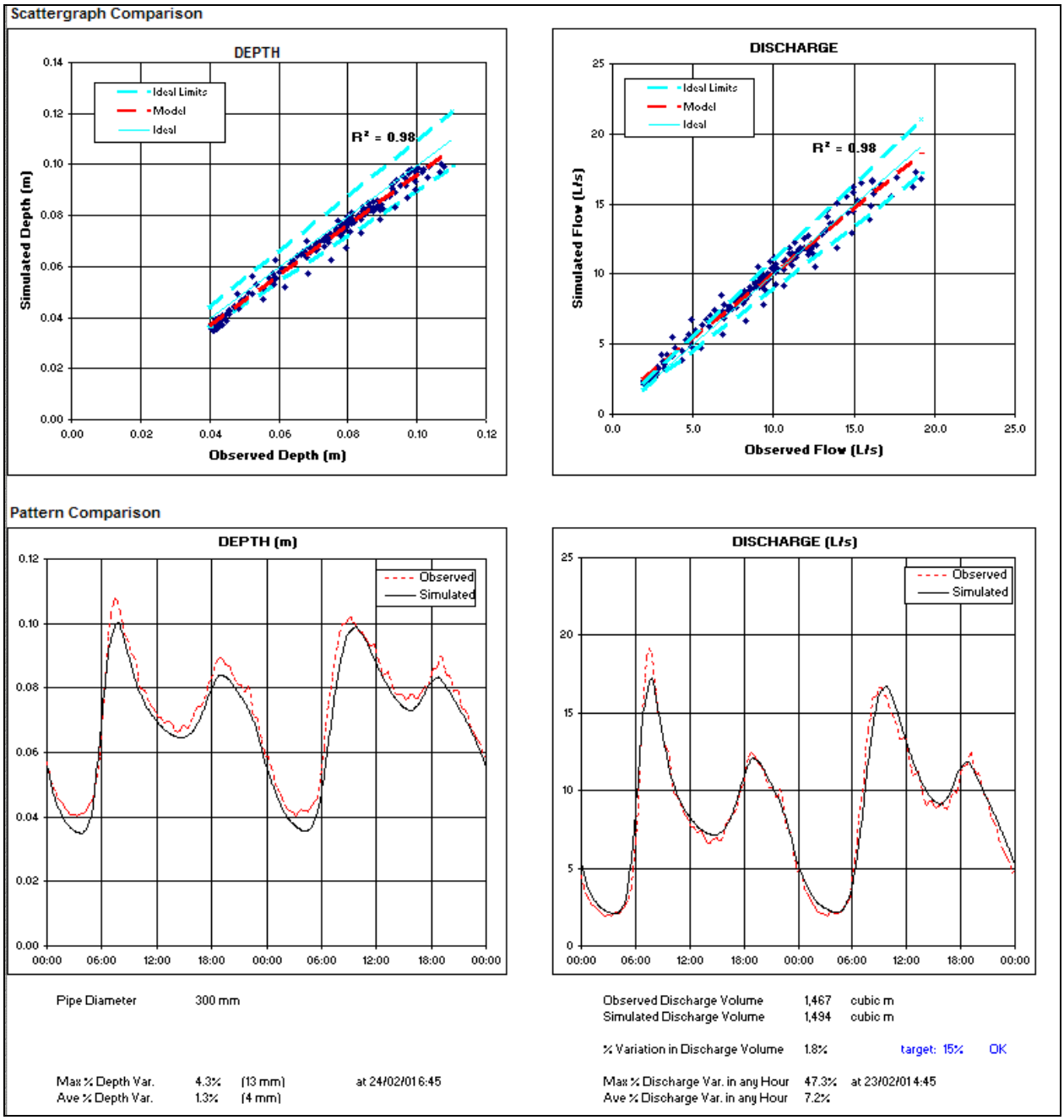

Figure 5 Typical Model Calibration Results in Standard Calibration Sheet Format.

6. CONCLUSIONS

A suite of 7 hydraulic models have been developed for the Brisbane sewer system which incorporate the catchments of S1 to S7. The models have been developed using the MOUSE sewer modelling package incorporating all pipes greater that 225mm in diameter and all significant pump stations and overflows.

The MOUSE models have been calibrated at 435 calibration stations which incorporate the available flow monitoring and pump station data. The models are suitable for the analysis of hydraulic conditions under the full range of dry weather flow hydraulic conditions.

The model development and calibration study represents one of the most significant calibrations for a model developed within the MOUSE system and demonstrates that the ability of the models to simulate large sewer systems with a high degree of reliability.

7. REFERENCES

City Design (BCC) and DHI Water and Environment Pty Ltd, 2003, *S1 and S2 West Wastewater Collection System MOUSE Modelling Study, Volume 1,* prepared for Brisbane Water, BCC.

City Design (BCC) and DHI Water and Environment Pty Ltd, 2004, *S2-East, S3,S5,S6 and S7t Wastewater Collection System MOUSE Modelling Study, Volume 1,* prepared for Brisbane Water, BCC.

The Institution of Engineers, Australia
8th National Conference on Hydraulics in Water Engineering
ANA Hotel Gold Coast, Australia 13-16 July 2004

Hydraulic and Ecological Modelling of the Pimpama River Estuary

S. Szylkarski
B.E., MEngSc., M.I.E.Aust.
State Manager, DHI Water and Environment Pty. Ltd., Australia.
J. Dorge
MSc. Biology.
DHI Water and Environment, Denmark.
D. Toomey
B.E.
Gold Coast City Council.
R. Burch
B.E., M.I.E.Aust.
Sinclair Knight Merz.

Abstract: The Gold Coast City Council through the Gold Coast Water Directorate is in the process of implementing the Northern Wastewater Strategy Reclaimed Water Scheme which is focused upon the development of beneficial water reuse activities across the Pimpama Woongoolba Floodplain, located between the Coomera River in the south and the Logan River to the north.

In order to determine the requirements of any reclaimed water reuse scheme the Council has commissioned an Ecological Study of the Pimpama River Estuary. The study will provide a scientific basis for determining the sustainable quantity and quality of reclaimed water, which may be released to the Pimpama River Estuary from the future Pimpama Water Reclamation Facility (WRF).

A numerical model of the Pimpama River estuary is being developed and calibrated to hydraulic, water quality and ecological measurements over a 12 month period. The model is being developed using a two dimensional (MIKE21) hydraulic model. The ecological model will be customised to the Pimpama River Estuary conditions enabling a dynamic simulation of the growth and decay of sea grass and the response of the sea grass to changes in water quality and eutrophic conditions.

The model will be used to assess the response of the Pimpama River Estuary to a range of release scenarios for the reclaimed water from the Pimpama WRF.

Keywords: Ecological Modelling, ECOLab, MIKE21, Pimpama River Estuary

1. INTRODUCTION

The primary objective of completing the Pimpama River Estuary Ecological Study is to provide scientific and technical information to determine the sustainable quantity of reclaimed water, which may be released to the Pimpama River Estuary from the future Pimpama Water Reclamation Facility (WRF), taking into consideration a wide range of constraints, including, but not necessarily limited to water quality, fisheries values and the ecological health of the estuarine environment.

The final recommendations to Council involve a 'specification' for the proposed Pimpama WRF in terms of the final quality of reclaimed water required from the facility, the volumes that may be released to the Pimpama River Estuary and the operational context under which the release is envisaged (i.e. it is expected that the release scenarios may differ between dry weather and wet weather conditions).

The first step involves determining the ecological health of the receiving waterway (Pimpama River Estuary) and characterising the ability of the waterway to accept a load from the plant without compromising the ecological health and environmental values of the Pimpama Estuary. That is, the load must be sustainable in terms of the ecological health of the Pimpama Estuary, under the various nominated operating conditions. This characterisation will then be used to formulate the treatment process of the Pimpama WWTP, including the quality performance specification and potential operating protocols. These protocols may be linked to prevalent climatic conditions.

The Study area is focussed upon the estuarine reach of the Pimpama River and the channels and islands forming the most southern extent of Moreton Bay (eg. Woogoompah Island), incorporating the general Broadwater and Jumpinpin region.

1.1 Overall Study Area Characteristics

The Pimpama River is located approximately 45 km southeast of the Brisbane CBD, between the Logan and Coomera Rivers. The Pimpama River drains a catchment area of approximately 13,070 ha with the headwaters located along the eastern edge of the Darlington Ranges some 29.3 km upstream of the mouth. The surrounding foothills within the upper catchment area contain a variety of small farms and rural residential areas. This system then meanders through the lower floodplain region, which has been modified for a variety of farming practices, particularly sugarcane production.

The tidal limit of the Pimpama River Estuary is located at a tidal barrage (floodgates) located approximately 4 km upstream from its confluence with Southern Moreton Bay.

Figure 1 – Pimpama River Estuary And Study Focus Area.

2. DATA COLLECTION PROGRAM

The data collection program for this study was aimed at providing sufficient information to:

- provide an understanding of the principal physical and ecological processes contributing to nutrient cycling in the estuary;
- provide a basis for the establishment of hydrodynamic and water quality models for the system;
- provide data for the calibration of system models; and
- provide data for fundamental nutrient balance calculations for the study area, as a means of cross-checking modelling results.

The data collection program was constrained by both budget and time, meaning that it was important that the collection program had to focus on collecting the most beneficial data within the timeframe available.

2.1 Hydrodynamic And Water Quality Monitoring

Ten tide gauges were deployed within the study area, five of which were located on study boundaries. Water level data was collected continuously for a period of three months to provide sufficient data for the tidal harmonics to be determined, to allow annual tidal cycles to be simulated. The three month tide data set was also utilised for model calibration.

Tide currents were measured using Acoustic Doppler Current Profiler (ADCP) technology at six locations in the study area. ADCP surveys were undertaken at each location during spring and neap tides in late September/ early October 2003.

Currents were measured approximately every 20 minutes along each transect over a 16 hour period that extended either side of low and high slack water.

The tide data collection equipment incorporated continuous water salinity measurement. This data was collected at the 10 tidal stations at the same periods as the tide data, providing information on the dynamics of water quality within the estuary. These data were used to calibrate the advection and dispersion characteristics of the estuary model.

Water samples were collected at the 10 sites throughout the study area each month for 12 months from July 2003. . Samples were analysed for a range of nutrients, suspended solids, chlorophyll-a, thermotolerant coliforms and E. coli.

2.2 Ecological Monitoring

Field inspections were undertaken during August 2003 to determine the spatial extent and species composition of seagrasses in the study area. Seagrass bed extents were surveyed using GPS, and spot sampling was undertaken.

In addition to this seagrass depth distribution, seagrass biomass was measured approximately every 3months at 12 sites from August 2003 to April 2004. This involved the sampling and measurement of seagrass biomass along each transect that traverses a range of water depths. At the time of each sampling, the water quality, species composition, epiphyte composition and sediment type was also recorded.

Following desk-top assessment of aerial photography and satellite imagery, field inspections were undertaken in October 2003 to determine the spatial extent and species composition and community structure of mangroves and salt marsh in the study area. Field survey of the boundaries of these areas was surveyed using hand-held GPS.

Macroinvertebrate surveys were undertaken on four occasions approximately three months apart, starting early July 2003. Eight sites were located along a clear estuarine gradient along the Pimpama River and the Broadwater. There were four other sites outside the study area with one site located in each of the following waterways: Logan River, Albert River, Coombabah Creek and Coomera River. These sites outside the study area provide comparative data from similar habitats that have been impacted to different degrees by catchment development. The Logan River and Albert River sites were chosen particularly to provide data on areas where nutrient concentrations are known to be relatively high, and may be impacting on benthic communities.

In the first sampling run, ten replicate samples were taken from each location to enable the number of replicates to be determined for subsequent events to provide the necessary statistical power. Samples were sorted and identified, and the diversity and trophic structure of the benthic communities described.

2.3 Sediment Biogeochemistry Sampling

Sediment biofacies were identified by sediment sampling of cross-sections within each major reach of the study area to determine the major biofacies and the approximate distribution. Seventy-six sites were sampled. Mapping of biofacies utilised the field data in conjunction with aerial photography and bathymetric information.

Sediment biogeochemistry was investigated at eight sites within the study area in winter (August 2003) and summer (February 2004). The sites were selected to be representative of the main biofacies in the estuary.

At each site, either benthic chambers or undisturbed cores were incubated on-site used to measure sediment gaseous and nutrient fluxes. Each site was sampled under dark and light conditions. Chamber and core incubations were undertaken with replicates in triplicate and duplicate respectively. The top 1 cm of each incubated core or chamber was sampled and analysed for Carbon, Total Nitrogen, Total Phosphorus, Chlorophyll-a, b, c and macrofauna.

Nutrient fluxes into and out of a mangrove creek system was measured over a 30 hour period. This approach provided a broad understanding of the likely nutrient cycling processes occurring in the mangrove systems, which would provide a good basis for modelling this element of the system as part of the estuary conceptual model development

2.4 Bathymetric Survey Data

The bathymetric survey information is used as the basis for the development of the model domain.

The bathymetric survey consisted of Airborne Laser Survey (ALS) of the study area on a 5m regular grid for all areas above 0 mAHD and hydro survey of the areas below 0 mAHD. The hydro survey consists of cross sections and longitudinal soundings for all significant channels within the study area. The soundings were also collected above the tidal flats during spring tides where navigable. The surveys were carried out in several stages with the final survey being conducted on 27 November 2003. The extent of the hydro survey is illustrated in Figure 2.

Figure 2 – Hydrosurvey Soundings within the study area.

3. ECOLOGICAL MODELLING

The development of a reliable ecological model is a primary outcome for the study and is essential for the study objectives to be met. The modelling is an evolutionary process which involves the adaptation of the model over the course of the study to produce a reliable analysis tool. Specifically the modelling objectives were:

- To provide guidance on the suitability of data collections sites;
- To make an evaluation of the most suitable modelling platform;
- To provide an understanding of the tidal characteristics; and
- To provide a tool for the assessment of water quality and ecological response to the discharge of treated wastewater to the estuary.

The MIKE21 model system developed by DHI Water and Environment is a two dimensional modelling system that incorporates hydraulic, transport, water quality and sediment process models. The MIKE21 modelling system was utilised in this study and specifically included the ECOLab module also developed by DHI. The ECOLab module is a model independent equation solver designed for ecological modelling that allows for tailor-made process descriptions to be incorporated directly into the model.

The ECOLab model structure was based on a conceptual model of the estuary nutrient cycling processes. This conceptual model was developed based on the results of the initial field investigation results, and on the observed conditions in the estuary. Refinement of the conceptual model and hence of the ECOLab module will be an integral part of the estuary model calibration and validation.

The first stage in the model evolution was the development of a simplistic two-dimensional model using existing bathymetric and tidal information. This preliminary model was used for the identification of the hydraulic conditions (depth, velocity, null zones), which was used to help assess the suitability of data collection sites. The initial model also provided an insight into the likely model simulation times, resolution and suitability of model boundary locations, and was used to analyse the importance of stratification in the estuary.

The second stage in the model evolution was the development of a detailed model bathymetry which was used in an evaluation of modelling platforms. In the absence of significant stratification, the modelling platform can be limited to a two-dimensional approach which provides a significant reduction in model simulation times. The comparison of suitable modelling platforms was limited to an evaluation between a Finite Difference (FD) and a Flexible Mesh (FM) modelling approach. It is feasible to apply either a finite difference model (using a nested solution) or a flexible mesh model to this application. The FD and FM models offer various advantages and disadvantages in relation to this study.

The third stage of the model evolution was the calibration of the selected model platform to hydraulic, water quality and ecological conditions during the data collection period. The successful calibration of the model requires an understanding of the overall environmental conditions within the estuary. The calibration procedure is essentially a learning process whereby the modeller develops an understanding of the dynamic conditions and adjusts the model to reproduce this behaviour.

The fourth and final stage of the model evolution is the application of the model as an assessment tool. The environmental boundary conditions will be modified to simulate expected and hypothetical conditions with the model, providing and assessment of the likely responses within the system. These responses can then be analysed deterministically and statistically to evaluate the overall impact on the future ecology of the Pimpama River Estuary.

3.1 Regional Model Development

The modelling process commenced with the development of a simplistic regional model of hydrodynamics and advection/dispersion. The purpose of the model was to provide guidance to the study team on the selection of sampling locations and expected hydrodynamic conditions. The model was also used to assess the likelihood of stratification within the Pimpama River estuary, and to obtain a preliminary appreciation of its flushing characteristics.

The development of the model was based on existing navigational charts and bathymetric data. The model is useful for the evaluation of the flow conditions and the study boundaries within the study area during the initiation of the model planning and was a crucial step in ensuring that the overall modelling and data collection requirements were understood from a broad perspective. The model was used extensively as a qualitative tool to allow for optimal planning of the study program.

3.2 Detailed Model Development

A "master" Digital Elevation Model (DEM) of 10m resolution was developed from the available hydrographic and ALS survey data. This DEM was used as the basis for all future model bathymetry generation. In some cases the DEM was insufficient to resolve the bathymetric conditions and seagrass, mangrove and biofacies mapping was used to confirm the bathymetric conditions.

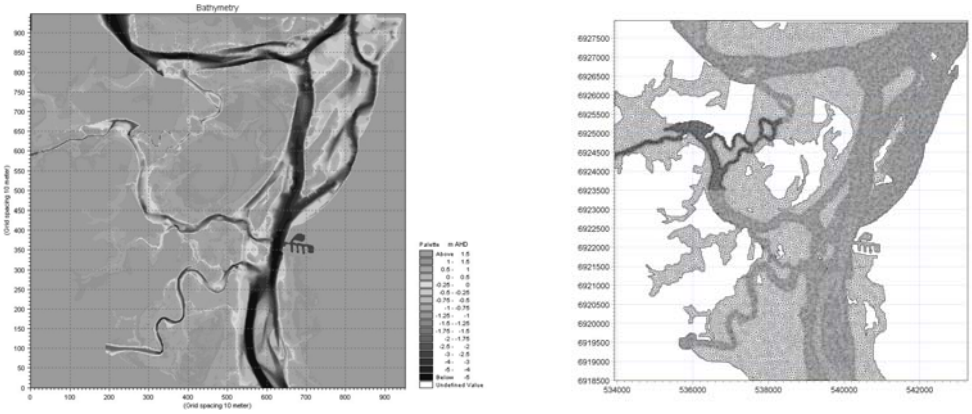

Figure 3 – Model Bathymetry In Finite Difference (Left) And Flexible Mesh (Right) Configurations.

The master DEM was then used to develop a series of nested Finite Difference (FD) models using the nested model facility as shown in Figure 3. An initial 10m nested model within a 30m outer model grid was developed. The 10m nested area covers the area between the Pimpama River and Jacobs Well Passage where the resolution of small tidal channels was required. Additional models were also developed that included 30m grid spacing over the whole study area, and nested 30m grid spacing within an outer 90m grid. Each of these models were developed and calibrated in order to assess the most appropriate modelling tool that provides a balance between resolution and acceptable simulation times.

A flexible mesh (FM) model bathymetry (Figure 3) was also developed on the basis of the 10 metre master DEM. The mesh was generated using a triangular mesh generator based on a constrained Delaunay triangulation. The computational domain was divided into a number of sub domains and different constraints applied for each domain. A maximum element area of 100 m2 was defined in the narrow channel areas covered by the 10m nested grid in the FD model, while in the remaining domain the maximum area in the channel sections was 900 m2 (equivalent to the 30 m grid in the MIKE 21 FD setup). For the floodplain zones a maximum elemental area constraint of 2500 m2 was applied. A total of 60,000 elements were generated in the final computational mesh which is shown in

3.3 Model Calibration

At the time of writing this paper the model has been calibrated for hydrodynamic and advection dispersion characteristics. Water quality and eutrophication model calibration will commence in April 2004 and be completed in the period through to July 2004

The FD 10m/30m hydrodynamic model was calibrated using water level and discharge data from 11 September to 29 November 2003. Water level calibration data were available for this entire period, while ADCP velocity and discharge data were available for the period from 26 September to 4 October 2003.

The calibration results were statistically analysed in order to assess the accuracy of the simulated results in comparison to observed water levels, discharges and velocities for the calibration period. An example of typical calibration result is presented in Figure 4. The figure shows the correlation of water levels for a typical gauging site over the 3 month tidal calibration period.

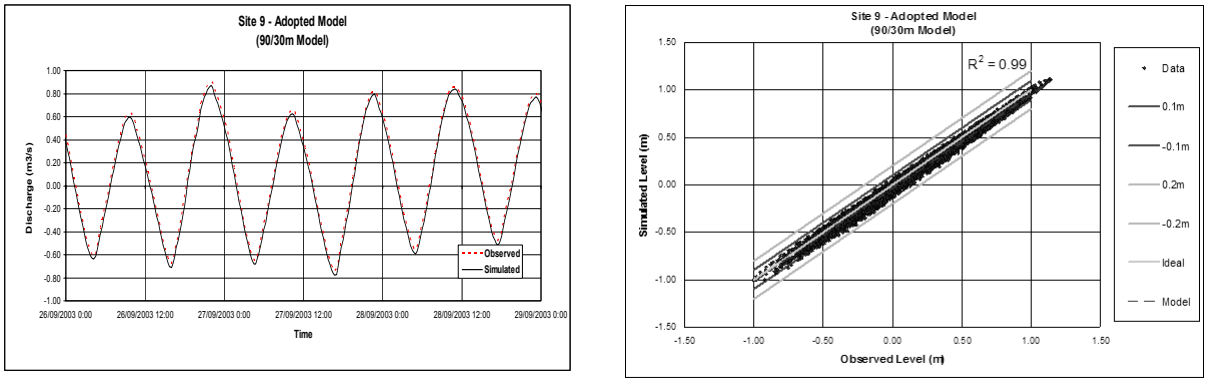

Figure 4 Water Level Calibration Results for a Typical Gauging Site.

The calibration results for water levels indicate an excellent calibration of the model at most sites, with R^2 values ranging from 0.94 to 1.00. A calculation of the Root Mean Squared Error (RMSE) and bias was also completed. The maximum root mean squared error (RMSE) is 0.091m which indicates that the water levels are generally accurate to within an accuracy of 0.1m.

The ADCP measurements were also processed to produce depth-averaged velocities (indicating current speed and direction) which can be compared directly to the simulated model results. Only qualitative comparisons are possible which nevertheless provide further indications of the strength of the model calibration. The ADCP velocity comparison can be used to check that the flow distribution across the channel is realistic. Two ADCP traverses were selected at each site for comparison, covering spring and neap tide conditions. The traverse timings were selected to coincide with maximum discharge conditions so that clear visual comparisons of the velocities could be made. A typical comparison of modelled and simulated velocities is present in Figure 5.

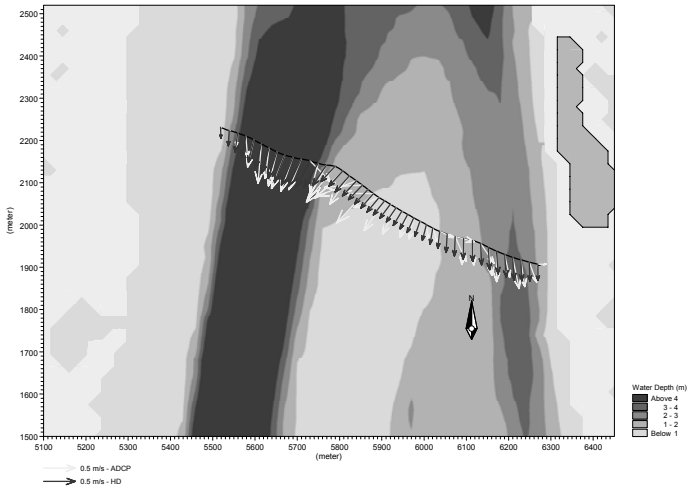

Figure 5 Velocity Comparison with Model and ADCP Measurements

3.4 Ecological Model Functionality

The ecological model consists of an 11 component water phase eutrophication model coupled to a benthic vegetation sub model and a sediment phase sub model. The 11 water phase components are subject to transport processes, and, thus integrated with the advection/dispersion calculations. The components of the eutrophication and benthic modules are listed in Table 1.

Table 1 Model Simulation Times.

Eutrophication Module	Benthic Module
PC - Phytoplankton Carbon	BC - Benthic Carbon (Macroalgae)
PN - Phytoplankton Nitrogen	BN - Benthic Nitrogen (Macroalgae)
PP - Phytoplankton Phosphorus	BP - Benthic Phosphorous (Macroalgae)
CH - Chlorophyll-a	EC - Shoot Biomass (Rooted Vegetation)
ZC - Zooplankton Carbon	NNEC - Number of shoots (Rooted Vegetation)
DC - Detritus Carbon	
DN - Detritus Nitrogen	
DP - Detritus Phosphorous	
IN - Ammonium/Ammonia & Nitrate/Nitrite	
IP - Phosphate	
DO - Dissolved Oxygen	

The eutrophication standard model is based on a mass preserving book-keeping system for the cycling of nitrogen, phosphorus and carbon within the various compartments of the water column. Compartments of nitrogen and phosphorus comprise a dissolved fraction, a dead organic fraction and an intracellular fraction of phytoplankton. Phytoplankton production is controlled by a description of the intracellular concentration of nitrogen and phosphorus, light availability, temperatures and it is possible to switch between different dominating phytoplankton species. The description of detritus C, N and P includes build up of detritus via death and sloughing of phytoplankton, zooplankton and benthic vegetation. Regeneration of nutrient from detritus and other transformation processes such as nitrification and denitrification are explicitly modelled. Dissolved oxygen is modelled based on the re-aeration at the water-air interface, primary production and respiration, nitrification, degradation of detritus and sediment oxygen demand.

The controlling factors for growth and death processes of benthic vegetation are incorporated in the model structure, and the interaction with the other components in the eutrophication module is an integral description of the model. The eutrophication model including the benthic vegetation sub-module is capable of describing the interspecific competition on nutrient uptake and nutrient availability between the rooted vegetation, macroalgae and the primary producers (phytoplankton) in the water column simulated in the water phase. The additional components are not subject to transport processes, and hence, including benthic vegetation does not occupy significant extra simulation time. A direct coupling between the light regime and the benthic vegetation is modelled. This means that impacts on seagrass of increased turbidity (e.g. modelled via the AD module) or increased phytoplankton production (modelled via the water phase sub-module) in the water phase is modelled explicitly.

The sediment model describes the nitrogen and phosphorous cycles as well as the linkage to nutrient concentrations in the water phase. In the model, nutrients cycling in the sediment are coupled to the modelled redox conditions and feedback mechanism from decomposition-nitrification-denitrification processes is modelled via a dynamic development of the aerobic (thickness of layer containing oxygen - KDO2) and oxic zone (thickness of layer containing nitrate). The simulated concentration distribution in the water column affects the processes occurring in the sediment, which again affect the concentration in the water column. The processes involved in the pathway from phytoplankton production in the water phase, deposition of organic material, turnover in sediment, oxygen consumption and nutrient fluxes between sediment and water phase, are all explicitly modelled. The thickness of the layers with oxygen and nitrate will influence the nutrient fluxes. The model is able to predict the flux of phosphate as a result of actual deposition of organic material, which affects the redox conditions, which again determines the adsorption of phosphate to iron. The actual flux of phosphate from sediment is a result of several sediment characteristics such as iron content, the pool of phosphorous, and the actual redox conditions. In many cases a pool of reversible phosphorus empties over a longer period following reduction in external nutrient loading.

The calibration of the water quality model will be made via adjustment of the model coefficients until a satisfactory accordance between observed and modelled data exists. The calibration efforts will focus on establishing correct diurnal variation in oxygen and the general concentration distribution of E.Coli within the estuary. The eutrophication model is a much more complex model compared with the water quality model thus the eutrophication calibration efforts are extensive. The proposed eutrophication model describes the light availability for the benthic vegetation as a function of phytoplankton biomass and concentration of detritus and suspended solids in the water phase. The calibration of the benthic vegetation sub-module will thus focus on firstly to establish a good agreement between modelled and observed secchi disk depth, secondly to establish accordance between the seagrass mapping and the modelled biomass distribution. This activity involves

adjustment of a limited, but sensitive, model coefficients. The dynamic structure of the modelling system changes in the Benthic Vegetation sub-module will also potentially change the results of the sediment/water phase part of the modelling complex. The sediment sub-module will be calibrated parallel with the water phase sub-module as the linkage between these two sub-modules is extensive.

3.5 Ecological Model Establishment

The initial establishment of the ecological module has been based on a conceptual model of the estuary nutrient cycling processes. The principal nutrient processes have been modelled using algorithms available within the ECOLab module, with appropriate modifications to reflect local characteristics. This model will be calibrated using the monthly water quality data collected over the 12 month sampling period. Further calibration of seagrass biomass production and distribution will be undertaken using the biomass sample results.

4. SIMULATION TIMES

Model run time is an important practical consideration in studies such as these. Single model runs can take up to several weeks to complete, making the calibration process and assessment of multiple scenarios unacceptably time-consuming.

To assess likely run times for the different model options, run times were calculated by carrying out a 1 day simulation for each of the models and then scaling the results for a 1 year simulation time period. The runtime estimates were calculated for two combinations of the models, HD/AD and AD/EU. The two simulation times are important because the eutrophication models can be calculated independently of the hydraulic model and therefore carried out as a standalone simulation. From the run time comparisons, it can be seen that the coarse 30m/90m model provides a dramatic decrease in simulation time compared to the other models. It is also noted that the FM model runs twice as slow as an equivalent FD model.

Table 2 Model Simulation Times.

Model	Type	HD/AD model 1 day	HD/AD model 1 year	AD/EU model 1 year
10/30 m grid	FD	1.66 hours	605 hours	2420 hours
30 m grid	FD	1.36 hours	499 hours	1996 hours
30/90 m grid	FD	6.4 minutes	39 hours	156 hours
FM	FM	3.35 hours	1221 hours	4886 hours

5. CONCLUSIONS

The modelling of the Pimpama River Estuary Ecological Study was carried out using a range of scales and types of models including finite difference (FD) and flexible mesh (FM) models. The models have been calibrated for hydraulics and transport process with a high degree of correlation found between observed and simulated state parameters for all scale models. The results show that a large scale model can be calibrated effectively in the Pimpama estuary whilst providing a significant reduction in simulation times. This is particularly important for eutrophication studies where the simulation time can be the governing conditions for a successful study outcome.

6. REFERENCES

DHI Water and Environment (2003). *MIKE21 Flow Model Reference Manual*, Version 2003.

DHI Water and Environment (2003). ECOLab *Reference Manual*, Version 2003.

Sinclair Knight Merz (2004). *Pimpama River Estuary Ecological Study, Milestone 2 Report*

The Institution of Engineers, Australia
8th National Conference on Hydraulics in Water Engineering
ANA Hotel Gold Coast, Australia 13-16 July 2004

DIVERSE DROP STRUCTURE APPLICATIONS IN AN OPEN CHANNEL

L. Toombes
B.E., Ph.D., Grad.I.E.Aust.
Engineer, Connell Wagner Pty. Ltd., Australia

Abstract: The Downstream Channel is a 27km diversion channel to convey discharge from the new Nam Theun II hydropower project to the Xe Bank Fai River. The design of this channel required a careful balance of hydraulics, operational requirements, geological constraints, and economics. A range of river training techniques, including riprap protection and velocity control weirs, were employed to manage scour in the channel, allowing the alignment and geometry of the channel to be optimised. Reservoirs can significantly alter the level of dissolved gases (eg oxygen, nitrogen, methane) present in the discharge waters, and can have a detrimental impact on aquatic life downstream. An aeration weir is to be constructed in the Downstream Channel to help equilibrate the dissolved gas levels in the discharge.

Keywords: Weir; Drop structure; River training; Water aeration; Oxygenation

1. INTRODUCTION

The Nam Theun II hydroelectric project is a new hydroelectric development located in central Laos. The Project is a trans-basin scheme, diverting water from the Nam Theun River catchment into the Xe Bang Fai River, and thereby benefiting from a 348m high head to drive generating units capable of producing a total of almost 6,000GWh per year. The project will generate 1070MW of power, of which approximately 995MW will be exported to Thailand with the balance going to the local Lao grid. Notable features of the project include:

- A power station with four 250MW units with Francis turbines to provide the Electricity Generating Authority of Thailand (EGAT) with up to 5,636GWh of electricity per year, as well as two 43MW units with Pelton turbines to provide Electricite du Laos (EDL) with up to 300GWh of electricity per year;
- A 138km double circuit 500kV transmission line to deliver power to EGAT, and a 70km long 115kV transmission line to deliver power to EDL;
- 16 major dams or weirs; and
- Over 34km of diversion channel and tunnels.

The power station will into a regulating pond formed by an earth rock embankment dam. The regulating dam will have two contiguous concrete discharge structures – one spilling into the continuation of the Nam Kathang River and the other into the Downstream Channel. Connell Wagner has been responsible for the hydraulic analysis of the Downstream Channel works, a 27km diversion channel to convey discharge from the Regulating Dam to the Xe Bang Fai River. The channel is designed to carry a normal operating flow of 315m^3/s, and larger discharges during flood events. The Downstream Channel is typically of trapezoidal cross-section, although the cross-section dimensions, channel grade and lining change along the channel. Several major structures are proposed for the Downstream Channel:

- A tri-level structure to convey flows in a local waterway, the Ban Itak, underneath the Downstream Channel, with a road bridge crossing the two waterways;
- An inverted siphon to convey the Downstream Channel discharge underneath the Nam Gnom River;
- An aeration weir located approximately 8km downstream of the regulating dam. The weir will serve the dual purpose of controlling a 2.4m change in channel invert elevation, while also aerating the discharge water to help improve water quality; and
- A 9.5m diameter tunnel excavated through a limestone massif 17km downstream of the regulating dam. The tunnel has a length of 700m.

Drop structures have been proposed to solve several challenges in the Downstream Channel that have been imposed by economic, geotechnical, or operational constraints.

2. DROP STRUCTURES FOR RIVER TRAINING AND VELOCITY CONTROL

2.1 Velocity, Flow Resistance and Channel Migration

Straight channels are rare in nature, but rather adopt a meandering alignment that may migrate with time. The degree of meandering depends upon, amongst other things, the typical velocities in the channel and the geomorphology of the terrain (eg bed material). In time, a channel will migrate until it reaches a quasi-stable alignment, where typical velocities no longer cause erosion. Ongoing migration of the channel may continue, particularly during large flood events.

The meandering of a channel impacts on flow velocities in two distinct ways:

- It increases the effective length of the channel, thereby reducing the average grade; and
- It increases the effective roughness of the channel, as changes in direction, eddy viscosity and other forces act to dissipate energy.

The latter is analogous to a macro-roughness or form roughness. In traditional one-dimensional hydraulic calculations, such as the Manning's Equation, form resistance and bed resistance are lumped together in the form of a single loss coefficient (eg Manning's n). CHOW (1973) indicates that the Manning's n of a channel with severe meandering may be up to 30% higher than a relatively straight channel. Manning's Equation is traditionally presented as:

$$V = \frac{1}{n}\left(\frac{D_H}{4}\right)^{2/3}\sqrt{S_f} \qquad (1)$$

For 'normal' or equilibrium flow conditions, the friction slope S_f is equal to the bed grade S_0.

2.2 Potential for Scour in the Downstream Channel

The downstream channel follows the general alignment of several natural streams in its trail across the local countryside. The new channel, however, is larger than these streams, and for simplicity of construction adopts a relatively straight alignment that will cut across the existing channels. Although the grade of the channel is relatively flat, the artificial nature of the channel – straight alignment, and smooth, regular section – implies that the resistance of the channel is relatively low. If left unchecked, velocities in the unlined channel would exceed the transport threshold of the erodable bed material.

The channel geometry is influenced by economics and geology as much as hydraulics. To minimise costs and the need to dump excess spoil, the downstream channel alignment is optimised with cut and fill balancing. In several areas the water surface level in the Downstream Channel will exceed the level of the existing topography, and levees are required to contain the channel discharge. Migration of the Downstream Channel, and the destruction of these levees, is clearly unacceptable.

2.3 River Training Mechanisms

'River Training' is a term used to describe techniques for limiting channel migration, traditionally by limiting velocities in the channel below the transport threshold of the bed material. Several techniques were investigated for the Downstream Channel.

2.3.1 Channel Scour Protection

There are a diverse variety of materials suitable for the protection of channels, ranging from concrete to rock to proprietary products. Due to the ready availability of rock from a nearby quarry, rock protection was determined to be the most economical. Both gabion mattresses (rock-filled wire baskets) and dumped riprap were considered. Gabion mattresses can generally tolerate higher velocities (the wire cages help resist uplift and motion of the rockfill) and use less material (the fabricated cages have better quality control than loose-dumped rock), but incur a higher fabrication cost. Again, the ready availability of rock material offset the benefits of the gabion mattresses, and dumped riprap was found to be more economical. Riprap with a D_{50} of 300mm and a layer thickness of 500mm should be adequate for velocities of 2.0m/s to 2.6m/s.

The riprap protection offered a number of hydraulic benefits as a bonus. As well as being able to resist relatively high velocities, dumped rock has a relatively high roughness, effectively increasing the resistance or Manning's n of the channel. Combined, these properties allowed acceptable velocities to be maintained in a relatively small channel cross-section, reducing the earthworks volumes and construction costs.

2.3.2 Velocity Control

Examination of Equation (1) (Manning's equation) suggests that there are numerous methods for influencing the flow velocity in a channel. Some methods, however are not as preferable as others.

It is difficult to produce a significant variation in the roughness of a channel, unless in the form of a channel lining such as that discussed in Section 2.3.1. So, from a purely hydraulic perspective, the simplest parameter to change is the geometry of the channel – the cross-sectional shape (D_H) and/or the grade (S_0). Both these factors, however, directly impact on the economics of the channel. It was therefore important to find the geometry that satisfies the hydraulic requirements and minimises construction costs.

A relatively common method of river training is to divide a channel with a steep gradient into a series of steps with a flatter grade. This technique is simply an imitation of nature – mountain streams can dissipate energy by eroding the bed into a series of drops, or natural steps. Although the creation of a 'stepped cascade' is traditional for river training, the grade of the Downstream Channel is already relatively flat. The limit of survey accuracy therefore makes the formation of flatter steps difficult within the construction tolerances.

A series of control weirs were spaced along each reach of the channel. Each weir formed a fixed point of 'control', and was used to raise the water level and reduce velocities upstream of the weir. The influence of the weir decreases with increased distance upstream, as the flow conditions in the channel approach equilibrium. The distance between the weirs is governed by the scour velocity of the channel bed material. The spacing could be increased by increasing the height of each weir, however this would also increase the channel depth required to contain the flow.

The water depths and velocities in the channel were predicted using standard backwater calculations, using the commercially available one-dimensional hydraulic analysis software package HEC-RAS (USACE 2003). The effect of the control weirs on water levels in a typical reach of the Downstream Channel is shown in Figure 1. The corresponding velocities are shown in Figure 2.

Sedimentation may occur behind each control weir. The long-term effect would be the natural formation of a stepped cascade profile. Although this is not necessarily undesirable by itself, it would nevertheless alter the hydraulic characteristics of the channel.

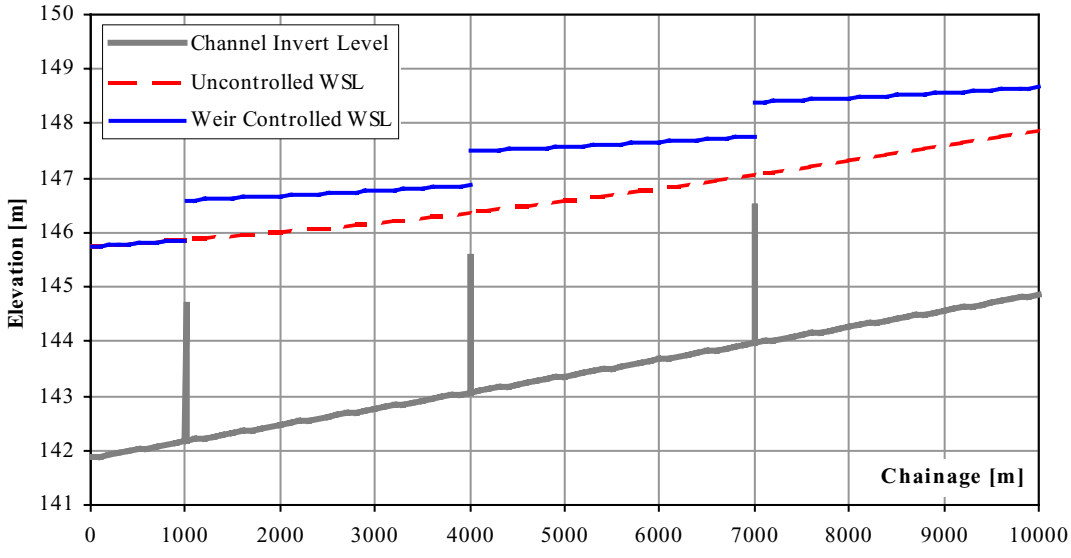

Figure 1 Typical Water Surface Levels (WSLs) in the Downstream Channel

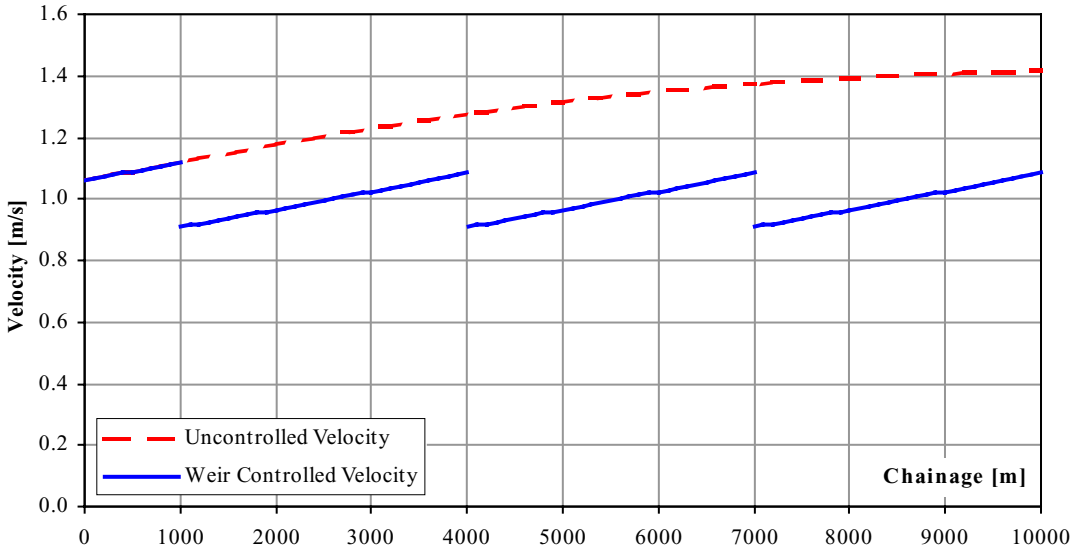

Figure 2 Typical Velocities in the Downstream Channel

2.4 Designs Proposed for the Downstream Channel

The ultimate design of the Downstream Channel geometry is still in the process of being optimised. Several more iterations are expected before the final balance of hydraulics, economics and geology is achieved. Currently, it is proposed to adopt a riprap lined channel for the upper 17km between the regulating dam and the tunnel. Downstream of the tunnel, across the Xe Bang Fai floodplain, an unlined channel is to be adopted. Control weirs are to be used to control the channel velocities.

Table 1 River Training Proposed for the Downstream Channel

Reach	Length [m]	Base [m]	Grade [%]	Velocity [m/s]	Lining	Control Weirs
Regulating dam to aeration weir	8000	20.0	0.08 to 0.1	2.1 to 2.3	Riprap	No
Aeration weir to tunnel	8000	21.5	0.08	1.1 to 2.15	Riprap	No
Tunnel to Xe Bang Fai River	9300	77.0	0.035	0.9 to 1.15	Unlined	Yes

3. DROP STRUCTURES FOR WATER AERATION

Dams have considerable impact on the gas transfer dynamics of the streams that they discharge into. The reservoir upstream of the dam acts to trap organic matter. The decomposition of this organic matter consumes oxygen, while releasing nitrogen, chlorine, and volatile organic compounds (VOCs) such as methane. Dissolved oxygen (DO) is one of the most important indicators of the quality of water in rivers and streams. High nitrogen and high VOC content are also detrimental to the presence of aquatic life. Consequently, it is often necessary to introduce an artificial mechanism downstream of large reservoirs to help aerate the water and restore gas concentrations to equilibrium concentrations.

3.1 Factors Influencing Gas Transfer at Drop Structures

The use of drop structures as aeration devices is relatively well recognised, although the precise details of the gas transfer mechanisms are less well understood. For a volatile gas (eg oxygen, nitrogen, VOC), the equation for gas transfer across an air-water interface may be written as:

$$\frac{\partial C}{\partial t} = K_L \, a \left(C_{sat} - C \right) \qquad (2)$$

The difference between the saturation concentration and the current concentration ($C_{sat} - C$) is commonly referred to as the *deficit*.

It is not the intention of this paper to go into details of air-water gas transfer, which have been discussed in numerous other documents including CHANSON (2001) and TOOMBES (2002). From Equation (2), the two key elements of air-water gas transfer are the interface area between the air and water, and the time that the air and water remain in contact. Drop structures, either single drops or multi-drop stepped cascades, are a relatively economical means of increasing the air-water contact area by entraining air bubbles into the water. There are several different mechanisms that contribute to air entrainment:

- At the upper surface of the free-falling jet;
- In the air-water shear-layer at the lower interface of the jet; and
- By 'plunging jet' where the jet impacts into the tailwater.

For a typical drop-structure with a relatively deep tailwater, the largest contributor is the plunging jet. Large volumes of air may be entrained along with the impacting jet, often 20% to 40% of the total volume of water. This air is entrained in the form of small bubbles, typically of the order of magnitude of 1mm to 10mm, and represents an enormous surface area. Depending on the impact velocity and angle and the depth of the tailwater, these bubbles may remain within the water for many seconds.

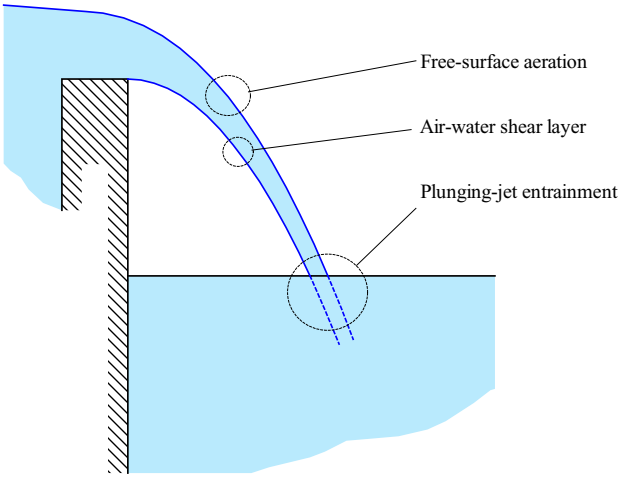

Figure 3 Typical Air Entrainment Mechanisms for a Drop Structure

3.2 Theoretical Estimates of Aeration Efficiency

Aeration efficiency is a measure of the ability of a structure to increase the dissolved gas concentration. There are two standard reporting methods: the deficit ratio r and the aeration efficiency E, defined in Equations (3) and (4) respectively.

$$r = \frac{C_{sat} - C_{US}}{C_{sat} - C_{DS}} \tag{3}$$

$$E = \frac{C_{DS} - C_{US}}{C_{sat} - C_{US}} = 1 - \frac{1}{r} \tag{4}$$

One of the major difficulties associated with predicting aeration efficiency of hydraulic structures is the problem of scale effects. As discussed above, the rate of gas transfer is proportional to the specific interface area, which is a function of both the total volume of entrained air and bubble size, which in turn are a complex function of many variables including impact velocities, viscous shear forces, surface tension and buoyancy to name a few. Dimensional analysis of a drop structure reveals that the aeration efficiency is a function of Froude, Reynolds and Weber numbers, which cannot be easily scaled simultaneously, as well as geometric and time scaling. Scaling effects are discussed by texts such as WOOD (1991) and CHANSON (1996), and it is recognised that large-scale modelling is required for accurate representation of air-water flows.

Nevertheless, numerous correlations of aeration efficiency have been published – generally empirical correlations of experimental data. Three of the more recognised correlations for oxygen transfer are AVERY and NOVAK (1978), NAKASONE (1987), and WATSON et al (1998):

$$r_{15} = 1 + k_{AN}\left(\frac{\rho_w}{\mu_w}(D_H)_i\sqrt{\frac{g\Delta H}{8}}\right)^{0.53}\left(\frac{2\Delta H}{(D_H)_i}\right)^{0.89} \quad (5)$$

$$\ln(r_{20}) = k_{N1}\Delta H^{k_{N2}}\left(\frac{q}{3600}\right)^{k_{N3}} d_t^{0.31} \quad (6)$$

$$r_{20} = 1.0 + 0.00107\left(\frac{d_t}{\Delta H}\right)^{0.70} Re_j^{0.3}\, Fr_j^{0.3} \quad (7)$$

where r_{20} is the deficit ratio (for oxygen) at 20ºC, ΔH is the difference in elevation between the water levels above and below the weir, q is the flowrate per unit width, ρ_w and μ_w are the density and viscosity of water, $(D_H)_i$ is the hydraulic diameter of the free-falling jet at impact, Re_j and Fr_j are the Reynolds and Froude numbers of the jet, and d_t is the tailwater depth. The coefficients k_{AN}, k_{N1}, k_{N2} and k_{N3} are reported below.

Table 2 Coefficient k_{AN} (AVERY and NOVAK 1978)

Water Salinity	k_{AN}
Tap Water	0.627×10^{-4}
Tap Water + 0.3% of $NaNO_3$	0.869×10^{-4}
Tap Water + 0.6% of $NaNO_3$	1.243×10^{-4}

Table 3 Coefficients k_{N1}, k_{N2} and k_{N3} (NAKASONE 1987)

ΔH [m]	q [m³/s]	k_{N1}	k_{N2}	k_{N3}
< 1.2	≤ 0.0653	0.0785	1.31	0.428
> 1.2	≤ 0.0653	0.0861	0.816	0.428
< 1.2	> 0.0653	5.39	1.31	-0.363
> 1.2	> 0.0653	5.92	0.816	-0.363

3.3 The Downstream Channel Aeration Weir

An aeration weir is planned for the Downstream Channel to safeguard the water quality of discharge into the Xe Bang Fai River. The weir is located approximately 8km downstream of the regulating dam.

The weir design has progressed through several iterations. The initial concept design nominated a labyrinth weir type. The main advantage of a labyrinth weir is that it provides a greater crest length (relative to the overall width of the weir) than a conventional weir. Aeration efficiency predictions using Equations (5), (6) and (7) put the efficiency of the weir between 55% and 65%. It should be noted that, due to the uncertainty surrounding aeration efficiency predictions and modelling, the aeration efficiency calculations were conducted not to guarantee aeration efficiency, but rather to provide a basis for comparison of different weir options.

Modifications to the vertical alignment of the Downstream Channel increased the height of the aeration weir above the tailwater level, providing a greater drop and consequently greater aeration efficiency. A revised weir geometry, adopting a conventional straight weir, was found to produce similar aeration efficiency estimates as the original concept design because of the greater drop height. The conventional weir geometry greatly reduced the cost of the weir construction.

Subsequent modifications to the channel geometry raised the water level downstream of the weir, once again modifying the aeration efficiency of the weir – this time for the worse. The third (and current) weir configuration, a U-shape weir with a total crest length of 340m but a width of only 20m, was adopted to increase the crest length and increase the aeration efficiency with the lower drop height. The aeration efficiency calculations indicate a similar efficiency to that obtained for the previous options.

Table 4 Theoretical Predictions of Aeration Efficiency (for Oxygen) of the Aeration Weir Options

Weir	Crest Length [m]	Drop Height [m]	Predicted Aeration Efficiency, E		
			Equation (5)	Equation (6)	Equation (7)
Labyrinth	360	2.1	55%	60%	64%
Conventional	140	2.5	61%	61%	64%
U-shape	340	1.5	49%	61%	59%

3.4 Other Factors Affecting Aeration of the Downstream Channel

The aeration efficiency estimates listed in Table 4 indicate that the proposed aeration weir should have an efficiency of approximately 60%. As illustrated in Equation (2), the rate of transfer of a volatile gas is proportional to the deficit. The efficiency of a structure can therefore only asymptote towards 100%, but never reach it.

The Downstream Channel is an artificial channel, and the ability to support aquatic life within the channel is not a major design consideration. Nevertheless, the discharge must not be detrimental to the water quality in the Xe Bang Fai River downstream. The aeration weir is not the only factor contributing to aeration of the discharge:

- The upper, riprap-lined reaches of the Downstream Channel will be relatively rough with a high flow velocity. Strong turbulent mixing should ensure that the fluid at the free surface (where gas transfer takes place) is constantly mixed, thereby increasing the rate of gas transfer compared to sluggish, smooth channels; and
- An additional drop structure is proposed downstream of the tunnel for energy dissipation purposes. This structure will also contribute to the aeration of the discharge waters. The efficiency of this structure has not been specifically investigated.

Although the contribution of these mechanisms are likely to not be as significant as the aeration weir, the overall effect, when combined with the aeration weir, should ensure that the water quality of the discharge into the Xe Bang Fai River is adequately maintained.

4. CONCLUSIONS

Connell Wagner has been responsible for the hydraulic design of the Downstream Channel, a 27km long diversion channel downstream of the Nam Thuen II Hydropower Station that conveys discharge from the power station to the Xe Bang Fai River. The design of this channel has posed a number of unique engineering challenges, imposed by constraints of geography, geology, operation and of course economics.

The first challenge encountered by the Downstream Channel is the desire to carry the design discharge in the smallest possible challenge across the most direct route. Channels with these characteristics are rare in nature, for the simple reason that a large discharge per unit width and a straight, regular channel generally results in high velocities. If the velocity is sufficient to cause erosion, the channel alignment will migrate and adopt a meandering alignment that both increases the channel length (decreases the average grade) and increases form resistance.

Such migration of the Downstream Channel was considered unacceptable, so ‘river training’ was required to maintain the integrity of the channel alignment. Two alternatives were examined:

- Riprap protection of the channel, which allows a higher velocity to be accommodated while also increasing the flow resistance; and
- Control weirs to regulate flow depths and velocities in the channel.

The current channel configuration proposed by Connell Wagner adopts both these techniques, in different areas, in order to provide the most economical and practical solution.

Care for the environment has become a significant influence on many projects. Reservoirs, particularly those with bottom outlets, can significantly change the levels of dissolved gas (oxygen, nitrogen, volatile organic compounds such as methane etc.) in the discharge waters from what would naturally occur in the river discharge. This can have a profound effect on aquatic life downstream of the dam. In order to help equilibrate the dissolved gas levels in the discharge, an aeration weir has been proposed for the Downstream Channel.

Aeration efficiency is a function of numerous variables, including the drop height (difference in elevation upstream and downstream of the weir) and discharge per unit width, and the weir configuration underwent several iterations in response to changes of the Downstream Channel alignment and geometry. The aeration efficiency of the weir has been estimated as approximately 60%, and in conjunction with free-surface aeration along the 27km channel and aeration at the tunnel outlet energy dissipator, should ensure the water quality of the discharge into the Xe Bang Fai River.

5. ACKNOWLEDGEMENTS

The author wishes to thank the Nam Theun Electricity Consortium (NTEC) and the Italian-Thai Development Public Company Ltd and Nishimatsu Construction Company Ltd (ITD-NCC Joint Venture) for their permission to publish the above information, and acknowledges Electricite de France (EDF) for their work on the design of the aeration weir.

6. REFERENCES

Avery, S.T. and Novak, CP. (1978). Oxygen Transfer at Hydraulic Structures, *Journal of Hydraulic Division*, ASCE, Vol 104, No HY11, pp. 1521-1540.
Chanson, H. (1996). *Air Bubble Entrainment in Free Surface Turbulent Shear Flows*, Academic Press, London, UK, 401p (ISBN 0-12-168110-6).
Chanson, H. (2001). *The Hydraulics of Stepped Chutes and Spillways*. 1st ed., Balkema, Lisse, The Netherlands, 384p (ISBN 90 5809 352 2).
Chow, V.T. (1973). *Open Channel Hydraulics*. International ed., McGraw-Hill Book Company, Singapore, 680p (ISBN 0-07-085906-X).
Nakasone, H. (1987). Study of Aeration at Weirs and Cascades, *Journal of Environmental Engineering*, ASCE, Vol 113, No. 1, pp. 64-81.
Toombes, L. (2002). *Experimental Study of Air-Water Flow Properties on Low-Gradient Stepped Cascades*, Ph.D Thesis, University of Queensland, 562p.
USACE (2003). *HEC-RAS River Analysis System v3.1.1* (hydraulic analysis software), US Army Corps of Engineers Hydraulic Engineering Centre, California.
Watson, C.C., Walters, R.W. and Hogan, S.A. (1998). Aeration Performance of Low Drop Weirs, *Journal of Hydraulic Engineering*, ASCE, Vol 124, No. 1, pp. 65-71.
Wood, I.R. (1991). *Air Entrainment in Free-Surface Flows* (IAHR Hydraulic Structures Design Manual No 4, Hydraulic Design Considerations), Balkema Publishers, Rotterdam, The Netherlands, 149p.

7. NOTATION

a	Specific interface area (air-water surface area per unit volume of air and water) [m²/m³]
C	Dissolved gas concentration
C_{DS}	Dissolved gas concentration downstream of a structure
C_{US}	Dissolved gas concentration upstream of a structure
C_{sat}	Concentration of dissolved gas in water at equilibrium
D_H	Hydraulic diameter [m]
d_t	Tailwater depth
E	Aeration Efficiency
Fr	Froude Number
K_L	Mass transfer coefficient or liquid film coefficient.
n	Coefficient representative of the channel resistance (Manning's number) [s/m$^{1/3}$]
Re	Reynolds Number
r	Deficit Ratio
S_f	Friction slope or energy grade
S_0	Bottom slope
V	Average cross-sectional velocity [m/s]
We	Weber number
ΔH	Difference in water elevation across a weir
μ_w	Dynamic Viscosity of water [Pa.s]
ρ_w	Density of water [kg/m³]

The Institution of Engineers, Australia
8th National Conference on Hydraulics in Water Engineering
ANA Hotel Gold Coast, Australia 13-16 July 2004

A New Generation, GIS Based, Open Flood Forecasting System

T. van Kalken
B.E., M.Sc. (Delft), MICE
Chief Engineer, DHI Water and Environment Pty Ltd
C. Skotner
M.Sc., Ph.D
Senior Engineer, DHI Water and Environment, Denmark
H. Madsen
M.Sc. Ph.D
Senior Engineer, DHI Water and Environment, Denmark

Abstract: This paper describes the development of a new generation flood forecast system based on an open interface approach. The system, "MIKE FLOODWATCH", is implemented in the ArcGIS environment utilising a variation of the ArcHydro geodatabase. The system can be linked directly to a range of telemetry and other hydrological databases which permits the seamless import and pre-processing of real time measurements, including rainfall radar and other grid-based data. The open interface allows the system to be coupled to virtually any hydrological or hydraulic model in order to obtain predictions of water levels and flows in the model domain. An advanced forecast dissemination module is capable of automatically posting forecasts via inter/intranets, SMS text, e-mail or fax. Complementing this system is the development of a new data assimilation module for the MIKE 11 hydrodynamic model. The module utilizes an efficient updating technique to improve the model state through a feedback process to match the available observations prior to the time of forecast and to automatically correct the model predictions into the forecast period. The system has recently been commissioned for the Flanders government in the Scheldt estuary in northern Belgium.

Keywords: Floods, real-time forecasting, GIS

1. INTRODUCTION

Accurate and reliable flow forecasting forms an important basis for efficient real-time river management, including flood control, flood warning, reservoir operation and river regulation. In order to achieve this objective, it has become a common practice to apply GIS based software that integrates data management and forecast modelling tools in a single environment known as a data management and forecast modelling shell. Such shells incorporate the ability to configure links to telemetry, manage and examine real-time data, register forecast modelling tools, carry out manual or scheduled forecast simulations, examine the results and publish selected data to a range of media; including web, fax, e-mail and SMS for mobile phones. Moreover, the systems can be used to carry out scenario analyses to provide early flood warnings, flood alleviation and other.

Complementing the forecast modelling shell are the forecast modelling tools used to compute e.g. a flood forecasts. The core of state-of-the-art operational flow forecasting systems is a hydrological/hydrodynamic simulation model that uses information of the current state of the river basin together with forecasts of the model forcing (precipitation, evapotranspiration and hydraulic model boundaries) to provide forecasts of the water levels and discharges in the river system. The forecast errors of such a system are related to errors in the current state of the river basin initialised by the simulation model, errors in the model forcing forecasts and errors related to the simulation model itself (such as model structural errors and use of non-optimal model parameters). In order to improve the estimate of the initial state of the system and to reduce the simulation errors in the forecast period a data assimilation procedure is often implemented in the forecast system. In general, data assimilation (often denoted model updating in hydrological applications) is a feedback process where the model prediction is conditioned to the observations of the river system (typically water levels and discharge measurements).

The combination of a resilient and robust forecast modelling shell and a forecast model tool that incorporates an accurate and fast updating technique constitutes a strong tool that can be used by flood managers to provide vital, sometimes life saving, information to local authorities and the vulnerable populace.
The paper is outlined as follows: In Section 2 a description is given of a new forecast modelling shell that integrates data management and forecast modelling methodologies in a GIS environment. The system is known as MIKE FLOODWATCH (DHI, 2000). In Section, 3 a new, fully adaptive error forecast technique is described, which has been incorporated into a data assimilation framework in MIKE 11 (Hartnack and Madsen, 2001; Madsen et al., 2003) and in Section 4 the forecast technique is applied in a real-time flood forecasting application in the Scheldt estuary in northern Belgium. Conclusions are given in Sections 5.

2. INTEGRATED DATA MANAGEMENT AND FORECAST MODELLING SHELL

Based on the concept for the existing MIKE FLOODWATCH, which has been applied in numerous projects world-wide, DHI Water & Environment has developed a new, modern and extremely robust forecast modelling shell with the objective to integrate data management, forecast models and dissemination methodologies in a single system.

The system, which is based on the common water resources relational database for management and storage of data, is fully integrated into ArcMap GIS 8.3 from ESRI, hence taking advantage of the newest GIS technology available on the market including modern scripting facilities and fast and robust methods for visualisation and processing of geographical data.

Real-time data including meteorological forecasts, radar imagery and telemetry data can be imported into the database and used e.g. as input to hydrologic and hydraulic forecasting models. Real-time data imported from external sources is quality assured according to user-defined quality criteria and stored in the system database.

In order to ensure a high level of openness and flexibility, the forecasting shell system makes consistent use of the EUROTAS industry file format for model interfacing. The systems may be used to execute any model type including meteorological weather models, hydrologic models, hydraulic and hydrodynamic models, advection-dispersion models, water quality models, forecasting models, error forecast models and others. Alternatively, models from other suppliers may be registered with MIKE FLOODWATCH and run within this environment.

System tasks such as import of real-time data from remote data acquisition stations, execution of forecast modelling tasks or dissemination of selected results to relevant parties (Figure 1) are handled consistently using a task scheduler that facilitates definition of the above tasks as well as common system tasks such as database maintenance and deletion of old instances of forecast modelling tasks, log messages etc.

Access restrictions can be defined for each user or group of users, hence making it possible to ensure that only suitably qualified and experienced staff can gain access to the parts of the system that require particular know-how. In turn, this adds to the philosophy of offering an extremely robust system that can operate in a range of user environments.

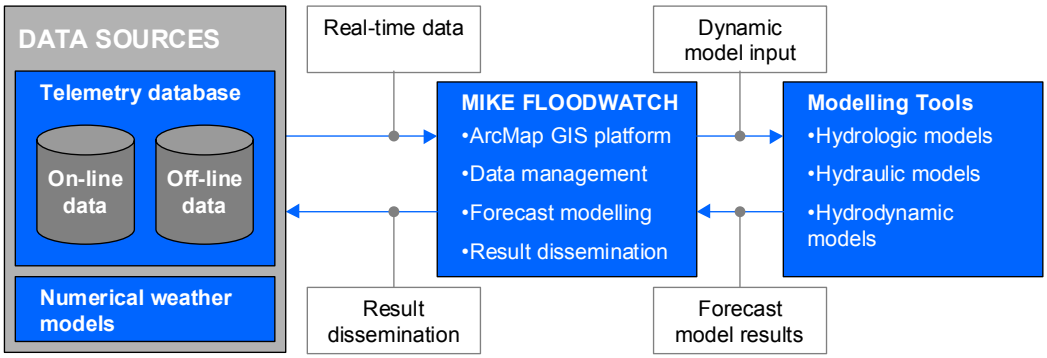

Figure 1 – MIKE FloodWatch links telemetry to models and automatically runs forecast operations

3. ADAPTIVE ERROR FORECAST METHOD

In this section a new, hybrid data assimilation procedure is presented that has been implemented in the MIKE 11 flood forecasting system developed at DHI Water and Environment (DHI, 2003). MIKE 11 is a comprehensive, one-dimensional modelling system for the simulation of flows, water quality and sediment transport in rivers and other water bodies (Havnø et al., 1995; DHI, 2003). The MIKE 11 system integrates different computational modules for the basic process descriptions such as hydrology, hydrodynamics, advection-dispersion etc. For flood forecasting applications the MIKE 11 hydrodynamic and rainfall-runoff modules are adopted.

Previous real time updating routines in MIKE 11 have relied upon a unique relation existing between water level and discharge at the updating point. The system analysed the deficit or excess of discharge compared to observations and applied corrective lateral inflows at the update points. The system has proved reliable in the past but suffered from two main drawbacks. Firstly, it could not be applied in areas affected by tides or backwater. Secondly, the process was iterative, requiring complete model simulation iterations in situations where two or more updating points were located along a single river reach.

To circumvent these inadequacies, a new general filtering framework has been developed for data assimilation. The new updating procedure in the filter is a succession of two steps. First, the model is employed to issue a one-time-step ahead forecast, following which the observed data are assimilated with the forecast to provide an updated state. The assimilation step is a linear combination of the data and the model in which the forecast error at the measurement point (denoted the innovation) is distributed to the entire model state using specified weighting functions. The formulation of the weighting functions is the most critical part of the filtering scheme, and different schemes mainly differ from each other in the way the gains are calculated. The most comprehensive linear assimilation scheme is the Kalman filter whereby the gains are determined based on a minimisation of the expected error of the updated state vector in terms of the errors of both model dynamics and data. In this case the weighting functions or Kalman gains are determined sequentially based on the dynamical evolution of the forecast covariance matrix of the state vector

In MIKE 11 the ensemble Kalman filter has been implemented (Hartnack and Madsen, 2001; Madsen et al., 2003). Experiences with the filter shows that the computational requirements for obtaining a proper representation of the covariance matrix are of the order of 100 model runs, which is often too computationally expensive in real-time applications. In this work, a very cost-effective filtering procedure has been developed based on predefined gain vectors that are assumed constant in time. In this case the filtering update is only slightly more expensive than a normal model run. Three different gain functions are assumed; a constant, a triangular, and a mixed exponential distribution as shown in Figure 2.

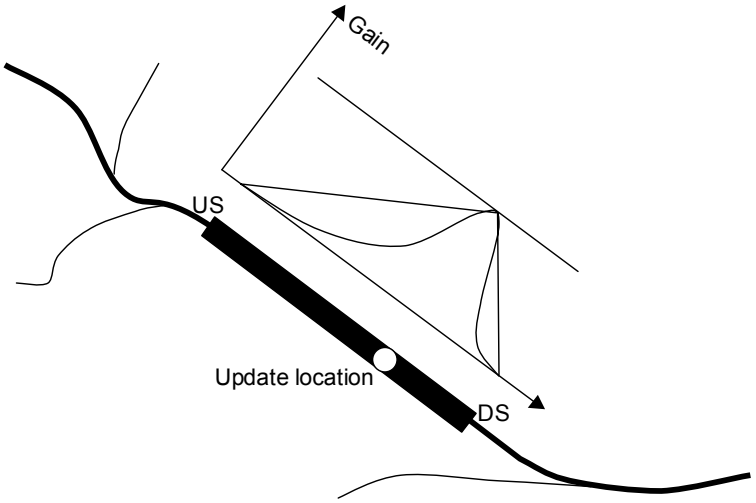

Figure 2 - Definition of Gain Function for a Measurement (Update) Location

The amplitude of the gain function at the measurement location should reflect the confidence of the observation as compared to the model forecast; that is, if the amplitude is equal to unity the measurement is assumed to be perfect, whereas for smaller amplitudes less emphasis is put on the measurement as compared to the model forecast. The distribution and the bounds of the gain function should reflect the correlation between the model forecast error at the measurement location and the errors at nearby grid points. In this work an amplitude of one is used.

The filtering procedure described above can be applied to update the state of the river system up to the time of forecast. Within MIKE 11, the filter can be applied at both discharge and water level points.This updated state can then be used as initial conditions for a model forecast. In this case, however, the forecast skills of the model will be limited to a time horizon where the initial conditions are washed out. To keep the model on the "right track" for a longer period the filtering procedure is combined with error forecasts at the measurement points. The principle of this combined approach is illustrated in Figure 3. At each update time step in the filtering period (prior to the time of forecast), the model innovation is acquired at all update locations. For each update location this gives rise to a time series of innovations that covers the filtering period up to the time of forecast (or the time of the last measurement). At the end of the filtering period, an error forecast model defined at each update location is then used to propagate the innovation in the forecasting period and update the affected state variables accordingly using the filtering algorithm. In real-time the error forecast models are applied at each measurement location from the time of the last observation to the end of the forecast period. Thus, the forecast methodology is insensitive to missing data; a situation which is commonly encountered in operational forecasting. In addition, the new module does not require additional model iterations, thereby reducing the time required to generate a forecast.

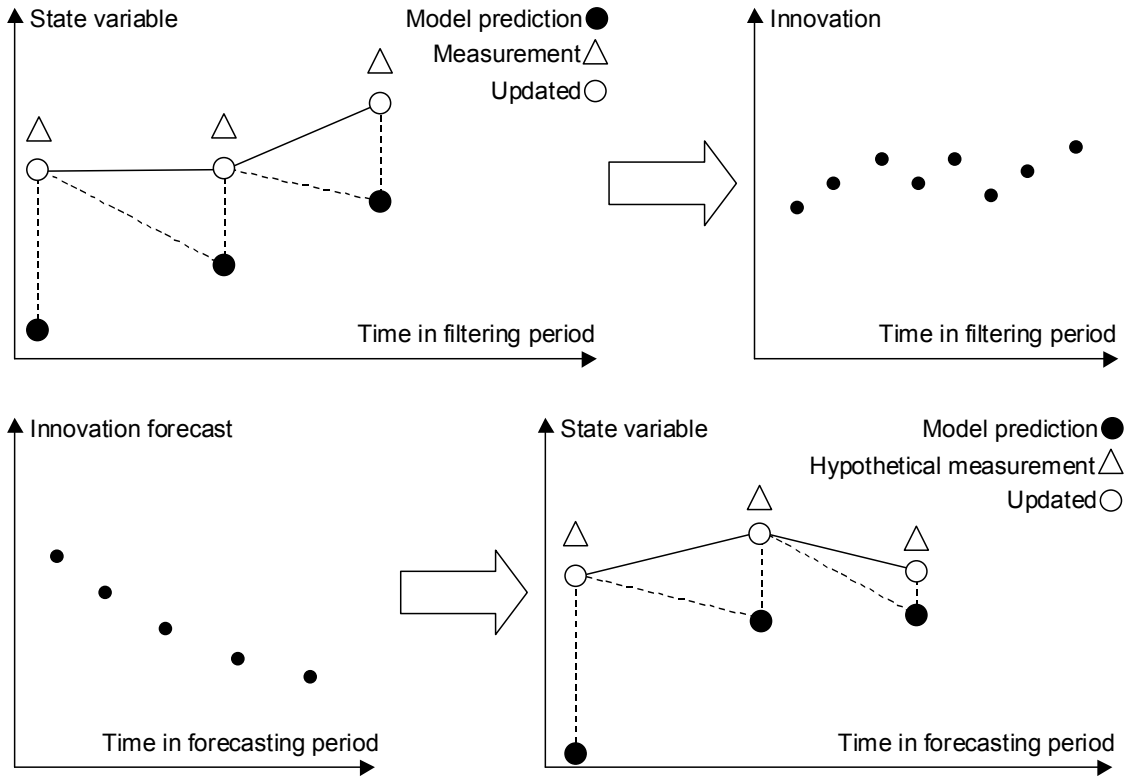

Figure 3 - Illustration of the Combined Filtering and Error Forecast Procedure

The error forecast model can be defined as a general linear or non-linear model with a one-step ahead prediction that depends on the previous errors or innovations, model states and model forcings. In order to ensure a fast, accurate and objective derivation of the error forecast models, fully automatic parameter estimation techniques have been incorporated. On the basis of a user-defined time window in the filtering period prior to the time of forecast, the parameters of the error forecast model are estimated. The error forecast models are updated when a new forecast is to be issued using time series of the most recent data. This allows the error forecast models to adapt from one forecast to the next based on the physical conditions prevailing at the time of forecast without any need for calibration or user

intervention in general. In the case of a linear error forecast model, the model parameters are estimated using least squares regression techniques. In the case of a non-linear model, the shuffled complex evolution (SCE) algorithm (Duan et al., 1992) is applied for the parameter optimisation.

4. FORECAST APPLICATION IN NORTHERN BELGIUM

The new updating technique as incorporated into MIKE 11 was used jointly with the forecast modelling shell, MIKE FLOODWATCH, to provide real-time forecasts of river stage and discharge at selected locations throughout the Scheldt estuary in Northern Belgium. The study area covers an area of more than 6500 km^2; including the major cities Brussels and Antwerp, ref. Figures 4 and 5. More than 40 catchments were identified in the study area, each of which was modelled using the NAM rainfall-runoff model to produce lateral inflows (both surface and subsurface flow) to the major rivers traversing the catchments.

The hydraulic model includes more than 500 km of rivers that meet with the Scheldt River, the mouth of which is located in the tidally affected estuary that adjoins the North Sea. More than 140 weirs and culverts have been included in the model to describe accurately the energy loss across structures and associated backwater effects. The model is resolved using approximately 8000 grid points (water level and discharge) and runs at a constant time step of 2 minutes. In the upstream part of the hydraulic model, which is not affected by the tide, updating is accomplished using a first order auto-regressive model, whereas in the downstream tidal area, the model innovations are known to exhibit a structured, harmonic behaviour, which justifies the use of the following biharmonic error forecast equation:

$$E_i = a+b*\cos(2*pi/(12.4/24)*t)+c*\sin(2*pi/(12.4/24)*t)+d*\cos(2*pi/(25.8/24)*t)+e*\sin(2*pi/(25.8/24)*t) \quad (1)$$

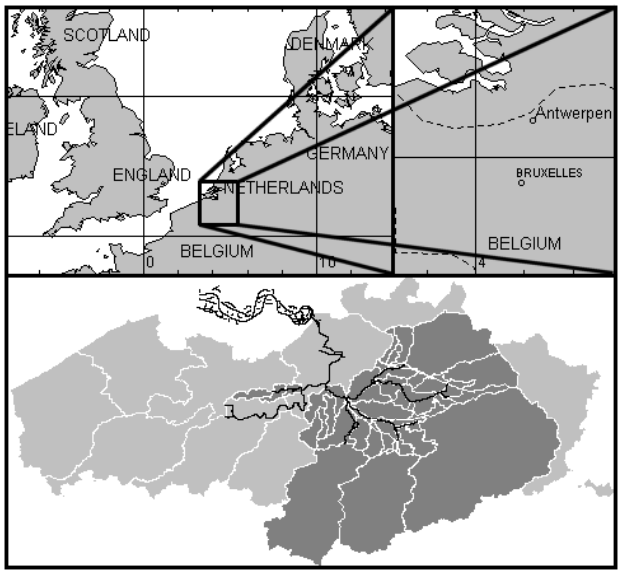

Figure 4 – Location of the Scheldt Esturary in Belgium showing model extent

in which E_i is the forecasted model error at the ith time level, a, b, c, d and e are coefficients to be estimated and t denotes time. For both measurement locations updating is accomplished using a triangular gain distribution with amplitude of one. Consequently, model updates will match the observations at the update locations in the filtering period prior to the time of forecast (or to the time of the last measurement).

The feasible parameter space of the estimated parameters is shown in Table 1. Moreover, the table shows a single instance of the estimated parameter set at Schelle-409 – a highly tidal update point located south of the city of Antwerp, just downstream of the confluence of the Scheldt and Rupel rivers. For the case shown in the table, the forecasting model was run using a simulation period of 14-01-2004 12:00:00 to 18-01-2004 12:00:00 with the time of the forecast set to 16-01-2004 12:00:00. Consequently, the model was used to provide a 48 hour forecast. For the purpose of testing the ability of the updating method to recover from erroneous model forcings or measurement

errors in general, a shift was introduced at the downstream model boundary to reflect the effect of a storm surge in the Scheldt estuary.

Parameter	Lower limit	Upper limit	Estimated
a [m]	-10	10	0.48378
b [m]	-5	5	0.25484
c [m]	-5	5	-0.16949
d [m]	-5	5	0.01513
e [m]	-5	5	-0.00005

Table 1 Feasible parameter space for the biharmonic error forecast model.

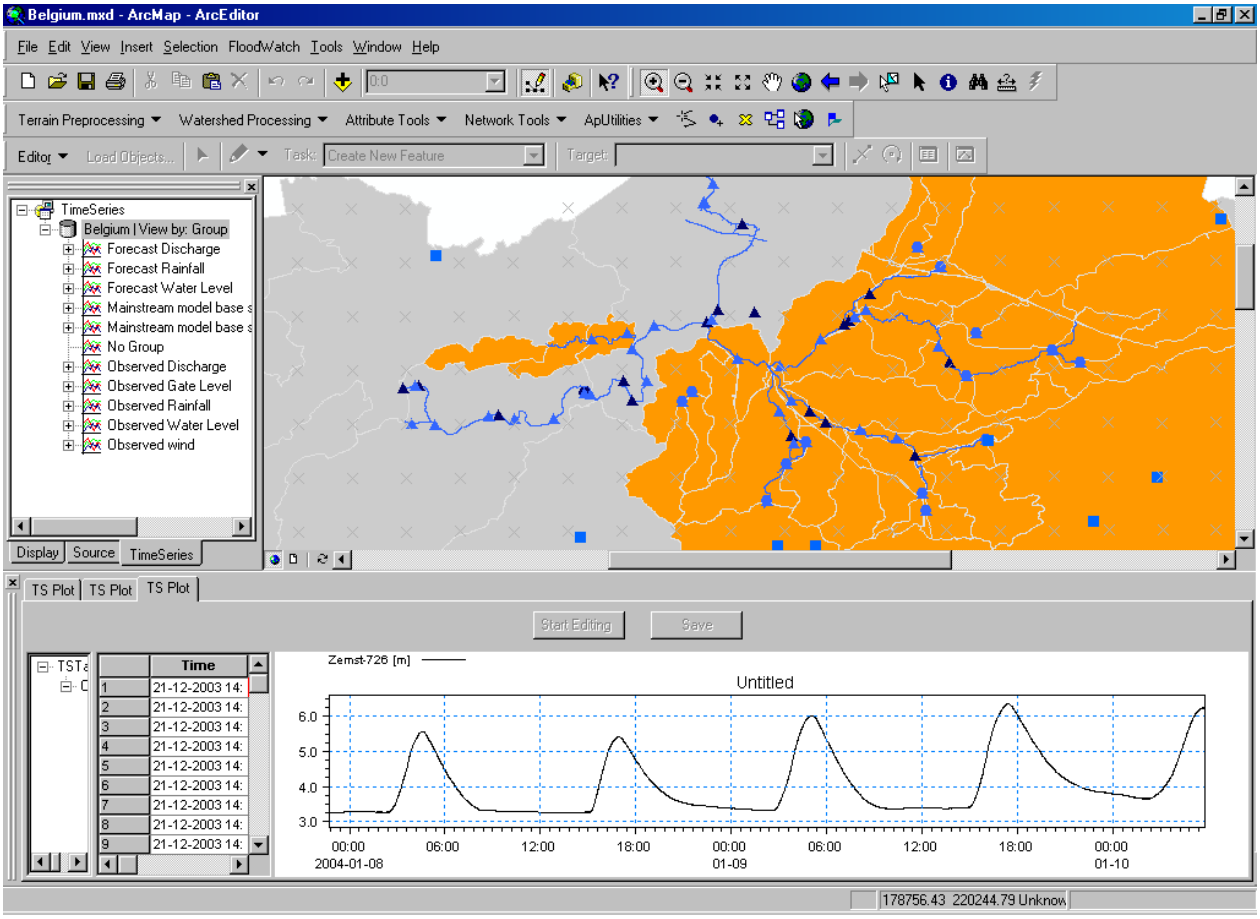

Figure 5 – Layout of the On-Line Data Management and Modelling System in the ArcMap GIS Environment

Figure 6 shows the measured and forecasted water levels at Schelle-409 with and without state updating. It is noted that the measurements consist of both valid data and missing data. Consequently, the example demonstrates that the updating method handles missing data - a feature that is useful in a real-time environment. In the case where updating is applied, the simulated water level is identical to the measured water level up to the time of the forecast. At the time of the forecast, or more generally, at the time of the last measurement, the parameters of the error forecast model are estimated automatically, (Table 1), using the optimisation algorithm described in Section 3. In the forecasting period, i.e. after 16-01-2004 12:00:00, the forecasted model innovation is applied in the filtering scheme

to produce a water level forecast that is significantly improved as compared with the situation where state updating is excluded.

In order to illustrate the concept of error forecasting, the observed and estimated model innovations at Schelle-409 are shown in Figure 7. Approximately 24 hours of acquired model innovations were used to optimise the parameters of the biharmonic error forecast equation (1), hence making it possible to estimate the model error in the forecasting period.

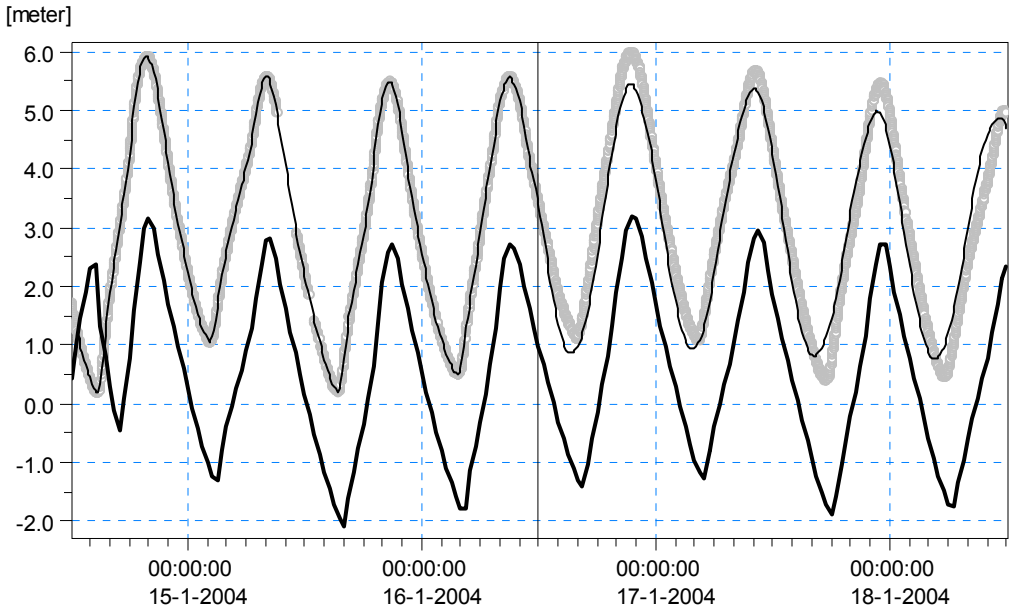

Figure 6 – Measured (○) and Forecasted (-) water level at Schelle-409 both with updating (thin line) and without updating (thick line). The time of forecast is at 16-01-2004 12:00:00

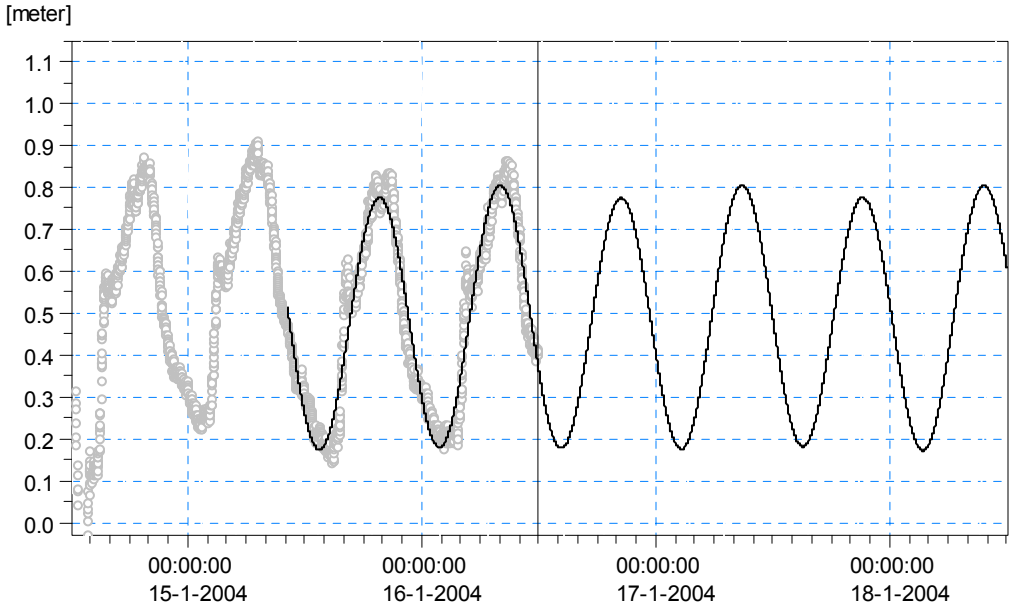

Figure 7 – Observed (○) and Estimated (-) Water Level Innovation at Schelle-409. The time of forecast is at 16-01-2004 12:00:00

5. CONCLUSIONS

A generic forecast modelling shell has been developed, which integrates robust data management facilities and forecast modelling technologies in a GIS based environment. The system facilitates easy access to a range of real-time data sources as well as the execution of modelling tools from different model suppliers. Complementing the forecast modelling shell, a new flood forecasting tool has been developed with the objective to provide fast, accurate and robust river forecasts in real-time. The forecasting technology, which has been integrated into a general data assimilation framework in the hydraulic model, applies an error forecasting technique to update the model state from one time step to the next. The new tool can be applied without restriction in tidal and backwater affected areas and does not require additional model iterations The system has been installed in a real-time data environment in northern Belgium.

6. REFERENCES

DHI, 2000, MIKE 11. Short description of MIKE FLOOD WATCH, DHI Software 2000, DHI Water & Environment.

DHI, 2003, MIKE 11. A modelling system for rivers and channels. Reference Manual, DHI Software 2003, DHI Water & Environment.

Duan, Q., Sorooshian, S., Gupta, V., 1992, Effective and efficient global optimization for conceptual rainfall-runoff models, Water Resour. Res., 28(4), 1015-1031.

Hartnack, J. and Madsen, H., 2001, Data assimilation in river flow modelling, 4th DHI Software Conference, 6-8 June, 2001, Scanticon Conference Centre, Helsingør, Denmark

Havnø, K., Madsen, M.N. and Dørge, J., 1995, MIKE 11 – a generalized river modelling package, Computer Models of Watershed Hydrology (ed. Singh, V.P.), Water Resources Publications, Colorado, 733-782.

Madsen, H., Rosbjerg, D., Damgård, J. and Hansen, F.S., 2003, Data assimilation in the MIKE 11 Flood Forecasting system using Kalman filtering, IAHS General Assembly, Sapporo, Japan, 3-11 July 2003.

The Institution of Engineers, Australia
8th National Conference on Hydraulics in Water Engineering
ANA Hotel Gold Coast, Australia 13-16 July 2004

Physical Modelling & Hydraulic Modifications to a Power Station Weed Settling Pond

J. W. Walker
B.E., MEngSci.
Senior Project Engineer, Water Research Laboratory, Civil and Environmental Engineering, University of NSW, Australia

Abstract: Cooling Water for Eraring Power Station (NSW) is sourced from Lake Macquarie, a nearby coastal saline lake. Prior to the water entering the power station it passes through a series of drum screens to remove weed, fish, sand and shell material. As part of the Power Stations environmental operating license, the fish must be returned to the lake and the weed removed for disposal. The Power Station constructed a small weed-settling pond into which the weed, fish, sand and shell material flowed. The weed-settling pond was linked to the lake by a 2km culvert. The envisaged concept was that the weed would settle in the pond and the fish would swim along the culvert back to the lake. However, much of the weed either floated or was neutrally buoyant, resulting in a large proportion of the weed being returned to the lake via the culvert. This paper discusses the recent successful modifications to the weed-settling pond.

Keywords: weed settling pond, fish, physical modelling.

1. INTRODUCTION

Eraring Power Station is located on the shores of Lake Macquarie in New South Wales, Australia. Water from the coastal lake is used as cooling water for the power station condensers. The cooling water system has the capacity to deliver up to 120kL/s. Prior to the cooling water being delivered to the condensers it passes through drum screens to remove weed, fish sand and shell material. The drum screens are cleaned using high-pressure water jets with a combined flow of 300L/s. The cleaning water and screened materials (i.e. weed, fish and sand) flow via a small culvert into a weed-settling pond measuring 10m long x 5m wide x 2m deep (Figure 1).

Figure 1 – Weed-Settling Pond (Pre-modification)

The weed-settling pond is linked to the lake by a 2km long trapezoidal channel (Figure 2). The operational concept is that the weed settles in the pond and the fish migrate along the channel and return to the lake. However, much of the weed either floats or is neutrally buoyant, resulting in a large proportion of the weed returning to the lake via the channel. In addition, the relative shallowness of the trapezoidal channel appears to act as a deterrent to the migration of the fish, with most species showing preference to the deeper water of the weed-settling pond.

Quantities and species of fish entering the pond vary significantly throughout the year. Similarly, weed inflow rates vary significantly during the year and are dependent on influences such as seasonal climatic changes and wind strength and direction. Maximum weed loads measured during the course of this study were in the order of $5m^3$/day.

The existing weed-settling pond has been in operation for some 20 years. The inefficiency of the settling pond in removing weed has resulted in odour and sedimentation problems associated with the accumulation of rotting weed at the channel outlet.

Modifications to the weed-settling pond were proposed to achieve two major objectives:

- Firstly, to minimise the transport of weed and sediments to the trapezoidal outlet channel, and;
- Secondly, to promote the passage of fish from the weed-settling pond to the trapezoidal outlet channel and continue downstream to Lake Macquarie.

Figure 2 - Section of Trapezoidal Channel

Eraring Power sought a solution that was non-mechanical and utilised the existing weed-settling pond. A concept to achieve the requirements of Eraring Power was developed and then tested using physical modelling tools. The final design has now been in successful operation for some 18 months.

2. CONCEPTUAL DESIGN

A simple schematic of the non-mechanical modifications to the existing pond for the purpose of removing the weed and allowing the fish to migrate downstream is shown in Figures 3 and 4. The proposed concept included two inlet sources of water. Water containing the weed and fish would enter at the upstream end of the pond via the existing inlet (Inlet A) and clean water (free of weed) would enter the pond downstream of the baffle plate (Inlet B).

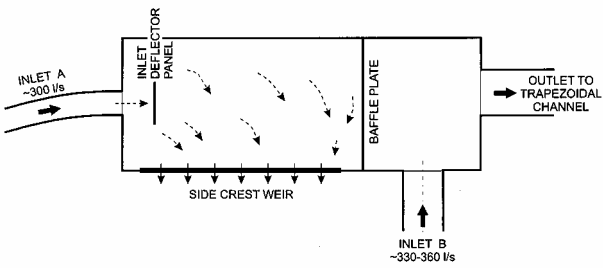

Figure 3 – Plan View of Conceptual Design

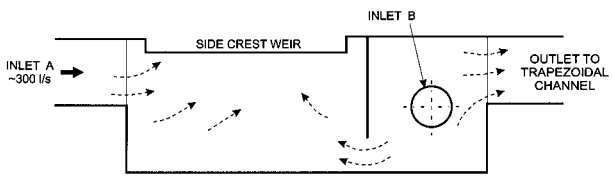

Figure 4 – Side Elevation of Conceptual Design

The flow rate at Inlet B would be sufficient to create a low flow in the upstream direction under the baffle plate as shown in Figure 4. As a result, weed entering the pond through Inlet A cannot pass beneath the baffle plate and then enter the downstream trapezoidal channel to Lake Macquarie. The fish, however, are capable of swimming against the low current beneath the baffle plate and thus return to Lake Macquarie.

Upstream of the baffle plate it was proposed to construct a broad side-crest weir. All water entering the pond through Inlet A would flow over the side-crest weir with the weed. The depth of flow over the side-crest weir would be minimised to ensure that the majority of the fish avoid this flow path, but deep enough to ensure that weed can pass over freely. The weed flowing over the weir could then be relatively easily captured for future disposal.

3. DESIGN REFINEMENT & PHYSICAL MODELLING

Advice was obtained from a fish biologist (Mallen-Cooper, 2000) on likely fish behaviour in the pond. It was recommended that to discourage fish from passing over the side-crest weir the depth of water over the weir should not exceed approximately 50mm. Also to promote the migration of all fish species (i.e. both bottom and near surface dwelling) a vertical 300mm slot was incorporated into the baffle plate shown in Figures 3 and 4.

3.1 Side Crest Weir Physical Model

A short section of the proposed side-crest weir was constructed at full prototype scale. To reduce the possibility of weed entanglement over the weir the crest was semi-circular in form with a diameter of 350mm.

Weed samples were collected from the weed-settling pond and a series of experiments conducted to assess the behaviour of weed flow over the weir for various crest water depths (Figure 5). Loosely placed weed flowed freely over the weir crest at water depths greater than 25mm. Small weed clumps required a water depth of 40mm to 50mm to flow relatively freely over the weir. To curtail weed blockage of the side-crest weir the minimum design water depth was set at 45mm. Thus, based on an inlet flow rate of 300L/s and a weir water depth of 45mm a weir length of 18m was determined (Walker, 2001). No testing was undertaken on fish behaviour over the weir.

Figure 5 – Weed Flow over Weir Crest

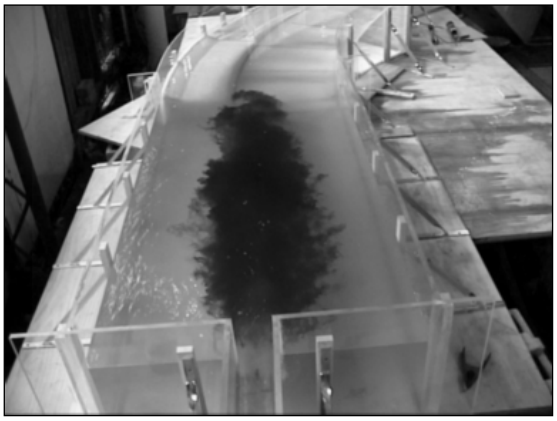

Figure 6 – Existing Weed-Settling Pond, Dye Test

3.2 Weed-Settling Pond Physical Model

As determined by Froudian similitude the existing weed-settling pond was constructed at an undistorted linear scale of 6. The model was constructed from clear acrylic sheeting and calibrated to replicate existing hydraulic performance. Dye tests and velocity measurements indicated a fast flowing near surface jet traversing down the centreline of the pond towards the exit channel (Figure 6). Measured mid-pond near surface velocities were typically in the order of 0.6m/s.

Modifications, optimisation and testing of the weed settling pond was undertaken over a period of time. The final design modifications to the weed settling pond are shown in Figure 7.

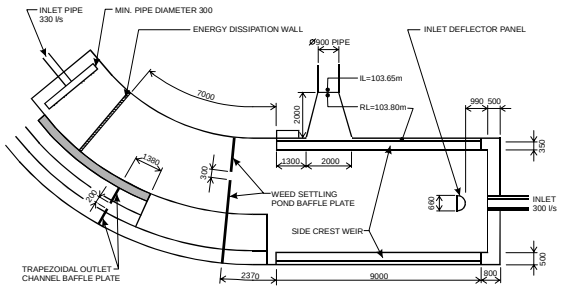

Figure 7 – Plan View of Final Design Modifications

The modifications are:

- 18m long side crest weir;
- side-crest weir channel and channel outlet;
- inlet deflector panel;
- weed-settling pond baffle plate;
- trapezoidal outlet channel baffle plates; and
- additional inflow of 330L/s.

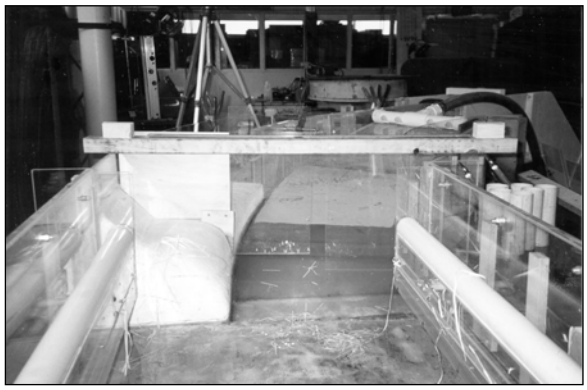

Figure 8 – Side-Crest Weir and Pond Baffle Plate

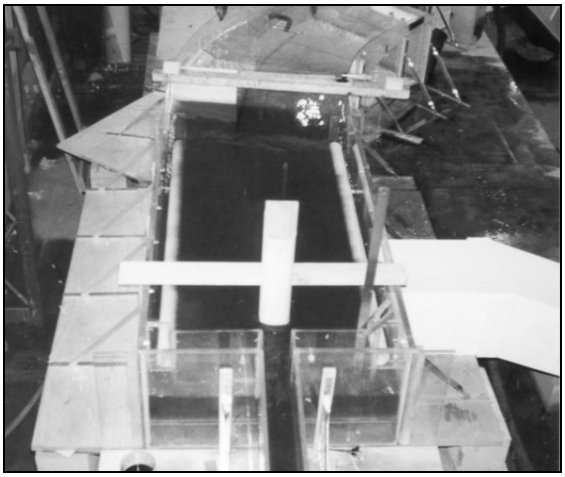

Figure 9 – Modified Weed Settling Pond, Dye Test

The modelled side-crest weir, side-crest weir channel and weed-settling pond baffle plate are shown in Figure 8. Note the slots in the baffle plate for fish passage.

Dye tests for the modified weed-settling pond indicate that water that enters via the inlet channel flows over the side crest weir. Almost no dye was observed to exit via the trapezoidal outlet channel as demonstrated in Figure 9. Shredded paper soaked in water was used successfully to simulate weed behaviour in the pond. Tests showed that the majority of the shredded paper flowed over the side-crest weir. The remainder of the shredded paper settled to the bed of the pond in small eddy zones located near the entrance to the pond. No shredded paper flowed into the trapezoidal outlet channel.

3.3 Maintenance Considerations

The operational water depth in both the existing and modified weed-settling pond is approximately 2m and the water depth at the entrance to the trapezoidal outlet channel is approximately 600mm. Fish in the existing weed settling pond generally demonstrate a reluctance to move from the deep pond to the shallow outlet channel. One possible way to encourage fish to move into the trapezoidal outlet channel is to decrease the water depth in the pond to the same depth as the outlet channel.

Physical modelling of the modified weed-settling pond was undertaken with the floor level of the pond raised to the same height as the invert level of the outlet channel. The hydraulic behaviour in the pond was similar to that without the raised floor level. However, from observations it was clear that weed deposition in the pond combined with the reduced storage volume of the pond would result in an increase in the frequency of maintenance. This outcome was not desirable and the concept of a raised floor level was not pursued further.

4. PROTOTYPE OPERATION

The modifications to the prototype weed-settling pond have been in operation for some 18 months. Weed passage down the trapezoidal channel has been eliminated. Whilst no surveys have been conducted on the fish, regular observations suggest that most fish are travelling down the trapezoidal channel and returning to the lake.

5. CONCLUSIONS

Model testing of the existing weed-settling pond located at Eraring Power Station demonstrated that with some modifications to the pond's design, weed can be prevented from entering the trapezoidal outlet channel and returning to Lake Macquarie. The concept of the modifications is based on the formation of a hydraulic barrier in the weed-settling pond. This hydraulic barrier prevents the passage of weed into the trapezoidal outlet channel, but allows fish to pass through the barrier with minimal hindrance.

Operation of the modified weed pond during the past 18 months has shown that the pond is now operating as initially intended.

6. ACKNOWLEDGEMENTS

WRL would like to thank Eraring Energy for their enthusiastic interest in this project and their permission to write and publish this paper.

7. REFERENCES

Mallen-Cooper, M. (2001), Optimising Passage of Fish and other Fauna in the Settling Pond of Eraring Power Station, June 2001, Fishway Consulting Services.

Mallen-Cooper, M. (2001), Notes on the Inspection of the Model of the Eraring Power Station Settling Pond at the Water Research Laboratory, Manly Vale, August 2001, Fishway Consulting Services.

Walker, J. W. (2001), Eraring Power Station Cooling Water Weed Settling Pond, Technical Report No 01/28, Water Research Laboratory, University of New South Wales.

The Institution of Engineers, Australia
8th National Conference on Hydraulics in Water Engineering
ANA Hotel Gold Coast, Australia 13-16 July 2004

Modelling Saturation Excess Runoff with SWAT

B.M. Watson
B.E., B.Sc., Grad.I.E.Aust.
Postgraduate Student, Deakin University, Australia
S. Selvalingam
B.Sc.(Eng), Ph.D., M.I.E.Aust.
Senior Lecturer, Deakin University, Australia
M. Ghafouri
B.Sc., M.Sc., Ph.D.
Lecturer, Deakin University, Australia

Abstract: The variable source area (VSA) concept of surface runoff generation is applicable in many catchments across southwest Victoria, Australia, where ephemeral, perched water tables develop due to the presence of duplex soils. SWAT, which is a catchment scale model that is widely used for predicting the response in stream yield to land use and climate changes, employs the curve number method to compute surface runoff. However the curve number method does not account for runoff generated from VSAs. This paper describes the implementation of a simple saturation excess runoff mechanism in SWAT that is consistent with the VSA concept. The modified model (SWAT-VSA) is applied to a semi-arid catchment in southwest Victoria dominated by duplex soils along with a version in which the curve number method is retained (SWAT-CN). SWAT-VSA and SWAT-CN predicted annual and monthly runoff volumes extremely well, while average results were achieved for the simulation of daily runoff. Overall it was concluded that both models performed equally well. However the advantage of SWAT-VSA is that it is based on the observed runoff generation mechanism of catchments in southwest Victoria unlike SWAT-CN.

Keywords: SWAT; saturation excess runoff; variable source areas; water balance model.

1. INTRODUCTION

Infiltration excess runoff is not a suitable mechanism to explain surface runoff generation in many catchments across southwest Victoria, Australia, because the infiltration capacity of the topsoil is usually much greater than the average rainfall intensity. Persistent failure to observe the occurrence of infiltration excess runoff in many catchments worldwide has prompted hydrologists to develop alternative models to account for runoff generation. Research has shown that the variable source area (VSA) concept is a more suitable mechanism to explain the generation of surface runoff for a variety of conditions (Dunne, 1983). VSAs are saturated portions of a catchment that give rise to the generation of saturation excess runoff. Rainfall that falls directly onto the saturated areas is readily transformed to surface runoff (Ormsbee and Khan, 1989). The temporal and spatial extent of VSAs is dynamic because they expand and contract in response to seasonal changes and even to rainfall events.

The VSA concept of surface runoff generation is particularly relevant to a significant proportion of temperate and semi-arid Australian catchments where the presence of duplex soils leads to the development of an ephemeral, perched water table at shallow depth (Raper and Kuczera, 1991). Duplex soils consist of a thin layer of permeable soil overlying a relatively impermeable layer of soil at a shallow depth. A lack of vertical flow capacity in the B horizon causes water to pond above the boundary between the A and B horizons, resulting in waterlogging and the development of an ephemeral, perched water table (Cox and McFarlane, 1995). The intersection of the perched water table with the ground surface gives rise to the formation of VSAs, from which saturation excess runoff is produced. Perched water tables have been widely observed in the field (Cox and McFarlane, 1995) and are considered to play a key role in the generation of surface runoff in catchments throughout southwest Victoria due to the prevalence of duplex soils across much of the region.

The results obtained from the application of hydrologic models, which are not capable of simulating saturation excess runoff, to catchments located in southwest Victoria would need to be reviewed with extreme caution, particularly when used for predictive purposes, because the physical assumptions pertaining to the model are largely incorrect in relation to the nature of these catchments (Stagnitti et al., 1992). It is essential that models account for the observed runoff generation mechanism of the catchment they are applied to, especially if the

principle motivation of the model application is to test alternative strategies to manage land use and climate change. Otherwise fundamentally erroneous conclusions may be reached and as a consequence the management strategies to be implemented could be seriously flawed and prevention of further environmental degradation may not be achieved.

The Soil and Water Assessment Tool (SWAT) is a catchment scale model that was developed to predict land use and climate change impacts on the water balance and water quality of large agricultural catchments (Neitsch et al., 2001). SWAT is a very powerful tool that is extensively used by government agencies worldwide to manage land and water resources at a regional scale. In Australia SWAT is becoming increasingly popular and has been identified as a promising model to predict land use and climate change impacts for catchments across southwest Victoria (Watson et al., 2003). SWAT uses the Soil Conservation Service (SCS) curve number method (USDA SCS, 1972) to compute surface runoff volume. The curve number method is an empirical formulation that is unable to distinguish between infiltration excess and saturation excess runoff (Endrey and Wood, 1999). Boughton (1989) reported an inherent limitation of the curve number method is the lack of any physical reality in its formulation and recommended that more physically based methods should be adopted instead to estimate surface runoff. Given the limitations associated with the curve number method and the need to account for the development of perched water tables and VSAs in models applied to catchments in southwest Victoria, it is imperative that SWAT is modified.

This paper describes the implementation of a simple saturation excess runoff mechanism into SWAT that is consistent with the VSA concept. The principle objective is to revise SWAT so that it is capable of reproducing the observed dynamics of surface runoff generation in catchments across southwest Victoria more closely. This study compares the performances of a version of SWAT that simulates saturation excess runoff (SWAT-VSA) and a version in which the curve number method is retained (SWAT-CN) when applied to a large-scale, semi-arid catchment in southwest Victoria. SWAT-VSA has only been applied to the one catchment so far, but it is intended for the model to be applied to more catchments across southwest Victoria in the future for further validation.

2. STUDY AREA

This pilot study was conducted in the Woady Yaloak River catchment in southwest Victoria, Australia (Figure 1). The source of the Woady Yaloak River is in the Central Victorian Highlands, where it proceeds to flow south over the basalt plains before eventually draining into Lake Corangamite, the largest permanent natural lake in Australia. Streamflow gauging stations are located at Pitfield (307 km^2) and Cressy (1157 km^2). The majority of land is used for agricultural purposes with grazing livestock (beef cattle, sheep and prime lambs) being the main commodity. There are large expanses of native eucalyptus forests also found across the north of the catchment. Soils throughout the catchment are predominantly duplex. The depth of most soil profiles (A and B horizons) across the catchment generally range between 1 m and 2 m. However isolated deeper pockets are found in some areas. The region has a Mediterranean climate with cold, wet winters and hot, dry summers. Average annual rainfall varies from 550 mm at Cressy to 700 mm at Ballarat. Average annual potential evaporation, measured by a Class A Pan situated 35 km south of Ballarat, is 1380 mm.

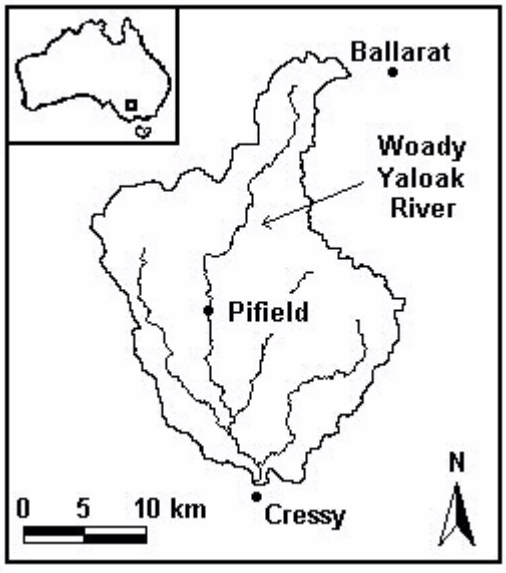

Figure 1 – Location Map of the Study Area.

3. MODIFICATION OF SWAT

SWAT is a distributed, long-term yield model that operates continuously on a daily time step. SWAT simulates the following hydrologic processes: climate, hydrology (evapotranspiration, surface runoff, percolation, lateral flow, and groundwater flow), routing, plant growth, and management practices. In SWAT a catchment is firstly divided into subbasins which are further divided into hydrologic response units (HRUs). HRUs are lumped land areas that have the same combination of land use and soil. Details of the VSA concept implemented in SWAT-VSA are presented in this section along with details of several additional modifications incorporated into both models.

3.1 Saturation Excess Runoff Mechanism

SWAT utilises the kinematic storage model of Sloan and Moore (1984) to simulate lateral flow. Sloan and Moore (1984) showed that the kinematic storage model can also be used to simulate saturation excess runoff. Ormsbee and Khan (1989) embedded the kinematic storage model into HEC-1 (U.S. Army Corps of Engineers, 1985) to simulate both saturation excess runoff and lateral flow. The hillslope conceptualisation used in CATPRO to simulate perched water tables is a generalization of the kinematic storage model (Mroczkowski et al., 1996). Extending the kinematic storage model in SWAT to simulate saturation excess runoff was considered to be a simple yet effective approach to account for VSAs. The current work was largely inspired by the elegant manner that CATPRO explicitly accounts for the dynamic nature of subsurface saturation and the relationship perched water tables have with VSAs.

The kinematic storage model of Sloan and Moore (1984) uses the mass continuity equation with the entire hillslope segment being the control volume. The hillslope, represented as a rectangular storage element, has a soil layer of constant depth D (mm) and an impermeable soil layer of length L (mm). The hillslope segment is orientated at an angle α. The kinematic wave approximation of saturated lateral flow assumes that the lines of flow in the saturated zone are parallel to the impermeable layer and the hydraulic gradient equals the bed slope (Figure 2a).

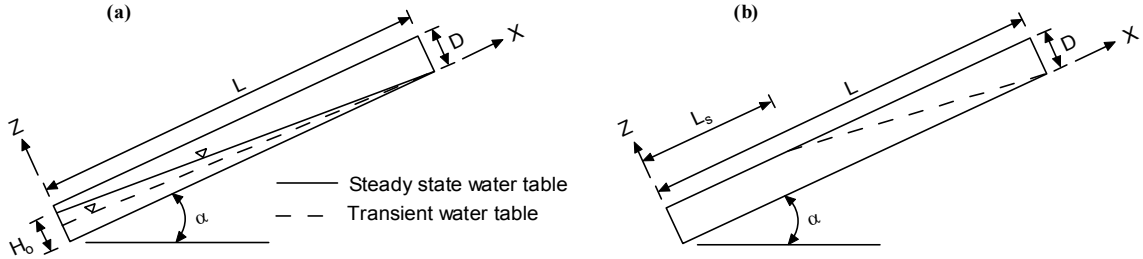

Figure 2 – The Kinematic Storage Model proposed by Sloan and Moore (1984): (a) without Saturation Excess Runoff; and (b) with Saturation Excess Runoff.

The mass continuity equation for the saturated component of the hillslope can be expressed as:

$$\frac{S_2 - S_1}{\Delta t} = iL - \frac{(q_1 + q_2)}{2} \tag{1}$$

where S is the drainable volume of water stored in the saturated zone per unit width (mm^2), Δt is the time step (1 day in the case of SWAT), i is the vertical input rate to the saturated zone (mm/d), q is the discharge per unit width (mm^2/d), and subscripts 1 and 2 denote the start and end of the time step. The storage volume S is found by:

$$S = H_o \ _d L/2 \tag{2}$$

where H_o is the water table depth at the outlet (mm) and θ_d (mm/mm) is the drainable porosity. The discharge at the outlet q is given by Darcy's law:

$$q = H_o v \tag{3}$$

where v is the velocity of flow at the outlet (mm/d) and is defined as:

$$v = K_{sat} \sin(\alpha) \tag{4}$$

where K_{sat} is the saturated hydraulic conductivity (mm/d). Substitution of (2) and (4) into (3) yields:

$$q = \frac{2SK_{sat} \sin(\alpha)}{\theta_d L} \tag{5}$$

Sloan and Moore (1984) modified the kinematic storage model to simulate saturation excess runoff when the water table intersects the ground surface (Figure 2b). Under these conditions (2) and (3) then become:

$$S = D\theta_d \left(L + L_s\right)/2 \tag{6}$$

$$q = iL_s + Dv \tag{7}$$

where L_s is the saturated slope length (mm). Substitution of (6) and (7) into (1) allows the saturated slope length L_s to be computed at the end of the time step:

$$L_{s2} = \frac{L_{s1}\left(D\theta_d / \Delta t - i\right) + 2iL - 2Dv}{D\theta_d / \Delta t + i} \tag{8}$$

Once L_s is known the discharge can be calculated using (7). An additional parameter, *sat_base*, was incorporated into SWAT-VSA to account for the permanently saturated portion of the hillslope located in the vicinity of the stream owing to baseflow from deeper aquifers. Kuczera et al., (1993) also added a parameter to CATPRO to represent the constantly saturated fraction of the hillslope. Currently *sat_base* is assumed to be constant and is added to L_s (after being multiplied by L first) whenever baseflow is present. In the model L_s is never allowed to exceed L.

3.2 Percolation

SWAT employs a storage routing technique to calculate the amount of water available for percolation to the underlying soil layer. Water is not permitted to flow vertically if the underlying layer is saturated. However water movement between layers is not limited by the hydraulic conductivity of the underlying layer. This means the amount of water that percolates can exceed the soil water drainage rate (K_{sat}) of the underlying layer. Consequently percolation will be overestimated. As outlined earlier, the B horizon of duplex soils has a distinct lack of vertical flow capacity that ultimately causes pondage on top of the B horizon. For some duplex soils in the immediate region of the study area the hydraulic conductivity of the A horizon can be four orders of magnitude greater than that of the B horizon (Williamson, 1979). Clearly the low hydraulic conductivity of the B horizon will impede percolation in these soils. To limit percolation when the drainage rate cannot move the total amount of water available for percolation, (9) and (10) were adopted from Maréchal and Holman (2002) and incorporated into both models:

$$per = \mathrm{Min}\left(K_{sat}^{i}, K_{sat}^{i+1}, per'\right) \tag{9}$$

where *per* is the amount of percolation to the underlying layer and *per'* is the amount of percolation calculated using the storage routing methodology. The amount of water that percolates past the bottom of the soil profile is given by:

$$per = \mathrm{Min}\left(K_{sat}^{i}, lbk, per'\right) \tag{10}$$

where *lbk* is the lower boundary hydraulic conductivity (mm/d).

3.3 Anisotropy

The hydraulic conductivity of anisotropic soils is not homogenous in the vertical and horizontal directions. Anisotropy has a significant influence on the movement of water in the soils of the Woady Yaloak River catchment, and generally in many of the soils across southwest Victoria (R. MacEwan, CLPR, personal communication, 2003). Eckhardt et al., (2002) introduced an anisotropy factor (*aniso*) into (5) to increase the amount of lateral flow produced on account of the horizontal hydraulic conductivity being greater than the vertical hydraulic conductivity. Given the importance of anisotropy in the soils of southwest Victoria, *aniso* was incorporated into SWAT-VSA and SWAT-CN. Values for *aniso* were limited to between 1 and 3. With the inclusion of *aniso*, (5) now becomes:

$$q = \frac{2SK_{sat}\sin\left(\alpha\right)aniso}{\theta_d L} \tag{11}$$

4. RESULTS AND DISCUSSION

SWAT-VSA and SWAT-CN were calibrated for the period 1978-1989 and validated for the period 1990-2001. Both model versions were calibrated with the aid of an automatic calibration scheme that uses the Shuffled Complex Evolution algorithm (Duan et al., 1992). The automatic calibration scheme, which was developed by van Griensven (2002), was taken from the yet to be released SWAT2004 (J. Arnold, USDA, personal communication, 2003) and incorporated into the base version adopted in this study, SWAT2000. For the sake of brevity only results from the application of the models at Cressy are presented. The observed and predicted runoff volumes for the calibration period are compared to one another in Figures 3 and 4 for annual, monthly and daily time steps.

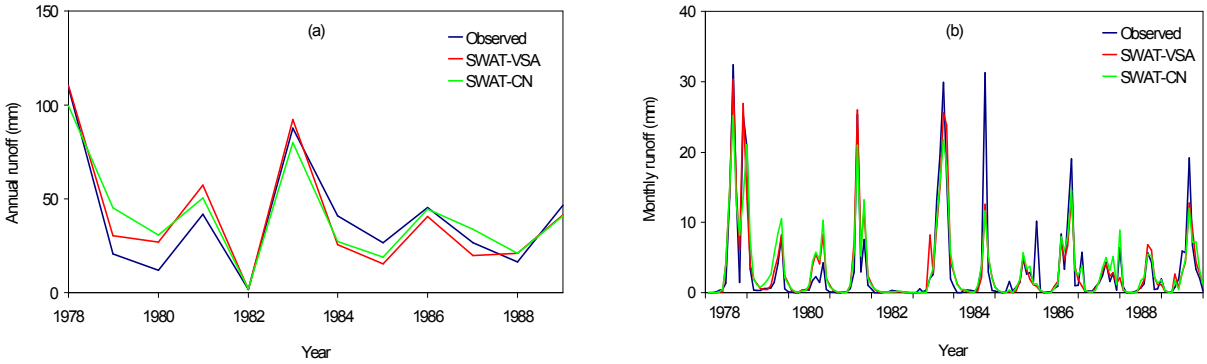

Figure 3 – Observed and Predicted Runoff at Cressy: (a) Annual Runoff; and (b) Monthly Runoff.

The performance of SWAT-VSA and SWAT-CN for predicting annual runoff volumes can be observed to be extremely good (Figure 3a). The results on a monthly time step are also very good, with the seasonal trends being accounted for relatively well (Figure 3b). It is evident that the annual and monthly runoff from the Woady Yaloak River catchment exhibits tremendous variability. Importantly both models have successfully captured this variability and have reproduced runoff exceptionally well over a long period of time. Daily runoff predictions for most years of the calibration and validation periods are considered to be reasonable overall (Figure 4), with peak events generally being underestimated by both models.

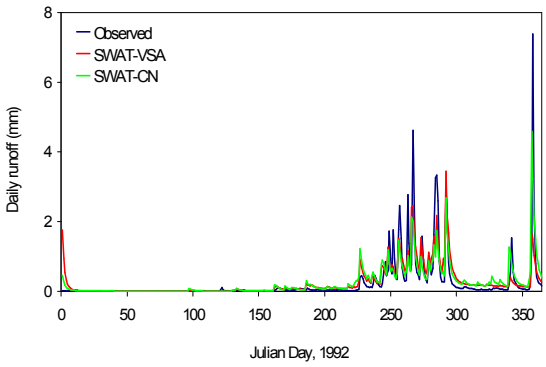

Figure 4 – Observed and Predicted Daily Runoff.

To quantify the performances of SWAT-VSA and SWAT-CN for predicting runoff two objective measures are employed: coefficient of efficiency (*CE*) and absolute deviation (*ADE*). The coefficient of efficiency is a measure of the variance while the absolute deviation is a measure of the average departure of predictions at every time step (Ndiritu and Daniell, 1999). A value of 1 for *CE* indicates a perfect fit, whereas for *ADE* zero indicates a perfect fit. The observed and predicted mean (Q_{obs} and Q_{pred}) and standard deviation (SD_{obs} and SD_{pred}) of annual, monthly and daily runoff volumes are presented in Table 1 along with the objective measures for the corresponding time scales.

Table 1 indicates that the mean runoff predicted by SWAT-VSA and SWAT-CN closely matched the mean observed runoff at each time scale. The performance of the models for preserving the standard deviation at the various time scales was considered acceptable, although both models slightly underestimated this statistic for monthly and daily runoff volumes. The *CE* values achieved by SWAT-VSA and SWAT-CN at annual and monthly time steps were equal to or greater than 0.80 for the calibration and validation periods, which are regarded as very good results since a *CE* value of between 0.7 and 0.8 indicates a relatively good fit (Krysanova et al., 1998). However on a daily time step only average results were achieved for *CE*, with values ranging from 0.44 to 0.55. Relatively similar values for *ADE* were achieved by the models for the calibration and validation periods. SWAT-VSA and SWAT-CN both performed extremely well for predicting annual and monthly runoff volumes whereas on a daily time step both models only performed moderately well. The average performance of both models for predicting daily runoff is not entirely down to inadequate model structures but may be partly attributed to limited data availability. The availability of specific data needed to operate SWAT, namely climatic

variables, management practices, and soil distribution and properties, is limited for the Woady Yaloak River catchment and it is therefore highly unlikely that daily predictions can be improved upon substantially regardless of any further modifications made to the model.

Table 1 – Statistics and Objective Measures used to Assess Performance of SWAT-VSA and SWAT-CN

Statistics[#] and Objective Measures	Calibration			Validation		
	Annual	Monthly	Daily	Annual	Monthly	Daily
SWAT-VSA						
Q_{obs}	39.61	3.30	0.108	28.98	2.42	0.079
Q_{pred}	40.20	3.35	0.110	28.25	2.35	0.077
SD_{obs}	31.18	6.42	0.456	25.68	5.38	0.375
SD_{pred}	32.07	5.64	0.296	26.87	4.56	0.208
CE	0.90	0.83	0.55	0.93	0.83	0.44
ADE	0.20	0.40	0.74	0.18	0.46	0.72
SWAT-CN						
Q_{obs}	39.61	3.30	0.108	28.98	2.42	0.079
Q_{pred}	41.18	3.43	0.113	29.58	2.47	0.081
SD_{obs}	31.18	6.42	0.456	25.68	5.38	0.375
SD_{pred}	26.75	5.00	0.243	27.43	4.42	0.215
CE	0.86	0.80	0.50	0.88	0.83	0.49
ADE	0.23	0.45	0.74	0.23	0.48	0.76

[#]Units of mean (Q) and standard deviation (SD) are in mm.

SWAT-VSA is consistent with the VSA concept in that runoff is only generated from the saturated portion of the hillslope. Figure 5 presents the average monthly hillslope saturation fraction of HRU 80 predicted by SWAT-VSA. The saturation fraction exhibits strong seasonal fluctuations, with peak values occurring in late winter and early spring when heavy rainfalls replenish the soil moisture of the A horizon. Figure 6 shows surface runoff was never generated from more than 43% of the total area of HRU80. The permenatly saturated area (*sat_base*) was determined to be 0.2%. from calibration. The occurrence of a drought with a recurrence interval of approximately one hundred years is responsible for the saturation fraction being equal to *sat_base* for all 1982.

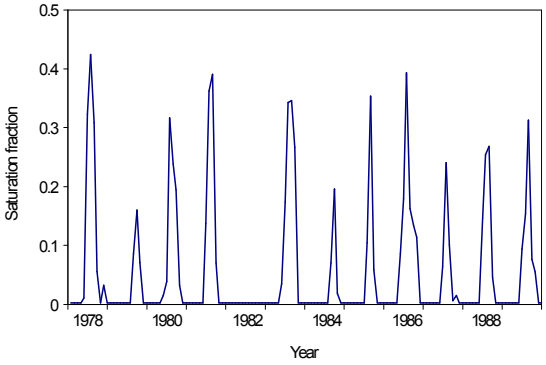

Figure 5 – Average Saturation Fraction of HRU80.

Overall SWAT-VSA and SWAT-CN have done a very good job at representing the long-term runoff of the Woady Yaloak River catchment, considering the tremendous variability of runoff on an annual and monthly basis and that floods and drought have occurred regularly throughout the evaluation period. Importantly the results from this study show that the kinematic storage model of Sloan and Moore (1984) can be extended in SWAT to predict saturation excess runoff successfully. Sloan and Moore (1984) reported that the kinematic storage model has sufficient features that would enable it to be incorporated into comprehensive watershed models, and in doing so would place these models on a more rational, physically correct and less empirical footing. This is reinforced by the assertion of Boughton (1989) that physically based approaches rather than the curve number method are more appropriate for water balance models. Replacement of the curve number method with the kinematic storage model removes some of the empiricism currently associated with SWAT while at the same time lending greater physical basis to the model.

When the curve number method is used to establish a long-term pattern of runoff from a long record of rainfall, as is done in SWAT, it is common practice to find, by trial and error, a set of curve numbers that produce a reasonable fit between the observed and predicted runoff. This can be easily achieved for gauged catchments but not so in the case of ungauged catchments. A significant problem inherent in the curve number method is the very high sensitivity of the predicted runoff to changes in the curve number, which in some cases can result in the amount of predicted runoff doubling when the curve number is increased by 10-15 (Boughton, 1989). With no opportunity for optimisation in ungauged catchments, the selection of suitable curve numbers remains a source of great uncertainty despite recommended values being published for different soils and land use classes (USDA SCS, 1972). The same problem applies when a hydrologic model, with the curve number method embedded in its formulation, is used to predict the response of runoff to changes in land use. To make predictions about future conditions the model must be forced to extrapolate beyond the conditions encountered in

the calibration period. However this means that selection of curve numbers for land use classes not present in the calibration period cannot be based on any optimised values. Utilisation of concepts that have greater physical basis, such as the kinematic storage model, can help overcome this limitation in curve number based models whose principle purpose is to predict land use change impacts.

It is important to stipulate that it is not the intention of this study to condemn the utilisation of the curve number method despite criticism of the method in the literature (Boughton, 1989). The curve number method is an effective, reliable and widely used method that is capable of producing good results, as was shown from this study. Instead it is proposed that utilising the kinematic storage model, rather than the curve number method, to calculate surface runoff in catchments dominated by duplex soils may be more appropriate. This is because the kinematic storage model can be interpreted in a manner that is more consistent with the VSA concept and saturation excess runoff, which are applicable in duplex soils. It is also important to mention here that 3-PG (Landsberg and Waring, 1997), a dynamic, process-based forest growth model, was integrated into both models to simulate the leaf area index and biomass of forests instead of the original plant growth module used in SWAT. Further details on this modification, which has major implications for the calculation of evapotranspiration, are to be presented in a forthcoming paper.

5. CONCLUSION

This paper outlined the extension of the kinematic storage model in SWAT to account for the development of ephemeral, perched water tables in duplex soils and the generation of VSAs and saturation excess runoff. The model simulating saturation excess runoff (SWAT-VSA) was applied to the Woady Yaloak River catchment along with a version that retained the curve number method (SWAT-CN). The results indicate that both models predicted annual and monthly runoff volumes extremely well while their performances for daily runoff predictions were only average. Although weaknesses in the model structures would undoubtedly be a factor, the limited availability of certain data sets would have also influenced the outcomes achieved on a daily time step. It is concluded that both models performed equally well and that no model produced significantly better results. This indicates that SWAT-VSA has great potential to be tested on more catchments across southwest Victoria where the VSA concept is the prevalent runoff generation mechanism. Since the surface runoff component of SWAT-VSA is based on the observed runoff generation mechanism of catchments in southwest Victoria, unlike that of SWAT-CN, it may be regarded as a more suitable model to utilise for the prediction of land use change impacts and testing alternative management strategies.

6. ACKNOWLEDGMENTS

The principle author would like to thank the following people: Dr Jeff Arnold (USDA) for help with SWAT and for supplying the automatic calibration subroutines; Dr Nicholas Coops (CSIRO) for assistance and advice on 3PG; and Richard MacEwan (CLPR) and Peter Dahlhaus (Dahlhaus Environmental Geology) for information on the soils and geology of the Woady Yaloak River catchment. The principle author also wishes to acknowledge the support of an Australian Postgraduate Award Scholarship.

7. REFERENCES

Boughton, W.C. (1989). A review of the USDA SCS curve number method. *Australian Journal of Soil Research*, Vol No. 27, pp. 511-23.

Cox, J.W. and McFarlane, D.J. (1995). The causes of waterlogging in shallow soils and their drainage in southwestern Australia. *Journal of Hydrology*, Vol No. 167, pp. 175-194.

Duan, Q., Gupta, V.K. and Sorooshian, S. (1992). Effective and efficient global minimalization for conceptual rainfall-runoff models. *Water Resources Research*, Vol No. 28, pp. 1015-1031.

Dunne, T. (1983). Relation of field studies and modeling in the prediction of storm runoff. *Journal of Hydrology*, Vol No. 65, pp. 25-48.

Eckhardt, K., Haverkamp, S., Fohrer, N. and Frede, H.-G. (2002). SWAT-G, a version of SWAT99.2 modified for application to low mountain range catchments, *Physics & Chemistry of the Earth, Part B: Hydrology, Oceans & Atmosphere*. Vol No. 27, pp. 641-644.

Endreny, T.A. and Wood, E.F. (1999). Distributed watershed modelling of design storms to identify nonpoint source loading areas. *Journal of Environmental Quality*, Vol No. 28, pp. 388-397.

Landsberg, J.J. and Waring, R.H. (1997). A generalised model of forest productivity using simplified concepts of radiation-use efficiency, carbon balance and partitioning. *Forest Ecology and Management*, Vol No. 95, pp. 209-228.

Krysanova, V., Müller-Wohlfeil, D.-I., & Becker, A. (1998). Development and test of a spatially distributed hydrological/water quality model for mesoscale watersheds. *Ecological Modelling*, Vol No. 106, pp. 261-289.

Kuczera, G., Raper, G.P., Breah, N.S. and Jayasuriya, M.D. (1993). Modelling yield changes after strip thinning in a mountain ash catchment: an exercise in catchment model validation. *Journal of Hydrology*, Vol No. 150, pp. 433-457.

Maréchal, D. and Holman, I.P. (2002). A soil hydrology-based catchment water resources model. In: *International Environmental Modelling and Software Society (IEMSs 2002)*, Lugano, Switzerland, pp. 452-457.

Mroczkowski, M., Raper, P. and Kuczera, G. (1996). *CATPRO – A Catchment Hydrosalinity Balance Model Version 2.0*. University of Newcastle, Newcastle, 46p.

Ndiritu, J.G. and Daniell, T.M. (1999). Assessing model calibration adequacy via global optimisation. *Water SA*, Vol No. 25, pp. 317-326.

Neitsch, S.L., Arnold, J.G., Kiniry, J.R. and Williams, J.R. (2001). *Soil and Water Assessment Tool Theoretical Documentation*, Grassland, Soil and Water Research Laboratory and Blackland Research Center, Temple 506p.

Ormsbee, L.E. and Khan, A.Q. (1989). A parametric model for steeply sloping forested watersheds. *Water Resources Research*, Vol No. 25, pp. 2053-2065.

Raper, G.P. and Kuczera, G. (1991). Groundwater recharge estimation using a lumped-parameter catchment process model. In: *First International Hydrology & Water Resources Symposium*, Perth, Australia, pp. 563-568.

Sloan, P.G. and Moore, I.D. (1984). Modeling subsurface stormflow on steeply sloping forested watersheds. *Water Resources Research*. Vol No. 20, pp. 1815-1822.

Stagnitti, F., Parlange, J.-Y., Steenhuis, T., Parlange, M.B. and Rose, C.W. (1992). A mathematical model of hillslope and watershed discharge. *Water Resources Research*, Vol No. 28, pp. 2111-2122.

USDA Soil Conservation Service. (1972). *National Engineering Handbook*, Hydrology, Section 4, Chapters 4-10.

U.S. Army Corps of Engineers (1985). *HEC 1 Users Manual*, U.S. Army Corps of Engineers, Davis.

van Griensven, A. (2002). *Developments Towards Integrated Water Quality Modelling River Basins*. PhD Dissertation. Vrije Universiteit Brussel, Brussels, 280p.

Watson, B.M., Selvalingam, S. and Ghafouri, M. (2003). Evaluation of SWAT for modelling the water balance of the Woady Yaloak River catchment. In: *Proceedings of MODSIM 2003*, Townsville, Australia, pp. 873-878.

Williamson, R.J. (1979). Soil Moisture and Hydrology of the Basalt Plains of Western Victoria. PhD Dissertation. University of Melbourne, Melbourne, 408p.

The Institution of Engineers, Australia
8th National Conference on Hydraulics in Water Engineering
ANA Hotel Gold Coast, Australia 13-16 July 2004

A Methodology for Predicting Berm Crest Elevation Fronting Coastal Lagoons

F.M. Weir
B.Sc. (Hons.)
Ph.D Student, School of Geosciences and Institute of Marine Science, University of Sydney, NSW 2006.
M.G. Hughes
B.Ec. (Hons.), Ph.D
Senior Lecturer, School of Geosciences and Institute of Marine Science, University of Sydney, NSW 2006.
T.E. Baldock
B.Eng. (Hons.), Ph.D
Lecturer, Division of Civil Engineering, University of Queensland, St Lucia, Brisbane, Qld 4072.

Abstract: This paper presents a method for predicting maximum probable berm crest elevation based primarily on offshore wave conditions. The approach uses a sediment transport criterion to identify berm-building wave conditions and an empirical equation for the total runup height to determine the maximum probable berm height; both require offshore wave conditions as input. The method is tested on five beach-lagoon systems located on the New South Wales central coast, as well as the extensive data set obtained at the US Army Corps Field Research Facility at Duck, North Carolina, USA with some success. Further development of the method is proposed by incorporating shoaling wave transformations and breaker wave conditions.

Keywords: Beach Berms, lagoons, wave run-up, swash, sediment transport

1. INTRODUCTION

Many lagoon entrances along the wave-dominated eastern seaboard of Australia naturally cycle between being briefly open to the sea or being closed off by a wave-built berm. Although this cycle of entrance condition is natural, it does cause significant environmental problems for lagoons with developed catchments. Some 70% of coastal lagoons in New South Wales have managed entrances, primarily to address the problem of foreshore flooding. Whilst lagoon opening may satisfy community concerns with respect to flooding, frequent artificial openings are having negative ecological impacts. At present coastal lagoon systems are still poorly understood, and past development practices have been incompatible with natural processes. The first step in developing sustainable management strategies for these coastal lagoon entrances is to obtain a reliable predictor for the maximum height of the wave-built berm, which controls maximum flood levels inside the lagoon.

The wave-built berm is an accretionary sedimentary feature located at the top of the beach-face, and is present on most steep beaches. In a series of laboratory experiments Bagnold (1940) demonstrated that the berm crest elevation is primarily dependent upon the wave runup height. Maximum wave runup occurs during increased wave set-up that accompanies spring high tides, and correspondingly Strahler (1966) showed an increase in berm elevation during spring tides. Utilising data from a field experiment at the US Army Corps of Engineers Field Research Facility (FRF) Holman and Sallenger (1985) found that the total wave runup (R_T) was proportional to a form of the Iribarren number ξ_o, so that during high tide:

$$R_T = H_o(0.8\xi_o + 0.11) \quad (1)$$

where

$$\xi_o = \beta / (H_o / L_o)^{1/2} \quad (2)$$

β is the beach face gradient, and H_o and L_o are the significant deep-water wave height and length, respectively.

The dependence of berm height upon wave runup leads to what is known as the berm-height paradox – i.e., increasing offshore wave heights increase the wave runup height and therefore the berm crest height, but the largest waves ultimately erode the beach face and result in a reduction in berm height (e.g. Bascom, 1954; Hughes and Turner, 1999; Komar, 1998). Successful prediction of the maximum berm crest elevation for management purposes requires an approach that both (a) quantifies the relationship between offshore wave height and berm height and (b) incorporates a prediction of the threshold condition that initiates offshore sediment transport and beach face erosion. A large number of criteria have been developed in the field and laboratory for the prediction of beach face erosion and accretion by wave-induced cross-shore sediment transport (e.g. Dalrymple, 1992; Hattori and Kawamata, 1980; Kraus et al., 1991; Sunamura and Horikawa, 1974). In an evaluation of some of these criteria, Jackson (1999) found that the criterion of Kraus et al. (1991) was the most effective at discriminating between erosion and accretion events:

$$H_o / wT = C\,(w / \sqrt{g\,H_o})^{2} \quad (3)$$

where w is the sediment fall velocity and g is the acceleration due to gravity. Based on data from 32 field sites Kraus et al. (1991) found that C is equal to 22,900 and that accretion takes place when:

$$H_O / wT < 3.2 \quad (4)$$

Maximum berm height at a given beach should thus equal maximum R_T at spring high tides combined with measured tidal elevations, for waves that fulfil the transport criteria (4).

2. DATA SET

2.1 FRF, Duck, North Carolina, USA

Detailed field measurements of the bathymetry and hydrodynamic conditions at the US Army Corp Field Research Facility (FRF) at Duck, North Carolina have been obtained continuously since 1981. Nearshore bathymetry at this site is characterised by relatively straight offshore contours, a moderate slope and a barred surf zone. Surveys along 26 shore perpendicular profile lines are conducted at monthly intervals, extending from the dune to approximately 950m offshore. For the purposes of this study 3 of the profiles at a spacing of 46m were used to obtain an alongshore average of berm crest elevation. Forty elevations were obtained for the period April 1998 to September 2003, with values ranging from 1.142 to 2.926m above the National Geodetic Vertical Datum (NGVD). Deep-water wave data for a period of 30 days prior to each survey was obtained from the Waverider buoy located 4km offshore in approximately 17m water depth. Sediment statistics were obtained from samples collected in the mid-tide region of the beach face during the DUCK94 experiment (Stauble and Cialone, 1996). This region of the beach face typically contains a bimodal gravel component along with a medium sized sand component with mean sediment size (D) of 0.3337mm.

2.2 Central Coast, NSW, Australia

The Australian study sites include five beach-lagoon systems on the New South Wales central coast, located between 50 and 90km north of Sydney, Australia. These are Wamberal Beach (Wamberal Lagoon), Terrigal Beach (Terrigal Lagoon), Avoca Beach (Avoca Lagoon), Copacabana Beach (Cockrone Lagoon) and Pearl Beach (Pearl Lagoon). These sites include a range of beach types and a wide range of exposure to a high-energy, deepwater wave climate. Monthly topographic surveys have been conducted during spring tides since July 2003 to measure berm height relative to the Australian Height Datum (AHD). Deep-water wave data was obtained from a Directional Waverider buoy located 12km offshore of Sydney in 85m water depth.

3. RESULTS

3.1 FRF, Duck

Berm height at the FRF had an average elevation of 2.20m and ranged from 1.142m to 2.926m NGVD (i.e. above mean sea level). Using (4) and a sediment fall velocity of 0.04344m s^{-1} it was determined that onshore sediment transport and potential berm building takes place when:

$$H_o / T < 0.139008 \quad (5)$$

This transport direction criterion was compared to visual estimates of profile change from the topographic surveys and it was found to have a 90% accuracy. Wave data during spring high tides (within the 30 days) prior to each survey were examined and the maximum deep water wave conditions that satisfied (5) was used to calculate the maximum R_T (including the tide level) using (1). A large number of berm heights actually exceed the predicted maximum runup height, but this likely reflects the error associated with (1) (see Holman and Sallenger, 1985). Linear regression was used to determine the relationship between berm height, B_h, and R_T, with the resulting equation represented by the centre line in Figure 1. Berm height and runup height are positively correlated with a correlation coefficient of R = 0.485, which is significant at the 95% confidence level. Approximately 75% of the variance remains unexplained, but is probably largely related to the uncertainty in predicting the maximum runup height from deepwater wave conditions (see Holman and Sallenger, 1985).

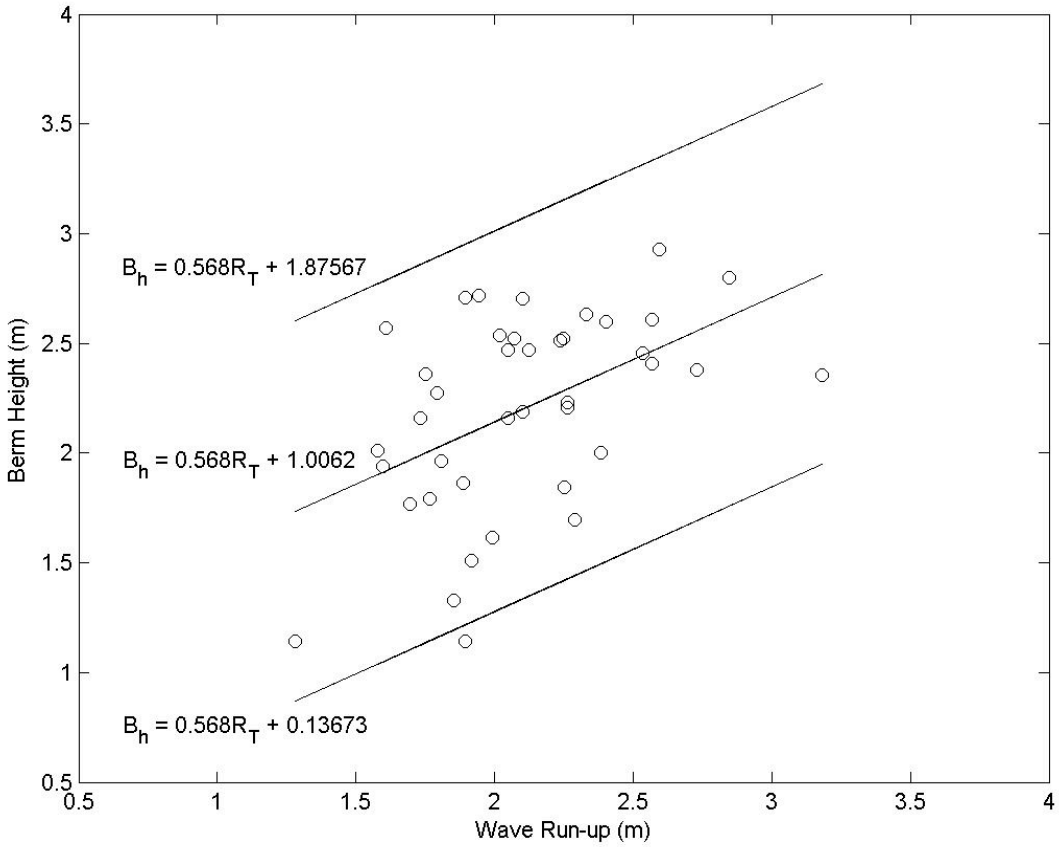

Figure 1 - Berm Height (B_h) Plotted Against Estimated Maximum Runup Height (R_T) At The FRF. The Centre Line Represents The Best Fit Equation, While The Upper and Lower Lines Represent The 95% Confidence Limits.

Assuming that 5 years of record is sufficiently long to yield something approaching the maximum probable berm height at the FRF, the regression model in Figure 1 indicates that this maximum berm height is 2.82m ± 0.87. The maximum berm height at the FRF site measured between 1990 and 2003 is 3.25m and within error of the predicted maximum.

3.2 Central Coast, NSW

Berm heights at the NSW beach-lagoon systems ranged from a minimum of 1.81m to 3.546m AHD (i.e., above mean sea level) at Pearl and Copacabana beaches respectively. This reflects a general pattern of berm height, with Pearl beach commonly displaying the lowest berm height and Copacabana the largest. This is attributed to the location and orientation of each beach; Copacabana is orientated towards the southeast and consequently receives waves directly from the dominant swell direction, while Pearl Beach is set back within the Broken Bay estuary and protected by an island.

The onshore sediment transport criterion (5) used to predict berm-building episodes at the FRF site is again utilised for the NSW beaches. This criteria was based on medium sized quartz sand, which typifies sediment

present on the NSW coastline. Figure 2 compares berm height on NSW beaches to predicted runup heights. Again berm height and runup height are positively correlated with a correlation coefficient of R = 0.452, which is significant at the 95% confidence level.

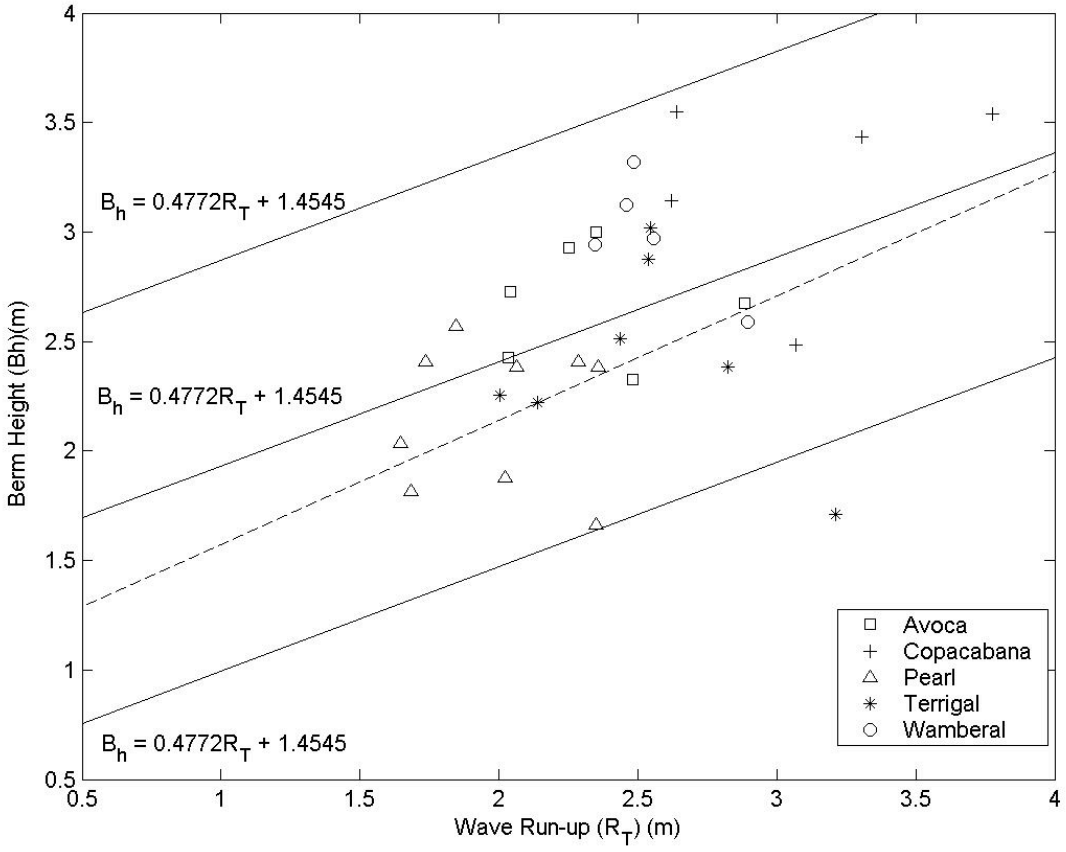

Figure 2 - Berm Height (B_h) Against Estimated Maximum Runup Height (R_T) At The NSW Beaches. The Centre Line Represents The Best Fit Equation, While The Upper and Lower Lines Represent The 95% Confidence Limit. The Dashed Line Represents The Best Fit Equation At The FRF.

Again, assuming that 1 year of record is sufficiently long to yield something approaching the maximum probable berm height at these NSW beaches, the regression model in Figure 2 indicates that the maximum berm height is 3.27m ± 0.94.

4. FURTHER DEVELOPMENT OF THE METHODOLOGY

While the methodology outlined in this paper is broadly successful, further refinement is necessary. This will be achieved through analysis of a large established data set of 20 years of topographic surveys of Narrabeen Beach, NSW, Australia, and continued analysis of the extensive data set at the US Army Corps Field Research Facility. In particular, time series of berm heights will be examined to identify only unequivocal berm-building episodes in the data set. Moreover, breaker wave conditions will be used to predict runup height more accurately than deepwater wave conditions. This will be done through scaling of (1) according to the wave shoaling/refraction coefficient or the formulation of a new wave run-up predictor based on wave breaker height. Breaker heights can be obtained from deepwater wave conditions using a public domain shoaling/refraction/diffraction model (e.g. REF/DIF; Kirby and Dalrymple, 1994). Example outputs from this REF/DIF model for the Copacabana embayment are shown in Figures 3 and 4, which clearly show wave shoaling, refraction and sheltering across the shoreface. Long term deepwater wave statistics can be used to determine the maximum possible breaker conditions capable of berm-building.

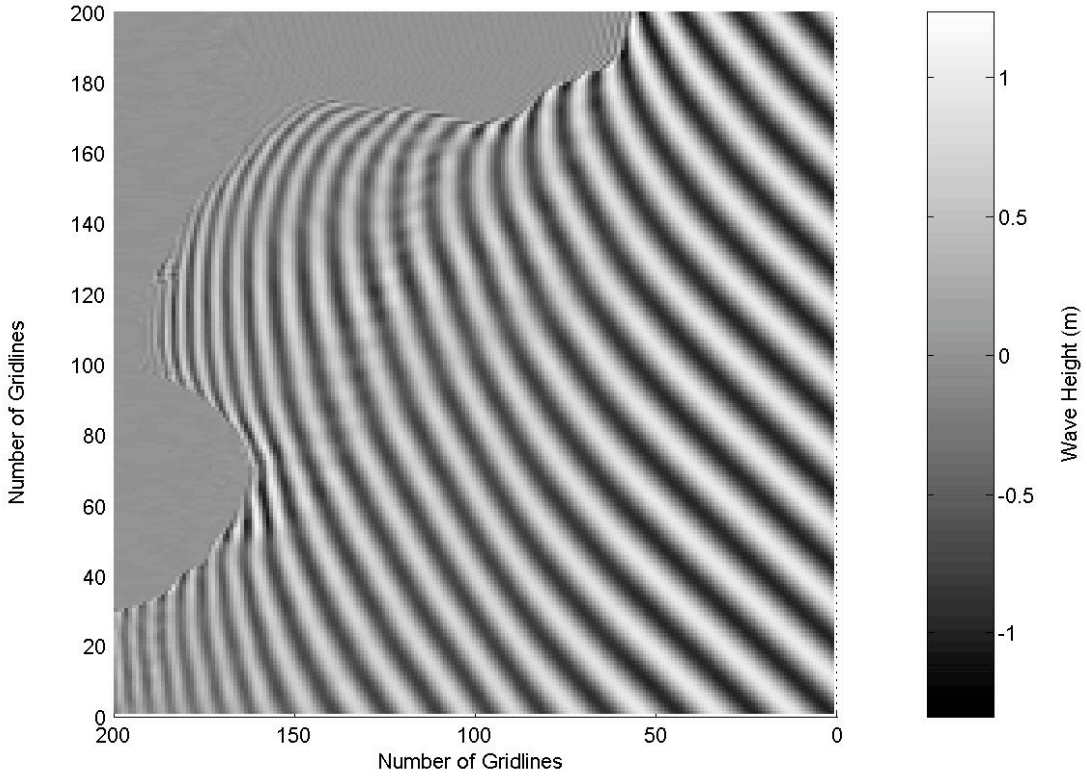

Figure 3 - An Example Of An Output From Freeware Program REF/DIF, Showing Waves With A Period Of 12 Seconds Approaching Copacabana Beach From The North East

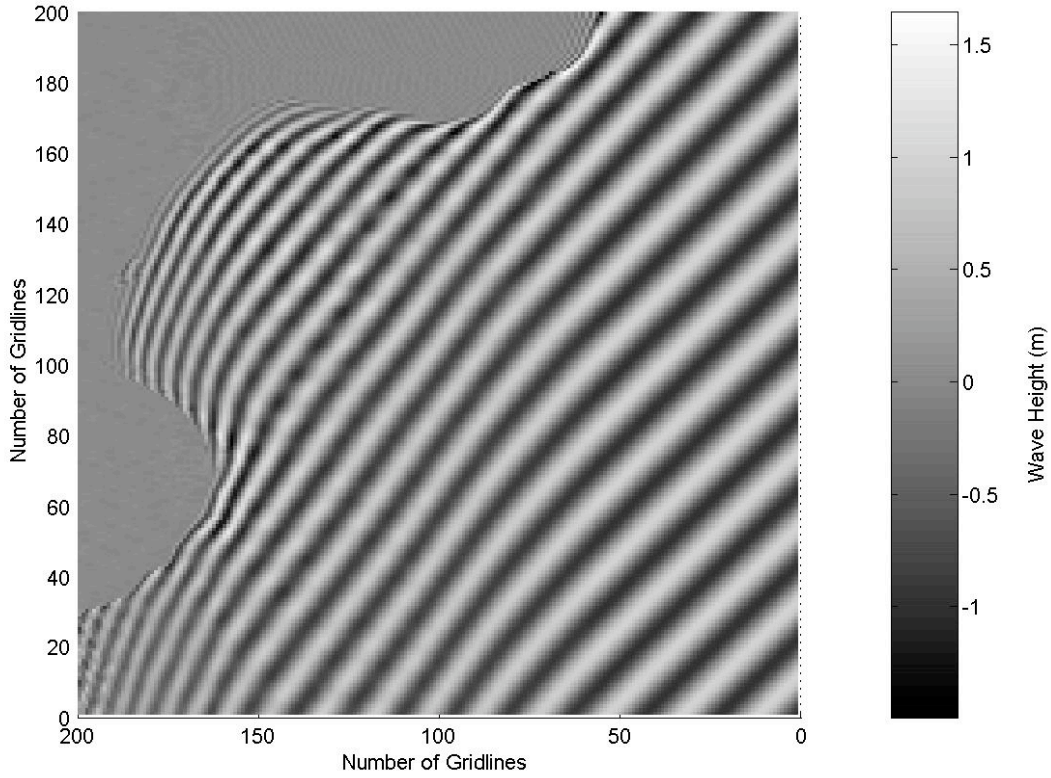

Figure 4 - An Example Of An Output From Freeware Program REF/DIF, Showing Waves With A Period Of 12 Seconds Approaching Copacabana Beach From The South East

5. CONCLUSIONS

This paper presents a new method of predicting the maximum possible berm height fronting a beach-lagoon system from deep-water wave statistics. The approach is based on predicting maximum wave run-up from an equation developed by Holman and Sallenger (1985) at the FRF at Duck, North Carolina. Maximum wave run-up during berm-building will most likely coincide with spring high tides; therefore offshore wave statistics during this portion of the tide cycle are used to predict the run-up maxima. The berm height paradox is circumvented through the use of the Kraus et al. (1991) sediment transport criterion. Using this criterion, it is possible to determine the maximum offshore wave height for which accretion occurs. The methodology was tested using data from both the FRF at Duck, USA, and five beach-lagoon systems located on the New South Wales central coast. The approach produced consistent results across the range of beaches studied, with the maximum probable berm height on the higher energy NSW beaches being some 0.4m higher that that at Duck, USA.

6. ACKNOWLEDGEMENTS

The US Army Corps of Engineers Field Research Facility provided the data from Duck, North Carolina. Sydney offshore wave data was collected and provided by the Manly Hydraulics Laboratory. Permission from the Department of Infrastructure, Planning and Natural Resources for use of this data is appreciated.

7. REFERENCES

Bagnold, R.A. (1940). Beach formation by Waves: Some model experiments in a Wave Tank. Journal Institution of Civil Engineers, Vol No. 15, pp.27-52

Bascom, W.H. (1953). Characteristics of Natural Beaches, *Proceedings of the 4th Coastal Engineering Conference*, ASCE., pp. 163-180.

Dalrymple, R.A. (1992). Prediction of storm/normal profiles. *Journal of Waterway, Port, Coastal, and Ocean Engineering*, ASCE, Vol. No. 118, pp. 193-200.

Hattori, M. and Kawamata, R. (1980). Onshore-offshore transport and beach profile change. In *Proceedings of the 17th Conference on Coastal Engineering*. ASCE, Sydney, Australia. pp. 1175-1193.

Holman, R.A. and Sallenger, A.H. (1985). Setup and Swash on a Natural Beach. *Journal of Geophysical Research*, Vol No. 90, pp. 945-953.

Hughes, M.G. and Turner, I. (1999). The Beachface, *Handbook of Beach and Shoreface Morphodynamics*, Short, A.D. (ed). John Wiley & Sons Ltd, New York, pp.119-144.

Jackson, N. (1999). Evaluation of Criteria for Predicting Erosion and Accretion on an Estuarine Sand Beach, Delaware Bay, New Jersey. *Estuaries*, Vol No. 22, pp. 215-223.

Kirby, J.T. and Dalrymple, R.A. (1994). *Combined refraction/diffraction model REF/DIF 1: Documentation and User's Manual*. Research Report No. CACR-94-22. Centre for Applied Coastal Research, Department of Civil Engineering, University of Delaware, Newark.

Komar, P.D. (1998). *Beach Processes and Sedimentation,* 2nd ed., Prentice Hall, New Jersey, 544p.

Kraus, N.C., Larson, M. and Kriebel, D.L. (1991). Evaluation of beach erosion and accretion predictors, *Coastal Sediments '91*. ASCE, Seattle, Washington, Vol No. 1, pp. 572-587.

Stauble, D.K. and Cialone, M.A. (1996). Sediment Dynamics and Profile Interactions: DUCK94. Proceedings of the 25th International Conference on Coastal Dynamics. Orlando, Florida. ASCE. Vol No. 4, pp. 3921-3934.

Strahler, A.N. (1996). Tidal Cycle of Changes on an Equilibrium Beach. *Journal of Geology*, Vol No. 74, pp. 247-268.

Sunamura, T. and Horikawa, K. (1974). Two-dimensional beach transformation due to waves. In *Proceedings of the 14th Conference on Coastal Engineering*. Copenhagen. pp. 920-938.

The Institution of Engineers, Australia
8th National Conference on Hydraulics in Water Engineering
ANA Hotel Gold Coast, Australia 13 16 July 2004

Aspects of Numerically Modelling Transcritical Flows

A.C. Wicht
School of Civil and Environmental Engineering, University of NSW
B. Cathers
B.E., Ph.D.,
Water Research Laboratory, School of Civil and Environmental Engineering, University of NSW

Abstract: Transcritical flows occur in open channels and consist of contiguous regions of subcritical and supercritical flow. In this paper, we compare the performance of two numerical models applied to the solution of the St Venant equations (ie 1D continuity and momentum). The models are based on two implicit finite difference (FD) schemes, viz Preissman's FD box scheme and the recently published NewC implicit FD scheme (V. Kutija & C. Hewett, Journal of Hydraulic Research, vol. 40, no. 2, 2002). The results from the two models are intriguingly different; while Preissman's box scheme goes unstable unless cognisance of the characteristics are taken into account, the NewC scheme (surprisingly) remains stable, and this is the reason that it has been recently proposed for the simulation of transcritical flows. The NewC results however, reveal water surface profiles which are superficially realistic but which may contain water surface profiles with spurious energy increases in some places, physically impossible backwater curves and missing hydraulic jumps. What we show in this paper is that there is a need to make recourse to energy considerations to properly assess the performance of the NewC FD scheme. A warning is therefore sounded over all solutions to transcritical flow regions which do not take account of the flow type when enforcing boundary conditions or which do not include forms of the energy equation in their solution.

Keywords: hydraulic numerical modelling, transcritical flow, finite difference schemes, characteristics

Notation:

h	stage (m)	R_h	hydraulic radius of the channel (m)
Q	flow (m^3/s)		Boussinesq coefficient
q	flow per unit width (m^2/s)	j	spatial index
y	(vertical) water depth (m)	n	temporal index
v	cross-sectionally averaged velocity (m/s)	Δt	time step (s)
z	elevation of bed above datum (m)	Δx	distance step (m)
C	Chezy coefficient ($m^{1/2}/s$)	g	acceleration due to gravity (m/s^2)
c	celerity (m/s)	K	conveyance (m^3/s)
A	channel area (m^2)	S	bedslope
b_s	channel width (m)	θ	temporal weighting factor

1. INTRODUCTION

Open channel flow consists of three flow regimes: critical, subcritical and supercritical. Subcritical flows are characterised by large flow depths and slow flow velocities, while the opposite is the case for supercritical flows. The Froude number (F) is defined by

$$F = \frac{v}{\sqrt{gy}} = \frac{v}{c} \tag{1}$$

and indicates whether a flow is supercritical (F>1), critical (F =1) or subcritical (F <1). Subcritical flows are the most common flow regime in natural and artificial open channel flows. Supercritical flows prevail in certain man-made hydraulic structures such as dam spillways. Critical flows occur in localised sections in natural constrictions or in man-made constrictions where it is desired to measure the flows based on measurements of depth alone such as at weirs or in flumes with a narrowed section. Critical flows occur in transitions between subcritical and supercritical flow. A reach of channel which contains both subcritical and supercritical flows is

called a *transcritical* flow region. In transcritical flows there is no requirement on the sequencing of the regions of sub- and supercritical flows.

Transcritical flows are relevant to dambreak problems, flows in channels controlled by a system of (remotely) controlled ('intelligent') gates for irrigation purposes and flows through hydraulic structures during floods. Transcritical flows are receiving increasing interest from the hydraulics community with the need for commercial codes (which are usually based on finite difference or finite element schemes) to reliably simulate them, without the introduction of artificially elevated levels of numerical diffusion to maintain numerical stability.

2. TRANSCRITICAL FLOWS

2.1 Characteristics and Information Paths for Transcritical Flows

In 1D open channel flow theory, the characteristics define the trajectories of information propagation and can be thought of as *information highways*. These information highways and the directions of information flow along them are different between subcritical and supercritical flows. The Froude number actually gives some indication of the direction of information flow in an open channel. The numerator in the definition for the Froude number is the flow velocity; the denominator is the wave celerity [$c = (gy)^{1/2}$], which is the speed at which surface waves (or pressure disturbances) travel. Thus the Froude number compares two speeds: the flow velocity in the channel to the wave celerity and there are two cases:

- In supercritical flow, $u > c$ and the two sets of surface disturbances (or information) travel at $(u \pm c)$ relative to the bank; both sets of disturbances propagate in the downstream direction since $(u \pm c)$ is always positive. The effect of this is that information cannot travel upstream.
- In contrast, for subcritical flows, $u < c$ and $(u \pm c)$ can be positive or negative. This means that surface disturbances can propagate upstream (as well as downstream) relative to a fixed point on the bank. Hence information (in the form of surface waves) can propagate upstream.

Transcritical flow can, therefore, be regarded as a region of channel containing two different regions of information flow. For some part of the channel, information will travel only downstream, and in the other parts information will travel both up- and downstream. This is the main factor which makes the modelling of transcritical flows so difficult since finite difference models rely on the transmission of information (boundary conditions) throughout the solution space in order to arrive at a unique solution to the set of governing equations.

Transcritical flows are most often modelled using a piece-wise approach. The whole channel is broken into sections, each of which has only one flow regime within it. To move between sections, energy considerations (eg hydraulic jump equations) are often used. The entire system is solved iteratively until a steady-state solution is reached.

The problems with this approach are that:

- unsteady solutions are difficult to address.
- internal boundary conditions must be supplied inside the channel, and the exact boundary condition requirements will vary between scenarios, and
- some knowledge of the intricacies of the particular programme used to calculate the flows is required before it can be safely said to give reliable answers. This means expense, uncertainty and time for any company using this kind of software.

In attempting to address some of these problems, Kutija and Hewett (Journal of Hydraulic Research, vol. 40, no. 2, 2002) have arrived at a different solution approach. In applying their NewC finite difference scheme to the flows in a channel containing transcritical flows, they were able to furnish one boundary condition at the start and end of the ***entire channel*** and come up with a stable solution to the discretised governing equations.

2.2 The NewC Scheme

The NewC finite difference scheme employs a staggered mesh and is one of many discretisations of the St Venant continuity and momentum equations in time and space. The NewC computational molecule is shown in Figure 1.

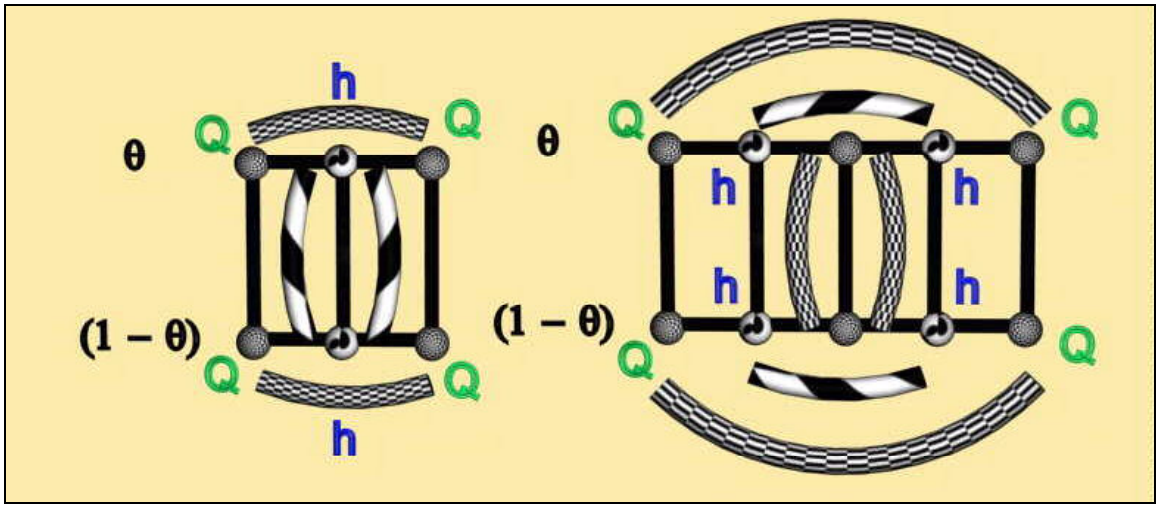

Figure 1 - NewC finite difference scheme computational molecule

The finite difference equations derived from this computational molecule are the same as those published by Kutija and Hewett for the NewC scheme (with the exception of a factor of ½ in the convective acceleration term, which is perhaps a typographical error). The NewC finite difference momentum and continuity equations follow:

$$Q_j^{n+1} - Q_j^n + \frac{\beta \Delta t}{2\Delta x} \frac{Q_j^{n+\frac{1}{2}}}{A_j^{n+\frac{1}{2}}} \left\{ \Theta \left(Q_{j+1}^{n+1} - Q_{j-1}^{n+1} \right) + (1-\Theta) \left(Q_{j+1}^{n} - Q_{j-1}^{n} \right) \right\} +$$

$$\frac{\Delta t}{\Delta x} g A_j^{n+\frac{1}{2}} \left\{ \Theta \left(h_{j+\frac{1}{2}}^{n+1} - h_{j-\frac{1}{2}}^{n+1} \right) - (1-\Theta) \left(h_{j+\frac{1}{2}}^{n} - h_{j-\frac{1}{2}}^{n} \right) \right\} + \Delta t g A_j^{n+\frac{1}{2}} \frac{Q_j^n \left| Q_j^{n+1} \right|}{\left(K_j^{n+\frac{1}{2}} \right)^2} = 0 \qquad (2)$$

NewC momentum equation

$$h_{j+\frac{1}{2}}^{n+1} - h_{j+\frac{1}{2}}^{n} + \frac{\Delta t (1-\Theta)}{b_s \Delta x} \left(Q_{j+1}^{n} - Q_j^{n} \right) + \frac{\Delta t \Theta}{b_s \Delta x} \left(Q_{j+1}^{n+1} - Q_j^{n+1} \right) = 0 \qquad (3)$$

NewC continuity equation

In arriving at these equations, some assumptions about the actual discretisations had to be made in addition to those explicitly stated by Kutija and Hewett. The discretised grid needs to supply water depths at non-nodal points, for example the water area at j, n + ½. Kutija and Hewett suggest that:

$$A_j^n = \frac{1}{2} \left(A_{j-\frac{1}{2}}^n + A_{j+\frac{1}{2}}^n \right) \qquad (4)$$

This is a reasonable approximation. In addition, no mention is made of how a water level is calculated at n + ½. If we take the average of n and n+1, there is a further complication, because the water level at n+1 is one of the things that the programme is trying to find. Therefore iteration has been used to obtain a value for A_j^{n+1}, and then this was averaged with A_j^n to obtain a value for $A_j^{n+1/2}$.

For comparison with the NewC scheme, Preissmann's box scheme was developed. Whilst this scheme can only handle subcritical flows (with one boundary condition at each end), or supercritical flows (with two boundary conditions at the upstream end), it serves as a contrasting comparison for the NewC scheme.

2.3 Tests and Results

2.3.1 Single Bedslope Tests

A number of simple tests for flows through a prismatic channel (i.e. constant bedslope, cross-sectional area and roughness) were conducted. They were aimed at:

- confirming the results presented by Kutija and Hewett, and
- verifying that the NewC calculation routines developed for this paper were the same in substance as those in the original reference.

2.3.1.1 Subcritical Flow Drawdown Curves

In the first test a steady, gradually varied flow (more specifically a drawdown curve) was simulated in a prismatic channel. The test conditions were: downstream depth, y_{ds} = 1m ; S = 0.002 ; Q = 100 m^3/s ; Chezy coefficient C = 50$m^{1/2}/s$, Δt = 100s and Δx = 60m. This data corresponds to an M2 backwater curve.

The NewC scheme, Preissmann's box scheme and the direct step method were all applied to this same problem. The three computational methods gave the same depths to within ± 6mm (i.e. a 12mm band) of each other for a subcritical drawdown curve. The results are displayed in Figure 2.

The results from NewC and Preissman's box scheme were determined by running the numerical models to steady state from an arbitrary initial condition of uniform flow. After time zero when the model was released from its initial conditions, the model results entered a transient phase in which waves and disturbances propagated up- and downstream, eventually settling down to a steady state solution. On the other hand, with the direct step method, there is no time stepping involved and the steady state solution is computed directly without a transient phase.

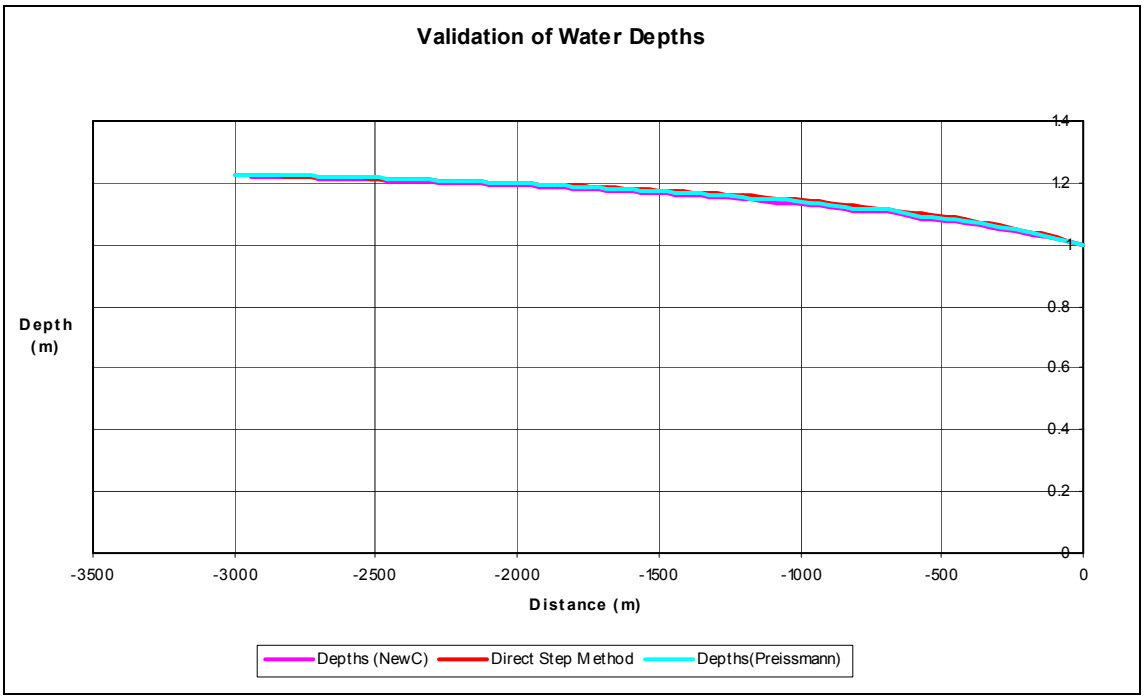

Figure 2: Drawdown curves computed by Preissman's box scheme, NewC and the direct step method.

2.3.1.2 Subcritical and Supercritical Uniform Flow Tests

The results published by Kutija and Hewett for uniform flow in supercritical and subcritical flow regimes were checked. The test conditions are in Table 1 below.

Q	*y_c (m)*	*Critical Slope*	*Slope*	*C* ($m^{1/2}/s$)	*y (m)*	*Froude N°*
50	0.29	0.0144	0.002	50	0.37	0.71
100	0.47	0.0088	0.01	50	0.34	1.59
250	0.86	0.0048	0.02	50	0.50	2.25
500	1.36	0.0032	0.03	50	0.70	2.75
1000	2.10	0.0023	0.04	50	1.00	3.16
1500	2.84	0.0016	0.05	50	1.13	3.99

Table 1: NewC results for various uniform flow conditions from Kujita and Hewett (2002)

Uniform flows were achieved in the majority of the channel by applying a constant flow at the upstream boundary and a weir-type equation at the downstream boundary.

The first major result which distinguishes the NewC scheme from other finite difference schemes, is obtained here. For the range of sub- and supercritical flow conditions in Table 1, NewC remained stable, even with a boundary condition imposed at each end of the reach and the supercritical Froude numbers ranging from about 1.6 to 4.0.

2.3.2 Multiple Bedslope, Steady State, Transcritical Tests

A steady state transcritical flow scenario published by Kutija and Hewett was also tested (Figure 3, right). The bed profile is the lowest of the three lines displayed in Figure 3; above it is the water surface and, (at left only) the total head line. Figure 3 at left shows the output from the NewC finite difference model developed for this paper [which coincides almost exactly with the published results].

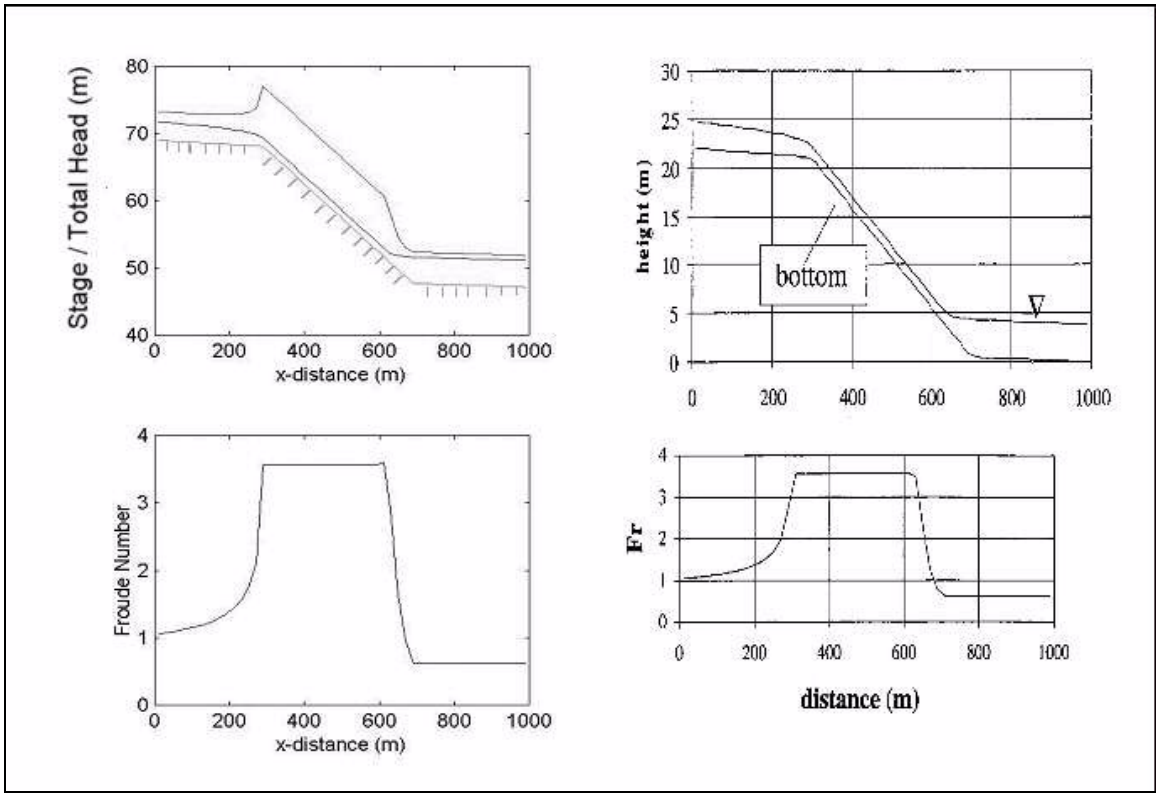

Figure 3: Multiple slope tests with transcritical flows: This Paper (L) (lowest curve is the bed, middle curve is the water surface and the top curve is the total head line.) Kutija and Hewett (2002) (R).
Conditions: Slope: 300m at 0.0033, 400m at 0.0510, 300m at 0.0016. Channel width = 100m
Upstream Q = $1500m^3/s$, Downstream Q = $200y^{3/2}$, C = $50m^{1/2}/s$, Δx = 20m, Δt = 10s

One parameter which was not plotted by Kutija and Hewett, but is plotted here as a check is the total head line. The 'jump' in total head at a chainage of about 300m is of critical importance; it indicates an increase in the total energy of the system, which cannot physically occur. The total head (H) at any point in the system is given by:

$$H = \frac{v^2}{2g} + y + z \tag{5}$$

so clearly either the flows or the water depths must be incorrect in Kutija's results. The flows are correct (they settle to the steady, imposed boundary flow condition value throughout), so the water depths generated in this model are incorrect.

Further experimentation performed on the energy jump indicated that:

- The energy jump is independent of the spatial mesh resolution.
- The difference in slope between the mild and steep slopes is the most important determinant of the jump magnitude.
- The flow magnitude also contributes to the spike magnitude.

A second feature of these results is a strange flow profile on the mild upper slope between chainage 0 and 300m. Despite the flow being supercritical on a mild slope, no backwater curve profile seems to match i.e. it is not an M3 curve, nor an M2, nor an M1 (see Figure 4). It is a physically impossible flow profile.

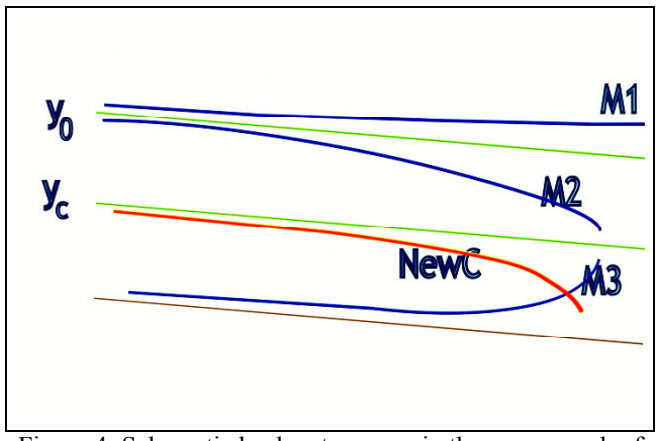

Figure 4: Schematic backwater curve in the upper reach of the transcritical flow test from chainage 0 – 300m

An additional problem with the results in Figure 3 is that the NewC finite difference model does not generate a hydraulic jump at the boundary between supercritical and subcritical flow.

2.4 Discussion

The NewC scheme can stably model flow that has Froude numbers spanning either side of unity with only one boundary condition at each end, regardless of whether the flow is supercritical or subcritical at the boundaries. This is a major achievement for a finite difference scheme.

Experimentation revealed that:

- stability of the NewC scheme is not assured when dealing with transcritical flows.
- at Courant numbers ($u\Delta t/\Delta x$) around 1 and with $\theta > 0.5$, the scheme is usually stable.
- imposing a downstream weir-type equation, rather than a non-normal depth, instability was less likely to develop.
- when the scheme does become unstable at very high Courant numbers ($u\Delta t/\Delta x \approx 100$), the instability was observed to be less severe than the rapidly growing instabilities seen when with $\theta < 0.5$, although oscillations developed in the water surface, in both the upstream and downstream directions.
- removal of the convective acceleration term in Preissman's box scheme yielded exactly the same numerical results as the NewC finite difference scheme (results not included here). The reason for this surprising result is yet to be determined.

2.4.1 Hydraulic Jumps

The absence of the hydraulic jump is unfortunate for the NewC scheme. NewC gives no discontinuity or upwards slope in the water surface at the supercritical to subcritical transition. This impacts very negatively on the usefulness of the NewC scheme because the location and magnitude of the hydraulic jumps are important aspects in assessing the steady-state flow profile of a transcritical flow.

Further downstream, the normal depth for the bedslope is correctly achieved. The achievement is not a significant one from a modelling perspective, because only one hand calculation per bedslope is required to arrive at the value in any case. There is no drop in the energy line around the location of the hydraulic jump, meaning that the flows immediately downstream of where the hydraulic jump should be located will have too much energy and accordingly, velocities and depths which are incorrect. The zone of suspect depths draws to an end only as the normal depth is approached.

To make NewC more accurate by including the hydraulic jump equation would be a difficult task. It would probably involve separating the reach into subcritical and supercritical zones, and, effectively, stitching them together using the hydraulic jump equation. For steady flows, this equation is:

$$\frac{y_2}{y_1} = \sqrt{8(F_1)^2 + 1} - 1 \tag{6}$$

The process would seem to be easier than with other schemes, because boundary conditions could be supplied at both ends of the reach always, but NewC's suspect supercritical modelling needs to be more fully investigated before it is used to evaluate supercritical sections using a boundary condition at each end. In addition, this approach would run counter to the fundamental simplicity that NewC is aiming for. The goal with NewC has been to simulate *all* flows with a boundary condition at each end of the reach, and discretisation of the reach into regions of subcritical and supercritical flow would undermine that simplicity.

2.4.2 Energy Artefacts

NewC produces energy "artefacts" (impossible jumps in the total head line) at changes between a mild and a steep slope. Energy or total head can never increase in the downstream direction without external input. Therefore, there must be an error in either the water heights or the flows at the transition point to produce the erroneous jump in energy. The flows are steady and correct at the input value, so the water levels must be incorrect on at least one side of the change in slope.

This highlights the fundamental issue, that supercritical flow perhaps cannot be adequately modelled with one boundary condition at each end of the reach. For these reasons, it is probable that the energy artefacts are manifestations of a system that is not simulating the physical information flow and therefore cannot be expected to simulate physical realities like a constantly decreasing total energy.

In a transcritical flow, the flow may (i) change from supercritical to subcritical flow or vice versa and (ii) be steady (with a stationary hydraulic jump if the flow is from supercritical to subcritical flow) or unsteady (with a travelling bore). When the flows are ***steady*** and there is a change from ***supercritical to subcritical*** flow, the transition is marked by the presence of a hydraulic jump. The loss in (mechanical) energy across the hydraulic jump varies with $(y_2 - y_1)^3$ where y_1 and y_2 are the depths either side of the jump. That the power is an ***odd*** number i.e. 3, is significant since it shows that energy considerations indicate the direction of flow or the '***arrow of time***'. That is, $(y_2 - y_1)^3$ is a quantity whose sign depends on the relative magnitude of y_1 and y_2. (Had the power been an ***even*** number, the energy loss would always be positive and therefore, considerations of energy would be unable to discern the direction of flow.) Obviously, the flow through a hydraulic jump is unable to gain energy without some external energy source i.e. there can only be an energy loss through a hydraulic jump. Consequently, any valid solution must satisfy the momentum equation and be compatible with energy losses across a hydraulic jump. It is interesting that unlike considerations of energy, momentum (and continuity) considerations do ***not*** give any information on the direction of flow. Hence a model based on momentum (and continuity) and applied to transcritical flow falsifies energy.

2.4.3 Suitability for Hydraulic Modelling Implementation

The NewC scheme is not suitable for implementation into a major hydraulic modelling code, such as those used commercially. The first problem would be stability. Using downstream depths and not a downstream weir equation can generate energy spikes at the downstream boundary and may trigger instabilities. This may frustrate attempts to implement NewC in major hydraulic models where a common approach is to allow any sort of boundary condition, but to keep the boundaries well away from the region of interest. NewC must also accurately model transitions (especially hydraulic jumps) and should have a constantly declining total head line. The great danger with this model is its seeming simplicity and propensity to give believable results. A cursory examination of NewC's results would reveal no problems. The water surface is smooth and continuous, with deeper water in places where, intuitively, the water should be flowing more slowly. Only on closer inspection do problems become apparent. An experienced hydraulic modeller or designer would baulk at the fact that there are no hydraulic jumps where they would be expected. Dangerously, however, this may seem to be the only fault with the model, and design could proceed based on the water surfaces outside the transition region. As has been shown, these regions give incorrect water surfaces *despite* intuitively looking plausible.

3. CONCLUSIONS

- NewC is able to stably model single slope sub- and super-critical flows with a single boundary condition at each end of the reach.
- Stability is not assured when modelling transcritical flows.
- NewC correctly produces the normal depth and a uniform flow rate when modelling transcritical flow.
- NewC produces erroneous backwater curves and impossible jumps in the total head of the system.
- NewC does not replicate hydraulic jumps.
- The scheme is not yet suitable for inclusion in a hydraulic modelling software package.

4. REFERENCES

Kutija and Hewett (2002), Modelling of supercritical flow conditions revisited: NewC Scheme, *Journal of Hydraulic Research*, Vol 40, pp145-152

Cunge, J., Holly, F. and Verwey, A. (1980) Practical Aspects of Computational River Hydraulics, Pitman Publishing, London, 436 pp

Kutija (1993), On the Numerical Modelling of Supercritical Flow, *Journal of Hydraulic Research*, Vol 31, pp841-848

Molinas and Yang (1985), Generalised Water Surface Profile Computations, Journal of Hydraulic Engineering, Vol 111, pp 381-397

The Institution of Engineers, Australia
8th National Conference on Hydraulics in Water Engineering
ANA Hotel Gold Coast, Australia 13-16 July 2004

Disaster Mitigation in Central Vietnam: Application of Two-dimensional Hydraulic Models

I.F. Wood
B.E., MEngSc
Senior Engineer, Kellogg Brown & Root Pty. Ltd., Australia
S.E. Murphy
B.E., MEngSc
Senior Engineer, Kellogg Brown & Root Pty. Ltd., Australia
N.H. Phuong
M.E.
Hydraulic Engineer, Institute of Water Resources Planning, Ministry of Agriculture & Rural Development, Vietnam

Abstract: The paper describes the application of two-dimensional hydraulic models as part of a floodplain management planning process for Quang Ngai Province, in coastal central Vietnam. In recent years significant flooding has caused many deaths and large losses, which have had the effect of limiting prospects for this already disadvantaged and vulnerable community. The Australian government's agency for international development, AusAID and the Government of Vietnam are jointly funding the Quang Ngai Natural Disaster Mitigation Project which aims to reduce vulnerability and improve the long-term prospects in the region. One component of this project is the development of floodplain management plans for the river systems of the densely populated and flood affected low land areas.

Two hydraulic models were developed using SOBEK from Delft|Hydraulics. These covered a total area of over 700km^2 containing a population of over 600,000 people. Discussion focuses on the innovative solutions applied to the challenges of developing large-scale models on a floodplain containing many features of hydraulic significance.

Keywords: Floodplain Management, Two-Dimensional Hydraulic Model, PEST Calibration, Quang Ngai, Vietnam

1. INTRODUCTION

Two separate 2-dimensional hydraulic models were developed for severely flood-affected regions of coastal Vietnam. The models were applied as part of the development of floodplain management plans for the Tra Khuc and Tra Bong Rivers in Quang Ngai Province.

Floodplain management planning is one component of the Quang Ngai Natural Disaster Mitigation Project which is jointly funded by the Australian government's agency for international development, AusAID and the Government of Vietnam. The overall objective of the Project is to reduce vulnerability and improve the long-term prospects for a community which in the past has been severely affected by flooding and other natural diasters. KBR (Kellogg Brown & Root Pty Ltd) was awarded the contract by AusAID to implement the project and commenced work in February 2003 with the establishment of a team and office in Quang Ngai city. This integrated project in natural disaster management is programmed to end in November 2005.

The floodplain management plan provides a "blueprint" for the future management of land based activities to limit the potential negative impact from on-going development on existing vulnerable flood prone communities. The plan also addresses the needs for disaster management planning at the Provincial Government level.

Two dimensional floodplain modelling and floodplain management planning are both relatively new concepts in this part of Vietnam. This, combined with the difficulties of obtaining reliable and consistent data and the sheer scale and complexity of the floodplain, created some unique and interesting challenges for the project hydraulic modelling team.

2. BACKGROUND

Quang Ngai Province (Figure 1) is located on the coast in Central Vietnam approximately 140 kms south of Da Nang. The Province has a total population of 1.2 million, of which 80% lives and works in small farming and fishing communities along the relatively flat coastal plain. Quang Ngai town itself has a population of 114,000 and is protected from small floods but a system of levees. In all, a population of over 600,000 (or 50% of the total province) is affected by flooding, and in some particularly vulnerable areas flood depths are over 3 m for 5 year and 10 year ARI events.

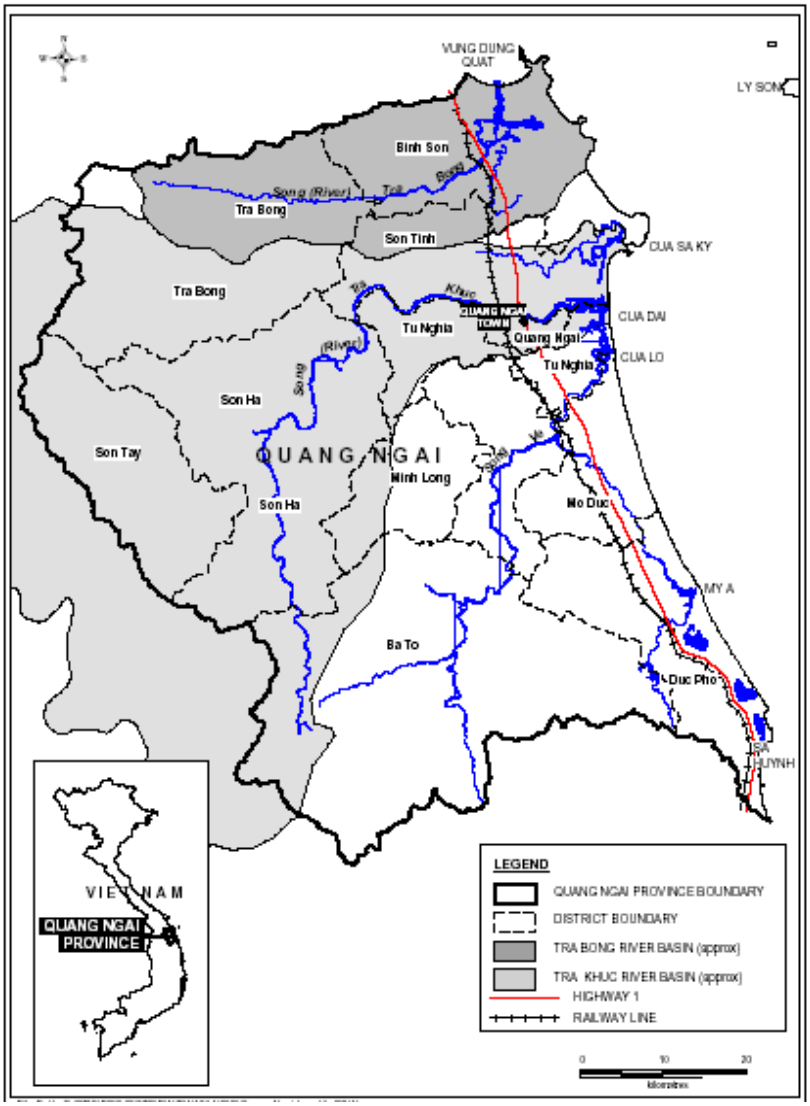

Figure 1 – Location Map

The combined pressures of poverty through low income-earning potential and the annual threat of disaster through flood or storm during the monsoon season have a severe impact on the prosperity and long term prospects of the region. For example, in the five year period from 1996 to 2000, natural disasters (mainly flooding) resulted in 325 deaths, the flooding of 207,000 houses, including the loss of 5,500 houses and the destruction or damage to 1,400 classrooms. Total damage costs for this period exceeded A$140 million. Poor families in rural areas are particularly vulnerable to the impacts of natural disaster because they have little capacity to absorb impacts such as the loss or damage to their dwellings, the loss of livestock or destruction of their crops.

It is because of the large impact on the rural poor that assistance through natural disaster mitigation is a key focus area for aid funding from many international donors. In particular, Central Vietnam has been targeted by the Australian government's agency for international development, AusAID through the A$15 million Quang Ngai Natural Disaster Mitigation Project.

The key components of the project are:

- a river basin management plan;
- community-based natural disaster management;
- "demonstration" infrastructure works including river bank protection, flood control dykes and a safe harbour for fishing vessels.

The river basin management plan in turn incorporates three parts: a floodplain management plan; a riverbank management plan and a fisheries infrastructure management plan. The hydraulic modelling discussed in this paper is a key feature of the floodplain management plan.

3. THE PROJECT AREA

The Project area encompasses three major river systems: Song Tra Khuc, Song Ve and Song Tra Bong. The catchment areas are 3,250 km^2, 1260 km^2 and 700 km^2 respectively. The rivers mainly run from West to East crossing the flat coastal plain which typically varies in width from 10 km to 16 km. The upper reaches of the catchments rise in the mountains to approximately 1400 m to 1600 m.

The climate is dominated by a strong monsoon from mid September to December. Of the total annual rainfall of 2400 mm at the coast, 1760 mm or 73% falls during the monsoon. In the highland areas of the upper catchment, the mean annual rainfall is in the order of 3500 mm.

The lower floodplains of the two larger rivers, the Tra Khuc and the Ve combine via a coastal waterway and a complex system of floodplain channels which drain collectively via a combination of three river mouths (refer Figure 2). The total flood affected lowland area of these two rivers is 350 km^2. While the Project area for the floodplain management plan only covers the Tra Khuc River, it was necessary to model both river systems.

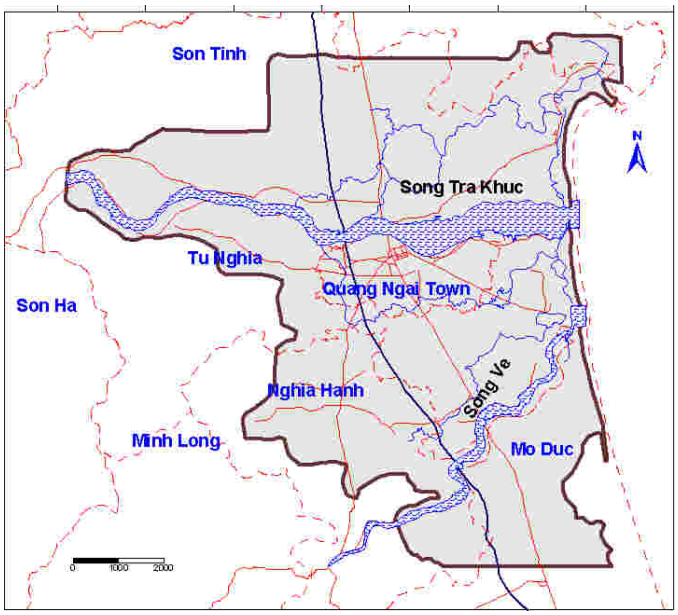

Figure 2 – Song Tra Khuc and Song Ve Model Area

The Tra Bong River lies 20km to the north and is not connected to the other systems (refer Figure 3). The Tra Bong River in the lower floodplain area bifurcates a number of times into a network of interconnected waterways. The flood-affected low land area is 75 km^2.

Flooding in both floodplain systems is strongly influenced by the embankments from main north-south rail and road routes. The embankments intersect the main direction of flow at right angles and are typically raised up to two metres above the surrounding floodplain to provide some flood immunity. In addition, development (land filling for residential and commercial purposes) tends to ribbon out along these main routes. Culverts and bridges are few and far between for the quantity of floodplain flow hence the combined effect is that there is considerable afflux across the embankments.

Other significant floodplain features include raised embankments for irrigation channels, flood protection levees around population centres and aquaculture ponds built out into the waterways in estuarine areas.

Infrastructure in the region is developing rapidly with several new proposals for major roads, industrial areas and further flood protection levees. Additionally in many estuary areas unplanned and unlicensed development of aquaculture ponds continues to encroach on the waterways. This ongoing development pressure, together with a perceived worsening of flooding over recent years, is the driving force behind the need for a coordinated whole-of-floodplain planning approach. A floodplain management plan requires a hydraulic model as the basis for assessment. Further, a two-dimensional hydraulic model was considered the only suitable approach to simulate the complex nature of the floodplain and the development options under consideration.

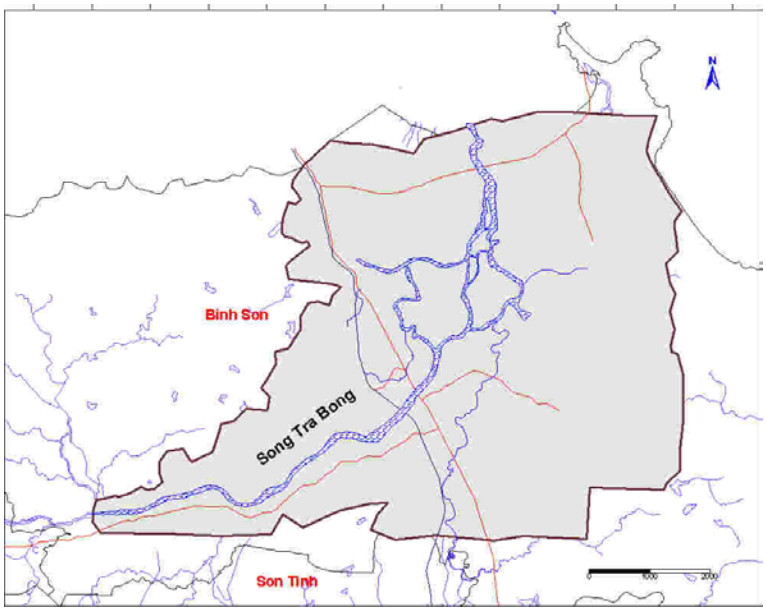

Figure 3 – Song Tra Bong Model Area

4. CHALLENGES FOR MODEL DEVELOPMENT

4.1 The Hydraulic Model

The selection of the most appropriate modelling software took into account many factors including costs, model capacity, model stability, run time, existing familiarity, software support and ease of use. An important factor in model selection was that technology transfer and capacity building were key outcomes for the Project. The modelling team included a Vietnamese expert from a central government agency who will ultimately inherit the software and hardware and will be responsible for maintaining the model. From this point of view key criteria were ease of use, flexibility, model documentation and ongoing software support and training.

After consideration of several alternatives, the SOBEK overland flow modelling package produced by Delft|Hydraulics was considered to be the most suitable. SOBEK features a robust 2-d finite difference algorithm plus the ability to incorporate 1-d elements, direct rainfall and meshed overlapping grids. Documentation, user interface and on-going support also met with requirements.

A daunting task at the commencement of the project was to take in the sheer scale of the project area. SOBEK operates with rectangular mesh with a fixed grid size over the floodplain area. The desire to have fine resolution to simulate delicate features was balanced against the constraints of run time and available data. The maximum feasible run time was considered to be 12 hours, and it was found that run times increase in a proportion greater than the square of the number of computational cells.

After several trials, the feasible maximum number of grid cells was found to be in the order of about 350,000. The adopted grid element sizes for the Tra Khuc and Tra Bong River models were 50x50 m and 30x30 m respectively. Run times were approximately 10 hours to simulate a 75 hour event (run on a 3.1GHz Dell Xeon).

4.2 Existing Spatial Information

The majority of the floodplain elevation data came from a previous survey conducted by others. While the total of 30,000 points from these surveys on the floodplain initially sounded impressive, it translated to an average point density of only 40 and 51 points per square kilometre on the Tra Khuc and Tra Bong floodplains respectively. Based on the adopted grid dimensions of 50 m and 30 m, the corresponding model point density is 400 and 1100 points per square kilometre respectively. Although the level of model detail on the floodplain is considered to be quite sparse, this density was considered adequate for the purposes of broad scale floodplain management planning.

Extensive checking and refinement of the x-y data associated with the floodplain information was undertaken to ensure consistency with known floodplain features. Coordinate projection systems are somewhat confusing in Vietnam with old data typically presented in a variety of different systems dating back to French and American periods of occupation. Further, not only is the projection system for new data (VN2000) incompatible with other international standards, but the information required to convert between systems is not available due to national security issues. These were among the many challenges at the early stage of the project which were frequently frustrating and time consuming, but were surmountable in the end.

4.3 New Survey Data

To make up for deficiencies in detail on the floodplain and to ensure that the most critical elements of the system were adequately modelled, an extensive survey of the main hydraulic features was commissioned. This included rivers and estuaries as well as the road, rail and irrigation channel embankments and culvert openings. Aerial survey technologies such as photogrammetry and laser altimetry were not an option for the project, so all survey was undertaken with traditional methods.

This new survey provided an additional 7,800 individually surveyed points made up of 1161 hectares of detailed survey, 645 cross sections of river and creek channels, 1030 cross sections on road, rail and channel embankments and details of 400 culverts and bridges.

Knowing by this stage that there were risks in assuming validity of the data, we undertook extensive cross checking of level information to ensure consistency. Numerous inconsistencies in level information from different sources were traced back to non-standard "standard" benchmarks, which initially created a degree of confusion. For example at one particular location five different levels were obtained from four separate sources of information. The numerous changes to level information during the course of model development required that the model topographic grid to be assembled in a very rigorous fashion so that the model could be re-assembled from its component parts in the event of a change.

A feature of the main river system is the fluvially active sandy river mouths on the Tra Khuc and Ve rivers. During the dry season coastal processes and tidal flows tend to fill in the river mouths, resulting in the Tra Khuc mouth being very small and the Ve mouth closing completely. While the modelling team was still contemplating how best to estimate mobilisation of the river and widening of the river mouth, we were fortunate to experience a relatively major flood event (in October 2003). So just three weeks after a dry season survey, the river mouths were re-surveyed to obtain the post flood profile. In the Tra Khuc scour reduced bed levels by up to 7 m and resulted in a net loss of 235,000 m^3 sediment from the river mouth area.

4.4 Model Development

Model grids for topographic data were generated using a Surfer® digital terrain model created from the survey data for the floodplains and the major waterways. Narrow linear features such as embankments and floodplain waterways were later inserted directly into the model grid using specifically written software to ensure the appropriate connectivity and continuity.

Details of 97 individual culverts and small bridges were also added directly into the model using software based on a generalised relationship developed between actual culvert opening width, model grid opening, orientation to the grid direction and a factored Manning's *n*.

The spatial distribution for the initial base values of Manning's *n* was generated from land use mapping information developed by the Province. Land uses such as rice paddy, other agriculture, forest, urban residential

and industrial were initially assigned a unique *n* value across the model grid generated using the Vertical Mapper™ spatial analysis tool in MapInfo®.

4.5 Model Calibration

The hydraulic models of the Tra Khuc/Ve River system and the Tra Bong River were calibrated to an extensive set of water level information from the major flood of December 1999. Flood levels for three major recent events (including the December 1999 event) are recorded on concrete flood marker posts at 32 locations throughout the floodplain. Flood level data was also available at an additional 583 locations which were surveyed from flood marks immediately following the 1999 event.

Inflow hydrology was based on rainfall routing models calibrated to recorded streamflow information upstream of the main floodplain on the Tra Khuc and Ve rivers. The quality of the streamflow data is considered good because a full-time staff of four people attend each gauging station and it is normal practice to conduct gaugings regularly during each significant flow event. Peak inflows during this event were 10,700 m^3/s, 2,600 m^3/s and 1,900 m^3/s on the Tra Khuc, Ve and Tra Bong rivers respectively.

This quantity of calibration data is quite unique for most modelling studies and so application of the automatic optimisation program PEST (Doherty, 2002) for the Tra Khuc River model was considered appropriate. Because run time is a key constraint to effective calibration, a "cut down" version of the Tra Khuc Model was created with a shortened hydrograph and less extensive floodplain. This version of the model adequately represented the core features of the floodplain immediately to either side of the river. By doing this run times were reduced to two hours which proved just feasible for the application of PEST.

PEST was used to calibrate Manning's *n* values for four separate sections of the main river plus the two dominant land use types. While initial optimisation iterations were quite effective, the calibration process tended to slow down with little further improvement for subsequent iterations. The PEST outcomes usefully highlighted deficiencies in the structure of the model as Manning's *n* values in certain locations were pushed past normally accepted bounds. This helped focus review to the particular areas of the model where problems were occurring. Thus PEST was applied in parallel with manual changes to the model topography (for example culvert relationships) to achieve an acceptable calibration of the model.

PEST proved to be a useful tool in calibration when used with the traditional calibration method of manual judgement by eye. The main constraint was the time required — often a single PEST optimisation iteration would require up to 12 model runs, taking over 24 hours. While the data set obtained in this study would be suitable for additional investigation of the applicability of PEST in two-dimensional hydraulic modelling.

5. MODEL APPLICATION

At the time of writing application of the model is still on-going. Design events were run over the range of 100 year ARI to 2 year ARI to map inundation for each event. For example Figures 4 and 5 show the depth and extent of flooding for a 100 year ARI event on the Tra Khuc and Tra Bong floodplains. Figures 6 and 7 show hazard maps generated from the product of depth and velocity. These were used to identify the major conveyance routes through the floodplain areas and to highlight problem areas and evacuation routes.

The 100 year ARI peak inflows were estimated at 18,000 m^3/s, 4,800 m^3/s and 2,600 m^3/s on the Tra Khuc, Ve and Tra Bong rivers respectively.

Additional testing of "what if" scenarios was undertaken with the model to investigate a variety of development scenarios including floodplain filling, new road proposals and flood protection levees. Selected opportunities for flood improvement works were also investigated. Large scale flood improvement works proved not feasible, hence the emphasis in flood management was a philosophy of "living with floods": harm minimisation, and management planning to ensure existing problems are not unduly exacerbated, and that looming development in the floodplains does not lead to disasters of even worse magnitude than experienced to date.

The Tra Bong model was also used to undertake hydraulic design of anti-salinity dyke works in the lower estuary, and assess the impact of the escalating development of aquaculture ponds in the estuary waterways.

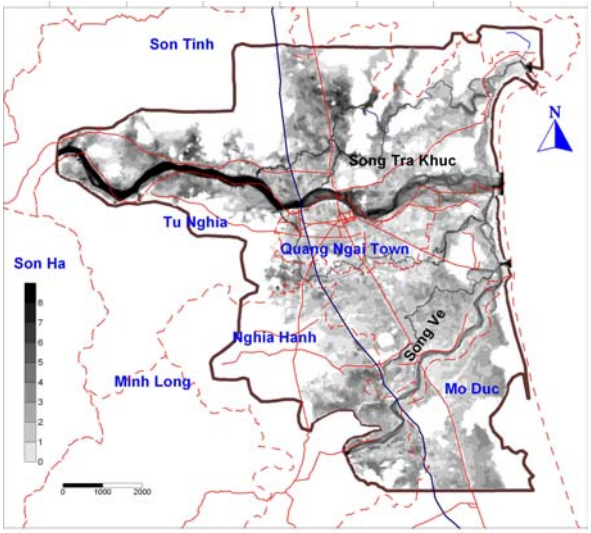

Figure 4 – Flood Depths and Extent of Flooding, Song Tra Khuc and Song Ve

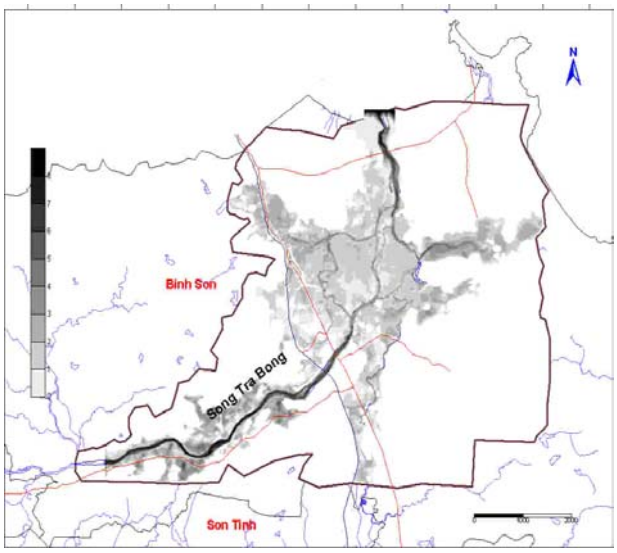

Figure 5 – Flood Depths and Extent of Flooding, Song Tra Bong

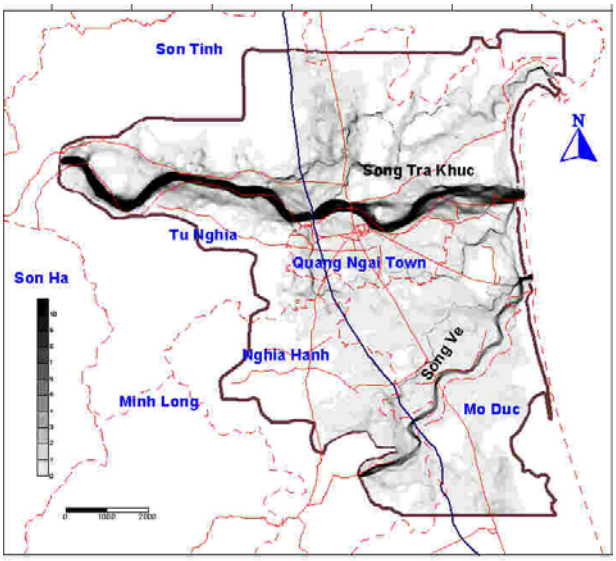

Figure 6 – Depth Velocity Product, Song Tra Khuc and Song Ve

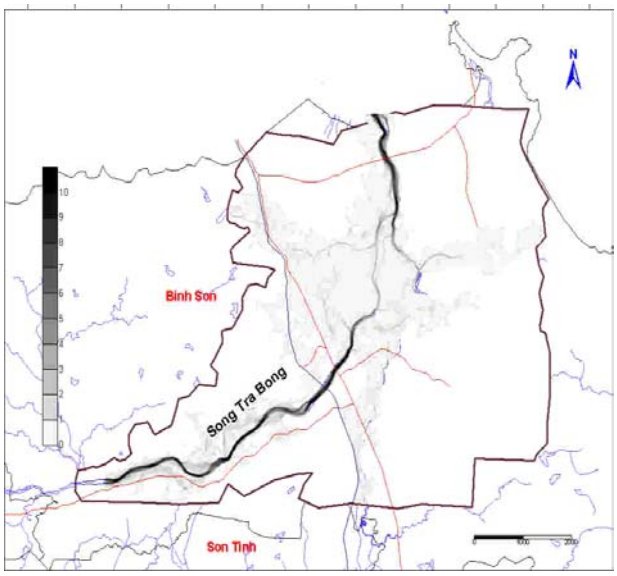

Figure 7 – Depth Velocity Product, Song Tra Bong

6. FLOODPLAIN MANAGEMENT PLANNING ISSUES

The key issue for floodplain management planning was to generate a sense of awareness in the government bodies and the general community that all activities in the floodplain are linked. These kinds of planning concepts are relatively new in an area which is developing rapidly. Communication was approached through a series of meetings with counterpart staff, and workshops with a wider range of stakeholders.

Despite some initial uncertainties, the general acceptance of planning concepts was quite encouraging. While not being insensitive to the hardships to some brought about by major flooding experienced during the course of the investigations, we were fortunate that this event fuelled the concept that structural works on the floodplain can have positive and negative impacts. In this instance, influential community figures spoke publicly about perceived worsening of flooding in some areas following the construction of levee works in a different area — exactly the message we had been trying to convey.

Through the workshop process we were able to introduce concepts such as the retention of floodway conveyance and the importance of flood storage volume. By dividing workshop attendees into small groups and issuing questionnaires we were also able to obtain feedback on issues such as acceptable levels of flood impact and

desirable flood immunity for different types of new development. This feedback formed the basis for developing a plan which was consistent with local expectations.

A key feature in establishing our credibility was having a 2-dimension hydraulic model and being able to present the results and outcomes of the modelling in a way that was easily understood.

7. CONCLUSIONS

Two-dimensional hydraulic models were developed for the floodplains of the Tra Khuc/Ve River system and the Tra Bong River in coastal central Vietnam. The combination of model scale and data uncertainty posed a unique set of challenges for model development. New technologies, in the form of specialist software and GIS tools, were used to assemble the model from its component features in a way that retained the critical hydraulic characteristics.

The availability of a large number of spatially distributed recorded flood levels enabled the use of the automatic parameter optimisation routine PEST to assist in the calibration process. Although model run time was a significant constraint to PEST optimisation, it proved to be a useful tool to highlight deficiencies in the model and target areas for further refinement.

The ability of the model to generate impressive looking and easily understood output proved invaluable in the consultation processes for the development of the floodplain management plan. Despite the fact that stakeholders were initially unfamiliar with the concepts involved in floodplain planning, a good rapport and understanding was quickly developed while using the model to illustrate critical issues.

The rewards from this Project will be on-going. Not only does the floodplain management plan provide lasting benefit to a community in need but our Vietnamese expert on the modelling team has received invaluable training in flood modelling over the 10 months of the project. The potentially lasting benefits of this are critical in a country where more than 50% of the total population is affected in some way by flooding.

8. REFERENCES

Doherty, J. (2002). *PEST Model-Independent Parameter Estimation,* Watermark Numerical Computing, 279p.

MapInfo Professional Version 7.0 User's Guide, MapInfo Corporation, 2002, Troy, New York, 759p.

Surfer Version 8 User's Guide, Golden Software Inc, 2002, Golden, Colorado, 640p.

Vertical Mapper User Guide, Northwood Technologies Inc and Marconi Mobile Ltd, 2001, Canada, 243p.

The Institution of Engineers, Australia
8th National Conference on Hydraulics in Water Engineering
ANA Hotel Gold Coast, Australia 13-16 July 2004

Numerical Modelling for Wave-Induced Pore Pressure in Marine Sediments: Case Study at East Coast in Australia

H. Zhang
B.E., Ph. D.
Lecturer, Griffith University, Australia
D.-S. Jeng
B.E., M. E., Ph.D.
Senior Lecturer, The University of Sydney, Australia

Abstract: In this paper, a case study for the wave-induced pore pressure in marine sediments is presented. An integrated three-dimensional model, combining wave model (SAWN) and soil model (PORO-WSSI), is established to investigate the wave-induced pore pressures in marine sediments. Based on the data in East Coast region in Australia, the distributions of the wave-induced pore pressure with different time intervals are presented. Also, the effects of the degree of saturation on the wave-induced pore pressure in marine sediments are examined through a parametric study.

Keywords: pore pressure, wave model, soil model, marine sediments

1. INTRODUCTION

The evaluation of the wave-induced pore pressure is important for numerous engineering issues. For example, the wave-induced pore pressure is the key factor in the determination of the seepage flow; stability of the seabed (including liquefaction and shear failure) near marine structures; modelling of water quality in marine environments etc.

Numerous investigations for the wave-induced seabed response have been carried out since the 1970's. Among these, analytical solutions, including un-coupled models (Liu, 1973), diffusion models (Moshagen and Torum, 1975), Biot consolidation models (Yamamoto et al., 1978; Mei and Foda, 1981; Jeng and Hsu, 1996), dynamic models (Jeng et al., 1999; Jeng and Cha, 2003; Lin and Jeng, 2004) have been proposed. The contribution and limitation of previous studies in the area have been systematically reviewed in Jeng (2003). However, all previous models have been limited to two-dimensional case, which can only represent part of the whole problem. Thus, a three-dimensional model for such a problem is desired.

In this paper, a three-dimensional wave model (SWAN) will be linked with the poro-elastic model for the wave-induced seabed response (PORO-WSSI) into a numerical model. In the new model, the wave-induced pore pressure in a three-dimensional coastal region (East Coast) can be calculated. Based on the proposed model, a series of parametric study will be conducted to provide a better understanding of wave-induced pore pressure in a porous seabed.

2. MODELS

2.1 Wave Model (SWAN)

SWAN is a numerical model, which provides estimates of the wave parameters in coastal areas, lakes and estuaries with given wind, bottom and current conditions. It is a spectral wave model based on the action density balance equation (Booij et al., 1999; Ris et al., 1999), which calculates wave transformation and set up. The version (Cycle 3, version 40.20) used in present study is the time dependent version released to public in 2003. It takes into account the wind wave growth, dissipation by white-capping, bottom friction and wave breaking. The quadruplets and triads wave-wave interactions are also included. Furthermore, the model can simulate the wave propagation processes such as, propagation through geographic space, refraction due to spatial variations in bottom and current, shoaling due to spatial variations in bottom and current, blocking and reflections by opposing currents, and transmission through, blocked by or reflection against sub-grid obstacles.

In SWAN the evolution of the wave spectrum is described by the spectral action balance equation, which for spherical coordinates is (Holthuijsen et al., 2003):

$$\frac{\partial N}{\partial t}+\frac{\partial c_\lambda N}{\partial \lambda}+(\cos\varphi)^{-1}\frac{\partial c_\varphi N}{\partial \varphi}+\frac{\partial c_\sigma N}{\partial \sigma}+\frac{\partial c_\theta N}{\partial \theta}=\frac{S}{\sigma} \tag{1}$$

with longitude, λ; latitude, φ; the wave direction (the direction normal to the wave crest of each spectral θ component); the relative frequency (as observed in a frame of reference moving σ with current velocity); action density spectrum, N(σ, θ); propagation velocities and in λ, φ, θ and σ space, c_λ, c_φ, c_θ and c_σ; the source term in terms of energy density representing effects of generation, dissipation and nonlinear wave-wave interactions. In present study, the main corresponding input source is wind energy as:

$$S_{in}=A+BE(\sigma,\theta) \tag{2}$$

where A and B depend on wave frequency and direction, and wind speed and direction. The dissipation of white capping and bottom friction are considered, but the depth induce breaking is not taken into account.

The dissipation form of wave energy can be expressed in terms of three different contributions. They are: whitecapping, $S_{ds,w}(\sigma, \theta)$, bottom friction $S_{ds,b}$ (σ, θ) and depth-induced breaking $S_{ds,br}(\sigma, \theta)$. The detailed information for the wave energy dissipation can be found in (Holthuijsen et al., 2003).

2.2 Soil Model (PORO-WSSI)

Numerous poro-elastic models for the wave-induced soil response have been developed since the 1970's. Recently, the second author has develop a series of analytical solutions and numerical models for the wave-induced seabed response around marine structures. In this study, we adopted the solutions of three-dimensional short-crested wave-induced soil response in am infinite seabed with the wave model (SWAN) to examine the wave-induced pore pressure in a three-dimensional coastal region.

In the PORO-WSSI model, the consolidation equation (Biot, 1941) is generally accepted as those governing the flow of compressible pore fluid in a compressible porous medium. For a three-dimensional problem, and treating the porous bed as hydraulically anisotropic, with same permeability in the x-, y- and z-directions, respectively, the governing equation can be expressed as

$$K\nabla^2 p-\gamma_w n_e \beta\frac{\partial p}{\partial t}=\gamma_w\frac{\partial \varepsilon}{\partial t} \tag{3}$$

where p is the wave-induced pore pressure; γ_w is the unit weight of the pore-water; n_e is the soil porosity; and ε is the volume strain defined by

$$\varepsilon=\frac{\partial u}{\partial x}+\frac{\partial v}{\partial y}+\frac{\partial w}{\partial z} \tag{4}$$

where u, v and w are the soil displacements in the x-, y-, and z-directions, respectively.

The compressibility of the pore fluid, β, is related to the apparent bulk modulus of the pore fluid K′ and the degree of saturation Sr , such that

$$\beta=\frac{1}{K_w}+\frac{1-S_r}{P_{wo}} \tag{5}$$

where K_w is the true bulk modulus of elasticity of water (which may be taken as 1.95×10^9 N/m², Yamamoto et al., 1978), P_{wo} is the absolute water pressure. If the soil skeleton is completely air-free, i.e. fully saturated, then β=1/Kw, since S_r=1.

The equations for overall equilibrium in a poro-elastic medium, relating to the effective stresses and pore pressure, are given by

$$\frac{\partial \sigma'_x}{\partial x} + \frac{\partial \tau_{xy}}{\partial y} + \frac{\partial \tau_{xz}}{\partial z} = \frac{\partial p}{\partial x} \tag{6}$$

$$\frac{\partial \tau_{xy}}{\partial x} + \frac{\partial \sigma'_y}{\partial y} + \frac{\partial \tau_{yz}}{\partial z} = \frac{\partial p}{\partial y} \tag{7}$$

$$\frac{\partial \tau_{xz}}{\partial x} + \frac{\partial \tau_{yz}}{\partial y} + \frac{\partial \sigma'_z}{\partial z} = \frac{\partial p}{\partial z} \tag{8}$$

where Cauchy stress tensor on the adjacent faces of a stress element consists of three effective normal stresses and six shear stress components. The shear stresses are expressed in double subscripts τ_{rs}, denoting the stress in the s-direction on a plane perpendicular to the r-axis.

To integrate two models into one, first, we must calculate the wave characteristics (including wave profile, wavelength, water particle velocities and wave pressure at the surface of the seabed). Once we have the wave characteristics, the soil model will be used to determine the wave-induced pore pressure, effective stresses and displacements etc.

3. CASE STUDY: EAST COAST, AUSTRALIA

In this study, the coastal region at East Coast in Australia is used as a case study. The calculated domain covers the longitude from -30.8 to -30.3, and the latitude from 153.3 to 153.7. The water depth varies from shallow water to deep water (up to 120 m), as shown in Figure 1.

With the information in Figure 1, the distribution of wave height and wave direction calculated from the wave model (SWAN) is plotted in Figure 2. The input data of soil characteristics and the grid size used in the wave model is given in Table 1.

Table 1-Input Data Of Numerical Models

Parameter	Values
Grid size in the x-direction	1000 m
Grid size in the y-direction	1000 m
Grid number in the x-direction	49
Grid number in the y-direction	61
Wind speed	20 m/sec
Wind direction	135 degree
Lowest frequency	0.0521 Hz
Highest frequency	1 Hz
Number of frequency	32
Significant wave height at boundaries	3 m
Peak wave period at boundaries	10 sec
Soil permeability	0.0001 m/sec
Shear modulus	10^7 N/m^2
Poisson's ratio	0.3
Soil porosity	0.4

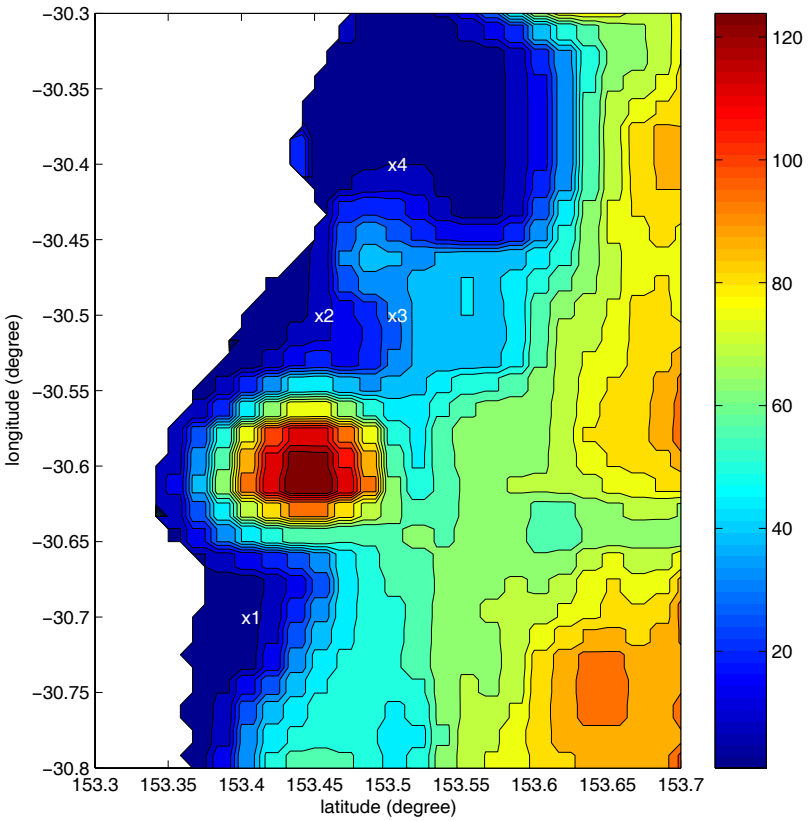

Figure 1- Topography Of East Coast Region In Australia.

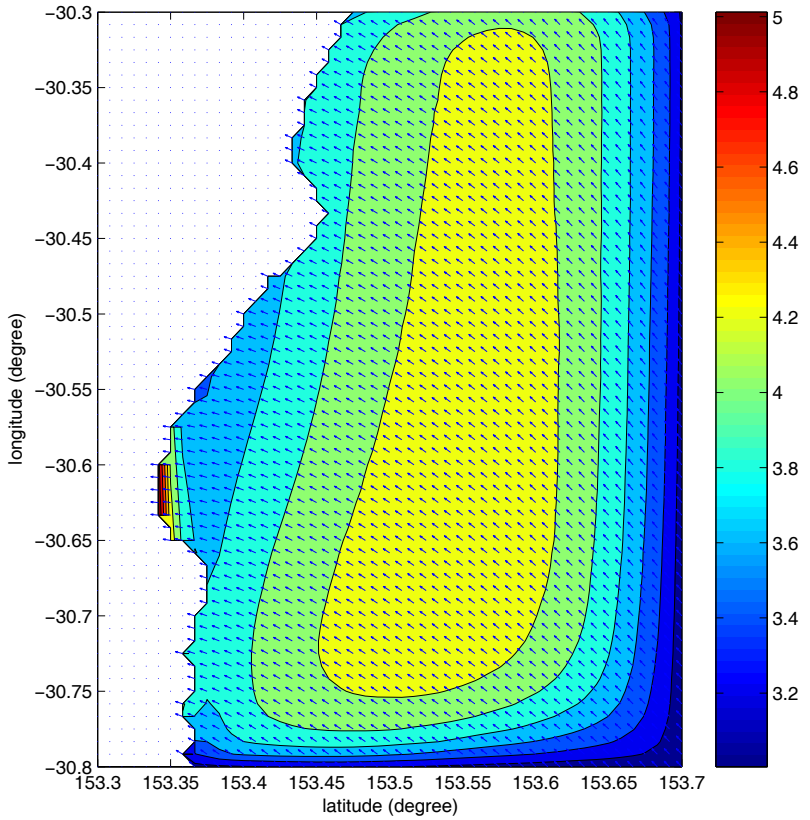

Figure 2-Distribution Of Wave Direction And Wave Height.

Based on the data given in Figures 1 and 2, we calculate the wave-induced pore pressure at different time intervals. Herein, we only present the contour distribution of the wave-induced pore pressure at time =2.25 sec in

Figure 3. The results presented in Figure 3 is at z=-1 m. As shown in Figure 3, two regions show the concentration of pore pressure. One is on the top area of Figure 3, and the other one is at the left corner. It is clear the results presented in Figure 3 cannot be predicted by the existing two-dimensional models.

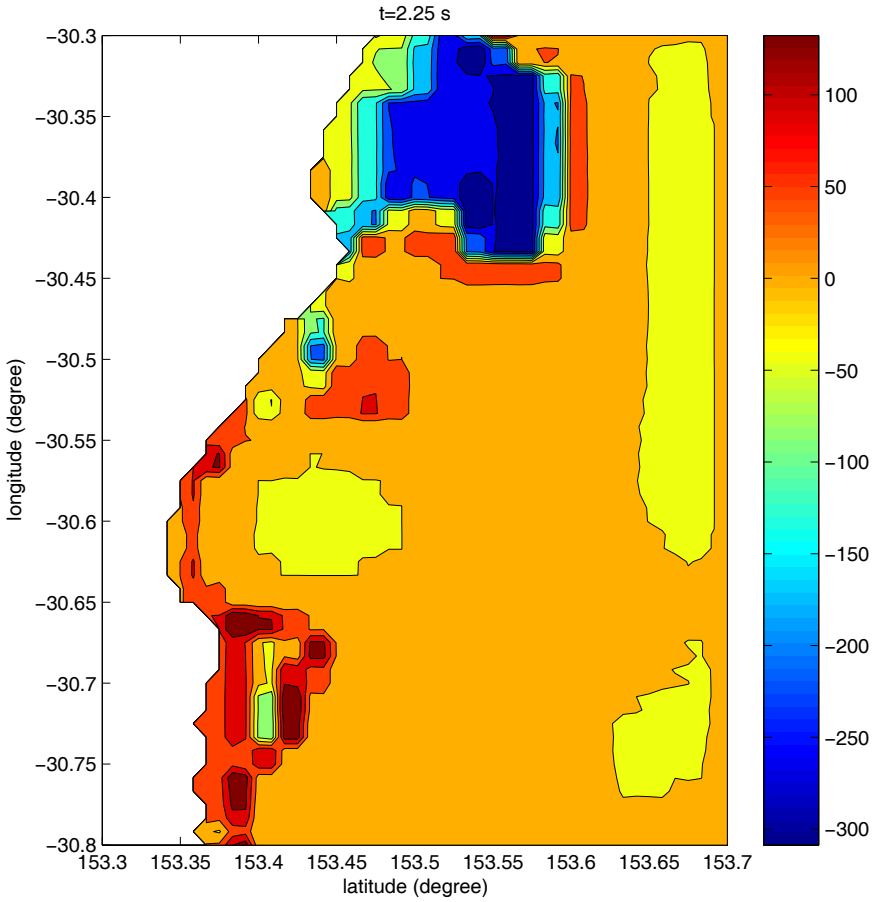

Figure 3-Contour Of The Wave-Induced Pore Pressure (S_r=0.95, Z=-1 m, T=2.25 sec)

To further investigate the influence of degree of saturation on the wave-induced pore pressure, we choose four different points as indicated in Figure 1. The distribution of the wave-induced pore pressure, p (N/m^2) versus time (sec) for various degree of saturation at different points are plotted in Figures 4-7.

As shown in Figure 4 (Point 1) and 5 (Point 2), there is a significant difference between fully saturation and nearly saturation (S_r=99%). However, this difference has been reduced at Point 3 and 4 (Figures 6 and 7). A general trend is observed in Figures 4-7. That is, the pore pressure decreases as the degree of saturation decreases near the peak of distribution. It also found that the magnitude of pore pressure at point 4 is much greater than other points.

4. CONCLUSIONS

In this paper, the wave model (SWAN) and soil model (PORO-WSSI) are linked together to investigate the wave-induced pore pressure in marine sediment in a three-dimensional domain. The data at east coast is used as the numerical example. With the new model, the contour distribution of the wave-induced pore pressure in a three-dimensional domain can be calculated, which cannot be done with the existing two-dimensional models. The significant influences of the degree of saturation on the pore pressure between fully saturated condition and nearly saturated conditions is also observed from Figures 4-7.

In this paper, only the preliminary results of the wave-induced pore pressure are presented. Another important issue, the wave-induced liquefaction, will be examined in the future study.

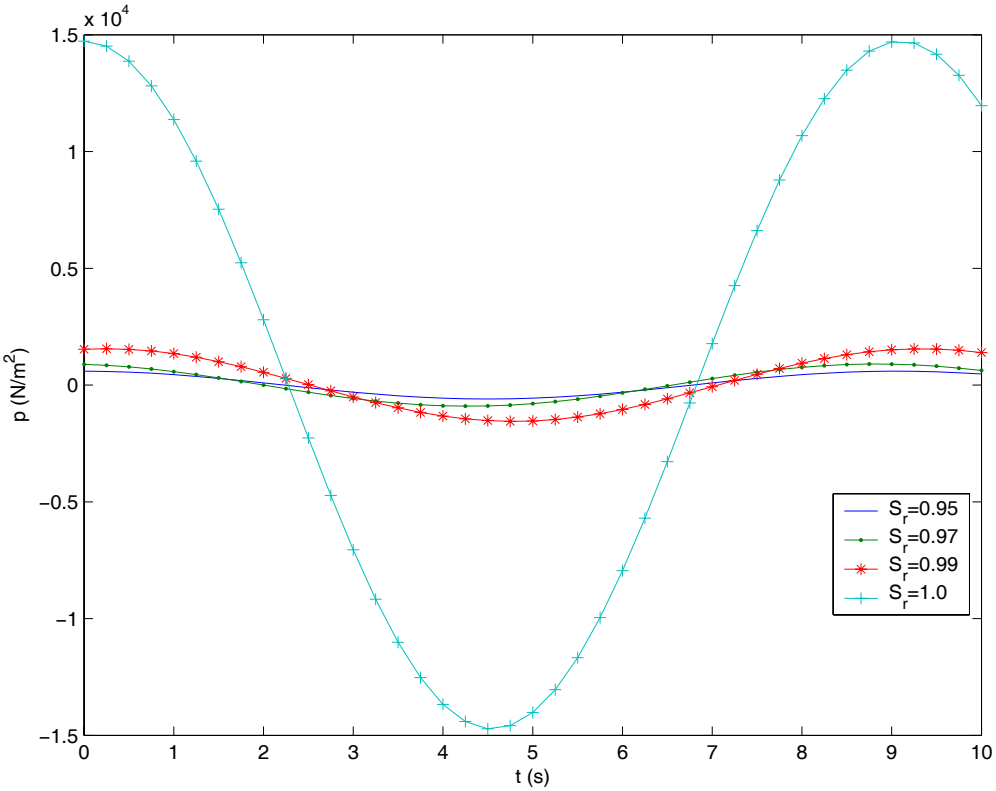

Figure 4-Distribution Of The Wave-Induced Pore Pressure Versus Time (Sec) For Various Degree Of Saturation At Point 1 (Referring To In Figure 1)

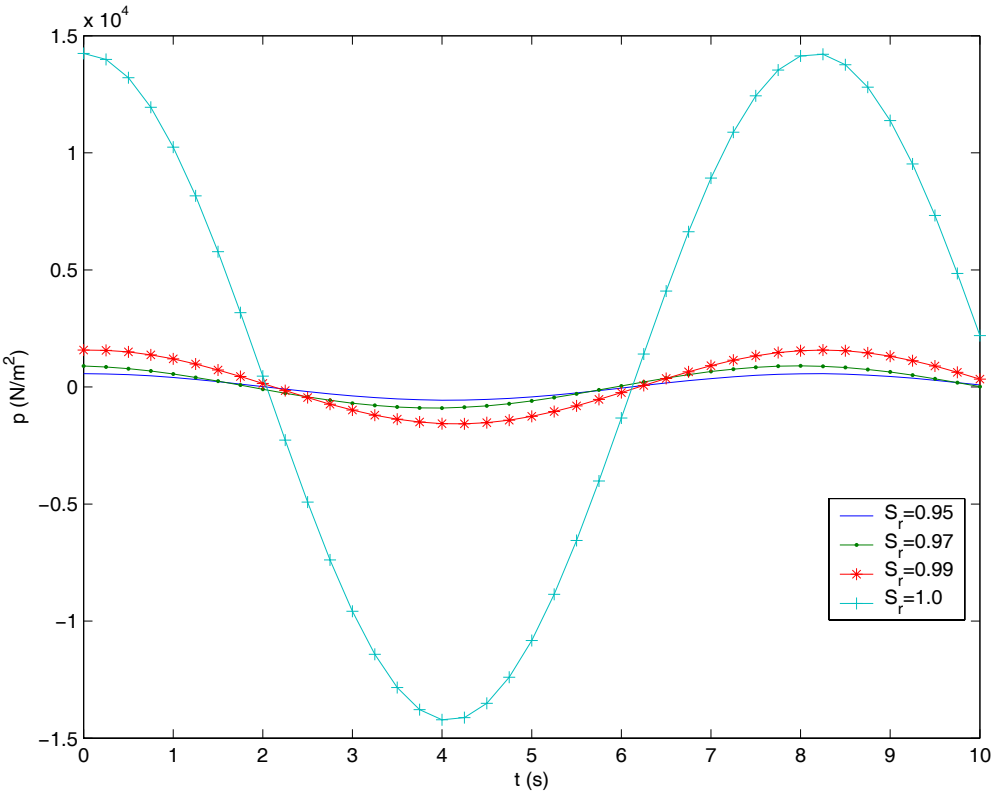

Figure 5-Distribution Of The Wave-Induced Pore Pressure Versus Time (Sec) For Various Degree Of Saturation At Point 2 (Referring To In Figure 1)

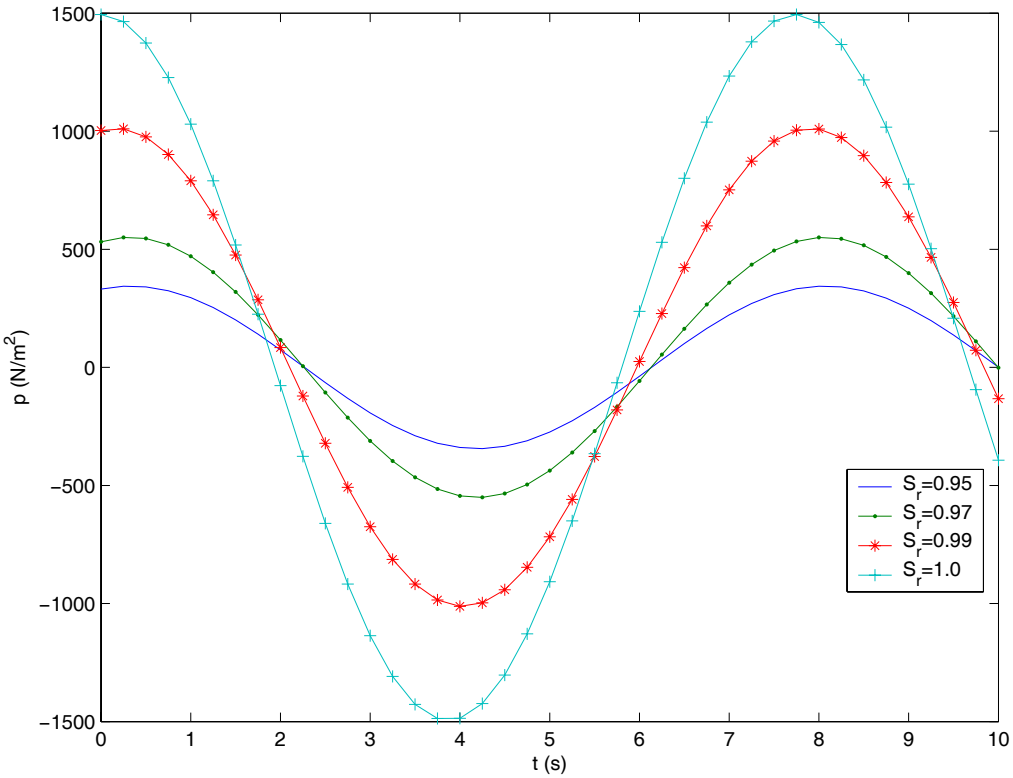

Figure 6-Distribution Of The Wave-Induced Pore Pressure Versus Time (Sec) For Various Degree Of Saturation At Point 3 (Referring To In Figure 1)

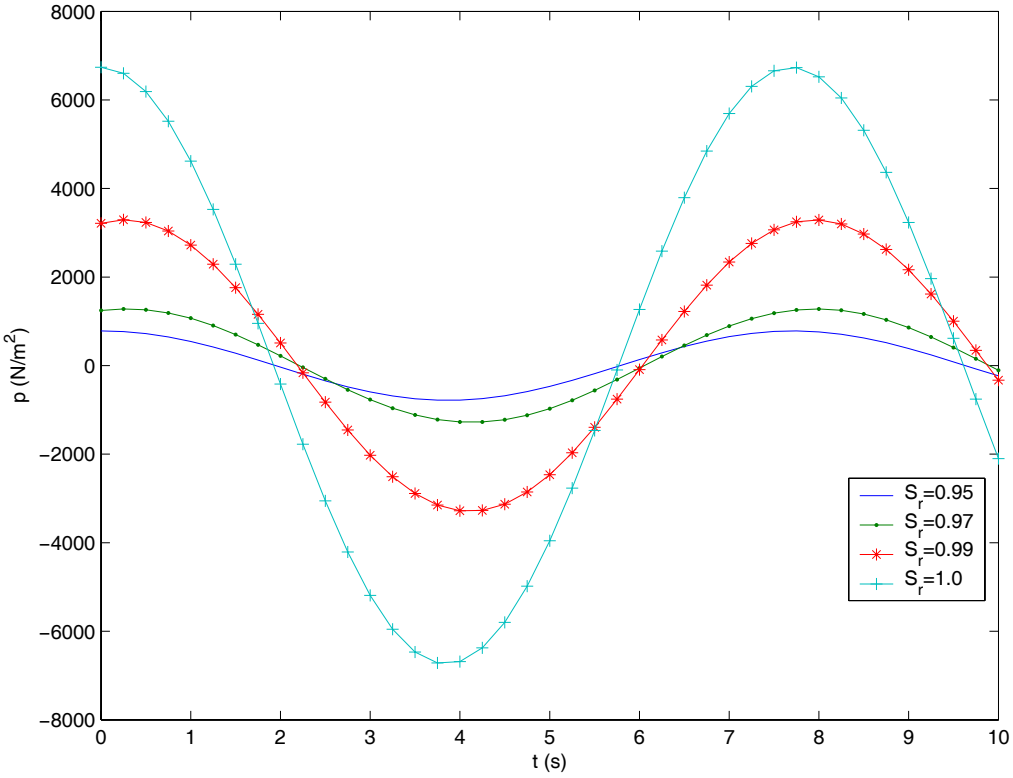

Figure 7-Distribution Of The Wave-Induced Pore Pressure Versus Time (Sec) For Various Degree Of Saturation At Point 4 (Referring To In Figure 1)

5. ACKNOWLEDGEMENTS

The second author is grateful for the support of Australian Research Council Large Grant Scheme (#A00104092)

6. REFERENCES

Biot, M. A. (1941) General theory of three-dimensional consolidation. *Journal of Applied Physics*, 12(2), 1550164

Booij, N.C., Ris, R.C., Holthuijsen, L.H., (1999). A third-generation wave model for coastal regions. Part I, Model description and validation. *Journal of Geophysical Research*, 104 (C4), 7649-7666.

Holthuijsen, L.H., Booij, N., Ris, R.C., Haagsma, I.J.G., Kieftenburg, A.T.M.M., Kriezi, E.E. (2003). *SWAN Cycle* III Version 40.20 User Manual. Delft University of Technology, The Netherlands.

Jeng, D.-S. (2003) Wave-induced seafloor dynamics. *Applied Mechanics Review*, 56(4), 407-429

Jeng, D.-S. and Cha, D. H. (2003). Effects of dynamic soil behaviour and wave non-linearity on the wave-induced pore pressure and effective stresses in porous seabed. *Ocean Engineering*, 30(16), 2065-2089.

Jeng, D.-S. and Hsu, J. R. C. (1996) Wave-induced soil response in a nearly saturated seabed of finite thickness. *Geotechnique*, 46(3), 427-440.

Jeng, D.-S., Rahman, M. S., Lee, T. L. (1999) Effects of Inertia forces on wave-induced seabed response. *International Journal of Offshore and Polar Engineering*, 9(4), 307-313.

Lin, M. and Jeng, D.-S. (2004) A 3-D model for ocean waves over a Columb-damping poroelastic seabed. Ocean Engineering, 31(5-6), 561-585.

Liu, P. L. F., (1973). Damping of water waves over porous bed. *Journal of Hydraulic Division, A.S.C.E.*, 99(12), 2263-2271.

Mei, C. C. and Foda, M. A. (1981). Wave-induced soil response in a fluid-filled poro-elastic solid with a free surface-a boundary layer theory. *Geophysical Journal of Royal Astron Society*, 66, 596-631.

Moshagen, H. and Torum, A. (1975). Wave induced pressures in permeable seabeds. *Journal of Waterway, Port, Coastal Engineering Division, A.S.C.E.*, 101(1), 49-57.

Ris, R.C., Holthuijsen, H. AND Booij, N., (1999). A third-generation wave model for coastal regions, Part II, Verification. *Journal of Geophysical Research*, 104 (C4), 7667-7681.

Yamamoto, T., H. L. Koning, H. Sellmejjer, E. V. Hijum, (1978). On the response of a poro-elastic bed to water waves. *Journal of Fluid Mechanics*, 87, 193--206.

The Institution of Engineers, Australia
8th National Conference on Hydraulics in Water Engineering
ANA Hotel Gold Coast, Australia 13-16 July 2004

Modelling The 3-Dimensional Flow Between The Nerang River Estuary And Burleigh Lakes System, Gold Coast

S.Zigic
ADEng., BEng
Director, Asia-Pacific ASA Pty. Ltd., Australia &
PhD Candidate, Griffith University Gold Coast Campus School of Engineering
B.A.King
BSc., Ph.D.,
Director, Asia-Pacific ASA Pty. Ltd., Australia
C.Lemckert
Bsc., MPhilSc., Ph.D
Senior Lecturer, Griffith University Gold Coast Campus School of Engineering

Abstract: A 3-dimensional numerical model (BFHYDRO) was employed to simulate the exchange between the Nerang River estuary and Burleigh Lakes system via an automated bi-directional hydraulic structure. To determine the accuracy and reliability of the model predictions, results were compared to measurements of surface elevation data at three stations within the lakes system. The model predictions were found to compare well to all stations. The high agreement between the measured and predicted datasets was particularly encouraging since it demonstrated the models ability to simulate the complex behaviour of the water as it flows through the hydraulic lock structure during each tidal cycle.

The outcomes of this project are expected to be highly beneficial, since it will allow managers to assess the influence that the hydraulic structure has upon the change in current flows, mixing and flushing dynamics, for present and future activities in this and other regions where such structures exist or are planned for.

Keywords: hydrodynamic, Nerang River, estuary, lake, modelling, hydraulic structure, three-dimensional

1. INTRODUCTION

The Nerang River estuary is the largest and most significant river and estuarine system within the Gold Coast, Australia, linking numerous man-made canal and lake environments (see Figure 1). The southern most branch of the estuary (approximately 18.5 km from the mouth) is connected to an artificial lake system (Burleigh Lakes system), via an automated bi-directional hydraulic structure referred to as 'Structure C'.

Structure C consists of four (4) box-cell culverts, each 3 m in width, 3 m in height and 11 m in length. Controlling the flow of water between the estuary and lake are four (4) 3 m by 3 m radial gates located on the lakeside of the culverts, each supporting a skin plate assembly used to separate the two (2) water bodies (see Figure 2). Each of the radial gates are programmed to allow water exchange 4 times per day between the lake and estuarine system, each for a period of 2 hours 12 minutes. The opening of the gates corresponds to the ebbing and flooding phases of the tides. Consequently, the structure limits the tidal velocities through the estuary and maintains the lake system as a brackish environment. Figure 2 shows a side profile schematic of Structure C, before and after the radial gates have been initiated.

This paper presents the extension of a two-dimensional (2D) vertically averaged model (BFHYDRO) used to simulate the inclusion of the hydraulic structure, and the complex exchange of water between the estuary and lake (Zigic et al., 2004) to three dimensions. A comparison is carried out between the model-predicted results to available observations within the lake.

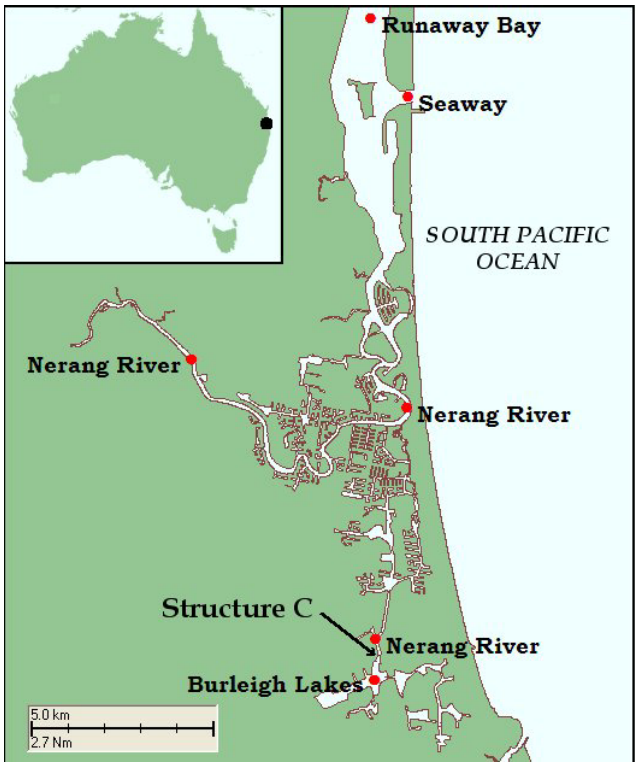

Figure 1 – Map of the study area and the location of the automated bi-direction hydraulic structure "Structure C".

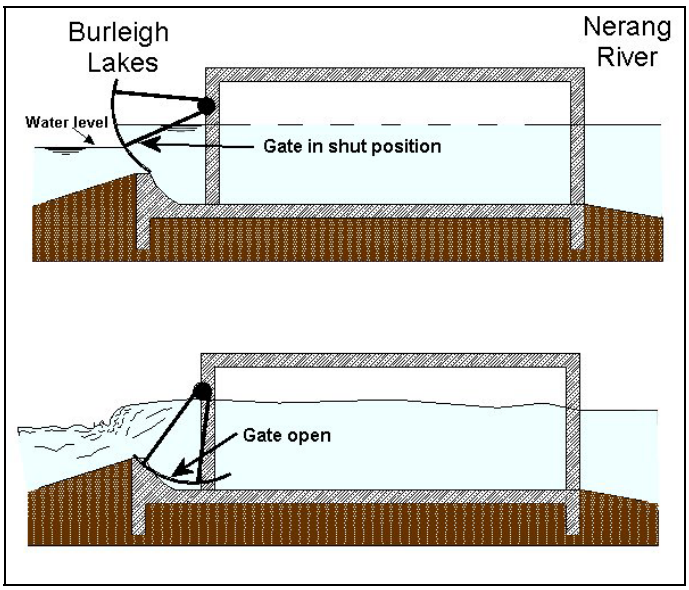

Figure 2 - A side profile schematic diagram illustrating the movement of a radial gate before (top) and after (bottom) they are initiated.

2. MODEL DESCRIPTION

To simulate the complex flow between the estuary and lake, a state-of-the art three-dimensional time-dependent, boundary fitted hydrodynamic model, BFHYDRO, was selected. BFHYDRO is used to generate tidal elevations, current velocities, salinity and temperature distributions for rivers, estuaries or coastal embayments. The three dimensional conservation of mass, momentum, salt and temperature equations are solved on a boundary fitted curvilinear grid system, allowing the user to match the model transformed co-ordinate system to the geometry of the water body. This boundary-fitted gridding method was particularly important to this study, due to the Nerang River extensive canal system (see Figure 1) and geometrically complex water body. Because tidal circulation is of primary importance in this study, baroclinic effects are neglected. The reader is referred to Muin and Spaulding (1997), Swanson (1986) and Swanson et al., (1998) for detailed presentation of the governing equations and other test cases of the BFHYDRO system.

The flow through the hydraulic structure cells are calculated entirely from the local water level gradients at each time-step, and not prescribed. Due to the nature of the structure, the broad crested weir formula (Chow, 1959) was used to best represent the exchange when the gates have opened (Zigic et al., 2004).

2.1 Hydrodynamic Grid Setup

The boundary fitted grid for the study area extends from Runaway Bay to the end of the Burleigh Lakes system (see Figure 1). The grid consists of 5134 active computational water cells. The boundary fitted grid for the Burleigh Lakes system is shown in Figure 3. The boundary fitted feature allows the user to match the grid to the shoreline boundary, as well as adjust the model grid resolution as desired. Thus, a fine grid resolution is used adjacent to Structure C (< 10m)to resolve the small scale features, and a much coarser resolution in the northern limits (between 150m to 200m) closer to the open boundaries at the Seaway and Runaway Bay. The boundary fitted grid for the Burleigh Lakes system is shown in Figure 3. The bathymetry data is mapped on the boundary fitted grid (see Figure 4). This gridding technique was employed to provide sufficient resolution near the mouth of the estuary and a fine resolution near the structure without compromising the numerical assumptions.

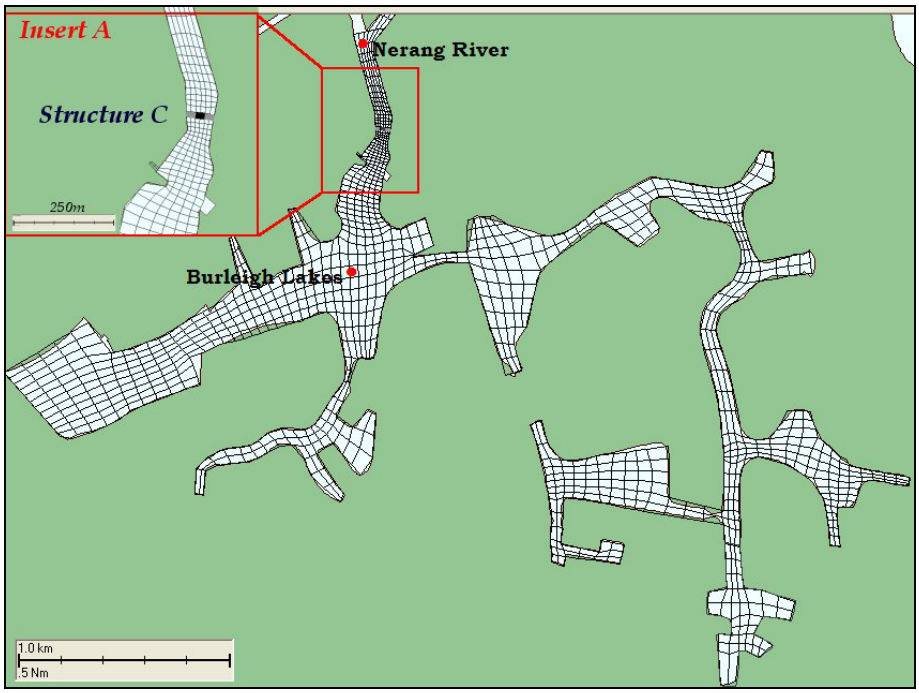

Figure 3 – Boundary fitted grid for the Burleigh Lakes system

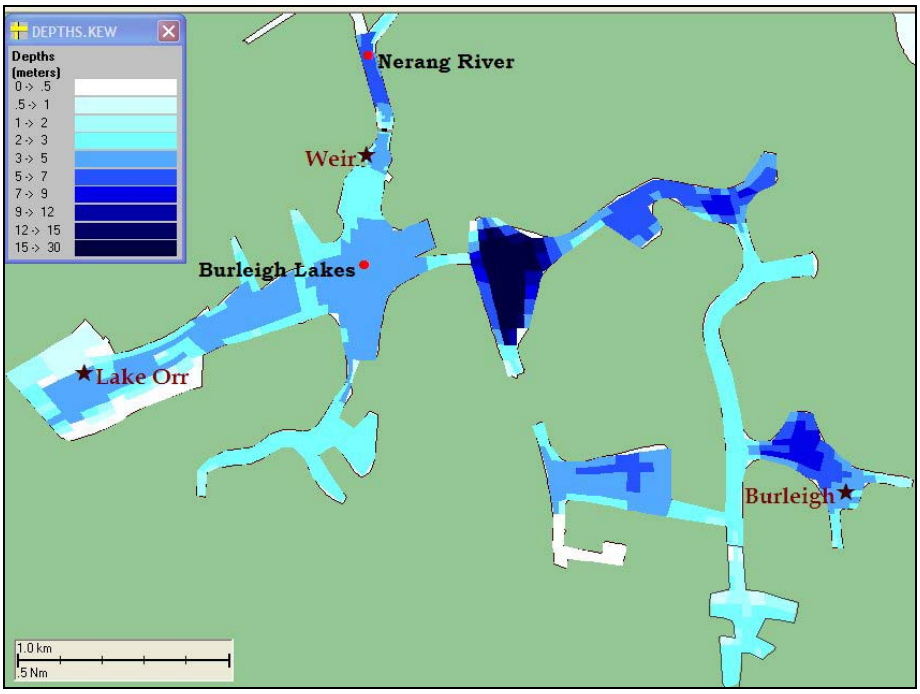

Figure 4 - Bathymetric grid used to define the Burleigh Lakes system. Note the red stars represent the location of the deployed tide gauges.

3. SOURCES OF AVAILABLE FIELD DATA

Time series of surface elevation data was collected between the 6-19 April 2002, at three (3) sites within the Burleigh Lakes system, for verifying the hydrodynamic model and quantifying the exchange between the estuary and the lake (refer to Figure 4). Gauges measuring temperature and depth (pressure) at 3 minute intervals, were placed approximately 150 m (referred to as Weir), 2200m (referred to as Lake Orr) and 4500m (referred to as Burleigh) upstream of the structure. Figure 5 shows a time series of measured surface elevation data between 6–19 April 2002, for three sites within the Burleigh Lakes system. During the 14-day field program the gates were open 44 times permitting water to enter and exit the Burleigh Lakes system.

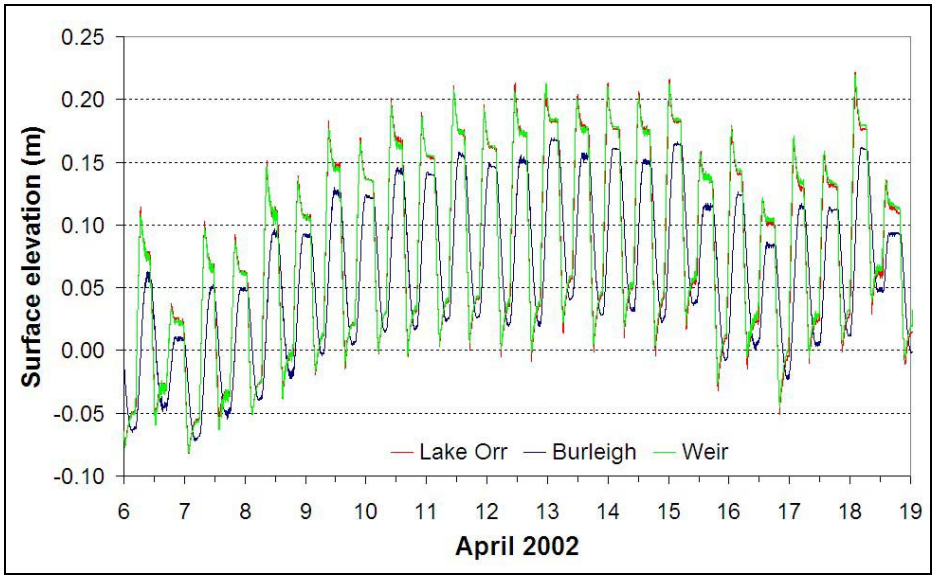

Figure 5 - A time series of the measured surface elevation data between 6– 19 April 2002, for three sites within the Burleigh Lakes system.

4. MODEL FORCING FUNCTIONS

The model forcing functions consist of tidal elevations along the open boundary at Runway Bay and Seaway. The tidal elevations are based on 22 major tidal constituents as reported by the Australian National Tidal

Facility. Since the loggings of the exact opening and closing times during the fourteen day period were not available, the times were deduced from the measured surface elevation data at Weir and were input directly into the model code (refer to Figure 5).

5. CALIBRATION-VALIDATION RESULTS

The measured surface elevation data was used as part of the calibration process, since flow data was unavailable. The quadratic bottom friction value was systematically adjusted between 0.001 and 0.01. Comparison between the model predicted surface elevation with the observed data showed that best results were obtained using a bottom friction coefficient of 0.007. The model was run over a 14-day period, with the initial two days used as a ramping period and a 60 second time step. Figures 6 and 7 show a snapshot of the predicted surface currents as vectors and colour contours during maximum ebb (water flowing out of the lake) and flood (water flowing into the lake) events, respectively with current speeds reaching up to 1 m/s (see Figure 8).

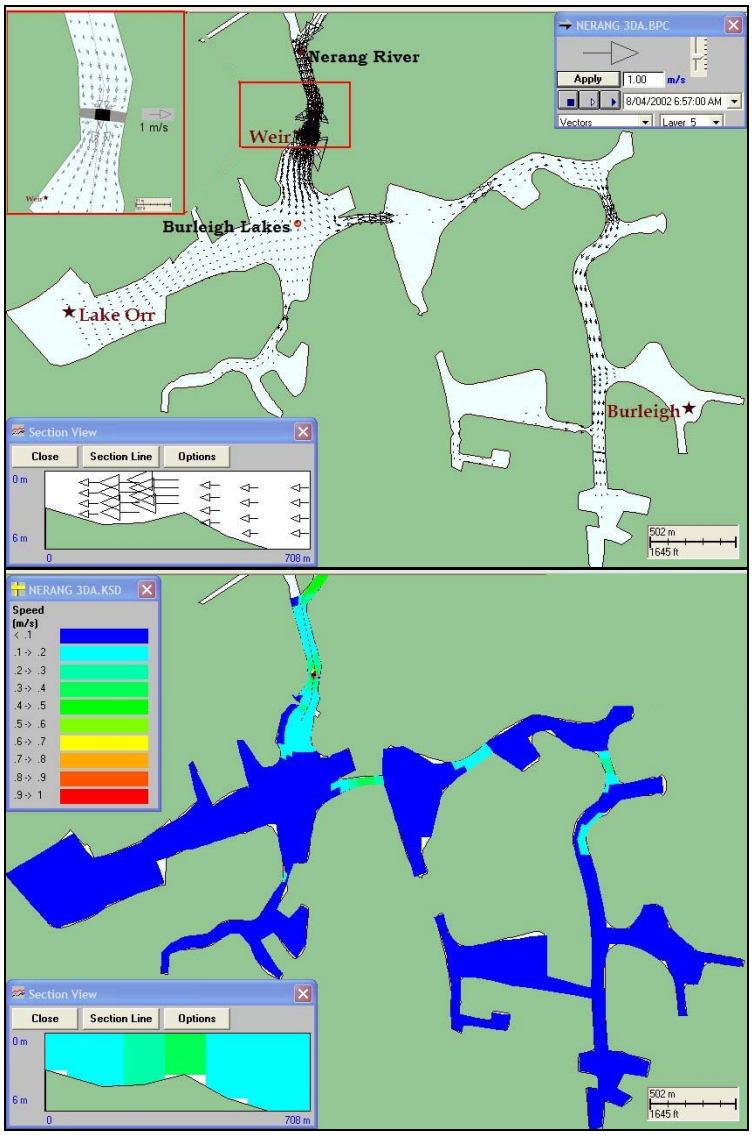

Figure 6 - Model predicted surface currents as (top) vectors; & (bottom) colour contours during maximum flood on the 8th April, 2002, 6:57 am. Note the bottom left inserts show a section view window along the dotted brown line.

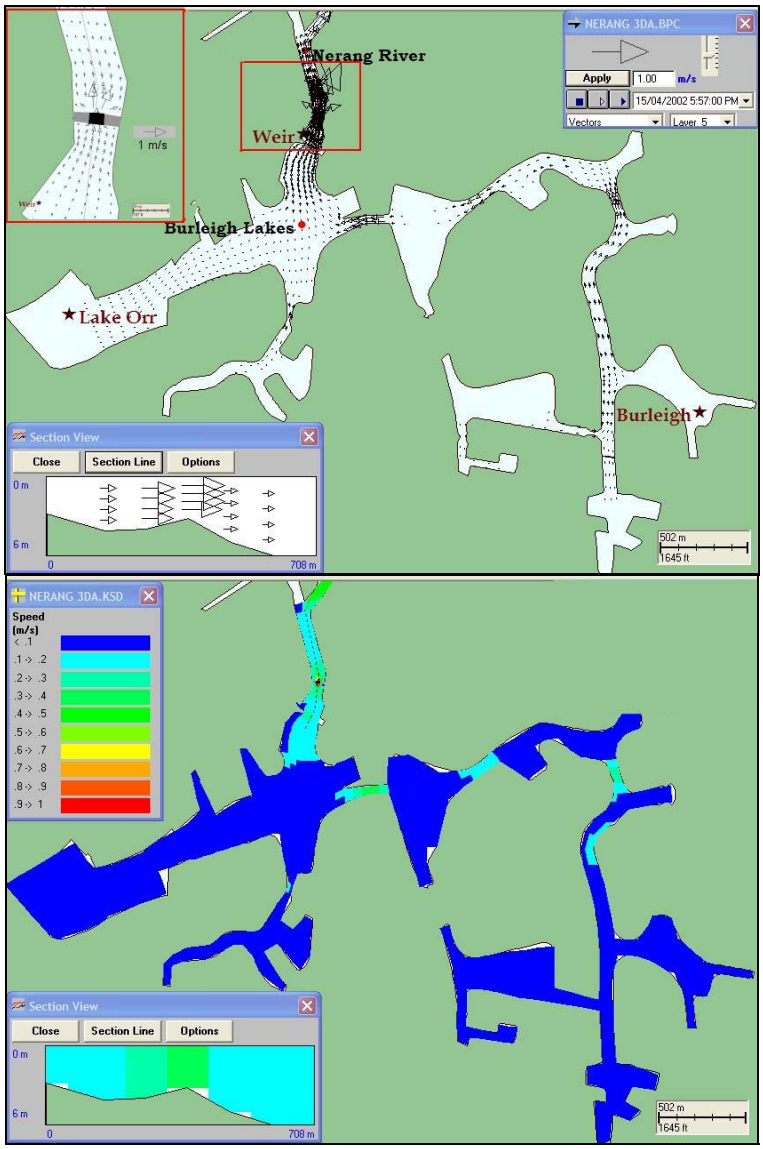

Figure 7 - Model predicted surface currents as (top) vectors; & (bottom) colour contours during maximum ebb on the 15th April, 2002, 5:57 pm. Note the bottom left inserts show a section view window along the dotted brown line.

Figures 9 – 11 show a comparison between the predicted and observed surface elevations at Weir, Lake Orr and Burleigh, respectively. The flow in and out of the lake for the 14-day simulation, resulting as a function of the opening and closing of the gates are well reproduced in the model at all stations. The correlation between the model predictions and the observed data at Weir and Lake Orr was greater than 87% and a surface elevation difference of less than 4 cm. The Burleigh predicted and observed correlation was 60% and a surface elevation difference of less than 5 cm. This lower correlation is due to the phase difference between the two datasets, which is due to the difficulty of the model replicating the constricted flow as the water moved under the bridge.

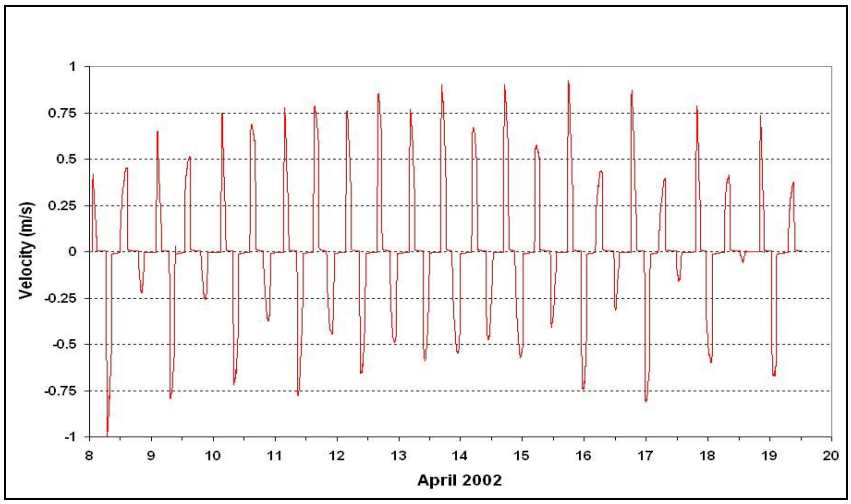

Figure 8 – Predicted surface current velocities immediately downstream of Structure C. Note negative currents represent the ebb tide.

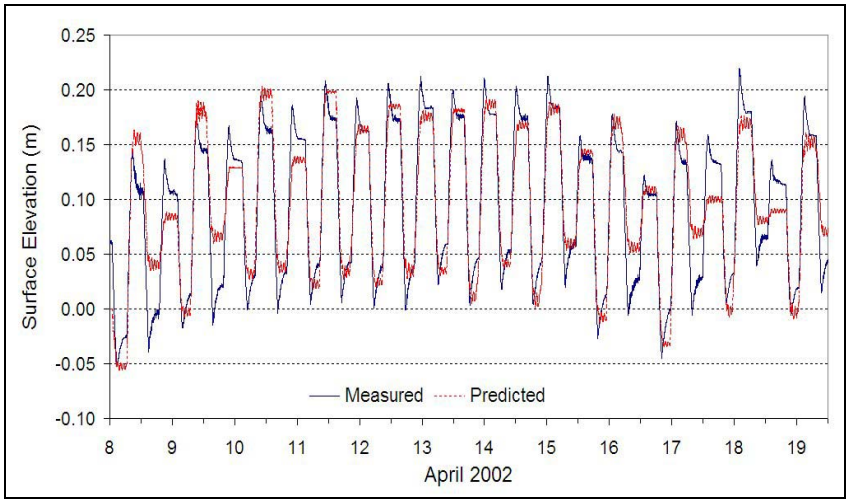

Figure 9 – Comparison of measured and predicted surface elevations at Weir.

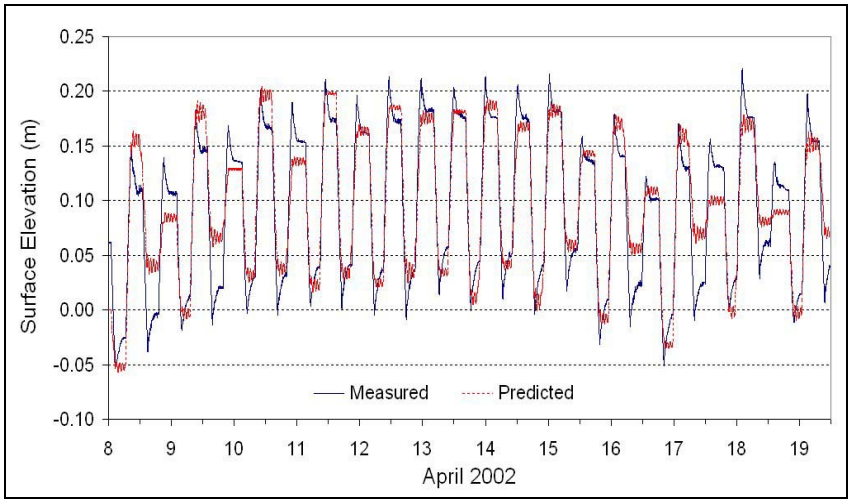

Figure 10 – Comparison of measured and predicted surface elevations at Lake Orr

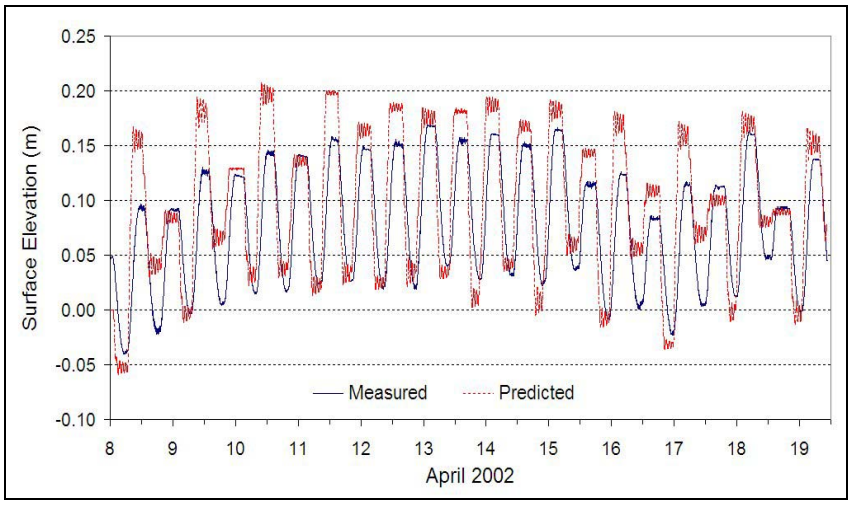

Figure 11 – Comparison of measured and predicted surface elevations at Burleigh.

6. CONCLUSIONS

A three-dimensional hydrodynamic model was applied to simulate the complex tidal exchange between the Nerang River estuary and the Burleigh Lakes system, with the inclusion of a bi-directional hydraulic lock structure. The predicted model surface elevations were found to compare favourably with the observed surface elevations at three stations in the Burleigh Lakes system. This was very encouraging since it demonstrated the models ability to simulate the complex behaviour of the water as it flows through the hydraulic lock structure during each tidal cycle.

7. ACKNOWLEDGEMENTS

The authors wish to thank Applied Science Associates Inc., who allowed us to use BFHYDRO model. Griffith University Gold Coast Campus (School of Engineering) and The Australian Research Council for their support. Discussions and assistance from Matthew Ward, Scott Langtry, Kathy Sheridan and Marc Zapata are gratefully acknowledged.

8. REFERENCES

Chow V T, (1959) Open Channel Hydraulics, McGraw Hill.

Muin, M. and Spaulding, M.L., 1997. Application of three dimensional boundary fitted circulation model to the Providence River. In: *Journal of Hydraulic Engineering,* Vol. 123, No. 1, January 1997, p. 13-20.

Swanson, J.C., Mendelsohn, D., Rines, H. and Schuttenberg, H., (1998). Mt. Hope Bay hydrodynamic model calibration and confirmation. Prepared for: New England Power Company, West Borough, MA, prepared by Applied Science Associates, Inc., Narragansett, RI.

Swanson, J. C. (1986). A three-dimensional numerical model system of coastal circulation and water quality. PhD dissertation, University of Rhode Island, Kingston, R.I.

Zigic, S., King., B and C. Lemckert (2004). Modelling the flow through a hydraulic structure. Submitted to the Journal of Estuarine Coastal Shelf Science.